

Pertanika Journal of
**SCIENCE &
TECHNOLOGY**

JST

VOL. 29 (4) OCT. 2021



PERTANIKA
JOURNALS

A scientific journal published by Universiti Putra Malaysia Press

PERTANIKA JOURNAL OF SCIENCE & TECHNOLOGY

About the Journal

Overview

Pertanika Journal of Science & Technology is an official journal of Universiti Putra Malaysia. It is an open-access online scientific journal. It publishes original scientific outputs. It neither accepts nor commissions third party content.

Recognised internationally as the leading peer-reviewed interdisciplinary journal devoted to the publication of original papers, it serves as a forum for practical approaches to improve quality on issues pertaining to science and engineering and its related fields.

Pertanika Journal of Science & Technology is a **quarterly** (*January, April, July, and October*) periodical that considers for publication original articles as per its scope. The journal publishes in **English** and it is open for submission by authors from all over the world.

The journal is available world-wide.

Aims and scope

Pertanika Journal of Science & Technology aims to provide a forum for high quality research related to science and engineering research. Areas relevant to the scope of the journal include: bioinformatics, bioscience, biotechnology and bio-molecular sciences, chemistry, computer science, ecology, engineering, engineering design, environmental control and management, mathematics and statistics, medicine and health sciences, nanotechnology, physics, safety and emergency management, and related fields of study.

History

Pertanika Journal of Science & Technology was founded in 1993 and focuses on research in science and engineering and its related fields.

Vision

To publish a journal of international repute.

Mission

Our goal is to bring the highest quality research to the widest possible audience.

Quality

We aim for excellence, sustained by a responsible and professional approach to journal publishing. Submissions can expect to receive a decision within 90 days. The elapsed time from submission to publication for the articles averages 180 days. We are working towards decreasing the processing time with the help of our editors and the reviewers.

Abstracting and indexing of Pertanika

Pertanika Journal of Science & Technology is now over 27 years old; this accumulated knowledge and experience has resulted the journal being abstracted and indexed in SCOPUS (Elsevier), Clarivate Web of Science (ESCI), EBSCO, ASEAN CITATION INDEX, Microsoft Academic, Google Scholar, and MyCite.

Citing journal articles

The abbreviation for Pertanika Journal of Science & Technology is *Pertanika J. Sci. & Technol.*

Publication policy

Pertanika policy prohibits an author from submitting the same manuscript for concurrent consideration by two or more publications. It prohibits as well publication of any manuscript that has already been published either in whole or substantial part elsewhere. It also does not permit publication of manuscript that has been published in full in proceedings.

Code of Ethics

The *Pertanika* journals and Universiti Putra Malaysia take seriously the responsibility of all of its journal publications to reflect the highest in publication ethics. Thus, all journals and journal editors are expected to abide by the journal's codes of ethics. Refer to *Pertanika's Code of Ethics* for full details, or visit the journal's web link at http://www.pertanika.upm.edu.my/code_of_ethics.php

Originality

The author must ensure that when a manuscript is submitted to *Pertanika*, the manuscript must be an original work. The author should check the manuscript for any possible plagiarism using any program such as Turn-It-In or any other software before submitting the manuscripts to the *Pertanika* Editorial Office, Journal Division.

All submitted manuscripts must be in the journal's acceptable similarity index range:
≤ 20% – PASS; > 20% – REJECT.

International Standard Serial Number (ISSN)

An ISSN is an 8-digit code used to identify periodicals such as journals of all kinds and on all media—print and electronic.

Pertanika Journal of Science & Technology: e-ISSN 2231-8526 (Online).

Lag time

A decision on acceptance or rejection of a manuscript is reached in 90 days (average). The elapsed time from submission to publication for the articles averages 180 days.

Authorship

Authors are not permitted to add or remove any names from the authorship provided at the time of initial submission without the consent of the journal's Chief Executive Editor.

Manuscript preparation

Most scientific papers are prepared according to a format called IMRAD. The term represents the first letters of the words *Introduction, Materials and Methods, Results, And Discussion*. IMRAD is simply a more 'defined' version of the "IBC" (*Introduction, Body, Conclusion*) format used for all academic writing. IMRAD indicates a pattern or format rather than a complete list of headings or components of research papers; the missing parts of a paper are: *Title, Authors, Keywords, Abstract, Conclusions, References, and Acknowledgement*. Additionally, some papers include *Appendices*.

The *Introduction* explains the scope and objective of the study in the light of current knowledge on the subject; the *Materials and Methods* describes how the study was conducted; the *Results* section reports what was found in the study; and the *Discussion* section explains meaning and significance of the results and provides suggestions for future directions of research. The manuscript must be prepared according to the journal's **Instruction to Authors** (http://www.pertanika.upm.edu.my/Resources/regular_issues/Regular_Issues_Instructions_to_Authors.pdf).

Editorial process

Authors who complete any submission are notified with an acknowledgement containing a manuscript ID on receipt of a manuscript, and upon the editorial decision regarding publication.

Pertanika follows a **double-blind peer-review** process. Manuscripts deemed suitable for publication are sent to reviewers. Authors are encouraged to suggest names of at least 3 potential reviewers at the time of submission of their manuscripts to *Pertanika*, but the editors will make the final selection and are not, however, bound by these suggestions.

Notification of the editorial decision is usually provided within 90 days from the receipt of manuscript. Publication of solicited manuscripts is not guaranteed. In most cases, manuscripts are accepted conditionally, pending an author's revision of the material.

As articles are double-blind reviewed, material that may identify authorship of the paper should be placed only on page 2 as described in the first-4-page format in *Pertanika*'s **Instruction to Authors** (http://www.pertanika.upm.edu.my/Resources/regular_issues/Regular_Issues_Instructions_to_Authors.pdf).

The journal's peer review

In the peer-review process, 2 to 3 referees independently evaluate the scientific quality of the submitted manuscripts. At least 2 referee reports are required to help make a decision.

Peer reviewers are experts chosen by journal editors to provide written assessment of the **strengths** and **weaknesses** of written research, with the aim of improving the reporting of research and identifying the most appropriate and highest quality material for the journal.

Operating and review process

What happens to a manuscript once it is submitted to *Pertanika*? Typically, there are 7 steps to the editorial review process:

1. The journal's Chief Executive Editor and the Editor-in-Chief examine the paper to determine whether it is relevance to journal needs in terms of novelty, impact, design, procedure, language as well as presentation and allow it to proceed to the reviewing process. If not appropriate, the manuscript is rejected outright and the author is informed.
2. The Chief Executive Editor sends the article-identifying information having been removed, to 2 to 3 reviewers. They are specialists in the subject matter of the article. The Chief Executive Editor requests that they complete the review within 3 weeks.

Comments to authors are about the appropriateness and adequacy of the theoretical or conceptual framework, literature review, method, results and discussion, and conclusions. Reviewers often include suggestions for strengthening of the manuscript. Comments to the editor are in the nature of the significance of the work and its potential contribution to the research field.

3. The Editor-in-Chief examines the review reports and decides whether to accept or reject the manuscript, invite the authors to revise and resubmit the manuscript, or seek additional review reports. In rare instances, the manuscript is accepted with almost no revision. Almost without exception, reviewers' comments (to the authors) are forwarded to the authors. If a revision is indicated, the editor provides guidelines for attending to the reviewers' suggestions and perhaps additional advice about revising the manuscript.
4. The authors decide whether and how to address the reviewers' comments and criticisms and the editor's concerns. The authors return a revised version of the paper to the Chief Executive Editor along with specific information describing how they have addressed' the concerns of the reviewers and the editor, usually in a tabular form. The authors may also submit a rebuttal if there is a need especially when the authors disagree with certain comments provided by reviewers.
5. The Chief Executive Editor sends the revised manuscript out for re-review. Typically, at least 1 of the original reviewers will be asked to examine the article.
6. When the reviewers have completed their work, the Editor-in-Chief examines their comments and decides whether the manuscript is ready to be published, needs another round of revisions, or should be rejected. If the decision is to accept, the Chief Executive Editor is notified.
7. The Chief Executive Editor reserves the final right to accept or reject any material for publication, if the processing of a particular manuscript is deemed not to be in compliance with the S.O.P. of *Pertanika*. An acceptance letter is sent to all the authors.

The editorial office ensures that the manuscript adheres to the correct style (in-text citations, the reference list, and tables are typical areas of concern, clarity, and grammar). The authors are asked to respond to any minor queries by the editorial office. Following these corrections, page proofs are mailed to the corresponding authors for their final approval. At this point, **only essential changes are accepted**. Finally, the manuscript appears in the pages of the journal and is posted on-line.

Pertanika Journal of

**SCIENCE
& TECHNOLOGY**

Vol. 29 (4) Oct. 2021



A scientific journal published by Universiti Putra Malaysia Press



EDITOR-IN-CHIEF

Luqman Chuah Abdullah
Chemical Engineering

CHIEF EXECUTIVE EDITOR

Mohammad Jawaid
Polymer Composites

UNIVERSITY PUBLICATIONS COMMITTEE

CHAIRMAN

Zulkifli Idrus

EDITORIAL STAFF

Journal Officers:

Kanagamalar Silvarajoo, *ScholarOne*
Siti Zuhaila Abd Wahid, *ScholarOne*
Tee Syin Ying, *ScholarOne*
Umni Fairuz Hanapi, *ScholarOne*

Editorial Assistants:

Ku Ida Mastura Ku Baharom
Siti Juridah Mat Arip
Zulinaardawati Kamarudin

English Editor:

Norhanizah Ismail

PRODUCTION STAFF

Pre-press Officers:

Nur Farrah Dila Ismail
Wong Lih Jiu

WEBMASTER

IT Officer:

Munir Hayat Md Bahrin

EDITORIAL OFFICE

JOURNAL DIVISION

Putra Science Park
1st Floor, IDEA Tower II
UPM-MTDC Technology Centre
Universiti Putra Malaysia
43400 Serdang, Selangor Malaysia.

Gen Enquiry

Tel. No: +603 9769 1622 | 1616

E-mail:

executive_editor.pertanika@upm.edu.my

URL: www.journals-jd.upm.edu.my

PUBLISHER

UPM Press

Universiti Putra Malaysia
43400 UPM, Serdang, Selangor, Malaysia.
Tel: +603 9769 8851
E-mail: penerbit@putra.upm.edu.my
URL: <http://penerbit.upm.edu.my>



ASSOCIATE EDITOR

2021-2023

Adem Kilicman
Mathematical Sciences
Universiti Putra Malaysia, Malaysia

Miss Laiha Mat Kiah
Security Services Sn: Digital Forensic, Steganography, Network Security, Information Security, Communication Protocols, Security Protocols
Universiti Malaya, Malaysia

Saidur Rahman
Renewable Energy, Nanofluids, Energy Efficiency, Heat Transfer, Energy Policy
Sunway University, Malaysia

EDITORIAL BOARD

2020-2022

Abdul Latif Ahmad
Chemical Engineering
Universiti Sains Malaysia, Malaysia

Hsiu-Po Kuo
Chemical Engineering
National Taiwan University, Taiwan

Mohd. Ali Hassan
Bioprocess Engineering, Environmental Biotechnology
Universiti Putra Malaysia, Malaysia

Ahmad Zaharin Aris
Hydrochemistry, Environmental Chemistry, Environmental Forensics, Heavy Metals
Universiti Putra Malaysia, Malaysia

Ivan D. Rukhlenko
Nonlinear Optics, Silicon Photonics, Plasmonics and Nanotechnology
The University of Sydney, Australia

Najafpour Darzi Ghasem
Bioprocess Technology, Chemical Engineering, Water and Wastewater Treatment Technology, Biochemical Engineering and Biotechnology, Bioethanol, Biofuel, Biohydrogen, Enzyme and Fermentation Technology
Babol Noshirvani University of Technology, Iran

Azlina Harun@Kamaruddin
Enzyme Technology, Fermentation Technology
Universiti Sains Malaysia, Malaysia

Lee Keat Teong
Energy Environment, Reaction Engineering, Waste Utilization, Renewable Energy
Universiti Sains Malaysia, Malaysia

Nor Azah Yusof
Biosensors, Chemical Sensor, Functional Material
Universiti Putra Malaysia, Malaysia

Bassim H. Hameed
Chemical Engineering: Reaction Engineering, Environmental Catalysis & Adsorption
Qatar University, Qatar

Mohamed Othman
Communication Technology and Network, Scientific Computing
Universiti Putra Malaysia, Malaysia

Biswajeet Pradhan
Digital image processing, Geographical Information System (GIS), Remote Sensing
University of Technology Sydney, Australia

Mohd Sapuan Salit
Concurrent Engineering and Composite Materials
Universiti Putra Malaysia, Malaysia

Norbahiah Misran
Communication Engineering
Universiti Kebangsaan Malaysia, Malaysia

Daud Ahmad Israf Ali
Cell Biology, Biochemical, Pharmacology
Universiti Putra Malaysia, Malaysia

Mohd Shukry Abdul Majid
Polymer Composites, Composite Pipes, Natural Fibre Composites, Biodegradable Composites, Bio-Composites
Universiti Malaysia Perlis, Malaysia

Roslan Abd-Shukur
Physics & Materials Physics, Superconducting Materials
Universiti Kebangsaan Malaysia, Malaysia

Hari M. Srivastava
Mathematics and Statistics
University of Victoria, Canada

Mohd Zulkifly Abdullah
Fluid Mechanics, Heat Transfer, Computational Fluid Dynamics (CFD)
Universiti Sains Malaysia, Malaysia

Wing Keong Ng
Aquaculture, Aquatic Animal Nutrition, Aqua Feed Technology
Universiti Sains Malaysia, Malaysia

INTERNATIONAL ADVISORY BOARD

2021-2024

CHUNG, Neal Tai-Shung
Polymer Science, Composite and Materials Science
National University of Singapore, Singapore

Mohamed Pourkashanian
Mechanical Engineering, Energy, CFD and Combustion Processes
Sheffield University, United Kingdom

Yulong Ding
Particle Science & Thermal Engineering
University of Birmingham, United Kingdom

Hiroshi Uyama
Polymer Chemistry, Organic Compounds, Coating, Chemical Engineering
Osaka University, Japan

Mohini Sain
Material Science, Biocomposites, Biomaterials
University of Toronto, Canada

ABSTRACTING AND INDEXING OF PERTANIKA JOURNALS

The journal is indexed in SCOPUS (Elsevier), Clarivate-Emerging Sources Citation Index (ESCI), BIOSIS, National Agricultural Science (NAL), Google Scholar, MyCite, ISC. In addition, Pertanika JSSH is recipient of "CREAM" Award conferred by Ministry of Higher Education (MoHE), Malaysia.

The publisher of Pertanika will not be responsible for the statements made by the authors in any articles published in the journal. Under no circumstances will the publisher of this publication be liable for any loss or damage caused by your reliance on the advice, opinion or information obtained either explicitly or implied through the contents of this publication. All rights of reproduction are reserved in respect of all papers, articles, illustrations, etc., published in Pertanika. Pertanika provides free access to the full text of research articles for anyone, web-wide. It does not charge either its authors or author-institution for refereeing/publishing outgoing articles or user-institution for accessing incoming articles. No material published in Pertanika may be reproduced or stored on microfilm or in electronic, optical or magnetic form without the written authorization of the Publisher.

Copyright ©2021 Universiti Putra Malaysia Press. All Rights Reserved.



Pertanika Journal of Science & Technology
Vol. 29 (4) Oct. 2021

Contents

Foreword <i>Mohammad Jawaid</i>	i
Mobile Application Development for Spectral Signature of Weed Species in Rice Farming <i>Nor Athirah Roslin, Nik Norasma Che'Ya, Nursyazyla Sulaiman, Lutfi Amir Nor Alahyadi and Mohd Razi Ismail</i>	2241
<i>Review article</i>	
Potential of <i>Syzygium polyanthum</i> (Daun Salam) in Lowering Blood Glucose Level: A Review <i>Nur Salsabeela Mohd Rahim, Ida Farah Ahmad and Terence Yew Chin Tan</i>	2261
Socio-Demographic Profile and Prevalence of Tuberculosis (TB) Treatment Outcomes among Tuberculosis/Human Immunodeficiency Virus (TB/HIV) Co-Infected Patients in Kelantan <i>Siti Romaino Mohd Nor, Mohd Rozi Husin, Mat Zuki Mat Jaeb and Nyi Nyi Naing</i>	2279
Physical Modelling of Flow and Head along with Dead-end and Looped Manifolds <i>Abdullah Amer, Thamer Ahmad Mohammad, Wissam Hameed Alawee and Nadhir Al-Ansari</i>	2295
A Combined Analytical Method for Intelligent Control of Friction Damped Structures <i>Kamyar Gharra, Karen Khanlari and Jafar Asgari Marnani</i>	2317
Classification of Existing Health Model of India at the End of the Twelfth Plan using Enhanced Decision Tree Algorithm <i>Ashok Kumar, Arun Lal Srivastav, Ishwar Dutt and Karan Bajaj</i>	2341
<i>Review Article</i>	
An Era of Recommendation Technologies in IoT: Categorisation by techniques, Challenges and Future Scope <i>Partibha Ahlawat and Chhavi Rana</i>	2355

A Novel Approach of Audio Based Feature Optimisation for Bird Classification <i>Murugaiya Ramashini, Pg Emeroylariffion Abas and Liyanage C De Silva</i>	2383
Behavioural Model for Decision-Makers' towards the Intention to Adopt Green Information Technology: A Preliminary Study <i>Abba Kyari Buba and Othman Ibrahim</i>	2409
Effect of Initial Carbon to Nitrogen Ratio on the Degradation of Oil Palm Empty Fruit Bunch with Periodic Addition of Anaerobic Palm Oil Mill Effluent Sludge <i>Muhamad Yusuf Hasan, Mohd Ali Hassan, Mohd Noriznan Mokhtar, Yoshihito Shirai and Azni Idris</i>	2435
Enhancement of Binding Affinity of Anti-Hapten Polyclonal IgG Recognizing Mitragnine using Affinity Purification <i>Radhiahtul Raehan Mustafa, Rashidah Sukor, Siti Mariam Mohd Nor, Nazamid Saari, Farina Mustaffa Kamal and Aliah Zannierah Mohsin</i>	2451
Response of Rubber Tree Saplings to Dolomite and Kieserite Application and K:Mg Ratio <i>Chakkrit Poonpakdee, Khwunta Khawmee and Jumpen Onthong</i>	2465
The Effect of the Operation Time, Orientation of Passenger and Body Mass Index on Passengers' Whole-Body Vibration on Urban Rail <i>Muhammad Nur Annuar Mohd Yunos, Mohd Azlis Sani Md Jalil, Nor Azali Azmir and Mifzal Nazhan Mazlan</i>	2481
Diffusion and Osmotic Permeability of Ion Exchange Membrane MK-40 Using Sodium Chloride Solution <i>Mohammed Qader Gubari, Haider Mohammed Zwain and Nadezda Vyacheslavovna Alekseeva</i>	2497
The Prediction of Chlorophyll Content in African Leaves (<i>Vernonia amygdalina</i> Del.) Using <i>Flatbed Scanner</i> and Optimised Artificial Neural Network <i>Retno Damayanti, Nurul Rachma, Dimas Firmanda Al Riza and Yusuf Hendrawan</i>	2509
The Effect of Storage Diversity on the Breaking Strength and Elongation of Polyamide Monofilament in Gill Net Fishing Gear <i>Herry Boesono, Fadhila Surya Layli, Agus Suherman, Bogi Budi Jayanto and Arief Yudhi Susanto</i>	2531

A Deep Learning Approach for Retinal Image Feature Extraction <i>Mohammed Enamul Hoque, Kuryati Kipli, Tengku Mohd Afendi Zulcaffle, Abdulrazak Yahya Saleh Al-Hababi, Dayang Azra Awang Mat, Rohana Sapawi and Annie Anak Joseph</i>	2543
Development of Micro-Spatial Electricity Load Forecasting Methodology Using Multivariate Analysis for Dynamic Area in Tangerang, Indonesia <i>Adri Senen, Christine Widyastuti, Oktaria Handayani and Perdana Putera</i>	2565
<i>Case study</i> Improving Performance in Construction Projects: A Case Study of Malaysian Public Projects <i>Aminah Md Yusof, Ali Raza Khoso, Samiullah Sohu, Shabir Hussain Khahro and Chang Saar Chai</i>	2579
Optimisation of Free Fatty Acid Removal in Nyamplung Seed Oil (<i>Callophyllum inophyllum</i> L.) using Response Surface Methodology Analysis <i>Ratna Dewi Kusumaningtyas, Haniif Prasetiawan, Radenrara Dewi Artanti Putri, Bayu Triwibowo, Siti Choirunisa Furi Kurnita, Nanda Dwi Anggraeni, Harumi Veny, Fazlena Hamzah and Miradatul Najwa Muhd Rodhi</i>	2605
A Comparative Study of Several EOF Based Imputation Methods for Long Gap Missing Values in a Single-Site Temporal Time Dependent (SSTTD) Air Quality (PM ₁₀) Dataset <i>Shamihah Muhammad Ghazali, Norshahida Shaadan and Zainura Idrus</i>	2625
Synthesis, Characterisation, and Density Functional Theory Study of Encapsulated Bioactive Components of Ginger <i>Triati Dewi Kencana Wungu, Damar Rastri Adhika, Meqorry Yusfi, Atsarina Larasati Anindya, Eduardus Bimo Aksono, Raden Roro Fosa Sarassina, Christofora Hanny Wijaya and Suprijadi</i>	2645
An Indoor Navigation Support for the Student Halls of Residence using Augmented Reality: A Design Perspective <i>Dinna Nina Mohd Nizam, Lim Wei Shin, Zaidatul Haslinda Abdullah Sani, Pornpon Thamrongrat and Nooralisa Mohd Tuah</i>	2659
Effects of Noise Pollution from Electric Backup Generators on the Operators' Health <i>Mahmmoud Ismail Mohammed and Muwafaq Ayesh Rabeea</i>	2675

The Demand Model of App-Based Transportation Household Scale in Semarang, Indonesia <i>Anita Ratnasari Rakhmatulloh, Diah Intan Kusumo Dewi, Wijayanti and Rosna Sari Pulungan</i>	2689
<i>Review article</i>	
Roles and Principles of Sterilisation Process in Palm Oil Mills <i>Yin Mee Thang, Robiah Yunus, Mohd Noriznan Mokhtar, David Ross Appleton, Ahmad Jaril Asis, Pei San Kong, Huey Fang Teh and Abdul Azis Ariffin</i>	2705
Utilisation of Oil Palm Fibre Biomass Waste as Additives in Foamed Concrete <i>Md Azree Othuman Mydin</i>	2723
Logistics and Freight Transportation Management: An NLP based Approach for Shipment Tracking <i>Rachit Garg, Arvind Wamanrao Kiwelekar and Laxman Damodar Netak</i>	2745
A Simulation Study on Modified Weibull Distribution for Modelling of Investment Return <i>Hamza Abubakar and Shamsul Rijal Muhammad Sabri</i>	2767
Analytical and Numerical Investigations of Mechanical Vibration in the Vertical Direction of a Human Body in a Driving Vehicle using Biomechanical Vibration Model <i>Maher Al-Baghdadi, Muhsin Jaber Jweeg and Muhannad Al-Waily</i>	2791
A Comparative Study on the Larvicidal Effects of <i>Piper sarmentosum</i> (Kaduk) Leaves Extracts against <i>Aedes aegypti</i> <i>Amelia Najiha Othman, Nur Farah Suryani Zainudin, Uswatun Hasanah Zaidan and Suhaili Shamsi</i>	2811
The Estimation of Iron Oxide Content in Soil based on Landsat 8 OLI TIRS Imagery in Wetland Areas <i>Deasy Arisanty, Aswin Nur Saputra, Akhmad Munaya Rahman, Karunia Puji Hastuti and Dedi Rosadi</i>	2829
Mathematical Modelling of Infra-Red Evaporation Characteristics of Wheat Straw Black Liquor <i>Surendra Pratap Singh, Mohammad Jawaid, Bhoomika Yadav and Mohd Supian Abu Bakar</i>	2845

Enhanced IoT-Based Climate Control for Oyster Mushroom Cultivation Using Fuzzy Logic Approach and NodeMCU Microcontroller <i>Muhammad Azizi Mohd Ariffin, Muhammad Izzad Ramli, Zarina Zainol, Mohd Nazrul Mohd Amin, Marina Ismail, Rosanita Adnan, Nor Diana Ahmad, Norhasiah Husain and Nursuriati Jamil</i>	2863
Participatory Design: Apps from The Older Adults to The Older Adults <i>Zaidatul Haslinda Abdullah Sani, Dinna@Ninna Mohd Nizam and Aslina Baharum</i>	2887
Development of Pulp Moulded Packaging Samples from Empty Fruit Bunch Fibre <i>Qiuyun Liu, Ceri Loxton, Amir Alzahari Mohamed, Mohammad Jawaid, Radek Braganca and Robert Elias</i>	2901
Empirical Model of Ground-Borne Vibration Induced by Commuter Railway Traffic <i>Mohd Khairul Afzan Mohd Lazi, Muhammad Akram Adnan and Norliana Sulaiman</i>	2913
<i>Review article</i>	
Impact of Climate Change on Migratory Birds in Asia <i>Nurhafizul Abu Seri and Azimah Abd Rahman</i>	2937
Enhanced Deep Hierarchical Long Short-Term Memory and Bidirectional Long Short-Term Memory for Tamil Emotional Speech Recognition using Data Augmentation and Spatial Features <i>Bennilo Fernandes and Kasiprasad Mannepalli</i>	2967
Proposed Methodology for End-of-Life Option using Multi Criteria Decision Analysis: A Study for General Paper Product <i>Salwa Mahmood, Muhammad Aizrul Ezuan Edirudzin and Nur Syamimi Jiran</i>	2993
Reduction of the Backing Gas Sequence as a Facile Method to Improve Corrosion Resistance in Duplex Stainless Steel (DSS) Weldment <i>Basuki Tri Laksono, Hendri Budi Kurniyanto, Purwa Sadewa and Riza Wirawan</i>	3013
Failure Rate Estimation for Transformer Population based on Health Index through Markov Model Approach <i>Nor Shafiqin Shariffuddin, Norhafiz Azis, Amran Mohd Selva, Muhammad Sharil Yahaya, Jasronita Jasni, Mohd Zainal Abidin Ab Kadir and Mohd Aizam Talib</i>	3029

Morphological Characteristics and Plant Species for Noise Reducer and Pb Metal Absorbers at Adisucipto Airport: Yogyakarta, Indonesia <i>Chales Torang Pandapotan, Siti Nurul Rofiqo Irwan and Eka Tarwaca Susila Putra</i>	3043 - 3057
Crack Behaviour of Self-Compacting Concrete (SCC) Beams Containing Eggshell in Flexural <i>Mohd Raizamzamani Md Zain, Oh Chai Lian, Lee Siong Wee, Norrul Azmi Yahya and Anizahyati Alisibramulisi</i>	3059
A Privacy Preserving Framework for Health Records using Blockchain <i>Chitra Karunakaran, Kavitha Ganesh, Sonya Ansar and Rohitha Subramani</i>	3081
Evaluation of Single Missing Value Imputation Techniques for Incomplete Air Particulates Matter (PM ₁₀) Data in Malaysia <i>Zuraira Libasin, Wan Suhailah Wan Mohamed Fauzi, Ahmad Zia ul-Saufie, Nur Azimah Idris and Noor Azizah Mazeni</i>	3099
Optimisation Design of Functionally Graded Sandwich Plate with Porous Metal Core for Buckling Characterisations <i>Emad Kadum Njim, Sadeq Hussein Bakhy and Muhannad Al-Waily</i>	3113
<i>Case Study</i> Anomaly Detection of Grid Connected Photovoltaic System Based on Degradation Rate: A Case Study in Malaysia <i>Mohamad Zhafran Hussin, Nor Diyana Md Sin, Hedzlin Zainuddin, Ahmad Maliki Omar and Sulaiman Shaari</i>	3143
Serious Game Conceptual Model of Brain-Based Learning for Halus Student <i>Saffa Raihan Zainal Abidin, Siti Fadzilah Mat Noor and Noraidah Sahari@Ashaari</i>	3161

Foreword

Welcome to the fourth issue of 2021 for the *Pertanika Journal of Science and Technology (PJST)*!

PJST is an open-access journal for studies in Science and Technology published by Universiti Putra Malaysia Press. It is independently owned and managed by the university for the benefit of the world-wide science community.

This issue contains 49 articles; two case studies, four review articles, and the rest are regular articles. The authors of these articles come from different countries namely India, Indonesia, Iran, Iraq, Japan, Malaysia, Nigeria, Pakistan, Russia, Saudi Arabia, Sweden, Thailand, and UK.

A regular article titled “A deep learning approach for retinal image feature extraction” was written by Mohammed Enamul Hoque and co-researchers from Universiti Malaysia Sarawak. This study proposes a retinal image feature, true vessel segments extraction approach exploiting the Faster Retinal Convolutional Neural Network. The fundamental Image Processing principles have been employed for pre-processing the retinal image data. A combined database assembling image data from different publicly available databases have been used to train, test, and evaluate this proposed method. This proposed method has obtained 92.81% sensitivity and 63.34 positive predictive value in extracting true vessel segments from the top first tier of colour retinal images. It is expected to integrate this method into ophthalmic diagnostic tools with further evaluation and validation by analysing the performance. Detailed information on this study can be found on page 2543.

The following article is on analytical and numerical investigations of mechanical vibration in the vertical direction of a human body in a driving vehicle using a biomechanical vibration model. In this study, analytical and numerical solutions for the dynamic biomechanical vibration model have been presented in detail to investigate and analyse the dynamic response of a human body when seated in a driving vehicle. The first simulation was an analytical solution by deriving the general equations of the motion of the vibration behaviour for the human body to calculate the natural frequency for individual parts. The second simulation was a finite element technique to calculate natural frequency and vibration modes for the human body under different frequency loads. The simulation results show that the mechanical response expected and predicted to respond to the human body is perfect using this biomechanical model in a vibratory environment as in a vehicle driving, which will help stimulate the quality and design of vibration insulator such as a seat. Complete information on this study is presented on page 2791.

Another article that we wish to highlight is “Failure rate estimation for transformer population based on health index through Markov model approach” by Nor Shafiqin Shariffuddin et al. from Malaysia. The condition parameters data extracted from 3,192 oil samples were analysed in this study. The samples were from 370 transformers with an age range between 1 and 25 years. Based on the Markov model prediction, the failure rate of the transformer population increases as the transformer’s age increases, and it begins to exceed the global average failure rates at 14 years. Overall, the Markov model can be considered a viable approach to predict transformer failure rates, and it can be used as an alternative option to determine the forecasted failure data. Detailed information on this study is presented on page 3029.

We anticipate that you will find the evidence presented in this issue to be intriguing, thought-provoking and useful in reaching new milestones in your own research. Please recommend the journal to your colleagues and students to make this endeavour meaningful.

All the papers published in this edition underwent Pertanika’s stringent peer-review process involving a minimum of two reviewers comprising internal as well as external referees. This was to ensure that the quality of the papers justified the high ranking of the journal, which is renowned as a heavily-cited journal not only by authors and researchers in Malaysia but by those in other countries around the world as well.

In the last 12 months, of all the manuscripts peer-reviewed, 36% were accepted. This seems to be the trend in PJST.

We would also like to express our gratitude to all the contributors, namely the authors, reviewers, Editor-in-Chief and Editorial Board Members of PJST, who have made this issue possible.

PJST is currently accepting manuscripts for upcoming issues based on original qualitative or quantitative research that opens new areas of inquiry and investigation.

Chief Executive Editor
Dr. Mohammad Jawaid
executive_editor.pertanika@upm.edu.my

Mobile Application Development for Spectral Signature of Weed Species in Rice Farming

Nor Athirah Roslin¹, Nik Norasma Che'Ya^{1*}, Nursyazyla Sulaiman¹,
Lutfi Amir Nor Alahyadi¹ and Mohd Razi Ismail²

¹Department of Agriculture Technology, Faculty of Agriculture, Universiti Putra Malaysia, 43400 UPM, Serdang, Selangor, Malaysia

²Institute of Tropical Agriculture and Food Security, Universiti Putra Malaysia, 43400 UPM, Serdang, Selangor, Malaysia

ABSTRACT

Weed infestation happens when there is intense competition between rice and weeds for light, nutrients and water. These conditions need to be monitored and controlled to lower the growth of weeds as they affected crops production. The characteristics of weeds and rice are challenging to differentiate macroscopically. However, information can be acquired using a spectral signature graph. Hence, this study emphasises using the spectral signature of weed species and rice in a rice field. The study aims to generate a spectral signature graph of weeds in rice fields and develop a mobile application for the spectral signature of weeds. Six weeds were identified in Ladang Merdeka using Fieldspec HandHeld 2 Spectroradiometer. All the spectral signatures were stored in a spectral database using Apps Master Builder, viewed using smartphones. The results from the spectral signature graph show that the jungle rice (*Echinochloa* spp.) has the highest near-infrared (NIR) reflectance. In contrast, the saromacca grass (*Ischaemum rugosum*) shows the lowest NIR reflectance. Then, the first derivative (FD) analysis was run to visualise the separation of each species, and the 710 nm to 750 nm region shows the highest separation. It shows that the weed species can be identified using spectral signature by FD analysis with accurate separation.

The mobile application was developed to provide information about the weeds and control methods to the users. Users can access information regarding weeds and take action based on the recommendations of the mobile application.

Keywords: Mobile application, rice farming, spectral signature, weed species

ARTICLE INFO

Article history:

Received: 30 September 2020

Accepted: 14 January 2021

Published: 22 September 2021

DOI: <https://doi.org/10.47836/pjst.29.4.01>

E-mail addresses:

norathirahroslin@gmail.com (Nor Athirah Roslin)

niknorasma@upm.edu.my (Nik Norasma Che'Ya)

sya_zyla@yahoo.com (Nursyazyla Sulaiman)

lutfiamirulmukminin@gmail.com (Lutfi Amir Nor Alahyadi)

razi@upm.edu.my (Mohd Razi Ismail)

* Corresponding author

INTRODUCTION

Rice is considered a security commodity. The national policy is to maintain a prudent level of self-sufficiency, 65% at minimum (Vaghefi et al., 2016). One-fifth of the world population or more than a billion households in Asia, Africa, and America rely on the rice systems as their primary source of employment and livelihoods. Apart from this, statistics have proven that the rice industry in Malaysia had created a stable income for the country. However, according to the Department of Statistics Malaysia in 2018, there is a decrease in the rice production in 2017 from 2,739 tonnes to 2,539 tonnes after one year. Many factors caused the decrease of production in paddy, such as climate change (Alam et al., 2012), the changes of planting method from transplanting to direct-seeding (Dilipkumar et al., 2018), field management (Yuhao et al., 2020), and weed infestation such as weedy rice (Man & Zain, 1998). The yield reduction is high if there is a high weed infestation in the rice field (Jabran et al., 2018). Furthermore, Sudianto et al. (2016) stated that similar to Southeast Asian countries, Malaysia faced problems with the infestation of weedy rice because the establishment methods changed from transplanting of seedlings to direct seedling. Ishak et al. (2013) stated that agricultural activities do not meet the optimal production of crops due to pest and weed issues, weather changes, extreme solar radiation, and exploration.

Weed is an infamous pest that affects yield production all around the world. Around 10% to 35% yield losses have been recorded in Malaysia (Karim et al., 2004). Infestations of weedy rice could cut harvests by 80% if not tested. It will be a crucial constraint to the United States and other world regions relying on rice production (Vigueira et al., 2019). The matter is severe as weed causes problems if farmers are not proactive in its management or control method. The wide adoption of the direct-seeding system has led to a substantially increased infestation and spread of millennial weeds in Malaysia, especially the establishment of weedy rice in the 1980s and after that (Ruzmi et al., 2017). During direct seeding, the threat of weed infestation is a cause of concern and is unavoidable (Matloob et al., 2015).

Precision agriculture is known as site-specific farming that has potential methods to manage crop fields (Tang et al., 2016). It is a combination of several technologies such as global positioning system (GPS), remote sensing (RS) technology, geographic information system (GIS), and physical sensors that collect data of growth traits and yield of fields and carries out various kinds of management (Lin et al., 2019). For example, Roslan et al. (2013) used microwave and machine vision application as the rapid detection method in determining the surface of *Dioscorea hispida* rhizome alkaloid content. They found that the method can be used to visualise the colours on the *D.hispida* rhizome peel. This technique is beneficial to many parties and solves ineffective traditional agricultural practices while increasing yield productivity. Productivity increase is essential with the rising human population. The demand for rice increases along with global rice farming and goods (Tang et al., 2016).

Weed Control Management in Rice Field

Weed control management is crucial to prevent yield losses. It cuts the cost of production while maintaining the quality of grain. Weed control management helps to reduce weed infestation and prevents the growth of weed seed banks in soil (Labrada, 2003). Poor weed management control affects crops negatively, causing competition between the crops and weeds for sunlight, nutrients, and water. In addition, it increases the cost of production for hired labour and input cost to control the weeds. Furthermore, it causes low yield due to the losses and lowers grain quality which lowers the price. Therefore, weed control should be implemented before planting the seed as early as possible to avoid weed infestation. During the land preparation stage, weed control should be applied to reduce weed infestation in the field. Weed control shall continue until planting the seed in the fields because weed growth is crucial until the paddy matures.

Weed Detection using Remote Sensing and Mobile Applications in Agriculture

Differences between weeds and crops are hard to detect because they have similar shapes and colour. Each weed species can be identified based on distinct spectral signatures. Remote sensing technology was used for weed detection using spectral reflectance and crop spectral reflectance (Bajwa et al., 2015). The colour infrared photography method provides a better weed screening between the crops (Medlin et al., 2000). Razali et al. (2009) opined that objects could be characterised using colour as a fundamental physical property. It is used to identify the maturity phase and harvesting process for products in agriculture. The light intensity could change the red-green-blue composition of agricultural products due to the variation of daylight. The colour and texture of a high-resolution red-green-blue image and reflectance of a low-resolution multispectral image are combined to detect weeds in rice fields. This combination will produce a fused red-green-blue and multispectral image combination with better weed discrimination features (Barrero & Perdomo, 2018). The reflective indices of the near-infrared spectrum are visible in the form of colour variability compared to the red-green-blue spectrum (Price, 1994). In addition, weed detections can be made through hyperspectral imaging (HSI), which captures data in hundreds of narrow bands, and has shown promising results when performing per-pixel classification (Wendel & Underwood, 2016). Each weed species has a unique spectral signature and reflectance (Figure 1). In addition, the leaf pigments, cell structure, and water content are different for each weed species. Based on these differences, weed species can be detected (Abdulridha et al., 2016). Unfortunately, most farmers cannot identify rice diseases, pests, and weeds in the fields because they have limited access to the latest data and information to control pests, especially weeds (Adesina et al., 1994).

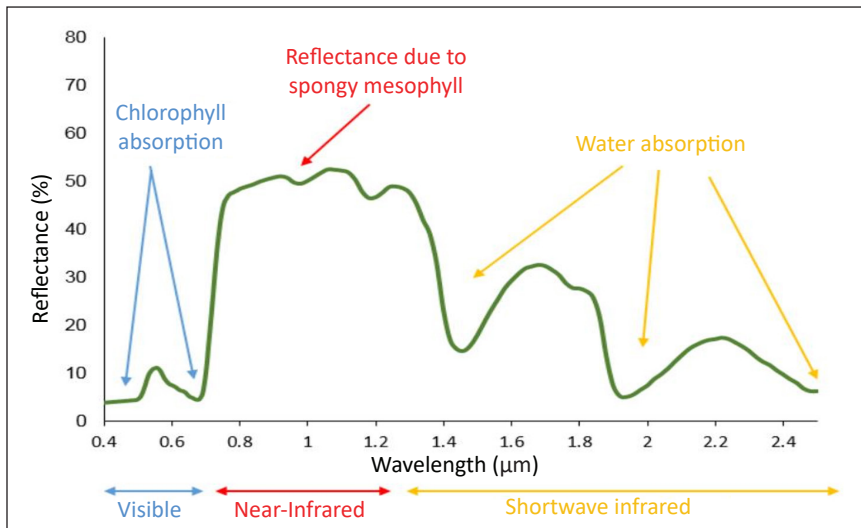


Figure 1. Vegetation spectral reflectance curve (Jensen, 2015)

The Development of Mobile Applications for Utilisation in the Rice Field

For the future of agriculture, the development of mobile applications is a significant initiative to create more advanced agriculture practices. The rapid growth of beneficial mobile applications and the advancement of mobile phones or smartphones, make these devices essential for farmers nowadays (Pongnumkul et al., 2015). Furthermore, most mobile applications are small in size. Therefore, they would not burden their smartphones and serve them with many features such as managing their data, machinery, orders, maps and navigation, and calendar (Desrial & Indriawardhana, 2019). Via an application that can detect a plant with a disease where it performs a survey and observation that minimises harm to the plants with a quick outcome. The result from the survey and observation can be a reference for the management of other crops in the future (Zhang et al., 2019).

Many rice-producing countries also have developed mobile applications. For example, Malaysia's advanced and available applications in Google Playstore are MARDI MyPerosakPadi, MARDI Padi Aerob, Rice Check Padi, and Agrimaths. These mobile applications can help users or farmers gain knowledge or information in managing paddy and rice from the start (planting) till the end (harvesting) (Rosle et al., 2019). Usually, in rice production, there is a problem with nutrient deficiency. Therefore, mobile applications can assist farmers to measure the correct levels of nitrogen in paddy plants (Dela Cruz, 2019). Other than that, high accuracy of grain counting can be done, providing quick results (Liu et al., 2017).

Weed infestation in crops is a serious matter to the farmers. It can cause many problems related to the plant from the start of planting up to the yield phase. Smartphones can increase farmers' income opportunities and solve vulnerabilities in the rural areas of less-developed

countries for smallholder farmers (Ramli et al., 2019). Identification of weed in crops is vital because it relates to the farmers' strategy and decision to manage the fields (Henson et al., 2017). Other than that, farmers can identify the weeds they are not familiar with by using a mobile application (Rahman et al., 2015). Table 1 shows the mobile apps for weed management in crop fields. WeedID and Padi2U provide information regarding weeds and how to control them. At the same time Adebayo et al. (2018) show the recommended weed management at different rice growth stages. Rahman et al. (2015) and Haug et al. (2014) used images to identify the weeds and recommend how to treat the weeds. All these applications are helpful but lack the spectral information of weed species. According to Su (2020), the spectral signature can be used to identify the weed species in high accuracy compared to image identification.

Spectral signature for plants is essential because it shows the unique value and the characteristics of the plant's species. The same goes for the weeds, as the spectral signature can be visualised using the spectral signature graph. Each spectral signature of weeds species has a different graph curve based on the specific characteristics. Therefore, a spectral library can be used to compare the reflectance of weeds and plants in a field and estimate the infestation percentage in the field (Yang & Kong, 2017). Furthermore, the spectral signature library can be used to discriminate and identify the plant location. Thus, the mapping of plant varieties can be done (Rao, 2008). The spectral signature graph is stored in the spectral signature library in a digital database to protect from loss and for easy access by researchers worldwide (Rossel et al., 2016). Digital database such as United States Geological Survey (USGS) Spectral Library Version 7 contains reflectance spectra including samples of minerals, rocks, soils, physically constructed, and mathematically

Table 1
Mobile application for weed management

Mobile application	Description
WeedID (Henson et al., 2017)	To identify weed using weed images, common name, scientific name, family name, weed characteristic, habitat, and method to control.
Padi2U (Athirah et al., 2020)	To identify common weed found in paddy by providing weed photo, common name, family name, description, weed habitat, and suggested method to control.
RiceAdvice-Weed Manager (Adebayo et al., 2018)	Provide recommended weed management at different rice growth stages. Weed information in the mobile application is based on farmers' knowledge. However, expert advice is provided for the best method to control the weed.
A mobile application using image analysis (Rahman et al., 2015)	Images captured and uploaded into the system, which identifies the image using a hierarchical system. The first level consists of non-experts and, the second level is from the experts.
Crop and weed identification using plant classification (Haug et al., 2014)	From the image captured by the user, the system will identify the weed and come out with the recommended method to control the weed.

computed mixtures, plants, vegetation communities, microorganisms, and artificial materials (Kokaly et al., 2017). Most conventional spectral libraries focus on minerals, and urban areas' temperature, where the primary information was soil. Examples of soil and minerals spectral libraries are ASTER Spectral Library, John Hopkin Spectral Library, Jet Propulsion Laboratory Spectral Library, MedSpec, and LILIAN (Adam, 2012). Vegetation spectral library was created in South China to store spectral data, different growth periods of various crops, and providing analysis with control strategy management of crops to the users (Chen et al., 2005).

Two spectral libraries of a selected tropical rainforest were designed and developed to store the data of vegetation spectra such as leaf condition, vigorous, and other physiological and biological parameters (Lau & Hashim, 2007). Other than that, the rubber trees disease spectral library was developed to identify the spread of disease in a large area (Jusoff et al., 2010). All spectral libraries were developed on particular observation and mostly are inaccessible to public users. However, the spectral library for weed species in rice farming is an excellent start to store all spectral signatures for current use and the future. Hence, we developed a mobile application for weed management to replace the prior paper-based system and provide a spectral signature database of weed species accessible via mobile application.

MATERIALS AND METHODS

The study area is located at Ladang Merdeka, Kampung Lundang Paku, Ketereh, Kelantan with coordinate $5^{\circ}59'3.0804''\text{N}$, $102^{\circ}12'24.0012''\text{E}$ and the total area of the field are $70,692.59 \text{ m}^2$ (Figure 2). The area is a well-organised plot, and the variety of the paddy

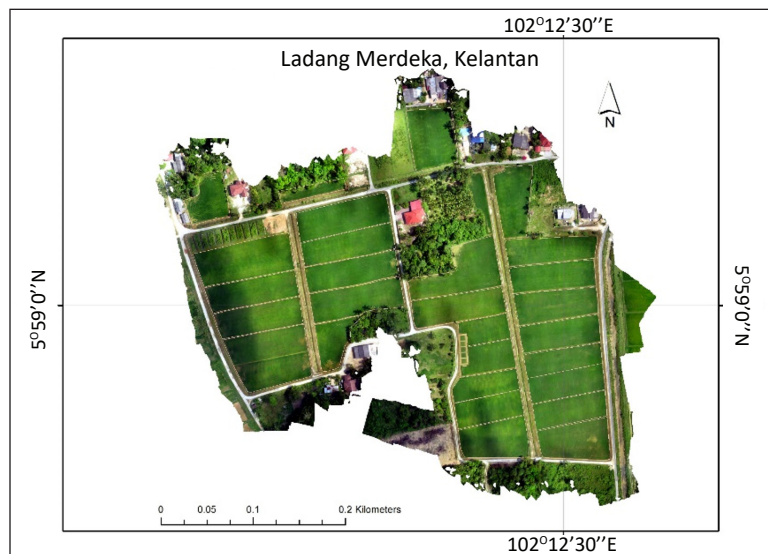


Figure 2. Experimental plot in Ladang Merdeka

seed is PadiU Putra. This paddy seed is a new variety, resistant to leaf blight disease, as discovered by UPM researchers.

Data Collection

Hyperspectral reflectance data were collected using a ASD FieldSpec® HandHeld 2 spectroradiometer (Malvern Panalytical, Cambridge, United Kingdom). The benefits of using FieldSpec® HandHeld 2 spectroradiometer is that it is cost-effective, user-friendly, versatile, and durable (ASDi, 2014). In addition, it has a highly sensitive detector array with a low stray light grating, a built-in shutter, DriftLock dark current compensation, and second-order filtering that produces a high signal-to-noise spectrum in under one second (ASDi, 2014) (Table 2).

Spectral signatures of weed were collected in 2018 at 9:00 am under the clear sky field conditions. The weed species collected were saromacca grass (*Ischaemum rugosum*), lesser fimbristylis (*Fimbristylis miliacea*), red sparangletop (*Leptochloa chinensis*), weedy rice (*Oryza sativa* L.), jungle rice (*Echinochloa* spp.), and flower of jungle rice (*Echinochloa* spp.) (Table 3). The calibration process was done using the white panel provided by the Analytical Spectral Device Corporation (ASD), Inc., Boulder, CO, USA. The white panel diffuses the reflection by nearly 100% of the incident light throughout the spectral range. In other words, the reflectance value of the white reference panel is nearly one at every wavelength (ASDi, 2014). Each weed was collected for ten samples at random between 5 cm distance of the optical sensor and the sample. This technique is used to avoid error and noise for data recording (Norasma, 2016).

Table 2
FieldSpec® HandHeld 2 Spectroradiometer properties (ASDi, 2014)

Specification	Information
Design	An ergonomic dual position “D” handle
Weight	1.17kg including batteries
Wavelength Range	325nm – 1075 nm
Accuracy	±1 nm
Optional GPS	Yes

Table 3
Weed species collected using a spectroradiometer (Analytical Spectral Device Corporation (ASD), Inc., Boulder, CO, USA)

Weed species	Abbreviation
Saromacca grass (<i>Ischaemum rugosum</i>)	IR
Lesser fimbristylis (<i>Fimbristylis miliacea</i>)	FM
Red sparangletop (<i>Leptochloa chinensis</i>)	LC
Weedy rice (<i>Oryza sativa</i> L.)	OSL
Jungle rice (<i>Echinochloa</i> spp.)	E
Flower of jungle rice (<i>Echinochloa</i> spp.)	FE

Data Analysis

All the raw data were transferred to a computer using a USB cable. First, the data was saved in a Microsoft Excel spreadsheet. Then, the data were binned into 10 nm spectral band each compared to 1 nm originally (Figure 3). Next, the spectral signature was visualised in the spectral reflectance graph for each species using Microsoft Excel. Then, the first derivative was run and visualised using Microsoft Excel as the steps below:

(a) Spectral Reflectance Visualisation

The spectral reflectance for all species was visualised graphically using Microsoft Excel step 3 (Figure 3).

(b) First Derivative Analysis

The first derivatives were calculated using Equation 1 in MS Excel and displayed in step 4 (Figure 3).

$$FD = \frac{R}{R} = \frac{Ry_2 - Ry_1}{\lambda x_2 - \lambda x_1} \tag{1}$$

Where:

FD = First Derivative

Ry₁, Ry₂ = Reflectance of the first and second reflectance pairs n1 and n2

λx₁, λx₂ = Wavelength of first and second reflectance pairs n1 and n2 n = Position of reflectance.

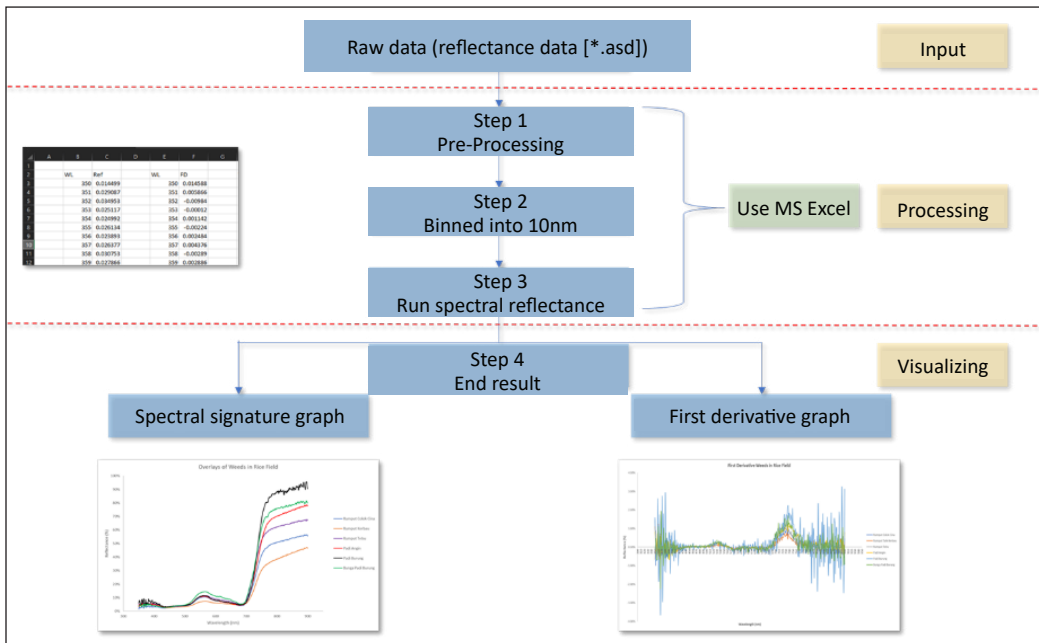


Figure 3. Hyperspectral data download and pre-processing (Lutfi, 2020)

Mobile App Development

The platform used to build this application is an online website called <https://masterappsbuilder.com>. This website is commercial software to develop a mobile application. It is user friendly and easy to use. Figure 4 shows the main menu of the website that contains the list of applications. The statistics data about the number of apps installed on Android and IOS devices is shown on the website. Other than that, it shows the number of visitors to the mobile application. The editor menu is shown after selecting the application on the list. The application menu contains a few functions: design, colours, features, application, and publication (Figure 4). The building application interface is located under the feature function menu. The data were stored in the database that can be displayed on the application through the function features (Figure 4).

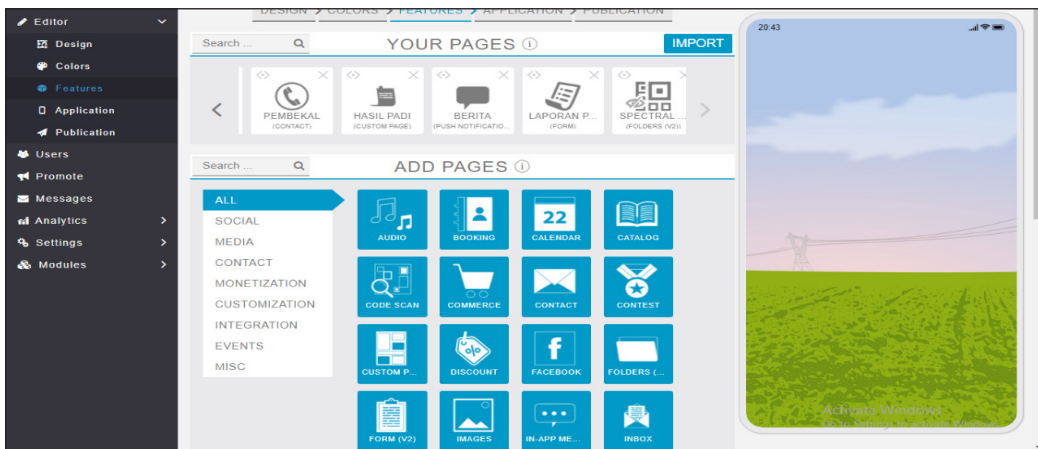


Figure 4. The application Editor feature and Feature menu in MasterAppBuilder

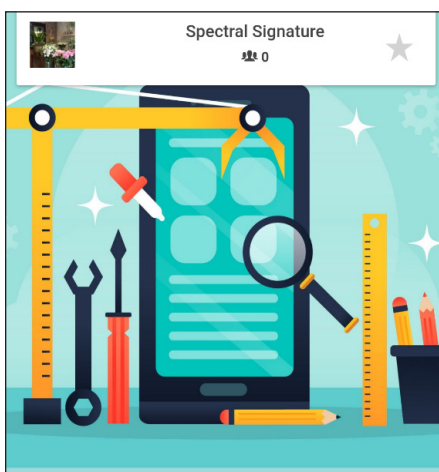


Figure 5. List of applications built-in the MasterAppBuilder website

Application preview is a preview interface for mobile apps using AMB previewer. It shows how the application works on the android or IOS device (Figure 5). On the previewer page, the user only can view the mobile apps without any editing features. This application can be downloaded at Google Playstore or Appstore in IOS.

RESULTS AND DISCUSSION

Spectral Signature Graph

The spectral reflectance profile is shown graphically for each type of weed (Figure 6), a low reflectance in the visible region with slight

peaks in the green region. An increase begins at 690 nm reaching the static line in the near-infrared region. It is an ordinary green plant spectral reflectance. The percentage difference in reflectance between weeds at one wavelength and weeds at another wavelength is enormous.

Species differences show up at specific wavelengths. For example, in the visible spectrum (450 nm to 700 nm), all weed spectral signatures were very similar, and many overlapped. At the same time, for the infrared region (700 nm to 990 nm), the spectra of different species are separated by their different wavelengths (Figure 6).

Jungle rice (*Echinochloa* spp.) had the highest NIR reflectance than other weed species (Figure 6). The second highest reflectance was its flower of jungle rice (*Echinochloa* spp.), followed by weedy rice (*Oryza sativa* L.). Lesser fimbristylis (*Fimbristylis miliacea*) had the lowest reflectance, followed by saromacca grass (*Ischaemum rugosum*). Finally, the red sparangletop (*Leptochloa chinensis*) had reflectance spectra from the other weeds (Figure 6).

Figures 7 to 12 show the spectral signatures for individual weed species such as saromacca grass (*Ischaemum rugosum*), lesser fimbristylis (*Fimbristylis miliacea*), red sparangletop (*Leptochloa chinensis*), weedy rice (*Oryza sativa* L.), jungle rice (*Echinochloa* spp.) and Jungle rice flowers (*Echinochloa* spp.) respectively.

Figure 13 shows the first derivative graph for each weed species. It clearly shows the 710 nm to 750 nm regions of the weed species separately. It can be an indicator to identify the weed species in this region. This region is known as the Near InfraRed region where it is related to the photosynthesis process. Since each weed is different, the significant bands for each weed can be seen in this region (710 nm to 750 nm). NIR is related to the biogeochemical and leaf pigments of the weed species (Jensen, 2015). Thus, this region is essential as an indicator to differentiate the weed species by using spectral signature.

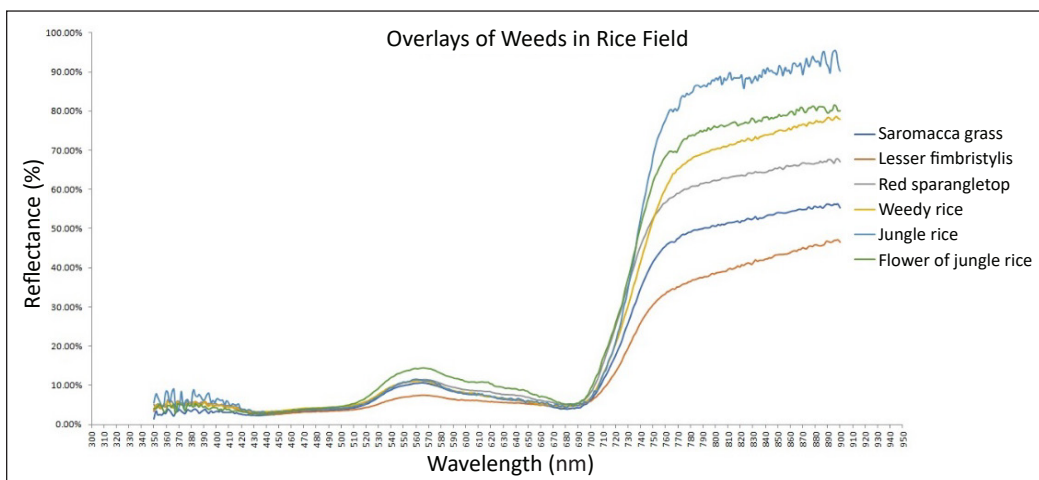


Figure 6. Overlays of spectral reflectance graph of weeds

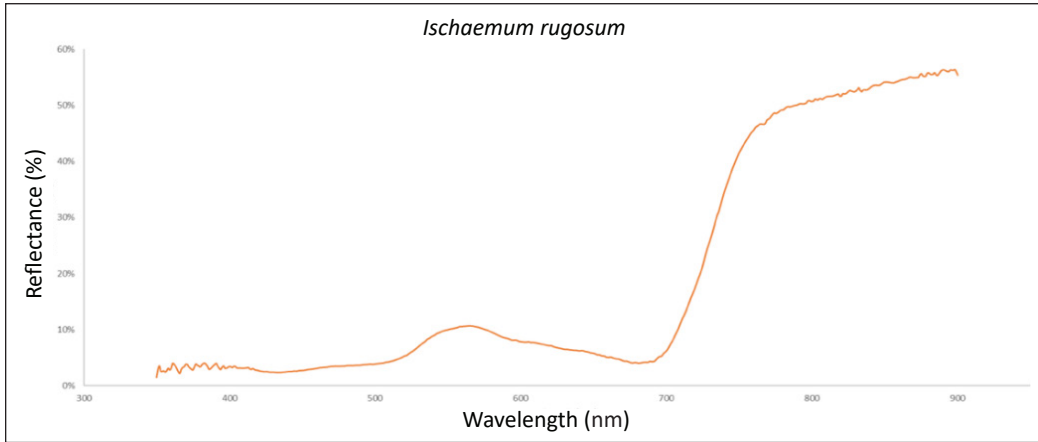


Figure 7. Spectral reflectance graph of Saromacca grass (*Ischaemum rugosum*) (Norasma et al., 2020)

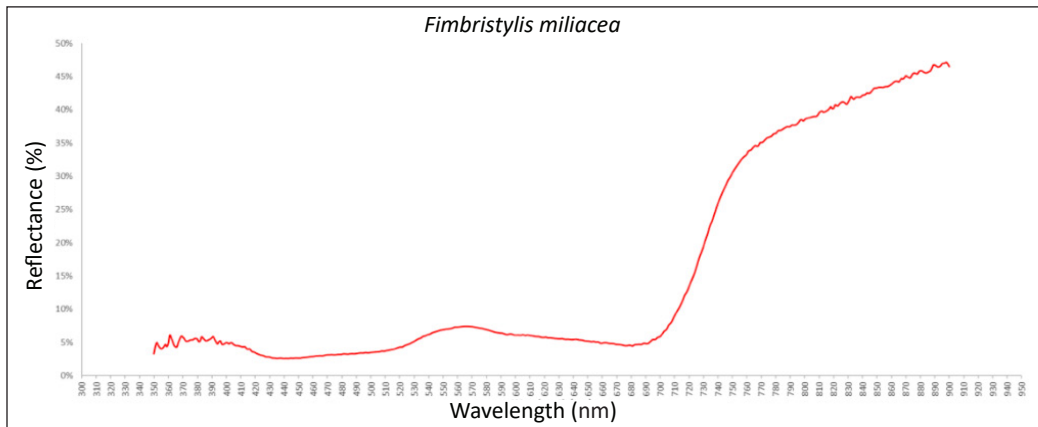


Figure 8. Spectral reflectance graph of Lesser fimbristylis (*Fimbristylis miliacea*) (Norasma et al., 2020)

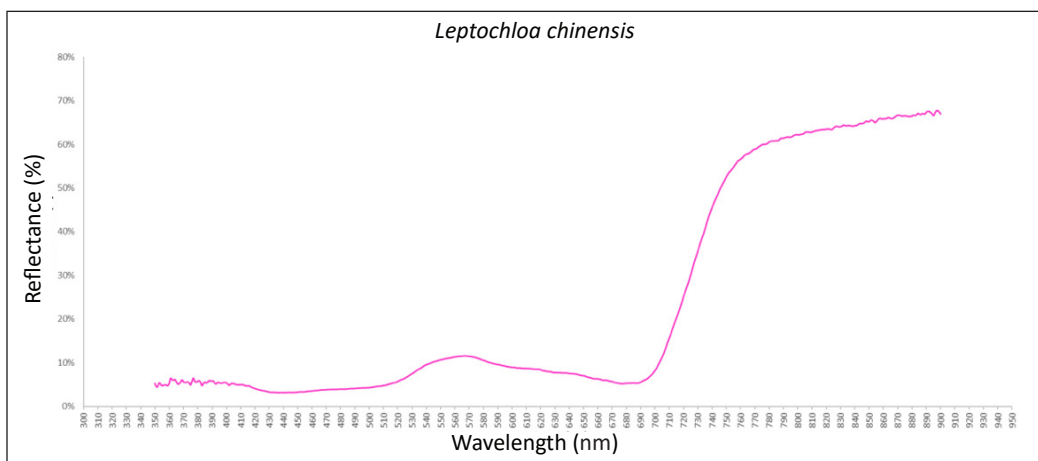


Figure 9. Spectral reflectance graph of Red sparangletop (*Leptochloa chinensis*) (Norasma et al., 2020)

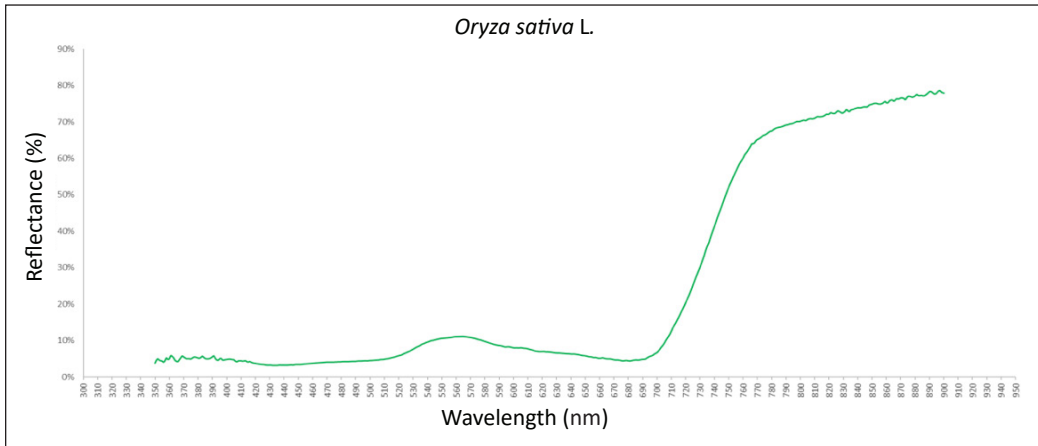


Figure 10. Spectral reflectance graph of Weedy rice (*Oryza sativa* L.)

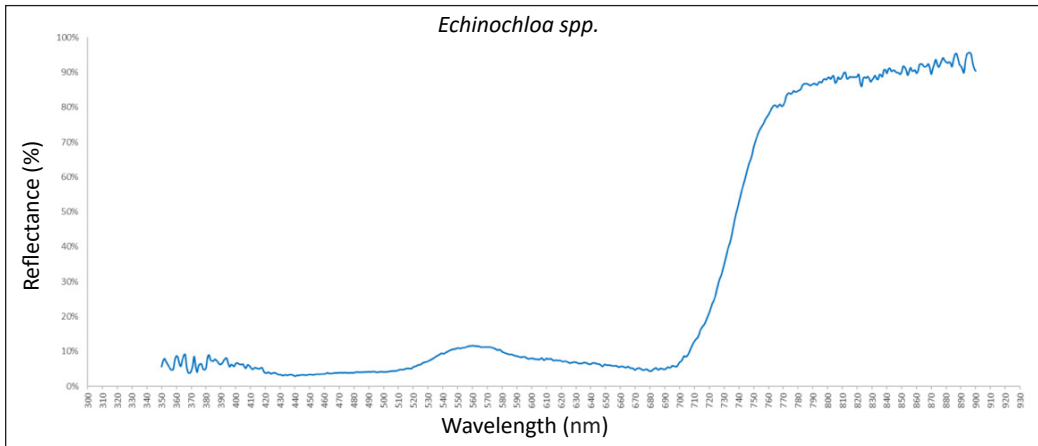


Figure 11. Spectral reflectance graph of Jungle rice (*Echinochloa* spp.)

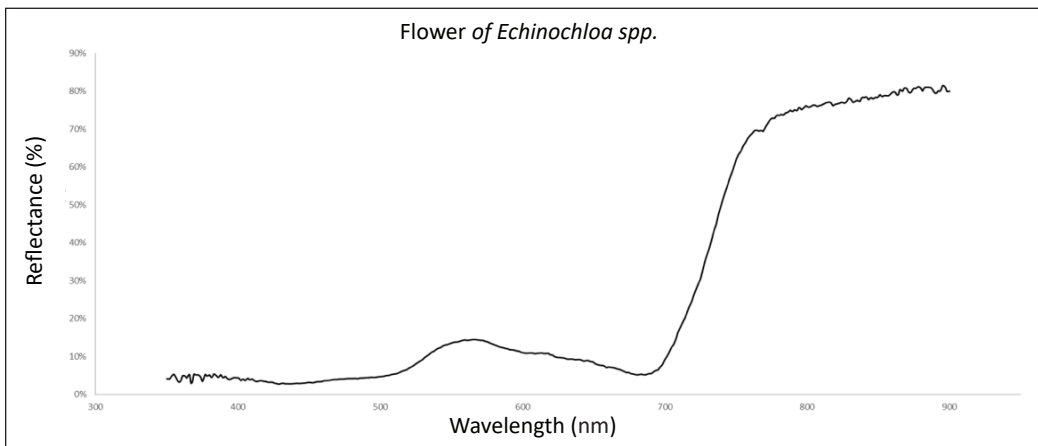


Figure 12. Spectral reflectance graph of Jungle rice's flowers (*Echinochloa* spp.)

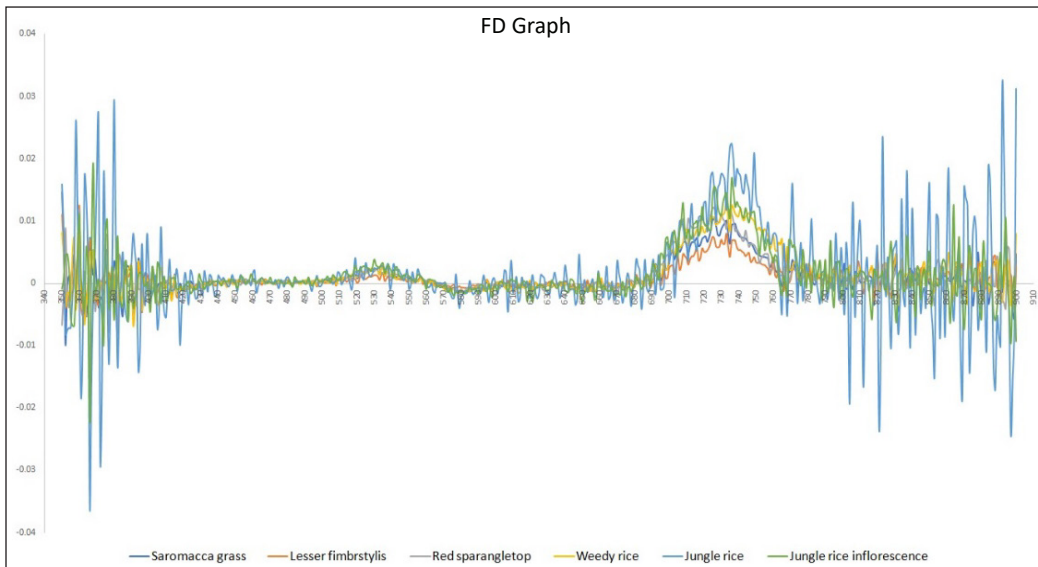


Figure 13. First derivative graph of weeds in KADA rice field

User Interface Mobile Application

A mobile app was successfully developed using the MasterAppBuilder. Figure 14 shows the main menu for the mobile app. It contains weed information, the spectral signature of weeds, and guidelines on how to control the weeds. The spectral library menu contains information about the six weeds that had been studied in the project. User can download the mobile application into their smartphones. The mobile application works by providing the image of the weed species, general name, scientific name, description, a method to control using a chemical application, and spectral signature graph of the weed species (Figure 14). Users can peruse the information provided in the mobile application to identify the weeds in their field based on the image and its description. A database of weed information, including spectral signatures is stored in this mobile application. Users can easily access it from their mobile devices. This mobile application offers a spectral signature graph that makes a difference compared with previous mobile apps available (Table 1). The WeedID developed by Henson et al. (2017) only provides the image of the weeds, its detailed description, and method to control. The same method was used to develop Padi2U mobile application, which offers the weed images, descriptions, and recommended methods to control (Athirah et al., 2020). The other mobile application developed was based on the image captured by the user. The system will identify the weed images and provide the method to control the weeds (Haug et al., 2014; Rahman et al., 2015). Thus, in this study, we introduce the spectral signature of six species of weeds that are commonly found in the study area. It can be a reference for the user to see the spectral signature of each weed.

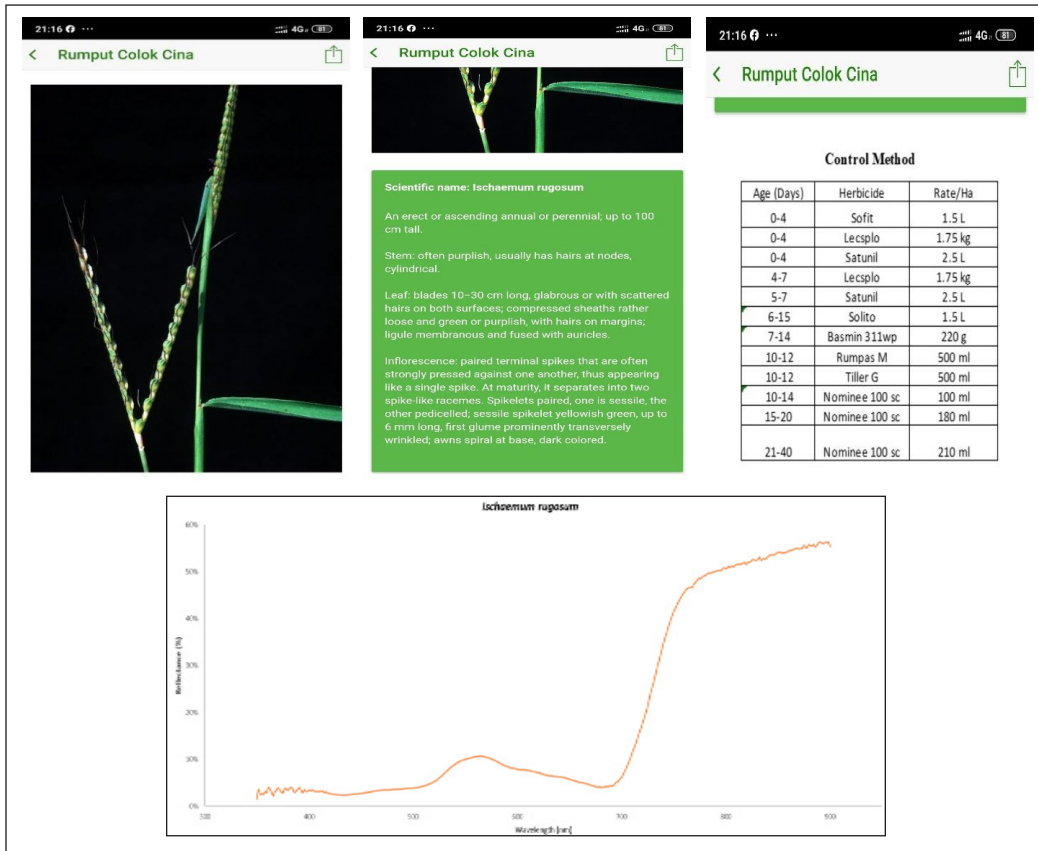


Figure 14. The content of menus, pictures, description, control method, and spectral signature graph (AMB Previewer)

CONCLUSION AND FUTURE DIRECTION

Detecting weeds visually in a large rice field area is challenging and time-consuming for farmers. In such a way, the use of mobile applications assists the user to manage weed effectively. This research project connects the spectral signature library and mobile applications that could be a potential use in modern technology to manage weeds in the field. The mobile application can display the spectral signature of the weed and suggest methods to control the weed using chemical control. Other than that, various methods of control can also be given through the mobile application to assist the farmers in overcoming the growth of weeds. Furthermore, the spectral signature can serve as a reference to detect weeds with a hyperspectral sensor in a shorter time instead of using the conventional method, which requires more time to detect the entire rice field thoroughly.

The mobile application can display the spectral signature of weeds, and such information is accessible to farmers via smartphones. Moreover, using a mobile phone or smartphone, users can easily compare the weed that had infested their field with the weed

information provided in the mobile application. In conclusion, the mobile application integrating spectral signature library can be a modus to display information about weed in the rice field.

Many challenges need to be overcome, such as the limitations in gaining raw data of the spectral signature of the weed in the rice field, the presence of various weeds in the field, the difference of control methods on each type of weed, and the conventional methods that the farmers are still using to detect weed. However, statistical analysis and vegetation index for the spectral reflectance analysis such as discriminant analysis, convolutional neural network (CNN), artificial neural network (ANN), and support vector machine (SVM) will increase the classification results.

ACKNOWLEDGEMENT

The authors wish to acknowledge Mr Mohd Zalyny Shah Noh and the financial support from the Ministry of Higher Education under Translational PADIU PUTRA Research Grant (Vote No: 5526500), Universiti Putra Malaysia GP-IPM (Vote No: 9611400) and Pest and Disease Monitoring Using Artificial Intelligent for Risk Management of Rice Under Climate Change” under the Long-Term Research Grant Scheme (LRGS), Ministry of Higher Education, Malaysia (LRGS/1/2019/UPM//2; vote number: 5545002). The authors also sincerely acknowledge the University Putra Malaysia for providing facilities.

REFERENCES

- Abdulridha, J., Ehsani, R., & De Castro, A. (2016). Detection and differentiation between laurel wilt disease, phytophthora disease, and salinity damage using a hyperspectral sensing technique. *Agriculture*, 6(4), Article 56. <https://doi.org/10.3390/agriculture6040056>
- Adam, S. N. B. (2012). *Design and development of an interactive digital spectral library* [Unpublished MSc dissertation]. Universiti Putra Malaysia, Malaysia.
- Adebayo, S., Ogunti, E. O., Akingbade, F. K., & Oladimeji, O. (2018). A review of decision support system using mobile applications in the provision of day to day information about farm status for improved crop yield. *Periodicals of Engineering and Natural Sciences*, 6(2), 89-99. <http://dx.doi.org/10.21533/pen.v6i2.183>
- Adesina, A. A., Johnson, D. E., & Heinrichs, E. A. (1994). Rice pests in the Ivory Coast, West Africa: Farmers' perceptions and management strategies. *International Journal of Pest Management*, 40(4), 293-299. <https://doi.org/10.1080/09670879409371902>
- Alam, M. M., Siwar, C., Toriman, M. E., Molla, R. I., & Talib, B. (2012). Climate change induced adaptation by paddy farmers in Malaysia. *Mitigation and Adaptation Strategies for Global Change*, 17(2), 173-186. <https://doi.org/10.1007/s11027-011-9319-5>
- ASDi. (2014). Handheld 2: Hand-held VNIR spectroradiometer. *FieldSpec*. Retrieved September 26, 2015, from <http://www.asdi.com/products/fieldspec-spectroradiometres/handheld-2-portable-spectroradiometer>

- Athirah, R. N., Norasma, C. Y. N., & Ismail, M. R. (2020). Development of an android application for smart farming in crop management. In *IOP Conference Series: Earth and Environmental Science* (Vol. 540, No. 1, p. 012074). IOP Publishing. <https://doi.org/10.1088/1755-1315/540/1/012074>
- Bajwa, A. A., Mahajan, G., & Chauhan, B. S. (2015). Nonconventional weed management strategies for modern agriculture. *Weed Science*, 63(4), 723-747. <https://doi.org/10.1614/WS-D-15-00064.1>
- Barrero, O., & Perdomo, S. A. (2018). RGB and multispectral UAV image fusion for Gramineae weed detection in rice fields. *Precision Agriculture*, 19(5), 809-822. <https://doi.org/10.1007/s11119-017-9558-x>
- Chen, S. S., Fang, L. G., Liu, Q. H., Chen, L. F., & Tong, Q. X. (2005). The design and development of spectral library of featured crops of South China. In *Proceedings 2005 IEEE International Geoscience and Remote Sensing Symposium, 2005. IGARSS'05.* (Vol. 2, pp. 4-pp). IEEE Publishing. <https://doi.org/10.1109/IGARSS.2005.1525234>
- Dela Cruz, G. B. (2019). Nitrogen deficiency mobile application for rice plant through image processing techniques. *International Journal of Engineering and Advanced Technology*, 8(6), 2950-2955. <https://doi.org/10.35940/ijeat.F8721.088619>
- Desrial, & Indriawardhana, P. A. K. (2019). Design of online application for agricultural machinery service based on android operating system. In *IOP Conference Series: Materials Science and Engineering* (Vol. 557, No. 1, p. 012023). IOP Publishing. <https://doi.org/10.1088/1757-899x/557/1/012023>
- Dilipkumar, M., Burgos, N. R., Chuah, T. S., & Ismail, S. (2018). Cross-resistance to imazapic and imazapyr in a weedy rice (*Oryza sativa*) biotype found in Malaysia. *Planta Daninha*, v36, Article e018182239. <https://doi.org/10.1590/S0100-83582018360100058>
- Haug, S., Michaels, A., Biber, P., & Ostermann, J. (2014). Plant classification system for crop/weed discrimination without segmentation. In *IEEE Winter Conference on Applications of Computer Vision* (pp. 1142-1149). IEEE Publishing. <https://doi.org/10.1109/WACV.2014.6835733>
- Henson, Y., Martin, R., Quinell, R., Van Ogtrop, F., Try, Y., & Tan, D. (2017, September 24-28). Development of a weed identifier mobile application for Cambodian rice farmers. In *Proceedings of the 18th Australian Society of Agronomy Conference* (pp. 1-4). Ballarat, Australia.
- Ishak, W. W., Hudzari, R. M., & Tan, M. Y. (2013). Development of an automation and control design system for lowland tropical greenhouses. *Pertanika Journal of Science & Technology*, 21(2), 365-374.
- Jabran, K., Uludag, A., & Chauhan, B. S. (2018). Sustainable weed control in rice. In *Weed Control* (pp. 276-287). CRC Press.
- Jensen, J. R. (2015). *Introductory digital image processing: A remote sensing perspective*. Prentice Hall Press.
- Jusoff, K., Yusoff, M. M., & Ali, N. H. M. (2010). Spectral signatures of leaf fall diseases in *Hevea brasiliensis* using a handheld spectroradiometer. *Modern Applied Science*, 4(2), 78-84.
- Karim, R. S., Man, A. B., & Sahid, I. B. (2004). Weed problems and their management in rice fields of Malaysia: An overview. *Weed Biology and Management*, 4(4), 177-186. <https://doi.org/10.1111/j.1445-6664.2004.00136.x>
- Kokaly, R. F., Clark, R. N., Swayze, G. A., Livo, K. E., Hoefen, T. M., Pearson, N. C., Wise, R. A., Benzel, W. M., Lowers, H. A., Driscoll, R. L., & Klein, A. J. (2017). *USGS spectral library version 7 data: US geological survey data release*. United States Geological Survey (USGS).

- Labrada, R. (2003). The need for improved weed management in rice. In *Proceedings of the 20th Session of the International Rice Commission* (pp. 181-189). FAO Publishing.
- Lau, A. M. S., & Hashim, M. (2007). The design and building of spectral library of tropical rain forest in Malaysia. In *The 28th Asian Conference on Remote Sensing 2007* (Vol. 2, pp. 1150-1157). Asian Association on Remote Sensing.
- Lin, C. Y., Chang, S. J., Lai, M. H., & Lu, H. Y. (2019, August 6-8). Overview of precision agriculture with focus on rice farming. In *International Workshop on ICTs For Precision Agriculture* (pp. 19-26). Selangor, Malaysia.
- Liu, T., Chen, W., Wang, Y., Wu, W., Sun, C., Ding, J., & Guo, W. (2017). Rice and wheat grain counting method and software development based on Android system. *Computers and Electronics in Agriculture*, *141*, 302-309. <https://doi.org/10.1016/j.compag.2017.08.011>
- Lutfi, A. N. A. (2020). *Mobile application development for spectral signature of weed species in rice* (Degree Thesis). Univerisiti Putra Malaysia, Malaysia.
- Man, A., & Zain, A. M. (1998). *Manual for the identification and control of padi angin (weedy rice) in Malaysia*. Malaysian Agricultural Research and Development Institute.
- Matloob, A., Khaliq, A., & Chauhan, B. S. (2015). Weeds of direct-seeded rice in Asia: problems and opportunities. *Advances in Agronomy*, *130*, 291-336. <https://doi.org/10.1016/bs.agron.2014.10.003>
- Medlin, C. R., Shaw, D. R., Gerard, P. D., & LaMastus, F. E. (2000). Using remote sensing to detect weed infestations in Glycine max. *Weed Science*, *48*(3), 393-398. [https://doi.org/10.1614/0043-1745\(2000\)048\[0393:URSTDW\]2.0.CO;2](https://doi.org/10.1614/0043-1745(2000)048[0393:URSTDW]2.0.CO;2)
- Norasma, C. Y. N. (2016). *Site-specific weed management using remote sensing* (PhD Thesis). The University of Queensland, Australia.
- Norasma, C. Y. N., Alahyadi, L. A. N., Fazilah, F. F. W., Roslan, S. N. A., & Tarmidi, Z. (2020). Identification spectral signature of weed species in rice using spectroradiometer handheld sensor. In *IOP Conference Series: Earth and Environmental Science* (Vol. 540, No. 1, p. 012091). IOP Publishing. <https://doi.org/10.1088/1755-1315/540/1/012091>
- Pongnumkul, S., Chaovalit, P., & Surasvadi, N. (2015). Applications of smartphone-based sensors in agriculture: A systematic review of research. *Journal of Sensors*, *2015*, Article 195308. <https://doi.org/10.1155/2015/195308>
- Price, J. C. (1994). How unique are spectral signatures? *Remote Sensing of Environment*, *49*(3), 181-186. [https://doi.org/10.1016/0034-4257\(94\)90013-2](https://doi.org/10.1016/0034-4257(94)90013-2)
- Rahman, M., Blackwell, B., Banerjee, N., & Saraswat, D. (2015). Smartphone-based hierarchical crowdsourcing for weed identification. *Computers and Electronics in Agriculture*, *113*, 14-23. <https://doi.org/10.1016/j.compag.2014.12.012>
- Ramli, N. S., Hassan, M. S., Man, N., Samah, B. A., Omar, S. Z., Rahman, N. A. A., Yusuf, S., & Ibrahim, M. S. (2019). Seeking of agriculture information through mobile phone among paddy farmers in

- Selangor. *International Journal of Academic Research in Business and Social Sciences*, 9(6), 527-538. <http://dx.doi.org/10.6007/IJARBSS/v9-i6/5969>
- Rao, N. R. (2008). Development of a crop-specific spectral library and discrimination of various agricultural crop varieties using hyperspectral imagery. *International Journal of Remote Sensing*, 29(1), 131-144. <https://doi.org/10.1080/01431160701241779>
- Razali, M. H., Ismail, W. I. W., Ramli, A. R., Sulaiman, M. N., & Harun, M. H. (2009). Development of image based modeling for determination of oil content and days estimation for harvesting of fresh fruit bunches. *International Journal of Food Engineering*, 5(2), Article 12. <https://doi.org/10.2202/1556-3758.1633>
- Roslan, S., Razali, M. H. H., Ismail, W. I. W., Abbas, Z., & Zainuddin, M. F. (2013). Rapid detection techniques for mechanical properties determination on surface of *Dioscorea hispida* rhizome. *Procedia Engineering*, 68, 446-452. <https://doi.org/10.1016/j.proeng.2013.12.205>
- Rosle, R., Norasma, C. Y. N., Roslin, N. A., Halip, R. M., & Ismail, M. R. (2019). Monitoring early stage of rice crops growth using normalized difference vegetation index generated from UAV. In *IOP Conference Series: Earth and Environmental Science* (Vol. 355, No. 1, p. 012066). IOP Publishing.
- Rossel, R. V., Behrens, T., Ben-Dor, E., Brown, D. J., Demattê, J. A. M., Shepherd, K. D., Shi, Z., Stenberg, B., Stevens, A., Adamchuk, V., Aichi, H., Barthes, B. G., Bartholomeus, H. M., Bayer, A. D., Bernoux, M., Bottcher, K., Brodsky, L., Du, C. W., Chappell, A., ... & Ji, W. (2016). A global spectral library to characterize the world's soil. *Earth-Science Reviews*, 155, 198-230. <https://doi.org/10.1016/j.earscirev.2016.01.012>
- Ruzmi, R., Ahmad-Hamdani, M. S., & Bakar, B. B. (2017). Prevalence of herbicide-resistant weed species in Malaysian rice fields: A review. *Weed Biology and Management*, 17(1), 3-16. <https://doi.org/10.1111/wbm.12112>
- Su, W. H. (2020). Advanced machine learning in point spectroscopy, RGB-and hyperspectral-imaging for automatic discriminations of crops and weeds: A review. *Smart Cities*, 3(3), 767-792. <https://doi.org/10.3390/smartcities3030039>
- Sudianto, E., Neik, T. X., Tam, S. M., Chuah, T. S., Idris, A. A., Olsen, K. M., & Song, B. K. (2016). Morphology of Malaysian weedy rice (*Oryza sativa*): Diversity, origin and implications for weed management. *Weed Science*, 64(3), 501-512. <https://doi.org/10.1614/WS-D-15-00168.1>
- Tang, J. L., Chen, X. Q., Miao, R. H., & Wang, D. (2016). Weed detection using image processing under different illumination for site-specific areas spraying. *Computers and Electronics in Agriculture*, 122, 103-111. <https://doi.org/10.1016/j.compag.2015.12.016>
- Vaghefi, N., Shamsudin, M. N., Radam, A., & Rahim, K. A. (2016). Impact of climate change on food security in Malaysia: economic and policy adjustments for rice industry. *Journal of Integrative Environmental Sciences*, 13(1), 19-35. <https://doi.org/10.1080/1943815X.2015.1112292>
- Vigueira, C. C., Qi, X., Song, B. K., Li, L. F., Caicedo, A. L., Jia, Y., & Olsen, K. M. (2019). Call of the wild rice: *Oryza rufipogon* shapes weedy rice evolution in Southeast Asia. *Evolutionary applications*, 12(1), 93-104. <https://doi.org/10.1111/eva.12581>

- Wendel, A., & Underwood, J. (2016). Self-supervised weed detection in vegetable crops using ground based hyperspectral imaging. In *2016 IEEE international conference on robotics and automation (ICRA)* (pp. 5128-5135). IEEE Publishing. <https://doi.org/10.1109/ICRA.2016.7487717>
- Yang, X. F., & Kong, C. H. (2017). Interference of allelopathic rice with paddy weeds at the root level. *Plant Biology*, *19*(4), 584-591. <https://doi.org/10.1111/plb.12557>
- Yuhao, A., Che'Ya, N. N., Roslin, N. A., & Ismail, M. R. (2020). Rice chlorophyll content monitoring using vegetation indices from multispectral aerial imagery. *Pertanika Journal of Science & Technology*, *28*(3), 779-795.
- Zhang, D., Wang, D., Du, Z., Huang, L., Zhao, H., Liang, D., Gu, C., & Yang, X. (2019). A rapidly diagnosis and application system of fusarium head blight based on smartphone. In *2019 8th International Conference on Agro-Geoinformatics (Agro- Geoinformatics)* (pp. 1-5). IEEE Publishing. <https://doi.org/10.1109/Agro-Geoinformatics.2019.8820529>



Review article

Potential of *Syzygium polyanthum* (Daun Salam) in Lowering Blood Glucose Level: A Review

Nur Salsabeela Mohd Rahim, Ida Farah Ahmad and Terence Yew Chin Tan*

Herbal Medicine Research Centre, Institute for Medical Research, National Institutes of Health, Ministry of Health Malaysia, Setia Alam, 40170 Shah Alam, Malaysia

ABSTRACT

Syzygium polyanthum is a herb widely used in Malaysia and Indonesia in cuisines. Traditionally, the herbal decoction of *S. polyanthum* (daun salam) leaves is often used by diabetic patients in Indonesia. Therefore, our objective is to evaluate the scientific evidence available for *S. polyanthum* in lowering blood glucose levels (BGL). We systematically searched Pubmed, Google Scholar, Scopus, CENTRAL, LILAC and clinicaltrials.gov databases up to 23rd October 2020 using the keywords “*Syzygium polyanthum*” and “antidiabetic”. From the selected 413 articles, eight studies involving rodents were included. All results showed a significant effect in lowering BGL without any adverse effects. The possible underlying mechanism of action is attributed to inhibiting intestinal glucose absorption and enhancing glucose uptake by the muscles. Chemical families responsible for the effect were determined as flavonoids, alkaloids and terpenoids. Thus, *S. polyanthum* leaves showed potential antidiabetic properties, but further research is required to identify the active compounds followed by the safety evaluation of this compound.

Keywords: Blood glucose level, daun salam, diabetic, *Syzygium polyanthum*

ARTICLE INFO

Article history:

Received: 03 November 2020

Accepted: 08 January 2021

Published: 22 September 2021

DOI: <https://doi.org/10.47836/pjst.29.4.02>

E-mail addresses:

sectradknow.hmrc@moh.gov.my (Nur Salsabeela Mohd Rahim)

idafarah@moh.gov.my (Ida Farah Ahmad)

terencetyc@moh.gov.my (Terence Yew Chin Tan)

* Corresponding author

INTRODUCTION

Diabetes mellitus (DM) is described as a deficiency of insulin production secreted by the pancreas or the inability of the body to use the insulin it produces (WHO, 2019). There are currently 420 million people globally with diabetes, with a mortality rate of 1.6 million in 2016 (Loke, 2020). This increase will occur due to population

growth, ageing, unhealthy diets, obesity and sedentary lifestyles (WHO, 2019). Asian countries make up more than 60% of the world's diabetic population (Ramachandran et al., 2012). This situation is due to a few factors, such as urbanisation and socioeconomic transition. Hence, they are prone to have more intra-abdominal fat accumulation and low muscle mass (Ramachandran et al., 2012).

According to the National Health and Morbidity Survey 2019 (NHMS, 2019), almost one in five Malaysian adults has diabetes. In addition, the survey found that 3.9 million Malaysian adults were diagnosed with diabetes, surpassing the 2014 prediction by Health Ministry that figure would not be reached until 2020 (Rashid, 2017).

There are two types of diabetes: Type 1 and Type 2. Type 1 diabetes (or juvenile/childhood-onset diabetes) is defined as the failure of the pancreas to produce insulin caused by hereditary factors or damage to the immune system (Berawi et al., 2017; WHO, 2019; & Widyawati et al., 2015a). Type 2 diabetes (non-insulin-dependent or adult-onset diabetes) is defined as the body's inability to respond appropriately to the action of insulin. Type 2 diabetes is much more common worldwide, accounting for around 90% of all diabetic patients, due to food intake habits, obesity, smoking and lack of physical activity (Berawi et al., 2017; WHO, 2019; & Widyawati et al., 2015a).

Despite using insulin and oral medications to control blood glucose, diabetes remains among the world's top 10 causes of death (Waly et al., 2010; WHO, 2019; & Widharna et al., 2015). In addition, DM is a risk factor for kidney, liver, and also contributes to the two-fold increase of coronary heart disease and vascular damage, which lead to 50% to 80% of the diabetes patient mortality (Emerging Risk Factors Collaboration, 2011; Duncan et al., 2003; Nwaneri et al., 2013; Rashid, 2017; & Whiteley et al., 2005).

Syzygium polyanthum belongs to the Myrtaceae family (The Plant List, 2012; Quattrocchi, 2012). Among others, species included in the genus *Syzygium* are *Eugenia atropunctata*, *Eugenia holmanii*, *Eugenia balsamea*, *Syzygium cymosum*, *Syzygium micranthum*, and *Syzygium pamtense* (The Plant List, 2012; Quattrocchi, 2012). *S. polyanthum* is widely distributed throughout Myanmar, Indo-China, Thailand, Malaysia, and Indonesia (Azwar, 2010), with a few familiar names, such as Indian laurel, Indonesian bay leaf, *daun salam*, *kelat samak*, *samak*, *serah*, *serai kayu*, *kelat putih*, *kelat merah*, *palong* (Malaysia), *manting*, *salam*, and *ubar serai* (Indonesia) (Malaysian Herbal Monograph Committee, 2017; The Plant List, 2012; & Quattrocchi, 2012).

Traditionally, *S. polyanthum* is widely used as a food ingredient in Indonesian and Malaysian cuisine and used to treat diabetes in Indonesia (Azwar, 2010). It is usually dried, crushed and extracted through soaking in boiled water (Dewijanti et al., 2018).

Other traditional uses include using the leaf and bark extracts of *S. polyanthum* for treating diarrhoea (Burkill, 1935). In addition, the poultices of the bark, root and leaves relieve itching (Burkill, 1935). The leaves contain polyphenols (flavonoids, terpenoids,

tannins) and saponin (Hikmah et al., 2016; Liem et al., 2015; Wahjuni et al., 2018; Widharna et al., 2015; Widyawati et al., 2015a & Yuliana, 2014). In medicinal plants. These polyphenols, saponins and coumarins have been reported to exhibit antidiabetic properties (Hikmah et al., 2016; Wahjuni et al., 2018; Yuliana, 2014).

Since *S. polyanthum* leaves are ethnobotanically used in treating diabetes in Indonesia and Malaysia (Dewijanti, 2018 & Burkill, 1935), the National Agency for Drug and Food Control in Indonesia highly regards this medicinal plant. Therefore, we conducted this study to evaluate the scientific evidence available for *S. polyanthum* in lowering blood glucose levels (BGL).

MATERIALS AND METHODS

This review was conducted under the Preferred Reporting Items for Systematic Reviews and Meta-Analysis (PRISMA) guidelines (Liberati et al., 2009).

Search Strategy

A literature search was conducted to identify relevant studies on *S. polyanthum* in lowering blood glucose. The following six electronic databases were searched for this purpose: Pubmed, Google Scholar, Scopus, CENTRAL, LILAC, and clinicaltrials.gov with two keywords (*Syzygium polyanthum* and antidiabetic) and their combinations (Table 1). The bird's eye view strategy was applied to identify all the antidiabetic properties of *S. polyanthum*. Relevant studies were further identified by going through the citations and lists of references in the related articles. All related articles found in English and Indonesian were included. Two authors independently conducted the literature search by dividing the databases list and followed by cross-checking to avoid redundancy. The search was done up to 23rd October 2020. The tentatively selected articles were reviewed for the inclusion criteria, peer-reviewed, and the articles that best met the criteria were carefully selected. The extensive literature search brought about 413 published articles (Table 1).

Study Selection

The PICOS (participants/patients, interventions, comparators, outcomes, study design) formula for the literature search was pre-determined through discussion by the authors. The selection of search terms was centred on participants and interventions for maximum sensitivity, as shown in Table 1. The search and inclusion/exclusion criteria are reported according to the Preferred Reporting Items for Systematic Reviews and Meta-Analyses (PRISMA) guidelines and presented in a PRISMA flow chart in Figure 1. The abstract of the searched articles was screened, followed by full-text reading for articles fulfilling the inclusion criteria. The inclusion criteria were based on samples, intervention, outcomes and study design. Articles published in English and Indonesian were reviewed and extracted.

Two authors conducted the screening process. Any disagreement was discussed with the third author, and a decision is agreed on. Both authors worked independently in analysing the eight studies and tabulated the extracted data (Table 2), and subsequently critically appraised the chosen papers together to reduce bias.

Selection of Samples and Intervention

1. Types of study sample: This review included using *S. polyanthum* as an intervention in animals induced with diabetes.
2. Types of intervention selected for this review include studies using any form/dosage of *S. polyanthum* intervention comparing it with diabetic medications.
3. Types of comparison: The comparison groups included (a) group with *S. polyanthum* compared with glibenclamide, (b) group with *S. polyanthum* compared with metformin, and (c) group with a combination of *S. polyanthum* with glibenclamide.

Selection of Outcomes

The outcome selected was the intervention ability and the comparators of *S. polyanthum* for lowering BGL in Type 2 diabetes in experimental studies.

Selection of Study Model

In vivo and human trials (if any) that evaluated the effectiveness of *S. polyanthum* in lowering BGL were included in this review.

Quality Assessment of Included Studies

The risk of bias (RoB) tool for animal intervention studies, i.e. SYRCLE's RoB tool, was used to assess the risk of bias of all included studies (Hooijmans et al., 2014b). Two independent authors performed a quality assessment of all included studies. Disagreements were resolved by discussion.

RESULTS

The search initially produced 413 potentially relevant studies (Table 1). However, 22 review articles were excluded immediately from these articles, as these contributed no additional data besides the original studies, which were already included. Another 111 studies were excluded based on duplication, vague references and unpublished work. Of the remaining 280 studies, 75 did not include antidiabetic studies, 120 did not use *S. polyanthum* species, and 77 involved other than *in vivo* studies. Conclusively, eight articles that fulfilled the inclusion criteria were included in this review (Hikmah et al., 2016; Liem

et al., 2015; Sutrisna et al., 2016; Wahjuni et al., 2018; Widharna et al., 2015; Widyawati et al., 2015a; Widyawati et al., 2015a; & Yuliana, 2014), as shown in the process of study selection (Figure 1).

The selected studied all used leaves extract of *S. polyanthum* in the form of extracts or decoction (Hikmah et al., 2016; Liem et al., 2015; Sutrisna et al., 2016; Wahjuni et al., 2018; Widharna et al., 2015; Widyawati et al., 2015a; Widyawati et al., 2015b; & Yuliana, 2014) and had comparable designs: in lowering BGL (Hikmah et al., 2016; Liem et al., 2015; Sutrisna et al., 2016; Wahjuni et al., 2018; Widharna et al., 2015; Widyawati et

Table 1
Search strategies used

Databases	Year of search	Keyword used	No. of studies in search
Pubmed	2015 – 2020	<i>Syzygium polyanthum</i> AND antidiabetic	3
Google scholar	2005 – 2020	<i>Syzygium polyanthum</i> AND antidiabetic	295
Scopus	2005 – 2020	<i>Syzygium polyanthum</i> AND antidiabetic	71
CENTRAL	2019	<i>Syzygium polyanthum</i> AND antidiabetic	1
LILAC	(No hit)	<i>Syzygium polyanthum</i> AND antidiabetic	0
Clinicaltrials.gov	2009 – 2020	<i>Syzygium polyanthum</i> AND antidiabetic	43
TOTAL SEARCH =			413

Note. As of 8th September 2020

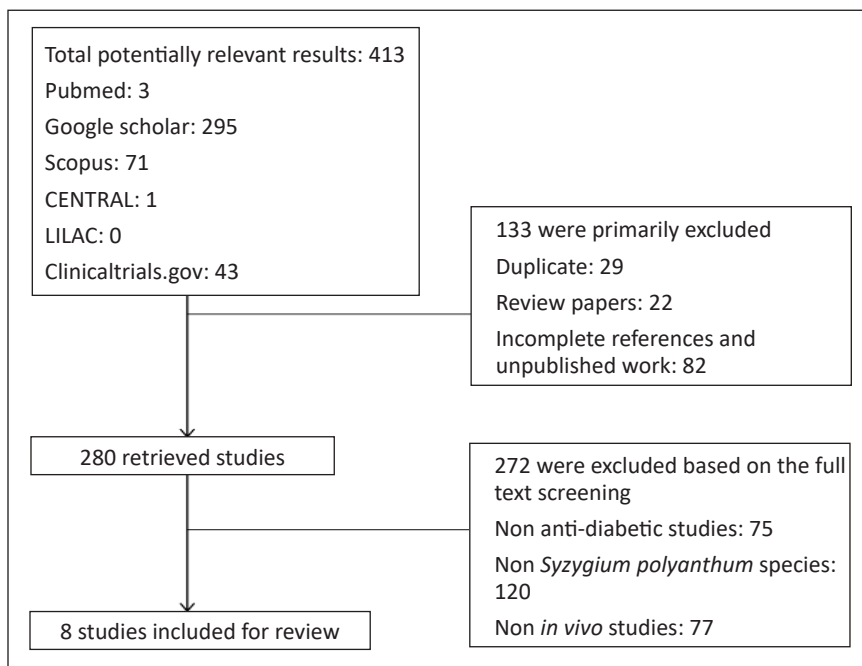


Figure 1. Preferred Reporting Items for Systematic Reviews and Meta-Analysis (PRISMA) flow diagram of study selection

al., 2015a; Widyawati et al., 2015b; & Yuliana, 2014), fasted animals were first induced with diabetes using alloxan (Hikmah et al., 2016; Liem et al., 2015; Sutrisna et al., 2016; Wahjuni et al., 2018; Widharna et al., 2015; Widyawati et al., 2015a; & Yuliana, 2014) or streptozotocin (Widyawati et al., 2015a & 2015b) followed by *S. polyanthum* mixture with glibenclamide (Hikmah et al., 2016 & Liem et al., 2015), different dosages of *S. polyanthum* extract alone (Sutrisna et al., 2016; Wahjuni et al., 2018; Widharna et al., 2015; Widyawati et al., 2015b; & Yuliana, 2014) or different extracts of *S. polyanthum* (Widyawati et al., 2015a) supplementation for a duration of 6 to 56 days. Only one study had a test period of seven hours (Widyawati et al., 2015a).

The results showed that oral administration of methanol extract of *S. polyanthum* leaves (1000 mg/kg body weight) did not significantly alter BGL in normal or intraperitoneally glucose-loaded male Sprague Dawley rats. However, in streptozotocin-induced (55 mg/kg b.w.) diabetic male Sprague Dawley rats (180 g to 250 g), administration of the extract in three doses (250, 500, 1000 mg/kg b.w.) twice daily for six days significantly ($p < 0.05$, $p < 0.01$, $p < 0.001$) and dose-dependently reduced fasting BGL compared to the control (normal saline, 10 mL/kg b.w.) (Widyawati et al., 2015b).

The aqueous extract of *S. polyanthum* leaves (200 mg/kg b.w.) administered orally to intravenous glucose-loaded average male Wistar rats (100 g to 150 g) showed a significantly ($p < 0.01$) reduction in BGL after 30 minutes. Glibenclamide administered at 0.45 mg/kg b.w. on the other hand, significantly ($p < 0.01$) reduced the BGL after 90 minutes compared to the regular control group (received drinking water) (Widharna et al., 2015).

Aqueous extract of *S. polyanthum* leaves (200 mg/kg b.w.) administered orally to alloxan-induced (150 mg/kg b.w.) diabetic male Wistar rats (100 g to 150 g) for 14 days significantly ($p < 0.01$) reduced their fasting BGL to 45% compared to untreated diabetic rats that received drinking water. However, oral administration of metformin (63 mg/kg b.w.) reduced fasting BGL to 48%, which showed no significant difference with the *S. polyanthum* extract (Widharna et al., 2015).

The combination of ethanol extract of *S. polyanthum* leaves (500 mg/kg b.w. and 750 mg/kg b.w.) with glibenclamide (0.65 mg/kg b.w.) administered orally to alloxan-induced (120 mg/kg b.w.) diabetic mice (*Mus musculus*) for 14 days significantly ($p < 0.05$) lowered fasting BGL by 230 ± 23.69 and 233.75 ± 9.93 mg/dL. This result is significant compared to the negative control (Na carboxymethyl cellulose (CMC) 0.5%) by 4 ± 6.82 mg/dL, positive control (glibenclamide alone) by 150.75 ± 11.34 mg/dL, combination of ethanol extract of *S. polyanthum* leaves (250 mg/kg b.w.) with glibenclamide (0.65 mg/kg b.w.) by 170 ± 10.51 mg/dL, and ethanol extract of *S. polyanthum* alone of 250, 500 and 750 mg/kg b.w. at 134 ± 4.61 , 151.25 ± 6.72 , and 158.75 ± 17.64 mg/dL, respectively (Liem et al., 2015).

The leaf decoction of *S. polyanthum* (1800 mg/kg b.w.) administered orally to alloxan-induced (120 mg/kg b.w.) diabetic male Wistar rats (180 gm to 200 g) for ten days

significantly ($p < 0.05$) lowered fasting BGL on hyperglycaemic rats as well as Kupffer cell count. However, it is not likely to give significant results in lowering pancreatic and kidney haemorrhage scores (Yuliana, 2014).

Petroleum ether, chloroform, and methanol extract of *S. polyanthum* leaves at a dose of 1000 mg/kg b.w. administered orally to intraperitoneal glucose-loaded average male Sprague Dawley rats (180 g to 250 g) for 30 minutes did not significantly alter the increase of BGL within 120 minutes after glucose loading (Widyawati et al., 2015a).

Aqueous extract of *S. polyanthum* leaves at a dose of (1000 mg/kg b.w.) administered orally to intraperitoneal glucose-loaded average male Sprague Dawley rats (180 g to 250 g) for 30 minutes significantly ($p < 0.05$) increase BGL (9.3 ± 0.38 mmol/L) compared to the control (normal saline, 10 mL/kg b.w.). Metformin with the administration of 500 mg/kg b.w. dose, on the other hand, significantly displayed better BGL inhibition after 90 minutes ($p < 0.01$) (5.3 ± 0.14 mmol/L) and 120 minutes ($p < 0.05$) (5.1 ± 0.19 mmol/L) compared to the control (normal saline, 10 mL/kg b.w.) with 6.4 ± 0.23 mmol/L after 90 minutes and 5.9 ± 0.13 mmol/L after 120 minutes (Widyawati et al., 2015a).

Methanol extract of *S. polyanthum* leaves (1000 mg/kg b.w.) administered orally to streptozotocin-induced (55 mg/kg b.w.) diabetic male Sprague Dawley rats (180 g to 250 g) for seven hours significantly ($p < 0.01$) decrease the fasting BGL compared to the diabetic control (normal saline, 10 mL/kg b.w.). Metformin, on the other hand, significantly reduced the blood glucose from the first hour ($p < 0.01$) to the seventh hour ($p < 0.001$) of the study (Widyawati et al., 2015a).

Ethanol extract of *S. polyanthum* leaves (62.5, 125, and 250) mg/kg b.w. administered orally to alloxan-induced (150 mg/kg b.w.) diabetic male Wistar rats for ten days significantly ($p < 0.05$) reduced BGL (114.3 ± 9.4 , 119.3 ± 23.4 , 119.3 ± 11.3) mg/dL (Sutrisna et al., 2016).

The combination of ethanol extract of *S. polyanthum* leaves (750 mg/kg b.w.) and glibenclamide (0.65 mg/kg b.w.) administered orally to alloxan-induced (70 mg/kg b.w.) diabetic male mice (*Mus musculus*) for 14 days shows significant ($p > 0.05$) mean difference of lowered fasting BGL (287.4 ± 65.05 mg/dL) compared to the negative control (Na CMC 0.5%) showing -78.8 ± 115.12 mg/dL, positive control (glibenclamide alone) (173.6 ± 60.55 mg/dL), ethanol extract of *S. polyanthum* leaves alone at (250, 500 and 750) mg/kg b.w. with 135.4 ± 28.89 , 163.2 ± 47.99 , 190.2 ± 46.98 mg/dL mean difference respectively, and the combination of ethanol extract of *S. polyanthum* leaves (250 and 500) mg/kg b.w. with glibenclamide (0.65 mg/kg b.w.) (237.4 ± 75.11 , 246 ± 23.09) mg/dL (Hikmah et al., 2016).

Aqueous extract of *S. polyanthum* leaves (5.0 mg/kg b.w./day) administered orally to alloxan-induced (125 mg/kg b.w.) diabetic Wistar rats for 56 days significantly ($p < 0.05$) lowered BGL (110.56 ± 1.68 mg/dL) than the control group (105.76 ± 2.53 mg/dL) (Wahjuni et al., 2018).

Figures 2 and 3 show the risk of bias assessment results of the eight studies included in this review. Six (75%) of the studies stated the studies have baseline characteristics based on this assessment. Since the backgrounds of the animals were essentially homogeneous,

	Selection bias - Sequence generation	Selection bias - Baseline characteristics	Selection bias - Allocation	Performance bias - Random housing	Performance bias - Blinding	Detection bias - Random outcome assessment	Detection bias - Blinding	Attrition - Incomplete outcome data	Reporting bias - Selective outcome reporting	Other bias
Hikmah 2016	?	+	?	+	?	?	?	?	+	+
Liem 2015	?	+	?	?	?	?	?	?	+	?
Sutrisna 2016	+	+	?	?	?	?	?	?	+	+
Wahjuni 2018	?	+	?	?	?	?	?	?	+	?
Widharna 2015	?	+	?	+	?	?	?	?	+	+
Widyawati, Pumawan 2015	+	+	?	?	?	?	?	?	+	+
Widyawati, Yusoff 2015	?	+	?	+	?	?	?	?	+	+
Yuliana 2014	?	+	?	?	?	?	+	?	+	?

Figure 2. Risk of bias assessment of included studies using SYRCLE tool

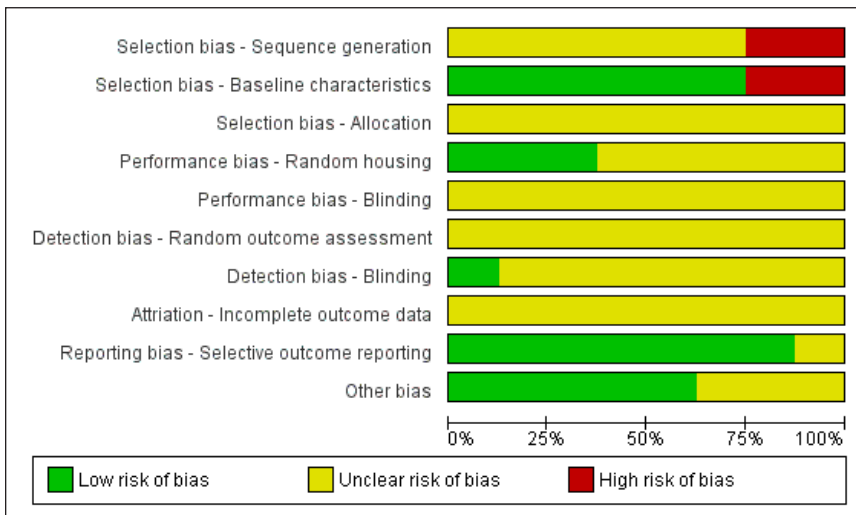


Figure 3. Risk of bias summary

Table 2
Data extraction table

Author, Year	Plant part	Type of extraction	Study subject	Induction of diabetes	Dosage	Comparison	p-value	Finding (s)
(Widyawati et al., 2015b)	Leaves	Methanol	Eighty-two healthy male Sprague Dawley rats weighing between 200 to 250 g	Streptozotocin-induced at 55 mg/kg b.w. intraperitoneally	125-1000 mg/kg b.w.	Glibenclamide, 10.00 mg/kg b.w. Metformin, 500.00 mg/kg b.w.	p < 0.01	Methanol extract of <i>S. polyanthum</i> leaves did not significantly alter the BGL in average and intraperitoneal glucose loaded rats, respectively. However, glibenclamide and metformin significantly reduced the BGL in normal and intraperitoneal-loaded glucose rats, respectively. Both methanol extract of <i>S. polyanthum</i> leaves and metformin, on the other hand, significantly reduced the fasting BGL in diabetic rats.
(Widhama et al., 2015)	Leaves	Aqueous	Eighty-four healthy male Wistar rats weighing between 100 to 150 g	Alloxan-induced at 150 mg/kg b.w. intravenously	200 mg/kg b.w.	Glibenclamide, 0.45 mg/kg b.w. Metformin, 63.00 mg/kg b.w.	p < 0.05	Both aqueous extract of <i>S. polyanthum</i> leaves and glibenclamide significantly lowered the BGL in intravenous glucose-loaded average rats. Aqueous extract of <i>S. polyanthum</i> leaves significantly reduced the fasting BGL while metformin did not significantly reduce the fasting BGL in diabetic rats.
(Liem et al., 2015)	Leaves	Ethanol	Thirty-two mice (<i>Mus musculus</i>)	Alloxan-induced at 120 mg/kg b.w. intraperitoneally	250-750 mg/kg b.w.	Glibenclamide, 0.65 mg/kg b.w.	p < 0.05	Combination of ethanol extract of <i>S. polyanthum</i> leaves with glibenclamide significantly lowered the fasting BGL in diabetic mice compared to glibenclamide alone.
(Yuliana, 2014)	Leaves	Aqueous	Twenty-four male Wistar rats weighing between 180 to 200 g	Alloxan-induced at 120 mg/kg b.w. intraperitoneally	900-2700 mg/kg b.w.	Untreated hyperglycemic rats	p < 0.05	Aqueous leaf decoction of <i>S. polyanthum</i> significantly lowered the fasting BGL in hyperglycemic rats.

Table 2 (continue)

Author, Year	Plant part	Type of extraction	Study subject	Induction of diabetes	Dosage	Comparison	p-value	Finding (s)
(Widyawati et al., 2015a)	Leaves	Petroleum ether, chloroform, methanol, aqueous	Seventy-five healthy male Sprague Dawley rats weighing between 180 to 250 g	Streptozotocin-induced at 55 mg/kg b.w. intraperitoneally	1000 mg/kg b.w.	Metformin, 500.00 mg/kg b.w.	p < 0.05 p < 0.01	Petroleum, chloroform, and methanol extract of <i>S. polyanthum</i> leaves did not significantly alter the increase of BGL in intraperitoneal glucose-loaded average rats. Aqueous extract of <i>S. polyanthum</i> leaves significantly altered the increase of BGL in intraperitoneal glucose-loaded average rats. Metformin significantly inhibited the BGL in intraperitoneal glucose-loaded average rats. Both methanol extract of <i>S. polyanthum</i> leaves and metformin, on the other hand, significantly reduced the fasting BGL in diabetic rats.
(Sutrisna et al., 2016)	Leaves	Ethanol	Forty healthy male Wistar rats	Alloxan-induced at 150 mg/kg b.w.	60–250 mg/kg b.w.	Glibenclamide, 0.63 mg/kg b.w.	p < 0.05	Ethanol extract of <i>S. polyanthum</i> leaves reduced BGL in diabetic rats.
(Hikmah et al., 2016)	Leaves	Ethanol	Forty healthy male mice	Alloxan-induced at 70 mg/kg b.w. intravenously	250–750 mg/kg b.w.	Glibenclamide, 0.65 mg/kg b.w.	p > 0.05	Combination of ethanol extract of <i>S. polyanthum</i> leaves and glibenclamide significantly lowered the BGL in diabetic mice compared to <i>S. polyanthum</i> leaves and glibenclamide alone.
(Wahjuni et al., 2018)	Leaves	Aqueous	Forty healthy Wistar rats	Alloxan-induced at 125 mg/kg b.w.	0.5–5.0 mg/kg b.w.	Glibenclamide, 0.18 mg/200g b.w.	p > 0.05	Aqueous extract of <i>S. polyanthum</i> leaves significantly reduced BGL in diabetic rats.

most of the studies did not describe the method of randomisation. None of the studies indicated whether the allocation was adequately concealed. As shown clearly in Figure 2, many items were scored as “unclear”, indicating that these animal studies’ reporting and presumably experimental design can be improved. Three (38%) of the studies did not state the source of the plant or extract, which gives a score of “unclear” in other bias.

DISCUSSION

Of the total eight studies we analysed, we found that different extracts of *S. polyanthum* leaves (aqueous, methanol, and ethanol) positively impact lowering the BGL in animal subjects. Out of the eight studies, the *S. polyanthum* leaves extract were conducted in average and diabetic rats to examine the hypoglycaemic (three studies) (Widharna et al., 2015; Widyawati et al., 2015a; & Widyawati et al., 2015b), intraperitoneal glucose tolerance test IPGTT (two studies) (Widyawati et al., 2015a & 2015b) and antihyperglycaemic (eight studies) (Hikmah et al., 2016; Liem et al., 2015; Sutrisna et al., 2016; Wahjuni et al., 2018; Widharna et al., 2015; Widyawati et al., 2015a; Widyawati et al., 2015b; & Yuliana, 2014). In addition, Sutrisna et al. (2016) reported that the most optimum dosage of ethanol extract of *S. polyanthum* leaves (62.5 mg/kg b.w.) administered to male Wistar rats reduced the BGL to 114.3 ± 9.4 mg/dL.

The phytochemical screening of *S. polyanthum* leaves extract contains tannins, flavonoids, alkaloids, and terpenoids (Hikmah et al., 2016; Liem et al., 2015; Wahjuni et al., 2018; Widharna et al., 2015; Widyawati et al., 2015b; & Yuliana, 2014). Each of these compounds has been shown to have a potential antidiabetic effect. A study reported that administering tannin from *Syzygium mundagam* bark significantly reduced the BGL of an STZ-induced diabetic rat model. It has been shown to have the antioxidant effect of tannin on reducing oxidative stress in diabetic animals supplemented with tannin fraction (TF) 200 mg/kg due to its hydrogen donating ability, which reduces the radical scavenging activity (Chandran et al., 2017; & Velayutham et al., 2012).

Flavonoids have been reported to possess antihyperglycaemic activity in STZ-induced diabetic rats through a few mechanisms of action attributable to the inhibition of α -glucosidase and the elevation of blood insulin levels (Khamchan et al., 2018; & Mohamed et al., 2015). Flavonoid compound (quercetin) present in *Syzygium cumini* seed (Chagas et al., 2015) and phenolic compound (gallic acid) present in *Syzygium samarangense* fruit (Khamchan et al., 2018) have been reported to regenerate pancreatic β -cells, thus may increase the secretion of insulin (Brahmachari, 2011; Jananie et al., 2011; & Yang & Kang, 2018). In addition, the animal study showed that flavonoids played similar functions to vitamin E by inhibiting peroxidation to liver microsomes in mice that experienced vitamin E efficiency (Duthie & Morrice, 2012). It is due to the stimulation of antioxidant enzymes catalase (CAT) and superoxide dismutase (SOD) activities or chemical structure where

double bond at two to three position conjugated with a 4-oxo function and hydroxyl groups at positions 3 and 5 in flavonoid contributes to its antiradical activity (Khamchan, 2018; Duthie & Morrice, 2012).

Alkaloid from *S. polyanthum* leaves has shown antidiabetic potential in STZ-induced diabetic rats (Widyawati et al., 2015b). Alkaloid compounds, namely polyhydroxyalkaloids (PHA), specifically casuarine 6-O- α -glucoside that are present in most Myrtaceae species such as *Syzygium malaccense*, *Syzygium oleosum*, *Syzygium paniculatum*, and *Syzygium cumini*. They could be induced in relatively high glucose uptake in mouse (β -TC6) pancreatic cell line and mouse (C2C12) myoblast skeletal muscle cells (Bhaskar et al., 2011; Jung et al., 2006; Kumar et al., 2013; & Porter et al., 2000). Alkaloid compounds play a role in reducing blood glucose transportation in the blood, stimulates glycogen synthesis and inhibits glucose synthesis by inhibiting enzyme glucose 6-phosphatase, fructose 1, 6-bifosfasaten and increase glucose oxidation through glucose 6-phosphate dehydrogenase (Kooti et al., 2016).

Oral administration of triterpenoid from *Syzygium malaccense* for 15 days results in a significant decrease of fasting BGL in STZ-induced diabetic rats (Bairy et al., 2005). Squalene, a triterpene that belongs to the terpenoid family present in *S. polyanthum* (Widyawati et al., 2015b) and *Mucuna pruriens* (Bhaskar et al., 2011), is responsible as an α -glucosidase inhibitor (Hou et al., 2009), which delay the absorbance of carbohydrates in the intestine subsequently decreasing the postprandial insulin level and also increase insulin insensitivity (Li et al., 2010; Nazaruk & Borzym-Kluczyk, 2014) and may increase insulin secretion (Li et al., 2010). Another underlying mechanism of *S. polyanthum* in reducing BGL may be inhibiting intestinal glucose absorption and enhancing glucose uptake by the muscles (Kooti et al., 2016).

However, few references suggest or deny the use of *S. polyanthum* leaves as a potential antidiabetic agent. The available articles have limitations in many aspects, and the results lack implications. Besides, no human studies are available, and only animal studies were included. Therefore, it is not easy to conduct any measure of consistency or subgroup analysis due to the more diverse nature of the animal studies, such as species used, design, and study characteristics (age, dose, schedule of administration). The risk of bias assessment of the animal studies conducted in this paper is vital to show the need to reduce the biases through methodological quality since most of the assessments gave “unclear” scores. Although safety data on *S. polyanthum* is limited, the only study by Widharna et al. (2015) revealed that combination of *S. polyanthum* and *Andrographis paniculata* leaves extract were free of acute oral toxicity up to 2000 mg/kg body weight and did not cause a change in behavioural activities of the animals. Other toxicity tests reported previously suggested that the extract of *S. polyanthum* was practically safe and non-toxic when tested on Wistar rats (Sumiwi et al., 2019). Therefore, based on the current empirical evidence, the potential

of *S. polyanthum* leaves alone or combined with glibenclamide has shown a significant lowering of blood glucose levels. However, this paper showed the need to improve the methodological quality of animal studies. It can be done by minimising or standardising the biological study characteristics of animal studies and reducing bias sources. By performing this, the original research can be applicable with high quality to be used for meta-analysis with reduced impact of bias (Hooijmans et al., 2014a).

CONCLUSION

In conclusion, the extract of *S. polyanthum* leaves alone or combined with glibenclamide may potentially exhibit a significant antidiabetic effect. However, although the leaves extract of *S. polyanthum* may be a promising agent for diabetes mellitus, further studies with a comprehensive methodology and results are needed to determine the phytochemicals involved, possible mechanisms of action, and safety assessment so that the results can be translated into clinical trials.

ACKNOWLEDGEMENT

The authors wish to extend their gratitude to the Director General of Health Malaysia, the Deputy Director-General of Health (Research & Technical Support), the Director of Institute for Medical Research, and the Head of Centre of Herbal Medicine Research Centre for their support and permission to publish this article.

REFERENCES

- Azwar, A. (2010). *Tanaman obat Indonesia* (Buku kedua ed.) [Indonesia Medicinal Plants (2nd Ed.)]. Selemba Medika.
- Bairy, K., Sharma, A., & Shalini, A. (2005). Evaluation of the hypoglycemic, hypolipidemic and hepatic glycogen raising effects of *Syzygium malaccense* upon streptozotocin induced diabetic rats. *Journal of Natural remedies*, 5(1), 46-51. <https://doi.org/10.18311/jnr/2005/414>
- Berawi, K. N., Shidarti, L., Nurdin, S. U., Lipoeto, N. I., & Wahid, I. (2017). Comparison effectiveness of antidiabetic activity extract herbal mixture of soursop leaves (*Annona muricata*), bay leaves (*Syzygium polyanthum*) and pegagan leaves (*Centella asiatica*). *Biomedical and Pharmacology Journal*, 10(3), 1481-1488. <https://dx.doi.org/10.13005/bpj/1256>
- Bhaskar, A., Nithya, V., & Vidhya, V. (2011). Phytochemical evaluation by GC-MS and antihyperglycemic activity of *Mucuna pruriens* on streptozotocin induced diabetes in rats. *Journal of Chemical and Pharmaceutical Research*, 3(5), 689-696.
- Brahmachari, G. (2011). Bio-flavonoids with promising antidiabetic potentials: A critical survey. *Research Signpost*, 661(2), 187-212.
- Burkill, I. H. (1935). *A dictionary of the economic products of the Malay Peninsula* (Vol. I (A - H)). Crown Agents for the Colonies.

- Chagas, V. T., França, L. M., Malik, S., & Paes, A. M. D. A. (2015). *Syzygium cumini* (L.) skeels: A prominent source of bioactive molecules against cardiometabolic diseases. *Frontiers in Pharmacology*, 6, Article 259. <https://doi.org/10.3389/fphar.2015.00259>
- Chandran, R., Parimelazhagan, T., & George, B. P. (2017). Antihyperglycemic activity of the bark methanolic extract of *Syzygium mundagam* in diabetic rats. *Alexandria Journal of Medicine*, 53(4), 317-324. <https://doi.org/10.1016/j.ajme.2016.12.001>
- Dewijanti, I. D., Artanti, N., Mangunwardoyo, W., Hanafi, M., Abbas, J., Megawati, M., Minarti, M., Musdalifah, D., & Meilawati, L. (2018). Bioactivities of *Syzygium polyanthum* (Wight) Walp leaf extract for decreasing diabetic risk. In *AIP Conference Proceedings* (Vol. 2024, No. 1, p. 020011). AIP Publishing LLC. <https://doi.org/10.1063/1.5064297>
- Duncan, B. B., Schmidt, M. I., Pankow, J. S., Ballantyne, C. M., Couper, D., Vigo, A., & Heiss, G. (2003). Low-grade systemic inflammation and the development of type 2 diabetes: The atherosclerosis risk in communities study. *Diabetes*, 52(7), 1799-1805. <https://doi.org/10.2337/diabetes.52.7.1799>
- Duthie, G., & Morrice, P. (2012). Antioxidant capacity of flavonoids in hepatic microsomes is not reflected by antioxidant effects *in vivo*. *Oxidative Medicine and Cellular Longevity*, 2012, Article 165127. <https://doi.org/10.1155/2012/165127>
- Emerging Risk Factors Collaboration. (2011). Diabetes mellitus, fasting glucose, and risk of cause-specific death. *New England Journal of Medicine*, 364(9), 829-841. <https://doi.org/10.1056/NEJMoa1008862>
- Hikmah, N., Yuliet, Y., & Khaerati, K. (2016). Pengaruh pemberian ekstrak daun salam (*Syzygium polyanthum* Wight.) terhadap glibenklamid dalam menurunkan kadar glukosa darah mencit (*Mus musculus*) yang diinduksi aloksan [Effect of administration of bay leaf extract (*Syzygium polyanthum* Wight.) on glibenclamide in reducing blood glucose levels of mice (*Mus musculus*) induced by alloxan.]. *Jurnal Farmasi Galenika (Galenika Journal of Pharmacy)(e-Journal)*, 2(1), 24-30.
- Hooijmans, C. R., Int'Hout, J., Ritskes-Hoitinga, M., & Rovers, M. M. (2014a). Meta-analyses of animal studies: An introduction of a valuable instrument to further improve healthcare. *Institute for Laboratory Animal Research Journal*, 55(3), 418-426. <https://doi.org/10.1093/ilar/ilu042>
- Hooijmans, C. R., Rovers, M. M., de Vries, R. B., Leenaars, M., Ritskes-Hoitinga, M., & Langendam, M. W. (2014b). SYRCLE's risk of bias tool for animal studies. *BMC Medical Research Methodology*, 14, Article 43. <https://doi.org/10.1186/1471-2288-14-43>
- Hou, W., Li, Y., Zhang, Q., Wei, X., Peng, A., Chen, L., & Wei, Y. (2009). Triterpene acids isolated from *Lagerstroemia speciosa* leaves as α -glucosidase inhibitors. *Phytotherapy Research: An International Journal Devoted to Pharmacological and Toxicological Evaluation of Natural Product Derivatives*, 23(5), 614-618. <https://doi.org/10.1002/ptr.2661>
- Jananie, R., Priya, V., & Vijayalakshmi, K. (2011). Determination of bioactive components of *Cynodon dactylon* by GC-MS analysis. *New York Science Journal*, 4(4), 1-5.
- Jung, M., Park, M., Lee, H. C., Kang, Y. H., Kang, E. S., & Kim, S. K. (2006). Antidiabetic agents from medicinal plants. *Current Medicinal Chemistry*, 13(10), 1203-1218. <https://doi.org/10.2174/092986706776360860>

- Khamchan, A., Paseephol, T., & Hanchang, W. (2018). Protective effect of wax apple [*Syzygium samarangense* (Blume) Merr. & LM Perry] against streptozotocin-induced pancreatic β -cell damage in diabetic rats. *Biomedicine & Pharmacotherapy*, 108, 634-645. <https://doi.org/10.1016/j.biopha.2018.09.072>
- Kooti, W., Farokhipour, M., Asadzadeh, Z., Ashtary-Larky, D., & Asadi-Samani, M. (2016). The role of medicinal plants in the treatment of diabetes: A systematic review. *Electronic Physician*, 8(1), 1832-1842. <https://doi.org/10.19082/1832>
- Kumar, A., Ilavarasan, R., Jayach, T., Deecaraman, M., Aravindan, P., Padmanabhan, N., & Krishan, M. (2013). Anti-diabetic activity of *Syzygium cumini* and its isolated compound against streptozotocin-induced diabetic rats. *Journal of Medicinal Plants Research*, 2(9), 246-249. <https://doi.org/10.5897/JMPR.9000093>
- Li, T. H., Hou, C. C., Chang, C. L. T., & Yang, W. C. (2010). Anti-hyperglycemic properties of crude extract and triterpenes from *Poria cocos*. *Evidence-Based Complementary and Alternative Medicine*, 2011, Article 128402. <https://doi.org/10.1155/2011/128402>
- Liberati, A., Altman, D. G., Tetzlaff, J., Mulrow, C., Gotzsche, P. C., Ioannidis, J. P. A., et al. (2009). The PRISMA statement for reporting systematic reviews and meta-analyses of studies that evaluate healthcare interventions: Explanation and elaboration. *British Medical Journal*, 2009, Article 339. <https://doi.org/10.1136/bmj.b2700>
- Liem, S., Yuliet, Y., & Khumaidi, A. (2015). Uji aktivitas antidiabetes kombinasi glibenklamid dan ekstrak daun salam (*Syzygium polyanthum* Wight.) terhadap mencit (*Mus musculus*) yang diinduksi aloksan [Antidiabetic activity of glibenclamide and bay leaf extract (*Syzygium polyanthum* Wight.) combination against mice (*Mus musculus*) induced by alloxan.]. *Jurnal Farmasi Galenika (Galenika Journal of Pharmacy) (e-Journal)*, 1(1), 42-47.
- Loke, A. (2020). Diabetes fact sheet. *World Health Organization*. Retrieved November 2, 2020, from <https://www.who.int/news-room/fact-sheets/detail/diabetes>
- Malaysian Herbal Monograph Committee. (2017). *Syzygium polyanthum* (Wight.) Walp. Retrieved February 27, 2019, from https://www.globinmed.com/index.php?option=com_content&view=article&id=106297:syzygium-polyanthum-wight-walp&catid=209&Itemid=143
- Mohamed, E. A., Ahmad, M., Ang, L. F., Asmawi, M., & Yam, M. F. (2015). Evaluation of α -glucosidase inhibitory effect of 50% ethanolic standardized extract of *Orthosiphon stamineus* Benth in normal and streptozotocin-induced diabetic rats. *Evidence-Based Complementary and Alternative Medicine*, 2015, Article 754931. <https://doi.org/10.1155/2015/754931>
- Nazaruk, J., & Borzym-Kluczyk, M. (2014). The role of triterpenes in the management of diabetes mellitus and its complications. *Phytochemistry Reviews*, 14(4), 675-690. <https://doi.org/10.1007/s11101-014-9369-x>
- NHMS. (2019). Non-communicable diseases, healthcare demand and health literacy: Key Findings. *National Health and Morbidity Survey 2019*. Retrieved November 2, 2020, from http://iptk.moh.gov.my/images/technical_report/2020/4_Infographic_Booklet_NHMS_2019_-_English.pdf

- Nwaneri, C., Cooper, H., & Bowen-Jones, D. (2013). Mortality in type 2 diabetes mellitus: Magnitude of the evidence from a systematic review and meta-analysis. *The British Journal of Diabetes & Vascular Disease*, 13(4), 192-207. <https://doi.org/10.1177/1474651413495703>
- Porter, E., Lughadha, E. N., & Simmonds, M. (2000). Taxonomic significance of polyhydroxyalkaloids in the Myrtaceae. *Kew Bulletin*, 55(3), 615-632. <https://doi.org/10.2307/4118779>
- Quattrocchi, U. F. L. S. (2012). *CRC world dictionary of medicinal and poisonous plants: Common names, scientific names, eponyms, synonyms, and etymology* (Vol. V R-Z). CRC Press.
- Ramachandran, A., Snehalatha, C., Shetty, A. S., & Nanditha, A. (2012). Trends in prevalence of diabetes in Asian countries. *World journal of Diabetes*, 3(6), 110-117. <https://doi.org/10.4239/wjd.v3.i6.110>
- Rashid, F. H. (2017, April 7). Almost 1 in 5 M'sian adults has diabetes: Health Ministry. *New Strait Times*. Retrieved November 2, 2020, from <https://www.nst.com.my/news/2017/04/228106/almost-1-5-msian-adults-has-diabetes-health-ministry>.
- Sumiwi, S. A., Zuhrotun, A., Hendriani, R., Rizal, M., Levita, J., & Megantara, S. (2019). Subchronic toxicity of ethanol extract of *Syzygium polyanthum* (Wight) Walp. leaves on Wistar rat. *The Indonesian Biomedical Journal*, 11(1), 30-35. <https://doi.org/10.18585/inabj.v11i1.458>
- Sutrisna, E., Trisharyanti, I., Munawaroh, R., & Suprpto, S. (2016). Antioxidant and antidiabetic activity of 70% ethanolic extract of *Syzygium polyanthum* (Wight) leaf from Indonesia. *International Journal of Research in Ayurveda and Pharmacy*, 7, 214-216.
- The Plant List. (2012). *Syzygium polyanthum* (Wight.) Walp. Retrieved February 27, 2019, from <http://www.theplantlist.org/tp11.1/record/kew-200120>
- Velayutham, R., Sankaradoss, N., & Ahamed, K. N. (2012). Protective effect of tannins from *Ficus racemosa* in hypercholesterolemia and diabetes induced vascular tissue damage in rats. *Asian Pacific Journal of Tropical Medicine*, 5(5), 367-373. [https://doi.org/10.1016/S1995-7645\(12\)60061-3](https://doi.org/10.1016/S1995-7645(12)60061-3)
- Wahjuni, S., Laksmiwati, A. M., & Manuaba, I. B. P. (2018). Antidiabetic effects of Indonesian bay leaves (*Syzygium polyanthum*) extracts through decreasing advanced glycation end products and blood glucose level on alloxan-induced hyperglycemic wistar rats. *Asian Journal of Pharmaceutical and Clinical Research*, 11(4), 340-343. <https://doi.org/10.22159/ajpcr.2018.v11i4.24084>
- Waly, M. I., Essa, M. M., & Ali, A. (2010). The global burden of type 2 diabetes: A review. *International Journal of Biological & Medical Research*, 1(4), 326-329.
- Whiteley, L., Padmanabhan, S., Hole, D., & Isles, C. (2005). Should diabetes be considered a coronary heart disease risk equivalent? Results from 25 years of follow-up in the Renfrew and Paisley survey. *Diabetes Care*, 28(7), 1588-1593. <https://doi.org/10.2337/diacare.28.7.1588>
- WHO. (2019). Diabetes mellitus. *World Health Organization*. Retrieved November 2, 2020, from <https://www.who.int/news-room/fact-sheets/detail/diabetes>
- Widharna, R. M., Tamayanti, W. D., Hendriati, L., Hamid, I. S., & Widjajakusuma, E. C. (2015). Antidiabetic effect of the aqueous extract mixture of *Andrographis paniculata* and *Syzygium polyanthum* leaf. *European Journal of Medicinal Plants*, 6(2), 82-91. <https://doi.org/10.9734/EJMP/2015/15601>

- Widyawati, T., Purnawan, W. W., Atangwho, I. J., Yusoff, N. A., Ahmad, M., & Asmawi, M. Z. (2015a). Anti-diabetic activity of *Syzygium polyanthum* (Wight) leaf extract, the most commonly used herb among diabetic patients in Medan, North Sumatera, Indonesia. *International Journal of Pharmaceutical Sciences and Research*, 6(4), 1698-1704. [https://doi.org/10.13040/IJPSR.0975-8232.6\(4\).1698-04](https://doi.org/10.13040/IJPSR.0975-8232.6(4).1698-04)
- Widyawati, T., Yusoff, N. A., Asmawi, M. Z., & Ahmad, M. (2015b). Antihyperglycemic effect of methanol extract of *Syzygium polyanthum* (Wight.) leaf in streptozotocin-induced diabetic rats. *Nutrients*, 7(9), 7764-7780. <https://doi.org/10.3390/nu7095365>
- Yang, D. K., & Kang, H. S. (2018). Anti-diabetic effect of cotreatment with quercetin and resveratrol in streptozotocin-induced diabetic rats. *Biomolecules & Therapeutics*, 26(2), 130-138. <https://doi.org/10.4062/biomolther.2017.254>
- Yuliana, T. W. (2014). Penurunan kadar glukosa darah dan hitung sel Kupffer tikus hiperglikemik setelah pemberian dekok daun salam [Decreased blood glucose levels and Kupffer cell count of hyperglycemic rats after consumption of bay leaf decoction]. *Jurnal Veteriner Desember*, 15(4), 541-547.



Socio-Demographic Profile and Prevalence of Tuberculosis (TB) Treatment Outcomes among Tuberculosis/Human Immunodeficiency Virus (TB/HIV) Co-Infected Patients in Kelantan

Siti Romaino Mohd Nor^{1,2}, Mohd Rozi Husin³, Mat Zuki Mat Jaeb⁴ and Nyi Nyi Naing^{1*}

¹Faculty of Medicine, Universiti Sultan Zainal Abidin, Medical Campus, Jalan Sultan Mahmud, 20400 UniSZA, Kuala Terengganu, Terengganu, Malaysia

²Clinical Research Centre Kelantan, Hospital Raja Perempuan Zainab II, 15586 Kota Bharu, Kelantan, Malaysia

³TB/Leprosy Sector, Jabatan Kesihatan Negeri Kelantan, 15200 Kota Bharu, Kelantan, Malaysia

⁴Respiratory Unit, Department of Medicine, Hospital Raja Perempuan Zainab II, 15586 Kota Bharu, Kelantan, Malaysia

ABSTRACT

In Kelantan, the prevalence of Tuberculosis (TB) treatment success rate among TB/HIV co-infection is still below the success target of the World Health Organisation (WHO). Our objective was to assess the socio-demographic profile and determine the prevalence of TB treatment outcomes among TB/HIV co-infected patients in Kelantan. The cross-sectional study involved secondary data from the MyTB online system from January 2014 to December 2018, carried out at TB/Leprosy Sector, State Health Department of Kelantan. The data were analysed using SPSS version 25.0 and STATA version 14. The ethics approval was obtained from the UniSZA Human Research Ethics Committee (UHREC) and Medical Research Ethics Committee (MREC) of Ministry of Health (MOH). There were 6,313 TB cases in Kelantan. Of these, 703 (11.1%) cases were TB/HIV co-infection. However, 36

cases were excluded, and 667 cases were evaluated based on inclusion and exclusion criteria. The mean (SD) age was 38.7 (7.9) years, and the mean duration of TB treatment was 202.8 (131.27) days. The prevalence of successful treatment was 57.1%, with 19.8% cases were cured, and another 37.3% cases were completed treatment. While the unsuccessful were 42.9%, with 10.1% cases were defaulted, and 32.8% cases died. The

ARTICLE INFO

Article history:

Received: 04 November 2020

Accepted: 01 April 2021

Published: 22 September 2021

DOI: <https://doi.org/10.47836/pjst.29.4.03>

E-mail addresses:

romainomn@gmail.com (Siti Romaino Mohd Nor)

mohdrozi@moh.gov.my (Mohd Rozi Husin)

matzu@gmail.com (Mat Zuki Mat Jaeb)

syedhatim@unisza.edu.my (Nyi Nyi Naing)

* Corresponding author

successful outcomes were significantly associated with the educational level, the anatomy of TB location, smoking status, DOTS by health care providers, source of notification, the place of treatment and method of detection. This study provides the basic data of patient's socio-demographic profiles, and the prevalence of TB treatment success in Kelantan is under international target by WHO of $\geq 90.0\%$.

Keywords: Co-infected patients, Human Immunodeficiency Virus, HIV, prevalence, socio-demographic, Tuberculosis, TB

INTRODUCTION

Tuberculosis (TB) is an infectious disease that remains a primary global health concern. Worldwide, TB is known as the top 10 cause of death, and each year millions of people fall sick with TB. In 2017, a total of 6.7 million people with TB were notified and reported to World Health Organization (WHO) by National TB Programmes (NTPs). Of these, 6.4 million had reported as new or relapse TB cases. This number has been increasing since 2013. Among people living with Human Immunodeficiency Virus (PLHIV), there were 464,633 TB cases, with 84% were on Anti-Retroviral Therapy (ART). As a result, the number of TB deaths among PLHIV has decreased by 44%, from 534 000 in 2000 to 300 000 cases in 2017. At the same time, HIV-negative people decreased by 29%, from 1.8 in 2000 to 1.3 million in 2017 (WHO, 2018a).

WHO recommends a Directly Observed Treatment Short-Course (DOTS) strategy to achieve a targeted cure rate. This strategy has shown improvement in the cure rate in many countries. TB treatment should be completed for six months, requires frequent clinic visits and monitoring, and may cause terrible experience side effects for the patients. It was challenging for patients to complete their TB treatment. However, the success rate of TB treatment in Malaysia is still below the Millennium Development Goal (MDG) target of 85% and much lower than the End TB Strategy success rate for 2025 of 90.0% (WHO, 2019).

To date, the treatment outcomes among TB patients with a range of success rates have been published in a few studies from different states of Malaysia. The success rate of TB treatment among TB/HIV co-infected patients is much lower than new TB patients in general (75% vs 83%). It highlights the need to improve TB and HIV services to save TB/HIV co-infected patients (WHO, 2018b). In the state of Kelantan alone, the treatment success rate in 2017 was only 27.9% (Jalal et al., 2017). Based on this, the method for improvement was needed, particularly in achieving a better cure rate.

The Regional Strategic Plan towards Ending TB has been implemented to achieve successful TB elimination by 2035. Therefore, TB and HIV programmes need to be strengthened by understanding the socio-demographic characteristics, and clinical

characteristics that may contribute to and affect the outcome of TB treatment. Many factors have affected poor treatment outcomes and treatment effectiveness, including demanding access to treatment, poor use of DOTS, poor communication between patients and health care providers, lack of incentives, lack of active search for lost patients, and limitations of supervision (Hannah et al., 2017; Liu et al., 2018; & Wen et al., 2018). In this regard, this study was conducted to assess the socio-demographic profile and determine the prevalence of TB treatment outcomes among TB/HIV co-infected patients in Kelantan.

MATERIALS AND METHODS

Study Design

The cross-sectional study involved the secondary data from MyTB online system. The population in this study consisted of all TB/HIV co-infected patients in Kelantan on January 2014 to December 2018. The selection of these subgroups of patients was based on the recommendation by WHO to evaluate patients separately for assessing the NTPs performance (Ministry of Health Malaysia, 2016). This study was conducted at State TB organiser, TB/Leprosy Sector, State Health Department of Kelantan (JKNK), Malaysia responsible for managing the MyTB online system registry.

Sample Size Determination and Sampling Method

All TB/HIV co-infected patients registered for TB treatment during the study period and fulfilled the inclusion and exclusion criteria. The single proportion formula $n = (Z/\Delta)^2 P(1-P)$; n = Minimum required sample size, Z = Value of standard normal distribution was 1.96, Δ = Precision of 0.05, P = proportion of success (27.9%) (Jalal et al., 2017). The minimum required sample size for the estimated proportion of successful treatment with a 95% confidence interval (CI) within a 5% point estimate was 309 patients. Assuming 15% of dropout, the number of the sample size needed was 364 patients. No probability sampling method was applied.

Study Procedure

The person in charge at TB/Leprosy Sector has retrieved and downloaded the data, including patient's socio-demographic characteristics, clinical characteristics and TB treatment outcome from MyTB online system into Microsoft Excel for patients identified as TB/HIV co-infection. However, the marital status was only recorded in TBIS 10A-1 Form but was unavailable in the MyTB online system. In addition, the data were not fully recorded for monthly income, with many missing data (91.0 %). Therefore, these two parameters were not reported. All the information needed in this study was extracted in December 2019.

Operational Definitions

According to the Clinical Practice Guidelines for Management of Tuberculosis by the Ministry of Health, Malaysia (2012), the following TB treatment outcome operational terms were used in this study:

1. Cured: Former smear-positive patient was cured in the last month of treatment and at least one previous occasion.
2. Completed treatment: A patient who has completed treatment has not meet the criteria for being classified as a cure or failure
3. Treatment failed: A patient whose sputum was smear-positive at five months or later during treatment.
4. Died: A patient who died for any reason during treatment.
5. Default: A patient who has interrupted treatment for two consecutive months or more.

In this analysis, treatment success outcome was defined as the sum of cured patients and those who completed treatment. In contrast, all the other outcomes (treatment failed, died, default) were considered unsuccessful.

Chest X-ray presentation upon diagnosis was categorised according to how severe the lesion appeared on the X-ray film. It was categorised into the followings:

1. No lesion if chest X-ray showed no lesions,
2. Minimal if chest X-ray showed a few lesions,
3. Moderate advance if chest X-ray showed many lesions,
4. Far advance if chest X-ray showed extensive lesions or miliary appearance, and
5. Not performed if chest X-ray was not done during the diagnosis

Inclusion and Exclusion Criteria

The inclusion criteria were TB and HIV patients aged ≥ 18 years old, tested positive for TB and HIV and confirmed TB. At the same time, the exclusion criteria were patients transferred to other treatment centres or who were still on TB treatment during the data collection (December 2019) because their treatment outcomes could not be determined. In addition, patients whose diagnoses were changed were also excluded because they were later discovered to have a different diagnosis.

Ethical Consideration

This study obtained ethics approval from the UniSZA Human Research Ethics Committee (UHREC) (UniSZA.C/2/UHREC/628-2 Jld 2 (20)) and Medical Research Ethics Committee (MREC) of MOH (NMRR-18-3464-42863). Privacy and confidentiality of patients were maintained by anonymising their identities.

Statistical Analysis

Data were analysed using IBM SPSS Statistics version 25.0 and STATA 14. The data were explored, checked and cleaned to detect any missing value or error. The categorical variables were summarized in frequency (n) and percentage (%). At the same time, the numerical variables were described in mean and standard deviation (SD) or median and interquartile range (IQR) depending on the normality of distribution. Prevalence was presented with percentage (%) with corresponding 95% CI. Inferential statistics were performed using either Pearson Chi-square or Fisher's exact test. The level of significant alpha was set at 0.05.

RESULTS

A total of 6,313 TB cases in Kelantan were registered in MyTB online system from January 2014 to December 2018. Of these, 703 (11.1%) cases were TB/HIV co-infection. However, 36 cases were excluded due to transfer out (3), change of diagnosis (24) and still ongoing treatment (9). Therefore, 667 cases were evaluated in this study based on inclusion criteria (Figure 1). Of these 667 cases, their ages ranged between 18 and 77 years, with a mean (SD) of 38.7 (7.9) years. While the range of the duration of TB treatment was 0 to 722 days, with a mean (SD) were 202.8 (131.27) days.

The majority of cases were male (88.5%), Malays (96.7%), with secondary level education (80.2%), living in the rural area (77.1%), unemployed (44.7%), have BCG scar (94.9%), new cases (82.8%), smoking (66.0%), under DOTS by health care providers (85.9%), received treatment from public hospitals (81.1%) and passive method detection (85.5%) (Figure 2). Only 3.1% of patients had diabetes, 1.3% given 2SHRZ and 5.5% under HAART treatment (Table 1).

In terms of the anatomy of TB location, there were 428 (64.2%) who had Pulmonary TB, 164 (24.6%) had Extra-Pulmonary TB, and 75 (11.2%) had both Pulmonary TB and Extra-Pulmonary TB. Meanwhile, chest X-ray results which are examined in Pulmonary TB and Extra-Pulmonary TB, showed there were 94 (14.1%) no lesion, 387 (58.0%) minimal, 171 (25.6%) moderate advance, 5 (0.7%) far advance and 10 (1.5%) not performed the diagnosis. From ten districts in Kelantan, the majority of them were from Kota Bharu (38.5%).

In this study, the prevalence of successful TB treatment among TB/HIV co-infected patients was 57.1%. The successful outcomes were achieved in 381 cases, with 132 (19.8%) cases cured and another 249 (37.3%) cases where treatment was completed. While the unsuccessful treatment outcomes were 42.9% achieved in 286 cases, with 67 (10.1%) cases were defaulted and 219 (32.8%) were cases of death. There were no treatment failure cases identified (Table 2).

The proportion of patients with successful outcomes in this study was significantly associated with level of education ($P = 0.018$), anatomy of TB location ($P = 0.015$), smoking status ($P = 0.004$), DOTS by health care providers ($P = < 0.001$), source of notification ($P = < 0.001$), place of treatment ($P = < 0.001$) and method of detection ($P = 0.043$). However, other socio-demographics and clinical characteristics were not significantly associated with treatment outcomes. Table 1 summarizes the socio-demographic characteristics and other related factors among all study subjects.

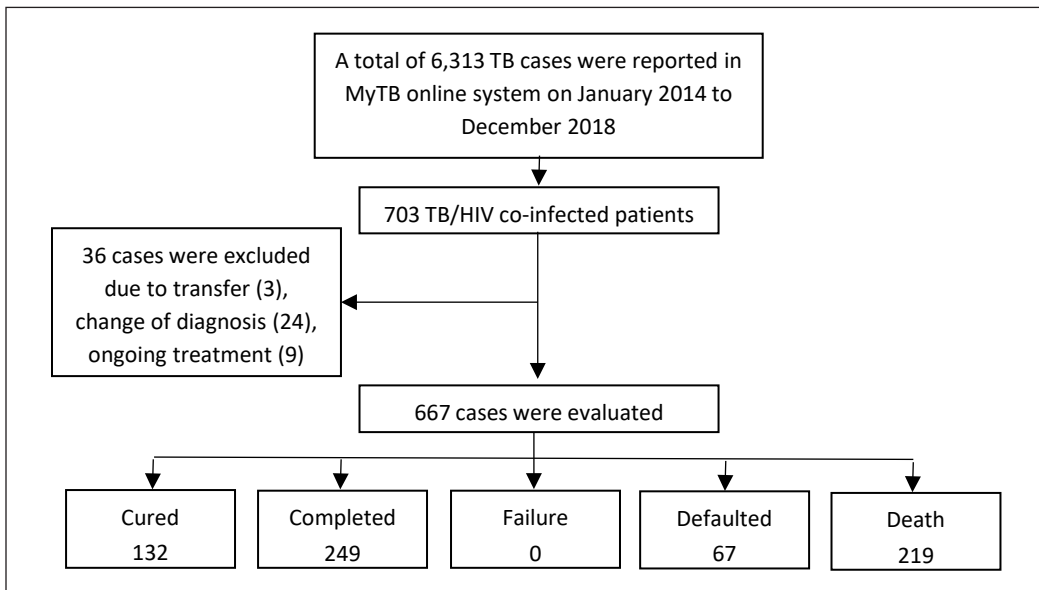


Figure 1. A schematic diagram for the selection of patients included

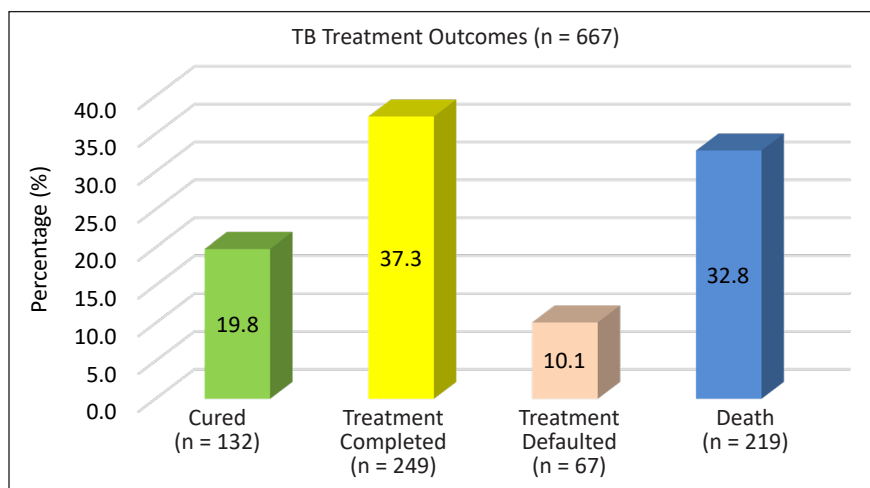


Figure 2. TB treatment outcomes among 667 TB/HIV co-infected patients in Kelantan in 2014 to 2018

Table 1
Socio-demographic and clinical characteristics among all study subjects (n = 667)

		Treatment Outcome n (%)		χ^2 (df)	P value
		Unsuccessful 286 (42.9%)	Successful 381 (57.1%)		
Gender	Male	256 (43.4)	334 (56.6)	0.545 (1)	0.460 ^a
	Female	30 (39.0)	47 (61.0)		
Race	Malays	276 (42.8)	369 (57.2)	0.062 (1)	0.804 ^a
	Non-Malays	10 (45.5)	12 (54.5)		
Level of education	No education	6 (50.0)	6 (50.0)	10.079 (3)	0.018^a
	Primary school	29 (39.2)	45 (60.8)		
	Secondary school	241 (45.0)	294 (55.0)		
	Tertiary level	10 (21.7)	36 (78.3)		
Residency	Urban	65 (42.5)	88 (57.5)	0.013 (1)	0.910 ^a
	Rural	221 (43.0)	293 (57.0)		
Occupation	Government servant	7 (25.0)	21 (75.0)	8.824 (4)	0.066 ^a
	Own business	38 (47.5)	42 (52.5)		
	Unemployed	132 (44.3)	166 (55.7)		
	Prisoner	24 (32.0)	51 (68.0)		
	Others	85 (45.7)	101 (54.3)		
Diabetes mellitus	No	279 (43.2)	367 (56.8)	0.807 (1)	0.369 ^a
	Yes	7 (33.3)	14 (66.7)		
BCG scar	No	13 (38.2)	21 (61.8)	0.315 (1)	0.574 ^a
	Yes	273 (43.1)	360 (56.9)		
HIV positive	Screening	270 (43.2)	355 (56.8)	0.419 (1)	0.518 ^a
	Verification	16 (38.1)	26 (61.9)		
Anatomy of TB location	Extra-pulmonary	76 (46.3)	88 (53.7)	8.373 (2)	0.015^a
	Pulmonary	168 (39.3)	260 (60.7)		
	Extra-pulmonary & pulmonary	42 (56.0)	33 (44.0)		
Chest X-ray status during diagnose	No Lesion	37 (39.4)	57 (60.6)		0.052 ^b
	Minimal	154 (39.8)	233 (60.2)		
	Moderately advanced	87 (50.9)	84 (49.1)		
	Far advanced	4 (80.0)	1 (20.0)		
	Not performed	4 (40.0)	6 (60.0)		
Case TB category	New case	232 (42.0)	320 (58.0)	0.988 (2)	0.610 ^a
	Relapse case	38 (46.3)	44 (53.7)		
	Case after treatment default	16 (48.5)	17 (51.5)		
Smoking status	No	80 (35.2)	147 (64.8)	8.193 (1)	0.004^a
	Yes	206 (46.8)	234 (53.2)		
Regime of treatment	2SHRZ	7 (77.8)	2 (22.2)		0.056 ^b
	2EHRZ	125 (45.3)	151 (54.7)		
	2HRZ	2 (66.7)	1 (33.3)		
	Others	152 (40.1)	227 (59.9)		

Table 1 (continue)

		Treatment Outcome n (%)		χ^2 (df)	P value
		Unsuccessful 286 (42.9%)	Successful 381 (57.1%)		
DOTs by Health care providers	No	77 (98.7)	1 (1.3)	119.631 (1)	< 0.001 ^a
	Yes	193 (33.7)	380 (66.3)		
HAART treatment	No	259 (44.0)	329 (56.0)	2.908 (1)	0.088 ^a
	Yes	11 (29.7)	26 (70.3)		
Source of notification	Public hospital	253(46.4)	292 (53.6)	15.673 (1)	< 0.001 ^a
	Public health clinic	32 (26.7)	88 (73.3)		
Place of treatment	Public hospital	249 (46.0)	292 (54.0)	< 0.001 ^b	
	Public health clinic	35 (28.5)	88 (71.5)		
	Private health sector	2 (66.7)	1 (33.3)		
Method of detection	Active	15 (51.7)	14 (48.3)	6.273 (2)	0.043 ^a
	Passive	251 (44.0)	319 (56.0)		
	Screening	20 (29.4)	48 (70.6)		
District	Kota Bharu	105 (40.90)	152 (59.1)	9.543 (9)	0.389 ^a
	Pasir Mas	22 (42.3)	30 (57.7)		
	Pasir Puteh	20 (47.6)	22 (52.4)		
	Tumpat	34 (43.0)	45 (57.0)		
	Bachok	20 (36.4)	35 (63.6)		
	Jeli	15 (55.6)	12 (44.4)		
	Kuala Krai	21 (55.3)	17 (44.7)		
	Machang	18 (36.0)	32 (64.0)		
	Tanah Merah	25 (52.1)	23 (47.9)		
	Gua Musang	6 (31.6)	13 (68.4)		

^a Pearson χ^2 was applied using SPSS version 25.0

^b Fisher's Exact Test was applied using STATA 14

The source of the notification included case from the district office (n=1) and case from private health sector (n=1). These two variables were excluded because of the small sample size.

Table 2

The prevalence of TB treatment outcomes among all study participants (n = 667)

Treatment outcome	Categories	n	Percentage (95% CI)
Successful	Cured	132	19.8 (16.78,22.82)
	Treatment Completed	249	37.3 (33.63,40.97)
	Total	381	57.1 (53.34,60.86)
Unsuccessful	Treatment Failure	0	0 (0,0)
	Treatment Defaulted	67	10.1 (7.83,12.37)
	Death	219	32.8 (30.98,34.62)
	Total	286	42.9 (39.14,46.66)

DISCUSSION

This study included a total of 667 cases, which were 381 successful and 286 unsuccessful TB treatment outcomes among TB/HIV co-infected patients. Unfortunately, published data on the treatment outcomes among TB/HIV co-infected patients in Kelantan were minimal. Therefore, the present study was designed to assess the socio-demographic profile and determine the prevalence of TB treatment outcomes among these high-risk groups in Kelantan. The results revealed significant differences in educational level, anatomy of TB location, smoking status, DOTS by health care providers, source of notification, and place of treatment. In addition, the method of detection was potentially associated with poor treatment outcomes in this study. However, other variables were not significantly associated with treatment outcomes.

The socio-demographic results in this study were similar to the results reported in the study among Pulmonary TB in Kelantan in 2011 in terms of gender, race, occupation status and smoking status, but contradict in terms of residency and death rate (Ronaidi et al., 2011). Among these 667 cases, 82.8% new TB cases were reported, which was similar to that observed in 2010 to 2012 among TB/HIV co-infected patients in Southwest Ethiopia (85.2%) (Abrha et al., 2015) and among TB/HIV co-infected patients in rural South Africa (84.9%) (Jacobson et al., 2015). However, it was lower compared to the study among Pulmonary Tuberculosis in Kelantan (90.0%) (Ronaidi et al., 2011) and the study among TB patients in Malaysian National TB Surveillance Database in 2012 (93.6%) (Liew et al., 2015).

The death rate in the present study was 32.8%, lower than reported in 2015 among TB patients (46.0%) (Liew et al., 2015), but higher than reported in 2015 among HIV co-infected patients at Mizan-Aman General Hospital, Southwest Ethiopia (5.5%) (Fiseha et al., 2015) and the study in 2020 among TB patients in Malaysia from 2014 to 2017 (10.2%) (Tok et al., 2020). Based on data from the MyTB online system, the number of TB deaths in this study was identified as; confirmed cases of death by TB and advanced HIV (24 cases), cases of death not caused by TB but caused by other factors such as delay in diagnosis, failure of multiple systems, mismanagement, opportunistic infections and others (136 cases), and cases have not identified the cause of death (59 cases). Hence, strengthening surveillance, supervision and health education to reduce death should be prioritised in healthcare systems. In addition, although efforts have been initiated for a high-risk group with the goal of early detection and prevention of TB complications (Liew et al., 2015), the impact of these efforts has not yet been seen in this study.

The previous studies reported prevalence of TB/HIV co-infection varied according to different study sites and study populations. This study has shown that 11.1% of patients having a TB/HIV co-infection. It was equivalent to the prevalence in Malaysia of HIV in new cases of TB (12.6%) in 2005 (WHO, 2008) and to the prevalence among TB patients

in Klang Valley, Malaysia in 2010 (11.8%) (Ismail & Bulgiba, 2013). However, it was higher than reported from 2014 to 2017 in Malaysia (6.0%) (Tok et al., 2020), from MOH in 2015 (5.9%) (Ministry of Health, 2015), and Maharashtra in 2017 (7.28%) (Warkari et al., 2017). However, this prevalence of TB/HIV co-infection in this study was lower than reported in Nigerian State of 20.5% (Oshi et al., 2014), Lagos Nigeria of 21.6% (Adejumo et al., 2017), Northern Ethiopia of 24.3% (Mekonnen et al., 2015), Ethiopia of 29.4% (Ali et al., 2016) and Malawi of 56.0% (Tweya et al., 2013).

Analysis of the study data demonstrated that the TB/HIV co-infected patients had poor treatment outcomes with a success rate of only 57.1%, which is lower than the WHO target set for MDG (85%) and far lower to End TB Strategy success rate for 2025 ($\geq 90.0\%$) (WHO, 2019). These results are almost similar to the study of 26,168 TB cases notified in Malaysia in 2017, 56.0% (WHO, 2018a), TB/HIV co-infected patients in the Klang Valley, 53.4% (Ismail & Bulgiba, 2013) and of TB patients enrolled at Nekemte Specialized Hospital, Western Ethiopia, 58.06% (Fekadu et al., 2020).

The success rate in this study was lower than in Malaysia from 2014 to 2017 (80.7%) (Tok et al., 2020), Ethiopia (88.2%) (Ali et al., 2016), North West Ethiopia (77.3%) (Sinshaw et al., 2017), South-East Nigeria (81.4%) (Duru et al., 2016), Western Ethiopia (60.7%) (Eyasu et al., 2014), and Northern Ethiopia (71.0%) (Belayneh et al., 2015). However, it was higher than the results obtained among 1,510 TB/HIV co-infection in Kelantan between 2003 to 2012 (27.9%) (Jalal et al., 2017), the Southern Region of Ethiopia (29.0%) (Fiseha et al., 2015), Nigeria (48.8%) (Ofoegbu & Odume, 2015) and the Eastern Region of Ghana (50.0%) (Ansa et al., 2012). It was also higher than reports from Ethiopia, from 6.3% to 20.0% (WHO, 2006; Ministry of Health Ethiopia, 2013).

According to the WHO Global Tuberculosis Report, the global treatment success rate for TB/HIV patients was 78.0% (WHO, 2017). The poor success rate observed in this study may be due to the high treatment default and death rates. In addition, the varying success rate between our findings and the results of other findings may be due to the difference in study design, characteristics and number of study participants involved in the study.

In this study, statistically significant differences between categories in TB treatment outcomes (unsuccessful and successful) were observed at the educational level. Treatment outcomes were mainly from individuals with a secondary educational level of more than 77% for both groups, 84.2% (241 out of 286) in the successful and 77.2% (294 out of 381) in the unsuccessful group. Another study found that lower levels of education were associated with unsuccessful treatment outcomes and mortality (Tok et al., 2020).

In comparison, pulmonary TB anatomy comprised most cases, 58.7% (168 out of 286) in the unsuccessful and 68.2% (260 out of 381) in the successful group. It contradicted the study done by others among TB patients (Fekadu et al., 2020; Tok et al., 2020). The presentations with pulmonary TB were often late resulting in poor treatment outcomes and increased risk of delay to start the treatment.

For smoking status, most cases were more than 60%, 72.0% (206 of 286) in the unsuccessful and 61.4% (234 of 381) in the successful group. Tok et al. (2020) found that smoking was associated with unsuccessful treatment outcomes. In this study, the nature of data collection for smoking was self-reporting by patients. Thus, it may have affected these findings. Smoking cessation efforts should be included in standard practice guidelines for TB case management.

In this study, the majority of respondents were under DOTS by health care providers for both groups. However, the cases were extremely higher under DOTS (99.7%) in the successful groups due to the full support and commitment from healthcare workers and patients. It is hoped that the DOTS would improve the cure rate in the future.

The notification source also showed a significant difference between the unsuccessful and successful groups, more than 76.6% reported from public hospitals than the public health clinics in both groups. It may be due to the diagnosis of TB cases were diagnosed entirely in the public hospital rather than the health clinic. In future, we also propose to engage all relevant stakeholders to notify the TB cases in line with the law in Malaysia, under Act 342: Prevention and Control of Infectious Diseases.

In terms of the place of treatment, most cases received the treatment in the public hospital for both groups. Only a few cases received treatment from the private health sector, 2 (0.7%) cases in the unsuccessful group and only 1 (0.3%) case in the successful group. This study finding is lower than reported in all patients registered in the 2012 Malaysian National TB Surveillance Database, 6.7% (Liew et al., 2015). The alternative to receiving the treatment in the private sector is not too much due to socio-economic factors. They need to pay a high cost of treatment in the private health sector. These observations are essential as the place of treatment affecting the outcomes of TB treatment.

In this study, the number of passive detection was higher in the unsuccessful and the successful group, 87.8% and 83.7%, respectively. The passive detection of TB cases was also identified as the factor associated with all-cause mortality among TB patients in Malaysia from 2014 to 2017 (Tok et al., 2020). Currently, the National Strategic Plan (NSP) for TB Control in Malaysia (2016 to 2020) had planned the strategic interventions to improve TB treatment outcomes, including efforts to enhance TB case detection. These efforts are ongoing to monitor their impact and subsequently plan for the next NSP from 2021 onwards.

Unemployed and other occupations had a higher proportion than government servants, own businesses and prisoners in both treatment groups. For all occupations, including the unemployed, the proportion in the successful group was higher than in the unsuccessful group. However, this was not statistically significant.

The study findings of TB treatment outcome were invariably differs from other studies conducted in other states due to multifactorial aspects such as socio-demography,

socio-economic, culture, level of knowledge, drugs used and tolerance to side effects. It also may have been influenced by local service provision settings of the TB patients population. Our findings indicate a need for a strategy to improve the treatment outcomes among TB/HIV co-infected patients with TB in collaborative activities. The basic data of the patient's socio-demographic and the prevalence of treatment outcome in this study can be used as a baseline to develop the further study. They may also contribute to the body of knowledge regarding the treatment outcomes. Healthcare facilities, particularly in Kelantan, could be encouraged to focus on these relevant areas for TB treatment so that a better outcome of TB treatment can be achieved in the future.

Nevertheless, our study had some limitations. The transfer of outpatients were subsequently excluded from our research, leading to a slight bias in our results. Secondary data was another drawback to this analysis. Patients' information was retrieved from the MyTB online system available in the TB/Leprosy Sector. The issue is the missing data (i.e., marital status and monthly income) cannot be minimized. Since their records were not available and their medical results were ambiguous, these variables could be included. It is hoped that future efforts to start capturing those variables could be made routinely.

CONCLUSION

This study provided the basic data of the patient's socio-demographic. The prevalence of the TB treatment success rate was 57.1%, which was under the international target by WHO of $\geq 90.0\%$. However, a high percentage of TB patients have died. It is a major public health issue that urgently needs to be resolved. It is essential to know the associated factors related to successful treatment. Further studies should be carried out, and intervention studies should be organised once the associated factors have been identified.

ACKNOWLEDGMENT

The authors wish to thank the Director-General of Health, Malaysia, for his kind permission to publish these research findings. Furthermore, our heartfelt thanks are extended to patients whose data were involved in this study.

REFERENCES

- Abrha, H., Tsehayneh, B., Massa, D., Tesfay, A., & Kahsay, H. (2015). Survival experience and its predictors among TB/HIV co-infected patients in Southwest Ethiopia. *Epidemiology (Sunnyvale)*, 5(3), 3-9. <https://doi.org/10.4172/2161-1165.1000191>
- Adejumo, O. A., Daniel, O. J., Otesanya, A. F., Adegbola, A. A., Femi-Adebayo, T., Bowale, A., Adesola, S., Kuku, O. O., Otemuyiwa, K. O., Oladega, S. N., Johnson, E. O., Falana, A. A., Dawodu, O., Owuna, H., Osoba, G., & Dacosta, A. (2017). Factors associated with TB/HIV co-infection among drug sensitive

- tuberculosis patients managed in a secondary health facility in Lagos, Nigeria. *African Journal of Infectious Diseases*, 11(2), 75-82. <https://doi.org/10.21010/ajid.v11i2.10>
- Ali, S. A., Mavundla, T. R., Fantu, R., & Awoke, T. (2016). Outcomes of TB treatment in HIV co-infected TB patients in Ethiopia: A cross-sectional analytic study. *BMC Infectious Diseases*, 16(1), Article 640. <https://doi.org/10.1186/s12879-016-1967-3>
- Ansa, G. A., Walley, J. D., Siddiqi, K., & Wei, X. (2012). Assessing the impact of TB/HIV services integration on TB treatment outcomes and their relevance in TB/HIV monitoring in Ghana. *Infectious Diseases of Poverty*, 1(1), 1-8. <https://doi.org/10.1186/2049-9957-1-13>
- Belayneh, M., Giday, K., & Lemma, H. (2015). Treatment outcome of Human Immunodeficiency Virus and Tuberculosis co-infected patients in public hospitals of eastern and southern zone of Tigray Region, Ethiopia. *Brazilian Journal of Infectious Diseases*, 19(1), 47-51. <https://doi.org/10.1016/j.bjid.2014.09.002>
- Duru, C. B., Uwakwe, K. A., Nnebue, C. C., Diwe, K. C., Merenu, I. A., Emerole, C. O., Iwu, C. A., & Duru, C. A. (2016). Tuberculosis treatment outcomes and determinants among patients treated in hospitals in Imo State, Nigeria. *OALib*, 03(06), 1-17. <https://doi.org/10.4236/oalib.1102754>
- Eyasu, E., Tadesse, B., & Tsedeke, W. (2014). Tuberculosis treatment outcomes among Tuberculosis/Human Immunodeficiency co-infected cases treated under directly observed treatment of short course in western Ethiopia. *Journal of AIDS and HIV Research*, 6(8), 164-171. <https://doi.org/10.5897/jahr2014.0312>
- Fekadu, G., Turi, E., Kasu, T., & Bekele, F. (2020). Impact of HIV status and predictors of successful treatment outcomes among Tuberculosis patients : A six-year retrospective cohort study. *Annals of Medicine and Surgery*, 60, 531-541. <https://doi.org/10.1016/j.amsu.2020.11.032>
- Fiseha, T., Gebru, T., Gutema, H., & Debela, Y. (2015). Tuberculosis treatment outcome among HIV co-infected patients at Mizan-Aman General Hospital, Southwest Ethiopia: A retrospective study fiseha. *Bioengineering & Biomedical Science*, 5(1), 1-4. <https://doi.org/10.4172/2155-9538.1000139>
- Hannah, H. A., Miramontes, R., & Gandhi, N. R. (2017). Sociodemographic and clinical risk factors associated with Tuberculosis mortality in the United States, 2009-2013. *Public Health Reports*, 132(3), 366-375. <https://doi.org/10.1177/0033354917698117>
- Ismail, I., & Bulgiba, A. (2013). Determinants of unsuccessful Tuberculosis treatment outcomes in Malaysian HIV-infected patients. *Preventive Medicine*, 57(SUPPL), S27-S30. <https://doi.org/10.1016/j.ypmed.2012.12.023>
- Jacobson, K. B., Moll, A. P., Friedland, G. H., & Sheno, S. V. (2015). Successful Tuberculosis treatment outcomes among HIV/TB coinfecting patients down-referred from a district hospital to primary health clinics in rural South Africa. *PLoS ONE*, 10(5), 1-11. <https://doi.org/10.1371/journal.pone.0127024>
- Jalal, T. M. T., Abdullah, S., Wahab, F. A., Dir, S., & Naing, N. N. (2017). Prevalence and factors associated with Tuberculosis treatment success among TB/ HIV co-infection in north-east Malaysia. *Malaysian Journal of Medical Sciences*, 24(6), 75-82. <https://doi.org/10.21315/mjms2017.24.6.9>
- Liew, S. M., Khoo, E. M., Ho, B. K., Lee, Y. K., Mimi, O., Fazlina, M. Y., Asmah, R., Lee, W. K., Harny, M. Y., Chinna, K., & Jiloris, F. D. (2015). Tuberculosis in Malaysia: Predictors of treatment outcomes in a national registry. *International Journal of Tuberculosis and Lung Disease*, 19(7), 764-771. <https://doi.org/10.5588/ijtld.14.0767>

- Liu, Y., Zheng, Y., Chen, J., Shi, Y., Shan, L. Y., Wang, S., Wang, W. B., Shen, X., & Zhang, Y. (2018). Tuberculosis-associated mortality and its risk factors in a district of Shanghai, China: A retrospective cohort study. *International Journal of Tuberculosis and Lung Disease*, 22(6), 655-660. <https://doi.org/10.5588/ijtld.17.0726>
- Mekonnen, D., Derbie, A., & Desalegn, E. (2015). TB/HIV co-infections and associated factors among patients on directly observed treatment short course in Northeastern Ethiopia: A 4 years retrospective study. *BMC Research Notes*, 8(1), 1-6. <https://doi.org/10.1186/s13104-015-1664-0>
- Ministry of Health. (2015). Global AIDS response progress report Malaysia 2015. In *Ministry of Health* (Issue March).
- Ministry of Health Ethiopia. (2013). *National TB/HIV sentinel surveillance one year report (July 2011 - June 2012)*. Ministry of Health Ethiopia.
- Ministry of Health Malaysia. (2012). *Clinical practice guidelines: Management of Tuberculosis* (3rd Ed.). Ministry of Health Malaysia.
- Ministry of Health Malaysia. (2016). *Clinical practice guidelines: Management of drug-resistant Tuberculosis* (1st Ed.). Ministry of Health Malaysia.
- Ofoegbu, O. S., & Odume, B. B. (2015). Tuberculosis patients at National Hospital Abuja Nigeria: A five year retrospective study. *South African Family Practice*, 57(1), 50-56. <https://doi.org/10.1080/20786190.2014.995913>
- Oshi, D. C., Oshi, S. N., Alobu, I., & Ukwaja, K. N. (2014). Profile, outcomes, and determinants of unsuccessful Tuberculosis treatment outcomes among HIV-infected Tuberculosis patients in a Nigerian State. *Tuberculosis Research and Treatment*, 2014, 1-8. <https://doi.org/10.1155/2014/202983>
- Ronaidi, N. M. N. N., Mohd, N. S., Mohammad, W. Z., Sharina, D., & Rosmawati, N. H. N (2011). Factors associated with unsuccessful treatment outcome of Pulmonary Tuberculosis in Kota Bharu, Kelantan. *Malaysian Journal of Public Health Medicine*, 11(1), 6-15.
- Sinshaw, Y., Alemu, S., Fekadu, A., & Gizachew, M. (2017). Successful TB treatment outcome and its associated factors among TB/HIV co-infected patients attending Gondar University Referral Hospital, Northwest Ethiopia: An institution based cross-sectional study. *BMC Infectious Diseases*, 17, 1-9. <https://doi.org/10.1186/s12879-017-2238-7>
- Tok, P. S. K., Liew, S. M., Wong, L. P., Razali, A., Loganathan, T., Chinna, K., Ismail, N., & Kadir, N. A. (2020). Determinants of unsuccessful treatment outcomes and mortality among Tuberculosis patients in Malaysia: A registry-based cohort study. *PLoS ONE*, 15(4), 1-14. <https://doi.org/10.1371/journal.pone.0231986>
- Twewa, H., Feldacker, C., Phiri, S., Ben-Smith, A., Fenner, L., Jahn, A., Kalulu, M., Weigel, R., Kamba, C., Banda, R., Egger, M., & Keiser, O. (2013). Comparison of treatment outcomes of new smear-positive Pulmonary Tuberculosis patients by HIV and antiretroviral status in a TB/HIV Clinic, Malawi. *PLoS ONE*, 8(2), Article e56248. <https://doi.org/10.1371/journal.pone.0056248>
- Warkari, P. D., Nakel, M. P., Mahajan, S. M., & Adchitre, S. A. (2017). Study of treatment outcome of Tuberculosis among HIV co-infected patients: A cross sectional study in Aurangabad City, Maharashtra. *International Journal Of Community Medicine And Public Health*, 4(12), 4466-4471. <https://doi.org/10.18203/2394-6040.ijcmph20175163>

- Wen, Yufeng, Zhang, Zhiping, Li, Xianxiang, Xia, Dan, Jun, M., Dong, Y., & Zhang, X. (2018). Treatment outcomes and factors affecting unsuccessful outcome among new Pulmonary smear positive and negative Tuberculosis patients in Anqing, China: A retrospective study. *BMC Infectious Diseases, 18*(104), 1-12. <https://doi.org/https://doi.org/10.1186/s12879-018-3019-7>
- WHO. (2006). *The stop TB strategy*. World Health Organization.
- WHO. (2008). *A revised framework to address TB-HIV co-infection in the Western Pacific Region*. World Health Organization.
- WHO. (2017). *Global Tuberculosis report 2017*. World Health Organization.
- WHO. (2018a). *Global Tuberculosis report 2018*. World Health Organization.
- WHO. (2018b). *TB-HIV factsheet 2018*. World Health Organization.
- WHO. (2019). *Global Tuberculosis report 2019: Executive summary*. World Health Organization.



Physical Modelling of Flow and Head along with Dead-end and Looped Manifolds

Abdullah Amer¹, Thamer Ahmad Mohammad^{1*}, Wissam Hameed Alawee² and Nadhir Al-Ansari³

¹Department of Water Resources Engineering, College of Engineering, University of Baghdad, 10070 Jadriyah, Baghdad, Iraq

²Department of Systems and Control Engineering, University of Technology, 10055 Industrial Street, Baghdad, Iraq

³Department of Civil, Environmental and Natural Resources Engineering, Lulea University of Technology, Lulea 971 87, Lulea, Sweden

ABSTRACT

In this study, physical models were designed and fabricated to investigate the hydraulic behaviour of dead-end and looped PVC manifolds. The physical models consisted of a water supply tank with overflow, PVC manifolds, steel supports, collection tank, pump, pressure sensors and valves to allow flow control. Throughout the study, the water level in the supply tank was kept constant. The hydraulic behaviour of dead-end manifolds was investigated using different spacing, S between outlets ($S=3\text{m}$, $S=2.5\text{m}$, $S=2\text{m}$, $S=1.5\text{m}$, and $S=0.75\text{m}$). The hydraulic behaviour of looped manifolds was investigated using a single outlet spacing of 1.5m . The comparison between the hydraulic behaviour of looped and dead-end manifolds was carried out using the data of the 1.5m outlet spacing. The value of uniformity, U for dead-end and looped manifolds was 82% and 92% , respectively. The value of friction ratio, f_n/f_1 , was found to be 33 and 0.18 for dead-end and looped manifolds, respectively. The experimental data of this study were used to validate selected formulae for

estimation of the friction correction factor (G Factor). The results showed that the equation proposed by Alazba et al. (2012) yielded the most satisfactory estimation. The performance of the selected formulae was tested using two statistical indices.

ARTICLE INFO

Article history:

Received: 05 December 2020

Accepted: 21 May 2021

Published: 22 September 2021

DOI: <https://doi.org/10.47836/pjst.29.4.04>

E-mail addresses:

a.rihan1910m@coeng.uobaghdad.edu.iq (Abdullah Amir)

tthamer@gmail.com (Thamer Ahmad Mohammad)

wissam_772005@yahoo.com (Wissam Hameed Alawee)

nadhir.alansari@ltu.se (Nadhir Al-Ansari)

* Corresponding author

Keywords: Dead-end manifold, friction correction factor, hydraulic behaviour, looped manifolds, statistical indices

INTRODUCTION

A manifold can be defined as a pipe with lateral openings (multiple outlets) distributed along its centreline with a known length, diameter and inlet pressure. Depending on the flow mechanism in the manifold, the manifold can be categorised as dividing, combining, parallel or a reverse flow type (Gandhi et al., 2012). Manifolds are used in various engineering applications. For example, in civil engineering, manifolds are widely used in water supply and wastewater projects. In contrast, mechanical engineering used manifolds for fuel distribution. In chemical engineering, manifolds are used for the distribution of chemicals to industrial units. In the design of manifolds, usually, the flow from outlets, coefficient of friction and the friction correction factor are assumed to be constant. Several experimental and mathematical studies have been carried out to investigate manifold hydraulics. The studies focused on the uniformity, hydraulics of sloped manifold and friction correction factor.

The uniformity was studied by Howland (1935), Mokhtari et al. (1997), Koh et al. (2003), Mostafa (2004), Provenzano and Pumo (2004), Maharudrayya et al. (2005), Hassan et al. (2014a), Hassan et al. (2014b), Hassan et al. (2014c), Tong et al. (2009), Sadeghi and Peter (2011), Hassan et al. (2015) and Alawee et al. (2016 & 2019). The impact of the coefficient of friction, friction head loss, manifold dimensions, and manifold slope on the flow from manifold outlets was studied by Mohammed et al. (2003), Keller and Bliesner (1990), Vallesquino and Luque-Escamilla (2002), Yildirim (2007), Alawee et al. (2020) and Sadeghi and Peters (2011). The friction correction factor is commonly used to calculate the total friction head loss along a manifold. Table 1 shows the formulae used to calculate the friction correction factor. Most of the studies referenced above were conducted on dead-end manifolds. Hence, there is a lack of studies on the hydraulics of looped manifolds. The effect of looping in a manifold is expected to reduce friction head losses and improve water flow uniformity. Therefore, an experimental study that compares the hydraulic performances of two different manifold designs is essential. This study will focus on the design, fabrication, installation, and operation of dead-end and looped manifolds. The data collected from the manifolds will be used to evaluate the uniformity, friction head losses, and validation of selected formulae for friction correction factors (Table 1).

MATERIALS AND METHODS

Description of the Experimental Setup

The physical model used in this study was fabricated in the University of Technology, Baghdad, Iraq workshop. The model was composed of a steel water supply tank (total volume = 3.9m³) with dimensions of 1.25m × 1.25m × 2.5m (length × width × height), and it was connected to a horizontal PVC pipe with a diameter of 25.4mm and a length of 18m. The 25.4mm diameter PVC pipe was levelled and laid horizontally on steel supports

Table 1
Selected formulae for friction correction factor

Author	Formula	Equation	Details
Christiansen (1942)	$G = \frac{1^m + 2^m + \dots + N^m}{N^{m+1}}$	1	N=number of outlets, m = power of velocity in friction head
Anwar (1999)	$G = \frac{1}{N^{m+1} + r^m} \sum_{k=1}^N (k + Nr)^m$	2	loss formula, r = outflow discharge to the total discharge, k = integer representing pipe section under consideration,
Oron and Walker (1981)	$G = 0.6387N^{-1.8916} + 0.35929$	3	
Valiantzas (2002)	$G = \frac{1}{m+1} \left[\left(1 + \frac{1}{2N}\right)^{m-1} - \left(\frac{1}{2N}\right)^{m+1} \right]$	4	
Mostafa (2004)	$G = \frac{N^2 + (N-1)^2 + (N-2)^2 + \dots + (N-(N-1))^2}{N^3}$	5	
Mohammed et al. (2003)	$G = \frac{\sum_{i=1}^{N-1} (N-1)^m}{N^{m+1}}$	6	$e=2.71$ and G = friction correction factor
Alazba et al. (2012)	$G = \frac{1 + \frac{1}{m}}{e\pi}$	7	

distributed at intervals of 1.15m. In order to maintain a constant water level of 2.76m in the supply tank, a 100mm diameter overflow PVC pipe was connected at the top of the tank. When the water level in the tank exceeded the level of 2.76m, the surplus water was discharged by gravity through the overflow pipe to a ground tank. Next, to keep the water level in the tank constant, recirculation of water was carried out by pumping the water stored in the ground tank to the supply tank via a 25.4mm diameter supply pipe. In practice, manifolds are subjected to a fixed head. For this reason, a constant head of 2.76m was maintained in the supply tank throughout this study.

In addition, heads greater than 2.76m would have been difficult to achieve due to a limited water supply capacity in the laboratory. Piezometers located at the pipe inlet and outlet were used to determine the head difference/friction head loss along the pipe. For five different velocities, data on friction head loss along the pipe without outlets were measured. The relationship between the friction head loss and the velocity was plotted on a log-log paper. Dead-end manifolds with 6mm diameter outlets distributed longitudinally along their centrelines were used in this study. In order to measure the head/pressure at each outlet, 6mm diameter holes were drilled on the opposite side of the outlets. Each opening was connected to a sensor that feeds into a data logger. The data logger was connected to a computer to obtain each outlet's instantaneous head/pressure readings. In addition, data on head and discharge along the length of dead-end manifolds with different outlet spacing (0.75m, 1.5m, 2.0m, 2.5m and 3.0m) were measured. Figure 1 shows a general three-

dimensional schematic drawing of the dead-end manifold used in this study. Triangular looped manifold, rectangular looped manifold and dead-end (straight) manifold were hydraulically assessed to study the impact of different manifold designs on flow uniformity and friction head losses.

The assessed manifolds had the same diameter (25.4mm), length (18m) and spacing between outlets (1.5m). In comparison, the water level in the supply tank was kept constant at 2.76m. Figures 2 and 3 show the configuration of triangular and rectangular looped manifolds. At the same time, Table 2 illustrates a sample of the sensors digital pressure reading. Each sensor can read a pressure between 0 to 26.85 kN/m² (30 psi)

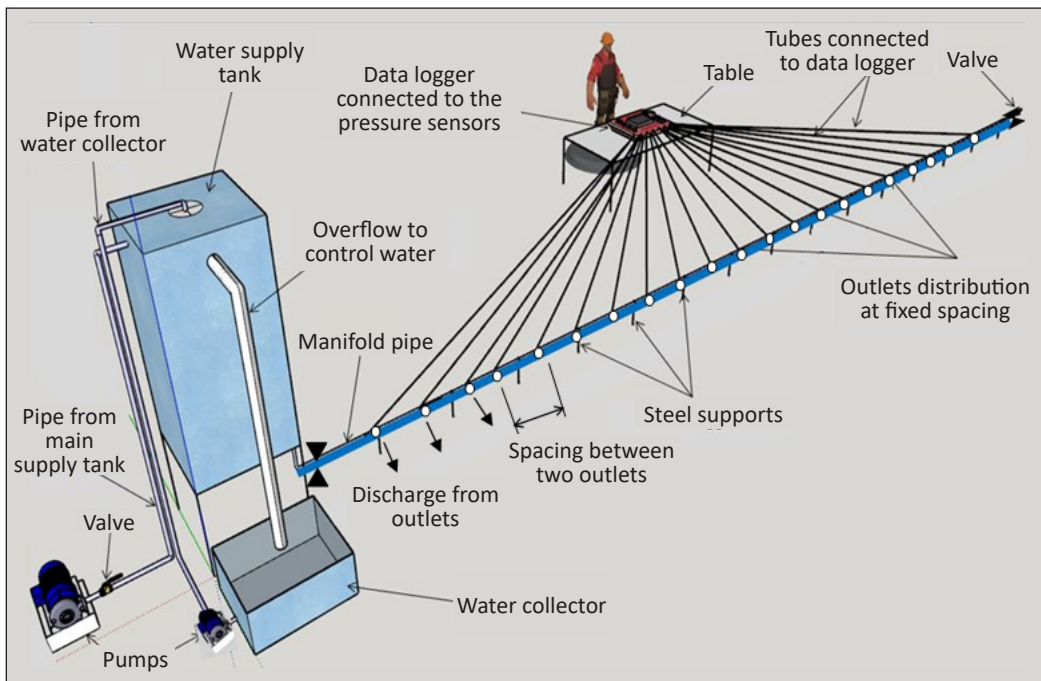


Figure 1. Three-dimensional schematic drawing for the dead-end manifold

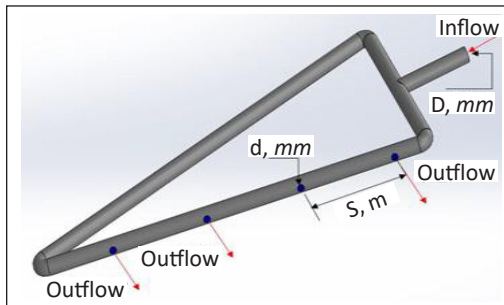


Figure 2. The triangular looped manifold
 Note. D is outlet diameter; d is manifold diameter; S is spacing between outlets

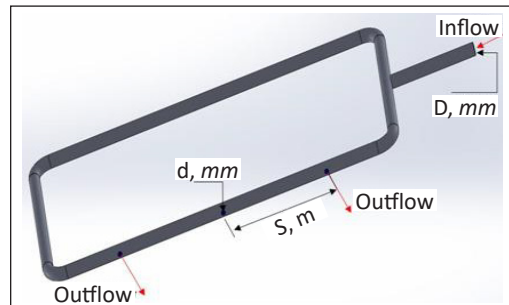


Figure 3. The rectangular looped manifold
 Note. D is outlet diameter; d is manifold diameter; S is spacing between outlets

Table 2
A sample of the sensors reading displayed on the computer screen

Date	Time	Sensors					
		1	2	3	4	5	6
22/10/2019	12:02:06 PM	0	0	0	0	0	0
22/10/2019	12:02:13 PM	3.57	3.61	3.46	3.68	3.68	3.57
22/10/2019	12:02:21 PM	3.64	3.71	3.46	3.46	3.68	3.53
22/10/2019	12:02:28 PM	3.68	3.68	3.57	3.57	3.64	3.5
22/10/2019	12:02:35 PM	3.64	3.64	3.46	3.46	3.68	3.53
22/10/2019	12:02:43 PM	3.68	3.68	3.82	3.57	3.57	3.5
22/10/2019	12:02:50 PM	3.64	3.64	3.46	3.46	3.68	3.53
22/10/2019	12:02:57 PM	3.64	3.71	3.46	3.46	3.46	3.46
22/10/2019	12:03:05 PM	3.5	3.5	3.68	3.68	3.57	3.57
22/10/2019	12:03:12 PM	3.57	3.61	3.46	3.68	3.57	3.46
22/10/2019	12:03:19 PM	3.68	3.86	3.64	3.57	3.46	3.46
22/10/2019	12:03:27 PM	3.68	3.82	3.57	3.57	3.57	3.46
22/10/2019	12:03:34 PM	3.64	3.86	3.57	3.46	3.46	3.46
22/10/2019	12:03:41 PM	3.64	3.71	3.46	3.46	3.46	3.46
22/10/2019	12:03:49 PM	3.46	3.68	3.68	3.57	3.64	3.57
22/10/2019	12:03:56 PM	3.68	3.68	3.68	3.57	3.64	3.5
22/10/2019	12:04:03 PM	3.64	3.86	3.57	3.46	3.46	3.46
22/10/2019	12:04:11 PM	3.68	3.68	3.57	3.57	3.57	3.5
22/10/2019	12:04:18 PM	3.64	3.64	3.46	3.46	3.68	3.53
22/10/2019	12:04:25 PM	3.68	3.86	3.64	3.57	3.46	3.46
22/10/2019	12:04:33 PM	3.64	3.61	3.46	3.46	3.68	3.57
22/10/2019	12:04:47 PM	3.68	3.79	3.5	3.46	3.5	3.68
22/10/2019	12:04:55 PM	3.82	3.86	3.64	3.5	3.46	3.46

with an accuracy of 3%. A piezometer was used to measure the pressure at each outlet to countercheck the readings obtained from the sensors. Hence, the head at the manifold outlet h_i is measured by a sensor and a piezometer. Figure 4 show samples of data collected by the sensors and piezometers along the length of a dead-end manifold. In contrast, Figure 5 shows the calibration curve for the sensors. Table 3 shows the experimental design of the study.

The Laboratory Measurements

The inlet valve controlled the flow from the tank to the manifolds (either dead-end or looped). The discharge from each manifold outlet, q_i , was measured using a container of known volume and a stopwatch. A digital thermometer measured the water temperature. The water temperature throughout this study ranged between 18 to 20°C. The temperature

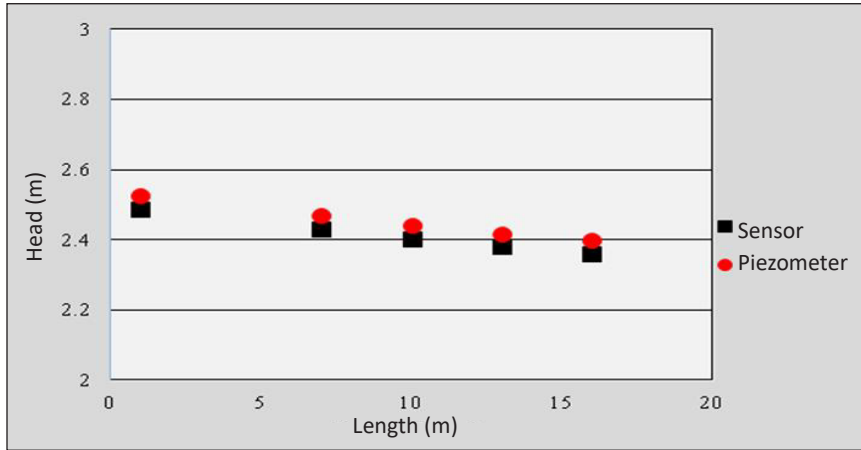


Figure 4. Sensors and piezometers readings for dead-end manifold with spacing, S of 3m

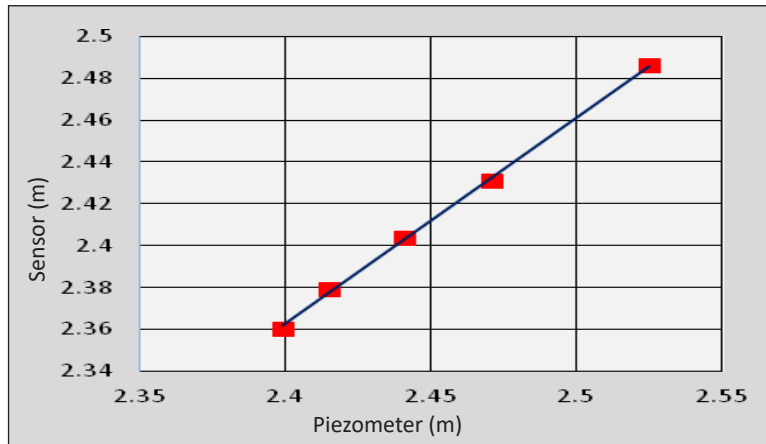


Figure 5. Sensor readings plotted against the piezometer readings for the dead-end manifold with spacing, S of 3m

Table 3
The experimental design

Model type	Diameter	Length	Spacing	Comments
Dead end manifold	25.4 mm	18 m	0.75 m	All manifolds and the normal pipe have the same material and subjected to same pressure at upstream
Dead end manifold	25.4 mm	18 m	0.75 m	
Dead end manifold	25.4 mm	18 m	1.5 m	
Dead end manifold	25.4 mm	18 m	2.0 m	
Dead end manifold	25.4 mm	18 m	2.5 m	
Dead end manifold	25.4 mm	18 m	3.0 m	
Looped triangular manifold	25.4 mm	18 m	1.5 m	
Looped rectangular manifold	25.4 mm	18 m	1.5 m	
Normal pipe (without outlets)	25.4 mm	18 m	1.5 m	

was used to determine the kinematic viscosity of the water. The kinematic viscosity is helpful in the calculation of the Reynolds number at different manifold segments. The difference in head between two successive outlets determines the friction head loss along the manifold segment. For similar flow conditions (discharge and inlet head) and geometry (length and diameter), friction head loss data on dead-end manifolds, looped manifolds and the pipe without outlets were used to calculate the G factors for the dead-end and looped manifolds. In addition, the data was used to validate selected formulae for the G factor.

RESULTS AND DISCUSSION

This study used high precision methods to measure the head and discharge along looped and dead-end manifolds. At each outlet, the discharge was recorded by taking an average of three measurements. At the same time, the head was taken by averaging approximately 30 readings. In addition, the Darcy Weisbach formula was used to calculate the coefficient of friction at different manifold segments. Although the Hazen Williams formula is widely used in the hydraulic design of manifolds (water-supply networks, sprinkler irrigation systems, and drip irrigation systems), its accuracy is affected by the fact that the resistance coefficient is assumed to be a constant value in the calculation of friction head loss in manifolds. Based on the manifold material, the Hazen Williams resistance coefficient is usually provided by the manufacturer. Whereas, if the Darcy Weisbach formula is used for the hydraulic design of manifolds, the value of the coefficient of friction is determined by calculating the Reynolds number and the relative roughness of the manifold. Discharge in manifolds usually decreases towards the dead-end. Hence, the Reynolds number also decreases, which leads to a changing coefficient of friction along the manifold. The values of Reynolds number at different segments of a manifold can be determined if the diameter, velocity, and kinematic viscosity of water at the segments are known.

The size of the PVC manifold used in this study was chosen to be 25.4mm diameter because most drip irrigation systems are designed with PVC manifolds of 25.4mm diameter. So, present study results will improve the hydraulic design of manifolds, particularly those used in drip irrigation systems.

Variation of Discharge and Head along the Dead-end Manifold

Figure 6 show the variations in the head, coefficient of friction and discharge along a dead-end manifold. Due to friction head loss, the head along the manifold is decreasing towards the dead-end. Hence, the discharge is decreasing towards the dead end, as shown in Figure 6. It is confirmed the fact that a discharge from a manifold's outlet, q_i is a function of the head at the outlet, h_i . The spacing between outlets, S is one of the main variables affecting the friction head loss and the variation in discharge along the manifold. In this study, for spacing between outlets, $S = 3$ m, a minimum difference of 5% was obtained between the

discharge of the first and last outlet of the dead-end manifold. In comparison, for $S=0.75$ m, the maximum difference was 18%. In this study, the uniformity of the flow along a manifold, U , is defined as the ratio of the discharge at the last manifold outlet, q_n , to that at the first outlet, q_1 . It can be expressed as Equation 8.

$$U = \frac{q_n}{q_1} \tag{8}$$

For the ideal case, U 's value is equal to 1, which indicates that the discharge from all manifold outlets is equal. However, in most cases, the value of U is not equal to 1. Therefore, the data on head and discharge at each manifold outlet were collected for various outlet spacing ($S=3$ m, $S=2.5$ m, $S=2$ m, $S=1.5$ m and $S=0.75$ m). For a maximum spacing of 3m and a minimum spacing of 0.75m, the uniformities were calculated and found to be approximately 95% and 82%, respectively.

The head difference between two successive outlets yielded the friction head loss along the manifold segment between these outlets. In contrast, the head difference between the first and last outlets determines the total friction head loss along the whole manifold. Figures 7, 8 and 9 show the variation of the head, head loss and discharge along with dead-end manifolds with various outlet spacing. For example, for $S=3$ m and $S=0.75$ m, the total friction head loss along with dead-end manifolds was 0.13m and 0.49m, respectively.

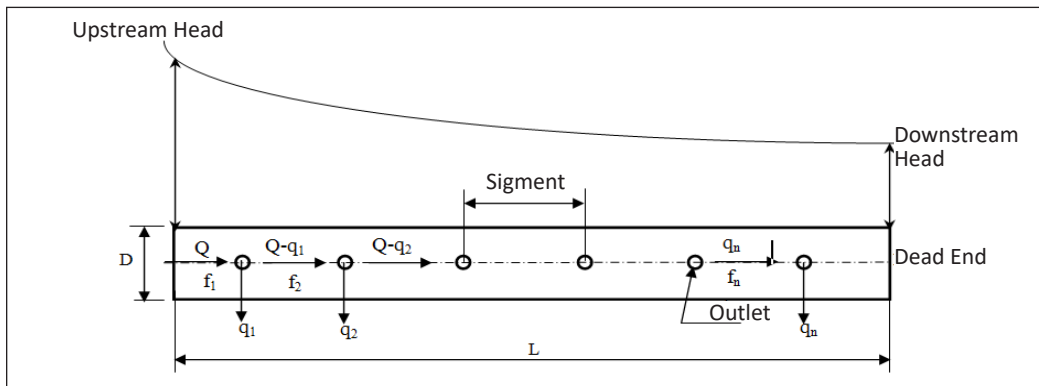


Figure 6. Variation of the head, coefficient of friction in the manifold segment, f_i and discharge from the outlet, q_i along with dead-end manifold (with diameter, d and length, L)

Variation of Discharge and Head along the Looped Manifolds

The distributions of head and discharge along looped manifolds were compared with those of dead-end manifolds. The looped rectangular and the triangular manifolds were symmetrical in geometry, as shown in Figures 2 and 3.

The distribution of head, total head loss and discharge along looped rectangular and triangular manifolds are shown in Figures 10, 11 and 12. The total friction head losses along

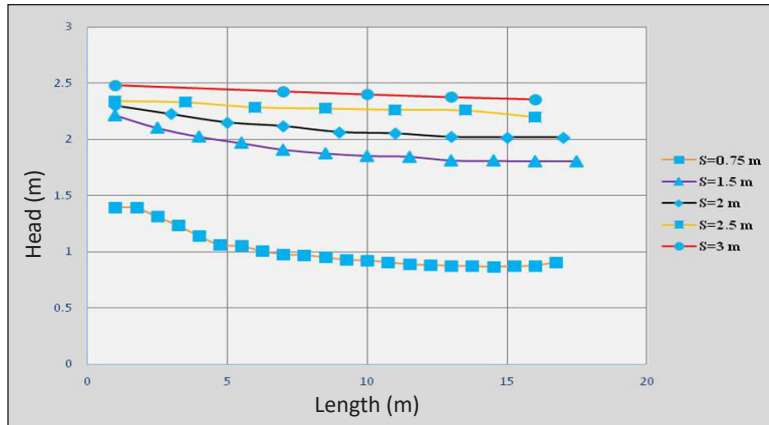


Figure 7. Variation of the head along the dead-end manifolds
 Note. S is the spacing between lines

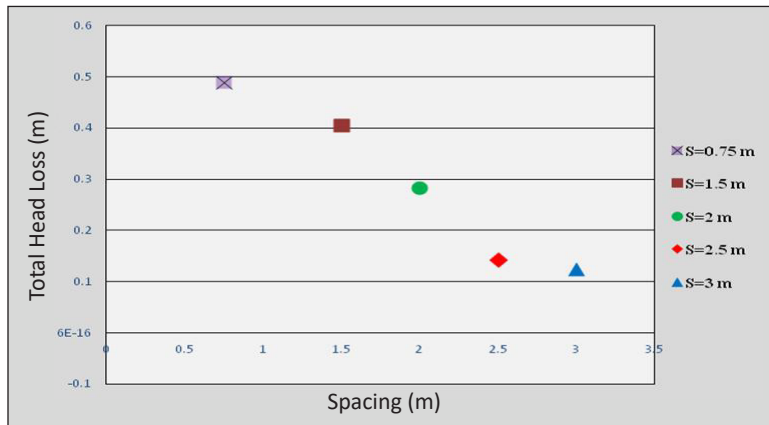


Figure 8. The impact of spacing between outlets on the friction head loss in the dead-end manifold
 Note. S is the spacing between lines

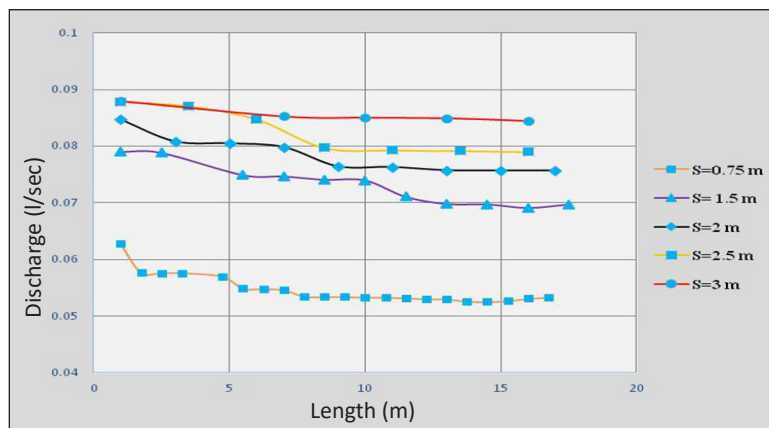


Figure 9. Variation of discharge along with the dead-end manifold
 Note. S is the spacing between lines

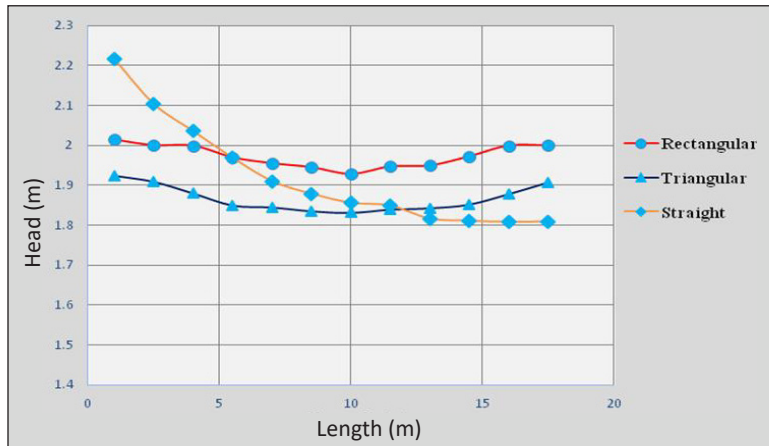


Figure 10. Variation of head along with looped manifolds

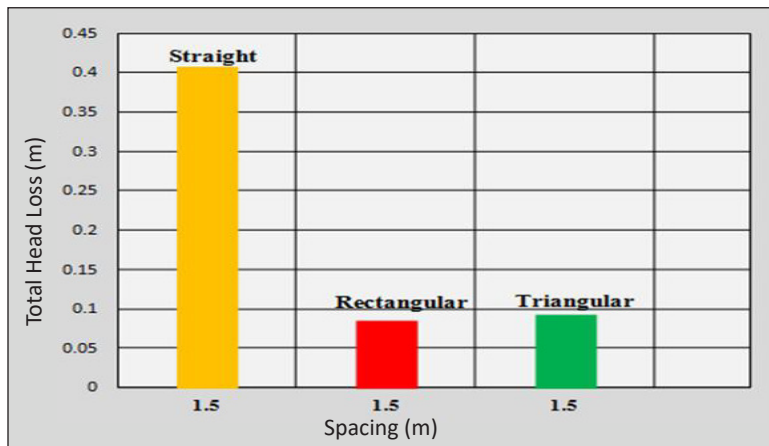


Figure 11. The total head loss in looped manifolds

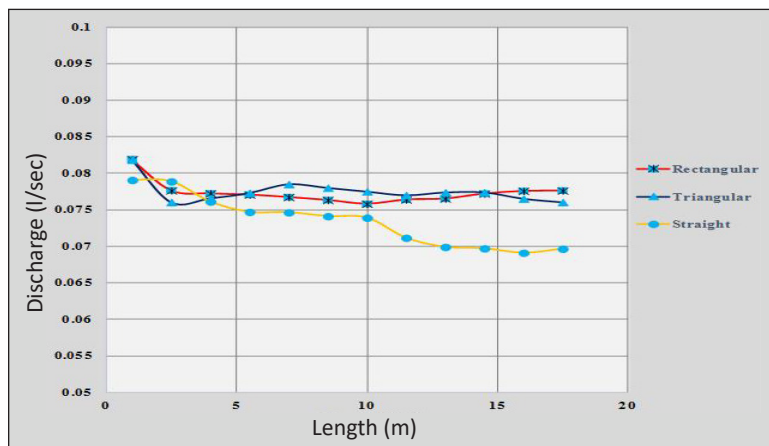


Figure 12. Variation of discharge along with looped manifolds

the triangular and rectangular looped manifolds were 0.071m and 0.092m, respectively. In comparison, the total friction head loss along the dead-end manifold with an outlet spacing of 1.5m, exact dimensions and flow conditions as the triangular and rectangular looped manifolds was found to be 0.41m only. Based on the above findings, the friction head loss in the dead-end manifold was greater than that in the looped manifold by almost 500%. In looped manifolds, the total discharge was divided between two branches of equal lengths of an identical number of outlets. This arrangement leads to reduced friction head losses and hence improved uniformity in the looped manifold. Figures 13 and 14 show the uniformity for dead-end and looped manifolds (rectangular and triangular).

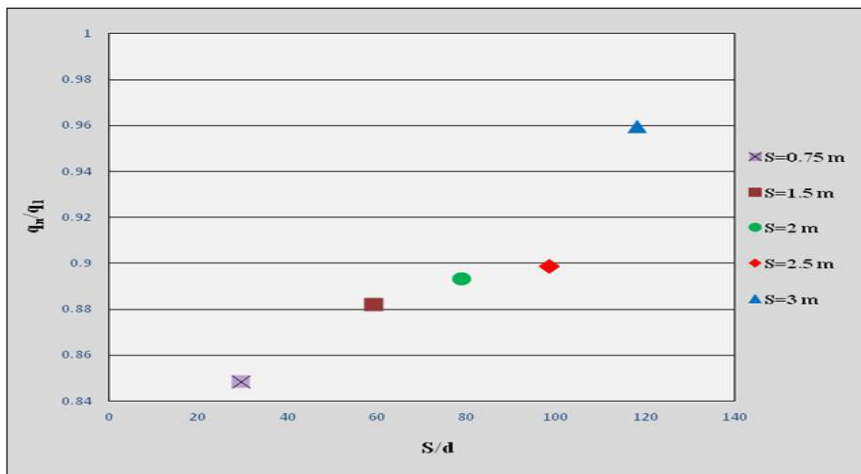


Figure 13. Variation of the uniformity coefficient, q_n/q_1 with spacing ratio, S/d for the dead-end manifold
 Note. S is the spacing in between outlets; d is the manifold diameter

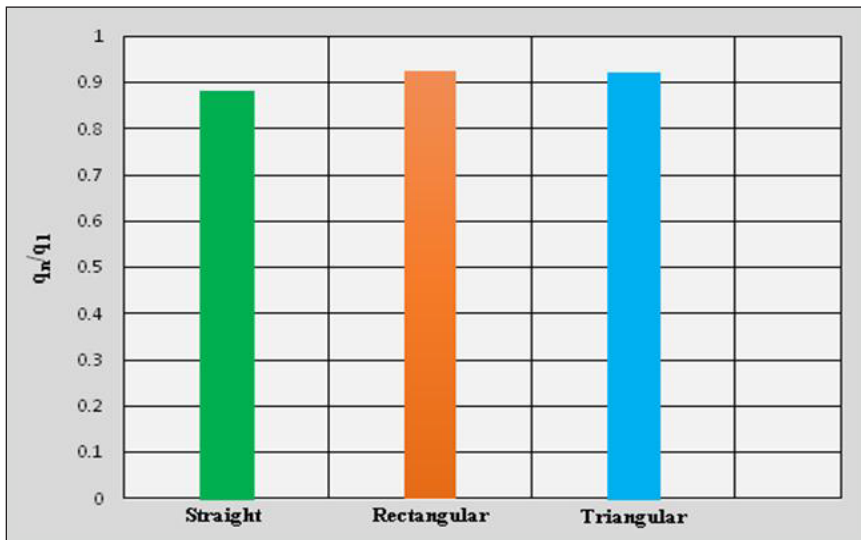


Figure 14. The uniformity coefficient, q_n/q_1 for dead-end (straight), rectangular, and triangular manifold types

The uniformities for the dead-end manifold, looped rectangular manifold and looped triangular manifold were calculated and found to be 82.8%, 91.7% and 92%, respectively. In looped manifolds, there was a gain in the head, which improved the uniformity value. The impact of different ranges of outlet spacing on head loss and uniformity was studied using a dead-end manifold. However, only one range of spacing between outlets (1.5m) was used to study the impact of looping on friction head loss and uniformity. The main objective of the comparison is to demonstrate the effect of looping in reducing the friction head loss and improving the uniformity along a manifold. Many previous studies assumed a constant coefficient of friction, f , while calculating the friction head loss in a manifold (Mohammed et al., 2003). In this study, the data collected from measurements of head and discharge along the manifold were used to calculate the values of coefficient of friction for different manifold segments by applying the Darcy Weisbach Equation 9 described below:

$$f_i = \frac{(h_f)_i d^5 g \pi^2}{8lQ_i^2} \quad (9)$$

where, f_i is coefficient of friction in a manifold segment i , $(h_f)_i$ is the friction head loss along with a manifold segment i , d is manifold diameter, g is the acceleration due to gravity, l is the segment length, Q_i is the discharge in a manifold segment, l and π is constant equal to 3.14.

The coefficient of friction varied widely along the dead-end and looped manifolds, the coefficient of friction in the first manifold segment, f_1 and that in the last segment, f_n can be used to illustrate the variations in the coefficient of friction along with the studied manifolds, the friction ratio, f_n/f_1 was calculated for the studied manifolds. Figures 15 and 16 show the relationship between the friction ratio, f_n/f_1 and the ratio S/d (outlet spacing, S /manifold

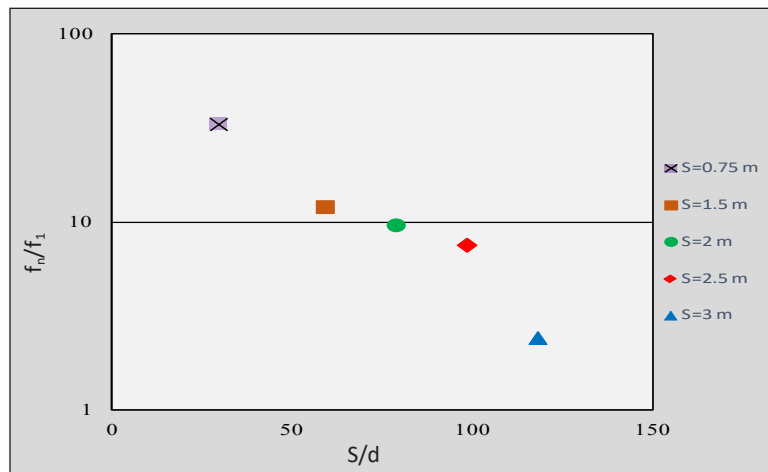


Figure 15. Variation of friction ratio, f_n/f_1 with spacing ratio, S/d in the dead-end manifolds
 Note. S is the spacing between outlets; d is the manifold diameter; f_1 is coefficient friction in the first manifold segment; f_n is the coefficient of friction in the first manifold

diameter, d). For dead-end manifold with a minimum spacing ($S=0.75\text{m}$), the friction ratio was maximum ($f_n/f_1=33$), while for maximum spacing ($S=3\text{m}$), the ratio was minimum ($f_n/f_1=0.18$). For an outlet spacing of 1.5m , the values of f_n/f_1 for rectangular and triangular looped manifolds were found to be 0.134 and 0.028 , respectively.

In this study, the Reynolds number was calculated using the following Equation 10:

$$(Re)_i = \frac{4Q_i}{\pi d \nu} \quad (10)$$



Figure 16. The friction ratio, f_n/f_1 for dead-end, rectangular, and triangular manifolds

where, the $(Re)_i$ is the Reynolds number, Q_i is the discharge in a manifold segment i , ν is the kinematic viscosity, d is the manifold diameter and π is constant equal to 3.14 .

In this study, the relative roughness of the PVC manifolds was kept constant since single diameter manifolds ($d=25.4\text{mm}$) were used. Figure 17 show the calculated coefficient of frictions and Reynold numbers at various manifold segments.

Under different flow conditions of the present study, the values of Reynolds number ranged from 4000 to 60640 , which indicates transitional and turbulent flow. A fitted curve that represents smooth pipe flow behaviour was set through the data. The relationship presented in Figure 17 confirms that the coefficient of friction for a smooth pipe is a

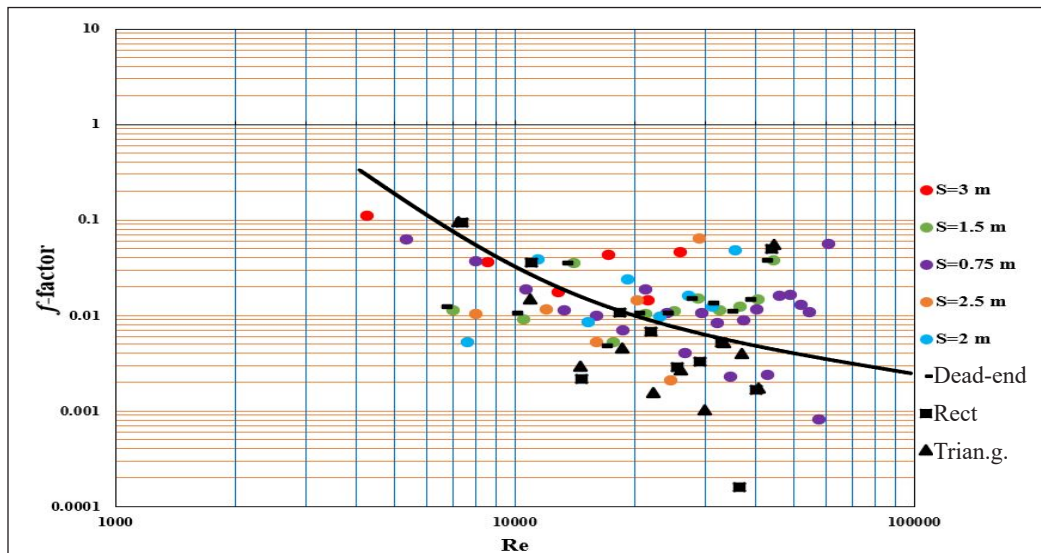


Figure 17. Moody diagram for the studied manifolds (relationship between coefficient of friction, f and Reynolds number, Re)

function of the Reynolds number only. It agree with the relationship given by Blasius for a smooth pipe (Streeter et al., 1998).

Friction Correction Factor for Dead-end and Looped Manifolds

The ratio between the total friction head loss in a manifold to that in a standard pipe having the same material, length, diameter and flow rate but without outlets is called friction correction factor. Researchers termed it the G factor, and it is calculated using Equation 11.

$$G_{\text{factor}} = (h_f)_m / (h_f)_p \quad (11)$$

where $(h_f)_m$ is the total friction head loss in the manifold and $(h_f)_p$ is the total friction head loss in the pipe without outlets.

The G factor can be used to simplify the calculation of friction head losses along a manifold. The present study used experimental data on friction head losses in standard PVC pipe (without outlets), dead-end manifolds and looped manifolds to determine the friction correction factor (G factor). Figure 18 shows the relationship on a log-log plot between friction head loss $(h_f)_p$ and the velocity, v along a PVC pipe without outlets.

The below relationship was obtained from five different discharge measurements taken during the experimental works (Equation 12).

$$(h_f)_p = 0.24 v^2 \quad (12)$$

The G factor for the dead-end manifold was calculated for different spacing, S between outlets ($S=3\text{m}$, $S=2.5\text{m}$, $S=2\text{m}$, $S=1.5\text{m}$ and $S=0.75\text{m}$), while for looped manifolds, only

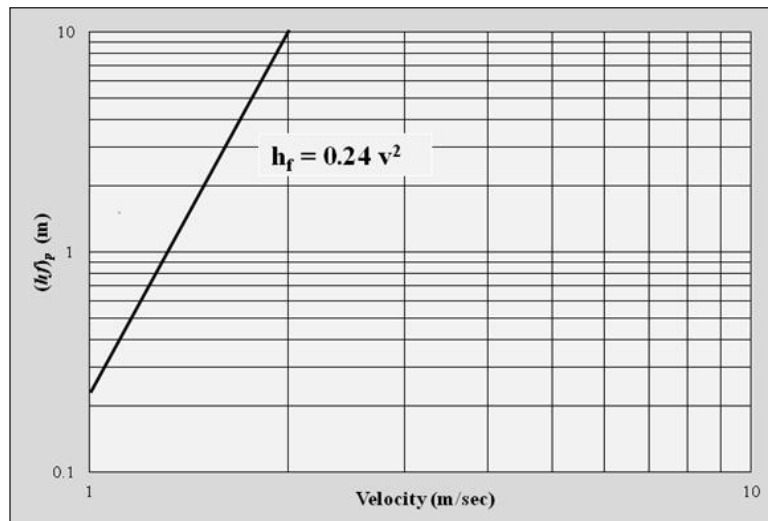


Figure 18. Relationship between the velocity, v and friction head loss for the PVC pipe without outlets $(h_f)_p$

one spacing was studied ($S=1.5\text{m}$). Table 4 and Figures 19 and 20 show the values of the G factor for the tested manifolds. The values of the G factor for the dead-end manifolds were significantly higher than those for looped manifolds.

The maximum value of the G factor in this study was found to be 0.608. It was obtained from friction head loss data of the dead-end manifold, while the minimum value was 0.112, and it was obtained from friction head loss data of the triangular looped manifold.

The values of the G factor in dead-end and lopped manifolds varied due to variation in friction head losses. The experimental data of the present study was used to validate selected formulae for estimation of the friction correction factor (G factor) for manifolds. For the

Table 4
Values of G factor for the studied manifolds

Manifold	L m	S m	N	$(h_f)_m$ m	$(h_f)_p$ m	G factor (from exp. data)
Dead-end	18	0.75	22	0.4888	1.3666	0.3577
Dead-end	18	1.5	12	0.4063	0.7315	0.5554
Dead-end	18	2	9	0.283	0.4655	0.6079
Dead-end	18	2.5	7	0.1436	0.3111	0.4616
Dead-end	18	3	6	0.1253	0.2487	0.5038
Dead-end	18	1.5	12	0.4071	0.7254	0.5612
Rectangular	18	1.5	12	0.0851	0.8049	0.1057
Triangular	18	1.5	12	0.0922	0.8242	0.1119
Dead-end	18	0.75	22	0.4888	1.3666	0.3577

L=manifold length, S=spacing between outlets, N=number of spacing, $(h_f)_m$ = friction head loss in manifold, $(h_f)_p$ = friction head loss in pipe without outlets, G=friction correction factor

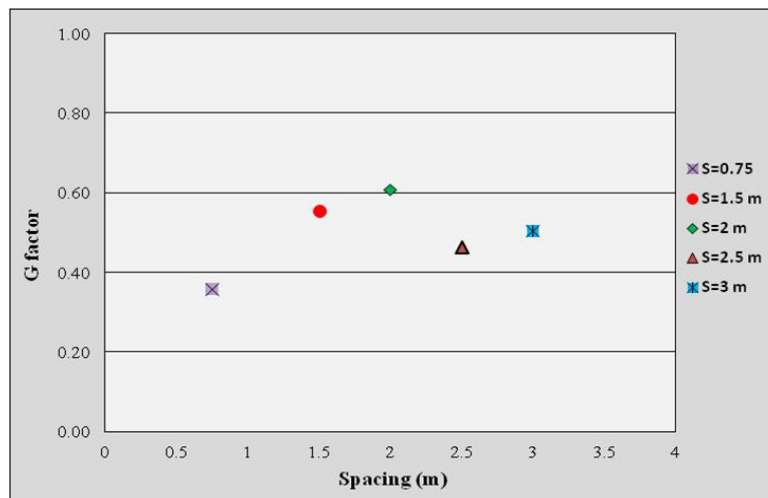


Figure 19. Variation of G factor (friction correction factor) with the outlet spacing, S for the dead-end manifold

dead-end manifolds used in this study, the G factor obtained from the experimental data for different outlet spacing was compared with that calculated using selected formulae, as shown in Table 5.

In this study, the tested formulae for the G factor were the formulae proposed by Christiansen (1942), Albertson et al. (1960), Mostafa (2004), Mohammed et al. (2003), Oron and Walker (1981), Valiantzas (2002), and Alazba et al. (2012). The G factor in

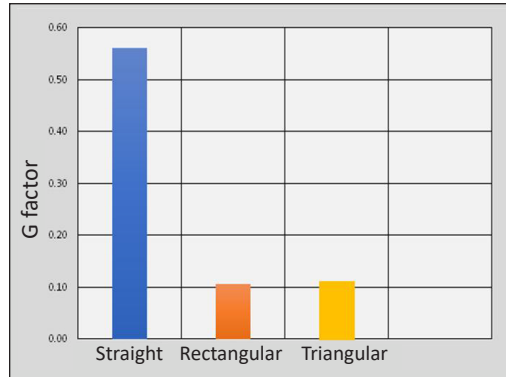


Figure 20. Values of G factor (friction correction factor) for the studied manifolds

Table 5
Values of G factor from the selected formulae and from the experimental data

	N=22	N=12	N=9	N=7	N=6
Experimental G factor	0.3577	0.5554	0.6079	0.4616	0.5038
Christiansen (1942)	0.3564	0.3762	0.3909	0.4082	0.4213
Albertson et al. (1960)	0.3333	0.3333	0.3333	0.3333	0.3333
Oron and Walker (1981)	0.3611	0.3651	0.3693	0.3754	0.3808
Valiantzas (2002)	0.3566	0.3767	0.392	0.4099	0.4236
Mostafa (2004)	0.3564	0.3762	0.3909	0.4082	0.4213
Mohammed et al. (2003)	0.311	0.2928	0.2798	0.2653	0.2546
Alazba et al. (2012)	0.5531	0.5732	0.5879	0.6047	0.6173

these formulae was either a function of the number of outlets in a manifold, N, only or a function of both number of outlets, N and the velocity exponent, m. Thus, the general relationship between the friction head loss, h_f and velocity, v in a pipe can be expressed in the following parabolic form (Equation 13):

$$h_f = Cv^m \tag{13}$$

where C is a constant number, and m is an exponent equal to 2 in Darcy Weisbach equation and 1.85 in Hazen Williams equation.

The comparison between Equations 12 and 13 determined that the value of the velocity exponent, m was 2.

Figure 21 show that most of the tested formulae underestimated the value of the G factor. Therefore, to study the impact of the outlets' number, N, on the G factor, the values were plotted as shown in Figure 22. For example, the value of the velocity exponent, m, was taken as 1.85 by Mostafa (2004), Alazba et al. (2012), and Sadeghi and Peters (2011).

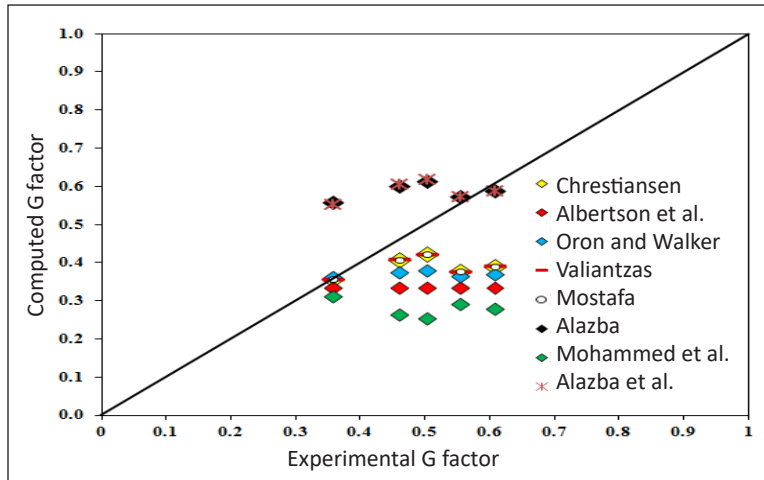


Figure 21. The validation of the selected G factor formulae

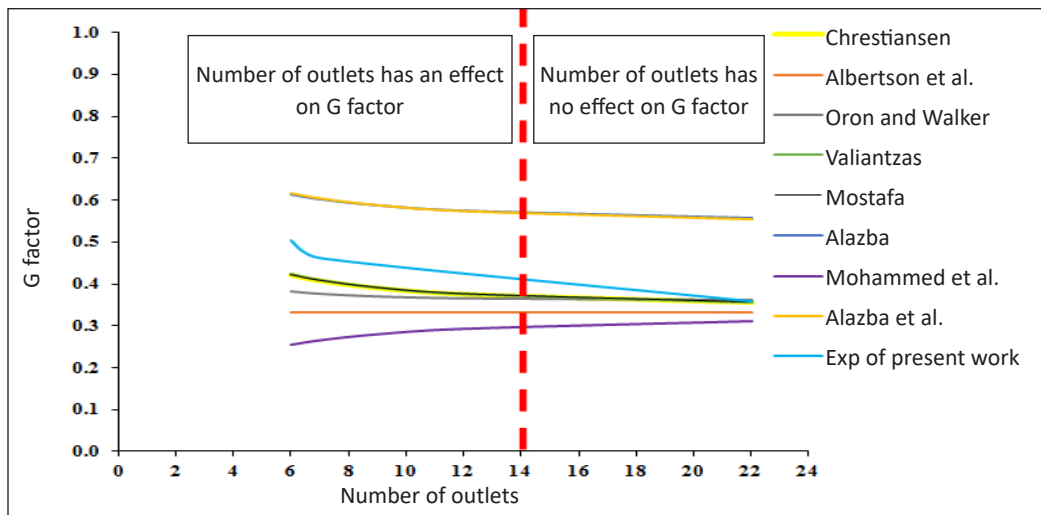


Figure 22. Variation of G factor with the number of manifold outlets

Statistical Tests

The agreement between the values of the experimental G factor and that computed from the application of selected formulae were tested using two statistical indices; the root mean square deviation (RMSD) (Equation 14) and normalised root mean squared deviation (NRMSD) (Equation 15).

$$RMSD = \sqrt{\frac{\sum_{i=1}^n (G_{e,i} - G_{c,i})^2}{n}} \quad (14)$$

$$\text{NRMSD} = \frac{\text{RMSD}}{G_{\max} - G_{\min}} \quad (15)$$

where $G_{e,i}$ represents the value of the experimental G factor, $G_{c,i}$ represents the values of computed G factor obtained from the tested formulae, n = number of experimental data, G_{\max} is the value of the maximum experimental G factor, G_{\min} is the value of the minimum experimental G factor.

In statistics, RMSD is commonly used to compare calculated and measured values and obtain an indication of the accuracy of the model predictions (Legates and McCabe, 1999). A low RMSD or NRMSD indicate an accurate prediction. Table 6 show the values of the selected statistical indices for all the tested formulae. Table 6 shows that the formulae proposed by Alazba et al. (2012) gave the lowest values for RMSD and NRMSD. These values were 0.120, 0.480, respectively. Based on the above results, it can be concluded that the Alazba et al. (2012) formula gave the most accurate estimation for the G factor.

Table 6
The statistical indices for the selected formulae of G factor

Formula for G Factor	RMSD	NRMSD
Christiansen (1942)	0.133	0.533
Albertson et al. (1960)	0.185	0.739
Oron and Walker (1981)	0.152	0.608
Valiantzas (2002)	0.132	0.529
Mostafa (2004)	0.133	0.533
Mohammed et al. (2003)	0.236	0.945
Alazba et al. (2012)	0.120	0.480

From the above discussion, the engineering significance of the present study can be summarised as:

1. The friction head loss and discharge variation along dead-end and looped manifolds were studied using reliable experimental data. The impact of looping of manifolds on uniformity and friction head losses was highlighted.
2. For both dead-end and looped manifolds, the experimental data confirmed that the coefficient of friction varied at various manifold segments. It confirms that using a constant value for the coefficient of friction along a manifold affects the accuracy of the hydraulic design. In addition, it is more suitable to use the Darcy Weisbach formula in the hydraulic design of manifolds as it allows for the use of different coefficient of friction values in the calculation. It is not possible in the Hazen Williams formula since it only assigns one value of the resistance coefficient along the entire manifold.

3. The manifold diameter used in this study was 25.4mm. The size and material of the manifold are widely used in drip irrigation systems around the world. So, the present study results can be used to improve the hydraulic design of drip irrigation systems.
4. The experimental data were used to validate selected formulae for the G factor, and a recommendation on the reliability of these formulae was given based on the statistical tests. Thus, it will assist manifold designers to apply a suitable formula.

CONCLUSION

The physical models of dead-end and looped PVC manifolds were designed and fabricated to test the variation of discharge and head losses along with these manifolds. For manifolds with the same length, diameter and material, the outlets spacing and manifold type (looped or dead-end) are the main factors affecting the friction head losses and uniformity. The study concluded a proportional relationship between spacing ratio, S/d (ratio of the spacing between outlets, S to manifold diameter, d), and the uniformity coefficient (q_n/q_1).

In addition, the experimental data showed that the uniformity increased in looped manifolds. The rectangular and the triangular looped manifolds yielded a uniformity of 92%. At the same time, a dead-end manifold with the same characteristics and flow conditions yielded a uniformity of 82%. The study also concluded that friction head losses were significantly less in looped manifolds than dead-end manifolds. For the same diameter, length, outlet spacing, material and inlet head, the friction head loss in the dead-end manifold was approximately 500% higher than that in the looped manifold because looping reduces the flow length and discharge. Therefore, the variation in the coefficient of friction along the dead-end manifold was significant. Hence, it should be considered in the hydraulic design. The maximum value of friction ratio, f_n/f_1 , was found to be 33. From collected data, the relationship between the Reynolds number and the coefficient of friction was found to be within the smooth region of Moody's diagram (Reynolds number between 4000 and 100000).

It was also found that the primary variable affecting the friction correction factor (G factor) is the spacing between outlets along the manifold (or the number of outlets). The study results show that when the number of outlets in a manifold was 14 or less, the impact was significant on the G factor. Also, the values of the G factor were significantly reduced in looped manifolds (rectangular or triangular). Validation of selected formulae of the G factor revealed that most of them underestimated the values of the G factor. Statistical tests were made to assess the performance of the selected formulae. The formula proposed by Alazba et al. (2012) yielded the most satisfactory estimation among the eight tested formulae. The tested formulae' performance was assessed using two statistical indices, and these indices were RMSD and NRMSD. The values of these indices for the equation of Alazba et al. (2012) were 0.120 and 0.480, respectively.

ACKNOWLEDGEMENT

The authors acknowledged the technical support provided by the Workshops and Training Center at the University of Technology, Baghdad, Iraq.

REFERENCES

- Alawee, W. H., Almolhem, Y. A., Yusuf, B., Mohammad, T. A., & Dhahad, H. A. (2020). Variation of coefficient of friction and friction head losses along a pipe with multiple outlets. *Water*, 12(844), 1-15. <https://doi.org/10.3390/w12030844>
- Alawee, W. H., Hassan, J. M., & Mohammad, W. S. (2016). Experimental and numerical study on the improvement of uniformity flow in a parallel flow channel. *Engineering and Technology Journal*, 34(5), 847-856.
- Alawee, W. H., Yusuf, B., Mohammad, T. A., & Dhahad, H. A. (2019). Variation of flow along a multiple outlets pipe with various spacing and inflow water head based on physical model. *Journal of Engineering Science and Technology*, 14(4), 2399-2409.
- Alazba, A. A., Mattar, M. A., El-Nesr, M. N., & Amin, M. T. (2012). Field assessment of friction head loss and friction correction factor equations. *Journal of Irrigation and Drainage Engineering, ASCE*, 138(2), 166-176. [https://doi.org/10.1061/\(ASCE\)IR.1943-4774.0000387](https://doi.org/10.1061/(ASCE)IR.1943-4774.0000387)
- Albertson, M. L., Bartion, J. R., & Simons, D. B. (1960). *Fluid Mechanics for Engineers*. Prentice Hall.
- Anwar, A. A. (1999). Factor G for pipeline with equally spaced multiple outlets and outflow. *Journal of Irrigation and Drainage Engineering, ASCE*, 125(1), 34-38. [https://doi.org/10.1061/\(ASCE\)0733-9437\(1999\)125:1\(34\)](https://doi.org/10.1061/(ASCE)0733-9437(1999)125:1(34))
- Christiansen, J. (1942). *Irrigation by sprinkling*. University of California, Agricultural Experiment Station Bulletin.
- Gandhi, M. S., Ganguli, A. A., Joshi, J. B., & Vijayan, P. K. (2012). CFD simulation for steam distribution in header and tube assemblies. *Chemical Engineering Research and Design*, 90(4), 487-506. <https://doi.org/10.1016/j.cherd.2011.08.019>
- Hassan, J. M., Mohamed, T. A., Mohammed, W. S., & Alawee, W. H. (2014a). Modeling the uniformity of manifold with various configurations. *Journal of Fluids*, 2014, Article 325259. <https://doi.org/10.1155/2014/325259>
- Hassan, J. M., Mohammed, W. S., Mohamed, T. A., & Alawee, W. H. (2014b). Review on single-phase fluid flow distribution in manifold. *International Journal of Science and Research*, 3(1), 325-330.
- Hassan, J. M., Mohammed, W. S., Mohamed, T. A., & Alawee, W. H. (2014c). CFD simulation for manifold with tapered longitudinal section. *International Journal of Emerging Technology and Advanced Engineering*, 4(2), 28-35.
- Hassan, J. M., Mohamed, T. A., Mohammed, W. S., & Alawee, W. H. (2015). Experimental and numerical study on the improvement of uniformity flow for three-lateral dividing manifold. *International Journal of Engineering and Technology*, 12(1), 29-37.

- Howland, W. E. (1935). Gain in head at take-offs. *Journal of the New England Water Works Association*, 49(1), Article 14.
- Keller, J., & Bliesner, R. D. (1990). *Sprinkle and trickle irrigation*. Springer Science + Business Media.
- Koh, J. H., Seo, H. K., Lee, C. G., Yoo, Y. S., & Lim, H. C. (2003). Pressure and flow distribution in internal gas manifolds of a fuel-cell stack. *Journal of Power Sources*, 115(1), 54-65. [https://doi.org/10.1016/S0378-7753\(02\)00615-8](https://doi.org/10.1016/S0378-7753(02)00615-8)
- Legates, D. R., & McCabe, J. (1999). Evaluating the use of “goodness-of fit” measures in hydrologic and hydroclimatic model validation. *Water Resources Research*, 35(1), 233-241. <https://doi.org/10.1029/1998WR900018>
- Maharudrayya, S., Jayanti, S., & Deshpande, A. P. (2005). Flow distribution and pressure drop in parallel-channel configurations of planar fuel cells. *Journal of Power Sources*, 144, 94-106. <https://doi.org/10.1016/j.jpowsour.2004.12.018>
- Mohammed, T. A., Noor, M. J. M. M., Halim, A. G., Badronnisa, Y., Soom, M. A. M., & Benzagta, M. A. M. (2003). Experimental study on the friction loss and uniformity of lateral discharge along a manifold. *Journal of Institution of Engineers Malaysia*, 64(2), 20-25.
- Mokhtari, S., Kudriavtsev, V. V., & Danna, M. (1997). Flow uniformity and pressure variation in multi-outlet flow distribution pipes. *Advances in Analytical, Experimental and Computational Technologies in Fluids, Structures, Transients and Natural Hazards*, 355, 113-122.
- Mostafa, E. A. (2004, March 26-28). Correction factor for friction head loss through lateral and manifold. In *Eighth International Water Technology Conference IWTC8* (pp. 735-749). Alexandria, Egypt.
- Oron, G., & Walker, W. (1981). Optimal design and operation of permanent irrigation systems. *Water Resources Research*, 17(1), 11-17. <https://doi.org/10.1029/WR017i001p00011>
- Provenzano, G., & Pumo, D. (2004). Experimental analysis of local pressure losses for microirrigation laterals. *Journal of Irrigation and Drainage Engineering*, 130, 318-324. [https://doi.org/10.1061/\(ASCE\)0733-9437\(2004\)130:4\(318\)](https://doi.org/10.1061/(ASCE)0733-9437(2004)130:4(318))
- Sadeghi, S. H., & Peters, T. (2011). Modified G and G_{avg} correction factors for laterals with multiple outlets and outflow. *Journal of Irrigation and Drainage Engineering*, ASCE, 137(11), 697-704. [https://doi.org/10.1061/\(ASCE\)IR.1943-4774.0000332](https://doi.org/10.1061/(ASCE)IR.1943-4774.0000332)
- Streeter, V. L., Wylie, E. B., & Bedford, K. W. (1998). *Fluid mechanics* (9th Ed.). McGraw-Hill Publishing Company.
- Tong, J. C. K., Sparrow, E. M., & Abraham, J. P. (2009). Geometric strategies for attainment of identical outflows through all of the exit ports of a distribution manifold in a manifold system. *Applied Thermal Engineering*, 29(17-18), 3552-3560. <https://doi.org/10.1016/j.applthermaleng.2009.06.010>
- Valiantzas, J. (2002). Continuous outflow variation along irrigation laterals: Effect of the number of outlets. *Journal of Irrigation and Drainage Engineering*, ASCE, 128, 34-42. [https://doi.org/10.1061/\(ASCE\)0733-9437\(2002\)128:1\(34\)](https://doi.org/10.1061/(ASCE)0733-9437(2002)128:1(34))

- Vallesquino, P., & Luque-Escamilla, P. L. (2002). Equivalent friction factor method for hydraulic calculation in irrigation laterals. *Journal of Irrigation and Drainage Engineering*, 128(5), 278-286. [https://doi.org/10.1061/\(ASCE\)0733-9437\(2002\)128:5\(278\)](https://doi.org/10.1061/(ASCE)0733-9437(2002)128:5(278))
- Yildirim, G. (2007). Analytical relationship for designing multiple outlets pipelines. *Journal of Irrigation and Drainage Engineering, ASCE*, 133(2), 140-154. [https://doi.org/10.1061/\(ASCE\)0733-9437\(2007\)133:2\(140\)](https://doi.org/10.1061/(ASCE)0733-9437(2007)133:2(140))

A Combined Analytical Method for Intelligent Control of Friction Damped Structures

Kamyar Gharra, Karen Khanlari* and Jafar Asgari Marnani

Department of Civil Engineering, Faculty of Technology and Engineering, Central Tehran Branch, Islamic Azad University, Tehran, Iran

ABSTRACT

Controlling structures and increasing the prognosis of their behaviour before natural disasters are the most critical issues in structural engineering. To that end, predicting the destructive effects of earthquakes on both acceleration and displacement of structures would be beneficial. This paper suggests an intelligent control system that realises simultaneous control of acceleration and displacement parameters. There are two modules in the system. First, the preserving module aims to estimate the crisis thresholds of acceleration and displacement based on the historical seismic data of each area. Second, the processing module finds the optimum value of the slip load of the friction damper so that both acceleration and displacement are controlled. We introduce an analytical method based on a matrix analysis approach and heuristic algorithm (MAHA) as a core of the processing module. MAHA would analyse the structure response, and the friction damper would determine the optimum slip load. The numerical and software simulation results for various one-bay and two-bay steel structures show that the proposed intelligent control system applies to multiple frictions damped structures under different earthquake records. In addition, a control level of 80% in acceleration and displacement of structures is achieved compared to an uncontrolled state. Moreover, the mentioned system enables the engineers to find appropriate friction dampers during the design of structures.

ARTICLE INFO

Article history:

Received: 22 December 2020

Accepted: 19 April 2021

Published: 22 September 2021

DOI: <https://doi.org/10.47836/pjst.29.4.05>

E-mail addresses:

kamyar.gharra75@gmail.com (Kamyar Gharra)

karen.khanlari@gmail.com (Karen Khanlari)

j_asgari@iauctb.ac.ir (Jafar Asgari Marnani)

* Corresponding author

Keywords: Analytical modelling, control system, damped friction structure, multi-degree of freedom

INTRODUCTION

There has been a difference in views among scientists in the earthquake and structural engineering (Domenico et al., 2020; Rashidi et al., 2020). Structural scientists focused

on strengthening structures, as well as the optimal design of buildings under earthquakes loads. The design of new buildings, including seismic restraint systems, is one of the new structural topics in recent decades (Nizic & Mestrovic, 2011; Majd et al., 2019; Sanghai & Pawade, 2020). These systems only act against various seismic vibrations without withstanding any static loads. In seismic restraint systems, dampers help to increase the loss of seismic energy entering the building. As a result, a desirable and durable structure can be achieved. The structures behave safely against all kinds of dynamic earthquake loads (Shaw, 1986; Pall, 1996; Fateh et al., 2016).

Friction dampers are classified as passive control systems and effectively control vibrations and reduce seismic responses. One of the most critical parameters in designing friction-damped structures is slip load. It has a significant impact on seismic and the level of non-elastic behaviour of the structure (Pasquin, 2004; Bhaskararao & Jangid, 2006).

In this regard, various researches have been done in recent years, including “The Seismic Reinforcement of Steel Frame Buildings using A Friction Damper by Lee S. et al. (2008). Scientists in earthquakes assess the response of acceleration and displacement between the floors of each structure. It was shown that the dissipated energy is effectively lost for a 10-story building with the proper distribution of dampers, and the structural behaviour is linear. In another study, Lee H. et al. (2008) investigated a base shear on designing a frictional damper system in a structure with elastic behaviour. They showed that the sliding load of the damper was determined with the shear of the floors in the initial bending frame. Also, it was shown that the distribution of slip load in proportion to the shear of the floor was effective. Hence, it could reduce the relative displacement of the floors by comparing the slip load’s uniform distribution.

Some investigations were conducted on optimising the performance of friction dampers within the structures. The use of heuristic algorithms in this domain emerged. Apostolakis and Dargush (2010) studied the optimal seismic design of steel bending frames with metal dampers or additional friction with a restraint system. They used a genetic algorithm to find the slip load of the structure. In order to evaluate the response of the optimised structure, they used the sum of the squares of the relative displacement or the acceleration of the floors. They compared three examples of bending frame models in pre and post improvement mode with the addition of dampers. The results showed that after the optimal design, the above response parameters were reduced. Also, the distribution of floor acceleration and relative displacement of floors was more uniform. In 2013 and 2015, two types of research were conducted by Fallah and Honarparst (2013) and Feliciano (2015). The purpose of these studies was to investigate the optimal slip load in multi-story buildings. They distributed the slip load in a structure using two modes; uniform and non-uniform. In both modes, the sum of slip loads in a structure was considered the same. Then, the optimal slip load was obtained in each case using a multivariate optimisation method.

In order to optimally design the location of friction dampers, several studies were conducted. For example, Lopez and Miguel (2015) found a method using the FireFly algorithm and the finite difference method on a ten-story building. Therefore, it was possible to obtain a suitable location for the damper to minimise the maximum displacement within the structure.

Kim and An (2016) conducted a study on nonlinear static and dynamic analyses of friction damped structures. They found the optimum position of friction dampers by genetic algorithm. They concluded that maximum roof displacement and the inter-story drift ratio were reduced by 30% and 40%, respectively. Perez et al. (2017a & 2017b) also worked on an optimisation method to control the failure probability of the friction-damped structure. The failure probability of the structure was defined by the criterion of increasing the amount of displacement between floors from 1% of the height of the first floor. The results for a three-story structure showed that optimising the damper location and frictional force could reduce the risk of failure by up to 80%.

Miguel and Lopez (2018) presented an approach to simultaneously optimise the frequency domain's frictional location and friction damper parameters. One of the advantages of Miguel's study was a significant reduction in computational time. The design was based on a six-story building. Variables such as force and displacement of the friction damper have been investigated. However, the results showed that the average displacement decreased by approximately 82%. Palacios et al. (2020) worked on protecting multiple adjacent buildings by using distributed damping systems. They reported about 50% in the overall inter story-drift of 40% in the overall acceleration peak-value.

As mentioned in the literature overview, they used the approximated model to identify the behaviour of friction damped structures. Moreover, they are limited to a specific region and individual structure parameters. This paper intends to advance previous research and propose an intelligent control system equipped with a combined analysis method. The novelty of the proposed control system is that it is designed parametric and more accurate. That means by varying the structures and earthquakes in each area, and we can put the relevant parameters. The system inputs include the number of stories, earthquake specifications, number of friction dampers, number of degrees of freedoms, allowable levels of acceleration, and displacements on that area. The outputs are optimum slip load, controlled acceleration, and displacement responses. The main objectives of the proposed idea are as follows:

- Implementing the intelligent control system that is knowledge-based, flexible, and in any geographical area. The system is composed of preserving and processing modules. The acceleration and displacement thresholds are analysed based on the historical seismic earthquake records of that region. Then, the processing module finds the optimum value of slip load so that acceleration and displacement are controlled jointly.

- Using an optimisation method in the core of the intelligent control system. It can work adaptively based on the variation of structural parameters and earthquake records.
- Combining matrix analysis of the reduced-order equation of motion, exact modelling of each friction joint, as well as a heuristic algorithm. This analytical approach gives the optimum value of slip load.
- Estimating the controlled response of structures during the structure design. It is based on the outputs of the intelligent control system and the appropriate friction damper in each structure.

The discussion of this paper will start by addressing the problem formulation. Second, the conceptual diagram of the intelligent control system and systematic parameters are described. Third, introducing the proposed MAHA as an effective solution for finding the optimum slip load of the friction damper. Fourth, the discussion will be based on the numerical results and simulation scenarios before being concluded.

METHODS

This study is conducted to realise an intelligent control system that applies to various structures in each area. First, the proposed system's substantial parameters, such as acceleration and displacement of structures, would be kept at an acceptable level. Then, the idea is proposed and formulated before introducing the combined analytical method to find the response of various structures.

Problem Formulation

Figure 1 depicts the conceptual diagram of the proposed intelligent control system. The system consists of two modules. First, the preserving module provides the set of processes to store, index, and access information. The information includes the data of seismic stations that measure the earthquake records. The data mining step can be started by creating a historical records of earthquakes in a specific area. In this step, the maximum acceleration and displacement levels on an area are detected.

Second, to process the acceleration and displacement levels on which the structures experienced minimum damage. Then, threshold levels are calculated and put into the processing module. In this module slip load of each story is defined as a decision variable. The primary role of this module is to find the optimum slip load of friction damper for designing an appropriate friction damper for that structure. To this end, first, the structure is analysed by the proposed matrix analysis method. Then acceleration and displacement responses are extracted. Finally, these responses are used as inputs of the optimisation method.

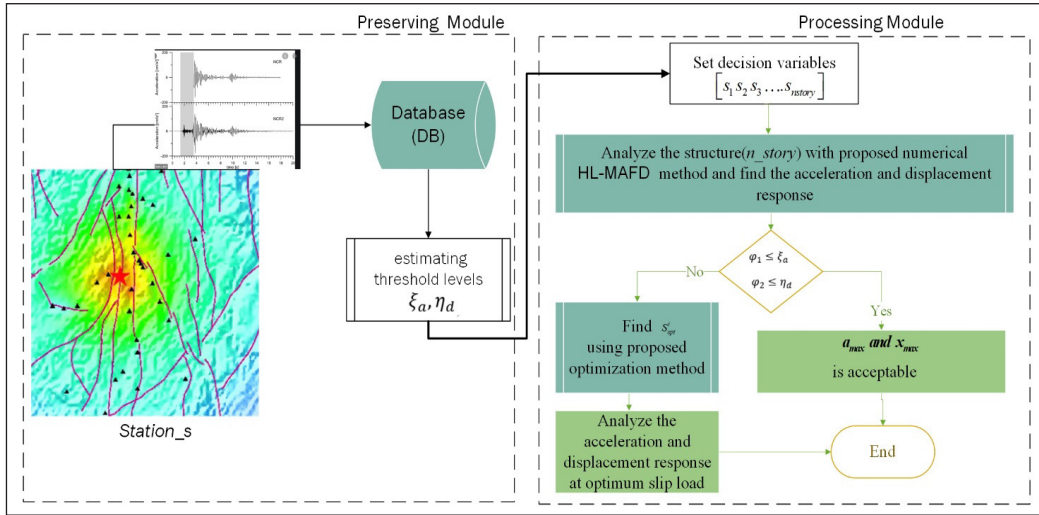


Figure 1. Conceptual diagram of the proposed intelligent control system

The output of the proposed intelligent control system is a controlled acceleration and displacement and an optimum value of slip load. This system can be set up in any area and can apply to various structures and earthquake records. To form a database, we have used the Seismic station data of Iran (For example, Manjil and Tabas) and El-Centro records.

The systematic parameters of this investigation are:

- Seismic station of Tabas and Manjil, (Station_s)
- SQL Database and Mathcad as a software medium, (DB)
- Server Core i7-8700 CPU at 3.20 GHz, 16 GB RAM, and a 480GB SSD hard drive, (processing module)
- Medium- size structures, (n_story)

The optimisation method raised to find the optimal slip load is defined in Equation 1a. This definition includes design variables, objective function, and constraints. Minimising the joint acceleration and displacement is considered an objective function. It is due to the behaviour of structures in the natural environment. The optimisation methods are designed in such a way to support various behaviour of structures under different earthquakes. Structures with higher natural frequency and short natural periods suffer higher acceleration. On the contrary, structures with lower natural frequency and long natural periods suffer higher displacement. So, in the proposed intelligent control system the objective function is designed based on the above considerations. Design variables include the force of friction dampers in different floors, threshold level of acceleration and displacement, relations (i) and (ii), as well as the minimum and maximum slip loads; constraint (iii).

$$Find \vec{S}, \vec{S} = [S_1 S_2 S_3 \dots S_{nstory}]$$

$$\text{Minimize } U(S) = [a_{max} \times x_{max}] \tag{1a}$$

Subject to

$$(i) \varphi_1 \leq \xi_a$$

$$(ii) \varphi_2 \leq \eta_d$$

$$(iii) S^{Min} \leq S_{opt}^i \leq S^{Max}$$

$S_1 S_2 S_3 \dots S_{nstory}$: decision variables that show slip load of each story;

a_{max} : maximum acceleration of structure;

x_{max} : maximum displacement of structure;

S^{Max} : maximum value of slip load;

S_{opt}^i : minimum value of slip load;

S_{opt}^i : optimum value of slip load;

$$\varphi_1 = \frac{|a_{max_d}|}{a_{max}} : \text{ratio of the maximum acceleration with damper to without damper;}$$

$$\varphi_2 = \frac{|x_{max_d}|}{x_{max}} : \text{ratio of the maximum displacement with damper to without damper;}$$

η_d : threshold level of displacement;

ξ_a : threshold level of acceleration.

$U(S)$ is the objective function that consists of displacement and acceleration, which is actually a non-linear function. The functions of x_{max} and a_{max} do not closed-form formulation (Equation 1b). In fact, displacement and acceleration response are derived from the general equation of motion in Equation 2 in the following sections.

$$U(S) = x_{max}(s). a_{max}(s) = x_{max}(s). \frac{d}{dt^2} x_{max}(s) \tag{1b}$$

Solving this equation is very complicated for MDOF (Multi Degree of Freedom) structures, especially the high-rise. For this purpose, the combined MAHA (Matrix Analysis and Heuristic Algorithm) is introduced based on the proposed HL-MAFD (Hysteresis Less-Matrix Analysis of Friction Damped structure) and a heuristic algorithm. The whole structure is first analysed by the proposed HL-MAFD algorithm, which is based on the basic principles of matrix analysis. In this step, the acceleration and displacement response will be obtained. Then, the optimum slip load in which both acceleration and displacement are controlled is obtained by a heuristic method. Figure 1 illustrates the conceptual flowchart of the proposed MAHA that performs based on the proposed HL-MAFD and SGA (search group algorithm).

Solving the Optimisation method

MAHA will find the appropriate slip load to meet the joint controlled response of acceleration and displacement of the structure. It is a combination of HL-MAFD, numerical matrix analysis, and a heuristic SGA. First, the initial response of acceleration and displacement of the structure is obtained from the HL-MAFD. In this method, an accurate system stiffness matrix is achieved to form the general equation of motion. Generally, when analysing friction braces in standard software, the shape of hysteresis curve is selected according to the manufacturer's specifications. Then the whole structure analysis is done according to the link of the structure (Bhaskararao & Jangid, 2006).

The innovation of the proposed approach compared to the previous ones is that the frictional element is first analysed numerically. The analysis is based on the basic principles of structural matrix analysis, structural dynamics, and relationships governing the general equation of motion at each time. In general, this approach is provided with a model for analysing frictional damper behaviour without the need for mechanical hysteresis curves. First, the motion general equation of the structure is formed. Then, the response of acceleration and displacement of the structure would be extracted. This response was obtained from solving the optimised formulation. The proposed method is a combination of the SGA (search group algorithm) and matrix analysis approach.

Numerical HL-MAFD

Figure 2 shows a structure equipped with a friction damper with N degrees of freedom (NDOF). Therefore, it is necessary to define additional freedom to perform dynamic analysis for friction joints in braces. By defining the degrees of freedom in the axial direction in Figure 2, the relative velocity of the two ends of the connection can be determined. Then, the frictional force can be determined with the help of the relative velocity of the two ends. After determining the frictional force, the force relations feedback is examined and applied as an external force to the system. Finally, the structure is analysed.

Regarding the methods used in SAP (Structural Analysis Program) or ETABS (Extended Three-Dimensional Analysis

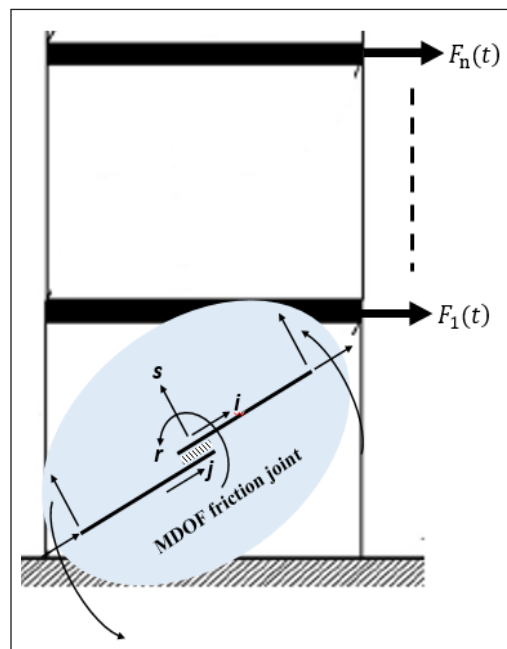


Figure 2. Structural model of a multi-degree of freedom with friction damper

of Building System) software, the proposed numerical analysis approach for structures with frictional elements do not require the use of an ideal hysteresis curve provided by the manufacturer. Therefore, in the proposed method, the behaviour of the damper is not predetermined according to its specifications. Instead, the system stiffness matrix is accurately obtained by considering the stiffness matrix of system components in proportion to master and slave freedom degrees.

The degrees of freedom considered in frictional elements include two degrees of axial freedom in the direction of frictional and one degree of vertical freedom. Also, one degree of rotational freedom is considered to prevent the friction link from breaking. The general motion equation is shown in Equation 2.

$$\overline{M} \ddot{x}(t) + \overline{K} x(t) + f(t) = F(t) \tag{2}$$

Where $f(t) = -\mu S \cdot \text{sign}(\dot{x})$ in which $f(t)$ is Friction force; S is slip load, and μ is a friction coefficient. M : mass matrix with the size of $NDOF \times NDOF$; K : stiffness matrix with the size of $NDOF \times NDOF$; $NDOF = m + s$; total Number of DOFs; m : number of master DOFs; s : number of slave DOFs; $x(t)$: acceleration response vector; $\dot{x}(t)$: velocity response vector; $\dot{x}(t)$: displacement response vector; $F(t)$: external force vector.

The degrees of freedom are divided into master and slave to perform static compression. It should be noted that dynamic loading is not performed on the slave degrees of freedom. In this case, the general motion equation can be partitioned into master and slave to form Equation 3.

$$\begin{bmatrix} M_{mm} & O_{sm} \\ O_{sm} & O_{ss} \end{bmatrix} \begin{bmatrix} \ddot{x}_m \\ \ddot{x}_s \end{bmatrix} + \begin{bmatrix} K_{mm} & K_{ms} \\ K_{sm} & K_{ss} \end{bmatrix} \begin{bmatrix} x_m \\ x_s \end{bmatrix} + \begin{bmatrix} O_m \\ f_s \end{bmatrix} = \begin{bmatrix} F_m \\ O_s \end{bmatrix} \tag{3}$$

- x_m : Displacement vector of master DOFs
- x_s : Displacement vector of slave DOFs
- K_{mm} , K_{ms} , K_{sm} and K_{ss} : Partitions of the Stiffness matrix
- M_{mm} : Main partition of the Mass matrix
- O_{ms} , O_{sm} and O_{ss} : Null partitions of the Mass matrix
- F_m : External forces vector on master DOFs
- f_s : Friction forces vector on slave DOFs
- O_s : Null partition of Friction forces vector
- O_m : Null partition of External forces vector

By expansion of Equation 3 we will have Equation 4a and 4b:

$$M_{mm} \ddot{x}_m + K_{mm} x_m + K_{ms} x_s = F_m \tag{4a}$$

$$K_{sm}x_m + K_{ss}x_s = f_s \tag{4b}$$

Arranging Equation 4b, the displacement vector of slave DOFs can be represented in terms of stiffness, displacement vector of master DOFs, and friction forces vector on slave DOFs as Equation 4c.

$$x_s = K_{ss}^{-1}(f_s - K_{sm}x_m) \tag{4c}$$

By applying the result of Equation 4c into Equation 4a, we obtain Equation 5.

$$M_{mm} \ddot{x}_m + (K_{mm} - K_{ms}K_{ss}^{-1}K_{sm})x_m = F_m - K_{ms}K_{ss}^{-1}f_s \tag{5}$$

So, comparing Equation 5 with traditional general motion equation, we can extract the condensed or reduced mass and stiffness matrices as Equation 6a and 6b.

$$M^* = M_{mm} \tag{6a}$$

$$K^* = K_{mm} - K_{ms}K_{ss}^{-1}K_{sm} \tag{6b}$$

Where $K_{mm}, K_{ms}, K_{ss}, K_{sm}, K_{ss}$ are submatrices of K_{sys} as shown in Equation (17). The reduced external force vector is defined as Equation 7.

$$F^* = F_m - K_{ms}K_{ss}^{-1}f_s \tag{7}$$

So, general motion equation of a system can be redefined based on master DOFs as Equation 8.

$$M^* \ddot{x}_m + K^* x_m = F^* \tag{8}$$

In the condensed general motion equation, the external force vector of master DOFs, F_m , is the seismic forces (i.e., earthquake). In the same way, the vector of forces related to slave DOFs, F_s , is the vector in which frictional forces are placed. To achieve the velocity of slave DOFs, \dot{x}_s , considering Equation 4b, we can obtain by differentiation of this vector as Equation 9.

$$x_s = K_{ss}^{-1}f_s - K_{ss}^{-1}K_{sm}x_m$$

$$\frac{d}{dt}x_s = K_{ss}^{-1}\frac{d}{dt}f_s - K_{ss}^{-1}K_{sm}\frac{d}{dt}x_m \tag{9}$$

Hence, we can consider that the vector of the frictional forces of slave DOFs is equal to zero ($\frac{d}{dt} f_s \cong 0$). So, we can approximately redefine the velocity vector of slave DOFs as Equation 10.

$$\dot{x}_s \cong -K_{ss}^{-1} K_{sm} \dot{x}_m \tag{10}$$

Considering Equation 10, we can define the velocity of slave DOFs in terms of the master DOFs. In fact, by this important relationship we can solve the condensed general motion equation in a lower degree.

Proposed MAHA

HL-MAFD numerical analysis approach was described in the previous section. So, we can find the answer to the acceleration and displacement of any structure based on the reduced general motion equation with the exact stiffness matrix. As mentioned in the conceptual diagram of Figure 1, the goal of the optimisation method is to find the value of acceleration and displacement of the structure in the optimum slip load. Figure 3 addresses

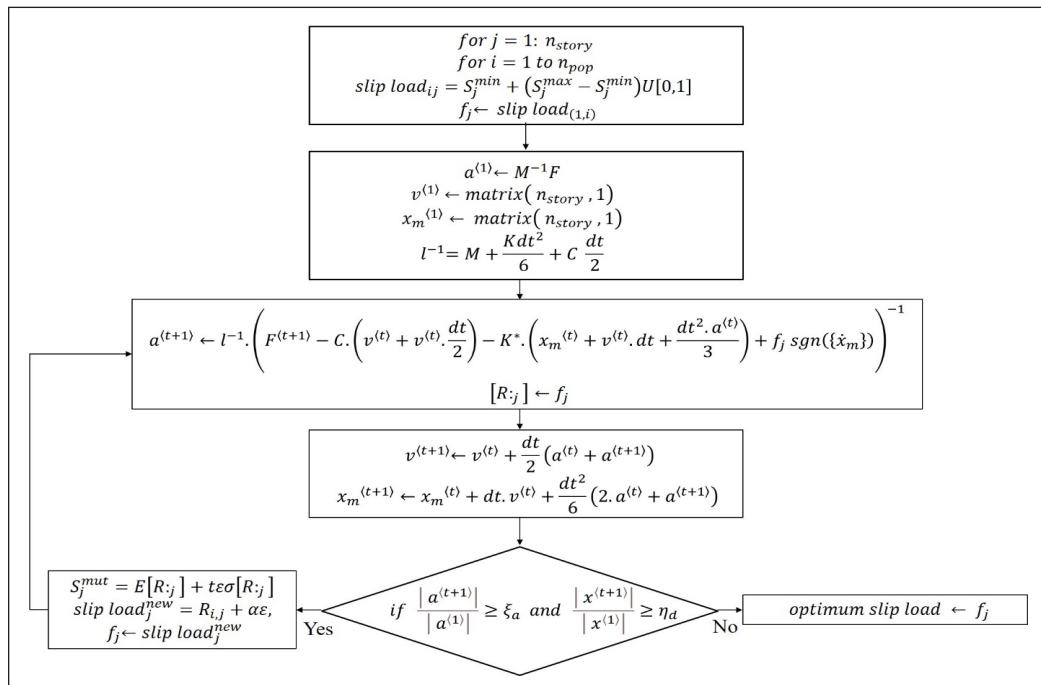


Figure 3. Flowchart of pseudo code of the MAHA

Note. n_{story} : number of stories; n_{pop} : number of initial populations of slip load; $U[1,0]$: uniform variable; E and σ : mean and variance; $slip load_{ij}$: generated population; R_j : j 'th column in search matrix; ε : random variable; t control coefficient of new variable; C : damping matrix $C \propto eigenvalue(M^{-1}K)$; γ, β : New marks coefficient

the functionality of the MAHA that is a combination of the proposed HL-MAFD and the heuristic SGA algorithm.

As can be seen in Figure 3, optimisation variables are the slip load of the structure. First, for each structure floor, an initial population is created for the slip load (n_{pop}). Then, acceleration and displacement values of the structure are obtained using the general motion equation obtained by the HL-MAFD at each time step. Also, the calculation of a sample stiffness matrix, \mathbf{K} , is given in Equation 16. Then, the acceleration and displacement output matrices are evaluated with the conditions mentioned in the optimisation method, defined as the minimum acceleration and displacement. If the condition does not satisfy, the amount of mutation will be determined for the slip load. Then, a new family will be formed for it. After that, the acceleration and displacement values will be calculated for the new values of slip load. This step repeats so that the condition is realised and the optimal slip load is obtained. Any variable that removes the objective function from the target range is more likely to be removed and replaced by a new variable. The values that are close to the optimal value would be stored in the search set ξ_a , and the slip load that meets the ξ_a, η_d would be the final one.

RESULTS AND DISCUSSION

Several scenarios have been studied and measured to verify the proposed analytical optimisation method. As mentioned in this paper, the proposed analytical algorithm HL-MAFD is used to obtain the structural response to extract the structural stiffness matrix. Then, the general equation of motion with reduced orders is solved at the optimum value of slip load. A 4-story structure with a friction damper is considered to depict the performance of a proposed approach. Two cases are analysed: an optimised slip load and a non-optimised. We show that the acceleration and displacement responses of the structure with optimised slip load can be controlled considerably comparing the non-optimised.

Figure 4 shows the desired structure, degrees of freedom, and nodes based on the proposed algorithm. A load of 30 kN

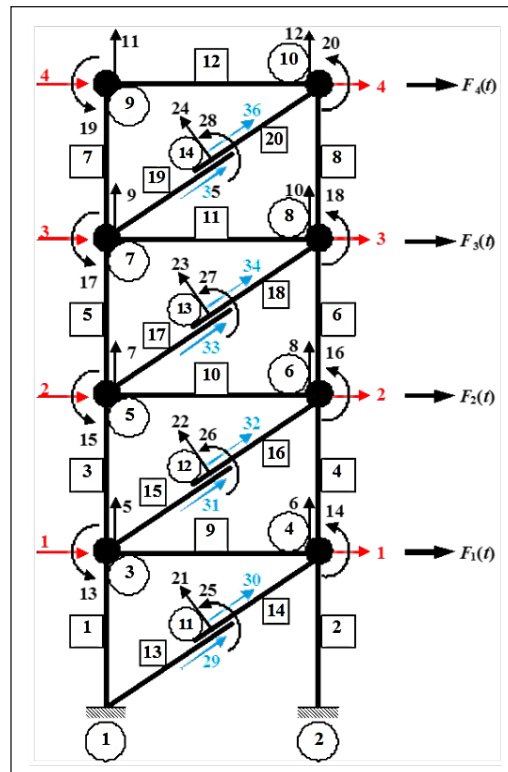


Figure 4. 4-story structure analysis under proposed method

is applied to each node. Also, the seismic hazard zonation factor is considered 0.2g. The cross-sections of the structure are designed based on the static distribution of force.

Simulations are done by Mathcad mathematical software. Various earthquake records with specific PGA are used as an external force. PGA (Peak Ground Acceleration) means maximum ground acceleration that occurred during earthquake at a location. PGA is equal

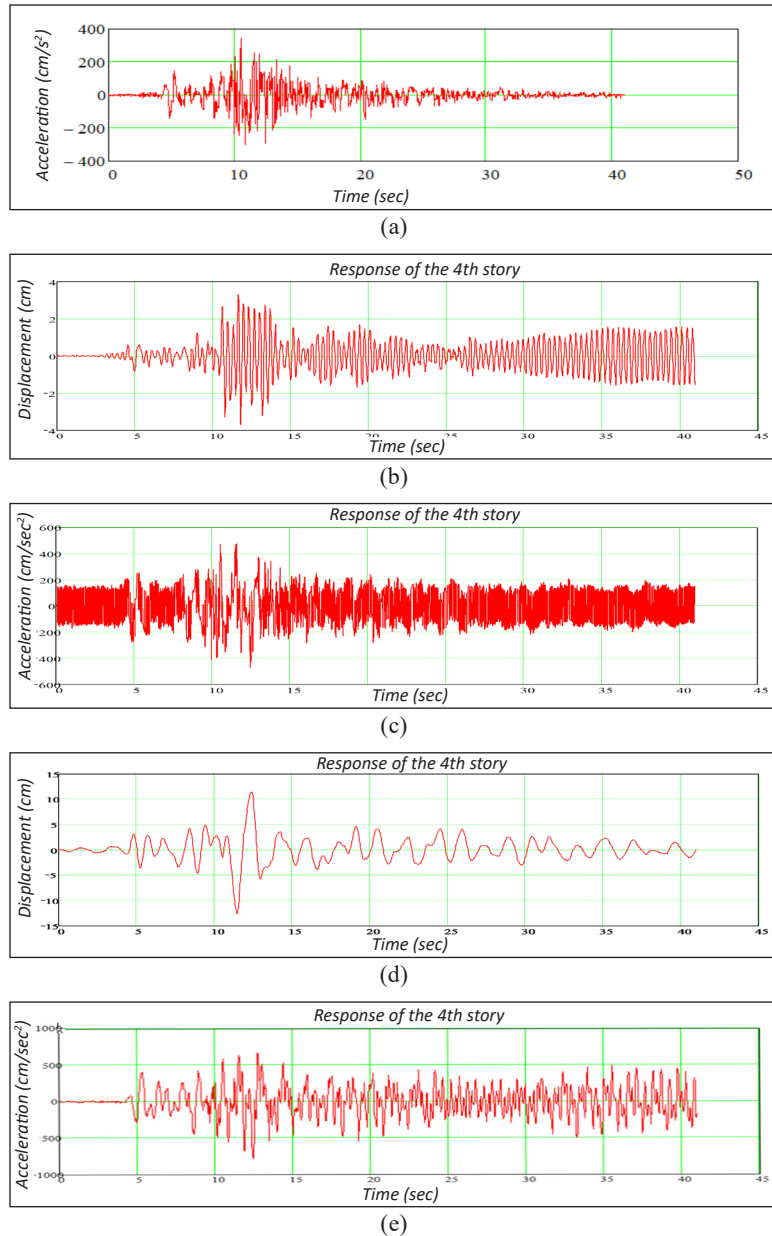


Figure 5. Measuring results of a four-story structure: (a) Tabas records; (b) Displacement with optimal slip load; (c) Acceleration with optimal slip load; (d) Displacement with non-optimised slip load; (e) Acceleration with non-optimised slip load

to the amplitude of the largest absolute acceleration recorded on an accelerogram during earthquake. Tabas earthquake mapping (1978), PGA 913.61 cm/s/s is shown in Figure 5a generated from earthquake records registered in the strongmotioncenter database. Figures 5b to 5c depict the acceleration and displacement responses for the case where the slip load is obtained from the optimisation method and the case where the slip load is randomly selected.

Table 1 shows the results of the simulations for a 4-story structure for three cases, bending frame, friction damper without optimal slip load, and the friction damper with optimal slip load.

In the friction damper model, the optimisation method is solved by considering the ratio of acceleration value and allowable displacement (conditions *i and ii*) equal to 0.3 and 0.25. The value of ξ_a and η_d in the optimisation method will limit the slip load equal to 2000 kgf. As can be seen, the measured reduction ratio of the acceleration amplitude and displacement of the structure is 0.272 and 0.205, respectively. Hence, the maximum amplitude of acceleration and displacement with friction damper at optimum slip load have been controlled compared to the non-friction damper structure.

As presented in Table 1, the acceleration and displacement amplitude ratio obtained from the optimisation method is 0.272 and 0.205, respectively. Furthermore, this indicates that they are less than the conditions defined in the optimisation method and the method meets constraints. The frequency responses of acceleration and displacement of a four-story structure in an optimised and a non-optimised slip load are shown in Figure 6. As shown in Figure 6, the number of peaks can be considerably controlled by using the friction damper in the structure and adjusting the slip load at the optimum level.

Moreover, to validate the results, further analyses were performed in 6 and 10-story structures with one and two bays. Figure 7 shows the acceleration and displacement responses of a 6-story structure that has been analysed by the proposed method. Further investigations have been carried out for 2-Bay structures under the earthquakes of Tabas, Manjil (1990- PGA: 128.21cm/s/s), and El-Centro (1940- PGA: 210.14 cm/s/s), as can be seen in Tables 2-4.

One of the main concepts of the proposed method is to show its potential to apply to various structures. To this end, we addressed the details of the analysis method for 4 and

Table 1
Four story result under Tabas Earthquake, $S=2000$, $\xi_a = 0.30$, $\eta_d = 0.25$

Frame Type	Top Displacement (cm)	Top Acceleration (cm/sec ²)
Bending	18.0	1742
Non-Optimum Frictional	12.717	789.012
Optimum Frictional	3.69	475.171
Obtained reduction ratio from optimisation method	0.205	0.272

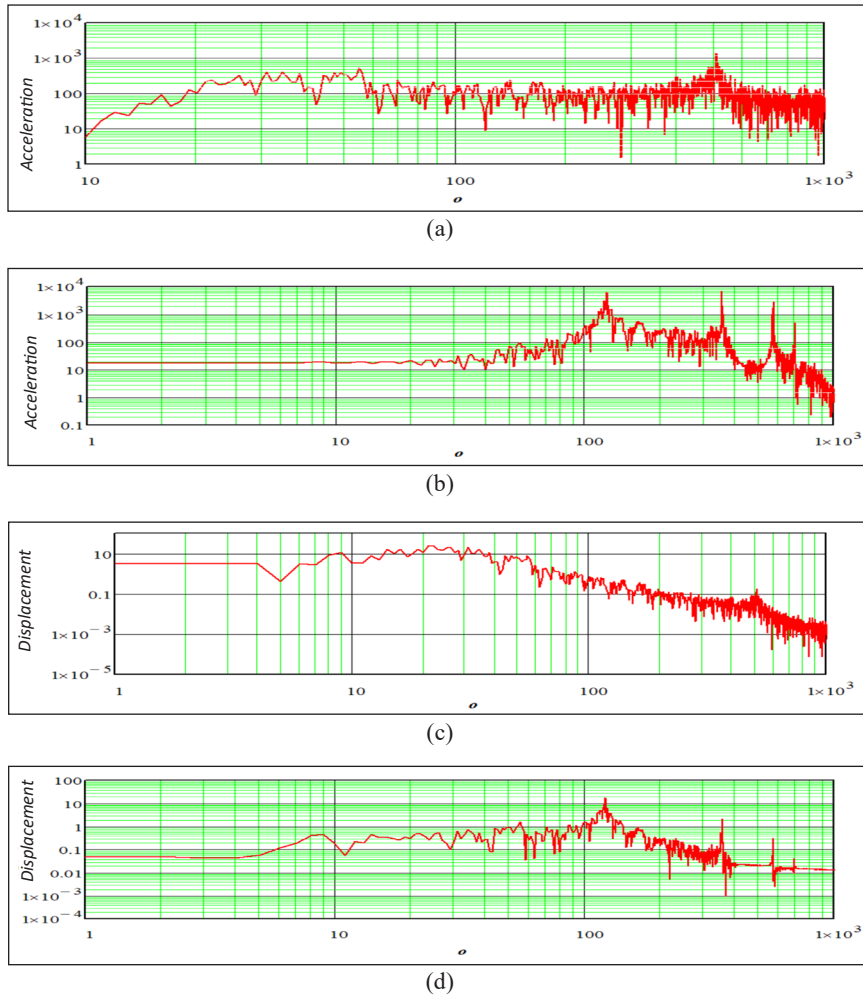


Figure 6. Frequency responses of a four-story building: (a) Acceleration with optimised slip load; (b) Acceleration without friction damper; (c) Displacement with optimised slip load; (d) displacement without friction damper

6 story structures in Figures 4 to 7. In each case, we compared the effect of non-optimum and optimum slip load on the response of acceleration and displacement. Then, simulations are extended to 2-Bay frames under different earthquakes. The results are shown in Table 2 to 4. The results show no control of acceleration and displacement on the bending frame (without friction damper).

Similarly, for the non-optimum friction frame, we do not have adequate control. In the third frame, “optimum frictional”, we can see the efficiency of the proposed method. That means the value of acceleration and displacement is reduced effectively compared to the bending frame. Since each earthquake has its specification and frequency spectrum, we have selected the most traditional ones in the world as a sample. As a result of the tectonic

condition of Iran, Tabas and Manjil earthquakes are considered. Similarly, El-Centro is considered an external force to show no limit on applying the proposed method. As explained in Equation 8, we can apply various earthquakes as external forces. Therefore, the reduced motion equation is applicable for analysing the structure under various earthquakes.

In all simulations, the structural response per optimal value of slip load can be found. Hence, the simultaneous control of acceleration and displacement of the structure would

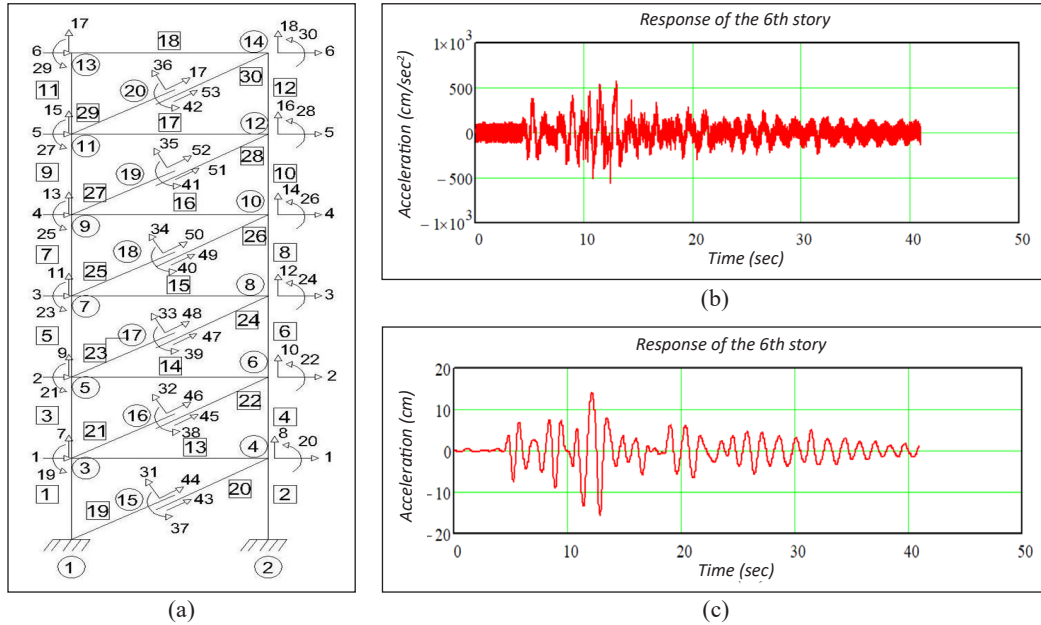


Figure 7. A six-story frame under Tabas earthquake $s=1800\text{kgf}$: (a) Analysed structure under proposed method; (b) Acceleration response; (c) Displacement response

Table 2
Six and Ten story results under Tabas $\xi_a = 0.30$ and $\eta_d = 0.25$

Number of Stories	Frame Type	Top Displacement (cm)	Top Acceleration (cm/sec ²)
6-story-1 Bay	Bending	50.4	1792
	Non-optimum Frictional	15.6	954
	Optimum frictional, S=1500	5.6	575
6-story-2 Bay	Bending	50.4	1956
	Non-optimum Frictional	16.7	954
	Optimum frictional, S=2500	13.1	565
10-story-1 Bay	Bending	70.7	2126
	Non-optimum Frictional	44.4	954
	Optimum frictional, S=2000	16.3	536
10-story-2 Bay	Bending	86	3075
	Non-optimum Frictional	36.9	2391
	Optimum frictional, S=2000	20.8	576

Table 3
 Four, Six, and Ten story results under Manjil $\xi_a = 0.30$ and $\eta_d = 0.25$

Number of stories	Frame Type	Top Displacement (cm)	Top Acceleration (cm/sec ²)
4-story-1 Bay	Bending	30.2	5325
	Non-optimum Frictional	12.7	1405
	Optimum Frictional, S=1000	7.4	451
4-story-2 Bay	Bending	21.7	3560
	Non-optimum Frictional	10.8	843
	Optimum Frictional, S=2000	4.7	437
6-story-1 Bay	Bending	30	2263
	Non-optimum Frictional	11.9	1316
	Optimum Frictional, S=1500	7.2	439
6-story-2 Bay	Bending	31.6	3895
	Non-optimum Frictional	18.5	1664
	Optimum Frictional, S=2000	9	437
10-story-1 Bay	Bending	30.5	2160
	Non-optimum Frictional	24.6	1162
	Optimum Frictional, S=1500	12.6	384
10-story-2 Bay	Bending	28.9	3808
	Non-optimum Frictional	18.4	890
	Optimum Frictional, S=2500	14.4	506

Table 4
 Four, Six, and Ten story result under El-Centro $\xi_a = 0.30$ and $\eta_d = 0.4$

Number of stories	Frame Type	Top Displacement (cm)	Top Acceleration (cm/sec ²)
4-story-1 Bay	Bending	30.3	2714
	Non-optimum Frictional	7.7	1449
	Optimum Frictional, S=1000	5.8	534
4-story-2 Bay	Bending	24	2683
	Non-optimum Frictional	8.4	1079
	Optimum Frictional, S=2000	5.7	581
6-story-1 Bay	Bending	36.5	4462
	Non-optimum Frictional	20.2	1159
	Optimum Frictional, S=1500	12	601
6-story-2 Bay	Bending	39.7	2734
	Non-optimum Frictional	19.2	1781
	Optimum Frictional, S=2000	15.5	578
10-story-1 Bay	Bending	81.8	2633
	Non-optimum Frictional	34.7	1864
	Optimum Frictional, S=1500	16.3	576
10-story-2 Bay	Bending	84.3	2353
	Non-optimum Frictional	46	1663
	Optimum Frictional, S=2500	23.6	547

be achieved. Figure 8 depicts the investigation results of changing the constraints in the optimisation method. By changing the values of ξ_a , η_d , the range of slip load can be determined to control the maximum amplitude and displacement values of the structure. The results illustrate that the optimum range of slip load of 1-bay structures is 1000 Kgf to 2000 Kgf. On the contrary, for 2-bay structures, this range was increased, and the optimum range was 2000 Kgf to 2500 Kgf. Thus, we can find the optimum slip load in each area with various allowable thresholds of acceleration and displacement.

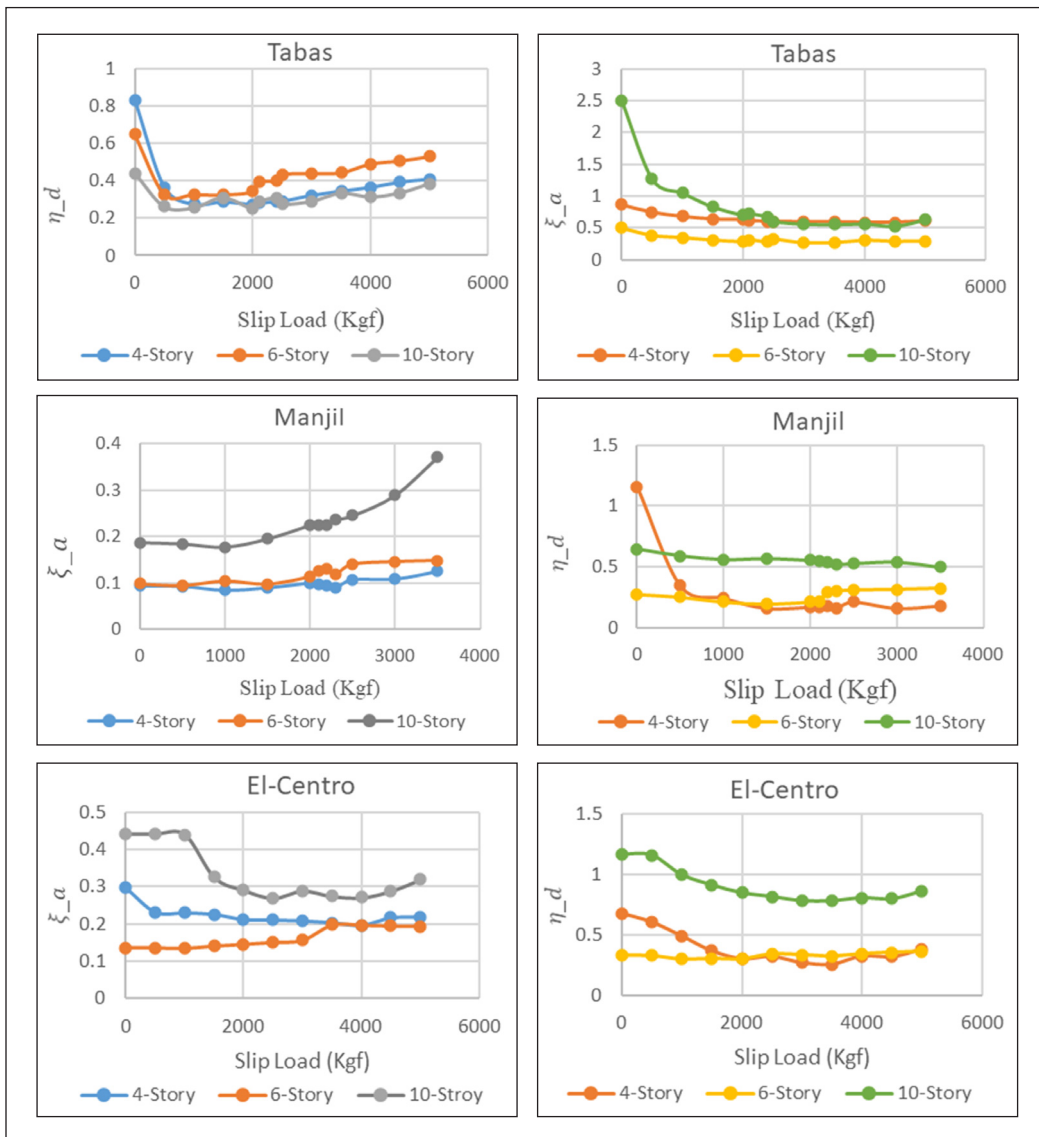


Figure 8. Variation of optimisation method constraints vs. slip load for 4, 6, and 10 story buildings under Tabas, Manjil, and El-Centro earthquakes

Table 5
Comparison of the proposed method with other references

Ref	Structure under Test	Displacement Reduction (%)	Acceleration Reduction (%)	Inter Story Drift Reduction (%)
Lee et al, 2008	6-story	-	31.8	66
This paper		80.1	80.3	84.2
Fallah & Honarparst, 2013	4-Story	40.3	19.6	35
This paper		80.1	80.3	84.2
Feliciano, 2015	6-story	69	71	-
This paper		68	86	70.1
Miguel & Lopez, 2018	4-story	82.73	-	81.8
This paper		80.1	80.3	84.2
Domenico, 2020	4-story	60	40	-
This paper		80.1	80.3	84.2
Sanghai & Pawade, 2021	6-story	-	-	33
This paper		68	86	70.1
Miguel & Pérez, 2017	9-story	72	70	83.3
This paper		81	80	86.2
Lopez & Miguel, 2015	10-story	66	-	76
This paper		80.07	78.12	79
Kim & An, 2016	4-story	30	-	40
This paper		80.1	80.3	84.2
Palacios et al. 2020	4-story	-	40	50
This paper		80.1	80.3	84.2

Table 5 shows a comparison between the results of this paper and other studies. The reduction ratio depicts how much the acceleration and displacement amplitudes can be controlled using optimised slip load compared to non-friction damped structures.

Furthermore, to assess the proposed MAHA and other investigations, 4, 6, 9, and 10-story buildings are analysed with the same situations as mentioned previously. Table 5 compared the result of a 4-story with the findings of Miguel and Lopez (2018), which shows that the proposed method of this paper can improve all three parameters above 80% simultaneously. Lopez and Miguel (2015) showed a 43% reduction of inter-story drift for a 6-story buildings, while this paper achieved 70%.

Lee H. et al. (2008) investigated un-damped and damped frames. They achieved a 31.8% and 43% reduction of maximum acceleration for 6-story and 4-story buildings, respectively. Also, they reported a 66% reduction of inter -story drift. Prez et al. (2017a) reported a 54% reduction in acceleration in controlled mode compared to uncontrolled. Miguel and Lopez (2018) resulted in an 80% reduction of acceleration and inter-story drift for a 4-story building. Sanghai & Pawade (2021) and Miguel & Pérez (2017), approved

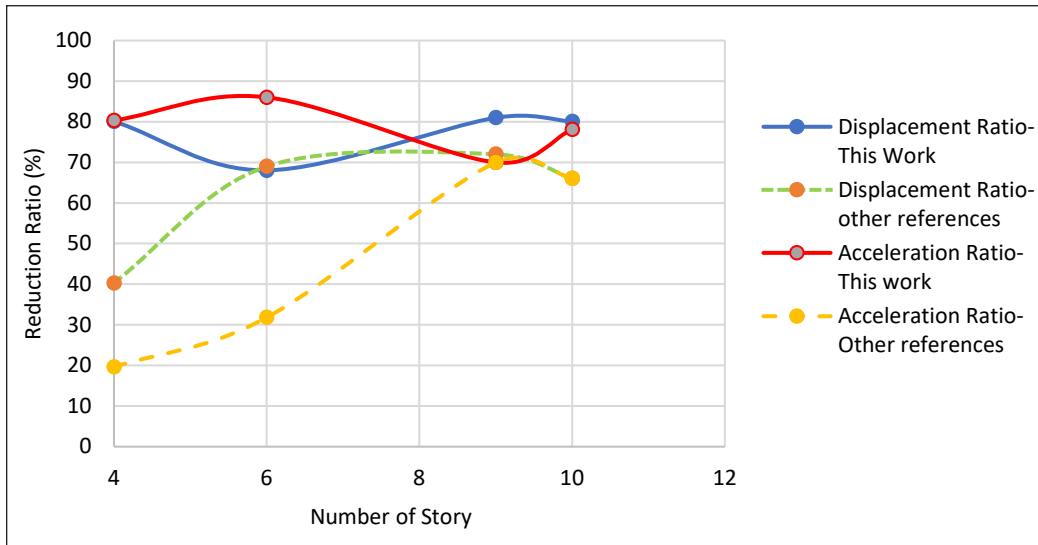


Figure 9. Comparison of results of this study with other references (Table 5)

that the displacement reductions are about 80% for 4, 9, and 10 stories scenarios. Palacios et al. (2020) reported about 50% and 40% reductions in the overall inter story-drift and acceleration peak-value, respectively. Kim & An (2016) concluded that maximum roof displacement and the inter-story drift ratio were reduced by 30% and 40%, respectively.

Moreover, to assess the effectiveness of the proposed method, numerical results are presented for 6, 9, and 10 stories. As can be seen in Table 5, the analogy of Sanghai & Pawade (2021), Miguel and Pérez (2017), and Lopez and Miguel (2015) approved that the displacement reductions of 82% and 80% can be achieved for 4, 9, and 10-stories scenarios, respectively. Regarding the acceleration, the reduction ratios are 80% and 78%. Also, the inter-story drift is investigated. It is under control in such a way that it is about 70% for all investigated structures.

The results of present work with the mentioned references has been comprised Table 5 and illustrated in Figure 9 to better depict the performance of the proposed optimisation method. Acceleration reduction ratios, based on this study, are higher than other references for various buildings. Moreover, the results for displacement reduction ratio for various investigated buildings show that the proposed method is more efficient than other references.

There are no height limitations and 4, 6, 9, and 10 stories are considered a prototype. As seen in Equations 2, 3, 17, 18, 19, and 20, the analysis is parametric, and the method is applicable for various numbers of stories (n_{story}). In fact, by increasing the number of buildings, the degree of freedom (DOFs) and relevant matrix dimension would be regenerated based on that building. However, it is worth noting that for tall buildings, there are specific considerations.

CONCLUSION

This paper proposed an intelligent control system that enabled simultaneous control of acceleration and displacement in a friction damped structure. The functionality of the proposed system was formulated as an optimisation method. A combined analysis approach named MAHA was presented to solve the problem, combining HL-MAFD and SGA's heuristic algorithm. Based on the results of this study, the following conclusions may be drawn:

- By using the proposed intelligent control system, the optimal value of slip load could be found that resulted in considerable control of acceleration and displacement of structures. The obtained results at these optimum slip loads showed the displacement reduction of 82% and 80% for 4, 6, 9, and 10 story structures, respectively. Regarding the acceleration, the reduction ratio is 80% and 78%. Also, the inter-story drift was investigated. It was under control in such a way that it was about 71% to 86% in all mentioned structures.
- The proposed approach was designed parametric and could be applied to various structures under different types of earthquakes. The numerical simulations concluded that the control system could be easily adjustable by changing optimisation method's acceleration and displacement ratio threshold.
- The proposed approach would be extended to tall and high-rise buildings regarding the high rise design considerations.
- By analysing the responses of structures under optimum slip load, the intelligent control system gives a statistical view of the behaviour of structures during the designing phase. The engineers could find the controlled responses of structures on that area and design a suitable friction damper based on the optimum slip load. Thus, this would be more beneficial in strengthening structures against earthquake damages in each specific area.
- The proposed control system would reduce the financial loss because of oversizing by allowing the slip load of friction damper to be designed based on the particular structure and area.

The proposed methodology is recommended as an effective and economical tool for controlling the damage of structures.

ACKNOWLEDGEMENT

The authors acknowledge the support of the Islamic Azad University of Central Tehran Branch.

REFERENCES

- Apostolakis, G., & Dargush, G. (2010). Optimal seismic design of moment-resisting steel frames with hysteretic passive devices. *Earthquake Engineering and Structural Dynamics*, 39(4), 355-376. <https://doi.org/10.1002/eqe.944>
- Bhaskararao, R., & Jangid, S. (2006). Seismic analysis of structures connected with friction dampers. *Journal of Engineering Structures*, 28(5), 690-703. <https://doi.org/10.1016/j.engstruct.2005.09.020>
- Domenico, D., Ricciardi, G., & Zhang, R. (2020). Recent advances in the design of structures with passive energy dissipation systems. *Journal of Applied Sciences*, 10, 1-6. <https://doi.org/10.3390/app10082819>
- Fallah, N., & Honarparst, S. (2013). NSGA-II based multi objective optimization in design of pall friction dampers. *Journal of Constructional Steel Research*, 89, 75-85. <https://doi.org/10.1016/j.jcsr.2013.06.008>
- Fateh, A., Hejazi, F., Ramanathan, R., & Jaffar, S. (2016). Seismic response of a light rail transit station equipped with braced viscous damper. *Pertanika Journal of Science & Technology*, 24(2), 273-283.
- Feliciano, C. (2015). Design optimization for plane structures equipped with friction dampers. *Institute Superior Tecnico, Lisboa, Portugal*, 1-10.
- Kim, J., & An, S. (2016). Optimal distribution of friction dampers for seismic retrofit of a reinforced concrete moment frame. *Advances in Structural Engineering*, 20(10), 1523-1539. <https://doi.org/10.1177/1369433216683197>
- Lee, H., Park, H., Lee, K., & Min, K. W. (2008). Allocation and slip load of friction dampers for a seismically excited building structure based on story shear force distribution. *Engineering Structures*, 30(4), 930-940. <https://doi.org/10.1016/j.engstruct.2007.03.020>
- Lee, S., Park, J., Moon, B., & Min, K. (2008). Design of bracing-friction damper system for seismic retrofitting. *Smart Structures and Systems*, 4(5), 685-696. <https://doi.org/10.12989/sss.2008.4.5.685>
- Logan, D. (2007). *A first course in the finite element method*. Nelson Publishing.
- Lopez, S., & Miguel, L. (2015). A firefly algorithm for the design of force and placement of friction dampers for control of man-induced vibrations in footbridges. *Journal of Optimization and Engineering*, 16(3), 633-661. <https://doi.org/10.1007/s11081-014-9269-3>
- Majd, A., Damerji, H., Hallal, J., & Fakhri, M. (2019). Effectiveness of friction dampers on the seismic behavior of high rise building vs shear wall system. *Engineering Reports*, 1(5), 1-14. <https://doi.org/10.1002/eng2.12075>
- Miguel, F., & Lopez, R. (2018). Methodology for the simultaneous optimization of location and parameters of friction dampers in the frequency domain. *Engineering optimization, Taylor and Francis Journal*, 50(12), 2108-2122. <https://doi.org/10.1080/0305215X.2018.1428318>
- Miguel, F., & Pérez, S. (2017). Optimization of location and forces of friction dampers. *REM International Engineering Journal*, 70(3), 273-279. <https://doi.org/10.1590/0370-44672015700065>
- Nizic, A., & Mestrovic, D. (2011). Seismic dampers in engineering structures. *Journal of the Croatian Association of Civil Engineering*, 63(7), 661-667.

- Palacios, F., Masswgu, J., Rossel, M., & Karimi, H. (2020). Distributed passive actuation schemes for seismic protection of multibuilding systems. *Journal of Applied Science*, 10(7), 1-30. <https://doi.org/10.3390/app10072383>
- Pall, S. (1996, June 23-26). Friction-dampers for seismic control of buildings a Canadian experience. In *Proceeding of the World Conference on Earthquake Engineering* (pp. 1-8). Montreal, Canada.
- Pasquin, C. (2004, August 1-6). Friction dampers for seismic rehabilitation of eaton's building. In *Proceeding of the World Conference on Earthquake Engineering* (pp. 1-10). Vancouver, Canada.
- Perez, S., & Miguel, L. (2017a). A new assessment in the simultaneous optimization of friction dampers in plane and spatial civil structures. *Journal of Mathematical Problems in Engineering*, 2017, Article 6040986. <https://doi.org/10.1155/2017/6040986>
- Perez, S., & Miguela, F. (2017b). Robust simultaneous optimization of friction damper for the passive vibration control in a Colombian building. *Journal of Procedia Engineering*, 199, 1743-1748. <https://doi.org/10.1016/j.proeng.2017.09.430>
- Rashidi, H., Khanlari, K., Zarfam, P., & Ashtiany, M. G. (2020). A novel approach of active control of structures based on the critically damped condition. *Journal of Vibration and Control*, 0(0), 1-13. <https://doi.org/10.1177/1077546320944300>
- Sanghai, S., & Pawade, P. (2020). Effectiveness of friction dampers on seismic response of structure considering soil-structure interaction. *Journal of the Croatian Association of Civil Engineering*, 72(1), 33-44. <https://doi.org/10.14256/JCE.1982.2017>
- Sanghai, S., & Pawade, P. (2021). Optimal placement of friction dampers in building using considering nonlinearity of soil. *Springer Journal of Innovative Infrastructure Solutions*, 6(28), 1-18. <https://doi.org/10.1007/s41062-020-00395-8>
- Shaw, S. (1986). On the dynamic response of a system with dry friction. *Journal of Sound and Vibration*, 108(2), 305-325. [https://doi.org/10.1016/S0022-460X\(86\)80058-X](https://doi.org/10.1016/S0022-460X(86)80058-X)

APPENDIX

Supplementary Data

To analyse the behaviour of the structure using the proposed method, we need to form a reduced general equation of motion as mentioned in Equation 8. To this end, we need to calculate the system stiffness matrix accurately. In the following, the analysis steps for a four-story structure with a frictional damper are addressed. The frame structure has been shown in Figure 4. The nodes matrix is shown in Equations 11 and 12. The number of elements (NEL) is 20, and the total number of degrees of freedom ($NDOF$) is 36.

$$NEL = 20, DOF = e + i = 36, e = 4, i = 32 \quad (11)$$

$$Nodes = \begin{pmatrix} 0 & 400 & 0 & 400 & 0 & 400 & 0 & 400 & 0 & 400 & 200 & 200 & 200 & 200 \\ 0 & 0 & 300 & 300 & 600 & 600 & 900 & 900 & 1200 & 1200 & 150 & 450 & 750 & 1050 \end{pmatrix} \quad (12)$$

Also, elements matrix is (Equation 13):

$$Elements = \begin{pmatrix} 1 & 2 & 3 & 4 & 5 & 6 & 7 & 8 & 3 & 5 & 7 & 9 & 1 & 11 & 3 & 12 & 5 & 13 & 7 & 14 \\ 3 & 4 & 5 & 6 & 7 & 8 & 9 & 10 & 4 & 6 & 8 & 10 & 11 & 4 & 12 & 6 & 13 & 8 & 14 & 10 \end{pmatrix} \quad (13)$$

The degree of freedom matrix and the member code matrix are the following (Equation 14 and 15):

$$DOF = \begin{pmatrix} 0 & 0 & 1 & 1 & 2 & 2 & 3 & 3 & 4 & 4 & 29 & 31 & 33 & 35 \\ 0 & 0 & 5 & 6 & 7 & 8 & 9 & 10 & 11 & 12 & 21 & 22 & 23 & 24 \\ 0 & 0 & 13 & 14 & 15 & 16 & 17 & 18 & 19 & 20 & 25 & 26 & 27 & 28 \end{pmatrix} \quad (14)$$

$$MCM^i = stack(DOF^{member_{2,j}}, DOF^{member_{3,j}}) \quad (15)$$

The total stiffness matrix of the structure that needs to solve the general equation of motion would be obtained via Equation 16:

$$K_{sys} = \sum_{i=1}^{NEL} T_i^T R_i^T k_i R_i T_i \quad (16)$$

Also, k_i is the member's stiffness matrix in rank of 6×6 (Logan, 2007). $K_{mm}, K_{ms}, K_{ss}, K_{sm}, K_{ss}$ are submatrices of K_{sys} and defined as Equation 17-20:

$$K_{mm} = submatrix(K_{sys}, 1, n_{story}, 1, n_{story}) \quad (17)$$

$$K_{ms} = submatrix(K_{sys}, 1, n_{story}, n_{story} + 1, DOF) \quad (18)$$

$$K_{sm} = submatrix(K_{sys}, n_{story} + 1, DOF, 1, n_{story}) \quad (19)$$

$$K_{ss} = submatrix(K_{sys}, n_{story} + 1, DOF, n_{story} + 1, DOF) \quad (20)$$

Finally, the K matrix is obtained according to Equation 6b.



Classification of Existing Health Model of India at the End of the Twelfth Plan using Enhanced Decision Tree Algorithm

Ashok Kumar*, Arun Lal Srivastav, Ishwar Dutt and Karan Bajaj

Chitkara University School of Engineering and Technology, Chitkara University, Himachal Pradesh, 174103 India

ABSTRACT

The high rate of urbanisation has increased the need for state-of-art health models that can meet the growing needs of society during any pandemic. Information-theoretic algorithms based on decision tree can mine the data to establish standards for the final decision by classifying the related data. Classification is an effective tool to analyse the existing health system in India's states and union territories. For this purpose, the data is categorised and then treated with the enhanced Shannon Entropy-based C4.5 decision tree algorithm to set some rules. These rules are capable of finding the major gaps in the health care systems after the analysis. Supposedly, these gaps are taken care of properly in the affected regions. In that case, the health care models will accomplish the endeavouring Sustainable Development Goals.

Keywords: C4.5 Algorithm, classification algorithms, decision tree, health model, Shannon entropy

ARTICLE INFO

Article history:

Received: 23 January 2021

Accepted: 24 May 2021

Published: 28 October 2021

DOI: <https://doi.org/10.47836/pjst.29.4.06>

E-mail addresses:

ashok.kumar@chitkarauniversity.edu.in (Ashok Kumar)
arun.srivastav@chitkarauniversity.edu.in (Arun Lal Srivastav)
ishwar.dutt1@chitkarauniversity.edu.in (Ishwar Dutt)
karan.bajaj@chitkarauniversity.edu.in (Karan Bajaj)

*Corresponding author

INTRODUCTION

There has been growth in unregulated private health service providers due to the high rate of urbanisation. Hence, it has become cumbersome for existing health models to meet high expectations and make a better choice from many service providers. Therefore, these primary health care services, which are easily accessible and the first point of contact, need to be improved to provide adequate care and achieve the expected health outcomes (Kruk et al., 2015; Mackintosh et al., 2016; Zeng et al., 2015).

Potential primary health care models can address the outbreak of the disease on time, before they become epidemic, through established and equipped delivery processes. Through such well-managed primary health care systems, there is a possible reduction in bad health in the worst-affected regions. Moreover, these systems can also support to get better health results (Kruk et al., 2010; Shi, 2012).

The importance of improving health systems is that the representatives of various regions recognised the United Nations' Millennium Development Goals during the Millennium Summit in September 2000. Their target is to monitor the development in the health sector and its outcome from 1990 to 2015 (Assembly, 2000).

Much remarkable work has been done to find the various issues in health care models that need to be taken care of. For example, some discussed the gaps within health care processes and their outcome by analysing the existing facilities and through several health care visits and found the low-quality standard in other domains like user experience, evidence-based care and population health management (Macarayan et al., 2018). Virus outbreaks in healthcare facilities for the elderly in Japan were analysed during the winter season of 2004 to 2005 (Okada et al., 2006). Regardless of many policies, women are not getting adequate quality maternity care; efforts are required to improve these care models (Alkema et al., 2016; Afulani et al., 2019).

Considerable efforts are required to address the issues and find the solution of developing an effective health care model. As an effective tool, data mining can deal with such issues by mining available health-related complex data sets. In data mining, various problems have been solved to extract potential knowledge from unorganised data, using various measures, like information-theoretic measures (Chen et al., 1996), local generalised quadratic distance metrics (Karim & Frank, 2017) and means like clustering of imbalanced high-dimensional media data (Sarka et al., 2018; Antonella & Mariangela, 2017; Panagiotis & Christos, 2016). Classification, which is one of the main objectives of data mining, is an effective tool to analyse the training set and study a classified model (Gondek & Hofmann, 2007; Zhang et al., 2006). Maria and Gunter (2016) found the decision tree algorithm as one of the most effective and commonly used key algorithms to build a predictive model among various classification algorithms. Initially, it is applied on a training set so that some classification criteria can be set and the unknown classes of the data are classified. The algorithm identifies, the appropriate property to every node by the gained information (Zhu & Wen, 2010). Refer Rokach and Maimon (2014) and Tzirakis and Tjortjis (2017) for more details about their advancements.

There are many studies on health care services to determine their effectiveness (Jamaludin et al., 2020; Jonsson et al., 2020). However, identifying the regions with a high density population, where the essential health services are more in demand, is another critical parameter that also requires immediate attention for the success of health care models. Furthermore, it will help in finding the sensitive areas during any pandemic. This purpose can be achieved by classifying the related data of the particular regions.

The present study has been motivated by the effectiveness of classification. So the data under consideration have been classified to analyse various parameters of health care models by bifurcating them in various ranges. The enhanced information theory-based classification algorithm C4.5 of data mining has been applied (Wu et al., 2008) to set some rules that are useful for reviewing and updating health care projects or models. The next part of the article includes the introductory part of the C4.5 algorithm compared to other classification methods. At the same time, in a later section, we categorise the attributes of data under consideration. Using the C4.5 algorithm, we have developed decision tree-based constraints. Finally, based on a set of rules obtained, a comparison of the resultant trees have been discussed, and the results with future scope have been concluded at last.

MATERIAL AND METHODS

C4.5 Algorithm

C4.5 algorithm plays a vital role in the development of the decision trees. Among the most commonly used decision tree algorithms, the ID3 algorithm (Quinlan, 1986) is mainly preferred for classification, while the C4.5 algorithm (Salzberg, 1994) is the modification or enhancement of the ID3 algorithm. C4.5 algorithm gets more popular when it is listed as the top 10 algorithms mentioned by Wu et al. (2008). The working procedure of this algorithm is the same as that of the ID3 algorithm. However, the only difference in the attribute selection criteria for a node is by using the split information.

Gained Information is evaluated using Shannon entropy (Shannon, 1948) and then gained ratio is calculated for each attribute. Finally, the attribute with the maximum gained ratio is used for classification. Then, the process is repeated further to develop its subtrees.

The C4.5 algorithm is preferred over other algorithms of classification due to the advantages mentioned in Table 1 (Sharma & Kumar, 2016):

Table 1
Performance of Different Decision Tree Algorithms

Features	Varma Entropy (Varma, 1966)	ID3 (Quinlan, 1986)	C4.5 (Quinlan, 1994)
Data Types	Discrete	Discrete	Discrete and Continuous
Speed	Average	Low	Fast
Pruning	Post Pruning	Post Pruning	Pre Pruning
Attribute Selection Criteria	Gained Information	Gained Information	Split info
Missing Values	Affects	Affects	No effect

Application in Health Model of India at the End of the Twelfth Plan

The data of India's different states and union territories that support the health system has been collected at the end of the Twelfth Plan (OGD, 2015) and is summarised in Table 3. This data is mainly categorised into two classes, C_1 and C_2 , where C_1 is classified as 'g' indicating good health care services. In contrast, C_2 is categorised as 'ng' that indicates 'not good' health care services. Based on the importance in health care models, four attributes (*the number of Primary Health Centers, Sub Centers and Community Health Centers functioning at the end of Twelfth Plan and Rural Population covered by Primary Health Centers*) from the data source have been selected. These attributes are essential in the process of decision making while selecting the appropriate region for health-related projects to be implemented based on the classification of the health model.

Associated average of health care for a particular region is considered 'good' if it is more than the national average. Otherwise, it is considered 'not good'. Finally, the three attribute classes are combined with the fourth having discrete values without any intervals and further are concluded as 'g' or 'ng' based on the majority as summarised in Table 2. Here A_1, A_2, A_3 and A_4 represent the four attributes, while case numbers (Case 1, Case 2 and so on) represents the various possible cases during the process of a class assignment to a particular region.

Table 2

Class Assignment Criteria

Regions	A_1	A_2	A_3	A_4	Classes of Health Care Services
Case 1	g	g	g	g	g
Case 2	g	g	g	ng	g
Case 3	g	g	ng	ng	ng
Case 4	g	ng	ng	ng	ng
Case 5	ng	ng	ng	ng	ng

Using the Shannon entropy-based C4.5 algorithm (Shannon, 1948), we developed a decision tree and compared it with Kumar et al. (2016), in which modified ID3 algorithm based on the Varma entropy measure (Varma, 1966) was used for specific values of two parameters such as α and β the same data with different specifications attributes. In the data used by Kumar et al. (2016), all the attributes have intervals, while in the present study, we deal with discrete values without intervals for one particular attribute. During the construction of the decision tree, the attributes data with discrete values have been divided at the threshold into two groups. Hence, only two branches emerge from it. In contrast,

in other attributes, branches are equal to the number of intervals and consequently result in more rules.

The first three attributes (*Primary Health Centers, Sub Centers and Community Health Centers*), based upon their values either less than or greater than the national average per unit population, are divided into four different ranges. Following are the details of all four attributes.

PHC stands for average population covered by *Primary Health Centers* functioning at the end of the Twelfth Plan, with four ranges: less than 26000, 26000-47000, 47001-61000 and greater than 61000.

SBC stands for average population covered by *Sub Centers* functioning at the end of the Twelfth Plan, with four ranges: less than 3600, 3600-4500, 4501-7100 and greater than 7100;

CHC is representing the average population covered by *Community Health Centers* functioning at the end of the Twelfth Plan with four ranges: less than 140000, 140000-220000, 220001-320000 and greater than 320000; and

RPHC is represents the average *Rural Population covered by Primary Health Centers* with discrete data without any interval and varies from 0 to 83808.

Table 3
Health Model of INDIA

Sr. no.	PHC	SBC	CHC	RPHC	Classes of Health Care Services
1	<26000	<3600	<140000	1077	ng
2	47001-61000	4501-7100	220001-320000	32979	g
3	<26000	4501-7100	<140000	9114	ng
4	26000-47000	4501-7100	140000-220000	26437	ng
5	47001-61000	>7100	>320000	4900	g
6	<26000	>7100	>320000	0	ng
7	26000-47000	4501-7100	140000-220000	25042	ng
8	47001-61000	4501-7100	>320000	26159	g
9	>61000	>7100	<140000	20132	ng
10	>61000	>7100	<140000	83808	g
11	>61000	4501-7100	>320000	26273	g
12	47001-61000	>7100	140000-220000	29961	ng
13	47001-61000	>7100	220001-320000	36364	g

Table 3 (Continued)

Sr. no.	PHC	SBC	CHC	RPHC	Classes of Health Care Services
14	<26000	<3600	<140000	12630	ng
15	<26000	4501-7100	140000-220000	14298	ng
16	>61000	>7100	140000-220000	75924	g
17	26000-47000	4501-7100	>320000	16780	ng
18	26000-47000	>7100	140000-220000	21075	ng
19	<26000	4501-7100	<140000	3535	ng
20	>61000	>7100	140000-220000	45426	g
21	>61000	>7100	220001-320000	33990	g
22	26000-47000	4501-7100	140000-220000	23784	ng
23	26000-47000	4501-7100	<140000	21958	ng
24	<26000	<3600	<140000	9218	ng
25	<26000	4501-7100	<140000	11171	ng
26	26000-47000	4501-7100	<140000	26797	ng
27	47001-61000	>7100	>320000	16467	g
28	>61000	>7100	140000-220000	40619	g
29	26000-47000	4501-7100	<140000	24736	ng
30	<26000	3600-4500	220001-320000	19042	ng
31	47001-61000	>7100	140000-220000	27195	ng
32	26000-47000	3600-4500	140000-220000	32291	ng
33	47001-61000	>7100	220001-320000	44414	g
34	26000-47000	4501-7100	140000-220000	27381	ng
35	>61000	>7100	220001-320000	68408	g

Now, by using Shannon entropy (Shannon, 1948), the amount of the information required for the object data is measured, using the following Equation 1:

$$I(C_1, C_2, C_3, \dots, C_c) = - \sum_{i=1}^c p_i \log_2 p_i, \quad (1)$$

with p_i represents the probability associated with each class.

In Table 3, the complete data is divided into two classes C_1 and C_2 where 13, 'g' is in C_1 and 22, 'ng' is in C_2 . Therefore

$$I(C_1, C_2) = \left(-\frac{13}{35}\right) * \log\left(\frac{13}{35}\right) - \left(\frac{22}{35}\right) * \log\left(\frac{22}{35}\right) = 0.951762676$$

Further, for the number of values, m_j in the range R_j of attribute A_k then entropy of A_k , $E(A_k)$ is given as Equation 2:

$$E(A_k) = \sum_{j=1}^r \frac{m_j}{N} \sum_{i=1}^c p_i \log_2 p_i \tag{2}$$

Here, association with the four different attributes are given as follows:

$$E(A_1) = E(PHC) = 0.309678301$$

$$E(A_2) = E(SBC) = 0.702953112$$

$$E(A_3) = E(CHC) = 0.685134682$$

$$E(A_4) = E(RPHC) = 0.378114904$$

Net gained information $Gain_info(A_k)$ for different attributes are given by Equation 3

$$Gain_info(A_k) = I(C_1, C_2, C_3, \dots, C_k) - E(A_k) \tag{3}$$

Hence, we have

$$Gain_info(A_1) = 0.642084374 \text{ bits}$$

$$Gain_info(A_2) = 0.248809563 \text{ bits}$$

$$Gain_info(A_3) = 0.266627993 \text{ bits}$$

$$Gain_info(A_4) = 0.573647772 \text{ bits}$$

Further, information of split, $Split_info(A_k)$ has been measured for each attribute using the following Equation 4

$$Split_info(A_k) = \sum_{j=1}^r \frac{m_j}{N} \log_2 \left\{ \frac{m_j}{N} \right\} \tag{4}$$

Therefore, we get

$$Split_info(A_1) = 1.993608561.$$

$$Split_info(A_2) = 1.587522864.$$

$$Split_info(A_3) = 1.926630222.$$

$$Split_info(A_4) = 0.863120569.$$

Net gained ratio information i.e. $Gain_ratio(A_k)$ for each attribute ' A_k ' is calculated using the Equation 5

$$Gain_ratio(A_k) = \frac{Gain_info(A_k)}{Split_info(A_k)} \tag{5}$$

Thus, we have

$$Gain_ratio(A_1) = 0.32207143 \text{ bits}$$

$$Gain_ratio(A_2) = 0.15672817 \text{ bits}$$

$$Gain_ratio(A_3) = 0.13839085 \text{ bits}$$

$$Gain_ratio(A_4) = 0.66462067 \text{ bits}$$

We note that the ratio of the fourth attribute is obtained with discrete values and without intervals. For example, RPHC is the maximum. Therefore this attribute is designated as the root of the decision tree and will divide the data initially into two parts at the threshold. Hence, only two branches will emerge for root. Further, the above process of gained ratio is repeated for branches or subtrees until we get the terminal nodes as 'g' or 'ng'. The resultant decision tree for the data in Table 3, using the C4.5 Algorithm, is given in Figure 1.

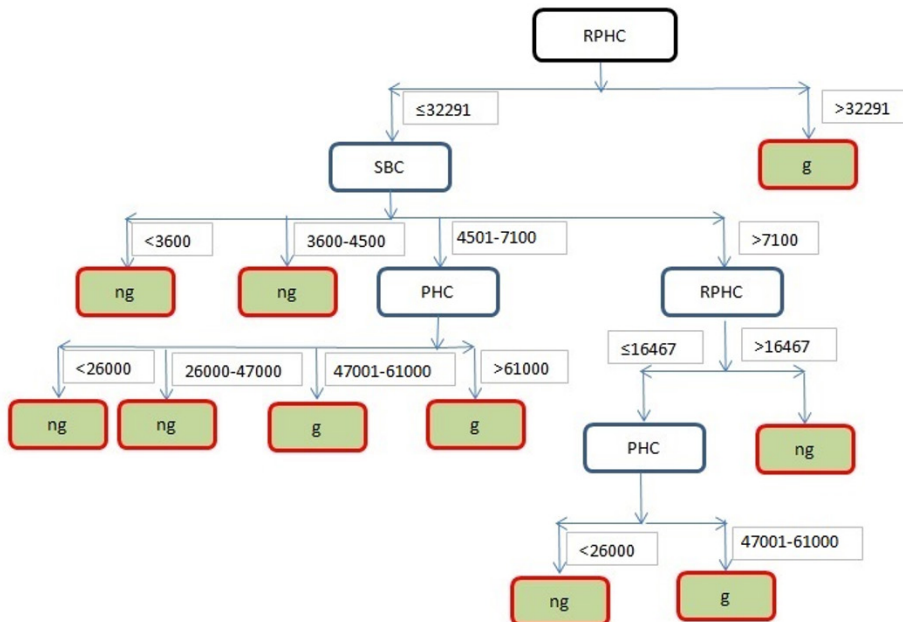


Figure 1. C4.5 Algorithm based Decision Tree

The decision tree obtained by Kumar et al. (2016) based on Varma (1966) is given in Figure 2, and for rules induced, we can refer to Kumar et al. (2016). Information required, entropy values, split information and gained information ratios are calculated for each attribute of the training data set. The root of the decision tree has the attribute with the highest gained ratio, and the other remaining attributes are arranged as in the nodes of its branches. The same procedure is repeated for the nodes of the branches. The rules formed while moving from the root towards the leaf or terminal node of the final decision tree are helpful in setting classification criteria. These classification rules form the strong base for the systematic analysis and the development of the system.

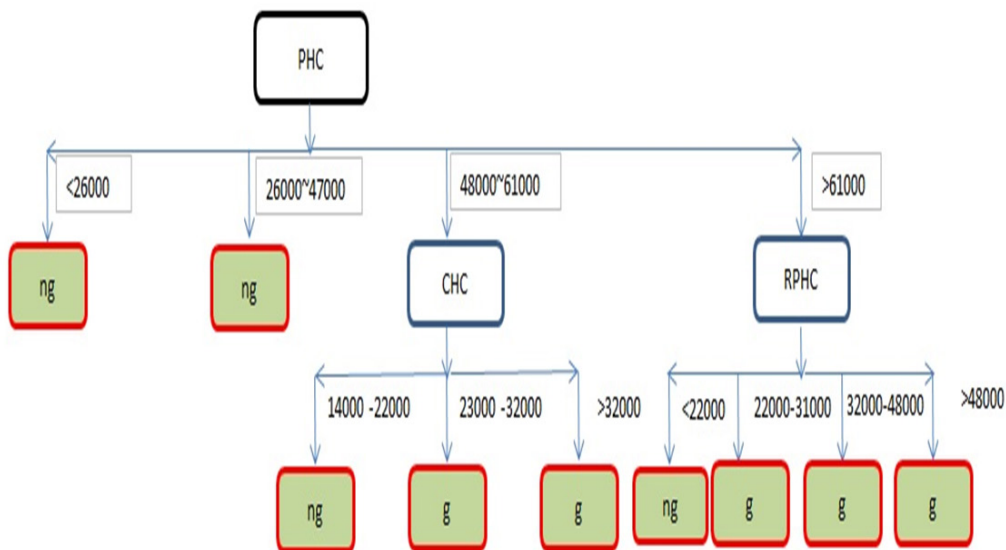


Figure 2. Varma Entropy-based Decision Tree

RESULTS AND DISCUSSION

Rules Induced

Some rules have been induced using ‘if-then’, based on the resultant C4.5 algorithm-based decision tree, given in Figure 1. Thus, further improving the decision making criteria during the evaluation or implementation of the health-related projects for the development of the health care system. These rules can be summarised as follows:

1. If RPHC is less than or equal to 32291 and SBC is less than 4500, then for any value of PHC and CHC, health care services are ‘not good’ in that region.

2. If RPHC is less than or equal to 32291 and SBC is within 4501 to 7100 and PHC is less than 47000, then for any value of CHC, health services are 'not good' in that region.
3. If RPHC is less than or equal to 32291 and SBC is within 4501 to 7100 and PHC is greater than 47000, then for any value of CHC, health services are 'good' in that region.
4. If RPHC is less than or equal to 32291 and SBC is greater than 7100, again RPHC is less than or equal to 16467 and PHC is less than 26000, then for any value of CHC, health services are 'not good' in that region.
5. If RPHC is less than or equal to 32291 and SBC is greater than 7100, again RPHC is less than or equal to 16467 and PHC is within 47001 to 61000, then for any value of CHC, health services are 'good' in that region.
6. If RPHC is less than or equal to 32291 and SBC is greater than 7100 and RPHC is more than 16467, then for any value of CHC, health services are 'not good' in that region.
7. If RPHC is greater than 32291 then for any value of SBC, PHC and CHC, health services are 'good' in that region.

The rules have been framed while moving from the root towards the terminating nodes in the resultant decision tree. Also, rules 4 and 5 can be further simplified by combining the conditions for RPHC as less than or equal to 16467. The regions with good health care models satisfy rules 3, 5 and 7, while rules 1, 2, 4 and 6 help identify the regions where health care models need to be updated.

Comparison between the Decision Trees

Two decision trees obtained by the modified ID3 algorithm based on Varma Entropy and C4.5 Algorithm have been compared and summarised in Table 4. Some conditions or rules have been formed with the help of decision trees so that the correct information can be collected. Thus, proper decisions can be made before implementing required policies or projects for the improvement of health care services. Furthermore, the rules obtained from the differently trained data (by considering the values of one attribute without intervals) and then applying the C4.5 Algorithm have resulted in more precise rules than those obtained by Kumar et al. (2016).

Table 4

Comparison of the Decision Trees

Sr. no.	Factors	Varma Entropy based Decision Tree	C4.5 Algorithm based Decision Tree
1	Attribute at root	PHC	RPHC
2	Minimum branch length	1	1
3	Maximum branch length	2	4
4	Smallest Rule	If 'PHC' less than 26000 then 'ng'	If 'RPHC' is greater than 32291 then 'g'
5	Largest Rule	If 'PHC' is greater than 61000 and 'RPHC' is greater than 48000 then 'g'	If 'RPHC' is less than or equal to 32291, 'SBC' is greater than 7100, 'RPHC' is greater than equal to 16467 and 'PHC' is less than 26000 then 'ng'.
6	Rules at depth 1	2	1
7	Rules at depth 2	7	2
8	Rules at depth 3	NA	5
9	Rules at depth 4	NA	2
10	Total number of Rules	5	8

CONCLUSION

The proper decision-making process is always helpful in the successful completion of time-bound projects. The selection of the appropriate classification method is based upon the nature of the training data set. The rules were based on the decision tree obtained by categorised data using the C4.5 algorithm is compared with that of the improved ID3 algorithm, based upon Varma entropy for a particular value of parameters. It was observed that, on using discrete values without intervals, better results are obtained. Thus, in comparison, if the C4.5 algorithm is used for classification, after categorisation of the collected data into different classes, more refined rules have been developed. Such rules help analyse the systematic and progressive development of any introduced system. It has been observed from the rules induced that available processes and measures need improvement in its current models to capture key elements of health facilities. Moreover, the unique features of regions where the health care models are in good condition can be implemented in those regions where improvement is required.

ACKNOWLEDGEMENT

Authors appreciate the incomparable support and inspiration by Honourble Chancellor Dr Ashok K. Chitkara and Honourble Pro-Chancellor Dr Madhu Chitkara, Chitkara University, Himachal Pradesh, India, to write this manuscript.

REFERENCES

- Afulani, P. A., Phillips, B., Aborigo, R. A., & Moyer, C. A. (2019). Person-centred maternity care in low-income and middle-income countries: Analysis of data from Kenya, Ghana, and India. *The Lancet Global Health*, 7(1), e96-e109. [https://doi.org/10.1016/S2214-109X\(18\)30403-0](https://doi.org/10.1016/S2214-109X(18)30403-0)
- Alkema, L., Chou, D., Hogan, D., Zhang, S., Moller, A. B., Gemmill, A., Fat, D. M., Boerma, T., Temmerman, M., Mathers, C., & Say, L. (2016). Global, regional, and national levels and trends in maternal mortality between 1990 and 2015, with scenario-based projections to 2030: A systematic analysis by the UN Maternal Mortality Estimation Inter-Agency Group. *The Lancet*, 387(10017), 462-474. [https://doi.org/10.1016/S0140-6736\(15\)00838-7](https://doi.org/10.1016/S0140-6736(15)00838-7)
- Antonella, P., & Mariangela, S. (2017). Weighted distance-based trees for ranking data. *Advances in Data Analysis and Classification*, 13(2), 427-444. <https://doi.org/10.1007/s11634-017-0306-x>.
- Assembly, U. G. (2000, September 6-8). United Nations millennium declaration. In *Millenium Summit of the United Nations*. New York.
- Chen, M. S., Han, J., & Yu, P. S. (1996). Data mining: An overview from a database perspective. *IEEE Transactions on Knowledge and Data Engineering*, 8(6), 866-883. <https://doi.org/10.1109/69.553155>
- Gondek, D., & Hofmann, T. (2007). Non-redundant data clustering. *Knowledge and Information Systems*, 12(1), 1-24. <https://doi.org/10.1007/s10115-006-0009-7>
- Jamaludin, M. H., Wah, Y. B., Nawawi, H. M., Yung-An, C., Rosli, M. M., & Annamalai, M. (2020). Classification of familial hypercholesterolaemia using ordinal logistic regression. *Pertanika Journal of Science & Technology*, 28(4), 1163-1177. <https://doi.org/10.47836/pjst.28.4.03>
- Jonsson, Å., Orwelius, L., Dahlstrom, U., & Kristenson, M. (2020). Evaluation of the usefulness of EQ-5D as a patient-reported outcome measure using the Paretian classification of health change among patients with chronic heart failure. *Journal of Patient-Reported Outcomes*, 4(1), 1-11. <https://doi.org/10.1186/s41687-020-00216-7>
- Karim, A., & Frank, P. F. (2017). Local generalized quadratic distance metrics: Application to the k-nearest neighbors. *Advances in Data Analysis and Classification*, 12(2), 341-363. <https://doi.org/10.1007/s11634-017-0286-x>.
- Kruk, M. E., Nigenda, G., & Knaul, F. M. (2015). Redesigning primary care to tackle the global epidemic of noncommunicable disease. *American Journal of Public Health*, 105(3), 431-437. <https://doi.org/10.2105/AJPH.2014.302392>
- Kruk, M. E., Porignon, D., Rockers, P. C., & Van Lerberghe, W. (2010). The contribution of primary care to health and health systems in low-and middle-income countries: A critical review of major primary care initiatives. *Social Science & Medicine*, 70(6), 904-911. <https://doi.org/10.1016/j.socscimed.2009.11.025>

- Kumar, A., Taneja, H. C., & Chitkara A. K. (2016, January 18-19). Analysis of health conditions using generalized information measure based ID3 algorithm. In *4th Annual International Conference on Operations Research and Statistics (ORS-2016)* (pp. 33-37). Singapore. https://doi.org/10.5176/2251-1938_OR16.11
- Macarayan, E. K., Gage, A. D., Doubova, S. V., Guanais, F., Lemango, E. T., Ndiaye, Y., Waiswa, P., & Kruk, M. E. (2018). Assessment of quality of primary care with facility surveys: A descriptive analysis in ten low-income and middle-income countries. *The Lancet Global Health*, *6*(11), e1176-e1185. [https://doi.org/10.1016/S2214-109X\(18\)30440-6](https://doi.org/10.1016/S2214-109X(18)30440-6)
- Mackintosh, M., Channon, A., Karan, A., Selvaraj, S., Cavagnero, E., & Zhao, H. (2016). What is the private sector? Understanding private provision in the health systems of low-income and middle-income countries. *The Lancet*, *388*(10044), 596-605. [https://doi.org/10.1016/S0140-6736\(16\)00342-1](https://doi.org/10.1016/S0140-6736(16)00342-1)
- Maria, T. G., & Gunter, R. (2016). Probabilistic clustering via Pareto solutions and significance tests. *Advance Data Analysis and Classification*, *12*(2), 179-202. <https://doi.org/10.1007/s11634-016-0278-2>.
- OGD. (2015). *Open government data (OGD) platform India*. Retrieved June 6, 2015, from <https://data.gov.in/>.
- Okada, M., Tanaka, T., Oseto, M., Takeda, N., & Shinozaki, K. (2006). Genetic analysis of noroviruses associated with fatalities in healthcare facilities. *Archives of Virology*, *151*(8), 1635-1641. <https://doi.org/10.1007/s00705-006-0739-6>
- Panagiotis, T., & Christos, T. (2016). T3C: Improving a decision tree classification algorithm's interval splits on continuous attributes. *Advances in Data Analysis and Classification*, *11*(2), 353-370. <https://doi.org/10.1007/s11634-016-0246-x>.
- Quinlan, J. R. (1986). Induction of decision trees. *Machine Learning*, *1*(1) 81-106. <https://doi.org/10.1007/BF00116251>
- Rokach, L., & Maimon, O. (2014). *Data mining with decision trees: Theory and applications*. World Scientific. <https://doi.org/10.1142/9097>
- Salzberg, S. L. (1994). C4.5: Programs for Machine Learning by J. Ross Quinlan. Morgan Kaufmann Publishers, Inc., 1993. *Machine Learning*, *16*, 235-240. <https://doi.org/10.1007/BF00993309>
- Sarka, B., Maia, Z., Peter, F., Thomas, O., & Christian, B. (2018). Clustering of imbalanced high-dimensional media data. *Advances in Data Analysis and Classification*, *12*(2), 261-284. <https://doi.org/10.1007/s11634-017-0292-z>.
- Shannon, C. (1948). A mathematical theory of communication. *The Bell System Technical Journal*, *27*(3), 379-423. <https://doi.org/10.1002/j.1538-7305.1948.tb01338.x>
- Sharma, H., & Kumar, S. (2016). A survey on decision tree algorithms of classification in data mining. *International Journal of Science and Research*, *4*(4) 2094-2097.

- Shi, L. (2012). The impact of primary care: A focused review. *Scientifica*, 2012, Article 432892. <https://10.6064/2012/432892>
- Tzirakis, P., & Tjortjis, C. (2017). T3C: Improving a decision tree classification algorithm's interval splits on continuous attributes. *Advances in Data Analysis and Classification*, 11(2), 353-370. <https://doi.org/10.1007/s11634-016-0246-x>
- Varma, R. S. (1966). Generalizations of Renyi's entropy of order α . *Journal of Mathematical Sciences*, 1(7), 34-48.
- Wu, X., Kumar, V., Quinlan, J. R., Ghosh, J., Yang, Q., Motoda, H., McLachlan, G. J., Ng, A., Liu, B., Philip, S. Y., & Zhou, Z. H. (2008). Top 10 algorithms in data mining. *Knowledge and information systems*, 14(1), 1-37. <https://doi.org/10.1007/s10115-007-0114-2>
- Zeng, J., Shi, L., Zou, X., Chen, W., & Ling, L. (2015). Rural-to-urban migrants' experiences with primary care under different types of medical institutions in Guangzhou, China. *PloS One*, 10(10), Article e0140922. <https://doi.org/10.1371/journal.pone.0140922>
- Zhang, J., Kang, D. K., Silvescu, A., & Honavar, V. (2006). Learning accurate and concise naïve Bayes classifiers from attribute value taxonomies and data. *Knowledge and Information Systems*, 9(2), 157-179. <https://doi.org/10.1007/s10115-005-0211-z>
- Zhu, P., & Wen, Q. (2010). Some improved results on communication between information systems. *Information Sciences*, 180(18), 3521-3531. <https://doi.org/10.1016/j.ins.2010.05.028>

Review Article

An Era of Recommendation Technologies in IoT: Categorisation by techniques, Challenges and Future Scope

Partibha Ahlawat* and Chhavi Rana

Department of Computer Science and Engineering, University Institute of Engineering and Technology, Maharishi Dayanand University, Rohtak, Haryana 124001, India

ABSTRACT

The evolution of the Internet of Things (IoT) accelerates the augmentation of data present on the Internet and possibilities for connections to the more dynamic and heterogeneous devices to the Internet. Recommendation technologies have proven their capabilities of digging the personalised information by proactive filtering in many application domains and can also be a backbone platform in IoT for identifying personalised things, services and relevant artefacts by prevailing over information overload problems. This paper is a comprehensive literature review that categorises IoT recommender systems by exploring the literature's different IoT based recommendation techniques. We conclude the paper by discussing the challenges and future scope for IoT based recommendations techniques to advancing and widening the frontiers of this research area.

Keywords: Context-awareness, IoT, knowledge-base, machine learning, recommender system, social IoT

ARTICLE INFO

Article history:

Received: 26 January 2021

Accepted: 30 July 2021

Published: 28 October 2021

DOI: <https://doi.org/10.47836/pjst.29.4.07>

E-mail addresses:

partibhakhatri@gmail.com (Partibha Ahlawat)

chhavi1jan@yahoo.com (Chhavi Rana)

*Corresponding author

ISSN: 0128-7680
e-ISSN: 2231-8526

INTRODUCTION

Internet of Things

The Internet of Things (IoT) is an integrated network of devices, things, physical objects with many embedded technologies. It is the junction of Internet-oriented vision, things oriented vision and semantics oriented vision (Čolaković & Hadžialić, 2018). IoT gives the addressable contribution in many applications and services like smart cities, smart homes, health monitoring,

wildlife monitoring, e-commerce, transport observations, building and home automation, manufacturing, agriculture, metropolitan scale development, energy management, environment monitoring, and medical enhancements. In the future, IoT will be responsible for hybridised the networks with its non-deterministic and dynamic nature that leads to the connection with billions of devices in a wide area of applications (Cha et al., 2017). Moreover, with the evolution of auto-organisation, self-learning, intelligent entities and virtual objects, IoT will act independently depending on the environment, context information and current circumstances.

Recommender Systems

Recommender System (RS) is the information filtering tool from collected data. The systems offers users and service providers the advantage of filtering the information from the dynamic, flexible, huge volume, rich and diverse data sources according to the users' observed behaviour, preferences and interest. There are many application domains where RS are implemented, like e-commerce, e-libraries, e-business services, e-learning, cognitive science, forecasting services, management science, and information retrieval systems. The recommendation process consists of three phases, i.e. information collection phase, learning phase and recommendation phase (Isinkaye et al., 2015). There are two most used recommendation techniques, collaborative filtering technique and content-based filtering technique. The collaborative filtering (CF) technique recognises the similarity between the users or items to provide recommendations. It is a domain-independent recommendation technique. Collaborative filtering techniques are further divided into memory-based techniques and model-based techniques. Content-based filtering technique takes care of the features or attributes of the items for recommendations. Instead of discovering the similarity between the users, it observes the similarity between the items by vector space model or probabilistic models. Both techniques are associated with limitations like a cold-start problem, data sparsity problem, scalability, content over specialisation and synonymy.

This paper presents a comprehensive review of the literature by exploring IoT recommenders according to a technique used. We finally represent the challenges and future scope related to this area. The rest of the paper is organised as to what are IoT recommender systems and differentiates them for the traditional recommender systems, discusses the various techniques of IoT recommender systems, presents some challenges and future scope.

IoT RECOMMENDER SYSTEMS

IoT generated data is dynamic and flexible, so the traditional recommendation techniques are ineffective and inefficient in IoT based services (Yao et al., 2019). IoT recommender systems are focused on recommendations of things and services (Mashal et al., 2015; Yao et

al., 2016). Recommendations in IoT reduce the personal efforts in discovering the exciting things and services according to user's personal preferences and are favourable for business enhancement and society development. IoT based recommendations require changes in the traditional recommendation methods based only on the characteristics of users and items. Kwon and Kim (2016) proposed a method by adding the characteristics of IoT in the form of social relationships between devices like POR (Partial Object Relationship), SOR (Social Object Relationship), C-LOR (Co-location Object Relationship), OOR (Object-Object Relationship), C-WOR (Co-Work ObjectR) in the traditional recommendation methods to configure a hybrid recommendation approach. Embedded systems of IoT scenarios can utilise the benefits of profile-driven and context-aware recommendations. The prediction quality of the existing recommendation algorithms is also improved by the availability of IoT characteristics and orthogonal data sources (Felfernig et al., 2017). Saleem et al. (2017) proposed a three-layer model by exploiting social IoT for recommendation services among various application domains of IoT. Cha et al. (2017) explained how the IoT platform is helpful for the collection of streaming and user contextual data for designing a real-time recommender system by geofencing. The experiment results of the proposed prototype model show that recommendation takes more time due to the usage of geofencing rather than using beacons.

A novel recommender system in the IoT was introduced by Frey et al. (2015) that deduce the users consumed physical objects by exploring the installed apps in their smartphones or tablets to build a digital inventory to recommend the physical things to new users. The proposed recommender system consists of two parts. The first is an app for data collection and sending recommendation notifications. The second is a server for data processing and to compute personalised recommendations. Sawant et al. (2017) introduced a basic architecture of IoT and CPS (Cyber-Physical System) with decision-making capabilities that provide recommendation services through SMS or Email. The proposed system architecture comprises four layers: selection layer, network layer, service layer and application layer. First the selection layer selects and filters the sensible data provided by users. Then, the network layer, broadcast the selected data to the Service layer. Third, the service layer processed the data using web services and feed the data to the application layer. Finally, the application layer interact with the users and suggest the services. Despite the remarkable advancements and research from the last decade IoT recommendations are complex as compared to the traditional (2D) recommender systems (Pratibha & Kaur, 2018). Table 1 explains how IoT recommender systems are different from traditional recommender systems (Yao et al., 2016; Yao et al., 2019; Felfernig et al., 2019; Felfernig et al., 2017).

Table 1

Differences between IoT Recommender Systems and Traditional Recommender Systems

Sr. No.	Parameters	IoT Recommender Systems (IoT RS)	Traditional Recommender Systems (2D RS)
1.	Recommended Object	Things, Services	Books, Movies, websites
2.	Dynamicity	Dynamic	Static
3.	Heterogeneity and Diversity	Heterogeneous and more Diverse	Homogeneous and less diverse
4.	Context-aware	Yes, need contextual information	Context less
5.	Accuracy	Less	More
6.	Security and Privacy	Should be more aware	Less Aware
7.	Multimodality	Interactive, Persuasive and Multimodal interface	Singleton Interface
8.	Distributed Nature	Yes	Centralised
9.	Spontaneity	More	Less
10.	Spatiotemporal Correlation	Yes, need to be taken care between things and users	Need not to be taken care
11.	Scalability	Yes	No
12.	Data Source	Streamed and orthogonal	Flat and Fixed

TECHNIQUES FOR IOT RECOMMENDER SYSTEMS

Many IoT RS techniques and models are proposed and implemented in the literature for things and services recommendations. To the best of our understanding, the paper has taken care of all available algorithms, models and approaches in IoT recommendations. We categorise the literature into the IoT recommendation techniques such as context-aware, knowledge-based, collaborative filtering-based, group-based, correlation-based, machine learning-based, graph-based and trust-based. The categorisation is according to the dynamic perspective taken care of in the purposed models of IoT recommender systems. The main dynamics for the recommendation techniques in IoT are context-awareness, characteristics of IoT things and applications, trust, IoT data representation and Social IoT.

Collaborative Filtering (CF) is one of the famous approaches used to design a recommender system. It involves depending on the history of users. Besides the challenges faced by the CF algorithms, they are used by some recommendation models in the IoT context. These days, RS are no longer personal recommender systems. Instead, they list

out the recommendations to a group of users and leads to group recommender systems. We consider the IoT RS, which exploits a group's desires and preferences within some correlation and gives suggestions to the whole group under Group-based Recommender Systems. The IoT RS, which exploit the functional knowledge about users, things (devices), IoT services and their identified relationships, are considered under the Knowledge-based IoT recommender Systems. We also put the ontology-based RS in this category, as ontology is the formal knowledge representation to build the IoT RS. Many frameworks of IoT RS have used the context-awareness of geographical locations, state of people, locations of physical objects, the identity of users, and leads to Context-aware IoT RS. Although Context-aware RS faces several challenges like context discovery, privacy issues and security threats, some researchers have used contextual information to develop the IoT-based Recommender Systems.

Some developed recommendation models used the graphical database model to represent the structural schema and relations among data. We consider such models under the Graph-based IoT recommender systems. Graph-based recommendation models have the capability of resolving scalability issues. Furthermore, the social networking application to the IoT creates the scope for a social relationship among things. The system models which suggest the recommendations by introducing the concept of socialisation between things, users and services are considered under the Correlation-based IoT recommendation systems. Machine Learning is an emerging and most desiring field to develop recommendation systems using human learning and real-world knowledge. With hybridisation, Machine Learning was also utilised by many traditional recommender systems to optimise their accuracy. Traditional recommendations techniques are not able to learn from the dynamic human activity pattern in IoT. However, machine learning with deep learning and reinforcement learning give promising opportunities for developing IoT RS. Many developed IoT RS models have extensively used machine learning, so we categorise them under the Machine learning-based IoT Recommender Systems. Figure 1 explains the taxonomy of the IoT recommender systems. The under given section will describe the techniques mentioned above by taking care of proposed models of the literature.

Context-aware IoT Recommender System

Context-aware recommendation techniques in IoT uses the contextual information regarding things, users, services and relationship. Integrating contextual information with traditional recommendation technologies results in multidimensional recommender systems with improved, efficient and accurate recommendations. Yavari et al. (2016) proposed an IoT based contextualised technique that involves Internet-scale data for fast decision making to provide personalised information to the users. Salman et al. (2015) suggested a proactive real-time context-aware RS that provide multi-type recommendation using neural

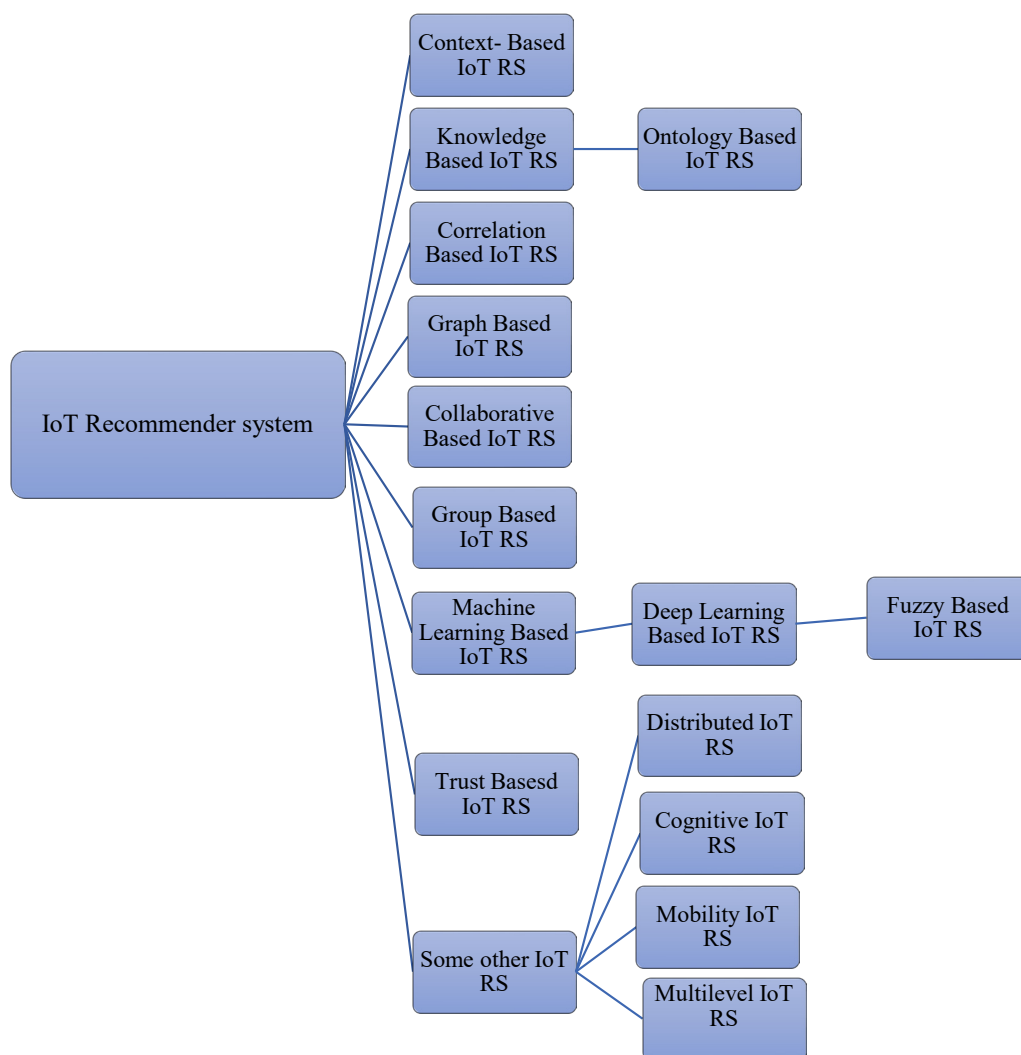


Figure 1. Taxonomy of IoT Recommender Systems

network reasoning power in the IoT paradigm. Twardowski and Ryzko (2016) presented a Multi-Agent System architecture for Big Data processing based mobile context-aware RS. Baltrunas et al. (2011) proposed Matrix Factorisation based context-aware RS, which provide interaction between items and context with less computational cost.

A scenario-based e-commerce recommendation model is introduced by Wu et al. (2019), based on customer interest and scenario-based contextual information in an IoT environment. Distributive cognitive theory is used to differentiate the sensitive scenario by establishing a multi-dimensional customer interest feature vector. Experimental result

shows that the model gives better recommendation accuracy and adaptable for high-quality recommendation services. Ravi et al. (2019) proposed a model CHXplorer composed of two building blocks, i.e., information management and multipurpose intelligent system. It is a mobile decision-support tool that provides practical recommendations to cultural heritage visitors.

Amato et al. (2013) proposed a Context-Aware Recommender System (CARS) model, assisted by users' preferences and multimedia information extracted from a mobile environment of cultural heritage. This model uses the hybrid recommendation technique combined with collaborative filtering over content-based filtering with similarity matrix k-nearest neighbour. Abu-issa et al. (2020) presented the design and implantation of a mobile-based application known as multi-type proactive CARS. It includes the user context and can provide multi-type recommendations. Zia et al. (2018) proposed an agent and context-based model for recommendations on Internet of vehicles scenario by using social and contextual network information. Context-awareness is a significant factor to upgrade the accuracy and efficiency of IoT recommender systems. Table 2 describes the context-aware recommender systems for IoT based scenarios.

Table 2

Context-aware IoT Recommender Systems

Model	Authors and Year	Technique used	Data set	Domain	Metrics
Contextualised Smart Parking Recommender (CSPR)	Yavari et al. (2016)	Context based filtering and aggregation	Melbourne City dataset	Smart city, parking space recommendation service	Query processing time
PMCARS (Proactive Multi-type Context-Aware Recommender System)	Salman et al. (2015)	Collaborative filtering, Neural network	Modeled data	Gas station and Restaurant recommendation	MSE (Accuracy)
RTRS (Real-time recommender system)	Cha et al. (2017)	Collaborative filtering, Cloud computing	Tourism data from city of Saint John in New Brunswick, Canada	Smart Tourism	Standard deviation

Table 2 (Continued)

Model	Authors and Year	Technique used	Data set	Domain	Metrics
MCARS (Mobile Context Aware RS)	Twardowski and Ryzko (2016)	Matrix-factorisation, Stochasting Gradient Descent (SGD)		Dietary/Fitness recommendation	
SERABCI	Wu et al. (2019)	Nearest Neighbour-based Collaborative filtering algorithm	B2C-Platform-Set	E-commerce	MAE
CHXplorer	Ravi et al. (2019)	User-based collaborative filtering		Cultural Heritage	Precision and Recall
MPCARS	Abu-issa et al. (2020)	Classification (Naïve Bayes classifier)	Survey based	Smart city	Accuracy

Knowledge-based IoT Recommender System

The knowledge base is the store of rules, facts and assumptions in a structured or unstructured manner. It is a kind of repository enabled for searching and processing. The object model used to represent the knowledge base is called ontology. A knowledge-based recommender system (KBRS) provides the recommendations by inputs user specifications, item attributes and domain knowledge. KBRS are generally used when sufficient ratings are not available for luxury things, financial services and real estate. Moreover, help to compensate for the Cold-Start problem (Aggarwal, 2016). Based on interface and knowledge, the knowledge base recommender systems are classified into two types, i.e., constraints-based (rule-based) recommender systems and case-based recommender systems. Constraints-base RS takes inputs in the form of constraints regarding item attributes and is matched with domain-specific rules to the user requirements. In Case-based RS, the user describes the specific cases as anchor points or targets. Similarity metrics are used on the item attributes to identify the similar items with the specified cases.

The result can be assumed as the new anchor point with interactive modification by the users to make the recommendation process more interactive. A utility-based recommender system is just a special case of KBRS. A utility function is deployed to calculate the liking probability of an item by the user. The selection of the appropriate utility function is the

main challenge, and the utility value for the target user is selected by the function called a priory. We consider the Ontology-based IoT recommender systems under the Knowledge-based IoT recommender systems as ontology is just an object-based description of the knowledge base. Ontology-based recommender systems are KBRS, which use ontological knowledge representation. Tarus et al. (2017) explained with their literature review that aggregation of the domain knowledge using ontology overcomes some of the limitations of conventional recommender systems.

Lee et al. (2019) proposed a recommendation model based on IoT users' implicit requests and information curation. The introduced model is divided into two parts. The first part reveals the requestor's desire by collective intelligence. The second part displays the recommendations compellingly. Franco (2017) explored an automatic and learning-based personalised recommender system using association rule mining techniques to recommend automation rules and feature the Smart Home applications (Franco, 2017). The rule is composed of trigger (only one), action (one or more) and state checks (zero or more). The proposed model includes the generalisation of rules, a similarity-threshold parameter to check the similarity of generalised rules (templates) and the application of an association rule mining algorithm (Apriori). The author developed a baseline non-personalised recommender system for evaluation and compared it with the proposed system with metrics Precision, Recall, F1-Score and Coverage. Subramaniaswamy et al. (2019) proposed a personalised recommender (ProTrip RS) for travellers by considering the user's parameters like travel sequence, motivations, actions, opinions and demographic information. The system has the capability of food suggestions based on personal choices, nutrition values and climate attributes, favourable for travellers with long term diseases and who follow a strict diet.

Recently Anthony Jnr (2020) suggested a Case-Based Reasoning (CBR) technique develop a recommender system for sustainable smart city planning. Case-based reasoning is a knowledge-based system that using similar prior cases to assess, solve or deduce the given problem. CBR uses predefined matching algorithms for searching similar cases from the case-based library. A typical CBR cycle is comprises of four phases: case retrieving, problem solution with a case, revise solution and retain the solution as a new case. Selvan et al. (2019) propose a system to develop fuzzy ontology-based RS to recommend drugs and food for diabetic patients using Type-2 fuzzy logic. The system was utilised by considering the uncertainty and heterogeneity attached with chronic patient's data collected by mobile and IoT devices. Table 3 explains some knowledge-based IoT recommender systems.

Table 3
Knowledge-Based IoT Recommender Systems

Model	Authors	Technique used	Data set	Domain	Metrics
An approach for better recommendation by revealing hidden desire and information curation	Lee et al. (2019)	Normalised Weighted Vector-mapping algorithm	Internet social community sites like GroupOn, Opentable	E-commerce	
IoTRS for Automation Rules	Franco (2017)	Apriori (Association rules mining Algorithm)	Muzzley automation rules dataset	Smart Home	Precision, Recall, F1-Score and Coverage
ProTripRS	Subramaniaswamy et al. (2019)	Hybrid filtering (CF+CBF+KBF)	Real climate-based dataset, food information and user dataset	E-Tourism	Precision, Recall, F-measure, Response time
CBR Recommender System	Anthony Jnr (2020)	Case based reasoning	Survey based data	Smart City	Std. deviation, Skewness, variance
FOPR for IoT	Selvan et al. (2019)	Type-2 Fuzzy logic	Chronic patients' dataset	IoT based Health care system	Recall, Precision, Accuracy, F-measure

Correlation-based IoT Recommender System

Correlation is defined as a mutual association between two or more things. The convergence of social networks and IoT develop the Social Internet of Things (SIoT). The SIoT adds correlations in practice for representing the interdependencies of the things or objects (devices), users and services. The inclusion of social networking aspects in the IoT discovers the automatically social relationship between objects and services to enhance information sharing, support for new applications and provide trustworthy network solutions (Roopa et al., 2019).

Saleem et al. (2017) developed a recommendation service to exploit SIoT by inferencing data from various IoT objects and services. The proposed framework is divided into three layers viz. perception layer, network layer and interoperability layer. The author discussed some implementation challenges in realising a proposed model, interoperability, trust, privacy, security, network management and navigability. Kang et al. (2016) proposed a social correlation group-based recommendation technique (SRS) by generating a target group with social correlation in services. The model uses the feature of social interest similarity and principles of CF and CBF. Authors define the social correlation group using their previous study and select the correlated nodes for the target service. The architecture of SRS consists of the Data Aggregation function to aggregate the data and the Data Abstraction function to build abstract data structure. Aggregated and Ontology Graph Manager manages abstracted data. Social correlation group is generated by Target Group function explained by the following Equations 1 and 2:

$$P(e1, c) = ve1 + \frac{\sum_{e2=1}^n sim(e1, e2)(ve2, c - ve2)}{\sum_{e2=1}^n mod(sim(e1, e2))} \quad (1)$$

Where,

$$sim(s, n) = \frac{\sum ps * pn}{mod(ps) * mod(pn)} \quad (2)$$

In this $sim(s, n)$ means how service requirement is close to user n and $P(e1, c)$ is predicted correlation for entity $e1$ on content c .

Forouzandeh et al. (2017) proposed a recommender system based on the relationship between users, objects, services and recommended an IoT device. Yao et al. (2016) discuss the solution of things recommendations problem in IoT by defining new properties of things of interest and build a framework based on unified probabilistic factors by putting together relations of IoT heterogeneous entities. Table 4 explains the correlation-based IoT Recommender Systems from the literature.

Table 4
Correlation-based IoT Recommender Systems

Model	Authors	Technique used	Data set	Domain	Metrics
SRS	Kang et al. (2017)	Collaborative filtering + Content-based filtering	MovieLens (SNS Domain+ IoT service+ media service	SIoT Applications	Prediction accuracy (MAE), Preference evaluation (MV), Hit ratio
IOTSRS	Forouzandeh et al. (2017)	Collaborative filtering (Pearson correlation)	Telus, Lbelium, BlueRover (IoT service companies)	IoT services	Precision, Recall, F-measure, RMSE
ToI Recommendation by LHR in IoT	Yao et al. (2016)	Probabilistic matrix factorization	WS university's CASAS dataset	Thing recommendations (E-commerce, Smart home)	MAE (Accuracy)

Graph-based IoT Recommender System

Graph-based Recommender Systems use undirected, highly connected graph that correlate between things as edges and items as nodes (Lee & Lee, 2015). Graph-based RS works in two stages which are Pre-processing Stage and Recommendation Stage. Graph-based RS has been used in different domains, mainly for tag recommendations by constructing a graph, users and resources. FolkRank is a well-known approach for tag recommendations designed by adapting Google's PageRank Algorithm. In traditional recommender systems, graph-based recommender system represents item and the user as a node in a graph by user set $U = \{u_1, \dots, u_n\}$ and item set $I = \{i_1, \dots, i_n\}$ to instantiate a bipartite graph $G = \langle V, E \rangle$ (Musto et al., 2016). There is a node for each user and item, so the total number of vertices is $|V| = |U| + |I|$. Undirected edges are connected between each item i and user u for users positive feedback, hence $E = \{(u, i) \mid \text{likes}(u, i) = \text{true}\}$ *likes* is the function for positive feedback given by user to item i . Chaudhari et al. (2017) proposed a privacy-aware Graph-based recommender system by exploiting the relations of content entities from user's history and with candidate content entities. A knowledge graph is used to encode the relations between entities. The proposed approach is not domain-based and can also be used for the search.

Mashal et al. (2015) introduced a graph-based service recommender system in the IoT that recommend services in applications like health care, energy monitoring. Weighted undirected tripartite graph-based model is used to define the IoT by tuple $I = (U; S; O; Y)$, here $U = \{u_1, \dots, u_m\}$ a user set, $S = \{s_1, \dots, s_k\}$ service set, $O = \{o_1, \dots, o_n\}$ object set with k service, m users and n objects. Ternary relation of these components is represented by Y is the subset of $U * S * O$. Vertices (V) are composed of services, objects, users and edges by $E = \{\{u, s\}, \{s, o\}, \{u, o\} \mid \{o, s, u\} \text{ belongs to } D\}$ D is a dataset. The weight value of edges is calculated by $\leftarrow dAw + (1 - d)p$, where A is the adjacency matrix, p is random suffer, d is a constant to control the random suffer from 0 or 1. Palaiokrassas et al. (2017) presented an innovative architecture that combines big data and user-generated data to make efficient recommendations using the Neo4j graph database for smart city-based applications.

Nizamkari (2017) presents a scalable recommendation technique by incorporating trust for service selection in SIoT. The result shows that the inclusion of trust into the recommender system increases coverage and accuracy compared to the traditional CF recommendation system. However, the proposed model suffers from a cold-start problem present in all types of CF recommender systems. Finally, Mashal et al. (2016) investigate that graph-based recommendation algorithms can give better results to develop an efficient and accurate recommender system for IoT to service recommendations and leverage the region of recommendations algorithms. Table 5 explains the graph-based recommender systems in IoT.

Table 5

Graph-based Recommender Systems

Model	Authors	Technique used	Data set	Domain	Metrics
Undirected tripartite graph-based RS	Mashal et al. (2015)	FolkRank (graph-based algo)		IoT based any application domain	MAE, RMSE, Recall, Precision
An IoT architecture personalised recommendations	Palaiokrassas et al. (2017)	Vector based Cosine or Euclidean similarity matrix	Neo4j, Node-Red data store	Smart cities	
GB trust enhanced RS	Nizamkari (2017)	Collaborative filtering (Pearson correlation)	LibimSeTi		MAE, RMSE, Coverage
IoT SRS	Mashal et al. (2016)	MPS, MPSU, MPSO, MPSUO, Servrank, User-based CF, object-based CF	Libeliu, Telus, BlueRover	IoT service domain	Recall, Precision

Collaborative IoT Recommender System

The traditional collaborative recommender systems out of the IoT context use the item rating explicitly mentioned by the user to find similar users (user-based technique) or similarities between the items (item-based technique). Nevertheless, Muñoz-Organero et al. (2010) proposed a system that uses the location and time of user and things instead of item rating to make collaborative recommendation compatible for IoT scenarios. The author uses the Pearson correlation similarity metric. The experiment results show that user-object interaction time and user locality are better than user rating in an IoT based environment. Choi et al. (2015) introduced a recommendation model based on Bandwagon Effect by exploiting the IoT information regarding item selection history without any extra actions. Bandwagon Effect shows its usefulness in conventional movie recommendation systems and is now also used in IoT recommender systems. The phenomenon of Bandwagon shows that fashionable information plays an important role to affect the personal choices for item selections, which means a person wants the same item when most people also want it.

Erdeniz et al. (2019) proposed a new recommender system for mobile health applications enabled by IoT, which gives recommendations about activity plans for improving individual health conditions. Table 6 represents the collaborative recommender systems for the IoT domain.

Although many studies used the CF technique, IoT RS based on CF suffers from some potential problems. These techniques are inefficient for IoT-based recommendations. The problems are scalability, cold start and data sparsity. IoT recommendation techniques should be scalable to deal as fast as possible with extensive dynamic data. A cold start problem occurs when new devices are added to the system without users' ratings. As the number of things increases, data sparsity problems can exist and affect the accuracy of IoT RS.

Table 6
Collaborative Recommender Systems

Model	Authors	Technique used	Data set	Domain	Metrics
CRS based on STS	Muñoz-Organero et al. (2010)	Pearson similarity metric	Synthesised Data set		Mean, Standard deviation
Bandwagon Effect based Recommendation MODEL (BERM)	Choi et al. (2015)	Collaborative filtering	GroupLens movie dataset	E-Marketing	
IoT RS for m-health (Virtual Coach)	Erdeniz et al. (2019)	Collaborative filtering (K-nearest neighbour)	Sample dataset from Quantified-Self	IoT enabled m-health application	

Group-based IoT Recommender System

A group-based recommender system provides recommendations to all the group members. The group is made by users with similar preferences, interests or likes. Shang et al. (2014) proposed a framework of a group-based recommender system beyond the anonymity and personalisation towards privacy preservation. The structure of the proposed model is divided into stages: preference exchange between peer to peer, preference aggregations within a group, inter-group recommendations, and local and personal recommendations. The last stage includes recommendations made by incorporating group social information and item content. So, groups can preserve individuals' private preference data by natural protection mechanisms from service providers. Elmisery et al. (2017) proposed a privacy-aware group-based RS for automatic finding interest groups in multimedia services with the

introduction of a middleware based on fog computing runs at the end-user side to exchange the user information for creating interest group and to facilitating recommendations without revealing his preference to other users. Generally, creating an interested group requires consumer's data that is a threat to their privacy.

Lee and Ko (2016) developed a recommender system for service selection to users in IoT enriched environment. However, aggregation of the user's preferences of a group is not suitable for an IoT environment, so the authors' design a user-based CF approach by considering a member organisation for the new neighbour group selected by MOGS (Member Organisation based Group Similarity) metrics such as common member-based, group size-based and member preference-based. Wang et al. (2020) described an average strategy-based group recommender system with preferential differences between group members using the trusted social network for preference corrections. Table 7 describes the IoT based group recommender systems.

Table 7

Group-based Recommender Systems

Model	Authors	Technique used	Data set	Domain	Metrics
Service Recommendation for UG in IoT using MOGS similarity metrics	Lee and Ko (2016)	User-based collaborative filtering	Synthesised data	IoT based application	Precision
GRS based on MPTSN (Member's preference for Trusted Social Network)	Wang et al. (2020)	RM based on IS, MF, IP, IFD	FilmTrust	IoT enabled Environment	MAE

Machine Learning-based IoT Recommender System

Machine learning is the ability of a computer system to automatically acquire knowledge to find solutions by accessing, looking, observing and recognising patterns of data from the database. Machine learning-based systems learn from past experiences without preprogramming and human interventions. There are two types of machine learning algorithms supervised (with labelled training data) and unsupervised (without labelled training data). Supervised learning is guided by a supervisor (trainer), data set acts as a supervisor to train the model. Regression, classification, decision tree, random

forest technique comes under supervised learning. In unsupervised learning, the model automatically learns patterns and relationships by observing the data structure. Clustering and association techniques come under unsupervised learning. Semi-supervised learning comes in the middle of unsupervised and supervised. The model is trained by combining the small labelled data with large non labelled data. Reinforcement learning sticks to learn from its experiences by taking steps when training data is not present.

Deep learning is an emerging machine learning technique that uses artificial neural networks and precisely assigns credit weights to the neural network layers to manifest the desired behaviour. Deep learning enables multiple processing layer computational models to learn from data representation in multiple abstraction levels. Deep learning also shows its potential in recommendation techniques with enhancing the efficiency and accuracy of RS. Recommender systems are flourishing by emerging deep learning techniques. Hence, deep learning pervasive nature help lifts the information retrieval systems and recommender systems (Ouhbi et al., 2018). Milano et al. (2020) present a literature review for ethical challenges for recommender systems like appropriate content, privacy, autonomy and personal identity, opacity, fairness and social effects.

Jabeen et al. (2019) proposed an IoT and community based efficient recommender system for diagnosing cardiac diseases and gave suggestions about the dietary and physical plan. Sewak and Singh (2016) suggested upgrading conventional recommenders into Optimal State recommender solutions to cope with the upcoming era of pervasive IoT and smart wear. The proposed architecture includes distributed and real-time machine learning for IoT based data to mitigate the challenges for optimal state recommender systems. The architecture uses some distributed advanced machine learning algorithms like distributed mini-batch SGD (Stochastic Gradient Descent), distributed Kalman filters. As all the components of the architecture are open source, they can run on the cloud for high flexibility, scalability and low cost that can be applied to IoT based industries. Barbin et al. (2020) proposed an RS based on the user's profile and service interest by making a decision tree for user classification. Ensemble learning techniques combine and rank the recommender system output, which improves the accuracy and efficiency of the recommendation technique. The result shows that the presented models enjoys higher accuracy than other recommendation model based on exact methods.

Guo and Wang (2020) proposed a deep Graph NN based social recommendation (GNN-SR) that deal with the challenge of neglecting the item's features correlation that can influence social group topologies. Their existing approaches for social recommendation use the quantified correlation between user preferences and social connections. Graph neural network method is used to encode user feature space graph and item feature space graph which is implanted into two latent factors of MF (Matrix Factorisation), used to resolve sparsity of item-user rating matrix. Huang et al. (2019) described a new

Multimodality Representation Learning-based Model (MRLM) to overcome the challenges of multimodality and heterogeneous information description of IoT items. The proposed model trains two submodules. First is GFRL (Global Feature Representation Learning) to represent the global features of users and items and accomplish three tasks, namely SoftMax classification, microscopic verification and triplet metric learning. Second is MFRL (Multimodal Feature Representation Learning) to refine global features of the item and produce multimodal final features from multimodal information description. MRLM consists of two phases, i.e., Data Processing and Model Training.

Experiments show the effectiveness of recommendations in IoT on two real-world data. First, Iwendi et al. (2020) propose a deep learning-based solution on health-oriented medical data for food recommendations to patients based on diseases and personal health features (weight, age, gender, cholesterol, fat, protein) implanting machine and deep learning algorithms. The Internet of Medical Things (IoMT) features is analysed and encoded before submitting to deep learning models. Second, Gladence et al. (2020) designed an RS for disabled and older people to provide home management assistant. NLP (Natural Language Processing) plays a vital role by acting as an interface between user and machine and enable the system to be controlled by the user's command. The proposed system is composed of integration of machine learning, cloud platform (Python-anywhere) and IoT. The framework comprises four layers, namely devious environment, cloud computing, and LAN server with Application Programming Interface for AI and smart devices. Table 8 describes Machine learning-based IoT recommender systems.

Table 8

Machine learning based IoT Recommender System

Model	Authors	Technique used	Data set	Domain	Metrics
IoT based EHRS	Jabeen et al. (2019)	Classification, Advice-based collaborative filtering	Hospital dataset	IoT based healthcare system	MAE, Precision, Recall, Accuracy
OSRS for IoT	Sewak and Singh (2016)	Supervised machine learning		IoT Based services, Smart Marketing	
EISRS	Barbin et al. (2020)	Classification (Binary decision tree), Association, Ensemble learning algo	Telus, Libelium, BlueRover	IoT service domain	Precision, Recall, F1-score, RMSE

Table 8 (Continued)

Model	Authors	Technique used	Data set	Domain	Metrics
GNN-SoR for IoT	Guo and Wang (2020)	Matrix factorisation, SGD (Stochastic gradient descent)	Epinions, Yelp, Flixter		RMSE, MAE, NDCG
MRLM	Huang et al. (2019)	Multilayer CNN, Cosine similarity	MovieLens-20M, BookCrossing		Recall, AUC (Area under ROC)
IoMT-APDRS	Iwendi et al. (2020)	LSTM deep learning	Health-base medical dataset	Smart healthcare	Recall, Accuracy, Precision, F1-measure
RSHA using IoT and AI	Gladence et al. (2020)	NLP (Natural Language Processing)		Smart Home Automation System	

Trust Aware IoT Recommender System

Trust is defined as reliance on the ability, integrity and nature of a thing (object), service or user necessary for social transactions in an IoT environment. Cryptography methods are not efficient to guarantee data/user security, trustworthiness and resistance in IoT based services (Mohammadi et al., 2019). So, for achieving the network's security trust evaluation, a rational recommendation for estimating friend node reliability should be employed at the node level. Furthermore, traditional security mechanisms cannot detect disrupt and malicious transmission in IoT scenarios. So, trust models are used to detect delusive behaviour by distinguishing honest nodes incorporated in the IoT devices.

Trust-based Recommender systems are developed to improve the recommendation quality by including the trustworthiness of users in the collaborative filtering technique. Two types of trust computation models –the reputation trust model and the relationship trust model, are incorporated in the trust-based recommender systems. Trust aware RS for IoT helps the users find reliable services by searching the entire scale-free trust network with high computational cost. Yuan et al. (2013) proposed an efficient search model called S_Searching based on the scalability freeness parameter of trust networks. A Skelton is made by choosing the highest degree nodes globally, and searching mechanisms for recommenders are conducted with this Skelton. With less computational cost and complexity, the S_Searching mechanism can find trustable recommender services. Many

Trust-based Recommendation models are not included in our literature survey because there is already a review paper for Trust-based recommendation systems in the IoT (Mohammadi et al., 2019).

Some Other IoT Recommender Systems

There are also some proposed models in literature with different recommendation techniques used in IoT based domain. Forestiero (2017) suggests a multi-agent-based RS utilising self-organising strategies and decentralisation for things recommendations in IoT. Locality preserving hash function maps similar things into similar bit-vectors managed by a cyber agent and converted based on an ad-hoc probability function. Result explains that the recommendation is fast, and the algorithm is scalable with constructive reorganisation for descriptors. Hamlabadi et al. (2018) proposed a framework of the Cognitive Recommender System (CRS) in the IoT. A cognitive system learns by employing in an unknown environment to improve its performance. The framework is distributed in three layers, namely Requirement layer, Thing System Layer (TSL), and Cognitive Process Layer (CPL). The proposed framework is flexible, cognitive, general-purpose and enabled for sharing. Saghiri et al. (2018). Suggested a recommender system on the IoT framework based on blockchain technology and cognitive systems. This framework consists of a requirement layer, cognitive process layer and things management layer embedded by IoT and blockchain technology.

Chirila et al. (2016) developed a recommendation mechanism for service recommendations to IoT devices enabled by web service interfaces. The proposed model uses broker-based architecture with semantic similarity-based filtering and clustering technique. Di Martino and Rossi (2016) proposed a Mobility Recommender System (MRS) based on scalable and distributed IoT architecture for ITS (Intelligent Transport System). The proposed architecture utilises road infrastructure based heterogeneous data (digital map and parking info) for recommendations.

Matsui and Choi (2017) proposed an RS that suggests indoor comfort products by exploiting HEMS (Home Energy Management System) data like indoor humidity, temperature, luminance, power consumption, and clothing quantity. Generally, people are not aware of the services related to the smart objects they purchased, so an RS can facilitate by recommending IoT services to grasp the connected smart objects (Noirie et al., 2017). Mashal et al. (2020) develop a recommendation system using a decision-making approach based on hybrid multi-criteria to suggest the most suitable IoT application. Additive weight methods and analytical hierarchy processes are used in the decision-making process. To overcome interoperability issues in IoT semantic web has been recognised as an emerging technology for service discovery (Kolbe et al., 2019). Cao et al. (2019) proposed a QoS (Quality of Service) aware service RS based on factorisation machine and relational model

to find a suitable web application programming interface for developing IoT mashup applications. Yan et al. (2019) proposed SIoT-SR (Service Recommendation) by adopting LSH (Locality-Sensitive Hashing) forest algorithm and collaborative filtering technique to discover the QoS data. It is a distributed approach and can face the privacy leakage problem. Hence, authors select LSH forest with self-correct parameters ability to enhance privacy, efficiency and accuracy.

DISCUSSION

In the last few years, there is an increase in applications of recommendation technologies for IoT application areas like smart marketing, smart home, smart tourism, smart healthcare systems, and smart cities development. We reviewed the main trends and techniques used by the published studies from 2013 to 2020. Some studies have made use of conventional recommendation approaches. However, there is a need for improvements in conventional methods to cope with the dynamic, heterogeneous and distributed IoT environment. Deep learning and reinforcement learning algorithms can provide promising results by capturing the users' temporal intentions.

As IoT Recommender Systems are in their infancy, there is a need to resolve the security and privacy issues to protect malicious activities over users' data. In most of the developed models in the literature, simulated data is used, as the accessing of real-time data is too complex. In most models, matrices like MAE (Mean Absolute Error), RMSE (Root Mean Squared Error), Precision and Recall are used to quantify the accuracy of the IoT RS. However, there is a lack of evaluation measures to quantify the IoT RS's productivity, diversity, scalability and adaptability. Therefore, IoT Recommendation techniques should evaluate the above parameters to be more applicable in IoT-based real-time application scenarios.

CHALLENGES AND FUTURE SCOPE

IoT technology enables various physical devices to talk and interact by creating new opportunities in many application domains. IoT technologies are desirable of an efficient and effective searching paradigm for helping users in extracting, visualising, recognising, decision making from non-standardised and high dimensional data. Therefore, there is a need for information filtering or decision-supporting tools to solve the information overloading problem in IoT based scenarios. However, developing an efficient, accurate and effective recommendation technique to meet users' desires faces many difficulties due to IoT characteristics like heterogeneity, real-time communication, scalability, mobility, dynamicity and correlation with things. Due to the problems mentioned above, recommender systems in IoT have not yet acquired as much effectiveness as they acquire in

non-IoT domains. Recommendations in IoT are dynamic, distributed, more context-aware and heterogeneous as compared to the traditional recommendations. Moreover, meeting these recommendations is a big challenge for the developers.

Instead of the above-said features of IoT based recommendations, they should also be persuasive, security and privacy-aware and interactive with a multimodal interface. Integration of the features mentioned above in the conventional recommendation techniques requires a more profound knowledge of the emerging trends (Deep learning, SIoT, ontology-driven knowledge base). Consideration of the SIoT for leveraging the heterogeneous relations of things with users, users with services, things with things and services with things is a good choice for extracting the user's preferences and choices. Nevertheless, implementation of SIoT based recommendations faces challenges like interoperability, trust and security, data discovery, social network management, self-healing and network navigability for streaming services (Saleem et al., 2017). Some researchers proposed context-aware recommender systems to incorporate contextual information in IoT recommendations. However, CARS in IoT also faces some issues: an accumulation of adequate data, context factor discovery, shortage of datasets availability, proactively informational filtering and privacy of users' contextual information. (Pratibha & Kaur, 2018). Due to the limited computational power of IoT devices, recommendation algorithms are located in clouds to support IoT apps recommendations and IoT workflows recommendations. For the recommendations of resource balancing in a particular IoT application domain, reconfiguration support recommendation algorithms should be deployed on the gateway only. For both purposes, the scalability of the recommendations algorithms creates an open challenge. The availability of a real IoT based dataset is also a challenge for the exact evaluation of algorithms. IoT has distributed nature and collects a considerable amount of data. However, data analysis methods of IoT scenarios are limited, so Big Data Analytics should be approached.

Hybridisations of the proposed IoT recommendations techniques like context-aware, knowledge-based, deep learning-based, trust-based, social correlation-based, group-based and graph-based and emerging technologies can lead to the solutions to some of the challenges mentioned above with improving the performance of IoT recommender systems. In the case of Internet connection failure, basic and most required functionalities should be available, so incorporating the recommendations functionalities on gateway can be a future work that leads to gateway autonomy property. Searching techniques can be combined with IoT recommendations for discovering user's preferences or implicit correlation with entities. The techniques are based on semantic analysis. When combined with the searching techniques, semantic analysis can enabled recommendation techniques and open a future direction for research. Most recommendation techniques do not force security and privacy constraints on the data. Blockchain-based cryptography has proved effective

security solutions in IoT environments. So, in future recommendations techniques based on blockchain supported distributed architecture can help in security and privacy concerns for user's collected data. Deep learning can provide customised and accurate recommendations, which is one of the emerging technologies for personalisation. Deep learning-based model can be deployed on an IoT device for edge computations or on a centralised server as a cloud-based learning model.

CONCLUSION

IoT is an emerging technology with future possibilities of enabling a large number of diverse devices connections results in the assemblage of dynamic and versatile data. Recommendations technologies can use this data for real-time and personalised suggestions about services, things and any relevant commodity in IoT-based scenario. This comprehensive literature review paper explains the existing recommendation techniques in the Internet of Things (IoT). The last section discussed some of the open issues and future scope to cope with IoT based recommendations' challenges. In conclusion, we can say that this literature survey will benefit a new researcher by widening the frontiers of required knowledge in this research field.

ACKNOWLEDGEMENT

The first author of the paper likes to say thanks to her guide cum supervisor Dr Chhavi Rana for guidance and supervision.

REFERENCES

- Abu-issa, A., Nawawreh, H., Shreth, L., Salman, Y., Hassounch, Y., Tumar, I., & Systems, A. R. (2020). A smart city mobile application for multitype, proactive, and context-aware recommender system. In *2017 International Conference on Engineering and Technology (ICET)* (pp. 1-5). IEEE Publishing. <https://doi.org/10.1109/ICEngTechnol.2017.8308181>
- Aggarwal, C. C. (2016). *Recommender systems*. Springer International Publishing. <https://doi.org/10.1007/978-3-319-29659-3>
- Amato, F., Mazzeo, A., Moscato, V., & Picariello, A. (2013). A Recommendation System for Browsing of Multimedia Collections in the Internet. In *Internet of things and inter-cooperative computational technologies for collective intelligence* (pp. 391-411). Springer. https://doi.org/10.1007/978-3-642-34952-2_16
- Anthony Jnr, B. (2020). A case-based reasoning recommender system for sustainable smart city development. *AI & Society*, 36, 159-183. <https://doi.org/10.1007/s00146-020-00984-2>
- Baltrunas, L., Ludwig, B., & Ricci, F. (2011). Matrix factorization techniques for context aware recommendation. In *Proceedings of the fifth ACM conference on Recommender systems* (pp. 301-304). Association for Computing Machinery. <https://doi.org/10.1145/2043932.2043988>

- Barbin, J. P., Yousefi, S., & Masoumi, B. (2020). Efficient service recommendation using ensemble learning in the Internet of things (IoT). *Journal of Ambient Intelligence and Humanized Computing*, *11*(3), 1339-1350. <https://doi.org/10.1007/s12652-019-01451-7>
- Cao, B., Liu, J., Wen, Y., Li, H., Xiao, Q., & Chen, J. (2019). QoS-aware service recommendation based on relational topic model and factorization machines for IoT Mashup applications. *Journal of Parallel and Distributed Computing*, *132*, 177-189. <https://doi.org/10.1016/j.jpdc.2018.04.002>
- Cha, S., Ruiz, M. P., Wachowicz, M., Tran, L. H., Cao, H., & Maduako, I. (2017). The role of an IoT platform in the design of real-time recommender systems. In *2016 IEEE 3rd world forum on Internet of things (WF-iot)* (pp. 448-453). IEEE Publishing. <https://doi.org/10.1109/WF-IoT.2016.7845469>
- Chaudhari, S., Azaria, A., & Mitchell, T. (2017). *An entity graph based Recommender System*. *AI Communications*, *30*(2), 141-149. <https://doi.org/10.3233/AIC-170728>
- Chirila, S., Lemnaru, C., & Dinsoreanu, M. (2016). Semantic-based IoT device discovery and recommendation mechanism. In *2016 IEEE 12th International Conference on Intelligent Computer Communication and Processing (ICCP)* (pp. 111-116). IEEE Publishing. <https://doi.org/10.1109/ICCP.2016.7737131>
- Choi, S. M., Lee, H., Han, Y. S., Man, K. L., & Chong, W. K. (2015). A Recommendation Model Using the Bandwagon Effect for E-Marketing Purposes in IoT. *International Journal of Distributed Sensor Networks*, *11*(7), Article 475163. <https://doi.org/10.1155/2015/475163>
- Čolaković, A., & Hadžialić, M. (2018). Internet of Things (IoT): A review of enabling technologies, challenges, and open research issues. *Computer Networks*, *144*, 17-39. <https://doi.org/10.1016/j.comnet.2018.07.017>
- Di Martino, S., & Rossi, S. (2016). An architecture for a mobility recommender system in smart cities. *Procedia Computer Science*, *58*, 425-430. <https://doi.org/10.1016/j.procs.2016.09.066>
- Elmisery, A. M., Rho, S., & Sertovic, M. (2017). Privacy aware group based recommender system in multimedia services. *Multimedia Tools and Applications*, *76*(24), 26103-26127. <https://doi.org/10.1007/s11042-017-4950-0>
- Erdeniz, S. P., Menychtas, A., Maglogiannis, I., Felfernig, A., & Tran, T. N. T. (2019). Recommender systems for IoT enabled quantified-self applications. *Evolving Systems*, *11*(2), 291-304. <https://doi.org/10.1007/s12530-019-09302-8>
- Felfernig, A., Erdeniz, S. P., Jeran, M., Akcay, A., Azzoni, P., Maiero, M., & Doukas, C. (2017). Recommendation technologies for IoT edge devices. *Procedia Computer Science*, *110*, 504-509. <https://doi.org/10.1016/j.procs.2017.06.135>
- Felfernig, A., Polat-Erdeniz, S., Uran, C., Reiterer, S., Atas, M., Tran, T. N. T., Azzoni, P., Kiraly, C., & Dolui, K. (2019). An overview of recommender systems in the Internet of things. *Journal of Intelligent Information Systems*, *52*(2), 285-309. <https://doi.org/10.1007/s10844-018-0530-7>
- Forestiero, A. (2017). Multi-Agent recommendation system in Internet of things. In *2017 17th IEEE/ACM International Symposium on Cluster, Cloud and Grid Computing (CCGRID)* (pp. 772-775). IEEE Publishing. <https://doi.org/10.1109/CCGRID.2017.123>
- Forouzandeh, S., Aghdam, A. R., Barkhordari, M., & Fahimi, A. (2017). Recommender system for users of Internet of Things (IOT). *International Journal of Computer Science and Network Security*, *17*(8), 46-51.

- Franco, D. A. I. (2017). *A recommender system for automation rules in the Internet of Things* (MSc Thesis). Instituto Superior Técnico, Portugal.
- Frey, R. M., Xu, R., & Ilic, A. (2015). A Novel Recommender System in IoT. In *2015 5th International Conference on the Internet of Things (IOT 2015)*. IEEE Publishing. <https://doi.org/10.3929/ethz-a-010561395>
- Gladence, L. M., Anu, V. M., Rathna, R., & Brumancia, E. (2020). Recommender system for home automation using IoT and artificial intelligence. *Journal of Ambient Intelligence and Humanized Computing*, 1-9. <https://doi.org/10.1007/s12652-020-01968-2>
- Guo, Z., & Wang, H. (2020). A deep graph neural network-based mechanism for social recommendations. *IEEE Transactions on Industrial Informatics*, 3203(c), 1-1. <https://doi.org/10.1109/tii.2020.2986316>
- HamlAbadi, K. G., Saghiri, A. M., Vahdati, M., TakhtFooladi, M. D., & Meybodi, M. R. (2018). A framework for cognitive recommender systems in the Internet of Things (IoT). In *2017 IEEE 4th international conference on knowledge-based engineering and innovation (KBEI)* (pp. 0971-0976). IEEE Publishing. <https://doi.org/10.1109/KBEI.2017.8324939>
- Huang, Z., Xu, X., Ni, J., Zhu, H., & Wang, C. (2019). Multimodal representation learning for recommendation in Internet of Things. *IEEE Internet of Things Journal*, 6(6), 10675-10685. <https://doi.org/10.1109/JIOT.2019.2940709>
- Isinkaye, F. O., Folajimi, Y. O., & Ojokoh, B. A. (2015). Recommendation systems: Principles, methods and evaluation. *Egyptian Informatics Journal*, 16(3), 261-273. <https://doi.org/10.1016/j.eij.2015.06.005>
- Iwendi, C., Khan, S., Anajemba, J. H., Bashir, A. K., & Noor, F. (2020). Realizing an efficient IoMT-assisted patient diet recommendation system through machine learning model. *IEEE Access*, 8, 28462-28474. <https://doi.org/10.1109/ACCESS.2020.2968537>
- Jabeen, F., Maqsood, M., Ghazanfar, M. A., Aadil, F., Khan, S., Khan, M. F., & Mehmood, I. (2019). An IoT based efficient hybrid recommender system for cardiovascular disease. *Peer-to-Peer Networking and Applications*, 12(5), 1263-1276. <https://doi.org/10.1007/s12083-019-00733-3>
- Kang, D., Choi, H., Choi, S., & Rhee, W. (2017). SRS : Social Correlation Group based Recommender System for Social IoT Environment. *International Journal of Contents*, 13(1), 53-61. <https://doi.org/10.5392/IJoC.2017.13.1.053>
- Kang, D., Choi, H., & Rhee, W. (2016). *Social Correlation Group Generation Mechanism in Social IoT Environment*. In *2016 Eighth International Conference on Ubiquitous and Future Networks (ICUFN)* (pp. 514-519). IEEE Publishing. <https://doi.org/10.1109/ICUFN.2016.7537086>
- Kolbe, N., Kubler, S., Robert, J., Le Traon, Y., & Zaslavsky, A. (2019). Linked vocabulary recommendation tools for Internet of things: A survey. *ACM Computing Surveys*, 51(6), 1-31. <https://doi.org/10.1145/3284316>
- Kwon, J., & Kim, S. (2016). Study on Recommendation in Internet of Things Environment. In *2015 7th International Conference on Multimedia, Computer Graphics and Broadcasting (MulGraB)* (pp. 13-14). IEEE Publishing. <https://doi.org/10.1109/MulGraB.2015.13>
- Lee, J. S., & Ko, I. Y. (2016). Service recommendation for user groups in Internet of things environments using member organization-based group similarity measures. In *2016 IEEE international conference on web services (ICWS)* (pp. 276-283). IEEE Publishing. <https://doi.org/10.1109/ICWS.2016.43>

- Lee, K., Lee, Y. S., & Nam, Y. (2019). A novel approach of making better recommendations by revealing hidden desires and information curation for users of Internet of things. *Multimedia Tools and Applications*, 78(3), 3183-3201. <https://doi.org/10.1007/s11042-018-6084-4>
- Lee, K., & Lee, K. (2015). Escaping your comfort zone: A graph-based recommender system for finding novel recommendations among relevant items. *Expert Systems with Applications*, 42(10), 4851-4858. <https://doi.org/10.1016/j.eswa.2014.07.024>
- Mashal, I., Alsaryrah, O., & Chung, T. Y. (2016). Analysis of recommendation algorithms for Internet of Things. In *2016 IEEE Wireless Communications and Networking Conference* (pp. 1-6). IEEE Publishing. <https://doi.org/10.1109/WCNC.2016.7564667>
- Mashal, I., Alsaryrah, O., Chung, T. Y., & Yuan, F. C. (2020). A multi-criteria analysis for an Internet of things application recommendation system. *Technology in Society*, 60, Article 101216. <https://doi.org/10.1016/j.techsoc.2019.101216>
- Mashal, I., Chung, T. Y., & Alsaryrah, O. (2015). Toward service recommendation in Internet of Things. In *2015 Seventh International Conference on Ubiquitous and Future Networks* (pp. 328-331). IEEE Publishing. <https://doi.org/10.1109/ICUFN.2015.7182559>
- Matsui, K., & Choi, H. (2017). A recommendation system with secondary usage of HEMS data for products based on IoT technology. In *2017 International Symposium on Networks, Computers and Communications (ISNCC)* (pp. 1-6). IEEE Publishing. <https://doi.org/10.1109/ISNCC.2017.8071982>
- Milano, S., Taddeo, M., & Floridi, L. (2020). Recommender systems and their ethical challenges. *AI & Society*, 35(4), 957-967. <https://doi.org/10.1007/s00146-020-00950-y>
- Mohammadi, V., Rahmani, A. M., Darwesh, A. M., & Sahafi, A. (2019). Trust-based recommendation systems in Internet of Things: a systematic literature review. *Human-centric Computing and Information Sciences*, 9(1), 1-61. <https://doi.org/10.1186/s13673-019-0183-8>
- Muñoz-Organero, M., Ramírez-González, G. A., Muñoz-Merino, P. J., & Delgado Kloos, C. (2010). A collaborative recommender system based on space-time similarities. *IEEE Pervasive Computing*, 9(3), 81-87. <https://doi.org/10.1109/MPRV.2010.56>
- Musto, C., Lops, P., Basile, P., de Gemmis, M., & Semeraro, G. (2016). Semantics-aware graph-based recommender systems exploiting linked open data. In *Proceedings of the 2016 conference on user modeling adaptation and personalization* (pp. 229-237). Association for Computing Machinery. <https://doi.org/10.1145/2930238.2930249>
- Nizamkari, N. S. (2017). A graph-based trust-enhanced recommender system for service selection in IOT. In *2017 International Conference on Inventive Systems and Control (ICISC)* (pp. 1-5). IEEE Publishing. <https://doi.org/10.1109/ICISC.2017.8068714>
- Noirie, L., Le Pallec, M., & Ammar, N. (2017). Towards automated IoT service recommendation. In *2017 20th Conference on Innovations in Clouds, Internet and Networks (ICIN)* (pp. 103-106). IEEE Publishing. <https://doi.org/10.1109/ICIN.2017.7899397>
- Ouhbi, B., Frikh, B., Zemmouri, E., & Abbad, A. (2018). Deep learning based recommender system. In *2018 IEEE 5th International Congress on Information Science and Technology (CiSt)* (pp. 161-166). <https://doi.org/10.1109/CIST.2018.8596492>

- Palaiokrassas, G., Karlis, I., Litke, A., Charlaftis, V., & Varvarigou, T. (2017). An IoT architecture for personalized recommendations over big data oriented applications. In *2017 IEEE 41st Annual Computer Software and Applications Conference (COMPSAC)* (Vol. 2, pp. 475-480). IEEE Publishing. <https://doi.org/10.1109/COMPSAC.2017.59>
- Pratibha, & Kaur, P. D. (2018). Towards incorporating context awareness to recommender systems in Internet of things. *Smart Innovation, Systems and Technologies*, 79, 771-780. https://doi.org/10.1007/978-981-10-5828-8_73
- Ravi, L., Vairavasundaram, S., Palani, S., & Devarajan, M. (2019). Location-based personalized recommender system in the Internet of cultural things. *Journal of Intelligent & Fuzzy Systems*, 36(5), 4141-4152. <https://doi.org/10.3233/JIFS-169973>
- Roopa, M. S., Pattar, S., Buyya, R., Venugopal, K. R., Iyengar, S. S., & Patnaik, L. M. (2019). Social Internet of Things (SIoT): Foundations, thrust areas, systematic review and future directions. *Computer Communications*, 139(September 2018), 32-57. <https://doi.org/10.1016/j.comcom.2019.03.009>
- Sawant, S. D., Sonawane, K. V., Jagani, T., & Chaudhari, A. N. (2017). Representation of recommender system in IoT using cyber physical techniques. In *2017 International conference of Electronics, Communication and Aerospace Technology (ICECA)* (Vol. 2, pp. 372-375). IEEE Publishing. <https://doi.org/10.1109/ICECA.2017.8212836>
- Saghiri, A. M., Vahdati, M., Gholizadeh, K., Meybodi, M. R., Dehghan, M., & Rashidi, H. (2018). A framework for cognitive Internet of Things based on blockchain. In *2018 4th International Conference on Web Research (ICWR)* (pp. 138-143). IEEE Publishing. <https://doi.org/10.1109/ICWR.2018.8387250>
- Saleem, Y., Crespi, N., Rehmani, M. H., Copeland, R., Hussein, D., & Bertin, E. (2017). Exploitation of social IoT for recommendation services. In *2016 IEEE 3rd World Forum on Internet of Things (WF-IoT)* (pp. 359-364). IEEE Publishing. <https://doi.org/10.1109/WF-IoT.2016.7845500>
- Salman, Y., Abu-Issa, A., Tumar, I., & Hassouneh, Y. (2015). A proactive multi-type context-aware recommender system in the environment of Internet of Things. In *2015 IEEE International Conference on Computer and Information Technology; Ubiquitous Computing and Communications; Dependable, Autonomic and Secure Computing; Pervasive Intelligence and Computing* (pp. 351-355). IEEE Publishing. <https://doi.org/10.1109/CIT/IUCC/DASC/PICOM.2015.50>
- Selvan, N. S., Vairavasundaram, S., & Ravi, L. (2019). Fuzzy ontology-based personalized recommendation for Internet of medical things with linked open data. *Journal of Intelligent and Fuzzy Systems*, 36(5), 4065-4075. <https://doi.org/10.3233/JIFS-169967>
- Sewak, M., & Singh, S. (2016). IoT and distributed machine learning powered optimal state recommender solution. In *2016 International Conference on Internet of Things and Applications (IOTA)* (pp. 101-106). IEEE Publishing. <https://doi.org/10.1109/IOTA.2016.7562703>
- Shang, S., Hui, Y., Hui, P., Cuff, P., & Kulkarni, S. (2014). Beyond personalization and anonymity: Towards a group-based recommender system. In *Proceedings of the 29th Annual ACM Symposium on Applied Computing* (pp. 266-273). <https://doi.org/10.1145/2554850.2554924>
- Subramaniaswamy, V., Manogaran, G., Logesh, R., Vijayakumar, V., Chilamkurti, N., Malathi, D., & Senthilselvan, N. (2019). An ontology-driven personalized food recommendation in IoT-based healthcare system. *Journal of Supercomputing*, 75(6), 3184-3216. <https://doi.org/10.1007/s11227-018-2331-8>

- Tarus, J. K., Niu, Z., & Mustafa, G. (2017). Knowledge-based recommendation: A review of ontology-based recommender systems for e-learning. *Artificial Intelligence Review*, 50(1), 21-48. <https://doi.org/10.1007/s10462-017-9539-5>
- Twardowski, B., & Ryzko, D. (2016). IoT and context-aware mobile recommendations using Multi-Agent Systems. In *2015 IEEE/WIC/ACM International Conference on Web Intelligence and Intelligent Agent Technology (WI-IAT)* (Vol. 1, pp. 33-40). IEEE Publishing. <https://doi.org/10.1109/WI-IAT.2015.120>
- Wang, X., Su, L., Zhou, Q., & Wu, L. (2020). Group recommender systems based on members' preference for trusted social networks. *Security and Communication Networks*, 2020, Article 1924140. <https://doi.org/10.1155/2020/1924140>
- Wu, X. Q., Zhang, L., Tian, S. L., & Wu, L. (2019). Scenario based e-commerce recommendation algorithm based on customer interest in Internet of things environment. *Electronic Commerce Research*, 1-17. <https://doi.org/10.1007/s10660-019-09339-6>
- Yan, B., Yu, J., Yang, M., Jiang, H., Wan, Z., & Ni, L. (2019). A novel distributed social Internet of Things service recommendation scheme based on LSH forest. *Personal and Ubiquitous Computing*, 1-14. <https://doi.org/10.1007/s00779-019-01283-4>
- Yao, L., Sheng, Q. Z., Ngu, A. H., & Li, X. (2016). Things of interest recommendation by leveraging heterogeneous relations in the Internet of things. *ACM Transactions on Internet Technology*, 16(2), 1-25. <https://doi.org/10.1145/2837024>
- Yao, L., Wang, X., Sheng, Q. Z., Dustdar, S., & Zhang, S. (2019). Recommendations on the Internet of Things: Requirements, challenges, and directions. *IEEE Internet Computing*, 23(3), 46-54. <https://doi.org/10.1109/MIC.2019.2909607>
- Yavari, A., Jayaraman, P. P., & Georgakopoulos, D. (2016). Contextualised service delivery in the Internet of things: Parking recommender for smart cities. In *2016 IEEE 3Rd world forum on Internet of things (WF-iot)* (pp. 454-459). IEEE Publishing. <https://doi.org/10.1109/WF-IoT.2016.7845479>
- Yuan, W., Guan, D., Shu, L., & Niu, J. (2013). Mehanizam pretraživanja preporučitelja za sustave sigurnih preporučitelja u Internetu stvari [Recommender searching mechanism for trust-aware recommender systems in Internet of things]. *Automatika*, 54(4), 427-437. <https://doi.org/10.7305/automatika.54-4.416>
- Zia, K., Muhammad, A., Saini, D. K., & Ferscha, A. (2018). Agent-based model of smart social networking-driven recommendations system for Internet of vehicles. In *International Conference on Practical Applications of Agents and Multi-Agent Systems* (pp. 275-287). Springer, Cham. <https://doi.org/10.1007/978-3-319-94580-4>

A Novel Approach of Audio Based Feature Optimisation for Bird Classification

Murugaiya Ramashini*, Pg Emeroylariffion Abas and Liyanage C De Silva

Faculty of Integrated Technologies, Universiti Brunei Darussalam, Jalan Tungku Link, BE1410, Brunei Darussalam

ABSTRACT

Bird classification using audio data can be beneficial in assisting ornithologists, bird watchers and environmentalists. However, due to the complex environment in the jungles, it is difficult to identify birds by visual inspection. Hence, identification via acoustical means may be a better option in such an environment. This study aims to classify endemic Bornean birds using their sounds. Thirty-five (35) acoustic features have been extracted from the pre-recorded soundtracks of birds. In this paper, a novel approach for selecting an optimum number of features using Linear Discriminant Analysis (LDA) has been proposed to give better classification accuracy. It is found that using a Nearest Centroid (NC) technique with LDA produces the optimum classification results of bird sounds at 96.7% accuracy with reduced computational power. The low computational complexity is an added advantage for handheld portable devices with minimal computing power, which can be used in birdwatching expeditions. Comparison results have been provided with and without LDA using NC and Artificial Neural Network (ANN) classifiers. It has been demonstrated that both classifiers with LDA outperform those without LDA. Maximum accuracies for both NC and ANN with LDA, with NC and the ANN classifiers requiring 7 and 10 LDAs to achieve the optimum accuracy, respectively, are 96.7%. However, ANN

classifier with LDA is more computationally complex. Hence, this is significant as the simpler NC classifier with LDA, which does not require expensive processing power, may be used on the portable and affordable device for bird classification purposes.

ARTICLE INFO

Article history:

Received: 3 February 2021

Accepted: 24 May 2021

Published: 28 October 2021

DOI: <https://doi.org/10.47836/pjst.29.4.08>

E-mail addresses:

ramashini@uwu.ac.lk (Murugaiya Ramashini)

emeroylariffion.abas@ubd.edu.bn (Pg Emeroylariffion Abas)

liyanage.silva@ubd.edu.bn (Liyanage C De Silva)

*Corresponding author

Keywords: Artificial neural network (ANN), bird sounds, classification, linear discriminant analysis (LDA), nearest centroid (NC)

INTRODUCTION

Birds have a considerable impact on our lives (Suthers, 2004). In the past, people had used bird sounds in their day-to-day life for stress recovery and as an attention restoration tool (Alvarsson et al., 2010). In addition, bird sounds were also used as alarms for severe weather changes and hazardous conditions (Vilches et al., 2006). They extracted this useful information from the birds' unique features and behaviours and their sounds due to their deep understanding and knowledge of birds and the environment, obtained through traditional knowledge and experiences from observing nature. However, nowadays, this knowledge is fast deteriorating and limited to only a few people due to our busy modern lifestyle and disengagement from nature.

Birdwatching, which includes identifying birds visually or by their sounds, has become a rapidly popular recreational activity. This activity positively impact the economy and the environment, especially for countries dependent on ecotourism. Tourists who visit destinations to meet their particular needs and share specific interests and motivation are called "niche tourists", and birdwatchers fall into such category. Birdwatchers may travel to specific destinations only for bird-watching purposes. The destination promotes the specific activity as one of its significant niche tourism activities (Butler, 2019). However, growing environmental changes, including potential timing mismatch for breeding, increase in ocean temperature, and the unavailability of sufficient food supply, have disrupted the bird population. As a result, it may affect the long-term sustainability of birdwatching and ecotourism. The future of ecotourism depends on wildlife tourism, such as birdwatching. It relies on the maintenance and well-being of the endemic species to draw tourists to the destinations (Kutzner, 2019). Lately, the focus has been given to surveillance and environmental monitoring related applications, with the rapid development of technologies such as artificial intelligence (Badi et al., 2019). Therefore, it is essential to find novel approaches that may strengthen the nature-based tour operators' resilience in the tourism industry and address the rapidly changing social and environmental conditions (Kutzner, 2019), It is also vital to have new technologies that can support visitors.

However, visual bird identification can be a difficult task, especially in a densely vegetated rainforest environment. Therefore, bird species identification based on sound may be a better option (Trifa et al., 2008). Consequently, audio-based bird classification has gotten the limelight in recent years.

Statistics can be computed over the audio bird-sound datasets to generate a single feature vector (Giannakopoulos & Pikrakis, 2014) that can identify the bird species. Then the relevant features extracted from sound are identified and grouped into a set of classes that it most likely fit. Depending on the application, different grouping algorithms, and feature extraction techniques may be used (Gerhard, 2003) with a wide range of supervised and unsupervised Machine Learning (ML) algorithms used for bird species identification.

For feature extraction, researchers have used time, frequency and also few cepstral domain features. Sharma et al. (2020) summarise the literature on audio signal processing for bird sound classification tasks, mainly focusing on feature extraction techniques.

Many researchers have used Artificial Neural Networks (ANNs) in their work. For example, Selouani et al. (2005) use Multi-Layer Perceptron (MLP) feedback loop to improve the architecture, using a set of selected features as input to produce different output for each species. Variations of ANN exist in the literature and have been used by many researchers to detect bird sounds (Ranjard & Ross, 2008; McIlraith & Card, 1997). Chou et al. (2008) use decision-based Neural Network (NN) to improve the accuracy of detection as well as processing time consumed by the model (Selouani et al., 2005). Probabilistic, backpropagation and Kohonen NNs have also been demonstrated by Terry and McGregor (2002). Priyadarshani et al. (2018) elaborate state of the art in bird recognition and describe the different techniques adopted over the years in their review article.

Despite the availability of many technologies, including audio signal processing and pattern recognition that have been used to study birds and their sounds, there are still plenty of research gaps in the identification of birds from their sounds due to the vast range and heritage distribution of bird species. Notably, the Borneo region is rich in biodiversity with unique and diverse animal life varieties, including many birds living in its dense and virgin tropical rainforest areas. Furthermore, although ecotourism is becoming a growing source of income for countries in the Borneo region, with bird watching as one of the main features of ecotourism in the area, there is no application using technology to assist visitors to this region.

This paper proposes a simple dimension-reduction technique, which can select the optimum feature combinations for dimension reduction purposes. When combined with two classification methods, Nearest Centroid (NC) and Artificial Neural Network (ANN), it can efficiently and effectively classify birds from their audio sounds. The proposed method has been demonstrated for the classification of 10 endemic bird species of the Borneo region. It has been shown that it can accurately identify these bird species, with a low requirement on computational power. Moreover, this is very significant, as currently, most researchers have utilised advanced and complex techniques, which require high computational power to classify bird sounds. While this is feasible for non-real-time applications with access to high-end equipment, real-time implementation of such techniques on simple portable devices has been proven very difficult.

Consequently, the proposed method may implement hardware solutions for real-time bird sound classification to assist bird watchers. The following section discusses the proposed methodology for the classification of bird sounds, composed of data collection, pre-processing, segmentation, feature extraction, dimensionality reduction and classification, followed by results and discussions and finally, the performance of the proposed method. The final section concludes the paper.

METHODOLOGY

It is necessary to pre-process the bird sound to extract essential properties as inputs to the classification model to classify a given unidentified bird sound according to its species. Pre-processing may involve passing the birds sound through a filter to remove unwanted noise and disturbance, segmenting the bird's sound into distinct parts and extracting important features from the bird sounds. Then, depending on the method adopted, selected bird sounds features may be fed directly onto the already-trained classification model to give the predicted species of the un-identified bird sound.

Figure 1 depicts a simplified process used for bird sound classification in this paper, categorised into the training of the classification model (training phase) and testing using the trained model (testing phase). Initially, the classification model is trained using a database of labelled bird sounds. Intuitively, the performance of the trained classification model in predicting unknown bird sounds shall depend on the quality of the training data, feature selections, as well as the classification model adopted. The collection of rich but reliable labelled bird sounds is a critical first step in classifying birds. Next, the labelled bird sounds are processed and used to provide selected features to train the chosen classification model. Generally, large extracted features would give better classification performance, albeit with extra computational complexity. In this regard, the dimensionality reduction technique shall be used to select combinations of the best features. Two classification models shall be adopted: Nearest Centroid (NC) and Artificial Neural Network (ANN) classifiers.

Data Collection, Pre-processing and Segmentation

The quality and quantity of bird sounds are essential to allow proper training of the classification model. However, biogenic, anthropogenic, and wind noise may influence the quality of the recordings such that bird sounds may be inaudible or only audible for a short period (Giannakopoulos & Pikrakis, 2014). Furthermore, bird sounds typically contain combinations of songs and calls, which may need to be pre-processed to obtain sections that are used for feature extraction and classification purposes. In this regard, signal pre-processing plays an important role.

Pre-filtered bird sounds are used for both training and testing phases. In the case of noisy data, researchers commonly use either low, high or bandpass filters, depending on the bird species being considered (Vilches et al., 2006), to selectively reduce noise level whilst preserving the quality of the intended bird sounds. Then, the uninterrupted bird sounds may need to be segmented into segments of homogeneous content (Giannakopoulos & Pikrakis, 2014) using quasi-periodic syllables of bird sounds. This process can be done manually (Trifa et al., 2008; Lee et al., 2008; Anderson et al., 1996) or automatically, depending on the applications. Automatic segmentation is generally preferred for real-time applications. Different methods may be adopted for segmentation, by taking advantage of the energy in

the time or frequency domain (Evangelista et al., 2015) and analysing autocorrelation and roll-off of the songs (Ranjard & Ross, 2008).

Whilst manual segmentation may be used for non-real-time applications, automatic segmentation of bird sounds is adopted in this paper by implementing an energy envelop based algorithm in the time domain, and removing unwanted silent periods, to give samples of bird sounds. Many researchers have previously used this iterative time-domain algorithm (Fagerlund & Laine, 2014; Fagerlund, 2007; Härmä et al., 2004). Segmentation is performed on the training the birds' sound dataset and testing bird sound dataset.

Feature Extraction

Most nature-related data, including bird sounds, are extensive and contain much redundancy. After segmentation of bird sounds into quasi-periodic syllables, the data need to be processed further before it can be made as input onto the classification models to remove as much redundant and irrelevant information as possible whilst retaining important properties to allow efficient classification of the data. This stage, commonly referred to as feature extraction, may involve the extraction of physical or perceptual features based on measurable and reported characteristics perceived by humans (Gerhard, 2003). The same features must be extracted from every dataset to allow like-for-like comparison between different datasets to facilitate classification. Generally, features may be extracted from the time-domain representation of the data or its corresponding frequency domain representation. Obviously, for frequency-domain features, syllables of the original time-based bird sounds need to be first converted into their frequency domain representation before their features are extracted. Features may also be obtained from different syllables of the same dataset.

Each sample of the birds sound is divided into overlapping frames to perform feature extraction. M different features are derived from each frame, consisting of time, frequency and quasi-periodic features. The time-domain features include Zero Crossing Rate (ZCR), Energy (E), and Entropy of energy, whilst Spectral Centroid, Spectral Spread, Spectral Entropy, Spectral Flux, Spectral Roll-off, Mel Frequency Cepstral Coefficients (MFCCs), and Chroma Vectors form the frequency domain features from each frame (Sharma et al., 2020). Apart from these features, Harmonic Ratio and Fundamental Period are also extracted (Giannakopoulos & Pikrakis, 2014).

A total of M distinct features are derived from each frame, which is then averaged over the length of the sample. Each sample belonging to one of the L species of bird considered. For the i^{th} sample of the training data, its features are represented in an M dimensional space, in a row vector x_i , where $x_i \in R^M$; with each sample classified as one of the L species of bird under consideration i.e. $c_i \in \{w_1, w_2, \dots, w_L\}$. Consequently, for training data with N samples, feature matrix $X = [x_1, x_2, \dots, x_N]$, where $X \in R^{N \times M}$ and class column

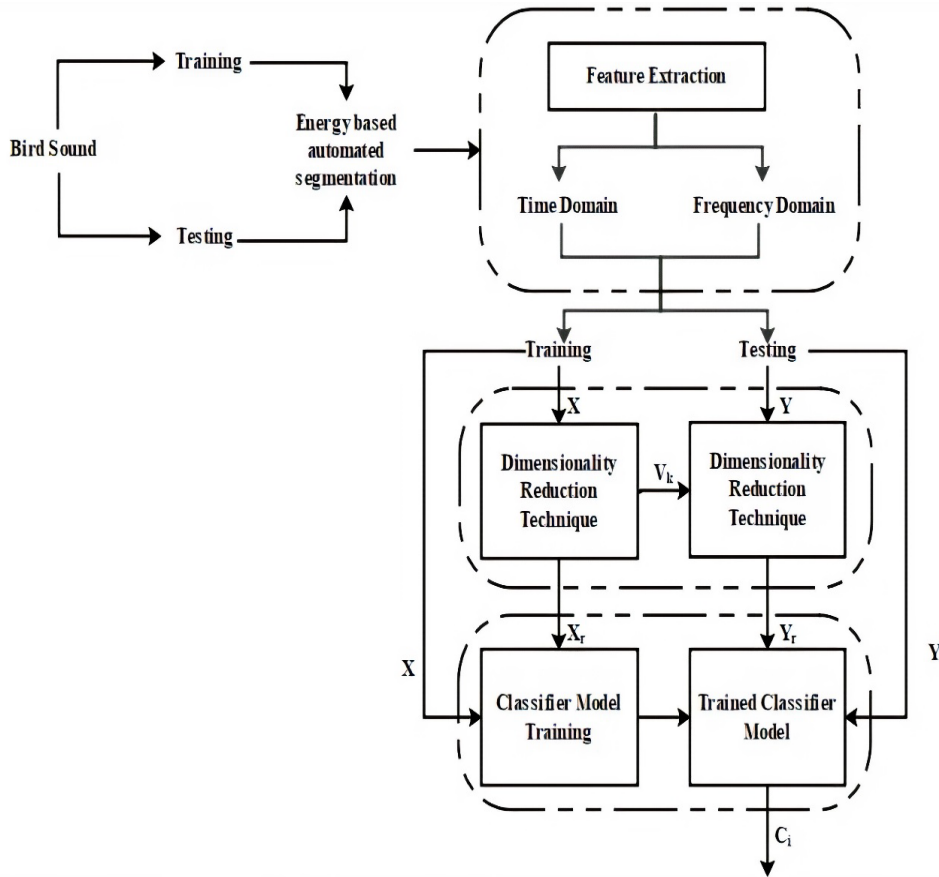


Figure 1. Proposed Methodology for Bird Sound Classification

vector $c \in R^N$ are used to populate feature information and species classification of all N segmented training samples, respectively.

Similar to the samples obtained from the training data, M features are also extracted from i^{th} test sample. This information is stored in an M dimensional space, in a row vector y_i , where $y_i \in R^M$. Each sample of the test data belongs to either one of the L species of birds under consideration. The classification model shall be performed predictions on species classification of the test sample, which has been previously pre-trained using the training data.

Dimensionality Reduction

For each training and testing sample, a feature row vector in an M dimensional space is obtained to describe the sample; forming feature matrix $X = [x_1, x_2, \dots, x_N]$, where

$X \in R^{N \times M}$ for the training dataset and $y_i \in R^M$ for each of the testing sample i . Of course, these M features from a single sample may be directly fed to the classification model of choice for either training or testing. However, not all of these M features are applicable, or may even contribute to the classification process in differentiating between the different species of birds. Nevertheless, the M features, which may contain plenty of redundant information, would surely increase computational complexity significantly.

An option would be to selectively truncate the number of features from M features to K features to reduce computational complexity of the classification process. For this purpose, numerous dimensionality reduction techniques (Tharwat et al., 2017) exist in the literature. These techniques may be generally categorised into unsupervised and supervised approaches. Commonly, the training dataset is used to determine the best set of K features from the original M features to feed into the classification process, Each of the K features is composed of a weighted combination of the original M features. This weighted combination derived from the training dataset shall then be used to determine the K features from the testing dataset.

Species classifications of the bird i.e. class column vector $c \in R^N$, are not taken into consideration in unsupervised dimensionality reduction processes, with information from the feature matrix $X = [x_1, x_2, \dots, x_N]$ only used to assist in choosing the best K features. Common unsupervised dimensionality reduction methods are Independent Component Analysis (Mogi & Kasai, 2013), Non-negative matrix factorisation (Ranjard & Ross, 2008; Ludeña-Choez et al., 2017) and Principal Component Analysis (PCA) (Lee et al., 2008; Milani et al., 2019). PCA is one of the most popular and widely used unsupervised dimensionality reduction method (Tan et al., 2012). It aims to project the original M dimensional feature matrix onto alternative orthogonal M dimensional space, by considering linear combinations of the M dimensional feature matrix with an objective of finding the alternative space, which gives the largest variance. Dimensionality reduction is achieved by selecting a reduced subset of K dimension, which accounts for as much variability to give a reduced dimension feature matrix $X_r \in R^{N \times K}$. Commonly, a projection matrix $V_k \in R^{M \times K}$ is obtained from PCA, which projects the original feature matrix $X_r \in R^{N \times K}$ onto the reduced dimension feature matrix $X_r \in R^{N \times K}$. The projection matrix may then be used to reduce the dimension of the testing data i ; from row vector y_i , where $y_i \in R^M$ to row vector $y_{r_i} \in R^K$.

On the other hand, supervised approach considers both features of the birds, i.e. the feature matrix $X = [x_1, x_2, \dots, x_N]$, as well as the species classifications, i.e. class column vector $c \in R^N$, to obtain a reduce set of K features from the original M features. Examples of supervised approaches include Neural Networks (NN), Mixture Discriminant Analysis (MDA) and Linear Discriminant Analysis (LDA) (Tharwat et al., 2017). Due to consideration of this extra information, the supervised approach can perform better in

applications that require the prediction of classes, such as bird species classification. Indeed, it has been shown that LDA outperforms PCA (Martinez & Kak, 2001), particularly in cases where the number of samples per class is small. Moreover, LDA works by selecting reduced dimensions, which accounts for as much variability across different classes, as possible, instead of across all samples, as used in PCA.

LDA transforms the original feature matrix $X \in R^{N \times M}$ of the training bird sounds, which lies in a M dimensional space, onto a reduced matrix $X_r \in R^{N \times K}$, which lies in a K dimensional space, where $K \leq M$. It is done by considering the classification c of the segmented bird sounds of the training data. Transformation using LDA is achieved via a two-step process: finding the suitable transformation matrix to achieved maximum class separability and selecting $K \leq M$ dimensions that best discriminate between the different classes. The first step translates into an optimisation problem to find the transformation matrix W which maximises the ratio of the between-class variance S_B to the within-class variance S_W , of the feature matrix X . Mathematically, this may be represented as the Fisher's criterion, as Equations 1 and 2

$$argmax_W \frac{W^T S_B W}{W^T S_W W} \tag{1}$$

where

$$W = S_W^{-1} \cdot S_B \tag{2}$$

The second step in LDA is to select the most significant dimensions of the matrix. This may be found by first finding the eigenvalues $\lambda = \{\lambda_1, \lambda_2, \dots, \lambda_M\}$ and eigenvectors $V = \{v_1, v_2, \dots, v_M\}$ of the transformation matrix W , using Equation 3

$$(W - \lambda_i) \cdot v_i = 0 \text{ for } i = 1, 2, \dots, M \tag{3}$$

The eigenvectors with the K highest eigenvalues are then chosen to construct the projection matrix $V_k \in R^{M \times K}$ to project the original feature matrix $X \in R^{N \times M}$ of the training bird sounds, onto a reduced dimension feature matrix $X_r \in R^{N \times K}$ using Equation 4

$$X_r = X \cdot V_k \tag{4}$$

The same projection matrix V_k , obtained from Equation 4, is also used to reduce the dimension of the i^{th} test bird sound $y_i \in R^M$ onto $y_{r_i} \in R^K$ using Equation 5

$$y_{r_i} = y_i \cdot V_k \tag{5}$$

It is noted that each element of $y_{r_i} \in R^K$ is a linear combinations of the original M features of the i^{th} test bird sound $y_i \in R^M$. Rather than directly reducing the number of features LDA allows a reduced number of combinations of features, as inputs onto the classification model.

Due to the potentially superior performance of the supervised approach, particularly LDA, compared to the unsupervised approach, LDA shall be considered the dimensionality reduction technique of choice in this paper. Different values of $K \leq M$ shall be chosen to be fed onto the classification process for training and testing, using two different classification models. Performance of the classification models using different values of K shall then be compared; in terms of accuracy in predicting unknown bird sound and computational complexity. It is noted that $K = M$ represents directly feeding the classification models with all the original M features without performing any dimensionality reduction, which forms the basis for comparisons.

It is highlighted that the training process is normally performed non-real-time. Hence, it has the luxury of training time required and using a processor with high processing power. On the other hand, the classification of bird sounds during the testing phase requires real-time processing with limited computing power. For this reason, developers usually are more concerned with the computational complexity during the testing phase.

Using LDA for the dimensionality reduction approach requires extra computation. However, the reduced dimensions being fed onto the classification process can reduce computation process during the classification. As can be seen from the dimension reduction process in Equation 5, each element of the vector $\mathcal{Y}_{r_i} \in R^K$ is composed of M multiplication and $(M - 1)$ addition operations. Since LDA reduces the dimensions to K , computational complexity of LDA during the testing phase is derived as $(M \cdot O(n^2) + (M - 1) \cdot O(n))$, where $O(n)$ is taken as the computational complexity for addition/subtraction operation and $O(n^2)$ as the computational complexities for multiplication/division operation, of an Arithmetic Logic Unit (ALU). Taking the features as type float i.e. $O(n) = O(n^2) = O(1)$, computational complexity can be simplified as $(2M - 1) \cdot K \cdot O(1)$. On the other hand, no extra computation is required for classification using all M features, i.e. without dimensionality reduction.

Classification

Generally, any machine learning technique aims to find the best function or mathematical model that may be used to classify bird species based on features of an unknown bird species. Training data is commonly used to derive this mathematical model. This phase is commonly referred to as the training phase. $K \leq M$ features from the training dataset, $K = M$ with representing using the classification models without any reduction to the dimensions of the original feature matrix may be used to derive the mathematical model. This mathematical model may then be used to classify unknown bird species in the inference phase, using similar $K \leq M$ features.

Two classification methods shall be considered in this paper: Nearest Centroids (NC), and Artificial Neural Network (ANN). Nearest Centroids (NC) are chosen due to their simplicity of implementation, requiring only the computation of centroids of each class

from the training dataset, with classification decisions based on the nearest distance of the unknown bird species centroids of the different classes. On the other hand, Artificial Neural Network (ANN) is a basic neural network. ANN uses the training dataset to determine an appropriate mathematical model using the concept of neurons.

Nearest Centroid (NC). NC is one of the simplest supervised classification methods. Class prediction of new unknown bird sound is assigned to the class of the centroids closest to the new unknown bird sound. At the initial stage, $K \leq M$ features from the training dataset are used to determine centroids or means for the different classes of birds. Given the feature matrix $\mathbf{X}_r \in \mathcal{R}^{N \times K}$ where $K \leq M$ with species classification column vector $\mathbf{c} = \{c_1, c_2, \dots, c_L\}$ used for training of the classifier model, centroid for species $w_j, j \in \{1, 2, \dots, L\}$, is represented by column vector $\boldsymbol{\mu}_j \in \mathcal{R}^K$ in the K dimensional space and is given by Equation 6:

$$\boldsymbol{\mu}_j = \frac{1}{|w_j|} \sum_{i \in w_j} \mathbf{x}_i \quad \forall j \in \{1, 2, \dots, L\} \tag{6}$$

where $|w_j|$ is the number of training bird sounds belonging to species class w_j . Centroids of the different species classification are then used for predicting unknown bird sounds. Feature vector $\mathbf{y}_{r_i} \in \mathcal{R}^K$ of the i^{th} test bird sound is used to predict its species classification \hat{c}_i , using Euclidian's distance calculation (Ramashini et al., 2019) as follows (Equation 7):

$$\hat{c}_i = \arg \min_{j \in \{1, 2, \dots, L\}} \|\boldsymbol{\mu}_j - \mathbf{y}_{r_i}\| \quad \hat{c}_i \in \{c_1, c_2, \dots, c_L\} \tag{7}$$

Although the training dataset is commonly very bulky, which is processed simultaneously during the training phase, it has the luxury of using a high-computing facility for processing due to its non-real-time nature. For this reason, the testing phase is more of a concern. As can be seen from Equation 7, NC involves the K subtraction operations to determine the distance of the i^{th} test bird sound to every centroids. Consequently, computational complexity of NC during the testing phase can be derived as $(L.K + 1)O(n) = (L.K + 1)O(1)$, for features of type float. It can be seen that complexity is proportional to the number of features K .

Artificial Neural Network (ANN). Alternative classification considered in this paper is ANN, which is one of the basic and prevalent supervised machine learning techniques that may be used for bird species classification. Figure 2 depicts a given layer of an ANN considered in this paper. $z^k(i)$ is the output of neuron i before the activation function in layer k , $a^k(i)$ is the output of neuron i after the activation function, n^k is the set of neurons in layer k , and $b^k(i)$ is the bias of neuron i in layer k . $\theta^k(i, j)$ is the weight between the output of neuron j in layer $k-1$ and neuron i in layer k . $g^k(z^k(i)), \forall i \in n^k$ is the activation function of every neuron in layer k of the ANN, and is used to provide non-linearity to the network (Equations 8 and 9),

$$z^k(i) = \sum_{j \in n^{k-1}} (\theta^k(i, j) \cdot a^{k-1}(j)) + b^k(i) \tag{8}$$

$$a^k(i) = g^k(z^k(i)) \tag{9}$$

These can alternatively be represented in matrix forms (Equations 10 and 11),

$$z^k = \theta^k \cdot A^{k-1} + b^k \tag{10}$$

$$A^k = g(z^k) \tag{11}$$

Where (Equations 12-18),

$$z^k = [z^k(1), z^k(2), \dots, z^k(|n^k|)]^T \tag{12}$$

$$\theta^k = \begin{bmatrix} \theta^k(1,1) & \dots & \theta^k(1, |n^{k-1}|) \\ \vdots & \ddots & \vdots \\ \theta^k(|n^k|, 1) & \dots & \theta^k(|n^k|, |n^{k-1}|) \end{bmatrix} \tag{13}$$

$$\theta^k = [\theta^k(i, j)] \forall (i \in n^k, j \in n^{k-1}) \tag{14}$$

$$A^k = \begin{bmatrix} a^k(1,1) & \dots & a^k(1, |n^k|) \\ \vdots & \ddots & \vdots \\ \theta a^k(|n^{k-1}|, 1) & \dots & a^k(|n^{k-1}|, |n^k|) \end{bmatrix} \tag{15}$$

$$A^k = [a^k(i, j)] \forall (i \in n^{k-1}, j \in n^k) \tag{16}$$

$$b^k = [b^k(1), b^k(2), \dots, b^k(|n^k|)]^T \tag{17}$$

$$g = [g^1(\cdot), g^2(\cdot), \dots, g^k(\cdot)]^T \tag{18}$$

In this paper, ANN with $K \leq M$ features in the input layer, 1 hidden layer and 1 output layer is considered, as depicted in Figure 2. The number of neurons in the output layer corresponds to the number of bird species considered. Elliot Sigmoid function is used as the input layer’s activation function (Elliott, 1993), which closely approximates the Hyperbolic Tangent or Sigmoid functions for small values. Whilst Softmax function is used as the output activation function in order to represent the probability distributions of a list of potential outcomes.

During the training phase of the ANN classifier, the objective is to find a set of weights θ^k so that the ANN can classify bird species accurately, using the training dataset as its basis. The ANN, together with this set of weights θ^k , then form the mathematical model used to classify unknown bird sound species during the testing phase.

Similar to NC, the testing phase of ANN represents a concern in terms of computational complexity, as it needs to be processed in real-time. The overall complexity is composed of the input-hidden and hidden-input layers, obtained using Equations 8 and 9, respectively, depending on the number of neurons. As there are K neurons at the input of the ANN, complexity of the input-hidden layer may be approximated as $KO(n^2) + KO(n)n^h + n^hO(g_h)$ where n^h is the number of neurons in the hidden layer and $O(g_h)$ is the complexity of the activation function in the hidden layer (depending on the function used). At the hidden-output layer, L represents the number of neurons at the output of the ANN. As such, complexity may be approximated as $(n^hO(n^2) + n^hO(n))L + L.O(g_o)$, where $O(g_o)$ is the complexity of the activation function in the output layer. Overall, complexity during the testing phase of the ANN is given by $(KO(n^2) + KO(n)n^h + n^hO(g_h) + (n^hO(n^2) + n^hO(n))L + L.O(g_o))$. Again, taking the features as type float, complexity can be simplified as $(2K + 2L)n^hO(1) + n^hO(g_h) + L.O(g_o)$. It can be seen that the complexity is also proportional to the number of features K that are being fed to the classification model as well as the number of neurons n^h in the hidden layer. Thus, there is no fixed relationship. Generally, the higher the number of features, i.e. the number of neurons in the input layer, the higher the number of neurons required in the hidden layer to achieve reasonable classification accuracy.

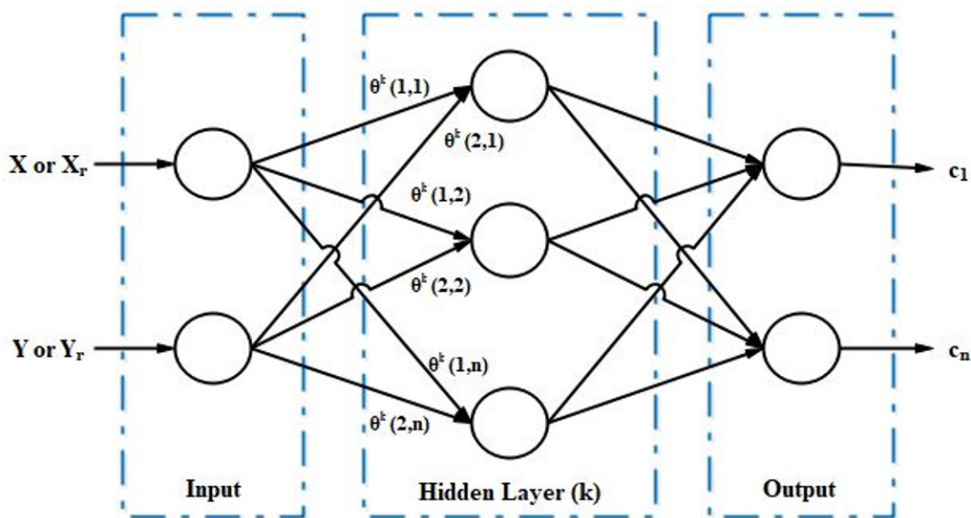


Figure 2. Artificial Neural Network (ANN) architecture adopted

RESULTS AND DISCUSSION

Ten $L = 10$ endemic bird species of the Borneo region have been selected, i.e. Rhinoceros Hornbill (RH), Hooded Pitta (HP), Savanna Nightjar (SN), Collared Owllet (CO), Collared Kingfisher (CK), Crested Serpent Eagle (CSE), Bornean Tree Pie (BTP), Bornean Spider Hunter (BSH), Malaysian Pied Fantail (MPF), and Malaysian Banded Pitta (MBP), with audio recordings collected from the xeno-canto (<https://www.xeno-canto.org/>) online database, which is one of the most frequently used online databases in bird sound classification related research (Ramashini et al., 2019; Sprengel et al., 2016; Lasseck, 2015; Stowell & Plumbley, 2014). These bird species represent some of the most commonly found birds in the region. Sponsored by the Xeno-Canto Foundation, the Xeno-Canto online database contains sound recordings of wild birds from all over the world verified by experts. These recordings are shared under various Creative Commons licenses, freely available online. Thus, they can be used for education and research purposes. The time duration of each bird sound sample varies, with standard recordings lasting for a few seconds. Metadata provided with the data has indicated that most samples are recorded with a 44 kHz sampling rate. Figure 3 shows the time and frequency domain representation of selected bird sounds.

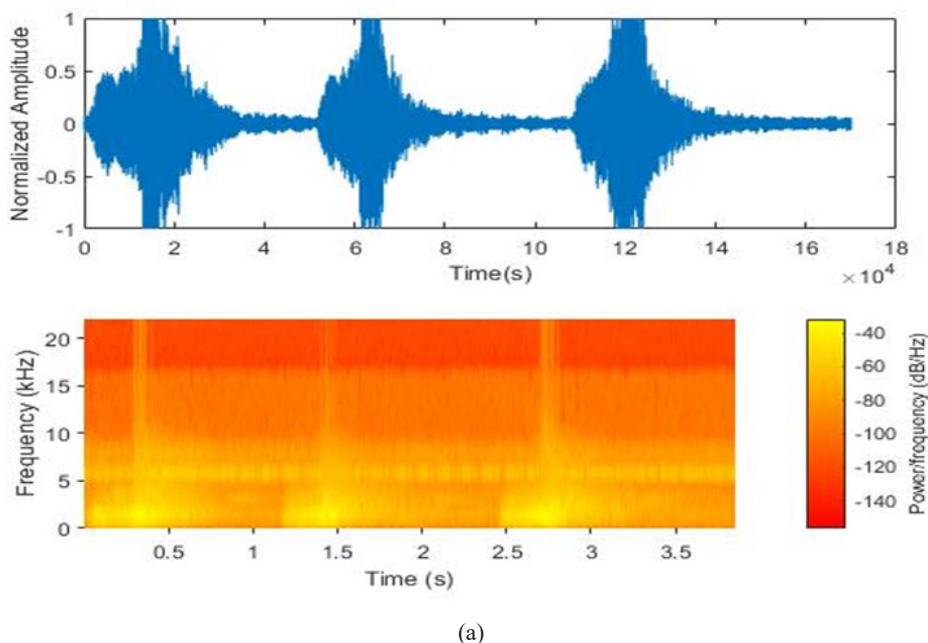
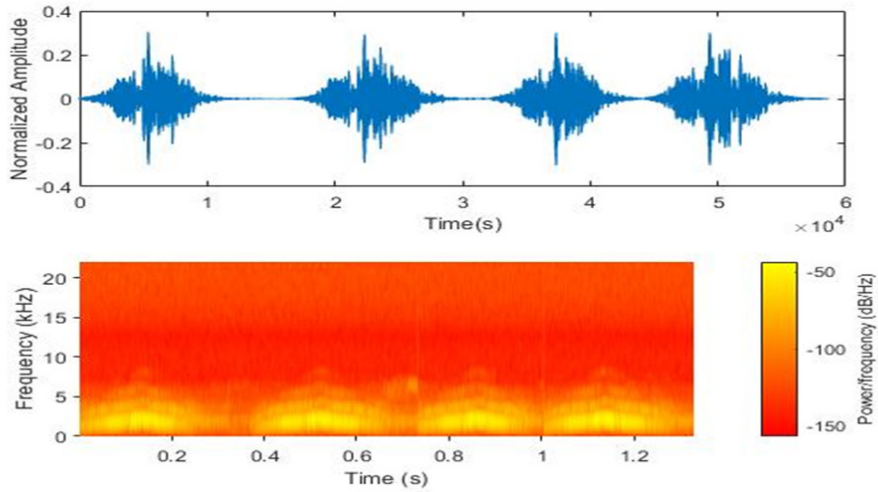
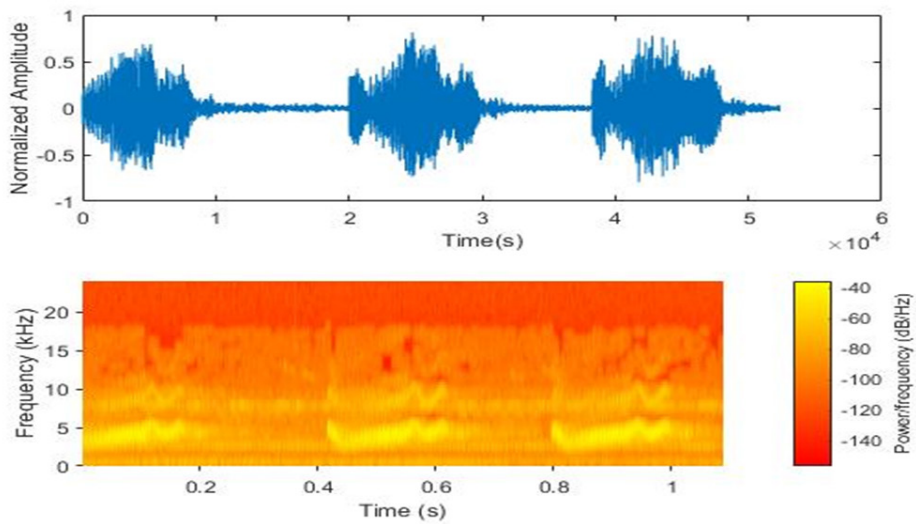


Figure 3. Time and frequency representation of bird samples; (a) Rhinoceros Hornbill (RH)



(b)



(c)

Figure 3. Time and frequency representation of bird samples; (b) Hooded Pitta (HP), (c) Savanna Nightjar (SN)

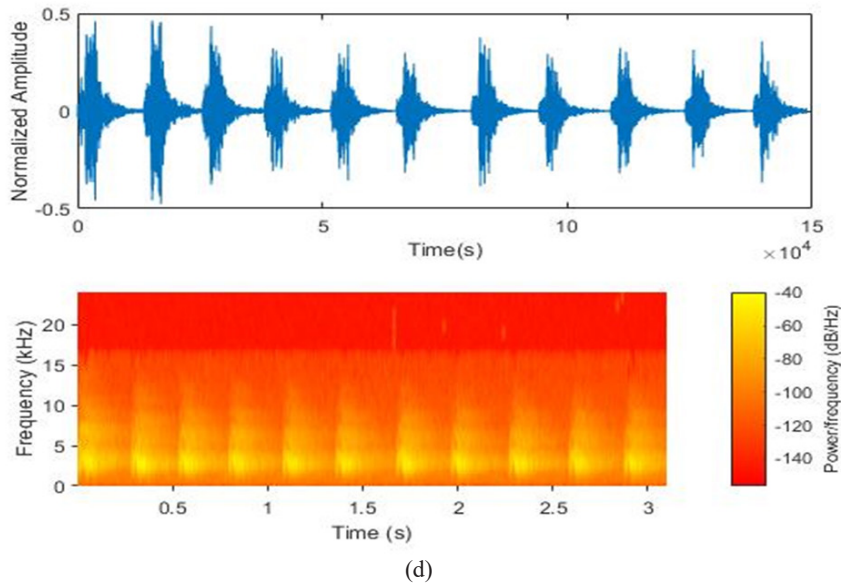


Figure 3. Time and frequency representation of bird samples; (d) Collared Kingfisher (CK)

The sounds are segmented using an energy-based automatic segmentation algorithm and divided into training and testing data sets. In this work, both 70:30 and 80:20 ratios of training to testing data are performed. In addition, 20% of the training dataset is chosen randomly for cross-validation purposes. The model is iteratively trained and validated on these different datasets. Furthermore, the training and testing data set are shuffled randomly multiple times to replicate the training and testing cycles with different combinations. These are done to avoid over-fitting as well as to ascertain the consistency of the result.

In total, 150 bird sounds have been used for training and testing, with 15 bird sounds for each class. $M = 35$ features have been extracted from each segment automatically, consisting of the frequency domain, time domain and other types of features, to form the training and testing feature matrices, giving the original feature matrix $X \in R^{N \times 35}$ of training bird sounds and the i^{th} test bird sound $y_i \in R^{35}$.

The original feature matrix $X \in R^{N \times 35}$ of the training bird sounds and the i^{th} test bird sound $y_i \in R^{35}$ can be fed directly to the classification algorithms. Alternatively, the dimensions may be first reduced using LDA to give a reduced matrix X_r . Similarly, in the testing phase, either the i^{th} test bird sound y_i can be fed directly, or it can be first reduced using the derived projection matrix V_k to give y_{r_i} ; incurring additional complexity of $69.K.O(1)$ in the testing phase. Obviously, reducing K reduces complexity during the classification stage but requires extra computation during its dimension reduction process. In the classification stage using NC classifier, computational complexity is given by $(10.K + 1)O(1)$, and is dependent on the number of features K that are fed onto the

NC classifier. On the other hand, computational complexity of ANN classifier is given by $(2K + 20)n^h O(1) + n^h O(g_h) + 10 \cdot O(g_o)$; dependent on both the number of features K that are fed onto the ANN classifier, as well as the number of neurons n^k in the hidden layer of the ANN classifier. Increasing K results in an increase in the computational complexity for both NC and ANN classifiers, and the larger the number of neurons n^k , the more complex the ANN model becomes. Elliot Symmetric Sigmoid and Softmax functions are used for the hidden and output layers of the ANN, respectively.

In the case of the NC classifier, feeding all 35 features to the classification model directly without reduction requires a complexity of $351 \cdot O(1)$ in the testing phase. However, introducing LDA to reduce the number of features prior to the classification stage, requires extra computation for the reduction process. As such, collectively, the computational complexity for both the dimension reduction and NC classification sharply increases from $351 \cdot O(1)$ to $2687 \cdot O(1)$ by reducing the number of features from 35 to 34 using LDA. However, complexity decreases as the number of features K fed onto the classification model are reduced further. For instance, reducing the number of features K fed onto the classification model to a certain limit would result in lower complexity than without using LDA. Table 1 shows the relationship between the number of features K fed onto the NC classifier and the resulting computational complexity, with and without LDA.

Testing accuracy of the NC classifier, with and without LDA, for different features K being fed, is given in Figure 4. NC classifier accuracy for without any reduction is 13.3% and 10% for 80:20 and 70:30 ratios of training to testing data, respectively. It can be seen that even with 1 LDA, the accuracy of the NC is much higher than without using LDA. Thus, this is because LDA projects the original matrix X and the test sound Y_i onto reduced dimensions matrix and vector that can best discriminate between different classes of bird sounds. Output matrix and vector are also ranked. The lower elements represent the most significant elements that may be used to discriminate between classes. As shown from Figure 4, improvement in accuracy is initially considerable with a small number of LDA features considered, up to a maximum accuracy upon which increasing the number of LDA features considered even further would result in a gradual reduction in accuracy using the NC classifier. Maximum accuracies of 96.7% with 7 LDA features, and 78% with 5-7 LDA features considered, are achievable for 80:20 and 70:30 ratios of training to testing data, respectively. With 7 LDA features considered, the computational complexity of the LDA/NC is $555 \cdot O(1)$.

Table 1 also gives the relationship between the number of features K fed onto the ANN classifier and the resulting computational complexity, with and without LDA. Whilst it is evident that complexity for NC reduces with the reduction in the number of LDA features K , it is not very straightforward with ANN. The complexity of ANN has a direct relationship with the number of LDA features K . However, it is also dependent on the number of neurons

n^h in the hidden layer with complexity increasing with the number of neurons n^h in the hidden layer. Figure 5 shows accuracies obtained using the ANN classifier with different values of n^h for $K = M = 35$, i.e. without LDA reduction. It can be seen that increasing the number of neurons n^h in the hidden layer does not necessarily improve the accuracy of the ANN model. The highest accuracy of 93.3% is achieved with $n^h = 100$. In fact, for a given number of features K , the number of neurons n^h in the hidden layer may need to be optimised to reach an optimal accuracy during the training phase.

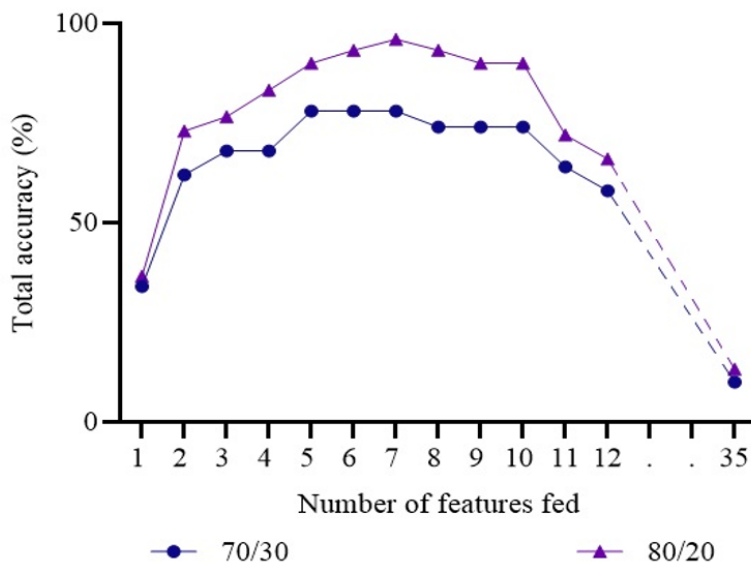


Figure 4. Testing accuracy obtained by Nearest Centroid (NC) for different number of Linear Discriminant Analysis (LDA) features K considered.

Table 1

The computational complexity of NC and ANN, with and without LDA reduction, for different number of inputs to the classification models for the testing phase

Inputs		Nearest Centroid (NC)	Artificial Neural Network (ANN)
w/o LDA	35	$351 \cdot O(1)$	$90 \cdot n^h O(1) + n^h O(g_h) + 10 \cdot O(g_o)$
	30	$2371 \cdot O(1)$	$(2070 + 80n^h)O(1) + n^h O(g_h) + 10 \cdot O(g_o)$
	25	$1976 \cdot O(1)$	$(1725 + 70n^h)O(1) + n^h O(g_h) + 10 \cdot O(g_o)$
W LDA	20	$1581 \cdot O(1)$	$(1380 + 60n^h)O(1) + n^h O(g_h) + 10 \cdot O(g_o)$
	15	$1186 \cdot O(1)$	$(1035 + 50n^h)O(1) + n^h O(g_h) + 10 \cdot O(g_o)$
	10	$791 \cdot O(1)$	$(690 + 40n^h)O(1) + n^h O(g_h) + 10 \cdot O(g_o)$
	5	$396 \cdot O(1)$	$(345 + 30n^h)O(1) + n^h O(g_h) + 10 \cdot O(g_o)$

Table 2 shows the optimum number of neurons n^h in the hidden layer and accuracies for a different number of LDA features. Generally, it can be seen that increasing the number of LDA features K also increases the number of neurons n^h in the hidden layer, which consequently results in an overall increase in complexity. In terms of accuracy, the initial increase in the number of LDA features K , increases accuracy until a maximum accuracy is reached, increasing K even further would result in a reduction in accuracy. Accuracies for different numbers of LDA features K for 70:30 and 80:20 ratios of training to testing data are given in Figure 6. Characteristics for both 70:30 and 80:20 ratios of training to testing data are similar with an initial increase in accuracy until an optimum is reached, beyond which accuracy starts to reduce.

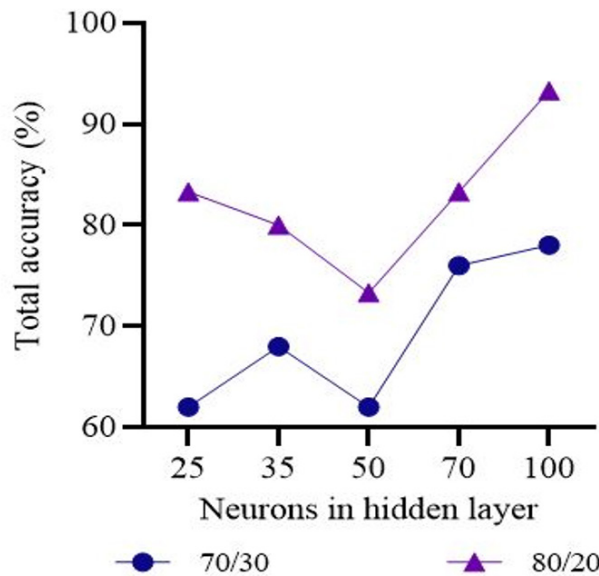


Figure 5. Testing accuracy obtained by Artificial Neural Network (ANN) for different number of neurons n^h in the hidden layer

Maximum accuracy obtained is 96.7% for 10 input LDA features with complexity of $1250.O(1) + 14.O(g_h) + 10.O(g_o)$. This is the same maximum accuracy obtained by NC classifier for 7 input LDA features with complexity of $555.O(1)$.

Comparing classification accuracies of NC and ANN classifiers with and without LDA, it can be seen that the selection of features using LDA improves performance significantly. Hence, this is especially true in the case of the NC classifier, where classification accuracy increased from 13.3% to 96.7% by using LDA. Thus, NC classification with 7 LDA and

ANN classification with 10 LDA, for 80:20 ratio of training and testing, produce the optimum testing accuracies.

Table 3 shows class-wise classification results of NC classifier with 7 LDA as input and ANN classifier with 10 LDA as input. It can be seen that the NC classifier wrongly predicted one sample of the bird BSH whilst the ANN classifier wrongly predicted one sample of the bird CO. Precision or P , i.e. the proportion of correct classification from the total predicted classification of a particular class. Recall or R , i.e. the proportion of correct classification from the actual total classification of a particular class, is another valuable measure of performance of a classification model. F_{SCORE} value of a particular class can be obtained from P and R as Equation 19,

$$F_{score} = \frac{2PR}{P + R} \tag{19}$$

Table 2

Computational complexity of artificial neural network (ANN) with linear discriminant analysis (LDA) reduction for the optimum number of neurons in the hidden layer n^h , for the testing phase

Input LDA, K	Neurons in Hidden Layer, n^h	Complexity	Accuracy (%)
1	3	$135.O(1) + 3.O(g_h) + 10.O(g_o)$	46.7
2	3	$210.O(1) + 3.O(g_h) + 10.O(g_o)$	73.3
3	4	$311.O(1) + 4.O(g_h) + 10.O(g_o)$	66.7
4	5	$416.O(1) + 5O(g_h) + 10.O(g_o)$	83.3
5	8	$585.O(1) + 8.O(g_h) + 10.O(g_o)$	76.7
6	9	$702.O(1) + 9.O(g_h) + 10.O(g_o)$	86.7
7	8	$755.O(1) + 8.O(g_h) + 10.O(g_o)$	90
8	8	$840.O(1) + 8.O(g_h) + 10.O(g_o)$	90
9	11	$1039.O(1) + 11.O(g_h) + 10.O(g_o)$	90
10	14	$1250.O(1) + 14.O(g_h) + 10.O(g_o)$	96.7
11	15	$1389.O(1) + 15.O(g_h) + 10.O(g_o)$	66.7
12	16	$1532.O(1) + 16.O(g_h) + 10.O(g_o)$	63.3

Figures 7 and 8 show the confusion matrices for NC classifier with 7 LDA inputs and ANN with 10 LDA inputs, respectively. As shown in Figure 7 for NC classification with 7 LDA, one sample from class 8, i.e. BSH bird, has been wrongly predicted as class 7, i.e. BTP bird. Subsequently, the precision value and F_{SCORE} for class 7 are 0.75 and 0.86, respectively, whilst for class 8, recall value and F_{SCORE} are 0.67 and 0.80, respectively. On

the other hand, as shown in Figure 8, ANN classification with 10 LDA wrongly predicted one sample of class 4, i.e. CO bird, as class 8, i.e. BSH bird. As a result, the precision value and F_{SCORE} for class 7 are 0.75 and 0.86, respectively. For class 4, the recall value and F_{SCORE} are 0.67 and 0.80, respectively.

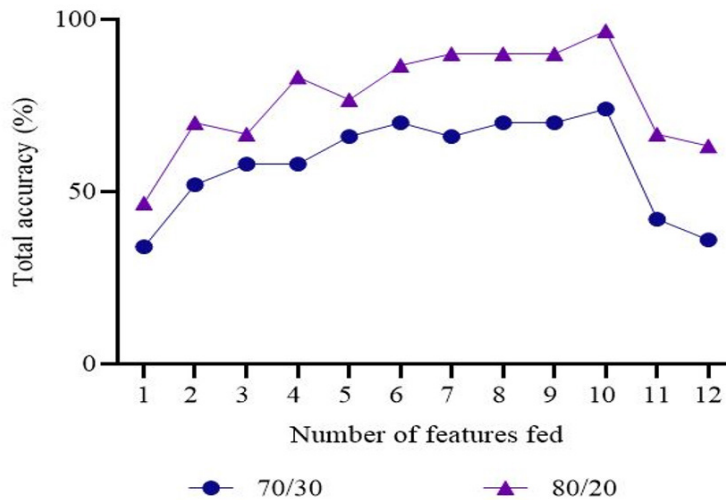


Figure 6. Testing accuracy obtained by the Artificial Neural Network (ANN) for different number of Linear Discriminant Analysis (LDA) features

Table 3

Class wise testing accuracy of Nearest Centroid (NC) classification with 7 Linear Discriminant Analysis (LDA) and Artificial Neural Network (ANN) classification with 10 Linear Discriminant Analysis (LDA)

Class Number	Birds Name	Testing Accuracy (%)	
		NC classification with 7 LDA features	ANN classification with 10 LDA features
1	RH	10	10
2	HP	10	10
3	SN	10	10
4	CO	10	6.7
5	CK	10	10
6	CSE	10	10
7	BTP	10	10

Table 3 (Continued)

Class Number	Birds Name	Testing Accuracy (%)	
		NC classification with 7 LDA features	ANN classification with 10 LDA features
8	BSH	6.7	10
9	MPF	10	10
10	MBP	10	10
Total Accuracy (%)		96.7	96.7

In the testing phase, NC and ANN classifiers with LDA give prediction accuracies of 96.7%. Each has one wrong prediction of the sample in different classes. Without LDA, the ANN classifier gives 93.3% accuracy with two wrong predictions. In contrast, the performance of an NC classifier without LDA is abysmal. Furthermore, in terms of computational complexity, both classifiers without LDA are comparatively less complex during the testing stage, than LDA. However, the complexity of the ANN classifier is always higher than the NC classifier, irrespective of using LDA as feature reduction, since its complexity depends on the number of neurons in both hidden and output layer and the activation function used.

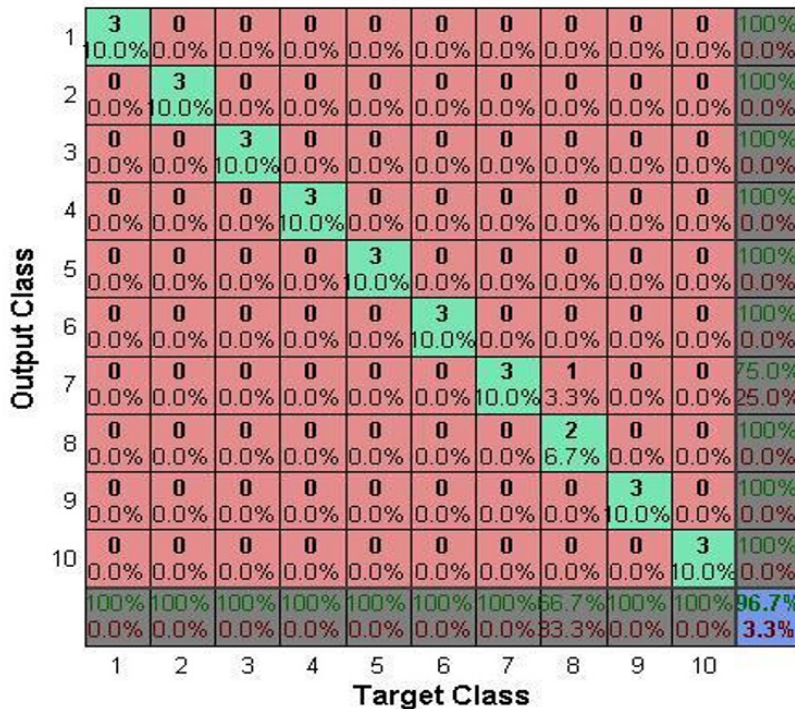


Figure 7. Testing confusion matrix: Nearest Centroid (NC) classification with 7 Linear Discriminant Analysis (LDA)

Output Class	1	3 0.0%	0 0.0%	0 0.0%	0 0.0%	0 0.0%	0 0.0%	0 0.0%	0 0.0%	0 0.0%	0 0.0%	100%
	2	0 0.0%	3 10.0%	0 0.0%	0 0.0%	0 0.0%	0 0.0%	0 0.0%	0 0.0%	0 0.0%	0 0.0%	100%
	3	0 0.0%	0 0.0%	3 10.0%	0 0.0%	0 0.0%	0 0.0%	0 0.0%	0 0.0%	0 0.0%	0 0.0%	100%
	4	0 0.0%	0 0.0%	0 0.0%	2 6.7%	0 0.0%	0 0.0%	0 0.0%	0 0.0%	0 0.0%	0 0.0%	100%
	5	0 0.0%	0 0.0%	0 0.0%	0 0.0%	3 10.0%	0 0.0%	0 0.0%	0 0.0%	0 0.0%	0 0.0%	100%
	6	0 0.0%	0 0.0%	0 0.0%	0 0.0%	0 0.0%	3 10.0%	0 0.0%	0 0.0%	0 0.0%	0 0.0%	100%
	7	0 0.0%	0 0.0%	0 0.0%	0 0.0%	0 0.0%	0 0.0%	3 10.0%	0 0.0%	0 0.0%	0 0.0%	100%
	8	0 0.0%	0 0.0%	0 0.0%	1 3.3%	0 0.0%	0 0.0%	0 0.0%	3 10.0%	0 0.0%	0 0.0%	75.0%
	9	0 0.0%	0 0.0%	0 0.0%	0 0.0%	0 0.0%	0 0.0%	0 0.0%	0 0.0%	3 10.0%	0 0.0%	100%
	10	0 0.0%	0 0.0%	0 0.0%	0 0.0%	0 0.0%	0 0.0%	0 0.0%	0 0.0%	0 0.0%	3 10.0%	100%
		100%	100%	100%	66.7%	100%	100%	100%	100%	100%	100%	96.7%
		0.0%	0.0%	0.0%	33.3%	0.0%	0.0%	0.0%	0.0%	0.0%	0.0%	3.3%
		1	2	3	4	5	6	7	8	9	10	
		Target Class										

Figure 8. Testing confusion matrix: Artificial Neural Network (ANN) classification with 10 Linear Discriminant Analysis (LDA)

CONCLUSION

Classification of birds using their sound is preferable as compared to visual identification, especially in dense forests. The general processing steps for bird sound classification are pre-processing, segmentation, feature extraction and classification. This paper aims to classify ten endemic Bornean birds by their sounds, collected from an online database and pre-processed to remove unwanted noise. Then, using an energy-based automated segmentation algorithm, the recordings are segmented for further processing. Thirty-five (35) acoustic features have been extracted from the segmented samples. The LDA has been used to reduce the dimensionality and select only the significant features before feeding the transformed features onto the classifier. The NC and ANN classifiers have been used for classification. It has been shown that both NC and ANN classifiers with LDA give 96.7% accuracy, which is comparatively higher than the performance of both classifiers without LDA in terms of testing accuracy.

Nevertheless, when computational complexity is considered, the simple NC classifier produces the same accuracy with the computational complexity of only 555.0(1), compared to the more complex ANN classifier. Thus, the NC classifier requires 7 LDAs to produce the optimum result. On the other hand, ANN’s computational complexity

is $1250.O(1)+14.O(g_h)+10.O(g_o)$, requiring 10 LDAs to give the optimum classification accuracy. The result is significant, as it indicates that the simple NC classifier with LDA can give optimum classification accuracy of 96.7% with relatively low computational power.

In future work, other classification approaches such as naive Bayes and decision trees may be combined with the proposed method to reinforce the benefit of using the proposed dimensionality optimisation method in improving accuracy whilst reducing complexity. Furthermore, the variety of bird species and more samples may also be considered to reflect the rich biodiversity in the Borneo region whilst implementing real-time bird sound classification.

ACKNOWLEDGEMENT

The corresponding author would like to thank Universiti Brunei Darussalam (UBD) for awarding the University Graduate Scholarship (UGS) to pursue a PhD at the university. Further, the author like to thank Uva Wellassa University, Sri Lanka, for their support in granting study leave for her PhD work at UBD.

REFERENCES

- Alvarsson, J. J., Wiens, S., & Nilsson, M. E. (2010). Stress recovery during exposure to nature sound and environmental noise. *International Journal of Environmental Research and Public Health*, 7(3), 1036-1046. <https://doi.org/10.3390/ijerph7031036>
- Anderson, S. E., Dave, A. S., & Margoliash, D. (1996). Template-based automatic recognition of birdsong syllables from continuous recordings. *The Journal of the Acoustical Society of America*, 100(2), 1209-1219. <https://doi.org/10.1121/1.415968>
- Badi, A., Ko, K., & Ko, H. (2019). Bird sounds classification by combining PNCC and robust Mel-log filter bank features. *Journal of the Acoustical Society of Korea*, 38(1), 39-46. <https://doi.org/10.7776/ASK.2019.38.1.039>
- Butler, R. W. (2019). Niche tourism (birdwatching) and its impacts on the well-being of a remote island and its residents. *International Journal of Tourism Anthropology*, 7(1), 5-20. <https://doi.org/10.1504/ijta.2019.10019435>
- Chou, C. H., Liu, P. H., & Cai, B. (2008). On the studies of syllable segmentation and improving MFCCs for automatic birdsong recognition. In *Proceedings of the 3rd IEEE Asia-Pacific Services Computing Conference, APSCC 2008* (pp. 745-750). IEEE Publishing. <https://doi.org/10.1109/APSCC.2008.6>
- Elliott, D. L. (1993). A better activation function for artificial neural networks. *ISR Technical Report TR 93-8*. Neuro Dyne, Inc.
- Evangelista, T. L., Priolli, T. M., Silla, C. N., Angelico, B. A., & Kaestner, C. A. (2015). Automatic segmentation of audio signals for bird species identification. In *2014 IEEE International Symposium on Multimedia* (pp. 223-228). IEEE Publishing. <https://doi.org/10.1109/ISM.2014.46>

- Fagerlund, S. (2007). Bird species recognition using support vector machines. *EURASIP Journal on Advances in Signal Processing*, 2007, 1-8. <https://doi.org/10.1155/2007/38637>
- Fagerlund, S., & Laine, U. K. (2014). New parametric representations of bird sounds for automatic classification. In *2014 IEEE International Conference on Acoustics, Speech and Signal Processing - Proceedings (ICASSP)* (pp. 8247-8251). IEEE Publishing. <https://doi.org/10.1109/ICASSP.2014.6855209>
- Gerhard, D. (2003). Audio signal classification: History and current techniques. *Technical Report TR-CS 2003-07*. University of Regina.
- Giannakopoulos, T., & Pikrakis, A. (2014). *Introduction to audio analysis: A MATLAB® approach*. Academic Press.
- Härmä, A., Somervuo, P., Harma, A., & Somervuo, P. (2004). Classification of the harmonic structure in bird vocalization. In *2004 IEEE International Conference on Acoustics, Speech, and Signal Processing (Vol. 5, pp. V-701)*. IEEE Publishing. <https://doi.org/10.1109/ICASSP.2004.1327207>
- Kutzner, D. (2019). Environmental change, resilience, and adaptation in nature-based tourism: Conceptualizing the social-ecological resilience of birdwatching tour operations. *Journal of Sustainable Tourism*, 27(8), 1142-1166. <https://doi.org/10.1080/09669582.2019.1601730>
- Lasseck, M. (2015). Improved automatic bird identification through decision tree based feature selection and bagging. *LifeCLEF*. Museum für Naturkunde Berlin.
- Lee, C. H., Han, C. C., & Chuang, C. C. (2008). Automatic classification of bird species from their sounds using two-dimensional cepstral coefficients. *IEEE Transactions on Audio, Speech and Language Processing*, 16(8), 1541-1550. <https://doi.org/10.1109/TASL.2008.2005345>
- Ludeña-Choez, J., Quispe-Soncco, R., & Gallardo-Antolín, A. (2017). Bird sound spectrogram decomposition through non-negative matrix factorization for the acoustic classification of bird species. *PLoS ONE*, 12(6), 1-20. <https://doi.org/10.1371/journal.pone.0179403>
- Martinez, A. M., & Kak, A. C. (2001). PCA versus LDA. *IEEE Transactions on Pattern Analysis and Machine Intelligence*, 23(2), 228-233. <https://doi.org/10.1109/34.908974>
- McIlraith, A. L., & Card, H. C. (1997). Birdsong recognition using backpropagation and multivariate statistics. *IEEE Transactions on Signal Processing*, 45(11), 2740-2748. <https://doi.org/10.1109/78.650100>
- Milani, M. G. M., Abas, P. E., & De Silva, L. C. (2019). Identification of normal and abnormal heart sounds by prominent peak analysis. In *Proceedings of the 2019 International Symposium on Signal Processing Systems* (pp. 31-35). Association for Computing Machinery. <https://doi.org/10.1145/3364908.3364924>
- Mogi, R., & Kasai, H. (2013). Noise-Robust environmental sound classification method based on combination of ICA and MP features. *Journal of Artificial Intelligence Research*, 2(1), 107-121. <https://doi.org/10.5430/air.v2n1p107>
- Priyadarshani, N., Marsland, S., & Castro, I. (2018). Automated birdsong recognition in complex acoustic environments: A review. *Journal of Avian Biology*, 49(5), 1-27. <https://doi.org/10.1111/jav.01447>
- Ramashini, M., Abas, P. E., Grafe, U., & De Silva, L. C. (2019). Bird sounds classification using linear discriminant analysis. In *2019 4th International Conference and Workshops on Recent Advances and Innovations in Engineering (ICRAIE)* (pp. 1-6). IEEE Publishing. <https://doi.org/10.1109/ICRAIE47735.2019.9037645>

- Ranjard, L., & Ross, H. A. (2008). Unsupervised bird song syllable classification using evolving neural networks. *The Journal of the Acoustical Society of America*, 123(6), 4358-4368. <https://doi.org/10.1121/1.2903861>
- Selouani, S. A. S. A., Kardouchi, M., Hervet, É., Roy, D., Hervet, E., & Roy, D. (2005). Automatic birdsong recognition based on autoregressive time-delay neural networks. In *2005 ICSC Congress on Computational Intelligence Methods and Applications* (pp. 1-6). IEEE Publishing. <https://doi.org/10.1109/CIMA.2005.1662316>
- Sharma, G., Umapathy, K., & Krishnan, S. (2020). Trends in audio signal feature extraction methods. *Applied Acoustics*, 158, Article 107020. <https://doi.org/10.1016/j.apacoust.2019.107020>
- Sprengel, E., Jaggi, M., Kilcher, Y., & Hofmann, T. (2016). Audio Based Bird Species Identification using Deep Learning Techniques. In *Working Notes of CLEF 2016* (pp. 547-559). Cross Language Evaluation Forum.
- Stowell, D., & Plumbley, M. D. (2014). Automatic large-scale classification of bird sounds is strongly improved by unsupervised feature learning. *PeerJ*, 2, Article e488. <https://doi.org/10.7717/peerj.488>
- Suthers, R. A. (2004). How birds sing and why it matters. In *Nature's Music: The Science of Birdsong* (pp. 272-295). Elsevier Academic Press. <https://doi.org/10.1016/B978-012473070-0/50012-8>
- Tan, L. N., Kaewtip, K., Cody, M. L., Taylor, C. E., & Alwan, A. (2012). Evaluation of a Sparse Representation-Based Classifier For Bird Phrase Classification Under Limited Data Conditions. In *Thirteenth Annual Conference of the International Speech Communication Association* (pp. 2522-2525). International Speech Communication Association (ISCA).
- Terry, A. M. R., & McGregor, P. K. (2002). Census and monitoring based on individually identifiable vocalizations: The role of neural networks. *Animal Conservation*, 5(2), 103-111. <https://doi.org/10.1017/S1367943002002147>
- Tharwat, A., Gaber, T., Ibrahim, A., & Hassanien, A. E. (2017). Linear discriminant analysis: A detailed tutorial. *AI Communications*, 30(2), 169-190. <https://doi.org/10.3233/AIC-170729>
- Trifa, V. M., Kirschel, A. N. G., Taylor, C. E., & Vallejo, E. E. (2008). Automated species recognition of antbirds in a Mexican rainforest using hidden Markov models. *The Journal of the Acoustical Society of America*, 123(4), 2424-2431. <https://doi.org/10.1121/1.2839017>
- Vilches, E., Escobar, I. A., Vallejo, E. E., & Taylor, C. E. (2006). Data mining applied to acoustic bird species recognition. In *18th International Conference on Pattern Recognition (ICPR'06)* (Vol. 3, pp. 400-403). IEEE Publishing. <https://doi.org/10.1109/ICPR.2006.426>



Behavioural Model for Decision-Makers' towards the Intention to Adopt Green Information Technology: A Preliminary Study

Abba Kyari Buba^{1,2*} and Othman Ibrahim¹

¹Department of Information Systems, School of Computing, Universiti Teknologi Malaysia, 81310 Skudai, Johor, Malaysia

²Faculty of Social and Management Science, Yobe State University, Nigeria

ABSTRACT

This preliminary survey investigates and validates the measurement model of factors influencing decision makers' intentions to adopt Green information technology (Green-IT) in manufacturing sectors in Nigeria. The Norm Activation Model (NAM) and Theory of Planned Behaviour (TPB) were used to explore the factors that could influence decision-makers' intention in adopting Green-IT. Using constructs from the NAM and TPB, this survey proposes a model for identified behavioural factors. A quantitative research approach with a data collection and analysis plan using a cross-sectional survey design was adopted. A sample of 30 decision-makers in the top three manufacturing industries in Nigeria was selected using a purposive sampling procedure for participation in the study. The data collected was analysed using Partial Least Square Structural Equation Modelling (PLS-SEM) to test the proposed model. The model was validated in two phases: (i) Initial Measurement Model and (ii) Modified Measurement Model. Findings revealed that Green-

IT Attitude, Subjective Norm, Ascription of Responsibility, Awareness of Consequences, Personal Norm, Environmental Concern, and Perceive Behavioural Control were the key elements of the behavioural intention model to adopt Green-IT, with 31 indicators having factor loadings of >0.5 , adequate internal consistency reliability, $CR > 0.7$, and Cronbach's Alpha, >0.7 . The result revealed convergent validity, and acceptable discriminant validity was assessed using $AVE > 0.5$ and Fornell-lacker's criterion.

ARTICLE INFO

Article history:

Received: 4 February 2021

Accepted: 5 July 2021

Published: 28 October 2021

DOI: <https://doi.org/10.47836/pjst.29.4.09>

E-mail addresses:

bkoriyell@gmail.com (Abba Kyari Buba)

othmanibrahim@utm.my (Othman Ibrahim)

*Corresponding author

The results from the full-scale study would contribute to developing a context-specific model to examine Green-IT adoption in developing nations.

Keywords: Adoption, green-IT, manufacturing industries managers, norm activation model, theory of planned behaviour

INTRODUCTION

Green-IT is about the genuine utilisation of IT to control the environmental sustainability of its operations, products, services, resources, systems, and production processes (Esfahani et al., 2015; Yang et al., 2019). According to De Luis et al. (2015) and Asadi et al. (2019), Green-IT is the solution that contributes actively to the reduction of pollution emissions (De Luis et al., 2015). Furthermore, Green-IT has been mentioned to provide solutions that could sustain a decrease in environmental footprints. Thus, enabling the firms to accept and adopt the changes in environmental regulations and expand the firm's competitiveness over time (Chen & Chang, 2014a; Chen & Chang, 2014b; Przychodzen et al., 2018; Yacob et al., 2018).

Green IT can be defined as Information Technology (IT), and Information System (IS) products, services, and practices to achieve sustainable development while focusing on energy proficiency for the used IT infrastructure (Anthony et al., 2020). Also, from other studies, Green-IT is regarded as the appropriate utilisation of IT for managing environmental sustainability to maximise the positive human behavioural impacts on the environment (Asadi et al., 2019; Esfahani et al., 2015; Guo et al., 2019; Yang et al., 2019). This process is achievable through designing, application, production, operation, and IT disposal, and products and services during their life cycle (Akman & Mishra, 2015; Seidel et al., 2013; Buba & Ibrahim, 2020; Yang et al., 2019). Green-IT solutions could sustain a decrease in environmental footprints, enable firms to accept and adopt the changes in environmental regulations, and expand the firm's competitiveness over time (Chen & Chang, 2014a; Chen & Chang, 2014b; Przychodzen et al., 2018; Yacob et al., 2018). Hence, Green-IT promotes work efficiency, business processes, deals with e-waste, IT-related emissions, and lower energy consumption (Dalvi-Esfahani et al., 2017a; Dalvi-Esfahani et al., 2017b; Sani et al., 2016). The forecasted benefits include competitive advantage, corporate sustainability in both the environment and the society (Gandhi et al., 2018; Kong et al., 2016; Nallusamy et al., 2016; Yang et al., 2019), lower waste and pollution and hence, energy conservation (Maruthi & Rashmi, 2015; Rehman & Shrivastava, 2013; Woo et al., 2014). Thus, this is achievable if Green-IT is made possible through its incorporation into the daily activities of an organisation.

Developing nations are lagging in technology diffusion, adoption, and implementation because of several challenges. A study mentions that this is because of internal or

external organisational practices (Singh & Sahu, 2020), while another study mentions cost issues, lack of knowledge, and awareness of sustainable development (Wang et al., 2018). A study conducted by Chen & Chang (2014a & 2014b) states that Greenhouse effects have increasingly become a major global issue due to concerns for environmental sustainability. Furthermore, there has been an establishment of the sustainability pillars (environmental, social, and economic). The international community urges companies to consider innovative methods and practices to sustain the environment (Aboelmaged & Hashem, 2019). Similarly, government policies, laws, and shareholders' pressures have been affecting the industries in trying to improve actions on environmental sustainability (Brandvik et al., 2019; Juschten et al., 2019). By integrating IT, innovations can shape the environmental circumstances and enable people to apply them (Huda, 2019; Przychodzen et al., 2018; Yacob et al., 2018). Research agrees that there is a benefit in the environment, economically and socially, which leads to sustainable development if Green-IT is utilised (Wang et al., 2018).

Besides, it entails managerial and human practices and organisational policies for sustainability (Singh & Sahu, 2020). However, despite Green-IT being able to handle environmental issues for economic fulfilment (Asadi et al., 2019; Chen & Chang, 2014a; Chen & Chang, 2014b; Guo et al., 2019), there has not been a fast adoption rate by manufacturing industries in developing countries to leverage these benefits. As a result, there is a gap in the adoption of Green-IT in developing countries, especially Nigeria. Furthermore, the effect of human behaviour in the adoption of Green-IT is an issue. Evolving technologies suffer numerous issues involving people's behaviour, which is equally critical for environmental sustainability (Chen & Chang, 2014a; Chen & Chang, 2014b; Yacob et al., 2018). Thus, the main goal of this study is to establish decision-makers' opinions for intention to adopt Green-IT.

The Objectives of the Study

This study concentrates on the following objectives:

1. To identify factors that influence the decision-makers to have intention in Green-IT adoption.
2. To analyse the relationship between the identified factors for the intention to adopt Green-IT.
3. To propose a behavioural model for the intention of adopting Green-IT to support the decision-makers.

Theoretical Background

To study the adoption of Green-IT by decision-makers, the author proposes a theoretical model based on a thorough review of the relevant literature. Based on research, cost-benefit

analyses do not adequately forecast pro-environmental action because their implementation decisions require value judgments, and well-known frameworks of individual adoption are not the best options for clarifying Green-IT incorporation in firms. The combination of the Theory of Planned Behaviour (TPB) and Norm Activation Model (NAM), which is developed in the sense of prosocial and environmentally responsible conduct and considerate conduct, will provide a more robust theoretical model that would clarify the implementation of Green-IT, as it involves value judgments and cost evaluations.

According to Ajzen and Fishbein (1980), the Theory of Planned Behaviour (TPB) emanates from the Theory of Reasoned Action (TRA), whereby TRA mentions that actions are entirely under volitional control, that individual behaviour results from the intent to do a behaviour. The intentions are determined by perceived behavioural control, attitudes, and subjective norms, as stated in the Theory of Planned Behaviour (TPB). In social and pro-environmental behaviour, the TPB is considered one of the most influential theories. Armitage and Conner (2001) have validated TPB in the pro-environmental behaviour context (Arvola et al., 2008; Asadi et al., 2015). The TPB is a well-established model to predict behaviour across various contexts and settings (Pavlou & Sawy, 2006). A general model is used to explain most human behaviours (Ajzen, 1991).

The Norm Activation Model (NAM) was developed about altruistic behaviour (Schwartz, 1977). The main component is personal norms which are achieved as being morally obligated rather than intent. They are utilised in NAM for individual behaviour prediction. From the model, the determination of personal norms occurs in two ways, awareness of consequences resulting from performing a particular behaviour and sensitiveness of control for indulging in a specific behaviour (Schwartz, 1977). Several studies posit NAM as a moderator model, while others use it for mediation (Onwezen et al., 2013). This theory has been most used to predict individual behaviour. The assumption is that personal norm drives a person's behaviour (Schwartz, 1977). Furthermore, being aware of the consequences, including ascription of responsibility, is important in initiating an individual's polite behaviour (Park & Ha, 2014).

Based on two concepts, TPB and NAM is an integrated theoretical model, which has been applied to environmental issues in previous studies. By including personal norms in the TPB model, predictability was increased when altruistic attitudes were evaluated (Arvola et al., 2008; Burns & Roberts, 2013; Kim & Hwang, 2020; Rezaei et al., 2019). Therefore, the NAM model addresses the flaw of the TPB, which is a lack of focus on the personal standard. As this research aims to examine the implementation of Green-IT policies within organisations based on the objective normative context of decision-makers, NAM has been selected for this research. In line with this, many works of literature have verified the efficiency of prediction in environmental behaviour using some information system theories like TPB and NAM (Asadi et al., 2015). These studies have identified that

when TPB and NAM are combined as mediators, they influence personal norms. Other studies have suggested that to identify behavioural intent. Actual behaviour must be an indicator (Akman & Mishra, 2014).

The researchers almost agreed that studying the intention of individuals would help organisation policymakers to identify how individuals can think and behave. Therefore, this paper aims to study the determinant of organisation management's intention in adopting Green-IT to their workplace.

Proposed Research Model

The incentive for adopting Green-IT intention was proposed. More so, it defined the factors and hypothesised the relationships among the model constructs. It commenced by pointing out some previous studies, which analysed the conceptual Green-IT adoption model development. A comprehensive review of the given constructs of TPB and NAM, which positively impacts the adoption of Green-IT within Nigerian manufacturing industries, has been realised. A pilot study was carried out to ensure the reliability of the instruments before the main data gathering. Figure 1 shows the proposed model.

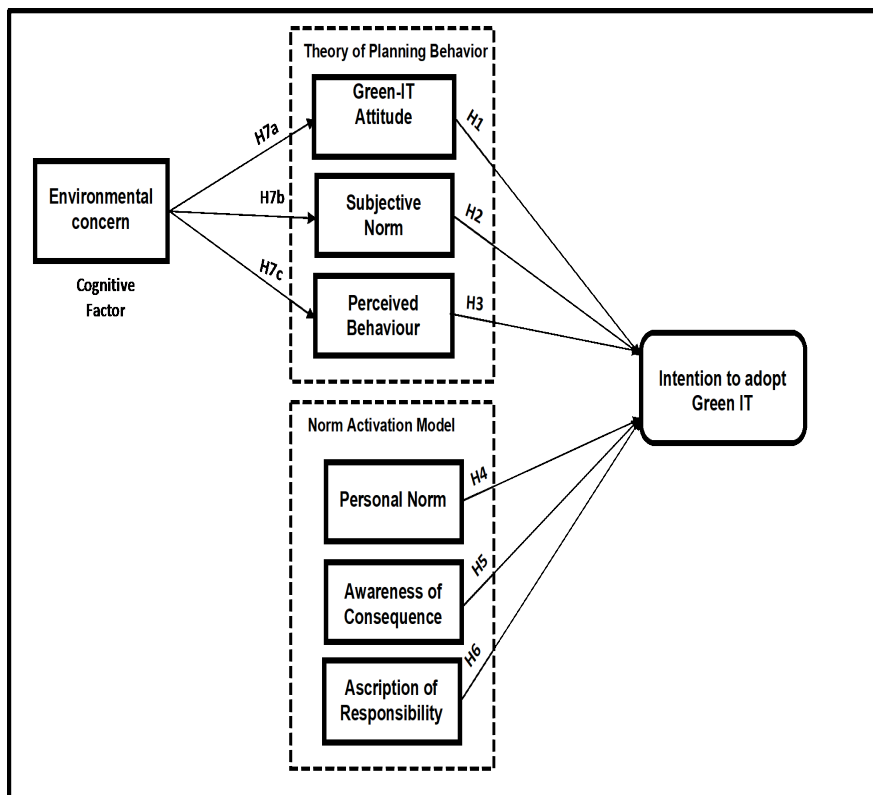


Figure 1. Initial proposed model

Hypotheses Development

Hypotheses 1: Attitude to Green-IT. The understanding of the benefit of Green-IT in solving environmental concerns by individuals has become protracted. The general public is more likely encouraged to develop a significant attitude considering the newly updated and acquired knowledge, which is also favourable towards Green-IT in recent times (Akman & Mishra, 2014; Ojo et al., 2019). Additionally, Bodur and Sarigöllü (2005) described that one of the best analysts of behaviour is their feelings and perception towards that particular behaviour (Reyes et al., 2013). Administrators of organisations and established businesses with a perception towards sustainability is a significant element to be used in attaining awareness on Green-IT challenges and related opportunities (Anthony Jr, 2019; Molla et al., 2008).

Previous researches have empirically reported that moral norm is a positive and significant element of the recognised concern and problematic awareness; likewise, the moral norm is an essential aspect of social behaviour or attitude (Chen & Tung, 2014; Steg & de Groot, 2010; Zhang et al., 2013). For example, it has been discovered that personal norm is a key factor that affects the assignment of responsibility and awareness level consequences (Ramstein et al., 2019). These identified moral obligations have an essential role to play in shaping favourable behaviour towards the environment. Following the Green-IT adoption, it can be recommended that as more business leaders are aware of the unfavourable consequences of environmental concerns, the higher they become more obliged to develop favourable behaviour towards the environment, thereby improving their potential to adopt Green-IT. Henceforth, based on these assertions, the researcher proposes the hypothesis below:

Hypothesis 1: The Attitude of Managers towards Green-IT will positively affect the intention to adopt Green-IT.

Hypotheses 2: Subjective Norm. The term subjective norm can be understood as a community burden involved in a specific behaviour (Ajzen, 1991). They influence behavioural intentions and are regarded as stimulants of the personal norm. Several empirical types of research have examined subjective norms' influence on the intention to purchase green commodities using the TPB (Zhang et al., 2019). Thus, this indicates that personal norms are influenced by other social environments and external support (Juschten et al., 2019; Koo et al., 2011). The term subjective norm is also considered an individual's attitude or perception about other important peoples' perception of their ability to perform specific tasks or behaviour exhibited in question. It means that an individual has thought about the simplicity or difficulty of a task or performing behaviour within the environment (Dezdar, 2017; Juschten et al., 2019). Previous investigations have confirmed the influence of the subjective norm on the intention or behavioural intention based on the

TPB and the TRA models (Ainin et al., 2015; Ajzen, 1991; Chow & Chen, 2009). A study conducted by Ainin et al. (2015) reported that the subjective norm is an essential factor in the possibility of mobile financing or banking adoption. The author indicates that a person who has perceived higher social pressure to implement Green-IT has a high positive and significant intention towards adopting it. Consequently, the researcher decides on this premise to develop the hypothesis stated below:

Hypothesis 2: Subjective norm will positively influence managers' intention to adopt Green-IT.

Hypotheses 3: Perceived Behaviour Control. Behavioural control as perceived by an individual is considered an essential aspect of TPB, also referred to as simplicity or ease of performing specific behaviours or otherwise (Lopes et al., 2019). The above assertion agrees with Ajzen (1991), who opined that the level of an individual's perceived behavioural control and behavioural intention correlation or association depends on the form of behaviour and the environmental factor (Asadi et al., 2019). In several past studies, Perceived Behavioural Control (PBC) was represented by several sub-factors, which included nature of the resources, time, and perceived level of uncertainty and inconveniences attached to action (Lin & Huang, 2012; Lopes et al., 2019; Sujata et al., 2019; Zhao et al., 2014).

Conversely, other scholars discovered entirely different relationships between PBC and product purchase intention. According to the scientific investigations, Zhang et al. (2019) mention that PBC and intention to purchase green products have no relationship. On the other hand, the study by Nasri and Charfeddine (2012) reveals that PBC specifies individual motives that are affected by one's perception of ease or difficulty of a particular behaviour and the perception of an individual towards successful performance of an activity or task. The PBC can affect the behaviour either directly or inversely via the intention of that particular behaviour. As established by past empirical studies, this research considers that the stronger PBC of an individual, the higher his probability of performing a specific task or behaviour. Thus, these lead to the following hypothesis:

Hypothesis 3: Perceived behaviour control will positively affect the managers' intention to adopt Green-IT.

Hypotheses 4: Personal Norm. Personal Norm (PN) refers to a feeling of moral commitment to undertake or avoid undertaking a particular behaviour or activity (Schwartz & Davis, 1981). Green-IT or issues related to the environment need the moral aspect of a person to exhibit a particular behaviour towards the environment, especially a favourable one (Asadi et al., 2019). Additionally, Harland et al. (2007) presume that prosocial or pro-environment behaviours of individuals are determined by their norms rather than by personal effect or benefit and cost evaluation. Therefore, PN is a specific behaviour

that needs to be prompted before assuming a position of relevance or responsibility in a community. Numerous researchers who studied intentions towards environmentally friendly behaviours stress that the direct predictor of an intention is the PN (Asadi et al., 2019).

Many studies have found that the critical factor affecting various pro-environment behaviours is a personal norm. For instance, it was reported that there is a strong association between PN and environmentally friendly behaviours in a general understanding (Abrahamse & Steg, 2009), definite environmental concerns such as conservations and green community, and a purchase (Asadi et al., 2019). Therefore, the following is hypothesised:

Hypothesis 4: The Personal Norm of managers will positively affect the intention to adopt Green-IT.

Hypotheses 5: Awareness of Consequences. The second variable to declare prosocial behaviour in NAM is Awareness of Consequences (AC). The AC refers to a situation where an individual becomes aware of how results affect others (Asadi et al., 2015; de Groot & Steg, 2009). Empirical studies have shown that persons with the express knowledge of the negative effect of environmental conditions on their lives have a favourable attitude towards becoming more environmentally friendly by adopting pro-environmental behaviours. For example, Asadi et al. (2019) suggested that every individual must be aware of the results of their environmental behaviour, especially in the future. The literature has further established that the individual awareness consequences are positively and significantly related to environmentally friendly behaviour (Agag, 2019; Harland et al., 2007). Therefore, once specific individuals became aware of the negative effect of environmental situations, they have a higher possibility of becoming more environmentally conscious and thereby adopting pro-environmental behaviour. In related research, Lauper et al. (2014) concluded that in consideration of imbibing and accepting eco-innovation, a positive, significant relationship exists between individual awareness of adverse consequences of the environmental situation and pro-environmental behaviour. Moreover, Dalvi-Esfahani et al. (2017a & 2017b) reported that a positive relationship which is also significant exists between personal norms and awareness of adverse consequences of the environmental concerns reveal an essential link between these variables. Thus, the researcher proposed the following hypothesis:

Hypothesis 5: Managers' awareness of consequences will positively influence the intention to adopt Green-IT.

Hypotheses 6: Ascription of Responsibility. Another critical variable in NAM is the Ascription of Responsibility (AR), as it affects prosocial behaviour among individuals. The ascription of responsibility is the feeling that an individual is developed towards a commitment to perform prosocial behaviour (Asadi et al., 2019). Following NAM

(Schwartz, 1977), the AR is a motivating factor for an individual to have a moral obligation and zeal to perform favourable environmental behaviour in addition to its impacts on environmentally friendly behaviours. Related empirical research conducted by Willuweit (2009) revealed an AR as a significant predictor of environmentally friendly behaviour. In similar research, Zhang et al. (2013) concluded that, based on the data obtained from the electricity users, AR increases their behaviour towards the environment. Thus, they become environmentally friendly and develop positive behaviour towards saving electricity. Other similar studies, such as de Groot and Steg (2009) and Han et al. (2015), showed that AR is essential in developing a person's moral capacity and motivating pro-social behaviour. Hence, the sixth hypothesis is developed as follows:

Hypothesis 6: Managers' AR will positively influence behavioural intention to adopt Green-IT.

Hypotheses 7: Environmental Concern. The available literature established a strong fact that Environmental Concern (EC) is an attitude towards environmental protection exhibited by an individual in a specific period (Zhang et al., 2019). The EC also refers to a universal perception or behaviour that triggers an individual to engage in activities that adequately protect the environment (Zhang et al., 2019). This attitude or concern is an essential aspect that influences people's behaviour to become pro-environment or environmentally friendly. With the recent concerns on the environmental problems that occur from time to time, such as the frequent occurrence of environmental-based issues, scholars are more conscious of the peoples' actions on related environmental specific issues (Maloney & Ward, 1973). Thus, there is a need to convince inhabitants to imbibe environmentally friendly behaviour. Ajzen and Fishbein (1980) suggested that a universal attitude such as EC does not influence a particular behaviour directly but inversely. Several past studies have found a positive and significant relationship between EC and behavioural intention to use green products (Lin & Huang, 2012; Sujata et al., 2019; Zhao et al., 2014). The EC is considered a solid cognitive factor to predict behavioural intention to purchase green products (Zhang et al., 2019). All the accessible empirical researches highlighted that EC favourably leads to positive behavioural intention to engage in pro-environmental behaviour and make effective decisions in purchasing green products. Hence, these posit the hypotheses below:

Hypothesis 7a: Environmental Concern will have a positive and significant influence on Green Attitude for behavioural intention to adopt Green-IT.

Hypothesis 7b: Environmental Concern will have a positive and significant influence on Subjective Norm for behavioural intention to adopt Green-IT.

Hypothesis 7c: Environmental Concern will have a positive and significant influence on Perceived Behaviour for behavioural intention to adopt Green-IT.

MATERIALS AND METHODS

Research Design

This study employed a positivist approach to advance the hypotheses, a priori assumptions to be statistically tested in the comprehensive study to validate the proposed model. This positivist method is selected because it concentrates on testing the concept (Brierley, 2017). It was utilised to validate the model's relationships by relating independent variables with dependent variables to adopt Green-IT. For this pilot study, the non-random purposive sampling technique was used. The study targets only the decision-makers in the manufacturing industries. It is a non-probability sampling technique, which guarantees the trust and proficiency of the informant (Tongco, 2007). Purposive sampling was the preferred method as the selection of the participants will be based on those who were fit to participate in the study. A survey was employed to gather the preliminary data from the targeted population of decision-makers in one of the manufacturing industries. The survey was developed according to the Norm Activation Model (NAM) by Schwartz (1977) and Theory of Planned Behaviour (TPB) by Ajzen and Fishbein (1980).

The primary data collection conducted later will be selecting the three top industries due to their expectation to be leading in substantial areas. These areas include amenities, infrastructure, environmental sustainability, and technology. Decision-makers also agree with the continuously changing environmental guidelines, among others. However, for this study, only one industry was selected as a case. The focus of the pilot study is to develop and validate the model and the instrument, and this data will not be included in the principal analysis. The study further used only samples obtained among the groups of decision-makers. Sampling is essential as it determines that more sample points attained could support analyses of diverse variables (Etikan et al., 2016). Additionally, every individual in the sampling is given an equal chance of being chosen as a respondent (Atkinson et al., 2005).

Data Collection Instrument

The instrument for this study is a constructed and validated questionnaire. The pilot study intends to get different insights from various decision-makers and ensure that the study is feasible. Six experts validated the survey instrument prior to the pilot study, which helped remove ambiguity. The instrument titled '*Intention to Adopt Green Information Technology Survey Questionnaire (INAGITEQ)*' was divided into two (2) sections, A and B. Section A contains items to assess respondents' general demographic information and includes gender, years of experience, educational attainment, and others. Section B contains items to measure the eight (8) constructs to develop the Behavioural Model for Decision-Makers towards the Intention to Adopt Green Information Technology. All the items generated were

developed using established procedures in the literature and the stakeholders' perspectives, who are specialists in the field of this study.

Intention to use the Green-IT Measures

The Intention to Adopt Green Information Technology Survey Questionnaire consists of eight (8) dimensions in line with updated measurement items from Zhu et al. (2013), Manavalan and Jayakrishna (2019), and Zhu et al., (2013). These dimensions are Green-IT Attitude, Subjective Norm, Ascription of Responsibility, Aware of Consequences, Personal Norm, Intention to Adopt, Environmental Concern, and Perceived Behavioural Control, with 40 items measuring the construct distributed among the eight (8) dimensions. A Five-point Likert scale (5=Strongly Disagree, 2=Disagree, 3=Neutral, 4=Agree, 5=Strongly Agree) was used to measure the extent to which they perceived their intention to use Green-IT, supported by the 40 items in the questionnaire. After several modifications, the instrument was subjected to content validity, construct validity, and reliability. The reports of construct validity and reliability are presented in this paper. The distributions of items within the dimensions are presented in Table 1.

Table 1

The measure of Intention to Adopt Green Information Technology

SN	Dimension/Construct	Measurement Items
1	Attitude	ATT1, ATT2, ATT3, ATT4, ATT5
2	Subjective Norm	SN1, SN2, SN3, SN4, SN5
3	Ascription of Responsibility	AR1, AR2, AR3, AR4, AR5
4	Aware of Consequences	AC1, AC2, AC3, AC4, AC5
5	Personal Norm	PN1, PN2, PN3, PN4, PN5
6	Intention to Adopt	INT1, INT2, INT3, INT4, INT5
7	Environmental Concern	EC1, EC2, EC3, EC4, EC5
8	Perceive Behavioural Control	PBC1, PBC2, PBC3, PBC4, PBC5

Participants

A pilot test consisted of thirty (30) respondents was conducted to achieve the construct validity and the reliability of the questionnaire. According to Baker et al. (2019), a sample size of 10–20% of the study's actual sample size is considered a reasonable number to participate in a pilot study. The sample size of the actual study is 280 decision-makers. Thus, 30 respondents represent about 10% of the actual sample size for the main study (280). The 30 decision-makers in the top three manufacturing industries in Nigeria were

selected using a purposive sampling procedure, which is a non-probability sampling approach. In the purposive sampling procedure, the researcher selects a “typical group” of individuals who might represent the larger population and then collects data from this group. This feature makes them well suited to small-scale, in-depth studies, as we will go on to show (Creswell & Plano-Clark, 2007). This purposive sampling involves identifying and selecting individuals or groups of individuals that are exceptionally knowledgeable about or experienced with a phenomenon of interest (Creswell & Plano-Clark, 2007). In addition to knowledge and experience, Kothari et al. (2020) note the importance of availability and willingness to participate and the ability to communicate experiences and opinions in an articulate, expressive, and reflective manner. The demographic information is presented in Table 2.

Administration and Data Analysis

Before the field administration of the instrument for validation purposes, several processes were followed, including content validation by experts, identification of target population for the pilot study selecting the appropriate sample, administration of the draft instrument, and reliability analysis, as reported. Thus, to examine the internal consistency reliability of the research instrument in this study, the data collected from the pilot testing was analysed using the SPSS 25 software and the Partial Least Squares Structural Equation Modelling (PLS-SEM) approach using SmartPLS to conduct a test on the reliability of the instrument by assessing the measurement model at both initial and modified levels. The results of the analysis provide preliminary information on whether the research instrument is suitable or otherwise.

Table 2

Demographic information of the respondents

	Variable Level	Frequency (n)	Percentage (%)
Sex	Male	20	66.7
	Female	10	33.3
Age	21-25 years	9	30.0
	26-30 years	13	43.3
	31-35 years	5	16.7
	More than 35	3	10.0

Table 2 (Continued)

	Variable Level	Frequency (n)	Percentage (%)
Level Education	College	4	13.3
	High school	4	13.3
	University	22	73.3
Experience	Less than 2 years	15	50.0
	Less than 4 years	3	10.0
	4-5 years	8	26.7
	9 years and above	4	13.3
Role	Lower Manager	26	86.7
	Middle Manager	2	6.7
	Top Manager	2	6.7

RESULTS AND DISCUSSIONS

Summary Statistics

The scale reliability was used to estimate the reliability of the “*Intention to Adopt Green Information Technology Survey Questionnaire (INAGITEQ)*”. The summary statistics are the descriptive information generated using descriptive statistical analyses. The summary of the statistics is presented in Table 3. The results show Mean, Minimum, Maximum, and Variance.

Table 3

Summary of Item Statistics

SN	Dimension/ Construct	Mean	Minimum	Maximum	Variance	N of Items
1	Green-IT Attitude	3.88	3.80	3.93	.004	5
2	Subjective Norm	3.55	3.47	3.63	.004	5
3	Ascription of Responsibility	3.68	3.63	3.70	.001	5

Table 3 (Continued)

SN	Dimension/ Construct	Mean	Minimum	Maximum	Variance	N of Items
4	Aware of Consequences	4.00	3.17	4.27	.221	5
5	Personal Norm	3.57	3.53	3.60	.001	5
6	Intention to Adopt	3.61	3.57	3.70	.004	5
7	Environmental Concern	3.59	3.53	3.67	.003	5
8	Perceived Behavioural Control	3.79	3.57	4.57	.192	5

Evaluating the Measurement Model

To assess the measurement model in this study, Partial-Least Square Structural Equation Modelling Approach was applied using SmartPLS 3.0 software. The central emphasis in assessment and goodness of the proposed measurement model is to assess the reliability and construct validity. Hair et al. (2017) defined construct validity as the correspondence between constructs and their indicators. It can also be seen as a necessary condition for developing and testing theory (Jarvis et al., 2003). The construct validity can be evaluated via discriminant and convergent validity. The measurement model of the study's constructs was validated in two major stages, which are (a) the Initial measurement model and (b) the Modified measurement model.

Initial and Modified Measurement Model

The proposed measurement model of the constructs in this research was assessed through item loadings, composite reliability (CR), and the average variance extracted (AVE). Item loadings of at least 0.7 showed acceptable indicator reliability for the measurement model. In addition, the factor loadings of the 40 items measuring eight (8) sub-constructs were assessed to validate the initial measurement model,

The assessment of the initial measurement model presents the indicators measuring the construct based on the analysis. Based on the analysis results measuring the construct of Intention to Adopt Green Information Technology, nine (9) items out of the 40 items measuring the constructs showed loadings of less than 0.7, indicating unsatisfactory loading, which violates the model factor loading requirement of 0.7. However, all the remaining 31 items showed a factor of 0.7 and above, satisfying the requirement (Hair et al., 2017).

Thus, the nine (9) items which failed the indicator reliability need to be deleted from the model. The PLS algorithm was rerun for the indicator items with external loadings of less than the threshold value of 0.7,

In line with the recommendation of Hair et al. (2017), if removing a particular item leads to an improvement in AVE and CR values, deletion of that item is essential. Hence, after conducting the PLS algorithm (Figure 2), the results showed that removing all the nine items improved the values of CR and AVE. Lastly, the remaining items were above the threshold by removing the nine poor items with external loadings of values lower than 0.70. The results of the indicator reliability measurement after removing the poor items are presented in Table 4.

Table 4

Modified Indicator Loadings

SN	Construct	Measurement Items	Outer Loadings
1	Attitude	ATT1	0.800
		ATT2	0.822
		ATT4	0.785
		ATT5	0.847
2	Subjective Norm	SN1	0.986
		SN3	0.947
		SN4	0.943
		SN5	0.987
3	Perceived Behavioural Control	PBC1	0.990
		PBC2	1.000
		PBC5	0.990
4	Aware of Consequences	AC1	0.981
		AC3	0.968
		AC4	0.945
		AC5	0.989
5	Personal Norm	PN1	0.988
		PN3	0.965
		PN4	0.943
		PN5	0.979
6	Ascription of Responsibility	AR1	0.981
		AR3	0.967
		AR4	0.945
		AR5	0.980

Table 4 (Continued)

SN	Construct	Measurement Items	Outer Loadings
7	Environmental Concern	EC1	0.984
		EC3	0.950
		EC4	0.939
		EC5	0.988
8	Intention to Adopt	INT1	0.988
		INT3	0.946
		INT4	0.950
		INT5	0.987
			0.987

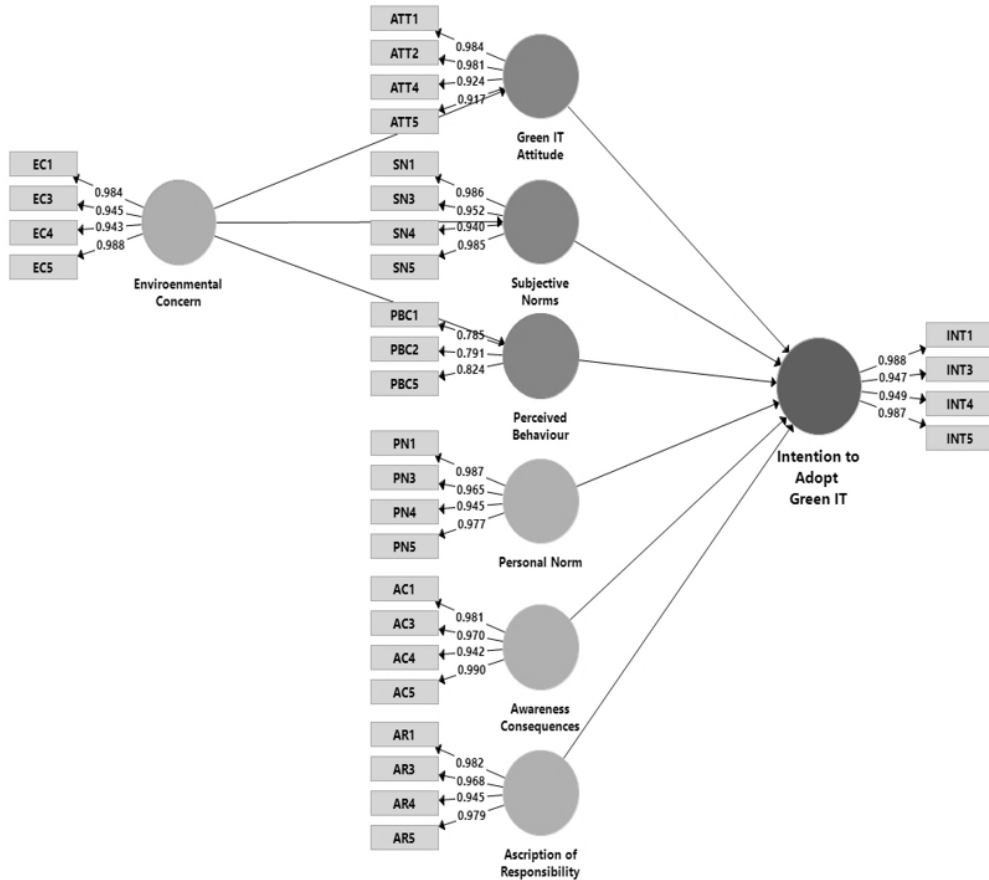


Figure 2. Modified Measurement Model

Internal Consistency Reliability

The assessment of the internal consistency reliability was performed alongside the benchmarks of composite reliability and Cronbach's alpha (α). As presented in Table 5, all identified constructs of the study met the satisfactory criteria of Cronbach's alpha and CR, which are supposed to be higher than 0.70. Thus, the results specify that all the indicators used to signify the constructs are reliable.

Table 5

Internal Consistency Reliability

SN	Construct	Cronbach's Alpha	Composite Reliability
1	Attitude	0.830	0.887
2	Subjective Norm	0.976	0.982
3	Perceived Behavioural Control	0.993	0.996
4	Aware of Consequences	0.980	0.985
5	Personal Norm	0.978	0.984
6	Ascription of Responsibility	0.978	0.984
7	Environmental Concern	0.976	0.982
8	Intention to Adopt	0.978	0.983

Convergent Validity

The convergent validity of the study's constructs is achieved by evaluating the values of AVE for each construct. In line with recommendations by Hair et al. (2017), this investigation considered the estimate of at least 0.5 as a good value for the AVE. As displayed in Table 6, the AVE values of all constructs exceeded the minimum value of 0.5, which means there is no issue regarding the convergent validity of the proposed measurement model.

Table 6

Convergent Validity

SN	Construct	Average Variance Extracted (AVE)
1	Attitude	0.663
2	Subjective Norm	0.933
3	Perceived Behavioural Control	0.987
4	Aware of Consequences	0.943
5	Personal Norm	0.938
6	Ascription of Responsibility	0.938
7	Environmental Concern	0.932
8	Intention to Adopt	0.937

Discriminant Validity

In line with the Voorhees et al. (2016) principle, the discriminant validity of the measurement model in this study was implemented. Any proposed measurement model of a study is regarded to have obtained substantial discriminant validity if the square roots of the AVE are higher than the association or correlations between the identified measure and all other measures in the model. Therefore, the evaluation was conducted on the discriminant validity for each factor.

The results indicated that all the AVE square roots were higher than the off-diagonal elements within their corresponding column and row. The values highlighted in bold in Table 7 show the values of cross-loadings and the Voorhees et al. (2016) criteria assessment. As indicated, the AVE's square roots and other values signify the intercorrelation between the constructs. This indicates that Voorhees et al., (2016) criterion are met. In this situation, the discriminant validity is achieved as the correlation among different constructs was low. Thus, with the satisfaction and assurance of discriminant validity, all the adjustments of the measurement model have been completed and can be used to run the structural model and test the hypotheses in this study.

Table 7

Discriminant validity (Fornell-Larcker's Standard)

	AC	AR	ATT	EC	INT	PBC	PN	SN
AC	0.971							
AR	0.367	0.969						
ATT	0.061	0.075	0.814					
EC	0.381	0.381	0.043	0.965				
INT	0.189	0.408	0.047	0.198	0.968			
PBC	-0.046	0.180	0.283	-0.047	0.082	0.993		
PN	0.365	0.591	0.067	0.379	0.389	0.169	0.969	
SN	0.367	0.193	0.163	0.393	0.062	-0.026	0.183	0.966

CONCLUSION

This study intends to find elements that influence the decision-makers to have intention in Green-IT adoption, analyse the relationship between the factors, and develop a valid and reliable model for adopting Green-IT to tackle environmental degradation. The findings from this preliminary study provide initial support for the model constructs and instruments in the assessment of factors influencing decision-makers to have the intention to adopt Green-IT to mitigate environmental degradation. The reliability coefficient for

the model constructs was established with a Cronbach's alpha value greater than 0.80 for all the constructs, higher than the minimum recommended value of 0.70 indicators (Hair et al., 2017; Akman & Mishra, 2014). The convergent and discriminant validity of all the constructs was established through the AVE and CR statistics. After deleting some poor misfit items, the AVE and CR values for all constructs were above the recommended minimum threshold.

Thus, all the constructs in the proposed model were appropriate for the final model to be validated in the main/full study. Following the comments and suggestions from academic experts and respondents to the pilot questionnaire, and the analysis is shown above, a final instrument has been designed for the proposed full-scale study. Moreover, the validation report of the Intention to Adopt Green Information Technology survey questionnaire is proposed to develop a Behavioural Model for Decision-Makers towards the Intention to Adopt Green Information Technology. Therefore, the results of the pilot studies show that, based on the established standards, the instrument is valid and reliable and can be considered a valid measuring instrument to collect relevant data in the full-scale study.

Previous researches on Green-IT have stressed the importance of Green-IT adaptation, especially in the decision-making process of mitigating environmental degradation and improvement in the manufacturing sector. Since the IT industry significantly impacts the environment, its utilisation growth is caused by massive energy consumption and reducing natural resources (Sanita et al., 2018). Based on previous research on the adoption of Green-IT (Przychodzen et al., 2018), introducing Green-IT to decision-makers has altered the manufacturing industries from traditional to modern. As a result, there has been rapid exhaustion of natural resources and awareness of environmental deterioration in the past (Przychodzen et al., 2018). It has led to an increase in the need for environmental responsibility. Therefore, the adoption of Green-IT by firms and industries has been a major topic among academics, decision-makers, and practitioners (Dalvi-Esfahani et al., 2017a; Dalvi-Esfahani et al., 2017b; Masri & Jaaron, 2017). Accordingly, Green-IT involves the efficient and practical design, manufacture, and use of computers, servers, and various peripherals to reduce environmental damage (Cai et al., 2013; Yang et al., 2019). Therefore, Green-IT is key for dealing with environmental damage (Przychodzen et al., 2018). For example, Dalvi-Esfahani et al. (2017a & 2017b) indicate that Green-IT adoption factors such as Environmental Concern, Green-IT Attitude, and Subjective Norm are significant when discussing the intention of individuals to adopt technologies. Asadi et al., (2019) argue that Perceived Behaviour Control, Personal Norm, Awareness of Consequence, and Ascription of Responsibility can also influence intention for adoption, as behavioural intent is explained for technology adoption.

The development and validation of the model and instrument is the first phase to evaluate the related factors that influence the stakeholders' behavioural intention to

adopt Green-IT. The investigator aims to utilise the instruments validated in this study to implement the survey in the main study using selected target groups of IT professionals who are the decision-makers in the Nigerian manufacturing industries. The effect of each construct in the proposed model on the adoption of Green-IT in Nigerian manufacturing industries will be examined. Their significance in the model will be validated by testing the proposed hypotheses using Partial Least Square Structural Equation Modelling (PLS-SEM). A final validated model will be created, used in future Green-IT adoption research in similar contexts. The model can also be used in future studies on Green-IT adoption in other sectors such as educational institutions, small and medium scale businesses, public services, and government agencies in Nigeria and beyond.

The results from the full-scale study will contribute to developing a context-specific model that can be used to examine Green-IT adoption and other technology-specific sectors in manufacturing industries in Nigeria and other developing nations. It will also contribute to the literature in Green-IT through relevant empirical evidence from the study's findings and provide the decision-makers with the basis for making specific decisions in the sector. In addition, the findings from the proposed study will be of significant importance to IT-based practitioners who are primarily service providers with valuable information and valid data, supported with scientific evidence to be used for any project in Green-IT. Finally, the study will contribute to the ongoing research into the best IT-based adoption models relevant in developing nations.

ACKNOWLEDGMENT

The author sincerely acknowledges the Universiti Teknologi Malaysia for providing space and facilities to support this research. He also thank other experts who contribute and provide support to this study.

REFERENCES

- Aboelmaged, M., & Hashem, G. (2019). Absorptive capacity and green innovation adoption in SMEs: The mediating effects of sustainable organisational capabilities. *Journal of Cleaner Production*, 220, 853-863. <https://doi.org/10.1016/j.jclepro.2019.02.150>
- Abrahamse, W., & Steg, L. (2009). How do socio-demographic and psychological factors relate to households' direct and indirect energy use and savings? *Journal of Economic Psychology*, 30(5), 711-720. <https://doi.org/10.1016/j.joep.2009.05.006>
- Agag, G. (2019). Understanding the determinants of guests' behaviour to use green P2P accommodation. *International Journal of Contemporary Hospitality Management*, 31(9), 3417-3446. <https://doi.org/10.1108/ijchm-09-2018-0755>
- Ainin, S., Jaafar, N. I., & Dezdar, S. (2015). Consideration of future consequences among managers in Iran and Malaysia. *Futures*, 71, 29-35. <https://doi.org/10.1016/j.futures.2015.06.003>

- Ajzen. (1991). Measuring oral health behaviour in Flemish health care workers: An application of the theory of planned behaviour. *Community Dental Health*, 25(2), 107-114. https://doi.org/10.1922/CDH_2120VandenBroucke08
- Ajzen, I., & Fishbein, M. (1980). *Understanding attitudes and predicting social behaviour*. Prentice-Hall.
- Akman, I., & Mishra, A. (2014). Green information technology practices among IT professionals: Theory of planned behavior perspective. *Problemy Ekorozwoju*, 9(2), 47-54.
- Akman, I., & Mishra, A. (2015). Sector diversity in green information technology practices: Technology acceptance model perspective. *Computers in Human Behavior*, 49, 477-486. <https://doi.org/10.1016/j.chb.2015.03.009>
- Anthony, B., Majid, M. A., & Romli, A. (2020). A generic study on green IT/IS practice development in collaborative enterprise: Insights from a developing country. *Journal of Engineering and Technology Management - JET-M*, 55(February), Article 101555. <https://doi.org/10.1016/j.jengtecman.2020.101555>
- Anthony Jr, B. (2019). Green information system integration for environmental performance in organizations. *Benchmarking: An International Journal*, 26(3), 1033-1062. <https://doi.org/10.1108/BIJ-05-2018-0142>
- Armitage, C. J., & Conner, M. (2001). Efficacy of the theory of planned behaviour: A meta-analytic review. *Journal of Applied Social Psychology*, 31(4), 471-499. <https://doi.org/10.1348/014466601164939>
- Arvola, A., Vassallo, M., Dean, M., Lampila, P., Saba, A., Lähteenmäki, L., & Shepherd, R. (2008). Predicting intentions to purchase organic food: The role of affective and moral attitudes in the theory of planned behaviour. *Appetite*, 50(2-3), 443-454. <https://doi.org/10.1016/j.appet.2007.09.010>
- Asadi, S., Hussin, A. R. C., Dahlan, H. M., & Yadegaridehkordi, E. (2015). Theoretical model for green information technology adoption. *ARPJ Journal of Engineering and Applied Sciences*, 10(23), 17720-17729.
- Asadi, S., Nilashi, M., Safaei, M., Abdullah, R., Saeed, F., Yadegaridehkordi, E., & Samad, S. (2019). Investigating factors influencing decision-makers' intention to adopt green IT in Malaysian manufacturing industry. *Resources, Conservation and Recycling*, 148(March), 36-54. <https://doi.org/10.1016/j.resconrec.2019.04.028>
- Atkinson, M. J., Kumar, R., Cappelleri, J. C., & Mass, S. L. (2005). Hierarchical construct validity of the treatment satisfaction questionnaire for medication (TSQM Version II) among outpatient pharmacy consumers. *Value in Health*, 8(SUPPL. 1), S9-S24. <https://doi.org/10.1111/j.1524-4733.2005.00066.x>
- Baker, D. H., Vilidaitė, G., Lygo, F. A., Smith, A. K., Flack, T. R., Gouws, A. D., & Andrews, T. J. (2019). *Power contours: Optimising sample size and precision in experimental psychology and human neuroscience*. arXiv.org.
- Bodur, M., & Sarigöllü, E. (2005). Environmental sensitivity in a developing country: Consumer classification and implications. *Environment and Behavior*, 37(4), 487-510. <https://doi.org/10.1177/0013916504269666>
- Brandvik, P. J., Storey, C., Davies, E. J., & Johansen, Ø. (2019). Combined releases of oil and gas under pressure: The influence of live oil and natural gas on initial oil droplet formation. *Marine Pollution Bulletin*, 140(February), 485-492. <https://doi.org/10.1016/j.marpolbul.2019.01.036>

- Brierley, J. A. (2017). The role of a pragmatist paradigm when adopting mixed methods in behavioural accounting research. *International Journal of Behavioural Accounting and Finance*, 6(2), 140-154. <https://doi.org/10.1504/ijbaf.2017.10007499>
- Buba, A. K., & Ibrahim, O. (2020). Behavioural model for decision-makers' intention to adopt green information technology in Nigerian manufacturing industries. *Science Proceedings Series*, 2(2), 166-171. <https://doi.org/10.31580/sps.v2i2.1721>
- Burns, S., & Roberts, L. (2013). Applying the theory of planned behaviour to predicting online safety behaviour. *Crime Prevention and Community Safety*, 15(1), 48-64. <https://doi.org/10.1057/cpcs.2012.13>
- Cai, S., Chen, X., & Bose, I. (2013). Exploring the role of IT for environmental sustainability in China: An empirical analysis. *International Journal of Production Economics*, 146(2), 491-500. <https://doi.org/10.1016/j.ijpe.2013.01.030>
- Chen, H. G., & Chang, J. (2014a). A study on green IT adoption. *Computer Science and Information Technology*, 2(8), 315-323. <https://doi.org/10.13189/CSIT.2014.020801>
- Chen, H. G., & Chang, J. (2014b). Exploring affecting factors on green IT adoption. In *International Conference on Knowledge Management in Organizations* (pp. 205-218). Springer. <https://doi.org/10.1007/978-3-319-08618-7>
- Chen, M. F., & Tung, P. J. (2014). Developing an extended theory of planned behavior model to predict consumers' intention to visit green hotels. *International Journal of Hospitality Management*, 36, 221-230. <https://doi.org/10.1016/j.ijhm.2013.09.006>
- Chow, W. S., & Chen, Y. (2009). Intended belief and actual behavior in green computing in Hong Kong. *Journal of Computer Information Systems*, 50(2), 136-141. <https://doi.org/10.1080/08874417.2009.11645392>
- Creswell, J. W., & Plano-Clark, V. (2007). *Designing and constructing mixed methods research*. Sage Publication.
- Dalvi-Esfahani, M., Ramayah, T., & Nilashi, M. (2017a). Modelling upper echelons' behavioural drivers of green IT/IS adoption using an integrated interpretive structural modelling – Analytic network process approach. *Telematics and Informatics*, 34(2), 583-603. <https://doi.org/10.1016/j.tele.2016.10.002>
- Dalvi-Esfahani, M., Ramayah, T., & Rahman, A. A. (2017b). Moderating role of personal values on managers' intention to adopt green IS: Examining norm activation theory. *Industrial Management and Data Systems*, 117(3), 582-604. <https://doi.org/10.1108/IMDS-02-2016-0049>
- de Groot, J., & Steg, L. (2009). Morality and pro-social behaviour: the role of awareness, responsibility and norms in the norm activation model. *Journal of Social Psychology*, 31(4), 425-449.
- De Luis, M. M., Cruz, A. J. A., Arcia, A. V. U., & Márquez, C. Y. (2015). Green information technology influence on car owners' behavior: Considerations for their operative support in collaborative eLearning and social networks. *Computers in Human Behavior*, 51, 792-802. <https://doi.org/10.1016/j.chb.2014.11.085>
- Dezdar, S. (2017). Green information technology adoption: Influencing factors and extension of theory of planned behavior. *Social Responsibility Journal*, 13(2), 292-306. <https://doi.org/10.1108/SRJ-05-2016-0064>

- Esfahani, M. D., Rahman, A. A., & Zakaria, N. H. (2015). Influence processes for practicing green information technology: Elaboration likelihood model. In *Pacific Asia Conference on Information Systems, PACIS 2015* (pp. 1-11). AIS Electronic Library (AISeL).
- Etikan, I., Musa, S. A., & Alkassim, R. S. (2016). Comparison of convenience sampling and purposive sampling. *American Journal of Theoretical and Applied Statistics*, *5*(1), 1-4. <https://doi.org/10.11648/j.ajtas.20160501.11>
- Gandhi, N. S., Thanki, S. J., & Thakkar, J. J. (2018). Ranking of drivers for integrated lean-green manufacturing for Indian manufacturing SMEs. *Journal of Cleaner Production*, *171*(June 2008), 675-689. <https://doi.org/10.1016/j.jclepro.2017.10.041>
- Guo, L., Xu, Y., Liu, G., Wang, T., & Du, C. (2019). Understanding firm performance on green sustainable practices through managers' ascribed responsibility and waste management: Green self-efficacy as moderator. *Sustainability (Switzerland)*, *11*(18), 1-16. <https://doi.org/10.3390/su11184976>
- Hair, J. F., Hult, G. T. M., Ringle, C. M., Sarstedt, M., & Thiele, K. O. (2017). Mirror, mirror on the wall: A comparative evaluation of composite-based structural equation modeling methods. *Journal of the Academy of Marketing Science*, *45*(5), 616-632. <https://doi.org/10.1007/s11747-017-0517-x>
- Han, H., Hwang, J., Kim, J., & Jung, H. (2015). Guests' pro-environmental decision-making process: Broadening the norm activation framework in a lodging context. *International Journal of Hospitality Management*, *47*, 96-107. <https://doi.org/10.1016/j.ijhm.2015.03.013>
- Harland, P., Staats, H., & Wilke, H. A. M. (2007). Situational and personality factors as direct or personal norm mediated predictors of pro-environmental behavior: Questions derived from norm-activation theory. *Basic and Applied Social Psychology*, *29*(4), 323-334. <https://doi.org/10.1080/01973530701665058>
- Huda, M. (2019). Empowering application strategy in the technology adoption: Insights from professional and ethical engagement. *Journal of Science and Technology Policy Management*, *10*(1), 172-192. <https://doi.org/10.1108/JSTPM-09-2017-0044>
- Jarvis, C. B., Mackenzie, S. B., Podsakoff, P. M., Giliatt, N., & Mee, J. F. (2003). a critical review of construct indicators and measurement model misspecification in marketing and consumer research. *Journal of Consumer Research*, *30*(2), 199-218. <https://doi.org/10.1086/376806>
- Juschten, M., Jiricka-Pürner, A., Unbehau, W., & Hössinger, R. (2019). The mountains are calling! An extended TPB model for understanding metropolitan residents' intentions to visit nearby alpine destinations in summer. *Tourism Management*, *75*(May 2018), 293-306. <https://doi.org/10.1016/j.tourman.2019.05.014>
- Kim, J. J., & Hwang, J. (2020). Merging the norm activation model and the theory of planned behavior in the context of drone food delivery services: Does the level of product knowledge really matter? *Journal of Hospitality and Tourism Management*, *42*(June 2019), 1-11. <https://doi.org/10.1016/j.jhtm.2019.11.002>
- Kong, T., Feng, T., & Ye, C. (2016). Advanced manufacturing technologies and green innovation: The role of internal environmental collaboration. *Sustainability (Switzerland)*, *8*(10), 9-11. <https://doi.org/10.3390/su8101056>
- Koo, C., Wati, Y., & Jung, J. J. (2011). Examination of how social aspects moderate the relationship between task characteristics and usage of social communication technologies (SCTs) in organizations. *International Journal of Information Management*, *31*(5), 445-459. <https://doi.org/10.1016/j.ijinfomgt.2011.01.003>

- Kothari, A., Mccutcheon, C., Boland, L., & Graham, I. D. (2020). *How we work together*. Integrated Knowledge Translation Research Network.
- Lauper, E., Moser, S., Fischer, M., & Matthies, E. (2014). Explaining car drivers' intention to prevent road-traffic noise: An application of the norm activation model. *Environment and Behavior*, 48(6), 826-853. <https://doi.org/10.1177/0013916515570476>
- Lin, P. C., & Huang, Y. H. (2012). The influence factors on choice behavior regarding green products based on the theory of consumption values. *Journal of Cleaner Production*, 22(1), 11-18. <https://doi.org/10.1016/j.jclepro.2011.10.002>
- Lopes, J. R. N., de Araújo Kalid, R., Rodríguez, J. L. M., & Ávila Filho, S. (2019). A new model for assessing industrial worker behavior regarding energy saving considering the theory of planned behavior, norm activation model and human reliability. *Resources, Conservation and Recycling*, 145, 268-278. <https://doi.org/10.1016/j.resconrec.2019.02.042>
- Maloney, M. P., & Ward, M. P. (1973). Ecology: Let's hear from the people: An objective scale for the measurement of ecological attitudes and knowledge. *American Psychologist*, 28(7), 583-586. <https://doi.org/10.1037/h0034936>
- Maruthi, G. D., & Rashmi, R. (2015). Green manufacturing: It's tools and techniques that can be implemented in manufacturing sectors. *Materials Today: Proceedings*, 2(4-5), 3350-3355. <https://doi.org/10.1016/j.matpr.2015.07.308>
- Manavalan, E., & Jayakrishna, K. (2019). A review of Internet of Things (IoT) embedded sustainable supply chain for industry 4.0 requirements. *Computers and Industrial Engineering*, 127(November 2017), 925-953. <https://doi.org/10.1016/j.cie.2018.11.030>
- Masri, H. A., & Jaaron, A. A. M. (2017). Assessing green human resources management practices in Palestinian manufacturing context: An empirical study. *Journal of Cleaner Production*, 143, 474-489. <https://doi.org/10.1016/j.jclepro.2016.12.087>
- Molla, A., Cooper, V., Corbitt, B., Deng, H., Peszynski, K., & Yen, S. (2008). E-readiness to G-readiness: Developing a green information technology readiness framework. In ACIS 2008 Proceedings (pp. 669-678). AIS Electronic Library (AISeL).
- Nallusamy, S., Ganesan, M., Balakannan, K., & Shankar, C. (2016). Environmental sustainability evaluation for an automobile manufacturing industry using multi-grade fuzzy approach. *International Journal of Engineering Research in Africa*, 19, 123-129. <https://doi.org/10.4028/www.scientific.net/JERA.19.123>
- Nasri, W., & Charfeddine, L. (2012). Factors affecting the adoption of Internet banking in Tunisia: An integration theory of acceptance model and theory of planned behavior. *Journal of High Technology Management Research*, 23(1), 1-14. <https://doi.org/10.1016/j.hitech.2012.03.001>
- Ojo, A. O., Raman, M., & Downe, A. G. (2019). Toward green computing practices: A Malaysian study of green belief and attitude among information technology professionals. *Journal of Cleaner Production*, 224, 246-255. <https://doi.org/10.1016/j.jclepro.2019.03.237>
- Onwezen, M. C., Antonides, G., & Bartels, J. (2013). The norm activation model: An exploration of the functions of anticipated pride and guilt in pro-environmental behaviour. *Journal of Economic Psychology*, 39, 141-153. <https://doi.org/10.1016/j.joep.2013.07.005>

- Park, J., & Ha, S. (2014). Understanding consumer recycling behavior: Combining the theory of planned behavior and the norm activation model. *Family and Consumer Sciences Research Journal*, 42(3), 278-291. <https://doi.org/10.1111/fcsr.12061>
- Pavlou, P. A., & El Sawy, O. A. (2006). From IT leveraging competence to competitive advantage in turbulent environments: The case of new product development. *Information Systems Research*, 17(3), 198-227. <https://doi.org/10.1287/isre.1060.0094>
- Przychodzen, W., Gómez-Bezares, F., & Przychodzen, J. (2018). Green information technologies practices and financial performance - The empirical evidence from German publicly traded companies. *Journal of Cleaner Production*, 201, 570-579. <https://doi.org/10.1016/j.jclepro.2018.08.081>
- Ramstein, C., Dominioni, G., Ettehad, S., Lam, L., Quant, M., Zhang, J., Mark, L., Nierop, S., Berg, T., Leuschner, P., Merusi, C., Klein, N., & Trim, I. (2019). *State and trends of carbon pricing 2019*. The World Bank. <https://doi.org/10.1596/978-1-4648-1435-8>
- Rehman, M. A., & Shrivastava, R. L. (2013). Green manufacturing (GM): Past, present and future (a state of art review). *World Review of Science, Technology and Sustainable Development*, 10(1-2-3), 17-55. <https://doi.org/10.1504/WRSTSD.2013.050784>
- Reyes-Rodríguez, M. L., Rivera-Medina, C. L., Cámara-Fuentes, L., Suárez-Torres, A., & Bernal, G. (2013). Depression symptoms and stressful life events among college students in Puerto Rico. *Journal of Affective Disorders*, 145(3), 324-330. <https://doi.org/10.1016/j.jad.2012.08.010>
- Rezaei, R., Safa, L., Damalas, C. A., & Ganjkanloo, M. M. (2019). Drivers of farmers' intention to use integrated pest management: Integrating theory of planned behavior and norm activation model. *Journal of Environmental Management*, 236(August 2018), 328-339. <https://doi.org/10.1016/j.jenvman.2019.01.097>
- Sani, D. A., Shahabi, H., Ahmad, B. A., Mirmokrih, S., & Ahmad, B. (2016). Application of geographic information system technology in controlling pipeline vandalism of oil and gas industry. *Research Journal of Information Technology*, 8(1), 39-46. <https://doi.org/10.3923/rjit.2016.39.46>
- Sanita, F., Udin, Z. M., & Hasnan, N. (2018). Green IT/S adoption within GSCM in Indonesian construction industry : An elucidation and practice. *Journal of Information System and Technology Management*, 2(6), 105-116.
- Schwartz, S. H. (1977). Normative influences on altruism. In *Advances in experimental social psychology* (Vol. 10, pp. 221-279). Academic Press. [https://doi.org/10.1016/S0065-2601\(08\)60358-5](https://doi.org/10.1016/S0065-2601(08)60358-5)
- Schwartz, H., & Davis, S. M. (1981). Matching corporate culture and business strategy. *Organizational Dynamics*, 10(1), 30-48. [https://doi.org/10.1016/0090-2616\(81\)90010-3](https://doi.org/10.1016/0090-2616(81)90010-3)
- Seidel, S., Recker, J., & Vom Brocke, J. (2013). Sensemaking and sustainable practicing: functional affordances of information systems in green transformations. *MIS quarterly*, 37(4), 1275-1299.
- Singh, M., & Sahu, G. P. (2020). Towards adoption of green IS: A literature review using classification methodology. *International Journal of Information Management*, 54(October 2019), Article 102147. <https://doi.org/10.1016/j.ijinfomgt.2020.102147>
- Steg, L., & de Groot, J. (2010). Explaining prosocial intentions: Testing causal relationships in the norm activation model. *British Journal of Social Psychology*, 49(4), 725-743. <https://doi.org/10.1348/014466609X477745>

- Sujata, M., Khor, K. S., Ramayah, T., & Teoh, A. P. (2019). The role of social media on recycling behaviour. *Sustainable Production and Consumption*, 20, 365-374. <https://doi.org/10.1016/j.spc.2019.08.005>
- Tongco, M. D. C. (2007). Purposive sampling as a tool for informant selection. *Ethnobotany Research and Applications*, 5, 147-158. <https://doi.org/10.17348/era.5.0.147-158>
- Voorhees, C. M., Brady, M. K., Calantone, R., & Ramirez, E. (2016). Discriminant validity testing in marketing: An analysis, causes for concern, and proposed remedies. *Journal of the Academy of Marketing Science*, 44(1), 119-134. <https://doi.org/10.1007/s11747-015-0455-4>
- Wang, W., Zhang, S., & Pasquire, C. (2018). *Factors for the adoption of green building specifications in China. International Journal of Building Pathology and Adaptation*, 36(3), 254-267. <https://doi.org/10.1108/IJBPA-06-2017-0027>
- Willuweit, L. (2009). *Promoting pro-environmental behavior: An investigation of the cross-cultural environmental behavior patterns. The case of Abu Dhabi* (MSc Thesis). Stockholm University, Sweden.
- Woo, C., Chung, Y., Chun, D., Han, S., & Lee, D. (2014). Impact of green innovation on labor productivity and its determinants: An analysis of the Korean manufacturing industry. *Business Strategy and the Environment*, 23(8), 567-576. <https://doi.org/10.1002/bse.1807>
- Yacob, P., Khor, S. C., Jaganathan, M., Maludin, N., & Nodesan, S. (2018, May 12-13). Small manufacturing firms sustainable green practices: Operationalization of sustainable value framework. In *ASIA International Multidisciplinary Conference 2018* (pp. 1-8). Johor Bahru, Malaysia.
- Yang, X., Li, Y., & Kang, L. (2019). Reconciling “doing good” and “doing well” in organizations’ green IT initiatives: A multi-case analysis. *International Journal of Information Management*, (May 2018), Article 102052. <https://doi.org/10.1016/j.ijinfomgt.2019.102052>
- Zhang, L., Fan, Y., Zhang, W., & Zhang, S. (2019). Extending the theory of planned behavior to explain the effects of cognitive factors across different kinds of green products. *Sustainability (Switzerland)*, 11(15), 1-17. <https://doi.org/10.3390/su11154222>
- Zhang, Y., Wang, Z., & Zhou, G. (2013). Antecedents of employee electricity saving behavior in organizations: An empirical study based on norm activation model. *Energy Policy*, 62, 1120-1127. <https://doi.org/10.1016/j.enpol.2013.07.036>
- Zhao, H. H., Gao, Q., Wu, Y. P., Wang, Y., & Zhu, X. D. (2014). What affects green consumer behavior in China? A case study from Qingdao. *Journal of Cleaner Production*, 63, 143-151. <https://doi.org/10.1016/j.jclepro.2013.05.021>
- Zhu, Q., Sarkis, J., & Lai, K. H. (2013). Institutional-based antecedents and performance outcomes of internal and external green supply chain management practices. *Journal of Purchasing and Supply Management*, 19(2), 106-117. <https://doi.org/10.1016/j.pursup.2012.12.001>

Effect of Initial Carbon to Nitrogen Ratio on the Degradation of Oil Palm Empty Fruit Bunch with Periodic Addition of Anaerobic Palm Oil Mill Effluent Sludge

Muhamad Yusuf Hasan^{1,2}, Mohd Ali Hassan^{1,3*}, Mohd Noriznan Mokhtar¹, Yoshihito Shirai⁴ and Azni Idris⁵

¹Department of Process and Food Engineering, Faculty of Engineering, Universiti Putra Malaysia, 43400 Serdang, Selangor, Malaysia

²Section of BioEngineering Technology, Universiti Kuala Lumpur, Malaysian Institute of Chemical and BioEngineering Technology, Vendor City, Taboh Naning, 78000 Alor Gajah, Melaka, Malaysia

³Department of Bioprocess Technology, Faculty of Biotechnology and Biomolecular Sciences, Universiti Putra Malaysia, 43400 Serdang, Selangor, Malaysia

⁴Department of Biological Functions and Engineering, Graduate School of Life Science and Systems Engineering, Kyushu Institute of Technology, 2-4 Hibikino, Wakamatsu-ku, Kitakyushu, Fukuoka 808-0196, Japan

⁵Department of Chemical and Environmental Engineering, Faculty of Engineering, Universiti Putra Malaysia, 43400 Serdang, Selangor, Malaysia

ABSTRACT

The objective of this study was to evaluate the effect of different initial carbon to nitrogen (C/N) ratios on the organic matter degradation during active co-composting of oil palm empty fruit bunch (OPEFB) and palm oil mill effluent (POME) anaerobic sludge. The initial C/N ratio was varied from 25:1, 35:1 and 45:1. Co-composting was conducted by

periodic addition of sludge to maintain the moisture content and enrich the compost product. The organic matter (OM), carbon to nitrogen profile and compost maturity index were analysed. The results showed that the initial C/N ratio of 35:1 was the best initial C/N ratio. In addition, the C/N ratio of 35:1 gave the best OM degradation. The appropriate amount of initial C/N ratio coupled with the correct composting process parameters such as daily mixing, suitable pH

ARTICLE INFO

Article history:

Received: 6 February 2021

Accepted: 10 May 2021

Published: 28 October 2021

DOI: <https://doi.org/10.47836/pjst.29.4.10>

E-mail addresses:

muhamadyusuf@unikl.edu.my (Muhamad Yusuf Hasan)

alihas@upm.edu.my (Mohd Ali Hassan)

noriznan@upm.edu.my (Mohd Noriznan Mokhtar)

shirai@life.kyutech.ac.jp (Yoshihito Shirai)

azni@upm.edu.my (Azni Idris)

*Corresponding author

and moisture content improved the organic matter degradation. It reduced the composting time from 40-60 days to 30 days.

Keywords: Anaerobic sludge, composting system, composting, oil palm empty fruit bunch, periodic addition

INTRODUCTION

Composting is a proven method to mitigate greenhouse gases emission by stabilising agricultural solid waste, landscape waste and food waste, which will otherwise be converted into methane and CO₂ (Kumar et al., 2010). Composting is a process of degradation of organic waste into a stable organic matter with the dynamic interactions among the physical, chemical and biological factors (Białobrzewski et al., 2015; Onursal & Ekinci, 2016). Thermophilic conditions generated during the process is a reflection of the biological heat of microbial growth and activity. Most agricultural solid wastes such as the OPEFB are not suitable for composting on their own due to the high lignocellulosic content and low nitrogen content. However, the degradability of the highly lignocellulosic feedstocks can be enhanced by co-composting with nitrogen-rich waste (Singh et al., 2010).

C/N is considered one of the essential parameters that can influence the process conditions in terms of nutrients for microbes, composting time and the final characteristics of the compost as a product (Cundiff & Mankin, 2003). OPEFB has been co-composted with several types of waste materials with comparatively high nitrogen content and low carbon, such as poultry litter, goat dung, cow dung and palm oil mill effluent (POME) (Alkarimiah & Rahman, 2014; Zainudin et al., 2013). The range of the initial C/N ratio from 64:1 until 22:1 have been studied, and the time for composting to achieve maturation was between 40-60 days. Composting period has been reduced by controlling other parameters, especially moisture content. This moisture addition can be achieved by adding anaerobic sludge POME regularly (Baharuddin et al., 2009). The work of Baharuddin et al. (2009) was significant as information on composting period can be deduced from moisture content and C/N. According to the findings of Zainudin et al. (2013), the addition of sludge POME contains indigenous microbes and nutrients. Since about June 2016, there are an estimated 75 composting plants, 2 of which use 90-100% POME and the rest only partially in Malaysia (Loh et al., 2017). Thus, lower C/N would eventually takes less time. This means less space is needed, less fuel is consumed, and labour costs are reduced. It would be more beneficial if the optimum C/N ratio for effective co-composting OPEFB can be determined.

This research aimed to investigate the initial effect of the C/N ratio using two different forms of waste with the periodic addition of POME sludge. Co-composting was performed in this work using OPEFB and POME anaerobic sludge as primary and co-substrate, respectively. Specific initial C/N ratios were selected, and sludge was applied periodically

until almost the end of the composting period. The profiles such as C/N ratio, the total mass of composting material, moisture content, oxygen concentration and temperature were analysed throughout the co-composting period.

MATERIALS AND METHODS

Raw Materials

Pressed and shredded OPEFB with a size range from 15 cm to 20 cm was obtained from Jugra Palm Oil Mill Sdn. Bhd. (Selangor, Malaysia), while POME anaerobic sludge was obtained from FELDA Besout (Perak, Malaysia).

Composting Set-Up

Figure 1 presents the compost reactor system used in this study. The system is comprised of an insulated 120 litres reactor capacity with a diameter and height of about 46 cm and 75 cm, respectively. The system is equipped with a 1.5 horsepower electrical motor, airflow meter, compressor pump for aeration and sludge pumps for sludge intake and leachate recycling. Airflow for aeration was controlled at 0.27 m³/h, which flowed through an air humidifier before aeration in the reactor. The temperature sensor and carbon dioxide sensor were purchased from STAN BURRAGE (UK) (Model CP11) and CO₂meter.com (USA) (Model K33/CM-0040), respectively.

Co-composting Procedure

The experiment was carried out using three different ratios of OPEFB to POME anaerobic sludge. The ratios were set to 1:4, 1:1 and 4:1, having an initial C/N ratio of about 25:1, 35:1, and 45:1, respectively. Experiments were performed in triplicate for each ratio. The mixture was loaded manually into the composter. POME anaerobic sludge was gradually pumped until it reached the required amount. The sludge was added about 10% of the total initial weight every 3 days for 8 days until a week before the 30th day of composting. The total amount of OPEFB and POME anaerobic sludge used was 50 kg as initial weight. Aeration was supplied every 3 days for 3 hours per day. The leachate was pumped to circulate the material (mainly water). It will help achieve homogeneity and maintain the moisture content of the composting material. The moisture content was maintained between 70-80%. Agitation was done for one hour per day. Aeration was subjected throughout the composting process to ensure the carbon dioxide was not more than 5% (Nakasaka et al., 1990). The pH was determined using a pH meter (Hanna Instruments, USA). One gram of composting sample was taken and mixed with 10 ml distilled water using a 25 ml falcon tube.

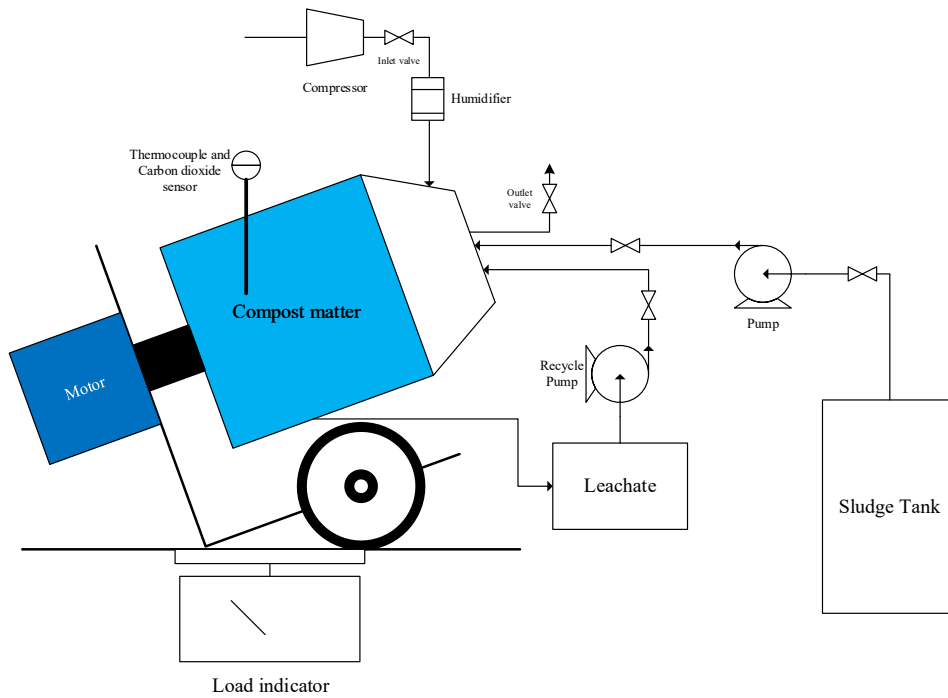


Figure 1. Schematic diagram of composting system

Analysis

Sludge acts as a medium to maintain the moisture content instead of using water. Each sample was dried at 105°C for 24 hours for moisture content analysis. The muffle furnace (KSL-1700X, MTI Corporation, USA) was used to measure the OM of compost material based on ignition loss at 550°C for 4 hours. The percentage of OM and total organic carbon (TOC) was determined using Equations 1 and 2:

$$OM_{\text{loss}}(\%) = 100 \cdot \frac{DM_0 \cdot OM_0 - DM_T \cdot OM_T}{DM_0 \cdot OM_0} \quad (1)$$

$$TOC = \frac{m_{OM} \times 100}{1.8} \quad (2)$$

For total nitrogen analysis of the sample, Total Kjeldahl Nitrogen (TKN) was carried out according to Kjeltec 2300 Analyser (FOSS Analytical AB, Sweden) manufacturer's manual. Cellulose and lignin content were determined using Fibertec 2010 and the Acid

Detergent Fibre (ADF) and Acid Detergent Lignin (ADL) methods, respectively (FOSS Analytical AB, Sweden). Moreover, since ADF contains both cellulose and lignin, whereas ADL contains only lignin, cellulose content was calculated by subtracting the value of ADF from the value of ADL. Mass of degradable organic matter (OM) with three different components, such as easily degradable OM content, slower (“moderate”) degradable OM, which is a cellulosic constituent and hardly degradable, which is lignin content within the co-composting material as defined by Talib et al. (2014).

Compost maturity was determined using the Solvita® compost maturity kit (Wood End® Research Laboratory Inc., Mt Vernon, Maine) at 25°C. The kit was used to measure carbon dioxide and ammonia emission using gel paddles. The compost maturity measurements were conducted in Solvita® jars, where the samples must be filled until the fill line. In addition, they must be in moist condition by following the manufacturer’s instruction (Guide to Solvita® testing for compost maturity index). Solvita® carbon dioxide and ammonia test paddles were carefully inserted into the jar without touching the gels part. The lid of the jar was closed tightly. The test paddles were allowed to remain at 25°C in the closed jar for 4 hours to allow any emissions to occur. The data was collected for detecting colour changes on the gel using a Solvita® digital colour reader. The reader detected colour changes for the Solvita® maturity index and emissions value for carbon dioxide and ammonia. The maturity index was measured over a scale of 1 to 8 for the carbon dioxide test result and 1 to 5 for the ammonia test result. The combined rating of the two scales result was assessed to determine the Solvita® maturity index (1-fresh, raw compost; 8-very stable compost).

Statistical Analysis

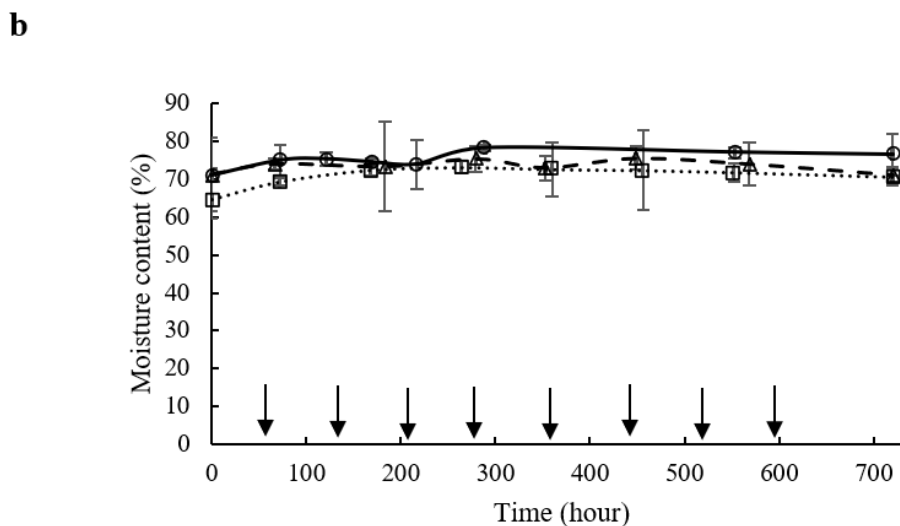
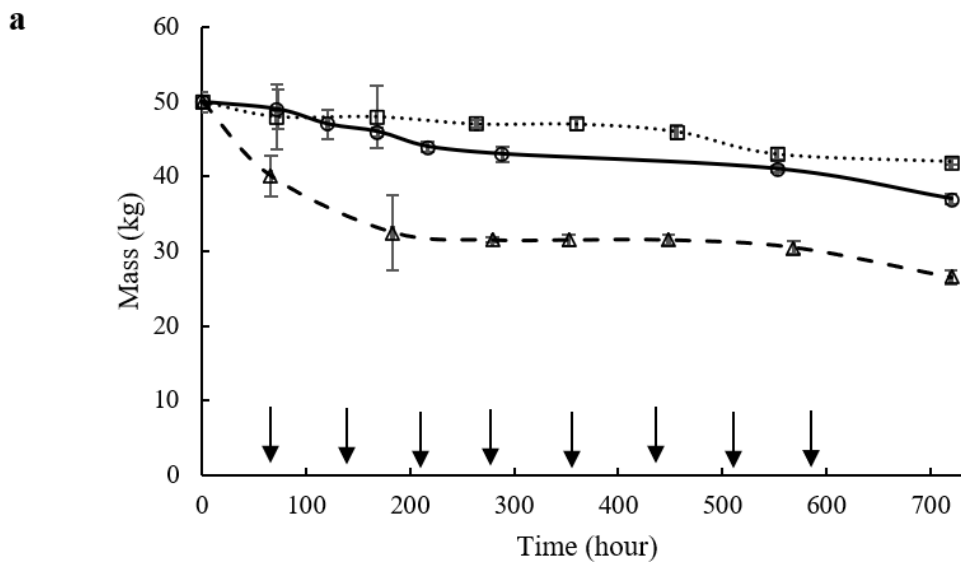
Statistical Analysis System Version 9.2 was used to analyse data collected for means and standard deviations using Analysis of Variance (ANOVA) at p0.05 for the treatment effect and post-hoc analysis by Duncan new multiple range test (DNMRT) for mean comparison.

RESULTS AND DISCUSSION

Compost Physico-chemical Evolution

The results for total mass curves at different initial C/N ratios during composting are presented in Figure 2a. The downward-facing arrows in the graph indicate the periodical additions of sludge during the process. The mass for the feedstock material with a 35:1 C/N ratio decreased at a much higher rate, followed by feedstock with the highest nitrogen content (25:1 C/N ratio) and lowest nitrogen content (45:1 C/N ratio). It can be seen that the decrease in mass was not necessary due to leachate runoff and evaporation, which causes the loss of moisture content as opposed to Figure 2b, where the level of moisture was almost maintained throughout the process. This is thought to be due to consumption of

easily and moderately degradable and remaining of hardly degradable fraction in organic matter as confirm this results obtained agreed with previous work carried out by Talib et al. (2014). As shown in Figures 4a and b, the C/N ratio of 35:1 has higher moderate OM than the C/N ratio of 25:1. However, recalcitrant carbon such as hard degradable OM mass in both C/N ratios was about the same. Hence, this explains why the ratio C/N of 35:1 decreased further due to biodegradable C/N ratio needing to be considered and not as total, assuming both nutrient sources are fully degradable as mentioned by Puyuelo et al. (2011).



c

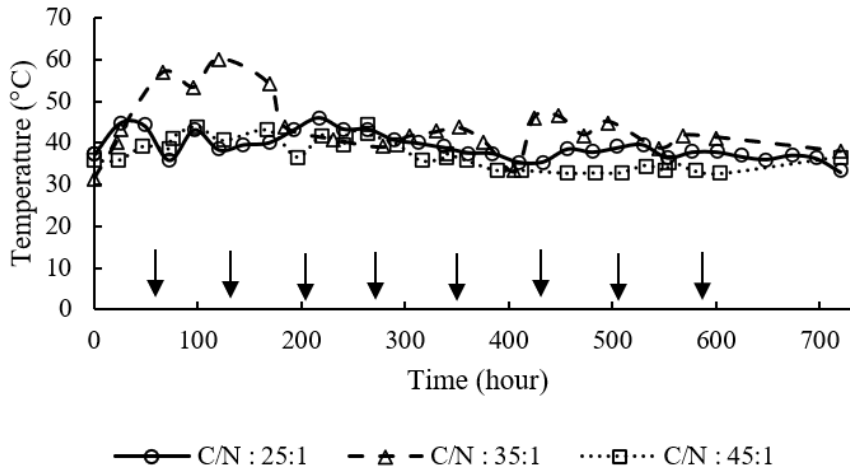


Figure 2. Profiles of mass, temperature and moisture content during the co-composting process. Arrows indicate periodical sludge addition

A moisture content plot of the periodical addition sludge into the compost reactor is shown in Figure 2b. After 150 hours or twice the addition of sludge, the moisture level was maintained in the range of 70 to 80%. The C/N ratio of 45:1 moisture content is the lowest compared to the other due to more OPEFB composition than sludge; the initial low moisture content was 65%. The other following C/N ratio has an initial adequate moisture content level of about 71%. The result suggests that the moisture content were relatively stable, probably due to the design of the compost reactor have fully insulated. Piping of inlet supplied gases was small within around 15 mm, and air supplied was only every 3 days interval which prevents moisture loss from evaporation. The inclined reactor position and the addition of sludge also contribute to water retention in the compost reactor. Another potential moisture loss is condensate, which was mainly produced during the thermophilic stage. It may drain as the leachate was less regulated due to experiment activity—only 3 days for 8 times, contributing to less water loss.

The variation of temperature profiles with three different initial C/N ratios of composting is shown in Figure 2c. C/N ratio of 35:1 achieved a high temperature of about 60°C before 100 hours of composting. The range of temperature within the thermophilic phase was above 40°C until 550 hours. Maximum temperatures of the C/N ratio for both 25:1 and 45:1 were found between 46°C and 44°C, which is lower than the 35:1 C/N ratio. As shown, the temperature keeps fluctuating between mesophilic and thermophilic phases until 720 hours. In general, the temperature profiles did not show a typical temperature pattern of co-composting. It represents the fluctuating temperature resulting from the

periodic addition of sludge every 3 days, and mechanical turning effects may contribute to heat loss. It is in agreement with the results reported by other researchers (Zervakis et al., 2013). The heating of compost is also related to the energy content of the substrate and degradability (Ryckeboer et al., 2003).

Hence, the composting rate also depends on the C/N ratio, where carbon is the source of energy and the main component of cell structure, and nitrogen is the second most significant element for cell growth and synthesis. The lower temperature may be due to less abundant nitrogen, which is associated with low microbial growth or quantity and less degradable of carbon such as the high composition of recalcitrant lignocellulose, which could contribute to a time delay to maturity (Zhou, 2017). All experiments were periodically added with sludge which assists in nutrient needs. However, the initial C/N ratio may also influence the time of process degradation. The obtained results support the use of control initial C/N ratio as a part of composting acceleration which agreed with those carried out by Zainudin et al. (2014) and Razali et al. (2012).

Figure 3a shows the carbon dioxide level during co-composting. The carbon dioxide level for 25:1 and 45:1 C/N ratios was higher than 5%, especially during the initial composting period (i.e. within 200 hours). After 300 hours, the carbon dioxide level drops below 4% until the end of composting. In the beginning period, the level of carbon dioxide increased, primarily in the thermophilic stage where the biodegradation process occurs. It indicates that the supply of oxygen from aeration and agitation for the composting system is appropriate. Lower aeration rates may negatively affect the OM degradation process. The resulting delayed thermophilic phase due to the rate of biological oxygen demand is higher than the rate of oxygen supply (Talib et al., 2014). Later period, carbon dioxide decreases due to less active aerobic oxygen-consuming microorganisms than the start of the process and an adequate supply of air which is expected to be below 5% of the carbon dioxide level as suggested by Nakasaki et al. (1990). Zainudin et al. (2017) also demonstrate that oxygen levels decrease during the thermophilic stage, and bacterial communities shift during different temperature phases. Because of the consistent interval supplies of aeration throughout the experiment, adding the sludge may not affect the oxygen levels.

The pH measurement was plotted in Figure 3b to represent the composting acidity or alkalinity. The range of pH throughout the composting period is about 8.11 to 8.99. All C/N ratio has slightly higher than neutral pH. The increase in pH measurement is associated with ammonia content due to biochemical reactions of nitrogen-containing materials producing ammonium hydroxide from ammonia-releasing proteolysis due to protein degradation, as explained by Razali et al. (2012). Increased pH also results in a lower C/N ratio than its higher ratio due to rapid metabolic degradation of organic matter and increased ammonium content due to nitrogen degradation (Gao et al., 2010; Tumuhairwe et al., 2009). The amount of nitrogen in composting continues to increase may be due to a concentration

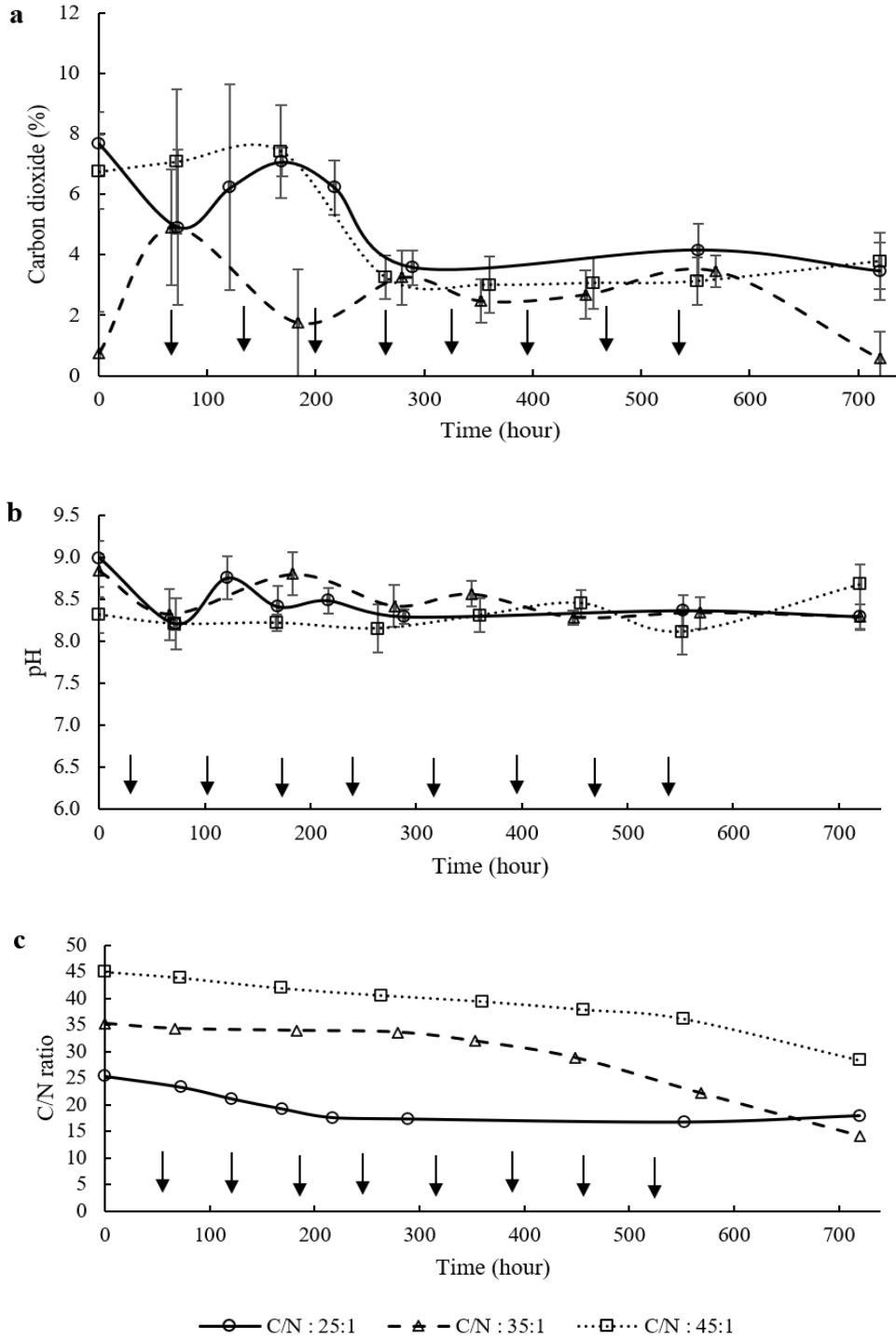
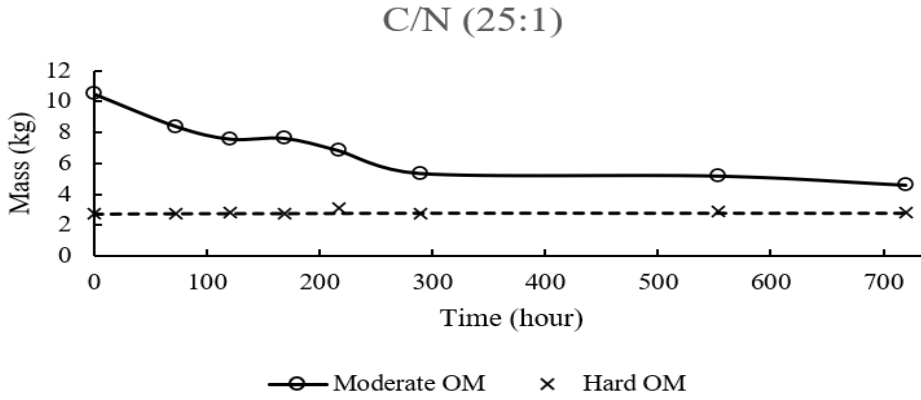


Figure 3. Changes in carbon dioxide, pH and C/N ratio during co-composting process. Error bar denotes standard deviation

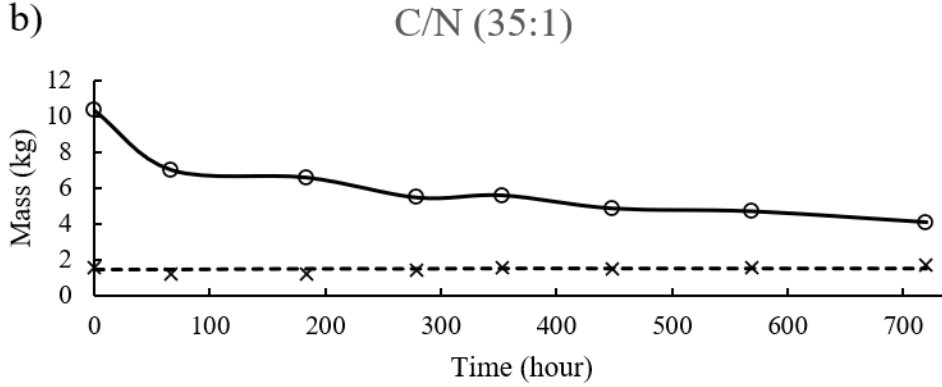
effect where carbon has a higher loss rate compared to nitrogen and causes an increase in the pH reading and the resulting decrease in the C / N ratio (Lin, 2008).

Figure 3c shows a C/N ratios profile during the co-composting. The initial C/N ratio of 35:1 has decreased lower value compared to other ratios. The initial C/N ratio of 45:1 has the slightest decrease compared to the others. The reduction of the C/N ratio indicates the decomposition of organic matter by microbial activity (Bernal et al., 2009). It indicates the initial C/N ratio plays a vital role in substrate ratio because carbon source and nitrogen source will provide a sufficient amount for mainly metabolism and growth of microorganisms, respectively. The results show that the periodic addition of sludge during the process did significantly impact the profiles. Due to anaerobic sludge, POME consists of main water consisting of 4% to 5 % solid content with of C/N ratio between 4:1 to 17:1. The finished product, compost, will reach a C/N ratio of below 20 is considered acceptable maturity and below 15 is preferable (Hock et al., 2009; Satisha & Devarajan, 2007). This indicator has been confirmed by Kumar et al. (2010), where C/N of 19 can still degrade more than 30% of organic matter if compost moisture is maintained at a minimum of 60%. Decreased C/N ratio of 35:1 is slightly higher than 25:1, which is 14:1 than 18:1. The value of degradation is significant with different letters between initial and final from the statistic analysis. The sludge composition is too high to limit aeration. The evidence of a carbon dioxide content for C/N of 25:1 and 45:1 higher than 35:1 can be explained in Figure 3a. Other possibilities are the composition of hardly degradable in the C/N ratio of 25:1 relatively higher than 35:1 as an exhibit in Figure 4. The maximum temperature for the initial C/N ratio of 25:1 and 45:1 is low. It may represent low biological activity towards organic matter depletion. As shown in Table 1, indications of an improved initial 35:1 degradation C/N ratio were obtained from the compost maturity index by using the Solvita maturity package. The values display the index of 6, which is the composting stage in the curing stage and is supported by the maximum loss of OM (74.15 %). These results also show that it is unnecessary to provide excessive sludge or OPEFB during initial composting as a partial quantity of both wastes can improve composting. Composting time was also reduced to 30 days.

a)



b)



c)

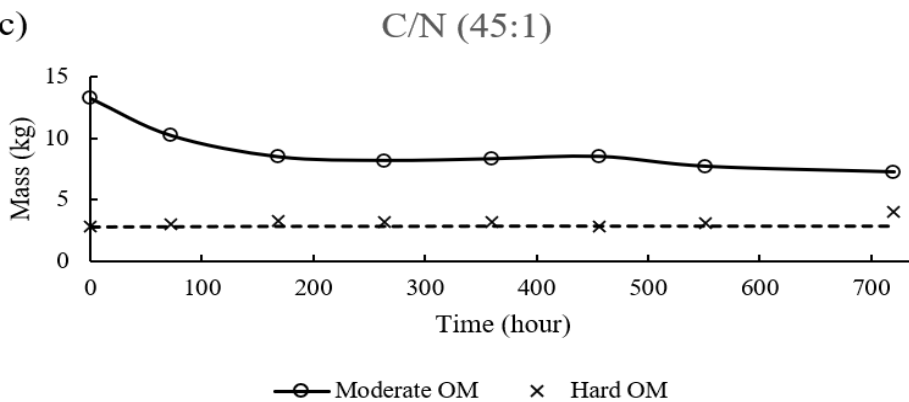


Figure 4. Organic Matter composition degradation

Table 1

Data for TOC, TKN, C/N ratio, OM loss, and Compost maturity index

Experiment	TOC (g/kg)		TKN (g/kg)		C/N ratio		OM loss (%)	Compost maturity index (interpretation)
	Initial	Final	Initial	Final	Initial	Final		
C/N(25:1)	516.70	475.90	20.33	26.49	25.41	17.95	63.25	Very Active
			± 0.11 ^b	± 0.49 ^b	± 2.78 ^a	± 4.84 ^a		
C/N(35:1)	514.40	424.29	14.59	30.00	35.26	14.13	74.15	Curing
			± 0.24 ^a	± 0.65 ^a	± 1.22 ^a	± 2.78 ^{d*}		
C/N(45:1)	516.70	483.50	11.50	17.00	44.98	28.41	49.63	Very active
			± 0.08 ^a	± 0.22 ^b	± 11.17 ^a	± 6.56 ^a		

Expression of results as means ± standard deviation

*Letters denotes significant differences across columns (p<0.05).

CONCLUSION

In this work, the initial C/N ratio was set up into three different levels. The experiment was designed using periodic addition of sludge to assess the effect of degradation organic matter composition and composting process parameters. This investigation showed that the initial C/N ratio of 35:1 obtained the best results in terms of degradation (reduce to 14:1) and achieved compost maturity into the curing stage. However, the appropriate amount of initial C/N ratio with control of the composting process parameter can contribute significantly to the C/N ratio profile. Furthermore, it is supported by the degradation of OM effectively compared to the high initial ratio. Thus, the 35:1 initial C/N ratio and below have a more significant impact on the degradation C/N ratio than higher ones. Since this work is only limited to its type and size of operation, therefore, for further works, variables and parameters of different types of composting operation are suggested to validate its operability on an industrial scale.

ACKNOWLEDGEMENT

The authors are once again grateful to the laboratory staff of Universiti Kuala Lumpur, Malaysia (UniKL), Universiti Putra Malaysia (UPM), and Kyushu Institute of Technology (Kyutech).

REFERENCES

- Alkarimiah, R., & Rahman, R. A. (2014). Co-composting of EFB and POME with the role of nitrogen-fixers bacteria as additives in composting process - A review. *International Journal of Engineering Science and Innovative Technology*, 3(2), 132-145.
- Baharuddin, A. S., Kazunori, N., Abd-Aziz, S., Tabatabaei, M., Rahman, N. A. A., Hassan, M. A., Wakisaka, M., Sakai, K., & Shirai, Y. (2009). Characteristics and microbial succession in co-composting of oil palm empty fruit bunch and partially treated palm oil mill effluent. *The Open Biotechnology Journal*, 3(1), 87-95. <https://doi.org/10.2174/1874070700903010087>
- Bernal, M. P., Alburquerque, J. A., & Moral, R. (2009). Composting of animal manures and chemical criteria for compost maturity assessment. A review. *Bioresource Technology*, 100(22), 5444-5453. <https://doi.org/10.1016/j.biortech.2008.11.027>
- Białobrzewski, I., Mikš-Krajnik, M., Dach, J., Markowski, M., Czekala, W., & Gluchowska, K. (2015). Model of the sewage sludge-straw composting process integrating different heat generation capacities of mesophilic and thermophilic microorganisms. *Waste Management*, 43, 72-83. <https://doi.org/10.1016/j.wasman.2015.05.036>
- Cundiff, J. S., & Mankin, K. R. (2003). Modeling the composting process. In *Dynamics of Biological Systems* (pp. 4.1-4.64). American Society of Agricultural Engineers.
- Gao, M., Liang, F., Yu, A., Li, B., & Yang, L. (2010). Evaluation of stability and maturity during forced-aeration composting of chicken manure and sawdust at different C/N ratios. *Chemosphere*, 78(5), 614-619. <https://doi.org/10.1016/j.chemosphere.2009.10.056>
- Hock, L. S., Baharuddin, A. S., Ahmad, M. N., Shah, U. K., Aini, N., Rahman, A., Abd-aziz, S., Hassan, M. A., & Shirai, Y. (2009). Physicochemical changes in windrow co-composting process of oil palm mesocarp fiber and palm oil mill effluent anaerobic sludge. *Australian Journal of Basic and Applied Sciences*, 3(3), 2809-2816.
- Kumar, M., Ou, Y. L., & Lin, J. G. (2010). Co-composting of green waste and food waste at low C/N ratio. *Waste Management (New York, N.Y.)*, 30(4), 602-609. <https://doi.org/10.1016/j.wasman.2009.11.023>
- Lin, C. (2008). A negative-pressure aeration system for composting food wastes. *Bioresource Technology*, 99(16), 7651-7656. <https://doi.org/10.1016/j.biortech.2008.01.078>
- Loh, S. K., Nasrin, A. B., Azri, S. M., Adela, B. N., Muzzammil, N., Jay, T. D., Eleanor, R. A. S., Lim, W. S., Choo, Y. M., & Kaltschmitt, M. (2017). First report on Malaysia's experiences and development in biogas capture and utilization from palm oil mill effluent under the economic transformation programme: Current and future perspectives. *Renewable and Sustainable Energy Reviews*, 74(September 2015), 1257-1274. <https://doi.org/10.1016/j.rser.2017.02.066>
- Nakasaka, K., Yaguchi, H., Sasaki, Y., & Kubota, H. (1990). Effects of oxygen concentration on composting of garbage. *Journal of Fermentation and Bioengineering*, 70(6), 431-433. [https://doi.org/10.1016/0922-338X\(90\)90128-J](https://doi.org/10.1016/0922-338X(90)90128-J)

- Onursal, E., & Ekinci, K. (2016). A kinetic study on how C/N ratio affects energy consumption of composting of rose oil-processing wastes with caged layer manure and straw. *Environmental Progress and Sustainable Energy*, 36(1), 129-137. <https://doi.org/10.1002/ep>
- Puyuelo, B., Ponsá, S., Gea, T., & Sánchez, A. (2011). Determining C/N ratios for typical organic wastes using biodegradable fractions. *Chemosphere*, 85(4), 653-659. <https://doi.org/10.1016/j.chemosphere.2011.07.014>
- Razali, W. A. W., Baharuddin, A. S., Talib, A. T., Sulaiman, A., Naim, M. N., Hassan, M. A., & Shirai, Y. (2012). Degradation of oil palm empty fruit bunches (OPEFB) fibre during composting process using in-vessel composter. *BioResources*, 7(2010), 4786-4805.
- Ryckeboer, J., Mergaert, J., Vaes, K., Klammer, S., Clercq, D., Coosemans, J., Insam, H., & Swings, J. (2003). A survey of bacteria and fungi occurring during composting and self-heating processes. *Annals of Microbiology*, 53(4), 349-410.
- Satisha, G. C., & Devarajan, L. (2007). *Effect of amendments on windrow composting of sugar industry pressmud*. 27, 1083-1091. <https://doi.org/10.1016/j.wasman.2006.04.020>
- Singh, R. P., Ibrahim, M. H., Esa, N., & Iliyana, M. S. (2010). Composting of waste from palm oil mill: A sustainable waste management practice. *Reviews in Environmental Science and Bio/Technology*, 9(4), 331-344. <https://doi.org/10.1007/s11157-010-9199-2>
- Talib, A. T., Mokhtar, M. N., Baharuddin, A. S., & Sulaiman, A. (2014). Effects of aeration rate on degradation process of oil palm empty fruit bunch with kinetic-dynamic modeling. *Bioresource Technology*, 169, 428-438.
- Tumuhairwe, J. B., Tenywa, J. S., Otabbong, E., & Ledin, S. (2009). Comparison of four low-technology composting methods for market crop wastes. *Waste Management*, 29(8), 2274-2281. <https://doi.org/10.1016/j.wasman.2009.03.015>
- Zainudin, M. H. M., Hassan, M. A., Tokura, M., & Shirai, Y. (2013). Indigenous cellulolytic and hemicellulolytic bacteria enhanced rapid co-composting of lignocellulose oil palm empty fruit bunch with palm oil mill effluent anaerobic sludge. *Bioresource Technology*, 147, 632-635.
- Zainudin, M. H. M., Hassan, M. A., Shah, U. K. M., Abdullah, N., Tokura, M., Yasueda, H., Shirai, Y., Sakai, K., & Baharuddin, A. S. (2014). Bacterial community structure and biochemical changes associated with composting of lignocellulosic oil palm empty fruit bunch. *BioResources*, 9(1), 316-335.
- Zainudin, M. H. M., Ramli, N., Hassan, M. A., Shirai, Y., Tashiro, K., Sakai, K., & Tashiro, Y. (2017). Bacterial community shift for monitoring the co-composting of oil palm empty fruit bunch and palm oil mill effluent anaerobic sludge. *Journal of Industrial Microbiology and Biotechnology*, 44(6), 869-877. <https://doi.org/10.1007/s10295-017-1916-1>
- Zervakis, G. I., Koutrotsios, G., & Katsaris, P. (2013). Composted versus Raw olive mill waste as substrates for the production of medicinal mushrooms: An assessment of selected cultivation and quality parameters. *BioMed Research International*, 2013, Article 546830. <https://doi.org/10.1155/2013/546830>

Zhou, J. M. (2017). The effect of different C/N ratios on the composting of pig manure and edible fungus residue with rice bran. *Compost Science & Utilization*, 205(2), 120-129. <https://doi.org/10.1080/1065657X.2016.1233081>



Enhancement of Binding Affinity of Anti-Hapten Polyclonal IgG Recognizing Mitragynine using Affinity Purification

Radhiahtul Raehan Mustafa¹, Rashidah Sukor^{1,2*}, Siti Mariam Mohd Nor³, Nazamid Saari¹, Farina Mustaffa Kamal⁴ and Aliah Zannierah Mohsin²

¹Department of Food Science, Faculty of Food Science and Technology, Universiti Putra Malaysia, 43400 UPM, Serdang, Selangor, Malaysia

²Laboratory of Food Safety and Food Integrity, Institute of Tropical Agriculture and Food Security, Universiti Putra Malaysia, 43400 UPM, Serdang, Selangor, Malaysia

³Department of Chemistry, Faculty of Science, Universiti Putra Malaysia, 43400 UPM, Serdang, Selangor, Malaysia

⁴Department of Veterinary Pathology and Microbiology, Faculty of Veterinary Medicine, Universiti Putra Malaysia, 43400 UPM, Serdang, Selangor, Malaysia

ABSTRACT

Antibodies are glycoproteins found in peritoneal fluid, serum, and blood. The antibody-based assay has been used for broad applications such as immunodiagnostic and other biomedical applications. Depending on the intended application, a highly purified polyclonal antibody could be used as an alternative. Purification of antibodies from anti-sera has been proven as one of the methods to enhance the binding affinity of antibodies towards its antigen. We report herein the enhancement of the binding affinity of anti-hapten polyclonal IgG recognizing mitragynine using affinity purification. Serum from the terminal bleed of New Zealand White (NZW) rabbits immunized with mitragynine conjugated with cationized-bovine serum albumin at methyl ester (C22-MG-cBSA), or aromatic ether modification (C9-MG-cBSA) were subjected to HiTrap Protein G affinity purification using fast protein

liquid chromatography (FPLC). The elution peak from chromatography fractions was analyzed using sodium dodecyl sulfate-polyacrylamide gel electrophoresis (SDS-PAGE) and Western blot. Here, we report the binding of polyclonal antibodies produced from inoculation of either C22-MG-cBSA or C9-MG-cBSA immunogens of which mitragynine-ovalbumin (MG-OVA) was used as coating antigen in the ELISA assay. Non purified anti-sera from C22-MG-cBSA-

ARTICLE INFO

Article history:

Received: 10 February 2021

Accepted: 05 July 2021

Published: 18 October 2021

DOI: <https://doi.org/10.47836/pjst.29.4.11>

E-mail addresses:

raehanmustafa@gmail.com (Radhiahtul Raehan Mustafa)

rashidah@upm.edu.my (Rashidah Sukor)

smariam@upm.edu.my (Siti Mariam Mohd Nor)

nazamid@upm.edu.my (Nazamid Saari)

farina@upm.edu.my (Farina Mustaffa Kamal)

aliahmohsin89@gmail.com (Aliah Zannierah Mohsin)

* Corresponding author

inoculated rabbits showed higher titer than C9-MG-cBSA at 1/128 000 and 1/32 000 dilutions, respectively. The affinity of purified poly-IgGs from rabbits immunized with C22-MG-cBSA showed a mean K_d value of 7.965×10^{-6} μ M, which was lower than those immunized with C9-MG-cBSA at mean K_d of 1.390×10^{-4} μ M. In addition, the purified poly-IgGs showed higher binding towards MG-OVA than non-purified anti-sera at comparable protein concentrations. These results indicated that the higher binding affinity of purified polyclonal IgG is due to the reduced competition among polyclonal antibodies with non-IgG proteins that co-existed in the non-purified anti-sera after the affinity purification.

Keywords: Affinity chromatography, ELISA, IgG purification, mitragynine, polyclonal antibody

INTRODUCTION

Mitragynine is the main alkaloid in *Mitragyna speciosa* (kratom), which contributes to human addiction. It is utilized in the same context as other drugs and is often misused as a substitute for commercial drugs (Meireles et al., 2019). This psychoactive compound could render psychotropic and toxic effects. Therefore, the determination of mitragynine in human biological samples (e.g., saliva, urine, and blood) is important to monitor kratom misuse. Immuno-based analytical methods such as enzyme-linked immunosorbent assay (ELISA) and immunoblotting offer high advantages for straightforwardly detecting the alkaloid. However, a high sensitivity, specificity, reliability, and robustness of these analytical methods depend on the quality of the antibodies as biorecognition molecules. Having high affinity of antibodies could prevent the non-specific binding of other proteins in ELISA. Therefore, it is crucial for indirect ELISA format for hapten (mitragynine) that involves the coating of diluted antibodies onto the plate surface.

Antibodies or immunoglobulin G (IgG)s are generally isolated from serum, plasma, egg yolk, and peritoneal fluid, which generally co-exist with other biomolecules and proteins such as albumin and salt that may interfere with the binding between antibodies and the target antigen (Arora et al., 2016). This problem causes non-specific background in many analytical techniques such as ELISA, reducing the detection signal or producing a false-positive result. Besides, antibodies with low sensitivity and specificity for their analyte can recognise other molecules structurally similar to the target analyte. Since kratom is usually consumed in a mixture of other substances, also known as kratom cocktails, the binding affinity of anti-mitragynine antibodies can be affected by kratom matrices or additives used in the cocktail. Thus, an efficient method for purifying antibodies is crucial for antibodies generation's high affinity and specificity.

Common techniques employed for antibody purification include ammonium sulphate precipitation, filtration, electrophoretic separation, and affinity chromatography (Tiller & Tessier, 2015). The choice of techniques is based on their key attributes, including size,

folding stability, solubility, binding affinity, isoelectric point (pI), and hydrophobicity of the antibody (Tiller & Tessier, 2015). Affinity chromatography is an effective separation tool for purifying individual molecules from a complex mixture, removing any unwanted proteins while maintaining the desired product consistency. It is a promising method for purifying antibodies from various animals, which employs different types of binding molecules (ligands) and solid phase support (matrices). It has significant advantages, including ease of operation, rapid, high yield and purity (> 90%), and excellent selectivity towards the target molecule. This method has been reported to be the most efficient technique for purifying antibodies (Arora et al., 2016; Lopez et al., 2019, Fishman & Berg, 2019).

Purification of antibodies from non-purified anti-sera has many advantages such as increased antibody concentration, purity, stability for long-term analysis and storage, as well as reduced non-specific background activities and variation lot to lot batch of the antibodies since polyclonal antibodies contain a mixture of the antibodies being produced (Fishman & Berg, 2019; Tiller & Tessier, 2015). However, the purification technique may and may not enhance the binding affinity of the antibody. As reported by Mustafaoglu et al. (2016), purification of antibodies did not improve the binding activity of the antibody due to the antibody activity (including both antigen detection and Fc recognition) was utterly preserved after purification. Limited studies were reported on the difference of binding affinity of purified poly-IgG or non-purified anti-sera in immunoassay. The choice of using purified antibodies or non-purified anti-sera in immuno-based assay depends on several factors, including the cost, availability of the target analyte in large quantity, personnel technical competency, and intended use of the assay. Therefore, this study aims to evaluate the binding affinity of non-purified anti-sera and purified poly-IgGs of anti-mitragynine polyclonal antibodies towards mitragynine conjugated with cationized-bovine serum albumin at different positions of mitragynine molecule, i.e., methyl ester (C22-MG-cBSA) and aromatic ether (C9-MG-cBSA).

MATERIAL AND METHODS

Materials and Reagents

All chemicals and reagents were of analytical grade. Mitragynine standard (98% purity) from Chromadex (Los Angeles, CA). Titermax Gold Adjuvant, Freund's Incomplete Adjuvant, ovalbumin (OVA), Tween 20 and 1-step ultra 3, 3', 5, 5'-tetramethylbenzidine (TMB) from Sigma Aldrich (St. Louis, MO). Alkaline phosphatase- and peroxidase-conjugated AffiniPure goat anti-rabbit (H+L) IgGs from Jackson ImmunoResearch Laboratories (West Grove, PA). Nitro blue tetrazolium chloride/5-bromo-4-chloro-3-indolyl phosphate (NBT/BCIP) chromogen and immobilon-P PVDF membrane from Merck (Darmstadt, Germany). Enhanced chemiluminescent (ECL) and HiTrap Protein G HP column from GE Healthcare (Uppsala, Sweden). Nunc Maxisorp 96-well microtiter plates from Thermo Fisher Scientific

(Waltham, MA). Coomassie Blue G-250, Tris, glycine and sodium dodecyl sulphate from Bio-Rad Laboratories (Hercules, CA). Ultra-pure water (18.2 M Ω .cm) from ELGA Lab Water (Lane End, UK).

Immunization of Animal

Animal studies were approved by the Institutional of Animal Care and Use Committee of Universiti Putra Malaysia (UPM/IACUC/AUP-R004). Mitragynine used as immunogen was modified at 16-COOCH₃ and 9-OCH₃ and conjugated to cBSA (Figure 1) according to Limsuwanchote et al. (2014) and Esteve-Turrillas et al. (2018) with slight modifications.

Four female 12-weeks old New Zealand White (NZW) rabbits (2 animals per immunogen) were immunized with the conjugated immunogen. The rabbit immunization protocol was carried out in accordance with polyclonal antibody production guidelines (Delahaut, 2017). Prior to the immunization procedure, rabbits were fed, primed and acclimatised for 14 days at the animal research facility, Faculty of Veterinary Medicine, Universiti Putra Malaysia, Serdang, Selangor. Pre-immune blood was collected prior to the first immunization and used as a negative control. For initial immunization, 500 μ g/mL of immunogen (MG-22-cBSA and MG-9-cBSA) was dissolved in 1 mL NaCl (0.9%) and mixed with an equal volume of Titermax gold adjuvant. Rabbits were immunized subcutaneously (SQ) with 1 mL (0.25 mL per site for four sites) of the prepared solution. The immunogens were prepared at 250 μ g/mL of antigen in Incomplete Freund's Adjuvant for subsequent immunization boosters. About five mL of blood per animal were collected after seven days of immunization via marginal ear vein. Rabbits were immunized at a one-month interval (28 days) with a total of 168 days of immunization protocol. Rabbits were euthanized by overdosage of pentobarbital via intracardiac injection. Approximately

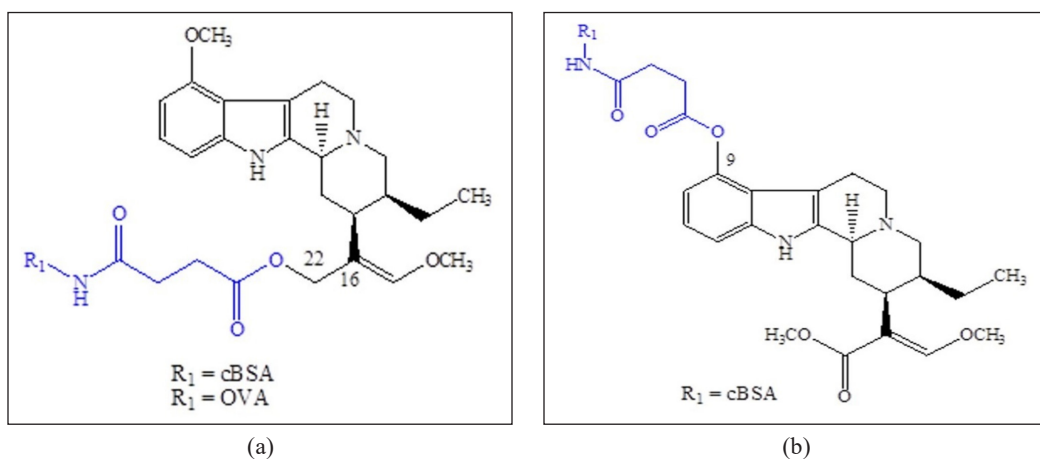


Figure 1. Mitragynine used as immunogen modified at two different molecule positions; (a) 16-COOCH₃ and (b) 9-OCH₃ and conjugated to cBSA. Mitragynine conjugated with OVA at 16-COOCH₃ was used as coating antigen in ELISA

80-120 mL of terminal sera per animal was collected through cardiac puncture. Blood was stored at 4°C (overnight) to clot and centrifuged for 20 mins at 1000 rpm. The non-purified anti-sera were stored in aliquots at -20°C until further use.

Sodium Dodecyl Sulphate-Polyacrylamide Gel Electrophoresis (SDS-PAGE)

The purity of purified poly-IgGs was examined after affinity chromatography by SDS-PAGE. According to the manufacturer's instructions, polyacrylamide (12%) was used as separation gel in reducing conditions (Bio-Rad Laboratories, Hercules, CA). Purified poly-IgGs (20 µg/mL) were prepared in SDS-PAGE sample buffer containing 2-mercaptoethanol as a reducing agent and heated at 95°C for 10 mins. The sample was electrophoresed at 110 V for 60 mins and stained with 0.1% Coomassie Brilliant Blue G-250 for 30 mins, and subsequently destained with methanol: acetic acid (4:1, v/v) until the background was clear.

Purification of Polyclonal IgGs

Non-purified anti-sera of rabbits from terminal bleed (10 mL) were pooled and dialyzed against PBS (pH 7.4) at 4°C with three times buffer changes. The non-purified anti-sera protein concentration was determined using NanoDrop ND-1000 (Thermo, Waltham, MA) at 280 nm. The non-purified anti-sera were subjected to affinity chromatography on ÄKTA Purifier 10 of Fast Protein Liquid Chromatography system (GE Healthcare Bio-Sciences, Pittsburg, PA) for IgG purification according to the manufacturer's instruction. Briefly, the binding buffer (20 mM sodium phosphate, pH 7) was mixed with an equal volume of the anti-mitragynine of non-purified anti-sera (5 mL), filtered (0.45 µm) and loaded onto a 1 mL of HiTrap Protein G HP column through a sample loop. The column was pre-equilibrated with the binding buffer (5 mL). The specific IgG in the non-purified anti-sera solution was allowed to bind to the protein G affinity column. After that, the unbound substances were washed by rinsing with the binding buffer at a flow rate of 1 mL/min at a five-column volume (5 mL). Bound IgGs were eluted using glycine-HCl (0.1 M, pH 2.7) and neutralized with Tris-HCl (1 M, pH 9). Purified poly-IgGs were collected during the elution peak generated and dialyzed (MWCO 12-14,000 Da) against PBS (pH 7.4) at 4°C within 24 hours and lyophilized. The weight of lyophilized IgGs was recorded and stored at -20°C until further use. The concentration of purified poly-IgGs was measured by NanoDrop ND-1000 at an absorbance value of 280 nm calculated using 1.35 as extinction co-efficient (ϵ) for rabbit IgG (Zhao et al., 2019).

Western Blot

According to the manufacturer's instructions, purified poly-IgGs from SDS-PAGE were further identified on Western blot (Bio-Rad Laboratories, Hercules, CA). Briefly, the

SDS gel was equilibrated in transfer buffer (5.76 g of Tris base, 2.95 g of glycine and 200 mL of methanol in 1 L of water) for 15 mins prior to transfer onto immobilon-P PVDF membrane. Next, a trans-blot semi-dry transfer cell (Bio-Rad Laboratories, Hercules, CA) was used to transfer the gel onto the membranes at 24 V and room temperature for 30 mins. Subsequently, non-specific binding on the membrane was blocked with skimmed milk (5%, w/v) in PBS and incubated with gentle shaking for 1 hour. Next, the membrane was washed three times with PBST and probed with alkaline phosphatase-conjugated AffiniPure goat anti-rabbit IgG (H+L) (1:1000, v/v). The membrane was further incubated with gentle shaking at room temperature for 2 hours. After the washing step, the protein bands were developed by the addition of NBT/BCIP substrate. The PVDF membrane was then rinsed with water and air-dried.

Indirect Enzyme-Linked Immunosorbent Assay (ELISA)

The humoral response of rabbit non-purified anti-sera of anti-mitragynine polyclonal antibodies was examined through indirect ELISA according to Mohsin et al. (2020), with slight modifications. The binding affinity of purified poly-IgGs from all rabbits was performed using total protein concentration at 5, 2.5 and 1.25 µg/mL of pre-immune anti-sera, non-purified anti-sera and purified poly-IgG from a terminal bleed of the rabbits. Ninety-six-well microtiter plates were coated with MG-OVA at 0.25 µg/mL (100 µL) in PBS (pH 7.4) and incubated overnight (16 hours) at 4°C. The plates were washed three times using PBS and blocked using skimmed milk (5% w/v, 250 µL) for 2 hours at room temperature with constant shaking (100 rpm). Pre-immune anti-sera, non-purified anti-sera and purified poly-IgG with dilution in PBS (100 µL) was added with total protein concentration at 5, 2.5 and 1.25 µg/mL, and incubated for 1 hour at 37°C. Next, goat anti-rabbit-HRP was added at 1/2500 (v/v) (0.16 µg/mL) and further incubated at similar condition. The plates were washed three times with PBST (PBS containing 0.01% Tween 20, 250 µL) between incubation. The ELISA reaction was initiated by adding 1-Step™ Ultra 3,3',5,5'-tetramethylbenzidine (TMB) substrate solution (100 µL) and the reaction was developed at room temperature for 20-30 mins in the dark. The reaction was quenched by the addition of 0.1 N HCl (100 µL). The absorbance was measured using a Multiskan FC microplate reader (Thermo Scientific, Waltham, MA) at 450 nm.

Data Analysis

All the samples were performed in triplicates ($n=3$). The absorbance of pre-immune anti-sera was used as a control (A_0). Results were analyzed using GraphPad Prism 5 (San Diego, CA) and one-site binding formula, $[Y=B_{max} * X / (K_d + X)]$ to evaluate the affinity constant (K_d) of purified poly-IgGs.

RESULTS AND DISCUSSION

Purification of IgGs

Purification of IgGs from non-purified anti-sera by protein G can be observed based on the solvent conductivity (mS/cm) and absorbance (mAU). The chromatographic profile, which showed the optimal condition of IgG purification, was in agreement with previous studies (Mohsin et al., 2020; Kang et al., 2016; Haddad et al., 2016). Figure 2 shows the chromatographic profile of the purified poly-IgGs using protein G affinity chromatography.

Approximately 1.49, 2.32, 2.16, and 1.73 mg/mL of purified poly-IgGs were obtained from 10 mL of non-purified anti-sera from the terminal bleed of rabbit 1, 2, 3, and 4, respectively. During purification, pH plays an important role to determine the purity and attributes of the purified-poly IgGs. The use of extreme pH (i.e., acidic or basic condition) in purification may degrade the IgGs, thus compromising the antigen recognition. This condition may also affect the functionality of the purified poly-IgGs (Lopez et al., 2019). A neutral pH of the binding buffer (pH 7.0, 20 mM sodium phosphate) was used due to the favourable condition of the binding at a pH close to physiological condition between protein-G and the antibody. Neutral condition of binding buffer (potassium phosphate) is essential for optimal antibody-antigen binding. Protein G was allowed to bind to IgGs in the non-purified anti-sera for 10 min (peak 1) with the binding buffer. During this step, IgG adsorption to protein G occurred through affinity attachment at a low flow rate of 1 mL/min. A longer incubation period using a low flow rate during the binding process is necessary for the maximum binding of the IgG with the protein G (Arora et al., 2017).

After binding IgG to protein G, the unbound non-specific molecule or weakly bound IgGs were further eliminated by washing the protein G column with 5 to 10 CV binding buffer. The unbound materials were eliminated, and the bound IgG was recovered by changing the buffer to acidic conditions. At this step, impurities and non-specific binding from other molecules in biological samples were successfully removed (Lopez et al., 2019). The elution step of affinity chromatography can be performed using a competitive ligand or non-specifically, such as adjusting the polarity of the solution, pH, ionic strength, and biomolecular chemical characteristics. The elution (peak 2) was performed by changing the ionic strength of the solution with the use of an elution buffer of 0.1 M glycine-HCl.

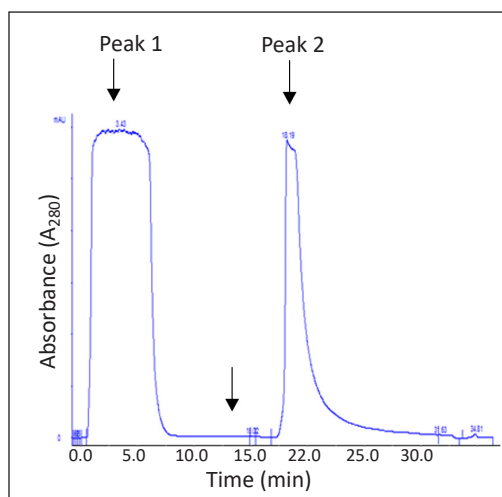


Figure 2. Chromatogram showing affinity chromatography using 20 mM of sodium phosphate (pH 7.0) (Peak 1) as binding buffer and elution (Peak 2) of IgG using 0.1 M glycine-HCl (pH 2.7) detected at 280 nm using HiTrap Protein G affinity

Increased salt concentration in the elution step elevated the ionic strength and weakened the protein G-IgG interactions (Mohsin et al., 2020).

Protein G-IgG binding dissociated by the positive charge of HCl at the acidic condition of the elution buffer. Therefore, during the elution step, the pH of the buffer was changed into acidic conditions using an elution buffer of pH 2.7. Acidic elution is most commonly used to elute purified poly-IgG due to favourable desorption and applies to most immunoglobulin species (Lopez et al., 2019). Nevertheless, the harsh acidic condition may lead to denaturation, alter the antigen-binding and conformational change, which cause aggregation to the IgGs (Arora et al., 2016). It was addressed by adding 1 M Tris-HCl (pH 9), which neutralized the IgGs condition, prevented loss of the IgGs activity, and maintained the IgGs structure.

SDS-PAGE and Western Blot of Purified Poly-IgGs

The purified poly-IgGs was assessed using SDS-PAGE and Western blotting under reducing condition. Figure 3 shows purified poly-IgG from four rabbits with two distinctive bands of the heavy and light chain of IgG at molecular weights of 50 and 25 kDa, respectively.

The basic structure of an antibody is made up of two identical heavy (H) chains (50 kDa) and light (L) chains (25 kDa) linked by disulfide bonds. The molecular weight of IgG in a non-reducing condition of SDS-PAGE is at 150 kDa (Arora et al., 2016). Using 2-mercaptoethanol in the sample buffer as a reducing agent caused the dissociation of disulphide bonds on the antibody structure. In addition, the evaluation of purified poly-IgGs allows for the observation of contamination with other serum proteins. In Figure 3, there was an absence of additional bands in the SDS-PAGE and immunoblot, which verified the purity of the IgG from the rabbit of non-purified anti-sera. These results were according to

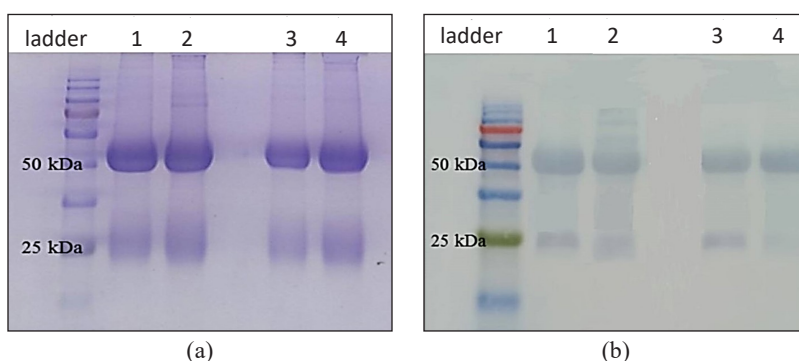


Figure 3. Characterisation of purified anti-mitragynine poly-IgGs. Two bands of 50 and 25 kDa, corresponding to the IgG heavy and light chains were shown on (a) SDS-PAGE (12% separating gel), and (b) Western blot developed on NBT-BCIP substrate. Lane 1 and 2: purified poly-IgGs of rabbit 1 and 2 immunised with C22-MG-cBSA; Lane 3 and 4: purified poly-IgGs of rabbit 3 and 4 immunised with C9-MG-cBSA. Each well was loaded with 5 µg/mL of purified poly-IgG

the previous studies, in which the pure IgG was obtained from polyclonal antibodies through affinity chromatography (Kang et al., 2016; Sadeghi et al., 2018, Mustafaoglu et al., 2016).

Binding Comparison of Non-Purified Anti-Sera and Purified Poly-IgGs towards Mitragynine

Purification of IgGs from anti-sera through affinity chromatography improved the binding affinity of the IgGs towards mitragynine at both C22- and C9-conjugated mitragynine (Figure 4). In addition, the purification was efficient in removing non-specifically bound protein to the ELISA plate, which interrupted the IgG-mitragynine binding. The binding of purified poly-IgGs from the four rabbits was compared with non-purified anti-sera from the terminal bleed by indirect ELISA, as shown in Figure 4.

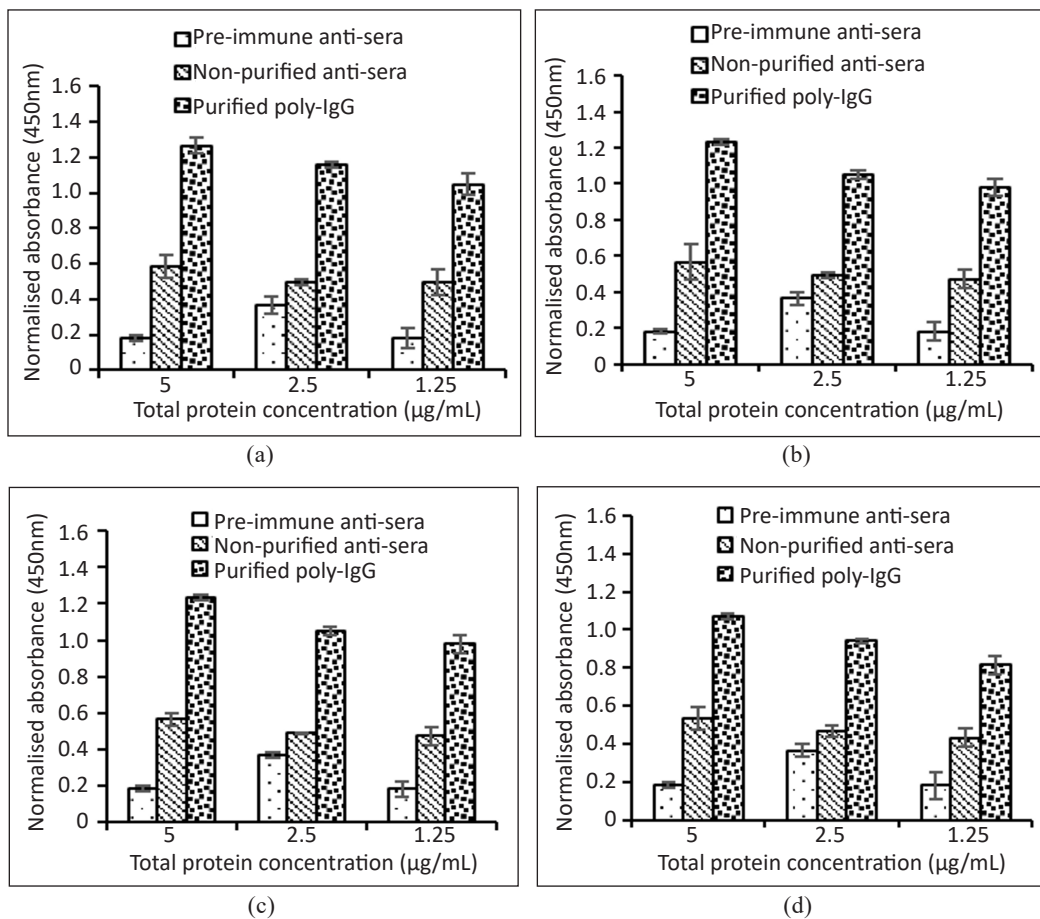


Figure 4. Binding comparison of non-purified anti-sera and purified poly-IgG of (a) rabbit 1 and (b) rabbit 2 immunized with C22-MG-cBSA and (c) rabbit 3 and (d) rabbit 4 immunized with C9-MG-cBSA. The non-purified anti-sera and purified poly-IgGs were from the terminal bleed of the rabbits. Pre-immune anti-sera were used as negative control. Normalized absorbance were obtained by subtracting background absorbance of pre-immune anti-sera. Values represent mean \pm SD of three readings.

Purified poly-IgGs showed a higher binding towards mitragynine-OVA than non-purified anti-sera at similar protein concentrations, which indicated that the affinity purification had improved the IgG binding. In addition, it was reported that approximately 75% of total IgGs were contained in a normal rabbit serum (Barker & Reisen, 2019). Hence, purification of the IgGs has successfully removed the unspecific protein, including serum albumin and other protein that co-existed in the non-purified anti-sera.

In the humoral response of IgG, the binding of anti-mitragynine poly-IgG in non-purified anti-sera towards mitragynine-cBSA conjugates are influenced by several important features. Firstly, the characteristic of the conjugates requires mitragynine-specific B cells and mitragynine-specific helper T cells. In addition, specific portions of hapten and carrier protein need to be associated to evoke an immune response physically. Secondly, the interaction occurs when the helper T cells bind to the B lymphocytes that only express major histocompatibility complex (MHC) class II molecules. Thus, the main factor inducing the humoral response of hapten-protein conjugates is an intrinsic determinant (hapten) recognized by B cells, and the other determinant is associated with MHC class II (carrier protein) recognized by T cell (Sanchez-Trincado et al., 2017).

An antibody molecule binds to the part of the antigen, which is called an antigenic epitope. The antibody recognizes the antigen-binding epitope at the antigen-binding site, which can be linear or conformational. Approximately 90% of B-cells epitopes are conformational, and only a small percentage of native antigens contain linear B-cell epitopes (Sanchez-Trincado et al., 2017). The antigen-binding sites were formed by folding the heavy and light chain variable domains, and the hypervariable domain will determine its complementary to the antigen.

The Binding Affinity of Purified Poly-IgGs

The affinity of the antibody, K_d is referred to the strength of the antibody binding towards its antigen. The higher binding affinity of the antibody indicates the lower K_d value (Laguna et al., 2015). Most small-sized antigens or haptens, such as toxins, hormones, and alkaloids, possess a single epitope that binds to each antibody. Therefore, the strength of the binding is determined solely by the affinity of the antibody towards the antigenic epitope. The K_d value for polyclonal antibodies is an average of the total IgGs, is either weaker or stronger than the average. Figure 5 depicts the K_d value of purified poly-IgGs from the four rabbits after affinity purification.

Based on Figure 5, mean K_d of purified poly-IgGs antibody showed higher binding affinity from rabbits immunized with C22-MG-cBSA at $7.965 \times 10^{-6} \mu\text{M}$ and rabbits immunized with C9-MG-cBSA cBSA at of $1.390 \times 10^{-4} \mu\text{M}$. It indicates that purification of poly-IgG from the non-purified anti-sera significantly enhanced the binding affinity of

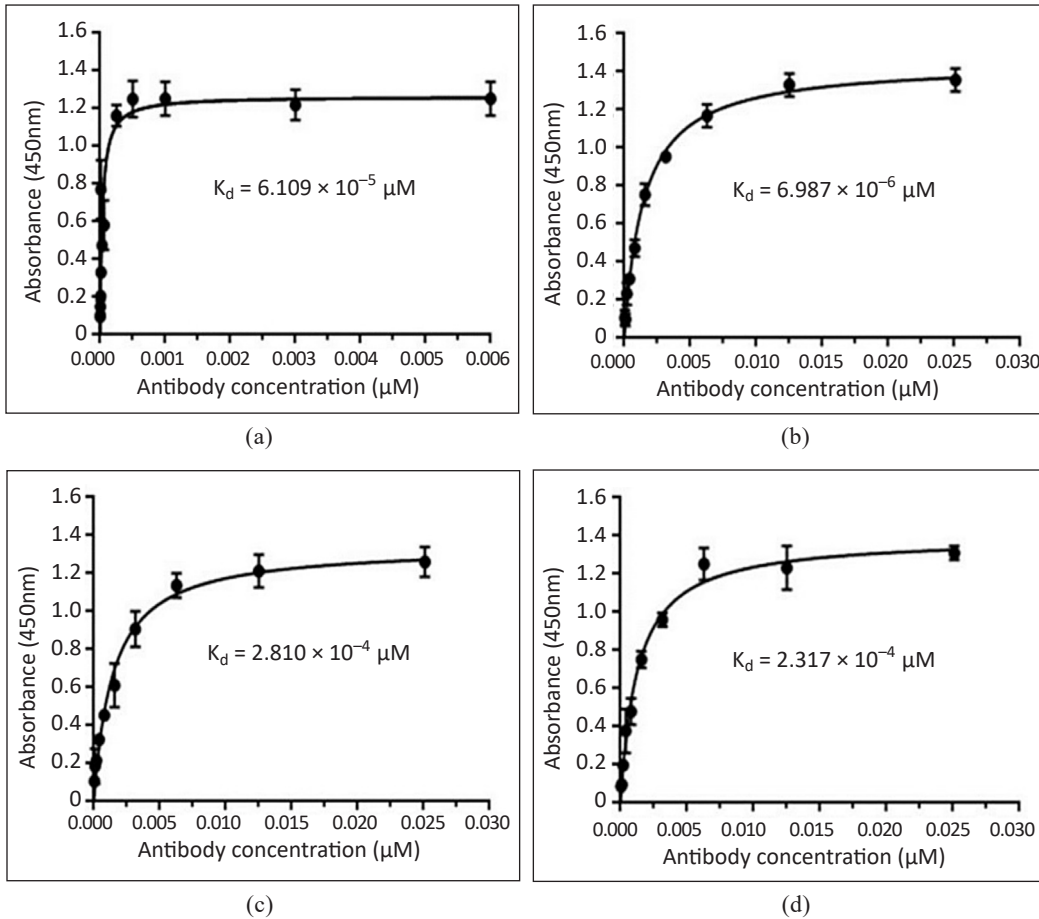


Figure 5. Binding affinity of purified poly-IgG for (a) rabbit 1 and (b) rabbit 2 immunized with C22-MG-cBSA and (c) rabbit 3 and (d) rabbit 4 immunized with C9-MG-cBSA.

the IgG towards the target antigen, i.e. mitragynine. The result obtained was in line with a previous study that reported that affinity purification of IgG from non-purified anti-sera enhanced the binding affinity of antibodies towards peptides (Mohsin et al., 2020).

In affinity purification of IgG, protein A and protein G, expressed in *Staphylococcus aureus* and *Streptococcus sp.*, respectively, are the most widely employed immunoglobulin-binding proteins (Fishman & Berg, 2019). It is due to the selectivity of the proteins towards IgG and the ability of the proteins to bind specifically to the F_c region of IgG (Choe et al., 2016). However, protein A has only two binding sites which can react to the antibodies. Furthermore, the interaction of protein A is not comparable to protein G for all the animal species. As a result, protein G's ability to bind and characteristics make it suitable for monoclonal and polyclonal antibody purification with lower affinity for protein A (Walls & Loughran, 2017).

Additionally, protein G has a high IgG binding specificity of many mammalian species (Choe et al., 2016). Therefore, it is a better choice due to its ability to bind to a broader range of IgG from eukaryotic species and IgG classes. Besides, specific binding of protein G at the F_c region of IgG in affinity chromatography exhibit minimal binding to albumin, resulting in high yield and high purified poly-IgG produced (Choe et al., 2016). The specificity binding of protein G to the F_c region of IgG makes them a good ligand for antibody purification.

Purification of IgG using affinity chromatography depends on the specific and reversible interaction between protein and its ligand, in this case, protein G and IgG. Protein G-affinity chromatography (coupled to agarose) using fast protein liquid chromatography (FPLC) is commonly used due to rapid and effective technique for the production of high purity antibodies (Fishman & Berg, 2019). The purification process allows only specific target antigen from a complex mixture to bind to the protein-G. The HiTrap protein G column efficiently removes albumin and other proteins from non-purified anti-sera, resulting in a higher binding affinity of the antibody. The eluted antibodies can be obtained in high purity using different salt concentrations, pH, and polarity (Arora et al., 2016).

CONCLUSION

Immunoglobulin (IgG) is applied in ELISA in several forms such as total IgG, serum, purified anti-sera, and specific IgG towards its antigen. Although polyclonal ELISA can be developed using non-purified anti-sera, this study had shown otherwise. The finding demonstrated that it is vital to purify antibodies to improve their affinity and prevent other protein that binds non-specifically to the low-signal plate of ELISA. A careful selection of IgG purification methods is also needed to avoid choosing non-representative populations of recovered IgGs. Since mitragynine IgG is not commercially available, the final product of purified anti-mitragynine IgG is an ideal and high-value biorecognition molecule in developing immuno-based detection methods such as ELISA. High-affinity anti-mitragynine IgG can also be a value-added molecule applied in portable sensor devices, which is yet to be reported. It will greatly benefit regulatory and enforcement agencies to monitor the misuse of kratom. Hence timely decisions can be made by the appropriate bodies.

ACKNOWLEDGMENTS

This work was financially supported by the Fundamental Research Grant Scheme (FRGS/2/2014/SG01/UPM/02/4) and MyBrain scholarship from the Ministry of Higher Education, Malaysia.

REFERENCES

- Arora, S., Saxena, V., & Ayyar B. V. (2016). Affinity chromatography: A versatile technique for antibody purification. *Methods*, *116*, 84-94. <https://doi.org/10.1016/j.ymeth.2016.12.010>
- Barker, C. M., & Reisen, W. K. (2019). Epidemiology of vector-borne diseases. In G. R. Mullen & L. A. Durden (Eds.), *Medical and veterinary entomology* (pp. 33-49). Academic Press. <https://doi.org/10.1016/B978-0-12-814043-7.00004-2>
- Choe, W., Durgannavar, T. A., & Chung, S. J. (2016). Fc-binding ligands of immunoglobulin G: An overview of high affinity proteins and peptides. *Materials*, *9*(12), Article 994. <https://doi.org/10.3390/ma9120994>
- Delahaut, P. (2017). Immunization - Choice of host, adjuvants and boosting schedules with emphasis on polyclonal antibody production. *Methods*, *116*, 4-11. <https://doi.org/10.1016/j.ymeth.2017.01.002>
- Esteve-Turrillas, F. A., Agulló, C., Mercader, J. V., Abad-Somovilla, A., & Abad-Fuentes, A. (2018). Rationally designed haptens for highly sensitive monoclonal antibody-based immunoanalysis of fenhexamid. *Analyst*, *143*(17), 4057-4066. <https://doi.org/10.1039/C8AN00827B>
- Fishman, J. B., & Berg, E. A. (2019). *Antibody purification and storage*. Cold Spring Harbor Laboratory Press. <https://doi.org/10.1101/pdb.top099101> Cold Spring Harb Protoc 2019
- Haddad, M., Soukkarieh, C., Khalaf, H. E., & Abbad, A. Q. (2016). Purification of polyclonal IgG specific for camelid's antibodies and their recombinant nanobodies. *Open Life Sciences*, *11*, 1-9. <https://doi.org/10.1515/biol-2016-0001>
- Kang, H. J., Choe, W., Min, J. K., Lee, Mi, Y., Kim, B. M., & Chung, S. J. (2016). Cyclic peptide ligand with high binding capacity for affinity purification of immunoglobulin G. *Journal of Chromatography A*, *1466*, 105-112. <https://doi.org/10.1016/j.chroma.2016.09.007>
- Laguna, M., Holgado, M., Hernandez, A. L., Santamaría, B., Lavín, A., Soria, J., Suarez, T., Bardina, C., Jara, M., Sanza, F. J., & Casquel, R. (2015). Antigen-antibody affinity for dry eye biomarkers by label free biosensing: Comparison with the ELISA technique. *Sensors*, *15*(8), 19819-19829. <https://doi.org/10.3390/s150819819>
- Limsuwanchote, S., Wungsintaweekul, J., Keawpradub, N., Putalun, W., Morimoto, S., & Tanaka, H. (2014). Development of indirect competitive ELISA for quantification of mitragynine in kratom (*Mitragyna speciosa* (Roxb.) Korth). *Forensic Science International*, *244*, 70-77. <https://doi.org/10.1016/j.forsciint.2014.08.011>
- Lopez, E., Scott, N. E., Wines, B. D., Hogarth, P. M., Wheatley, A. K., Kent, S. J., & Chung, A. W. (2019). Low pH exposure during immunoglobulin G purification methods results in aggregates that avidly bind Fcγ Receptors: Implications for measuring Fc dependent antibody functions. *Frontiers in Immunology*, *10*, Article 2415. <https://doi.org/10.3389/fimmu.2019.02415>
- Meireles, V., Rosado, T., Barroso, M., Soares, S., Gonçalves, J., Luís, Â, Caramelo D., Simao, A. Y., Fernandez, N., Duarte, A. P., & Gallardo E. (2019). *Mitragyna speciosa*: Clinical, toxicological aspects and analysis in biological and non-biological samples. *Medicine*, *6*(1), Article 35. <https://doi.org/10.3390/medicines6010035>

- Mohsin, A. Z., Sukor, R., Selamat, J., Hussin, A. S. M., Ismail, I. H., Jambari, N. N., & Mustafa-Kamal, F. (2020). Generation of high affinity anti-peptide polyclonal antibodies recognizing goat α_{s1} -casein. *Molecules*, 25(11), Article 2622. <https://doi.org/10.3390/molecules25112622>
- Mustafaoglu, N., Kiziltepe, T., & Bilgicer, B. (2016). Antibody purification via affinity membrane chromatography method utilizing nucleotide binding site targeting with a small molecule. *Analyst*, 141(24), 6571-6582. <https://doi.org/10.1039/C6AN02145J>
- Sadeghi, S., Aghebati-Maleki, L., Nozari, S., & Majidi, J. (2018). A methodological approach for production and purification of polyclonal antibody against dog IgG. *Veterinary Research Forum*, 9(1), 13-18.
- Sanchez-Trincado, J. L., Gomez-Perosanz, M., & Reche, P. A. (2017). Fundamentals and methods for T- and B-cell epitope prediction. *Journal Immunological Research*, 8, 1-14. <https://doi.org/10.1155/2017/2680160>
- Tiller, K. E., & Tessier, P. M. (2015). Advances in antibody design. *Annual Review of Biomedical Engineering*, 17, 191-216. <https://doi.org/10.1146/annurev-bioeng-071114-040733>
- Walls, D., & Loughran, S. T. (Eds.). (2017). *Protein chromatography: Methods and protocol*. Humana Press.
- Zhao, Y., Sun, X., Marquis, C. P., & Lee, N. A. (2019). Development of a sensitive sandwich ELISA specific to 2S albumin (Ana o 3) as a stable protein marker for cashew nut residue detection in pre-packaged food products. *Food Control*, 96, 432-440. <https://doi.org/10.1016/j.foodcont.2018.09.038>

Response of Rubber Tree Saplings to Dolomite and Kieserite Application and K:Mg Ratio

Chakkrit Poonpakdee, Khwunta Khawmee and Jumpen Onthong*

Agricultural Innovation and Management Division, Faculty of Natural Resources, Prince of Songkla University, Songkhla, 90110 Thailand

ABSTRACT

This study aimed to examine the effect of the application of dolomite and kieserite on the growth and nutrient uptake of rubber tree saplings and the relationship between K:Mg ratios in soils and nutrient uptake. The experiment followed a completely randomized design with five replicates. Budded stumps of RRIM 600 rubber were planted in soil with low extractable Mg ($< 0.30 \text{ cmol}_c \text{ kg}^{-1}$). Kieserite application at a rate of $0.5 \text{ cmol}_c \text{ Mg kg}^{-1}$ significantly promoted the greatest sapling height, stem diameter, Mg and S concentrations, and leaf chlorophyll levels. High kieserite application rates ($1.0 \text{ cmol}_c \text{ Mg kg}^{-1}$) were more likely to decrease K and N uptake significantly. Applying dolomite ($0.5 \text{ cmol}_c \text{ Mg kg}^{-1}$) also significantly increased rubber growth compared with the control treatment but the significant increases were lower than those for kieserite application. Applying K at 72, 108, and 180 mg kg^{-1} significantly increased leaf K concentration, but significantly decreased Mg concentrations. Therefore, rubber plantations should apply Mg at a rate of $0.5 \text{ cmol}_c \text{ Mg kg}^{-1}$ in the form of kieserite, and a ratio of K:Mg 2:1 is suitable for promoting rubber tree growth.

Keywords: Dolomite, K:Mg ratio, kieserite, plant nutrition, rubber tree sapling

ARTICLE INFO

Article history:

Received: 24 March 2021

Accepted: 05 July 2021

Published: 18 October 2021

DOI: <https://doi.org/10.47836/pjst.29.4.12>

E-mail addresses:

chakkrit.p@psu.ac.th (Chakkrit Poonpakdee)

khwunta.k@psu.ac.th (Khwunta Khawmee)

jumpen.o@psu.ac.th (Jumpen Onthong)

* Corresponding author

INTRODUCTION

Para rubber is an important economic crop in Thailand. Fertiliser is a key factor in the success of rubber tree plantations. In the past, mixed chemical fertilisers that contained nitrogen (N), phosphorus (P), potassium (K), and magnesium (Mg) were recommended in Thailand (Rubber Research Institute of Malaya, 1963). After 1978, Mg

was removed from the mixed chemical fertilisers used because the amount of Mg available in the soil was sufficient (Nualsri et al., 1982). Mixed chemical fertiliser 20-8-20 or 29-5-18 (N, P₂O₅, K₂O, respectively) was recommended for immature and mature rubber trees grown in traditional rubber cultivation areas (Rubber Research Institute of Thailand, 2019). In tropical soils that experience high weathering and soil leaching are low in basic cation (K⁺, Na⁺, Ca²⁺, and Mg²⁺) content (Brady & Weil, 2008). Therefore, intensive rubber cultivation up to the second or third plantation cycles without Mg application will lead to a low concentration of available Mg in the soil.

Magnesium (Mg) is crucial for plants. Approximately 75% of leaf Mg is involved in protein synthesis, and 15-20% of total Mg is associated with chlorophyll pigments, Mg act primarily as a cofactor of a series of enzymes responsible for photosynthetic carbon fixation and metabolism (Marschner, 1995). In plants, Mg²⁺ is a vital component of chlorophyll and is responsible for activating more than 300 enzymes (e.g., RNA polymerases, ATPases, protein kinases, phosphatases, glutathione synthase, and carboxylases). It also regulates ion transport and cation balance in plants (Bose et al., 2011). A ton of fresh latex rubber contains 5 kg of Mg (Kungpisdan, 2011). Therefore, continued rubber cultivation results in available soil Mg slowly decreasing through plant uptake for growing and production. The optimal available soil Mg is 0.30 cmol_c kg⁻¹, but most rubber trees growing in Thailand only have access to Mg amounts lower than this optimal soil Mg level (Kungpisdan et al., 2013). In soil with low Mg content, kieserite (MgSO₄·7H₂O) at the rate of 80 g tree⁻¹ year⁻¹ has been recommended for rubber plantations in Thailand (Rubber Research Institute of Thailand, 2019).

Potassium (K) is the macronutrient for the growth and latex production of a rubber tree. A ton of latex contained 25 kg of K (Kungpisdan, 2011). Excessive Mg application antagonises K uptake (Ding et al., 2006; Tandon, 1992). The application of a high dose of K fertiliser to soil also decreases the concentration of leaf Mg (Marschner, 1995). Conversely, excess Mg fertiliser application decreases leaf K concentrations (Kungpisdan & Buranatum, 1998). In fruits and vegetables, the ratios of Mg to K have proven to be more accurate in indicating the quality response than Mg status by itself (Gerendás & Führs, 2013). There have been no reports relating to the effects of Mg on growth and the antagonism between K and Mg in rubber tree saplings. Therefore, the balance between K and Mg in the soil needs to be studied. Therefore, the objectives of this study included the following: 1) to investigate the effect of the form of Mg administered on the growth and nutrient translocation in the soil to rubber saplings, and 2) to evaluate the optimal ratio of soil K: Mg. The knowledge gained from this research can lead to an improved understanding of Mg and K fertiliser management in rubber growing soils.

MATERIALS AND METHODS

Soil Sampling

Khlong Thom soil series (Km: Fine-loamy, kaolinitic, isohyperthermic Typic Kandiodults) was collected at a depth of 0-30 cm from rubber plantation soil in Songkhla province, Thailand. The soil samples were air-dried, passed through a 10-mesh sieve for physicochemical properties analysis, and then passed through a 3/4 mesh for pot experiments.

Effect of Dolomite and Kieserite Application on Growth of Rubber Tree Saplings

Budded stumps of the RRIM 600 rubber tree were planted in 30 L plastic pots filled with 28 kg of air-dried soil. The experiment used a completely randomized design (CRD) with five replicates containing five treatments each 1) without Mg application as the control treatment; 2-3) Mg application at the rates of 0.5 and 1.0 cmol_c kg⁻¹ in the form of dolomite (CaMg(CO₃)₂), and 4-5) Mg application at the rates of 0.5 and 1.0 cmol_c kg⁻¹ in the form of kieserite (MgSO₄·H₂O). The sources of N (100 mg N kg⁻¹) P (40 mg P₂O₅ kg⁻¹) and K (100 mg K₂O kg⁻¹) were added in the form of urea (46-0-0), triple superphosphate (0-46-0), and potassium chloride (0-0-60) as top dressings in all treatments for optimal nutrition levels. Distilled water was used for watering until harvesting (6 months).

Effect of K:Mg Ratio on Growth of Rubber Tree Saplings

Five treatments at different K:Mg ratios were applied (Table 1). Extractable K and Mg levels in the Khlong Thom soil series were 10.2 and 16.0 mg kg⁻¹, respectively. The K:Mg ratios (4.5:1, 2:1, and 3:1) were adjusted using KCl and kieserite to K₇₂:Mg₁₆, K₇₂:Mg₃₆, K₁₀₈:Mg₃₆, K₁₈₀:Mg₃₆, and K₁₈₀:Mg₆₀.

Table 1
Initial extractable K and Mg in soil and K:Mg ratio

Treatment	Ratio K:Mg	Initial concentration (mg kg ⁻¹)		Fertiliser application (g 28 kg ⁻¹ soil)	
		K*	Mg*	KCl	Kieserite
K ₇₂ : Mg ₁₆	4.5:1	10.2	16.0	3.5	0.0
K ₇₂ : Mg ₃₆	2:1	10.2	16.0	3.5	3.6
K ₁₀₈ : Mg ₃₆	3:1	10.2	16.0	5.5	3.6
K ₁₈₀ : Mg ₃₆	5:1	10.2	16.0	9.5	3.6
K ₁₈₀ : Mg ₆₀	3:1	10.2	16.0	9.5	7.8

Note: * Initial extractable K and Mg concentrations in the soil before fertiliser application based on treatment.

Growth Rate

Sapling height and stem diameter at 10 cm above the bud union were recorded. The number of leaves, whorls and petioles were also recorded along with the rubber tree symptoms after dolomite and kieserite application. The differences in sapling height and stem diameter between the beginning and end of cultivation (6 months) were considered to compare the effect of dolomite and kieserite on the growth of the rubber tree saplings.

Soil and Plant Analysis

Soil samples passed through a 10 mesh sieve (particles < 2 mm) were used to analyse the soil pH (soil: water = 1:5 w/v), organic matter (Walkley and Black method), total N (Kjeldahl method), available phosphorus (Bray II) and extractable K, Ca, and Mg (1M NH₄OAc pH 7.0). In addition, plant sections consisting of the leaf, petiole, stem, primary root, and lateral root were separated. The plant samples were oven-dried at 80°C for 72 h. Each plant section was weighed, ground, and passed through a 20 mesh sieve then digested with H₂SO₄ to calculate the total N (Kjeldahl method), and for mixed acid (HNO₃:HClO₄ = 3:1 v/v) for P, K, Ca, Mg, and S analysis (Jones Jr, 2001).

Statistical Analysis

The growth rates, nutrients in the soil, and the rubber tree saplings are presented herein as mean values of five replications with their standard deviations. The plant dried weights and nutrient concentrations were used to calculate the efficiency of plant nutrition uptake in the rubber tree saplings. Analysis of Variance (ANOVA) was used to test the difference among treatments. Means were separated using the Test of Mean Comparison, which is Duncan's Multiple Range Test (DMRT) at $P \leq 0.05$.

RESULTS

Soil Chemical Properties

After Mg application, the soil chemical properties revealed that the soil Mg concentrations significantly increased according to the Mg application rates (Table 2). However, Mg application rates of 0.5 and 1.0 cmol_c kg⁻¹ in the kieserite formula significantly increased the soil available Mg concentrations from 0.12 cmol_c kg⁻¹ (control) to 0.68 and 1.19 cmol_c kg⁻¹, respectively. While dolomite application significantly increased the Mg levels to 0.27 and 0.36 cmol_c kg⁻¹, respectively. Moreover, dolomite application at both 0.5 and 1.0 cmol_c kg⁻¹ increased the soils' available Mg level and enhanced their pH value from 4.6 to 5.1 and 5.6, respectively. The extractable Ca from 0.32 cmol_c kg⁻¹ to 0.49 and 0.60 cmol_c kg⁻¹, respectively.

Table 2
Soil chemical properties after dolomite and kieserite application

Treatment	pH (1:5)	EC (dS m ⁻¹)	Total N (g kg ⁻¹)	Avail. P (mg kg ⁻¹)	Extr. K [-----]	Extr. Mg cmol _c kg ⁻¹ -----]	Extr. Ca
Mg 0 cmol _c kg ⁻¹ (control)	4.6±0.8 c	0.11±0.01 c	0.33±0.05	10.80±1.30	0.23±0.06	0.12±0.01 d	0.32±0.02 c
Mg 0.5 cmol _c kg ⁻¹ (dolomite)	5.1±0.1 b	0.12±0.01 c	0.33±0.08	10.36±1.62	0.25±0.08	0.27±0.02 cd	0.49±0.03 b
Mg 1.0 cmol _c kg ⁻¹ (dolomite)	5.6±0.2 a	0.12±0.01 c	0.36±0.06	9.27±1.51	0.25±0.04	0.36±0.01 c	0.60±0.03 a
Mg 0.5 cmol _c kg ⁻¹ (kieserite)	4.6±0.1 c	0.19±0.01 b	0.34±0.04	10.87±2.43	0.26±0.06	0.68±0.20 b	0.35±0.03 c
Mg 1.0 cmol _c kg ⁻¹ (kieserite)	4.5±0.1 c	0.26±0.01 a	0.37±0.06	10.03±1.82	0.26±0.04	1.19±0.19 a	0.34±0.02 c
F-test	*	*	NS	NS	NS	*	*
C.V. (%)	2.75	19.66	9.19	13.88	21.91	23.4	7.56

Note: * Significantly different ($P \leq 0.05$); NS = not significantly different ($P > 0.05$). Different letters in each column indicate significant difference by DMRT at $P \leq 0.05$

Effect of Dolomite and Kieserite on Growth of Rubber Tree Saplings

Dolomite and kieserite applications significantly promoted the growth of rubber tree saplings (Table 3). The height and diameter of the saplings tended to increase compared with the control, and the numbers of leaves, petioles, and whorls significantly increased following the application of both dolomite and kieserite. The number of leaves on the rubber tree saplings significantly increased by 9-20 leaves, the number of petioles by 9-19.5, and the number of whorls by 0.8-1 compared to the control treatment. However, the application of 1.0 cmol_c Mg kg⁻¹ of dolomite led to the yellowing of leaf structures between veins. While the veins remain green. These abnormal symptoms were similar to those typical of Mg deficiency but simultaneously occurred in the upper and lower leaves. Yellowing was apparent in the leaves, petioles, and stems. Later, those rubber tree saplings shed their leaves and died (Figure 1c).

Kieserite application significantly promoted the growth of the rubber tree saplings in terms of their shoots and roots (Figures 1a & 1b) more than the application of dolomite (Table 3). After 6 months, the height and stem diameter of the saplings treated with kieserite at an application rate of 0.5 cmol_c Mg kg⁻¹ displayed the highest values (51.01 cm and 3.69 mm, respectively). A kieserite application rate of 1.0 cmol_c Mg kg⁻¹ resulted in 30.33 cm and 2.07 mm, and the control treatment resulted in values of 26.72 cm and 1.31 mm, for height and stem diameter, respectively. Moreover, a similar effect was recorded for the numbers of leaves, whorls, and petioles.

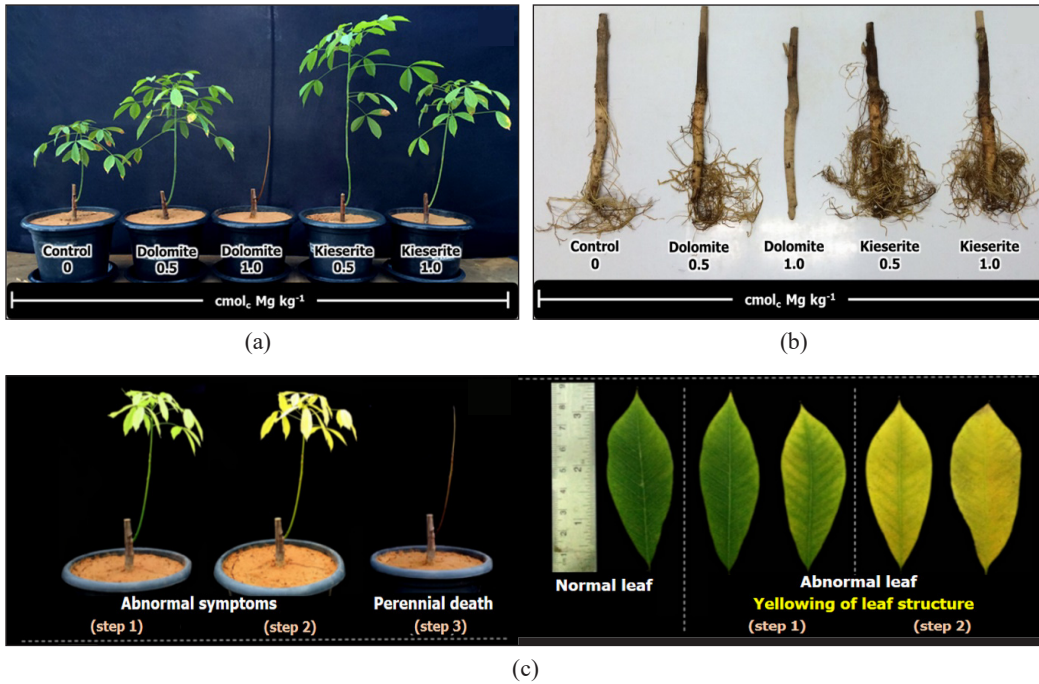


Figure 1. Effect of dolomite and kieserite application on shoots (a) and roots (b) of rubber tree saplings and abnormal symptoms of rubber tree sapling (c) after dolomite application ($1.0 \text{ cmol}_c \text{ kg}^{-1}$)

Table 3
Effect of dolomite and kieserite on growth of rubber tree sapling

Treatment	Height (cm)	Diameter (mm)	Number of		
			Leaf	Petiole	Whorl
Mg $0 \text{ cmol}_c \text{ kg}^{-1}$ (control)	26.72±3.25 b	1.31±0.55 b	13.50±2.58 b	25.50±2.54 b	1.00±0.20 b
Mg $0.5 \text{ cmol}_c \text{ kg}^{-1}$ (dolomite)	28.13±2.58 b	1.85±0.68 b	22.50±4.77 ab	34.50±3.31 ab	1.80±0.40 a
Mg $1.0 \text{ cmol}_c \text{ kg}^{-1}$ (dolomite)	ND	ND	ND	ND	ND
Mg $0.5 \text{ cmol}_c \text{ kg}^{-1}$ (kieserite)	51.01±4.26 a	3.69±0.87 a	33.00±9.53 a	45.00±4.66 a	2.00±0.60 a
Mg $1.0 \text{ cmol}_c \text{ kg}^{-1}$ (kieserite)	30.33±3.32 b	2.07±0.55 b	23.25±5.11 ab	35.25±8.54 ab	2.00±0.40 a
F-test	*	*	*	*	*
C.V. (%)	32.71	38.13	34.76	31.54	16.60

Note: * Significantly different ($P \leq 0.05$). Different letters in each column indicate a significant difference at $P \leq 0.05$ by DMRT. ND = No data because the rubber tree died. Each parameter value was calculated by considering the difference in values between the cultivation's beginning and end (6 months)

Dolomite application ($0.5 \text{ cmol}_c \text{ Mg kg}^{-1}$) significantly increased the biomass (Table 4). The primary roots and petioles significantly increased to 28.29 and 1.67 g tree^{-1} , respectively. Whereas for the control treatment, it was 17.31 and 0.66 g tree^{-1} , respectively (Table 4). Kieserite application at both 0.5 and $1.0 \text{ cmol}_c \text{ Mg kg}^{-1}$ significantly increased the dry weight of the above-ground biomass and the root sections (Table 4). Kieserite application at a rate of $0.5 \text{ cmol}_c \text{ Mg kg}^{-1}$ significantly increased the primary roots, leaves, stems, lateral roots, and petioles to 51.22 , 10.09 , 12.48 , 7.76 , and 1.57 g tree^{-1} , respectively.

Comparing dolomite and kieserite ($0.5 \text{ cmol}_c \text{ Mg kg}^{-1}$) revealed that kieserite application caused a significant increase in root and above-ground biomass to 58.97 and $24.14 \text{ g tree}^{-1}$, respectively. In contrast, dolomite application resulted in 30.96 and $11.87 \text{ g tree}^{-1}$ (Table 4).

Effect of Dolomite and Kieserite on Plant Nutrition Uptake and Total Chlorophyll Content

Dolomite application at the rate of $0.5 \text{ cmol}_c \text{ Mg kg}^{-1}$ significantly increased leaf Mg concentration from 1.48 g kg^{-1} (control) to 3.85 g kg^{-1} . Leaf Ca concentration increased to 8.29 g kg^{-1} . Whereas for the control treatment, it was 5.18 g kg^{-1} (Table 5). Kieserite application rates of 0.5 and $1.0 \text{ cmol}_c \text{ Mg kg}^{-1}$ significantly enhanced leaf Mg concentration to 4.09 and 4.50 g kg^{-1} , respectively. Whereas leaf Mg concentration in the control treatment was 1.48 g kg^{-1} . Moreover, kieserite application significantly increased leaf S from 0.67 g kg^{-1} (control) to 1.18 and 1.67 g kg^{-1} for kieserite application rates of 0.5 and $1.0 \text{ cmol}_c \text{ Mg kg}^{-1}$, respectively. However, kieserite applications of 0.5 and $1.0 \text{ cmol}_c \text{ Mg kg}^{-1}$ significantly decreased K uptake from 20.01 g kg^{-1} to 15.79 and 12.58 g kg^{-1} , respectively. Total leaf Mg (4.09 g kg^{-1}) and leaf S (1.18 g kg^{-1}) for saplings that received $0.5 \text{ cmol}_c \text{ kg}^{-1}$ application of kieserite were higher than that for saplings to which dolomite was applied (Mg 3.85 and S 0.75 g kg^{-1} , respectively). However, kieserite application significantly decreased leaf K content (15.79 g kg^{-1}) compared with dolomite application (20.07 g kg^{-1}) and the control treatment (20.01 g kg^{-1}). The chlorophyll concentrations in the saplings which received kieserite applications at the rates of 0.5 and $1.0 \text{ cmol}_c \text{ Mg kg}^{-1}$ were 2.80 and 2.88 mg dm^{-2} , respectively, and were higher than those to which dolomite was applied at the rate of $0.5 \text{ cmol}_c \text{ kg}^{-1}$ (2.08 mg dm^{-2}) and the control treatment (1.79 mg dm^{-2}).

Ratio of K:Mg on Plant Growth Rate and Nutrient Concentration in Leaves

The 2:1 ratio of K:Mg provided the greatest height and stem diameter not significantly increased between the beginning and end of cultivation (6 months) of the rubber tree saplings (Table 6). Increasing K application rates tended to significantly increase leaf K concentrations (Table 6). However, increasing the soil K application rates caused the Mg leaf concentrations to significantly decrease. Thus, the lowest leaf Mg concentration (1.26

Table 4
Effect of dolomite and kieserite on the dry weight of rubber tree sapling

Treatment	Dry weight (g tree ⁻¹)							
	Leaf	Petiole	Stem	Primary root	Lateral root	Shoot	Root	Whole plant
Mg 0 cmol _c kg ⁻¹ (control)	5.12±1.82 b	0.66±0.22 b	4.28±1.37 b	17.31±2.75 c	2.57±0.13 b	10.06±2.64 b	19.88±2.67 c	29.45±8.82 d
Mg 0.5 cmol _c kg ⁻¹ (dolomite)	5.89±2.15 b	1.67±0.66 a	4.32±1.53 b	28.29±4.19 b	2.68±0.50 b	11.87±3.00 b	30.96±4.64 b	42.84±7.53 c
Mg 1.0 cmol _c kg ⁻¹ (dolomite)	ND	ND	ND	ND	ND	ND	ND	ND
Mg 0.5 cmol _c kg ⁻¹ (kieserite)	10.09±2.36 a	1.57±0.90 a	12.48±2.86 a	51.22±3.54 a	7.76±2.83 a	24.14±5.50 a	58.97±1.80 a	83.11±8.59 a
Mg 1.0 cmol _c kg ⁻¹ (kieserite)	6.71±1.51 b	1.39±0.82 a	12.51±0.74 a	33.03±2.65 b	3.57±0.77 b	20.61±2.37 a	36.60±3.35 b	57.21±2.11 b
F-test	*	*	*	*	*	*	*	*
C.V. (%)	31.95	29.70	23.93	11.51	20.07	21.58	8.95	9.96

Note: * Significantly different (P ≤ 0.05). Different letters in each column indicate a significant difference at P ≤ 0.05 by DMRT; ND = No data because the rubber tree died

Table 5
Effect of dolomite and kieserite on leaf nutrient concentration and total chlorophyll content

Treatment	Leaf nutrient concentration								Total chlorophyll content (mg dm ⁻²)
	N	P	K	Mg	Ca	S	[----- g kg ⁻¹ -----]		
Mg 0 cmol _c kg ⁻¹ (control)	40.66±3.53 a	1.25±0.74	20.01±2.56 a	1.48±0.35 b	5.18±0.89	0.67±0.22 c	1.79±0.04 b		
Mg 0.5 cmol _c kg ⁻¹ (dolomite)	39.46±2.74 a	1.32±0.66	20.07±3.55 a	3.85±0.74 a	8.29±0.77	0.75±0.11 c	2.08±0.53 b		
Mg 1.0 cmol _c kg ⁻¹ (dolomite)	ND	ND	ND	ND	ND	ND	ND		
Mg 0.5 cmol _c kg ⁻¹ (kieserite)	40.93±3.11 a	1.42±0.25	15.79±2.66 b	4.09±0.84 a	4.85±0.62	1.18±0.32 b	2.80±0.21 a		
Mg 1.0 cmol _c kg ⁻¹ (kieserite)	33.71±1.85 b	1.30±0.51	12.58±3.41 c	4.50±0.77 a	5.19±0.58	1.67±0.57 a	2.88±0.37 a		
F-test	*	NS	*	*	NS	*	*		
C.V. (%)	24.23	11.08	13.33	19.96	34.32	23.53	16.05		

Note: * Significantly different (P ≤ 0.05); NS = not significantly different (P > 0.05). Different letters in each column indicate significant difference by DMRT at P ≤ 0.05; ND = No data because the rubber tree died

Table 6
Effect of K:Mg ratio on growth rate and leaves nutrient concentration

Treatment	Ratio	Height ^a (cm)	Stem diameter ^a (mm)	N	P	K (g kg ⁻¹)	Mg	Ca
K ₇₂ :Mg ₁₆	4.5:1	44.13 ± 3.53	5.55 ± 1.70	40.51 ± 4.31	0.48 ± 0.05	19.74 ± 1.60 b	3.67 ± 1.09 a	6.06 ± 0.82
K ₇₂ :Mg ₃₆	2:1	49.56 ± 3.11	6.29 ± 2.20	36.16 ± 4.61	0.45 ± 0.20	21.41 ± 2.73 b	3.38 ± 1.22 a	6.48 ± 1.61
K ₁₀₈ :Mg ₃₆	3:1	44.00 ± 5.22	6.17 ± 3.21	36.97 ± 5.73	0.54 ± 0.19	29.27 ± 2.63 a	3.20 ± 1.21 a	7.68 ± 0.58
K ₁₈₀ :Mg ₃₆	5:1	38.80 ± 4.87	5.60 ± 2.77	41.41 ± 3.52	0.47 ± 0.11	27.82 ± 3.53 a	1.26 ± 0.19 b	7.61 ± 0.60
K ₁₈₀ :Mg ₆₀	3:1	ND	ND	ND	ND	ND	ND	ND
F-test		NS	NS	NS	NS	*	*	NS
C.V. (%)		12.28	5.97	11.19	35.34	11.06	35.53	14.32

Note: * Significantly different (P ≤ 0.05); NS = not significantly different (P > 0.05). Different letters in each column indicate significant difference by DMRT at P ≤ 0.05; ND = No data because the rubber tree died

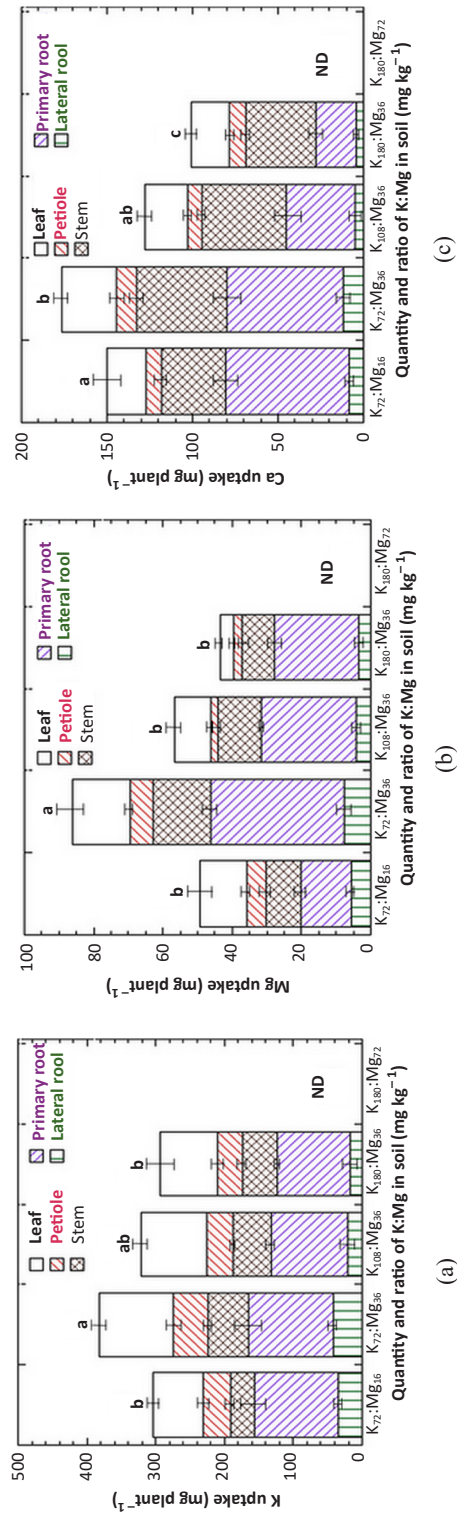


Figure 2. Effect of quantity and ratio of soil K: Mg (mg kg⁻¹) on K (a), Mg (b), and Ca uptake (c)
Note. ND = no data because the rubber tree died

mg kg⁻¹) resulted from a K application rate of 180 mg kg⁻¹, with Mg applied at a level at 36 mg kg⁻¹ (ratio 5:1).

The primary roots had the highest K concentration, followed (in decreasing order) by leaves, stems, petioles, and lateral roots. The highest K uptake (333.53 mg tree⁻¹) occurred with the K application rate of 72 mg kg⁻¹ with 36 mg kg⁻¹ Mg (ratio 2:1). In contrast, the lowest K uptake (279.08 mg tree⁻¹) was recorded for the K application rate of 72 mg kg⁻¹ with 16 mg kg⁻¹ Mg (ratio 2:1) (Figure 2a). Plant K was lowest (43.27 mg tree⁻¹) based on a K application rate of 180 mg kg⁻¹ with 36 mg kg⁻¹ Mg (ratio 5:1). Mg uptake was highest (78.51 mg tree⁻¹) for the Mg application rate of 36 mg kg⁻¹ with 72 mg kg⁻¹ K (ratio 2:1). On the other hand, Mg uptake significantly decreased with an increasing K application rate (Figure 2b). The highest Mg content was found in the primary roots, followed (in descending order) by stems, leaves, petioles, and lateral roots (Figure 2b).

Ca uptake was highest in the primary roots, followed by (in descending order) stems, leaves, petioles, and lateral roots. Thus, the K application rate of 72 mg kg⁻¹ with 36 mg kg⁻¹ Mg (ratio 2:1) promoted the highest plant Ca content (166.14 mg tree⁻¹). Nevertheless, increasing the K application rate from 72 mg kg⁻¹ to 108 and 180 mg kg⁻¹ with Mg applied at 36 mg kg⁻¹ (ratios of 3:1 and 5:1, respectively) caused sapling Ca to significantly decreased to 125.24 and 97.62 mg tree⁻¹, respectively (Figure 2c).

DISCUSSION

Soil Chemical Properties

Applying both dolomite and kieserite significantly increased the extractable Mg in the soil (Table 2). For the same rate of dolomite and kieserite application, the available soil Mg levels were higher in those to which kieserite was applied compared to those receiving dolomite. The solubility of kieserite in water is higher than that of dolomite. Therefore, the Mg content in the kieserite was liberated more rapidly than that of the dolomite. Moreover, the Mg content was gradually released, leading to improved plant growth in the saplings to which kieserite was applied (Figures 1a & 1b). Dolomite application significantly enhanced the level of available Mg in the soil and significantly increased the soil pH value and Ca concentration in soil (Table 2).

Growth of Rubber Tree Saplings and their Mg Concentration

The application of kieserite promoted the growth of the rubber tree saplings in terms of their height, stem diameter, number of leaves, whorls and petioles, and the dry weight of both their shoot and root sections (Tables 3 & 4) compared to those grown with dolomite application. In addition, the application of Mg in the soil significantly increased the leaves Mg (Table 5). The result is similar to the results for Mg application to para rubber

(Bueraheng et al., 2018), citrus (Xiao et al., 2014; Zheng et al., 2015), and rice (Ding et al., 2006). Mg is an element that is highly mobile in plants, particularly in green sections, such as leaves. Therefore, the application of Mg led to a significant increase in total chlorophyll in leaves (Table 5). This result was similar to those previously reported for Mg application in citrus (Xiao et al., 2014), rice (Moreira et al., 2015; Yuchuan et al., 2008), strawberry plants (Choi & Latigui, 2008), pepper (Anza et al., 2005) and maize (Jezek et al., 2015). Mg levels in leaves ranging between 0.25% and 1.0% are considered sufficient for plants (Yash, 1998). Kieserite contains an S content of 27%. In soils with a coarse texture and a low organic matter content, S deficiency is common (Brady & Weil, 2008). Therefore, kieserite application at rates of 0.5 and 1.0 cmol_c Mg kg⁻¹ significantly increased the S content in leaves (Table 5). Although the optimal S level for rubber has not been reported, the optimal leaf S was reported to be within a range of 2.5-10.0 g kg⁻¹ for general plants (Yash, 1998).

Applying kieserite at a rate of 0.5 cmol_c Mg kg⁻¹ significantly decreased the K concentrations in leaves (Table 5). However, excess dolomite application (1.0 cmol_c Mg kg⁻¹) caused the death of the rubber saplings (Figure 1a). The optimal soil available Mg for rubber plantations has been reported as being 0.08-0.21 cmol_c Mg kg⁻¹ (Krishnakumar & Potty, 1992). Therefore, rubber tree saplings receiving dolomite at the rate of 1.0 cmol_c Mg kg⁻¹ may have Mg toxicity on plant growth because of excess soil Mg. Moreover, excess Mg application inhibits translocation of other nutrients from roots to shoots (Marschner, 1995). These results are in line with previous studies, which have found that excess lime application led to negative effects on plant growth, particularly on maize and barley (Kovacevic et al., 2006), the growth of which tended to decrease after an increase in lime application rates.

In Mg deficient rice, leaves displayed decreased chlorophyll concentrations, photosynthetic activity, and soluble protein. However, leaf concentrations of soluble sugars and malondialdehyde (MDA) and the activities of superoxide dismutase, catalase, and peroxidase increased (Yuchuan et al., 2008). Moreover, it has been reported that Mg inhibition of root elongation has implications for hydroponic procedures when screening for Al tolerant soybean germplasm (Silva et al., 2001). In this study, excess dolomite application at a rate of 1.0 cmol_c Mg kg⁻¹ to the soil-grown rubber saplings led to their death after only 2 months. In the initial stage, light yellow colouration developed along the marginal veins of both the upper and lower leaves, similar to the symptoms of Mg deficiency. Subsequently, the leaves, petioles, and stems displayed yellow colouration and the saplings developed lateral root rot. In the final stage, the saplings shed their leaves, and death occurred (Figure 1c).

Effect of K:Mg Ratio on Growth and Nutrient Concentration in Leaves of Rubber Tree Saplings

Most soils in Thailand are acidic, with low K, Na, Ca, and Mg base saturation. Ion exchange equilibria, desorption and adsorption in acid soils are crucial to understanding crop production leaching and nutrient management dynamics. The antagonistic effect between soil Mg-K and Ca-K interaction can be explained by the differences in their ionic mobility and ion competition for plant uptake (Tandon, 1992). Therefore, excessive application of Mg to soil often reduces K translocation by plants (Tandon, 1992). In this research, K application rates ranging from 72 mg kg⁻¹ to 108 and 180 mg kg⁻¹ significantly enhanced K leaf concentrations (Table 6). Similar results have been reported in other studies with high rates of K fertiliser application in the soil also significantly increasing K concentrations in para rubber leaves (Kungpisdan & Buranatum, 1998). On the other hand, a high rate of K application to the soil significantly decreased the leaf Mg concentration (Table 6). This result was similar to those achieved with pummelo (Nguyen et al., 2016), cabbage, celery and lettuce (Inthichack et al., 2012), orchids (Poole & Seeley, 1978), and crested wheatgrass (Robbins & Mayland, 1993). Therefore, a high rate of K fertiliser application may cause an Mg deficiency in plants.

In Thailand, leaf Mg:K ratios in rubber grown in lowlands and uplands were 3.81:1 and 3.25:1, respectively. Whereas in the soils, they were 2.87:1 and 6.99:1 (Robbins & Mayland, 1993). While, the optimal K:Mg ratio in rice leaves has been found to range between 22 and 25 (Ding et al., 2006). Moreover, the exchangeable Ca:Mg ratio should be 6:1 in maize growing soils (Osemwota et al., 2007) and at a ratio of 1:2-1:1 for celery (Li et al., 2013). Further, the ratios of K:Mg-based on soil type were suggested as 1.2:1 in sandy soils, 1:1 in sandy loam and loamy soils, 0.7:1 in clay soils, and 2.2:1 in peat soils (Loide, 2004), which accords with the findings in the present study that a ratio of K:Mg of 2:1 in sandy loam was suitable for promoting nutrient uptake in rubber trees (Figure 2).

Further, K caused negative interaction between Mg and Ca. Therefore, a high soil K concentration affects Mg translocation from soil to plant. The inhibition of Mg uptake from K fertilisation reduced leaf tissue concentrations of Mg and the development of bacterial spots in tomato plants (Engelhard & Woltz, 1989). Moreover, the Ca:Mg ratio in the culture solution for soybean plants which promotes the best growth, was found to be 3:10 (Hashimoto, 2012). Therefore, the quantity and ratio of K and Mg should be considered in fertilisation in rubber growing soils because K and Mg management is important in promoting growth and plant health.

CONCLUSION

Mg application in the form of kieserite and dolomite significantly promoted rubber tree growth. The results indicated that rubber trees grew better following the application

of kieserite than after the application of dolomite. Moreover, kieserite application was beneficial for chlorophyll and S content. The optimal Mg application rate was found to be 0.5 cmol_c Mg kg⁻¹ in the form of kieserite and at a ratio of K:Mg of 2:1, which was suitable for promoting rubber tree growth. However, further study of the S sensibility from kieserite application is required to increase knowledge regarding the management of rubber growing soils.

ACKNOWLEDGEMENTS

This research was supported by the Natural Rubber Innovation Research Institute, Prince of Songkla University (Grant No NAT600394S).

REFERENCES

- Anza, M., Riga, P., & Garbisu, C. (2005). Time course of antioxidant responses of *Capsicum annuum* subjected to a progressive magnesium deficiency. *Annals of Applied Biology*, *146*(1), 123-134. [https://doi: 10.1111/j.1744-7348.2005.04023.x](https://doi.org/10.1111/j.1744-7348.2005.04023.x)
- Bose, J., Babourina, O., & Rengel, Z. (2011). Role of magnesium in alleviation of aluminium toxicity in plants. *Journal of experimental botany*, *62*(7), 2251-2264. [https://doi:10.1093/jxb/erq456](https://doi.org/10.1093/jxb/erq456)
- Brady, N. C., & Weil, R. R. (2008). *The nature and properties of soils*. Prentice Hall.
- Bueraheng, H., Onthong, J., & Khawmee, K. (2018). Effect of magnesium on manganese uptake and growth of rubber trees. *Journal of Agricultural Research and Extension*, *35*(1), 12-22.
- Choi, J. M., & Latigui, A. (2008). Effect of various magnesium concentrations on the quantity of chlorophyll of 4 varieties of strawberry plants (*Fragaria ananassas* D.) cultivated in inert media. *Journal of Agronomy*, *7*(3), 244-250.
- Ding, Y., Luo, W., & Xu, G. (2006). Characterisation of magnesium nutrition and interaction of magnesium and potassium in rice. *Annals of Applied Biology*, *149*(2), 111-123. [https://doi:10.1111/j.1744-7348.2006.00080.x](https://doi.org/10.1111/j.1744-7348.2006.00080.x)
- Engelhard, A. W., & Woltz, S. S. (1989). Management of Fusarium wilt of vegetables and ornamentals by macro and microelements. In A. W. Engelhard (Ed.), *Soil Borne Plant Pathogens: Management of Diseases with Macro- and Microelement* (pp. 18-32). APS Press.
- Gerendás, J., & Führs, H. (2013). The significance of magnesium for crop quality. *Plant Soil*, *368*(1), 101-128. [https://doi:10.1007/s11104-012-1555-2](https://doi.org/10.1007/s11104-012-1555-2)
- Hashimoto, Y. (2012). Studies on the magnesium metabolism of crops (Part 1) the balance among magnesium, calcium and potassium in free and bound forms at the flowering stage of soy-bean plants. *Soil Science and Plant Nutrition*, *2*(1), 123-130.
- Inthichack, P., Nishimura, Y., & Fukumoto, Y. (2012). Effect of potassium sources and rates on plant growth, mineral absorption, and the incidence of tip burn in cabbage, celery, and lettuce. *Horticulture, Environment, and Biotechnology*, *53*(1), 135-142. [https://doi:10.1007/s13580-012-0126-z](https://doi.org/10.1007/s13580-012-0126-z)

- Jezeck, M., Geilfus, C. M., Bayer, A., & Muhling, K. H. (2015). Photosynthetic capacity, nutrient status, and growth of maize (*Zea mays* L.) upon MgSO₄ leaf-application. *Frontiers in Plant Science*, 5(1), 1-10. <https://doi.org/10.3389/fpls.2014.00781>
- Jones Jr, B. (2001). *Laboratory guide for conducting soil tests and plant analysis*. CRC Press.
- Kovacevic, V., Banaf, D., Kovacevic, J., Lalic, A., Jurkovic, Z., Krizmanic, M. (2006). Influences of liming on maize, sunflower and barley. *Cereal Research Communications* 34(1), 553-556. <https://doi.org/10.1556/CRC.34.2006.1.138>
- Krishnakumar, A. K., & Potty, S. N. (1992). Nutrition of Hevea. In M. R. Sethuraj & N. M. Mathew (Eds.), *Natural Rubber: Biology, and Technology* (pp. 239-262). Elsevier Science Publishers.
- Kungpisdan, N. (2011). *Fertilizer recommendation for para rubber tree*. Department of Agriculture Press.
- Kungpisdan, N., & Buranatum, W. (1998). *Study of optimal N, P, K, and Mg fertilization in mixed-cultivation of rubber plantation in Kho Hung soil series*. Department of Agriculture Press.
- Kungpisdan, N., Rattanachaoat, M., Pramkasin, P., Kilruk, T., Junaumpond, L., & Thongpu, A. (2013). *Development of plant nutrition management for rubber tree*. Department of Agriculture Press.
- Li, Y. Q., Qin, J., Mattson, N. S., & Ao, Y. S. (2013). Effect of potassium application on celery growth and cation uptake under different calcium and magnesium levels in substrate culture. *Scientia Horticulturae*, 158(1), 33-38.
- Loide, V. (2004). A bout the effect of the contents and ratios of soil's available calcium, potassium and magnesium in liming of acid soils. *Agronomy Research*, 2(1), 71-82.
- Marschner, H. (1995). *Mineral nutrition of higher plants*. Academic Press.
- Moreira, W. R., Bispo, W. M. D., Rios, J. A., Debona, D., Nascimento, C. W. A., Rodrigues, & F. A. (2015). Magnesium-induced alterations in the photosynthetic performance and resistance of rice plants infected with *Bipolaris oryzae*. *Scientia Agricola*, 72(4), 328-333. <https://doi.org/10.1590/0103-9016-2014-0312>
- Nguyen, H., Maneepong, S., & Suranilpong, P. (2016). Nutrient uptake and fruit quality of pummelo as influenced by ammonium, potassium, magnesium, zinc application. *Journal of Agricultural Science*, 8(1), 1-10.
- Nualsri, L., Suwanmonkol, P., Tainukul, V., & Panmanee, K. (1982). Fertilization recommendation in A.D. 1982. *Para Rubber Journal*, 3(1), 4-25.
- Osemwota, I. O., Omued, J. A. I., & Ogboghodo, A. I. (2007). Effect of calcium/magnesium ratio in soil on magnesium availability, yield, and yield components of maize. *Communications in Soil Science and Plant Analysis*, 38(19-20), 2849-2860. <https://doi.org/10.1080/00103620701663081>
- Poole, H. A., & Seeley, J. G. (1978). Nitrogen, potassium and magnesium nutrition of three orchid genera. *Journal of American Society for Horticulture Science*, 103(1), 1-7.
- Robbins, C. W., & Mayland, H. F. (1993). Calcium, magnesium, and potassium uptake by crested wheatgrass grown on calcareous soils. *Communications in Soil Science and Plant Analysis*, 24(9-10), 915-926.
- Rubber Research Institute of Malaya. (1963). Revised manuring programme for replantings. *Rubber Research Institute Bulletin*, 67, 79-85.

- Rubber Research Institute of Thailand. (2019). *Academic information of rubber in 2019*. Rubber Research Institute Department of Agriculture Press.
- Silva, I. R., Smyth, T. J., Israel, D. W., & Rufty, T. W. (2001). Altered aluminum inhibition of soybean root elongation in the presence of magnesium. *Plant and Soil*, 230(1), 223-230. <https://doi.org/10.1023/a:1010384516517>
- Tandon, H. L. S. (1992). *Management of nutrient interactions in Agriculture*. Fertiliser Development and Consultation Organization Press.
- Xiao, J. X., Hu, C. Y., Chen, Y. Y., Yang, B., & Hua, J. (2014). Effects of low magnesium and an arbuscular mycorrhizal fungus on the growth, magnesium distribution and photosynthesis of two citrus cultivars. *Scientia Horticulturae*, 177(1), 14-20. <https://doi.org/10.1016/j.scienta.2014.07.016>
- Yash, P. K. (1998). *Handbook of reference methods for plant analysis*. CRC Press.
- Yuchuan, D., Chunrong, D., Wen, C., Yanshou, L., Xiaoli, W., Ping, R., & Guohua, X. (2008). High potassium aggravates the oxidative stress induced by magnesium deficiency in rice leaves. *Pedosphere*, 18(3), 316-327.
- Zheng, C. S., Lan, X., Tan, Q. L., Zhang, Y., Gui, H. P., & Hu, C. X. (2015). Soil application of calcium and magnesium fertilizer influences the fruit pulp mastication characteristics of Nanfeng tangerine (*Citrus reticulata* Blanco cv. Kinokuni). *Scientia Horticulturae*, 191(1), 121-126. <https://doi.org/10.1016/j.scienta.2015.05.008>



The Effect of the Operation Time, Orientation of Passenger and Body Mass Index on Passengers' Whole-Body Vibration on Urban Rail

Muhammad Nur Annuar Mohd Yunos*, Mohd Azlis Sani Md Jalil, Nor Azali Azmir and Mifzal Nazhan Mazlan

Faculty of Mechanical and Manufacturing Engineering, Universiti Tun Hussein Onn Malaysia, 86400 Batu Pahat, Johor, Malaysia

ABSTRACT

Urban rail is a widely used public transportation; the vibration from frequent rides may impact passengers. The rail vehicle's vibrations can cause human fatigue and result in severe musculoskeletal problems to the passenger. This paper aims to identify the effects of passenger orientation, operation time and body mass index on passengers' whole-body vibration on an urban rail in Malaysia. Real-time monitoring of the whole-body vibration was conducted using 2³ full factorial designs of the experiment, which was analysed statistically using Minitab Software. The overall result of this study is that the passengers in a seated position had greater exposure to whole-body vibration, which is 0.3686 ms⁻² than standing passengers, 0.2965 ms⁻². Also, passengers tend to be exposed to greater vibration during an off-peak time of 0.4063 ms⁻², than a peak time of 0.3706 ms⁻². Lastly, overweight passengers were exposed to greater vibration, of 0.4063 ms⁻², than passengers within the ideal weight range of 0.4000 ms⁻². This study has statistically proven that all the factors were significantly influenced the vibration exposure to the passenger. The most significant factor towards the vibration exposure is the "Body Mass Index (BMI)", in which

the p-value is less than 0.001. This study concludes that the whole-body vibration of a passenger is affected by the orientation of the passenger, operation time and body mass index of passengers on urban rail service.

ARTICLE INFO

Article history:

Received: 26 March 2021

Accepted: 05 July 2021

Published: 08 October 2021

DOI: <https://doi.org/10.47836/pjst.29.4.13>

E-mail addresses:

muhdnurannuar@gmail.com (Muhammad Nur Annuar Mohd Yunos)

azlis@uthm.edu.my (Mohd Azlis Sani Md Jalil)

azali@uthm.edu.my (Nor Azali Azmir)

mifzalnazhan7@gmail.com (Mifzal Nazhan Mazlan)

* Corresponding author

Keywords: Human factors, public transportation, rail ergonomics, ride comfort, whole-body vibration

INTRODUCTION

In the era of globalisation, railway systems have become one of the most important public transportation; it is the main mode of transportation chosen by people, notably in highly developed countries (Ismail et al., 2010). Light Rail Transit (LRT) is the preferable mode of transport, especially in urban areas, as it is sustainable, improves travel options and facilitates swift mobility (Fateh et al., 2016). However, passenger comfort has become one of the essential factors in the competition with other modes of transportation (Dumitriu, 2013). Therefore, passenger comfort has become a priority among train operators. Based on previous researches, one of the major factors that affect passenger comfort level in trains is the vibration and vibration behaviour of the vehicle (Kim et al., 2009; Munawir et al., 2017). Not only vibration reduces the quality of the ride experience of the passenger, but it also affects the passenger's health (Zhou et al., 2016).

Passengers tend to experience health problems such as lower back pain with prolonged exposure to high-magnitude vibration caused by the trains (Nuawi et al., 2011). Vibration can also cause human fatigue and may result in severe musculoskeletal problems to the passenger (Mohajer et al., 2017). In trains, vibration is transmitted to the passengers through the floor, seats and backrests (Kumara et al., 2013).

Whole-body Vibration (WBV)

Whole-body vibration (WBV) is defined as the situation where the whole body experiences the effect of vibration when supported by a vibrating surface (Azlis-Sani et al., 2015). WBV can be transmitted to the whole body of the passenger through seats, backrests and the floor of the vehicle (Munawir et al., 2017). It can also be transmitted by standing and sitting in the vehicle (Smith et al., 2005). The effects of the whole-body vibration depended on the position of the passenger's body inside the train (Griffin & Erdreich, 1991). Therefore, WBV was considered an important factor in passenger comfort as it is largely produced in the railway vehicle (Kim et al., 2009).

In the last two decades, a few major problems were found to occur in the human body due to exposure to whole-body vibration. Whole-body vibration increased the risk of having lower back pain and spine structural injury (Gągorowski, 2010; Schwarze et al., 1998). Some researchers have found that lower back pain due to whole-body vibration depended on the passenger's body mass index (BMI) because the spine supports most bodyweight (Mortimer et al., 2001; Pradhan et al., 2017).

Therefore, whole-body vibration should be measured to determine the value of vibration exposed to the passenger/driver inside the train. The whole-body vibration can be measured at three supporting surfaces: the seatback, the seat pan and the feet (Pradhan et al., 2017). The measurement procedure of whole-body vibration can be referred to in the international standard ISO 2631-1:1997 (Park et al., 2013). This measurement procedure can calculate whole-body vibration experienced by the passenger and crew in the railway industry.

ISO 2631-1:1997 is a standard that focuses on mechanical vibration and mechanical shock. This standard provides the evaluation and analysis of the human exposure to whole-body vibration in relation to human health and comfort, the probability of vibration perception and the incidence of motion sickness (ISO, 1997). According to this standard, the frequency range, which is transmitted to the seated body as whole-body vibration is between 0.5 Hz to 80 Hz (ISO, 1997). Figure 1 shows the biocentric axes of the human body in seated and standing positions.

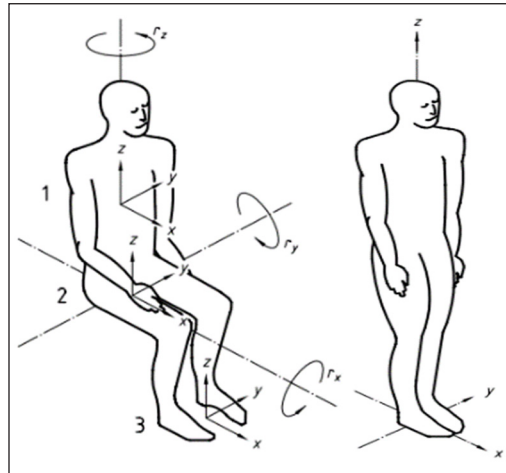


Figure 1. The biocentric axes of the human body in seated and standing positions (ISO, 1997)

Therefore, the objective of this study is to study the effect of passenger orientation, operation time and BMI of passengers towards the whole body vibration in urban rail services.

MATERIALS AND METHODS

Real-time Monitoring

Real-time monitoring is a process of data collection from the actual real operation of the services. This study underwent real-time monitoring of the whole-body vibration in Kuala Lumpur urban rail. This line consists of 37 stations along the 45.1 km track with a driverless automatic system.

Instruments

This study used a triaxial accelerometer with a seat pad, and the Human Vibration Meter (HVM 100). Before the measurement was taken, the triaxial accelerometer was calibrated by using an Accelerometer Calibrator Kristler 8921. There are three (3) sets of triaxial accelerometers connected with three (3) individual HVM. The first triaxial accelerometer was attached to the seat where the subject sat. Meanwhile, the other one was attached to the floor under the feet of the other subject. Finally, the last set was attached to the floor under the seat to prevent anyone from step on it. All instruments used are shown in Figures 2(a) and 2(b); the measurement location inside the coach is shown in Figure 3.

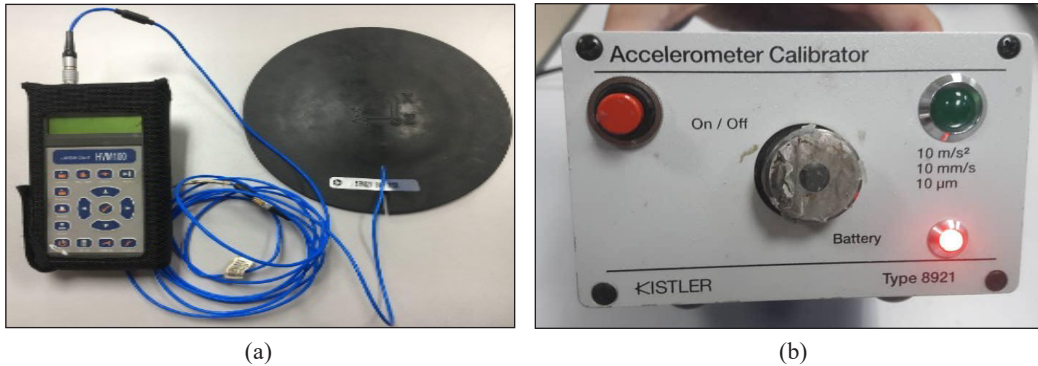


Figure 2. (a) HVM and Triaxial Accelerometer; and (b) Accelerometer Calibrator Kristler 8921

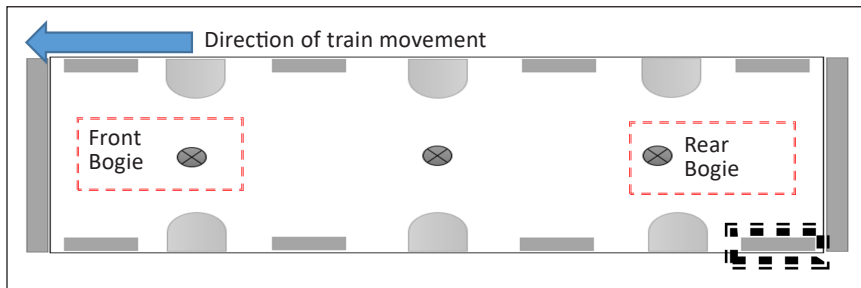


Figure 3. Locations of the measurements

Body Mass Index (BMI)

This study had chosen two subjects which represent BMI for normal and overweight. Details of the subject are shown in Table 1.

Table 1
Detail of subject

Subject	Height	Weight	BMI	Level
A	1.70 m	65 kg	22.5	Normal
B	1.84 m	100 kg	29.5	Overweight

Operation Time

This study was conducted at two different operation times: peak and off-peak operation hours. Based on previous research, peak hours are between 7:00 am to 9:00 am and 4:30 pm to 6:30 pm. Meanwhile, off-peak hours are outside the peak time (Wang et al., 2016).

Orientation of Passenger

Real-time monitoring began with installing two triaxial accelerometers on the floor and the passenger seat, based on ISO 2631-1. After that, both subjects would take their positions according to the procedure. For example, one subject sat on the seat pad while another stood on the seat pad, as seen in Figures 4(a) and 4(b).

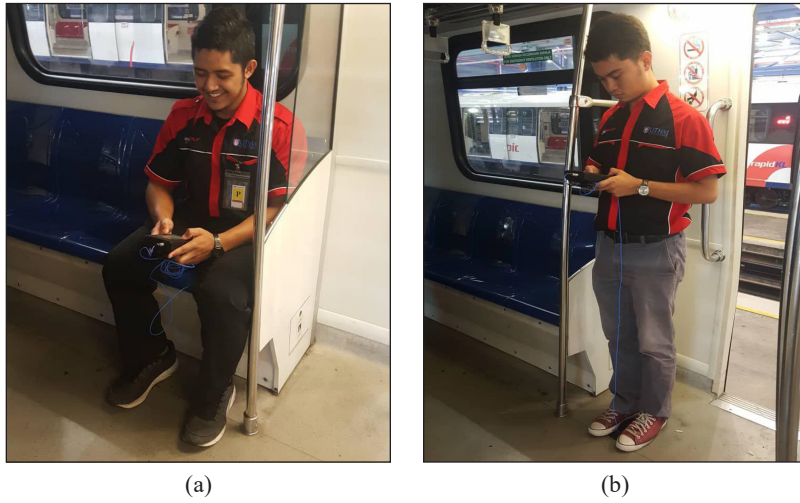


Figure 4. (a) Seating positions; and (b) Standing positions

Full Factorial Experimental Design

This study underwent 2³ full factorial experiment designs, as per showed in Table 2.

The monitoring of the whole-body vibration took place along the route with, the region between each station labelled as a section. Table 3 summarises the labelling of each section.

Table 2
Design of experiment

Case	Operation Time	Orientation	BMI
1	Peak	Standing	Normal
		Seating	Overweight
2	Off-peak	Standing	Overweight
		Seating	Normal
3	Off-peak	Standing	Normal
		Seating	Overweight
4	Peak	Standing	Overweight
		Seating	Normal

Table 3
Sections of the urban rail route

Station	Section	Station	Section	Station	Section
Station A	Start	Station N	13	Station AA	26
Station B	1	Station O	14	Station BB	27
Station C	2	Station P	15	Station CC	28
Station D	3	Station Q	16	Station DD	29
Station E	4	Station R	17	Station EE	30
Station F	5	Station S	18	Station FF	31
Station G	6	Station T	19	Station GG	32
Station H	7	Station U	20	Station HH	33
Station I	8	Station V	21	Station II	34
Station J	9	Station W	22	Station JJ	35
Station K	10	Station X	23	Station KK	36
Station L	11	Station Y	24		
Station M	12	Station Z	25		

Data Analysis

Data analysis for this study involved calculating few parameters, which was done manually by following guidelines from ISO (1997).

This study measured the vibration on three (3) axes of the passenger and weighted acceleration that combines all the axes needed to calculate for further analysis. The formula used is shown in Equation 1. The weighting for the calculation is different between seating and vertical orientation, as shown in Table 4.

Table 4
Weighting for different orientation

Orientation	Weighting		
	X-axis	Y-axis	Z-axis
Seating	1.4	1.4	1.0
Standing	1.0	1.0	1.0

$$a_w = \sqrt{(ka_x)^2 + (ka_y)^2 + (ka_z)^2} \tag{1}$$

Daily Vibration Exposure A (8)

This study calculated the Daily Vibration Exposure A (8) to monitor vibration exposure to the passenger on the urban rail. The formula used to calculate A (8) is shown in Equation 2.

$$A(8) = a_w \left[\frac{T}{T_0} \right]^{\frac{1}{2}} \tag{2}$$

Statistical Analysis

This study analyses the factorial design by using Minitab Software. There are 3 findings shall be presented from the statistical analysis of the full factorial design.

Significant effect of the variables

The result shall be presented by showing the Pareto Chart. The reference line drew on the chart indicates which factors that are tested in this study are significant.

Level of statistically significant association between the variables

This study developed 2 hypothesis statements which are listed below:

H₀ = There is no statistically significant association between the variables.

H₁ = There is a statistically significant association between the variables.

The decision to accept the hypothesis statement is based on the p-value of the analysis, where the significant level (α) is equivalent to 5% or 0.05.

Level of Model Fits Data

This study shall examine the goodness-of-fit statistic of the data in the model summary. The result shall be present in terms of the value of R^2 .

RESULT

This study presented the result from two processes: real-time monitoring and statistical analysis.

Daily Vibration Exposure

Figure 5 shows the result of daily vibration exposure for normal seated and standing passengers during peak hours. It is clearly shown that the value of the vibration exposure for the seated passenger is greater at most of the sections than the standing passenger. The greatest value of vibration exposure for the seating passenger is in Section 33 (0.014 ms^{-2}); for the standing passenger is in Section 1 (0.013 ms^{-2}).

Figure 6 shows the daily vibration exposure for normal seated and standing passengers during off-peak hours. It is clearly shown that the value of the vibration exposure for the

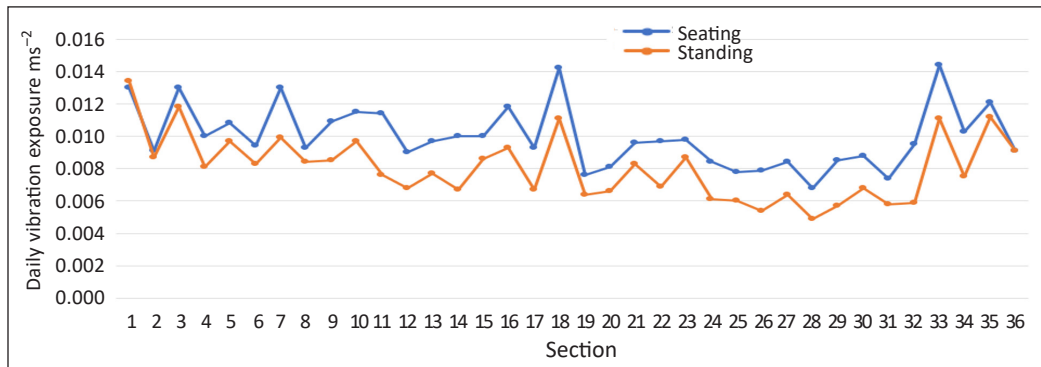


Figure 5. Daily vibration exposure for normal seated and standing passengers during peak hours

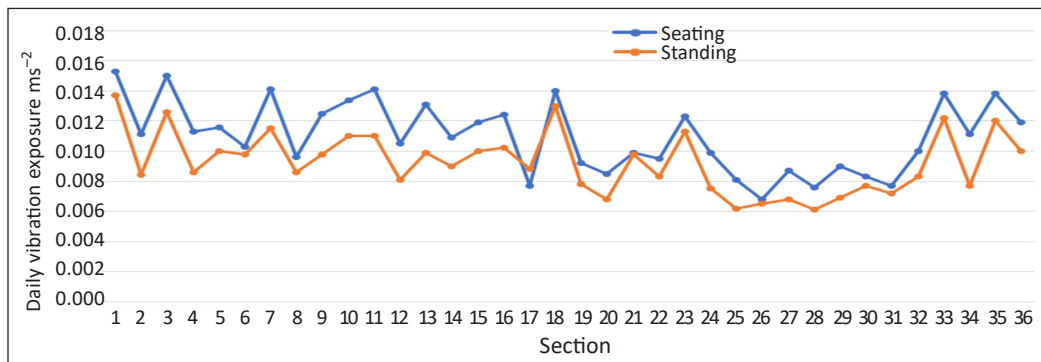


Figure 6. Daily vibration exposure for normal seating and standing passengers during off-peak time

seated passenger is greater at 35 sections than the standing passenger. The greatest value of vibration exposure for the seated passenger is in Section 3 (0.016 ms^{-2}), while for the highest value for standing passengers is in Section 1 (0.013 ms^{-2}).

Figure 7 shows the daily vibration exposure for overweight seated and standing passengers during peak hours. There is only one section where the standing passenger was exposed to higher daily vibration than to the seated passenger; the value is higher for the seated passenger than the standing passenger in the other 35 sections. The greatest value of vibration exposure for the seated passenger is in Section 1 (0.015 ms^{-2}) while, for the standing passenger is in Section 1 (0.013 ms^{-2}).

Figure 8 shows the daily vibration exposure for overweight seated and standing passengers during off-peak hours. It is clearly shown that the value of the vibration exposure for the seated passenger is greater in most of the sections than the standing passenger. The greatest value of vibration exposure for the seated passenger is in Section 1 (0.015 ms^{-2}), while for the standing passenger is in Section 1 (0.014 ms^{-2}).

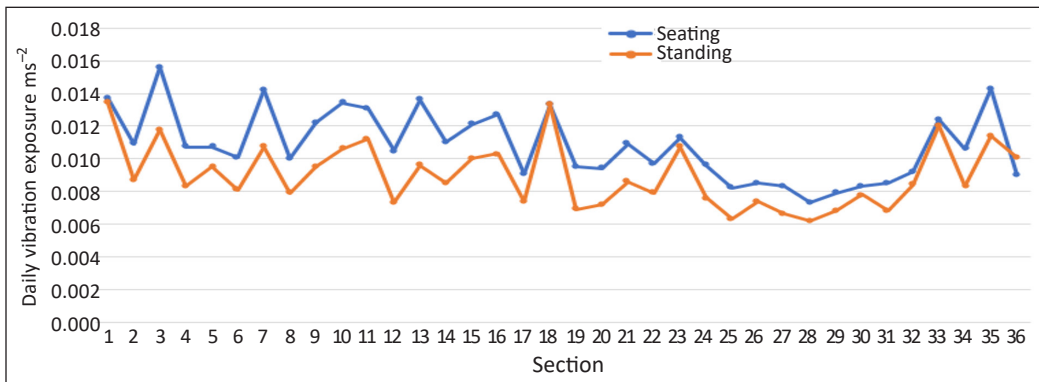


Figure 7. Daily vibration exposure for overweight seated and standing passengers during peak hours

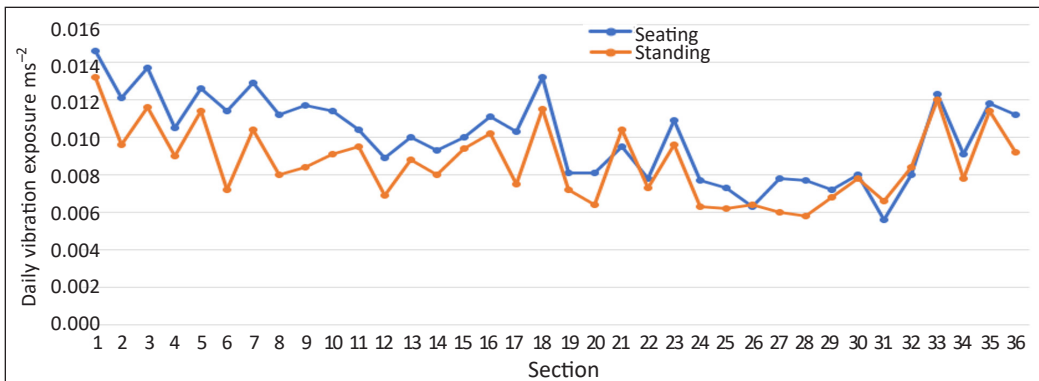


Figure 8. Daily vibration exposure for overweight seated and standing passengers during off-peak hours

Overall Daily Vibration Exposure

Figure 9 shows normal passengers' overall daily vibration exposure for orientations (seated and standing) and both operation hours. During peak hours, normal seated passenger was exposed to 0.3686 ms^{-2} of vibration while standing passenger was exposed to 0.2965 ms^{-2} . Besides that, during off-peak hours, the seated passenger was exposed to 0.4000 ms^{-2} while the standing passenger was exposed to 0.3326 ms^{-2} . Thus, it shows that seated passenger was exposed to greater vibration than standing passenger for both operation hours.

Figure 10 shows the overall daily vibration exposure for overweight passenger for both orientation and operation hours. While seated, the overweight passengers was exposed to about 0.3706 ms^{-2} of vibration during peak hours and 0.4063 ms^{-2} for the same orientation during off-peak hours. While standing, the overweight passenger was exposed to 0.3187 ms^{-2} of whole-body vibration during peak hours than 0.3409 ms^{-2} during off-peak hours. It clearly shows that overweight passengers are exposed to greater whole-body vibration while seated than standing and experience greater exposure during off-peak hours than peak hours.

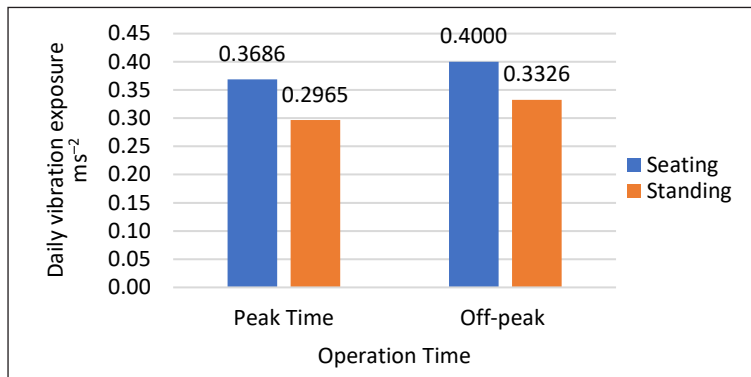


Figure 9. Overall A (8) for normal passenger

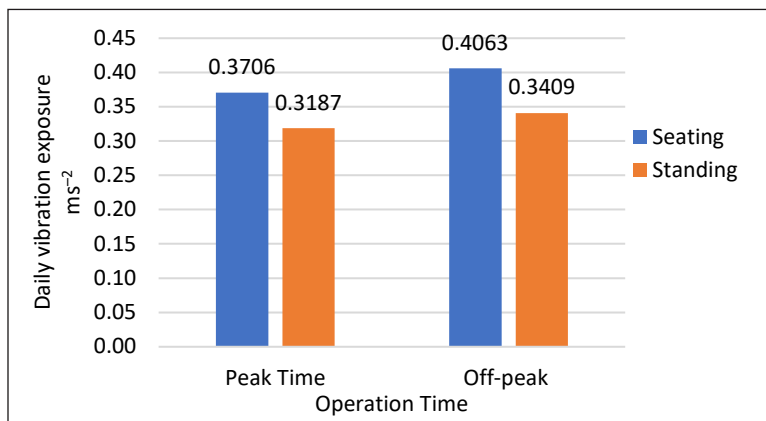


Figure 10. Overall A (8) for overweight passenger

Figure 11 shows the result of overall daily vibration exposure for the seated passenger. The result shows that the normal seated passenger was exposed to 0.3686 ms^{-2} of daily vibration exposure during peak hours than the seated overweight seated, 0.3706 ms^{-2} . Meanwhile, during off-peak hours, the normal seated passenger was exposed to 0.4000 ms^{-2} and the overweight seated passenger was exposed to 0.4063 ms^{-2} . Therefore, it can be concluded that the overweight passenger was exposed to greater daily vibration exposure than the normal seating passenger during both operation hours.

Figure 12 shows the result of overall daily vibration exposure for the standing passenger. During peak hours, the normal standing passenger was exposed to 0.2965 ms^{-2} of daily vibration exposure, and the overweight standing passenger was exposed to 0.3187 ms^{-2} . Meanwhile, during off-peak hours, the normal standing passenger was exposed to 0.3326 ms^{-2} and the overweight seated passenger was exposed to 0.3409 ms^{-2} . Therefore, it can be concluded that the overweight passenger tends to receive a greater daily vibration exposure than the normal seated passenger during both operation hours.

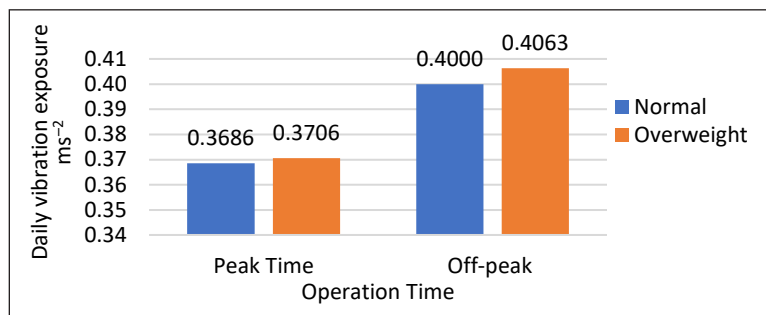


Figure 11. Overall A (8) for seating passenger

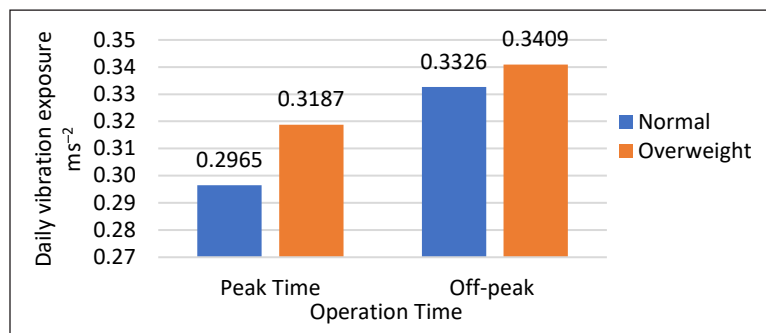


Figure 12. Overall A (8) for standing passenger

2³ Full Factorial Design

Significant Effect of the Variables. Figure 13 shows the Pareto Chart from the 2³ full factorial design analysis. The chart shows that all three (3) factors are statistically significant ($\alpha = 0.05$). The chart also shows that the largest effect on the passenger's

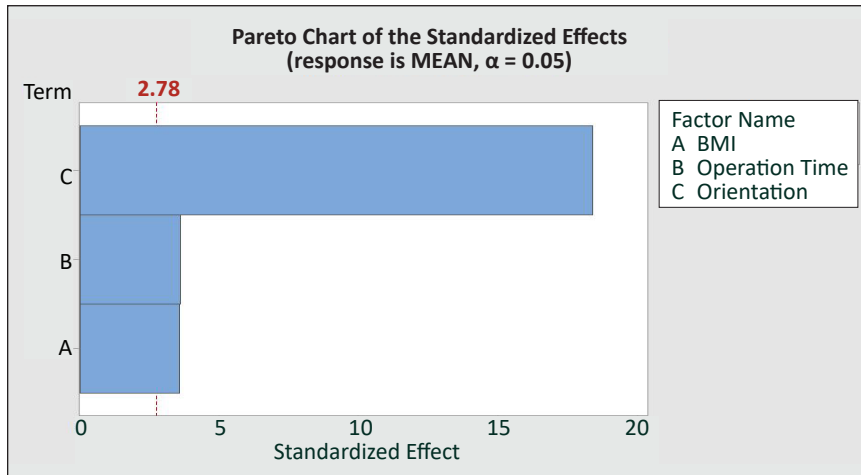


Figure 13. Pareto Chart

whole body vibration exposure is the body mass index, followed by operation time. The orientation of the passenger is the smallest because it extends the least in the Pareto Chart.

Level of Statistically Significant Association between the Variables. There are three (3) hypothesis statements that are tested in this full factorial design analysis which are:

Body Mass Index (BMI)

H_0 = There is no statistically significant association between Body Mass Index (BMI), Operation Time and Orientation of Passenger.

H_1 = There is a statistically significant association between Body Mass Index (BMI), Operation Time and Orientation of Passenger.

Operation Time

H_0 = There is no statistically significant association between Operation time, Body Mass Index (BMI) and Orientation of Passenger.

H_1 = There is a statistically significant association between Operation time, Body Mass Index (BMI) and Orientation of Passenger.

Orientation of Passenger

H_0 = There is no statistically significant association between Orientation of Passenger, Body Mass Index (BMI) and Operation Time.

H_1 = There is a statistically significant association between Orientation of Passenger, Body Mass Index (BMI) and Operation Time.

Table 5
Coded coefficients

Term	Effect	Coef	SE Coef	T-Value	P-Value	VIF
Constant		0.37944	0.00157	241.63	0.000	
BMI	0.01125	0.00563	0.00157	3.58	0.023	1.00
Operation Time	0.01136	0.00568	0.00157	3.62	0.022	1.00
Orientation	-0.05776	-0.02888	0.00157	-18.39	0.000	1.00

Table 5 shows that the coded coefficients from the Minitab result. The result shows that the main effect of BMI, Operation and Orientation of passengers are statistically significant which are the value of p-value are less than $\alpha = 0.05$. Therefore, the decision for the hypothesis statement is H_0 is rejected for all the variables where there is a statistically significant association between Body Mass Index (BMI), Operation Time and Orientation of Passenger.

Level of Model Fits Data. In these results in Table 6, the value of R^2 is 98.91%, indicating that the model provides a good fit for the data.

Table 6
Model summary

S	R-sq	R-sq(adj)	R-sq(Pred)
0.0044417	98.91%	98.10%	95.65%

DISCUSSION

Real-time Monitoring

Orientation of Passenger. For the normal passenger, it is found that during peak hours, the daily vibration exposure for the seated passenger is 0.3686 ms^{-2} while the standing passenger was exposed to 0.2965 ms^{-2} . It shows that the seated passenger was exposed to 24% more daily vibration than the standing passenger during peak hours. Besides that, during off-peak hours, the seated passenger was exposed to 0.4 ms^{-2} while the standing passenger was exposed to 0.3326 ms^{-2} . It shows that the seated passenger was exposed to 20% greater daily vibration than the seated passenger. It is due to greater surface exposure toward the seated passenger than the standing passenger.

For the overweight passenger, it is found that during peak hours, the daily vibration exposure for the seated passenger is 0.3706 ms^{-2} while the standing passenger was exposed to 0.3187 ms^{-2} . Therefore, it shows that the seated passenger was exposed to 16% greater daily vibration than the standing passenger during peak hours. Besides that, during off-peak hours, the seated passenger was exposed to 0.4063 ms^{-2} while the standing passenger was exposed to 0.3409 ms^{-2} . Thus, it shows that the seated passenger was exposed to 19% greater daily vibration than the seated passenger.

From both results, it was found that the seated passenger was exposed to greater daily vibration than the standing passenger. This result corresponds with previous research, where

the researcher found that the seated passenger gained higher vibration than the standing passenger (Hasnan et al., 2018). This phenomenon is caused by a difference in the area of contact between both orientations. A seated passenger has fewer body parts exposed to the vibrating surface, such as the buttock, feet and back. Meanwhile, the passenger in a vertical orientation only has one area of contact: their feet (Kumar & Saran, 2014).

Operation Time

For the normal weight passenger, it was found that in the seated orientation, the daily vibration exposure during peak hours is 0.3686 ms^{-2} while during off-peak hours is 0.4 ms^{-2} . Therefore, it shows that the seated orientation caused 8% greater daily vibration exposure during off-peak hours than peak hours. Besides that, the standing passenger was exposed to 0.2965 ms^{-2} during peak hours and 0.3326 ms^{-2} during off-peak hours. Therefore, it shows that the vertical orientation caused 12% greater daily vibration exposure during off-peak hours than peak hours.

For the overweight passenger, it was found that in the seated orientation, the daily vibration exposure during peak hours is 0.3706 ms^{-2} and 0.4063 ms^{-2} during off-peak hours. It shows that the seated orientation causes 9% greater daily vibration exposure during off-peak hours than peak hours. Besides that, in the vertical orientation, the passenger was exposed to 0.3187 ms^{-2} of vibration during peak hours and 0.3409 ms^{-2} during off-peak hours. It shows that the vertical orientation causes 7% greater daily vibration exposure during off-peak hours than peak hours.

Therefore, from both results, it was found that the passenger tends to be exposed to greater daily vibration during off-peak hours than peak hours in both orientations. It is due to the difference in the overall mass of the train between both operation hours. The overall mass of the train is greater during peak hours than during off-peak hours. Therefore, during peak hours, the numbers of passengers board the train were higher than during off-peak hours. When the mass decreases, the vibration will increase (Tuladhar et al., 2018). It is why the train's vibration transmission rate is higher during off-peak hours than during peak hours. Other than that, the speed of the train differs during both operation hours. The train arrives every three minutes during peak hours and every eight minutes during off-peak hours. However, the number of operating trains is the same during both operation hours. It shows that the train travels slower during off-peak hours than peak hours. When the train speed decreases, the vibration will increase (Karakasis et al., 2005).

Body Mass Index of Passenger

For the seated passenger, it was found that the normal weight passenger was exposed to 0.3686 ms^{-2} of vibration during peak hours, while the overweight passenger was exposed to 0.3706 ms^{-2} . However, during off-peak hours, the normal weight passenger was exposed

to 0.4000 ms^{-2} of vibration, and the overweight passenger was exposed to 0.4063 ms^{-2} . Thus, it shows that the overweight passenger experienced slightly greater exposure to daily vibration than normal passengers during both operation hours.

In the vertical orientation, the daily vibration exposure during peak hours for the normal weight passenger was 0.2965 ms^{-2} while the overweight passenger was 0.3187 ms^{-2} . It shows that the overweight passenger was exposed to 7% greater daily vibration during peak hours than the normal weight passenger. Besides that, during off-peak hours, the normal passenger was exposed to 0.3326 ms^{-2} of vibration, and the overweight passenger was exposed to 0.3409 ms^{-2} . Therefore, it shows that the overweight passenger was exposed to slightly greater daily vibration than the normal passenger during both operation hours.

CONCLUSION

This study concludes that passenger orientation has a significant effect on daily vibration exposure. In addition, the seated passenger was exposed to greater whole-body vibration than the standing passenger. Operation hours have a significant effect on the daily vibration exposure. Daily vibration exposure was greater during off-peak hours than during peak hours. Lastly, the overweight passenger experienced greater whole-body vibration than the normal weight passenger. All the variables are statistically significant and shall affect the value of whole-body vibration of the urban rail passenger.

ACKNOWLEDGEMENT

The authors were supported by the Post Graduate Research Grant (GPPS) by Universiti Tun Hussein Onn Malaysia. The authors would also like to thank Rapid Rail Sdn Bhd and Prasarana Malaysia Berhad for their contribution and participation in this study. The authors declare that there is no conflict of interest.

REFERENCES

- Azlis-Sani, J., Zaid, M. F., Yahya, M. N., Ismail, S. M. S. S. M., Ahmad Tajedi, N. A., Aziz, R. A., & Zein, R. M. (2015). Evaluation of whole body vibration and back pain problem among light rapid transit (LRT) Drivers. *Applied Mechanics and Materials*, 773-774, 845-849. <https://doi.org/10.4028/www.scientific.net/amm.773-774.845>
- Dumitriu, M. (2013). Evaluation of the comfort index in railway vehicles depending on the vertical suspension features. *Annals of Faculty Engineering Hunedoara*, 11(4), 23-32.
- Fateh, A., Hejazi, F., Ramanathan, R. A., & Jaffar, M. S. (2016). Seismic response of a light rail transit station equipped with braced viscous damper. *Pertanika Journal of Science and Technology*, 24(2), 273-283.
- Gągorowski, A. (2010). Simulation study on stiffness of suspension seat in the aspect of the vibration assessment affecting a vehicle driver. *Logistics and Transport*, 11, 55-62.

- Griffin, M. J., & Erdreich, J. (1991). Handbook of Human Vibration. *The Journal of the Acoustical Society of America*, 90 (4), Article 2213. <https://doi.org/10.1121/1.401606>
- Hasnan, K., Bakhsh, Q., Ahmed, A., Ali, D., & Jamali, A. R. (2018). Analysis of WBV on standing and seated passengers during off-peak operation in KL monorail. *IOP Conference Series: Materials Science and Engineering*, 324(1), 2-7. <https://doi.org/10.1088/1757-899X/324/1/012003>
- Ismail, A. R., Nuawi, M. Z., How, C. W., Kamaruddin, N. F., Nor, M. J. M., & Makhtar, N. K. (2010). Whole body vibration exposure to train passenger. *American Journal of Applied Sciences*, 7(3), 352-359. <https://doi.org/10.3844/ajassp.2010.352.359>
- ISO, I. (1997). *2631-1: Mechanical vibration and shock-evaluation of human exposure to whole-body vibration-Part 1: General requirements*. ISO.
- Karakasis, K., Skarlatos, D., & Zakinthinos, T. (2005). A factorial analysis for the determination of an optimal train speed with a desired ride comfort. *Applied Acoustics*, 66(10), 1121-1134. <https://doi.org/10.1016/j.apacoust.2005.02.006>
- Kim, Y. G., Choi, S., Kim, S. W., Kim, Y. M., & Park, T. W. (2009). An experimental study on the ride comfort of the Korean high-speed train. *Experimental Techniques*, 33(6), 30-37. <https://doi.org/10.1111/j.1747-1567.2008.00419.x>
- Kumar, V., & Saran, V. H. (2014). Influence of reading format on reading activity under uniaxial whole body vibration. *International Journal of Industrial Ergonomics*, 44(4), 520-527. <https://doi.org/10.1016/j.ergon.2014.05.004>
- Kumara, V., Saranb, V. H., & Guruguntla, V. (2013, December 18-20). Study of vibration dose value and discomfort due to whole body vibration exposure for a two wheeler drive. In *Proceedings of the 1st International and 16th National Conference on Machines and Mechanisms (iNaCoMM2013)* (pp. 947-952). IIT Roorkee, India.
- Mohajer, N., Abdi, H., Nahavandi, S., & Nelson, K. (2017). Directional and sectional ride comfort estimation using an integrated human biomechanical-seat foam model. *Journal of Sound and Vibration*, 403, 38-58. <https://doi.org/10.1016/j.jsv.2017.05.019>
- Mortimer, M., Wiktorin, C., Pernold, G., Svensson, H., & Vingård, E. (2001). Sports activities, body weight and smoking in relation to low-back pain: A population-based case-referent study. *Scandinavian Journal of Medicine and Science in Sports*, 11(3), 178-184. <https://doi.org/10.1046/j.1524-4725.2001.110308.x>
- Munawir, T. I. T., Samah, A. A. A., Rosle, M. A. A., Azlis-Sani, J., Hasnan, K., Sabri, S. M., Ismail, S. M., Yunos, M. N. A. M., & Bin, T. Y. (2017). A comparison study on the assessment of ride comfort for LRT passengers. In *IOP Conference Series: Materials Science and Engineering* (Vol. 226, No. 1, p. 012039). IOP Publishing. <https://doi.org/10.1088/1757-899X/226/1/012039>
- Nuawi, M. Z., Ismail, A. R., Nor, M. J. M., & Rahman, M. M. (2011). Comparative study of whole-body vibration exposure between train and car passengers: A case study in malaysia. *International Journal of Automotive and Mechanical Engineering*, 4, 490-503.
- Park, M., Fukuda, T., Kim, T., & Maeda, S. (2013). Health risk evaluation of whole-body vibration by ISO 2631-5 and ISO 2631-1 for operators of agricultural tractors and recreational vehicles. *Industrial Health*, 51(3), 364-370. <https://doi.org/10.2486/indhealth.2012-0045>

- Pradhan, S., Samantaray, A. K., & Bhattacharyya, R. (2017). Evaluation of ride comfort in a railway passenger vehicle with integrated vehicle and human body bond graph model. In *ASME International Mechanical Engineering Congress and Exposition* (Vol. 58479, p. V012T16A013). American Society of Mechanical Engineers. <https://doi.org/10.1115/IMECE2017-71288>
- Schwarze, S., Notbohm, G., Dupuis, H., & Härtung, E. (1998). Dose-response relationships between whole-body vibration and lumbar disk disease - A field study on 388 drivers of different vehicles. *Journal of Sound and Vibration*, 215(4), 613-628. <https://doi.org/10.1006/jsvi.1998.1602>
- Smith, D. L., Chang, J., Cohen, D., Foley, J., & Glassco, R. (2005, November 6-10). A simulation approach for evaluating the relative safety impact of driver distraction during secondary tasks. In *12th World Congress on ITS* (pp. 1-12). San Francisco, California.
- Tuladhar, S. R., Khomchuk, P., & Sivananthan, S. (2018). *Estimating passenger loading on train cars using accelerometer*. ArXiv Publishing.
- Wang, X., Fan, T., Li, W., Yu, R., Bullock, D., Wu, B., & Tremont, P. (2016). Speed variation during peak and off-peak hours on urban arterials in Shanghai. *Transportation Research Part C: Emerging Technologies*, 67, 84-94. <https://doi.org/10.1016/j.trc.2016.02.005>
- Zhou, C., Dai, P., Wang, F., & Zhang, Z. (2016). Predicting the passenger demand on bus services for mobile users. *Pervasive and Mobile Computing*, 25(2013), 48-66. <https://doi.org/10.1016/j.pmcj.2015.10.003>

Diffusion and Osmotic Permeability of Ion Exchange Membrane MK-40 Using Sodium Chloride Solution

Mohammed Qader Gubari^{1,2}, Haider Mohammed Zwain^{3*} and Nadezda Vyacheslavovna Alekseeva²

¹Department of Fuel and Energy Engineering Technologies, Technical College Kirkuk, Northern Technical University, Mosul, Iraq

²Department of Technological Processes, Devices and Technosphere Safety, Tambov State Technical University, Tambov, Russia

³College of Water Resources Engineering, Al-Qasim Green University, 51013 Al-Qasim Province, Babylon, Iraq

ABSTRACT

Cation exchange membrane (MK-40) is a commercial membrane with a fixed group that is an important part of the electrodialysis (ED) process. Sodium chloride (NaCl) diffusion and osmotic permeability for MK-40 was studied. A cell containing two compartments was used to analyse the properties of the MK-40 membrane fixed between them. Furthermore, the influence of temperature, NaCl concentration, and operating time on MK-40 properties was investigated. The results showed that the highest diffusion permeability coefficient of NaCl was 7.37×10^{-9} (m²/s), and the maximum osmotic permeability coefficient of distilled water was 43.8×10^{-9} (m²/s) at NaCl solution concentration of 0.1 M and 50°C. Generally, the permeability was constant beyond 60 min of operational time. Additionally, the minimum diffusion permeability coefficients of the MK-40 membrane fell by about 22% over time when the concentration of NaCl solution was 1 M at 25°C. To conclude,

membrane properties in the ED process depend on the two electrodes (a cathode and an anode), without the diffusion of salts particles. Meanwhile, the most important properties of cation exchange membranes (CEMs) used in electrodialysis are increased membrane efficiency when water and salts transport decrease through CEMs, which leads to a decrease in energy consumption. Thus, the MK-40 membrane showed a good

ARTICLE INFO

Article history:

Received: 29 March 2021

Accepted: 05 July 2021

Published: 08 October 2021

DOI: <https://doi.org/10.47836/pjst.29.4.14>

E-mail addresses:

mohammedqader1983@gmail.com (Mohammed Qader Gubari)

haider.zwain@wrec.uoqasim.edu.iq (Haider Mohammed Zwain)

alexjewan.nadja@gmail.com (Nadezda Vyacheslavovna

Alekseeva)

* Corresponding author

properties due to its low diffusion permeability for concentrated NaCl solution at elevated temperatures and minimum reduction in diffusion permeability of concentrated NaCl solution over time.

Keywords: Cation exchange membrane (MK-40), diffusion permeability, electrical conductivity, osmotic permeability, sodium chloride

INTRODUCTION

Industrial application of ion exchange membranes (IEMs) started with saltwater desalination, and membranes are widely used in many fields such as drinking water treatment, treated wastewater treatment, amino acid demineralisation, sugar liquor demineralisation, whey demineralisation, and purification of organic matter. Saline water desalination is the most appropriate and commonly used fundamental technology of these applications (Tanaka, 2011). Recent years have seen extensive use of IEMs in processes such as electro dialysis (ED), diffusion dialysis, dialysis of Donnan, and capacitive deionisation (Chaabouni et al., 2015). Owing to their chemical stability, water transport properties and desirable ion, IEMs have recently attracted considerable interest in membrane-based technologies (Geise et al., 2014a).

MK-40 is one of the heterogeneous cation ion exchange membranes in the form of a flat sheet (Vasil'eva et al., 2013). MK-40 composites are developed based on KU-2 cation exchange resins (a matrix of polystyrene (PS) cross-linked with divinylbenzene (DVB) and fixed groups), polyethylene and nylon (Melnikov et al., 2018). MK-40 rejects an ion with the same charge (co-ions) and enables the passage of oppositely charged ion (counter-ions) (Geise et al., 2014b). The main application of MK-40 in processes of water desalination (Andreeva et al., 2020). On the other hand, IEMs are considered a key component of electro dialysis (ED) systems. Their contribution to the process's overall cost may be as large as 40 to 50 % (Mikhaylin & Bazinet, 2016). Therefore, the application of technologies utilizing IEMs is typically defined by the transport properties and costs of IEMs.

IEMs are mainly affected by several parameters: temperature, solution concentration, electrical conductivity, and flux time. Temperature is one of the most important characteristics that can affect the electrical conductivity and fluid flow, and the characteristics of IEMs. Therefore, it is very important to optimise the temperature (Karimi & Ghassemi, 2016). For instance, Guesmi et al. (2010) reported that different temperatures (10, 25, and 40°C) had significantly affected the ion exchange equilibrium of the system with CMX cation exchange membrane involving monovalent and divalent ions. Nevertheless, the salt concentration also influences the diffusion permeability, conductivity, and ion transport numbers (Sarapulova et al., 2019). For example, Geise et al. (2013) found that when the salt concentration increased from 0.58 to 58 g/L, the permeability of sodium chloride decreased by 16% in uncharged hydrogel and increased by more than 10% in charged polymers.

In this regard, diffusion and osmotic permeability are key indicators for IEMs characteristics. It can be measured by two-compartments cells used for calculating diffusion and osmotic permeability coefficients. The values of diffusion and osmosis depend on the size of the system, and on the concentration profiles of dilute and concentrate solutions, which are set by the application of the ED system (Chehayeb et al., 2019). Many methods have been used to determine the effect of solution properties on membrane diffusion permeability, such as solution concentration, temperature and flux time. For example, Kingsbury et al. (2018) studied the permeability of water and salt simultaneously using a two-chamber cell. One-half of the cells consisted of a NaCl solution, while the other half consisted of distilled water. In addition, a concentrated NaCl solution was selected to optimise the osmosis rate and promote water transport measurements. Furthermore, the non-flow two-chamber cell was used by Melnikov et al. (2018) to analyse the permeability of the diffusion. Half of the cell consisted of salt or acid, while the second half consisted of distilled water.

From the literature, permeation of co-ions of NaCl via diffusion and water by osmosis is a non-ideal movement that cannot be regulated by electrical fields and thus decreases the performance of electrochemical processes. Consequently, limiting non-ideal transport of water and salt (osmosis and salt diffusion) is a key objective to study the effect of some parameters on CEM (MK-40) performance (Gubari et al., In Press). To date, there are a few researchers who have evaluated the effect of discharged feed solutions and different distilled water temperatures on diffusion and osmotic permeability of CEMs in the ED process to verify the effectiveness of membrane separation. Therefore, this study aims to investigate the diffusion and osmotic permeability of MK-40 membrane, employing two compartments cell, using NaCl solution and distilled water, at different salt concentrations (0.1, 0.5 and 1 M) and different distilled water temperatures (25 and 50°C).

MATERIALS AND METHODS

Membranes and Reagents

The MK-40 membrane is effective for small-scale water desalination due to its low cost and long lifetime (Gubari et al., 2021). The copolymerisation of polystyrene obtained by Ion-exchange materials in the MK-40 membrane with divinylbenzene. “Shchekinoazot” (Russian) manufactured this membrane in the form of flat sheets (Vasil’eva et al., 2013). MK-40 membrane pore size distribution indicates two maxes, the first one approximately 10 nm and corresponding to micro and mesoporous, and the second relates to macropores around 1000 nm in sizes. The pores of the membrane MK-40 are positioned within the sulfonated ion-exchange particles (MK-40). The second pores type is the spaces in a membrane between various particles (Nikonenko et al., 2019). Table 1 collects the main features of commercial MK-40 membranes (Pismenskaya et al., 2012). In this study,

distilled water (electric conductivity of $4.5 \mu\text{S cm}^{-1}$; $\text{pH} = 5.5$; 25°C) and NaCl ($\geq 99.7\%$ purity) at different concentrations were used.

Table 1
Properties of commercial MK-40 membrane

Membrane	Cation exchange (MK-40)
Ion exchange groups, bulk	$-\text{SO}_3^-$
Idem, surface	$-\text{SO}_3^-$
Thickness, μm	480 ± 10
Ion exchange capacity, mM cm^{-3} wet	1.7 ± 0.1
Ion exchange material surface fraction of, %	22 ± 3
Contact angle, degrees	55 ± 3
Particular conductivity in solution 0.5 M NaCl , $\text{mS}\cdot\text{cm}^{-1}$	7.7 ± 0.3
Diffusion permeability, $10^{-8} \text{ cm}^2 \cdot \text{s}^{-1}$	6.7 ± 0.4

Salt and Water Penetration Measurements

The coefficients of salt diffusion were determined from the calculation of the self-diffusion, taking into account the diluting effects of osmosis in the gradient of salt concentration. In other word, the flow of water from the distilled water compartment dilutes the salt concentration in the other compartment over time, and reduces the driving force of diffusion and osmosis (Kingsbury et al., 2018). The permeability of diffusion was established by the amount transferred by the membrane of a substance over a surface unit per unit of time. Thus, the permeability coefficients of membranes for salt diffusion can be determined by the formula given in Equation 1 of the experimental salt permeability obtained from the reference for a steady flow of liquid from the salt compartment to the distilled water compartment (Alekseeva et al., 2012).

$$P_s = \frac{C_2 \cdot V_2 \cdot X}{(C_1 - C_2) \cdot S \cdot t} \quad (1)$$

where: P_s is NaCl diffusion permeability, (m^2/s); C_1 and C_2 are the total concentration of the components in salt solution and water, respectively (mol/m^3); V_2 is the volume of water at the end of the experiment (m^3); S is membrane operating area (m^2); X is the membrane thickness (m); t is the test time (s).

The water flow from compartment filled with distilled water to compartment filled with NaCl solution is measured by the change in the amount of solution in horizontal capillaries over a given period. The osmotic permeability coefficient is determined by Equation 2 (Alekseeva et al., 2012).

$$P_w = \frac{n_w \cdot X}{(C_1 - C_2) \cdot S \cdot t} \quad (2)$$

where: P_w is distilled water osmotic permeability (m^2/s); n_w is the moles of distilled water transferred (mol). It was measured from volume change in the distilled water compartment.

Experimental Setup

Before the operational process, MK-40 is cleaned with a carbon tetrachloride solution and wait 15 minutes for the membrane to dry, and then cleaned with an ethanol solution and wait 15 minutes for the membrane to dry. After that, the membranes are placed in a saturated solution of sodium chloride (NaCl) for 24 hours and then placed in distilled water for 24 hours. Subsequently, MK-40 is placed in (0.1 M) of NaOH solution for 24 hours and then placed in distilled water for 24 hours. Then, the MK-40 is placed in (0.1 M) of HCl solution for 24 hours and then placed in distilled water until a neutral reaction. In the operational process, membrane coupons were fixed in the cell for 24 hours before operation to achieve pseudo-stable osmosis and diffusion.

In this experiment, a two-compartment cell was employed to study the permeability characteristics of MK-40, as shown in Figure 1. In order to do so, NaCl as a salt solution and distilled water as solvent were used. The volumes of the left half-cell contained NaCl solution, and the right half-cell contained distilled water were 550 cm^3 each. The membrane area was 31.4 cm^2 , and its thickness was 1 mm. The cell was connected to the

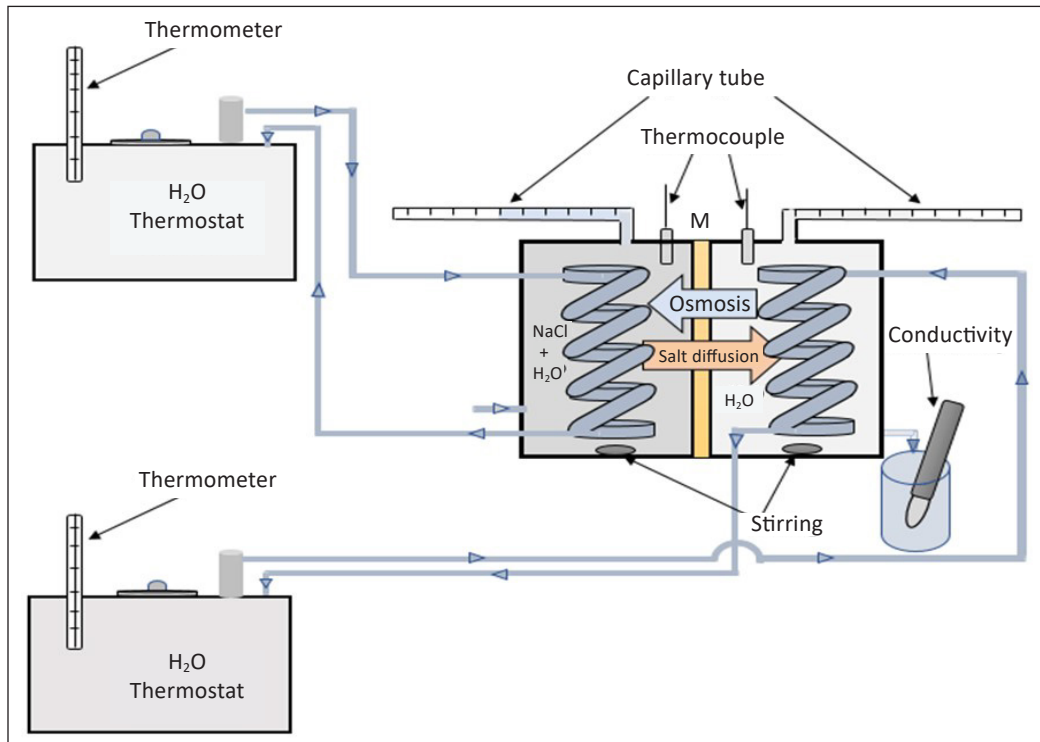


Figure 1. Schematic experiment diagram of two-compartment cell

thermostat box to maintain the cell temperature, and each compartment was connected to the thermocouple to measure temperature of the compartments. Different concentrations of NaCl (0.1, 0.5 and 1 M) and temperatures of distilled water (25 and 50°C) were selected to monitor diffusion and osmotic rates.

The two compartments were immediately filled with new solutions and distilled water. Once an operation began, the NaCl solution chamber and the distilled water chamber were stirred at 300 rpm with magnetic stir bars. The salt diffusion coefficient and osmotic water coefficient were determined due to water moving into the high concentrated compartment due to the osmosis process, while the salt diffused through the membrane into the distilled water compartment due to a concentration gradient. Each compartment of the cell was sealed and connected to a capillary tube, which made it possible to measure the volume change in the compartment with high accuracy. Then, the conductivity of distilled water compartment was measured over 15 min transition periods for each experiment, and the calibration curve using NaCl standard solutions converted these conductivity measurements to salt concentration. Finally, the salt diffusion coefficient and distilled water osmotic coefficient were measured using Equations 1 and 2, respectively.

RESULTS AND DISCUSSION

There are many properties of ion exchange membrane that influence salt diffusions, such as membrane chemical structure and water content. Diffusion of salt and osmosis of solvent are key factors that lead to variations in permeability of commercial MK-40 membrane. This study used, NaCl as a salt and water as a solvent, and the results were discussed below.

Diffusion Permeability of NaCl

Diffusion permeability coefficients of NaCl were calculated using Equation 1. Figure 2 presents the NaCl diffusion permeability coefficients at two distilled water temperatures (25 and 50°C), NaCl concentrations (0.1, 0.5 and 1 M), and 20 min transition periods. Over operational time of 20 to 100 min, when NaCl concentration was 0.1, 0.5 and 1 M, Figure 2 (a) showed that NaCl diffusion permeability coefficient decreased from 2.31×10^{-9} to 1.76×10^{-9} (m²/s), 2.19×10^{-9} to 1.62×10^{-9} (m²/s) and 1.97×10^{-9} to 1.53×10^{-9} (m²/s) at temperatures of 25°C, respectively. During the same operational period, at NaCl concentration of 0.1, 0.5 and 1 M, Figure 2 (b) illustrated that NaCl diffusion permeability coefficient declined from 7.37×10^{-9} to 3.88×10^{-9} (m²/s), 6.41×10^{-9} to 3.54×10^{-9} (m²/s) and 5.41×10^{-9} to 3.15×10^{-9} (m²/s), when temperature was 50°C, respectively.

Drop-in NaCl diffusion permeability coefficients could be due to water flux from diluted water compartment to salt solution compartment, lowering the driving force for diffusion and osmosis (Kingsbury et al., 2018). After about 60 min of operational time, NaCl diffusion permeability coefficients were approximately constant for both temperatures

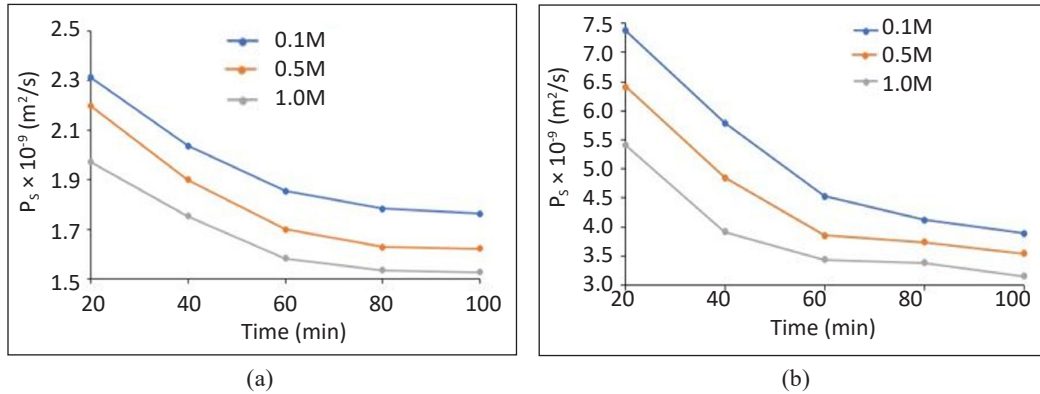


Figure 2. NaCl diffusion permeability coefficients at two different distilled water temperatures, (a) 25°C and (b) 50°C, using different NaCl concentrations, 0.1, 0.5, and 1 M, over 100 min operational time

because of concentration polarisation resulting from increased salt concentration in the boundary layer near the surface of the membrane (Melnikov et al., 2018). It prevents salt penetration through the membrane, explaining why the diffusion permeability was approximately constant after 60 minutes of operation.

MK-40 membrane showed low permeability to NaCl, which results in minimising energy losses in the electrodialysis process. In comparison, Kamcev et al. (2018) investigated NaCl diffusion permeability coefficients of cation exchange membrane (CR61), using a high NaCl concentration of 1 M. They found that diffusion permeability coefficients were 1.7×10^{-10} (m^2/s).

Figures 2(a) and 2(b) both revealed that a higher temperature of 50°C has led to higher permeability than 25°C. It could be because the higher temperature can enhance the permeation rate and accelerate the ions transport across membranes (Luo et al., 2010). To date, there are very few studies reporting the diffusion permeability of membranes at high temperatures. It can be noticed that higher salt concentration has significantly decreased the diffusion permeability coefficients of MK-40 membrane. Over an operational period of 20-100 min, when the NaCl concentration increased from 0.1 M to 1 M, NaCl diffusion permeability coefficients of the MK-40 membrane fell by about 24%-22% and 47%-41%, for the temperature of 25 and 50°C, respectively. It indicates that the MK-40 membrane is uncharged due to decreased polymer's water content as salt concentration increases. In contrast to charged membranes, when salt concentration increases, the salt diffusion permeability coefficients increase (Geise et al., 2013).

Tanaka (2011) investigated that when the temperature of ion exchange membranes such as Selemion CMR/ASR and Neoccepta CIMS/ACS3 increased from 25°C to 50°C, the overall hydraulic permeability was increased from $(1.116 \times 10^2$ to $1.937 \times 10^2)$ $cm^4 \cdot eq^{-1} \cdot s^{-1}$ and $(1.254 \times 10^2$ to $1.835 \times 10^2)$ $cm^4 \cdot eq^{-1} \cdot s^{-1}$. It confirms that when using a higher operating temperature, the membrane's diffusion permeability will increase, which will

lead to a decrease in the efficiency of the MK-40 membrane. According to Gatapova et al. (2020), an ion-exchange membrane (MK-40) diffusion permeability coefficient for a NaCl solution under thermostatic and thermodynamic conditions has been investigated. They found a significant difference in diffusion coefficient values when operating at the same temperature compared to the temperatures difference on both sides.

Osmatic Permeability of Solvent

Various experiments were performed to investigate the transport of solvents in ion-exchange membranes (Alekseeva et al., 2012, Kingsbury et al., 2019). In this study, the water transport occurs as free water (osmosis), not as bound water (electro-osmosis). The osmotic permeability coefficients of distilled water were calculated using Equation 2. Over an operational period of 20-100 min, Figure 3 showed the osmotic permeability coefficients of distilled water at two distilled water temperatures (25 and 50°C), NaCl concentrations (0.1, 0.5 and 1 M), and 20 min transition periods. Over operational time of 20 to 100 min, when NaCl concentration was 0.1, 0.5 and 1 M, Figure 3 (a) showed that NaCl osmotic permeability coefficient decreased from 3.57×10^{-9} to 1.58×10^{-9} (m^2/s), 2.09×10^{-9} to 0.8338×10^{-9} (m^2/s) and 0.948×10^{-9} to 0.2×10^{-9} (m^2/s) at temperatures of 25°C, respectively. On the other hand, under the same operating conditions, at NaCl concentration of 0.1, 0.5 and 1 M, Figure 3 (b) illustrated that the NaCl diffusion permeability coefficient declined from and 43.8×10^{-9} to 21.13×10^{-9} (m^2/s), 29.66×10^{-9} to 9.75×10^{-9} (m^2/s) and 10.53×10^{-9} to 3.73×10^{-9} (m^2/s), when the temperature was 50°C, respectively.

Decreasing osmotic permeability coefficients could be due to high salt concentration gradients lead to increase water flux from diluted water compartment to salt solution compartment due to osmosis (Kingsbury et al., 2018). Therefore, it is concluded that salt concentration's gradients should be essentially low to minimise the distilled water's flow

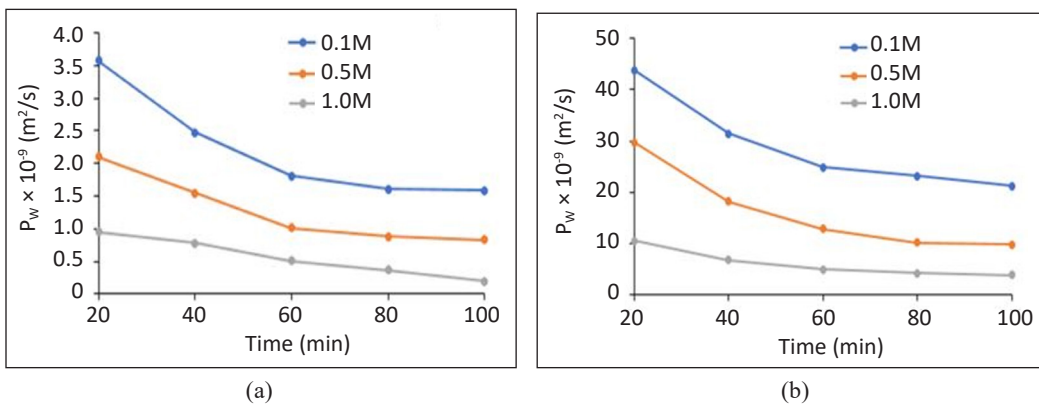


Figure 3. Water permeability coefficients at two different distilled water temperatures, (a) 25°C and (b) 50°C, using different NaCl concentrations, 0.1, 0.5, and 1 M, over 100 min operational time

due to osmosis, which increases the osmotic permeability coefficient. Furthermore, it could be due to concentration polarisation resulting from increased NaCl concentration in the membrane boundary layer (Melnikov et al., 2018). Osmotic permeability coefficients were also approximately constant for both temperatures (25°C and 50°C) after 60 minutes of operation.

A few studies have examined the influence of temperature on osmotic performance. Zhao and Zou (2011) studied the effect of temperature on membrane performance during osmosis desalination, and their results confirmed that the flux increases with increasing temperature. Kingsbury et al. (2018) investigated the water permeability coefficient of CEM (Nafion N115) using 4 M of NaCl solution; the results were 1.13×10^{-10} (m²/s). It can be concluded that the CEM membrane type (MK-40) has a low permeability to water, which results in minimising energy losses. It is noted that an increase in the overall NaCl solution concentration and an increase in distilled water temperature significantly affect osmotic permeability coefficient. Eventually, the findings showed that higher permeability of water was correlated with higher permeability of salt.

CONCLUSION

The diffusion and osmotic permeability have been successfully studied to characterize the heterogeneous cation exchange membrane (MK-40) using different concentrations of NaCl solution and distilled water temperatures. Salt concentration and water temperature were among the most important parameters affecting the diffusion and osmotic permeability of MK-40. The uncharged MK-40 membrane had low permeability to salt, which results in minimising energy losses. Nevertheless, the MK-40 membrane revealed that as the salt concentration of the external solution decreases, the diffusion permeability of the membrane increases. Since osmotic pressure is a linear function of solution concentration, osmotic water transfer increases linearly with increasing salt concentration. On the other hand, the temperature and flux time affected the diffusion and osmosis permeability of the membrane. For example, at a distilled water temperature of 50°C, the osmotic permeability coefficient of MK-40 was significantly higher than at 25°C.

ACKNOWLEDGEMENT

Authors wish to thank Tambov State Technical University-Russia for facilitating the laboratory work and Northern Technical University-Iraq for the fund.

REFERENCES

- Alekseeva, N. V., Arkhipov, A. I., & Borisov, P. A. (2012). Study of diffusive and osmotic permeability of MK-40 and MA-40 electrodialysis membranes in two-component solutions of Copper, Zinc, Nickel and Sodium salts. *Вестник ТГТУ*, 18(4), 923-927.

- Andreeva, M. A., Loza, N. V., Pis'menskaya, N. D., Dammak, L., & Larchet, C. (2020). Influence of surface modification of MK-40 membrane with polyaniline on scale formation under electro dialysis. *Membranes*, 10(7), 1-14. <https://doi.org/10.3390/membranes10070145>
- Chaabouni, A., Guesmi, F., Louati, I., Hannachi, C., & Hamrouni, B. (2015). Temperature effect on ion exchange equilibrium between CMX membrane and electrolytes solutions. *Journal of Water Reuse and Desalination*, 5(4), 535-541. <https://doi.org/10.2166/wrd.2015.008>
- Chehayeb, K. M., & Lienhard, J. H. (2019). On the electrical operation of batch electro dialysis for reduced energy consumption. *Environmental Science: Water Research & Technology*, 5(6), 1172-1182. <https://doi.org/10.1039/C9EW00097F>
- Gatapova, N. T., Dzhubari, M. K., & Alekseeva, N. V. (2020). A study of diffusion permissibility of MK-40 membrane in thermodynamic conditions. *Вестник ТГТУ*, 26(4), 619-628.
- Geise, G. M., Freeman, B. D., & Paul, D. R. (2013). Sodium chloride diffusion in sulfonated polymers for membrane applications. *Journal of Membrane Science*, 427, 186-196. <https://doi.org/10.1016/j.memsci.2012.09.029>
- Geise, G. M., Paul, D. R., & Freeman, B. D. (2014a). Fundamental water and salt transport properties of polymeric materials. *Progress in Polymer Science*, 39(1), 1-42. <https://doi.org/10.1016/j.progpolymsci.2013.07.001>
- Geise, G. M., Cassidy, H. J., Paul, D. R., Logan, B. E., & Hickner, M. A. (2014b). Specific ion effects on membrane potential and the permselectivity of ion exchange membranes. *Physical Chemistry Chemical Physics*, 16(39), 21673-21681. <https://doi.org/10.1039/C4CP03076A>
- Gubari, M. Q., Zwain, H. M., Alekseeva, N. V. & Baziyani, G. I. (2021). Features of feed concentration and temperature effects on membranes operation in electro dialysis systems – A review. *Journal of Physics: Conference Series*, 1973(1), 012178.
- Gubari, M. Q., Zwain, H. M., Al-Zahiwat, M. M., & Alekseeva, N. V. (2021). Characteristics of the MK-40 and MA-40 membranes for industrial wastewater treatment - A review. *Ecological Engineering & Environmental Technology*, 22(1), 39-50. <https://doi.org/10.12912/27197050/132095>
- Guesmi, F., Hannachi, C., & Hamrouni, B. (2010). Effect of temperature on ion exchange equilibrium between AMX membrane and binary systems of Cl⁻, NO₃⁻ and SO₄²⁻ ions. *Desalination and Water Treatment*, 23(1-3), 32-38. <https://doi.org/10.5004/dwt.2010.1837>
- Kamcev, J., Paul, D. R., Manning, G. S., & Freeman, B. D. (2018). Ion diffusion coefficients in ion exchange membranes: Significance of counterion condensation. *Macromolecules*, 51(15), 5519-5529. <https://doi.org/10.1021/acs.macromol.8b00645>
- Karimi, L., & Ghassemi, A. (2016). How operational parameters and membrane characteristics affect the performance of electro dialysis reversal desalination systems: The state of the art. *Journal of Membrane Science and Research*, 2(3), 111-117. <https://doi.org/10.22079/JMSR.2016.20309>
- Kingsbury, R. S., Bruning, K., Zhu, S., Flotron, S., Miller, C. T., & Coronell, O. (2019). Influence of water uptake, charge, manning parameter, and contact angle on water and salt transport in commercial ion exchange membranes. *Industrial & Engineering Chemistry Research*, 58(40), 18663-18674. <https://doi.org/10.1021/acs.iecr.9b04113>

- Kingsbury, R. S., Zhu, S., Flotron, S., & Coronell, O. (2018). Microstructure determines water and salt permeation in commercial ion-exchange membranes. *ACS Applied Materials & Interfaces*, *10*(46), 39745-39756. <https://doi.org/10.1021/acsami.8b14494>
- Luo, J., Wu, C., Wu, Y., & Xu, T. (2010). Diffusion dialysis of hydrochloride acid at different temperatures using PPO-SiO₂ hybrid anion exchange membranes. *Journal of Membrane Science*, *347*(1-2), 240-249. <https://doi.org/10.1016/j.memsci.2009.10.029>
- Melnikov, S., Kolot, D., Nosova, E., & Zabolotskiy, V. (2018). Peculiarities of transport-structural parameters of ion-exchange membranes in solutions containing anions of carboxylic acids. *Journal of Membrane Science*, *557*, 1-12. <https://doi.org/10.1016/j.memsci.2018.04.017>
- Mikhaylin, S., & Bazinet, L. (2016). Fouling on ion-exchange membranes: Classification, characterization and strategies of prevention and control. *Advances in Colloid and Interface Science*, *229*, 34-56. <https://doi.org/10.1016/j.cis.2015.12.006>
- Nikonenko, V., Nebavsky, A., Mareev, S., Kovalenko, A., Urtenov, M., & Pourcelly, G. (2019). Modelling of ion transport in electromembrane systems: Impacts of membrane bulk and surface heterogeneity. *Applied Sciences*, *9*(1), Article 25. <https://doi.org/10.3390/app9010025>
- Pismenskaya, N., Melnik, N., Nevakshenova, E., Nebavskaya, K., & Nikonenko, V. (2012). Enhancing ion transfer in overlimiting electro dialysis of dilute solutions by modifying the surface of heterogeneous ion-exchange membranes. *International Journal of Chemical Engineering*, *2012*, Article 528290. <https://doi.org/10.1155/2012/528290>
- Sarapulova, V., Shkorkina, I., Mareev, S., Pismenskaya, N., Kononenko, N., Larchet, C., Dammak, L., & Nikonenko, V. (2019). Transport characteristics of Fujifilm ion-exchange membranes as compared to homogeneous membranes AMX and CMX and to heterogeneous membranes MK-40 and MA-41. *Membranes*, *9*(7), Article 84. <https://doi.org/10.3390/membranes9070084>
- Tanaka, Y. (2011). Ion-exchange membrane electro dialysis for saline water desalination and its application to seawater concentration. *Industrial & Engineering Chemistry Research*, *50*(12), 7494-7503. <https://doi.org/10.1021/ie102386d>
- Vasil'eva, V. I., Akberova, E. M., Zhiltsova, A. V., Chernykh, E. I., Sirota, E. A., & Agapov, B. L. (2013). SEM diagnostics of the surface of MK-40 and MA-40 heterogeneous ion-exchange membranes in the swollen state after thermal treatment. *Journal of Surface Investigation. X-ray, Synchrotron and Neutron Techniques*, *7*, 833-840. <https://doi.org/10.1134/S1027451013050194>
- Zhao, S., & Zou, L. (2011). Effects of working temperature on separation performance, membrane scaling and cleaning in forward osmosis desalination. *Desalination*, *278*(1-3), 157-164. <https://doi.org/10.1016/j.desal.2011.05.018>



The Prediction of Chlorophyll Content in African Leaves (*Vernonia amygdalina Del.*) Using *Flatbed Scanner* and Optimised Artificial Neural Network

Retno Damayanti*, Nurul Rachma, Dimas Firmanda Al Riza and Yusuf Hendrawan

Department of Agricultural Engineering and Biosystem, Faculty of Agricultural Technology, Universitas Brawijaya, Jl. Veteran, Malang, East Java, 65145 Indonesia

ABSTRACT

African leaves (*Vernonia amygdalina Del.*) is a nutrient-rich plant that has been widely used as a herbal plant. African leaves contain chlorophyll which identify compounds produced by a plant, such as flavonoids and phenols. Chlorophyll testing can be carried out non-destructively by using the SPAD 502 chlorophyll meter. However, it is quite expensive, so that another non-destructive method is developed, namely digital image analysis. Relationships between chlorophyll content and leaf image colour indices in the RGB, HSV, HSL, and Lab* space are examined. The objectives of this study are 1) to analyse the relationship between texture parameters of red, green, blue, grey, hue, saturation(HSL), lightness (HSL), saturation(HSV), value(HSV), L*, a*, and b* against the chlorophyll content in African leaves using a flatbed scanner (HP DeskJet 2130 Series); and 2) built a model to predict chlorophyll content in African leaves using optimised ANN through a feature selection process by using several filter methods. The best ANN topologies are 10-30-40-1 (10 input nodes, 40 nodes in hidden layer 1, 30 nodes in hidden layer 2, and 1 output node) with a trainlm on the learning function, tansig on the hidden layer, and purelin on the output layer. The selected topology produces MSE training of 0.0007 with

R training 0.9981 and the lowest validation MSE of 0.012 with R validation of 0.967. With these results, it can be concluded that the ANN model can be potentially used as a model for predicting chlorophyll content in African leaves.

ARTICLE INFO

Article history:

Received: 01 April 2021

Accepted: 12 July 2021

Published: 08 October 2021

DOI: <https://doi.org/10.47836/pjst.29.4.15>

E-mail addresses:

damayanti@ub.ac.id (Retno Damayanti)

nrlrachma@student.ub.ac.id (Nurul Rachma)

dimasfirmanda@ub.ac.id (Dimas Firmanda Al Riza)

yusufhendrawan@gmail.com (Yusuf Hendrawan)

* Corresponding author

Keywords: African leaves, artificial neural network, chlorophyll, flatbed scanner

INTRODUCTION

African leaves (*Vernonia amygdalina*) is a medicinal plant and belongs to the Asteraceae family. African leaf is also called bitter leaf since it has a bitter smell and taste (Danladi et al., 2018). African leaf can grow to a height of more than 10 m with a stem diameter of 40 cm, and its bark will be grey to brown. The leaves are green, elliptical in shape, about 4-15 × 1-4 cm in size, 0.2-4 cm long petiole, and serrated at the edges. The cultivation of African leaves is usually carried out through stem cuttings from the parent plants that are more than one year old (Nursuhaili et al., 2019). As a medicinal plant, African leaves are widely used as an antifeedant, antischistosomal, antiplasmodial, antioxidant, anti-inflammatory, antidiabetic and anticancer drug (Oyeyemi et al., 2017). Chlorophyll is a green leafy substance in plants that absorb and convert light energy into chemical energy (Pavlovic et al., 2014). Chlorophyll absorbs light, especially red and blue, from the visible light spectrum (Luimstra et al., 2018). Green colour (around 550 nm) is not absorbed but is reflected to give chlorophyll a special colour (Rajalakshmi & Narasimhan, 2013).

The results of the previous research stated that chlorophyll content and leaf ageing levels could be used to identify the content of compounds produced by plants, including flavonoids, phenols (Abdulkadir et al., 2015), nitrogen (Cartelat et al., 2005), and can be used as a parameter for the quality of green vegetables during storage (Limantara et al., 2015). Common chlorophyll conventional testing is conducted by extracting a chlorophyll before it then measures by UV-VIS spectrophotometry. Besides than that, utilising a chlorophyll meter is another method to measure chlorophyll content (Uddling et al., 2007). Chlorophyll meter measures transmitted light of the leaves at 650 nm and 940 nm then processes it, using a microprocessor, to measure the amount of chlorophyll content (Borhan et al., 2017). Even though several conventional chlorophyll testing has shown a proven result, there are several drawbacks such as being destructive, requires a lengthy process and being costly. Therefore, to overcome these issues, this research proposes another method that is non-destructive, rapid and cheaper computer vision assessment; this includes colour and texture analysis (Hendrawan et al., 2019a). Digital colour analysis for plant leaf colour has become an increasingly popular and effective method for evaluating foliar nutrition and health in response to environmental stresses (Hu et al., 2010). In this study, the computer vision approach uses a flatbed scanner for image acquisition. The machine vision method is very effective because it will not destruct the object. A flatbed scanner is considered fast, assessable on the market, cheap, and not dependent on external light conditions (Dalen, 2006). The flatbed scanner has recently been widely used for image analysis purposes, including rice classification (Dalen, 2006), leaf surface area estimation (Kaur et al., 2014), prediction of chlorophyll content in potato plants (Yadav et al., 2010), and testing the purity of rice seeds (Widiastuti et al., 2018).

Detecting green leaves in a natural environment is more difficult since the leaves are similar to the background in colour. Leaf colour is a good indicator of plant health, and it

can be used to predict the leaf's chlorophyll. The chlorophyll can be predicted by analysing the distribution of colour components [Red (R), Green (G), Blue (B), Hue(H), Saturation (S), and Intensity (I)] of the leaf images. Texture analysis using the grey level co-occurrence matrix (GLCM) method is dominant at the grey level, The GLCM method is developed on colour images, known as the colour co-occurrence matrix (CCM) method. Based on the research of (Hendrawan et al., 2019b), colour texture analysis (CCM) provides additional image characteristics above the grey level representation (GLCM). It has been proven to measure biological objects effectively. Artificial neural network (ANN) modelling with the backpropagation (BP) learning algorithm is utilised in applying this method. The BP algorithm is a simple iterative learning algorithm that works well on complex data. During the training, weights are arranged iteratively to minimise errors (Setti & Anjar, 2018). Image analysis and the ANN method have now been widely applied to identify chlorophyll. Grunenfelder et al. (2006) used colour indices to assess the chlorophyll development and greening of fresh market potatoes. Barman and Choudhury (In Press) analyse the distribution of colour to predict the chlorophyll of citrus leaf. Hassanijalilian et al. (2020) estimate chlorophyll of soybean leaves infield with smartphone digital imaging and machine learning. Mohan and Gupta (2019) predict chlorophyll content on rice and obtained more efficient results than using linear regression models Samli et al. (2014) applied ANN to predict chlorophyll concentrations *a*, Gupta and Pattanayak (2017) used ANN to project chlorophyll content in potato plants non-invasively, Damayanti et al. (2020) predicted chlorophyll content in cassava leaves using ANN, and also Peng and Yi (2019) which has predicted chlorophyll content in pomegranate leaves based on digital image analysis and ANN.

However, there is no research identification a chlorophyll African leave by using machine vision yet. This study aims to: 1) analyse the relationship between the texture of the feature of red, green, blue, grey, hue, saturation_(HSL), lightness_(HSL), saturation_(HSV), value_(HSV), L*, a*, and b* on the chlorophyll content of African leaves using a flatbed scanner (HP DeskJet 2130 Series); and 2) develop a model to predict chlorophyll content in African leaves using ANN which has been optimised through the feature selection process by using multiple filter methods.

MATERIAL AND METHODS

In order to process the data, Lenovo Z40-72 Laptop was utilised with AMD A10-7300 processor specifications (1.9 GHz/Turbo 3.2 GHz) and 4 GB DDR3 @ 1600 MHz memory capacity; flatbed scanner of HP DeskJet 2130 series to acquire digital image imagery; chlorophyll meter SPAD 502 with a measuring area of 2×3 mm and a maximum sample thickness of 1.2 mm for *real-time* measurement of chlorophyll content of leaves as comparative data; Paint Microsoft software to convert image formats to bitmap (BMP)

and to change image resolution; self-built software based on Visual Basic 6.0 (Microsoft) for image feature extraction; Waikato Environment for Knowledge Analysis (WEKA 3.8) software for the feature selection process; and Matlab R2014a software for the ANN design process. African leaves, as samples, were obtained from the Merjosari area, Lowokwaru District, Malang City, East Java, Indonesia. The difference in leaf colour texture is a parameter to determine chlorophyll content. This study's leaf colour texture difference can be categorised into three parts: 1) the shoot, 2) the middle, and 3) the base. 3 to 4 leaves from the top and bottom of the plant were taken, while the middle leaves were taken from the leaves between the top and bottom of the plant. Twenty leaves were taken for each category, so that there are 60 African leaves were needed in this study.

The real-time measurement, using SPAD 502 chlorofilmeter, is considered for comparative study. The leaves are clipped to SPAD 502 chlorofilmeter, and the sensor will provide a chlorophyll content index (CCI) to detect chlorophyll. Simultaneously, chlorophyll measurement is done after image data acquisition by flatbed scanner HP DeskJet 2130 series. This scanner uses a CIS sensor (CMOS Image Sensor) which bring more benefits such as requires low power and voltage, gives low price and provides detail image because of its smaller pixel size (Shakeri et al., 2012). The flatbed scanner is considered assessable on the market, easy to use, stable when acquiring images and does not depend on external light conditions (Widiastuti et al., 2018) and low cost. The acquired image is saved in bitmap format. The data augmentation process was carried out on 60 images. Data augmentation is one of the processes in image processing to increase the number of samples and improve modelling performance (Shorten & Taghi, 2019). Various augmentation techniques include cutting (*cropping*), rotation, illumination, scaling and colouring (Okafor et al., 2018). In this study, the cutting and rotating images technique of African leaves were used. A total of 60 images that have been acquired were then divided into two parts by using Paint software with an image resolution of 300×300 pixels comprising 120 images of African leaves (Figure 1). Furthermore, the rotation process (at an angle of 0°, 90°, 180° and 270°) from 120 pictures was conducted (Figure 2), providing 480 total images.

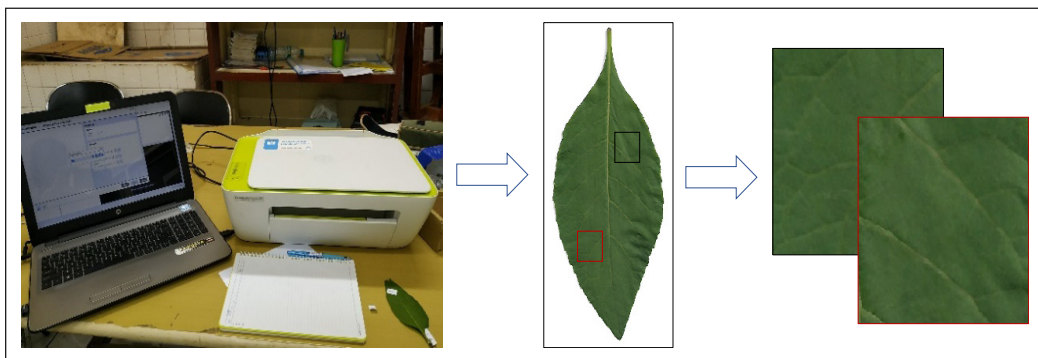


Figure 1. Image acquisition and augmentation process of cutting images of African leaves

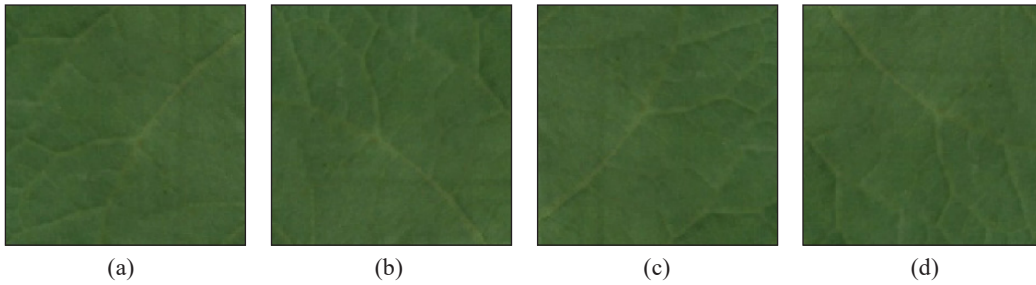


Figure 2. The results of rotating augmentation of African leaf image images on rotation: (a) 0°, (b) 90°, (c) 180°, (d) 270°

The value of the textural features of the acquired image saved in bitmap format will then be extracted. Colour texture analysis is an important method in computer vision that can be used for object recognition, surface defect detection, or pattern recognition (Armi & Shervan, 2019). The results of texture feature extraction are entropy, energy, contrast, homogeneity, sum mean, variance, correlation, maximum probability, inverse difference moment and cluster tendency on each colour-space which includes red, green, blue, grey, hue, saturation_(HSL), lightness_(HSL), saturation_(HSV), value_(HSV), L*, a* and b* (Hendrawan et al., 2018). The ten texture features used in this study are based on Harlick (Haralick et al., 1973) texture Equations 1-10 (Hendrawan & Haruhiko, 2009):

$$Entropy = - \sum_i^M \sum_j^N P [i, j] \log P [i, j] \quad (1)$$

$$Energy = \sum_i^M \sum_j^N P^2 [i, j] \quad (2)$$

$$Contrast = \sum_i^M \sum_j^N (i - j)^2 P [i, j] \quad (3)$$

$$Homogeneity = \sum_i^M \sum_j^N \frac{P [i, j]}{1 + |i - j|} \quad (4)$$

$$Sum\ Mean = \frac{1}{2} \sum_i^M \sum_j^N (iP [i, j] + jP [i, j]) \quad (5)$$

$$Variance = \frac{1}{2} \sum_i^M \sum_j^N ((i - \mu)^2 P [i, j] + (j - \mu)^2 P [i, j]) \quad (6)$$

$$Correlation = \sum_i^M \sum_j^N \frac{(i - \mu)(j - \mu)P [i, j]}{\sigma^2} \quad (7)$$

$$Inverse\ Difference\ Moment = \sum_i^M \sum_j^N \frac{P [i, j]}{|j - k|^k} \quad i \neq j \quad (8)$$

$$Cluster\ Tendency = \sum_i^M \sum_j^N (i + j - 2\mu)^k P [i, j] \quad (9)$$

$$Maximum\ Probability = Max_{i, j}^{M, N} P [i, j] \quad (10)$$

Where: $P_{(i, j)}$ is the element of (i, j) normalised *co-occurrence matrix*, μ and σ are *mean* and the *standard deviation* of pixel elements are as in Equations 11-13:

$$P[i, j] = \frac{N(i, j)}{M} \quad (11)$$

$$\mu = \sum_i^M i \sum_j^N P[i, j] \quad (12)$$

$$\sigma = \sum_i^M (i - \mu)^2 \sum_j^N P[i, j] \quad (13)$$

Where: $N_{(i,j)}$ is the amount calculated in the image with the pixel intensity i followed by the pixel intensity j at a displacement of one pixel to the left, and M is the total number of pixels.

The definition of texture features (Hendrawan et al., 2019b) are as follows: entropy measures the randomness of the grey level distribution; *energy* measures the number of repeated pairs or measures the level of texture uniformity; contrast measures the local contrast in the image; homogeneity measures the local homogeneity of a pixel pair; sum mean calculates the average grey level of a colour image; variance shows the distribution of the grey level distribution; correlation shows the correlation between two pixels in a pixel pair; different inverse moment shows the refinement of the image; cluster tendency measures the grouping of images that has similar grey levels, and maximum probability is the result of the most dominant pixel pair in the image.

From the feature extraction process, 120 texture features were obtained consisting of 10 texture features for red, green, blue, grey, hue, saturation_(HSL), saturation_(HSV), value, lightness, L^* , a^* and b^* then sorted from 1 to 120 orderly. Next, feature selection (a preprocessing image data) using WEKA 3.8 to select ANN input. These methods will delete outliers and chose highly important data features to fit the requirement of the learning function (Garner, 1995). In this research, feature selection uses the filter method consisting of Chi-Squared Attribute Evaluator, Correlation Attribute Evaluator, ReliefF Attribute Evaluator and Gain Attribute Evaluator. Feature selection is considered an effective and efficient procedure for optimising data mining and machine learning. The purpose of feature selection is to reduce irrelevant, redundant, and noise features to get better learning performance, produce higher accuracy and produce a simpler model (Wang et al., 2016). The method does not rely on learning algorithms and data characteristics, and this is not affected by other features but solely based on rank (Li et al., 2017). The output from feature selection was then used as ANN input to produce the model.

Network topology was the design, and the lowest mean square error (MSE) validation data was set. Four hundred eighty digital images were divided into 75% (360 images) and 25% (120 images) for training data and validation data, respectively, to prevent overfitting (Xu & Royston, 2018). Input data, taken from feature selection, were then modelled using ANN (Matlab R2014a) to predict the chlorophyll content of African leaves. However, after feature selection performing another preprocessing data, in this case, was normalisation, is important to standardise the data scale. The input and output data were switched on a scale of -1 to +1 to avoid a significant weight change during the ANN training process.

Sensitivity analysis was carried out by using variations of the learning rate, momentum, the number of nodes on the hidden layer and the number of hidden layers. This study used 10 types of learning functions to obtain a suitable learning function to predict the chlorophyll content of African leaves.

RESULTS AND DISCUSSION

Based on the measurement of chlorophyll content, the difference of each leaf colour texture reflected its chlorophyll content (Figure 3). Chlorophyll content contributed to the greenish level of the leaf, meaning that the denser the green colour, the more chlorophyll on the leaf. On the contrary, pale green or yellowish-green leaves expressed low chlorophyll content. Therefore, this parameter was important to measure chlorophyll content using computer vision (Barman et al., 2018). Based on Figure 4, it can be seen that the increase chlorophyll content follows the increase of difference in leaf colour. The average chlorophyll content in (1) leaves' shoot was 41.2 CCI; (2) the middle part of the leaves was 46.3 CCI; and (3) leaves' base was 51.2 CCI. Therefore, the insignificant green colour difference on African leaves was equated to the low level of chlorophyll interval. According to Pavlovic et al. (2014), changes in chlorophyll content can be influenced by several factors, including physiological, morphological (age and position of leaves) and abiotic (temperature, relative humidity, and light quality) factors.

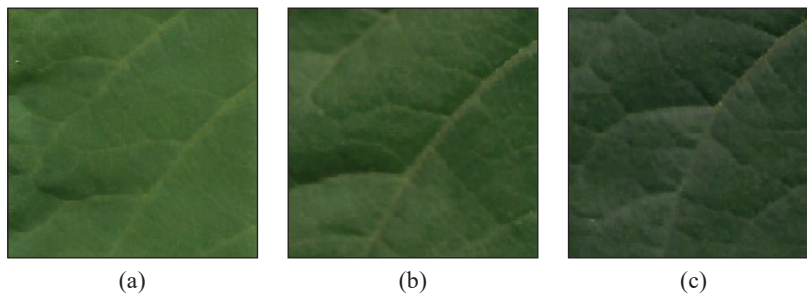


Figure 3. The results of image acquisition of African leaf images: (a) the shoot, (b) the middle, (c) the base

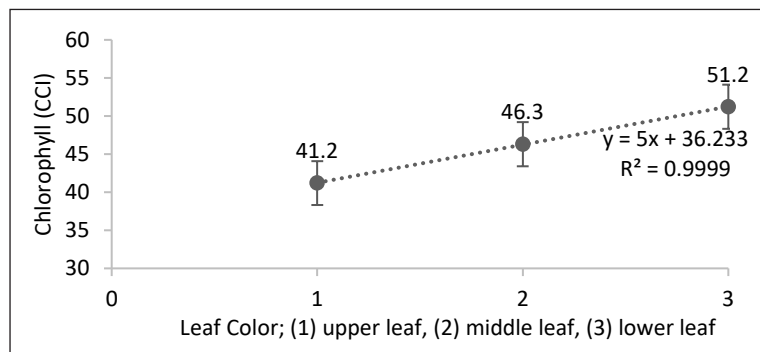


Figure 4. Graph of the relationship between chlorophyll content and leaf colour texture category

The augmented image data was then proceeded to feature extraction, and the results were 120 textural features. However, only selected textural features with the filter method proposed a fast, efficient and non-dependent learning algorithm to predict chlorophyll content in African leaves (Kumar & Rama, 2014; Mendoza et al., 2018). This study utilised the filter method based on four evaluation attributes: chi-squared attribute evaluator, correlation attribute evaluator, ReliefF attribute evaluator, and gains attribute evaluator. The top 10 best feature for each evaluation attribute was chosen. Table 1 shows the feature selection for each evaluation attribute used. Table 1 illustrates $b^*_{(Lab)}$ Energy with the evaluation attribute ReliefF has a strong correlation to chlorophyll content in African leaves with weight accounting for 0.3431. After obtaining the weight and ranking for each feature, the features selected in Table 1 were modelled using ANN using the trial and error method to define the best combination of features-subset which later for chlorophyll prediction; the lowest validation MSE was also considered as a robust model. Trial and error on ANN modelling on preliminary research generated the best ANN topology, consisting of 30 nodes on the first hidden layer, 40 nodes on the second hidden layer, with the learning function of trainlm, tansig activation function in each hidden layer, and purelin on the output layer; learning rate 0.1; and momentum 0.5 (Hendrawan et al., 2019c). Table 2 shows that the entire 120 texture features configuration created higher validation MSE compare with feature selection. Compare with three other evaluation attribute (Table 2), ReliefF produces the lowest validation MSE using 10 ANN input was 0.0025. The highest validation MSE is in the evaluation attribute Gain Ratio with 2 ANN input was 0.7469. Therefore, feature selection was important to optimise the performance of the ANN model. Based on these results, 10 textural features in the evaluation attribute ReliefF were used as input of ANN modelling to predict chlorophyll content in African leaves. Moreover, ReliefF gives more benefits such as dealing with nominal or continuous features, handling lost data and tolerating noise (Mendoza et al., 2018).

From the trial and error results on the feature selection process (Table 2), we obtain the best combination of 10 textural features that have a high correlation against the chlorophyll content of African leaves. The ten textural features include b^* energy, b^* correlation, b^* entropy, $\text{saturation}_{(HSV)}$ sum mean, $\text{saturation}_{(HSL)}$ sum mean, blue sum mean, sum mean hue, maximum hue probability, correlation hue, and red correlation. Figure 5a shows the relationship of chlorophyll content to b^* energy. The results stated that the value of b^* energy decrease with the increase in chlorophyll content. Another thing, the low b^* energy value indicated that the uniformity of texture on African leaves was also low. Figure 5a also tells that the value of b^* energy has a negative correlation with a determination coefficient of 0.0297. As for the relationship of chlorophyll content to the b^* correlation (Figure 5b), b^* correlation increase with the increase of chlorophyll content, the increase of b^* correlation showed that the correlation among pixels on African leaves was high.

Table 1
Result of feature selection using the filter method

No.	Attribute Evaluator	Search Method	Textural features	Weight	Rank
1.	<i>Chi-Squared Attribute Evaluator</i>	<i>Ranker</i>	b* Energy	1568.4034	1
			b* Entropy	1040.8304	2
			b* Correlation	1004.3086	3
			Saturation _(HSV) Energy	558.246	4
			Hue Energy	496.8733	5
			Hue Entropy	476.624	6
			a* Entropy	388.9211	7
			a* Energy	373.5219	8
			Saturation _(HSV) Sum Mean	373.3694	9
			a* Maximum Probability	354.2468	10
2.	<i>Correlation Attribute Evaluator</i>	<i>Ranker</i>	b* Energy	0.1554	1
			b* Entropy	0.1187	2
			Hue Entropy	0.0881	3
			b* Inverse	0.0862	4
			Saturation _(HSV) Sum Mean	0.0857	5
			Hue Energy	0.0827	6
			b* Correlation	0.0822	7
			a* Maximum Probability	0.0777	8
			Red Entropy	0.0762	9
			Red Maximum Probability	0.076	10
3.	<i>ReliefF Attribute Evaluator</i>	<i>Ranker</i>	b* Energy	0.3431	1
			b* Correlation	0.2717	2
			b* Entropy	0.2643	3
			Saturation _(HSV) Sum Mean	0.2543	4
			Saturation _(HSL) Sum Mean	0.2205	5
			Blue Sum Mean	0.211	6
			Hue Sum Mean	0.2055	7
			Maximum hue probability	0.205	8
			Hue Correlation	0.2026	9
			Red Correlation	0.2007	10
4.	<i>Gain Ratio Attribute Evaluator</i>	<i>Ranker</i>	b* Energy	0.4125	1
			b* Entropy	0.319	2
			b* Correlation	0.2209	3
			Hue Entropy	0.1669	4
			Saturation _(HSV) Sum Mean	0.1604	5
			Blue Maximum Probability	0.1571	6
			b* Inverse	0.1559	7
			Hue Energy	0.1534	8
			Red Maximum Probability	0.1483	9
			Saturation _(HSV) Energy	0.1453	10

Table 2
Trial and error ANN performance using textural feature selection

No.	Attribute Evaluator	Search Method	Input	MSE training	MSE validation
1.	-	-	All features (120 inputs)	0.0094	0.5193
2.	Chi-Squared Attribute Evaluator	Ranker	Feature rank 1-2	0.0097	0.7465
			Feature rank 1-3	0.0097	0.0818
			Feature rank 1-4	0.0093	0.0174
			Feature rank 1-5	0.0089	0.0136
			Feature rank 1-6	0.0063	0.0121
			Feature rank 1-7	0.0098	0.0149
			Feature rank 1-8	0.0058	0.0117
			Feature rank 1-9	0.0060	0.0076
			Feature rank 1-10	0.0033	0.0046
			3.	Correlation Attribute Evaluator	Ranker
Feature rank 1-3	0.0098	0.0063			
Feature rank 1-4	0.0099	0.1236			
Feature rank 1-5	0.0090	0.0254			
Feature rank 1-6	0.0066	0.0237			
Feature rank 1-7	0.0055	0.0249			
Feature rank 1-8	0.0090	0.0165			
Feature rank 1-9	0.0094	0.0166			
Feature rank 1-10	0.0092	0.0166			
4.	ReliefF Attribute Evaluator	Ranker			
			Feature rank 1-3	0.0098	0.0624
			Feature rank 1-4	0.0090	0.0172
			Feature rank 1-5	0.0081	0.0159
			Feature rank 1-6	0.0099	0.0125
			Feature rank 1-7	0.0016	0.0026
			Feature rank 1-8	0.0083	0.0092
			Feature rank 1-9	0.0099	0.0108
			Feature rank 1-10	0.0015	0.0025
			5.	Gain Ratio Attribute Evaluator	Ranker
Feature rank 1-3	0.0097	0.0818			
Feature rank 1-4	0.0099	0.0217			
Feature rank 1-5	0.0091	0.0160			
Feature rank 1-6	0.0064	0.0099			
Feature rank 1-7	0.0088	0.0225			
Feature rank 1-8	0.0077	0.0211			
Feature rank 1-9	0.0092	0.0265			
Feature rank 1-10	0.0069	0.0220			

Moreover, b^* correlation has a positive correlation with a coefficient of determination of 0.1593. When it comes to the relationship between b^* entropy and chlorophyll (Figure 5c), b^* entropy increases with the increase of chlorophyll content. The higher b^* entropy value indicated that the roughness of the texture of the African leaves was high. From Figure 5c, it can also be seen that b^* entropy has a positive correlation with a determination coefficient of 0.0332.

In Figure 5d, it can be seen that the relationship of chlorophyll content to sum mean saturation_(HSV). The results showed that the sum mean saturation_(HSV) decrease with the increased chlorophyll content, the decreasing sum mean saturation_(HSV) shows that the level of grey saturation_(HSV) in African leaves was low. From Figure 5d, it can also be seen that sum mean saturation_(HSV) has a negative correlation with a determination coefficient of 0.3449.

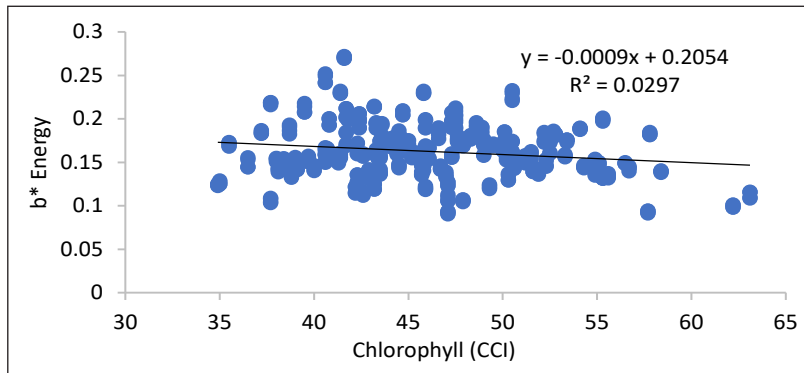
In Figure 5e, it can be seen the relationship of chlorophyll content to sum mean saturation_(HSL). The results showed that the sum mean saturation_(HSL) decreased with the increase in chlorophyll content. The decreasing sum mean saturation_(HSL) indicates that the saturation_(HSL) of the grey level of African leaves is low. From Figure 5e, it can also be seen that sum mean saturation_(HSL) has a negative correlation with a determination coefficient of 0.3376.

In Figure 5f, it can be seen the relationship of chlorophyll content to blue sum mean. The results showed that the value of the sum mean blue decreased with the increase in chlorophyll content. Decreasing the blue_(RGB) sum mean indicates that the level of blue in African leaves is low. From Figure 5f, it can also be seen that the blue sum mean has a negative correlation with a determination coefficient of 0.208.

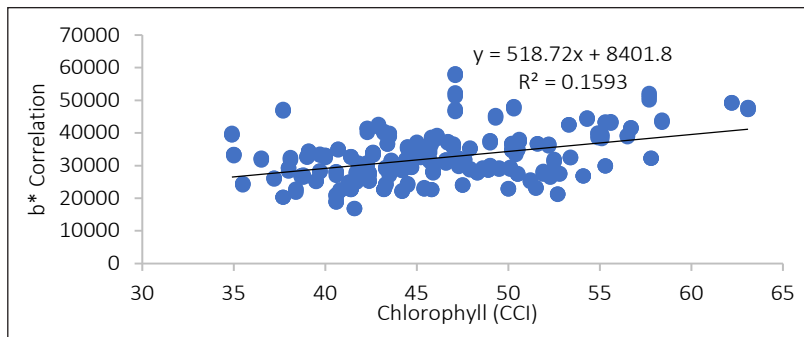
Figure 5g, it can be seen the relationship of chlorophyll content to hue sum mean. The results showed that the hue sum mean value decrease with the increase in chlorophyll content. The decrease of the hue sum mean showed that the grey level of hue on African leaves is low. From Figure 5g, it can also be seen that the hue sum mean has a negative correlation with a determination coefficient of 0.0557.

In Figure 5h, it can be seen the relationship of chlorophyll content to the maximum hue probability. The results show that the maximum hue probability value decreases with the increase in chlorophyll content. The decrease of maximum hue probability value indicated that the dominant hue pixel pair is getting lower or irregular on African leaves. In Figure 5h, it can also be seen that the maximum hue probability has a negative correlation with a coefficient of determination of 0.1022. In Figure 5i, it can be seen the relationship of chlorophyll content to hue correlation. The results showed that the value of hue correlation increased with the increase in chlorophyll content. The increase of hue correlation showed that the correlation between hue on African leaves was high. From Figure 5i, it can also be seen that the hue correlation has a positive correlation with a determination coefficient of 0.1648.

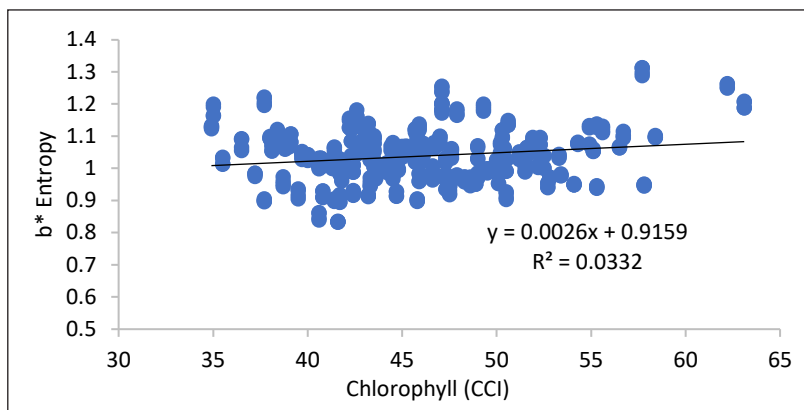
In Figure 5j, it can be seen the relationship of chlorophyll content to red correlation. The results showed that the red correlation value increase with the increase in chlorophyll content. The increasing red correlation value showed that the correlation between red on African leaves was high. Hendrawan and Murase (2009) have stated that during the photosynthesis process, plants absorb red wavelengths to reflect more green wavelengths.



(a)

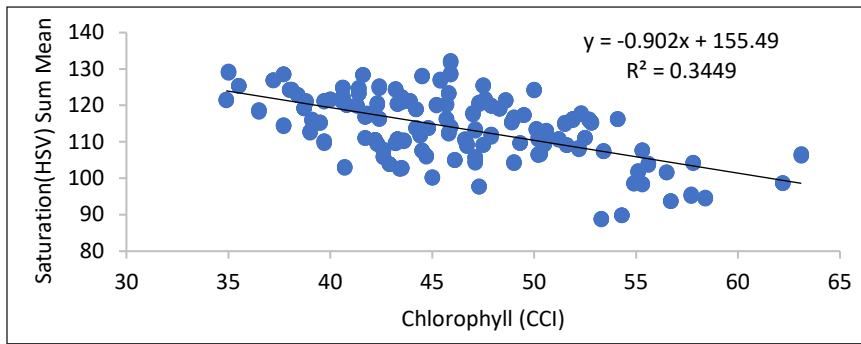


(b)

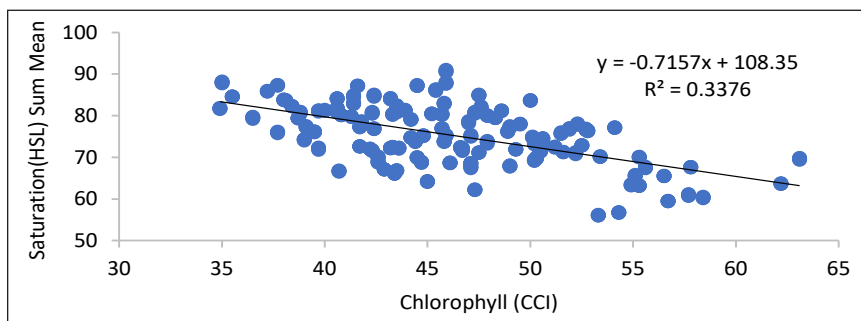


(c)

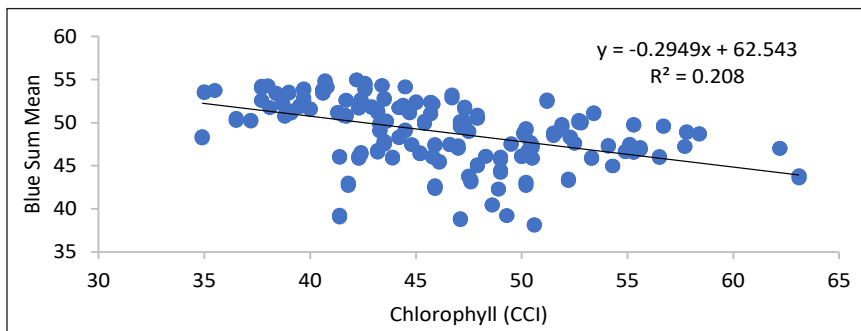
Figure 5. The relationship between chlorophyll content on the 10 best textural features: (a) b* energy, (b) b* correlation, and (c) b* entropy,



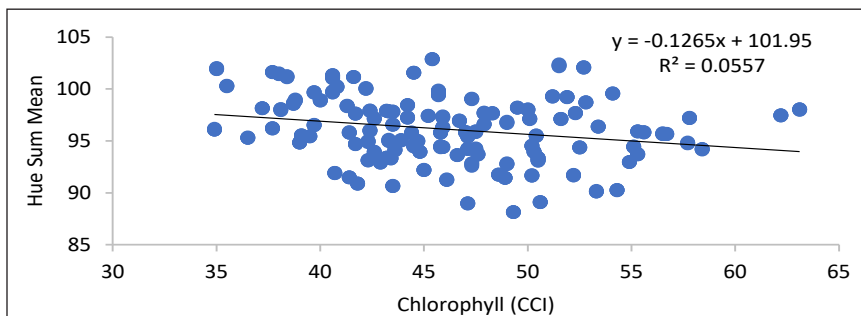
(d)



(e)

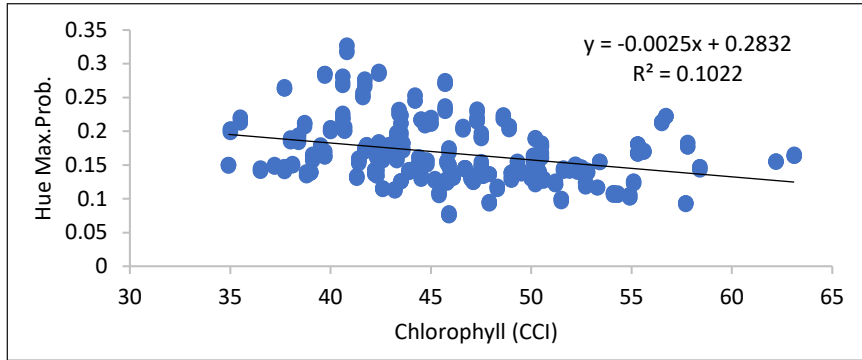


(f)

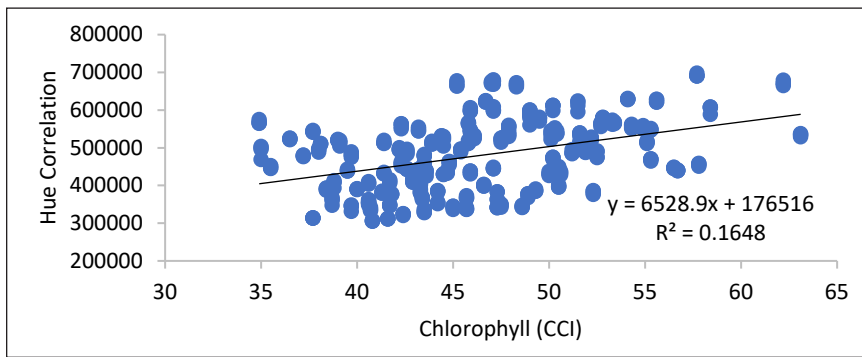


(g)

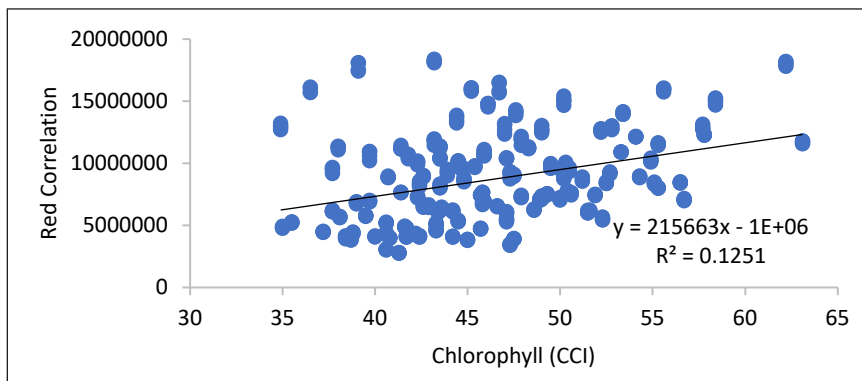
Figure 5. (continue) The relationship between chlorophyll content on the 10 best textural features: (d) saturation_(HSV) sum mean and (e) saturation_(HSL) sum mean, (f) blue sum mean, and (g) hue sum mean



(h)



(i)



(j)

Figure 5. (continue) The relationship between chlorophyll content on the 10 best textural features: (h) maximum hue probability, (i) hue correlation, and (j) red correlation.

Thus, the more red is absorbed, the higher the green colour is formed. From Figure 5j, it can also be seen that the red correlation has a positive correlation with a determination coefficient of 0.1251. Based on the linearity of the relationship between chlorophyll content on textural features, the resulting coefficient of determination is low.

In Table 3, it can be seen that the trial and error results on the learning function. Table 3 shows that trainlm (Lavenberg-Marquardt) is more accurate than other learning functions with the smallest MSE validation, which was 0.0032, and the largest validation R was 0.9925. Trainlm updates weights and biases based on Jacobian Matrix calculations. Trainlm is a simpler and more efficient learning function because the solution to matrix equations is a built-in function. The next sensitivity analysis process is the selection of activation function.

Table 3
Trial and error on the learning function selection

No.	Learning Function	R Training	R Validation	MSE Training	MSE Validation
1	Traincgb (Conjugate Gradient BP with Powell – Beale Restart)	0.9719	0.9716	0.0096	0.0099
2	Traincgf (Conjugate BP with Fletcher Reeves Update)	0.9711	0.9704	0.0099	0.0103
3	Traincgp (Conjugate Gradient BP with Polak Ribiere Update)	0.9709	0.9706	0.0100	0.0104
4	Traingd (Gradient Descent BP)	0.9794	0.9781	0.0100	0.0114
5	Traingda (Gradient Descent with Adaptive Learning Rate BP)	0.9708	0.9699	0.0100	0.0106
6	Traingdm (Gradient Descent with momentum Adaptive Learning)	0.9709	0.9702	0.0100	0.0103
7	Traingdx (Gradient Descent with Momementum Adaptive Learning)	0.9707	0.9698	0.0100	0.0105
8	Trainlm (Lavenberg Marquadt BP)	0.9934	0.9925	0.0034	0.0032
9	Trainoss (One Step Secant BP)	0.9708	0.9700	0.0100	0.0104
10	Trainrp (Resilient BP)	0.9712	0.9672	0.0098	0.0113
11	Trainscg (Scaled Conjugate Gradient BP)	0.9708	0.9708	0.0100	0.0101

The activation function is a function used to determine the output based on the input. In the ANN-BP algorithm, three common activation functions are the purelin function (linear), logsig (binary sigmoid) function, and tansig (bipolar sigmoid) function. Thus, the activation function can significantly improve the performance of ANN modelling. In trial and error, the activation function is randomly paired to obtain the lowest validation MSE.

In Table 4, the selection of activation function can be known by learning function using trainlm. Common activation functions were tansig and logsig for the hidden layer and purelin for the output layer. Moreover, this statement is in line with the result of the research, where tansig and purelin was chosen for hidden layers and output layer, respectively. It provided the lowest validation MSE (0.0032) and the highest validation R (0.9925). A study from Jaber et al. (2019) stated that the configuration of tansig and purelin resulted in the decrease of MSE training and validation equates with the increase

in epoch with the best performance on epoch 2487, which resulted in R training of 0.9995 and R validation of 0.99994.

The determination of the best ANN topology is determined by a combination of input variables, output variables, learning functions, activation functions, learning rate, momentum, number of the hidden layer and nodes in the hidden layer, which is appropriate so that it produces low MSE values and high determination coefficient (Jaber et al., 2019). However, a standard method has not been found to produce the best combination for each study by now. Therefore, to get the best topology, it is necessary to do *trial and error* on a certain subject (Kato et al., 2015). The results of *trial and error* to predict chlorophyll content in African leaves can be seen in Table 5. Table 5 shows the best topology results comprising 10-40-30-1 (10 input variables, 40 nodes on hidden layer 1, 30 nodes in

Table 4
Trial and error to determine activation function

Learning function	Activation function			R Training	R Validation	MSE Training	MSE Validation
	Hidden Layer 1	Hidden Layer 2	Output Layer				
Trainlm	Tansig	Tansig	Purelin	0.9934	0.9925	0.0034	0.0032
	Tansig	Tansig	Tansig	0.9780	0.9764	0.0078	0.0085
	Tansig	Tansig	Logsig	0.8050	0.8086	0.1647	0.1658
	Logsig	Logsig	Purelin	0.9735	0.9727	0.0093	0.0094
	Logsig	Logsig	Tansig	0.9778	0.9753	0.0078	0.0085
	Logsig	Logsig	Logsig	0.8050	0.8067	0.1647	0.1658

Table 5
Trial and error to determine learning rate and momentum

Learning Rate	Momentum	ANN Structure	R Training	R Validation	MSE Training	MSE Validation
0.1	0.5	10>>30>>1	0.9757	0.9739	0.0085	0.0089
		10>>40>>1	0.9799	0.9797	0.0078	0.0073
		10>>30>>40>>1	0.9945	0.9933	0.0020	0.0025
		10>>40>>30>>1	0.9873	0.9856	0.0055	0.0066
		10>>40>>40>>1	0.9771	0.9744	0.0085	0.0094
	0.9	10>>30>>1	0.9789	0.9765	0.0075	0.0086
		10>>40>>1	0.9796	0.9783	0.0080	0.0080
		10>>30>>40>>1	0.9908	0.9895	0.0034	0.0038
		10>>40>>30>>1	0.9981	0.9967	0.0007	0.0012
		10>>40>>40>>1	0.9808	0.9795	0.0068	0.0075

the hidden layer 2, and 1 variable output, which resulted in the lowest validation MSE compared to other topology designs. Therefore, the best ANN topology model is used to predict chlorophyll content in African leaves. The lowest validation MSE is 0.0012, with an R of 0.9967, meaning that the correlation reaches 99.67% between the input and output variables. The results also showed that two hidden layers topology provided higher accuracy than one hidden layer.

Figure 6 presents a graph of the relationship between epoch and MSE in the training process to predict chlorophyll content in African leaves. The graph shows the learning process during training from the best topology was 10-40-30-1. The maximum number of iterations used was 10000 with an MSE goal was 0.01, where learning will stop when reaching either the 10000th iteration or 0.01 of the MSE goal. The convergent learning process in the 8th iteration with the resulting MSE training value of 0.00068112. It shows that learning reaches the MSE goal in the 8th iteration within 4 seconds. According to Damayanti et al. (2020), a good learning process decreased the MSE but iterations, so the learning graph will show a decrease in linear lines. Determination of epoch and goals based on previous research (Hendrawan et al., 2019c) stated that validated MSE with the goal of 0.01 was considerably accurate for predicting objective functions. Nevertheless, extremely low MSE can cause overfitting.

In Figure 7a, the blue line shows the regression plot of the training data simulation result. In contrast, the blue line in Figure 7b shows the regression plot of the validation data simulation result. Figure 7b shows the regression plot of the simulation results of the validation data. The two graphs show the distribution of data close to the linear fit line, which shows the accuracy of prediction as they are closer to the actual value; the closer the R-value, the more robust the correlation. For example, in Figure 7a, the R was 0.99806, which means a correlation of 99.806%.

In Figure 7b, the correlation coefficient is 0.99671, which means a correlation of 99.671%. According to Schober et al. (2018), there were several R criteria: 0.00 to 0.10 can be ignored, 0.10 to 0.39 was weak, 0.40 to 0.69 was moderate, 0.70-0.89 was strong, and 0.90-1.00 was robust. Therefore, the research results showed a robust correlation between textural features (input) and chlorophyll content (output). Figure 8 shows the best topology results with the lowest validation MSE to predict chlorophyll content in African leaves.

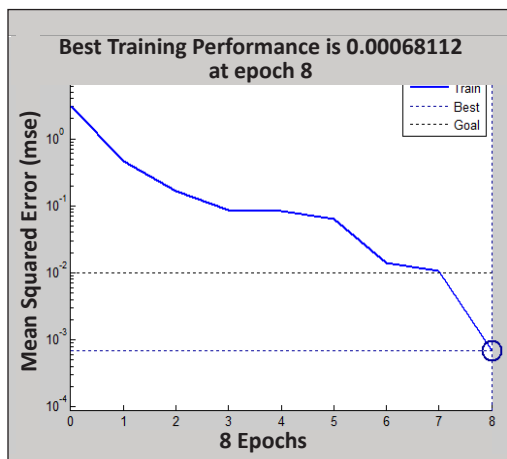


Figure 6. Learning process of ANN model to predict chlorophyll content in African leaves

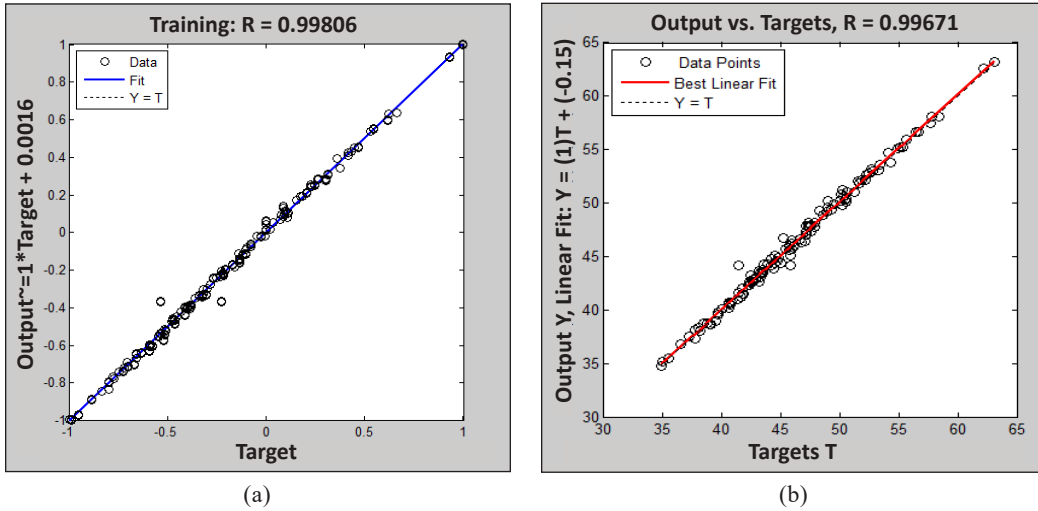


Figure 7. Simulation results of regression plots: (a) data training; (b) data validation

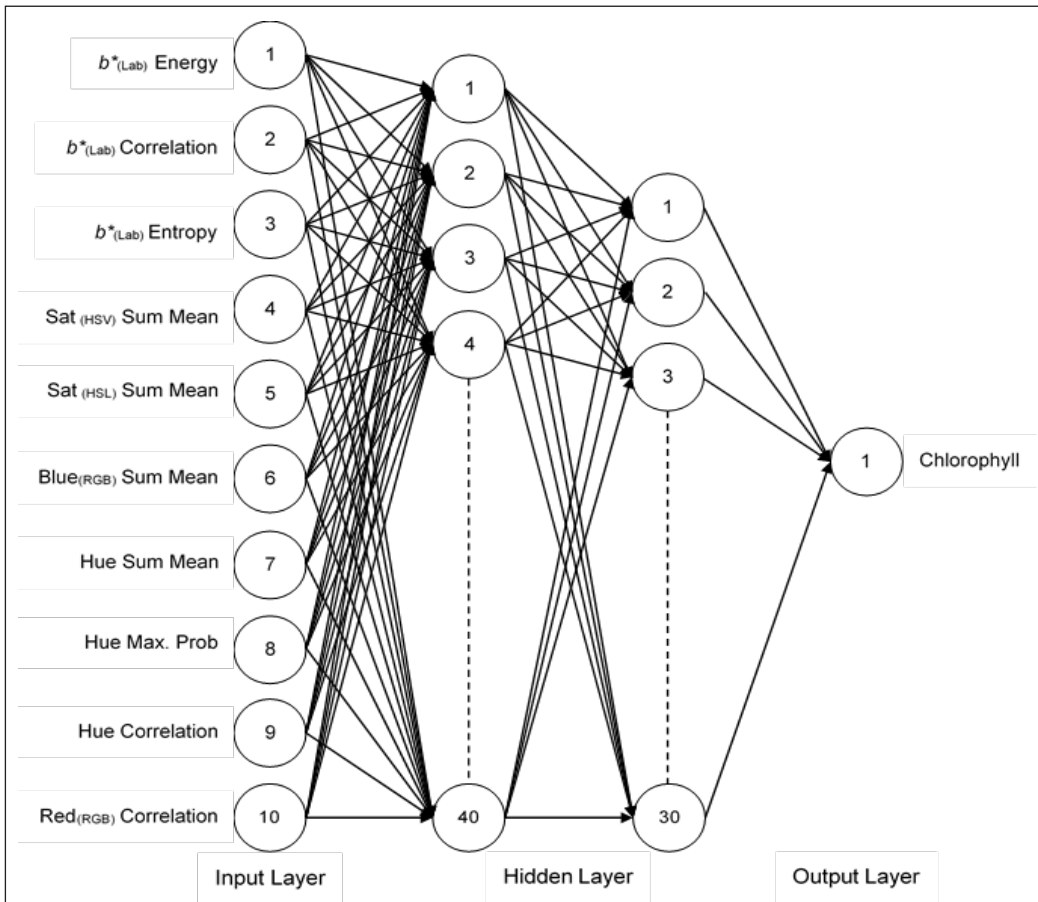


Figure 8. ANN-BP structure to predict chlorophyll content in African leaves

CONCLUSION

The best combination of 10 textural features input in ANN modelling to predict chlorophyll content in African leaves, among others, b* energy, b* correlation, b* entropy, saturation_(HSV) sum mean, saturation_(HSL) sum mean, blue sum mean, hue sum mean, maximum hue probability, hue correlation, and red correlation. Those ten textural features were obtained from selecting 120 textural features using feature selection with filter method ReliefF. Based on the research results, the best ANN topology was 10-40-30-1 (10 input layers, 40 nodes in hidden layer 1, 30 nodes in hidden layer 2, and 1 output layer). The selected learning function was trainlm, while the best activation function uses tansig in the hidden layer and purelin in the output layer. The selected ANN topology produced low MSE training of 0.0007 with R training of 0.9981, and the lowest validation MSE was 0.0012 with R validation of 0.9967. From these results, it can be concluded that there was a robust correlation of 99.67% between textural features (input) and chlorophyll content (output). Therefore, the topology can be potentially used as a model for predicting chlorophyll content in African leaves.

ACKNOWLEDGEMENT

The authors wish to acknowledge support from the Department of Agricultural Engineering, Faculty of Agricultural Technology, Universitas Brawijaya, for the assistance given during the research. This study was funded by the Associate Professor Research Grant Program (Hibah Doktor Lektor Kepala 2020), Universitas Brawijaya, the Ministry of Research, Technology, and Higher Education of the Republic of Indonesia.

REFERENCE

- Abdulkadir, A. R., Sarwar, M. J., & Dhiya, D. Z. (2015). Effect of chlorophyll content and maturity on total phenolic, total flavonoid contents and antioxidant activity of *Moringa oleifera* Leaf (Miracle Tree). *Journal of Chemical and Pharmaceutical Research*, 7(5), 1147-1152.
- Armi, L., & Shervan, F. E. (2019). Texture image analysis and texture classification methods - A review. *International Online Journal of Image Processing and Pattern Recognition*, 2(1), 1-29.
- Barman, U., & Choudury, R. D., (In Press). Smartphone image based digital chlorophyll meter to estimate the value of citrus leaves chlorophyll using linear regression, LMBP-ANN and SCGBP-ANN. *Journal of King Saud University – Computer and Information Sciences*. <https://doi.org/10.1016/j.jksuci.2020.01.005>
- Barman, U., Ridip, D. C., Arunav, S., Susmita, D., Bijon, K. D., Barna, P. M., & Golap, G. B. (2018). Estimation of chlorophyll using image processing. *International Journal of Recent Scientific Research*, 9(3), 24850-24853. <https://doi.org/10.24327/IJRSR>
- Borhan, M. S., Panigrahi, S., Satter, M. A., & Gu, H. (2017). Evaluation of computer imaging technique for predicting the SPAD readings in potato leaves. *Information Processing in Agriculture*, 4(4), 275-282. <https://doi.org/10.1016/j.inpa.2017.07.005>

- Cartelat, A., Cerovic, Z. G., Goulas, Y., Meyer, S., Lelarge, C., Prioul, J. L., Barbottin, A., Jeuffroy, M. H., Gate, P., Agati, G., & Moya, I. (2005). Optically assessed contents of leaf polyphenolics and chlorophyll as indicators of nitrogen deficiency in wheat (*Triticum aestivum* L.). *Field Crops Research*, *91*, 35-49. <https://doi.org/10.1016/j.fcr.2004.05.002>
- Dalen, G. V. (2006). Characterisation of rice using flatbed scanning and image analysis. *Food Policy, Control, and Research*, *6*, 149-186.
- Damayanti, R., Sandra, & Dahlena, E. (2020). The artificial neural network to predict chlorophyll content of cassava (*Manihot esculenta*) leaf. In *IOP Conference Series: Earth and Environmental Science* (Vol. 475, No. 1, p. 012012). IOP Publishing. <https://doi.org/10.1088/1755-1315/475/1/012012>
- Danladi, S., Muhammad, A. H., Idris, A. M., & Umar, I. I. (2018). *Vernonia amygdalina* Del: A mini review. *Research Journal of Pharmacy and Technology*, *11*(9), 4187-4190. <https://doi.org/10.5958/0974-360X.2018.00768.0>
- Garner, S. R. (1995, April 18-21). WEKA: The waikato environment for knowledge analysis. In *Proceedings of the New Zealand computer science research students conference* (Vol. 1995, pp. 57-64). University of Waikato, Hamilton.
- Grunenfelder, L., Hiller, L. K., & Knowles, R. (2006). Color indices for the assessment of chlorophyll development and greening of fresh market potatoes. *Postharvest Biology and Technology*, *40*(1), 73-81. <https://doi.org/10.1016/j.postharvbio.2005.12.018>
- Gupta, S. D., & Pattanayak, A. K. (2017). Intelligent image analysis (IIA) using artificial neural network (ANN) for non-invasive estimation of chlorophyll content in micropropagated plants of potato. *In Vitro Cellular & Developmental Biology-Plant*, *53*, 520-526. <https://doi.org/10.1007/s11627-017-9825-6>
- Haralick, R. M., Shanmugam, K., & Dinstein, I. H. (1973). Textural features for image classification. *IEEE Transactions on Systems, Man, and Cybernetics*, *3*(6), 610-621. <https://doi.org/10.1109/TSMC.1973.4309314>
- Hassanijalilian, O., Igathinathane, C., Doetkott, C., Bajwa, S., Nowatzki, J., & Esmaceli, S. A. H. (2020). Chlorophyll estimation in soybean leaves infield with smartphone digital imaging and machine learning. *Computer and Electronics in Agriculture*, *174*, 1-12. <https://doi.org/10.1016/j.compag.2020.105433>
- Hendrawan, Y., Amini, A., Maharani, D. M., & Sandra. (2019a). Intelligent non-invasive sensing method in identifying coconut (*Coco nucifera* var. Ebunea) ripeness using computer vision and artificial neural network. *Pertanika Journal of Science & Technology*, *27*(3), 1317-1339.
- Hendrawan, Y., Fauzi, M. R., Khoirunnisa, N. S., Andreane, M., Hartianti, P. O., Halim, T. D., & Umam, C. (2019b). Development of colour co-occurrence matrix (CCM) texture analysis for biosensing. *IOP Conference Series: Earth and Environmental Science*, *230*, 1-8. <https://doi.org/10.1088/1755-1315/230/1/012022>
- Hendrawan, Y., Widyaningtyas S., & Sucipto, S. (2019c). Computer vision for purity, phenol, and pH detection of Luwak Coffee green bean. *TELKOMNIKA*, *17*(6), 3073-3085. <http://dx.doi.org/10.12928/telkomnika.v17i6.12689>
- Hendrawan, Y., & Haruhiko, M. (2009). Precision irrigation for sunagoke moss production using intelligent image analysis. *Environmental Control in Biology*, *47*, 21-36. <https://doi.org/10.2525/ecb.47.21>

- Hendrawan, Y., Sakti, I. M., Wibisono, Y., Rachmawati, M., & Sandra. (2018). Image analysis using color co-occurrence matrix textural features for predicting nitrogen content in spinach. *TELKOMNIKA*, 16(6), 2711-2723. <http://dx.doi.org/10.12928/telkomnika.v16i6.10326>
- Hu, H., Liu, H. Q., Zhu, J. H., Yao, X. G., Zhang, X. B., & Zheng, K. F. (2010). Assesment of chlorophyll content based on image color analysis, comparison with SPAD-502. In *2010 2nd International Conference on Information Engineering and Computer Science* (pp. 1-3). IEEE Publishing. <https://doi.org/10.1109/ICIECS.2010.5678413>
- Jaber, A. A., Ahmed, A. M. S., & Hussein, F. M. A. (2019). Prediction of hourly cooling energy consumption of educational buildings using artificial neural network. *International Journal on Advanced Science Engineering Information Technology*, 9(1), 159-166. <https://doi.org/10.18517/ijaseit.9.1.7351>
- Kato, J., Hiroya, H., Shinsuke, T., Kenjiro, T., & Takashi, K. (2015). Analytical sensitivity in topology optimization for elastoplastic composites. *Structural and Multidisciplinary Optimization*, 52(3), 507-526. <https://doi.org/10.1007/s00158-015-1246-8>
- Kaur, G., Salim, D., Amandeep, S. B., & Derminder, S. (2014). Scanner image analysis to estimate leaf area. *International Journal of Computer Application*, 107(3), 5-10. <https://doi.org/10.5120/18729-9963>
- Kumar, C. S., & Rama, R. J. S. (2014). Application of ranking based attribute selection filters to perform automated evaluation of descriptive answers through sequential minimal optimization models. *ICTACT Journal on Soft Computing*, 5(1), 860-868. <https://doi.org/10.21917/IJSC.2014.0122>
- Li, J., Kewei, C., Suhang, W., Fred, M., Robert, P. T., Jiliang, T., & Huan, L. (2017). Feature selection: A data perspective. *ACM Computing Surveys*, 50(6), 94:1-94:45. <https://doi.org/10.1145/3136625>
- Limantara, L., Martin, D., Renny, I., Indriatmoko., & Tatas, H. P. B. (2015). Analysis on the chlorophyll content of commercial green leafy vegetables. *Procedia Chemistry*, 14, 225-231. <https://doi.org/10.1016/j.proche.2015.03.032>
- Luimstra, V. M., Schuurmans, J. M., Antonie, M. V., Klass, J. H., Jef, H., & Hans, C. P. M. (2018). Blue light reduce photosynthetic efficiency of cyanobacteria through an imbalance between photosystems I and II. *Photosynthesis Research*, 138(2), 177-189. <https://doi.org/10.1007/s11120-018-0561-5>
- Mendoza, R. J. P., Daniel, R., & Luis, D. M. (2018). Distributed reliefF-based feature selection in spark. *Knowledge and Information System*, 57, 1-20. <https://doi.org/10.1007/s10115-017-1145-y>
- Mohan, P. J., & Gupta, S. D. (2019). Intelligent image analysis for retrieval of leaf chlorophyll content of rice from digital images of smartphone under natural light. *Photosynthetica*, 57(2), 388-398. <https://doi.org/10.32615/ps.2019.046>
- Nursuhaili, A. B., Nur, A. S. P., Martini, M. Y., Azizah, M., & Mahmud, T. M. M. (2019). A review: Medicina valur, agronomic practices and post-harvest handlings of *Vernonia amygdalina*. *Food Research*, 3(5), 380-390. [https://doi.org/10.26656/fr.2017.3\(5\).306](https://doi.org/10.26656/fr.2017.3(5).306)
- Okafor, E., Lambert, S., & Marco, A. W. (2018). An analysis of rotation matrix and colour constancy data augmentation in classifying image of animals. *Journal of Information and Telecommunication*, 2(4), 465-491. <https://doi.org/10.1080/24751839.2018.1479932>

- Oyeyemi, I. T., Akinbiyi, A. A., Aderiike, A., Abimbola, O. A., & Oyetunde, T. O. (2017). *Vernonia amygdalina*: A folkloric herb with anthelmintic properties. *Beni-Suef University Journal of Basic and Applied Sciences*, 7(1), 43-49. <https://doi.org/10.1016/j.bjbas.2017.07.007>
- Pavlovic, D., Bogdan, N., Sanja, D., Hadi, W., Ana, A., & Dragana, M. (2014). Chlorophyll as a measure of plant health: Agroecological aspects. *Pestic Phytomed*, 29(1), 21-34. <https://doi.org/10.2298/PIF1401021P>
- Peng, Y., & Yi, W. (2019). Prediction of the chlorophyll content in pomegranate leaves based on digital image processing technology and stacked sparse autoencoder. *International Journal of Food Properties*, 22(1), 1720-1732. <https://doi.org/10.1080/10942912.2019.1675692>
- Rajalakshmi, K., & Narasimhan, B. (2013). Extraction and estimation of chlorophyll from medicinal plants. *International Journal of Science and Research*, 4(11), 209-212. <https://doi.org/10.21275/v4i11.nov151021>
- Samli, R., Nuket, S., Selcuk, S., & Vildan, Z. K. (2014). Applying artificial neural networks for the estimation of chlorophyll-a concentrations along the Istanbul Coast. *Polish Journal of Environmental Studies*, 23(4), 1281-1287.
- Schober, P., Christa, B., & Lothar, A. S. (2018). Correlation coefficients: Appropriate use and interpretation. *Anesthesia & Analgesia*, 126(5), 1763-1768. <https://doi.org/10.1213/ANE.0000000000002864>
- Setti, S., & Anjar, W. (2018). Analysis of backpropagation algorithm in predicting number of internet users in the world. *Jurnal Online Informatika*, 3(2), 110-115. <https://doi.org/10.15575/join.v3i2.205>
- Shakeri, M., Mohammad, M. A., Nasima, S., Mamun, M., & Syedul, M. A. (2012). Advanced CMOS based image sensors. *Australian Journal of Basic and Applied Sciences*, 6(7), 62-72.
- Shorten, C., & Taghi, M. K. (2019). A survey on image data augmentation for deep learning. *Journal of Big Data*, 6(60), 1-48. <https://doi.org/10.1186/s40537-019-0197-0>
- Uddling, J., Alfredsson, J. G., Piikki, K., & Pleijel, H. (2007). Evaluating the relationship between leaf chlorophyll concentration and SPAD-502 chlorophyll meter readings. *Photosynthesis Research*, 91(1), 37-46. <https://doi.org/10.1007/s11120-006-9077-5>
- Wang S., Tang J., & Liu H. (2016). Feature selection. In C. Sammut & G. Webb (Eds.), *Encyclopedia of Machine Learning and Data Mining* (pp. 1-9). Springer.
- Widiastuti, M. L., Aris, H., Endah, R. P., & Satriyas, I. (2018). Digital image analysis using flatbed scanning system for purity testing of rice seed and confirmation by grow out test. *Indonesian Journal of Agricultural Science*, 19(2), 49-56. <http://dx.doi.org/10.21082/ijas.v19n2.2018.p49-56>
- Xu, Y., & Royston, G. (2018). On splitting training and validation set: a comparative study of cross-validation, bootstrap and systematic sampling for estimating the generalization performance of supervised learning. *Journal of Analysis and Testing*, 2, 249-262. <https://doi.org/10.1007/s41664-018-0068-2>
- Yadav, S., Yasuomi, I., & Snehasish, D. G. (2010). Estimation of the chlorophyll content of micropropagated potato plants using RGB based image analysis. *Plant Cell Tissue and Organ Culture*, 100, 183-188. <https://doi.org/10.1007/s11240-009-9635-6>

The Effect of Storage Diversity on the Breaking Strength and Elongation of Polyamide Monofilament in Gill Net Fishing Gear

Herry Boesono^{1*}, Fadhila Surya Layli¹, Agus Suherman¹, Bogi Budi Jayanto¹ and Arief Yudhi Susanto²

¹Department of Fisheries Resources Utilization, Faculty of Fisheries and Marine Science, Diponegoro University, Semarang, Central Java 50275, Indonesia

²PT. Arteria Daya Mulia (ARIDA), Cirebon, West Java 45113, Indonesia

ABSTRACT

The study aimed to determine the breaking strength and elongation of polyamide monofilament 0.44 mm in dry condition after treating with open and close storage. This study was an experimental study that refers to SNI ISO 1805: 2010 method. Data collection was done in the dry condition with two yarn samples from different treatments and one sample as a control. Each treatment was done 10 times of repetition. The test material was collected in one mesh. Then the locking distance was adjusted with the mesh size. The breaking strength and elongation score were tested using an autograph. The study found the breaking strength on polyamide nets stored closely was higher than open storage samples. On the other, the elongation value on monofilament polyamide nets stored closely was lower than open storage samples. There was an effect on different storage methods against polyamide breaking strength (sig 0.00), which was lower than α (0.05). Different storage methods also affected the elongation score of polyamides (sig 0.00) < α (0.05). In conclusion, there was an effect on different storage methods, open or close storage, against breaking and elongation strength of polyamide monofilament 0.4 mm.

Keywords: Breaking strength, elongation, fish, gill net, polyamide, synthetic fibre

ARTICLE INFO

Article history:

Received: 15 March 2021

Accepted: 06 July 2021

Published: 08 October 2021

DOI: <https://doi.org/10.47836/pjst.29.4.16>

E-mail addresses:

herryboesono@gmail.com (Herry Boesono)

fadhilasuryalayli@gmail.com (Fadhila Surya Layli)

Lpgsuherman2@gmail.com (Agus Suherman)

bogipsp002@gmail.com (Bogi Budi Jayanto)

ariefyudhisusanto@yahoo.co.id (Arief Yudhi Susanto)

* Corresponding author

INTRODUCTION

There are two types of fishing gear based on basic materials, such as natural and synthetic fibre. Natural fibre is made up of natural material without any chemical process or transformation. Natural fibre can be obtained from plants or animals bodies—however,

synthetic fibre is obtained from the polymerisation process of monomers. Natural fibres are not being used as the primary material of fishing gear due to low material durability. Therefore, synthetic fibre is more commonly used to make fishing gear compared to natural fibre. Synthetic is a scientific and technical term for a chemical process, such as chemical elements that have been combined and strengthened by the factory with new properties (Puspito, 2009). Synthetics fibres are essential substances like phenol, benzene, acetylene, prussic acid, and chlorine. Basic materials that make up artificial fibre are known as synthetic fibre (Ardidja, 2010).

The durability of synthetic yarn is seen from its breaking strength and elongation score. Yarn breaking strength and elongation score are the value of yarn synthetic durability against the tensile force (Klust, 1987). Breaking strength is tested by a machine with different capabilities against the maximum load that can be borne (Ramos, 1999). Elongation is the elasticity value of synthetic yarn. Therefore, the breaking strength and elongation score is an important part that needs to be considered. If the value of breaking strength is high and has low elongation, it can increase material effectivity (Sari et al., 2017). A synthetic fibre made from chemicals to be the primary material of fishing gear commonly used by fishermen is polyamide, polyethylene, and polyvinyl chloride. Those materials are from plastics type low-density polyethylene (LDPE) (Mainnah et al., 2016).

One of the fishing gear made from polyamide as the primary material is a gill net. A gillnet is a rectangular fishing gear made from polyamide monofilament or multifilament with the same mesh size. A gillnet is a type of gilled gear because fish mostly catch on the gill cover as its way of passing through the net (Brant, 1984). A gillnet is installed vertically against the water surface and block the direction of fish movement (Making et al., 2014). Fishing nets are a passive catching tool (Nurdin, 2009) with a completed buoy, ballast, head, and under the rope or without under rope to block fish direction movement to be cached to the net (Fachrudin, 2012). Polyamide or nylon material is chosen as the basic material of the gill net due to its characteristic that fits like a basic material of the gill net (Rahmadhani et al., 2017).

Gillnet can be used or operated by big boat fishermen or on an industrial scale and small boat/traditional fishers. Drop net or setting step is done in a few hours in accordance with the fishermen that operate it (Sulaeman, 2008). The installation step of the net is started by the drop of marker buoy tied up with slingshot. The piece drops one by one until the net is entirely spread and soaked for a few hours. The next step is a net withdrawal that starts from the marker buoy, pulled using a roller. When the net is withdrawn, the catch is taken (Putra, 2007). Traditional fishers with their small boat in Tambaklorok, Semarang City, have different habits in storing the fishing gear, either open or closed storage. Open storage is a way of keeping the habit of fishers that store the gill net on the boat without being covered, where close storage is when the gill net is stored on the boat that is covered by cloth and tarpaulin.

The improvement in the use of synthetic yarn still has a weakness. Synthetic fibres can experience a quality decline due to environmental factors such as ultraviolet (UV) light exposure. UV affected the value of fibre synthetic breaking strength (Al-Oufi et al., 2003). Furthermore, direct and continuous sunlight exposure can cause weathering. Weathering can modify and ruin the structure of polymer molecules, which finally caused the loss of the strength and extensibility, durability, and general performance of polyamide yarn (Thomas & Hridayanathan, 2006). Based on the weakness of synthetic yarn, it is necessary to test the polyamide yarn on the gill net, which is stored in a different place to find a suitable gill net storage method and make the gill net last longer. Synthetic materials have been rapidly developed in the fishing industry and able to make the industry smoother. The improvement of the use of synthetic fibre is currently being considered because of its characteristic that it is difficult to be rot, which affects the environment (Kim et al., 2016). Therefore, the present study aimed to determine the breaking strength and elongation of polyamide monofilament 0.44 mm in dry condition after treating with open and close storage.

MATERIALS AND METHODS

Materials

Materials used in the study were net samples obtained from fishers that used polyamide gill net 0.4 mm and 6 months of service life. Samples were collected from different storage treatments on a different boat, kept closed (using a tarpaulin) and kept openly (Figure 1). Sampling was conducted in Tambaklorok Village, North Semarang District, Semarang City, Central Java. Tambaklorok gill net fishers have been an arrest operation for 6 to 7 hours per day and off on Friday. Gillnet used a basic gill net that usually changed after 1 to 2 years and repaired every day off or when severe damage was found in the gill net. In addition, mesh samples were taken from the net body, which was still good or not yet damaged.



Figure 1. Net sample

Experimental Design

The experimental design was a method used in this study and to know the effect of different storage methods on the durability of the gill net. The study was conducted by finding samples in accordance with the original conditions of the object of research. The field survey was done to find gill net that is being stored differently. Samples were chosen based on the difference between open and closed storage, with several variables that must be equated. In addition, variables must be correlated, such as gillnet, service life, usage time, mesh size, and net diameter. Sample test results were compared with test results of unused nets as control (deemed according to the standard) to see the differences in test results.

The test of the samples was done in the quality control room PT ARIDA. The materials used were net samples obtained from fishers using polyamide material of gill net 0.4 mm, have the same operational life from different storage treatments on the boat, namely closed storage (using a tarpaulin) and open storage. The test was done in the dry condition against net samples from three groups, including the control group (untreated net), net samples being treated with open storage (open storage group), and net samples with closed storage (closed storage group). There were 10 repetitions of each group according to SNI ISO 1805:2010, at least 10 times valid repetitions against each sample test that must be done (Indonesia National Standard, 2010). The following process was materials tested obtained from one mesh of each test. Breaking strength and elongation were tested using a breaking strength machine and Trapezium II application.

Data Analysis

The hypothesis of the study was:

1. Breaking strength

H_0 : no effect found in different treatments against yarn breaking strength.

H_1 : different treatments affected yarn breaking strength.

2. Elongation

H_0 : no effect found in different treatments against yarn elongation.

H_1 : different treatments affected yarn elongation.

The data analysis was done to know the effect of different treatments against breaking strength and elongation of polyamide yarn by Kruskal-Wallis of the non-parametric test (because data results do not spread normally). The process of data analysis was done using SPSS Software with the following decision-making rules:

- Know the effect of treatments on breaking strength and elongation (Kruskal-Wallis test) with a probability of 0.05.

Asymp. Value sig>0.05, then H_0 was accepted.

Asymp. Value sig<0.05, then H_0 was rejected.

- Know the comparison between factors (Mann-Whitney test) with a probability of 0.05.
 Asymp. Value sig>0.05, then Ho was accepted.
 Asymp. Value sig<0.05, then Ho was rejected.

RESULTS AND DISCUSSION

General View of the Sample Collection Location

Sample collection was done in Tambaklorok Village, North Semarang District, Semarang City, Central Java. Mostly, the profession of the population were fishermen. The fishing gear used by Tambaklorok fishermen were varied; one of those was gill net fishing gear. Tambaklorok fishers stored their gill net by covering it with tarpaulin and tied it not to be stolen and damaged. Some fishermen who use the gill net almost every day usually store it openly to reduce their time to open or close the cover after being used. The fishermen did not consider the effect of the storage method on net durability. The fishermen only consider its age and level of damage or replace or repair the fishing gear.

The Autograph Machine Test Results

Autograph machine output showed a time graph; therefore, it can be seen whether the net breaks at a standard time or not and at what range of tensile strength values caused the net to break.

Figure 2 showed the new nets in 10 times test would break at strength 5-6 Kgf in 20-23 seconds. The unused nets showed

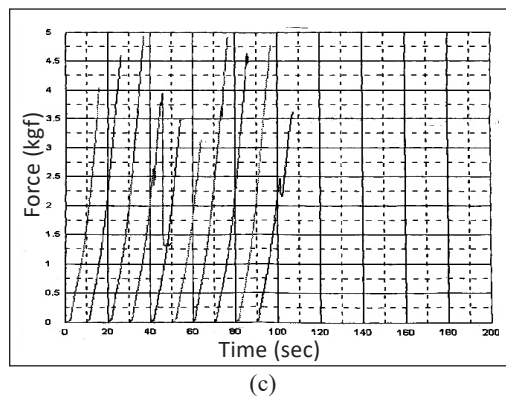
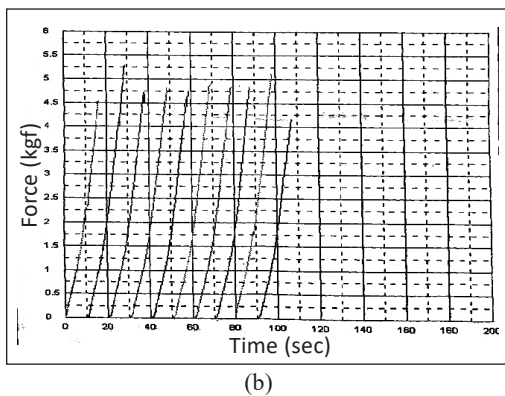
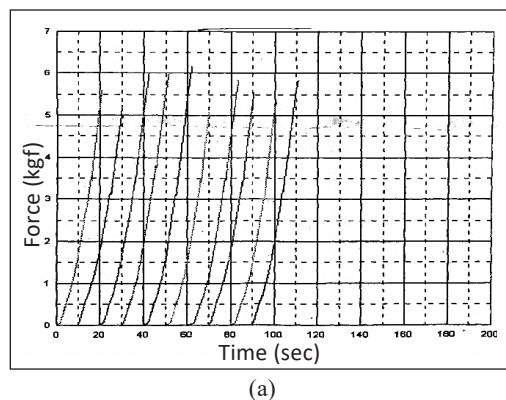


Figure 2. Graph of autograph machine test results: (a) Graph of unused nets test results; (b) Closed storage net test result graph; (c) Graph of open storage net test results

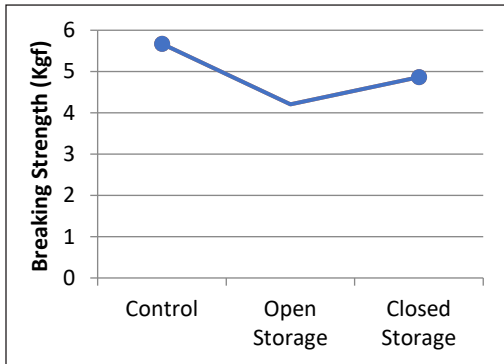


Figure 3. Average of breaking strength

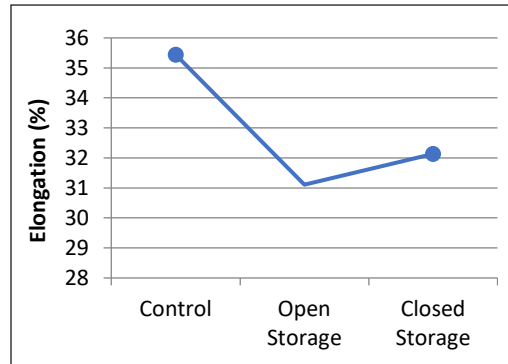


Figure 4. Elongation average graph

good resistance. Figure 3 showed that the gill net stored closely on 10 times test would break at strength 4-5 Kgf in less than 20 seconds. The breaking strength of this group was lower than the control group. Figure 3 showed that net in open storage after 10 times test would break at strength 3-4 Kgf in less than 20 seconds. Based on Figure 4, the graph declined after breaking due to the durability reduction of the net stored openly. Thus, the open storage method of nets showed lower durability compare to nets that stored closely.

Breaking Strength of Nets in Different Storage. The breaking strength test was done by giving a load to the net until the net breaks so that the maximum load received by the net can be seen. The breaking strength test was done in 3 groups (Figure 3). The unused nets as control were compared with treated nets, whether open storage treatment or closed storage. The test was done according to the National Standard of Indonesia (NSI), and the results were shown in Table 1.

Table 1
Breaking strength test results

No	Breaking strength value (Kgf)		
	Unused nets	Open storage	Closed storage
1	5.09	3.15	4.54
2	5.25	3.49	4.72
3	5.34	3.63	4.77
4	5.55	3.96	4.81
5	5.6	4.04	4.82
6	5.83	4.6	4.85
7	5.86	4.64	4.86
8	6	4.78	4.91
9	6.01	4.91	5.13
10	6.16	4.93	5.31
Average	5.67	4.21	4.87

Kgf = Kilogram Force

Breaking strength value declined after the nets being used (Figure 3). The decline of its breaking strength is caused by many factors, such as net material quality or usage factor. Quality factor influenced by material quality used to make the net because each net has a different structure. Usage factor was a factor that affects net breaking strength after being used. Immersion nets also influenced the decline of nets breaking strength.

Elongation of Nets in Different Storage. Elongation nets test was done in 3 groups as the groups in breaking strength test. Unused nets was a control that being compared with open and closed nets storage. The test was done according to NSI with wet test method at 20°-21°C room temperature and 100 force load. Based on the elongation test, the results are shown in Table 2.

Table 2
Net elongation test results

No	Elongation (%)		
	Unused nets	Open storage	Closed storage
1	33.27	27.25	28.67
2	33.9	27.84	30.82
3	34.33	30.62	31.26
4	34.51	30.84	31.34
5	34.64	31	32.51
6	34.95	31.58	32.92
7	35.64	32.28	33.2
8	36.71	32.88	33.5
9	37.46	33.07	33.5
10	38.96	33.74	33.64
Average	35.44	31.11	32.14

The results of the nets elongation value test showed a decline after being used (Figure 4). The elongation value was lower not because of a better elongation, but the nets were already not elastic. The breaking strength of open storage nets was lower so that with the same strength, the nets would break before reaching the breaking strength standard, so the elongation was small. It also can be observed physically; the mesh shifted because the elongation nets and breaks easily because the breaking strength value of nets open storage was low.

The elongation value of the tested nets was decreased after use. The smaller elongation value is not because the elongation is getting better but, the net is no longer experiencing elongation. The breaking strength value in an openly stored net is getting smaller so that with the same strength, the net will break before reaching the standard breaking strength and then the elongation value is small. The mesh has physically shifted because the net is

stretched and breaks because the breaking strength value of the net kept open is also small. According to Ardidja (2010), threads with high elasticity can return to their original shape and size or leave a small elongation. This condition also guarantees whether the mesh size remains constant and can maintain its strength.

Treatments Effect on Breaking Strength. The results of the non-parametric through Kruskal-Wallis test ($\alpha=0.05$) showed the breaking strength affected differently by the treatments. The polyamide nets showed P-value < 0.05 or 0.000 , which means H_0 was rejected and H_1 accepted. It shows the different storage methods that affected breaking strength.

The Mann-Whitney test was done to know the treatment that gave the actual effect on breaking strength nets. Based on this test, control, open storage, and closed storage treatments showed the results in Table 3. The results showed that the breaking strength of each treatment showed significant differences. In the group of open storage, nets showed a lower breaking strength value than closed storage nets breaking strength, so closed storage was preferred to maintain the quality of the net.

Table 3
Mann Whitney test results of treatments effect on breaking strength

Groups	Z-value count	P-value	Indication
Control vs Open	-3.780	0.000	Significantly different
Control vs Closed	-3.553	0.000	Significantly different
Open vs Closed	-2.231	0.026	Significantly different

Treatments Effect on Elongation. The analysis of non-parametric using Kruskal-Wallis with 5% test level ($\alpha = 0.05$) showed that the nets elongation of all group were affected. Polyamide yarn showed P-value < 0.05 (0.000), which means H_0 was rejected and H_1 accepted (different storage methods affected elongation score). Mann-Whitney test results were shown in Table 4.

Table 4
Mann Whitney test results of treatments effect on elongation

Groups	Z-value count	P-value	Indication
Control vs Open	-3.554	0.000	Significantly different
Control vs Closed	-3.704	0.000	Significantly different
Open vs Closed	-1.286	0.199	Not significantly different

The population majority was fishermen and catching tools they operated, such as arad fishing gear, gill net, and trammel net (Putri et al., 2018). The basic gill net was a catching tool to catch demersal fish. Fish that could be cached by Tambaklorok fishermen using a

basic gill net were *Nibeal biflora* and *Rastrellinger* sp. The catch target of basic gill net was demersal fish such as *Nibeal biflora* and *Leiognathidae*. The catch of basic gill net in northern waters such as pelagic fish, including *Rastrellinger* sp. (Gunawan et al., 2016).

The way of how gill net catch was fish spun into the nets, making the net elastics (has lower breaking strength because the maximum load that can be borne was also getting smaller). Breaking strength was the maximum strength that needs to break the material in a test that uses tension. The unit of breaking strength is a kilogram of force (Kgf) (Fadhari et al., 2015). Yarn with high elasticity can be back to the first shape and size or leaving little elongation. That condition also guaranteed whether net mesh size was constant and maintained its strength (Aridja, 2010).

Open storage nets usually done on the boat reduced the breaking strength faster than closed storage. It was caused by the polyamide material that was susceptible to UV light. A good gill net has a high breaking strength value, meaning that the net can withstand a greater load. The best fishing gear yarn was yarn with low durability but had a high breaking strength value (Fadhari et al., 2015).

The results of statistical elongation data analysis showed the different elongation scores between new and used nets. The elongation score was reduced due to the application of the net. This result showed that open storage has a lower elongation score but did not break in the standard time and meet the standard charts. The elongation score of open and closed storage did not differ significantly because the breaking strength of both groups reduced that affected elongation and experienced construction modification such as cover shift due to use. Too high elongation can modify nets construction such as cover shift and mesh size. Stretched nets make the mesh size bigger so that the fish can easily catch (Fadhari et al., 2015).

CONCLUSION

The breaking strength of Polyamide monofilament 0.4 mm nets that have been stored openly and closely were 4.21 Kgf and 4.81 Kgf, respectively. The elongation score of Polyamide monofilament 0.4 mm nets that have been stored openly and closely were 32.14% and 31.11%, respectively. There was a different storage effect on breaking strength of Polyamide monofilament 0.4 mm nets. The nets of closed storage showed a higher breaking strength compare to open storage. In addition, there was a different storage effect on the elongation of Polyamide monofilament 0.4 mm nets. The nets of closed storage showed a higher elongation compare to open storage. The suggestion of this study was to store the gill net closely and avoid direct sunlight exposure.

ACKNOWLEDGMENTS

The authors wish to thank Fakultas Perikanan dan Ilmu Kelautan Universitas Diponegoro, Lembaga Penelitian dan Pengabdian Masyarakat (LPPM) Universitas Diponegoro dan PT. Arteria Daya Mulia (ARIDA) Cirebon City, West Java, Indonesia.

REFERENCES

- Al-Oufi, H., McLean, E., Kumar, A. S., Claereboudt, M., & Al-Habsi, M. (2003). The effects of solar radiation upon breaking strength and elongation of fishing nets. *Fisheries Research*, 6(1), 115-119. [https://doi.org/10.1016/S0165-7836\(03\)00103-6](https://doi.org/10.1016/S0165-7836(03)00103-6)
- Ardidja, S. (2010). *Bahan alat penangkap ikan* [Fishing equipment material]. STP Press.
- Brant, A. V. (1984). *Fish catching methods of the world*. Fishing News Books Ltd.
- Fachrudin, H. (2012). *Petunjuk teknis perikanan tangkap: Identifikasi jaring insang (Gill net)* [Capture fisheries technical instructions: Gill net identification]. Balai Besar Penangkapan Ikan.
- Fadhari, A., Isnaniah, I., & Nofrizal, N. (2015). Study on strength broke and elongation yarn PA (Polyamide) with addition of skin stem extract salam (*Syzygium polyanthum*) with different concentration. *Jurnal Online Mahasiswa Fakultas Perikanan dan Ilmu Kelautan Universitas Riau*, 2(1), 1-12.
- Gunawan, A. A., Ismail, I., & Jayanto, B. B. (2016). Analisis finansial usaha perikanan jaring klitik (Gill net dasar) dan jaring nilon (Gill net permukaan) di pangkalan pendaratan ikan (PPI) Tanjungsari Kabupaten Pemalang, Jawa Tengah [Financial analysis of fishery business clitic nets (Basic gill nets) and nylon nets (Surface gill nets) at the Tanjungsari fish landing base (PPI) Pemalang Regency, Central Java]. *Journal of Fisheries Resources Utilization Management and Technology (JFRUMT)*, 5(2), 48-54.
- Indonesia National Standard. (2010). *SNI ISO 1805. Alat penangkap ikan berbahan jaring –Penentuan gaya putus mata jaring* [Fishing equipment made from nets - Determination of net eye breaking force]. Indonesia National Standard.
- Kim, S., Kim, P., Lim, J., An, H., & Suuronen, P. (2016). Use of biodegradable driftnets to prevent ghost fishing: Physical properties and fishing performance for yellow croaker. *Animal Conservation*, 19(4), 309-319. <https://doi.org/10.1111/acv.12256>
- Klust, G. (1987). Bahan jaring untuk penangkakan ikan [Material for fishing nets]. In Tim BPPI Semarang (Trans.), Bagian proyek pengembangan teknik penangkapan ikan (Edisi 2) [Fishing technique development project section (2nd Ed.)]. Balai Penangkapan Ikan.
- Mainnah, M., Diniyah, D., & Iskandar, B. H. (2016). Perpaduan serat daun nanas (*Ananas Comosus*) dan kitosan sebagai material alat penangkapan ikan ramah lingkungan [Combination of pineapple leaf fiber (*Ananas Comosus*) and chitosan as environmentally friendly fishing equipment material]. *Marine Fisheries*, 7(2), 149-159.
- Making, A. D. L., Asriyanto, A., & Yulianto, T. (2014). Pengaruh perbedaan mata jaring (Mesh size) gillnet terhadap cara tertangkap ikan kembung perempuan (*Scomber neglectus*) di perairan Morodemak, Kabupaten Demak [The effect of difference in mesh size of gillnet on how to catch female mackerel fish

- (*Scomber Neglectus*) in Morodemak waters, Demak Regency]. *Journal of Fisheries Resources Utilization Management and Technology (JFRUMT)*, 3(4), 120-129.
- Nurdin, E. (2009). Perikanan tuna skala rakyat (Small scale) di prigi, Trenggalek-Jawa Timur [Small scale tuna fishery in prigi, Trenggalek-East Java]. *BAWAL: Widya Riset Perikanan Tangkap*, 2(4), 177-183. <http://dx.doi.org/10.15578/bawal.2.4.2009.177-183>
- Puspito, G. (2009). Perubahan sifat-sifat fisik mata jaringan insang hanyut setelah digunakan 5, 10, 15, dan 20 tahun [Changes in the physical properties of the eye gill tissue after being used for 5, 10, 15, and 20 years]. *Jurnal Penelitian Sains*, 12(3), 1-6. <https://doi.org/10.26554/jps.v12i3.172>
- Putra, I. (2007). *Deskripsi dan analisis hasil tangkapan jaring millenium di Indramayu* [Description and analysis of millennium net catches in Indramayu]. Institut Pertanian Bogor.
- Putri, V. L., Kurohman, F., & Fitri, A. D. P. (2018). Efisiensi teknis dan selektivitas alat tangkap jaring insang (Gillnet) terhadap komposisi hasil tangkapan di perairan Semarang [Technical efficiency and selectivity of gillnet fishing equipment on composition of catches in Semarang waters]. *Saintek Perikanan: Indonesian Journal of Fisheries Science and Technology*, 13(2), 126-132. <https://doi.org/10.14710/ijfst.13.2.126-132>
- Rahmadhani, T., Syofian, I., & Nasution, P. (2017). Studi perubahan panjang benang jaring polyamide (PA) yang direndam didalam air tawar dan air laut [Study of changes in length of polyamide net yarn (PA) soaked in freshwater and sea water]. *Jurnal Online Mahasiswa Fakultas Perikanan dan Ilmu Kelautan Universitas Riau*, 4, 1-12.
- Ramos, J. M. L. (1999). Chemical and physical properties of synthetic fibres most commonly used in fishing gear, with reference to their use in cape Verde fisheries. *Fisheries Training Program*, 1, 1-26.
- Sari, V. A. P., Boesono, H., & Setiyanto, I. (2017). Analisis pengaruh media perendaman benang PA multifilamen D21 terhadap kekuatan putus (Breaking strength) dan kemuluran (Elongation) dengan metode SNI ISO 1805: 2010 [Analysis of the effect of soaking media for PA multifilament D21 yarn on breaking strength and elongation with SNI ISO 1805: 2010 method]. *Journal of Fisheries Resources Utilization Management and Technology*, 6(4), 168-174.
- Sulaeman, M. (2008). *Jaring insang [Gill net]* (3rd Ed.). Institut Pertanian Bogor.
- Thomas, N. S., & Hridayanathan, C. (2006). The effect of natural sunlight on the strength of polyamide 6 multifilament and monofilament fishing net materials. *Fisheries Research*, 1(2-3), 326-320. <https://doi.org/10.1016/j.fishres.2006.06.012>



A Deep Learning Approach for Retinal Image Feature Extraction

Mohammed Enamul Hoque^{1*}, Kuryati Kipli¹, Tengku Mohd Afendi Zulcaffle¹, Abdulrazak Yahya Saleh Al-Hababi², Dayang Azra Awang Mat¹, Rohana Sapawi¹ and Annie Anak Joseph¹

¹Department of Electrical and Electronics Engineering, Faculty of Engineering, Universiti Malaysia Sarawak, 94300 UNIMAS, Kota Samarahan, Sarawak, Malaysia

²Faculty of Cognitive Sciences and Human Development, Universiti Malaysia Sarawak, 94300 UNIMAS, Kota Samarahan, Sarawak, Malaysia

ABSTRACT

Retinal image analysis is crucially important to detect the different kinds of life-threatening cardiovascular and ophthalmic diseases as human retinal microvasculature exhibits remarkable abnormalities responding to these disorders. The high dimensionality and random accumulation of retinal images enlarge the data size, that creating complexity in managing and understating the retinal image data. Deep Learning (DL) has been introduced to deal with this big data challenge by developing intelligent tools. Convolutional Neural Network (CNN), a DL approach, has been designed to extract hierarchical image features with more abstraction. To assist the ophthalmologist in eye screening and ophthalmic disease diagnosis, CNN is being explored to create automatic systems for microvascular pattern analysis, feature extraction, and quantification of retinal images. Extraction of the true vessel of retinal microvasculature is significant for further analysis, such as vessel diameter and bifurcation angle quantification. This study proposes a retinal image feature, true vessel

segments extraction approach exploiting the Faster RCNN. The fundamental Image Processing principles have been employed for pre-processing the retinal image data. A combined database assembling image data from different publicly available databases have been used to train, test, and evaluate this proposed method. This proposed method has obtained 92.81% sensitivity and 63.34 positive predictive value in extracting true vessel segments from the top first tier of colour retinal images. It is expected to

ARTICLE INFO

Article history:

Received: 21 March 2021

Accepted: 12 July 2021

Published: 08 October 2021

DOI: <https://doi.org/10.47836/pjst.29.4.17>

E-mail addresses:

hqenam.unimas@gmail.com (Mohammed Enamul Hoque)

kkuryati@unimas.my (Kuryati Kipli)

ztmafendi@unimas.my (Tengku Mohd Afendi Zulcaffle)

ysahabdulrazak@unimas.my (Abdulrazak Yahya Saleh Al-Hababi)

amdazra@unimas.my (Dayang Azra Awang Mat)

srohana@unimas.my (Rohana Sapawi)

jannie@unimas.my (Annie Anak Joseph)

* Corresponding author

integrate this method into ophthalmic diagnostic tools with further evaluation and validation by analysing the performance.

Keywords: Cardiovascular disease, convolutional neural network, deep learning, feature extraction, retinal imaging

INTRODUCTION

Medical imaging offers the way of visual inspections of diseases state. Retinal image analysis is recognised as a significant part of the medical imaging discipline as some of the severe cardiovascular diseases such as Diabetic Retinopathy (DR), Hypertensive Retinopathy (HR), and Ischemic Stroke (IS) can be detected by analysing the degradation of retinal microvasculature in a non-invasive manner (Abbasi-sureshjani et al., 2016; James, 2000; Witt et al., 2006). Researches revealed that some distinct funduscopic disorders such as arteriovenous (AV) nicking, exudates, Cotton Wool Spots (CWS), vessel widening, microaneurysm, changes in bifurcation angles, and focal arteriolar narrowing in the retina are found as closely associative to the above-mentioned cardiovascular diseases though the different vascular risk factors and blood pressure are in control (De Silva et al., 2011; Henderson et al., 2011). Ong et al. (2013) demonstrated that the risk of stroke and hypertensive retinopathy are optimally assistive. However, Baker et al. (2008) and Wang et al. (2011) investigated that even this can be the cause of stroke fatality in people who are not suffering from the stroke risk factors. Therefore, deviations in the retinal artery and vein diameter are strongly recommended as the great cause of stroke (Kipli et al., 2018).

Image Processing (IP) techniques are being exploited to extract the human retina's qualitative and quantitative image features. However, most of the developed IP-based techniques are not fully automated and time-consuming, which are still considered the limitations of retinal image analysis. In biomedical imaging such as AI-based radiology, IP is excitingly contributing as the radiological diagnosis depends on different imaging modalities. As ophthalmology has a salient similarity with radiology, AI is being explored to develop new methods to assist ophthalmic practitioners in predicting fatal cardiovascular disease and other notable threatening events for vision loss. However, random acquisition of retinal image data and its high dimensionality create a heap of retinal data. This massive data accumulation is throwing the data management challenge to ophthalmologists. DL has been introduced to develop intelligent tools by integrating various task-driven AI algorithms to manage these tremendous-sized data in a more acceptable, safe, and efficient way.

The Artificial Neural Network (ANN) technique is employed to construct Deep Neural Network (DNN) exploiting multiple layers that analyse the image feature hierarchy from higher to lower level vice-versa (Goodfellow et al., 2016; Buduma & Locascio, 2017). The multi-layered DL structures process nonlinear data to analyse and classify many data patterns, extract and classify both supervised and unsupervised data features. The small

units of ANN, artificial neuron, produce real-valued activations that have been utilised to construct DNN forming parameterized functions such as Rectified Linear Units (ReLUs), sigmoid, Tangent Hyperbolic (tanh), and softmax (Abadi et al., 2016; Ghesu et al., 2016; Schmidt-Erfurth et al., 2018). The integrated artificial neurons in each layer of DNN are needed to train for defraying information with high-level representation and more abstraction from the network's first to the last layers. Convolutional Neural Network (CNN) is a form of feed-forward DNN consisting of convolution, pooling, and fully connected layers developed primarily to deal with image data. Convolutional Neural Network employs backpropagation to learn complex image features hierarchies and patterns automatically and adaptively.

The AI applications based on CNN are being developed extensively for retinal image analysis, especially for disease state gradation, microvasculature segmentation, and feature extraction. There are two types of recently developed DL algorithms for ophthalmic abnormality detection such as image-based and lesion-based. The lesion-based algorithms are trained with previously known features such as exudates, haemorrhages, and microaneurysms. Image-based algorithms are also known as black-box algorithms, and this kind of system is trained with manually graded retinal images that generate an output indicating the disease state (Fenner et al., 2018). To classify the Age-related Macular Degeneration (AMD), Grassmann et al. (2018) developed a DL algorithm exploiting six different CNN models such as Visual Geometry Group (VGG), Inception-V3, AlexNet, ResNet V-2, ResNet, and GoogLeNet that obtained 94.30% accuracy and 84.20% sensitivity on Cooperative Health Research on the Region of Augsburg (KORA) data set. Niemeijer et al. (2007) and Abramoff et al. (2016) developed a CNN algorithm to detect DR signs, exudates, haemorrhages, and neovascularisation, combining VGG and AlexNet that recorded 90.7% accuracy, 82.7% sensitivity, and 96.8% sensitivity, 87% specificity, 0.98 AUC respectively. Gargeya & Leng (2017) and Pratt et al. (2016) proposed a customised CNN model, Gulshan et al. (2016) used Inception-V3 for DR detection, and Ting et al. (2017) developed a CNN model to detect referable and vision-threatening DR while Takahashi et al. (2017) modified GoogLeNet for DR grading. The proposed model of Ting et al. (2017) showed 90.5%, 100%, 96.4%, 93.2% sensitivity and 91.6%, 91.1%, 87.2%, 88.7% specificity for referable DR, vision-threatening DR, glaucoma and AMD detection respectively. The performance of Gargeya & Leng (2017) was recorded as 94% sensitive and 98% specific to DR detection. The work of Ting et al. (2017) seems inconsistent for the implementation in ophthalmic tools as their data set was not graded by the experts. Their work did not consider the great DR signs such as microaneurysms, haemorrhages to analyse and identification of macular oedema was poor, which are the strong limitations of the model of Ting et al. (2017).

In retinal image analysis, segmentation is an important step as the segmented image is further utilised for qualitative and quantitative feature detection. Melinsca et al. (2015)

and Zhu et al. (2017) developed deep max-pooling CNN and Extreme Learning Machine (ELM) based retinal image segmentation algorithms that obtained 94.66% and 96.00% accuracy, respectively. The work of Zhu et al. (2017) has been evaluated on Retinal Images for Screening (RIS) and found as time effective. For semantic segmentation of retinal image Dense U-net, a DL approach has been introduced. Wang et al. (2019) proposed a Dense U-net model employing image patch-based technique for segmentation that obtained 0.9511 and 0.9538 accuracy, 0.7986 and 0.7914 sensitivity, and 0.9736 and 0.9722 specificity for DRIVE and STARE databases, respectively. Wang et al. (2019) model used a sequential reconstruction strategy to reconstruct the segmented patches at the output end. An optimized deep CNN approach had been introduced by Badawi & Fraz (2019) for AV classification and obtained the best accuracy, 98%, for the AVR DV dataset. Exploiting Recurrent Residual CNN (RRCNN) and Recurrent CNN (RCNN) Alom et al. (2018) developed U-Net-based semantic segmentation algorithms, while Oliveira et al. (2018) developed a CNN model for data augmentation and prediction. Both algorithms of Badawi & Fraz (2019) and Oliveira et al. (2018) obtained the best result for the STARE database. However, the sensitivity of Oliveira et al. (2018) has slightly deviated while performing cross-training on STARE and DRIVE datasets. In the vessel segmentation model of Wang et al. (2015), CNN and Random Forest (RF) have been ensembled where CNN was dedicated to detecting hierarchical features, and RF contributed as a classifier. Wang et al. (2015) evaluated the DRIVE and STARE database and obtained 0.9767 and 0.9813 accuracy, 0.8173 and 0.8104 sensitivity, and 0.9733 and 0.9791 specificities for both databases, respectively. Maji et al. (2015) combined Denoising Auto-Encoder (DAE) and RF to develop a hybrid DL model for vessel detection and showed 93.27% accuracy. Guo et al. (2019), Mo and Zhang (2017) and Yan et al. (2019) proposed supervised CNN models, and Lahiri et al. (2016) proposed an unsupervised Deep Neural Ensemble Network. The work of Guo et al. (2019) and Lahiri et al. (2016) obtained 95.60% and 95.33% accuracy on the DRIVE database, respectively, while the work of Yan et al. (2019) showed the best outcome, 0.9638 accuracies, 0.7735 sensitivity, and 0.9857 specificities for STARE database. Though the work of Mo & Zhang (2017) showed robustness in segmentation and faster processing speed, the algorithm showed slightly lower accuracy for a cross-training on CHASE DB1 and DRIVE database, respectively. It is assumed that the wider arteriolar orientation, poor vessel contrast, and non-uniform background illumination of the CHASE DB1 image can cause a deviation in the accuracy.

Retinal Image feature identification is crucially important for visual analysis of the impairment in the microvascular structure of the human retina. In order to decide on cardiovascular disease or other ophthalmic abnormalities from retinal image analysis, diagnostic methods must have consistency in detecting the interesting features such as CWS, haemorrhages, exudates, vessel widening, and microaneurysm. Most of the retinal

image feature detection algorithms based on DL have been developed to detect retinal lesions. To detect haemorrhages, Van Grinsven et al. (2016) trained their 5-layered CNN model with both selective and non-selective retinal image samples. Van Grinsven et al. (2016) evaluated their Selective Sampling CNN (SeSCNN) and Non-Selective Sampling CNN (NSeSCNN) model's performance on Kaggle and Messidor databases for different false positive values. It was recorded that the SeSCNN performed better than NSeSCNN.

The developed Neural Network (NN) architecture combining Logistic Regression (LR) with Radial Basis Function (RBF) of García et al. (2009a) obtained 88.1% accuracy, 70.4% positive predictive value, and 100% sensitivity in retinal hard exudate detection. The image-based exudate detection of Osareh et al. (2009) obtained 96% sensitivity, and 94.6% positive predictive value, and this performance is better than their lesion-based detector. Tan et al. (2017) evaluated their 10-layered CNN model for exudates, microaneurysms, and haemorrhages detection on CLEOPETRA that showed 87.58% sensitivity for exudate detection and 62.37% sensitivity for haemorrhages and microaneurysm detection. The Fuzzy C-means and ANN-based DL model of Osareh et al. (2003) was 93% sensitive to exudate detection and 95% sensitive to detect lesions in retinal images. To detect both image-based and lesion-based hard exudates, Van Grinsven et al. (2016) investigated Multi-Layer Perceptron (MLP), Support Vector Machine (SVM), RBF, and NN classifier.

For retinal image feature detection cross-entropy function, regularisation for MLP and RBF had been used in the investigation of Van Grinsven et al. (2016). Among these models, MLP obtained better results, 97.01% accuracy, 100% sensitivity, and 92.59% positive predictive value, compared to SVM, RBF, and NN classifier. The training of MLP was more complex than RBF. It could be happened due to the slow convergence as the effects of different weights and the presence of nearly flat regions in the error function of MLP. As the legacy of Van Grinsven et al. (2016), García et al. (2010) investigated Majority Voting (MV) schema (MV), SVM, RBF, and MLP for microaneurysm and haemorrhages detection. According to the investigation of García et al. (2010), MV and RBF can be recognised as successful feature detectors. However, training these two detectors is expensive, and between these two, RBF can be considered the best feature detector.

It is important to comprehend the suitable AI methods before implementation to obtain the expected results as implementing these methods is complex, and we need to train the methods recurrently. Supervised, unsupervised, and reinforcement learning are the available techniques for training the AI method. In terms of data processing proficiency, SVM is considered the most suitable and popular supervised learning algorithm compared to other existing algorithms such as ANN, K-nearest Neighbour (KNN), Naïve Bayes classifier, Decision Tree, Fuzzy Logic, and Random Forest. On the other hand, clustering algorithms and association rules are suitable for noisy and low-quality data processing that are the most used unsupervised learning algorithm to develop DL models for medical data processing.

The selection of DL methods to develop AI machines for retinal image analysis must be empirical regarding the retinal image data characteristics, number of parameters for training the algorithms, and length of the training period. For medical image analysis tools, ANN is suitable to implement in DL compared to the logistic regression because of the non-linear operation ability of ANN in high dimensional image data processing, dealing with noisy data, and securing higher prediction accuracy. Recurrent Neural Network (RNN) and CNN have been more efficient in cardiovascular disease state prediction, and abnormal feature detection by analysing retinal and brain MR images (Krittanawong et al., 2017).

The development of appropriate DL-based retinal image segmentation and feature extraction methods is crucially important to understand the complex hierarchical microvasculature of the human retina that can maximise the retinal abnormalities detection result. The highly varied retinal image dataset due to the poor acquisition method can affect the performance of DL models. To avoid this complication, appropriate annotation of characteristics features is significant while preparing the training data. According to the literature study, no DL-based retinal image feature detection method has been reported that can segment retinal microvasculature and extract qualitative and quantitative image features simultaneously. The existing retinal image feature detection algorithms had been developed to detect retinal lesions such as hemorrhages, microaneurysms, and exudates as a single feature. Various CNN models such as recurrent CNN, deep CNN utilise different non-linear functions that obtained comparatively better feature extraction results than the logistic regression approach.

The existing retinal image feature detection methods of García et al. (2009a), García et al. (2010), García et al. (2009b), and Osareh et al. (2009) obtained the best detection performance for image-based criterion compared to the lesion-based criterion. It can be happen due to the lesion's low pixel intensity as the lesion is annotated alone from the whole image. Moreover, pixel-wise ground truth estimation in the lesion-based criterion is cumbersome that can degrade the training accuracy and consequently obtain poor feature detection performance. Though the CNN-based feature detection model showed better performance than the statistical analysis, there are some limitations of this newly developed technology in terms of overfitting training data and lengthy processing due to the utilisation of more parameters. Reducing hidden layers from the CNN architecture and increasing training data can potentially solve the data overfitting problem.

All the recently introduced DL models for feature detection have been investigated to select the suitable CNN architecture for this study. This paper proposes a DL approach for retinal image feature extraction employing the Faster-RCNN method. This proposed method has been designed to extract true vessel segments as retinal image features from the multiple locations of the first top tier of colour retinal images. To train, test, and evaluate the performance of this proposed method, colour retinal images from different publicly

available databases have been extracted. The development of this DL approach is aimed to integrate into our previous work the IP algorithm for retinal vessel diameter quantification of different interesting locations of retinal images for creating a fully automated vessel diameter quantification method (Hoque et al., 2019; Hoque et al., 2018; Kipli et al., 2020). The applied methodology, including training and testing for the development of this proposed DL method, is explained in detail in the following section. The obtained results are briefly described, and the evaluation and critical analysis of the performance are also added consecutively. Figure 1 illustrates the graphical representation of the Faster RCNN model.

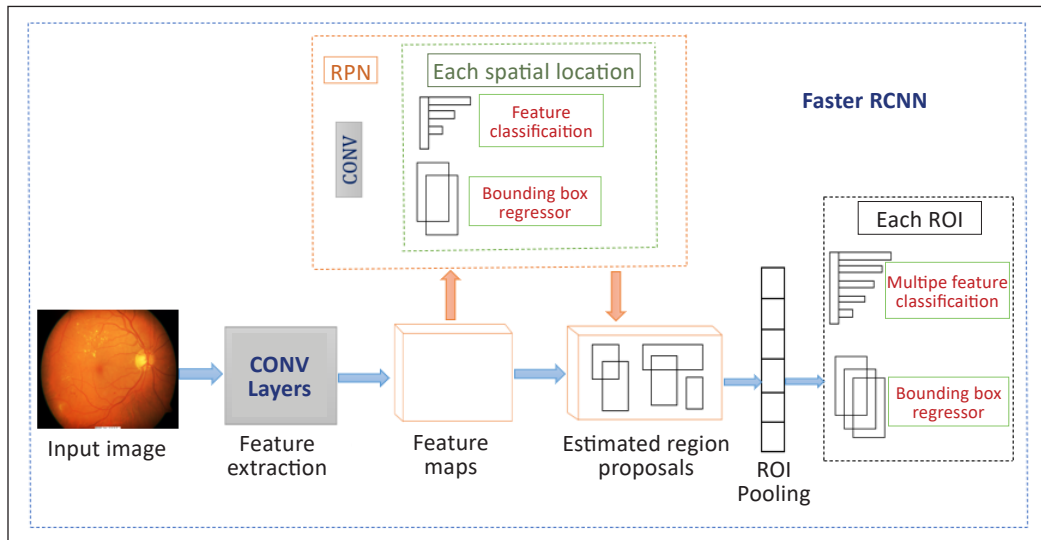


Figure 1. Graphical representation of Faster RCNN model

MATERIALS AND METHODS

The existing IP techniques, and the recently developed DL method, Faster-RCNN, were combined to develop this proposed method. A collection of normal, healthy, and abnormal, pathological, images from the different databases such as High-Resolution Fundus Image Database (HRFID), Digital Retinal Images for Vessel Extraction (DRIVE), Structured Analysis of the Retina (STARE), and MESSIDOR database were used in this research to train, test and validate the proposed DL model. Four hundred fifty images had been used for training and testing this algorithm. These 450 images were divided to form training and testing datasets where the training dataset contained 270 images, and the testing dataset contained 180 images. Both the training and testing dataset consisted of normal and pathological retinal images. Figure 2 describes the involved steps in this proposed method.

At the preprocessing stage, Contrast Limited Adaptive Histogram Equalization (CLAHE) was employed to enhance the quality of the input image. After that, the enhanced image was resized following the DL algorithm’s requirement, [224 224 3], and estimated

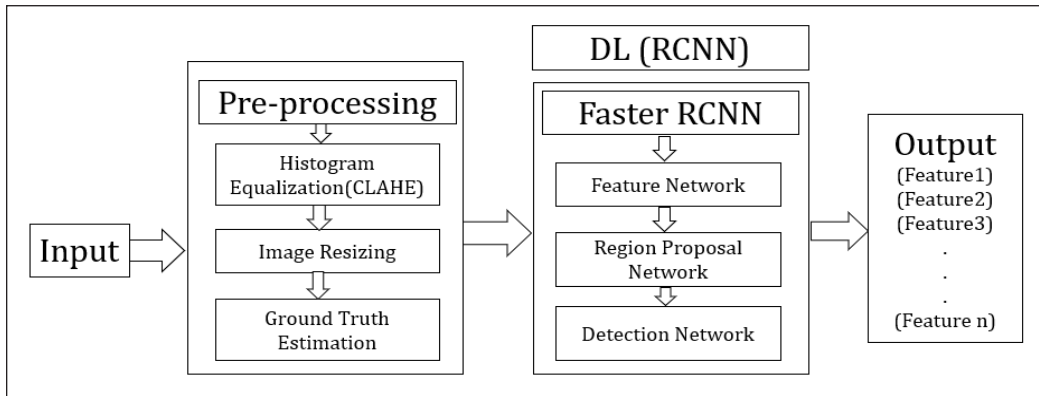


Figure 2. Proposed method

the GroundTruth from that image to extract the features, true vessel, using image labeller apps of MATLAB.

The main vessels of the top first tier were considered Region of Interest (ROI) of all the images. The multiple vessel segments of that ROI were annotated as the ground truth by using bounding boxes. These images with annotated ground truth were augmented to use as training data for securing better performance. A previously developed Faster-RCNN had been trained in this project to detect the expected features of retinal images. Figure 3 demonstrates the graphical representation of the proposed method.

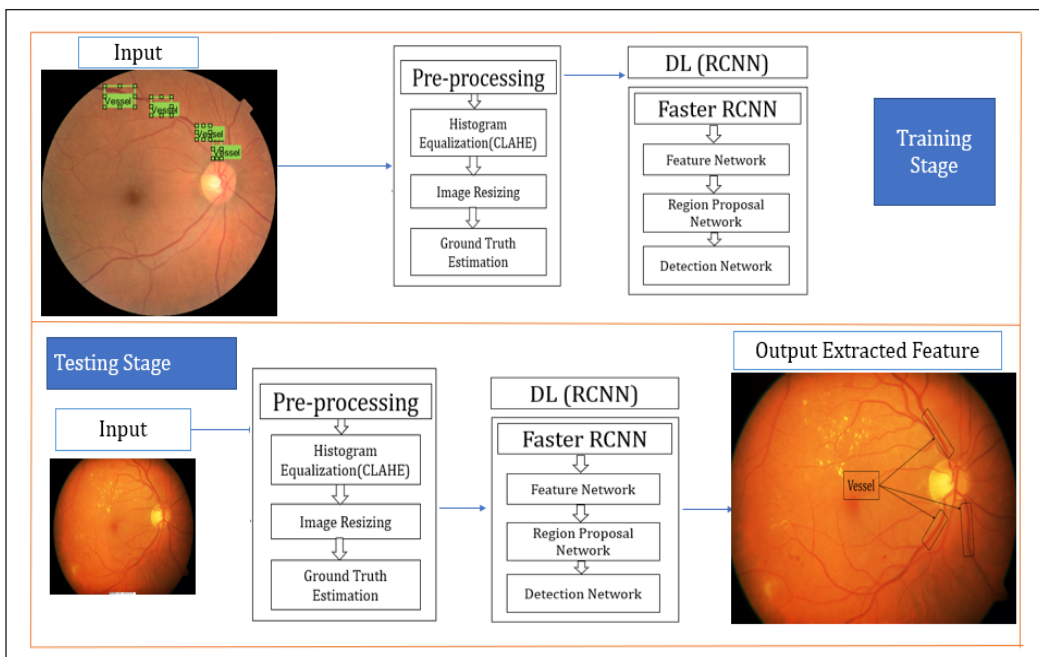


Figure 3. Graphical representation of the proposed method

DL Network (Region-based Convolutional Neural Network, RCNN)

Faster RCNN is the updated version of RCNN developed to detect multiple objects from a single image. To construct DL architecture for this research, Faster RCNN had been used. Faster RCNN uses a separate network, Region Proposal Network (RPN), to detect the region proposals from the feature maps provided by the convolutional layer. The RoI pooling layer reshapes the detected region proposals. It passes these to the fully connected layer, softmax, and linear regression layer that classifies the features and predicts the offset values for the bounding boxes. The Faster RCNN model is the composition of three different modules that are fully convolutional network, feature network, to generate feature maps from the input image, RPN to generate bounding boxes that contain different features or objects extracted from feature maps, and Detection Network that takes input from both RPN and feature network to detect the expected features. This entire system for feature detection is a single unified network.

Feature Network (Convolutional Layer)

The tasks were performed in three different stages to develop the proposed model in this research. First, a Fast R-CNN had been created, and further an RPN was added, and finally, the RPN and detection network was trained. To perform the convolutional operation, a Fast R-CNN, ResNet-50 (Residual Network-50), was trained to produce the feature maps further fed into RPN to generate the region proposals. ResNet-50 is a model of CNN that consists of 50 layers of different fundamental operations of CNN methodology such as convolution, pooling, activation, and fully connected layers. The input size of the images that is suitable for the network is $224 \times 224 \times 3$. The kernel sizes for the initial convolution and max-pooling of the ResNet were considered as 7×7 and 3×3 , respectively, with stride 2 for both convolution and max pooling. The network architecture starts after initial steps that consist of three different residual blocks, and each of the blocks contains three convolution layers performed with 64, 64, and 256 Kernel, respectively. In order to design the deeper ResNet, the bottleneck architecture was used instead of using all 3×3 convolution layers as a standard residual block. In the bottleneck architecture of the residual block, three convolution layers, 1×1 , 3×3 , and 1×1 convolution, is stacked one over another for each residual function. 1×1 is used to reduce the input dimension before performing the 3×3 convolution, and then another 1×1 convolution layer is used to preserve the original shape. The size of the stride, stride 2, reduces the height and width of the input to half and doubles the channel width for the following stages. There are 4, 6, and 3 residual blocks in stages 2, 3, and 4, respectively. The network has an average pooling layer followed by a fully connected layer as the final layer.

Region-based Proposal Network (RPN)

RPN contains 3 convolution layers that take the feature map as input are generated from the feature network and produces region proposals with bounding boxes containing the potential features. In order to generate the region proposal, a sliding window of 3×3 size kernel was used for each location of the feature map and 9 ($K=9$) anchor boxes with three different scales of 128, 256, and 512, and 3 aspect ratios of 1:1, 1:2, and 2:1 were used for each location. In addition, a box-class layer, cls layer, results in $2K$ scores that the anchor boxes contain an object or not, and a box regression layer, reg layer, results in $4K$ for the coordinates of K boxes. Figure 4 illustrates the operational block diagram of RPN.

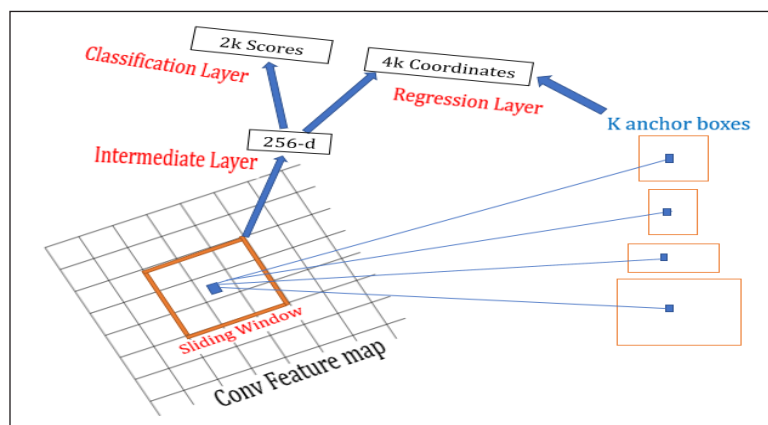


Figure 4. Operational block diagram of RPN

Detection Network

Fast RCNN had been adopted to construct the detection network where two sibling layers get input from the feature network and RPN. The output proposals from the pooling layer were fed to the classification layer, softmax classification, and linear regression layer, bounding box regression layer of the detection network as a batch. The softmax classification layer classifies the RoI pooling layer output, RoI bounding box, by computing the probability distribution, $p = (p_0, \dots, p_k)$ over the $K+1$ class throughout the fully connected layer. The bounding box regression layer is responsible for predicting the bounding boxes, by computing the regression offsets for each object class. The regression layer generates 4 bounding box offsets that can be explained as $t_i^k = (t_x^k, t_y^k, t_w^k, t_h^k)$ where $i=x,y,w,h$, and (x,y) denotes the coordinates of the top left corner of the bounding box and w and h denote the width and height of the bounding box respectively.

Training DL Network

To train the proposed DL method stochastic gradient descent training algorithm had been used with an initial learning rate of 1×10^{-3} Twenty epoch and 400 iterations for each

epoch were performed to accomplish the whole training process. The mini-batch size was set to 3. As the Faster RCNN had been used in this research, the standard cost function was used to calculate the training loss. The whole training procedures for the entire network are briefly described in the following sections.

Training RPN

The number of anchors was reduced to train the RPN. Initially, the anchors were assigned by a binary class label threshold. Further, the values of Intersection over Union (IoU) of primary and predicted bounding boxes of anchors were considered to reduce the number of anchors. The IoU measures the overlap between the primary and the predicted boundary boxes. If the value of IoU is greater than 0.4, then the anchor is assigned as a positive label while the anchor is assigned as a negative label if the value of IoU is lower than 0.3. The rest anchors that do not satisfy this condition were not considered for the RPN training process. Thus, the multi-task training loss for RPN combines the losses in classification and regression operation calculated by Equation 1.

$$L(\{P_i\}, \{t_i\}) = \frac{1}{N_{cls}} \sum_i L_{cls}(p_i, p_i^*) + \lambda \frac{1}{N_{reg}} \sum_i p_i^* L_{reg}(t_i, t_i^*) \quad (1)$$

Here λ is the balancing parameter to balance the weights of L_{cls} and L_{reg} roughly. L_{cls} is the classification loss which is log loss over two different classes of anchor, object, or not an object. The term i represents the index number of mini-batch, where p_i denotes the output label from the classification layer for i^{th} anchor and p_i^* denotes the ground-truth label. The label of both p_i and p_i^* is binary, 1 or 0 where 1 indicates a boundary box is an object, and 0 indicates the boundary box is not an object. L_{reg} is the regression loss considered for calculation if the anchor is an object, where t_i^* is the regression target, ground-truth coordinate for the regression layer, and t_i outputs of the learned regression layer.

After the sampling of anchors, the region proposals with that sampled anchors were fed to the Region of Interest (RoI) pooling. The RoI pooling layer employs max pooling to extract the fixed-sized feature maps with the size of (N, 7, 7, 512) for each proposal. Here N, is the number of Region proposals from RPN. Figure 5 illustrates the operation of the RoI pooling layer.

Training Detection Network

The threshold values of IoU were set to 0.1 to 0.5 to label the ROIs as background To train the detection network. The RoI was labelled as foreground when the IoU is above 0.5. Bounding box targets, ground truth boxes were also generated following the same approach of RPN. The multitask loss L was calculated for each labelled RoI to estimate

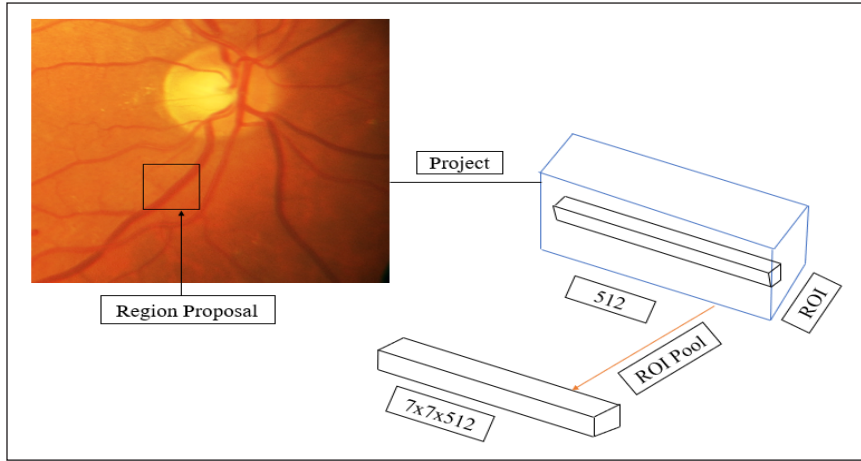


Figure 5. Operation of RoI pooling layer

the loss during training the detection network. The loss in the classification layer had been calculated by a cross-entropy or log loss, while the smooth L_1 loss had calculated regression loss for bounding box regression. The multitask loss L was calculated by Equation 2,

$$L(p, u, t^u, v) = L_{cls}(p, u) + \lambda[u \geq 1]L_{loc}(t^u, v) \quad (2)$$

Here $L_{cls}(p, u)$ is log loss and $L_{cls} = -\log p_u$ where u is the true feature class in the bounding box. $L_{loc}(t^u, v)$ is the loss of the regression layer, which is calculated by smooth L_1 loss. The balancing parameter is denoted by λ , u represents the class, and v represents the bounding box regression targets for class u . The term $[u \geq 1]$ determines the true bounding box regression targets. When $u=0$, the regression loss is considered 0 because there were no ground-truth boxes for the background. The bounding box regression loss, $L_{loc}(t^u, v)$, was computed by Equation 3,

$$L_{loc}(t^u, v) = \sum_{i \in \{x, y, w, h\}} \text{smooth}L_1(t_i^u - v_i) \quad (3)$$

Where smooth L_1 was determined by Equation 4,

$$\text{Smooth}L_1(x) = \begin{cases} 0.5x^2 & \text{if } |x| < 1 \\ |x| - 0.5 & \text{otherwise,} \end{cases} \quad (4)$$

Smooth loss L_1 was used because it is less sensitive to outliers, and $\lambda=1$ was set to balance the two losses. Finally, the ground truth regression target v_i was normalised for the mean as zero and unit variance.

The 4 Step alternating training method (Ren et al., 2017) was further employed to the RPN and Detection Network simultaneously to share the weights of convolution layers of the two networks between themselves. In the first step of this training method, the RPN

was trained as described in the section, **Training RPN**. Then, an ImageNet pre-trained model was used to initialise the RPN and fine-tuned end-to-end for the region proposal task in step 1. Next, the proposals generated in step 1 were used by Fast RCNN to train the detection network in step 2, which the ImageNet pre-trained model also initialised. Although, as in these training steps, the two networks do not share convolution layers, the detection network was used to initialise to train RPN in the third step. In this step, the shared convolution layers were fixed and fine-tuned the unique layers to RPN. In the final step, step 4, the unique convolution layers of Fast RCNN were also fine-tuned following the fixed shared convolutional layers. In this way, a unified network, Faster RCNN, was formed where both networks share the same convolution layers.

RESULT

The training performance was measured for each iteration of each epoch of the training stage. The training loss and the Root Mean Squared Error (RMSE) after the final epoch were recorded as 0.3446 and 0.17. It was observed that the training performance of the proposed network had increased over time and reached 99.4% training accuracy after 7 training epochs. After the completion of training, the proposed method had been tested on two different datasets, healthy and unhealthy datasets. The healthy dataset had been created extracting images from DRIVE, and the images for the unhealthy dataset were taken from Kaggle. These two unknown datasets consisted of 700 images. The proposed method was able to detect the true vessel from both healthy and unhealthy images. Figure 6 demonstrates the images, healthy and unhealthy, with the true detected vessel. The testing performance of the proposed method for these two unknown datasets was also recorded. Table 1 represents the testing performance of the proposed method for the unknown dataset.

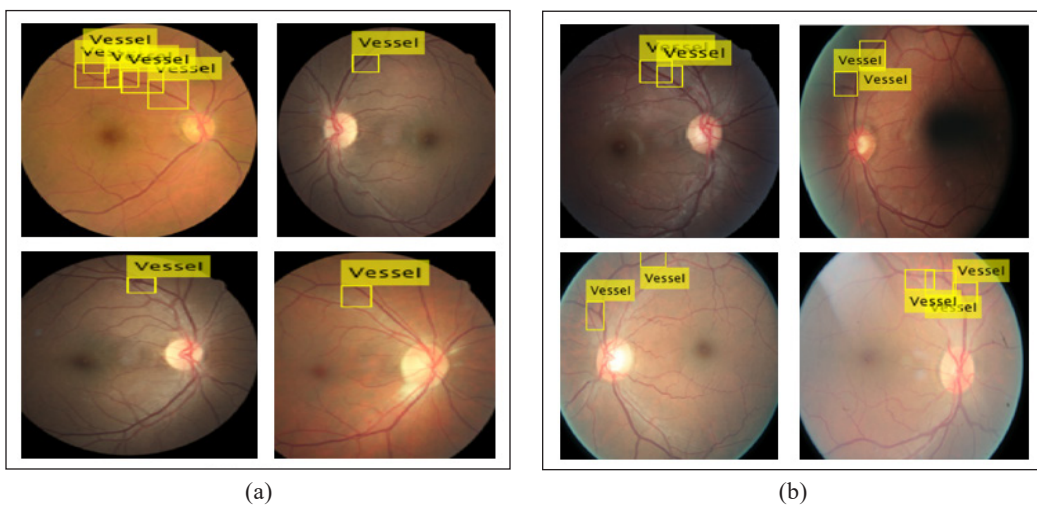


Figure 6. Test images: (a) healthy and (b) unhealthy with the true detected vessel

In Table 1, columns 1,2 and 3 represent the datasets, Se, and PPV of the proposed method. The network successfully detected the true vessel from the interesting location of those images. Figure 7 shows the retinal images with the true detected vessel from multiple locations.

Table 1
Testing performance of the proposed method for the unknown dataset

Dataset	Se (Mean value, %)	PPV (Mean value, %)
Healthy Dataset	90.53	61.22
Unhealthy Dataset	88.16	60.67

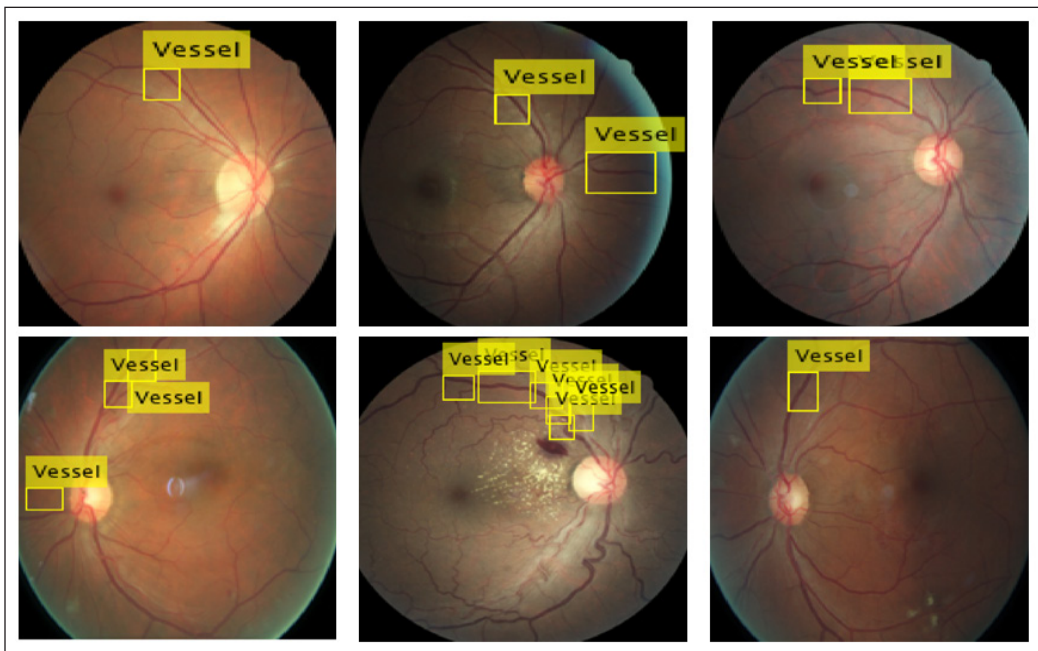


Figure 7. Retinal Images with the true detected vessel from multiple locations

Sensitivity (Se) and Positive Predictive Value(PPV) had been calculated to evaluate the performance of the proposed DL method. In addition, the testing dataset that was pre-processed for use in this research had been used for testing and calculating the performance measurement matrices. Table 2 illustrate the performance comparison between the recently developed methods and the proposed method.

In Table 2, columns 1,2,3 and 4 representing the author’s information, applied method, features extracted, and result, respectively. According to column 3 of Table 2, it is seen that most of the methods were developed to detect different features such as haemorrhages, exudates, microaneurysms, and the proposed method focused on true vessel detection.

Table 2
Comparison of proposed method performance and existing methods

Author	Method Applied	Extracted Feature	Result (Mean Value %)	
			Se	PPV
(Tan et al., 2017)	CNN (10 Layered)	Exudates	87.58	
		Haemorrhages Microaneurysm	62.57	
(García et al., 2010)	Logistic Regression (MLP, RBF, SVM and combining these three NNs using an MV schema)	Haemorrhages, Microaneurysm		
		Image-based	100	56
		Lesion-based	86.01	51.99
		Retinal Exudates (Image-Based)	96.00	94.60
(García, Sánchez, Poza, et al., 2009)	Logistic Regression RBFNN	Retinal Hard Exudates (Lesion-Based)	92.10	86.40
		Retinal Hard Exudates (Image-Based)	100	70.4
(García, Sánchez, López, et al., 2009)	Logistic Regression MLP, RBFNN, SVM	Retinal Hard Exudates (Lesion-Based)		
		MLP	88.14	80.72
		RBF	88.49	77.41
		SVM	87.61	83.51
		Retinal Hard Exudates (Image-Based)		
		MLP	100	92.59
		RBF	100	81.48
		SVM	100	77.78
(Van Grinsven et al., 2016)	SeSCNN NSeSCNN	Haemorrhages, SeSCNN (FP*1)	78.60	
		Haemorrhages, SeSCNN(FP0.1)	51.10	
		Haemorrhages NSeSCNN(FP1)	75.30	
		Haemorrhages, NSeSCNN (FP0.1)	31.60	
Proposed Method	Faster RCNN	True vessel	92.81	63.34

Though all methods are dedicated to detecting different features, their performance is tabulated here as the retinal image feature detector.

DISCUSSION AND CONCLUSION

Faster RCNN is primarily introduced for multiple object detection from a single image. In this proposed method, this Faster RCNN has been used as a feature detector dedicated to extracting true vessels from interesting locations of retinal images. As this study is the pre-step of developing an automated retinal vessel diameter quantification algorithm, the ROIs for true vessels from different locations are considered during ground truth estimation following the recommendation of local clinical experts and the manually marked ROIs

of (Al-Diri et al., 2008). It is seen from the performance analysis table, Table 2 that the proposed method obtained 92.81% sensitivity and 62.34% PPV. Furthermore, the proposed method showed better performance as a feature extractor compared to the lesion-based feature extractor of García et al. (2010) and García et al. (2009b), and the exudates detector of Van Grinsven et al. (2016).

Though the proposed method's performance is slightly lower than some of the mentioned feature extractors in Table 2, the result is still comparable and considered for further development. In Figure 5, the unhealthy images contain the diabetic lesion, so the microvascular structure cannot be extracted more precisely. The performance of the proposed method with the unknown datasets was also satisfactory. The proposed method obtained 90.53% and 88.16% Se, and 61.22% and 60.67% PPV for both healthy and unhealthy datasets (Table 1), respectively. It is seen that the performance of the proposed method for anonymous healthy and unhealthy data is slightly lower than the data that were pre-processed initially for training and testing the proposed method. For the healthy dataset, this deviation was happened due to the algorithm's execution with the anonymous data that were not pre-processed initially. The cause of the deviation in the performance of a proposed method for an unhealthy dataset is due to retinopathies and lesions.

Attaining maximum results is challenging due to the highly complex and hierarchical structure of retinal images. The proposed method had been trained with a comparatively small dataset that consists of 270 images containing healthy and pathological signs. As it is suggested to train the DL method with a large dataset, data augmentation had been performed to secure the best training performance. The obtained testing performance of the proposed method showed consistency as the testing dataset contained both normal retinal images and images with abnormality. Data pre-processing is considered one of the most crucial parts of DL algorithm development. Therefore, it is highly expected to use primary data and perform a better operation for data pre-processing such as enhance data quality by histogram equalisation and efficient ground truth estimation for training, testing, and validating the proposed method.

To increase the robustness of the proposed method, utilising a large dataset is highly recommended, and training options should be empirical. It is recommended to configure the training option by setting with more epochs, high Verbose-Frequency to secure the maximum result. Due to the inefficient retinal image acquisition, annotating the background and foreground appears to be a major challenge, and the parameter values of positive and negative overlapping need to be focused on for more accurate feature detection. In order to secure the best detection result, different ranges for positive and negative overlapping have been explored in this study. It was investigated that the range [0 0.3] for negative overlapping and [0.4 1] for positive overlapping is the best suit for training the proposed algorithm. As the retinal vessel detection is considered a small object and the difference

between the background and true vessel pixel values is less, the positive overlap range needs to be larger to distinguish the expected objects during training the system. Though the obtained result is satisfactory, this study has some limitations, such as lack of primary retinal image data and highly configured hardware with efficient graphics computing units that are crucially important for higher detection accuracy and speed up the training process. To further development this proposed method, it is recommended to use a large dataset of real images containing healthy retinal images and retinal images with the abnormality. It is expected to integrate this proposed method in clinical tools with further development, evaluation, and validation.

ACKNOWLEDGMENT

It is at this moment declared that this paper had not been submitted anywhere for publication, and there is no conflict of interest for publishing this paper. The authors would like to thank University Malaysia Sarawak (UNIMAS) and Fusionex International for supporting this research through UNIMAS-Fusionex Research Grant (RG/F02/FUSX/01/2019).

REFERENCE

- Abadi, M., McMahan, H. B., Chu, A., Mironov, I., Zhang, L., Goodfellow, I., & Talwar, K. (2016). Deep learning with differential privacy. *Proceedings of the ACM Conference on Computer and Communications Security, 24-28-Octo(Ccs)*, 308-318. <https://doi.org/10.1145/2976749.2978318>
- Abbasi-sureshjani, M. F. S., Romeny, H., & Sarti, A. (2016). Analysis of vessel connectivities in retinal images by cortically inspired spectral clustering. *Journal of Mathematical Imaging and Vision*, 56(1), 158-172. <https://doi.org/10.1007/s10851-016-0640-1>
- Abràmoff, M. D., Lou, Y., Erginay, A., Clarida, W., Amelon, R., Folk, J. C., & Niemeijer, M. (2016). Improved automated detection of diabetic retinopathy on a publicly available dataset through integration of deep learning. *Investigative Ophthalmology and Visual Science*, 57(13), 5200-5206. <https://doi.org/10.1167/iovs.16-19964>
- Al-Diri, B., Hunter, A., Steel, D., Habib, M., Hudaib, T., & Berry, S. (2008). A reference data set for retinal vessel profiles. In *2008 30th Annual International Conference of the IEEE Engineering in Medicine and Biology Society* (pp. 2262-2265). IEEE Publishing. <https://doi.org/10.1109/IEMBS.2008.4649647>
- Alom, M. Z., Hasan, M., Yakopcic, C., Taha, T. M., & Asari, V. K. (2018). *Recurrent residual convolutional neural network based on U-Net (R2U-Net) for medical image segmentation*. ArXiv Publishing.
- Badawi, S. A., & Fraz, M. M. (2019). Multiloss function based deep convolutional neural network for segmentation of retinal vasculature into arterioles and venules. *BioMed Research International*, 2019, Article 4747230. <https://doi.org/10.1155/2019/4747230>
- Baker, M. L., Hand, P. J., Wang, J. J., & Wong, T. Y. (2008). Retinal signs and stroke: Revisiting the link between the eye and brain. *Stroke*, 39(4), 1371-1379. <https://doi.org/10.1161/STROKEAHA.107.496091>

- Buduma, N., & Locascio, N. (2017). *Fundamentals of deep learning: Designing next-generation machine intelligence algorithm*. O'Reilly Media Inc.
- De Silva, D. A., Manzano, J. J. F., Liu, E. Y., Woon, F. P., Wong, W. X., Chang, H. M., Chen, C., Lindley, R. I., Wang, J. J., Mitchell, P., Wong, T. Y., & Wong, M. C. (2011). Retinal microvascular changes and subsequent vascular events after ischemic stroke. *Neurology*, *77*(9), 896-903. <https://doi.org/10.1212/WNL.0b013e31822c623b>
- Fenner, B. J., Wong, R. L. M., Lam, W. C., Tan, G. S. W., & Cheung, G. C. M. (2018). Advances in retinal imaging and applications in diabetic retinopathy screening: A review. *Ophthalmology and Therapy*, *7*(2), 333-346. <https://doi.org/10.1007/s40123-018-0153-7>
- García, M., López, M. I., Álvarez, D., & Hornero, R. (2010). Assessment of four neural network based classifiers to automatically detect red lesions in retinal images. *Medical Engineering and Physics*, *32*(10), 1085-1093. <https://doi.org/10.1016/j.medengphy.2010.07.014>
- García, M., Sánchez, C. I., Poza, J., López, M. I., & Hornero, R. (2009a). Detection of hard exudates in retinal images using a radial basis function classifier. *Annals of Biomedical Engineering*, *37*(7), 1448-1463. <https://doi.org/10.1007/s10439-009-9707-0>
- García, M., Sánchez, C. I., López, M. I., Abásolo, D., & Hornero, R. (2009b). Neural network based detection of hard exudates in retinal images. *Computer Methods and Programs in Biomedicine*, *93*(1), 9-19. <https://doi.org/10.1016/j.cmpb.2008.07.006>
- Gargeya, R., & Leng, T. (2017). Automated identification of diabetic retinopathy using deep learning. *Ophthalmology*, *124*(7), 962-969. <https://doi.org/10.1016/j.ophtha.2017.02.008>
- Ghesu, F. C., Krubasik, E., Georgescu, B., Singh, V., Zheng, Y., Hornegger, J., & Comaniciu, D. (2016). Marginal space deep learning: Efficient architecture for volumetric image parsing. *IEEE Transactions on Medical Imaging*, *35*(5), 1217-1228. <https://doi.org/10.1109/TMI.2016.2538802>
- Goodfellow, I., Bengio, Y., & Courville, A. (2016). *Deep Learning*. MIT Press.
- Grassmann, F., Mengelkamp, J., Brandl, C., Harsch, S., Zimmermann, M. E., Linkohr, B., Peters, A., Heid, I. M., Palm, C., & Weber, B. H. F. (2018). A deep learning algorithm for prediction of age-related eye disease study severity scale for age-related macular degeneration from color fundus photography. *Ophthalmology*, *125*(9), 1410-1420. <https://doi.org/10.1016/j.ophtha.2018.02.037>
- Gulshan, V., Peng, L., Coram, M., Stumpe, M. C., Wu, D., Narayanaswamy, A., Venugopalan, S., Widner, K., Madams, T., Cuadros, J., Kim, R., Raman, R., Nelson, P. C., Mega, J. L., & Webster, D. R. (2016). Development and validation of a deep learning algorithm for detection of diabetic retinopathy in retinal fundus photographs. *JAMA - Journal of the American Medical Association*, *316*(22), 2402-2410. <https://doi.org/10.1001/jama.2016.17216>
- Guo, S., Wang, K., Kang, H., Zhang, Y., Gao, Y., & Li, T. (2019). BTS-DSN: Deeply supervised neural network with short connections for retinal vessel segmentation. *International Journal of Medical Informatics*, *126*, 105-113. <https://doi.org/10.1016/j.ijmedinf.2019.03.015>
- Henderson, A. D., Bruce, B. B., Newman, N. J., & Biousse, V. (2011). Hypertension-related eye abnormalities and the risk of stroke. *Reviews in Neurological Diseases*, *8*(404), 1-9. <https://doi.org/10.3909/rind0274>

- Hoque, M. E., Kipli, K., Zulcaffle, T. M. A., Mat, D. A. A., Joseph, A., Zamhari, N., Sapawi, R., & Arafat, M. Y. (2019). Segmentation of retinal microvasculature based on iterative self-organizing data analysis technique (ISODATA). In *2019 International UNIMAS STEM 12th Engineering Conference (EnCon)* (pp. 59-64). IEEE Publishing. <https://doi.org/10.1109/EnCon.2019.8861259>
- Hoque, M. E., Kipli, K., Zulcaffle, T. M. A., Sapawi, R., Joseph, A., Abidin, W. A. W. Z., & Sahari, S. K. (2018). Feature extraction method of retinal vessel diameter. In *2018 IEEE-EMBS Conference on Biomedical Engineering and Sciences (IECBES)* (pp. 279-283). IEEE Publishing. <https://doi.org/10.1109/IECBES.2018.8626660>
- James, M. (2000). Cost effectiveness analysis of screening for sight-threatening diabetic eye disease. *BMJ*, *320*(7250), 1627-1631. <https://doi.org/10.1136/bmj.320.7250.1627>
- Kipli, K., Hoque, M. E., Lim, L. T., Mahmood, M. H., Sahari, S. K., Sapawi, R., Rajae, N., & Joseph, A. (2018). A review on the extraction of quantitative retinal microvascular image feature. *Computational and Mathematical Methods in Medicine, 2018*, Article 4019538. <https://doi.org/10.1155/2018/4019538>
- Kipli, K., Hoque, M. E., Lim, L. T., Zulcaffle, T. M. A., Sahari, S. K., & Mahmood, M. H. (2020). Retinal image blood vessel extraction and quantification with Euclidean distance transform approach. *IET Image Processing*, *14*(15), 3718-3724. <https://doi.org/10.1049/iet-ipr.2020.0336>
- Krittanawong, C., Zhang, H. J., Wang, Z., Aydar, M., & Kitai, T. (2017). Artificial intelligence in precision cardiovascular medicine. *Journal of the American College of Cardiology*, *69*(21), 2657-2664. <https://doi.org/10.1016/j.jacc.2017.03.571>
- Lahiri, A., Roy, A. G., Sheet, D., & Biswas, P. K. (2016). Deep neural ensemble for retinal vessel segmentation in fundus images towards achieving label-free angiography. In *2016 38th annual international conference of the IEEE engineering in medicine and biology society (EMBC)* (pp. 1340-1343). IEEE Publishing. <https://doi.org/10.1109/EMBC.2016.7590955>
- Maji, D., Santara, A., Ghosh, S., Sheet, D., & Mitra, P. (2015). Deep neural network and random forest hybrid architecture for learning to detect retinal vessels in fundus images. In *2015 37th annual international conference of the IEEE Engineering in Medicine and Biology Society (EMBC)* (pp. 3029-3032). IEEE Publishing. <https://doi.org/10.1109/EMBC.2015.7319030>
- Melinsca, M., Prentasic, P., & Loncaric, S. (2015). Retinal vessel segmentation using deep neural networks. In *Proceedings of the 10th International Conference on Computer Vision Theory and Applications (VISAPP-2015)* (pp. 577-582). Science and Technology Publications. <https://doi.org/10.5220/0005313005770582>
- Mo, J., & Zhang, L. (2017). Multi-level deep supervised networks for retinal vessel segmentation. *International Journal of Computer Assisted Radiology and Surgery*, *12*(12), 2181-2193. <https://doi.org/10.1007/s11548-017-1619-0>
- Niemeijer, M., Van Ginneken, B., Russell, S. R., Suttorp-Schulten, M. S. A., & Abramoff, M. D. (2007). Automated detection and differentiation of drusen, exudates, and cotton-wool spots in digital color fundus photographs for diabetic retinopathy diagnosis. *Investigative Ophthalmology and Visual Science*, *48*(5), 2260-2267. <https://doi.org/10.1167/iovs.06-0996>

- Oliveira, A., Pereira, S., & Silva, C. A. (2018). Retinal vessel segmentation based on fully convolutional neural networks. *Expert Systems with Applications*, *112*, 229-242. <https://doi.org/10.1016/j.eswa.2018.06.034>
- Ong, Y. T., Wong, T. Y., Klein, R., Klein, B. E., Mitchell, P., Sharrett, A. R., Couper, D. J., & Ikram, M. K. (2013). Hypertensive retinopathy and risk of stroke. *Hypertension*, *62*(4), 706-711. <https://doi.org/10.1161/HYPERTENSIONAHA.113.01414>
- Osareh, A., Mirmehdi, M., Thomas, B., & Markham, R. (2003). Automated identification of diabetic retinal exudates in digital colour images. *British Journal of Ophthalmology*, *87*(10), 1220-1223. <http://dx.doi.org/10.1136/bjo.87.10.1220>
- Osareh, A., Shadgar, B., & Markham, R. (2009). A computational-intelligence-based approach for detection of exudates in diabetic retinopathy images. *IEEE Transactions on Information Technology in Biomedicine*, *13*(4), 535-545. <https://doi.org/10.1109/TITB.2008.2007493>
- Pratt, H., Coenen, F., Broadbent, D. M., Harding, S. P., & Zheng, Y. (2016). Convolutional neural networks for diabetic retinopathy. *Procedia Computer Science*, *90*(July), 200-205. <https://doi.org/10.1016/j.procs.2016.07.014>
- Ren, S., He, K., Girshick, R., & Sun, J. (2017). Faster R-CNN: Towards real-time object detection with region proposal networks. *IEEE Transactions on Pattern Analysis and Machine Intelligence*, *39*(6), 1137-1149. <https://doi.org/10.1109/TPAMI.2016.2577031>
- Schmidt-Erfurth, U., Sadeghipour, A., Gerendas, B. S., Waldstein, S. M., & Bogunović, H. (2018). Artificial intelligence in retina. *Progress in Retinal and Eye Research*, *67*(May), 1-29. <https://doi.org/10.1016/j.preteyeres.2018.07.004>
- Takahashi, H., Tampo, H., Arai, Y., Inoue, Y., & Kawashima, H. (2017). Applying artificial intelligence to disease staging: Deep learning for improved staging of diabetic retinopathy. *PLoS ONE*, *12*(6), 1-11. <https://doi.org/10.1371/journal.pone.0179790>
- Tan, J. H., Fujita, H., Sivaprasad, S., Bhandary, S. V., Rao, A. K., Chua, K. C., & Acharya, U. R. (2017). Automated segmentation of exudates, haemorrhages, microaneurysms using single convolutional neural network. *Information Sciences*, *420*(August), 66-76. <https://doi.org/10.1016/j.ins.2017.08.050>
- Ting, D. S. W., Cheung, C. Y. L., Lim, G., Tan, G. S. W., Quang, N. D., Gan, A., Hamzah, H., Garcia-Franco, R., Yeo, I. Y. S., Lee, S. Y., Wong, E. Y. M., Sabanayagam, C., Baskaran, M., Ibrahim, F., Tan, N. C., Finkelstein, E. A., Lamoureux, E. L., Wong, I. Y., Bressler, N. M., ... & Wong, T. Y. (2017). Development and validation of a deep learning system for diabetic retinopathy and related eye diseases using retinal images from multiethnic populations with diabetes. *JAMA - Journal of the American Medical Association*, *318*(22), 2211-2223. <https://doi.org/10.1001/jama.2017.18152>
- Van Grinsven, M. J. J. P., Van Ginneken, B., Hoyng, C. B., Theelen, T., & Sánchez, C. I. (2016). Fast convolutional neural network training using selective data sampling: Application to hemorrhage detection in color fundus images. *IEEE Transactions on Medical Imaging*, *35*(5), 1273-1284. <https://doi.org/10.1109/TMI.2016.2526689>
- Wang, C., Zhao, Z., Ren, Q., Xu, Y., & Yu, Y. (2019). Dense U-net based on patch-based learning for retinal vessel segmentation. *Entropy*, *21*(2), 1-15. <https://doi.org/10.3390/e21020168>

- Wang, J. J., Baker, M. L., Hand, P. J., Hankey, G. J., Lindley, R. I., Rohtchina, E., Wong, T. Y., Liew, G., & Mitchell, P. (2011). Transient ischemic attack and acute ischemic stroke: Associations with retinal microvascular signs. *Stroke*, *42*(2), 404-408. <https://doi.org/10.1161/STROKEAHA.110.598599>
- Wang, S., Yin, Y., Cao, G., Wei, B., Zheng, Y., & Yang, G. (2015). Hierarchical retinal blood vessel segmentation based on feature and ensemble learning. *Neurocomputing*, *149*(PB), 708-717. <https://doi.org/10.1016/j.neucom.2014.07.059>
- Witt, N., Wong, T. Y., Hughes, A. D., Chaturvedi, N., Klein, B. E., Evans, R., McNamara, M., McG Thom, S. A., & Klein, R. (2006). Abnormalities of retinal microvascular structure and risk of mortality from ischemic heart disease and stroke. *Hypertension*, *47*(5), 975-981. <https://doi.org/10.1161/01.HYP.0000216717.72048.6c>
- Yan, Z., Yang, X., & Cheng, K. T. (2019). A three-stage deep learning model for accurate retinal vessel segmentation. *IEEE Journal of Biomedical and Health Informatics*, *23*(4), 1427-1436. <https://doi.org/10.1109/JBHI.2018.2872813>
- Zhu, C., Zou, B., Zhao, R., Cui, J., Duan, X., Chen, Z., & Liang, Y. (2017). Retinal vessel segmentation in colour fundus images using Extreme Learning Machine. *Computerized Medical Imaging and Graphics*, *55*(2017), 68-77. <https://doi.org/10.1016/j.compmedimag.2016.05.004>



Development of Micro-Spatial Electricity Load Forecasting Methodology Using Multivariate Analysis for Dynamic Area in Tangerang, Indonesia

Adri Senen^{1*}, Christine Widyastuti¹, Oktaria Handayani¹ and Perdana Putera^{2,3}

¹Electrical Engineering Department, Institut Teknologi PLN, Menara PLN, Jl. Lingkar Luar Barat, Duri Kosambi, Cengkareng, Jakarta Barat 11750, Indonesia

²Agricultural Technology Department, Politeknik Pertanian Negeri Payakumbuh, Jalan Raya Negara km 7 Tanjung Pati 50 Kota Sumatera Barat 26271, Indonesia

³Electrical and Electronic Engineering Department, University of Nottingham, PEMC building Jubilee Campus Nottingham NG8 1BB, United Kingdom

ABSTRACT

Dynamic population and land use significantly affect future energy demand. This paper proposes a suitable method to forecast load growth in a dynamic area in Tangerang, Indonesia. This research developed micro-spatial load forecasting, which can show load centres in microgrids, estimate the capacity and locate the distribution station precisely. Homogenous grouping implemented the method into clusters consisted of microgrids. It involves multivariate variables containing 12 electric and non-electric variables. Multivariate analysis is conducted by carrying out Principal Component Analysis (PCA) and Factor Analysis. The forecasting results can predict load growth, time, and location, which can later be implemented as the basis of a master electricity distribution plan because it provides an accurate long-term forecast.

Keywords: Dynamic area, load forecasting, micro-spatial, multivariate

ARTICLE INFO

Article history:

Received: 09 April 2021

Accepted: 05 July 2021

Published: 08 October 2021

DOI: <https://doi.org/10.47836/pjst.29.4.18>

E-mail addresses:

adrisenen@itpln.ac.id (Adri Senen)

christinewidyastuti@gmail.com (Christine Widyastuti)

oktaria@itpln.ac.id (Oktaria Handayani)

perdana.putera@nottingham.ac.uk (Perdana Putera)

* Corresponding author

INTRODUCTION

Demographic change combined with the depletion of our natural resources is remodelling how society in using energy. As the population increases or decreases, accurate load forecasting is the first step in planning the expansion of electric power to estimate energy demand or prioritise

renewable energy installation acceleration in the future and reduce the negative effect of global warming (Lagaaij, 2018).

By far, one of the most trending methods is sectoral load forecasting. This technique is straightforward but lacks accuracy in areas with impoverished data available and dynamic service areas. It means on an area with rapid change on land use because of economic growth and population, the results are still macro and cannot precisely depict load centres in smaller area service (grid) and cannot determine the substation's location.

Therefore, a smaller area or micro-spatial technique may play an essential role in ensuring load forecast. Methods to forecast small area loads fall into two major categories (Carvalho et al., 2016; Fu et al., 2018; Kobylinski et al., 2020), trending and simulation. Trending methods work with present and past-small area load data, extrapolating past load growth trends to project future load. It uses some techniques like time series (Avazov et al., 2019), curve fitting (El Kafazi et al., 2017), ARIMA (Al Amin & Hoque, 2019). The proposed model has the capability of filtering datasets and improving forecasting performance. However, these forecast methods do not deal with the area with no historical data and do not show the interaction of factors that influence load growth. However, the current method is more accurate when it is used for short-term load forecasting. It did not show the interaction of factors that affect the load growth. Generally, the load forecasting algorithm is built by involving 2 to 4 variables and ignored changes in land use and spatial planning. The result is biased in the medium and long term when applied to power distribution networks in the dynamic area.

The latest method facilitates forecasting based on the value of past requests and other factors that influence it, for instance, population and weather (Mukhopadhyay et al., 2017). For time-series data that have two or more variables. Certainly, it would not be too appropriate if the analysis was done using time series models (Avazov et al., 2019) because it does not rule out the possibility of interrelationships between one data with the other data. Therefore, multivariate models were needed. The models included in the multivariate analysis are more complicated than the univariate models (Jimenez et al., 2019). The multivariate model itself can be in the form of bivariate data analysis (only two-time series data) and the form of multivariate data (more than two-time series data). Multivariate models include transfer function models, intervention analysis, Fourier analysis, spectral analysis and vector time series models. Microspatial simulation methods (Babcock et al., 2013; Jimenez et al., 2019) perform detailed multivariate modelling. They work with land-use, demographic, geographic and end-use information in addition to electrical load data and attempt to reproduce, or simulate, the process of growth.

This paper developed a suitable methodology for areas experiencing dynamic regional use changes (urban area) while still involving many variables that influence the load growth itself. The case study in this article is Tangerang, Indonesia. The micro-spatial method is

based on clustering to show and simulate different factors that cause load growth for each cluster, according to the area's characteristics. Whilst the previous method simulated the factors causing the same load growth for each grid, even though, in reality, each cluster has different regional characteristics. Moreover, the factors that cause load growth have not directly shown a correlation to load growth. Therefore, this methodology fits to project load growth over a small area with an accurate forecast result. The number of load points can be estimated on each grid according to its geographic structure. In addition, the accumulation of load growth in every grid is considered the region's growth (macro).

METHODS

Microspatial simulation methods of small area load forecasting employ a land use or class-based customer framework. This method often utilises an “urban model” of population, commerce, and socio-economic factors to explain and forecast changes in the magnitude and location of various classes of electric load growth. Information on land use pattern development is then used to project or forecast future load growth. This method is best suited to a high spatial resolution grid of cells, long-range forecasting, and it is appropriate for multi-scenario planning. In contrast to trending methods, simulation requires substantially more well-organised data in databases and is collected systematically and adequately. Generally, these methods divide the service area into a smaller set of areas (grid). The size of the grid depends on data availability and load forecasting methods that will be used.

Load forecasting methods use land-use simulation, project type and load density into electrical service areas based on existing and future land use exchange. As a result, load growth can be determined in a smaller area, and the forecasting results are precise. The development of load growth will be presented into load density in every grid per year review.

Models and Parameters

The forecast is initially begun by collecting and compiling variables into a grid. The variables consist of existing land use conditions expressed as a large percentage (representing geography and land use aspect), residential (representing demographic aspect), PDRB (representing economic aspect), and electric load demand present in each grid (size of grids is subdistrict). End review data refers to a neighbourhood and hamlet called RT/RW (Rencana Tata Ruang dan Wilayah).

Grid values have been arranged and compiled based on the grid data to determine grids subdivision (clustering analysis). The goal is to merge grids that have the same characteristics. This grid forms one cluster. The next step is analysing variables based on principal component analysis (PCA) in every cluster. It helps to understand the covariance structure in the original variables and/or create a smaller number of variables using this

structure. The technique will produce dominant variables to load density in every cluster. After that, variables will be used to calculate load density growth models. Every model that is produced will do a standard statistic test to ensure the model is correct. The load density, as a result, will be projected into electric load per year in the future based on the land use in every grid.

Data Requirement

Data are divided into two major groups generally: electrical data and nonelectrical data. Electrical data used in this methodology consist of load per sector (residential, commercial, industry and public) and load density in sub-districts. Non-electrical data consists of residential numbers, PDRB, land use for each subdistrict and RT/RW's data.

The selection and determination of the variables used are based on existing data in each predicted area. It is understood that the techniques developed are generally implemented in developed areas, where data collection is updated regularly. However, in developing countries, there will be problems with the availability of such data. It is exacerbated by the demand for the availability of electrical energy that is so fast to support the regional economic level.

The method is basically can use many variables (more than 12 as implemented in this article). However, in determining the variable, some characteristics of the variable must be known. In this study, the characteristic of the variables is derived from determining the estimated error of the predetermined model by testing on the residual value whether it is normally distributed.

Micro-Spatial Load Forecasting Using Multivariate Analysis

Identification Stage. *Clustering Analysis.* Cluster analysis classifies a set of observations into two or more mutually exclusive unknown groups based on combinations of interval variables. The purpose of cluster analysis is to discover a system of organising observations (grid) into groups, where members share properties in common. It is cognitively easier to predict the behaviour or properties of objects based on group membership in which all of them share similar properties. On the other hand, it is generally cognitively difficult to deal with individuals and predict behaviour or properties based on observations of other behaviours or properties. The procedure of clustering analysis consists of the following steps:

- Arranging distance matrix (matrix's size is $N \times N$) of which the element is euclidean's distance between N object. Name this matrix as a space matrix

$$D = \{d_{ij}\}; ij = 1,2,3,\dots,N$$

- Computing minimum space matrix above. Then, combine both as one group. If the group with minimum space are group U and V, it will form a new group (UV). The space revision method is Euclidean space which usually uses space between objects (Equation 1).

$$d_{ij} = \sqrt{\sum_{k=1} (v_{ik} - v_{jk})^2} \quad [1]$$

Based on Equation 1, the lowest Euclidean space shows that grid relation is close.

Repeat steps a and b counted (N-1) numbers until all objects stay in one group. Finally, write every result of clustering C_i .

- Clustering results and subdividing strength (C_i) can be drawn into a dendrogram. Based on the dendrogram, we can determine numbers of clusters and their members of Principal Component Analysis (PCA)

Principal Components Analysis (PCA). PCA shows influencing variables at each cluster by reducing the number of dimensions without losing variables information. As a result, the variables do not influence load density significantly and will be put out of load density models. In order to derive simple models but still represent all of the variables.

In case if the original variable has a different set of measurements, the principal component is degraded from correlation matrix R. It is needed orthogonal transformation of data into a standard form (Equation 2):

$$Z_{ij} = \frac{x_{ij} - \bar{x}_j}{s_j} \quad [2]$$

Determination of principal components numbers is based on a cumulative variance proportion of 75% or more than the total variant.

Factor Analysis. Factor analysis is used to reduce a large set of variables to a more meaningful, smaller set of variables (development of PCA). Variables that are correlated with one another, which are also largely independent of other subsets of variables, are combined into factors. Factors are generated to be representative of the underlying processes that have created the correlations among variables. It can be written as Equation 3:

$$\gamma_{ij} = a_{ij} \sqrt{\lambda_j} \quad [3]$$

Estimation Stage and Mathematics Model. Determination Mathematics Model. The determination mathematics model is the prediction of loading in electric power commonly

exposed in a linear model. Based on this, model construction can be formulated in terms of double regression, which is built based on mathematics model, that is Equation 4:

$$Y = b_1 + b_2X_2 + b_3X_3 + \dots + b_kX_k + e \quad [4]$$

This mathematics model is a group linear equation with a multivariable and simplified in a matrix, written as Equation 5:

$$Y = Xb + e \quad [5]$$

Where:

$$\gamma = \begin{bmatrix} \gamma_1 \\ \gamma_2 \\ \gamma_3 \\ \cdot \\ \cdot \\ \cdot \\ \gamma_n \end{bmatrix} \quad b = \begin{bmatrix} b_1 \\ b_2 \\ b_3 \\ \cdot \\ \cdot \\ \cdot \\ b_k \end{bmatrix} \quad e = \begin{bmatrix} e_1 \\ e_2 \\ e_3 \\ \cdot \\ \cdot \\ \cdot \\ e_n \end{bmatrix}$$

In order to get b values, sum square deviation has to be minimised as Equation 6:

$$\sum e_i^2 = e'e = (Y - Xb)'(Y - Xb) \quad [6]$$

Where, $e' = Y(Xb)'$, so that (Equation 7)

$$b = (X'X)^{-1}X'Y \quad [7]$$

Correlation Analysis. Correlation analysis determines which variable has a stronger correlation (significant) with the initial response. So this variable will be possible to give a significant effect. So correlation with X and Y written as Equation 8:

$$r_{XY} = \frac{Cov_{XY}}{S_X S_Y} \quad [8]$$

If $r > 0,5$, that variable will have a significant effect on the load density variable. However, that limit is not absolute as it depends on the condition and variable needed.

Examination and Mathematics Model Test. Examination and mathematics model test are done to examine whether statistically, mathematics model has been proper or not, using F test (parameter test), t-test (parameter coefficient test) and multicollinearity test (Jimenez et al., 2019; Sun et al., 2017).

Forecasting Stage. Variable Trend. To get load density growth every year based on the model before, the first step in this process is to make a trend in each variable (except the area variable) to get growth model every year from each variable. Then, selecting the best trend from each variable is made based on the smallest error value (MAPE).

Land use alteration is trended based on RT/RW from a related area, RT/RW data use are up to 2010, and change of land use between 2011 – 2016 is seen from the growth trend area from several years before.

Load Density for Cluster Forecasting Base on Mathematics Model. Based on the result from the getting variable, the trend growth model variable is used to predict load density in each cluster. This model agrees with the model that has been derived previously.

Calculation of Peak Load Forecasting. The result of forecasting density per year from this cluster is used to calculate the load density of each area at the same cluster. Change of wide-area refers to RT/RW data.

The following process calculates of the total power of the political district by adding power in each sector (residential, commercial industry and public) at the political district. Mathematically can be written as Equation 9:

$$P_{total}(t) = C_f(P_R(t) + P_B(t) + P_1(t) + P_S(t)) \quad [9]$$

RESULT AND DISCUSSION

Forming Cluster

The forming cluster aims to group objects (districts) into clusters in which each cluster consists of districts with homogeneous characteristics.

Object (districts) grouping is conducted using the clustering technique. Results of the correlation matrix process between district variables are described in the dendrogram below in Figure 1.

Results from clustering obtained 5 clusters with an entire grid of 114 districts. Further, load forecasting will be implemented in each cluster for the next ten years. The sample taken for this research is the calculation of cluster 4.

Principal Component and Factor Analysis

PCA is performed after grids are obtained. Then, it is applied by transforming original variables into new variables (principal component) in the form of a linear combination that reduces and explains the variance of original variables. Results of the correlation matrix process of each variable at each cluster towards load density per district and component matrix are described in Tables 1 and 2, respectively.

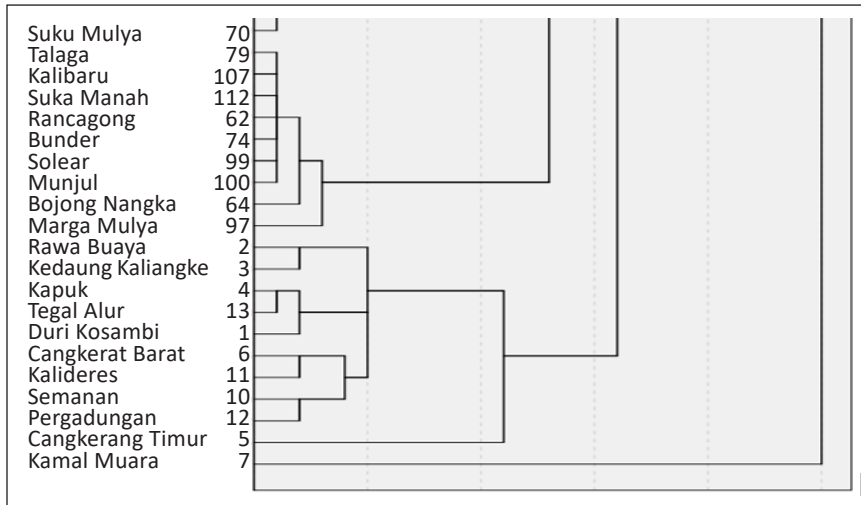


Figure 1. Dendrogram of forming cluster

Table 1
Total variance explained

Component	Initial eigenvalues			Extraction sums of squared loadings		
	Total	Var	Cumulative %	Total	Var (%)	Cumulative (%)
1	5.054	50.540	50.540	5.054	50.540	50.540
2	2.803	28.034	78.574	2.803	28.034	78.574
3	1.864	18.637	97.211	1.864	18.637	97.211
4	.204	2.040	99.251			
5	.064	.640	99.891			
6	.011	.109	100.000			
7	.000	.000	100.000			
8	.000	.000	100.000			
9	.000	.000	100.000			
10	.000	.000	100.000			

Table 2
Rotated component matrix

Variable	Complement		
	1	2	3
Residential	.963	-.188	.122
L_Residential	.961	-.229	-.082
L_Industry	.027	.963	.220
L_Commercial	.013	.083	.994
L_Social	-.430	.871	-.118
PDRB	.978	.083	.081
AL_Residential	.961	-.229	-.082
AL_Industry	.027	.963	.220
AL_Commercial	.013	.083	.994
AL_Social	-.430	.871	-.118

Further, PCA is grouped with its factors as depicted in the Table 3.

Table 3
Factor analysis

Cluster	Principal component		
	Component 1	Component 2	Component 3
4	PDRB	Industrial area	Commercial area
	Residential area	Industrial load	Commercial load
	Residential Load	Social load	
	Household	Social area	

Several variables are used in *Exploratory Factor Analysis*. It is derived from the Measurement of Sampling Adequacy (MSA) in the Anti-Image Matrices table. Variables eligible to use Exploration Factor Analysis are variables with MSA values more than 0.500, as in Table 4.

Table 4
Anti-image Matrices

Variable	Value
Area size	0,548
Industrial Land Use	0,618
Business Land Use	0,630
PDRB	0,656
Industrial load	0,548
Business load	0,596
Social load	0,578

The scree plot in Figure 2 shows the number of factors formed from the component points that have more than one eigenvalue. For example, three-component points have an Eigenvalue of more than one, so one factor is formed.

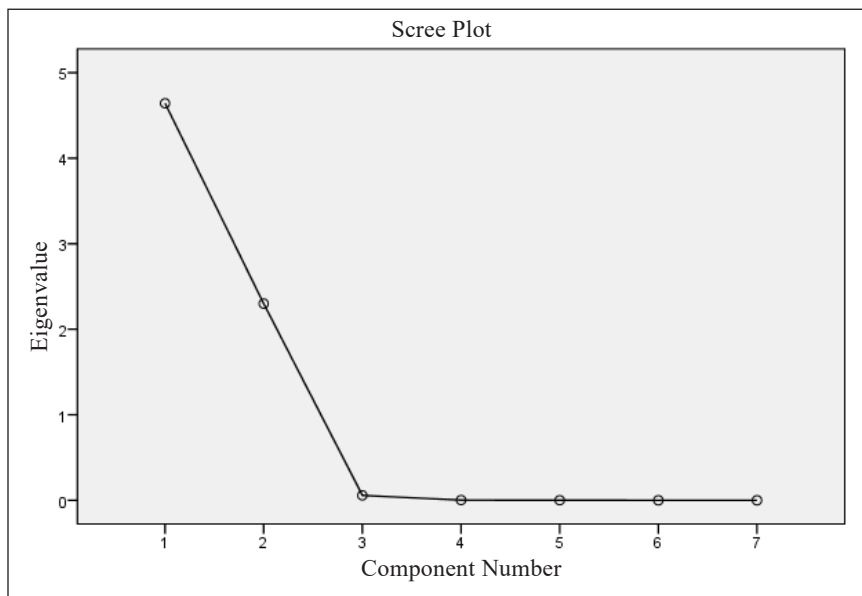


Figure 2. Scree Plot Eigenvalue

The statistical test shows that each factor has the greatest value of 0.5. For example, component one, two and three is 0.901, 0.732 and 0.799 respectively with the first factor 54.5%, the second factor 22.6% and the third factor 18, 7%.

Correlation Analysis

The analysis correlation coefficient of each variable towards the response variable (load density) obtains variables whose correlation with the initial response is close. They are housing (land use), a social area (land use), commerce and average load of electricity for business. The calculation results show that variables can explain the variance from a rating value of 96.1 %, which is statistically good.

Variable Testing

Regression coefficients parameter (t-test) is conducted to identify variables that significantly affect the initial rating value (load density). From the results, it can be seen that the parameter's significance contribution to initial rating value. Results of the parameter are seen in Table 5.

Table 5
Testing of regression coefficients parameter

Model	t-test	sig.	VIF
(Constant)	6.68	0.003	
Residential	-4.92	0.008	9.4
Social	-2.63	0.058	2.0
Commerce	5.38	0.006	8.1
Business	4.79	0.009	1.3

Based on the testing of regression coefficients parameter using variables and significance α level set at 5%, the results show that the significant parameters are constant with an average industry load because P-value is smaller than $\alpha = 0.05$. In addition, after multicollinearity (VIF) analysis was conducted, there was no multicollinearity detected as $1 < VIF < 10$.

Load Density Forecasting Process

It is important to calculate the trend of each variable (except the land-use variable) to obtain load density growth annually based on the acquired model. Therefore, it aims to obtain annual model growth per year of each variable. The selection of the best trend of each variable depends on the smallest error (MAPE). According to the trend results at each variable (except land use using RT/RT), the forecast for load density is illustrated in Figure 3.

Calculation of Load Growth of Each Grid

Annual peak load forecasting of each district is described in Tables 6 and 7. Load density forecasting per year obtained in this cluster is used to calculate the load density of each sector of the respective cluster. After the density of each sector is acquired, we can estimate

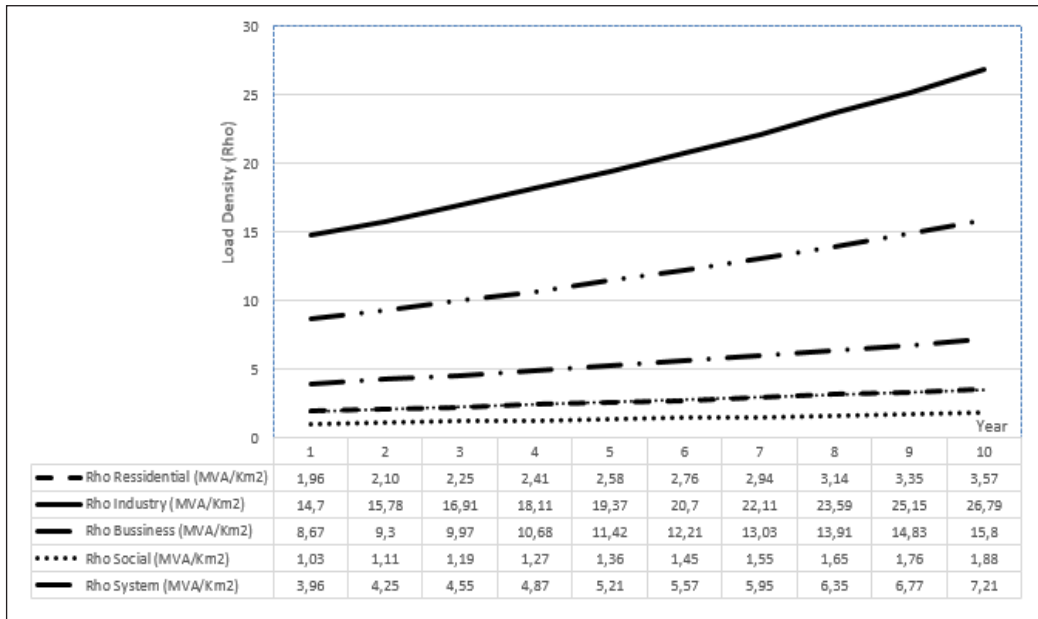


Figure 3. Load density curve per sector (MVA / Km²)

Table 6
Peak load forecasting year 1 – 5

Grid	Year				
	1	2	3	4	5
	Load (MVA)	Load (MVA)	Load (MVA)	Load (MVA)	Load (MVA)
Rawa Buaya	26.38	28.32	30.35	32.50	34.77
Kapuk	40.85	43.84	47.00	50.33	53.83
Kamal Muara	59.52	63.89	68.48	73.33	78.44
Kedaung Kaliangke	26.38	28.32	30.35	32.50	34.77
Kedoya Utara	18.31	19.65	21.06	22.55	24.13
Kembangan Utara	19.68	21.13	22.65	24.25	25.94
Semanan	33.79	36.27	38.88	41.63	44.53
Pegadungan	33.61	36.07	38.67	41.41	44.29
Tegal Alur	43.90	47.12	50.51	54.09	57.86

Table 7
Peak load forecasting year 6 to 10

Grid	Year				
	6	7	8	9	10
	Load (MVA)	Load (MVA)	Load (MVA)	Load (MVA)	Load (MVA)
Rawa Buaya	37.16	39.67	42.33	45.13	48.08
Kapuk	57.53	61.43	65.54	69.87	74.44

Table 7 (continue)

Grid	Year				
	6 Load (MVA)	7 Load (MVA)	8 Load (MVA)	9 Load (MVA)	10 Load (MVA)
Kamal Muara	83.83	89.51	95.50	101.81	108.47
Kedaung Kaliangke	37.16	39.67	42.33	45.13	48.08
Kedoya Utara	25.78	27.53	29.37	31.31	33.36
Kembangan Utara	27.72	29.60	31.58	33.67	35.87
Semanan	47.59	50.81	54.21	57.80	61.58
Pegadungan	47.33	50.54	53.92	57.49	61.25
Tegal Alur	61.83	66.02	70.44	75.10	80.01

the energy of every sector in each district by multiplying load density per sector with the size of its sector (district) at each cluster. Meanwhile, the change of sector size per year is adjusted to the area and space planning.

Methodology Comparison Testing

Forecasting results are compared to other methodologies to ensure the development of this methodology. In this case, trending methods and Gompertz analysis. The test results can be seen in Table 8.

Table 8
Methodology comparison testing

Historical data	Load data (MVA)	Trending MAPE	Gompertz MAPE	Microspatial simulation MAPE
1	600.33	0.002	0.0685	3.4E-05
2	621.80	0.003	0.0346	4.3E-05
3	644.10	0.001	0.0022	2.1E-04
4	667.13	0.001	0.0284	3.1E-04
5	690.66	0.001	0.0573	1.2E-03
6	715.31	0.002	0.0833	1.2E-04
Mov. Avg. Pcntg. error		0.126%	4.571%	0.032%

This test compares forecasting results to the history of the actual data before. The results show that load forecasting methodology base on land use simulation has a smaller error (0.032%) than trending methods (0.126%) or Gompertz analysis (4.571%). Generally, the error tolerance level statistically has prediction under 10% (Kartikasari & Prayogi, 2018). Thus, it can be inferred that the prediction model obtained is sufficient.

CONCLUSION

The development of micro-spatial load forecasting based on multivariate analysis is extended from the macro, sectoral load forecasting method, which can provide solutions and information such as load calculation, time of the incident, and its location in higher precision. Therefore, it is more appropriate to be applied as a basic tool in developing electrical distribution plan for a dynamic area such as Tangerang.

Comparing to micro-spatial load forecasting methods, which have already been developed before (Kobylinski et al., 2020; Raza et al., 2020; Sun et al., 2017), this method has a complicated algorithm solution, but returning with the more accurate result and reducing the problem with a big volume counting process.

The complication rate rises occurs because the clustering algorithm was done before the principal component analysis process (from the previous method). As a result, the level of complicity became N times, in which N indicated the number of clusters.

This method will be more accurate to be implemented in the smaller area because the base of the load variable is the load density of the service area (in this case study, it used sub-district as the smallest area).

ACKNOWLEDGEMENTS

The authors would like to thank the Ministry of Education and Culture of Indonesia and Institut Teknologi PLN for supporting this project.

REFERENCES

- Al Amin, M. A., & Hoque, M. A. (2019). Comparison of ARIMA and SVM for short-term load forecasting. In *2019 9th Annual Information Technology, Electromechanical Engineering and Microelectronics Conference (IEMECON)* (pp. 1-6). IEEE Publishing. <https://doi.org/10.1109/IEMECONX.2019.8877077>
- Avazov, N., Liu, J., & Khousainov, B. (2019). Periodic neural networks for multivariate time series analysis and forecasting. In *2019 International Joint Conference on Neural Networks (IJCNN)* (pp. 1-8). IEEE Publishing. <https://doi.org/10.1109/IJCNN.2019.8851710>
- Babcock, C., Matney, J., Finley, A. O., Weiskittel, A., & Cook, B. D. (2013). Multivariate spatial regression models for predicting individual tree structure variables using LiDAR data. *IEEE Journal of Selected Topics in Applied Earth Observations and Remote Sensing*, 6(1), 6-14. <https://doi.org/10.1109/JSTARS.2012.2215582>
- Carvalho, J. P., Larsen, P. H., Sanstad, A. H., & Goldman, C. A. (2016). *Load forecasting in electric utility integrated resource planning*. LBNL Publications.
- El Kafazi, I., Bannari, R., Abouabdellah, A., Aboutafail, M. O., & Guerrero, J. M. (2017). Energy production: A comparison of forecasting methods using the polynomial curve fitting and linear regression. In *2017 International Renewable and Sustainable Energy Conference (IRSEC)* (pp. 1-5). IEEE Publishing. <https://doi.org/10.1109/IRSEC.2017.8477278>

- Fu, Q., Lai, R., Shan, Y., & Geng, X. (2018). A spatial forecasting method for photovoltaic power generation combined of improved similar historical days and dynamic weights allocation. In *2018 IEEE Innovative Smart Grid Technologies - Asia (ISGT Asia)* (pp. 1195-1198). IEEE Publishing. <https://doi.org/10.1109/ISGT-Asia.2018.8467889>
- Jimenez, J., Pertuz, A., Quintero, C., & Montana, J. (2019). Multivariate statistical analysis based methodology for long-term demand forecasting. *IEEE Latin America Transactions*, *17*(01), 93-101. <https://doi.org/10.1109/TLA.2019.8826700>
- Kartikasari, M. D., & Prayogi, A. R. (2018). Demand forecasting of electricity in Indonesia with limited historical data. *Journal of Physics: Conference Series*, *974*, Article 012040. <https://doi.org/10.1088/1742-6596/974/1/012040>
- Kobylinski, P., Wierzbowski, M., & Piotrowski, K. (2020). High-resolution net load forecasting for micro-neighbourhoods with high penetration of renewable energy sources. *International Journal of Electrical Power & Energy Systems*, *117*, Article 105635. <https://doi.org/10.1016/j.ijepes.2019.105635>
- Lagaaaj, A. (2018). Accelerating solar for decelerating climate change in time. In *2018 IEEE 7th World Conference on Photovoltaic Energy Conversion (WCPEC) (A Joint Conference of 45th IEEE PVSC, 28th PVSEC & 34th EU PVSEC)* (pp. 2392-2394). IEEE Publishing. <https://doi.org/10.1109/PVSC.2018.8547702>
- Mukhopadhyay, P., Mitra, G., Banerjee, S., & Mukherjee, G. (2017). Electricity load forecasting using fuzzy logic: Short term load forecasting factoring weather parameter. In *2017 7th International Conference on Power Systems (ICPS)* (pp. 812-819). IEEE Publishing. <https://doi.org/10.1109/ICPES.2017.8387401>
- Raza, M. Q., Mithulananthan, N., Li, J., & Lee, K. Y. (2020). Multivariate ensemble forecast framework for demand prediction of anomalous days. *IEEE Transactions on Sustainable Energy*, *11*(1), 27-36. <https://doi.org/10.1109/TSSTE.2018.2883393>
- Sun, X., Ouyang, Z., & Yue, D. (2017). Short-term load forecasting based on multivariate linear regression. In *2017 IEEE Conference on Energy Internet and Energy System Integration (EI2)* (pp. 1-5). IEEE Publishing. <https://doi.org/10.1109/EI2.2017.8245401>

Case study

Improving Performance in Construction Projects: A Case Study of Malaysian Public Projects

Aminah Md Yusof¹, Ali Raza Khoso^{1,2*}, Samiullah Sohu³, Shabir Hussain Khahro⁴ and Chang Saar Chai⁵

¹Department of Structure and Materials, School of Civil Engineering, Faculty of Engineering, Universiti Teknologi Malaysia (UTM), 813100 Johor Bahru, Malaysia

²Department of Civil Engineering, Mehran University of Engineering & Technology Jamshoro, 76062 Pakistan

³Department of Civil Engineering, Quaid-e-Awam University of Engineering Science & Technology, Larkana Campus, 67480 Pakistan

⁴College of Engineering, Prince Sultan University, Riyadh, 11586 Saudi Arabia

⁵Swinburne University of Technology, Sarawak Campus, Kuching, 93350 Malaysia

ABSTRACT

Studies have worked out measures to curb the poor performance problems. However, it is hard to investigate the actual reasons because of the diverse construction culture of different countries. This research aims to develop a framework for mitigating the problems triggering the poor performance via a novel classification. An empirical analysis of mean and relative importance index (RII) was performed in SPSS of collected data from 56 public projects in Malaysia from 2003 to 2014. Qualitative and quantitative data was analysed from Audit General's Reports, interviews, a pilot survey, and a full-scale experts' survey. Findings from research investigated that the most influential factors affecting poor performance are not genuinely linked with those investigated from Audit

General's Report except a few. Furthermore, the study findings conclude that related financial problems and construction stage from project life cycle contribute to poor performance. The potential mitigation measures are worked out and validated via focused group discussions with experts. Finally, a framework was developed that emphasised Competent, Commitment, Communication, Comfort and Collaboration

ARTICLE INFO

Article history:

Received: 07 April 2021

Accepted: 05 July 2021

Published: 08 October 2021

DOI: <https://doi.org/10.47836/pjst.29.4.19>

E-mail addresses:

aminahyusof@utm.my (Aminah Md Yusof)

raza.ali@graduate.utm.my (Ali Raza Khoso)

sohoosamiullah@gmail.com (Samiullah Sohu)

shkhahro@psu.edu.sa (Shabir Hussain Khahro)

cschai@swinburne.edu.my (Chang Saar Chai)

* Corresponding author

(5Cs) to mitigate the poor performance issues. The study is limited to identifying factors contributing to poor performance; however, relevant responsible stakeholders should also need to be identified in the future.

Keywords: Framework, Malaysia, mitigations, poor performance, project performance, public sector

INTRODUCTION

The construction industry in Malaysia contributes to socio-economic growth and shares 4% to 6% of the country's Gross Domestic Product (GDP) (Alaloul et al., 2020). However, the industry desperately suffers from various underlying problems such as overrun of time, cost, quality, safety, and disputes that lead to poor performance in the sector. The problem of poor performance is so severe and inescapable that none of the regions on the globe is under an exception. Several past studies believe that only 2.5% of projects in the world are delivered on time and within the estimated budget (Gunnoe et al., 2016). Therefore, it is a big question mark on the performance of the construction sector.

Project performance is an indispensable goal of every project where success is measured from innumerable parameters which are still conflicting, such as the most common are time, cost, and quality (Mellado & Lou, 2020; Unegbu et al., in press). Nevertheless, due to the lack of consensus on measuring project performance, there are many diverse opinions on what to include as performance and success measurement parameters. In the past, financial indicators were seen as the sole parameters to measure project performance, and later time, quality and satisfaction of end-users were added. However, the Malaysian public sector has continuously reported a low-performance sector (Takim, 2009). Besides, Malaysia aims to boost its economy and elevate its status from a developing to a developed nation. With this aim, the government had propelled its National Transformation Plan (NTP) that includes the Government Transformation Plan (GTP) and Economic Transformation Program (ETP). GTP and ETP are designed to address all obstacles to achieve Vision 2020. This master plan brought together several mega projects in the country to boost the economy. However, several impediments hindered the road to successful project performance.

Construction projects typically suffered from severe time and cost overrun problems and quality and safety issues, especially after modern construction, which has brought more complexity. Owing to the peculiar nature of industry and modern construction challenges, the problems of poor construction are increasing at a higher pace. Therefore, the government needs to ensure that projects are completed on time, with stipulated cost, meeting designed quality and general requirements. On the contrary, the current scenario is inverted, and the Malaysian construction industry has not witnessed successful projects. Sambasivan and Soon (2007) claimed that 17.3% of projects completed in 2005 suffered severe time problems related delay in Malaysia. Data from government and industry revealed that

around 65% of public projects suffered from an overrun of time and budget, which leads to conflicts (Rahman et al., 2013). Akhund et al. (2017, 2019) found that time and cost overrun are common in many developing economies. Memon et al. (2014) identified that issues in design and documentation, finance-related problems, project management and contract problem are only factors for Malaysian construction projects. Othman and Ismail (2014) found that several projects suffered from delays in Malaysia, leading to poor performance.

A report published by the National Audit Department (2009) stated that 11 public projects in Malaysia were abandoned due to cost overrun issues, low quality, and failure to comply with specifications. Also, nine of them encountered severe delays, seven projects have problems with quality, and six were not executed according to the specification. The report further stated that the said factors are reoccurring each time, and no suitable measures have been adopted yet to counteract. However, a few past studies have identified few major reasons behind the poor performance in Malaysia, such as delay (Alaloul et al., 2020; Sambasivan & Soon, 2007; Hooi & Ngui, 2014), cost overrun (Alaloul et al., 2020; Shehu et al., 2014), and quality (Alaloul et al., 2020).

Causes, as mentioned earlier and the report of the National Audit Department (2009), triggered that public projects in Malaysia are struggling with severe problems associated with project performance. It enlightens the need to explore the actual reasons behind the poor project performance, which would overcome the weakness in the industry and further show a better insight into the industry. The study aims to explore a novel classification of poor performance causes and design a framework that is a way forward to mitigate the problems and a sound indicator of the country's economic growth. To the best of our knowledge, a similar work particularly targeting the performance of the Malaysian public sector from past completed projects is not available in the pages of literature. Also eventually, limited studies have focused on exploring the factors of poor performance in Malaysia. Further, the factors of one region could not be investigated for other countries owing to differences in culture, political situation, and economic condition. Moreover, the study is not limited to this extent. However, it contributes to the literature by designing a novel classification of poor performance factors, which were not discussed extensively. The classification exclusively targets the actors, processes, and institutions re-classified from the project life cycle phases.

A REVIEW OF PROJECT PERFORMANCE

Poor Performance Measurement in Construction Projects

Construction projects agonise from several problems that are directly and indirectly allied with project performance. In order to investigate the performance of a project, it is vital to design the factors that affect the project performance as standard measuring guidelines or benchmarking factors (Unegbu et al., in press). Many studies in the past have worked

out factors affecting poor performance in construction in different countries (Le, 2020; Lopes et al., 2011; Shiferaw & Klakegg, 2013). For example, Ahzahar et al. (2011) found that in Malaysia, shortage of resources and low quality of materials are prevalent causes of project failure.

Puspasari (2005) revealed eight major classifications of factors that govern the project performance, i.e. characteristics owner related factors, labour and materials-related factors, contractor-related factors, consultant-related factors, project procurement, and external environment-related factors. Gamil and Rahman (2020) classified the poor performance factors into the following categories; governmental and administrative factors, management and leadership, human resources, stakeholders, and materials and machinery. Enshassi et al. (2009) worked out that delays in material availability, project leadership challenges, escalation in material prices, inexperienced and less qualified team members, poor quality of equipment, and raw materials are leading problems associated with project performance. Sweis (2013) exclusively focused on contractor related factors and believe that contractors have a prime role in project performance. It is also witnessed by Khoso and Yusof (2020), who claimed that project success is directly connected with contractors. Jaffar et al. (2011) found from review research that lack of technical capability, poor coordination, lack of integration and communication, and insufficient equipment are key causes of project failure. Faridi and El-Sayegh (2006) found that shortage of human resources, poor site management and supervision, poor leadership, and equipment failure are key causes that affect a project outcome. Enshassi et al. (2009) relate unavailability of resources, delays, leadership problems, escalation in material prices, inexperienced staff, poor equipment and, materials with project performance. Besides, Khoso et al. (2021a, 2021b) relate project performance to contractor selection issues in public projects.

The performance in construction projects also measured with different factors and performance criteria such as time, quality, cost and safety (Yeung et al., 2009), design, rework percentage, safety, time and cost (Kang et al., 2008), and customer requirements and satisfaction (Ling et al., 2006). Further, McDermot et al. (2020) listed out 12 factors affecting poor performance such as poor planning, insufficient skilled labour, wrong estimates, poor defining of scope, communication gap among stakeholders, cash flow problem, failure to estimate risks, poor change control, bureaucracy, problems in the proper ground investigation, improper project delivery system, accountability in decision-making. Other major underlying factors are incapable project manager, changes in design, related financial problems, contract management system issues, additional work, inefficient planning and scheduling, material shortage, unavailability of skilled labours, delay in construction, cite problems, wrong estimation, incapable contractor and inexperienced client, and poor team qualification (Yue, 2018). Finally, Gadisa and Zhou (2020) worked out the 58 most occurring factors and classified them into major criteria: as ineffective contract

management, incompetency of client, problems in the procurement process, construction material related problems, stakeholder’s coordination problem, performance measuring indicators, external environment, and incapable contractor.

Iron Triangle in Project Performance

The success or failure of any project is evaluated on certain parameters where the time, cost, and quality (known as Iron Triangle) have a dominant role, and many researchers evaluated the performance based on Iron Triangle. Mellado and Lou (2020), and Unegbu et al. (in press) believe that time overrun is referred to as a delay, which reflects the excessive time that exceeds the stipulated time of a project. Studies believe that time overrun is a severe cause of project performance (Akhund et al., 2018; Sambasivan & Soon, 2007). Issues of time overrun are not related to a single party; however, clients, consultants, contractors related factors are responsible. Doloi et al. (2012) explored several factors related to time overrun. Many other studies have also encountered the problem of time overrun, such as Bajjou and Chafi (2020), Soewin and Chinda (2018), and Girma et al. (2017). Besides, many studies believe that construction projects have a poor record in terms of the budgeted cost. The problem of cost overrun is a global challenge, and these problems are encountered by Akhund et al. (2019), Li et al. (2011), and Niazi and Painting (2017). In addition to time, cost, quality is another major indicator of project performance. Many studies have worked out possible causes of poor quality in construction projects (Alubaid et al., 2018; Callistus et al., 2014; Khoda et al., 2016). Furthermore, Alaloul et al. (2020) also developed poor performance factors based on time, cost and quality parameters. Figure 1 summarises the reviewed factors from the literature.

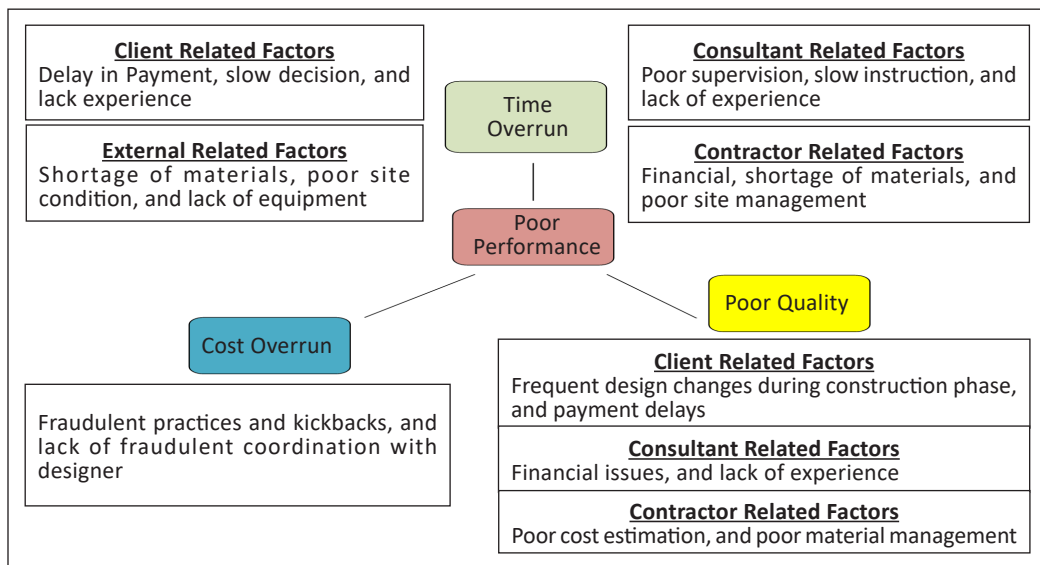


Figure 1. Time, cost, and quality related factors for project performance

RESEARCH METHODOLOGY

A project success and failure are continuously assessed with specific tools that eventually require explicit criteria or performance indicators. This study investigates the poor performance evaluating criteria or indicators, and designs a framework to mitigate the problems. This scientific research follows a mixed-mode research methodology where the essence of qualitative and quantitative are assorted together. This work employs qualitative mode during preliminary analysis, whereas the quantitative approach was applied during the survey phase.

Unfolding of the literature revealed a few studies focused on poor performance measurement; therefore, to have a larger set of previous research for the sake of more reliability of primary data, the Malaysian Audit General's Report (2003-2014) (www.audit.gov.my) was reviewed together. Both printed and electronic documents were collected and profoundly reviewed. Likewise, in other analytical methods, the analysis of the documents requires data that is suitable to examine, with meaningful interpretation, elicit meaning, high understanding, and empirical knowledge. The Malaysian Audit General's Report formed a basis for this study where in addition to other past studies, factors influencing poor performance were listed out. Extracted factors were clustered into phases of the project life cycle. Figure 2 illustrates the followed methodology.

Preliminary Data Collection

The preliminary data source includes the auditor report from 2003 to 2014. A systemic documents analysis followed this step. The reviewed audit institution was established to strengthen the government financial management system. This institution aims to carry out audits of public projects self-regulating and submits the reports to State legislatures. Since the institution audits 25 ministries, this study only focused on a limited part related to building construction and factors related to poor performance were extracted. From 2003 to 2014, a total of 56 projects were selected from the reports. Only the most frequent occurrence factors from past projects were compiled together for better understanding purposes. It adds the tally to the 75 most influential factors. The preliminary data was validated from this report, followed by site visits and meetings with experienced personnel.

Questionnaire Design

A larger set of data can easily be gathered via a questionnaire survey method within a short period. Compared to interviews, the survey is a more reliable tool that removes the chances of data biases. The data obtained from literature and Audit General Reports together facilitated in designing of the questionnaire. The survey tool was originally reviewed by an academic team consisting of university professors. The collected preliminary data assimilate in a quantitative format where respondents were expected to reply on a numeric five-point

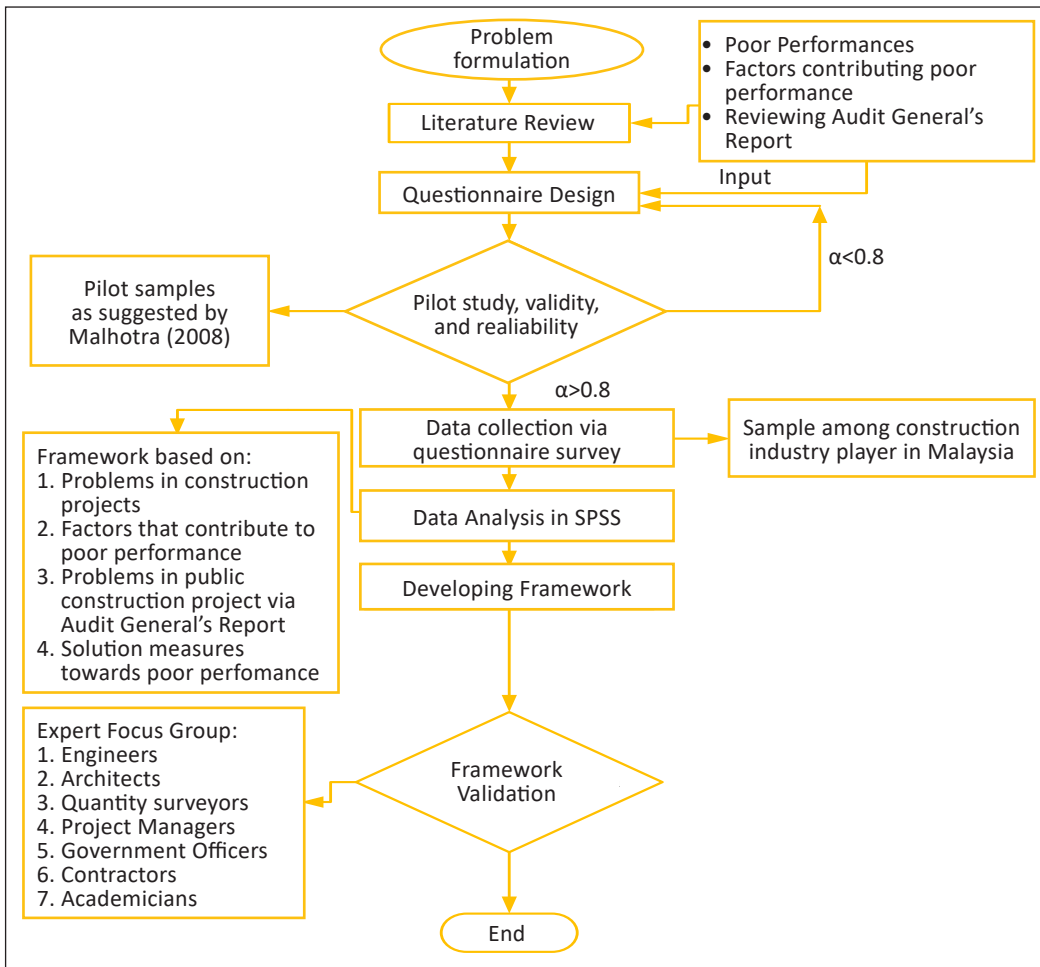


Figure 2. The research methodology

Likert scale of equal interval (where; 5>4>3>2>1; 5: strongly agree; 1: strongly disagree). The questionnaire was designed in the following three sections.

Part 1: This part aims to collect the respondent demographic background such as their organisation type, experience, project description, and designation.

Part 2: In this section, respondents were asked to provide their opinions based on a five-point Likert scale. This part aims to identify the most influential factors leading to poor performance in the public construction project. The factors were classified into five phases of the project life cycle.

Part 3. This section aims to cover the potential mitigation measures to improve the poor performance in the public construction project in Malaysia. Responses were gathered on a similar five-point Likert scale where 5>4>3>2>1; 5: extremely important; 1=not important.

Pilot Survey and Data Reliability

The questionnaire was tested on a smaller group before floating to a larger sample. Therefore, a pilot study offers insight for the researcher, which further clarify the research directions. It is constructive as it also warns whether projects could fail if research protocols are not followed. For this research, a pilot survey was conducted among 40 respondents, according to Hill (1998), who suggested 10 to 30 responses are positive for survey-based research. Cronbach's alpha test was performed in SPSS to validate the research data.

Data Collection from Surveys

The samples from a larger population working on various construction projects in Malaysia were determined. Since it was impossible to target all populations, a targeted population method such as the purposive sampling method was adopted, marking the specific responses based on the researcher's judgement. It also assures that only the person with specific knowledge and experience are followed. Client, consultant and contractor groups were involved in this survey. A total of 210 questionnaire surveys were sent via physical meetings, emails, WhatsApp, and an online survey tool. The survey took more than two months to complete where 137 successful responses were gathered.

Analysis Method

Scientific research follows a suitable analysis approach to convert the data into information and later into knowledge by interpretation. Collected data were analysed using average index (A.I) and relative important index (RII) methods. A.I approached was applied to compute the most influential factor. A factor is treated according to its respective value of A.I according to Rogers (2003), A.I value above 3.1 is considered significant. Later, the RII was calculated, where a value of above 60% (0.6) was considered agreed (Jarkas & Bitar, 2012).

ANALYSIS AND DISCUSSION

Analysis on Poor Performance Factors from Audit General's Report Past Projects

This section demonstrates poor performance factors from the past 56 projects overviewed and investigated from Auditor General's Report. Analysis of the top ten factors based on their occurrence is presented in Figure 3. The analysis from the report witnessed that the quality of construction deteriorates in almost every project with the highest rate of re-occurrence (n) (i.e. n=53/56). It is followed by 'construction not accordance with contract specification' (n= 45). There is a clear relationship between the first two factors. The quality deteriorates owing to ignoring the terms and conditions as prescribed in the documents. Such events lead to conflicts among parties and results in delays and overrun of budget.

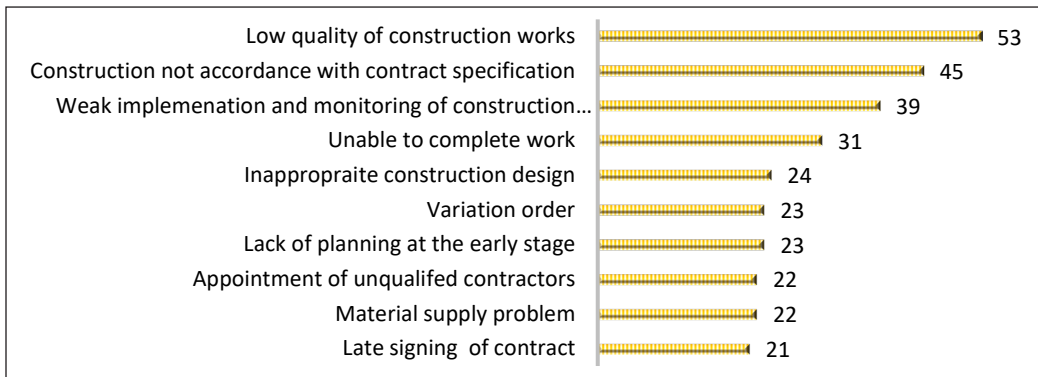


Figure 3. Poor performance factors in Malaysian public project from 56 projects

The third most occurred factor is also related to the second one. The problem of weak implementation and monitoring is the result of non-compliance with contract conditions. Also, results show that contractors could not perform work in more than 50% of selected projects. It is also witnessed from the data that construction design was inappropriate in n=24 projects. There is a linear relationship between these two causes. The majority of projects are abandoned or delays due to problems in design. It leads to time and cost overrun problems, which are later resolved through variation order as shown in n=23 projects from the investigation of the report.

The further analysis found that in Malaysia, most problems related to poor performance are due to lack of planning which is triggered owing to the incapable contractor. In n=22 projects, the capable contractor was not chosen. These findings also witnessed that many problems occur due to contractors' improper selection during the contract stage of the project life cycle. The least cited factor, i.e. late signing of the contract, is also considered one of the major reasons. It leads to delays in construction.

Analysis on Poor Performance Factors based on Stages of Project Life Cycle

Five stages of the project life cycle were considered, and factors were classified to each stage according to the suitability with the stage. Each stage was analysed individually and discussed below. The reliability was measured in SPSS using Cronbach's alpha method as an internal measure of consistency. For this case, the reliability of each data of the project life cycle stage was computed independently. As a result, data reliability varies from 0.808 to 0.972 in different stages of the project life cycle.

Early Investigation Stage Factors

This stage is critical for a project as it involves feasibility, early project planning, seeking funding sources, and various decisions involve in this stage. The data on the poor performance factor is analysed via A.I and RII as shown in Table 1.

Table 1
Analysis of poor performance factors of early investigation stage

Factors (Cronbach's alpha=0.808)	A.I.			RII	Ranking
	Contractor	Consultant	Client		
Land acquisition delays	3.80	3.95	4.00	78.60	1
Poor early stage planning	3.90	4.00	3.80	78.00	2
Lack of project funding	3.95	4.05	3.60	77.85	3
Ignoring experts' views during early planning	3.80	3.60	3.71	73.90	4
Delays in drawing, and bill of quantities	4.00	3.30	3.73	72.90	5
Late appointment of consultant	3.60	3.50	3.50	70.45	6
problems in understanding requirement from client	3.40	3.47	3.70	70.40	7
Poor site location	3.30	3.45	3.66	69.00	8

Land acquisition is ranked the highest poor performance factor. This problem generally requires a longer time to resolve because of several stakeholders such as landowners, government, and court of law. Furthermore, the agreement of the owner on offered compensation is also seen as a fundamental problem. These complications were unswervingly linked with the delays as construction could not be underway unless site ownership was transferred to the government. Poor early-stage planning is another crucial reason found from the analysis. The right planning predicts the future events of the entire project, and a contingency plan can also be prepared to mitigate any unwilling event in the future. On the other hand, poor planning affects the entire project with respect to time, cost, and quality and ultimately leads to project failure. Lack of project funding is ranked third most influential problem. Public projects often suffered from this problem as poor planning in an early investigation to seek the fund leads to delays in project completion. The delay is also directly linked with a cost overrun and other contractual problems such as change orders and extension of time. The ranking of the remaining poor performance factors is shown in Table 1.

Design Stage Factors

Table 2 illustrates the analysis results of the design stage. From the analysis, it is found that the public projects in Malaysia are frequently suffered from site investigation issues. Site investigation is the responsibility of all parties such as clients, consultants and contractors. The majority of problems in site investigation are often due to the geotechnical or ground investigation, such as related to deep soil investigation, which decides the choice of foundation. As a result, there is a likelihood of large variation in project cost comparing to early estimation. It happens when the client and its partner, i.e. consultants, overlooked the site and appropriate investigation is not performed. Besides, the mistakes in design

are seen as another major reason. Without proper drawing, it is not possible to carry out construction work. It often leads to re-work as consultants re-design the project in the middle of construction, and the project again goes back to the approval stage. This process affects the entire structure of the project, and many problems of time, cost overrun, and conflicts occur between the parties. Also, delays in the preparation of drawing is another major reason revealed from the analysis. Such delays often result in delays in projects, and further problems happen when a project contract is awarded to the contractor, and still, the drawings are incomplete.

Table 2
Analysis of poor performance factors of design stage

Factors (Cronbach's alpha=0.897)	A.I.			RII	Ranking
	Contractor	Consultant	Client		
Poor site investigation	3.90	3.80	3.70	76.00	1
Design mistakes and overlooked	4.00	3.55	3.80	75.20	2
Design preparation delays	3.90	3.63	3.67	74.60	3
Incomplete drawings	3.86	3.65	3.60	74.00	4
Lack of project information	3.75	3.65	3.70	73.75	5
Non cleared specification	4.00	3.45	3.57	73.45	6
Poor construction design	3.80	3.60	3.54	73.15	7

Contract Stage Factors

Poor performance factors under the contract stage are demonstrated in Table 3. The problem of incapable selection of a contractor is observed as the most significant in public sector construction. Typically, the public sector selects the contractor based on the lowest bid award, which is under criticism for the last two decades. As a result, the technical capabilities of contractors are given less weightage over their bid price. Incapable contractors often quote less bid price, which attracts the public client owing to the funds belonging to the public. However, it is never a wise decision in the long run and not suitable for a project as the contractors want more profit later, so reduce the quality and seek more change orders and other reasons to pay them more. Besides, budget estimation mistake is another problem during contract stage. There are two different but interlinked scenarios related to this problem; the prior is related to the client and later with the contractor. The prior scenario transpires when a client with its partner consultant estimates a wrong project cost and prepare their bill of quantities accordingly. At the same time, in the latter case, the incapable contractor quotes already a minimum budget to win the contract. Therefore, mistakes in budget and resource planning alongside a selection of incapable contractors further trigger poor performance. Such factors lead to conflict among contractor and client as the contractor would cry for additional budget seek more change or variation orders.

Late approval is another crucial factor contributing to poor performance. It is considered the main problem in the public sector as the procedures there are very complex. The public sector is burdened with additional formalities than the private sector. Also, in public sector, funds belong to public. Therefore, thorough audit and monitoring have often delayed the process. The factor of the inaccurate bid price is also linked with mistakes in budget and resources. The contract is a major stage that mostly leads to severe problems if it does not handle properly.

Table 3
Analysis of poor performance factors of contract stage

Factors (Cronbach's alpha=0.903)	A.I.			RII	Ranking
	Contractor	Consultant	Client		
Selection of incapable contractor	3.95	4.00	4.00	80.00	1
Mistakes in budget and resource planning	4.10	3.90	3.60	78.00	2
Late approvals	4.00	3.80	3.82	77.00	3
Inaccurate bid price	3.91	3.80	3.75	76.50	4
Weak contract system	3.80	3.70	3.50	73.30	5
Late appointment of contractors	3.79	3.75	3.29	73.20	6
Inappropriate methods by contractor	3.72	3.60	3.50	72.10	7
Late in signing of contract documents	3.50	3.40	3.50	68.32	8

Construction Stage Factors

Construction is seen as the most challenging job as it involves the highest resources in terms of human resources, budget, equipment, time management, and monitoring jobs. The analysis results of factors of poor performance in the construction stage are shown in Table 4. Furthermore, the A.I. values of the top 5 factors are illustrated in Figure 4.

The related financial problems are the most persuasive in the construction stage, such as cash flow issues and payment delays. Since construction consumes the highest amount of resources, any interruption in cash flow can harm project progress. The contractor relies on regular payment from the client, and when payment is delayed, the entire project gets affected. Such issues lead to time delays and later transpire into conflicts. Variation order is also observed as the most critical factor in the construction stage. Several factors are correlated to variation order, such as changes in design, method, and scope. When variations are proposed in the construction stage, the contractor seeks variation orders that ultimately cause delay of work, overrun of cost, chances of conflicts, and lower the quality. The client must ensure that early planning is performed prudently and sensibly so that the problems in the construction stage may be avoided.

Effective decision-making has a key role in a project, and any delay in decision making directly impacts a project. All processes such as endorsing drawings, contract documents,

terms and conditions, work orders, and payments are based on clients' decision. Slow decision making indicates that delays in the entire project as the factors act as a chain. Therefore, the client must ensure that there is no due pending decision. Apart from this, quality is also seen as a top factor affecting poor performance. Quality is always connected with cost and time. Problems of cash flow, late payment, variation order and slow decision making increased the time and cost and parallel affect the quality of a project. Whenever a project is affected by delays or an overrun in the budget, the contractor would reduce the quality to expedite the work and meet the budget. Several other reasons were found as the most critical factors in the construction stage. See Table 4 for further details.

Table 4
Analysis of poor performance factors of construction stage

Factor (Cronbach's alpha=0.972)	RII	Ranking	Factor (Cronbach's alpha=0.972)	RII	Ranking
Issues related to cash flow	83.00	1	Coordination issue between contractor and supplier	75.91	19
Late payment delivery	81.00	2	Incompetency to complete work	75.81	20
Variation order	80.00	3	Coordination issue between contractor and sub-contractors	75.50	21
Slow decision making	79.51	4	Non-availability of technical supervisor	75.29	22
Low quality work	79.32	5	Changes in sub-contractor's appointment	75.20	23
Changes in design	79.00	6	Escalation in material prices	75.00	24
Lacking in project monitoring	78.55	7	Appointment delay in sub-contractors	74.50	25
Less workers	78.44	8	Work permits problem	74.47	26
Site management issues	78.40	9	Site problems	73.60	27
Delay in approvals	78.27	10	Issues in material supply	73.58	28
Non-compliance with standards methods	77.83	11	Training issues of team	72.30	29
Delay in design approval	77.40	12	Problems in proper and timely instructions to workers	71.70	30
Non-availability of qualified personnel	77.30	13	Delays in issuing documents	71.40	31
Delays from sub-contractors	77.10	14	Higher extension of time (EOT) approvals	71.00	32
Communication gap between local authorities	77.00	15	Safety negligence on site	68.70	33
Delay in starting work	76.49	16	Non-availability of workers' accommodation	68.63	34
Ignoring contract specified conditions	76.18	17	Security problems at site	68.50	35
Contractor and consultant coordination problem	75.91	18	Lack of storage capacity at site	68.47	36

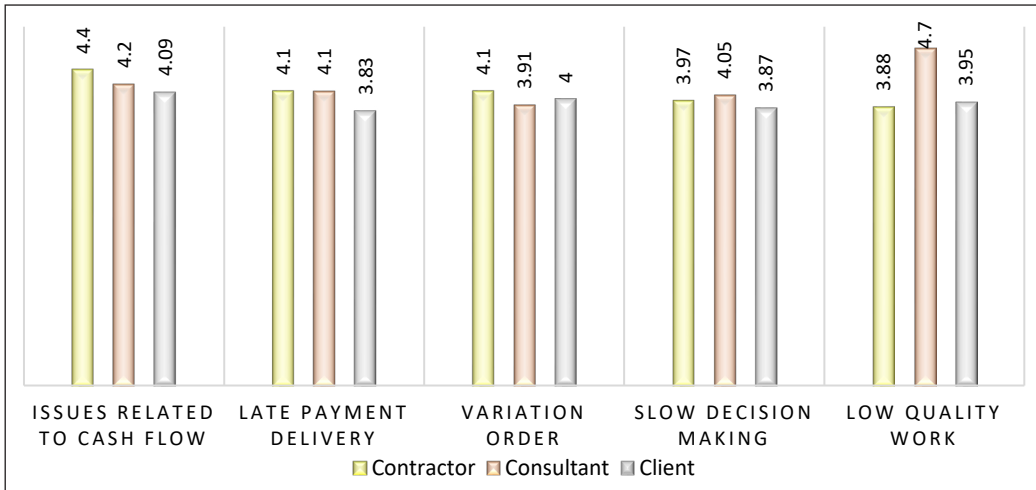


Figure 4. A.I. of top five factors of poor performance of construction stage

Handing Over Stage Factors

It is the last stage of a project life cycle. When the contractor has finalised their work, they will hand the project to the owner or client. Several factors are associated with this stage that leads to poor performance, as shown in Table 5. Financial related problems are again ranked the most critical in this stage, likewise construction. Generally, the problem of finances is equally important for all stages. During the handing over the stage, it is common to find defects in finished work. The contractor is obliged and bonded by contract to repair the defective works. Sometimes, the defects occur after handing over the stage, which in many cases is difficult to deal with and leads to conflicts and court of law. The problem of poor monitoring is found as another critical factor in this stage too. The proper monitoring at this stage may save the client from many problems which later may arise. Another pressing issue is payment to the worker. Normally, when the project is about to end, and the contractor is still waiting for the payment from the client, this issue arises. Later, the handing over goes to the delay due to the conflict between the worker and contractor. Several other factors mentioned in Table 5 are responsible for delays, cost overruns, conflicts, quality issues, and other contractual problems.

Table 5
Analysis of poor performance factors of handing over stage

Factors (Cronbach's alpha=0.951)	A.I.			RII	Ranking
	Contractor	Consultant	Client		
Financial problems	4.00	4.10	3.80	79.12	1
Defects in work	4.00	3.85	3.80	78.00	2
Poor monitoring	3.87	3.82	3.91	76.00	3

Table 5 (continue)

Factors (Cronbach's alpha=0.951)	A.I.			RII	Ranking
	Contractor	Consultant	Client		
Payment issue to workers	3.80	3.80	3.81	75.85	4
Inefficient supervision	3.90	3.70	3.69	74.81	5
Not completing repair work within defective liability period	3.69	3.80	3.71	74.21	6
Delays in making decision against contractors	3.80	3.70	3.70	74.18	7
Testing and commissioning in pending	3.80	3.65	3.65	73.30	8
Issuing completion certificate before actual complete	3.65	3.70	3.50	72.50	9
Poor facilities/equipment	3.55	3.50	3.60	70.75	10
Delays in issuance of certificate of non-compliance	3.66	3.50	3.51	70.70	11
Liquidated payment variation due to delay	3.60	3.70	3.30	70.40	12
Certificate of non-compliance approval by no-authorized party	3.72	3.52	3.40	69.80	13
Incomplete project report	3.60	3.50	3.45	69.50	14
Daily activity log book is incomplete	3.50	3.52	3.41	69.31	15
Overpayment to contractor	3.20	3.55	3.40	67.20	16

A NOVEL CLASSIFICATION OF FACTORS OF POOR PERFORMANCE

The analysis and discussion are based on an approach of factor identification, where classification is based on stages of the project life cycle. However, this section proposed a novel classification which is of more interest as this particular focuses on the responsible party or process behind such as stakeholder, process, or institution. Therefore, a unique classification of the factors mentioned earlier factors in the form of actor related factors, process-related factors, and related institutional factors is presented below.

Actors play a vital role in any project. Discussions with experts sorted the factors as mentioned earlier according to a novel classification. According to experts, 25 factors are re-classified into actor related factors. Reclassification found that 64% of actor related factors are only from the construction stage, whereas 20% are from handing over, 12% under the design phase, and the remaining 4% from the early investigation stage. Highly ranked factors under this classification are; 'issues related to cash flow', 'slow decision making', 'changes in design'. These poor performance factors are directly linked to the project actors as caused by their non-seriousness or incapacibilities.

Process related factors are viewed differently as these factors are associated with sequence or chain of events. Twenty-six factors are re-classified as process-based factors, which contributes 35% of total performance-related factors. From the analysis, construction

related factors dominant the other stages with 34.61% of factors. Furthermore, six out of ten significant factors are only from the construction stage. The top three factors under this category are ‘late payment delivery’, ‘variation order’, and ‘low quality work’. These poor performance factors are linked with the process, as they occurred owing to a sequence or chain of events.

Institutional factors are categorised based on norms, entity, rules, and the government or their related factors. Likewise, for actors and processes, most factors from the institutional classification are based on the construction stage with 45.83%. The top-ranked factors under this classification are ‘selection of incapable contractor’, ‘lacking in project monitoring’, and ‘site management issues’. These factors are directly linked with institutional factors because they are based on weakness in norms, standards, and rules. Furthermore, the government and relevant ministry also contribute to these factors owing to their weak regulations. Table 6 illustrates the re-classification of poor performance factors into a novel classification based on actors, process, and institutional factors.

Table 6
Poor performance factors based on novel classification of actor, process, and institutional factors

Factors	RII	Stage	Overall Ranking	New Ranking
1. Actor based classification				
Issues related to cash flow	83.00		1	1
Slow decision making	79.51	Construction	5	2
Changes in design	79.00		6	3
Less workers	78.44		11	4
Defects in work	78.00	Handing over	14	5
Non-availability of qualified personnel	77.30		20	6
Delays from sub-contractors	77.10	Construction	21	7
Ignoring contract specified conditions	76.18		27	8
Poor site investigation	76.00	Design	28	9
Contractor and consultant coordination problem	75.91		29	10
Coordination issue between contractor and supplier	75.91	Construction	30	11
Incompetency to complete work	75.91		31	12
Coordination issue between contractor and sub-contractors	75.50		33	13
Design mistakes and overlooked	75.20	Design	35	14
Changes in sub-contractor’s appointment	75.20	Construction	36	15
Appointment delay in sub-contractors	74.50		38	16
Not completing repair work within defective liability period	74.21	Handing over	43	17
Incomplete drawings	74.00	Design	45	18

Table 6 (continue)

Factors	RII	Stage	Overall Ranking	New Ranking
Issuing completion certificate before actual complete	72.50	Handing over	55	19
Problems in proper and timely instructions to workers	71.70	Construction	57	20
Problems in understanding requirement from client	70.40	Early investigation	66	21
Incomplete project report	69.50	Handing over	68	22
Daily activity log book is incomplete	69.31		69	23
Safety negligence on site	68.70	Construction	72	24
Lack of storage capacity at site	68.47		73	25
2. Process based classification				
Late payment delivery	81.00		2	1
Variation order	80.00	Construction	4	2
Low quality work	79.32		6	3
Financial problems	79.12	Handing over	7	4
Land acquisition delays	78.60	Early investigation	10	5
Delay in approvals	78.27	Construction	13	6
Mistakes in budget and resource planning	78.00	Contract	15	7
Non-compliance with standards methods	77.83	Construction	18	8
Delay in design approval	77.40		19	9
Late approvals	77.00	Contract	22	10
Inaccurate bid price	76.50		25	11
Design preparation delays	74.60	Design	41	12
Lack of project information	73.75		47	13
Issues in material supply	73.58	Construction	48	14
Non-cleared specification	73.45	Design	49	15
Testing and commissioning in pending	73.30	Handing over	50	16
Poor construction design	73.15	Design	52	17
Delays in drawing, and bill of quantities	72.90	Early investigation	54	18
Inappropriate methods by contractor	72.10	Contract	58	19
Delays in issuing documents	71.40	Construction	59	20
Poor facilities/equipment	70.70	Handing over	62	21
Delays in issuance of	70.66	Handing over	63	22
Late appointment of consultant	70.45	Early investigation	64	23
Certificate of non-compliance approval by no-authorized party	69.80	Handing over	67	24
Non-availability of workers' accommodation	68.63	Construction	71	25
Late in signing of contract documents	68.32	Contract	74	26
3. Institutional based classification				
Selection of incapable contractor	80.00	Contract	3	1

Table 6 (continue)

Factors	RII	Stage	Overall Ranking	New Ranking
Lacking in project monitoring	78.55	Construction	9	2
Site management issues	78.40		12	3
Poor early stage planning	78.00	Early investigation	16	4
Lack of project funding	77.85		17	5
Communication gap between local authorities	77.00	Construction	23	6
Delay in starting work	76.49		24	7
Poor monitoring	76.00	Handing over	26	8
Payment issue to workers	75.85		32	9
Non-availability of technical supervisor	75.29	Construction	34	10
Escalation in material prices	75.00		37	11
Inefficient supervision	74.81	Handing over	39	12
Work permits problem	74.47	Construction	40	13
Delays in making decision against contractors	74.18	Handing over	42	14
Ignoring experts' views during early planning	73.90	Early investigation	44	15
Site problems	73.60	Construction	46	16
Weak contract system	73.30	Contract	51	17
Late appointment of contractors	73.20		53	18
Training issues of team	72.30	Construction	56	19
Higher extension of time (EOT) approvals	71.00		60	20
Liquidated payment variation due to delay	70.40	Handing over	65	21
Safety negligence on site	68.70	Construction	61	22
Poor site location	69.00	Early investigation	70	23
Overpayment to contractor	67.20	Handing over	75	24

POTENTIAL MITIGATION MEASURES TO IMPROVE POOR PERFORMANCE

This section presents the potential measures that can effectively improve the poor performance in construction projects. The measures have been designed keeping in view the identified factors of poor performance in the Malaysian public sector. First, a survey from experts was conducted to identify the most effective measures. Second, the identified most suitable measures were later validated in focused group discussions consisting of engineers, architects, quantity surveyors, project managers, government officers, contractors, and academicians. Finally, the most effective mitigation measures found from the analysis are demonstrated in Table 7.

PROPOSED FRAMEWORK TO IMPROVE POOR PERFORMANCE IN PUBLIC PROJECTS

Framework development is inspired by the intention of delivering the public project on time, with stipulated cost, standard quality, with no conflicts and fewer chances of

Table 7
Mitigation measures to improve poor performance

No.	Mitigation measure	RII	No.	Mitigation measure	RII	No.	Mitigation measure	RII
1	Appropriate project planning	89.0	14	Effective supervision	84.0	27	Complete planning for preconstruction stages	82.3
2	Project focus on time, quality and cost	88.1	15	Timely site inspection	83.9	28	Inspect ground conditions during early investigation stage	82.0
3	Good communication among stakeholders	87.5	16	Maximum avoidance of communication gap	83.7	29	Need to improve contract award system	82.0
4	Appropriate management of site	87.2	17	Priority on client's need	83.6	30	Frequent training to staff	81.9
5	Committed leadership	87.0	18	Implementation of appropriate construction method	83.4	31	Inspecting past experience of team	81.5
6	Completeness of drawings	86.5	19	Hiring of experienced and skilled technical staff	83.3	32	Timely arranging of progress meetings	81.0
7	Appointment of skilled labours	85.3	20	Sound coordination between parties	83.0	33	Quality management system's implementation	80.8
8	Very clear specification	85.2	21	Strict implementation of planning	82.9	34	Clear contract terms	80.6
9	Settle land acquisition issues in the beginning	85.0	22	Strict adherence on construction ethics	82.8	35	Risk prevention strategies	80.4
10	Proper strategic planning	84.9	23	Controlling mechanism	82.7	36	Focus on HR department	79.8
11	Effective team utilisation	84.7	24	Hiring experienced sub-contractors	82.6	37	Sound design	79.2
12	Providing a clear information	84.3	25	Good quality equipment usage	82.5	38	Implementation of latest technology	78.0
13	Proper allocation of resources	84.2	26	Research, training and developments	82.5			

project failure. The framework was developed with the assistance of potential mitigation measures suggested by experts. Performance is a function of ability and motivation, where ability may be defined based on an individual’s aptitude and the inputs supplied by the organisation, such as training. In contrast, motivation is a product of desire and commitment. The inability may be due to various factors such as; extremely challenging tasks, lack of skills, knowledge, and aptitude, no improvement over passage of time, and strong effort but no performance. Therefore, ability must be improved to a certain extent to meet the intended performance. Besides, motivation is a function of morale, commitment, and a high motivation drives to successful completion of the task. Henceforth, it should be ensured to motivate individual and involved parties throughout the project. This research proposed a framework where to ensure higher performance. One has to follow the mentioned sequence of activities as shown in Figure 5.

As the project begins and all the major stakeholders are identified, the client must make sure that a performance management policy has been formulated. It should encompass the project schedule, end-user satisfaction, budget performance, technical performance, training, learning, and motivation. Next, each active part must be called to share the policy.

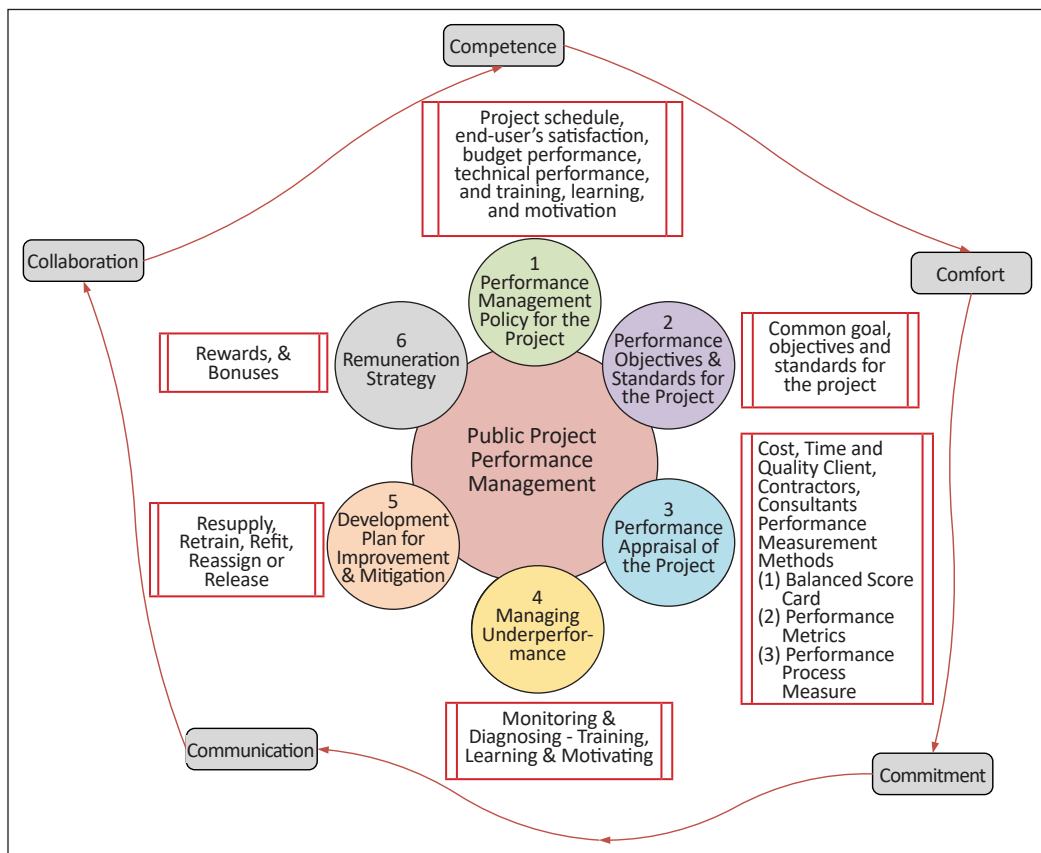


Figure 5. Framework for improving public project performance

The very next step is to establish performance objectives and standards. The performance policy, as well as the objectives, must be carefully designed based on contracts. The performance objectives must be established based on common goals, shared mission, and values that benefit the involved parties equally. It can motivate each party to work harder, and they would start owning the project. The next step in the framework process is appraising the performance for immediate actions against any mishaps. The following approaches can be achieved.

- Balanced Score Card
- Performance Metrics, and
- Performance Process Measure

The next step in the framework is measuring the underperformances. Any mishap, if identified, its alternative approach must be effectively implemented, such as a shortage of materials. The underperformance can be attributed to several factors, such as the ability. There are five possible directions to overcome performance problems that are associated with ability. It refers to the development plan and learning development activities such as; resupply, retrain, refit, reassign, and release. The final step in the framework is implementing a remuneration strategy such as bonuses, rewards, incentives, recognition, and motivation. The remuneration strategies aim to boost the morale of the individual, and this would enhance productivity.

In addition to the steps mentioned above, the proposed framework integrates the concept of Competence, Comfort, Commitment, Communication and Collaboration (5Cs). The concept of 5Cs must be the foundation of each project. *Competence* is the basis of many organisations according to which employees are the most valuable asset in the firm. A project manager is a major employee in a project, and its competency could not be overlooked. A project manager must possess enough skills such as leadership, technical, and ethics. *Comfort* is based on the concept that the resources, efforts, and leaderships align well with project performance. Besides, *commitment* ensures that all involved stakeholders and levels of the organisational hierarchy are willing to manage, perform, and operate the required facilities in harmony. The commitment is a driving force that keeps the project on a track that leads to performance. The dissemination of information to internal and external parties are done via *communication*. Effective communication throughout the project and especially in the early phases, have a positive influence on performance. Several conflicts and problems arise owing to the miss-communication factor. Finally, *collaboration* is also equally valuable for a project. Several collaborative tools play a vital role, such as seminars, training, workshops, and team-building activities. Such tools are also fruitful in dispute resolutions, problem-solving, enhancing a win-win scenario, and risk balancing. Therefore, collaboration is a strategy to resolve the problems mutually.

CONCLUSION

This research aims to identify factors contributing to poor performance in public projects in Malaysia and develop a framework for mitigating the problems triggering the poor performance via a novel classification. The research identified 75 most influential poor performance factors for Malaysian public sectors. Fifty-six past projects were investigated from Audit General's report (2003 to 2014). The factors were classified into project life cycle stages. From the study findings, it was concluded that the highest factors belonged to the construction stage. The related financial issues are found as the most contributing factor in poor performance. The study found a contradiction in the findings of Audit General's Report factors and those identified in this study. According to the Audit General's Report, most poor performance issues are due to low quality, contractual issues, weak implementation, and monitoring work. However, the survey results found the majority of factors related to financial issues.

Henceforth, the severity and occurrence of factors investigated in this study do not link with those available in the reports. Nonetheless, respondents agreed with some factors which were also observed critical from the survey, such as variation order, selection of incapable contractor, variation order, design issues, financial issues, and poor monitoring. Therefore, the study re-classified the factors into a novel classification based on actor, process, and institution. This classification is imperative to understand the actual and precise problems related to poor performance. Furthermore, researchers and policymakers could easily trace the problems, and responsible departments can be identified, such as actors, processes or institutions. In addition to this, other major findings of this research are in the form of mitigation measures. Thirty-eight most effective solutions are ranked from the survey analysis. Based on the mitigation measures, a framework is designed from the experts' opinion. The framework operates on the principle of performance management, which relates the ability and motivation and consisting of six major steps. Moreover, the framework is supported by 5Cs, i.e., Competence, Comfort, Commitment, Communication and Collaboration. In future, the reports from State and Federal statutory bodies may be considered for further analysis. Furthermore, detailed research could be conducted where exclusive stakeholders are identified who is responsible for poor performance.

ACKNOWLEDGEMENT

The authors wish to thank Dr. Nurul Alifah Binti Jatarona for her countless assistance in collecting the data.

REFERENCES

- Ahzahar, N., Karim, N. A., Hassan, S. H., & Eman, J. (2011). A study of contribution factors to building failures and defects in construction industry. *Procedia Engineering*, 20, 249-255. <https://doi.org/10.1016/j.proeng.2011.11.162>

- Akhund, M. A., Khoso, A. R., Khan, J. S., Imad, H. U., & Memon, K. M. (2019). Prompting cost overrun factors during PCP in construction projects. *Indian Journal of Science and Technology*, 12(4), 1-7. <https://doi.org/10.17485/ijst/2019/v12i4/140936>
- Akhund, M. A., Khoso, A. R., Memon, U., & Khahro, S. H. (2017). Time overrun in construction projects of developing countries. *Imperial Journal of Interdisciplinary Research (IJIR)*, 3(4), 1-6.
- Akhund, M. A., Imad, H. U., Memon, N. A., Siddiqui, F. H., Khoso, A. R., & Panhwar, A. A. (2018). Contributing factors of time overrun in public sector construction projects. *Engineering, Technology & Applied Science Research*, 8(5), 3369-3372.
- Alaloul, W. S., Liew, M. S., Zawawi, N. A. W., Mohammed, B. S., Adamu, M., & Musharat, M. A. (2020). Structural equation modelling of construction project performance based on coordination factors. *Cogent Engineering*, 7(1), 1-20. <https://doi.org/10.1080/23311916.2020.1726069>
- Alubaid, F. A. R. S., Alhadeethi, R. H. F., & Alnajjar, A. J. (2018). Evaluating the quality control related factors to engineering defects in construction projects in Jordan. *International Journal of Civil Engineering and Technology*, 9(6), 923-937.
- Bajjou, M. S., & Chafi, A. (2020). Empirical study of schedule delay in Moroccan construction projects. *International Journal of Construction Management*, 20(7), 783-800. <https://doi.org/10.1080/15623599.2018.1484859>
- Callistus, T., Felix, A. L., Ernest, K., Stephen, B., & Andrew, A. C. (2014). *Factors Affecting Quality Performance of Construction Firms in Ghana: Evidence from Small-Scale Contractors*. *Civil and Environmental Research, IISTE*, 6, 18-23.
- Doloi, H., Sawhney, A., Iyer, K. C., & Rentala, S. (2012). Analysing factors affecting delays in Indian construction projects. *International Journal of Project Management*, 30(4), 479-489. <https://doi.org/10.1016/j.ijproman.2011.10.004>
- Enshassi, A., Mohamed, S., & Abushaban, S. (2009). Factors affecting the performance of construction projects in the Gaza strip. *Journal of Civil Engineering and Management*, 15(3), 269-280. <https://doi.org/10.3846/1392-3730.2009.15.269-280>
- Faridi, A. S., & El-Sayegh, S. M. (2006). Significant factors causing delay in the UAE construction industry. *Construction Management and Economics*, 24(11), 1167-1176. <https://doi.org/10.1080/01446190600827033>
- Gadisa, B., & Zhou, H. (2020). Exploring influential factors leading to the poor performance of public construction project in Ethiopia using structural equation modelling. *Engineering, Construction and Architectural Management*, 28(6), 1683-1712. <https://doi.org/10.1108/ECAM-12-2019-0689>
- Gamil, Y., & Rahman, I. A. (2020). Assessment of critical factors contributing to construction failure in Yemen. *International Journal of Construction Management*, 20(5), 429-436. <https://doi.org/10.1080/15623599.2018.1484866>
- Girma, S. E., Shahid, T. S. Z., & Neeraj, J. K. (2017). Critical factors affecting schedule performance: A case of Ethiopian public construction projects - engineers' perspective. *Engineering, Construction and Architectural Management*, 24(5), 757-773. <https://doi.org/10.1108/ECAM-03-2016-0062>
- Gunnoe, J., Kashiwagi, D. T., & Kashiwagi, J. (2016). Job order contracting performance and industry analysis. *IOSR Journal of Business and Management*, 18(09), 103-115. <https://doi.org/10.9790/487x-180902103115>

- Hill, R. (1998). What sample size is “enough” in internet survey research? *Interpersonal Computing and Technology: An Electronic Journal for the 21st Century*, 6(3-4), 1-12.
- Hooi, L. W., & Ngui, K. S. (2014). Enhancing organizational performance of Malaysian SMEs. *International Journal of Manpower*, 35(7), 973-995. <https://doi.org/http://dx.doi.org/10.1108/IJM-04-2012-0059>
- Jaffar, N., Tharim, A. H. A., & Shuib, M. N. (2011). Factors of conflict in construction industry: A literature review. *Procedia Engineering*, 20, 193-202. <https://doi.org/10.1016/j.proeng.2011.11.156>
- Jarkas, A. M., & Bitar, C. G. (2012). Factors affecting construction labor productivity in Kuwait. *Journal of Construction Engineering and Management*, 138(7), 811-820. [https://doi.org/10.1061/\(asce\)co.1943-7862.0000501](https://doi.org/10.1061/(asce)co.1943-7862.0000501)
- Kang, Y., O'Brien, W. J., Thomas, S., & Chapman, R. E. (2008). Impact of information technologies on performance: Cross study comparison. *Journal of Construction Engineering and Management*, 134(11), 852-863. [https://doi.org/10.1061/\(asce\)0733-9364\(2008\)134:11\(852\)](https://doi.org/10.1061/(asce)0733-9364(2008)134:11(852))
- Khoda, A., Lou, B., Parvishi, A., & Sarami, R. (2016). Fuzzy analysis of construction cost of quality in Iran focused on building materials quality. *IIOAB Journal*, 7(Suppl 4), 367-373.
- Khoso, A. R., & Yusof, A. M. (2020). Extended review on contractor selection in construction projects. *Canadian Journal of Civil Engineering*, 47(7), 771-789. <https://doi.org/10.1139/cjce-2019-0258>
- Khoso, A. R., Yusof, A. M., Chai, C., & Laghari, M. A. (2021a). Robust contractor evaluation criteria classification for modern technology public construction projects. *Journal of Public Procurement*, 21(1), 53-74. <https://doi.org/10.1108/JOPP-06-2020-0053>
- Khoso, A. R., Yusof, M. A., Leghari, M. A., Siddiqui, F., & Sohu, S. (2021b). Public tendering practices, issues and directions - A case of Pakistan construction sector. *Pertanika Journal of Science and Technology*, 29(1), 123-147. <https://doi.org/10.47836/pjst.29.1.07>
- Le, N. (2020). Vietnam construction industry performance issues and potential solutions. *Journal for the Advancement of Performance Information and Value*, 9(2), 7-20. <https://doi.org/10.37265/japiv.v9i2.27>
- Li, Y. Y., Chen, P. H., Chew, D. A. S., Teo, C. C., & Ding, R. G. (2011). Critical project management factors of aec firms for delivering green building projects in Singapore. *Journal of Construction Engineering and Management*, 137(12), 1153-1163. [https://doi.org/10.1061/\(asce\)co.1943-7862.0000370](https://doi.org/10.1061/(asce)co.1943-7862.0000370)
- Ling, F. Y., Ibbs, C. W., & Hoo, W. Y. (2006). Determinants of international architectural, engineering, and construction firms' project success in China. *Journal of Construction Engineering and Management*, 132(2), 206-214. [https://doi.org/10.1061/\(asce\)0733-9364\(2006\)132:2\(206\)](https://doi.org/10.1061/(asce)0733-9364(2006)132:2(206))
- Lopes, J. P., Oliveira, R. A., & Abreu, M. I. (2011, June 20-23). The construction industry and the challenges of the millennium development goals. In *Management and Innovation for a Sustainable Built Environment* (pp. 1-14). Amsterdam, The Netherlands.
- McDermot, E., Agdas, D., Díaz, C. R. R., Rose, T., & Forcael, E. (2020). Improving performance of infrastructure projects in developing countries: An ecuadorian case study. *International Journal of Construction Management*, 0(0), 1-15. <https://doi.org/10.1080/15623599.2020.1797985>

- Mellado, F., & Lou, E. C. W. (2020). Building information modelling, lean and sustainability: An integration framework to promote performance improvements in the construction industry. *Sustainable Cities and Society*, 61(May), Article 102355. <https://doi.org/10.1016/j.scs.2020.102355>
- Memon, A. H., Rahman, I. A., Abdullah, M. R., Asmi, A., & Azis, A. (2014). Factors affecting construction cost performance in project management projects: Case of MARA large projects. *International Journal of Civil Engineering and Built Environment*, 1(1), 2289-6317.
- National Audit Department. (2009). Synopsis on the audit of the federal government's financial statement, financial management and activities of federal ministries/departments and management of government companies 2009. *Auditor General's Report Federal 2009*. National Audit Department Malaysia.
- Niazi, G. A., & Painting, N. (2017). Significant factors causing cost overruns in the construction industry in Afghanistan. *Procedia Engineering*, 182, 510-517. <https://doi.org/10.1016/j.proeng.2017.03.145>
- Othman, A., & Ismail, S. (2014). Delay in government project delivery in Kedah, Malaysia. *Recent Advances in Civil Engineering and Mechanics*, 248-254.
- Puspasari, T. R. (2005). *Factors causing the poor performance of construction project* (Unpublished Master project Report). Universiti Teknologi Malaysia, Malaysia.
- Rahman, I. A., Memon, A. H., Tarmizi, A., & Karim, A. (2013). Significant factors causing cost overruns in large construction projects in Malaysia. *Journal of Applied Sciences*, 13(2), 286-293. <https://doi.org/10.3923/jas.2013.286.293>
- Rogers, E. M. (2003). The innovation-decision process. In *Diffusion of innovations* (5th Ed., pp. 168-218). Free Press.
- Sambasivan, M., & Soon, Y. W. (2007). Causes and effects of delays in Malaysian construction industry. *International Journal of Project Management*, 25(5), 517-526. <https://doi.org/10.1016/j.ijproman.2006.11.007>
- Shehu, Z., Endut, I. R., & Akintoye, A. (2014). Factors contributing to project time and hence cost overrun in the Malaysian construction industry. *Journal of Financial Management of Property and Construction*, 19(1), 55-75. <https://doi.org/10.1108/JFMPC-04-2013-0009>
- Shiferaw, A. T., & Klakegg, O. J. (2013). Project evaluation: Accomplishments, shortfalls, and lessons learned in housing development projects in Ethiopia. *Journal of Management in Engineering*, 29(3), 289-301. [https://doi.org/10.1061/\(asce\)me.1943-5479.0000138](https://doi.org/10.1061/(asce)me.1943-5479.0000138)
- Soewin, E., & Chinda, T. (2018). Factors affecting construction performance: Exploratory factor analysis. In *IOP Conference Series: Earth and Environmental Science* (Vol. 140, No. 1, p. 012102). IOP Publishing. <https://doi.org/10.1088/1755-1315/140/1/012102>
- Sweis, G. J. (2013). Factors affecting time overruns in public construction projects: The case of Jordan. *International Journal of Business and Management*, 8(23), 120-129. <https://doi.org/10.5539/ijbm.v8n23p120>
- Takim, R. (2009). The management of stakeholders' needs and expectations in the development of construction project in Malaysia. *Modern Applied Science*, 3(5), 167-175.

- Unegbu, H. C. O., Yawas, D. S., & Dan-asabe, B. (in press). An investigation of the relationship between project performance measures and project management practices of construction projects for the construction industry in Nigeria. *Journal of King Saud University - Engineering Sciences*. <https://doi.org/10.1016/j.jksues.2020.10.001>
- Yue, C. K. (2018). Major construction delay factors in Portugal, the UK, and the US. *Practice Periodical on Structural Design and Construction*, 23(4), Article 04018024. [https://doi.org/10.1061/\(asce\)sc.1943-5576.0000389](https://doi.org/10.1061/(asce)sc.1943-5576.0000389)
- Yeung, J. F., Chan, A. P., & Chan, D. W. (2009). Developing a performance index for relationship-based construction projects in Australia: Delphi study. *Journal of Management in Engineering*, 25(2), 59-68. [https://doi.org/10.1061/\(ASCE\)0742-597X\(2009\)25:2\(59\)](https://doi.org/10.1061/(ASCE)0742-597X(2009)25:2(59))

Optimisation of Free Fatty Acid Removal in Nyamplung Seed Oil (*Callophyllum inophyllum* L.) using Response Surface Methodology Analysis

Ratna Dewi Kusumaningtyas^{1*}, Haniif Prasetiawan¹, Radenrara Dewi Artanti Putri¹, Bayu Triwibowo¹, Siti Choirunisa Furi Kurnita¹, Nanda Dwi Anggraeni¹, Harumi Veny², Fazlena Hamzah² and Miradatul Najwa Muhd Rodhi²

¹Chemical Engineering Department, Faculty of Engineering, Universitas Negeri Semarang, Kampus Sekaran, Gunungpati, Semarang 50229, Indonesia

²School of Chemical Engineering, College of Engineering, Universiti Teknologi Mara (UiTM), 40450 Shah Alam, Selangor, Malaysia

ABSTRACT

Nyamplung seed (*Callophyllum inophyllum* L.) oil is a prospective non-edible vegetable oil as biodiesel feedstock. However, it cannot be directly used in the alkaline catalysed transesterification reaction since it contains high free fatty acid (FFA) of 19.17%. The FFA content above 2% will cause saponification reaction, reducing the biodiesel yield. In this work, FFA removal was performed using sulfuric acid catalysed esterification to meet the maximum FFA amount of 2%. Experimental work and response surface methodology (RSM) analysis were conducted. The reaction was conducted at the fixed molar ratio of nyamplung seed oil and methanol of 1:30 and the reaction times of 120 minutes. The

catalyst concentration and the reaction temperature were varied. The highest reaction conversion was 78.18%, and the FFA concentration was decreased to 4.01% at the temperature of 60°C and reaction time of 120 minutes. The polynomial model analysis on RSM demonstrated that the quadratic model was the most suitable FFA conversion optimisation. The RSM analysis exhibited the optimum FFA conversion of 78.27% and the FFA content of 4%, attained at the reaction temperature, catalyst concentration, and reaction time of 59.09°C,

ARTICLE INFO

Article history:

Received: 31 March 2021

Accepted: 15 July 2021

Published: 08 October 2021

DOI: <https://doi.org/10.47836/pjst.29.4.20>

E-mail addresses:

ratnadewi.kusumaningtyas@mail.unnes.ac.id (Ratna Dewi Kusumaningtyas)

haniif.prasetiawan@mail.unnes.ac.id (Haniif Prasetiawan)

dewi.artanti@mail.unnes.ac.id (Radenrara Dewi Artanti Putri)

bayu.triwibowo@mail.unnes.ac.id (Bayu Triwibowo)

schoirunisafurikurnita@gmail.com (Siti Choirunisa Furi Kurnita)

nandadwianggraeni@gmail.com (Nanda Dwi Anggraeni)

harumi2244@uitm.edu.my (Harumi Veny)

fazlena@salam.uitm.edu.my (Fazlena Hamzah)

miradatul@salam.uitm.edu.my (Miradatul Najwa Muhd Rodhi)

* Corresponding author

1.98% g/g nyamplung seed oil, and 119.95 minutes, respectively. Extrapolation using RSM predicted that the targeted FFA content of 2% could be obtained at the temperature, catalyst concentration, and reaction time of 58.97°C, 3%, and 194.9 minutes, respectively, with a fixed molar ratio of oil to methanol of 1:30. The results disclosed that RSM is an appropriate statistical method for optimising the process variable in the esterification reaction to obtain the targeted value of FFA.

Keywords: Biodiesel, Box-Behnken, esterification, FFA, quadratic model, RSM, sulfuric acid

INTRODUCTION

Population, economic, and industry growth have intensified the global energy demand. To date, fossil energy still dominates the energy supply worldwide (Ghasemian et al., 2020). However, crude oil production in some countries shows a declining trend, which is not in balance with the energy need. Besides, the utilisation of fossil fuel currently also faces an environmental challenge as its combustion becomes the major source of carbon dioxide emission. Carbon dioxide is among the most dominant greenhouse gasses, contributing to global warming and climate change (Paraschiv & Paraschiv, 2020). The issues on the fossil fuel supply depletion and the negative environmental effect of fossil fuel utilisation have led to the increasing interest in renewable energy research. In recent days, many countries implement the policy to use fossil fuel and biofuel blending to ensure energy sustainability and security. Biodiesel is a viable biofuel that can be used as pure or in blends with diesel fuel. This alternative fuel is prospective for large scale production and application since it is non-toxic, low sulfur and aromatics content, biodegradable, and simple to use. Moreover, it holds neutral carbon characteristics, a high flash point that ensures safety in handling and storage, good lubricity, and high oxygen (Corach et al., 2017; Dey et al., 2021). Application of biodiesel/diesel fuel blends in diesel engines shows a good combustion, performance and emission reduction, especially for B20 or 20% biodiesel in the biodiesel-diesel fuel mixture (Mubarak et al., 2021).

Biodiesel is a fatty acid methyl ester derived from vegetable oils and/or animal fats. Most of the current industrial production of biodiesel from vegetable oils is achieved through transesterification (Aboelazayem et al., 2018; Demirbas, 2006). Theoretically, in transesterification, at least three moles of alcohol are required to achieve complete conversion of one mol of triglycerides to alkyl esters (Islam et al., 2014). The most common catalyst for biodiesel production is an alkaline catalyst such as KOH, NaOH, or solid base catalyst. The transesterification process using an alkaline catalyst is cheap and easy.

Some potential biodiesel feedstocks in Indonesia are crude palm oil, jatropha oil, and coconut oil. However, currently, the non-edible vegetable oil is preferred as biodiesel raw material to avoid the conflict between food and energy need (Kusumaningtyas et al., 2014). Among Indonesia's the prospective local non-edible oil for biodiesel production

is nyamplung (*Calophyllum inophyllum* L.) seed oil (Musta et al., 2017; Silitonga et al., 2014). *Calophyllum inophyllum* L is extensively planted in Indonesia, and the nyamplung seed oil can be purchased from the local farmers (Ong et al., 2019). In addition, Atabani and César (2014) reported that *Calophyllum inophyllum* methyl ester blended with diesel fuel (B10 and B20) revealed good properties and good engine performance and emission in diesel machines.

However, crude nyamplung seed oil (CNSO) usually contains gum and high free fatty acid (FFA). A high amount of FFA in the feedstock is not desirable in alkaline catalysed transesterification since it can react with the base catalyst, yielding the soap and diminishing the biodiesel yield. The desired amount of FFA in alkaline-catalyst is less than 0.5% to less than 3% w/w of oil (Arora et al., 2015). Generally, the maximum tolerable amount of FFA in base-catalysed transesterification is 2%. Thus, a pre-treatment step is necessary to reduce the FFA content in nyamplung seed oil to a maximum level of 2% prior to transesterification reaction. FFA removal in CNSO can be conducted through an esterification reaction using methanol in the presence of an acid catalyst. There are several types of acid catalysts for FFA esterification. They are categorised into the homogenous acid catalysts, for instance, sulfuric acid, para-toluene sulfonic acid, phosphoric acid, and hydro, and HCl (Harun et al., 2018; Murad et al., 2018) and the heterogenous ones, such as Amberlyst 15, sulfated zirconia, niobic acid, zeolite, and tin (II) chloride (Banchero & Gozzelino, 2018; Dal Pozzo et al., 2019; Kusumaningtyas et al., 2014). Homogenous catalyst, particularly sulfuric acid, has been found as an efficient and economic catalyst for FFA esterification both at laboratory and industrial scales (Banani et al., 2015; Chai et al., 2014; Gebremariam & Marchetti, 2018).

Therefore, sulfuric acid was selected as the catalyst for the FFA removal via the esterification reaction of CNSO oil in this work. The investigation included experimental work and the analysis using response surface methodology (RSM) to determine the optimal operation condition, which yielded the targeted FFA final value of 2%. The final FFA level was aimed at 2% since it is the maximum acceptable FFA value for the subsequent transesterification reaction to avoid undesired saponification reaction. The work comprised the detailed analysis of several polynomial models on RSM to reveal the most appropriate model for optimisation. The study on the FFA esterification in CNSO in the presence of a sulfuric acid catalyst which involves the comprehensive analysis and selection of the various polynomial models in RSM for process optimisation, has never been reported in the literature.

MATERIALS AND METHODS

Materials

The material used in this work were: crude nyamplung seed oil, phosphoric acid (from Merck), methanol (industrial grade, form local supplier), ethanol (analytical grade, from

Merck), KOH (analytical grade, from Merck), oxalic acid (analytical grade, from Merck), sulfuric acid (analytical grade, from Merck), distilled water (analytical grade, from a local supplier), and phenolphthalein indicator (analytical grade, from Merck).

Nyampung Seed Oil Characterisation

Prior to the esterification reaction, the crude nyamplung seed oil was first degummed using phosphoric acid to remove its gum content, resulting in refined nyamplung seed oil (RNSO). Both CNSO and RNSO were then characterised to reveal their properties. First, the fatty acid composition was determined using Gas Chromatography-Mass Spectroscopy (GC-MS Perkin Elmer, GC Clarus 680, MS Clarus SQ 8T), similar to our previous work (Kusumaningtyas et al., 2016). Next, density measurement was conducted using a pycnometer (Taghizade, 2016). Then, viscosity determination was carried out using viscometer bath Stanhope-Seta KV6 tube 350 CFO. Finally, acid value tests were accomplished based on the AOCS acid-base titration method (Banchero & Gozzelino, 2018).

Degumming

Initially, 500 ml CNSO was introduced into 500 mL beaker glass and heated using a hot plate at 70°C. Next, sulfuric acid with a concentration of 0.3% w/w was added. The mixing was kept for 25 minutes using a magnetic stirrer to ensure the completion of the degumming reaction. After the reaction finished, the CNSO was inputted into the separating funnel and added with warm distilled water (40-50°C in temperature) for purification. The mixture of the degummed CNSO and water was settled for 24 hours until the gum was separated. Then, the two layers were formed. The top and bottom layers were refined nyamplung seed oil (RNSO) and gum, respectively. To remove the water content, the RNSO was then heated using the oven at 105°C until it reached the constant weight.

FFA Removal

The FFA removal was conducted via an esterification reaction with methanol employing sulfuric acid. First, RNSO and methanol were weighed to obtain the molar ratio of RNSO and methanol of 1:30. Then, RNSO was introduced into the three necks flask batch reactor and heated until it reached the reaction temperature. On the other flask, methanol was also heated at an exact temperature. When both RNSO and methanol attained the reaction temperature, methanol was then poured into the reactor. The reaction temperatures were varied at 40°C, 50°C, and 60°C. Afterwards, the sulfuric acid catalyst was added at a specific concentration (1%, 3%, 5%, 7% w/w RNSO). The reaction was carried out for 120 minutes. A constant mixing using a magnetic stirrer with a speed of 1000 rpm was performed to certify the homogeneous reaction. The total experimental running was 7

experiments with different operating conditions. The sample was taken periodically every 10 minutes for each experiment. Hence, the total sampling number was 31 times. The reaction conversions were calculated based on the FFA content of the sample using the procedure of our previous work. The FFA content of the samples was calculated using the standard KOH titration (Kusumaningtyas et al., 2018).

RSM

RSM using Design Expert 11 software was employed for statistical calculation using three different variables (reaction temperature, catalyst concentration, and reaction time) based on the Box-Behnken methodology (BBD). The four polynomials models in the RSM, namely linear, interactive (2FI), quadratic, and cubic, were evaluated to determine the most appropriate model for optimisation. The selected model was applied in this work.

RESULT AND DISCUSSION

CNSO and RNSO Characterization

The properties of CNSO and refined nyamplung seed oil (RNSO), which has undergone a degumming process, were demonstrated in Table 1. The degumming process aims for reducing the gum content. Besides, degumming has also brought about a better characteristic of the oil feedstock. It can be observed in Table 1, the density viscosity, acid number, and acidity of the RNSO were lower than CNSO. The decreasing value of density happened due to the losses of some heavy compounds such as gum. The degumming process also caused a lighter colour of the oil. It was due to removing the compounds which significantly affected the oil colour (Lamas et al., 2016). Thus, the degumming process has shown a better characteristic of the oil feedstock, leading to an effective transesterification reaction and a higher quality of biodiesel product.

Table 1
Properties of CNSO and RNSO

Properties	CNSO (Before Degumming)	RNSO (After Degumming)
Density (kg/m ³)	906	898
Viscosity (mm ² /s)	60.39	59.04
Acid Number (mg KOH/g)	0.38	0.36
Acidity (%)	19.18	18.39

The fatty acid composition in CNSO was determined using GC-MS, and the result was exhibited in Table 2. Based on this composition, the molecular weight of CNSO can be calculated. It was found that CNSO molecular weight was 869.74 g/mol and the most dominant fatty acid in CNSO were oleic acid and linoleic acids. It is in good agreement with

the fatty acid composition found by Aparamarta et al. (2020). The fatty acid composition was merely performed for the CNSO. Fatty acid analysis for the RNSO was discounted. Based on the slightly altering of the acid number of CNSO and RNSO exhibited in Table 1, it can be assumed that the degumming process did not significantly change the fatty acid composition.

Table 2
CNSO fatty acid composition

Fatty acid	Molecular Weight (g/mol)	Area (%)
Palmitic acid	256.2228	15.51
Linoleic acid	280.45	28.94
Oleic acid	282.52	40.55
Stearic acid	284.47	14.39
Arachidic acid	312.54	0.60

Esterification of FFA: Effect of Catalyst Concentration

FFA removal was conducted via esterification reaction of RNSO and methanol in the presence of a sulfuric acid catalyst. Sulfuric acid catalyst concentration was varied at 1%, 3%, 5%, and 7% w/w RNSO with the molar ratio of RNSO: methanol of 1: 30 and temperature of 40°C, 50°C, and 60°C. Encinar et al. (2021) suggested the sulfuric acid catalyst concentration of 0.5% to 2% for the feedstock with an FFA content of 10.7%. The higher sulfuric catalyst concentration can be employed for the higher acidic vegetable oils. The molar ratio of oil to methanol referred to Chai et al. (2014), recommended the molar ratio of oil to methanol in the range of 1:20 to 1:60. Specifically, Marchetti & Errazu (2008) proposed the molar ratio of 1:30 as the optimal condition. On the other hand, the reaction temperature ratio was adjusted to the boiling point of the methanol. The reaction was run for 120 minutes, as suggested by Chai et al. (2014). The effect of catalyst concentration on the FFA conversion is demonstrated in Figure 1.

In Figure 1, reaction conversion increased at the catalyst concentration from 1% to 3%. It was due to the decreasing of the activation energy by the addition of the catalyst. Thus, the collision between the particles was increased, resulting in a higher possibility of reaction occurrence. Accordingly, it enhanced the reaction rate and FFA conversion. On the other hand, the apparent reaction conversion declined on the higher reaction concentration (5% to 7%) since the excessive amount of catalyst could provoke the side reaction and reduce the FFA conversion (Widiarti et al., 2017). The excessive employment of catalysts will correspondingly bring about the difficulty and higher costs in the product separation. Based on the experiments, it was revealed that the optimum catalyst concentration was 3%, which resulted in the FFA conversion of 78.18% at the temperature of 60°C with a reaction time of 120 minutes. The FFA content of such operation conditions was 4.01%. This value

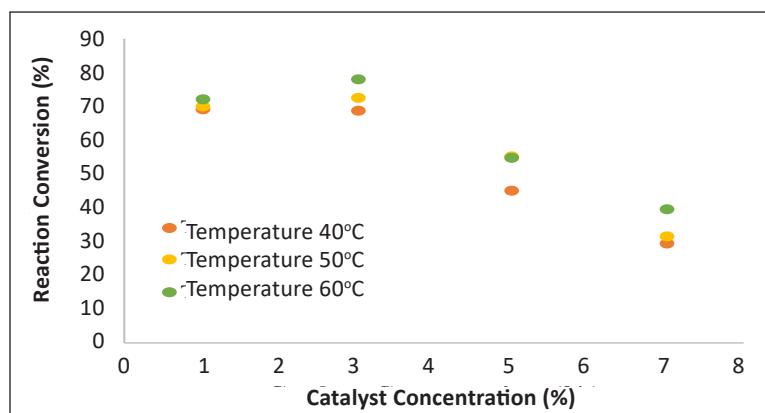


Figure 1. Effect of Catalyst Concentration on the FFA Conversion at the Reaction Time of 120 Minutes and Molar Ratio of RNSO to Methanol of 1:30

has not satisfied the maximum allowable FFA content of 2% for the transesterification reaction yet. Therefore, further, observation was conducted at different temperatures and reaction times.

Esterification of FFA: Effect of Temperature and Reaction Time

The influence of the reaction temperature and time was presented in Figure 2. It is shown that the higher the reaction temperature, the higher removal of FFA occurred. This phenomenon was because the higher reaction temperature will increase the molecular motion of each reactant species, improving the kinetics energy. Therefore, the increase in the reaction temperature raised the FFA conversion. This fact also agreed with the Arrhenius law, which states that the reaction rate is equivalent to the reaction temperature. Encinar et al. (2021) described that this phenomenon was common for the endothermic reaction. According to Le Chatelier's principle, the equilibrium shifts to the product formation as the temperature rises.

As shown in Figure 2, it was also found that the FFA conversion enhanced with the reaction time, but the enhancement was slower from 60 to 120 minutes. It means that the reaction was approaching the chemical equilibrium point at 120 minutes. Based on catalyst concentration alteration (Figure 1) as well as the temperature and reaction time variation (Figure 2), it was revealed that the best conversion was achieved at the catalyst concentration of 3%, molar ratio of RNSO to methanol of 1:30, reaction temperature of 60°C, and reaction time of 120 minutes with the FFA conversion of 78.18% and the FFA content of 4.01%. This result was in line with our previous work that reported that the optimum condition of FFA removal in kapok randu seed oil using methanol reactant and the sulfuric acid catalyst was 60°C, and reaction time of 120 minutes (Kusumaningtyas et al., 2019). The promising way to enhance the reaction conversion is by increasing the reaction

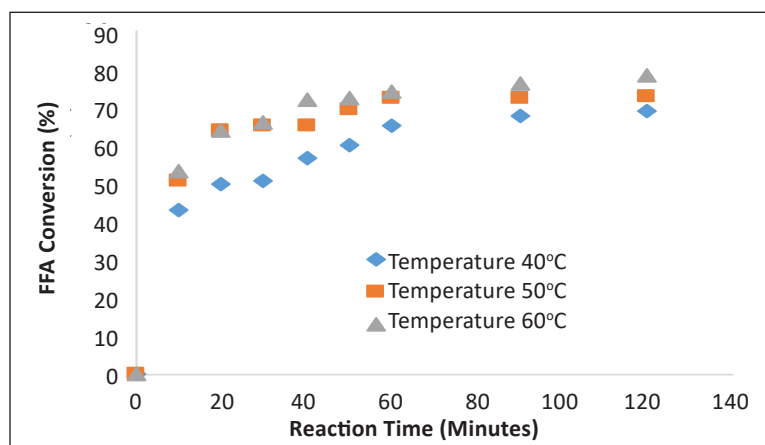


Figure 2. Effect of Temperature and Reaction Time on the FFA Conversion at the Catalyst Concentration of 3% w/w and Molar Ratio of RNSO and Methanol of 1:30

temperature to 65°C and applying a higher molar ratio of the reactants, as accomplished by Chai et al. (2014). In this work, the lowest FFA content obtained among all the experiments conducted was 4.01%. It did not match FFA content's standard limitation for base catalysed transesterification (2%). Therefore, response surface methodology optimisation was then carried out to predict the optimum operating condition of the esterification reaction, yielding the 2% FFA content of RNSO.

RSM Analysis

The result of the FFA removal was under the targeted value of FFA content (maximum 2%). Thus, RSM will be beneficial for designing the operating condition to achieve the targeted conversion. RSM is a set of mathematical and statistical tools that can be used to develop an empirical model that correlates the reaction conversion or product yield with the significant process parameters (Veljković et al., 2019). The application of this tool is valuable to reduce the experimental cost (Liu et al., 2018). However, there are several models provided for optimisation using RSM. Hence, a suitable model should be selected. In this work, four polynomial models (linear, interactive or 2FI, quadratic, and cubic) in RSM were evaluated to determine the most suitable model which fitted the experimental data. Similar models were also tested by Maran & Priya (2015) and Ahmad et al. (2020).

In this study, the best polynomial model will be useful for future work to design the experiment condition and improve the conversion of the reaction. A combination of the effects of the 3 independent variables (catalyst concentration, temperature, and reaction time) on the FFA esterification in RNSO using sulfuric acid catalyst were investigated to select the model. These variables were used to optimise using RSM since they were the main parameters studied in experimental work. Experiments with the different combinations

of the three variables were conducted and calculated statistically using an experimental design based on the Box-Behnken Methodology (BBD). The BBD is a self-reliant quadratic design which does not involve implanted factorial (Rodríguez-Ramírez et al., 2020). This complete factorial design is the most commonly applied in RSM optimisation (Veljković et al., 2019). The experimental design using BBD is shown in Table 3.

Table 3

Experimental Design Using Box-Behnken Methodology (BBD), which equipped with the experimental data and predictive result

Run	Temperature (A)	Catalyst Concentration (B)	Time (C)	FFA Conversion, %		% Error	FFA Content, %		% Error
				Exp	Prediction		Exp	Prediction	
1	60	3	60	74.07	74.10	0.05	4.77	4.97	4.25
2	60	3	120	78.18	78.75	0.73	4.02	4.24	5.46
3	40	3	60	64.9	66.67	2.73	6.46	6.30	2.52
4	50	5	120	55.41	56.88	2.65	8.21	8.44	2.76
5	40	3	120	68.7	71.00	3.35	5.76	5.61	2.53
6	40	5	90	44.97	47.97	6.67	10.13	9.94	1.88
7	60	5	90	52.56	56.84	8.14	8.73	8.35	4.30
8	50	1	120	69.96	72.15	3.13	5.53	5.22	5.66
9	40	1	90	66.8	64.84	2.94	6.11	6.54	7.10
10	50	5	60	52.56	52.08	0.91	8.73	9.09	4.07
11	60	1	90	71.85	71.14	0.98	5.18	5.43	4.83
12	50	3	90	72.17	73.36	1.64	5.12	5.15	0.53
13	50	1	60	66.48	67.98	2.25	6.17	5.99	3.00

The four polynomial models, namely linear, interactive (2FI), quadratic, and cubic, were used to predict the response variable to the experimental data. In addition, two types of tests, i.e., a sequential model sum of squares and model summary, were used as the basis for the polynomial model determination, which is suitable for optimising the FFA conversion. The result is shown in Tables 4 and 5, respectively.

Based on the result shown in Tables 4 and 5, it was acquired that the quadratic model was justified as the most suitable model for optimising the FFA content and conversion in the esterification using a sulfuric acid catalyst. The basis of the selection of the quadratic model was the lowest p-value, the highest value of adjusted R^2 , and the highest value of predicted R^2 . Table 4 reveals that the quadratic model provided the lowest p-value. Table 5 shows that the quadratic model provided the highest value of adjusted R^2 . Meanwhile, the predicted R^2 for the quadratic model did not appear in Table 5 since the value was precisely closed to 1. In contrast, the actual R^2 were not presented in Table 5 since this table depicted the summary of the model test. Therefore, the actual R^2 values were advanced investigated based on the values of predicted R^2 . Based on the values of the p-value, adjusted R^2 , and

Table 4
Sequential model sum of squares test

Component	Sum of square	DF	Mean Square	F-value	p-value	Remarks
Sequential Sum of Square for FFA Content						
Mean	554.72	1	554.72			
Linear	25.51	3	8.50	5.08	0.0250	Suggested
2FI	0.0595	3	0.0198	0.0079	0.9989	
Quadratic	14.16	3	4.72	16.85	0.0221	Suggested
Cubic	0.8404	3	0.2801			Aliased
Residual	0.0000	0				
Total	595.30	13	45.79			
Sequential sum of square for FFA Conversion						
Mean	54097.44	1	54097.44			
Linear	753.08	3	251.03	5.08	0.0249	Suggested
2FI	1.74	3	0.5787	0.0078	0.9989	
Quadratic	417.93	3	139.31	16.83	0.0222	Suggested
Cubic	24.83	3	8.28			Aliased
Residual	0.0000	0				
Total	55295.02	13	4253.46			

Table 5
Model summary test

Component	Std. Dev	Adjusted R ²	Predicted R ²	Press	Remarks
Model Summary of FFA Content					
Linear	0.0250	0.5050	0.2313	Suggested	0.0250
2FI	0.9989	0.2604	-0.8490	-	0.9989
Quadratic	0.0221	0.9172	-	Suggested	0.0221
Cubic	-	-	-	Aliased	-
Model summary of FFA Conversion					
Linear	0.0249	0.5051	0.2314	Suggested	0.0249
2FI	0.9989	0.2606	-0.8492	-	0.9989
Quadratic	0.0222	0.9171	-	Suggested	0.0222
Cubic	-	-	-	Aliased	-

predicted R² attained, the quadratic model was found the most suitable model and further analysed using ANOVA. This finding is in line with the result analysis of Maran & Priya (2015), which suggested that the quadratic model was the most appropriate.

The empirical model, expressed using the quadratic model with the interaction obtained from the experimental data based on the RSM, was modified into a polynomial equation. The final equation for FFA content and FFA conversion optimisation is presented in Equations 1 and 2, respectively.

$$\text{FFA Content (\%)} = 16.5 - 0.306 A - 2.2 B + 0.014 C - 0.0059 AB - 0.000042 AC + 0.0005 BC + 0.0026 A^2 + 0.54 B^2 - 0.00014 C^2 \quad (1)$$

$$\text{FFA Conversion (\%)} = 10.63 + 1.66 A + 11.91B - 0.081 C + 0.032 AB + 0.00026 AC + 0.0026 BC - 0.014 A^2 - 2.94 B^2 + 0.00075 C^2 \quad (2)$$

Statistical analysis for the quadratic model using ANOVA regression model is shown in Table 6.

Table 6
ANOVA regression model to predict the FFA conversion using sulfuric acid catalyst

Source	Sum of square	Degree of Freedom	Mean square	F value	p-value	Remarks
ANOVA for FFA Content						
Model	39.73	9	4.41	15.76	0.0221	significant
X ₁	4.15	1	4.15	14.80	0.0310	
X ₂	20.51	1	20.51	73.22	0.0034	
X ₃	0.8515	1	0.8515	3.04	0.1796	
X ₁₂	0.0552	1	0.0552	0.1971	0.6871	
X ₁₃	0.0006	1	0.0006	0.0022	0.9653	
X ₂₃	0.0036	1	0.0036	0.0129	0.9169	
X ₁ ²	0.1486	1	0.1486	0.5306	0.5191	
X ₂ ²	10.69	1	10.69	38.16	0.0085	
X ₃ ²	0.0343	1	0.0343	0.1224	0.7495	
Residual	0.8404	3	0.2801			
Cor Total	40.57	12				
Adeq prec	12.46					
ANOVA for FFA Conversion						
Model	1172.75	9	130.31	15.74	0.0222	significant
X ₁	122.38	1	122.38	14.79	0.0310	
X ₂	605.35	1	605.35	73.14	0.0034	
X ₃	25.35	1	25.35	3.06	0.1784	
X ₁₂	1.61	1	1.61	0.1949	0.6888	
X ₁₃	0.0240	1	0.0240	0.0029	0.9604	
X ₂₃	0.0992	1	0.0992	0.0120	0.9197	
X ₁ ²	4.37	1	4.37	0.5278	0.5201	
X ₂ ²	315.17	1	315.17	38.08	0.0086	
X ₃ ²	1.04	1	1.04	0.1258	0.7463	
Residual	24.83	3	8.28			
Cor Total	1197.58	12				
Adeq prec	12.46					

The F-value of the model was 15.76, indicating that the model was significant. There was only 2.22% of noise potential, which could cause the model unsuccessful in predicting the value of the response variable (FFA conversion). The p-value was 0.022 (< 0.05), designating that the variables were significant to the model. In this study, the influential variables were A, B, and B². Table 6 also demonstrates the value of adeq precision. Adeq precision measures the signal ratio to the disturbance (noise), and its value is expected to be higher than 4. A ratio of 12.46 resulted in this work, denoted that the inputted signal was appropriate.

Validation of the model capability in predicting is necessary to ensure the accuracy of the model approach. Figure 3 shows the model validation by comparing the predicted result with the experimental data. Figure 3(a) demonstrates that the predictive value based on the model's calculation was close to the experimental data. It was indicated by the

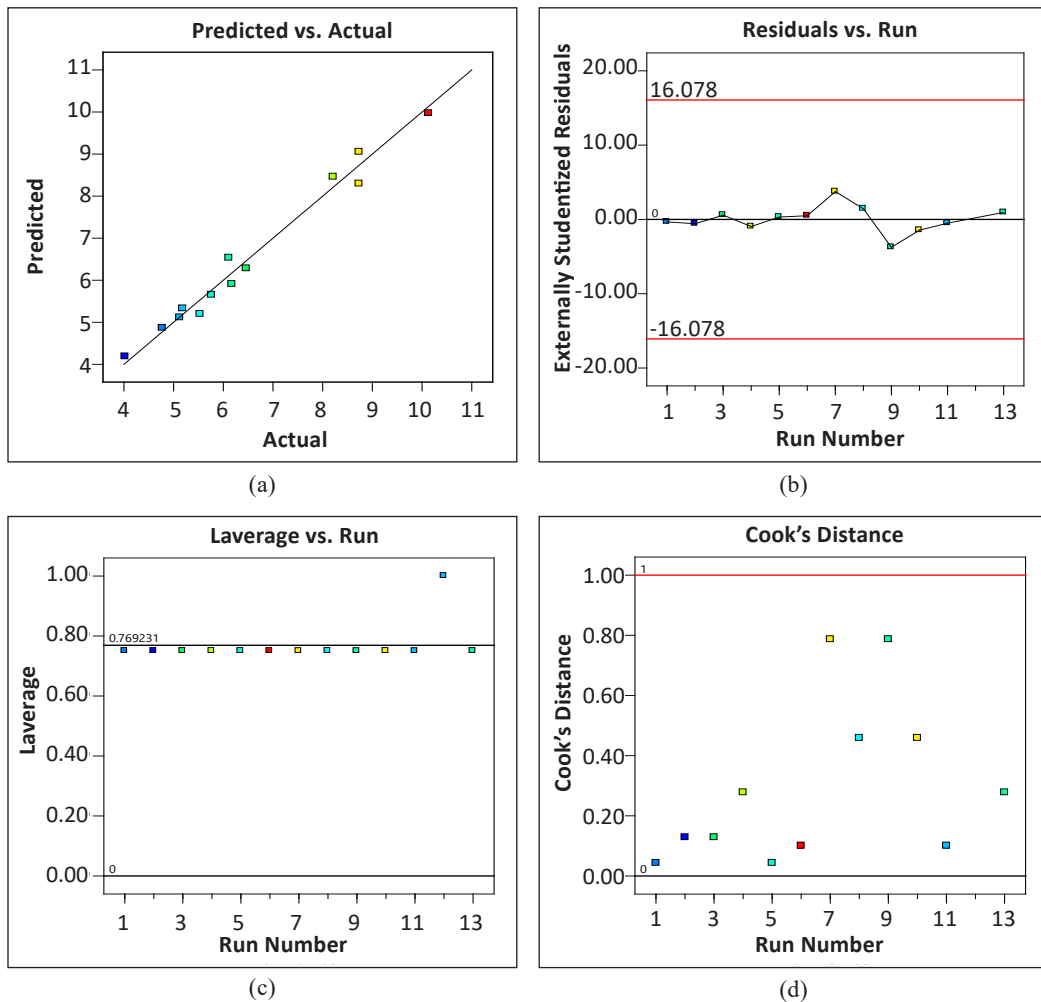
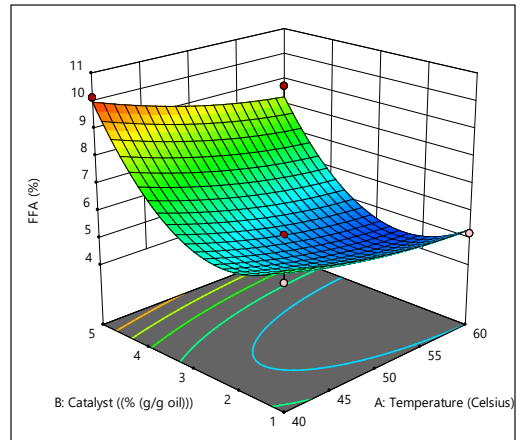


Figure 3. The Result of the Diagnoses for the Quadratic Model Approach

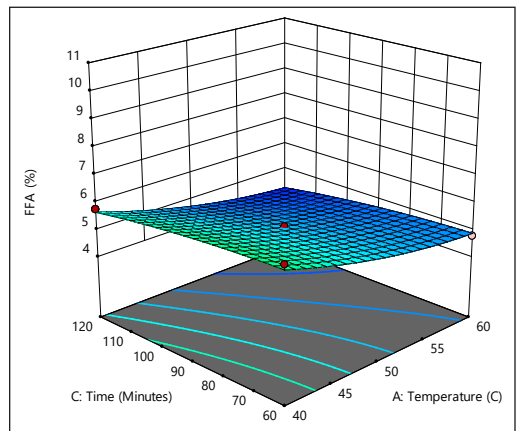
point of the prediction and experimental response values just about the 45° line. It specified that the proposed model was successfully identified the correlation of the input variables (catalyst concentration, reaction temperature, and reaction time) to the response (reaction conversion).

The model suitability was further determined by constructing a plot between the externally studied residuals and the prediction value. Figure 3(b) exhibits that all the data were under the limit, meaning that the model was suitable. As shown in Figure 3(c), all the leverage parameters were less than 1. It denoted that there was no significant error that could affect the model approach. Figure 3(d) presents that all the points were under the expected Cook's Distance Parameter. It implied that there is no significant error in observation in taking the experimental data. All the results of the model diagnoses demonstrated that the quadratic model developed in this analysis was appropriate for FFA content and FFA conversion optimisation in the FFA esterification using a sulfuric acid catalyst. The graphical illustration, termed response surface, is frequently used to justify the individual and cumulative influences of the experimental variables and their successive effect on the response (Liu et al., 2014).

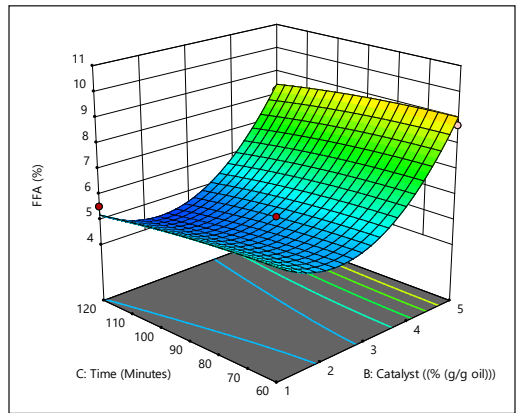
The significant variables affecting the FFA content and conversion were temperature and catalyst concentration as demonstrated in Figures 4 and 5. It can be observed that the FFA content reduced and, in contrast, the FFA conversion rose due to the temperature increase up to



(a)



(b)



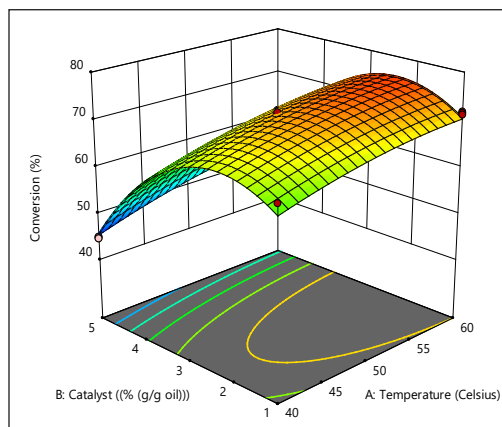
(c)

Figure 4. Three dimensional (3D) response surface of the effect of the process condition to the FFA content. (a) Reaction time = 90 min; (b) Catalyst concentration = 5 (g/g RNSO); and (c) Reaction temperature = 50°C.

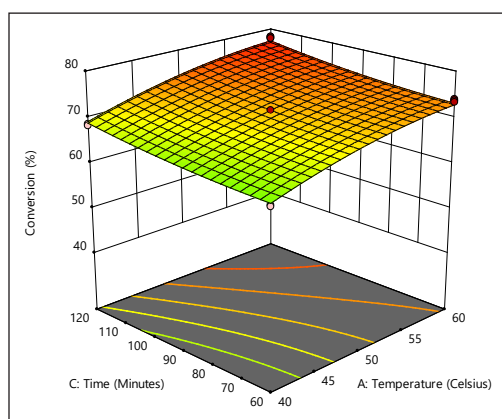
60°C. Additionally, increasing catalyst concentration from 1 to 3% significantly enhanced the FFA conversion and lowered the FFA content. However, an additional amount of catalyst employment did not result in the higher reaction conversion and the FFA removal. Reaction time considerably improved the reaction conversion and FFA removal from 0 to 60 minutes. After 60 minutes, reaction time slightly affected the esterification reaction.

In this work, the Derringer method was employed for the FFA conversion and FFA removal optimisation in the esterification using a sulfuric acid catalyst. In the complex system, various experimental variables have to be considered simultaneously to determine the optimum condition. It is known as a multi-response problem based on Multi-criteria Decision Making. In this case, the desirability approach is often employed as a vigorous instrument for optimisation in a multi-response system. The Derringer method is among the popular desirability method. The desirability function values are between 0 and 1. The value 0 means that the factors provided an undesired response. On the other hand, the value 1 indicates the optimal condition of the parameter evaluated (Amdoun et al., 2018).

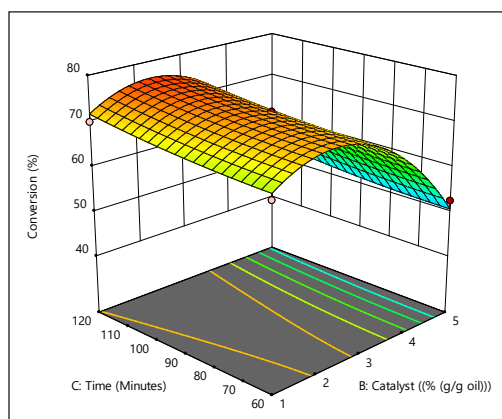
Based on the RSM simulation, it was revealed that the optimum conversion and the FFA content were 78.27% and 4%, respectively, achieved at the reaction temperature of 59.09 °C, catalyst concentration 1.98% g/g RNSO, and reaction time of 119.95 minutes. At this operation condition, the value of the desirability ramp



(a)



(b)



(c)

Figure 5. Three dimensional (3D) Response surface of the effect of the process condition to the FFA conversion. (a) Reaction time = 90 min; (b) Catalyst concentration = 5 (g/g RNSO); and (c) Reaction temperature = 50°C.

was 1 (Figure 6). The result fitted the experimental data and indicated the accuracy of the model. A similar method of optimisation applying desirability function was also described by (Mourabet et al., 2017).

Extrapolation was performed using RSM to predict the operating conditions and achieve a maximum of 2% FFA content. As shown in Figure 7, the FFA content can be lowered up to 2% with the reaction condition as follows: reaction temperature, catalyst concentration,

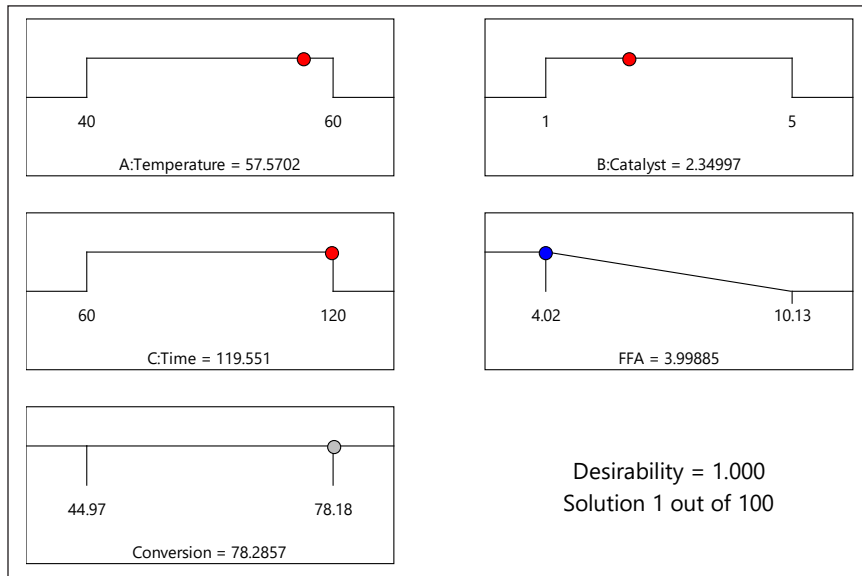


Figure 6. Optimisation of FFA conversion using RSM (Quadratic model)

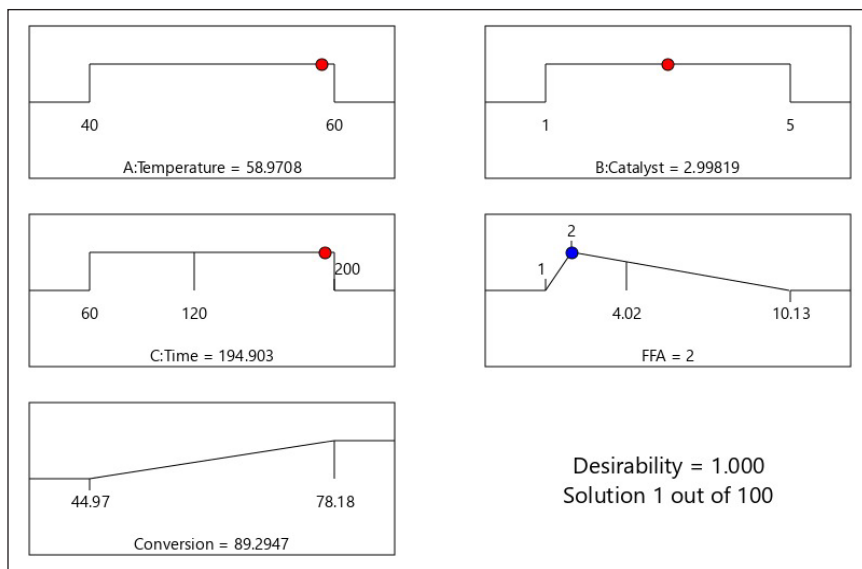


Figure 7. RSM prediction of operation condition on the FFA esterification using sulfuric acid catalyst to decrease the FFA content to 2%

and reaction time were 58.97°C, 3%, and 194.9 minutes, respectively, whereas the molar ratio of oil to methanol was fixed at 1:30. Therefore, the FFA conversion achieved was estimated at 89.3%.

The result has shown that RSM is simple and effective for process optimisation. Furthermore, the RSM and desirability function combination lead to the more accurate finding of the optimal condition. The identical deduction was reported by Amdoun et al. (2018). This study is significant in providing the optimum operating condition for reducing the FFA in CNSO to fulfil the allowable level of FFA content before being used as feedstock for biodiesel production via base catalysed transesterification reaction.

CONCLUSION

The experimental work of FFA esterification in RNSO with methanol in the presence of sulfuric acid catalyst has shown the optimal reaction condition at the reaction temperature of 60°C, a reaction time of 120 minutes, the molar ratio of RNSO) to methanol of 1:30, and the reaction times of 120 minutes, which yielded the reaction conversion of 78.18% and the FFA concentration of 4.01%. This value did not match the maximum acceptable FFA content value for alkaline catalysed transesterification (2%). The RSM was performed to estimate the optimal operation condition for achieving the FFA content of 2%. The RSM model analysis demonstrated that the quadratic model was the most suitable for optimising this process in future work. The RSM extrapolation predicted that the FFA content of 2% could be obtained at the reaction temperature, catalyst concentration, reaction time of 58.97°C, 3%, and 194.9 minutes, respectively, and the fixed molar ratio of oil to methanol of 1:30.

ACKNOWLEDGMENT

The funding resource from the Research and Community Service Institute (LPPM) of Universitas Negeri Semarang through Collaborative Research Scheme (UNNES-UiTM Matching Grant) with Contract Number of 101.23.4/UN37/PPK.3.1/2020 is highly acknowledged.

REFERENCES

- Aboelazayem, O., Gadalla, M., & Saha, B. (2018). Biodiesel production from waste cooking oil via supercritical methanol: Optimisation and reactor simulation. *Renewable Energy*, *124*, 144-154. <https://doi.org/10.1016/j.renene.2017.06.076>
- Ahmad, A., Rehman, M. U., Wali, A. F., El-Serehy, H. A., Al-Misned, F. A., Maooda, S. N., Aljawdah, H. M., Mir, T. M., & Ahmad, P. (2020). Box–Behnken response surface design of polysaccharide extraction from *Rhododendron arboreum* and the evaluation of its antioxidant potential. *Molecules*, *25*(17), Article 3835. <https://doi.org/10.3390/molecules25173835>

- Amdoun, R., Khelifi, L., Khelifi-Slaoui, M., Amroune, S., Asch, M., Assaf-ducrocq, C., & Gontier, E. (2018). The desirability optimization methodology: A tool to predict two antagonist responses in biotechnological systems: Case of biomass growth and hyoscyamine content in elicited datura starmonium hairy roots. *Iranian Journal of Biotechnology*, *16*(1), 11-19. <https://doi.org/10.21859/ijb.1339>
- Aparamarta, H. W., Gunawan, S., Husin, H., Azhar, B., & Aditya, H. T. (2020). The effect of high oleic and linoleic fatty acid composition for quality and economical of biodiesel from crude *Calophyllum inophyllum* oil (CCIO) with microwave-assisted extraction (MAE), batchwise solvent extraction (BSE), and combination of MAE-BSE meth. *Energy Reports*, *6*, 3240-3248. <https://doi.org/10.1016/j.egy.2020.11.197>
- Arora, R., Toor, A. P., & Wanchoo, R. K. (2015). Esterification of high free fatty acid rice bran oil: Parametric and kinetic study. *Chemical and Biochemical Engineering Quarterly*, *29*(4), 617-623. <https://doi.org/10.15255/CABEQ.2014.2117>
- Atabani, A. E., & César, A. D. S. (2014). *Calophyllum inophyllum* L. - A prospective non-edible biodiesel feedstock. Study of biodiesel production, properties, fatty acid composition, blending and engine performance. *Renewable and Sustainable Energy Reviews*, *37*, 644-655. <https://doi.org/10.1016/j.rser.2014.05.037>
- Banani, R., Youssef, S., Bezzarga, M., & Abderrabba, M. (2015). Waste frying oil with high levels of free fatty acids as one of the prominent sources of biodiesel production. *Journal of Materials and Environmental Science*, *6*(4), 1178-1185.
- Banchero, M., & Gozzelino, G. (2018). A simple pseudo-homogeneous reversible kinetic model for the esterification of different fatty acids with methanol in the presence of Amberlyst-15. *Energies*, *11*(7), Article 1843. <https://doi.org/10.3390/en11071843>
- Chai, M., Tu, Q., Lu, M., & Yang, Y. J. (2014). Esterification pretreatment of free fatty acid in biodiesel production, from laboratory to industry. *Fuel Processing Technology*, *125*, 106-113. <https://doi.org/10.1016/j.fuproc.2014.03.025>
- Corach, J., Sorichetti, P. A., & Romano, S. D. (2017). Permittivity of diesel fossil fuel and blends with biodiesel in the full range from 0% to 100%: Application to biodiesel content estimation. *Fuel*, *188*, 367-373. <https://doi.org/10.1016/j.fuel.2016.10.019>
- Dal Pozzo, D. M., Azevedo Dos Santos, J. A., Júnior, E. S., Santos, R. F., Feiden, A., Melegari De Souza, S. N., & Burgardt, I. (2019). Free fatty acids esterification catalyzed by acid Faujasite type zeolite. *RSC Advances*, *9*, 4900-4907. <https://doi.org/10.1039/c8ra10248a>
- Demirbas, A. (2006). Biodiesel production via non-catalytic SCF method and biodiesel fuel characteristics. *Energy Conversion and Management*, *47*(15-16), 2271-2282. <https://doi.org/10.1016/j.enconman.2005.11.019>
- Dey, S., Reang, N. M., Das, P. K., & Deb, M. (2021). A comprehensive study on prospects of economy, environment, and efficiency of palm oil biodiesel as a renewable fuel. *Journal of Cleaner Production*, *286*, Article 124981. <https://doi.org/10.1016/j.jclepro.2020.124981>
- Encinar, J. M., Nogales-Delgado, S., & Sánchez, N. (2021). Pre-esterification of high acidity animal fats to produce biodiesel: A kinetic study. *Arabian Journal of Chemistry*, *14*(4), Article 103048. <https://doi.org/10.1016/j.arabjc.2021.103048>

- Gebremariam, S. N., & Marchetti, J. M. (2018). Techno-economic feasibility of producing biodiesel from acidic oil using sulfuric acid and calcium oxide as catalysts. *Energy Conversion and Management*, 171(June), 1712-1720. <https://doi.org/10.1016/j.enconman.2018.06.105>
- Ghasemian, S., Faridzad, A., Abbaszadeh, P., Taklif, A., Ghasemi, A., & Hafezi, R. (2020). An overview of global energy scenarios by 2040: Identifying the driving forces using cross-impact analysis method. *International Journal of Environmental Science and Technology*, 1-24. <https://doi.org/10.1007/s13762-020-02738-5>
- Harun, F. W., Jihadi, N. I. M., Ramli, S., Hassan, N. R. A., & Zubir, N. A. M. (2018). Esterification of oleic acid with alcohols over Cu-MMT K10 and Fe-MMT K10 as acid catalysts. In *AIP Conference Proceedings* (Vol. 1972, No. 1, p. 030025). AIP Publishing LLC. <https://doi.org/10.1063/1.5041246>
- Islam, A., Taufiq-Yap, Y. H., Chan, E. S., Moniruzzaman, M., Islam, S., & Nabi, M. N. (2014). Advances in solid-catalytic and non-catalytic technologies for biodiesel production. *Energy Conversion and Management*, 88, 1200-1218. <http://dx.doi.org/10.1016/j.enconman.2014.04.037>
- Kusumaningtyas, R. D., Aji, I. N., Hadiyanto, H., & Budiman, A. (2016). Application of tin(II) chloride catalyst for high FFA jatropha oil esterification in continuous reactive distillation column. *Bulletin of Chemical Reaction Engineering & Catalysis*, 11(1), 66-74. <https://doi.org/10.9767/brec.11.1.417.66-74>
- Kusumaningtyas, R. D., Akbar, M. H., & Widjanarko, D. (2019). Reduction of FFA in kapok randu (*Ceiba pentandra*) seed oil via esterification reaction using sulfuric acid catalyst: Experimental and kinetics study. *Jurnal Bahan Alam Terbarukan*, 8(2), 156-166.
- Kusumaningtyas, R. D., Handayani, P. A., Rochmadi, Purwono, S., & Budiman, A. (2014). Tin(II)chloride catalyzed esterification of high FFA jatropha oil: Experimental and kinetics study. *International Journal of Renewable Energy Development*, 3(2), 7581. <https://doi.org/http://dx.doi.org/10.14710/ijred.3.2.75-81>
- Kusumaningtyas, R. D., Prasetiawan, H., Pratama, B. R., Prasetya, D., & Hisyam, A. (2018). Esterification of non-edible oil mixture in reactive distillation column over solid acid catalyst: Experimental and simulation study. *Journal of Physical Science*, 29(II), 212226. <https://doi.org/10.21315/jps2018.29.s2.17>
- Lamas, D. L., Constenla, D. T., & Raab, D. (2016). Effect of degumming process on physicochemical properties of sunflower oil. *Biocatalysis and Agricultural Biotechnology*, 6(March), 138-143. <https://doi.org/10.1016/j.bcab.2016.03.007>
- Liu, J., Wang, J., Leung, C., & Gao, F. (2018). A multi-parameter optimization model for the evaluation of shale gas recovery enhancement. *Energies*, 11(3), Article 654. <https://doi.org/10.3390/en11030654>
- Liu, W., Yin, P., Liu, X., & Qu, R. (2014). Design of an effective bifunctional catalyst organotriphosphonic acid-functionalized ferric alginate (ATMP-FA) and optimization by Box-Behnken model for biodiesel esterification synthesis of oleic acid over ATMP-FA. *Bioresource Technology*, 173, 266-271. <https://doi.org/10.1016/j.biortech.2014.09.087>
- Maran, J. P., & Priya, B. (2015). Comparison of response surface methodology and artificial neural network approach towards efficient ultrasound-assisted biodiesel production from muskmelon oil. *Ultrasonics Sonochemistry*, 23, 192-200. <https://doi.org/10.1016/j.ultsonch.2014.10.019>

- Marchetti, J. M., & Errazu, A. F. (2008). Esterification of free fatty acids using sulfuric acid as catalyst in the presence of triglycerides. *Biomass and Bioenergy*, 32(9), 892-895. <https://doi.org/10.1016/j.biombioe.2008.01.001>
- Mourabet, M., El Rhilassi, A., El Boujaady, H., Bennani-Ziatni, M., & Taitai, A. (2017). Use of response surface methodology for optimization of fluoride adsorption in an aqueous solution by Brushite. *Arabian Journal of Chemistry*, 10, S3292-S3302. <https://doi.org/10.1016/j.arabjc.2013.12.028>
- Mubarak, M., Shaija, A., & Suchithra, T. V. (2021). Experimental evaluation of *Salvinia molesta* oil biodiesel/diesel blends fuel on combustion, performance and emission analysis of diesel engine. *Fuel*, 287, Article 119526. <https://doi.org/10.1016/j.fuel.2020.119526>
- Murad, P. C., Hamerski, F., Corazza, M. L., Luz, L. F. L., & Voll, F. A. P. (2018). Acid-catalyzed esterification of free fatty acids with ethanol: An assessment of acid oil pretreatment, kinetic modeling and simulation. *Reaction Kinetics, Mechanisms and Catalysis*, 123(2), 505-515. <https://doi.org/10.1007/s11144-017-1335-3>
- Musta, R., Haetami, A., & Salmawati, M. (2017). Biodiesel hasil transesterifikasi minyak biji Nyamplung (*Calophyllum inophyllum*) dengan metanol [Biodiesel of the transesterification product of *Calophyllum inophyllum* seed oil from kendari using methanol solution]. *Indonesian Journal of Chemical Research*, 4(2), 394-401. <https://doi.org/10.30598/ijcr.2017.4-rus>
- Ong, H. C., Milano, J., Silitonga, A. S., Hassan, M. H., Shamsuddin, A. H., Wang, C. T., Indra Mahlia, T. M., Siswanto, J., Kusumo, F., & Sutrisno, J. (2019). Biodiesel production from *Calophyllum inophyllum*-*Ceiba pentandra* oil mixture: Optimization and characterization. *Journal of Cleaner Production*, 219, 183-198. <https://doi.org/10.1016/j.jclepro.2019.02.048>
- Paraschiv, S., & Paraschiv, L. S. (2020). Trends of carbon dioxide (CO₂) emissions from fossil fuels combustion (coal, gas and oil) in the EU member states from 1960 to 2018. *Energy Reports*, 6, 237-242. <https://doi.org/10.1016/j.egy.2020.11.116>
- Rodríguez-Ramírez, R., Romero-Ibarra, I., & Vazquez-Arenas, J. (2020). Synthesis of sodium zincsilicate (Na₂ZnSiO₄) and heterogeneous catalysis towards biodiesel production via Box-Behnken design. *Fuel*, 280, Article 118668. <https://doi.org/10.1016/j.fuel.2020.118668>
- Silitonga, A. S., Ong, H. C., Mahlia, T. M. I., Masjuki, H. H., & Chong, W. T. (2014). Biodiesel conversion from high FFA crude *Jatropha curcas*, *Calophyllum inophyllum* and *Ceiba pentandra* oil. *Energy Procedia*, 61, 480-483. <https://doi.org/10.1016/j.egypro.2014.11.1153>
- Taghizade, Z. (2016). *Determination of biodiesel quality parameters for optimization of production process conditions*. Polytechnic Institute of Bragança.
- Veljković, V. B., Veličković, A. V., Avramović, J. M., & Stamenković, O. S. (2019). Modeling of biodiesel production: Performance comparison of Box–Behnken, face central composite and full factorial design. *Chinese Journal of Chemical Engineering*, 27(7), 1690-1698. <https://doi.org/10.1016/j.cjche.2018.08.002>
- Widiarti, N., Suryana, L. A., Wijayati, N., Rahayu, E. F., Harjito, H., Wardhana, S. B., Prasetyoko, D., & Suprpto, S. (2017). Synthesis of SrO.SiO₂ catalyst and its application in the transesterification reactions of soybean oil. *Bulletin of Chemical Reaction Engineering & Catalysis*, 12(2), 299-305. <https://doi.org/10.9767/brec.12.2.804.299-305>



A Comparative Study of Several EOF Based Imputation Methods for Long Gap Missing Values in a Single-Site Temporal Time Dependent (SSTTD) Air Quality (PM10) Dataset

Shamihah Muhammad Ghazali^{1*}, Norshahida Shaadan^{1,2} and Zainura Idrus¹

¹Center for Statistical and Decision Science Studies, Faculty of Computer & Mathematical Sciences, Universiti Teknologi MARA, 40450, Shah Alam, Selangor, Malaysia

²Business Analytics Research Group, Faculty of Computer & Mathematical Sciences, Universiti Teknologi MARA, Bukit Ilmu, 18500, Machang, Kelantan, Malaysia

ABSTRACT

Missing values are often a major problem in many scientific fields of environmental research, leading to prediction inaccuracy and biased analysis results. This study compares the performance of existing Empirical Orthogonal Functions (EOF) based imputation methods. The EOF mean centred approach (EOF-mean) with several proposed EOF based methods, which include the EOF-median, EOF-trimmean and the newly applied Regularised Expectation-Maximisation Principal Component Analysis based method, namely R-EMPCA in estimating missing values for long gap sequence of missing values problem that exists in a Single Site Temporal Time-Dependent (SSTTD) multivariate structure air quality (PM10) data set. The study was conducted using real PM10 data set from the Klang air quality monitoring station. Performance assessment and evaluation of the methods were conducted via a simulation plan which was carried out according to four percentages (5, 10, 20 and 30) of missing values with respect to several long gap sequences (12, 24, 168 and 720) of missing points (hours). Based on several performance indicators such as RMSE, MAE, R-Square and AI, the results have shown that R-EMPCA outperformed the other methods. The results also conclude that the proposed EOF-median and EOF-trimmean have better performance than the existing EOF-mean based method in which EOF-trimmean is the

best among the three. The methodology and findings of this study contribute as a solution to the problem of missing values with long gap sequences for the SSTTD data set.

ARTICLE INFO

Article history:

Received: 16 April 2021

Accepted: 05 July 2021

Published: 08 October 2021

DOI: <https://doi.org/10.47836/pjst.29.4.21>

E-mail addresses:

shamihah.ghazali@gmail.com (Shamihah Muhammad Ghazali)

shahida@tmsk.uitm.edu.my (Norshahida Shaadan)

zainura@tmsk.uitm.edu.my (Zainura Idrus)

* Corresponding author

Keywords: Air quality, empirical orthogonal functions, imputation, long gap missing values, PM10

INTRODUCTION

Usually, missing values in the air quality data set occurs when the values are unobserved, or the values were missing due to several reasons such as failure of monitoring instruments during some bad seasonal weather, computer system crashes, routine maintenance, human errors, calibration process and staying off-line for several days at the monitoring stations (Ghazali et al., 2020; Shaadan & Rahim, 2019). The impact of the missing data on the statistical analysis results depends on the mechanism that made the data to be missing and on the way the data analyst deals with them (Plaia & Bondi, 2006). In environmental studies, three types of missing data were taken into account, which is Missing Completely at Random (MCAR), Missing at Random (MAR) and Missing Not at Random (MNAR). For most air quality data sets, the mechanism of missing air quality data is MAR; the probability of a missing that a value is not dependent on the missing part themselves (Josse & Husson, 2016; Plaia & Bondi, 2006; Shaadan et al., 2015).

In the presence of missing data, treatment to replace the missing values is crucial in many fields, especially in air quality data sets where high percentages of data are being missed with long gap sequences (Ghazali et al., 2020). Many existing imputation methods that deal with missing values were proposed in the literature. The methods include a simple approach such as using mean or median substitution, a model-based approach including Regression-based imputation (REGEM), nearest neighbour (NN), K-nearest neighbour (KNN), expectation-maximisation (EM), maximum likelihood method and other hybrids methods (Junninen et al., 2004). Ruggieri et al. (2013) claimed that the Empirical Orthogonal Functions (EOF) based method is among the most promising method of imputing missing values to solve long gap sequences of missing data present in the air quality data set. Several applications of EOF methodology on the observed data by a Singular Value Decomposition (SVD) in handling the missing values have been discussed in several areas. However, the issue of long gap missingness in air quality data set and the experimentation is limited in the number. Moreover, long gaps of missingness often occur due to a longer sequence of hours, which is more than 6 hours and occur within several days or weeks and months (Bartzokas et al., 2003).

A study conducted by Beckers and Rixen (2003) was among the earliest investigation that used EOF calculations and procedures to fill in missing data. The study had used the imputation method in spatial-temporal data sets in the oceanographic field of studies. Next, another research was conducted by Sorjamaa et al. (2010) that proposed an improved EOF methodology for filling missing values in spatial-temporal climates data sets using EOF Pruning which was based on an original linear projection method. Among other closely related research that is continuously being explored was the paper by Beckers and Rixen (2003), Hannachi et al. (2007), Sorjamaa et al. (2010), Ruggieri et al. (2010) and Di Salvo et al. (2016). In Ruggieri et al. (2013), the authors proposed spatial-temporal Functional

Principal Component Analysis (FPCA) and used the EOF procedure to fill in long gap sequences of missing data to investigate the temporal variation of multiple pollutant datasets measured at multi-site and multivariate at the same time.

Even though the large proportion of missing values and long gap sequences of missing values have been considered in the above studies, noticeably, the scope was mostly focused on the imputation methods for Multi-site and Spatial-temporal Multivariate data structures. In a study by Bai et al. (2020), the authors propose a novel gap-filling method that used the EOF procedure; the method is known as diurnal cycle constrained empirical orthogonal function (DCCEOF) that used to fill in missing data gaps in hourly PM_{2.5} concentration of air quality data and the data existed the long gaps about 40% of days missing in the dataset.

However, the study data was focused on the time series of hourly PM_{2.5} datasets. Therefore, another kind of air quality data format identified as Single Site Temporal Time-Dependent (SSTTD) was rarely highlighted. Meanwhile, for Malaysia, the recorded format of air quality data set for an air quality monitoring station for a single pollutant is usually in the form of SSTTD. The pollutant observations were normally recorded and arranged into daily (row) by hourly (column) matrix format. In conclusion, the application of EOF based methods and their capacity has not yet been explored and compared to be used in the imputation analysis when long gap sequences are present in the SSTTD format air quality data sets. An example of missing values in SSTTD format is shown in Table 1.

Table 1
Example of daily by hourly recorded PM₁₀ data within 24 hours

Day	Hour							
	Hour 1	Hour 2	Hour 3	Hour 4	Hour 5	.	.	Hour 24
Day 1	30	40	60	70	90	.	.	140
Day 2	20	NA	NA	NA	NA	.	.	120
Day 3	50	70	90	NA	NA	.	.	NA
.
.
Day n	70	80	NA	NA

Thus, to fill the gap, in this paper, several EOF based methods are employed to find the most appropriate method for a good reconstruction of long sequences of missing values in SSTTD multivariate air quality data format with the application for PM₁₀ air pollutant data set.

MATERIAL AND METHODS

Data and Study Area

The data used in this study is a real secondary air quality data of particulate matter with a size 10 micrometre and smaller called PM₁₀ measured in $\mu\text{g m}^{-3}$ of Klang air quality

monitoring station. The data was obtained from the Air Quality Division of the Department of Environmental (DOE) Malaysia. The data was recorded using a Continuous Ambient Air Quality Monitoring (CAQM) system by Alam Sekitar Malaysia Sdn. Bhd. (ASMA), a private sector authorised by the DOE. For experimentation analysis in this study, a complete data set was identified for Klang station, consisting of 479 days observations with 11,496 hourly cell records from 1st June 2014 up to 24th April 2015 and will be treated as reference data.

Figure 1 shows the location of Klang station in the Malaysia map with longitude and latitude (N03°00.620', E101° 24.484'). Klang station is located at Sekolah Menengah Perempuan Raja Zarina, Klang, Selangor. The area is surrounded by the crowded industries, residential and commercial areas. Klang station was chosen in this study because this station is among the popular stations with high PM₁₀ levels recorded by DOE.

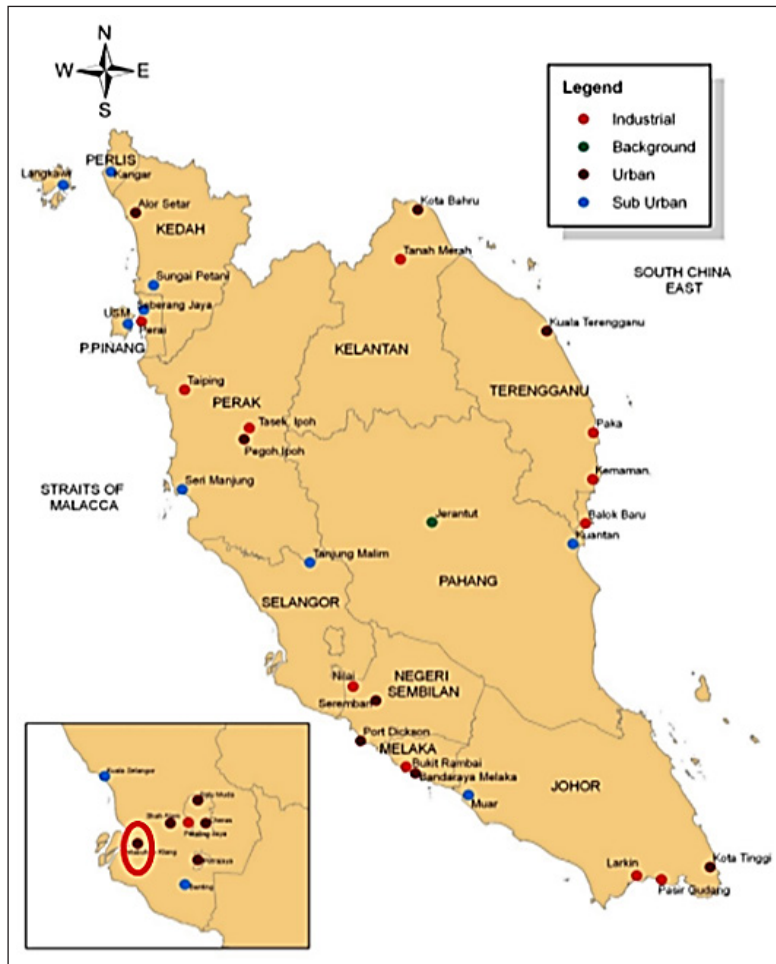


Figure 1. Location maps of air quality monitoring stations, including Klang station (i.e. highlighted in red circle). (Source: Malaysia Environmental Quality Report, 2013)

Methodology Framework

In order to achieve the research objective, the following steps of procedure as depicted in Figure 2 was employed in this study. The research methodology consists of four phases of stages; phase 1: Obtaining reference data, phase 2: Generating missing data pattern, phase 3: Imputing missing values and phase 4: Performance comparison.

Phase 1 step aims to prepare a reference data set for experimentation purposes to compare imputation methods. The reference data must be such a compulsory procedure to validate the performance of the imputation method with better accuracy (Shaadan et al., 2015). This study used a whole PM10 data set of hourly-recorded observations at the Klang air quality monitoring station as a reference data set. Selecting the reference data for this study begins with understanding and viewing the whole structure of the SSTTD data and only selecting the data with a complete case. As mentioned earlier, the selected reference

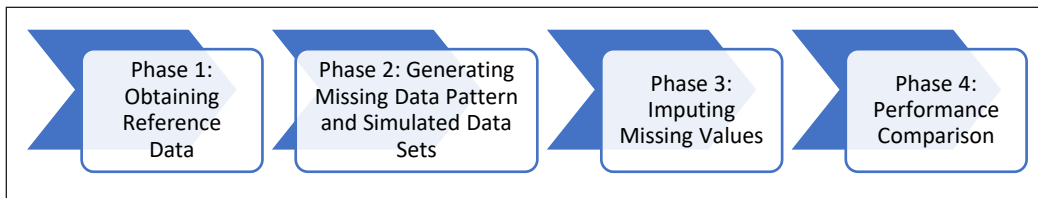


Figure 2. The methodology framework for research analysis

data for Klang station consists of 479 days observations with 11,496 hourly cell records from 1st June 2014 up to 24th April 2015. In phase 2, the simulations of artificial missing data set with several designed patterns were conducted. The patterns were generated according to several percentages of missing values of 5%, 10% and 30% with a different gap size of a sequence of missing points (i.e. hourly points) within 12 (half day), 24 (1 day), 168 (1 week) and 720 (1 month) period. Therefore, 16 missing values patterns need to be designed in this study, as shown in Table 2. Each design pattern will be generated into 100 simulated or artificial datasets.

In the next step, in phase 3, missing values imputation with the existing EOF-based method and several proposed EOF-

Table 2
Sixteen different patterns of missing generated data

Pattern of missingness	Percentages of missingness (%)	Gap length of missingness (hours)
P05_G12	5	12 (half day)
P05_G24	5	24 (1 day)
P05_G168	5	168 (1 week)
P05_G720	5	720 (1 month)
P10_G12	10	12 (half day)
P10_G24	10	24 (1 day)
P10_G168	10	168 (1 week)
P10_G720	10	720 (1 month)
P20_G12	20	12 (half day)
P20_G24	20	24 (1 day)
P20_G168	20	168 (1 week)
P20_G720	20	720 (1 month)
P30_G12	30	12 (half day)
P30_G24	30	24 (1 day)
P30_G168	30	168 (1 week)
P30_G720	30	720 (1 month)

based methods were applied. The analysis was executed on the 100 simulated data sets for each missing pattern obtained in phase 2. The number of simulated missing data sets of 100 for each pattern is decided to be used, following the experimentation conducted by the study of Di Salvo et al. (2016) and Shaadan et al. (2015). Other researchers could also increase the size of the simulated data sets for further detailing the sensitivity analysis, but this sensitivity analysis is not the scope of this research. In this study, the objective of this experimentation based on these 100 simulated data sets for each different designed pattern is to evaluate the performance of the imputation methods towards the consistency of the performance results. Thus, further, validate the performance obtained based on the average value approach, which at the same time can be used to evaluate the performance of the methods towards the complexity of the missing patterns.

Several performance indicators will then be applied to assess the performance of the imputation at phase 4, which includes Root Mean Square Error (RMSE), Mean Absolute Error (MAE), Coefficient of Determination (R-Square) and Agreement Index (AI).

Imputation Methods

Empirical Orthogonal Functions (EOF) Method. The Empirical Orthogonal Functions is a deterministic method for reconstructing the new data matrix through data reduction and identifying temporal variation relationships in the data. In solving the missing values, the EOF allows a linear, continuous projection to a high-dimensional space. The EOF method is performed using Singular Value Decomposition (SVD) by extracting the salient empirical modes of variation from the temporal dependent singular vectors of the data matrix and construct a new set of variables that capture most of the observed variance from the data through a linear combination of the original variables. In understanding the concept of EOF, let us consider a data matrix \mathbf{X} containing the observations, which is arranged such that the element of SSTTD data field t, h of the matrix called $x(t, h)$ where t and h denote respectively time and hours position and M is the number of modes contained in the field, using an optimal set of basis functions of temporal dependent $U_k(s)$ and expansion functions of time $C_k(t)$, as below in Equation 1:

$$x(t, h) = \sum_{k=1}^M C_k(t) U_k(s) \quad (1)$$

In this study, the EOF is performed on SVD. The SVD aims to extract the loading of the principal components, EOFs time (score) and EOFs temporal (loading). SVD is computed for the 2 dimensional of temporal dependent singular vectors of the $n \times p$ data matrix \mathbf{X} , where n is the time-series (days), and p is the temporal-dependent (hours), U and V are a collection of eigendecomposition of vectors of \mathbf{X} , as in Equation 2:

$$\hat{\mathbf{X}} = \mathbf{UDV}^* = \sum_{k=1}^r \rho_k \mathbf{a}_{tk} \mathbf{u}_k \tag{2}$$

The column $\mathbf{a}_k = (a_{1k}, a_{2k}, \dots, a_{nk})$ of \mathbf{U} which the score and $\mathbf{u}_k = (u_{k1}, u_{k2}, \dots, u_{kp})$ of \mathbf{V} which the loading are respectively the left and right singular vectors of the data matrix \mathbf{X} . \mathbf{D} is the diagonal matrix with the singular values ρ in its diagonal, the diagonal elements are $\lambda_1 \geq \lambda_2, \dots, \geq \lambda_r \geq 0$ of \mathbf{D} , are singular values of \mathbf{X} . Where r is the smaller dimension of \mathbf{X} with $r \leq \min(n, p)$ is the rank of \mathbf{X} . The singular values and the singular vectors have been sorted in decreasing order.

From the SVD, the EOF removes the noise from the data. Only the selected singular values and vectors are used for the reconstruction of a new data matrix. This study selects the optimal number of dimension k 'th using Generalised Cross-Validation (GCV) methods. The GCV value can be interpreted as a classical model selection criterion where the residual sum of squares is penalised by the number of degrees of freedom. Equation 3 is as follows:

$$GCV(S) = \frac{np \sum_{i=1}^n \sum_{j=1}^p (x_{ij} - (\hat{x}_{ij})^S)^2}{np - p - nS - pS + S^2 + S} \tag{3}$$

The EOF cannot be directly used with a database that contains missing values. In the common practice, in the existing EOF imputation method, the column mean was normally treated as the initial value for the missing cells (Beckers & Rixen, 2003; Ruggieri et al., 2010; Sorjamaa et al., 2010). However, the existing EOF imputation method has a drawback because it uses data matrix centralisation based on statistic mean for EOF computation. To be applied for the air quality dataset, the existing EOF need to be improved because the dataset often consists of extreme observations due to climatic variations and random processes. In this study, a robust statistic of statistic median and trimmed mean is employed in the matrix centralisation computation and proposed as initial values for the missing values. In this paper, four EOF-based imputation methods are introduced, and the capability of the methods for estimating missing values for long gap missingness problems in Malaysia air quality of SSTTD multivariate datasets is investigated. The existing of EOF method based on the mean (EOF-mean) is compared with the several proposed EOF based on median (EOF-median), EOF based on the trimmed mean (EOF-trimmean) and the newly applied Regularised Expectation-Maximisation Principal Component Analysis (R-EMPCA), which an iterative-based imputation method that is iteratively performing the EOF analysis by means of EM algorithm on the incomplete data sets. Up until now, the performance of R-EMPCA is not yet being explored for solving long gap missingness problems in air quality with SSTTD datasets.

The Existing method: EOF based on the Mean (EOF-mean) Method. Given that a few data points are missing with a long gap of missingness, the aim was to replace the missing value x_{miss} at time t with a value on the estimated data point from EOF based imputation, which $x_{ij}(t, h)$ at the same time t is missing, where $\hat{x}_{miss} = x_{ij}(t, h)$. This procedure of EOF-mean starts from allows the generated missing values at time t to be initially replaced with the mean of the observed values column. Next, the completed data are centralised using the mean centralisation. Then, the EOF procedure is applied to the centralised data matrix, and a new reconstructed matrix of the EOF-mean is built. Finally, the formula for the initial values of the mean column is written as Equation 4:

$$Mean, \bar{x} = \frac{\sum_{k=1}^n x_{ki}}{n} \tag{4}$$

The Proposed Methods: EOF based on Median (EOF-median) and EOF based on Trimmed Mean (EOF-trimmean) Methods. These methods propose an enhancement approach on the existing EOF-mean by using a different strategy in the initialisation step. The EOF-median and EOF-trimmean initially replace the missing values using robust median statistics trimmed mean, respectively, before performing any EOF procedure. The enhancement focuses on using the values from the median and trimmed mean of the observed values as the initial values to replace missing values in the data matrix \mathbf{X} . These initial values are calculated from the available data in the dataset to form a completed data matrix. Finally, the completed data are centralised using the median and trimmed mean centralisation, respectively. The formula for the initial values of the median column is written as Equation 5:

$$Median, m = l + \left(\frac{\frac{N}{2} - F_l}{f_m} \right) \times C \tag{5}$$

where l is the lower-class boundary of the median class, N is the total frequency, F_l is the cumulative frequency before the median class, f_m is the class width of the median class and is the frequency of the median class. Another proposed method is EOF-trimmean. The formula for the initial values of the trimmed mean column is written as Equation 6:

$$Trimmedmean, T = \frac{1}{R} * \sum_{|k|+1}^{n-|k|} X_{ij} \tag{6}$$

where n is the number of observations, k is an integer of the trim proportion with the calculation of $k = n\alpha$ with α the percentages to trim, and R is the denominator of trimmed

mean where $R = n - 2k$. In particular, the algorithm of EOF-based methods to impute the missing values using the different initialisation approach by applying three different initial values, which are column mean, the proposed median and trimmed mean, can be stated as follows in Table 3.

Table 3
Algorithm of EOF-mean, EOF-median and EOF-trimmean methods

<p>Start</p> <p>Step 1: Identify the missing values, x_{miss} in the data matrix \mathbf{X}_M.</p> <p>Step 2: Initial values are filled into missing using the column mean/median/trimmed mean (hours), of the data matrix \mathbf{X} and turned into a new completed matrix \mathbf{X}_M.</p> <p>Step 3: After the initial value replacement, centralised the data matrix \mathbf{X}_M by subtracting the new completed matrix \mathbf{X}_M using the column mean/median/trimmed mean of \mathbf{X}_M.</p> <p>Step 4: Computed a Singular Value Decomposition (SVD) in Equation 2 on the centralised matrix \mathbf{X}_M.</p> <p>a) The loading and scores EOFs \mathbf{U} and \mathbf{V} are extracted from the SVD</p> <p>b) An optimal number of EOFs are selected using cross validation method of GCV formula in Equation 3.</p> <p>The selected EOF loadings and EOF scores are used to make the reconstruction by multiply the loadings and scores and adding the subtracted column mean/median/trimmean to form a new reconstructed data matrix \mathbf{X}_M.</p> <p>Step 5: Replace the missing values, x_{miss} in the data matrix \mathbf{X} by their new estimated value obtained from the reconstructed data matrix \mathbf{X}_M of EOF-mean/ EOF-median/ EOF-trimmean.</p> <p>End</p>
--

The Newly Applied: Regularised Expectation-Maximisation Principal Component Analysis (R-EMPCA) Method. Another application of the EOF-based imputation method proposed in this study to solve the long gap of missingness is the Regularised Expectation Maximisation Principal Component Analysis (R-EMPCA), with the regularised iterative EOF approach that was previously introduced in Josse & Husson (2016). However, this method is not yet explored for solving the long gap missing data problem.

Generally, the regularised iterative EOF is very similar to iterative EOF. Both methods use an iterative approach and are based on the EOF model, extracting the EOF score and loading. This regularised iterative method starts with the initialisation step of the missing values by mean values. Then, an estimation step of the parameters where the appropriate optimal number of EOFs modes is predefined from the temporal covariance matrix. The third step is the imputation step of missing values. The estimation of the mean matrix for the missing values is to be updated after each iteration during the imputation process. Finally, the last step is to reconstruct the new matrix of completed data using the updated or converge mean matrix from the imputation step. The R-EMPCA has extended the normal EOF analysis by replacing the centralisation process by using a weighted least squares criterion as in Equation 7:

$$\mathbf{W}_{n \times p} * (\mathbf{X}_{n \times p} - \hat{\mathbf{X}}) \|_2^2: \text{rank}(\mathbf{r}) \leq \mathbf{S} \tag{7}$$

Then the missing values are imputed in an iterative loop with the fitted matrix with noise variance as Equation 8:

$$\hat{x}_{ij} = \sum_{s=1}^S \left(\sqrt{\lambda_s^\ell} - \frac{(\hat{\sigma}^2)^\ell}{\sqrt{\lambda_s^\ell}} \right) \times u_{is}^\ell v_{js}^\ell, \tag{8}$$

The noise variance estimated as Equation 9:

$$(\hat{\sigma}^2)^\ell = \frac{\| \mathbf{X}^{\ell-1} - \mathbf{U}^\ell \mathbf{D}^\ell (\mathbf{V}^\ell)^* \|^2}{np - n\mathbf{S} - p\mathbf{S} + \mathbf{S}^2}, \tag{9}$$

$\mathbf{1}_{n \times p}$ is a matrix filled with values one. In addition, only the missing values are replaced with estimated values, and the mean matrix is re-centred and updated after each iteration to give the same weight to each variable. Then, the estimation and imputation steps are repeated until the difference between two successive estimated matrices is less than the threshold or the iteration number exceeds the maximum fixed iterations. The algorithm for R-EMPCA is shown in Table 4. Thus, the iteration will make full use of useful information in the process of missing values imputation.

Table 4

Summary of the R-EMPCA algorithm of the EOF based method by applying an iterative approach for filling the missing values

<p>Start</p> <p>Step 1: An optimal number of EOFs are selected using cross validation method of GCV formula in Equation 3</p> <p>Step 2: Identify the missing values, x_{miss} in the data matrix \mathbf{X}.</p> <p>Step 3: Initialisation $\ell = 0$. Initial values are substituted into missing values using the mean of the column (hours), \bar{x}_{mean} of the original data matrix \mathbf{X}.</p> <p>Step 4: The step $\ell \geq 1$ are:</p> <ul style="list-style-type: none"> a) Performing the reconstruction of PCA analysis to estimates EOF scores and loadings using the SVD formula in Equation 2. b) Missing values are imputed with the fitted values with the noise variance estimated. Then, update and replace the missing values in the data matrix \mathbf{X} by their new estimated values from the reconstruction. <p>Step 5: Step at 4(a) of estimation of parameters by SVD and 4(b) the imputation step are repeated until the convergence criterion is fulfilled.</p> <p>Step 6: Replace the missing values, x_{miss} in the data matrix \mathbf{X} with the new estimated value, $\hat{\mathbf{X}}_{R.EMPCA}$ obtained from the final reconstruction of data matrix</p>
--

Performance Evaluation

The performance indicator involved in this study is Root Mean Square Error (RMSE), Mean Absolute Error (MAE), Coefficient of Determination (R-Square) and Agreement

Index (AI) from (Junninen et al., 2004) are considered. The formulas for the performance indicator are given by the following Equations 10-13:

$$RMSE = \sqrt{\frac{\sum_{i=1}^n (x_i - \hat{x}_i)^2}{n}} \quad (10)$$

$$MAE = \frac{\sum_{i=1}^n |x_i - \hat{x}_i|}{n} \quad (11)$$

$$R\text{-Square} = \left[\frac{1}{N} \frac{\sum_{i=1}^n (\hat{x}_i - \bar{\hat{x}}_i)(x_i - \bar{x}_i)}{\sigma_{\hat{y}} \sigma_y} \right]^2 \quad (12)$$

$$AI = 1 - \left[\frac{\sum_{i=1}^n (\hat{x}_i - x_i)^2}{\sum_{i=1}^n (|\hat{x}_i - \bar{\hat{x}}_i| + |x_i - \bar{x}_i|)^2} \right] \quad (13)$$

where \hat{x}_i is the observed value, \hat{x}_i is the imputed value, \bar{x}_i indicates the average of the actual data, and $\bar{\hat{x}}_i$ is the average of the imputed data with σ_y and $\sigma_{\hat{y}}$ are their standard deviations respectively. RMSE and MAE are used to assess the accuracy of the methods by looking at the residuals (i.e. the difference between the imputed and the observed values). At the same time, R-Square measures the imputation methods capability in predicting or estimating missing observation while AI measures the correlation between the imputed and the observed value. The ideal imputation method is the one that gives small error measures; the RMSE and MAE and high R-Square and AI.

RESULTS AND DISCUSSION

This section discusses the performance results of the imputation methods. The imputation methods were applied for the Klang station dataset, and the experiment was conducted for each missing data pattern using all four EOF based imputation methods. The results were then calculated as average results of the 100 simulated datasets for each missing pattern. The following Table 5 and Figure 3 represent the average score of each performance indicator based on error measures, the RMSE and MAE, while Figure 4 shows the performance based on R-Square and AI. The complexity evaluation was conducted according to the performance of the methods with respect to the different patterns of missing values with different levels of % and gap size—from low to higher percentage and from small long gap to larger long gap.

Table 5 indicates the average RMSE, MAE, R-Square and AI values for the four EOF methods computed from 100 artificial data sets for each missing pattern. Overall, the

R-EMPCA method has a very excellent performance indicated by the lowest RMSE and MSE values and the highest R-Square compared to the other three methods; the EOF-mean, EOF-median and the EOF-trimmean. Furthermore, it shows a stronger capability of the R-EMPCA method to estimate the missing values with higher accuracy and higher predictive power for each type of missing pattern except that for pattern P30_G720, whereby all methods are shown to have quite a similar performance for this pattern. Figures 3 and 4 also shows that among the EOF-mean, EOF-median and EOF-trimmean, the proposed EOF-trimmean method having a better performance, which are indicated by lower RMSE and MAE values and higher AI and R-Square values in comparison with EOF-mean and EOF-median methods. Therefore, this study has proven that the R-EMPCA method is the most suitable imputation method for a data set with a long missingness gap.

Noticeably, in this investigation, the value of R-square for R-EMPCA is not more than 0.7 for all the sixteen patterns of missingness. At the same time, the AI is relatively high with 0.78744 for the P05_G12 and become lower as this result depends on the pattern of missingness. It is also observed that there is a reduction in the performance of the methods when the proportion of missingness increases as the gap size increases. These findings are supported by Junger and Ponce de Leon (2015), who mentioned that the performance of the estimated value would be decreased when the missing values and the gap size increase in the data set. Even though the R-EMPCA method is found the best in terms of performance, it is believed that R-Square and the AI values recorded are due to the performance's ability when the methods experimented within the condition of long gap missingness situation. The results would be much better when the method is applied for a not so complex missing data set (i.e. data set with a small percentage and short gap sequence of missingness).

EOF-mean was the worst identified imputation method among the EOF-based imputation methods, while the proposed EOF-median has moderate performance. The following Figures 5-7 provide the analysis of the consistency of the results.

Table 5
Performances of four methods of imputation according to missing data pattern

Patters	Performance Indicators	Klang Station			
		EOF-mean	EOF-median	EOF-trimmean	R-EMPCA
P05_G12	RMSE	38.11721	38.97415	38.70757	25.95430
	MAE	23.87387	22.07330	22.07434	11.46257
	R-Square	0.00835	0.00831	0.00904	0.59141
	AI	0.15670	0.23467	0.21502	0.78744
P05_G24	RMSE	38.17311	38.95518	38.68937	31.85556
	MAE	24.51937	22.82607	22.82319	17.80248
	R-Square	0.00359	0.00334	0.00383	0.33962
	AI	0.20054	0.23440	0.21749	0.61509
P05_G168	RMSE	35.96443	35.55519	35.37376	35.07408

Table 5 (continue)

Patters	Performance Indicators	Klang Station				
		EOF-mean	EOF-median	EOF-trimmean	R-EMPCA	
	MAE	25.80377	24.20227	24.17143	24.81692	
	R-Square	0.00033	0.00037	0.00050	0.05371	
	AI	0.32522	0.30319	0.29982	0.39352	
P05_G720	RMSE	35.92638	35.08161	34.91106	35.77932	
	MAE	27.10393	25.70282	25.60557	26.94752	
	R-Square	0.00038	0.00012	0.00023	0.01623	
	AI	0.31892	0.33314	0.32900	0.33561	
	P10_G12	RMSE	39.01976	40.12672	39.85329	27.39822
		MAE	24.05786	22.29393	22.29608	12.15135
R-Square		0.01373	0.01258	0.01378	0.55831	
	AI	0.13102	0.23574	0.21656	0.77262	
	P10_G24	RMSE	39.29177	40.49170	40.19496	33.11227
		MAE	24.74710	23.15876	23.14616	18.23082
R-Square		0.00616	0.00505	0.00567	0.32431	
	AI	0.14871	0.24123	0.22060	0.59886	
	P10_G168	RMSE	37.30235	37.02084	36.84009	36.42588
		MAE	25.52515	23.44938	23.47681	24.51017
R-Square		0.00049	0.00043	0.00077	0.05335	
	AI	0.27288	0.24343	0.23635	0.34863	
	P10_G720	RMSE	34.89105	34.16551	33.98925	34.73723
		MAE	24.72334	23.01038	22.95128	24.55034
R-Square		0.00014	0.00007	0.00017	0.01111	
	AI	0.31434	0.29831	0.29199	0.33000	
	P20_G12	RMSE	41.37989	42.57698	42.29561	31.44141
		MAE	24.34981	22.69193	22.68838	13.96214
R-Square		0.02221	0.02054	0.02184	0.46850	
	AI	0.13507	0.24032	0.22357	0.71544	
	P20_G24	RMSE	41.47086	42.63278	42.35331	35.52967
		MAE	24.96108	23.25652	23.25844	18.62116
R-Square		0.00953	0.00754	0.00844	0.29630	
	AI	0.12609	0.22980	0.21189	0.56698	
	P20_G168	RMSE	39.36883	39.98125	39.72529	38.47219
		MAE	25.08108	23.43837	23.41567	24.09854
R-Square		0.00049	0.00042	0.00060	0.05056	
	AI	0.19992	0.24278	0.22545	0.28785	
	P20_G720	RMSE	37.01653	36.37736	36.20709	36.84366
		MAE	24.82146	22.53450	22.54400	24.62451
R-Square		0.00014	0.00005	0.00018	0.00971	

Table 5 (continue)

Patters	Performance Indicators	Klang Station			
		EOF-mean	EOF-median	EOF-trimmean	R-EMPCA
P30_G12	AI	0.27432	0.26486	0.25474	0.29133
	RMSE	40.66486	41.86543	41.58401	31.40857
	MAE	24.02346	22.40867	22.40350	14.25771
	R-Square	0.03081	0.02896	0.03038	0.44710
P30_G24	AI	0.14768	0.25175	0.23628	0.70575
	RMSE	41.52809	42.65726	42.37999	36.08452
	MAE	24.76144	23.02723	23.03267	18.84405
	R-Square	0.01278	0.01076	0.01168	0.27366
P30_G168	AI	0.11905	0.22828	0.20970	0.54812
	RMSE	40.38344	40.76528	40.54024	39.51843
	MAE	25.45146	23.41158	23.43521	24.44615
	R-Square	0.00070	0.00044	0.00078	0.04593
P30_G720	AI	0.19293	0.20585	0.19629	0.27885
	RMSE	40.96781	41.25684	41.00958	40.79544
	MAE	26.15329	24.69441	24.62649	25.94850
	R-Square	0.00012	0.00005	0.00015	0.01002
	AI	0.24747	0.26452	0.25627	0.26770

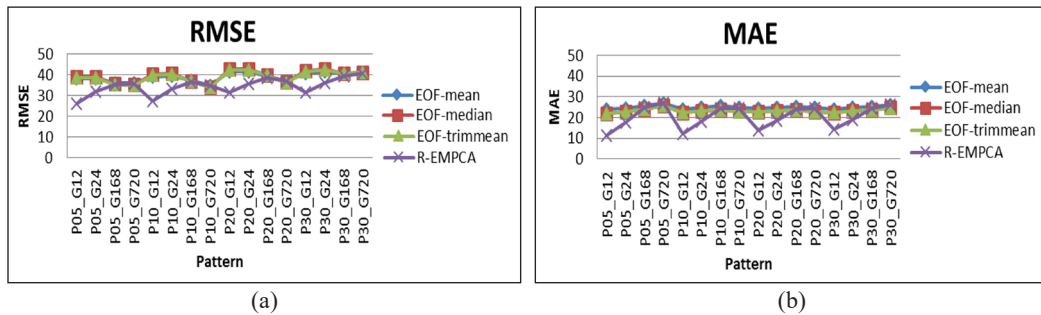


Figure 3. Imputation methods performance based on average error measures: (a) RMSE; and (b) MAE

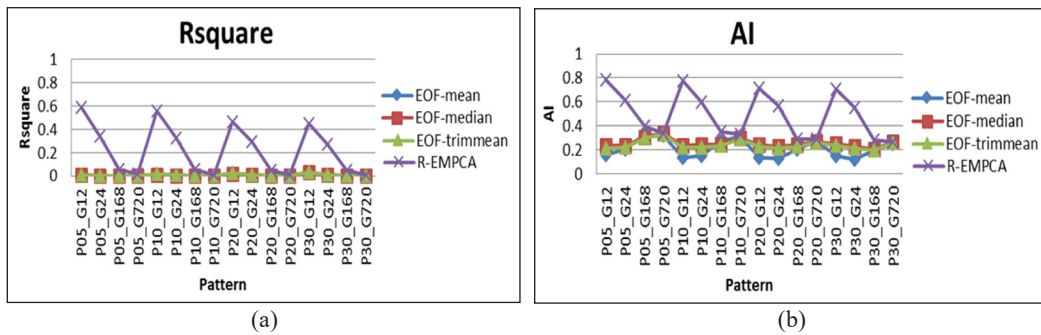


Figure 4. Imputation methods performance based on correlational measures: (a) R-Square; and (b) AI

As depicted in Figure 5, the distribution of RMSE for each method shows an increasing pattern when the proportion and the gap size increase. Among the four methods, R-EMPCA clearly shows the lowest RMSE median for the data set with gap sizes 12 and 24 at levels of missing percentage (5, 10, 20, and 30). However, for the data set with a larger gap size, 168 and 720, R-EMPCA has shown a slight reduction in the performance indicated by a slight increase in RMSE score. The RMSE distribution also has a consistently decreasing performance pattern for EOF-mean, EOF-median and EOF-trimmean methods when the gap size increases. Figure 5 also shows that the distribution pattern of RMSE for all methods are similar for the largest missing gap size with 720 consecutive missing points (i.e. within a month duration of missingness).

In contrast, R-EMPCA keeps a better performance at different percentages of missingness and gap sizes of missingness when the RMSE produce the lowest error amongst other methods. It can be seen from the boxplots that EOF-mean, EOF-median and EOF-trimmean at all levels of missingness patterns have quite a similar pattern of boxplot where the lower and the upper whisker show a similar range. In addition, EOF-trimmean shows a lower median and variance compared to the EOF-mean and EOF-median. On the other hand, the median of EOF-mean shows slightly higher compared to the EOF-median and EOF-trimmean. Therefore, EOF-trimmean outperforms the EOF-median in estimating missing values for long gap missingness, whereas EOF-mean demonstrates the worst performances.

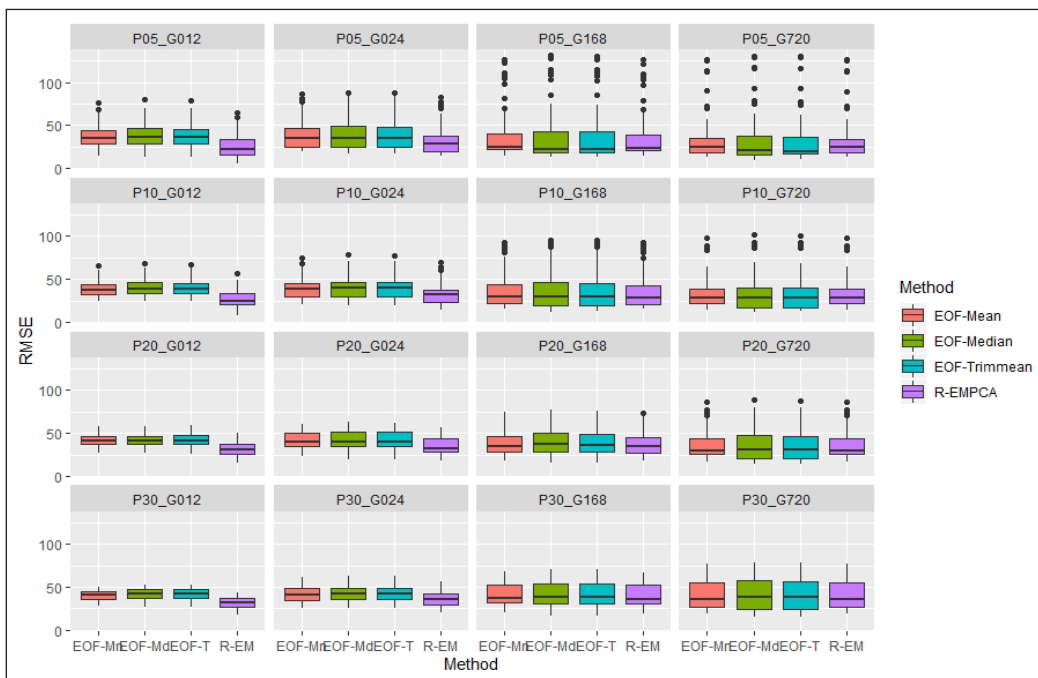


Figure 5. Box plot on RMSE distribution

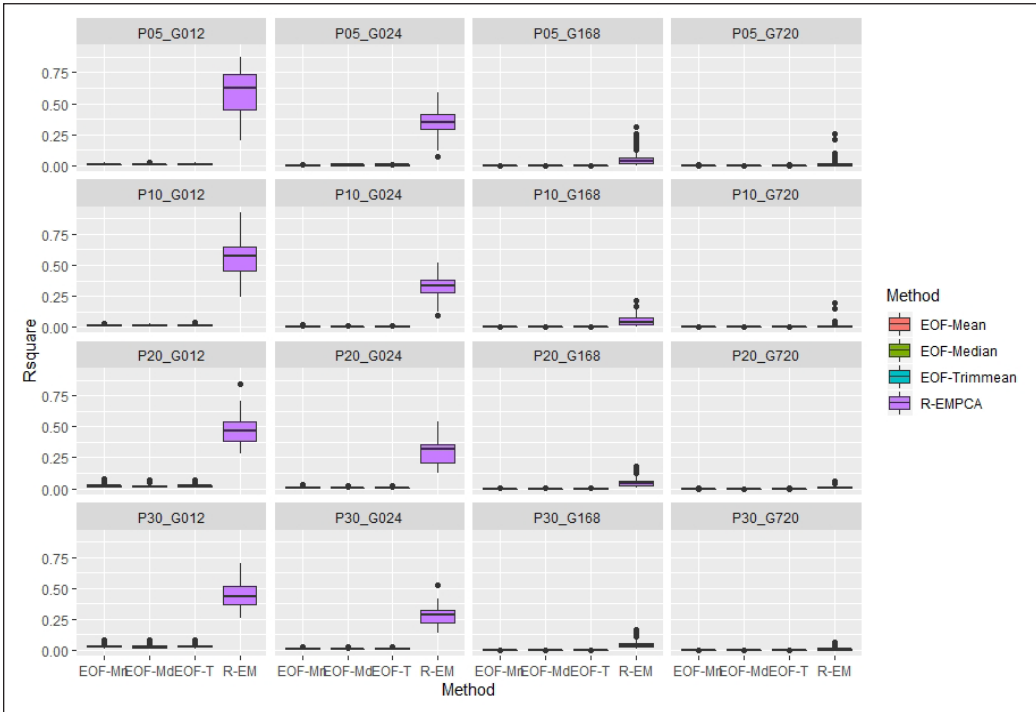


Figure 6. Box plot on R-Square distribution

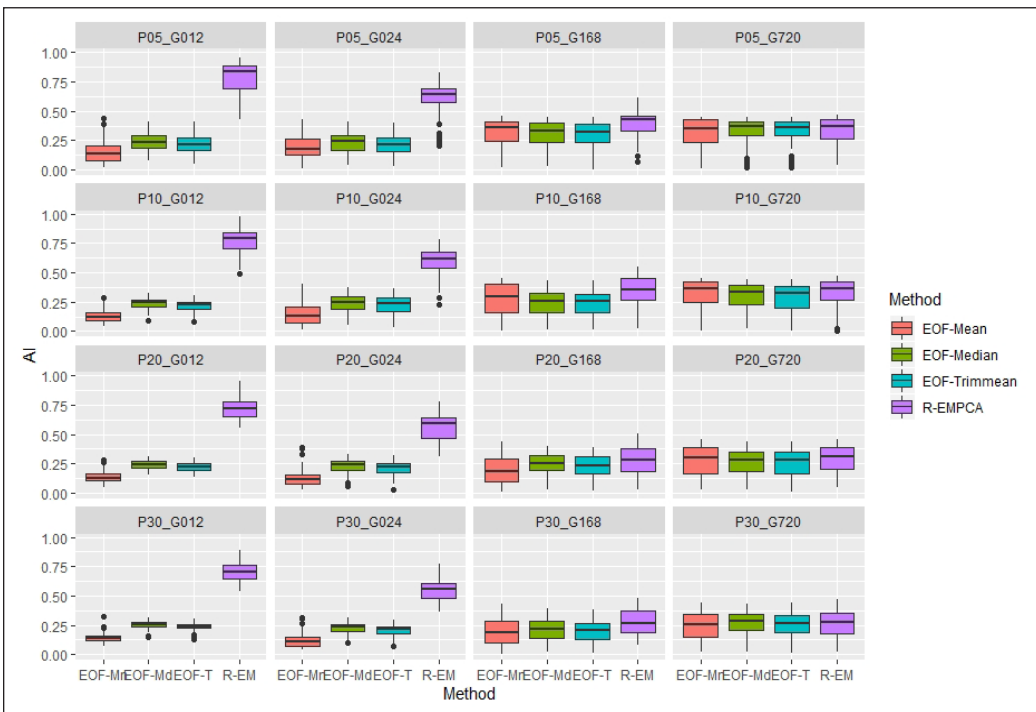


Figure 7. Box plot on AI distribution

The summary of the boxplot of R-Square score distribution for four EOF based imputation methods is shown in Figure 6. A higher value of R-Square that close to 1 indicates that the estimated values were almost close to the observed values, the boxplot of R-Square showed that R-EMPCA outperforms EOF-mean, EOF-median and EOF-trimmean with the highest value of R-Square for all the patterns of missingness from 12 gaps to 720 gaps of missingness. This plot directly explained that R-EMPCA has a good performance in terms of accuracy measure of R-Square for the generated long gap of missing data. However, the other three EOF-mean, EOF-median and EOF-trimmean, show a very short and thin boxplot, indicates that these three methods have a very low median and variance below that 0.01.

The pattern is also similar for AI score distribution. As shown in Figure 7, R-EMPCA possessed a very excellent AI score (high score) for missing data set with 12 and 168 gap sizes. However, the performance gradually decreased as gap size increase at all levels of missing percentage. Among the EOF-mean, EOF-median and EOF-trimmean, the EOF-mean has the lowest AI median for gap size 12 and 168 but having equal performance with EOF-median and EOF-trimmean when gap size increase to 168 and 720, indicated by quite similar median values. The results shown in Figures 5 to 7 have provided evidence and justification for the consistency of the imputation results obtained to validate and support the findings as summarised from Figures 3 and 4. These results indicate that R-EMPCA has consistent results as the best imputation method. EOF-trimmean is the second-best imputation method for the long gap missingness problem in the air quality dataset in Klang station.

CONCLUSION

In this study, four EOF-based imputation methods, which are EOF-mean, EOF-median, EOF-trimmean and R-EMPCA, were used and compared for the treatment of long gap missing values problem for a Single-Site Temporal Time-Dependent (SSTTD) type of multivariate air quality (PM10) data using real data set of Klang air quality monitoring station. The results have found that R-EMPCA outperformed the other EOF based methods, including the existing method, EOF-mean and the two proposed methods, EOF-median and EOF-trimmean, in some long gap sizes. The performance of R-EMPCA has proven its superiority as the method having the best result for not so large missing gap but gradually decrease and become at par with the other methods for enormous gap size; such as for one month (720 hourly consecutive missing points). However, the results also lead to a conclusion that the proposed EOF-median and EOF-trimmean give better performance as compared to the existing EOF-mean based method. Overall, the R-EMPCA provides a realistic and promising way to handle the long gap missingness presented in multivariate hourly air quality (PM10) of SSTTD data sets. To conclude, the use of various applications

on the imputation techniques based on the characteristics of the air quality dataset is recommended. A more general comparison of this method with many other different methodologies such as smoothing techniques or functional data analysis approach will be conducted in the future to evaluate further the performance and accuracy of the R-EMPCA method in handling long gaps of missingness. The data set was used generally in the experimentation without considering the seasonal influence on the imputed values. However, for the application in practice, it is suggested to apply the method according to season.

ACKNOWLEDGEMENTS

The authors gratefully acknowledge the Department of Environment Malaysia (DOE) for providing the information and data.

REFERENCES

- Bai, K., Li, K., Guo, J., Yang, Y., & Chang, N. B. (2020). Filling the gaps of in situ hourly PM_{2.5} concentration data with the aid of empirical orthogonal function analysis constrained by diurnal cycles. *Atmospheric Measurement Techniques*, 13(3), 1213-1226. <https://doi.org/10.5194/amt-13-1213-2020>
- Bartzokas, A., Darula, S., Kambezidis, H. D., & Kittler, R. (2003). Sky luminance distribution in Central Europe and the Mediterranean area during the winter period. *Journal of Atmospheric and Solar-Terrestrial Physics*, 65(1), 113-119. [https://doi.org/10.1016/S1364-6826\(02\)00283-3](https://doi.org/10.1016/S1364-6826(02)00283-3)
- Beckers, J. M., & Rixen, M. (2003). EOF calculations and data filling from incomplete oceanographic datasets. *Journal of Atmospheric and Oceanic Technology*, 20(12), 1839-1856. [https://doi.org/10.1175/1520-0426\(2003\)020<1839:ECADFF>2.0.CO;2](https://doi.org/10.1175/1520-0426(2003)020<1839:ECADFF>2.0.CO;2)
- Di Salvo, F., Plaia, A., Ruggieri, M., & Agro, G. (2016). Empirical orthogonal function and functional data analysis procedures to impute long gaps in environmental data. In *Studies in Theoretical and Applied Statistics, Selected Papers of the Statistical Societies* (pp. 3-13). Springer. https://doi.org/10.1007/978-3-319-27274-0_1
- Ghazali, S. M., Shaadan, N., & Idrus, Z. (2020). Missing data exploration in air quality data set using R-package data visualisation tools. *Bulletin of Electrical Engineering and Informatics*, 9(2), 755-763. <https://doi.org/10.11591/eei.v9i2.2088>
- Hannachi, A., Jolliffe, I. T., & Stephenson, D. B. (2007). Empirical orthogonal functions and related techniques in atmospheric science: A review. *International Journal of Climatology: A Journal of the Royal Meteorological Society*, 27(9), 1119-1152. <https://doi.org/10.1002/joc.1499>
- Josse, J., & Husson, F. (2016). missMDA: A package for handling missing values in multivariate data analysis. *Journal of Statistical Software*, 70(1), 1-31. <https://doi.org/10.18637/jss.v070.i01>
- Junger, W. L., & Ponce de Leon, A. (2015). Imputation of missing data in time series for air pollutants. *Atmospheric Environment*, 102, 96-104. <https://doi.org/10.1016/j.atmosenv.2014.11.049>

- Junninen, H., Niska, H., Tuppurainen, K., Ruuskanen, J., & Kolehmainen, M. (2004). Methods for imputation of missing values in air quality data sets. *Atmospheric Environment*, 38(18), 2895-2907. <https://doi.org/10.1016/j.atmosenv.2004.02.026>
- Malaysia Environmental Quality Report. (2013). *Air Quality*. Department of Environment Malaysia.
- Plaia, A., & Bondi, A. L. (2006). Imputation of missing values in air quality data sets. In *XLIII Riunione Scientifica Della Società Italiana Di Statistica* (pp. 667-670). CLEUP Publishing.
- Ruggieri, M., Plaia, A., Di Salvo, F., & Agró, G. (2013). Functional principal component analysis for the explorative analysis of multisite-multivariate air pollution time series with long gaps. *Journal of Applied Statistics*, 40(4), 795-807. <https://doi.org/10.1080/02664763.2012.754852>
- Ruggieri, M., Di Salvo, F., Plaia, A., & Agró, G. (2010). EOFs for gap filling in multivariate air quality data: a FDA approach. In *Compstat 2010* (pp. 1557-1564). Physica-Verlag.
- Shaadan, N., Deni, S. M., & Jemain, A. A. (2015). Application of functional data analysis for the treatment of missing air quality data. *Sains Malaysiana*, 44(10), 1531-1540. <https://doi.org/10.17576/jsm-2015-4410-19>
- Shaadan, N., & Rahim, N. A. (2019). Imputation analysis for time series air quality (PM10) data set: A comparison of several methods. In *Journal of Physics: Conference Series* (Vol. 1366, No. 1, p. 012107). IOP Publishing. <https://doi.org/10.1088/1742-6596/1366/1/012107>
- Sorjamaa, A., Lendasse, A., Cornet, Y., & Deleersnijder, E. (2010). An improved methodology for filling missing values in spatiotemporal climate data set. *Computational Geosciences*, 14(1), 55-64. <https://doi.org/10.1007/s10596-009-9132-3>



Synthesis, Characterisation, and Density Functional Theory Study of Encapsulated Bioactive Components of Ginger

Triati Dewi Kencana Wungu^{1,2*}, Damar Rastri Adhika^{2,3}, Meqorry Yusfi^{2,4}, Atsarina Larasati Anindya², Eduardus Bimo Aksono⁵, Raden Roro Fosa Sarassina⁶, Christofora Hanny Wijaya⁷ and Suprijadi^{2,4}

¹Department of Physics, Nuclear Physics and Biophysics Research Group, Faculty of Mathematics and Natural Sciences, Institut Teknologi Bandung, Jl. Ganesa 10 Bandung 40132, Indonesia

²Research Center for Nanosciences and Nanotechnology, Institut Teknologi Bandung, Jl. Ganesa 10 Bandung 40132, Indonesia

³Department of Engineering Physics, Advanced Material Research Group, Faculty of Industrial Technology, Institut Teknologi Bandung, Jl. Ganesa 10 Bandung 40132, Indonesia

⁴Department of Physics, Instrumentation and Computational Physics Research Groups, Faculty of Mathematics and Natural Sciences, Institut Teknologi Bandung, Jl. Ganesa 10 Bandung 40132, Indonesia

⁵Faculty of Veterinary, Universitas Airlangga, C Campus, Jl. Mulyorejo Surabaya, 60115 Indonesia

⁶Diploma Program of Economics and Business, Universitas Gadjah Mada, Yogyakarta, Indonesia

⁷Department of Food Science and Technology, Bogor Agricultural University, Bogor, Indonesia

ABSTRACT

In this paper, we encapsulated ginger bioactive components in maltodextrin nanocapsules. Ginger nanocapsules were characterised using Transmission Electron Microscope (TEM) and Particle Size Analyser (PSA). The results show that the nanoparticles have a generally globular shape with particle size under 200 nm. In addition, the simulation of gingerol and dextran, as a representative for maltodextrin, was also investigated using Density Functional Theory (DFT) calculation. From the DFT calculation, gingerol exhibited a physisorption

interaction with dextran by forming hydrogen bonds. Furthermore, the density of state analysis shows that the gingerol-dextran system has a conductive-like behaviour that promotes the nanocapsules' cell uptake.

Keywords: DFT, encapsulation, ginger, gingerol, TEM

ARTICLE INFO

Article history:

Received: 17 April 2021

Accepted: 05 July 2021

Published: 08 October 2021

DOI: <https://doi.org/10.47836/pjst.29.4.22>

E-mail addresses:

triatidewi@fi.itb.ac.id; triati6579@gmail.com

(Triati Dewi Kencana Wungu)

damar@tf.itb.ac.id (Damar Rastri Adhika)

MEQORRYUSFI@sci.unand.ac.id (Meqorry Yusfi)

ATSARINALARASATIANDINDYA@gmail.com

(Atsarina Larasati Anindya)

EDUARDUS-B-A-H@fkh.unair.ac.id (Eduardus Bimo Aksono)

FOSA.SARASSINA@ugm.ac.id (Raden Roro Fosa Sarassina)

CHANNYWIJAYA@apps.ipb.ac.id (Christofora Hanny Wijaya)

supri@fi.itb.ac.id (Suprijadi)

* Corresponding author

INTRODUCTION

Ginger (*Zingiber officinale* Roscoe) has been widely used for beverages, food, and medicine since ancient times due to its

health benefits (White, 2007). Ginger is ubiquitously grown in Indonesia due to the suitable climate for ginger cultivation; therefore, ginger-based products are widely popular among Indonesians, particularly those who seek to use it for medicinal purposes. Traditionally, people process ginger by boiling the roots in water to get the extract as herbal drink or using ginger roots directly in foods as a spice. However, these traditional processing methods need a large amount of ginger to produce the desired benefit, not to mention the short durability of the processed product. It is, therefore, necessary to seek new methods for ginger processing to enable its effective utilisation.

Bioactive compounds of ginger include hydrophobic phenolic compounds (gingerol, shogaol, gingerdiol, and gingerdione) and hydrophilic polysaccharides (Kou et al., 2018). Gingerol has many pharmacological benefits such as antioxidant, anticancer, anti-inflammation, analgesic, and antipyretic (Shahrajabian et al., 2019). The main challenge to utilize hydrophobic compounds such as gingerol in the pharmaceuticals and the food industry is the low bioavailability and sustainability of these hydrophobic compounds that can be overcome by using the nanoencapsulation technique. Nanoencapsulation is one of the most recent techniques that can be an excellent strategy to protect hydrophobic compounds against unsuitable environments and processing conditions such as light, high temperature, and humidity. In addition, the Nanoencapsulation technique could also enhance the bioavailability of hydrophobic compounds such as controlled release, improvement in water solubility, and increase in antioxidant activity (Rezaei et al., 2019).

In practice, nanoencapsulation involves incorporating of ingredients, bioactive compounds, or other desired materials into the encapsulated material for the delivery of the contents at the appropriate time (King, 1995). On the other hand, encapsulation is a process to entrap active agent within another wall material to improve the quality of foods by protecting micronutrients through processing and storage until the foods are consumed (Ghayour et al., 2019; Ahmad et al., 2019; İnanç Horuz & Belibağlı, 2018). The wall material used for coating or encapsulating ginger bioactive compounds must be food-grade, biodegradable, and form a barrier between the internal phase and its surroundings (Nedovic et al., 2011). It may be made from sugars, proteins, gums, and natural and modified polysaccharides, but polysaccharides are the most widely used.

Since previous studies of encapsulation technique show the stability of functional food components and toxicity reduction (Suganya & Anuradha, 2017), nano-encapsulated ginger bioactive compounds could theoretically exhibit faster gastrointestinal absorption compared to the traditionally processed ginger, as well as a slower degradation without compromising its unique taste and flavour (Lakshmi et al., 2012). Therefore in this study, a maltodextrin-based nanoencapsulation method of ginger bioactive compounds was performed to synthesise ginger nanocapsules used in a food product. Synthesised nanocapsules were then characterised using Particle Size Analyser (PSA) and Transmission Electron Microscope (TEM) to clarify the shape and size of the nanoparticle.

To understand the encapsulation process of nano-encapsulated ginger bioactive compounds, theoretical methods from an atomistic scale point of view can help describe the interaction within the system (Setzer, 2010; Khayer & Haque, 2020; Michailidou et al., 2020). Thus, to seek the physical-chemical properties and the electronic properties and elucidation of interaction between ginger bioactive compounds and nanocapsule wall, we performed a computational analysis based on a quantum-mechanical description of the electron-core interaction using the Density Functional Theory (DFT) method. It has been predicted that DFT could offer to solve advanced quantum chemistry and material science problems.

MATERIALS AND METHODS

Materials

n-hexane (CAS-No:110-54-3) and Tween 80 (CAS-No:9005-65-6) were obtained from Merck KGaA (Germany). Maltodextrin was obtained from a local commercial market. Both reagents, *n*-hexane and Tween 80, used without purification because it is already in the pro-analysis grade category. While for maltodextrin, there is no purification to maintain the low production cost, especially for mass-scale production.

Nanoencapsulation of Ginger Bioactive Components

Fresh ginger was washed, cut, and dried at 60°C for 24 hours. The dried ginger was soaked in *n*-hexane for 24 hours to extract the bioactive compounds, which were put in a rotary evaporator at 70°C and 150 rpm to eliminate the solvent. The evaporated extract was then prepared to create nanocapsules with maltodextrin as the capsule material. The first step of nanoencapsulation was preparing oil-in-water nanoemulsion based on the method described by Silva et al. (2011) and Jaganathan and Kumar (2017) with slight modifications described as follows. First, an organic solution of 0.3% (w/w) extract was dissolved in *n*-hexane at 40°C. Then, an aqueous solution of 0.5% (w/w) Tween 80 in the distilled water was prepared. The organic solution was then added to the aqueous solution with the volume ratio of 1:6 and homogenised by ultrasonication at 20 kHz to create the oil-in-water nanoemulsion. Next, the *n*-hexane was removed from the nanoemulsion using a rotary evaporator at 70°C and 150 rpm. The next step was to create a separate maltodextrin solution by adding 2% maltodextrin and 0.5% Tween 80 to 100 ml distilled water. Finally, the maltodextrin solution was added dropwise to oil-in-water nanoemulsion under constant stirring at 2000 rpm for 3 hours. The final ginger nanocapsule dispersion was stored at 4°C before being characterised.

Nanocapsule Characterisation

PSA. The ginger nanocapsule dispersion was diluted in distilled water until it reached 0.1% to 1% (w/w) concentration and homogenised with ultrasonication at 20 kHz for 2 min. Then, the dispersion was placed in a disposable plastic cuvette, and PSA measurements were done with Horiba SZ-100 Particle Size Analyser. The settings used for the measurements were as follows: water as the dispersion medium, measurement temperature 25°C, three measurement repeats, and monodisperse and narrow size range for the calculations.

Morphological Analysis using TEM. TEM Hitachi HT7700 at the Research Center for Nanoscience and Nanotechnology, Bandung Institute of Technology, was used for morphological observation of ginger nanocapsules. The operational voltage was set to 100 kV with the magnification of 40,000 times. The diluted nanocapsule dispersion used for PSA characterisation was further thinned by distilled water and then sonicated for about 5 min to prevent the agglomeration of nanocapsules. After that, 2-3 drops from the thinned dispersion were dropped onto a carbon-coated TEM copper grid. The nanocapsules were observed with TEM after the n-hexane was evaporated from the TEM grid.

Model and Computational Analysis on the Nanocapsule System

Gingerol was reported as the main bioactive compound in ginger roots and had antioxidant, analgesic, anti-inflammatory, and antipyretic properties (Kundu & Surh, 2009; Ippoushi et al., 2003; Koo et al., 2001; Suekawa et al., 1984). Therefore, the model used in our calculation was limited to gingerol ($C_{17}H_{26}O$) as the representative bioactive compound and dextran ($H(C_6H_{10}O_5)_3OH$) as the encapsulation material. Aside from maltodextrin, the use of dextran was also considered in the calculation. All calculations were performed using the density functional theory (DFT) with plane-wave basis set as implemented in the Vienna Ab-initio Simulation Package (VASP) (Kresse & Furthmüller, 1996a; Kresse & Furthmüller, 1996b). The projector augmented wave (PAW) method was used, and the generalised gradient approximation (GGA) within the Perdew-Burke-Ernzerhof (PBE) functional was applied for the exchange-correlation energy (Blöchl, 1994; Perdew et al., 1996). The energy cutoff used was 520 eV, and the Brillouin zone was sampled using $3 \times 3 \times 3$ k-points of Monkhorst-Pack grids (Monkhorst & Pack, 1976). In this work, optimisation was done for gingerol alone and dextran alone. We designed a gingerol-dextran system after the optimisation was done by combining gingerol and dextran in an extensive vacuum system, as shown in Figure 1. Then, a full relaxation calculation was done to get the optimised gingerol-dextran system.

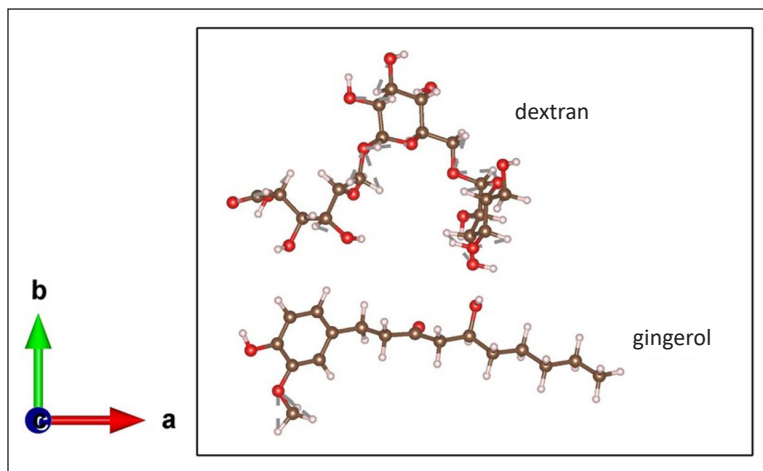


Figure 1. (Color online). The initial structure of the gingerol-dextran system

The binding energy of dextran on gingerol, E_b , was determined using Equation 1:

$$E_b = E_{(\text{gingerol-dextran})} - [E_{(\text{gingerol})} + E_{(\text{dextran})}] \quad [1]$$

where $E_{(\text{gingerol-dextran})}$ is the total energy of gingerol-dextran system, $E_{(\text{gingerol})}$ is the total energy of isolated gingerol, and $E_{(\text{dextran})}$ is the total energy of isolated dextran.

RESULT AND DISCUSSION

Nanocapsule Characterisation

Size distribution and homogeneity particle characterisation were done with a PSA and transmission electron microscopy (TEM to determine the nanocapsules' shape). PSA was employed to determine the average particle size and overall size distribution of the nanocapsules. This method can provide a more extensive statistical sampling size than electron microscopy observation and therefore, is useful for quantitative judgments.

The particle size distribution profile (Figure 2) shows that most of the nanocapsules (39.518 %) are in the 50-100 nm range. 1.11% of the nanocapsules were observed at the smallest measurement size range of 0 to 49 nm, and 0.059% of the nanocapsules were observed at the biggest measurement size range of 551 to 600 nm. Overall, the nanocapsules were measured in all size ranges in varying degrees of frequency, which means the nanocapsules are possibly not homogenous. It could be caused by inadequate optimisation of the ultrasonication process, which produced a non-uniform droplet size of the ginger extract before being encapsulated by maltodextrin. However, we cannot discount the possibility that some nanocapsules measured at the more extensive size ranges were aggregates. However, the percentage of the nanocapsules measured under the size of 200

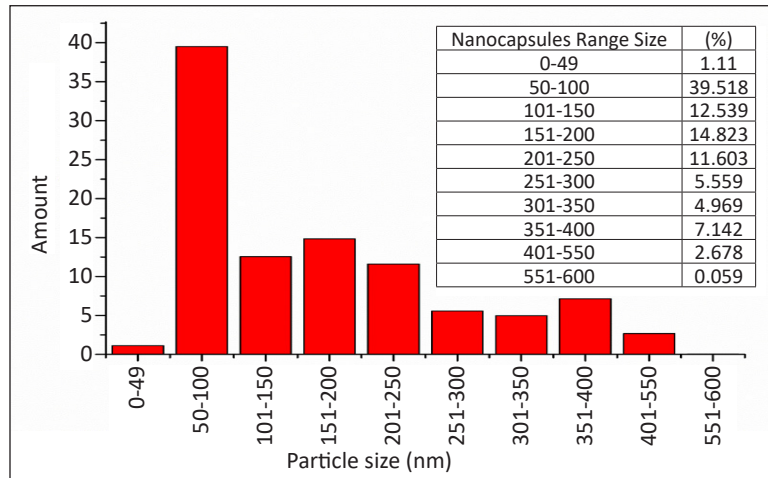


Figure 2. Distribution of nanocapsule size

nm was 67.99%, which means the encapsulation was successfully performed in the nanoscale range.

Polydispersity Index (PI) of nanocapsules solution was measured at 0.347, showing that the particle size on the solution has a good size distribution. PI values range from 0 to 1, where the PI value < 0.1 shows a very homogeneous particle size. Materials intended for general purposes require PI values of 0.3 and 0.5 (Shah et al., 2014). The PI value of 0.347 in this study shows that the ginger nanocapsule particle size distribution is already acceptable for the intended purpose as food products.

As PSA only measures the diameter of the nanocapsules, there was also the possibility that the synthesised nanocapsules were not globular in shape, which made the size measurement varied. Therefore, qualitative analysis by TEM was employed to see the shape of the nanocapsule, to ensure the encapsulation of the ginger bioactive compounds inside the maltodextrin walls, and, to a lesser degree, confirming the size of the nanocapsules measured by PSA.

TEM results in Figure 3 show that the nanocapsules have a perfectly globular shape. The dark area located at the centre of the nanocapsule indicates the bioactive component at the core of the nanocapsules. The dark circle surrounding the outer surface of the nanocapsule

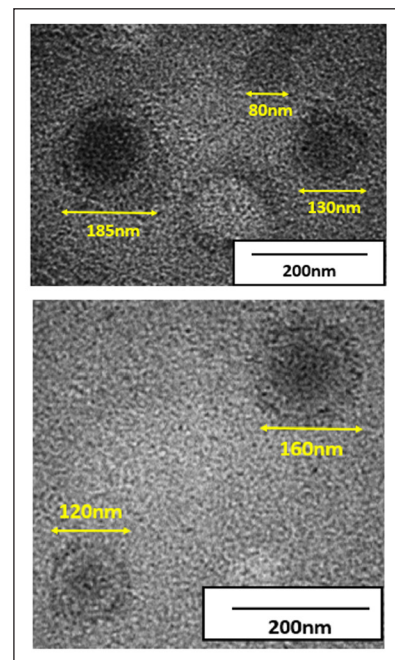


Figure 3. The TEM results showing nanocapsules

is composed of maltodextrin, which acts as a shell material for the nanocapsules. The observed nanocapsule size was small enough to categorise the nanocapsules as nano-scaled particles, even though TEM observation also shows slight varieties on nanocapsule size.

Computational Result

Geometry. The DFT studies confirmed the interaction between dextran and gingerol, wherein the binding energy of dextran on gingerol is -0.34 eV. The initial and optimised structures of gingerol-dextran are shown in Figures 4 and 5. It was observed that the interaction between dextran and gingerol occurred via the rotation of the hydroxyl moiety

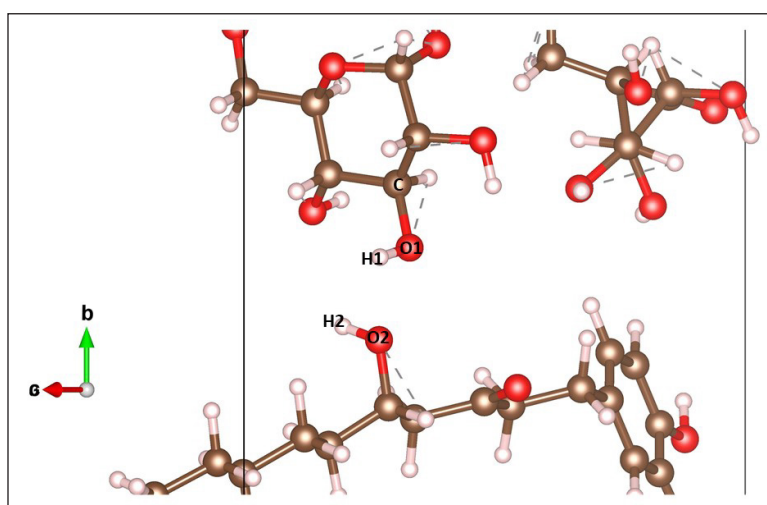


Figure 4. (Colour online). The initial structure of the gingerol-dextran system. For clarity, some atoms are not involved in both dextran and gingerol

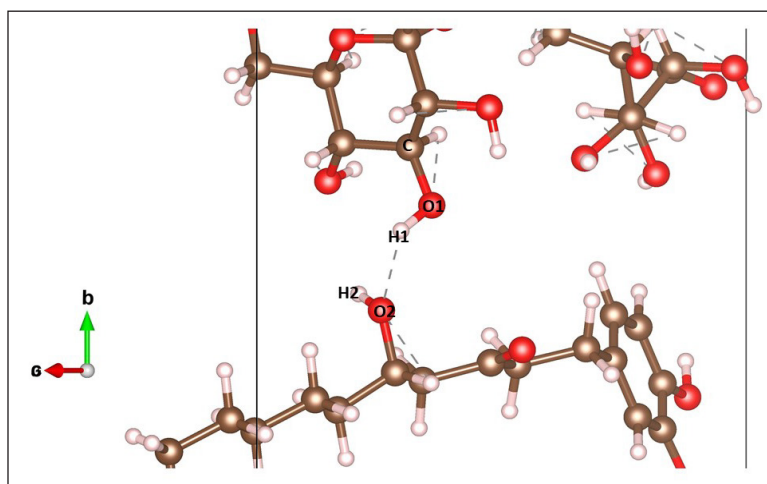


Figure 5. (Colour online). The optimised structure of the gingerol-dextran system. For clarity, some atoms are not involved in both dextran and gingerol

from dextran (O_1H_1) towards the oxygen moiety from gingerol (O_2). This rotation was due to Coulombic repulsive interaction between a dextran (H_1) and a hydrogen atom from gingerol (H_2) hydrogen atom. As listed in Table 1, the O_1H_1 rotation increased the $C-O_1-H_1$ angle by 5.94° , and this caused the H_1 to approach the oxygen moiety from gingerol and form a hydrogen bond with a length of 2.01 \AA . This hydrogen bond is considered physisorption because of its relatively large distance. Table 1 also shows that the H_1-O_2 bond length was shortened by 0.1 \AA , indicating the initiation of the encapsulation process. As the encapsulation was formed by physisorption, it should be theoretically accessible for the nanocapsules to be dissolved after consumption.

Table 1
The O-H, H-H, O-O bond lengths and C-O-H angle before and after dextran bind to gingerol

	O_1-O_2 (Å)	H_1-H_2 (Å)	H_1-O_2 (Å)	$C-O_1-H_1$ (deg)
Before	2.10	2.39	2.11	107.82
After	2.60	2.33	2.01	113.76

Density of States. The density of states analysis was employed to study the electronic structure of the gingerol-dextran system. Figure 6 shows the density of states (DOS) of isolated gingerol, isolated dextran, and gingerol-dextran systems. The DOS intensity near the Fermi level for isolated gingerol and isolated dextran is much higher than in the gingerol-dextran system. Furthermore, the peak height decreased when dextran and gingerol were bound together—from Figure 6, isolated gingerol, isolated dextran, and bound gingerol-dextran show conductive-like behaviours as shown by the density of states crossing the Fermi level.

In biological environments, conductivity is especially relevant to cell membrane permeability. It is because conductivity depends on the particle surface charge, which is one of the major variables determining particle uptake into the cells, particularly in human cells.

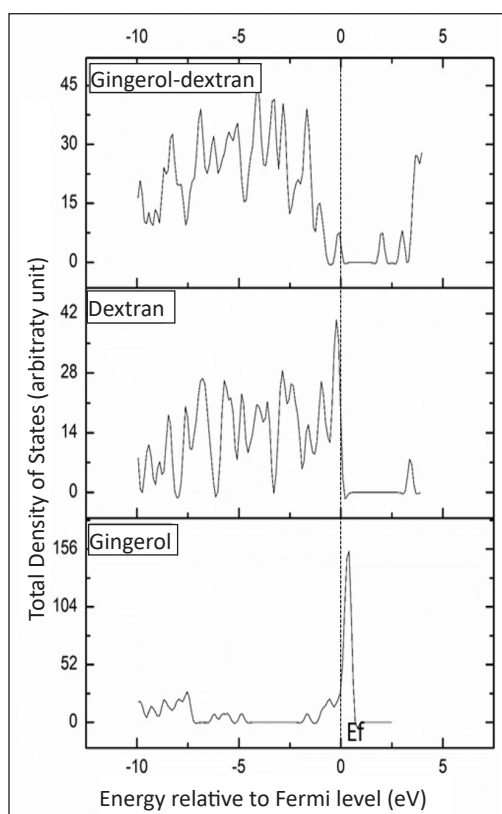


Figure 6. The total density of states of gingerol, dextran, and gingerol-dextran. The Fermi level is set to zero axes.

Nanoparticle Surface Charge and Cell Uptake

Nanoparticle uptake into cells is affected by several factors, including shape, size, and surface charge. The outer structure of animal cells consists of a phospholipid bilayer barrier and transmembrane proteins, which regulate whether the particle may be imported inside or exported outside the cell. The DFT calculation result, particularly from the density of states, shows that the interaction within the nanoparticle (between the dextran and gingerol) exhibits conductive-like behaviour, assuming that changing ions in molecules will affect the electronic structure of the nanoparticle and thus the cell uptake. A previous computational model shows that the negative charge of the phospholipid bilayer is relatively stable at a specific location due to the depth of the potential wells where the ions can be found (Pekker & Shneider, 2014), thus tweaking the surface charge of the nanoparticle will have a major effect on its interaction with the cell surface, and by extension, the cell uptake.

Admittedly, the surface charge of the phospholipid bilayer varies significantly in different cells and species as a result of the heterogeneous spatial distribution of macromolecular structures across the phospholipid bilayer (Klausen et al., 2016). However, as a general rule, this phospholipid bilayer has polar heads facing the external environment and lipid tails in the reverse direction. The interaction between polar or charged nanoparticles with the polar heads of the phospholipid bilayer is usually strong enough to make the nanoparticles unable to pass this barrier freely, and the nanoparticles tend to adhere to the membrane surface. These nanoparticles possibly use active transport methods of cell uptake with the aid of transmembrane proteins. Likewise, less charged nanoparticles are more easily passed through the cell membrane.

The nanoparticles used in this study are intended for gastrointestinal absorption to circulate in the cardiovascular system. Therefore, the nanoparticles should not strongly adhere to the gastrointestinal cell membrane surface. We can assume that more conductive nanoparticles will adhere to the cell membrane surface due to strong surface charge interactions and thus are difficult to penetrate further into the mucosal cells. Less charged nanoparticles are predicted to pass more easily through this barrier and thus are more desirable. The benefits and disadvantages of nanoparticles' ability to pass the cell membrane depend on the intended use. As a carrier for drugs intended to treat stomach ulcers, it is indeed more advantageous to have the nanoparticles adhere to the cell membrane surface, as the ulcer lies on the surface. On the other hand, nanoparticles are intended to reach systemic circulation. Therefore, they have to pass the cell membrane barrier.

It has been observed that the cell uptake mechanism differs between positively and negatively charged nanoparticles. In contrast, the positively charged particles tend to stick to the inner hydrophobic part of the phospholipid bilayer; negatively charged particles usually only interact with the outer hydrophilic surface and are difficult to pass the phospholipid bilayer (Tatur et al., 2013). From our DFT study, it can be seen that the nano-encapsulated ginger is less conductive compared to free gingerol. Less conductive particles tend not to

adhere strongly to either the phospholipid bilayer's inner hydrophobic or outer hydrophilic side. Therefore, they can be assumed to be able to pass through the phospholipid bilayer. Although a certain amount of conductivity is still needed to adhere to the outer hydrophilic side in the first stage of absorption through the phospholipid bilayer, predicting the exact conductivity value needed for optimal absorption through the phospholipid bilayer is beyond the scope of this study.

Other studies observed that the cell uptake of nanoparticles was more influenced by individual cell membrane composition than the different uptake routes taken by the nanoparticles of different charges (Fröhlich, 2012). However, these two factors may also be linked. Furthermore, the relations between nanoparticle surface charge and cell viability has also been recently explored, with increasing evidence to support that higher nanoparticle charge content may lead to structural cell damage to some extent (Tatur et al., 2013; Fröhlich, 2012; Hosseinidoust et al., 2015), which urges the need to tailor the surface charge of nanoparticles, such as by encapsulation. Our study proves that nano-encapsulated gingerol is less charged than free gingerol, and based on the previous studies by Tatur et al. (2013), Fröhlich (2012), Hosseinidoust et al. (2015), it can be inferred that nano-encapsulation of gingerol potentially lessens structural damage. However, further studies of nano-encapsulation with different materials should be done before we can safely assume that this is caused by nano-encapsulation and not a singular observation from a specific nano-encapsulated material.

SUMMARY AND CONCLUSION

In this study, we conducted the synthesis and characterisation of nano-encapsulation of ginger bioactive components and computational studies to analyse the geometry and the density of states of the ginger-dextran system. The bioactive components of ginger were encapsulated by maltodextrin. Particle characterisation was done using a PSA and TEM. PSA results show that the particle size of the ginger nanocapsules had a relatively homogenous particle distribution, with most of the particles measured under 200 nm. TEM observation confirms the nano-scale size of the ginger nanocapsules and shows that the ginger nanocapsules are perfectly globular in shape. The DFT calculation of the dextran-ginger system was conducted to measure the electronic properties and geometric structure. The hydrogen bond formation between dextran and gingerol indicates that the ginger nanocapsules were formed via physisorption. The density of states analysis shows that the gingerol-dextran system has a conductive-like behaviour to promote cell membrane permeability of the nanocapsule system. Ginger nanocapsules have similar characteristics to the gingerol-dextran system. Hence, they are expected to have a good cell membrane permeability to be easily absorbed by human cells.

ACKNOWLEDGEMENT

The Institut Teknologi Bandung supports this work through a research scheme of Indonesia Collaboration Research 2018 with the contract number 011/WCU-ITB/LL/II/2018 and Riset Unggulan ITB 2018. All calculations and experiment facilities were done in Research Centre for Nanosciences and Nanotechnology, Institut Teknologi Bandung, Indonesia.

REFERENCES

- Ahmad, M., Mudgil, P., Gani, A., Hamed, F., Masoodi, F. A., & Maqsood, S. (2019). Nano-encapsulation of catechin in starch nanoparticles: Characterization, release behavior and bioactivity retention during simulated *in-vitro* digestion. *Food Chemistry*, *270*, 95-104. <https://doi.org/10.1016/j.foodchem.2018.07.024>
- Blöchl, P. E. (1994). Projector augmented-wave method. *Physical Review B*, *50*(24), 17953-17979. <https://doi.org/10.1103/PhysRevB.50.17953>
- Fröhlich, E. (2012). The role of surface charge in cellular uptake and cytotoxicity of medical nanoparticles. *International Journal of Nanomedicine*, *2012*(7), 5577-5591. <https://doi.org/10.2147/IJN.S36111>
- Ghayour, N., Hosseini, S. M. H., Eskandari, M. H., Esteghlal, S., Nekoei, A. R., Hashemi Gahruei, H., Tatar, M., & Naghibalhossaini, F. (2019). Nanoencapsulation of quercetin and curcumin in casein-based delivery systems. *Food Hydrocolloids*, *87*, 394-403. <https://doi.org/10.1016/j.foodhyd.2018.08.031>
- Hosseinidoust, Z., Alam, M. N., Sim, G., Tufenkji, N., & Van De Ven, T. G. M. (2015). Cellulose nanocrystals with tunable surface charge for nanomedicine. *Nanoscale*, *7*(40), 16647-16657. <https://doi.org/10.1039/c5nr02506k>
- İnanç Horuz, T., & Belibağlı, K. B. (2018). Nanoencapsulation by electrospinning to improve stability and water solubility of carotenoids extracted from tomato peels. *Food Chemistry*, *268*, 86-93. <https://doi.org/10.1016/j.foodchem.2018.06.017>
- Ippoushi, K., Azuma, K., Ito, H., Horie, H., & Higashio, H. (2003). [6]-Gingerol inhibits nitric oxide synthesis in activated J774.1 mouse macrophages and prevents peroxynitrite-induced oxidation and nitration reactions. *Life Sciences*, *73*(26), 3427-3437. <https://doi.org/10.1016/j.lfs.2003.06.022>
- Jaganathan, A., & Kumar, S. M. (2017). Nano bioactive compounds to enrich antioxidant methods in food science. *IJIRST-International Journal for Innovative Research in Science & Technology*, *3*(10), 239-246.
- Khayer, K., & Haque, T. (2020). Density functional theory calculation on the structural, electronic, and optical properties of fluorene-based azo compounds. *ACS Omega*, *5*(9), 4507-4531. <https://doi.org/10.1021/acsomega.9b03839>
- King, A. H. (1995). Encapsulation of food ingredients. *ACS Symposium Series*, *590*, 26-39. <https://doi.org/10.1021/bk-1995-0590.ch003>
- Klausen, L. H., Fuhs, T., & Dong, M. (2016). Mapping surface charge density of lipid bilayers by quantitative surface conductivity microscopy. *Nature Communications*, *7*(1), 1-10. <https://doi.org/10.1038/ncomms12447>

- Koo, K. L. K., Ammit, A. J., Tran, V. H., Duke, C. C., & Roufogalis, B. D. (2001). Gingerols and related analogues inhibit arachidonic acid-induced human platelet serotonin release and aggregation. *Thrombosis Research*, 103(5), 387-397. [https://doi.org/10.1016/S0049-3848\(01\)00338-3](https://doi.org/10.1016/S0049-3848(01)00338-3)
- Kou, X., Ke, Y., Wang, X., Rahman, M. R. T., Xie, Y., Chen, S., & Wang, H. (2018). Simultaneous extraction of hydrophobic and hydrophilic bioactive compounds from ginger (*Zingiber officinale* Roscoe). *Food Chemistry*, 257, 223-229. <https://doi.org/10.1016/j.foodchem.2018.02.125>
- Kresse, G., & Furthmüller, J. (1996a). Efficiency of ab-initio total energy calculations for metals and semiconductors using a plane-wave basis set. *Computational Materials Science*, 6(1), 15-50. [https://doi.org/10.1016/0927-0256\(96\)00008-0](https://doi.org/10.1016/0927-0256(96)00008-0)
- Kresse, G., & Furthmüller, J. (1996b). Efficient iterative schemes for ab initio total-energy calculations using a plane-wave basis set. *Physical Review B - Condensed Matter and Materials Physics*, 54(16), 11169-11186. <https://doi.org/10.1103/PhysRevB.54.11169>
- Kundu, J. K., & Surh, Y. J. (2009). Molecular basis of chemoprevention with dietary phytochemicals: Redox-regulated transcription factors as relevant targets. *Phytochemistry Reviews*, 8(2), 333-347. <https://doi.org/10.1007/s11101-009-9132-x>
- Lakshmi, S., Rampriya, S., & Baskar, V. (2012). Nano drug system of shogaol for transdermal delivery enhancement. *Journal of Biological and Information Sciences*, 1(2), 12-17.
- Michailidou, G., Ainali, N. M., Xanthopoulou, E., Nanaki, S., Kostoglou, M., Koukaras, E. N., & Bikiaris, D. N. (2020). Effect of poly(vinyl alcohol) on nanoencapsulation of budesonide in chitosan nanoparticles via ionic gelation and its improved bioavailability. *Polymers*, 12(5), 1101-1123. <https://doi.org/10.3390/polym12051101>
- Monkhorst, H. J., & Pack, J. D. (1976). Special points for Brillouin-zone integrations. *Physical Review B*, 13(12), 5188-5192. <https://doi.org/10.1103/PhysRevB.13.5188>
- Nedovic, V., Kalusevic, A., Manojlovic, V., Levic, S., & Bugarski, B. (2011). An overview of encapsulation technologies for food applications. *Procedia Food Science*, 1, 1806-1815. <https://doi.org/10.1016/j.profoo.2011.09.265>
- Pekker, M., & Shneider, M. N. (2014). The surface charge of a cell lipid membrane. *Journal of Physical Chemistry & Biophysics*, 5(2), 177-183. <https://doi.org/10.4172/2161-0398.1000177>
- Perdew, J. P., Burke, K., & Ernzerhof, M. (1996). Generalized gradient approximation made simple. *Physical Review Letters*, 77(18), 3865-3868. <https://doi.org/10.1103/PhysRevLett.77.3865>
- Rezaei, A., Fathi, M., & Jafari, S. M. (2019). Nanoencapsulation of hydrophobic and low-soluble food bioactive compounds within different nanocarriers. *Food hydrocolloids*, 88, 146-162. <https://doi.org/10.1016/j.foodhyd.2018.10.003>
- Setzer, W. N. (2010). A DFT analysis of thermal decomposition reactions important to natural products. *Natural Product Communications*, 5(7), 993-998. <https://doi.org/10.1177/1934578x1000500701>
- Shah, R., Eldridge, D., Palombo, E., & Harding, I. (2014). Optimisation and stability assessment of solid lipid nanoparticles using particle size and zeta potential. *Journal of Physical Science*, 25(1), 59-75.

- Shahrajabian, M. H., Sun, W., & Cheng, Q. (2019). Clinical aspects and health benefits of ginger (*Zingiber officinale*) in both traditional Chinese medicine and modern industry. *Acta Agriculturae Scandinavica, Section B - Soil & Plant Science*, 69(6), 546-556. <https://doi.org/10.1080/09064710.2019.1606930>
- Silva, H. D., Cerqueira, M. A., Souza, B. W. S., Ribeiro, C., Avides, M. C., Quintas, M. A. C., Coimbra, J. S. R., Carneiro-Da-Cunha, M. G., & Vicente, A. A. (2011). Nanoemulsions of β -carotene using a high-energy emulsification- evaporation technique. *Journal of Food Engineering*, 102(2), 130-135. <https://doi.org/10.1016/j.jfoodeng.2010.08.005>
- Suekawa, M., Ishige, A., Yuasa, K., Sudo, K., Aburada, M., & Hosoya, E. (1984). Pharmacological studies on ginger. I. Pharmacological actions of pungent constituents, (6)-gingerol and (6)-shogaol. *Journal of Pharmacobio-Dynamics*, 7(11), 836-848. <https://doi.org/10.1248/bpb1978.7.836>
- Suganya, V., & Anuradha, V. (2017). Microencapsulation and nanoencapsulation: A review. *International Journal of Pharmaceutical and Clinical Research*, 9(3), 233-239. <https://doi.org/10.25258/ijpcr.v9i3.8324>
- Tatur, S., MacCarini, M., Barker, R., Nelson, A., & Fragneto, G. (2013). Effect of functionalized gold nanoparticles on floating lipid bilayers. *Langmuir*, 29(22), 6606-6614. <https://doi.org/10.1021/la401074y>
- White, B. (2007). Ginger: An overview. *American Family Physician*, 75(11), 1689-1691.



An Indoor Navigation Support for the Student Halls of Residence using Augmented Reality: A Design Perspective

Dinna Nina Mohd Nizam^{1*}, Lim Wei Shin¹, Zaidatol Haslinda Abdullah Sani¹, Pornpon Thamrongrat² and Nooralisa Mohd Tuah¹

¹Faculty of Computing and Informatics, Universiti Malaysia Sabah, 87000 W.P.Labuan, Malaysia

²School of Informatics, Walailak University, Nakhon Si Thammarat, 80161 Thailand

ABSTRACT

Augmented Reality (AR) technology has become increasingly popular due to its potential use in an indoor environment. AR technology enables virtual information, such as navigation instructions, to be merged into the actual environment via a mobile screen. Using an AR-based Indoor Navigation speeds uptime while also being interactive in searching for a particular building location. Every year when new semester students enrol in the university, some students will have difficulty finding a particular location on the campus. The most searched for building upon arrival at the university is the student halls of residence. While searching for it, students waste time asking others for information or looking for a nearby campus map. Therefore, this project investigates the requirements needed for an AR-based indoor navigation application to be applied within the student halls of residence and identifies technical issues through a small-scale prototype development within a small navigational area. Seventy-one students participated in the feasibility study by responding to a set of questionnaires related to the Student Residence AR

indoor navigation application. At the same time, four users with and without previous experience with AR applications evaluated the prototype application. The results identified that the more the students have difficulty searching, the more they require additional time to reach their destination and seek help from others, an excellent reason to implement the Student Residence AR indoor navigation. In addition, the prototype evaluation results discussed issues related to arrow path confusion, distance accuracy,

ARTICLE INFO

Article history:

Received: 13 April 2021

Accepted: 30 July 2021

Published: 08 October 2021

DOI: <https://doi.org/10.47836/pjst.29.4.23>

E-mail addresses:

dinna@ums.edu.my (Dinna Nina Mohd Nizam)

bwhiteshin1997@gmail.com (Lim Wei Shin)

linda.sani@ums.edu.my (Zaidatol Haslinda Abdullah Sani)

pornpon.th@wu.ac.th (Pornpon Thamrongrat)

alisa.tuah@ums.edu.my (Nooralisa Mohd Tuah)

* Corresponding author

assistive guideline, and software development challenges in AR development that could be beneficial to future developers and researchers.

Keywords: AR indoor navigation, AR prototype development, augmented reality, design perspective, student halls of residence

INTRODUCTION

Augmented Reality (AR) navigation technology has allowed indoor navigation in buildings for various users and environments. AR indoor navigation has guided users to navigate easily within complex buildings (Gerstweiler, 2018). Verma et al. (2020) carried out an AR indoor navigation application within a hospital and reported that the application provided a better user experience to the users rather than 2D Maps. Meanwhile, Yoon et al. (2019) reported that implementing an AR indoor application through a smartphone for visually impaired people was significant, and they presented a guideline for future studies. The latter motivates our study to apply an AR indoor navigation application in student residence halls in a branch campus.

Every year when new students enrol into the university, there will be those who will have some difficulty searching for a specific location on the campus. The most searched for building upon arriving on campus is the student halls of residence. Upon arrival and registration, a student begins to search for their accommodation to keep their bulky belongings. Roaming around in search of a building with their belongings in hand would not be a pleasant first-day experience at the campus for them. Furthermore, the environment layout of campus as compared to hospital wards and hotel rooms are quite different. Hospitals prioritise the safety of their patients; hence rooms are designed differently. Some have single rooms, double rooms, and a whole ward layout, while hotels have different room layouts. In this study, every room in the student halls of residence has the same layout. Therefore, this study aims to comprehend the requirements for university students implementing a Student Residence AR indoor navigation application. The contribution of this study is threefold; first, analyse the possibility of implementing the Student Residence AR indoor navigation application among the students. Second, to identify the user requirements needed for the Student Residence AR indoor navigation application among the students. Third, to identify technical requirements for developing a Student Residence AR indoor navigation application through a pilot study before implementing it on a bigger scale.

AR is the technology that blends the real-world environment with the virtual world via digital objects (Siltanen, 2012). It is a technology platform that integrates digital visual content into the real-world environment of the user. AR has brought significant advancement in several application areas such as education (Sani et al., 2020; Cai et al., 2019; Vargas et

al., 2020), health care (Bui et al., 2021; Gerup et al., 2020), tourism (Williams et al., 2020; Yung & Khoo-Lattimore, 2019), and also in navigation support (Satriadi et al., 2019). In addition, AR technology can be used for both indoor and outdoor activities (Arantes & Lamounier Jr, 2018).

AR in navigation has helped people by giving them a reference or direction in wayfinding, which has changed how people explore a new place. Currently, AR navigation applications are widely performed outdoors, such as for test car navigations (Uchida et al., 2017), pedestrian wayfinding (Dong et al., 2021; Tran & Parker, 2020), and sightseeing navigations (Kato & Yamamoto, 2020; Sasaki & Yamamoto, 2021). Nevertheless, indoor navigation has also gained plausible attention in research as well as in technology adoption. For example, Codina et al. (2019) investigated AR navigation in buildings for emergencies or low visibility conditions and reported that AR navigation was significantly beneficial for the staff in finding their ways in that state of urgency or particular events. Furthermore, de Oliveira et al. (2017) added the usefulness of indoor AR navigation for users with limited mobility, such as wheelchair users sustained safe navigation.

Additionally, this paper surveyed a number of AR navigation articles in the literature to comprehend the AR application in the field. Table 1 summarises the surveyed articles and their study objectives and outcome or results obtained from the study. Findings show that indoor navigation can be used widely, whether it is for any navigation purposes or direction precision and effectiveness. Therefore, this study has strong support in implementing a Student Residence AR indoor navigation application, particularly for students entering the student halls of residence for the first time.

There are six types of AR technology, and they are classified into two categories (Figure 1); triggered-based and view-based augmentation (Edwards-Stewart et al., 2016). The widely known triggered-based augmentations are the marker-based AR and location-based AR, while the general view-based augmentation is the markerless AR. The marker-based AR approach uses a marker presented in a paper-based or physical object to trigger the augmentation (Siltanen, 2012). In comparison, the location-based AR is activated by the Global Positioning System (GPS) location and pairs the desired destination (Chanphearith & Santoso, 2016). Thus, the combination of GPS, compass sensors, trackers, and computer displays determines the location-based AR implementation (Billinghurst et al., 2014).

Conversely, the markerless AR method uses a real-world static view or real-life object as a marker. Thus, the tracking method combines the natural features of a particular real-life object by detecting the targeted object's edges, corners, and texture (Jumarlis & Mirfan, 2018). In addition, markerless AR also uses GPS and compass to provide data based on the user's location. This data then determines what AR contents the user receives in a particular area, producing maps and directions at the end.

Table 1
 Summary of several indoor augmented reality navigation studies

Articles	Study Objective	Outcome/ Result
D. Khan et al. (2019)	Time efficiency/ Distance accuracy	AR navigation is efficient, accurate, and user friendly.
Codina et al. (2019)	Distance accuracy	AR system is useful in low visibility situations and proved to be helpful.
Vidhyavani et al. (2019)	Object recognition accuracy	The mobile camera allows various objects to be supplied into the AR application.
R. U. Khan et al. (2019)	Human cognitive workload/ Time efficiency	Indoor AR system provides useful information without having any physical equipment or connection.
Ghantous et al. (2018)	Distance accuracy	AR navigation results are positive and satisfying.
Gerstweiler (2018)	Distance accuracy	Good performance was reported in guiding users with AR.
De Oliveira et al. (2016)	Optimal routes	AR has the ability to identify the best routes and reduce potential hazards for wheelchair users.
Yang & Saniie (2017)	Distance accuracy/ Position estimation	The position estimation error is reduced by a larger AR marker or by using higher resolution images.

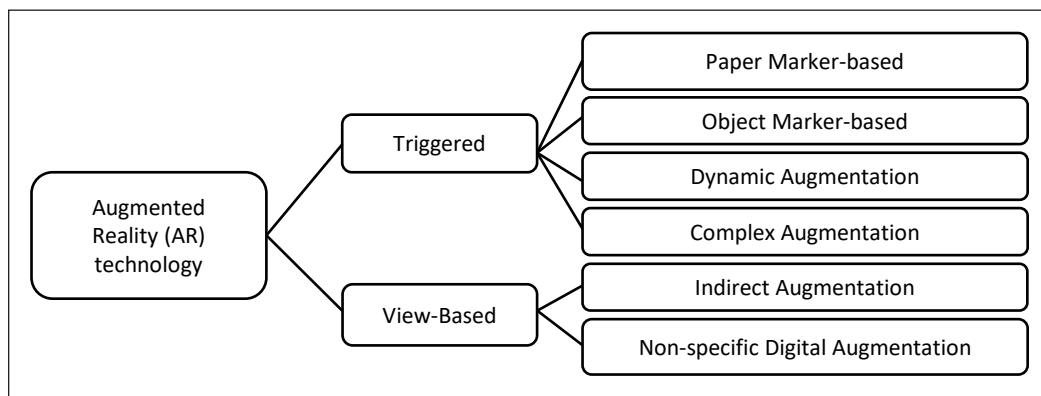


Figure 1. Augmented reality technologies classified by Edwards-Stewart et al. (2016)

The Student Residence AR indoor navigation application will adapt the marker-based AR technology to trigger augmentation for this current study. A marker-based AR technology is more relevant for a dedicated indoor navigation system that does not demand extensive installation or strong wireless connections.

MATERIALS AND METHODS

Figure 2 illustrates the study as a whole, consisting of four phases: Initial phase, Design phase, Implementation phase, and Evaluation phase. However, this paper only reports the first two phases; the initial phase and the design phase. The initial phase includes reviewing

the literature, reviewing previous AR navigation studies, and conducting a preliminary investigation to identify user requirements reported in the results and discussion section. In the design phase, a small scale prototype pilot was built and implemented to identify technical requirements before building the larger scale prototype for the student halls of residence. As continuous work from this study, the following articles will report the other two phases; implementation and evaluation.

In the initial phase, using a simple random sampling approach, seventy-one students participated in the preliminary feasibility study conducted among 1,900 university students living in the student halls of residence of the branch campus. Online questionnaires were distributed across Year 1 to Year 4 students via google forms. Unfortunately, only a few students completed the questionnaires due to the Covid-19 Pandemic, which forced most students to return home. Approximately 36 male and 35 female students answered the survey question. The questions were divided into three sections: (1) Demographic profile, (2) User experience on current halls of residence system, and (3) User opinion on a Student Residence AR indoor navigation application. The outcomes of this feasibility study are discussed in the results and discussion section.

In the design phase, the Student Residence AR indoor navigation application utilises marker-based technology. Software such as Unity 3D and Visual Studio is used in the development of the application. Vuforia SDK package is added to the Unity 3D application to enable augmented reality functions. C# Programming Language is also used to write

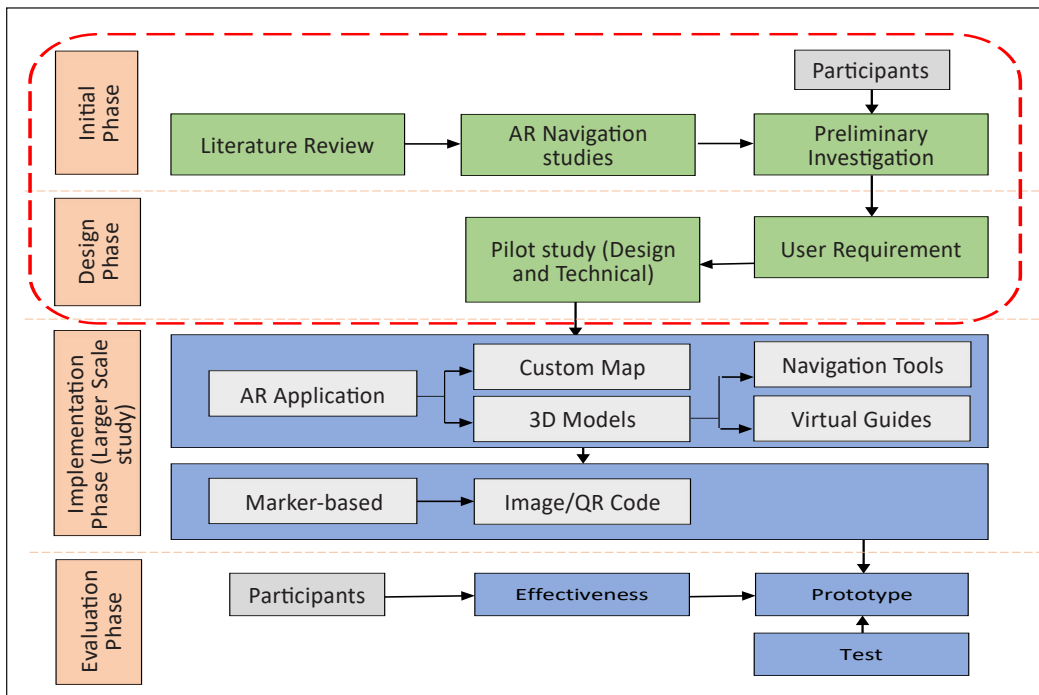


Figure 2. Conceptual Design of the entire work and focus of this paper is indicated in the red dashed line area

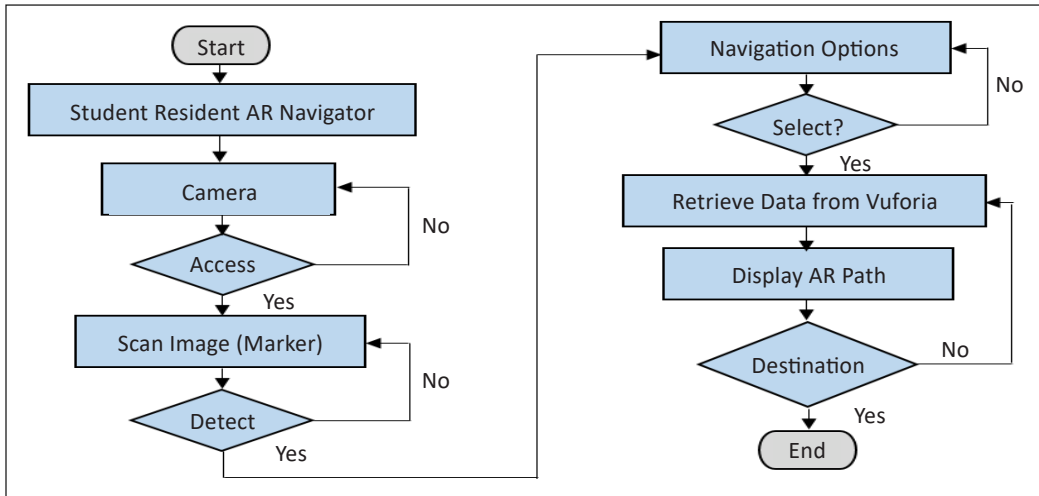


Figure 3. The application algorithm flow for both the small-scale and large-scale prototype

scripts that allow certain functions to be called on the application’s component (object). Before a large-scale application is developed in the implementation phase, a small-scale prototype was developed and reported in this paper. This small-scale prototype was done to identify technical issues and to optimise resources.

Figure 3 presents the algorithm flow for both the small-scale prototype and the large-scale Student Residence AR indoor navigation application. This application uses the AR-codes as markers because they are much easier to be recognised by the camera and user. The AR code, known as the Augmented Reality Code, is a 2D barcode in the form of pixel squares in a box and redirects the user to an AR website or mobile application. Once the Student Residence AR indoor navigation application recognises the marker (scans image) and identifies the user location at this point, the application displays the navigation options (e.g., Living Room, Store, Kitchen, Room, Room 2). After a selection has been made, the application calculates both the marker’s position and destination. The position of the computer-generated content can be affected by any change in the position of the real-world object. Therefore, the more refined the application can identify a particular physical object, the more accurate the digital data layout will be. These calculations and measurements are conducted through the Vuforia Engine Platform. Whenever a user changes routes by accident, the Vuforia Engine Platform recalculates the destination and displays the user’s corrected path.

RESULTS AND DISCUSSION

A preliminary study was conducted to assess the feasibility of implementing a Student Residence AR indoor navigation application for students in the student halls of residence. Table 2 demonstrated that students had difficulty finding their particular room when they

first arrived at the university’s halls of residence. In addition, there was a significant relationship between Searching Difficulty and both Genders ($\chi^2(1) = 5.04$; $p < .05$), with female students struggling more than male students.

Table 3 reports Searching Difficulty and the practice student applied when searching a particular room in the residence halls. The relation between Searching Difficulty and Searching Support practice was significant, $\chi^2(4) = 24.26$; $p < .01$. From the data, the majority of students struggled with searching and sought assistance from others. There were only a few students who had no problems.

Table 2
Searching difficulty of both genders

Genders	Yes	No	Chi - Square
Male (n=36)	27	9	df = 1
Female (n=35)	33	2	$\chi^2 = 5.04$,
Total	60	11	$p = .02$

Table 3
Searching difficulty on searching support

	No.	Had Difficulty	No Difficulty	%	Chi-Square
By Floor Map	26	23	3	23.9	df = 4
Ask Help From Others	39	39	0	35.8	$\chi^2 = 24.26$,
Own Explore	38	30	8	34.9	$p = .00$
No Need Assistance	6	3	3	5.5	
Total	109			100	

Table 4
Searching difficulty on time spent and AR awareness

	Searching Difficulty	Yes	No	Chi - Square
Need (Spends) More Time	Had Difficulty	44	16	df = 1
	No Difficulty	4	7	$\chi^2 = 5.80$,
	Total	48	23	$p = .01$
AR-Based Indoor Navigation Awareness	Had Difficulty	33	27	df = 1
	No Difficulty	10	1	$\chi^2 = 0.09$,
	Total	43	28	$p = .93$

Table 4 reports the number of students having difficulty finding their particular room when they first arrived at the university’s residence halls and the need to have extra time when searching. The result shows a significant association between the two variables, $\chi^2(1) = 5.80$; $p < .01$. It indicates that when students are having difficulty searching, they will require additional time. Also in Table 4 reports the number of students having difficulty searching and their awareness of existing AR-based indoor navigation applications. There was no significant association between the number of students who had difficulty searching and their awareness, $\chi^2(1) = 0.09$; $p > .05$. However, Table 4 shows that students who had difficulty searching are primarily aware of AR-based indoor navigation in the

Table 5
AR usage experience and preferable method when finding room of both genders

	Genders	Yes	No	Chi - Square
Experience in using existing AR Indoor Application	Male (n=36)	3	33	df = 1
	Female (n=35)	1	34	$x^2= 1.00,$
	Total	4	67	$p = .32$
Preferable Method (Conventional Vs AR)	Male (n=36)	29	7	df = 1
	Female (n=35)	27	8	$x^2= 0.12,$
	Total	56	15	$p = .72$

market. Therefore, it could be a good reason for fostering the Student Residence AR indoor navigation.

Table 5 reports the students' experience in using any existing AR-based indoor navigation applications. Both male and female students have never used any AR-based indoor navigation applications, and the proportion between both genders shows no difference, $x^2(1) = 1.00$; $p > .05$. Also, Table 5 reports the preferable practice of searching for a room in the residence halls between conventional or an AR-based indoor navigation application. Again, there is no difference in proportion ($x^2(1) = 0.12$; $p > .05$) between both genders as to the preferable practice in searching a room. Nevertheless, both genders show interest in using a Student Residence AR indoor navigation application within the campus.

The preliminary study results reported that most of the respondents were aware and interested in having an AR-based indoor navigation application. Although most respondents have not previously experienced or used AR-based indoor navigation applications such as the proposed Student Residence AR indoor navigation application, they are still interested in using it because of its convenience. This preliminary study also identified that the more the students have difficulty searching, the more they require additional time to reach their destination and seek help from others. Only a tiny percentage of students did not ask for assistance when they first arrived at the university's halls of residence.

Furthermore, a small-scale prototype of the Student Residence AR indoor navigation application within a house was developed to test and identify technical requirements for a more significant scale application development. The aim was to minimise the technical errors that could result in a delay or ineffective large-scale application. Figure 5 presents the interfaces and flow of the application.

Figure 4(a) shows the homepage of the Student Residence AR indoor navigation application prototype. Figure 4(b) shows the 'Scan page' of the application where users need to search for the AR marker and scan it via their phone camera. The marker is used to trigger the application. It will then load and direct the user to the 'Selection page', as shown in Figure 4(c). Here, users are required to choose one of the destinations (e.g., Living Room, store and kitchen). Once a preferable destination has been selected, users are directed

to the 'Path Display pages', as shown in Figures 4(d) and 4(e). These pages show the path with arrows leading to the preferred destination. Users can follow the arrows until they reach the intended destination. Upon arrival at the destination, a message 'You've reached Destination' will appear, as shown in Figure 4(f). Users can then quit the application by going back to the 'Selection Page' and tap on the 'Exit' button, as shown in Figure 4(g).

In this prototype development, the canvas allows users to interact with the AR device via buttons, as presented in Figure 5. Panel 1 and 2 of the canvas layers have different button functions that help direct users to specific destinations.

Also, a floor plane (the 3D flat surface in Unity) is created to allow the application to understand the navigational area, as shown in Figure 6. The blue area of the floor plane represents walkable areas, whereas the pink and grey 3D objects represent non-walkable areas. A baking process is carried out to allow the application to understand these two distinct areas. In addition, the AR camera object is used as a first-person view of the application and acts as a virtual human on the floor plane. In this situation, the AR camera object will also move when the user moves the application.

Furthermore, to guide the users to go from the current location to the destination location via the indoor application, a navigation controller script was created using the C# programming language to display a 3D path. Nevertheless, in this prototype, the line was replaced with an arrow-pattern-like path to make it more visible and pleasant for the users

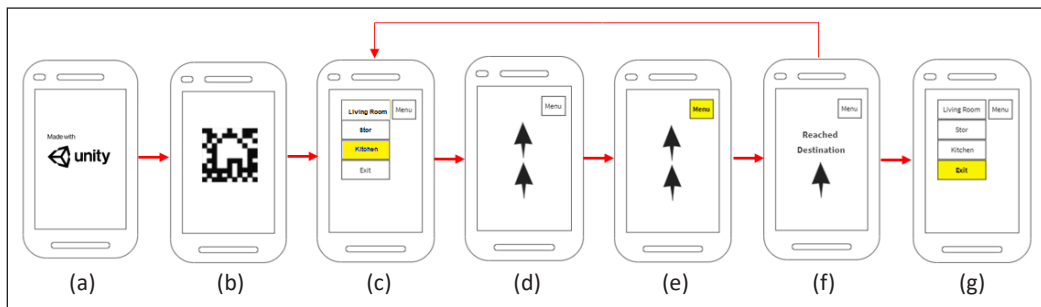


Figure 4. Interface design and the AR Indoor navigation prototype flow

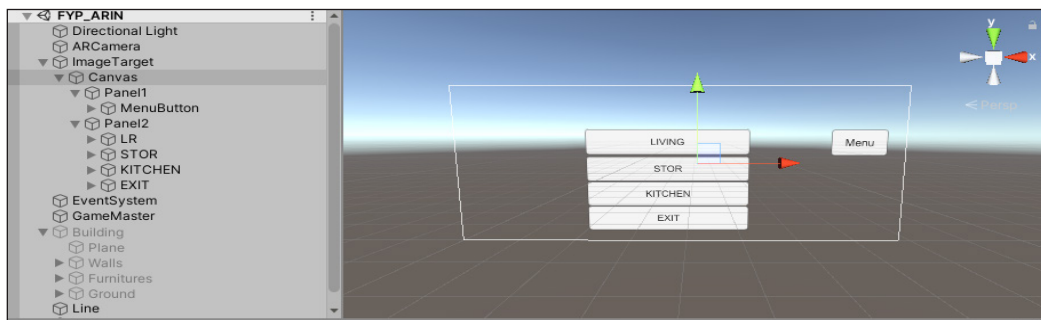


Figure 5. Panel 1 and Panel 2 of the Canvas layers created

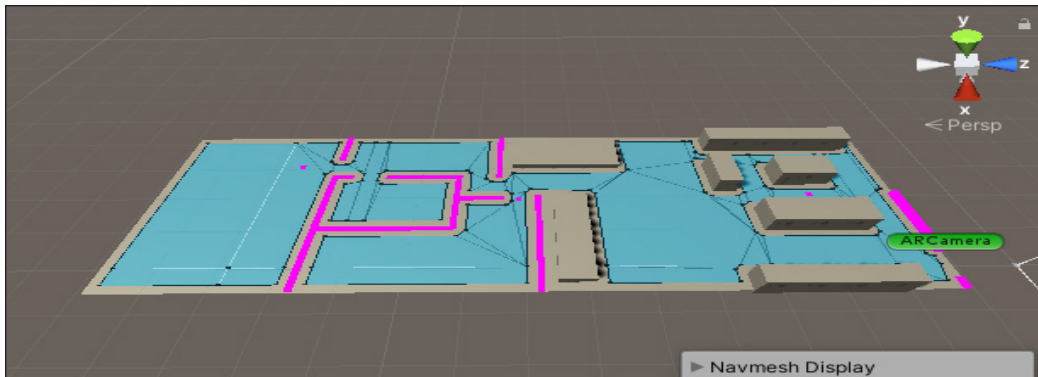


Figure 6. The walkable and non-walkable area of the floor plane

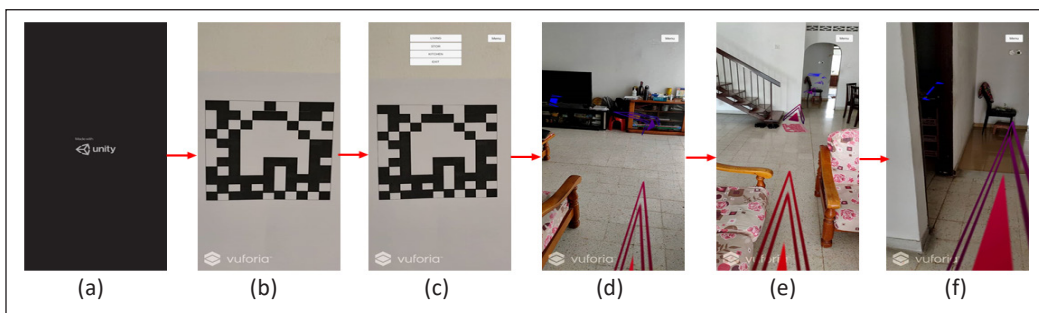


Figure 7. The Student Residence AR indoor navigation application demonstration

[Figures 7(d), 7(e) and 7(f)]. A voice narrative is also integrated along the arrow-pattern-like path to assist navigation. Demonstration of the AR-based indoor navigation prototype, which leads to the kitchen of a house (pilot scale), is presented in Figure 7.

Four evaluators were involved in the prototype test. Two of the evaluators had experience with AR development, one had used AR before, and the other had never used any AR application before. In a closed experimental area, the evaluators were given the AR-based indoor navigation application and were informed to use the application to reach a destination. However, the evaluators had no idea how the closed experimental area was set up. Overall, the development of a small-scale prototype resulted in a number of practical technical issues.

Improving Arrow Paths

Although the arrow path correctly directs users to their destination with the help of the voice narration, the arrow-pattern-like path makes it irritating and confusing for users to follow because the arrow-pattern-like path occasionally appears in mid-air or above eye level when panned around. Since it is critical to avoid potential user confusion when designing a UI navigation app (Huang et al., 2020), the arrow-pattern-like path will be

improved in the large-scale development phase by including a standard line alongside the arrow-pattern-like path to avoid confusion.

Distance Accuracy

Two evaluators discovered problems with distance accuracy due to the small number of AR markers used in the navigation and floor plane to reach the destination. Compared to markerless AR navigations that use GPS, this indoor navigation employs AR markers. However, the number of AR markers used will affect the distance accuracy as each AR marker can only cover a small navigation area. According to Rehman & Cao (2017), a more complex environment and longer route may improve accuracy and performance. Therefore, for large-scale development, more AR markers are needed to reduce distance accuracy errors.

Assistive Guidelines

The application was confusing in the beginning because the evaluators did not know what to do. This situation made the application challenging to use and non-user-friendly. Therefore, in the large-scale project, it is necessary to add an assistive guideline to provide users with clear step-by-step recommendations when using the application in contrast to Rehman and Cao (2017) suggestion of not to use any assistive guideline to study retention routes in indoor navigations.

Complicated Software Development Kit

Both AR Core and Vuforia are useful software development kits (SDKs) that enable AR application development. However, the AR navigation in the pilot study is developed using Unity. When using AR Core, all AR components were stored in separate folders causing the developer to unfold each folder, learn one by one, understand and use each component. However, when using Vuforia, the components were nicely arranged on a fixed panel in Unity, ready to be used. This arrangement makes the development process easier and smoother. Furthermore, AR Core dedicates to location-based navigation using SLAM (Simultaneous Localisation and Mapping) algorithms (Morar et al., 2020). In contrast, Vuforia dedicates to marker-based navigations using their plane-find technology, as in Figure 6 (Vuforia Library, 2021). Therefore, Vuforia will be applied in the large-scale development due to the project implementation in an indoor static environment.

The implementation of this small-scale prototype revealed a few other issues that must be addressed before moving forward with the large-scale prototype in the university. Because the student residence halls cover such a large area, multiple routes may arise when using the AR indoor navigation application. As a result, a more complicated rerouting process is required. One solution to this could include a feature in the application that

allows users to choose a route based on the total time to get to their destination before continuing their journey. Aside from that, the ease of use of the AR indoor navigation application should also be taken into consideration. Allowing the user to interact with the app with ease will increase engagement and encourage long-term usage. Incorporating a mixed reality environment, such as allowing users to interact with the application using gesture recognition or an assistant avatar, could be convenient. However, keeping confusion and burden to a minimum should be regarded.

CONCLUSION

Searching for a place or room in the student halls of residence for new students is sometimes an unpleasant experience, especially when there is so much luggage to carry during registration. This paper aims to perform a feasibility study of applying a Student Residence AR indoor navigation application and identify technical issues through a small scale prototype development within a small navigational area. The four critical issues discussed include improving arrow paths, distance accuracy, assistive guidelines, and software development kit difficulty.

The next phase of this study is to implement the Student Residence AR indoor navigation application on a larger scale, the university's halls of residence, and to evaluate the application among new students entering the university. In addition, the Covid-19 Pandemic has introduced a new norm for physical distancing in the fight against the outbreak. Therefore, this application may embrace physical distancing during this challenging time, and at the same time, expose the student to a virtual campus environment.

ACKNOWLEDGEMENT

The authors would like to express their gratitude to Universiti Malaysia Sabah (UMS) for providing the necessary resources for this research. Thank you also to all of the undergraduates who volunteered their time and effort with this study.

REFERENCES

- Arantes, W. V., & Lamounier Jr, E. A. (2018). A strategy for the use of indoor and outdoor augmented reality location systems applied to smartphones. *IEEE Latin America Transactions*, 16(5), 1460-1467. <https://doi.org/10.1109/TLA.2018.8408442>
- Billinghurst, M., Clark, A., & Lee, G. (2014). A survey of augmented reality. *Foundations and Trends in Human-Computer Interaction*, 8(2-3), 73-272. <https://doi.org/10.1561/11000000049>
- Bui, D. T., Barnett, T., Hoang, H. T., & Chinthammit, W. (2021). Tele-mentoring using augmented reality technology in healthcare: A systematic review. *Australasian Journal of Educational Technology*, 37(4), 81-101. <https://doi.org/10.14742/ajet.6243>

- Cai, S., Liu, E., Yang, Y., & Liang, J. C. (2019). Tablet-based AR technology: Impacts on students' conceptions and approaches to learning mathematics according to their self-efficacy. *British Journal of Educational Technology, 50*(1), 248-263. <https://doi.org/10.1111/bjet.12718>
- Chanphearith, S., & Santoso, A. J. (2016). Analysis and implementation of location-based augmented reality mobile application for searching tourist attractions and culinary places in Phnom Penh. *International Journal of Computer Science Trends and Technology (IJCTST), 4*(6), 126-136.
- Codina, M., Castells-Rufas, D., Carrabina, J., Salmon, I., Ayuso, N., Guerendiain, A., & Alvarez, G. (2019). Augmented reality for emergency situations in buildings with the support of indoor localization. In *Multidisciplinary Digital Publishing Institute Proceedings* (Vol. 31, No. 1, p. 76). MDPI Publishing. <https://doi.org/10.3390/proceedings2019031076>
- de Oliveira, L. C., Andrade, A. O., de Oliveira, E. C., Soares, A. B., Cardoso, A., & Lamounier Jr, E. A. (2017). Indoor navigation with mobile augmented reality and beacon technology for wheelchair users. In *2017 IEEE EMBS International Conference on Biomedical & Health Informatics (BHI)* (pp. 37-40). IEEE Publishing. <https://doi.org/10.1109/BHI.2017.7897199>
- de Oliveira, L. C., Soares, A. B., Cardoso, A., de Oliveira Andrade, A., & Lamounier Jr, E. A. (2016). Mobile augmented reality enhances indoor navigation for wheelchair users. *Research on Biomedical Engineering, 32*(2), 111-122. <https://doi.org/10.1590/2446-4740.01515>
- Dong, W., Wu, Y., Qin, T., Bian, X., Zhao, Y., He, Y., Xu, Y., & Yu, C. (2021). What is the difference between augmented reality and 2D navigation electronic maps in pedestrian wayfinding? *Cartography and Geographic Information Science, 48*(3), 225-240. <https://doi.org/10.1080/15230406.2021.1871646>
- Edwards-Stewart, A., Hoyt, T., & Reger, G. M. (2016). Classifying different types of augmented reality technology. *Annual Review of CyberTherapy and Telemedicine, 14*(January), 199-202.
- Gerstweiler, G. (2018). Guiding people in complex indoor environments using augmented reality. In *2018 IEEE Conference on Virtual Reality and 3D User Interfaces (VR)* (pp. 801-802). IEEE Publishing. <https://doi.org/10.1109/VR.2018.8446138>
- Gerup, J., Soerensen, C. B., & Dieckmann, P. (2020). Augmented reality and mixed reality for healthcare education beyond surgery: An integrative review. *International Journal of Medical Education, 11*, 1-18. <https://doi.org/10.5116/ijme.5e01.eb1a>
- Ghantous, M., Shami, H., & Taha, R. (2018). Augmented reality indoor navigation based on Wi-Fi trilateration. *International Journal of Engineering Research & Technology (IJERT), 7*(07), 396-404.
- Huang, B. C., Hsu, J., Chu, E. T. H., & Wu, H. M. (2020). Arbin: Augmented reality based indoor navigation system. *Sensors (Switzerland), 20*(20), 1-20. <https://doi.org/10.3390/s20205890>
- Jumarlis, M., & Mirfan, M. (2018). Implementation of markerless augmented reality technology based on android to introduction lontara in marine society. In *IOP Conference Series: Earth and Environmental Science* (Vol. 156, No. 1, p. 012017). IOP Publishing. <https://doi.org/10.1088/1755-1315/156/1/012017>
- Kato, Y., & Yamamoto, K. (2020). A sightseeing spot recommendation system that takes into account the visiting frequency of users. *ISPRS International Journal of Geo-Information, 9*(7), Article 411. <https://doi.org/10.3390/ijgi9070411>

- Khan, D., Ullah, S., & Nabi, S. (2019). A generic approach toward indoor navigation and pathfinding with robust marker tracking. *Remote Sensing*, *11*(24), 1-21. <https://doi.org/10.3390/rs11243052>
- Khan, R. U., Oon, Y. B., Madihie, A., & En, C. S. (2019). Indoor navigation systems using annotated maps in mobile augmented reality. *International Journal of Innovation, Creativity and Change*, *8*(2), 1-14.
- Morar, A., Balutoiu, M. A., Moldoveanu, A., Moldoveanu, F., Butean, A., & Asavei, V. (2020). Evaluation of the ARCore indoor localization technology. In *2020 19th RoEduNet Conference: Networking in Education and Research (RoEduNet)* (pp. 1-5). IEEE Publishing. <https://doi.org/10.1109/RoEduNet51892.2020.9324849>
- Rehman, U., & Cao, S. (2017). Augmented-reality-based indoor navigation: A comparative analysis of handheld devices versus google glass. *IEEE Transactions on Human-Machine Systems*, *47*(1), 140-151. <https://doi.org/10.1109/THMS.2016.2620106>
- Sani, Z. H. A., Huiyi, A. S., Hong, T. S., Nizam, D. N. M., & Baharum, A. (2020). Design and development of an augmented reality application to learn Mandarin. *European Journal of Molecular & Clinical Medicine*, *7*(8), 3814-3826.
- Sasaki, R., & Yamamoto, K. (2021). Sightseeing navigation system from normal times to disaster outbreak times within urban tourist areas in Japan. *Applied Sciences*, *11*(10), Article 4609. <https://doi.org/10.3390/app11104609>
- Satriadi, K. A., Ens, B., Cordeil, M., Jenny, B., Czauderna, T., & Willett, W. (2019). Augmented reality map navigation with freehand gestures. In *2019 IEEE Conference on Virtual Reality and 3D User Interfaces (VR)* (pp. 593-603). IEEE Publishing. <https://doi.org/10.1109/VR.2019.8798340>
- Siltanen, S. (2012). *Theory and applications of marker-based augmented reality: Licentiate thesis* (Issue 3). VTT Technical Research Centre of Finland.
- Tran, T. T. M., & Parker, C. (2020). Designing exocentric pedestrian navigation for AR head mounted displays. In *Extended Abstracts of the 2020 CHI Conference on Human Factors in Computing Systems* (pp. 1-8). ACM Publishing. <https://doi.org/10.1145/3334480.3382868>
- Uchida, N., Tagawa, T., & Sato, K. (2017). Development of an augmented reality vehicle for driver performance evaluation. *IEEE Intelligent Transportation Systems Magazine*, *9*(1), 35-41. <https://doi.org/10.1109/MITS.2016.2601943>
- Vargas, J. C. G., Fabregat, R., Carrillo-Ramos, A., & Jové, T. (2020). Survey: Using augmented reality to improve learning motivation in cultural heritage studies. *Applied Sciences*, *10*(3), Article 897. <https://doi.org/10.3390/app10030897>
- Verma, P., Agrawal, K., & Sarasvathi, V. (2020). Indoor Navigation using augmented reality. In *Proceedings of the 2020 4th International Conference on Virtual and Augmented Reality Simulations* (pp. 58-63). ACM Publishing. <https://doi.org/10.1145/3385378.3385387>
- Vidhyavani, A., Stanly, S., Pandey, A. K., & Choudhury, S. (2019). Combination of real and virtual world for indoor navigation using mobile application. *International Journal of Engineering and Advanced Technology*, *8*(4), 307-310.
- Vuforia Library. (2021). *Using ARCore with Vuforia engine*. Retrieved May 20, 2021, from <https://library.vuforia.com/articles/Solution/arccore-with-vuforia.html>

- Williams, M., Yao, K. K. K., & Nurse, J. R. C. (2020). *Developing an Augmented reality tourism app through user-centred design (extended version)*. ArXiv Publishing.
- Yang, G., & Saniie, J. (2017). Indoor navigation for visually impaired using AR markers. In *2017 IEEE International Conference on Electro Information Technology (EIT)* (pp. 1-5). IEEE Publishing. <https://doi.org/10.1109/EIT.2017.8053383>
- Yoon, C., Louie, R., Ryan, J., Vu, M. K., Bang, H., Derksen, W., & Ruvolo, P. (2019). Leveraging augmented reality to create apps for people with visual disabilities: A case study in indoor navigation. In *The 21st International ACM SIGACCESS Conference on Computers and Accessibility* (pp. 210-221). ACM Publishing. <https://doi.org/10.1145/3308561.3353788>
- Yung, R., & Khoo-Lattimore, C. (2019). New realities: A systematic literature review on virtual reality and augmented reality in tourism research. *Current Issues in Tourism*, 22(17), 2056-2081. <https://doi.org/10.1080/13683500.2017.1417359>



Effects of Noise Pollution from Electric Backup Generators on the Operators' Health

Mahmmoud Ismail Mohammed¹ and Muwafaq Ayesh Rabeea^{2*}

¹Faculty of Science, University of Mosul, Mosul, 41002, Iraq

²Faculty of Applied sciences, University Of Anbar, Anbar 31001, Iraq

ABSTRACT

Noise is a harmful pollutant that leads to an unsanitary environment in urban areas. Electric backup generators, widely used in developing countries, have been one of the most common noise sources. This study identifies workers' public health in public electrical backup generators in Mosul City, Iraq. Workers' health was assessed by measuring blood parameters, including Hb, RBCs, WBCs, PLT, and PCV. In addition, other biochemical parameters have been tested, such as; TP, ALB, F.B.S, Bilirubin, Blood Urea, and Cholesterol. General Urine Examination (GUE) was implemented for all samples. The results show a significant change in the blood samples studied compared to the control sample. Hb increased to 15.72 ± 0.9 and 16.12 ± 0.74 g/dl, at noise levels 92.5 and 94.8 dB, respectively, compared to the control group (14.07 ± 0.20 g/dl). RBCs and PLT increased with the high noise level, whereas TP shows a decrease of about 6.43 ± 0.46 and 6.75 ± 0.14 g/dl at 92.5 and 94.8 dB, respectively, compared to the control group. Similarly, F.B.S, blood urea, and total cholesterol were increasing compared to the control group. Depending on the results obtained, up to 30% of the workers tested have severe hearing troubles. This percentage was classified as acute Hypacusis (57%), severe Hypacusis (40%), and complete deafness (3%). Therefore, public electrical backup generators, which were randomly distributed in the public areas of developing countries, are a source of noise pollution.

Keywords: Biochemical parameters, blood, generator, noise pollution

ARTICLE INFO

Article history:

Received: 28 March 2021

Accepted: 25 August 2021

Published: 08 October 2021

DOI: <https://doi.org/10.47836/pjst.29.4.24>

E-mail addresses:

mahjsbio74@uomosul.edu.iq (Mahmmoud Ismail Mohammed)

muw88@uoanbar.edu.iq (Muwafaq Ayesh Rabeea)

* Corresponding author

INTRODUCTION

People living in cities have risen over the last few decades, which has caused a number of health problems (Flies et al., 2019). In addition, the urban environment has become increasingly crowded, leading to a significant increase in pollution problems

such as heat, noise, and air pollution. Therefore, these areas need continuous assessment and suggest technologies to reduce pollutants' exposure and density risks (Hussien et al., 2020; Mohammed et al., 2020; Paull et al., 2020).

Noise pollution is defined as a heterogeneous mixture of unwanted continuity sounds, usually due to industrial progress. This type of pollution is closely related to developed places, especially industrial places. Noise pollution has been placed in the second grade after water pollution in the cities. The technological development had resulted in many risks, despite the significant benefits provided by the urban technology to humankind, the advanced achievements that contributed to man's well-being, and the provision of his requirements. Still, there are great dangers and problems brought by this technology between its folds and contributed to causing great suffering for most of humanity. Noise is considered the most dangerous environmental pollutants and one type of physical environmental pollution due to its negative impact on psychological health. It also has physiological and social effects on humans. It is an invented pollution component that resulted from modernity's progress that depends on the use of machines, tools, means of transportation, conductors, and traffic signals that led to making significant changes in the sound environment (Adimalla et al., 2020; Dzhambov & Dimitrova, 2016; Eduardo et al., 2015).

The World Health Organization (WHO) has announced that large cities' noise has harmful impacts on public health. These effects depend on the period and level of exposure of a person. WHO also reported that the acceptable limit for daily exposure to noise in residential areas is 55dB (van Kempen et al., 2018; WHO, 2011). Noise at a certain sound level could cause damage to the ability of human hearing. When a person is subjected to a sound with an intensity of 85 dB, he starts getting disturbed, and when the intensity of the sound becomes more than 90 dB, the body organs start getting impacted. Continuous exposure to high sound levels, which caused further damage to the nerve cells in the inner ear, caused people to be deaf. The nerve cells are gradually eroded, and this issue has been known as neurodevelopmental hearing loss (Dzhambov et al., 2016; Sygna et al., 2014).

Noise is linked to a number of industries, such as textile and cement industries, as workers in such factories are exposed to the noise of more than 90-115dB, causing psychological and organic influences with temporary or permanent hearing loss (Jadaan et al., 2016; Vladimir & Madalina, 2019). In addition, airports and highways in many countries have been recorded as a major noise source with a measuring sound between 56-65dB (Amoatey et al., 2020). Backup electric power generators are diesel-powered outdoor machines that supply temporary electrical power up to a specific voltage (Ashmore & Dimitroulopoulou, 2009; Cuesta & Cobo, 2000). During statutory power outages, most people depend on these types of generators to meet their commercial, industrial, and domestic electricity needs (Parvathi & Gopalakrishnan, 2003). However, the noise caused

by aerodynamic forces generated in such machines, which can reach 92.4 dB (Ibhadode et al., 2018), has a detrimental effect on the health of their operators. Therefore, the risk of exposure to noise from these sources, which may cause serious health problems for workers, must be assessed. Therefore, this study aimed to evaluate some blood parameters (biological and biochemical) for workers in public electrical backup generators. In addition, the workplace conditions have been assessed based on the slight hearing problems and the severe hearing problems resulting from this type of noise.

MATERIAL AND METHODS

Mosul is Iraq's second-largest city, with a population of around 1,800,000. It is located on the Tigris River in northern Iraq and was chosen as a case study to assess the effects of backup generator noise on the workers' health.

Eighty blood and urine samples were collected from operators of electrical backup generators in the study area. Men 35 and 40 years of age, with no social differences were targeted in this study. The collected samples were divided into two groups based on working time and noise levels. The first group consists of 60 samples, while the second group consists of 20 samples, as shown in Table 1.

Table 1
Classification of the number of samples collected

Working	Noise level	
	94.8 dB	92.5 dB
15 years	15	15
10 years	15	15

The apparatus of sound level determination (Testo-815) was used to measure acoustic noise intensity level. In addition, the blood pressure was spatially checked using a Mercury Sphygmomanometer with a stethoscope (Yuyue) (Measurement range: 0-300mmHg and Sensitivity: >2.25 mmHg).

The total protein amount was estimated using a ready-made analysis kit from the English company (Fortress/ UK). The method includes forming a coloured complex resulting from the interaction of the protein in the serum with a solution of basic copper potassium tartrate (Cu^{++} ions in the basic environment). It is known as the biorite detector to give a complex of purple colour whose intensity is proportional to the amount of protein, and the intensity of the solution is measured at the wavelength (550) nanometres (Arneson & Brickell, 2007). The bilirubin concentration was estimated using ready-made Kit solutions. The method is based on bilirubin's interaction with the reagent Diazotized sulfalinic acid to form the Azobilirubin coloured compound. Dimethyl sulfoxide (DMSO) was added to estimate the total bilirubin (Arneson & Brickell, 2007). The intensity was measured at a wavelength of (550 nm), proportional to the amount of bilirubin present in the blood serum. The ALB concentration was determined using the Bromocresol green method, in which a ready-made test kit was used from a company from (Biolab /France). It depends

on the amount of albumin that binds with the reagent (3, 3', 5, 5'-tetrabromocresol green) (Bromocresol green) BCG). The Albumin-BCG complex, which is green in colour, was measured at a wavelength of 630 nm (Arneson & Brickell, 2007). The enzymatic method (Urease-Modified Berthelot Reaction) was used to quantify urea.

The method includes ready-made solutions from the French company (Biomérieux) containing the enzyme urease, which releases ammonia into the basic environment. Ammonia reacts with salicylate and hypochlorite to form 2, 2-dicarboxyindophenol, measured at a wavelength (580) nanometres by a spectrophotometer. The total serum cholesterol was determined using the Kit from Biolab/France. It is an enzymatic method based on converting cholesterol and cholesterol esters to the tincture of Quinoneimine. The analysis kit contains the enzyme cholesterol esterase, which works on the analysis of cholesterol in the blood serum into cholesterol and fatty acids and in the presence of oxygen and cholesterol oxidase, which works on free cholesterol due to the first reaction to cholesterol-4-en-3-one and hydrogen peroxide. The formed peroxide interacts with phenol and 4-amino antipyrine in the presence of the peroxidase enzyme (peroxidase); a pink colour is formed resulting from the compound (Quinoneimine), and the intensity of the colour is directly proportional with the concentration of cholesterol in serum (Richmond, 1973). 10 ml of urine was taken and placed in a test tube and was centrifuged for 3 minutes, then we kept the precipitate, which is placed on a glass slide, and a microscopic examination was performed on it to know the types of cells in the urine sample (Brunze, 2016).

A practical experiment was carried out using a random design. The obtained data were statistically analysed for each of the studied groups using the Duncan Multiple Range Test. The results were considered significant at the probability level ≤ 0.05 , using SAS's statistical program (Asker et al., 2021).

RESULTS AND DISCUSSION

Nowadays, the Iraqi environment can be considered a dangerous source of psychological and physiological impact on a person's health due to traffic chaos and the high intensity of electric generators. Noise is sonic waves that are transferred as electro-signals into the neurofibrils. The signals reach the cortex agitating its cells. Due to this agitation, such signals are passed to the Autonomic Nervous System, causing a malfunction of the Endocrine glands. Consequently, hormones of Adrenaline, Noradrenalin, Cortisol, and Growth are raised (Brink et al., 2019). The study area's noise level is 94.8dB at some locations and 92.5dB at other locations.

The Noise Effect on the Hearing Sense

The continuous directed exposure to certain force sound waves can reduce the ability to hear or cause the deaf. The high intensity of sound can cause damage to the nerve cells of the

inner ear. Consequently, the nerve cells are gradually eroded, and the exposed person will be deaf. The noise in such sites is an influential impact on workers' health and performance. Psychological disturbances can be suffered as it distracts minds, and causes distress, dissatisfaction, increased nervousness, and sensitivity. The noise can also cause gradual damage in the eardrums, causing hard pain for the worker (Evandt et al., 2017; Gori et al., 2014; Oguntunde et al., 2019). The workers in the study area are suffering psychological tension due to the high noise. In addition, the immune system can be affected, leading to less protection to the body, including the middle ear causing buzzing and deafness. The impact of noise levels at 85,120-90 and < 100dB is caused by hearing loss (gradually), disturbances, and torturous pain in the eardrum, respectively (Esch et al., 2002; Sohrabi & Khreis, 2020). Researchers have found that among five workers working in high noise factories, one suffered from hearing loss. The sudden noise from severe explosions greater than 140dB could also cause heart problems in heart patients (Maschke et al., 2002).

The generators' sites' noise intensity is measured to be 94.8 and 92.5dB, which lies at the level of 90-120dB. There are many effects noted depending on the noise intensity. Although 40% of the tested workers do not suffer from any impacts, 60% suffer from discomfort and slight disturbances, 30% suffer from severe hearing problems. Therefore, severe hearing problems have been shown that those with severe Hypacusis are 40%, and an acute Hypacusis is 56.66%, while complete deafness is 3.33%, as in Figure 1.

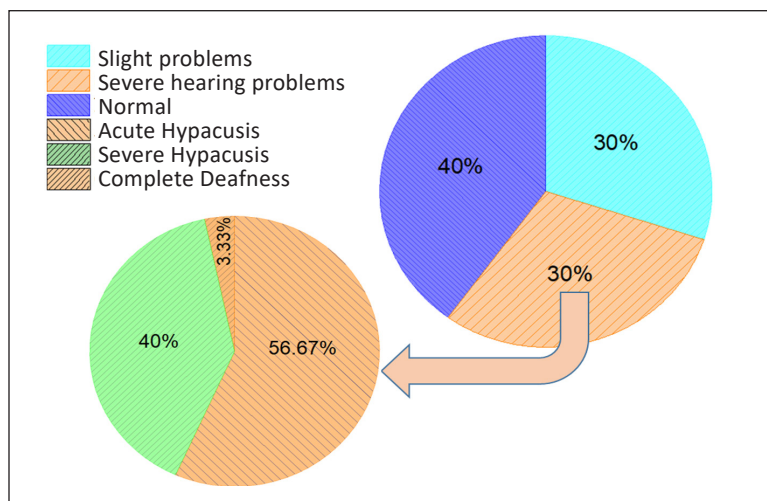


Figure 1. Percentage of people with hearing problems

The Noise Effect on Blood Pressure and the Number of Heartbeats

As shown in Figure 2, the operators working in such sites who suffer from high blood pressure were 40%, and the rate of the heartbeats increased to 41%. In the places where workers are exposed to high noises, the risk of heart disease has increased due to the

increased tension that causes the release of Cortisol hormones, changes in the heart rate, and the widening of blood arteries. Consequently, there is a relationship between exposure to noise, high blood pressure, and heart function disorders. In addition, exposure to a high-sudden noise could cause several physiological reactions within the human body, including adrenaline secretion, high blood pressure, increased heart beating rate, and breathing rate. Previous studies in this field found that workers exposed to noise ranging from 90-100dB per day suffer from high blood pressure (Dzhambov & Dimitrova, 2017; Gori et al., 2014; van Kempen et al., 2018).

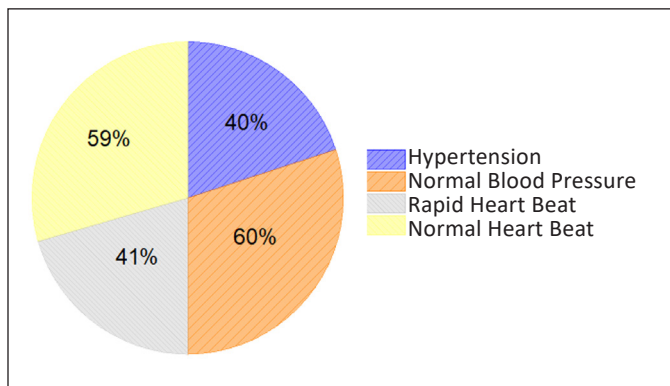


Figure 2. Impact of noise level on the heartbeat (mm Hg) and hypertension (bpm)

The Noise Effect on Hb, PCV and RBCs

The results shown in Table 2 illustrated the concentrations of these variables changes in operators' blood according to the noise levels. For example, Hb highest concentration reaches 16.12 ± 0.74 according to the noise intensity of 94.8dB, while the lowest concentration of Hb was about 15.72 ± 0.9 at 92.5dB. In comparison, PCV ranges from 12.41 to 9.28% at different noise levels 94.8 and 92.5dB. On the other hand, RBCs reached 5.82 ± 0.2 and 5.67 ± 0.28 at 92.5 and 94.8dB, respectively. Besides the relationship between the noise level and the period work, the first group (15 years) showed the highest increase in Hb reached 13.67% compared to their values in the second group's blood (10 years), 0.7%. Thus, the workers are exposed to noise at different levels, with increasing of the working periods affects the production of red blood cells, leading to changes in the blood components, which usually causes injury (Dongre et al., 2011; Le & Hattingh, 1983).

The Noise Effect on WBCs and PLT

Table 2 shows that the number of WBCs and PLT showed a significant increase compared to the control groups. The highest values reach 8.38 ± 1.5 and 207.75 ± 37.73 at 94.8dB, while the lowest values reach 7.67 ± 0.36 and 165.75 ± 16.37 at 92.5dB, respectively. However, the control group's values were (5.87 ± 0.07) and (137.5 ± 3.23) . Regarding the periods

of exposure, the first group showed the highest values at 8.72 ± 0.68 and 211.75 ± 36.34 compared to the second group that reaches 7.3 ± 0.7 and 161.75 ± 15.77 . Working with a high noise level of more than 70dB for more than 8 hours per day affects the immune system's functions and thus increases WBCs, especially lymphatic ones. In addition, exposure to noise leads to changes in the blood components and, eventually, grows PLT that occurs in response to the effort caused by bulging blood cells (Brook & Rajagopalan, 2009; Xiao et al., 2016).

Table 2
Impact of noise level and work-years on some blood components

Parameter		Noise level (94.8)dB	Noise level (92.5)dB	Working years (15)	Working years (10)	Control
Hb g/dl	Av \pm St error	16.12 \pm 0.74	15.72 \pm 0.9	16.65 \pm 0.75*	14.4 \pm 0.6	14.07 \pm 0.20*
	Con %	114.57	111.72	114.57	102.34	100
	Increase%	14.57	11.72	14.57	2.34	-
PCV %	Av \pm St error	48.45 \pm 2.22	47.1 \pm 2.71	49.42 \pm 2.27	46.2 \pm 1.8	43.1 \pm 0.21
	Number%	112.41	109.28	114.66	107.19	100
	Increase%	12.41	9.28	14.66	7.19	-
RBCs *10 ⁶ /mm ³	Av \pm St error	5.82 \pm 0.2*	5.67 \pm 0.28	5.72 \pm 0.12*	5.16 \pm 0.4	5.12 \pm 0.13*
	Number%	113.67	110.74	111.71	100.78	100
	Increase%	13.67	10.74	11.71	0.78	-
WBC cells per μ l	Av \pm St error	8.38 \pm 1.5*	7.67 \pm 0.36	8.72 \pm 0.68*	7.3 \pm 0.7	5.87 \pm 0.07*
	Number%	142.75	130.66	148.55	124.36	100
	Increase%	42.75	30.66	48.55	24.36	-
PLT *10 ³ /mm ³	Av \pm St error	207.75 \pm 37.73	165.75 \pm 16.37	211.75 \pm 36.34	161.75 \pm 15.77	137.5 \pm 3.22
	Number%	151.09	120.54	154	117.63	100
	Decrease%	51.09	20.54	54	17.63	-
Bilirubin (mg/dl)		2.60 \pm 0.27	2.27 \pm 0.16*	2.33 \pm 0.17*	2.37 \pm 0.19	2.82 \pm 0.13*
Total Bilirubin (mg/dl)		1.11 \pm 0.27*	0.75 \pm 0.24	1.07 \pm 0.42*	0.77 \pm 0.24	0.73 \pm 0.01*
Conjugated Bilirubin (mg/dl)		0.59 \pm 0.15	0.29 \pm 0.11	0.50 \pm 0.12	0.47 \pm 0.17	0.17 \pm 0.04
Unconjugated Bilirubin (mg/dl)		0.40 \pm 0.20	0.33 \pm 0.12	0.55 \pm 0.18	0.26 \pm 0.12	0.24 \pm 0.06

The Noise Effect on TP and Urea

As shown in Table 3, the results revealed that TP concentrations decrease at different noise intensity levels compared to the control group. Urea concentrations showed an increase in serum of operators compared to the control group. The decrease in TP is 10.24% and 14.5%, according to the noise levels 94.8 and 92.5dB, respectively. The highest urea concentration reached 55.1 ± 0.65 at 94.8dB compared to the lowest concentration of 39.5 ± 0.06 at 92.5dB. Many environmental pollutants, including noise pollution, affect the formation of proteins in the liver, which is one of the liver's most critical functions. The amino acids are

necessary for the formation of proteins, as any defect in this member's work will negatively affect the process of protein formation. Therefore, lower concentrations, which in turn will increase the level of urea as a final product of the amino acid metabolism (Allouche et al., 2011; Anetor et al., 2009; Oiamo et al., 2015).

The Noise Effect on Concentrations of FBS, ALB, and Cholesterol

According to the results, as shown in Table 3, it was found out that the glucose and albumin concentrations increased based on the noise intensity. The highest values reached 13.21 and 9.25% at a noise intensity of 94.8dB. Meanwhile, there was an increase in FBS and ALB concentrations, reaching 21.26 and 2.5%, respectively. Regarding the effect periods work, the first group increased 45.11 and 8.75% compared to the second group, 14.39 and 3.5%. In this field, previous studies have proved that noise exposure has many physiological reactions in humans, including an imbalance in the regulation of the composition of carbohydrates and the effects on the glucose levels in the blood. Therefore, patients with diabetes respond with more sensitivity than others to such noise pollutions (Roswall et al., 2018). At the same time, the cholesterol concentrations have reached the highest values, 16.8%, at a noise level of 94.8dB, as shown in Table 3. The noise levels at 92.5dB showed an increase in cholesterol concentrations in the operators' serum, reaching 5.57%. Concerning the work duration, the first group revealed an increased rate of 13.40 % compared to the second group, 8.20%. The noise pollution resulting from the noises of the various engines caused a high concentration of fat in the serum. This rise has a relationship with some factors, including exposure to noise of different levels and exposure to industrial pollutants (Yeatts et al., 2007).

The Noise Effect on Concentrations of Total Bilirubin and Conjugated Bilirubin

The results shown in Table 3 reported a clear rise in the concentrations of total bilirubin and conjugated bilirubin in the serum of operators exposed to different levels of severity of noise in comparison to the control group. The rise in bilirubin concentrations reached 1.11 ± 0.27 and 0.75 ± 0.24 , according to the different noise intensities 94.8 and 92.5dB compared to the control group (0.73 ± 0.01). Whereas the conjugated bilirubin reached the highest concentration of 0.59 ± 0.15 at 94.8dB. Whilst, the lowest concentration reached 0.29 ± 0.11 at 92.5dB compared to the control group (0.17 ± 0.04). This increase results from the malfunction that affects the liver and leads to a lack of the liver's ability to secrete bilirubin which clogs the bile ducts and the disease known as hepatic jaundice (Arjunan & Rajan, 2020).

Table 3
Impact of noise level and work-years on some of the biochemical variables

Parameter		Noise level (94.8)dB	Noise level (92.5)dB	Working years (15)	Working years (10)	Control
T.P g/dl	Av ± St error	6.75±0.14	6.43±0.46*	6.75±0.42	6.44±0.22*	7.52±0.15*
	Concentration%	89.76	85.50	89.76	85.63	100
	Decrease %	-10.24	-14.5	-10.24	-14.37	-
Urea mg/dl	Av ± St error	55.1±0.65*	39.5±0.06	50.8±0.84	41.0±0.34	36.5±0.22*
	Concentration%	150.95	108.21	139.17	112.32	100
	Increase %	50.95	8.21	39.17	12.32	-
F.B.S mg/dl	Av ± St error	72.3±6.7	67.5±3.23	86.52±10.1	68.2±4.8	59.62±18.7
	Concentration%	121.26	113.21	145.11	114.39	100
	Increase %	21.26	13.21	45.11	14.39	-
Alb g/dl	Av ± St error	4.37±0.17	4.10±0.59	4.35±0.48	4.14±0.4	4.00±0.9
	Concentration%	109.25	102.50	108.75	103.5	100
	Increase %	9.25	2.50	8.75	3.5	-
Total Cholesterol mg/dl	Av ± St error	183.87 ±25.87	167.5 ±23.1	179.75 ±24.16*	171.5 ±11.92*	158.5 ±0.64*
	Concentration%	116	105.67	113.40	108.20	100
	Increase %	16	5.67	13.40	8.20	-

The Effect of Noise on the Functions of the Kidney

Figure 3 indicates urine analysis for the operators, which shows different types of cells in the urine. The Pus cells revealed the highest percentage of 35% then, the RBCs were 30%, the Epith cells were 20%, and finally, the crystals were 15%. Exposure to successive and high sounds leads to changes in the body systems. It affects the kidney structure, causing the penetration of proteins from blood to urine through the kidney's glomeruli. Consequently, this situation created signs of imbalance in the kidney's functionality lead to observing these different types of cells in the urine (Farong et al., 2018). However, causing much disorder

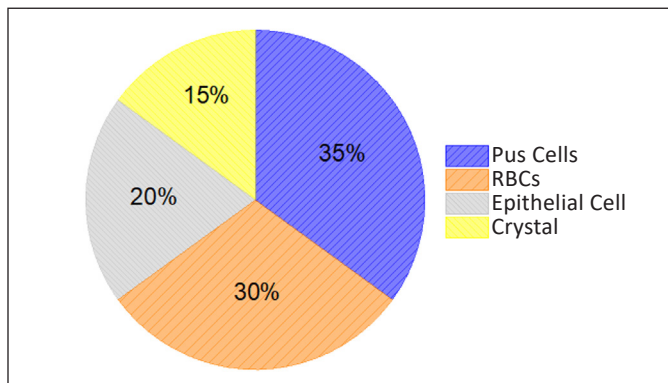


Figure 3. The percentage of various cells in the urine

and abnormal impacts in the human body are related to this type of noise pollution, which is the response to the physiological damage-causing sediment of many kinds of stuff in the urinary tracts, thereby increasing the possibility of salt sediments in the urinary tracts especially in the case of ureter and bladder inflammation. The workers in such places do not have good personal hygiene habits and are not committed to stopping eating protein or meat. Also, the workers do not regularly visit doctors and medical centres.

CONCLUSION

Previously, it has not been directly addressed such this type of pollution caused by (random distributed backup electrical generators) in the Middle East. Therefore, this study can be considered the first to highlight such pollution, which can cause severe health conditions after long-term exposure. The exposure of these noise sources leads to significant differences in some blood parameters (Hb, RBCs, WBCs, PLT, PCV, TP, ALB, FBS, Bilirubin, Blood Urea, and Cholesterol. It was confirmed by comparing the control group results with those of the exposed group (workers). The noise intensity of the measured sites has reached 94.8 and 92.5dB. The first noise level, 94.8dB, showed a higher effect than the second level, 92.5dB. The operators exposed to the noise for 15 years are affected more than those with less exposure time (10 years). Therefore, it is recommended that workers take precautionary measures in the workplace (the backup electrical generators), including temporary work that involves various employment conditions, i.e. on-call and seasonal work.

ACKNOWLEDGEMENTS

The authors wish to express their gratitude to the College of Sciences at the University of Mosul for their unwavering support throughout this research project.

REFERENCES

- Adimalla, N., Qian, H., Nandan, M. J., & Hursthouse, A. S. (2020). Potentially toxic elements (PTEs) pollution in surface soils in a typical urban region of south India: An application of health risk assessment and distribution pattern. *Ecotoxicology and Environmental Safety*, 203(126), Article 111055. <https://doi.org/10.1016/j.ecoenv.2020.111055>
- Allouche, L., Hamadouche, M., Touabti, A., & Kennouf, S. (2011). Effect of long-term exposure to low or moderate lead concentrations on growth, lipid profile and liver function in albino rats. *Advances in Biological Research*, 5(6), 339-347.
- Amoatey, P., Omidvarbona, H., Baawain, M. S., Al-Mayahi, A., Al-Mamun, A., & Al-Harthy, I. (2020). Exposure assessment to road traffic noise levels and health effects in an arid urban area. *Environmental Science and Pollution Research*, 27(28), 35051-35064. <https://doi.org/10.1007/s11356-020-09785-y>

- Anetor, J. I., Yaqub, S. A., Anetor, G. O., Nsonwu, A. C., Adeniyi, F. A. A., & Fukushima, S. (2009). Mixed chemical-induced oxidative stress in occupational exposure in Nigerians. *African Journal of Biotechnology*, 8(5), 821-826. <https://doi.org/10.4314/ajb.v8i5.59972>
- Arjunan, A., & Rajan, R. (2020). Noise and brain. *Physiology and Behavior*, 227(July), Article 113136. <https://doi.org/10.1016/j.physbeh.2020.113136>
- Arneson, W. L., & Brickell, J. M. (2007). *Clinical Chemistry: A laboratory perspective*. F.A. Davis Company.
- Ashmore, M. R., & Dimitroulopoulou, C. (2009). Personal exposure of children to air pollution. *Atmospheric Environment*, 43(1), 128-141. <https://doi.org/10.1016/j.atmosenv.2008.09.024>
- Asker, A. S., Tawfeeq, A. A., Alhamdani, H. A. A. A., & Alhamdani, A. A. (2021). Effect of addition of ginger (*Zingiber officinale*) and vitamin E on level of cortisol, ADA enzyme and liver enzymes in Awassi ewes. *IOP Conference Series: Earth and Environmental Science*, 761(1), Article 012087. <https://doi.org/10.1088/1755-1315/761/1/012087>
- Brink, M., Schäffer, B., Vienneau, D., Foraster, M., Pieren, R., Eze, I. C., Cajochen, C., Probst-Hensch, N., Röösli, M., & Wunderli, J. M. (2019). A survey on exposure-response relationships for road, rail, and aircraft noise annoyance: Differences between continuous and intermittent noise. *Environment International*, 125(February), 277-290. <https://doi.org/10.1016/j.envint.2019.01.043>
- Brook, R. D., & Rajagopalan, S. (2009). Particulate matter, air pollution, and blood pressure. *Journal of the American Society of Hypertension*, 3(5), 332-350. <https://doi.org/10.1016/j.jash.2009.08.005>
- Brunze, N. A. (2016). *Fundamentals of urine and body fluid analysis-e-book* (4th Ed.). Elsevier.
- Cuesta, M., & Cobo, P. (2000). Active control of the exhaust noise radiated by an enclosed generator. *Applied Acoustics*, 61(1), 83-94. [https://doi.org/10.1016/S0003-682X\(99\)00062-6](https://doi.org/10.1016/S0003-682X(99)00062-6)
- Dongre, N. N., Suryakar, A. N., Patil, A. J., Ambekar, J. G., & Rathi, D. B. (2011). Biochemical effects of lead exposure on systolic & diastolic blood pressure, heme biosynthesis and hematological parameters in automobile workers of North Karnataka (India). *Indian Journal of Clinical Biochemistry*, 26(4), 400-406. <https://doi.org/10.1007/s12291-011-0159-6>
- Dzhambov, A. M., & Dimitrova, D. D. (2016). Exposure-response relationship between traffic noise and the risk of stroke : A systematic review with meta-analysis. *Arhiv za higijenu rada i toksikologiju*, 67(2), 136-151.
- Dzhambov, A. M., & Dimitrova, D. D. (2017). Crossmark. *Environmental Research*, 152(August 2016), 244-255. <https://doi.org/10.1016/j.envres.2016.10.024>
- Dzhambov, A. M., Dimitrova, D. D., & Mihaylova-alakidi, V. K. (2016). Public health: Burden of sleep disturbance due to traffic noise in Bulgaria. *Folia Medica*, 57(3/4), 264-269. <https://doi.org/10.1515/folmed-2015-0049>
- Eduardo, P., Fiedler, K., Henrique, P., & Zannin, T. (2015). Evaluation of noise pollution in urban traffic hubs - Noise maps and measurements. *Environmental Impact Assessment Review*, 51, 1-9. <https://doi.org/10.1016/j.eiar.2014.09.014>
- Esch, T., Stefano, G. B., Fricchione, G. L., & Benson, H. (2002). Stress in cardiovascular diseases. *Medical Science Monitor*, 8(5), RA93-RA101.

- Evandt, J., Oftedal, B., Krog, N. H., Skurtveit, S., Nafstad, P., Schwarze, P. E., Skovlund, E., Houthuijs, D., & Aasvang, G. M. (2017). Road traffic noise and registry based use of sleep medication. *Environmental Health*, 16(1), 1-12. <https://doi.org/10.1186/s12940-017-0330-5>
- Farong, Y., Xin, Y., Zuoping, L., Xiuzhen, L., Mingren, X., & Denglou, L. (2018). Effects of noise pollution on functions of the liver and kidney of rats. *Meteorological and Environmental Research*, 9(4), 41-43. <https://doi.org/10.19547/j.issn2152-3940.2018.04.010>
- Flies, E. J., Mavoa, S., Zosky, G. R., Mantzioris, E., Williams, C., Eri, R., Brook, B. W., & Buettel, J. C. (2019). Urban-associated diseases: Candidate diseases, environmental risk factors, and a path forward. *Environment International*, 133(October), Article 105187. <https://doi.org/10.1016/j.envint.2019.105187>
- Gori, T., Babisch, W., Basner, M., & Mu, T. (2014). Cardiovascular effects of environmental noise exposure. *European Heart Journal*, 35(13), 829-836. <https://doi.org/10.1093/eurheartj/ehu030>
- Hussien, B. M., Rabeaa, M. A., & Farhan, M. M. (2020). Characterization and behavior of hydrogen sulfide plumes released from active sulfide-tar springs, Hit-Iraq. *Atmospheric Pollution Research*, 11(5), 894-902. <https://doi.org/10.1016/j.apr.2020.02.001>
- Ibhadode, O., Tenebe, I. T., Emenike, P. C., Adesina, O. S., Okougha, A. F., & Aitanke, F. O. (2018). Assessment of noise-levels of generator-sets in seven cities of South-Southern Nigeria. *African Journal of Science, Technology, Innovation and Development*, 10(2), 125-135. <https://doi.org/10.1080/20421338.2017.1400711>
- Jadaan, K. S., Msallam, M., & Abu-Shanab, D. A. (2016). The impact of road traffic noise on hospital workers. *Indian Journal of Science and Technology*, 9(1), 1-8. <https://doi.org/10.17485/ijst/2016/v9i1/79259>
- Le, F., & Hattingh, J. (1983). Comparative haematology of some South African birds. *Comparative Biochemistry and Physiology - Part A: Physiology*, 74(2), 443-448. [https://doi.org/10.1016/0300-9629\(83\)90628-X](https://doi.org/10.1016/0300-9629(83)90628-X)
- Maschke, C., Harder, J., Ising, H., Hecht, K., & Thierfelder, W. (2002). Stress hormone changes in persons exposed to simulated night noise. *Noise Health*, 5(17), 35-45. <https://doi.org/https://www.noiseandhealth.org/text.asp?2002/5/17/35/31836>
- Mohammed, M. I., Yousif, S. W., & Rabeaa, M. A. (2020). Physiological and biochemical changes analysis to labors blood samples in plastics recycling factory in Mosul-Iraq. *Journal of Global Pharma Technology*, 10(06), 281-288.
- Oguntunde, P. E., Okagbue, H. I., Oguntunde, O. A., & Odetunmibi, O. O. (2019). A study of noise pollution measurements and possible effects on public health in Ota Metropolis, Nigeria. *Open Access Macedonian Journal of Medical Sciences*, 7(8), 1391-1395. <https://doi.org/10.3889/oamjms.2019.234>
- Oiamo, T. H., Luginaah, I. N., & Baxter, J. (2015). Cumulative effects of noise and odour annoyances on environmental and health related quality of life. *Social Science & Medicine*, 146, 191-203. <https://doi.org/10.1016/j.socscimed.2015.10.043>
- Parvathi, K., & Navaneetha Gopalakrishnan, A. (2003, December 15-17). Studies on control of noise from portable power generator. In *Proceedings of the Third International Conference on Environment and Health, Chennai, India* (pp. 328-338). Chennai, India.

- Paull, N., Krix, D., Torpy, F., & Irga, P. (2020). Can Green Walls Reduce Outdoor Ambient Particulate Matter, Noise Pollution and Temperature? *International Journal of Environmental Research and Public Health*, *17*(14), Article 5084. <https://doi.org/10.3390/ijerph17145084>
- Richmond, W. (1973). Preparation and properties of a cholesterol oxidase from *Nocardia* sp. and its application to the enzymatic assay of total cholesterol in serum. *Clinical Chemistry*, *19*(12), 1350-1356. <https://doi.org/10.1093/clinchem/19.12.1350>
- Roswall, N., Raaschou-nielsen, O., Solvang, S., & Tjønneland, A. (2018). Long-term exposure to residential railway and road traffic noise and risk for diabetes in a Danish cohort. *Environmental Research*, *160*(August 2017), 292-297. <https://doi.org/10.1016/j.envres.2017.10.008>
- Sohrabi, S., & Khreis, H. (2020). Burden of disease from transportation noise and motor vehicle crashes: Analysis of data from Houston, Texas. *Environment International*, *136*(February), Article 105520. <https://doi.org/10.1016/j.envint.2020.105520>
- Sygná, K., Marit, G., Aamodt, G., Oftedal, B., & Hjertager, N. (2014). Road traffic noise, sleep and mental health. *Environmental Research*, *131*, 17-24. <https://doi.org/10.1016/j.envres.2014.02.010>
- van Kempen, E., Casas, M., Pershagen, G., & Foraster, M. (2018). WHO environmental noise guidelines for the European region: A systematic review on environmental noise and cardiovascular and metabolic effects : A summary. *International Journal of Environmental Research and Public Health*, *15*(2), Article 379. <https://doi.org/10.3390/ijerph15020379>
- Vladimir, M., & Madalina, C. (2019). Optimizing urban landscapes in regard to noise pollution. *Procedia Manufacturing*, *32*, 161-166. <https://doi.org/10.1016/j.promfg.2019.02.197>
- WHO. (2011). *Burden of disease from environmental noise*. World Health Organization.
- Xiao, J., Li, X., & Zhang, Z. (2016). Daly-based health risk assessment of construction noise in Beijing, China. *International Journal of Environmental Research and Public Health*, *13*(11), Article 1045. <https://doi.org/10.3390/ijerph13111045>
- Yeatts, K., Svendsen, E., Creason, J., Alexis, N., Herbst, M., Scott, J., Kupper, L., Williams, R., Neas, L., Cascio, W., Devlin, R. B., & Peden, D. B. (2007). Coarse particulate matter (PM_{2.5-10}) affects heart rate variability, blood lipids, and circulating eosinophils in adults with asthma. *Environmental Health Perspectives*, *115*(5), 709-714. <https://doi.org/10.1289/ehp.9499>



The Demand Model of App-Based Transportation Household Scale in Semarang, Indonesia

Anita Ratnasari Rakhmatulloh^{1*}, Diah Intan Kusumo Dewi¹, Wijayanti² and Rosna Sari Pulungan¹

¹Department of Urban and Regional Planning, Faculty of Engineering, Diponegoro University, Semarang, Prof. Soedarto, Tembalang, Semarang 50275, Central Java, Indonesia

²Department of Architecture, Faculty of Engineering, Diponegoro University, Semarang, Prof. Soedarto, Tembalang, Semarang 50275, Central Java, Indonesia

ABSTRACT

In the development of transportation systems, Application-Based Transportation is an innovation to adapt to technological advances. It offers users an alternative mode that is cheap, easy, and flexible according to their needs. The Application-based travel demands can be seen from its socio-economic and travel characteristics. In Indonesia, previous studies have concentrated on study areas on a city scale, with diverse land use classifications not only on the residential area which is the most users of app-based transportation. The modelling results in this study were obtained from spatial simulation and partial linear regression analysis with the T-test as the final stage of analysis. As a result, demand for App-Based Transportation is affected by two factors which include age and travel costs. They are inversely proportional to the frequency of travel. In this case, this mode is mostly used by the population with young age and low cost of travel. Also, this mode is only used on short-distance trips and trips during rush hour in the morning. During the afternoon rush hour, the trip is transferred to public transportation, which has a lower cost. Therefore,

this study aims to determine the application-based transportation demand model for household units in Tlogosari, Semarang, Indonesia. An additional in-depth study is needed to be carried out on the degree of motorcycle safety to improve services.

ARTICLE INFO

Article history:

Received: 30 March 2021

Accepted: 05 August 2021

Published: 18 October 2021

DOI: <https://doi.org/10.47836/pjst.29.4.25>

E-mail addresses:

anita.ratnasari.r@gmail.com (Anita Ratnasari Rakhmatulloh)

diah.intan@pwk.undip.ac.id (Diah Intan Kusumo Dewi)

wijayanti_jaft@yahoo.co.id (Wijayanti)

onapulungan@gmail.com (Rosna Sari Pulungan)

* Corresponding author

Keywords: App-based transportation, demand, household unit

INTRODUCTION

For convenience and flexibility, the significant growth of the urban population has been accompanied by an increase in the number of private vehicle use. High mobility has led to various environmental problems such as congestion, air pollution, lack of parking space, high accident rates, and excessive energy consumption (Zhao et al., 2018). In developing countries such as Indonesia, public transportation tends to be inefficient in cost and time (Rithoma & Rakhmatulloh, 2013). This condition was also supported by Jaśkiewicz and Besta (2014), who discovered that public transportation is not optimal due to various factors. It includes travel time, inadequate cleanliness, access, travel safety, and less than optimal driver ability. In addition, public transportation is considered difficult to access due to its location, which tends to be far from the user's home (Cheng & Chen, 2015).

As a result of the industrial revolution 4.0 and the development of technology, App-Based Transportation was developed to solve increasingly massive personal use and less optimal quality of service for public transportation modes. The implementation of an app-based transportation model connects motorists and drivers using only the applications on smartphones. Furthermore, the development of App-Based Transportation in the world is often referred to as "ridesharing" or "peer-to-peer mobility" with the concept of sharing rides with the same destination. However, this term is considered inappropriate with the development of technology and science. The driver and passenger do not share the same destination, but the driver provides a service similar to a limousine or taxi (Regina & Clewlow, 2018). In 2013, California Public Utilities officially terminated the service as Transportation Network Companies (TNCs), recently referred to as "ride-hailing." Also, the term ridesourcing is an app-based transportation system that provides transportation services on demand with higher reliability and less waiting time (Rayle et al., 2014). The number of terms that appear implementing application-based transportation modes has led to a misperception of implementing the concept in various countries. Furthermore, the same source stated that it could replace private and complement public transportation in reaching areas it cannot serve. The App-Based Transportation services were also chosen due to the reduced waiting time with a door-to-door system. It is cheaper, faster, and require half the waiting time compared to traditional taxi services (Smart et al., 2015; Hou et al., 2016; Anderson, 2014). Also, this service is trackable; therefore, it is advantageous compared to other modes because it reduces parking demand, improves driver welfare by providing new jobs, and affects user travel patterns and travel destinations (Henao, 2017).

Like other modes of transportation, App-Based Transportation relies heavily on user demand characteristics to provide its services. Furthermore, socio-economic characteristics and user movement patterns influence these requests. Age is one of the socio-economic factors that most influence the travel demand for users of App-Based Transportation modes (Efthymiou et al., 2013). Meanwhile, Rayle et al. (2014) stated that parents tend not to be

adept at using technology. Therefore, the ability to use App-Based Transportation services such as ridesourcing decreases with age. Apart from age, Shaheen et al. (2016) discovered that employment status is the next factor most influences App-Based Transportation modes. Furthermore, work activities and the implications for the income generated will influence a person to use App-Based Transportation modes. According to Lavieri et al. (2018), a person with low income tends not to use App-Based Transportation services due to the consideration of travel costs. On the other hand, a person with high and middle income tends to use these services. Also, it was discovered that most users do not own private vehicles, forcing them to choose App-Based Transportation modes as their daily mobility mode. Meanwhile, Lekshmi et al. (2016) identified the five variables that most significantly influence the choice of these modes. It includes age, income, vehicle ownership, travel time, and travel costs.

In addition to the socio-economic factors, users' travel demand trends can also be seen based on movement patterns such as travel destinations. Users often use it for social/recreational activities, including going to bars, restaurants and concerts, and family and friends gatherings (Rayle et al., 2014). It is also the case in Slovakia, which shows that the average travel time spent on recreational purposes is more significant than travelling for work or other activities (Šimeček, 2019). According to Lavieri et al. (2018), areas with a high density, such as residential areas, are the origin of App-Based Transportation users. Furthermore, land use should be considered as one of the factors that make a person travel. Generally, it can be concluded that age, gender, vehicle ownership, travel time, travel costs, employment status, income, vehicle ownership, and purpose of travel are some of the variables that affect the demand for App-Based Transportation trips (Rayle et al., 2014; Lekshmi et al., 2016; Shaheen et al., 2016; Efthymiou et al., 2013; Lavieri et al., 2018).

Based on Figure 1, the application of App-Based Transportation in the Southeast Asia region commenced in 2010 with the presence of Gojek in Indonesia. Furthermore, this has continued to increase since 2013 in various countries and systems. For example, Grab in Malaysia, the Philippines, Cambodia, Gotaxi in Myanmar, Viviantaxi in Laos, and Comfortdelgro in Vietnam (Phun et al., 2018). For example, in Malaysia, application-based transportation is dominated by cars with a ride-sharing system to alleviate traffic congestion. The availability of transportation rules also has a significant impact. App-Based Transportation in Malaysia only reaches a few cities, such as Johor Bahru, Kuala Lumpur, Kinabalu City, Penang, and Melaka (GrabCarMalaysia, 2018). The study carried out by Sakaran et al. (2018) used socio-economic factors such as gender, age, and monthly income to identify an App-Based Transportation demand model in Kinabalu City, Malaysia. The results showed that the demand for App-Based Transportation in Kinabalu City was dominated by female residents aged 30 years with lower middle income. Meanwhile, the study carried out by Adam et al. (2020) in the City of Penang and Bayan Lepas, Penang

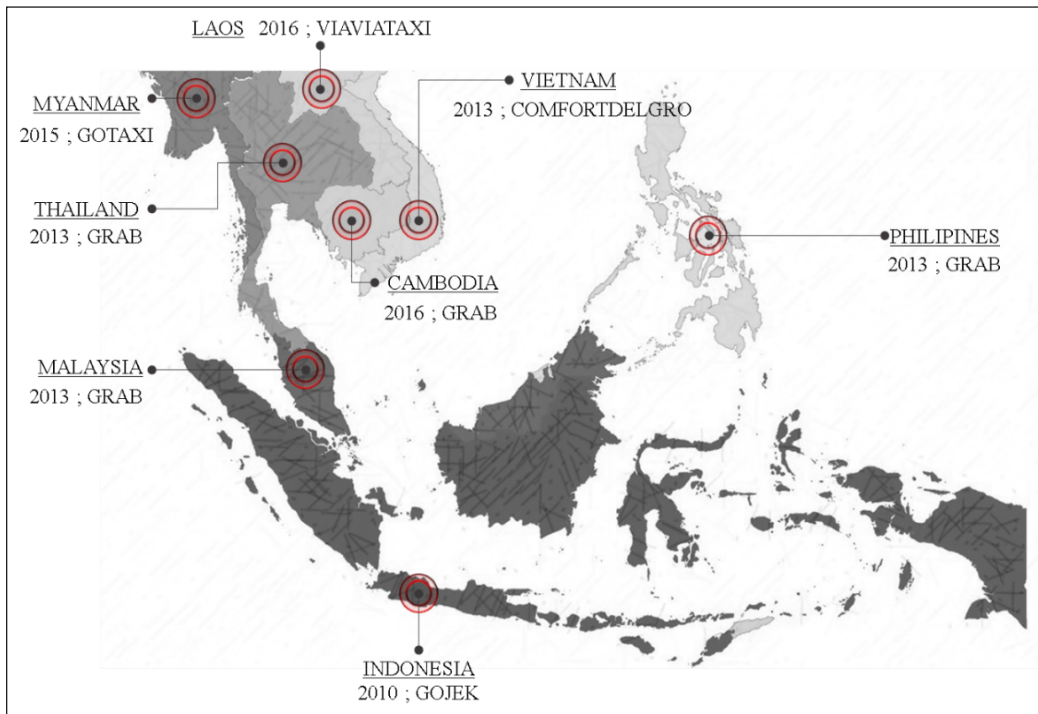


Figure 1. Application of App-Based Transportation in Southeast Asian countries

showed that factors that influence App-Based Transportation demand are user age, gender, and vehicle ownership. With the dominance of 21 to 30 years and women, most are not private vehicles owners.

The embryo for the growth of App-Based Transportation in Indonesia commenced with the existence of Uber Taxi. However, along with technological developments and society's current needs, the existence of Uber Taxi has been displaced by Gojek and Grab platforms (Ristantia & Hayah, 2018). Figure 1 shows that the Gojek application has been operating since 2010. However, the on-demand system commenced operating in 2015. Meanwhile, Grab commenced operating in Indonesia in 2014. These two platforms are growing, wherein in 2018, Gojek and Grab had served 62 districts/cities and approximately 100 districts/cities, respectively. As of December 2017, the Grab and Gojek application services users reached 9.7 million (Bohang, 2017). In Indonesia, Semarang City is one of the cities with the highest internet usage, with an average contribution of 64% of usage per year and 93% of the population using smartphones to access the internet network (Sukma, 2016). That has become one of the factors that have influenced the rapid increase in App-Based transportation modes in the city of Semarang in the last quinquennium. Unlike what happened in Kinabalu City, Malaysia, App-Based Transportation in the city of Semarang mostly uses motorbikes, which often leads to problems such as congestion. Furthermore,

the use of technology in its operation causes the App-Based Transportation mode to depend heavily on user demands related to a person's characteristics and needs.

The concept of App-Based Transportation mode procurement has the advantage of reducing transportation costs, reducing fuel consumption, minimising air pollution, and reducing congestion provided that the user demand is well controlled (Morency, 2007; Caulfield, 2009; Chan & Shaheen, 2012). Furthermore, the household unit is one of the smallest areas that determine the travel demand characteristics of transportation modes users in more detail. However, most study on App-Based Transportation demand characteristics, especially in Indonesia, is still limited to a regional or city scale, leading to more generalised characteristics. Therefore, this study aims to select the analysis area to the household level to obtain a demand model with more specific characteristics towards App-Based Transportation modes, especially in Semarang. Moreover, this study question that needs to be answered in this case is what factors affect the travel demand of users of household-scale application-based transportation modes in the Tlogosari Household Semarang, user characteristics (gender, age, income, vehicle ownership, typo of work) and travel characteristics (purpose of trip, mode choice, travel time, travel distance, cost).

METHODOLOGY

Semarang Study Area

App-Based Transportation usually only focuses on service targets in massive downtown areas in economic activity (Hall & Krueger, 2016). However, the growing demand for community movement has led to this service reaching more suburbs on a smaller scale, such as households. Previous studies have been dominated by observations of App-Based Transportation service demand models on a larger scale including cities to countries. Therefore, it is necessary to obtain a smaller study scope, such as households that need to be carried out to pay attention to the community's need for more detailed transportation. For example, Figure 2 shows that Semarang City is one of the cities in Indonesia that dominates land use in the form of settlements. Therefore, the basis for using this transportation application serves many household units and the surrounding area. Furthermore, Tlogosari Household is a form of household unit in Semarang with a dense activity every day in an area and a high-density level. Therefore, the intensity of the movement is relatively high. It was supported by Lavieri et al. (2018) that areas with a high density, such as residential areas, are the origin of App-Based Transportation services.

Since 1986, this housing has been built by the Government of Indonesia and implemented by Perum Perumnas Regional V. This was a form of providing justice-based housing, especially for the middle to lower class. The housing with 170.74 hectares was included in Muktiharjo Kidul and Tlogosari Kulon Village, Pedurungan District, Semarang City, Central Java, Indonesia, which can be seen in Figure 2. Based on the data obtained

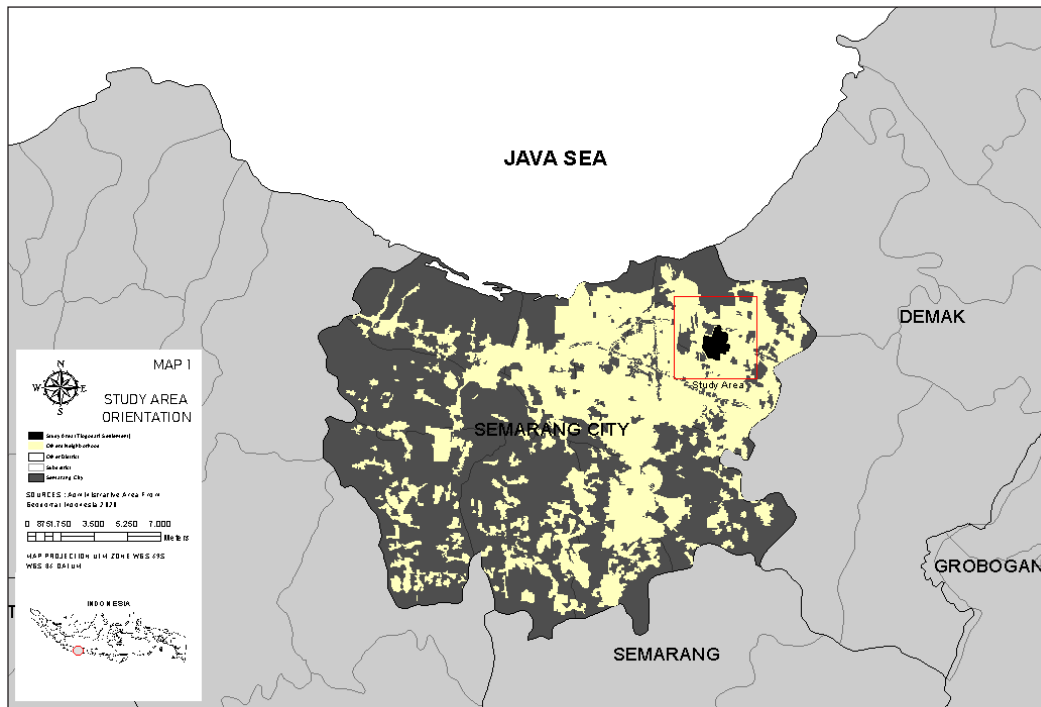


Figure 2. Study area orientation of Tlogosari Household

from the field survey, there are 9,598 and 7,445 Heads of Families in Tlogosari Kulon and Muktiharjo Kidul District, respectively. Furthermore, both districts are dominated by people of productive age (<50 years). The dominant livelihoods in this area are entrepreneurs and service providers, labourers, and traders. A large number of school-age and working (productive) population has led to this area being traversed by commuters. Therefore, the application-based mode of transportation was selected as an alternative for daily transportation to work and school.

Quantitative Analysis

This study implemented quantitative methods with nonprobabilistic sampling techniques. That is, these techniques do not provide equal opportunities for population members. Also, the accidental sampling technique was used in which the sample's determination is carried out by chance. Sampling is based on whom the user meets while carrying out this study (Leedy & Ormrod, 2010). Furthermore, this technique was used because the study population, in this case, the exact number of the App-Based Transportation users at Tlogosari Household, was unknown. The number of samples in this study was 100 respondents, with sampling carried out at community activity centres, including parks, rice fields, and residential areas. Based on Figure 2, it can be seen that main roads, public

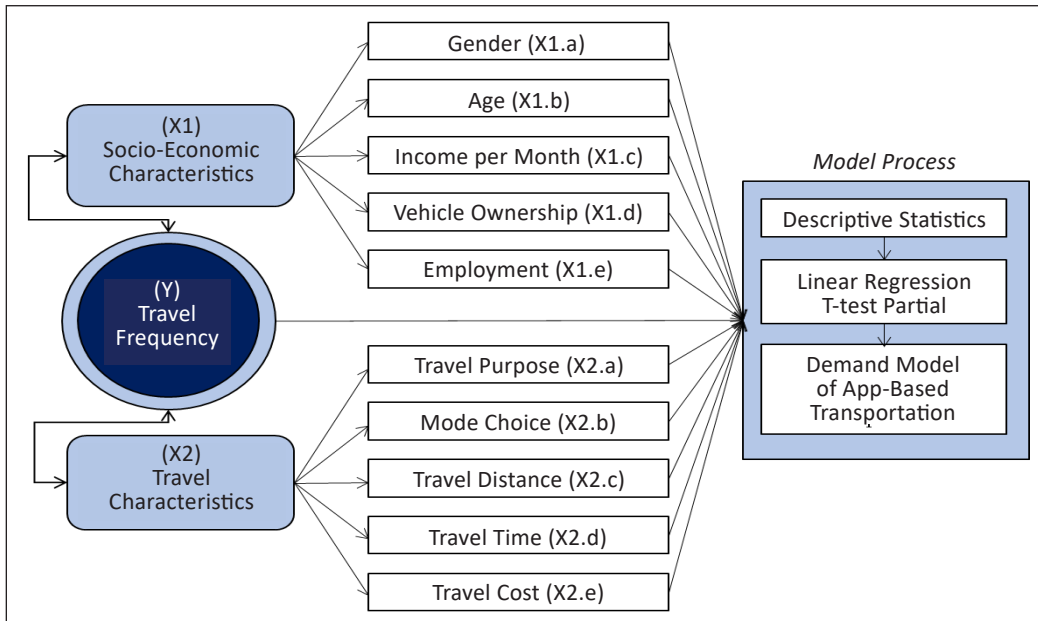


Figure 3. Study variable for app-based transportation

spaces, and trade and service locations are sample points with activities that tend to be massive. Therefore, the App-Based mode of transportation has a higher chance of being in these locations. The variables used in this study were based on previous literature studies' results which can be seen in Figure 3.

Furthermore, the acquisition of study data was processed by quantitative methods, i.e., linear regression utilising mathematical data processing applications. This study was built based on a simple analytical approach using descriptive statistical analysis and linear regression analysis. The depiction of data acquisition results combined the concept of descriptive diagrams and spatial data simulation to clarify the real conditions in the field. Meanwhile, implementing the linear regression analysis method is quite suitable for identifying the factors that influence App-Based Transportation demand. It is because it involves the dependent and independent variables in the process. In data analysis, the linear regression implemented the partial t-test method by looking at the T value and significant results to examine the relationship between variables. These variables are related to the T-Test > T-Table value, and the significance value is greater than 0.05 (> 0.05). Furthermore, the dependent variable used was the frequency of modal usage in a week (Y), and the independent variables are age, gender, type of occupation, income, vehicle ownership, the purpose of travel, travel time, mode choice, and travel costs. The linear regression process results will obtain a model with the equation, as seen in Equation 1.

$$Y = a + bn(Xc.d) + e \quad [1]$$

Where;

Y : the frequency of mode usage within a week

a : constant

bn : coefficient (b1-b10)

Xc.d : number of variables (X1: socio-economic characteristics; X2: travel characteristics)

e : another variable that is not observed/detected by the observer

RESULT AND DISCUSSION

Identification of User Characteristics

The characteristics of App-Based Transportation users can be divided into two types of variables: the users' socio-economic variables and travel characteristics. The socio-economic variables consist of gender, age, income, vehicle ownership, and type of work. Meanwhile, travel characteristics can be divided into destinations, travel times, mode choice, and travel costs. The travel frequency, in this case, is a dependent variable that affects those in the socio-economic and travel characteristics. Based on Figure 4, it shows that from its characteristics, users of the App-Based Transportation in Tlogosari Household are dominated by female residents with ages ranging from 17 to 25 years, have status as students, have an income of between 1 to 3 million rupiah, and own private vehicles, especially motorcycle. Furthermore, the female population tends to use app-based transportation more than the male population. That can be due to the large number of female residents that cannot use private vehicles. This condition is the same as what happened in Kinabalu City, Malaysia. The female population dominates the App-Based Transportation modes because of the ease of access, convenience, and most of them cannot use private vehicles (Adam et al., 2020).

Half of the respondents are in the young age group (17 to 25 years). 51% of respondents, followed by the 26 to 35 years age group (20%), and the age group 12 to 16 years (13%), with the old age group as the smallest. This young age group's dominance is in line with the activities carried out by that age group, which is higher than that of other age groups. With the high activity level, young age groups often use transportation modes (App-Based Transportation) compared to other age groups. Furthermore, based on the study carried out by Rayle et al. (2014), the elderly have limitations in using technology. Therefore, it is challenging to use App-Based Transportation. As one of the cities with the highest level of internet consumption in Indonesia, the Semarang City community's opportunity to use App-Based Transportation is relatively high.

Student residents dominate the young population (17-25 years) in Tlogosari Household, and some of them head to the city centre to access education. Also, the door-to-door system causes parents to feel safer choosing this type of transportation as their child's

main transportation to and from school. Furthermore, the student-age population that does not have an income causes the income of App-Based Transportation users in Tlogosari Household to be from the middle to lower level. Based on the study carried out by Rayle et al. (2014), App-Based Transportation in various countries was mostly used for recreational purposes than for schools. It is due to differences in systems, cultures, and customs between Indonesia and other countries, in which this type of transportation in other countries operates more cars than motorbikes.

Apart from being reviewed based on the user's socio-economic condition, trip characteristics are another variable in identifying App-Based Transportation modes in Tlogosari Household. Generally, Figure 4 shows that App-Based Transportation is widely used in the morning, i.e. during the busy hours of activity from 06.00-09.59 WIB. Furthermore, the population aged 17 to 25 led to app-based transportation to travel to or from school. During peak hours, most of them use this mode of transportation as an alternative to their mobility. Motorcycles are the most popular mode of transportation, which account for 76% of all trips, compared to just 24% for cars. Because the cost system is adjusted to the distance travelled in which the farther the distance, the more expensive the price will be issued, the residents of Tlogosari Household, on average, only use it at a distance of 4 to 8 kilometres. Therefore, the travel costs incurred to use App-Based Transportation in a day average only around 10 to 20 thousand IDR according to the abilities and needs of Tlogosari Household residents.

The Origin-Destination (O-D) analysis aids the examination of movement patterns according to land use in an area. An additional analysis variable that can better understand App-Based Transportation users' travel patterns in Tlogosari Household. This was carried

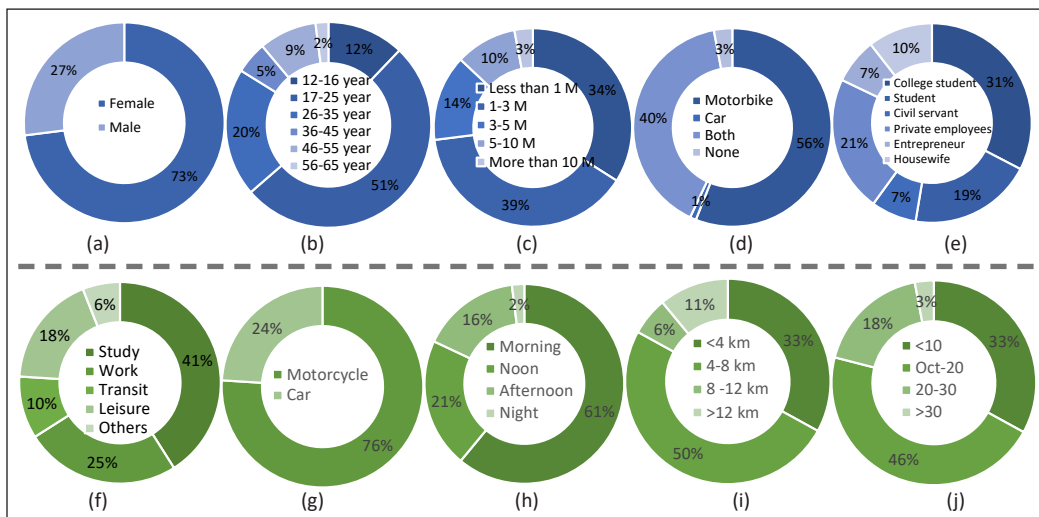


Figure 4. Socio Economic characteristics (blue) and travel characteristics (green); (a) gender, (b) age, (c) income (IDR), (d) vehicle ownership, (e) type of work, (f) purpose of trip, (g) travel frequency for a week, (h) travel time, (i) travel distance, (j) cost (thousand IDR).

out to support the regional development policy for Semarang, which is contained in the Regional Regulation of the City of Semarang Number 14 of 2011 concerning the Spatial Plan for the city from 2011-2031. Generally, the purpose of travel for App-Based Transportation users at Tlogosari Household is to go to areas with land use as trade and services and offices, transportation, education, industry, and surrounding settlements. Furthermore, the trips made were only limited to the closest areas identified in the previous section, which states that the average distance travel. Based on Figure 5 in the symbol D, the most prominent travel attraction for App-Based Transportation users in Tlogosari Household is in the central area of Semarang City with the use of the largest land for offices and trade and services (including education). Also, it can be indicated that there was a rotating demand-pull in the downtown area. This is because of the area of the facilities' completeness, and diversity of land uses that are offered compared to other areas around Tlogosari Household.

The population density in the centre of Semarang City is getting more significant due to travel attractions from its surrounding area of the Tlogosari Household. The areas with high density tend to be locations with much mobility. Therefore, the use of App-Based Transportation modes is potentially higher than in areas with low density (Lavieri et al., 2018). The App-Based Transportation originating from Tlogosari Household is part

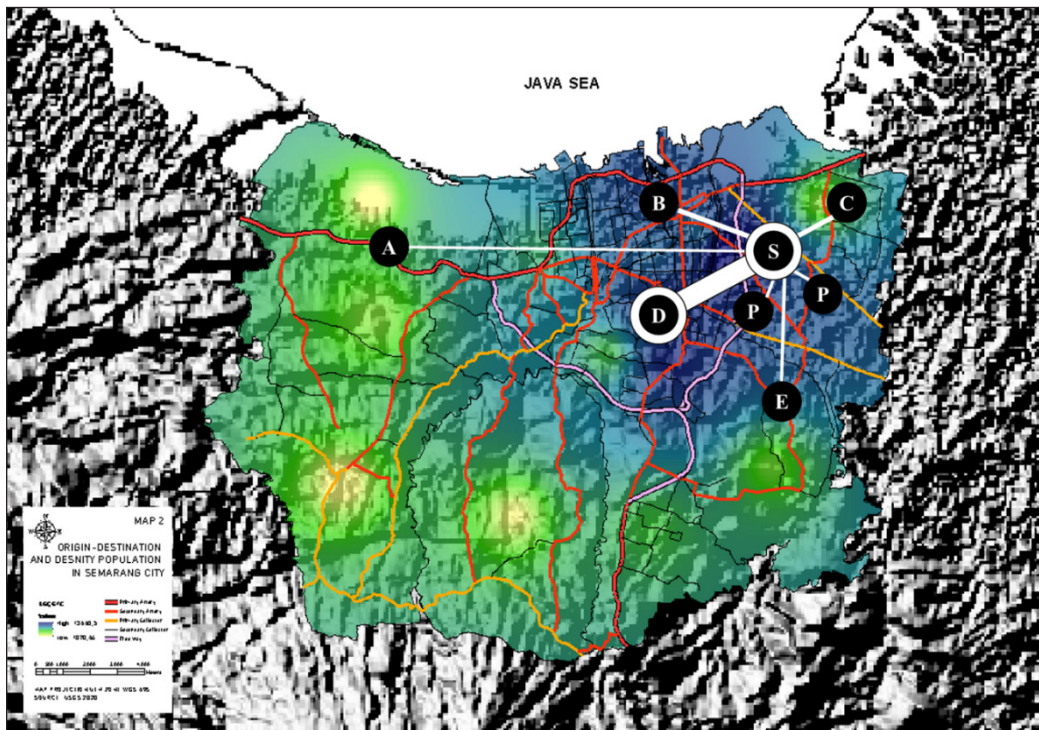


Figure 5. Trip origin-destination (OD) app-based transportation in Semarang City; (S) Tlogosari settlement; (a) industrial area, (b) station; (c) terminal; (d) city centre; (e) educational area; (p) other settlement

of the Transit-Oriented Development (TOD) concept in Semarang City. Furthermore, the Household-scale movements in the area contribute to improving the TOD system by integrating public transportation centres such as stations and terminals for further movement. Based on Figure 5, travel attraction also occurs at locations with industrial land uses. It implies that App-Based Transportation has also become a forum for the labour movement in Semarang. Therefore, land use is an essential factor to be considered in planning an App-Based Transportation system. A person's movement is strongly influenced by the needs of activities for specific land uses.

Travel Demand Model Analysis

The linear regression analysis of the partial T-test was carried out using the frequency of trips by the app-based transportation users per week on eight independent variables. It was in the form of the socio-economic characteristics (gender, age, income, type of work) and travel characteristics (purpose of trip, mode choice, travel distance, cost). Previously, the data normality test was carried out, and two variables with abnormal patterns were discovered, namely vehicle ownership and travel time. However, they were not included in the regression process. After testing the eight dependent variables with good normality, two variables that directly affected the increase in user travel requests in age and travel costs were obtained (Table 1). From the Collinearity Statistics component in Table 1, all tested variables did not show signs of multicollinearity. It is because the Tolerance and VIF value were >0.10 and <10.00 , respectively. It indicated that the independent variables, especially cost and age, did not have a strong correlation.

$$Y = 7.226 - 0.54 (X1.b) - 0.795 (X2.e) \quad [2]$$

Based on the results of the regression equation shown in Equation 2, several findings of the travel demand model are obtained in the form of:

- The constant 7.226 showed that provided the independent variable is considered constant, the average App-Based Transportation demand is 7.226,
- The age regression coefficient (X1.b) of -0.54 indicates that a yearly increase in age will reduce App-Based Transportation demand by 0.54.
- The travel cost regression coefficient (X2.e) of -0.795 indicated that each additional trip cost of 1 IDR reduces fashion demand by 0.795.

In developing countries such as Indonesia, the age and cost of travel are highly considered by App-Based Transportation users. The young population contributes more to increasing users of transportation modes to the household scale in Semarang City. It also proves that Semarang's position as one of the highest contributors to internet users affects the ease of access of its people to App-Based Transportation. Although the equation results showed that the other eight variables were not affected, they indirectly contributed to the

Table 1
Linear regression results

Model	Unstandardized Coefficients	Standardized Coefficients	T	Sig.	Collinearity Statistics
Code	B	Beta			Tolerance
(Constant)	7.226	0.762	9.483	0.000	-
Socio-Economic Characteristics (X1)					
X1.a Gender	0.078	0.177	0.046	0.437	0.663
X1.b Age	-0.054	0.023	-0.226	-2.360	0.020
X1.c Income	-0.047	0.077	-0.071	-0.616	0.539
X1.e Work	-0.097	0.057	-0.220	-1.719	0.089
Travel Characteristics (X2)					
X2.a Purpose of Trip	0.026	0.075	0.039	0.350	0.727
X2.b Mode Choice	0.103	0.194	0.058	0.531	0.597
X2.c Distance	0.070	0.074	0.100	0.949	0.345
X2.e Cost	-0.795	0.248	-0.307	-3.202	0.002

Note. Dependent variable: frequency, number of T table 1.860

Table 2
Correlation of indicators

Model	Coefficient Correlations ^a							
	Mode Choice	Travel_Purpose	Cost	Gender	Travel Distance	Income	Age	Work
Correlations	Mode Choice	1.000	0.031	0.125	0.013	-0.152	-0.185	-0.138
	Travel_Purpose	0.092	1.000	0.049	0.113	-0.057	0.102	-0.365
	Cost	0.031	1.000	-0.121	-0.243	0.010	-0.086	-0.014
	Gender	0.125	-0.121	1.000	-0.004	-0.203	0.065	0.110
	Travel_Distance	0.013	-0.243	-0.004	1.000	0.022	-0.021	0.089
	Income	-0.152	0.010	-0.203	0.022	1.000	-0.234	-0.177
	Age	-0.185	-0.086	0.065	-0.021	-0.234	1.000	-0.361
	Work	-0.138	-0.014	0.110	0.089	-0.177	-0.361	1.000

^aDependent variable: frequency

age and travel costs variables' influence. Based on Table 2 shows that others influence the formation of several independent variables in the study. Furthermore, the variables that produced a correlation value of <0.05 are considered to have a close relationship with another one. The variable of travel costs is related to the choice of the transportation mode used, the purpose of the trip, income of service users which is also relevant to the type of work. Meanwhile, the user age variable relates to a person's ability to travel or the distance between locations. It is because older people tend to have limited mobility compared to younger ones.

These results are relevant to the study carried out by Sakaran et al. (2018) in Kinabalu City, Malaysia, which states that the factors that influence travel demand for App-Based Transportation modes are age and income (indirectly related to travel costs). It was also supported by Lavieri et al. (2018) statement, which states that basic income is a factor that influences people in choosing to use transportation. In this case, low-level people tend to choose cheap and affordable transportation due to the low cost of travel. It suggests that the area scale between urban and household has the same result. Although the policies and concepts for providing App-Based Transportation modes that are implemented are also different, Kinabalu City uses more cars. Meanwhile, in Indonesia, especially in Tlogosari Household Semarang, there is more usage of motorbikes.

The number of motorcycles used in app-based transportation is due to the relatively affordable price compared to cars. As a developing country, prices are considered for local people in choosing the mode of transportation. It has led to the procurement of application-based transportation in Indonesia, especially in the Tlogosari Semarang Household, which is very vulnerable to the safety and security of passengers. Furthermore, several platforms, such as Gojek, have provided safety insurance for drivers and passengers in the event of an accident while using the service (Gojek.com, 2019). In addition, vehicle equipment and safety standards have been implemented. It includes mandatory use of national standard helmets, special raincoats, and ensuring motorcycles meet operating requirements or are in good condition. Surprisingly, a feature is provided in the application to report complaints about the condition of the motorbike or service driver if it is not satisfactory for the company to follow up. Certainly, further study is still needed on the safety factor in application-based transportation, especially motorcycle services. It is because there are still many violations of service standards on application-based transportation in Indonesia.

CONCLUSION

The travel demand model derived from the App-Based Transportation in the Tlogosari Household area household unit produces two factors: age and travel costs, which can directly affect user demand. Both socio-economic and travel characteristics influence each other and are formed through the influence of other variables. Furthermore, the frequency

of travel requests is inversely proportional to the variable age and travel costs. Therefore, the older a person is or, the cheaper the transportation costs, the more frequent the use of transportation modes in Tlogosari Household will increase. In detail, it was discovered that students were the population that dominated the usage of application-based transportation from the point of its generation (Tlogosari Household). It often occurs in the morning because of the ease of access to technology and to save travel time. However, application-based transportation to Tlogosari Household decreased in the afternoon because most students return with their working parents or use public transportation such as Bus Rapid Transit.

Furthermore, this study also discovered a strong influence of land use at the point of attraction on the choice of application-based transportation as a mode of the residents' movement in Tlogosari Household and its surroundings. The downtown area that is dominant in land use as trade and services were the strongest attraction as a point of awakening for the movement of application-based transportation users. Apart from trade and services, land use as education also plays an important role in influencing the use of application-based transportation because most users are students. Furthermore, acknowledging the characteristics of the demand for App-Based Transportation modes on the household scale can guide the government and stakeholders to make detailed plans in providing these modes by the characteristics of users in the future. Also, the cost variable is very sensitive and influences the public in choosing motorcycle services in application-based transportation. In consideration, further study is suggested to be carried out on the safety of motorcycles to improve services of the app-based transportation implementation, especially in Indonesia.

ACKNOWLEDGEMENTS

This study was financially supported by The Faculty of Engineering, Diponegoro University, Indonesia, through Excellent Research Grant 2019.

REFERENCES

- Adam, M., Kee, D. M. H., Junaina, I., Fadhilah, N., Uwais, N., Al Rashidi, F., Al Shammari, H., Quttainah, M. A., Srivastava, A., & Pandey, R. (2020). The influence of customer satisfaction on Grab services in Malaysia. *International Journal of Tourism and Hospitality in Asia Pasific (IJTHAP)*, 3(2), 26-37. <https://doi.org/10.32535/ijthap.v3i2.820>
- Anderson, D. N. (2014). "Not just a taxi"? For-profit ridesharing, driver strategies, and VMT. *Transportation*, 41(5), 1099-1117. <https://doi.org/10.1007/s11116-014-9531-8>
- Bohang, F. K. (2017). Berapa jumlah pengguna dan pengemudi Go-Jek? [*How many Go-Jek users and drivers?*]. Retrieved January 18, 2021, from <https://tekno.kompas.com/read/2017/12/18/07092867/berapa-jumlah-pengguna-dan-pengemudi-go-jek?page=all>

- Caulfield, B. (2009). Estimating the environmental benefits of ride-sharing: A case study of Dublin. *Transportation Research Part D: Transportation Environment*, 14(7), 527-531. <https://doi.org/10.1016/j.trd.2009.07.008>
- Chan, N., & Shaheen, S. A. (2012). Ridesharing in North America: Past, present, and future. *Transportation Reviews*, 32(1), 93-112. <https://doi.org/10.1080/01441647.2011.621557>
- Cheng, Y. H., & Chen, S. Y. (2015). Perceived accessibility, mobility, and connectivity of public transportation systems. *Transportation Research Part A: Policy and Practice*, 77, 386-403. <https://doi.org/10.1016/j.tra.2015.05.003>
- Efthymiou, D., Antoniou, C., & Waddell, P. (2013). Factors affecting the adoption of vehicle sharing systems by young drivers. *Transport Policy*, 29, 64-73. <https://doi.org/10.1016/j.tranpol.2013.04.009>
- Gojek.com. (2019). *A complete guide for GoRide's passenger insurance claim*. Retrieved June 04, 2021, from <https://www.gojek.com/blog/goride/asuransi/>
- GrabCarMalaysia. (2018). *About GrabCar*. Retrieved February 06, 2021, from <https://www.GrabCar.com/my/about/>
- Hall, J. V., & Krueger, A. B. (2016). *An analysis of the labor market for Uber's driver partners in the United States*. National Bureau of Economic Research.
- Henao, A. (2017). *Impacts of ridesourcing - Lyft and Uber - On transportation including VMT, mode replacement, parking, and travel behavior*. University of Colorado.
- Hou, J., Zhao, H., Zhao, X., & Zhang, J. (2016). Predicting mobile user's behaviors and locations using dynamic Bayesian networks. *Journal of Management Analytics*, 3(3), 191-205. <https://doi.org/10.1080/23270012.2016.1198242>
- Jaśkiewicz, M., & Besta, T. (2014). Heart and mind in public transport: Analysis of motives, satisfaction and psychological correlates of public transportation usage in the Gdańsk-Sopot-Gdynia Tricity Agglomeration in Poland. *Transportation Research Part F: Traffic Psychology and Behaviour*, 26, 92-101. <https://doi.org/10.1016/j.trf.2014.06.012>
- Lavieri, P. S., Dias, F. F., Juri, N. R., Kuhr, J., & Bhat, C. R. (2018). A model of ridesourcing demand generation and distribution. *Transportation Research Record Journal of the Transportation Research Board*, 2672(46), 31-40. <https://doi.org/10.1177/0361198118756628>
- Leedy, P. D., & Ormrod, J. E. (2010). *Practical research: Planning and design*. Pearson Education.
- Lekshmi, G. R. A., Landge, V. S., & Kumar, V. S. (2016). Activity based travel demand modeling of Thiruvananthapuram urban area. *Transportation Research Procedia*, 17, 498-505. <https://doi.org/10.1016/j.tpro.2016.11.100>
- Morency, C. (2007). The ambivalence of ridesharing. *Transportation*, 34(2), 239-253. <https://doi.org/10.1007/s11116-006-9101-9>
- Phun, V. K., Masui, R., & Yai, T. (2018). Operational Characteristics of paratransit services with ride-hailing apps in Asian developing cities: The Phnom Penh case. *Journal of Transportation Technologies*, 8(04), 291-311. <https://doi.org/10.4236/jtts.2018.84016>

- Rayle, L., Shaheen, S., Chan, N., Dai, D., & Cervero, R. (2014). Just a better taxi? A survey-based comparison of taxis, transit, and ridesourcing services in San Francisco. *Transport Policy*, 45, 168-178. <https://doi.org/10.1016/j.tranpol.2015.10.004>
- Regina, R., & Clewlow, G. S. (2018). *Disruptive transportation: The adoption, utilization, and impacts of ride-hailing in the United States*. Institute of Transportation Studies.
- Ristantia, N. S., & Hayah, Z. (2018). Smart mobility dalam pengembangan transportasi berbasis aplikasi online di Indonesia [Smart mobility in transportation development based on online application in Indonesia]. *Ruang*, 4(3), 237-246.
- Rithoma, A. R., & Rakhmatulloh, A. R. (2013). Kajian rute angkutan umum di Banyumanik Semarang terkait transportasi yang berkelanjutan [A study of public transportation routes in banyumanik semarang regarding sustainable transportation]. *Jurnal Pembangunan Wilayah dan Kota*, 9(1), 65-73.
- Sakaran, S. S., Noor, H. M., & Eboy, O. V. (2018). Socioeconomic factors that affect usage of Grabcar services in Kinabalu City, Sabah. *Malaysian Journal of Business and Economics*, 5(2), 65-77.
- Shaheen, S., Cohen, A., & Zohdy, I. (2016). *Shared mobility: Current practices and guiding principles*. (No. FHWA-HOP-16-022). Federal Highway Administration.
- Šimeček, M. (2019). Discrete choice analysis of travel behaviour. *Transactions on Transport Sciences*, 10(1), 5-9. <https://doi.org/10.5507/tots.2019.001>
- Smart, R., Rowe, B., Hawken, A., Kleiman, M., Mladenovic, N., Gehred, P., & Manning, C. (2015). *Faster and cheaper: How ride-sourcing fills a gap in low-income Los Angeles neighborhoods faster and cheaper*. BOTEC Analysis Corp.
- Sukma, D. (2016). *Data Gfk: 9 dari 10 orang Indonesia internetan lewat smartphone* [Gfk data: 9 out of 10 Indonesians surf through smartphones]. Retrieved February 12, 2021, from <https://arenalte.com/berita/industri/data-gfk-terbaru-2016-pengguna-smartphone-indonesia/>
- Zhao, M., Yin, L., An, S., Wang, J., & Feng, D. (2018). Ridesharing problem with flexible pickup and delivery locations for app-based transportation service: Mathematical modeling and decomposition methods. *Hindawi Journal of Advanced Transportation*, 2018, Article 6430950. <https://doi.org/10.1155/2018/6430950>

Review article

Roles and Principles of Sterilisation Process in Palm Oil Mills

Yin Mee Thang^{1,2}, Robiah Yunus^{1,3*}, Mohd Noriznan Mokhtar⁴, David Ross Appleton², Ahmad Jaril Asis², Pei San Kong², Huey Fang Teh² and Abdul Azis Ariffin^{1,5}

¹Institute of Advanced Technology, Universiti Putra Malaysia, 43400 UPM Serdang, Selangor, Malaysia

²Sime Darby Plantation Berhad, Plantation Tower, No 2, Jalan PJU 1A/7, Ara Damansara, 47301 Petaling Jaya, Selangor, Malaysia

³Institute of Plantation Studies, Universiti Putra Malaysia, 43400 Serdang, Selangor, Malaysia

⁴Faculty of Engineering, Universiti Putra Malaysia, 43400 Serdang, Selangor

⁵Dolphin International Berhad, 17 & 19, Jalan Puteri 5/20, Bandar Puteri, 47100 Puchong, Selangor, Malaysia

ABSTRACT

Sterilisation in palm oil mills is considered a pre-treatment process as it affects stripping efficiency and oil quality. Although sterilisation technology has been well-established in the palm oil milling industry, the roles and principles of sterilisation, particularly related to the chemical changes in fruits and stalks occurring during the process, have been rarely reported. The review begins with the background literature on the biochemical properties of the FFBs, such as the compositions of binding carbohydrates and the phenomena of natural fruit detachment. Followed by the harvesting practice to understand the type of FFBs supplied to the industry. In addition, a comparison of the well-established conventional and alternative sterilisation technologies and sterilisation functions is critically

reviewed and assessed. Establishing the current sterilisation process initiatives to address the natural fruit's separation more efficiently in palm oil mills is important. Particularly visualise sterilisation as a breakup of specific binding carbohydrates that leads to strippability. It will provide a further understanding of the sterilisation mechanism, which would benefit the palm oil miller in optimising the processing of fresh fruit bunches. The information provided in this review is necessary to

ARTICLE INFO

Article history:

Received: 02 April 2021

Accepted: 19 August 2021

Published: 18 October 2021

DOI: <https://doi.org/10.47836/pjst.29.4.26>

E-mail addresses:

robiah@upm.edu.my (Robiah Yunus)

thangyinmee@gmail.com (Yin Mee Thang)

noriznan@upm.edu.my (Mohd Noriznan Mokhtar)

david.ross.appleton@simeidarbyplantation.com (David Ross Appleton)

ahmadjarilasis@gmail.com (Ahmad Jaril Asis)

sylvia.kong.peisan@simeidarbyplantation.com (Pei San Kong)

teh.huey.fang@simeidarbyplantation.com (Huey Fang Teh)

docazis7@gmail.com (Abdul Azis Ariffin)

* Corresponding author

mitigate the percentage of unstripped bunches and reduce the oil losses and ultimately enhance the oil extraction rate.

Keywords: Abscission, fresh fruit bunch, palm oil, pre-treatment, sterilisation

INTRODUCTION

Natural fruit detachment in oil palm fruit at the abscission zone occurs in two stages (Henderson & Osborne, 1994; Henderson & Osborne, 1990; Osborne et al., 1992). Fruit separation at a fruit base usually occurs one to three days earlier than in any other position. All harvested FFBS delivered to palm oil mills must be processed regardless of any degree of ripeness to prevent further deterioration of their quality. Therefore, an optimum sterilisation process is important to strip all unripe and ripening fruits from the stalk.

In a typical palm oil milling process, different operations are involved to mechanically extract the oil from fleshy mesocarp fibres of fresh fruit bunches (FFBs). The oil extracted is crude palm oil (CPO). Generally, these involve sterilisation of the FFBs followed by stripping; the stripped fruits undergo digestion and mechanical pressing. Finally, the clarification step is to separate the oil phase from the mixture of oil-water, purification to remove FFBs debris, drying to remove the moisture until the acceptable level. Then the oil would be stored in a storage tank (Siew, 2011, Vincent et al., 2014).

A good sterilisation process has a large impact on the efficiency and effectiveness of the downstream milling process, particularly the strippability of the palm oil fruits and the final oil quality (Babatunde et al., 1988; Siew, 2011; Ariffin, 1991; Vincent et al., 2014). Sterilisation is the heart of the palm oil milling process. Most of the technology development in the palm oil milling industry so far has focused primarily on the alternative sterilisation techniques which aimed at improving the OER (Vincent et al., 2014; Sivasothy et al., 2005; Hadi et al., 2012; Sukaribin & Khalid, 2009; Omar et al., 2017). Still, many incidences of unstripped bunches (USB), where some fruits are still attached to the stalk, occur due to inefficient sterilisation. It suggests that the reasons underlying the high USB issues are not well understood. The oil loss due to USB is reported that approximately 0.77% of the total oil loss occurs in a palm oil mill (Walat & Ng, 2013). It equates to RM 306.5 million based on an average CPO price of RM 2,000 in 2019 (MPOB, 2019).

So far, no attempt has been made to assess the fundamental issues that underline the oil palm fruit strippability or separation in these sterilisers. For instance, the effects of sterilisation conditions on the degradation of binding carbohydrates at the abscission zone of oil palm fruits are not well known. In addition, the conversion of lignocellulosic fibres into simpler sugars affects strippability as it facilitates the detachment of fruits from the bunch. Furthermore, no study on the suitability of current sterilisation parameters in processing the FFBs with different ripeness levels is available. Sterilisation could facilitate the rupture of the cell wall and the release of oil (Owolarafe & Faborode, 2008). Therefore,

a greater understanding of the chemical changes in fruit bunches, particularly the binding carbohydrates at the abscission zone, is necessary to align the sterilisation parameters with mimicking the separation of the natural fruits to gain insights on how to optimise the sterilisation process best to improve the strippability.

ABSCISSION OF OIL PALM UPON RIPENING

Oil palm is a sessile drupe; it produces a bunch containing 1000 to 3000 oil palm fruits. Oil deposition in the mesocarp starts at about 15 weeks after pollination (WAP) and continues until fruit maturity at around 20-22 WAP (Sambanthamurthi et al., 2000; Teh et al., 2013). The bunch at this stage is ready for harvesting—lipid content accumulated up to the optimum level. At the same time, sugars such as glucose and fructose and the moisture were decreased to a deficient level. As a result, the carotene content was fluctuated during the development stage and recorded as about 600 ppm to 700 ppm at 20 WAP onwards. The tocopherols and tocotrienols were increased from 20 WAP onwards (Sambanthamurthi et al., 2000).

Natural fruit detachment at the abscission zone occurs in oil palms in two stages (Henderson & Osborne, 1994; Henderson & Osborne, 1990; Osborne et al., 1992). The abscission zone of oil palm is shown in Figure 1. The first stage of abscission is induced at the junction of the fruit and its pedicel, which is regulated by ethylene. It is observed that in ripening fruit, some of the cells are loosely associated at pedicel while others still adhered along the fruit-based pedicel junction. At this point, the fruit is firmly held within the surrounding cup of the rudimentary androecial ring, the tepals, bracteoles, and spiny floral bract; full cell communication remains.

Nevertheless, in the second stage, the cells in this whole perimeter change the cell wall adhesion when the fruit is ripe and then abscised. It generally occurs at the inner face of the rudimentary androecial ring, and this second stage of separation is not directly

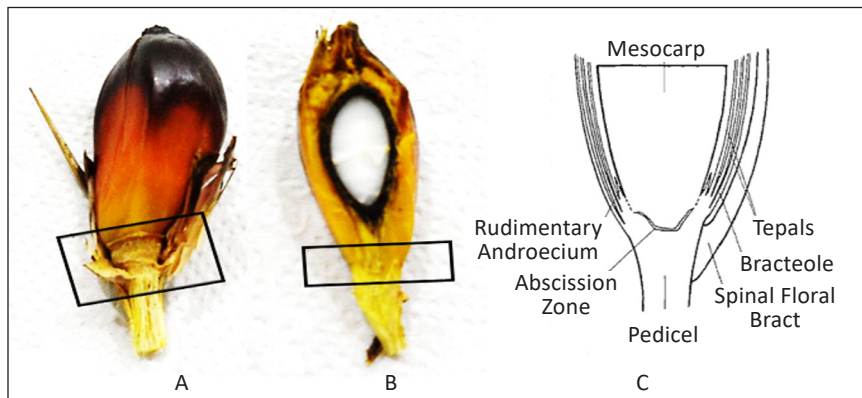


Figure 1. Abscission layer (rectangle area) of an oil palm fruit. A, with tepal attached; B, halve view, C, abscission zone

responsive to ethylene. Hence, it suggested that regulating saccharide fragments or other degradation products of middle lamella or cell wall hydrolase such as endo- β -1, 4-glucan hydrolase initiate the second stage cell separation after the first stage (Payasi et al., 2009; Roongsattham et al., 2012). Henderson et al. (2001) found that high pectic polysaccharides are present in the oil palm abscission zone compared to those adjacent mesocarp and pedicel tissue to the abscission zone. They also reported that the cell walls of the abscission zone contain high levels of unmethylated pectin and polygalacturonase enzyme expression during fruit ripening and fruit detachment.

Fruit separation at a fruit base usually occurs one to three days earlier than in any other position. Therefore, even when cell separation at the fruit base is complete, the fruit is not shed (Henderson & Osborne, 1990; Henderson & Osborne, 1994; Osborne et al., 1992). However, unripe fruit will not separate at any position. As a result, this non-synchronous detachment of oil palm fruit as each fruit ripens raises a problem internal harvesting schedule due to the lack of reliable ripeness indicators of these many-fruited bunches in oil palm estates (Sambanthamurthi et al., 2000; Tan et al., 2010; Razali et al., 2012; Zulkifli & Ropandi, 2001). In oil palm plantations, the detachment and fall of the ripe fruit from its oil palm fruit bunches are taken to indicate the readiness for harvesting.

All harvested FFBs delivered to palm oil mills must be processed regardless of any degree of ripeness to prevent further deterioration of their quality. Therefore, an understanding of bunch ripening is important if harvesting is done correctly (Corley & Tinker, 2003; Ariffin, 2010). Furthermore, an optimum sterilisation process is important to strip all unripe and ripening fruitlets from the stalk. Therefore, characterisation of FFBs prior to the sterilisation process is in need. However, no study has sought a profiling pattern between the binding carbohydrates characteristics and the manual ripeness determinations of FFBs delivered to the palm oil mill. These FFBs may differ from those of controlled bunches from the trial plot because of unidentified bunch age and containing a certain degree of damage due to the handling during transportation. Research mainly focuses on palm biomass lignocellulosic composition after the oil extraction.

STERILISATION PROCESS IN PALM OIL MILLS

Conventional Steriliser Technology

The most common sterilisation process in palm oil mills is in pressure vessels of varying designs: cylindrical vessels lying in horizontal, vertical, tilting or oblique positions, and spherical vessels. All sterilisers share similar operating parameters of 40 psi to 45 psi and residence time of 60 minutes to 90 minutes (Hassan et al., 1994; Halim et al., 2009). In addition, different steam cycles such as single, double, and triple peaks are put in place to improve the heat transfer during the sterilisation by stripping off the air trapped inside the steriliser to enhance further sterilisation efficiency. Sterilisation also can be operated

as a continuous process that works at a lower steam pressure, such as atmospheric steam pressure (Vincent et al., 2014; Sivasothy et al., 2005).

The horizontal steriliser is the most commonly used in palm oil mills. It has a single hinged door at one end in which the FFBs are cooked by direct contact with steam (Halim et al., 2009). The FFBs are spread out uniformly in the cages with a low stacking height. When the pressurised steam is injected, it can reach out to different directions and corners of the contents within the cages. Low stacking height also minimises fruit bunch compression, which consequently minimises the bruising of the fruits. However, poor air removal is observed, especially during the earlier venting stage of the sterilisation. Thus, to remove the air from the pockets of space within the stacked fruit bunches, high steam consumption is required when using horizontal sterilisers, which operate using multiple-peak cycles. KM (2013) reported that about 360 kg to 400 kg of process steam per tonne of FFB is required for a horizontal steriliser operating at a steam temperature of 143°C and 4 bar absolute steam pressure in a triple-peak cycle. The disadvantage of a horizontal steriliser is the extensive maintenance and labour cost (cages management).

Aside from horizontal sterilisers, FFBs can also place directly into tall vertical sterilisers without steel cages. The vessel's height is restricted by the height of the building and the limited space of the loading ramp. Due to the stacking height in vertical sterilisers, the rate of bruised FFBs is high. It is reported that about 305 kg to 355 kg of steam per tonne of FFB was required for vertical sterilisers operating at a steam temperature of 143°C in triple-peak cycles for about 60 minutes (KM, 2013).

Meanwhile, a smaller capacity is allowable in spherical sterilisation, specifically a 25 m³ spherical steriliser enclosed with a top opening for filling the FFBs and a bottom condensate drain. It can be rotated 360 degrees to facilitate both FFBs feeding and discharge through a single door. Spherical steriliser consumes 220 to 250 kg of steam per ton of FFB over a steaming time of 60 minutes in a two-peak cycle (CIMG, 2015, Kumaradevan et al., 2015).

According to Sivasothy et al. (2005), Tan et al. (1999), and Hadi et al. (2012), the batch sterilisation required a longer steaming period and vast quantities of steam to heat the steriliser cage as well as to ensure complete heating up to the inner layer of the bulky FFB. Therefore, it is slow and inefficient as compared to the continuous sterilisation process. Continuous sterilisation is an alternative to batch process sterilisation, where it is operated at atmospheric pressure (Sivasothy et al., 2005; Sivasothy et al., 2006; Loh, 1994). This type of sterilisation is carried out in a heating chamber subjected to steam at atmospheric pressure continuously. FFBs are transported to a double-roll crusher for crushing before entering the heating chamber to expose to steam at atmospheric pressure through a scraper conveyor. The crushing of FFBs facilitates steam penetration into the inner layers of the fruit bunch (Sivasothy et al., 2006; Sivasothy & Rohaya, 2000, Fatin et al., 2014).

The crushed bunches are immediately pre-heated to 60°C to facilitate deaeration, minimise the amount of air entering the chamber, and ensure that the temperature in the

continuous sterilisation chamber is close to saturated steam. The bunches are heated for about 60 minutes inside the chamber using live steam. The bottom of the feed conveyor is filled with water to seal against steam loss (Sivasothy et al., 2005; Sivasothy et al., 2006). A continuous stream of steam gives consistent steam at the required temperature in a continuous steriliser. Consequently, steam consumption is the highest among the different sterilisers due to prolonged exposure time. It is reported that about 300 kg to 360 kg of steam per tonne of FFB was required for a continuous steriliser operating at a steam temperature of 98°C for about 60 minutes.

In addition, a continuous steriliser requires the second stage of post-heating to maintain a high temperature of stripped fruits to complete its heat treatment (Sivasothy et al., 2006; KM, 2013). Furthermore, Fatin et al. (2014) reported that better heat penetration in the chopped FFBs enhances strippability after sterilisation; however, the chopped FFBs must be sterilised within 30 minutes to preserve a good quality of the palm oil. Sivasothy et al. (2006) indicated that fewer unstripped bunches (USB) were noticed in conventional sterilisation (2.13%) as opposed to continuous sterilisation (24.1%) at the early stage of development in continuous sterilisation. A summary of sterilisation technology in the oil palm industry is tabulated in Table 1.

The continuous sterilisation process is fundamentally different from the batch process in how the material flows. In general, a palm oil mill operating for about 16 hours to 20 hours a day depends on the availability of FFBs and other factors, which diminishes the advantages of continuous sterilisation. The disruption of FFBs supply will result in the loss of the throughput and efficiency of the operation (Aziz, 2003). In addition, issues such as high steam consumption, the extra cost associated with additional facilities such as the bunch crusher and moving scraper conveyor, pre-heating section, the double process of uncooked bunches need to be addressed to make the continuous sterilisation more economically viable.

Table 1
Summary of current sterilisation technology

Characterisation	Horizontal	Vertical	Spherical	Tilting	Continuous
Cooking time	Standard 100-120 mins	Standard >120 mins	Short 60 mins	Short 60-80 mins	Short 70-85 mins
Pressure	High 40 psi	High 30-40 psi	High 45 psi	High 40-45 psi	Atmospheric
Numbers of pressure peak cycle	Triple	Triple	Double	Triple	Single
Presence of cage	Yes	No	No	No	No
Steam consumption	High 360-400 kg/ MT FFB	Moderate 305-355 kg/ MT FFB	Low 220-250 kg/ MT FFB	Low 200 kg/MT FFB	Moderate 300-360 kg/ MT FFB

Alternatives to Steriliser Technology

Intensive studies are carried out to replace the conventional sterilisation process in palm oil mills. Sterilisation technology such as dry heating or coupled with solvent extraction was studied by Chow and Ma (2007) and Hadi et al. (2012). Sivasothy et al. (2006) and Hadi et al. (2012) found that the content of free fatty acid (FFA) of CPO obtained from continuous sterilisation and dry heating are similar to that obtained using conventional batch sterilisation. However, extreme dry heating can potentially cause the burning of oil palm fruits and difficulty in depericarping operation. Therefore, optimum heating time is crucial to loosen the nut from its mesocarp and keep the kernel in good condition for further processing at the same time.

Microwave energy is used in the low-temperature microwave sterilisation approach (Sarah & Taib, 2013; Sukaribin & Khalid, 2009; Umudee et al., 2013). This approach is operated at a low temperature of 100°C as it is aimed to preserve the oil quality compared to the conventional sterilisation that operated at 140°C (Vincent et al., 2014; Chow & Ma, 2007). Sukaribin and Khalid (2009) found that microwave radiation can detach the fruits from the bunch without damage to the other regions of the bunch. They found that the abscission zone contains the highest dielectric properties than other regions, leading to higher microwave power absorbed at this region. The moisture content at the abscission zone was found almost 5 to 7 times higher than the mesocarp, helped in conducting the ionic constituents, subsequently contributed to the enhancement in the dielectric properties. These properties provide a good heating effect to detach the fruits from the stalk. Strippability of 80% was observed after 12 and 14 minutes heating with 1.5 kW and 1kW microwave power, respectively. Khalid et al. (1996) suggested having separate microwave heating for FFBs and losing fruits due to their moisture content variation. Lengthy microwave heating exposure, similar to dry heating, would cause the burning of the oil palm fruits. However, current microwave and dry heating only accommodate spikelets or small amounts of fruitlets at one time. Therefore, industrial-scale microwaves and ovens should be studied to confirm their feasibility for sterilisation FFBs.

Waterless sterilisation, which uses supercritical carbon dioxide, autoclave, and enzymes to recover oil from fresh and sterilised palm fruits, was also reported in literature pieces. For example, Omar et al. (2017) reported the complete inactivation of lipase-producing microbes in ripe loose fruits using supercritical carbon dioxide at 10 MPa pressure, at 80°C for 60 minutes. The treated fruits were found in shinning and glossy appearance with the presence of β -carotene.

Domínguez et al. (1994) reported that mixtures of enzymes were used to degrade the cell wall materials to enhance the oil extractability from oilseeds. Enzymes commonly used are hemicellulolytic or cellulolytic enzymes such as amylase, glucanase, protease, pectinase. It is possible via hydrolysis of the cell wall materials to facilitate the release of oil. Eshtiaghi

et al. (2015) investigated the oil extraction using commercially available enzymes such as Cellic CTec2 (a blend of cellulases, beta-glucosidases, and hemicellulose), Cellic HTec2 (endoxy lanase with soluble hemicellulose specificity), and Pectinex Ultra SP-L (an enzyme with rich pectolytic activities). Oil recovery of 88% was achieved by treating the sterilised fruit with the mixtures of Cellic CTec2, Cellic HTec2, and Pectinex Ultra SP-L at the ratio of 0.46: 0.34: 0.2. The enzyme loading was set as 30 mg /10 g substrate, substrate loading of 50% w/v, pH 4.8, and 2 hours of incubation at 50°C. Silvamany and Jahim (2015) proposed that the enzyme type and concentration and the enzymatic treatment time were important for oil extraction from palm mesocarp to reduce the remaining pressed pulp. The cellulose concentration ranging from 0.05% to 0.15% reduced about 13% to 18% of the remaining pressed pulp, respectively, after 4 hours of enzyme treatment at 50°C. Oil recovery of 88% to 95% was reported with different concentrations of cellulase, respectively.

It is revealed that successful applications of new technology can increase yield without compromising the quality of the oil extracted. The effluent generated in the milling process could also be reduced effectively by applying these technologies. However, these approaches require expensive technological advancement and are mostly still in their early stage; some approaches are labour intensive. Sultana (2007) stated that the best heating method for sterilisation is to use wet steam. Sterilisation under high humidity conditions is effective— hydrolysis and denaturation occur at lower heat and shorter exposure times than in the absence of water.

FUNCTIONS OF STERILISATION

Deactivation of Lipase

The level of FFA is one of the major indications of oil quality. Therefore, various experiments were conducted to study the level of FFA during fruit development. As a result, active endogenous lipase in the oil palm mesocarp was reported (Mohankumar et al., 1990; Henderson & Osborne, 1991; Sambanthamurthi et al., 1991). Furthermore, lipase activity in the oil palm mesocarp is found synchronised with triacylglycerol biosynthesis. The lipase activity was determined at 16 weeks after anthesis (WAP), reached a maximum level at 21 WAP, and declined after 21 WAP.

Therefore, sterilisation's initial objective was to inhibit lipase activity in the pulp (Mongana report, 1955). It can be easily achieved by heating the palm fruits to about 60°C. Sambanthamurthi et al. (1991) and Chong and Sambanthamurthi (1993) suggested that lipolytic enzyme is possibly only present in ripe fruits. Therefore, its activity could be related to the degree of ripeness of the fruit. They investigated the loose, ripe, and unripe fruits, which were bruised and left at ambient temperature for 4 hours, followed by sterilisation and then oil extraction. It was revealed that the FFA in the unripe bruised fruits was 0.16%, which is relatively low compared to 2.06% of FFA of ripe bruised fruits.

Notably, 9.45% of FFA was observed in loose bruised fruits. Henderson and Osborne (1990) also reported hydrolase inside the palm fruit that can hydrolyse valuable triglycerides of the mesocarp to undesirable FFA. The autocatalytic and enzymatic hydrolysis occurred spontaneously at a temperature of less than 50°C, in the presence of moisture, dirt, and infection by microbes such as *Pseudomonas fluorescens* and *Geotrichum candidum* that are capable of splitting fat (Menon, 2013).

Ngando-Ebongue *et al.* (2006) found that the calcium-dependent lipase is abundantly present in the mesocarp and represents a few per cent of total proteins. Lipase is compartmentalised within the cell and only comes into contact with the oil if cell membranes are damaged (Mongana Report, 1955; Corley & Tinker, 2003). Therefore, FFB must be processed immediately after harvesting to prevent an unacceptable rise of FFA in oils. In addition, the enzyme is brought into contact with oil when the fruit is bruised, which can be caused by falling on the ground during harvesting, loading, transportation, and discharge from the lorry into steriliser cages (Ngando-Ebongue *et al.*, 2006; Hadi *et al.*, 2009).

Loosening of Fruits and Softening of Mesocarp Tissue

The second objective of sterilisation is to soften the mesocarp tissues and loosen the fruits to facilitate the subsequent mechanical stripping step. The deformation properties of both the abscission and mesocarp layers are affected markedly by the thermal softening process. After sterilisation, the fruit's fracturability at both abscission and mesocarp layers was reduced by 18% and 51%, respectively (Abbas *et al.*, 2006). Furthermore, the hardness values of the sterilised fruitlets for both abscission and mesocarp layers were reduced by approximately 84% compared to that of the fresh fruitlets. In addition, the adhesiveness values for both sterilised abscission and mesocarp layers were reduced by 91% and 60%, respectively, as compared to that of fresh fruit.

Facilitating Separation of Mesocarp Layer from Kernel Shell

On top of the sterilisation as mentioned earlier, sterilisation, helps isolate the mesocarp layer from the kernel shell to minimise kernel breakage at the oil pressing stage (Sivasothy *et al.*, 1992). The heat penetrates the nut that might affect the quality of nut-cracking through triple peak sterilisation. If the fruit is hot and the kernel shell may be sufficiently elastic to deform temporarily during pressing. If the fruits are well-cooked using triple peak sterilisation, wet nuts with 15% moisture in the nut and 20% moisture in the kernel can be cracked with 98% cracking efficiency without any broken kernels. Therefore, to minimise nut breakage during pressing, the digested fruit should be at about 100°C at the press station (Menon, 2013).

A NEW PERSPECTIVE OF STERILISATION AS A CHEMICAL REACTION SYSTEM

Different types of sterilisation technology have distinct pros and cons. For instance, issues with an uneven steam distribution occur in horizontal sterilisation, and many bruised FFBs are found in vertical sterilisation. Therefore, chopped FFBs are required prior to sterilisation in continuous sterilisers. Furthermore, research and development are still needed in microwave-assisted sterilisation and enzymatic sterilisation. Multiple pressure cycles with optimum air sweeping and bleed off enhance strippability, but high steam consumption is required in batch sterilisation. In addition, extreme sterilisation conditions lead to water loss and result in poor strippability. Applications of new technology can increase yield and without compromising the quality of the oil extracted. However, the incidences of USB are yet to address, as the efficiency of sterilisation was evaluated by measuring the percentage of USB.

Therefore, the heat transfer phenomena during sterilisation need to be investigated. Poor milling efficiency could be due to the typical palm oil milling process. The stalk is processed together with the FFB, which may cause difficulties of heat penetration, especially to those fruits located at the centre of a large and compact bunch. In addition, insufficient steam supply reduces the steam temperature to the sterilisers. As a result, the heat transmitted to the FFBs might be insufficient to achieve good sterilisation within the fixed period; this will eventually affect the FFBs strippability as reflected in the percentage of USB. Arif et al. (2016) observed that less heat was transferred inside the FFB stalks ($0.00054^{\circ}\text{C/s}$ to $0.00977^{\circ}\text{C/s}$) as compared to sections near or beside the stalk ($0.01988^{\circ}\text{C/s}$ to $0.02228^{\circ}\text{C/s}$). Moreover, fluctuation of heat transfer was observed due to inconsistent steam penetration towards the inside of the FFBs stalk. Babatunde et al. (1988) performed a comparative study that revealed 52% of the sterilised fruits were stripped after sterilisation at 100°C for 120 minutes, compared to about 95% of fruits stripped after 50 minutes of sterilisation at 130°C .

Low strippability was observed if air occluded in the bunch did not remove efficiently; this is due to low thermal conductivity caused by the compact nature of the fruits. The thermal conductivity of air is about 10 times lower than that of oil and 30 times lower than water. Ariffin (1991) and Sivasothy et al. (1992, 1994) reported that the introduction of the pollination by the weevil, *Elaeidobius Kamerunicus*, in 1981 had increased the difficulty of heat penetration to larger and more closely packed multi-layer fruitlets during sterilisation. Therefore, it is important to remove as much air as possible during sterilisation. Air not only acts as a barrier to heat transfer, but oil oxidation increases considerably at high temperatures. Therefore, it can affect the quality, such as the poor bleachability of the product oil. In a horizontal steriliser, different air-steam mixture compositions are observed at various points of the sterilising process after a short time of sweeping, ranging from 0.1

L to 200 L of air/kg of steam from the top to the bottom of the steriliser. Therefore, it is also important to monitor the evacuation of the air content during the sterilisation process slowly and progressively. It is suggested to sweep the air with steam for 10 minutes at a rate of 100 kg/hr to expel almost 90% of air from the steriliser (Menon, 2012; Menon, 2013). Concurrently, the condensate formed will also need to be removed from the vessel to prevent it from interfering with the heat transfer within the steriliser (Sivasothy et al., 1992).

The sterilisation temperature is vital as a sufficiently high temperature is required (above 100°C) for an optimum period (more than 50 minutes) to allow the heat to penetrate the pericarp, especially into the attachment point of the fruits to the stalk. The research found that an hour is required for the bunch core to reach a temperature of 130°C to 135°C (Babatunde et al., 1988; Sivasothy et al., 2005; Leuenberger, 2001; Vincent et al., 2014). However, the optimum temperature and duration required for certain weights and sizes of FFBs are not well known in the actual situation. As there is no indication when the 100% strippability has reached during the sterilisation. Hence, the chances of getting a USB still occur.

Therefore, let us look at sterilisation from a different angle. Particularly visualise sterilisation as a breakup of specific binding carbohydrates that leads to strippability. Sterilisation is viewed as a chemical reaction where the binding carbohydrates are degraded, as illustrated in Figure 2 (modified from Hubbe et al., 2018; D’Alessandro E & Pliego Jr, 2018). Carbohydrates are commonly divided into monosaccharides, oligosaccharides, and polysaccharides. Monosaccharides are polyhydroxy-aldehydes or–ketones, generally with an unbranched carbon chain. Glucose, fructose, and galactose are their common representatives. In contrast, oligosaccharides are carbohydrates obtained from <10 carbohydrate units, formally dehydrated to form monosaccharides. While polysaccharides, consisting of numerous monosaccharides that can up to > 10 units. Hence, the polysaccharides are often considerably less soluble in water than mono- and oligosaccharides. The well-known representatives are starch, cellulose, and pectin (Belitz et al., 2009). Elevated temperatures with sufficient water enhanced

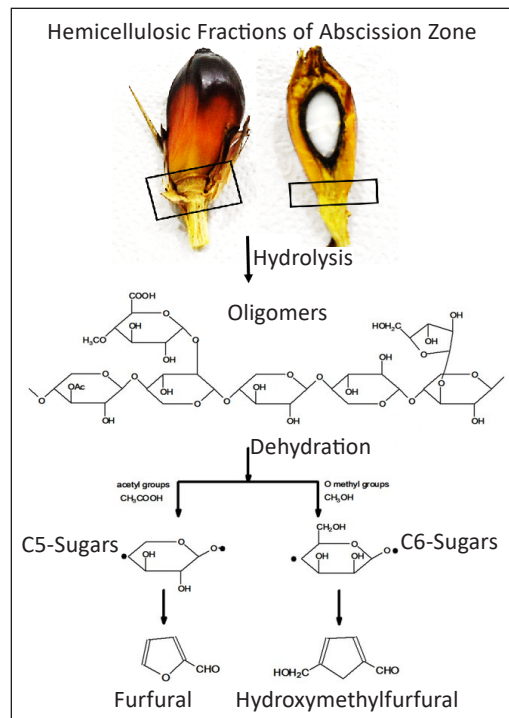


Figure 2. Schematic presentation of a breakdown of binding carbohydrates at the abscission zone of FFB

the hydrolysis of cell wall materials into oligo-intermediates before the formation of monomers such as glucose and xylose (Mittal et al., 2009; Jacobsen & Wyman, 2000; Lloyd & Wyman, 2003; Hubbe et al., 2018; D'Alessandro & Pliego Jr, 2018). Some can be further dehydrated and produce hydroxymethylfurfural and furfural (Lloyd & Wyman, 2003).

It is assumed that better heat penetration efficiency during the sterilisation process will result in a higher rate of degradation of lignocellulosic fibres to sugars, thus a higher percentage of strippability. The energy supplied into the steriliser is used to break the binding carbohydrates of the abscission zone, and therefore the fruit can be mechanically detached from the stalk. The heat penetration induces a breakage of the cells connecting the fruit to the stalk during the sterilisation stage. An effective sterilisation process can ensure optimum hydrolytic degradation of the binding carbohydrates within fruits to stalk and consequently maximising the detachment of fruits. However, limited research has been done on the heat treatment to enhance the depolymerisation of cell walls during sterilisation. The binding carbohydrates of oil palm fruits were investigated by Silvamany and Jahim (2015). The result showed that the sterilised oil palm fruits contain extractive, moisture, hemicellulose, α -cellulose, and soluble lignin, as tabulated in Table 2.

On the other hand, Thang et al. (2017) reported that the water-soluble sugar content from oil palm fruits subjected to autoclave treatment ranged from 3.2% to 3.6%. Sucrose and glucose were found between 0.34% and 0.54% for all samples. The water-soluble sugar content was found slightly higher than non-structural carbohydrates due to the hydrolysis of cell wall materials during high-temperature autoclaves. Babatunde et al. (1988) reported that the cell wall materials of the fruit tissue could be depolymerised at temperatures above 48°C and dehydrated at temperatures above 115°C. Besides, the degradation of binding carbohydrates at the abscission zone of FFBs during sterilisation could be established by analysing the sugars compositions in the steriliser condensates. The sugars may be leached into the steriliser condensate during the sterilisation or degraded. Ariffin et al.

Table 2
Composition analysis of palm mesocarp

Characterisation	%
Total lipid content	56.68
Soluble sugars	2.89
Total structural carbohydrates	13.76
Glucan	8.27
Xylan	4.52
Arabinan	0.97
Soluble lignin	3.58
Insoluble lignin	0.038
Water extractive	17.16
Ethanol extractive	17.98

Table 3
Sugar content in steriliser condensate and sludge

Sugar	Condensate (ppm)	Sludge (ppm)
Glucose	120.54	170.75
Fructose	123.59	175.96
L-Sorbose	139.53	197.44
D-Ribose	166.48	251.47
L-Arabinose	149.85	233.06
D-Galactose	160.16	248.02
Maltose	265.28	411.35
Xylose	133.48	207.35
Mannose	137.94	256.37

(1993) reported that various soluble sugars were analysed in steriliser condensate and sludge obtained from palm oil mill (Table 3). It has been evidenced that sterilisation via hydrolysis of the binding carbohydrates facilitates the release of oil.

Therefore, the mechanism of the heating process and its relationship with cell walls degradation to enhance strippability should be further investigated. FFBs delivered to the mills comprise fruits with different degrees of ripeness. Hence, an optimum sterilisation process is important to ensure all fruits at different ripeness levels are being stripped from the stalk. This action allows specific chemical changes such as rupture of vessels, swelling or elongation of the connecting tissue cells, and modification of pectic compounds (Mongana Report, 1955; Hassan et al., 1994). In addition, the composition of the sugars of the sterilised fruit or the condensate could be used as an indicator to optimise the sterilisation parameter to achieve 100% strippability with zero USB.

CONCLUSION

This review has summarised the current steriliser technologies used in palm oil mills, including horizontal, vertical, spherical and continuous sterilisers. The roles and principles of the sterilisation process in palm oil mills have also been elucidated. To date, it can be concluded that horizontal sterilisers (batch process) and continuous sterilisers (continuous process) are the most promising technologies owing to their large scale production and ability to produce crude palm oil with low FFA. Potential replacements for conventional sterilisers such as solvent extraction and microwave-assisted sterilisation to improve the oil extraction rate and reduce oil losses have also been studied. However, the effects of sterilisation conditions on FFBs with different ripeness categories based on the chemical changes in the binding carbohydrates at the abscission zone and relate the effects to the fruits strippability should be evaluated. An effective and optimised sterilisation process with sufficient heat penetration at the point of abscission zone ensure hydrolytic degradation of these binding carbohydrates and maximise of the detachment of fruits from the bunch to be developed.

ACKNOWLEDGEMENTS

The authors are grateful to Sime Darby Plantation Bhd and Universiti Putra Malaysia LRGS 5526100 for the guidance, encouragement, and funding for the success and permission to publish this paper.

REFERENCES

- Abbas, S. A., Ali, S., Halim, S. I. M., Fakhru-Razi, A., Yunus, R., & Choong, T. S. Y. (2006). Effect of thermal softening on the textural properties of palm oil fruitlets. *Journal of Food Engineering*, 76(4), 626-631. <https://doi.org/10.1016/j.jfoodeng.2005.06.013>

- Arif, H., Wahad, M. A., & Sobri, T. M. (2016a). Model validation for temperature profile inside FFB during sterilization for palm oil mill process. *Journal of Engineering and Applied Sciences*, 11(15), 9029-9038.
- Ariffin, A. A. (1991). Chemical changes during sterilization process affecting strippability and oil quality. Seminar on Developments in Palm Oil Milling Technology and Environmental Management. Genting Highlands (pp.2-12). PORIM.
- Ariffin, A. A. (2010, May 11-13). *Ripeness standards and palm fruit maturity affecting oil extraction rate (OER)*. [Paper Presented] 2011 International Conference and Exhibition of Palm Oil, Jakarta, Indonesia.
- Ariffin, A. A., Rosnah, M. S., Muhamadiyah, B., Zailan, W. O. W., & Hasamudin, W. H. W. (1993, August 18-19). *Biochemical study of sterilizer condensate and sludge from palm oil mill*. [Paper Presented]. 1993 National Seminar on Advances in Environmental Control Technology, Kuala Lumpur, Malaysia.
- Aziz, M. K. A. (2003). *The study of heat penetration in palm oil fruitlets by developing a new technique for measuring oil content in fruitlet during sterilization process*. Universiti Teknologi Malaysia Institutional Repository.
- Babatunde, O. O., Ige, M. T., & Makanjuola, G. A. (1988). Effect of sterilization on fruit recovery in oil palm fruit processing. *Journal of Agricultural Engineering Research*, 41(2), 75-79. [https://doi.org/10.1016/0021-8634\(88\)90190-4](https://doi.org/10.1016/0021-8634(88)90190-4)
- Belitz, H., Grosch, W., & Schieberle, P. (2009). Carbohydrates. In H. Belitz, W. Grosch, & P. Schieberle (Eds.), *Food Chemistry* (pp. 248-339). Springer. <http://dx.doi.org/10.1007/978-3-540-69934-7>
- Chong, C. L., & Sambanthamurthi, R. (1993). Effects of mesocarp bruising on the rate of free fatty acid release in oil palm fruits. *International Biodeterioration & Biodegradation*, 31, 65-70. [https://doi.org/10.1016/0964-8305\(93\)90015-T](https://doi.org/10.1016/0964-8305(93)90015-T)
- Chow, M. C., & Ma, A. N. (2007). Processing of fresh palm fruits using microwaves. *Journal of Microwave Power Electromagnetic Energy*, 40(3), 165-173. <https://doi.org/10.1080/08327823.2005.11688538>.
- CIMG. (2015). *3C spherical FFB sterilizer 2.0 – A cost-efficient tool in palm oil extraction in the 21st century*. CIMG Resources Sdn Bhd. Retrieved August 19, 2013, from <http://spherical-sterilizer-palm-oil-mill.blogspot.com/2015/03/3c-spherical-ffb-sterilizer.html>
- Corley, R. H. V., & Tinker, P. B. (2003). The products of the oil palm and their extraction. In *The Oil Palm* (pp. 445-466). Blackwell Publishing.
- D'Alessandro E., & Pliego Jr, J. (2018). Fast screening of solvents for simultaneous extraction of furfural, 5-hydroxymethylfurfural and levulinic acid from aqueous solution using SMD solvation free energies. *Journal of the Brazilian Chemical Society*, 29(2), 430-434. <http://dx.doi.org/10.21577/0103-5053.20170140>
- Domínguez, H., Núñez, M. J., & Lema, J. M. (1994). Enzymatic pretreatment to enhance oil extraction from fruits and oil seeds: A review. *Food Chemistry*, 49(3), 271-286. [https://doi.org/10.1016/0308-8146\(94\)90172-4](https://doi.org/10.1016/0308-8146(94)90172-4)
- Eshtiaghi, M. N., Paoplook, K., Yoswathana, N., & Kuldiloke, J. (2015). Enhanced oil extraction from palm fruit mesocarp using technical enzymes. *International Journal of Advances in Science Engineering and Technology*, 3(1), 42-45.

- Fatin, S. A., Rosnah, S., & Robiah, Y. (2014). The effect of storage time of chopped oil palm fruit bunches on the palm oil quality. *Agriculture and Agricultural Science Procedia*, 2, 165-172.
- Hadi, N. A., Ng, M. H., Choo, Y. M., & Ma, A. N. (2012). Dry heating of palm fruits: Effect on selected parameters. *American Journal of Engineering and Applied Sciences*, 5(2), 128-131.
- Hadi, S., Ahmad, D., & Akande, F. B. (2009). Determination of the bruise indexes of oil palm fruits. *Journal of Food Engineering*, 95, 322-326. <https://doi.org/10.3844/ajeassp.2012.128.131>
- Halim, S., Mustafa, K., & Noor, A. (2009). Research work on steam accumulator in palm oil mill. *European Journal of Scientific Research*, 37(4), 542-552.
- Hassan, A. H., Basiron, Y., Sukaimi, J., Loke, K. H., Salleh, H., & Hasan, N. B. (1994). Sterilization. In *Palm Oil Factory Process Handbook Part 1 – General Description of the Palm Oil Milling process* (pp. 17-29). Palm Oil Research Institute of Malaysia.
- Henderson, J., & Osborne, D. (1990). Cell separation and anatomy of abscission in the oil palm, *Elaeis guineensis* Jacq. *Journal of Experimental Botany*, 41(223), 203-210.
- Henderson, J., & Osborne, D. J. (1991). Lipase activity in ripening and mature fruit of the oil palm. Stability *in vivo* and *in vitro*. *Phytochemistry*, 30(4), 1073-1078. [https://doi.org/10.1016/S0031-9422\(00\)95175-6](https://doi.org/10.1016/S0031-9422(00)95175-6)
- Henderson, J., & Osborne, D. J. (1994). Inter-tissue signalling during the two-phase abscission in oil palm fruit. *Journal of Experimental Botany*, 42(276), 943-951.
- Henderson, J., Davies, H. A., Heyes, S. J., & Osborne, D. J. (2001). The study of a monocotyledon abscission zone using microscopic, chemical, enzymatic and solid state ¹³C CP/MAS NMR analyses. *Phytochemistry*, 56(2), 131-139. [https://doi.org/10.1016/S0031-9422\(00\)00447-7](https://doi.org/10.1016/S0031-9422(00)00447-7)
- Hubbe, M., Pizzi, A., Zhang, H., & Halis, R. (2018). Critical links governing performance of self-binding and natural binders for hot-pressed reconstituted lignocellulosic board without added formaldehyde: A review. *Bioresources*, 13(1), 2049-2115.
- Jacobsen, S. E., & Wyman, C. E. (2000). Cellulose and hemicellulose hydrolysis models for application to current and novel pretreatment processes. *Applied Biochemistry and Biotechnology*, 84, 81-96. <https://doi.org/10.1385/ABAB:84-86:1-9:81>
- Khalid, K. B., Zahariah, Z., & Yusof, W. D. W. (1996). Variation of dielectric properties of oil palm mesocarp with moisture content and fruit maturity at microwave frequencies. *Elaeis*, 8(2), 83-91.
- KM. (2013). Selection of sterilizer technology for energy efficient operation of palm oil mills. ENERGYWISE. Retrieved September 23, 2013, from <http://rank.com.my/energywise/?p=310#sthash.XLTPqAJj.dpbs>.
- Kumaradevan, D., Chuah, K. H., Moey, L. K., Mohan, V., & Wan, W. T. (2015). Optimising the operational parameters of a spherical steriliser for the treatment of oil palm fresh fruit bunch. *IOP Conference Series: Materials Science and Engineering*, 88, 1-6.
- Leuenerger, H. (2001). *Physical basic of steam sterilization*. Retrieved August 18, 2015, from <http://www.pharma.unibas.ch/technology/index.html>.
- Lloyd, T., & Wyman, C. E. (2003). Application of a depolymerization model for predicting thermochemical hydrolysis of hemicellulose. *Applied Biochemistry and Biotechnology*, 105, 53-67. <https://doi.org/10.1385/ABAB:105:1-3:53>

- Loh, T. W. (1994, July 7-8). Innovative methods in oil processing/ oil palm industry. In *Proceedings of the 1994 PORIM National Palm Oil Milling and Refining Technology Conference* (pp. 75-80). Kuala Lumpur, Malaysia.
- Menon, N. R. (2012). Innovation potentials in palm oil mill design. *Palm Oil Engineering Bulletin*, 104, 21-34.
- Menon, N. R. (2013). Process review: Part 1. *Palm Oil Engineering Bulletin*, 108, 21-34.
- Mittal, A., Chatterjee, S. G., Scott, G. M., & Amidon, T. E. (2009) Modeling xylan solubilization during autohydrolysis of sugar maple and aspen wood chips: Reaction kinetics and mass transfer. *Chemical Engineering Science*, 64(13), 3031-41. <https://doi.org/10.1016/j.ces.2009.03.011>
- Mohankumar, C., Arumugan, C., & Kaleysaraj, R. (1990). Histological localization of oil palm fruit Lipase. *Journal of the American Oil Chemists' Society*, 67(10), 665-669. <https://doi.org/10.1007/BF02540419>
- Mongana Report (1955). *Research on production & storage of palm oil*. Institute for the advancement of Scientific Research in Industry & Agriculture.
- MPOB. (2019). *Oil extraction rate*. Malaysia Palm Oil Board.
- Ngando-Ebongue, G. F., Dhouib, R., Carrière, F., Zollo, P. H. A., & Arondel, V. (2006). Assaying lipase activity from oil palm fruit (*Elaeis guineensis* Jacq.) mesocarp. *Plant Physiology and Biochemistry*, 44(10), 611-617. <https://doi.org/10.1016/j.plaphy.2006.09.006>
- Omar, A. K. M., Norsalwani, T. L. T., Khalil, H. P. S. A., Nagao, H., Zuknik, M. H., Hossain, M. S., & Norulaini, N. A. N. (2017). Waterless sterilization of oil palm fruitlets using supercritical carbon dioxide. *The Journal of Supercritical Fluid*, 126, 65-71. <https://doi.org/10.1016/j.supflu.2017.02.019>
- Osborne, D. J., Henderson, J., & Corley, R. H. V. (1992). Controlling fruit-shedding in the oil palm. *Endeavour*, 16(4), 173-177. [https://doi.org/10.1016/0160-9327\(92\)90044-P](https://doi.org/10.1016/0160-9327(92)90044-P)
- Owolarafe, O., & Faborode, M. (2008). Micro-structural characterisation of palm fruit at sterilisation and digestion stages in relation to oil expression. *Journal of Food Engineering*, 85(4), 598-605.
- Payasi, A., Mishra, N. N., Chaves, A. L. S., & Singh, R. (2009). Biochemistry of fruit softening: An overview. *Physiology and Molecular Biology of Plants*, 15(2), 103-113. <https://doi.org/10.1007/s12298-009-0012-z>
- Razali, M. H., Halim, A. S. M. A., & Roslan, S. (2012). A review on crop plant production and ripeness forecasting. *International Journal of Agriculture and Crop Sciences (IJACS)*, 4(2), 54-63
- Roongsatham, P., Morcillo, F., Jantasuriyarat, C., Pizot, M., Moussu, S., Jayaweera, D., Collin, M., Gonzalez-Carranza, Z. H., Amblard, P., Tregear, J. W., Tragoonrung, S., Verdeil, J., & Tranbarger, T. J. (2012). Temporal and spatial expression of polygalacturonase gene family members reveals divergent regulation during fleshy fruit ripening and abscission in the monocot species oil palm. *BMC Plant Biology*, 12(150), 1-15. <https://doi.org/10.1186/1471-2229-12-150>
- Sambanthamurthi, R., Let, C. C., Cheang, O. K., Huat, Y. K., & Rajan, P. (1991). Chilling-induced lipid hydrolysis in the oil palm (*Elaeis guineensis*) mesocarp. *Journal of Experimental Botany*, 42(242), 1199-1205. <https://doi.org/10.1093/jxb/42.9.1199>
- Sambanthamurthi, R., Sundram, K., & Tan, Y. A. (2000). Chemistry and biochemistry of palm oil. *Progress in Lipid Research*, 39(6), 507-558.

- Sarah, M., & Taib, M. R. (2013). Enzymatic destruction kinetics of oil palm fruits by microwave sterilization. *International Journal of Chemical Engineering and Applications*, 4(3), 129-133. <https://doi.org/10.7763/IJCEA.2013.V4.278>
- Siew, W. L. (2011). *Edible oil processing - Palm oil milling process*. The AOCS Lipid Library.
- Silvamany, H., & Jahim, J. M. (2015). Enhancement of palm oil extraction using cell wall degrading enzyme formulation. *Malaysian Journal of Analytical Sciences*, 19(1), 77-87.
- Sivasothy, K. Ma, A. N., Maycock, J. H., & Koichiro, Y. (1994) Combined sterilization-stripping process. *Palm Oil Development*, 19, 20-29.
- Sivasothy, K., Basiron, Y., Suki, A., Taha, R. M., Hwa, T. Y., & Sulong, M. (2006). Continuous sterilization: The new paradigm for modernizing palm oil milling. *Journal of Oil Palm Research*, (Special Issue), 144-152.
- Sivasothy, K., Halim, R. M., & Basiron, Y. (2005). A new system for continuous sterilization of oil palm fresh fruit bunches. *Journal of Oil Palm Research*, 17, 145-151.
- Sivasothy, K., Hasan, M., & Yaacob, M. (1992). Overview of automation in a palm oil mill - The sterilisation process. *Computing & Control Engineering Journal*, 3(1), 45-52. doi.org/10.1049/cce:19920016
- Sivasothy, K., & Rohaya, M. H. (2000, May 18-19). *Crushing and sterilization of fresh fruit bunches: a promising approach for continuous sterilization*. [Paper presentation]. 2000 International Planters Conference, Kuala Lumpur, Malaysia.
- Sukaribin, N., & Khalid, K. (2009). Effectiveness of sterilisation of oil palm bunch using microwave technology. *Industrial Crops and Product*, 30(2), 179-183. <https://doi.org/10.1016/j.indcrop.2009.05.001>
- Sultana, Y. (2007). *Pharmaceutical microbiology and biotechnology-sterilization method and principles*. Semantic Scholar.
- Tan, Y., Kuntom, A., Siew, W., Yusof, M., & Chong, C. (1999). Present status of crude palm oil quality in Malaysia. In *Proceedings of the PORIM International Palm Oil Congress* (pp.203-211). PORIM.
- Tan, Y. A., Low, K. W., Lee, C. K., & Low, K. S. (2010). Imaging technique for quantification of oil palm fruit ripeness and oil content. *European Journal of Lipid Science and Technology*, 112(8), 838-843. <https://doi.org/10.1002/ejlt.201000020>
- Teh, H. F., Neoh, B. K., Hong, M. P., Low, J. Y., Ng, T. L., Ithnin, N., Thang, Y. M., Mohamed, M., Chew, F. T., Yusof, H. M., Kulaveerasingam, H., & Appleton, D. R. (2013). Differential metabolite profiles during fruit development in high-yielding oil palm mesocarp. *PLoS One*, 8(4), Article e61344. <https://doi.org/10.1371/journal.pone.0061344>
- Thang, Y. M., Ariffin, A. A., Appleton, D. R., Asis, A. J., Mokhtar, M. N., & Yunus, R. (2017). Determination of sugars composition in abscission zone of oil palm fruit. In *IOP Conference Series: Materials Science and Engineering* (Vol. 206, No. 1, p. 012034). IOP Publishing.
- Umudee, I., Chongcheawchamnan, M., Kiatweerasakul, M., & Tongurai, C. (2013). Sterilization of oil palm fresh fruit using microwave technique. *International Journal of Chemical Engineering and Applications*, 4(3), 111-113. <https://doi.org/10.7763/IJCEA.2013.V4.274>

Yin Mee Thang, Robiah Yunus, Mohd Noriznan Mokhtar, David Ross Appleton,
Ahmad Jaril Asis, Pei San Kong, Huey Fang Teh and Abdul Azis Ariffin

- Vincent, C. J., Shamsudin, R., & Baharuddin, A. S. (2014) Pretreatment of oil palm fruits: A review. *Journal of Food Engineering*, 143, 123-131. <https://doi.org/10.1016/j.jfoodeng.2014.06.022>.
- Walat, O., & Ng, S. B. (2013). Palm oil mill OER and total oil losses. *Palm Oil Engineering Bulletin*, 108, 10-16.
- Zulkifli, A. R., & Ropandi, M. (2001). Fully stripped bunches in palm oil mills. *MPOB Information Series*, 111(127), 1-2.

Utilisation of Oil Palm Fibre Biomass Waste as Additives in Foamed Concrete

Md Azree Othuman Mydin

School of Housing, Building and Planning, Universiti Sains Malaysia, 11800, Penang, Malaysia

ABSTRACT

Worldwide, the construction industry has acknowledged the future demand for lightweight construction materials, with high workability, self-compacting, and environmentally friendly. Given this demand, recent innovative material namely foamed concrete (FC), has been found to reduce normal concrete's weight potentially. However, while FC made with Ordinary Portland Cement has good compressive strength, other characteristics such as tension are relatively weak given the number of micro-cracks. Therefore, the study focused on the potential use of oil palm fibres in FC regarding their durability and mechanical properties. Notably, one of the major issues faced in the construction of reinforced FC is the corrosion of reinforcing steel which affects the behaviour and durability of concrete structures. Hence, in this study, oil palm fibres were added to improve strength and effectively reduce corrosion. Five types of fibre generated from oil palm waste were considered: oil palm trunk, oil palm frond, oil palm mesocarp and empty fruit bunch consisting of the stalk and spikelets. Specimens with a density of 1800 kg/m³ were prepared in which the weight fraction of the fibre content was kept constant at 0.45% for each mixture. Testing ages differed in testing and evaluating the parameters such as compressive strength, flexural strength, tensile strength, porosity, water absorption, drying shrinkage and ultrasonic pulse velocity. The results showed that the incorporation of oil palm fibre in FC helped reduce water absorption, porosity and shrinkage while enhancing the compressive, flexural and tensile strength of FC.

Keywords: Bending, compression, foamed concrete, oil palm fibre, porosity, water absorption

ARTICLE INFO

Article history:

Received: 06 April 2021

Accepted: 05 July 2021

Published: 18 October 2021

DOI: <https://doi.org/10.47836/pjst.29.4.27>

E-mail address:

azree@usm.my

INTRODUCTION

Concrete is one of the main materials used in the construction sector, given its versatility in terms of production and its environmental protection and recyclability. Concrete is still preferred as a material used

for construction compared to timber, steel or composite materials. Naturally, concrete has higher compressive strength but lower tensile strength. Structures constructed from concrete materials also have a long service life. Composite's responses are formed when the concrete is incorporated with reinforced steel bars, and in this way, all types of actions can be sustained. However, the average concrete density is around 2400 kg/m^3 , which often causes issues in larger open floor plans and high-rise buildings since it will be penalised due to its weight towards the project (Suhendro, 2014). It has become a major issue in the construction industry for the past few years, as the demand for high-rise buildings increases from year to year. Consequently, researchers and engineers continue to focus on addressing and overcoming this issue. Hence, foamed concrete (FC) has become the latest advanced material that could minimise the self-weight of the concrete. It can be made to have a density between 800 kg/m^3 to 1800 kg/m^3 (Serri et al., 2014). These characteristics have attracted building material manufacturers for construction applications. Therefore, oil palm fibre is one of the additives included in the FC mixture to enhance its properties.

In Malaysia's agricultural sector, oil palm is one of the main exports, which has helped develop the industry and the economy. Lignocellulosic biomass generated from oil palm industries comprises cellulose, hemicellulose, and lignin and is often referred to as plant biomass (Mohammadhosseini et al., 2016). Oil palm trunks (OPT), oil palm fronds (OPF), empty fruit bunches (EFB) and palm pressed fibres (PPF), palm shells, and palm oil mill effluent (POME) are included in this classification. However, major dumping issues result given the presence and volume of oil palm waste. Therefore, to solve this issue regarding biomass waste, the waste from the by-product of oil palm can be utilised as the infill material in FC to enhance its properties (Momeen et al., 2016). FC is a cellular cemented material acquired through the introduction of preformed foam into the cementitious matrix. Combining these materials leads to air voids built up within the material's underlying microstructure (Mahzabin et al., 2018). These natural fibres substitute other traditional additives such as steel and glass fibres which have previously been expansively utilised. This change in tendency is due to the added value that natural fibres bring to these materials, particularly from sustainability.

There is increasing attention to developing concrete bonded natural lignocellulosic fibre composites with improved durability and mechanical properties. These fibres provide a superior contact surface with the cement matrix, which significantly enhances its bond, gaining a more homogeneous material, thus, having better mechanical properties. The inclusion of lignocellulosic fibres, such as coconut fibre, oil palm fibre and jute fibre as reinforcement in cement-based composites, has been studied to in part substitute the synthetic counterparts, particularly glass and polymeric fibres in construction materials. Though, in addition to the problem of durability, there is the issue of the interface between the fibres with the cementitious matrix (Ezerskiy et al., 2018). Furthermore, the mechanical

features of cement-based composites strengthened with natural fibres not only depend on the properties of the fibre itself but also on the degree to which an applied load is spread to the fibres by the matrix phase (Ferreira et al., 2017).

Moreover, deviations in the mechanical properties over time can transpire due to microstructural instabilities in the fibre–matrix boundary and bulk, as a sign of the continued hydration process in the fibre surroundings (Hasan et al., 2020). First, though, the growing porosity value of the cement composite in the interfacial region arises, as there is a variation of the water to binder proportion (Hospodarova et al., 2018). Then, there is a further encounter for the fibre-cement; the lignocellulosic fibres' hydrophilic nature hinges on the lumens, sorptivity, irregularity, chemical compounds and superficial energy in the fibre–matrix boundary (Karade & Aggarwal, 2011). Therefore, it is crucial to control the fibre–matrix interface with lignocellulosic fibre, unlike synthetic fibres such as glass fibre. Lignocellulosic fibres have substantial disparities in chemical composition, diameter, and superficial coarseness ensuing in the important smattering in fibre mechanical properties (Li et al., 2020). For instance, with a non-uniform cross-section and composition along the longitudinal axis, the tensile strength of the oil palm trunk fibre is diverse between 115 to 165 MPa. The lignocellulosic fibre reinforcement bonding in cement-based materials remain comparatively unmapped (Mahmud et al., 2021).

Therefore, problems between the lignocellulosic fibre interface and matrix must be analysed inversely from composites reinforced with synthetic fibres, though comparable durability and mechanical strictures can be employed (Onuaguluchi & Banthia, 2016). The contact can ensue over three mechanisms: mechanical coupling of the two materials, physical coupling such as van der Waals interaction, and covalent bonding between the fibre and the matrix (Kochova et al., 2020). These interactions produce an interphase region which is a three-dimensional region near the fibre with properties different from either the fibre or the matrix (Hasan et al., 2021)

In recent years, foresight groups worldwide have recognised the future demand for light, durable, economical and environmentally friendly construction materials to enhance eco-friendly products. It is anticipated that the current study will benefit many players in the construction industry, especially manufacturers and contractors since they can derive the benefits of the newly formed construction materials (Kamaruddin et al., 2018). FC has several advantageous properties such as low self-weight, especially for low densities, which are important in renovation operations and lowering the loads in the building's structural elements. As such, the oil palm fibres aid in reinforcing the FC and help to enhance the tensile and flexural strength of the FC.

According to Mohammadhosseini et al. (2016), the strength of EFB spikelet fibres is higher than the EFB stalk, whereas the extension at the failure of the fibre from the stalk is more than that of the fibre from the spikelet. OPT fibre was found to be suitable

reinforcement given the high tensile strength (300-600 N/mm²) retained by OPT, which is regarded as high compared to other natural fibres. OPT also has a high density (1200 kg/mm³), which signifies that the fibre has a strong and high lignin content (23.03%). Moreover, it is considered strong as lignified cellulose fibres hold their strength better than delignified fibres (Majid et al., 2012). Hence this research aims to examine the durability and mechanical properties of FC incorporating different types of biomass waste of the palm oil fibre, namely the stalk, spikelet, frond, trunk and mesocarp.

MATERIALS AND METHOD

Materials

FC is a mixture of lightweight cellular mortar and stable foam. Ordinary Portland Cement (OPC), fine sand, clean water and preformed foam are the main materials used to form FC. The cement used in this mixture is Type 1 Portland Cement under British Standard BS12 (British Standard Institution, 1996), and a portable foaming generator is used to produce the stable foam practically. In this study, a synthetic foaming agent, as the foaming agent, was used to produce the foam. This type of foaming agent is suitable to produce FC since it has a density of 1000 kg/m³ and above. The ratio of foam to water applied was 1:30. This colourless liquid has a specific gravity of 1.05 and is a foaming agent containing sodium sulphate that eases foam formation. Previously, foam generators were used as a preform foaming agent and to mix the synthetic foam with water.

Next, the foam was then applied to the mortar and mixed for 5 minutes. The mixing rotation speed was subsequently decreased to prevent the occurrence of defects. The weight of the foam used in this study was 65 g/litre for each design mix. In addition, the fine aggregate used in this study was natural fine sand obtained through a local distributor. The fine sand had been sieved during the material preparation. The appropriate size of fine aggregates or fine sand used was 1.18 mm using a sieving machine according to British Standard BS882 (British Standard Institution, 1992). Clean water free from debris and other organic materials was used to mix and cure the process in this study. The water-cement ratio was 0.45 based on previous studies that claimed that this ratio could achieve reasonable workability of FC. Oil palm fibres were used in vast quantities of oil palm biomass such as oil palm trunk (OPT), an oil palm frond (OPF), oil palm mesocarp (OPM) and empty fruit bunch (EFB) consisting of the stalk and spikelets generated by the oil palm industry in Malaysia.

The OPF and OPT were produced from oil palm plantations, while the oil palm EFB was from oil palm processing. The OPM is residue attained from oil palm fruits after extracting the oil. All these fibres were extracted and processed in factories and supplied from a local supplier. The fibres were cleaned and rinsed five times using tap

water beforehand to eliminate any unwanted debris (Figure 1). The fibres were then sun-dried for about 72 h until thoroughly dried. Only natural fibres were used in this study, having a length of around 3 cm and 0.01 mm in diameter. The weight fraction used was 0.45% by weight of the total mix. The chemical composition and mechanical properties of these fibres are shown in Table 1. Figure 2 visualises the SEM micrograph images of different types of fibre used in this investigation.



Figure 1. Fibres were properly washed to remove unwanted residue and debris

Table 1
Chemical composition and mechanical properties of fibres

Composition	Fronde fibre	Trunk fibre	Mesocarp fibre	Spikelets fibre	Stalk fibre
Lignin (%)	21.4 ± 0.6	20.1 ± 0.8	31.4 ± 3.8	23.6 ± 0.5	17.8 ± 0.7
Cellulose (%)	31.7 ± 4.1	34.4 ± 0.8	24.5 ± 0.7	25.1 ± 2.6	33.1 ± 0.6
Hemicellulose (%)	34.3 ± 1.2	14.3 ± 1.6	31.7 ± 4.4	26.2 ± 1.5	32.8 ± 2.2
Extractives (%)	2.5 ± 0.4	2.4 ± 0.3	4.3 ± 0.2	2.7 ± 0.3	3.2 ± 0.4
Diameter (µm)	296	275	382	358	329
Density (kg/m ³)	660	635	804	758	722
Tensile strength (MPa)	96	67	139	116	82
Young's modulus (MPa)	6753	3828	14367	10305	5831
Elongation at break (%)	14.4	17.5	9.6	11.5	14.7

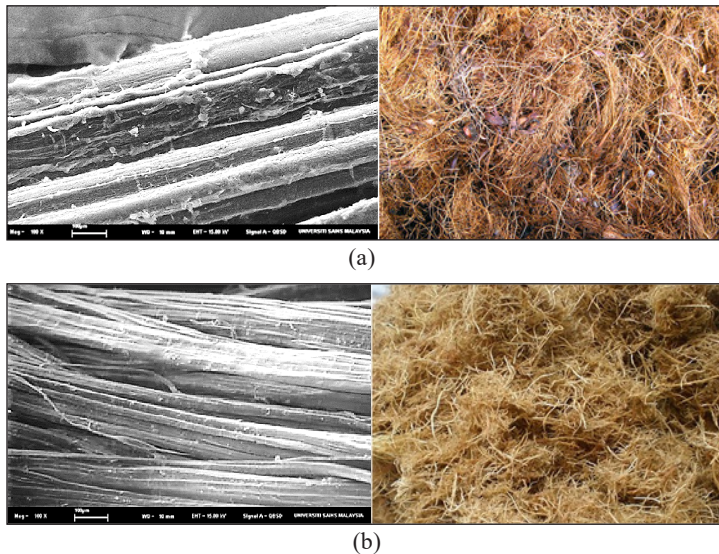


Figure 2. SEM micrograph of different types of fibre used in this study: (a) mesocarp fibre; and (b) stalk fibre

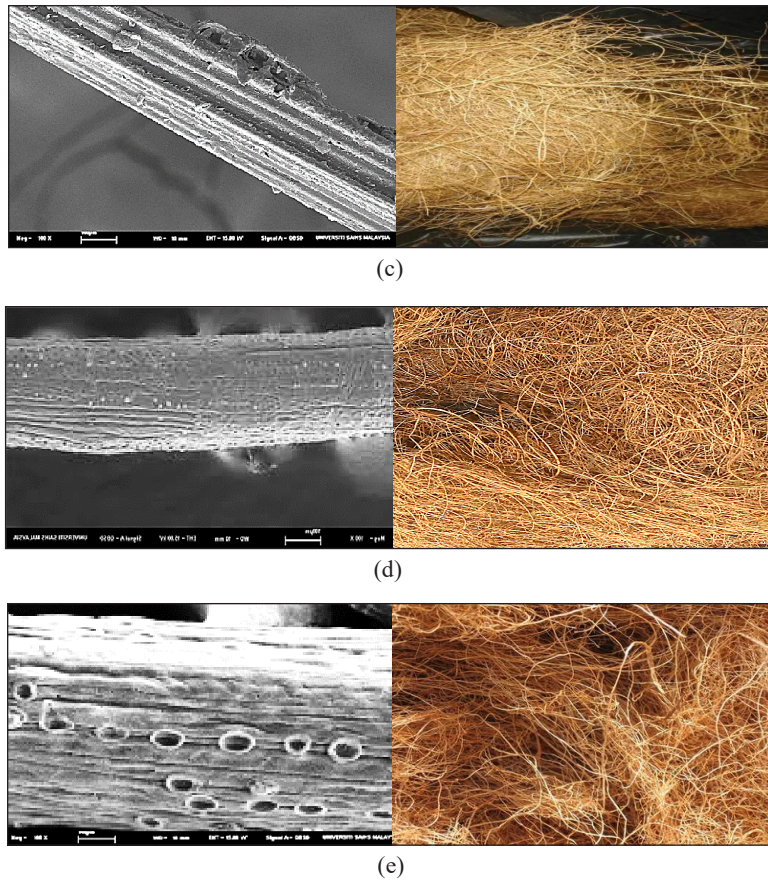


Figure 2 (continue). SEM micrograph of different types of fibre used in this study: (c) frond fibre; (d) trunk fibre; and (e) spikelets fibre

Mix Design

A total of 6 mixes were prepared in this research. The density used was kept constant at 1800 kg/m^3 . The fibre weight fraction (weight-to-weight ratio) used in this study was 0.45%. For all mixes, the sand-cement ratio was 1:1.5, and the water-cement ratio was kept constant at 0.45 because it gave adequate workability through the flow table test (Figure 3). The desirable spread for this flow table test is between 20-25cm. For this assessment, spreads of 22 to 24 cm were achieved. Table 2 shows the proportions of the mix used in this study.



Figure 3. Flow table test

Table 2
Mix proportions

Type	Target Density (kg/m ³)	Actual mix Density (kg/m ³)	Percentage of Fibre (%)	Mix ratio (S: C: W)	Cement weight (kg)	Fine sand (kg)	Water (kg)	Fibre weight (kg)
Control	1800	1793	-	1:1.5:0.45	39.81	59.72	17.92	-
FronD	1800	1805	0.45	1:1.5:0.45	39.81	59.72	17.92	0.529
Trunk	1800	1799	0.45	1:1.5:0.45	39.81	59.72	17.92	0.529
Mesocarp	1800	1813	0.45	1:1.5:0.45	39.81	59.72	17.92	0.529
Spikelet	1800	1811	0.45	1:1.5:0.45	39.81	59.72	17.92	0.529
Stalk	1800	1809	0.45	1:1.5:0.45	39.81	59.72	17.92	0.529

Testing

The tests performed in this study involved examining the durability and mechanical properties of the oil palm fibres. The water absorption test, porosity test, ultrasonic pulse velocity (UPV) test and drying shrinkage test were undertaken to examine the durability properties of FC. In addition, destructive tests that included the compression test, flexural test and splitting tensile test were also conducted in determining the mechanical properties of FC. Tables 3 and 4 show details of the specimens and standard codes of these tests for the durability properties and mechanical properties tests.

Table 3
Durability properties test

Type of Test	Specimen	Code	Description
Porosity	Cylinder (45 mm diameter × 50 mm height)	British Standard BS1881-122 (British Standard Institution, 1983)	The specimens are fully submerged in the vacuum chamber for 48 h after being removed from the oven and cooled. The mass in water and mass in the air is then recorded.
Water Absorption	Cylinder (75 mm diameter × 100 mm height)	British Standard BS1881-122 (British Standard Institution, 1983)	The specimens are placed in an oven for 72 h. After being removed and cooled, specimens are weighed and immediately immersed in the tank. The specimens are left immersed for 30 min. Then, after being removed from the water, the specimens are weighed again.
Drying Shrinkage	Prism (75 mm × 75 mm × 275 mm)	ASTM International C878 (ASTM International, 2014)	A spherical gauge plugs are attached at both ends of the specimens to facilitate length change measurements.
UPV	Prism (100 mm × 100 mm × 500 mm)	British Standard BS12504-4 (British Standard Institution, 2004)	The ultrasonic pulse velocity (UPV) is examined by measuring the propagation velocity of a transmitted longitudinal ultrasonic pulse across the cross-sectional area. The transducers are placed for testing at a length of 0.5 m.

Table 4
Mechanical properties test

Type of Test	Specimen	Code	Description
Compression Test	Cube (100 mm × 100 mm × 100 mm)	British Standard BS12390-3 (British Standard Institution, 2011)	Compressive strength test of FC is performed using GoTech GT-7001-BS300 Universal Testing Machine. The maximum load and compressive strength are recorded.
Flexural Test	Prism (100 mm × 100 mm × 500 mm)	ASTM International C293 (ASTM International, 2016)	Flexural strength test of FC is conducted using GoTech GT-7001-C10 Universal Testing Machine. The maximum load and flexural strength are recorded.
Splitting Tensile Test	Cylinder (100 mm diameter × 200 mm height)	ASTM International C496 (ASTM International, 2017)	Tensile strength test of FC is accomplished using GoTech GT-7001-BS300 Universal Testing Machine. The maximum load and splitting tensile strength are recorded.

RESULTS AND DISCUSSION

Water Absorption

The water absorption percentage in FC specimens is shown in Figure 4. It is seen that the mesocarp fibre results had the lowest percentage of water absorption at 7.94%, followed by the percentage of the water absorption of the spikelet fibre at 7.99%. It shows a slight difference between spikelet fibre and mesocarp fibre at 0.05%. The control mix resulted in the highest rate of water absorption of 9.18%. Among all five fibres considered in this study, trunk fibre led to the highest water absorption capacity of FC (9.09%). These results can be related to the chemical composition of the fibre itself. With reference to Table 1, the percentage of cellulose will directly affect the water absorption of fibre reinforced FC. For instance, the cellulose content in trunk fibre is the highest (34.4%), while cellulose content in mesocarp fibre is the lowest (24.5%). Fibre with high cellulose content has a greater diffusion coefficient and transport capacity; thus, it absorbs more water. Additionally, according to Elrahman et al. (2019), water absorption is highly dependent on the voids in the composite itself; the water fills the empty voids quickly by capillary action until the voids are limited. However, with the addition of oil palm fibres, the water absorption in FC can be reduced compared to the control specimens without fibre. Fu et al. (2020) concurred that as fibre content increases, water absorption would increase. This proposition is also supported by Hamad (2014) that water absorption increases as the fibre content increases.

Therefore, in this research, the percentage of fibre content is held constant at 0.45%, the optimum percentage that allows good water absorption in FC. On the other hand, moisture diffusion occurs by transmitting fluid molecules through the porous structure, although this process is inhibited by the required number of fibres that fill up the void in the FC matrix. However, an abundant amount of fibre may cause capillary transport into the gaps and flaws at the interface between the fibre and matrix (Jalal et al., 2017).

During this process, the effect of water begins with the swelling of the fibre after moisture absorption continues with the matrix micro-crack around the swollen fibres. Then, the capillary mechanism, water molecules flow along with the fibre-matrix interface, causing water diffusion through the bulk matrix. Finally, the water-soluble substances leach from the fibres, causing ultimate fibre-matrix debonding. It may result in a reduction of the mechanical properties of the concrete.

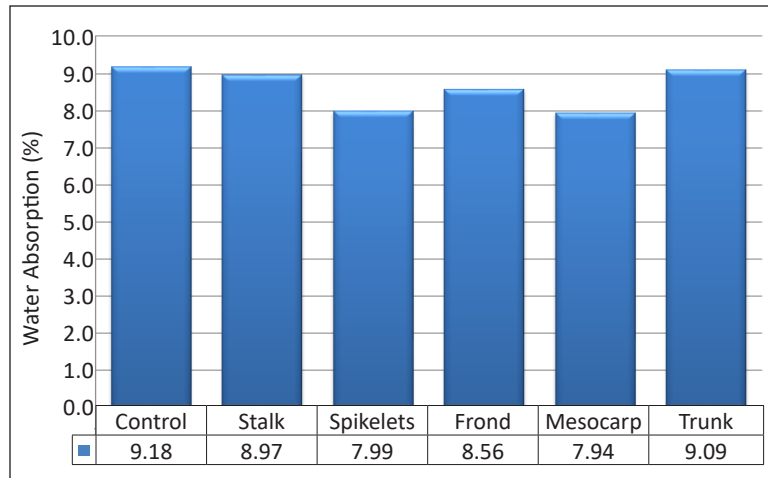


Figure 4. Influence of different parts of oil palm fibre on water absorption of 1800 kg/m³ density FC

Porosity

Figure 5 shows the result for the percentage of porosity in FC. Based on this result, FC, including all parts of oil palm fibre, resulted in a lower porosity percentage than the control mix. According to Lim et al. (2013), porosity and pore size distribution in FC may be reduced by using admixtures. Therefore, the inclusion of oil palm fibres helped to initiate blocked pore structures to reduce the diameter of openings and reduce the permeability of the concrete structure. Thus, it can be concluded that the inclusion of fibre can reduce porosity in FC. With reference to Figure 5, the control specimen recorded the highest porosity of 25.91%. The addition of mesocarp fibre gave the lowest porosity of 22.45%, while trunk fibre inclusion led to the highest porosity reading of 24.78%. Same as water absorption, the cellulose content in fibre plays an important role and affects the porosity of FC. When the oil palm fibres were exposed to a process of water absorption, this cellulose swelled. As a result of the swelling, microcracks can appear in a brittle matrix in the cementitious composite of FC, leading to the largest transport of water through the fibre matrix interface and giving high porosity. The formation of microcracks in FC matrix at the interface region, induced by cellulose fibre swelling, can upsurge the diffusion transference of water via them. Additionally, a capillarity mechanism becomes active; water molecules flow through the fibre and FC matrix interface, leading to a greater diffusivity. The difference

of diffusion coefficient values for the same fibre weight fraction in FC can be explained again due to the scattering of natural constituents of the fibre itself.

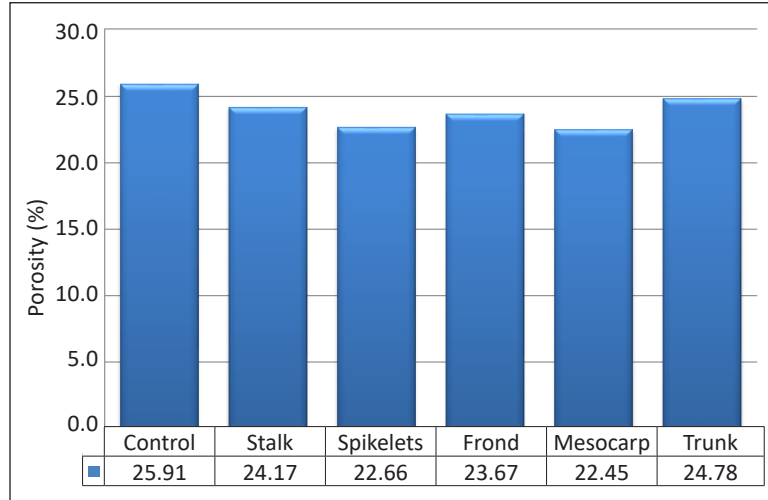


Figure 5. Influence of different parts of oil palm fibre on porosity of 1800 kg/m³ density FC

Ultrasonic Pulse Velocity

Based on the result shown in Figure 6 below, the highest reading of the UPV is influenced by the mesocarp fibre. A UPV test was conducted to determine the quality of concrete. From Figure 6, the ultrasonic pulse velocity result with the addition of mesocarp fibre was the highest (3217m/s), followed by spikelets (3208m/s), stalk (2995m/s), frond (2966m/s) and lastly, the trunk fibre (2945m/s). The control mix only achieved ultrasonic pulse velocity reading of 2894m/s. According to Moon et al. (2015), concrete with a UPV value between 3500-4000 km/s is in the range reflecting good to a perfect type of concrete; thus, FC with the addition of mesocarp fibre is categorised as good and of a high-quality concrete grade. It shows that the control mix is considered a poor quality of concrete. Therefore, the inclusion of fibre can enhance the quality of concrete. The UPV allows the examination of material homogeneity and ease in the diagnosis of defects. It also allows for examining material homogeneity and ease in the diagnosis of defects. The UPV method is when the material passes through the propagation of a high-frequency sound wave. Wave speed varies according to material density allowing for porosity estimation and discontinuity detection. The quality of most building materials is related to their rigidity. The measurement of UPV can be used to measure concrete structures' quality, estimate the mechanical properties, compressive strength and modulus of elasticity.

The ultrasonic pulse velocity results obtained from this experimental work can be linked with the cross-section diameter of the fibres themselves. The cross-section diameter of fibre in harden cement matrix will influence the ultrasonic pulse velocity of FC. Individual

cells in fibre cross-sections of larger diameter will fill the gaps well between the void cells of FC and led to a denser cementitious composite, which at the same time improved the ultrasonic pulse velocity of FC (Mydin & Mohd Zamzani, 2018). The inclusion of natural fibres contributes to the modification of the pore structure of FC, leading to reduced gel pores in FC. Among the five types of oil palm fibre considered in this research, mesocarp fibre has the largest cross-section diameter of $382\mu\text{m}$, followed by spikelets fibre ($358\mu\text{m}$), stalk fibre ($329\mu\text{m}$), frond fibre ($296\mu\text{m}$) and trunk fibre ($275\mu\text{m}$). So, it can be seen that the larger the diameter of the fibre, the better will be the result of the ultrasonic pulse velocity. Natural fibre like oil palm is flexible and small in diameter. Intrinsically, they create a small matrix of aggregates within the larger FC matrix. If ultrasonic pulse flows through FC via the cement paste, the fibres create a more tortuous path. The more tortuous the path, the longer it takes for the ultrasonic pulse to traverse through it.

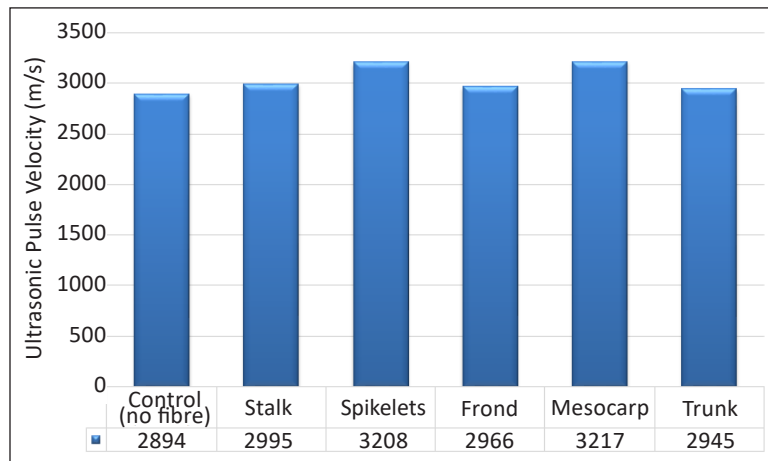


Figure 6. Influence of different parts of oil palm fibre on UPV of 1800 kg/m^3 density FC

Drying Shrinkage

Figure 7 shows the result of the drying shrinkage for FC with a density of 1800 kg/m^3 and different parts of oil palm fibre. The drying shrinkage of FC with mesocarp fibre increased significantly until day 28 of the testing age. On day 28, the drying shrinkage of this mixture exceeds the drying shrinkage that occurs in the FC with the inclusion of spikelet fibre. It can be seen from Figure 7 that all drying shrinkage in the FC with the inclusion of oil palm fibres slightly increases after day 28 until day 60. It is due to the concrete specimens' condition during the first seven days, which were not fully hardened, while on day 28 onwards, the concrete specimens hardened completely, thus slowing the shrinkage in the concrete (Tangchirapat & Jaturapitakkul, 2010). Based on Figure 7, the control mix experienced the highest drying shrinkage in the FC. The absence of solid aggregate in FC makes the particles in FC become closer with the evaporation of water; hence, it increases the shrinkage value of the FC.

However, with the addition of oil palm fibres, drying shrinkage in FC can be reduced. Previous studies proved that the inclusion of fibre restricts drying shrinkage. According to Munir et al. (2015), fibre can retain water, thus delaying the water evaporation rate and reducing drying shrinkage. From Figure 4, spikelets and mesocarp fibres gave the best result in terms of drying shrinkage. Spikelets and mesocarp fibres have excellent young's modulus and elongation at break (Table 1). Elongation at break of mesocarp fibre was only 9.6% and for mesocarp fibre was 11.5%. The other fibres got higher elongation at break. For instance, elongation at break of trunk fibre was 17.5%, almost double that of mesocarp fibre. Therefore, fibre with lower elongation at break percentage will not shrink much when combined with FC cementitious material.

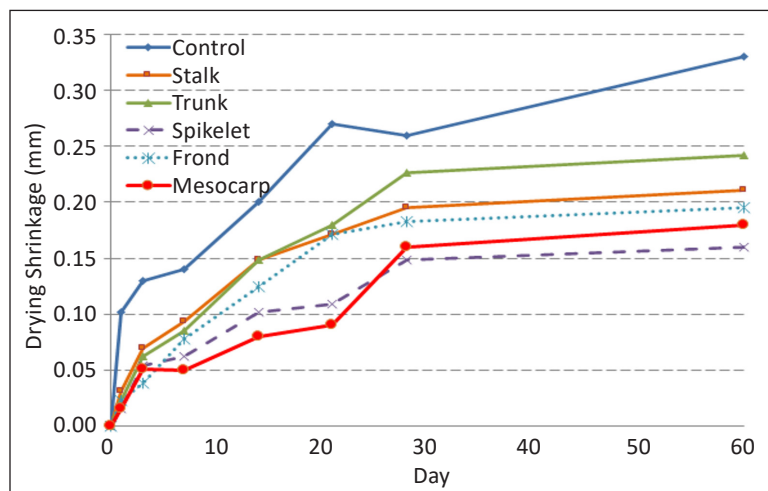


Figure 7. Influence of different parts of oil palm fibre on drying shrinkage of 1800 kg/m³ density FC

Compressive Strength

The result of the compressive strength of FC with the addition of oil palm fibres is shown in Figure 8, where there is a noticeable improvement in the compressive strength of FC beginning from day seven until day 60 of the testing age. It can be seen that FC, without the addition of oil palm fibre, has the lowest compressive strength compared to other mixtures. With the addition of mesocarp fibre, FC achieved the highest compressive strength of 30% increment compared to the control specimen at day 28, followed by FC with the addition of spikelet fibre (21% increment). Besides, there is also a noticeable increase in compressive strength at 16%, 11% and 7% of the FC specimens, including the frond, stalk, and trunk, respectively, at day 28. Here, the fibres and the cement matrix achieved high compaction, which resulted in good mix homogeneity with 0.45% fibre inclusion. This finding is also supported by Muthusamy & Zamri (2016), who proved that compressive strength and bulk density are slightly enhanced with low fibre content ranging between 0.3% to 1.5%.

These results were expected to be related to the young's modulus of the fibres. Mesocarp fibre has the highest young's modulus, 14367 MPa, compared to other fibres from oil palm biomass waste. When relating to the single fibre test results in Table 1, mesocarp fibre has the highest value of young's which was 14367 MPa, followed by spikelet (10305 MPa), frond (6753 MPa), stalk (5831 MPa) and trunk (3828 MPa), thus directly contributing to the higher compressive strength of foamed concrete. By adding mesocarp fibre which has the highest young's modulus in FC, the resistance of the composite has been suppressed. This result may be explained because fibre with higher young's modulus provides greater rigidity to the FC matrix.

However, if the fibre content exceeds 0.5%, the compressive strength of mortar samples is reduced, as proven by other studies. According to Mydin et al. (2016a), the high addition of fibre into the concrete mixture will retard the hydration process, thus resulting in low strength concrete. Although it also gains strength after a certain concrete age. As FC contains void gaps of a wide range of sizes and shapes in the matrix and micro-cracks at the transition zone between the matrix, the addition of fibre can aid in the failure of the mode under compression stress (Thakrele, 2014). Therefore, based on the result obtained in this study, it can be concluded that all FC mixes undergo strength development based on age.

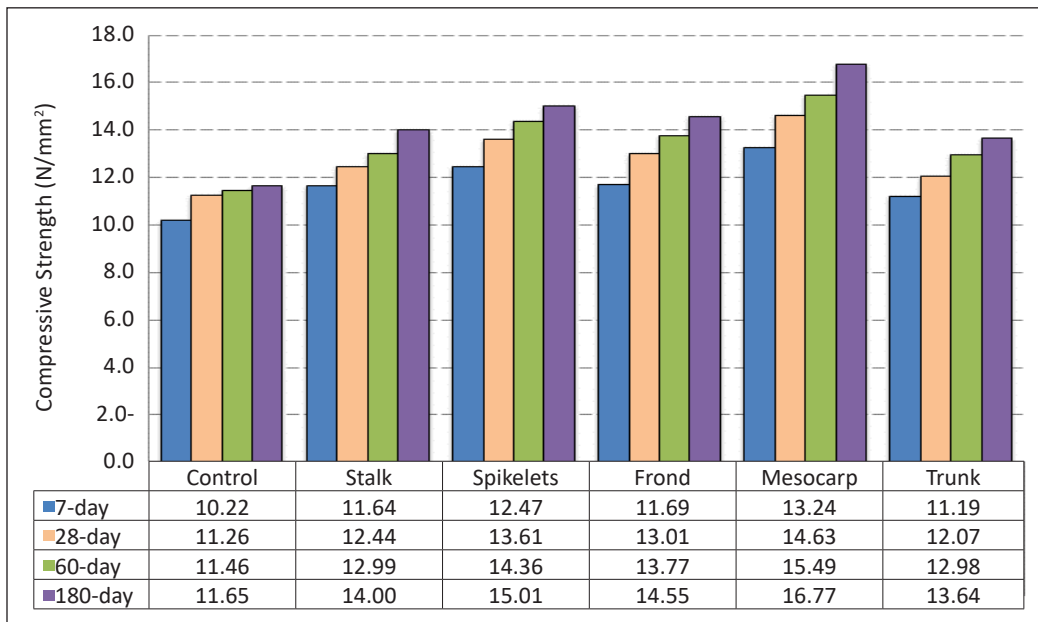


Figure 8. Influence of different parts of oil palm fibre on axial compressive strength of 1800 kg/m³ density FC

Flexural Strength

Figure 9 shows the result of the FC specimens' flexural strength with oil palm fibre. The FC specimens with the inclusion of mesocarp fibre show the highest flexural strength compared to the other mixtures. The control mix obtained the lowest flexural strength showing only

a slight increment along with the testing age. However, FC specimens with the addition of oil palm fibres show a significant increment in flexural strength by age. Moreover, there is a noticeable increase of compressive strength at 41%, 74%, 67% and 37% of the FC specimens, including stalk fibre, spikelet fibre, frond fibre and trunk fibre, respectively, at day 28 compared to control specimen. The highest flexural strength at day 28 was achieved with the inclusion of mesocarp fibre with an enhancement of 96% compared to the control specimen.

These results were likely to be related to the tensile strength of the fibres presented in Table 1. Mesocarp fibre has the highest tensile strength, 139 MPa, among other fibres from oil palm biomass waste considered in this research. The tensile strength of a single fibre is defined as the ability of the fibre to resist a force that tends to pull it apart. So, the stronger fibre entanglement such as mesocarp fibre will sturdily keep the fibres together and create tougher fibre–matrix adhesion, which leads to excellent flexural strength properties to the FC specimens under the applied load. Meanwhile, trunk fibre has the lowest tensile strength (67 MPa), followed by a stalk (82 MPa), frond (96 MPa) and spikelet (116 MPa). This relatively low transverse stiffness of fibre creates weak planes of failure for a much stiffer matrix, thus exhibiting the lowest percentage of flexural strength enhancement. Hence, the results obtained increases the possibility that mesocarp fibre is the most effective fibre that can provide stronger fibre gripping in a longer period, thus delaying fracture in composites at early of day seven under flexural.

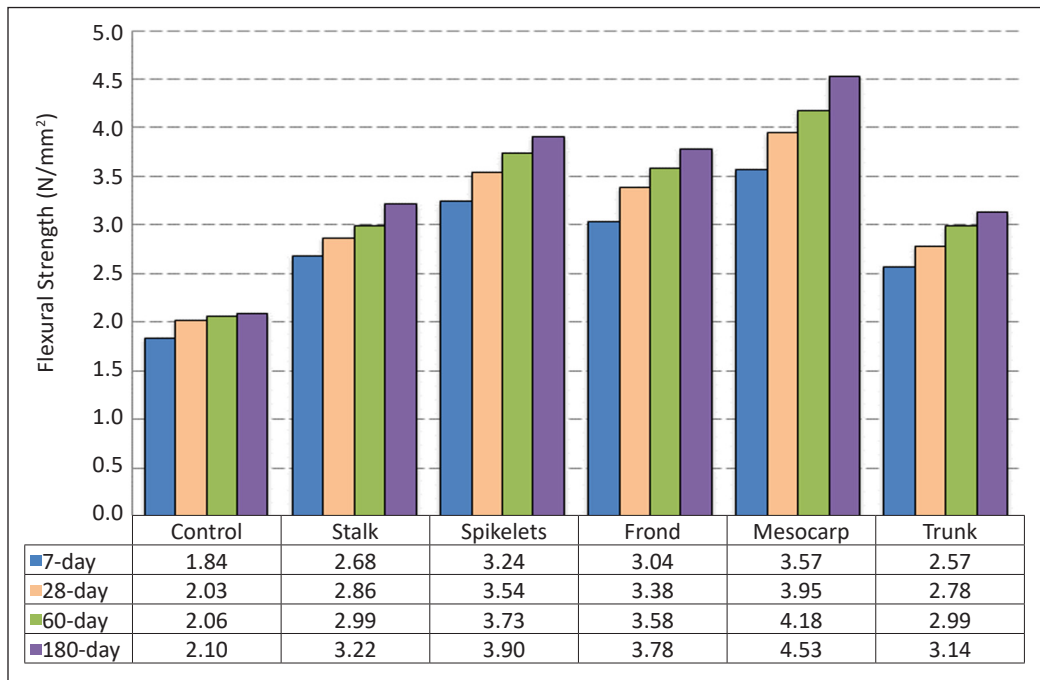


Figure 9. Influence of different parts of oil palm fibre on the flexural strength of 1800 kg/m³ density FC

Ramamurthy et al. (2009) reported that the flexural strength of FC ranges between 15% and 35% of its compressive strength. Whereas in the current research, the flexural strength of FC is between 20-28% of its compressive strength. The fibre in FC is to strengthen FC mass and transfer the basic material character from brittle to ductile elastic-plastic. Fibre contributes towards enhancing the flexural strength of FC. However, excessive fibre content may also reduce bonding and deterioration (Mydin et al., 2016b). The use of a 0.45% volumetric fraction of fibre content can be considered an optimal percentage for this type of concrete based on the increment of compressive strength and flexural strength. The increase of flexural strength is compatible with the compressive strength increase. High flexural strength is due to reducing porosity in FC mixes (Sari & Sani, 2017). Therefore, based on the result of the strength obtained, it can be concluded that the inclusion of fibre can enhance flexural strength by age.

Splitting Tensile Strength

Figure 10 displays the trend of increasing splitting tensile strength in FC, including different parts of oil palm fibre. Based on the result, the FC specimens with mesocarp fibre achieved the highest tensile strength, whereas the control mix obtained the lowest tensile strength. As for the other specimens, each mix achieved a noticeable increment in tensile strength at 22%, 20%, 20% and 18% of FC with the addition of stalk fibre, spikelet fibre, frond fibre and trunk fibre, respectively.

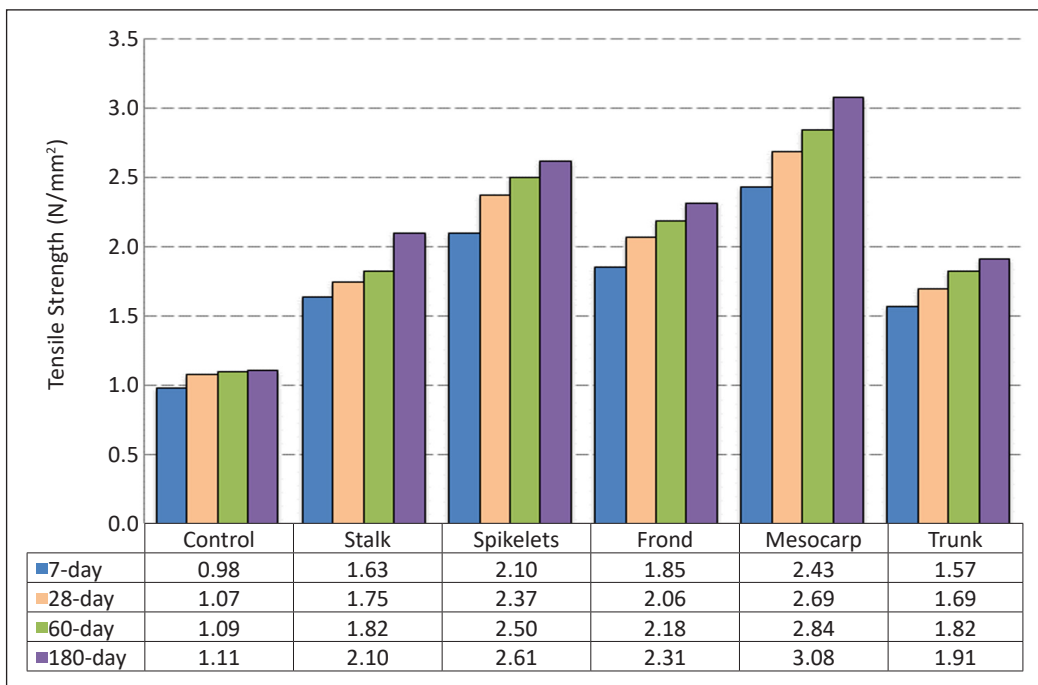


Figure 10. Influence of different parts of oil palm fibre on the tensile strength of 1800 kg/m³ density FC

In this research, the splitting tensile strength of FC is 60% of its flexural strength. As shown in Table 1, the elongation at break for mesocarp fibre is low, resulting in high tensile strength (Müller et al., 2014). Elongation at break expresses the ability of fibre to resist changes of shape without crack formation. Natural fibre such as oil palm fibre is more rigid, thus enhancing the splitting tensile strength (Memon et al., 2018). FC is known to have low tensile strength and brittle nature. However, based on the data recorded in this study, the tensile strength was shown to increase due to oil palm fibres slightly. The increase of tensile strength is due to the increase in toughness of concrete due to the presence of oil palm fibres, where 0.45% of fibre content enhances the increment of tensile strength in FC by promoting optimum pozzolanic reaction with OPC content, thus producing denser and stronger concrete. The data obtained in this study indicate that the addition of oil palm fibres enhances the tensile strength of FC.

Correlation Between Water Absorption and Porosity

As shown in Figure 11 below, the relationship between the two variables is almost linear. It shows that lower density mixtures absorb significantly higher percentages of water compared to those with higher densities. According to Jhatial et al. (2017), water absorption can be expressed as either an increase in mass per unit of dry mass or an increase per unit volume. In normal concrete, water absorption results are most likely to be relatively similar, no matter how they are expressed. However, in FC mixtures, there will be a remarkable contrast if expressed by both expressions. The researchers also claimed that FC mixtures with high porosity do not necessarily result in high-water absorption. Kim et al. (2010) also agreed that there was no clear relationship between water absorption and porosity. However, a linear correlation exists between them. The pore structure of the cement

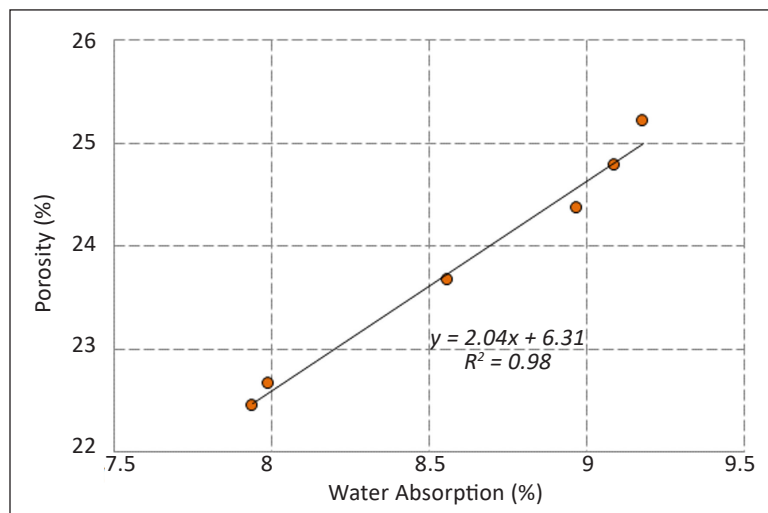


Figure 11. Correlation between water absorption and porosity of 1800 kg/m³ density FC

matrix affects both water absorption and porosity. The distribution of liquid occurs at the surface and flows into the interior. Therefore, this proves that surface water absorption has a significant influence on porosity. In addition, internal water absorption may have little impact on the porosity of FC.

Correlation Between Compressive Strength and Porosity

Air voids, capillary pores and gel pores are conditions found in the pore structure of cement-based materials, in which the pores are randomly sized, organised and attached. Porosity is recognised as one of the major elements that directly affect the strength and durability of cement-based materials. Based on Figure 12, it can be observed that the lower porosity of concretes with sufficient binding material content leads to a higher strength of concretes.

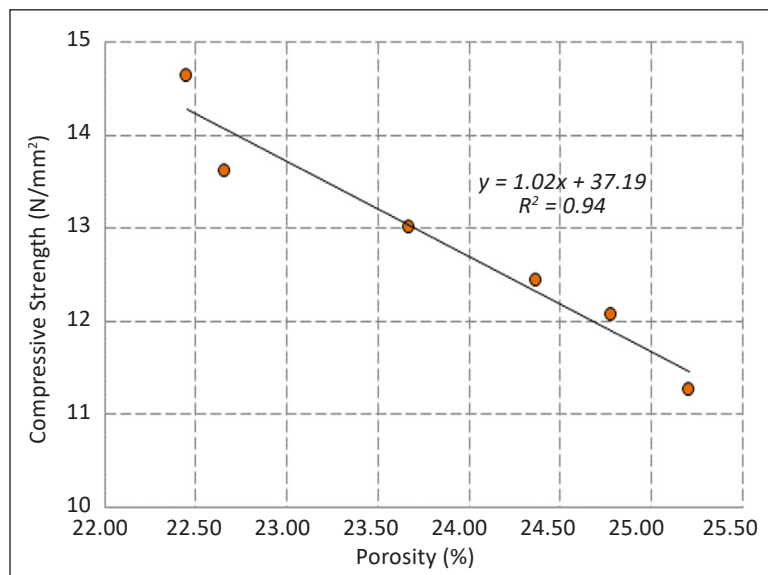


Figure 12. Correlation between compressive strength and porosity of 1800 kg/m³ density FC

Correlation Between Flexural Strength and Water Absorption

The relationship between flexural strength and porosity is shown in Figure 13 below, where the behaviour of flexural strength is similar to compressive strength. As water absorption increases, flexural strength will decrease. The development of molecules that retaliate and dismantle their chemical stability is the result of high-water absorption. A product consisting of solid and pore systems is obtained through the hydration reaction of cement (Jalal et al., 2017). The pathway for the transfer of fluid into concrete is supplied by opening the network of the cement paste matrix, and its development depends on several considerations, such as the initial condition and its duration, testing age and climatic exposure during drying and conditioning of concrete (Kamaruddin et al., 2018).

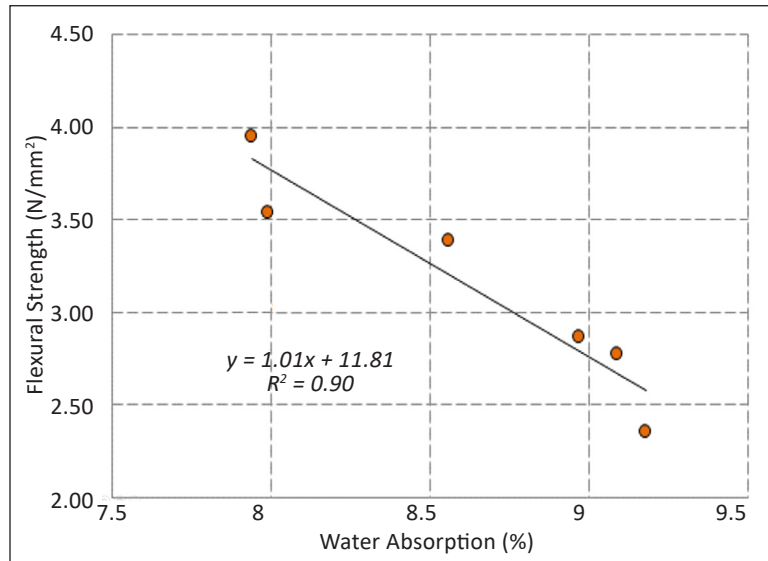


Figure 13. Correlation between flexural strength and water absorption of 1800 kg/m³ density FC

CONCLUSION

In this research, with mesocarp fibre, FC attained remarkable results, which proved that the addition of fibre in FC could enhance its properties. FC with mesocarp fibre acquired the lowest water absorption percentage at 7.94%, followed by the percentage of water absorption in spikelet fibre at 7.99%. It shows slight differences between spikelet fibre and mesocarp fibre at 0.05%. For porosity, FC, including all parts of oil palm fibre, resulted in a lower porosity percentage than the control mix. The inclusion of oil palm fibres helps to initiate occluded opening structures to minimise the diameter of openings and reduce permeability through the concrete structure. The highest reading of UPV was influenced by mesocarp fibre. A UPV test was conducted to evaluate the quality of concrete where the FC with the addition of mesocarp fibre was categorised as a good and high-quality concrete grade with a reading of 3.217 km/s. Drying shrinkage of FC with the addition of mesocarp fibre increased significantly until day 28 of the testing age. The drying shrinkage of FC with the inclusion of oil palm fibres slightly increased after day 28 until day 60. In addition, the FC without the addition of oil palm fibre had the lowest compressive strength compared to the other mixtures. With the addition of mesocarp fibre FC achieved the highest compressive strength, followed by FC with spikelet fibre. Here, the fibres and the cement matrix were expected to achieve high compaction, leading to good homogeneity in the mixture with 0.45% fibre inclusion. The addition of fibre in FC strengthens FC mass and modifies the basic material character from fragile to ductile elastic-plastic. As such, the addition of fibre contributes to enhancing the flexural strength of FC. However, excessive fibre content may lead to reduce bonding and disintegration.

ACKNOWLEDGEMENT

The author gratefully acknowledges financial support for this research provided by Universiti Sains Malaysia under Bridging Grant (Ref. No. 304/PPBGN/6316230).

REFERENCES

- ASTM International. (2014). *ASTM C878 / C878M-14a: 2014. Standard test method for restrained expansion of shrinkage-compensating concrete*. ASTM International
- ASTM International. (2016). *ASTM C293 / C293M-16: 2016. Standard test method for flexural strength of concrete (using simple beam with center-point loading)*. ASTM International.
- ASTM International. (2017). *ASTM C496 / C496M-17: 2017. Standard test method for splitting tensile strength of cylindrical concrete specimens*. ASTM International.
- British Standard Institution. (1983). *BS 1881-122: 1983. Testing concrete. Method for determination of water absorption*. British Standards Institute.
- British Standard Institution. (1992). *BS 882: 1992. Specification for aggregates from natural sources for concrete*. British Standards Institute.
- British Standard Institution. (1996). *BS 12: 1996. Specification for Portland cement*. British Standards Institute.
- British Standard Institution. (2004). *BS 12504-4: 2004. Testing concrete. Determination of ultrasonic pulse velocity*. British Standards Institute.
- British Standard Institution. (2011). *BS 12390-3: 2011. Testing hardened concrete. Compressive strength of test specimens*. British Standards Institute.
- Elrahman, M. A., El Madawy, M. E., Chung, S. Y., Sikora, P., & Stephan, D. (2019). Preparation and characterization of ultra-lightweight foamed concrete incorporating lightweight aggregates. *Applied Sciences*, 9(7), 1-12. <https://doi.org/10.3390/app9071447>
- Ezerskiy, V., Kuznetsova, N. V., & Seleznev, A. D. (2018). Evaluation of the use of the CBPB production waste products for cement composites. *Construction and Building Materials*, 190(30), 1117-1123. <https://doi.org/10.1016/j.conbuildmat.2018.09.148>
- Ferreira, S. R., De Andrade, S. F., Lima, P. R. L., & Filho, R. D. T. (2017). Effect of hornification on the structure, tensile behavior and fiber matrix bond of sisal, jute and curaua' fiber cement based composite systems. *Construction and Building Materials*, 139, 551-561. <https://doi.org/10.1016/j.conbuildmat.2016.10.004>
- Fu, Y., Wang, X., Wang, L., & Li, Y. (2020). Foam concrete: A state-of-the-art and state-of-the-art practice review. *Advances in Materials Science and Engineering*, 2020, Article 6153602. <https://doi.org/10.1155/2020/6153602>
- Hamad, A. J. (2014). Materials, production, properties and application of aerated lightweight concrete. *International Journal of Materials Science and Engineering*, 2(2), 152-157. <https://doi.org/10.12720/ijmse.2.2.152-157>

- Hasan, K. M. F., Horvath, P. G., & Alpar, T. (2020). Potential natural fiber polymeric nanobiocomposites: A review. *Polymers*, 12(5), Article 1072. <https://doi.org/10.3390/polym12051072>
- Hasan, K. M. F., Horvath, P. G., & Alpar, T. (2021). Lignocellulosic fiber cement compatibility: A state-of-the-art review. *Journal of Natural Fibers*, 1-26 <https://doi.org/10.1080/15440478.2021.1875380>
- Hospodarova, V., Singovszka, E., & Stevulova, N. (2018). Characterization of cellulosic fibers by FTIR spectroscopy for their further implementation to building materials. *American Journal of Analytical Chemistry*, 9(6), 303-310. <https://doi.org/10.4236/ajac.2018.96023>
- Jalal, M. D., Tanveer, A., Jagdeesh, K., & Ahmed, F. (2017). Foam concrete. *International Journal of Civil Engineering Research*, 8(1), 1-14.
- Jhatial, A. A., Inn, G. W., Mohamad, N., Alengaram, U. J., Mo, K. H., & Abdullah, R. (2017). Influence of polypropylene fibres on the tensile strength and thermal properties of various densities of foamed concrete. In *IOP Conference Series: Materials Science and Engineering* (Vol. 271, No. 1, p. 012058). IOP Publishing. <https://doi.org/10.1088/1757-899X/271/1/012058>
- Kamaruddin, S., Goh, W. I., Jhatial, A. A., & Lakhari, M. T. (2018). Chemical and fresh state properties of foamed concrete incorporating palm oil fuel ash and eggshell ash as cement replacement. *International Journal of Engineering & Technology*, 7(4.30), 350-354. <https://doi.org/10.14419/ijet.v7i4.30.22307>
- Karade, S., & Aggarwal, L. (2011). Cement-bonded lignocellulosic composites for building applications. *Metals Materials and Processes*, 17(2), 129-140. <https://doi.org/10.1016/j.conbuildmat.2010.02.003>
- Kim, Y., Jiong, H., Jae, L., & Heeyou, B. (2010). Mechanical properties of fiber reinforced lightweight concrete containing surfactant. *Advances in Civil Engineering*, 10, 1-9. <https://doi.org/10.1155/2010/549642>
- Kochova, K., Gauvin, F., Schollbach, K., & Brouwers, H. (2020). Using alternative waste coir fibres as a reinforcement in cement fibre composites. *Construction and Building Materials*, 231, Article 117121. <https://doi.org/10.1016/j.conbuildmat.2019.117121>
- Li, Q., Ibrahim, L., Zhou, W., Zhang, M., Fernando, G. F., Wang, L., & Yuan, Z. (2020). Holistic solution to natural fiber deterioration in cement composite using hybrid treatments. *Cellulose*, 27(7), 981-989. <https://doi.org/10.1007/s10570-019-02813-2>
- Lim, S. K., Tan, C. S., Lim, O. Y., & Lee, Y. L. (2013). Fresh and hardened properties of lightweight foamed concrete with palm oil fuel ash as filler. *Construction and Building Materials*, 46, 39-47. <https://doi.org/10.1016/j.conbuildmat.2013.04.015>
- Mahmud, S., Hasan, K. M. F., Jahid, M. A., Mohiuddin, K., Zhang, R., & Zhu, J. (2021). Comprehensive review on plant-fiber reinforced polymeric biocomposites. *Journal of Materials Science*, 56, 7231-7264. <https://doi.org/10.1007/s10853-021-05774-9>
- Mahzabin M. S., Hock, L. J., Hossain, M. S., & Kang, L. S. (2018). The influence of addition of treated kenaf fibre in the production and properties of fibre reinforced foamed composite. *Construction and Building Materials*, 178, 518-528. <https://doi.org/10.1016/j.conbuildmat.2018.05.169>
- Majid, A., Anthony, L., Hou, S., & Nawawi, C. (2012). Mechanical and dynamic properties of coconut fibre reinforced concrete. *Construction and Building Materials*, 30, 814-825. <https://doi.org/10.1016/j.conbuildmat.2011.12.068>

- Memon, I. A., Jhatial, A. A., Sohu, S., Lakhari, M. T., & Hussain, Z. (2018). Influence of fibre length on the behaviour of polypropylene fibre reinforced cement concrete. *Civil Engineering Journal*, 4(9), 2124-2131. <https://doi.org/10.28991/cej-03091144>
- Mohammadhosseini, H., Awal, A. S. M. A., & Sam, A. R. M. (2016). Mechanical and thermal properties of prepacked aggregate concrete incorporating palm oil fuel ash. *Sadhana*, 41(10), 1235-1244. <https://doi.org/10.1007/s12046-016-0549-9>
- Momeen, M., Islam, U., Mo, K. H., & Alengaram, U. J. (2016). Durability properties of sustainable concrete containing high volume palm oil waste materials. *Journal of Cleaner Production*, 137, 167-177. <https://doi.org/10.1016/j.jclepro.2016.07.061>
- Moon, A. S., Varghese, V., & Waghmare, S. S. (2015). Foam concrete as a green building material. *International Journal for Research in Emerging Science and Technology*, 2(9), 25-32.
- Müller, H. S., Breiner, R., Moffatt, J. S., & Haist, M. (2014). Design and properties of sustainable concrete. *Procedia Engineering*, 95, 290-304. <https://doi.org/10.1016/j.proeng.2014.12.189>
- Munir, A., Abdullah, Huzaim, Sofyan, Irfandi, & Safwan. (2015). Utilization of palm oil fuel ash (POFA) in producing lightweight foamed concrete for non-structural building material. *Procedia Engineering*, 125, 739-746. <https://doi.org/10.1016/j.proeng.2015.11.119>
- Muthusamy, K., & Zamri, N. A. (2016). Mechanical properties of oil palm shell lightweight aggregate concrete containing palm oil fuel ash as partial cement replacement. *KSCE Journal of Civil Engineering*, 20(4), 1473-1481. <https://doi.org/10.1007/s12205-015-1104-7>
- Mydin, M. A. O., & Zamzani, N. (2018). Coconut fiber strengthen high performance concrete: Young's modulus, ultrasonic pulse velocity and ductility properties. *International Journal of Engineering & Technology*, 7(2), 284-287. <https://doi.org/10.14419/ijet.v7i2.23.11933>
- Mydin, M. A. O., Musa, M., & Ghani, A. N. A. (2016a). Fiber glass strip laminates strengthened lightweight foamed concrete: Performance index, failure modes and microscopy analysis. In *AIP Conference Proceedings* (Vol. 2016, No. 1, p. 020111). AIP Publishing LLC. <https://doi.org/10.1063/1.5055513>
- Mydin, M. A. O., Noordin, N. M., Utaberta, N., Yunos, M. Y. M., & Segeranazan, S. (2016b). Physical properties of foamed concrete incorporating coconut fibre. *Jurnal Teknologi*, 78(5), 99-105. <https://doi.org/10.11113/jt.v78.8250>
- Onuaguluchi, O., & Banthia, N. (2016). Plant-based natural fibre reinforced cement composites: A review. *Cement and Concrete Composite*, 68, 96-108. <https://doi.org/10.1016/j.cemconcomp.2016.02.014>
- Ramamurthy, K., Nambiar, E. K. K., & Ranjani, G. I. S. (2009). A classification of studies on properties of foam concrete. *Cement and Concrete Composites*, 31(6), 388-396. <https://doi.org/10.1016/j.cemconcomp.2009.04.006>
- Sari, K. A. M., & Sani, A. R. M. (2017). Applications of foamed lightweight concrete. *MATEC Web of Conferences*, 97, 1-5. <https://doi.org/10.1051/mateconf/20179701097>
- Serri, E., Mydin, M. A. O., & Suleiman, M. Z. (2014). Thermal properties of oil palm shell lightweight concrete with different mix designs. *Jurnal Teknologi*, 70(1), 155-159. <https://doi.org/10.11113/jt.v70.2507>

- Suhendro, B. (2014). Toward green concrete for better sustainable environment. *Procedia Engineering*, 95, 305-320. <https://doi.org/10.1016/j.proeng.2014.12.190>
- Tangchirapat, W., & Jaturapitakkul, C. (2010). Strength, drying shrinkage, and water permeability of concrete incorporating ground palm oil fuel ash. *Cement and Concrete Composites*, 32(10), 767-774. <https://doi.org/10.1016/j.cemconcomp.2010.08.008>
- Thakrele, M. H. (2014). Experimental study on foam concrete. *International Journal of Civil, Structural, Environmental and Infrastructure Engineering Research and Development*, 4(1), 145-158.

Logistics and Freight Transportation Management: An NLP based Approach for Shipment Tracking

Rachit Garg^{1,2*}, Arvind Wamanrao Kiwelekar¹ and Laxman Damodar Netak¹

¹Department of Computer Engineering, Dr. Babasaheb Ambedkar Technological University, Lonere Maharashtra, India

²Center for Advanced Technologies and Innovation, ATA Freight Line India Pvt. Ltd., Pune, Maharashtra, India

ABSTRACT

Tracking and tracing systems have become basic services for most logistics companies and are particularly essential for the shipping and logistics industry. Dynamic logistics management today need constant supervision and management of continuously-changing supply chains that motivate the necessity of goods-centric logistics monitoring and tracking, which guarantees a chance to improve transparency and control of a company's multiple logistical activities. However, operational inefficiencies due to the conventional monitoring system for the supply chain management can also result in sales loss, higher cost, poor customer service—and eventually lower profits. Based on research literature, this paper aims to provide a novel approach for tracking and tracing shipment in a logistics organisation by implementing deep natural language processing concepts. The study aims to allow the stakeholders to think in new ways in their organisation and helping them to have a powerful influence on tracking and tracing to make the best decision possible at the right time. The proposed method is compared based on the accuracy of identifying the query, and results are significantly acceptable. This study is of related interest to researchers, academicians, and practitioners.

Keywords: Logistics and deep NLP, NLP, natural language processing, natural language query, speech-to-text, tracking system

ARTICLE INFO

Article history:

Received: 19 April 2021

Accepted: 15 July 2021

Published: 18 October 2021

DOI: <https://doi.org/10.47836/pjst.29.4.28>

E-mail addresses:

rachit.garg.nitttr@gmail.com (Rachit Garg)

awk@dbatu.ac.in (Arvind Wamanrao Kiwelekar)

ldnetak@dbatu.ac.in (Laxman Damodar Netak)

* Corresponding author

INTRODUCTION

The way business operates worldwide has experienced dramatic changes over the past decade, with conventional industrial, political, and geographical borders almost vanishing. The logistics sector was not left

untouched by such changes under global market conditions. Global business logistics played a crucial role in adapting to the changing consumer demand in globalisation and mass adaptation. In times of globalisation, businesses increasingly need versatility and agility to satisfy the rising needs of adaptation and fluctuating consumer demand (Klein & Thomas, 2009). The dynamics of worldwide supply chains have ensured that their manageability has increased (Artto et al., 1998). Supply chains are becoming more complex worldwide (Christopher & Peck, 2004). As a result, a company's success depends more and more on its supply network, and 'individual companies are no longer competing as independent entities but as supply chains (Lambert & Cooper, 2000). The world in which logistics and transport managers find themselves is very different today from just a few years ago. Today's managers in the Logistics service industry have several challenges and opportunities in dramatic contrast to a decade ago. It is, therefore, no wonder that many managers have not entirely adapted to the changing world and have missed chances and success deficits. The prospect of exploiting the transport role as a crucial strategic factor in the supply chain is prominent among the list of missed opportunities. With globalisation, the nature of services, and higher consumer expectations, businesses turn their supply chain into the epicentre of industry innovation using state-of-the-art technologies.

Rising technological advances are widening industry-wide, and logistics and the supply chain can be the most affected industries. Renowned for the substantial use of manual procedures and the vast volume of data processed at various locations and in different ways, logistics has the most significant advantage from adopting emerging technology and pursuing the most creative logistics trends. As digitalisation takes hold and consumer expectancies grow, logistic companies are witnessing a period of unparalleled transition. Innovations make it possible to be more competitive and collaborative, and they re-form the market in ways that only start to emerge. Many advances in current logistics at the global and local level motivate the need for more transparency in supply chain structures or collaboration with creative logistical service providers (Klumpp et al., 2011).

The transparency of the supply chain is the ability to monitor a wide range of goods during transport to obtain a simple overview of each stage of the process. It helps businesses enhance their customer support and cost control through continuous inventory management, constructive status updating, interruption limits, and risk reduction (Gnimpieba et al., 2015). Without adequate systems, businesses face enormous challenges because the requisite supply chain transparency cannot be guaranteed (Baresi et al., 2016). Shipping and tracking are additionally centre segments of a board network like a modern supply chain management system intended to fulfil clients. Tracking shipments in service to customers is considered significant for suppliers and essential to efficient supply networks. Transportation tracking is an integral part of customer service and is essential for logistical services. The tracking system makes it easier to identify the shipment location and informs the client in due course.

The application of information management over the entire strategy of the logistics can be improved by monitoring the carriers in real-time and tracking them.

Responses to questions like “Where is my shipment? Furthermore, “When is my shipment coming?” in logistics is usually not adequately accurate and thus reduces the productivity of logistics service providers. As logistics is dynamic and requires numerous transport modes and carriers, improving productivity and saving the supply chain’s expense is essential to connect between various parties and use real-time data. Product timely delivery is a significant factor in the happiness of customers. Higher levels of customer loyalty contribute to better engagement of consumers and company repeat. Technical solutions will play a key role by increasing the distribution pace and keeping consumers aware of the product delivery plan. It can also provide the customer with a platform for tracking orders, enhancing a sense of self-sufficiency and control for a customer, and translating customer services for saving logistical organisation time and money. Using technology to gain more insight into all aspects of the industry and make data-driven decisions based on real-time information and innovation brings productivity across the logistics process. The information-sharing framework enables manufacturers to improve cooperation with their partners in real-time.

More businesses integrate technologies into their supply chain management processes to remain globally competitive and at the forefront of a complex business environment. AI is a central component of the revolution of Industry 4.0. Organisations can use artificial intelligence (AI) to help turn the unpredictable into the envisaged.

This paper aims to develop further the above concepts and apply an intelligent transport management conceptual model. The purpose of this paper is twofold: first, the analysis and presentation of the deficiencies of conventional tracking systems in logistics networks and second, to propose a new approach for constructing solutions for tracking in logistics networks. This paper is present in six sections. Section 2 discusses the theory of tracking systems by identifying the existing tracking systems from the literature. Section 3 discusses the motivation behind the use of Natural Language Processing (NLP). Section 4 discusses the method of implementation. Section 4 and 5 discuss the objective and significance of this study. Section 6 discusses the method of implementation. The study results are present in section 7 of this paper, and we finally conclude in Section 8 by drawing the future research directions.

LITERATURE REVIEW

There is rising interest in monitoring delivery and supplying consumers with tracking information. It is an essential customer service factor often viewed as industry practices instead of a possible competitive benefit for logistics service providers (LSPs). Industries spend substantial resources to provide their consumers with monitoring services (Töyrylä,

1998). It allows consumers to trace and track transportation shipments in transit and, therefore, schedule and control their activities. Tracking means the IT-supported systems to determine object status in the manufacturing or logistic company's physical supply chain. A track-and-trace framework for managing interconnected logistical networks is essential and enhances customer support (Shamsuzzoha et al., 2013). In the early days of tracking, a communications system for calling service providers and tracking shipments is an example of technology to add value (Kerr, 1989). EDI and LMS were widespread for regulating the shipment and decision-making (Sullivan & Fordyce, 1989). Loebbecke and Powell (1998) introduced the TRANSP-TRACK approach for seamless tracking that also uses EDI. It is a technological solution to tracking issues in a logistics chain (Loebbecke & Powell, 1998). Alexander's intelligent tracking system includes gathering information using RFID, GIS, GPS, and improving tracking efficiencies (Brewer et al., 1999). Chadil et al. (2008) provide the use of a model client-server in the real-time monitoring system. It is an integrated approach to detect shipment location information regularly sent to a server utilising a GPS/GPRS module. This study implements a tracking system using the GPS, GPRS, and Google Earth software for displaying locations (Chadil et al., 2008). A hybrid cargo level tracking system is an infrastructure-based solution that achieves greater precision and lower overall expenses than the existing system. The concept covers some advances and the newest generation of existing infrastructure (Yang et al., 2010).

The literature describes real-time tracking and tracing in various ways. Baresi et al. (2016) define traceability by an attribute that enables the shipment's current position to be determined. According to Shamsuzzoha et al. (2013), tracking refers to the product's positioning because it has value and risk of loss. Supply chain networks are an integral approach to coordinating material and product handling and monitoring from source to the final customer (Baresi et al., 2016).

According to Klein et al., tracking of shipments typically takes place via terrestrial systems (Klein & Thomas, 2009). All terrestrial systems are based on and implemented on Earth, whereas satellite-based systems need spatial hardware. Terrestrial systems issue status messages only when they complete each process phase. Mainly satellite-based systems, such as GPS, monitor larger cargo units, covering longer distances (Kothris, 2001). Auto-ID technologies allow the positioning of shipments in the supply chain. According to the study, Auto-ID networks are the subsystem of the logistics system (Shamsuzzoha et al., 2013). A logistics system is an effective freight transfer accompanied by an information flow. GPS trackings are commonly accepted and used for outdoor monitoring, which many articles have already adopted (Sultana et al., 2016).

At the same time, a supply chain network manages large volumes of items. It requires a distribution strategy to minimise the related logistics and labour costs in handling customer claims (Ko et al., 2011). Barcodes, QR codes, WSN, RFID, and GPS successfully monitor

and trace logistics. All these systems collect critical monitoring data like temperature, moisture, and position automatically and continuously (He et al., 2009; Jedermann et al., 2006). RFID technology provides certain distinct advantages to other forms of detecting systems, and for virtually any business enterprise, the potential of RFID technology can bring exciting possibilities. For product safety, visibility, and traceability, many industries use RFID technology. A mature RFID-solution technology allows structural enhancements across many logistics and supply chain systems. However, RFID systems are disadvantaged even with certain benefits as they entail high investment costs and lack data protection (Yuksel & Yuksel, 2011). Musa et al. (2014) provide a thorough overview of product visibility in the supply chain, outlining different criteria, processes, and architectures. Figure 1 depicts the evolution of the logistics tracking system.

Researchers and standardizing organisations still look ahead aggressively to establish global monitoring strategies (Huvio et al., 2002). Company managers have described this monitoring framework to boost their business by enhancing consumer loyalty and incorporating IT. However, most tracking systems are for the advantage of a particular entity, and therefore the tracing and tracking of multi-organisational ecosystems is not available (Kärkkäinen et al., 2004). As a result, companies are only able to monitor their shipments. Larger organisations have developed their monitoring scheme that typically uses the same solution with the same problems. Many companies concentrating on designing global supply chain management solutions construct their systems around a server that acts as a central storage point for monitoring data. Blockchain is an emerging technology to address a range of logistics problems (Christidis & Devetsikiotis, 2016; Kim & Laskowski, 2018). It is due to blockchain’s highly secure, trustworthy, unchangeable, collective repository, and global accessibility features. These characteristics are critical for logistics policymakers and provide end-to-end monitoring capability during transport,

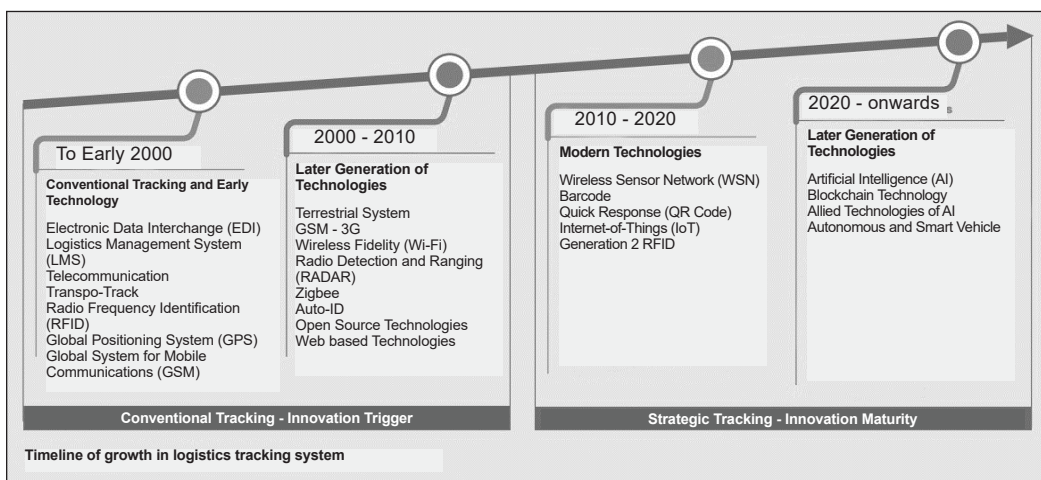


Figure 1. Timeline of growth in logistics tracking system (GEP, 2018)

accountability, and decentralised activity without intermediary intervention (Abbas et al., 2020; Betti et al., 2019; Zhao et al., 2016).

Contemporary tracking systems may perform well if a single organisation manages products, but global supply chain networks do not fit conventional tracking approaches. Multi-company supply networks are typically carried out via a Web page to make tracking information accessible, leading to manual customer interrogation (Ruiz-Garcia et al., 2010). Automated monitoring systems should be there in the customer's operating systems for the tracking systems. It is generally, though, prolonged and sometimes time-consuming. The industry deals with various issues, including transparency in supply chains, with many end customers unaware of the origins of their shipments, complicated processes involving intermediate freight brokers, and a lack of accountability in losses is an often challenging and opaque process. Logistics and shipping networks use information systems to a different degree. A planning and tracking system must be in place to succeed in various operations and assist decision-making at different points in the supply chain.

Artificial Intelligence (AI) and its subsets are no longer science fiction; they are a digital future for many businesses. Organisations, particularly those in the logistics sector, are on the verge of implementing AI-based solutions to streamline and redefine all of their core objectives. Artificial intelligence is a broad technology phrase that refers to transforming a massive amount of data into actionable insight through algorithmic processing. For the supply chain industry, Natural Language Processing (NLP) provides various advantages. Intelligent products are eventually the secret to saving and monitoring data to the final destination. NLP is computer software that interprets, perceives, and deduces context from human language intelligently and sensitively. NLP is used to analyse text, allowing machines to understand how humans communicate. There are numerous uses of NLP in the business world, including speech comprehension, information extraction, text generation, question answering, sentiment analysis, classification, speech-to-text translation and vice versa, and knowledge acquisition (Chowdhary, 2020; Clark et al., 2010; Garg et al., 2021b; Liu et al., 2017).

NLP is an ideal tool for tackling massive amounts of valuable data. Thus, any organisation that recognises the importance of data analysis—from a single text to a collection of documents that must be summarised—will benefit from NLP. NLP capabilities transform unstructured text into actionable information. Additionally, NLP technology can assist a platform in precisely managing user expectations to boost user satisfaction effectively. NLP is now increasingly being applied to medical education, which has helped to accelerate this process over the past several years. The potential of the NLP to facilitate FOAM (Free Open-Access Medical Education) materials integration with more traditional curricular components (Chary et al., 2019).

Thessen et al. defined the use of NLP to extract biological information such as cellular processes, taxonomy names, and morphological features in their work. According to them,

using natural language processing in biodiversity study promise to develop a semantic web for biology (Thessen et al., 2012). Biomedical and clinical text processing is a significant application area for natural language processing. Neuman et al. (2019) presented ScispaCy as a rapid and robust biomedical model. It is a specialised natural language processing library designed to address the core text processing requirements in the biomedical area (Neumann et al., 2019). In another study, Garg et al. (2021a) proposed a model for personalising news for the logistics business. It is a model that determines the importance of marine news by extracting data from corpora using statistics and deep learning methods. The study employs a natural language processing methodology to recommend news to various stakeholders in a busy media environment (Garg et al., 2021a).

MOTIVATION BEHIND NLP IN LOGISTICS TRACKING

The fourth party logistics company (4PLs) is ideal for handling all the customers' supply chains. It thus serves as their only interface to a diverse network of logistics services providers across various forms: water (sea and barge), air, road, and rail. This position poses considerable challenges for efficient freight transport planning and control while maintaining adequate service standards. Real-time monitoring data is essential to achieve this type of operational excellence.

Industries are on the verge of investing a significant budget in providing their consumers with tracking services. This monitoring and tracking enable the service providers' customers to identify the shipments in transit; thus, they schedule and control their activities. New tracking solutions may work well in managing products by one organisation, but the tracking of global supply chain networks does not follow conventional tracking approaches. Logistics organisations are spending a considerable amount on value-added services like tracing and tracking to their customers. These services play a significant role in satisfying customer demands as customers can locate shipments in transit; hence, they plan and monitor their operations. Many companies use traditional tracking approaches to handle goods by one company, but this approach might not work well to track global supply chain networks (Goll & Bolte, 2020).

The world economy is on a stunning turnaround. Brexit and the USCMA's approval would possibly allow freight and global distribution programs to shift towards regional and more localised solutions (Bank, 2019). In 2021, global shipping technology will be a hot topic, and logistics partners need to recognise the best approach diligently. Delays and inefficiencies can vary from few days to weeks in current shipment management processes. It provides a significant opportunity and a necessity to incorporate technology and automation solutions that make timely decisions in the supply chain. This need gap requires developments from the processing of natural languages and machine learning. The Machine Learning (ML) and NLP algorithms can quickly transform large numbers of unstructured

text into workable insights (Garg et al., 2021c). Natural language technologies have gained substantial focus from business, academia, and government since their inception. Natural language processing for the supply chain and distribution can be implemented in several respects. As supply chains produce broad data sets, it is vital to consult this data to optimise the supply chain correctly. NLP encourages users to ask difficult questions and guides them through the data to provide insights into answering them. It is also easier to simplify customer service with natural language processing. Stakeholders ask questions, and NLP responds to or directs them through the correct details. It decreases administrative costs of customer service centres and increases the supply chain's satisfaction (Garg et al., 2021b).

The automation of information-based tasks is one of the most popular and efficient NLP usage cases. The advantages of NLP range not just from operational efficiencies and productivity but also from more operational data analysis to a modest benefit. We propose an NLP-based supply chain management solution for NLP-enabled smart tracking based on the fundamental need for a pragmatic solution to the supply chain and widespread NLP technological adoption in various fields (Kota, 2019). NLP-enabled smart tracking may benefit in the following way.

Monitor Shipment Movement

NLP algorithms can monitor changes in the shipment in real-time and help to manage master data accurately.

Reduce Language Barriers

Most companies operate globally, and language barriers can impede the efficiency of processes. To minimise barriers to regional languages, NLP can translate the question from one language to another language.

Tailored Stringent Delivery Expectations

Clients want to know where their orders are and receive the most accurate delivery expectations within tighter delivery periods. In a convenient time frame, users cannot expect the quickest delivery but instead precision. These challenges go well beyond the world of consumers, as they probably have learned from corporations like Walmart, which have similar suppliers' standards.

More Effective Order Tracking and Delivery

The technology provides consistency across the entire production chain to improve insight in any aspect of the market and make real-time data-driven decisions. In supply chain management, the net effect of using technology includes decreased inventory costs, reduced

operating capital requirements, and improved client satisfaction. For all the candidates, this is undoubtedly a victory.

In value-added supply chain management and logistics systems, industry markets today are diverse. In recent years, technological advancement has helped meet the increasing demands of tracking and tracing the logistics or transport chains. Therefore, in terms of effective logistics network management and customer demand, the value of tracking and tracing shipments is considered reasonably large for manufacturing companies (Lund et al., 2019).

RESEARCH OBJECTIVE

The study aims to examine the implementation of natural language processing in a logistics organisation to develop a natural language-based solution to tracking or tracing shipments in the logistics industry. The study's objective is to allow users to ask shipment-related questions and guide them through the data; providing workable insights to answer those questions enhances the customer experience in a logistic organisation. This research consists of a location monitoring module used to coordinate shipment tracking. Another objective of this study is to create an intelligent system that covers the core application of Natural Language Processing (NLP) to meet smart logistics services.

RESEARCH SIGNIFICANCE

Technology has a significant role to play in this new age for every industry to thrive. As the market is competitive, knowing the client base is critical. Since the prediction of consumer demand and its fulfilment has become complicated, it can be a tedious activity without good cooperation between different business partners. Supply chain management needs to provide the information of products at every stage of the logistics chain and have the correct details related to tracking the object. Each business needs to be aware of the product's physical position in the supply chain while preserving a sensitive relationship between the third party and the client and balancing costs and time. This study will help to achieve the management of transportation in the supply chain. From an academic viewpoint, the study contributes to NLP's potential in identifying information related to shipment in the logistics industry.

METHOD OF IMPLEMENTATION

The paper's work is conducted in Python. The experiment environment consists of Intel Core i5-4590 CPU, memory is 4 GB, and the operating system is Windows 7 professional. This study is a prototype system executed on a sample dataset created from original AIS (Automatic Identification System) data. The process is described broadly in two phases: Phase one involves speech recognition and generating SQL queries from the natural

language; Phase 2 includes the results. The second phase is mainly a DBMS system that runs the SQL query over the database. Figure 2 depicts the pictorial representation of steps in implementation. The steps of implementation are as follows:

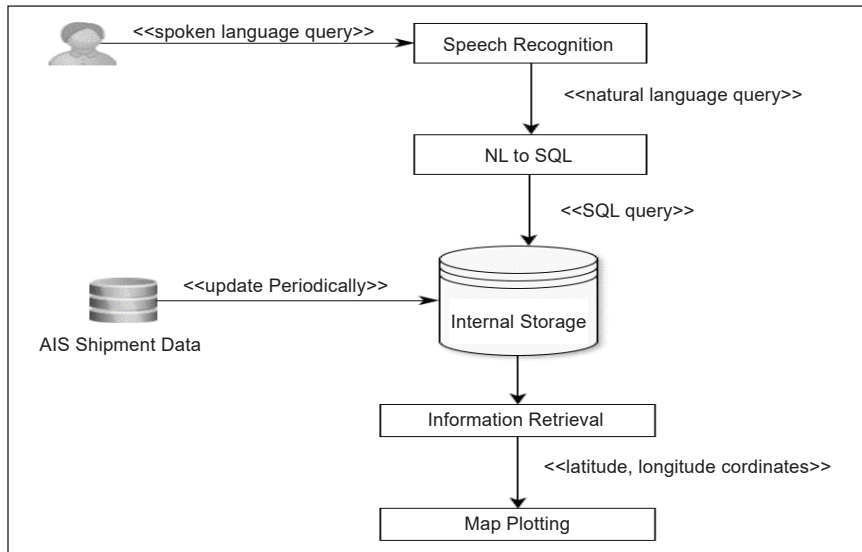


Figure 2. Steps in implementation

Data Sources

This experiment uses the dataset of shipment. The dataset is created by considering the original dataset available from AIS and all logistics companies for tracking and other shipment details. Automatic Identification Systems (AIS) monitor ship traffic to improve the safety of navigation worldwide. With these systems, planners can handle long-term movement patterns in the ocean (MarineCadastre.gov, 2013). The original dataset includes a large number of columns. Some of the primary columns are (Flag, IMO, ENI, MMSI, Call sign, Carrier, Vessel Name, Vessel Type, Time of latest Position, Destination Port, Loading Port, Built, Latitude, Longitude, Current port, global Area, Local Area, Reported Destination, Speed, Draught, Course, Navigational status, Length, Width, Capacity, Current Port Country). For this study, the original dataset is trimmed to few columns, including Port of Loading (POL), Port of Destination (POD), Carrier, Latitude, Longitude (Table 1). Another database having the serial number and status of the shipment is defined in Table 2. The serial of the 'shipment' table has a key reference with the serial of the 'status' table. The data description is given below. Once the data is collected, a machine learning or deeper learning algorithm is not recommended to be directly fitted from raw text data. First, we have to pre-process the text by passing the raw data to a series of filters implemented in Python. Once the data is preprocessed, it is available for further processing. The pre-processing of data mainly includes removing punctuation and lowering the case of data.

Table 1
Structure of table 'shipment' for database entry

Field Name	Data Type	Description
Serial	Numeric	Serial no. of Shipment (key reference with status.serial)
Shipmentid	Alphanumeric	Shipment No. For ex. OEIN101 (Ocean Export India-Shipment Serial No.)
Mode	Alphabetic	Mode of Transportation (Ocean/Road/Air)
Trade	Alphabetic	Trading Mode (Import/Export)
Country	Alphabetic	Country of Trade
Source	Alphabetic	Port of Loading (POL)
Destination	Alphabetic	Port of Destination (POD)
Carrier	Alphabetic	Name of the Carrier
IsTransshipped	Boolean (Yes/No)	Movement of container from one vessel to another
latitude	Decimal	Latitude Coordinate
longitude	Decimal	Longitude Coordinate

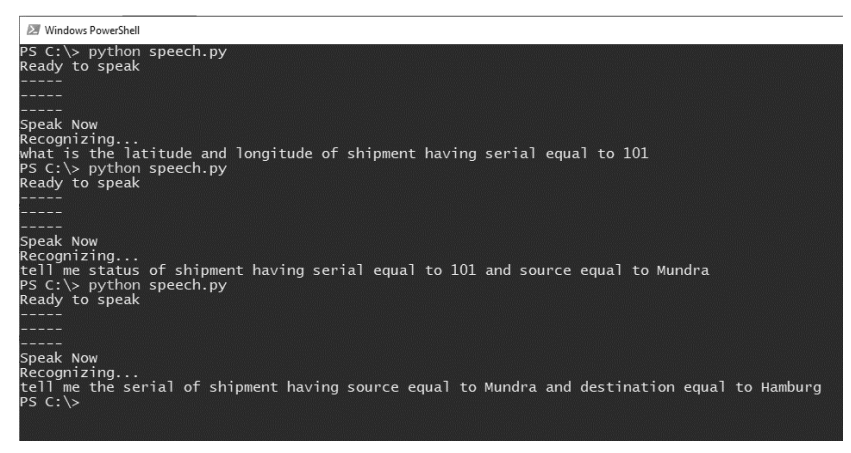
Table 2
Structure of table 'status' for database entry

Field Name	Data Type	Description
Serial	Numeric	Serial no. of Shipment (key reference with shipment.serial)
Status	Alphabetic	Status of shipment (intransit, reached, delivered)

Speech to Natural Language Text Conversion

The cleaned data is now ready for use with different pre-processing techniques. The primary and essential feature of any speech recognition device is text information extraction. Speech is the most popular communication, and most people rely on speech to communicate. The system of speech recognition primarily converts spoken languages into text. The deep neural network models are standard for speech-to-text conversion. Speech recognition attempts to translate a source speaker's speech into the target language text while retaining the linguistic content (Huang et al., 2019).

Speech recognition recognises spoken terms and sentences and translates them into text readable by a human being. This study uses the *SpeechRecognition* library to convert speech into text in a Python environment. The advantage of using this library is that no machine learning algorithm has to be developed from starting. Furthermore, this library has easy wrappers for several popular speech recognition APIs (such as Google Cloud Speech API, IBM Speech to Text). Literature shows the quick increases in implementations of speech-to-text (S2T) tasks in end-to-end sequence-to-sequence (S2S) modelling (C. Wang et al., 2020). Figure 3 shows the snapshot of implementing speech recognition to convert speech into text.



```

Windows PowerShell
PS C:\> python speech.py
Ready to speak
-----
Speak Now
Recognizing...
what is the latitude and longitude of shipment having serial equal to 101
PS C:\> python speech.py
Ready to speak
-----
Speak Now
Recognizing...
tell me status of shipment having serial equal to 101 and source equal to Mundra
PS C:\> python speech.py
Ready to speak
-----
Speak Now
Recognizing...
tell me the serial of shipment having source equal to Mundra and destination equal to Hamburg
PS C:\>

```

Figure 3. Speech recognition implementation to convert speech into text

Converting Natural Language Text to a Query Language

Relational databases store an immense amount of information and form the backbone of financial and customer affairs monitoring applications such as Customer Relationship Management (CRM). The Natural Language Interface (NLI), a research field on the intersection of natural language processing and human-computer interactions, aims to develop ways for people to communicate through natural language with computers (Bai et al., 2021; Li et al., 2019). This study reports one specific feature of the NLI used for relation databases: translating natural language queries into SQL. Thus, non-expert users may interact with the framework and database using NLI to the database. However, access to connection databases requires knowledge of database query language as it is essential, but for a naive user, it is challenging to expertise it (Ahkhouk et al., 2020).

NLI encourages users to ask questions in a natural language without knowing the database structure or the complicated machine language. Questions entered in a natural language are translated in a formal query language in a statement (W. Wang et al., 2020). This study uses the *ln2sql* approach for generating structured query language. *ln2sql* is an NLP tool to convert a natural language query into a database query. This tool takes a natural language sentence as an input and converts that into a valid SQL. The other inputs for a tool include a SQL dump file for database modelling, a language configuration file for language learning, and a thesaurus file for keyword filtering. A database dump is a file with a table configuration record and database info. This tool is an English implementation of a French paper that translates French to SQL (*fr2sql*) (Couderc & Ferrero, 2015). The Graphical User Interface (GUI) interface of *ln2sql* in Figure 4. Figure 4 depicts the conversion of a natural language query to a database query.

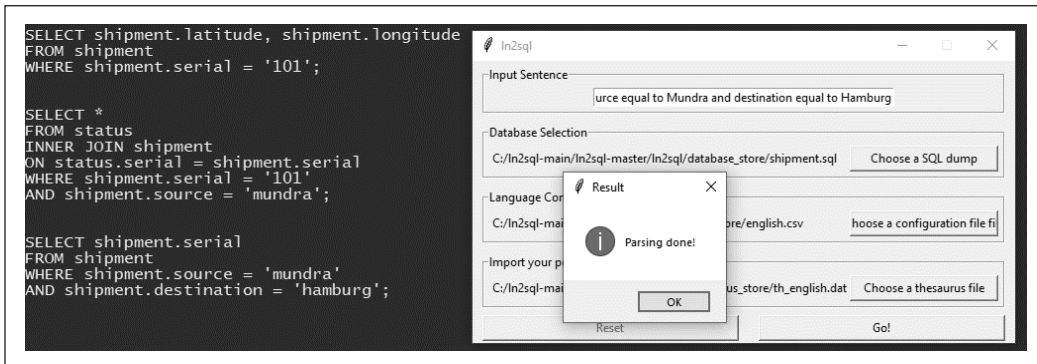


Figure 4. Converting Natural language to query language

RESULTS AND DISCUSSION

As the output from the previous step, we have a database query converted from natural language. After query formation, it is executed to generate the necessary data by the DBMS. This study offers an environment in which a user may ask a question in English, French, Turkish which will be translated into English and interpreted by multiple modules to form an equivalent SQL query that supports naïve users to find a more manageable solution and collaborative. It entirely depends on the use cases, and the applications could be limitless. The Google API can collect data, generate the vector from the database file, and display it on Google MAP view on any GUI platform. The plotting can also be done by using various other libraries on the R platform if, in any case, anyone does not want to consume Google API. The Google API is programmable so that the required performance can be shown in locations vs time or tracking waypoints for the desired logistics. Once the natural language query is translated into a database query, the user can also retrieve tracking information. This study allows users to ask various questions related to the shipment. Table 3 depicts the result generated from executing the natural language query on the proposed system. We have executed the system and gathered the answers for a random natural language query. The results are divided into three categories based on accuracy—High, Medium, Poor. The test case consists of users who know database concepts and related queries. The 20 such users named as known users tested the system by asking two questions each using speech recognition and verified the resulting outcome of the converted query. The ten such queries for a better understanding of readers are shown in Table 3.

- **High:** The correct SQL statement generation from natural language is marked as ‘High’
- **Medium:** The generated SQL statements that are partially correct are marked as ‘Medium’
- **Poor:** The wrongly generated SQL statements or failed to generate are marked as ‘Poor’

Table 3
Result generated from executing NL query on the proposed system

Natural Language Query	Generated Query	Desired Result	Decision Comment
what is status of shipment of serial 101	SELECT *	SELECT *	Medium
	FROM status	FROM status	
	INNER JOIN shipment	INNER JOIN shipment	
	ON status.serial = shipment.serial	ON status.serial = shipment.serial	
	WHERE shipment.serial = OOV;	WHERE shipment.serial = 101;	
what is the latitude and longitude of shipment having serial equal to 101	SELECT shipment.latitude, shipment.longitude	SELECT shipment.latitude, shipment.longitude	High
	FROM shipment	FROM shipment	
	WHERE shipment.serial = '101';	WHERE shipment.serial = '101';	
tell me the serial of shipment having source equal to Mundra and destination equal to Hamburg	SELECT shipment.serial	SELECT shipment.serial	High
	FROM shipment	FROM shipment	
	WHERE shipment.source = 'mundra'	WHERE shipment.source = 'mundra'	
	AND shipment.destination = 'hamburg';	AND shipment.destination = 'hamburg';	
tell me shipment serial where source equal to Mundra and destination equal to Hamburg	SELECT *	SELECT shipment.serial	Poor
	FROM shipment	FROM shipment	
	WHERE shipment.serial = 'hamburg'	WHERE shipment.source = 'mundra'	
	AND shipment.source = 'mundra'	AND shipment.destination = hamburg;	
	AND shipment.destination = OOV;		
what is transport of all export trade shipment	SELECT shipment.transport, shipment.trade	SELECT shipment.transport	Medium
	FROM shipment;	FROM shipment	
		WHERE shipment.trade = 'export';	
tell me shipment latitude and longitude where serial equal to 101	List index out of range	SELECT shipment.latitude, shipment.longitude	Poor
		FROM shipment	
		WHERE shipment.serial = '101';	

Table 3 (continue)

Natural Language Query	Generated Query	Desired Result	Decision Comment
tell me status of shipment having serial equal to 101 and source equal to Mundra	SELECT *	SELECT *	High
	FROM status	FROM status	
	INNER JOIN shipment	INNER JOIN shipment	
	ON status.serial = shipment.serial	ON status.serial = shipment.serial	
	WHERE shipment.serial = '101'	WHERE shipment.serial = '101'	
tell me serial of all shipment	SELECT shipment.serial	SELECT shipment.serial	High
	FROM shipment;	FROM shipment;	
tell me all the status	SELECT *	SELECT *	High
	FROM status;	FROM status;	
What is latitude and longitude of all shipment having country equal to India	SELECT shipment.latitude, shipment.longitude	SELECT shipment.latitude, shipment.longitude	High
	FROM shipment	FROM shipment	
	WHERE shipment.country = 'india';	WHERE shipment.country = 'india';	

The test set accuracy is shown in Table 4. Test set carries those questions which a known user queries. Overall, the system’s accuracy is acceptable, but further investigation on query reformulation with AIS may improve accuracy. Figure 5 depicts the accuracy graph.

Table 4 Accuracy of the result generated from the proposed system

Query Category	Accuracy
High	60%
Medium	20%
Poor	20%

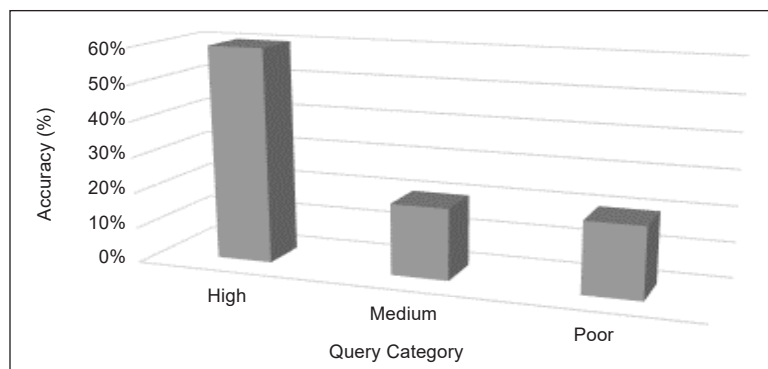


Figure 5. Accuracy of generated SQL queries with respect to desired result

THEORETICAL CONTRIBUTION

Logistics industries are shipping millions of tons of material and goods every year. Due to different risks of damage, delay, and burglary in shipping transit, income, productivity and goods are often lost. The reliability of delivery today plays a crucial role in improving customer service. While it has been possible to track shipments in real-time via modern tracking solutions, these solutions ensure easy monitoring and analysis by providing real-time tracking of shipment location. However, the solutions remain not widely spread throughout the industry. These solutions use GPS, RFID, terrestrial systems, and logistics databases to ascertain the shipment's position at any time, but usually extremely complicated, slow, and time-consuming. This study provides an overview of the logistics tracking and management theory. The philosophy of logistics management is not a universal measure. Instead, it combines interdisciplinary knowledge and analysis that addresses the customers' motivating needs and the organisational processes to achieve broader corporate goals. There is an increasing range of methods available for tracking. However, these methods appear to complicate the problems, fail to focus on what is essential, and are burdensome for those concerned, so they do not produce lasting results. In extension to current literature, this study aims to implement AI's technological advancements using NLP to enhance the shipment tracking and management system in a logistics organisation. This research helps define the ability of NLP to track the shipment using speech recognition to provide the status of shipment in real-time and also help the stakeholders in identifying actionable insights for effective logistics network management and customer demand. This study will help the stakeholders track the shipment at ease without searching the shipment status from master data.

IMPLICATION FOR PRACTICE

The transparency of the supply chain allows a large variety of goods to be monitored during transport to obtain a simple overview of each process step. If a customer is aware of the exact location of a shipment, destination, and intended route, he can alter plans for future shipments and respond to changing circumstances immediately. Using technology to gain more knowledge of every aspect of the industry and make data-driven decisions based on information and innovation in real-time brings productivity throughout the logistics process. A combination of real-time tracking and an easy-to-use system gives naïve users the confidence they need. This study aims to enhance or bring shipment tracking to perfection in a logistics company. The study will also identify the possibilities of implementing the NLP approach and its potential for logistics tracking systems. It will give them the momentum to pursue long-term action plans and to take action to secure fast gains. The study will also assist them in the following way.

- Transparency in delivery—allows all stakeholders to have access to information across the supply chain
- Enable end-users to make decisions in real-time
- Remove Language Barrier—caused by barriers to regional languages
- Reduced cost of trading and logistics operations and their timeframes
- Ease of doing business

CONCLUSION AND FUTURE RESEARCH DIRECTIONS

The growth of supply chain technologies has taken an exciting turn. The available technologies can change existing company operation speed, versatility, and productivity and allow innovative business models and services. In this paper, the method aims at offering a roadmap for refining transport decisions using an advanced supply chain approach. This study aims to develop an intelligent process for supervision, to track and trace the shipment. Furthermore, it provides a method that can be used to collect and communicate logistical information. This study's findings will provide valuable insight for designing more successful road-sea chain monitoring strategies focused on detected criteria and organisational challenges. Another objective of this study is to establish a partnership between the trade partners and supply chain carriers to minimise the inefficiency of physical delivery and enhance supply chain stability. However, the authors recognise that more empirical research and application are needed to validate or refute this approach's perceived advantages. The research can be further expanded through the development of an SCM-customized data analysis engine. Since the work is underway, it needs more research to ascertain its efficacy using real-time AIS data, expecting to anticipate it in the next update of this research. Our future work focuses on semantic query reformulation and query expansion and incorporates predictive analysis for routing prediction.

ACKNOWLEDGEMENT

The authors are grateful to the reviewers for providing valuable comments to improve the paper.

REFERENCES

- Abbas, K., Afaq, M., Khan, T. A., & Song, W. C. (2020). A blockchain and machine learning-based drug supply chain management and recommendation system for smart pharmaceutical industry. *Electronics*, 9(5), Article 852. <https://doi.org/10.3390/electronics9050852>
- Ahkouk, K., Machkour, M., & Antari, J. (2020). Inferring SQL queries using interactivity. In *Proceedings of the 3rd International Conference on Networking, Information Systems & Security* (pp. 1-7). ACM Publishing. <https://doi.org/10.1145/3386723.3387820>

- Artto, K., Heinonen, R., Arenius, M., Kovanen, V., & Nyberg, T. (1998). *Global project business and the dynamics of change*. Technology Development Centre Finland and Project Management Association Finland.
- Bai, T., Ge, Y., Guo, S., Zhang, Z., & Gong, L. (2021). Enhanced natural language interface for web-based information retrieval. *IEEE Access*, 9, 4233-4241. <https://doi.org/10.1109/ACCESS.2020.3048164>
- Bank, W. (2019). Trade integration as a pathway to development? *LAC Semiannual Report*. World Bank.
- Baresi, L., Meroni, G., & Plebani, P. (2016). A GSM-based approach for monitoring cross-organization business processes using smart objects. In *International Conference on Business Process Management* (pp. 389-400). Springer. https://doi.org/10.1007/978-3-319-42887-1_32
- Betti, Q., Khoury, R., Halle, S., & Montreuil, B. (2019). Improving hyperconnected logistics with blockchains and smart contracts. *IT Professional*, 21(4), 25-32. <https://doi.org/10.1109/MITP.2019.2912135>
- Brewer, A., Sloan, N., & Landers, T. L. (1999). Intelligent tracking in manufacturing. *Journal of Intelligent Manufacturing*, 10(3), 245-250. <https://doi.org/10.1023/A:1008995707211>
- Chadil, N., Russameesawang, A., & Keeratiwintakorn, P. (2008). Real-time tracking management system using GPS, GPRS and Google earth. In *2008 5th International Conference on Electrical Engineering/Electronics, Computer, Telecommunications and Information Technology* (Vol. 1, pp. 393-396). IEEE Publishing. <https://doi.org/10.1109/ECTICON.2008.4600454>
- Chary, M., Parikh, S., Manini, A. F., Boyer, E. W., & Radeos, M. (2019). A review of natural language processing in medical education. *Western Journal of Emergency Medicine*, 20(1), 78-86. <https://doi.org/10.5811/westjem.2018.11.39725>
- Chowdhary, K. R. (2020). Natural language processing. In *Fundamentals of Artificial Intelligence* (pp. 603-649). Springer. https://doi.org/10.1007/978-81-322-3972-7_19
- Christidis, K., & Devetsikiotis, M. (2016). Blockchains and smart contracts for the internet of things. *IEEE Access*, 4, 2292-2303. <https://doi.org/10.1109/ACCESS.2016.2566339>
- Christopher, M., & Peck, H. (2004). Building the resilient supply chain. *The International Journal of Logistics Management*, 15(2), 1-14. <https://doi.org/10.1108/09574090410700275>
- Clark, A., Fox, C., & Lappin, S. (2010). *The handbook of computational linguistics and natural language processing*. Wiley-Blackwell. <https://doi.org/10.1002/9781444324044>
- Couderc, B., & Ferrero, J. (2015, June 22-25). fr2sql: Interrogation de bases de données en français [Querying databases in French]. In *22ème Traitement Automatique des Langues Naturelles* (pp. 1-13). Caen, France.
- Garg, R., Kiwelekar, A. W., Netak, L. D., & Bhate, S. S. (2021a). Personalization of news for a logistics organisation by finding relevancy using NLP. In V. K. Gunjan & J. M. Zurada (Eds.), *Modern Approaches in Machine Learning and Cognitive Science: A Walkthrough: Latest Trends in AI, Volume 2* (pp. 215-226). Springer. https://doi.org/10.1007/978-3-030-68291-0_16
- Garg, R., Kiwelekar, A. W., Netak, L. D., & Bhate, S. S. (2021b). Potential use-cases of natural language processing for a logistics organization. In V. K. Gunjan & J. M. Zurada (Eds.), *Modern Approaches in Machine Learning and Cognitive Science: A Walkthrough: Latest Trends in AI, Volume 2* (pp. 157-191). Springer. https://doi.org/10.1007/978-3-030-68291-0_13

- Garg, R., Kiwelekar, A. W., Netak, L. D., & Ghodake, A. (2021c). i-Pulse: A NLP based novel approach for employee engagement in logistics organization. *International Journal of Information Management Data Insights*, 1(1), Article 100011. <https://doi.org/10.1016/j.jjime.2021.100011>
- GEP. (2018). *Artificial intelligence and its impact on procurement and supply chain: A comprehensive study*. Retrieved May 9, 2020, from <https://www.gep.com/white-papers/artificial-intelligence-impact-on-procurement-supply-chain>
- Gnimpieba, Z. D. R., Nait-Sidi-Moh, A., Durand, D., & Fortin, J. (2015). Using internet of things technologies for a collaborative supply chain: Application to tracking of pallets and containers. *Procedia Computer Science*, 56, 550-557. <https://doi.org/10.1016/j.procs.2015.07.251>
- Goll, D. C., & Bolte, N. O. (2020). *Potential analysis of track-and-trace systems in the outbound logistics of a Swedish retailer* (MSc Thesis). Jonkoping University, Sweden.
- He, W., Tan, E. L., Lee, E. W., & Li, T. Y. (2009). A solution for integrated track and trace in supply chain based on RFID & GPS. In *2009 IEEE Conference on Emerging Technologies & Factory Automation* (pp. 1-6). IEEE Publishing. <https://doi.org/10.1109/ETFA.2009.5347146>
- Huang, W. C., Hayashi, T., Wu, Y. C., Kameoka, H., & Toda, T. (2019). *Voice transformer network: Sequence-to-sequence voice conversion using transformer with text-to-speech pretraining*. ArXiv Publishing.
- Huvio, E., Grönvall, J., & Främling, K. (2002, June 13-14). Tracking and tracing parcels using a distributed computing approach. In *Proceedings of the 14th Annual Conference for Nordic Researchers in Logistics (NOFOMA'2002)* (pp. 29-43). Trondheim, Norway.
- Jedermann, R., Behrens, C., Westphal, D., & Lang, W. (2006). Applying autonomous sensor systems in logistics - Combining sensor networks, RFIDs and software agents. *Sensors and Actuators A: Physical*, 132(1), 370-375. <https://doi.org/10.1016/j.sna.2006.02.008>
- Kärkkäinen, M., Ala-Risku, T., & Främling, K. (2004). Efficient tracking for short-term multi-company networks. *International Journal of Physical Distribution & Logistics Management*, 34(7), 545-564. <https://doi.org/10.1108/09600030410552249>
- Kerr, A. (1989). Information technology - Creating strategic opportunities for logistics. *International Journal of Physical Distribution & Materials Management*, 19(5), 15-17. <https://doi.org/10.1108/EUM00000000000319>
- Kim, H. M., & Laskowski, M. (2018). Toward an ontology-driven blockchain design for supply-chain provenance. *Intelligent Systems in Accounting, Finance and Management*, 25(1), 18-27. <https://doi.org/10.1002/isaf.1424>
- Klein, T., & Thomas, A. (2009). Opportunities to reconsider decision making processes due to auto-ID. *International Journal of Production Economics*, 121(1), 99-111. <https://doi.org/10.1016/j.ijpe.2008.04.017>
- Klumpp, M., Kandel, C., & Bioly, S. (2011). A model for mystery shipping in logistics. In *9th International Industrial Simulation Conference 2011, ISC 2011* (pp. 180-184). EUROSIS Publishing.
- Ko, J. M., Kwak, C., Cho, Y., & Kim, C. O. (2011). Adaptive product tracking in RFID-enabled large-scale supply chain. *Expert Systems with Applications*, 38(3), 1583-1590. <https://doi.org/10.1016/j.eswa.2010.07.077>

- Kota, L. (2019). Artificial intelligence in logistics. *Advanced Logistic Systems - Theory and Practice*, 12(1), 47-60. <https://doi.org/10.32971/als.2019.004>
- Kothris, D. (2001). Performance assessment of terrestrial and satellite based position location systems. In *Second International Conference on 3G Mobile Communication Technologies (3G 2001)* (pp. 211-215). IET Digital Library. <https://doi.org/10.1049/cp:20010043>
- Lambert, D. M., & Cooper, M. C. (2000). Issues in supply chain management. *Industrial Marketing Management*, 29(1), 65-83. [https://doi.org/10.1016/S0019-8501\(99\)00113-3](https://doi.org/10.1016/S0019-8501(99)00113-3)
- Li, J., Wang, W., Ku, W. S., Tian, Y., & Wang, H. (2019). SpatialNli: A spatial domain natural language interface to databases using spatial comprehension. In *Proceedings of the 27th ACM SIGSPATIAL International Conference on Advances in Geographic Information Systems* (pp. 339-348). ACM Publishing. <https://doi.org/10.1145/3347146.3359069>
- Liu, D., Li, Y., & Thomas, M. A. (2017). A Roadmap for natural language processing research in information systems. In *Proceedings of the 50th Hawaii International Conference on System Sciences*. HICSS Publishing. <https://doi.org/10.24251/HICSS.2017.132>
- Loebbecke, C., & Powell, P. (1998). Competitive advantage from IT in logistics: The integrated transport tracking system. *International Journal of Information Management*, 18(1), 17-27. [https://doi.org/10.1016/S0268-4012\(97\)00037-6](https://doi.org/10.1016/S0268-4012(97)00037-6)
- Lund, S., Manyika, J., Woetzel, J., Bughin, J., Krishnan, M., Seong, J., & Muir, M. (2019). *Globalization in transition: The future of trade and value chains*. McKinsey Global Institute.
- MarineCadastre.gov. (2013). *AIS data handler*. BOEM Publishing.
- Musa, A., Gunasekaran, A., & Yusuf, Y. (2014). Supply chain product visibility: Methods, systems and impacts. *Expert Systems with Applications*, 41(1), 176-194. <https://doi.org/10.1016/j.eswa.2013.07.020>
- Neumann, M., King, D., Beltagy, I., & Ammar, W. (2019). *Scispacy: Fast and robust models for biomedical natural language processing*. ArXiv Publishing.
- Ruiz-Garcia, L., Steinberger, G., & Rothmund, M. (2010). A model and prototype implementation for tracking and tracing agricultural batch products along the food chain. *Food Control*, 21(2), 112-121. <https://doi.org/10.1016/j.foodcont.2008.12.003>
- Shamsuzzoha, A. H. M., Ehres, M., Tenkorang, R. A., Nguyen, D., & Helo, P. T. (2013). Performance evaluation of tracking and tracing for logistics operations. *International Journal of Shipping and Transport Logistics*, 5(1), 31-54. <https://doi.org/10.1504/IJSTL.2013.050587>
- Sullivan, G., & Fordyce, K. (1989). Logistics management system: Continuous flow manufacturing using knowledge based expert systems. In *Proceedings of the 2nd International Conference on Industrial and Engineering Applications of Artificial Intelligence and Expert Systems-Volume 2* (pp. 520-522). ACM Publishing. <https://doi.org/10.1145/67312.67313>
- Sultana, S., Tahsin, M., Reza, T., & Hossam-E-Haider, M. (2016). An innovative implementation of indoor positioning system using GPS. In *2016 3rd International Conference on Electrical Engineering and Information Communication Technology (ICEEICT)* (pp. 1-4). IEEE Publishing. <https://doi.org/10.1109/CEEICT.2016.7873117>

- Thessen, A. E., Cui, H., & Mozzherin, D. (2012). Applications of natural language processing in biodiversity science. *Advances in Bioinformatics*, 2012, 1-17. <https://doi.org/10.1155/2012/391574>
- Töyrylä, I. (1998). Realising the potential of traceability - A case study research on usage and impacts of product traceability. In *Acta Polytechnica Scandinavica Mathematics and Computing Series* (Vol. 97). Helsinki University of Technology.
- Wang, C., Tang, Y., Ma, X., Wu, A., Okhonko, D., & Pino, J. (2020). *fairseq S2T: Fast Speech-to-text modeling with fairseq*. ArXiv Publishing.
- Wang, W., Tian, Y., Wang, H., & Ku, W. S. (2020). A natural language interface for database: Achieving transfer-learnability using adversarial method for question understanding. In *2020 IEEE 36th International Conference on Data Engineering (ICDE)* (pp. 97-108). IEEE Publishing. <https://doi.org/10.1109/ICDE48307.2020.00016>
- Yang, G. H., Xu, K., & Li, V. O. K. (2010). Hybrid cargo-level tracking system for logistics. In *2010 IEEE 71st Vehicular Technology Conference* (pp. 1-5). IEEE Publishing. <https://doi.org/10.1109/VETECS.2010.5493655>
- Yuksel, M. E., & Yuksel, A. S. (2011). RFID technology in business systems and supply chain management. *Journal of Economic and Social Studies*, 1(1), 53-71. <https://doi.org/10.14706/JECOSS11115>
- Zhao, J. L., Fan, S., & Yan, J. (2016). Overview of business innovations and research opportunities in blockchain and introduction to the special issue. *Financial Innovation*, 2(1), Article 28. <https://doi.org/10.1186/s40854-016-0049-2>



A Simulation Study on Modified Weibull Distribution for Modelling of Investment Return

Hamza Abubakar* and Shamsul Rijal Muhammad Sabri

School of Mathematical Sciences, Universiti Sains Malaysia, 11800 USM, Pulau Pinang, Malaysia

ABSTRACT

The Weibull distribution is one of the most popular statistical models extensively applied to lifetime data analysis such as survival data, reliability data, wind speed, and recently in financial data, due to its flexibility to adaptably imitate different families of statistical distributions. This study proposed a modified version of the two-parameter Weibull distribution by incorporating additional parameters in the internal rate of return and insurance claims data. The objective is to examine the behaviour of investment return on the assumption of the proposed model. The proposed and the existing Weibull distribution parameters have been estimated via a simulated annealing algorithm. Experimental simulations have been conducted mimicking the internal rate of return (IRR) data for both short time (small sample) and long-term investment periods (large samples). The performance of the proposed model has been compared with the existing two-parameter Weibull distribution model in terms of their R-square (R^2), mean absolute error (MAE), root mean squared error (RMSE), Akaike's information criterion (AIC), and the Kolmogorov-Smirnov test (KS). The numerical simulation revealed that the proposed model outperformed the existing two-parameter Weibull distribution model in terms of accuracy, robustness, and sensitivity. Therefore, it can be concluded that the proposed model is entirely suitable for the long-term investment period. The study will be extended using the internal rate of return real data set. Furthermore, a comparison of the various Weibull distribution parameter estimators such as metaheuristics or evolutionary algorithms based on the proposed model will be carried out.

Keywords: Extended Weibull distribution, investment growth rate, maximum likelihood, simulated annealing

ARTICLE INFO

Article history:

Received: 25 April 2021

Accepted: 05 July 2021

Published: 18 October 2021

DOI: <https://doi.org/10.47836/pjst.29.4.29>

E-mail addresses:

zeeham4u2c@yahoo.com (Hamza Abubakar)

rija@usm.my (Shamsul Rijal Muhammad Sabri)

* Corresponding author

INTRODUCTION

Many physical systems have been observed to generate data that follow the statistical distributions, such as Weibull distribution (Datsiou & Overend, 2018). Real-world

phenomena are often defined using statistical distributions. Since statistical distributions are useful, their principles are extensively studied, and new distributions are created. However, there is still much interest in creating more flexible statistical distribution models to address different types of real-life data (Liao et al., 2020). Recently, researchers in statistical modelling have proposed different model approaches for generating new distributions data analysis. The purpose was to improve the ability to match complex phenomena in the data with high skewness and kurtosis. These extensions allow for greater flexibility when modelling specific data applications. Some studies are conducted on the generalised distribution classes in describing various phenomena (Elmahdy & Aboutahoun, 2013; Alzaatreh et al., 2013; Chauhan & Malik, 2017; Hashmi et al., 2019). It is simple and flexible in handling problems involving computing the modified or extended statistical distributions due to the computational and analytical resources provided in various programming software such as Python, Matlab, R, and Mathematica. A thorough review of methods for generating distributions was conducted by Lee et al. (2013).

Various researchers have developed new families of distributions for different reasons by incorporating one or more parameters into existing distributions. Adding extra parameter(s) to the current probability distribution has been shown to increase the distribution's versatility and goodness of fit. Several studies were carried out by scholars on the modification or extension of the existing Weibull model. This extension and modifications are well documented in the extant literature. A study by Phani (1987) has often been considered as one of the pioneering studies. The effort of his study was to find a match between two groups of fused silica optical fibres in terms of tensile strength. Following the work of Phani was the study by Marshall and Olkin (1997), who extended the Weibull distribution model by introducing additional parameters to the existing standard Weibull distributions.

Finally, Hirose (2002) proposed another extended Weibull distribution. The aim was to avoid the difficulties which appear in the conventional Weibull distribution models. Another study by Sarhan and Zaindin (2009) was proposed on the new version distribution named modified Weibull distribution. The study was a generalisation of exponential, Rayleigh, linear failure rate, and Weibull. A five-parameter distribution model named a beta modified Weibull distribution was studied by Bidrama et al. (2013). Wang and Elbatal (2015) proposed a new class of lifetime distributions by compounding the modified Weibull, and geometric distributions called the modified Weibull geometric distribution. Another three-parameter Weibull moment exponential (WME) distribution was proposed by (Hashmi et al., 2019). The proposed distribution is flexible because of various shapes of hazard rate functions. Finally, Guerra et al. (2020) proposed two new general families of statistical distributions model based on the unit interval system. A lifetime distributions model, called Marshall-Olkin extended inverse Weibull (MOEIW) distribution was proposed by Okasha and Basheer (2020). The reliability analysis of the new model is examined by employing

various functions, including a compound of survival function, reversed hazard rate function, mean inactivity time and strong mean inactivity time. Recently, another suitable distribution for modelling the carbon fibres data was proposed by Almetwally (2021). The proposed distribution combined the inverse Rayleigh distribution and the extended odd Weibull family to formulate the extended odd Weibull inverse Rayleigh (EOWIR) distribution with three parameters. Abubakari et al. (2021) proposed a distribution-based model based on five parameters named the modified beta flexible Weibull extension distribution (MBFWED). The extended version of the Weibull distribution is increasingly becoming an effective tool for modelling lifetime data. The modification is useful in lifetime analysis (reliability analysis), insurance, economy, finance, and engineering (Almazah et al., 2021).

However, there are a plethora of studies on the application of applications and uses of metaheuristics algorithm (MA) and artificial intelligence (AI) based techniques. These studies include a simulated algorithm (Abbasi et al. 2006), genetic algorithm (Alzaeemi & Sathasivam 2020) and election algorithm (EA) (Sathasivam et al., 2020; Abubakar et al., 2020a; Abubakar Danrimi, 2021) and artificial dragonfly algorithm (Abubakar et al., 2020b). One of the purposes of incorporating MA was to maximise the fitness function for optimal representation. Studies on metaheuristics algorithms in parameters estimation include the earlier work (Thomas, 1995). Genetics algorithms (GAS) was used to determine the parameters of Weibull distribution. Abbasi et al. (2006) proposed estimation of Weibull distribution parameters using simulated annealing for failure distribution modelling in reliability studies. Okafor et al. (2018) proposed metaheuristics named Particle Swarm Optimisation Algorithm (PSOA) in estimating the Weibull distribution parameters for failure distributive analysis. Freitas de Andrade et al. (2019) proposed the use of heuristic optimisation search algorithms such as Cuckoo Search Optimisation (CSO), Harmony Search (HS), Ant Colony Optimisation (ACO) and Particle Swarm Optimisation (PSO) in estimating the parameters of Weibull distribution. Recently, a new metaheuristics optimisation algorithm method, Social Spider Optimisation (SSO), was used in (Alrashidi et al., 2020) to estimate Weibull distribution parameters. Artificial bee colony (ABC) was by Yonar and Pehlivan (2020) based on the ML estimation of the 3-p Weibull distribution. Guedes et al. (2020) compared the performance of four metaheuristic optimisation algorithms; Migrating Birds Optimisation (MBO), Cuckoo Search (CS), Harmony Search (HS) and Imperialist Competitive Algorithm (ICA). Furthermore, a genetic algorithm (GA) with particle swarm optimisation (PSO) was recently used by Kaba and Suzer (2021) in searching for the root-mean-square error using the cumulative distribution function, and many more are increasingly becoming effective tools for optimisation and parameter estimation problem.

With the aim of extending the existing Weibull distribution model, this study proposes another modified version of the model by incorporating the growth rate parameter on the

original two-parameter. To the best of the author's knowledge, no study has been conducted on modifying the two-parameter Weibull distribution by imposing a growth rate on the original version. In our work, Simulated annealing (SA) based on Abbasi et al. (2006) will be utilised in estimating the parameters of the modified Weibull distribution based on simulated data set mimicking the internal rate return (IRR). However, simulated data based on internal rate return (IRR) has never been analysed based on the new version Weibull distribution (WD) assumption. Therefore, this study is brand-new, focusing on the stock investment modelling on the assumption of the modified Weibull distribution model. The present work aims to evaluate the potentiality of investment return distributed based on the proposed Weibull distribution model. The contributions of the present work include (i) modification of the existing Weibull distribution by imposing growth rate parameters and (ii) estimating the parameters of the proposed Weibull distribution model using a simulated annealing algorithm. This study will benefit investment decision-makers in making appropriate investment decisions with minimum risk and higher investment returns to the insurance company for evaluating investment claims and setting premiums at a level that will cover these claims, and leave an ample profit for shareholders.

MATERIALS AND METHODS

Weibull Distribution Model

Let x_i be a random sample of size N from IRR data. Let $F(x_i, \alpha, \beta, \eta)$ denote the cumulative density function (CDF) of Weibull distribution (WD) presented in Equation 1 as follows,

$$F_{Weibull}(x_i, \alpha, \beta, \eta) = \begin{cases} 1 - e^{-\left(\frac{x_i - \alpha}{\eta}\right)^\beta} & , x_i > \alpha \\ 0 & , x_i \leq \alpha \end{cases} \quad (1)$$

where $f(x_i, \alpha, \beta, \eta)$ is used to define the corresponding probability density function (PDF) presented in Equation 2 as follows,

$$f_{Weibull}(x_i, \alpha, \beta, \eta) = \begin{cases} \frac{\beta}{\eta} \left(\frac{x_i - \alpha}{\eta}\right)^{\beta-1} e^{-\left(\frac{x_i - \alpha}{\eta}\right)^\beta} & , x_i > \alpha \\ 0 & , x_i \leq \alpha \end{cases} \quad (2)$$

In our study, x_i is the internal rate of return (IRR) data generated over investment period t ; $\beta > 0$ is the shape parameter (slope/threshold); $\eta > 0$ is defined as the scale parameter (characteristic life) of the distribution showing how spread the internal rate of return (IRR) data is over investment period, and $\alpha \geq 0$ is used to denote the location of the distribution. The Weibull PDF satisfies the following properties:

- (i) Weibull distributions function f is decreasing with $f(x_t) \rightarrow \infty$ as $x_t \rightarrow 0$ when the value of shape parameter is $0 < \beta < 1$,
- (ii) Weibull distributions function f is decreasing with $f(x_t) \rightarrow 1$ as $x_t \rightarrow 0^+$ when the value of shape parameter is $\beta = 0$
- (iii) Weibull distributions when $\beta = 0$ the Weibull distribution function f increases and later decreases, with a maximum value at the mode as $x_t = \eta \left(1 - \frac{1}{\beta}\right)^{\frac{1}{\beta}}$
- (iv) For all $f(x_t) \rightarrow 0$ as $x_t \rightarrow 0^+$.

In the case where the parameter $\alpha = 0$, the PDF in Equation (2) reduces to 2-parameter Weibull distribution in Equation 3,

$$f_{Weibull}(x_t, \beta, \eta) = \begin{cases} \frac{\beta}{\eta} \left(\frac{x_t}{\eta}\right)^{\beta-1} e^{-\left(\frac{x_t}{\eta}\right)^\beta}, & x_t \geq 0, \beta, \eta > 0 \\ 0 & , x_t \leq \alpha \end{cases} \quad (3)$$

with the respective CDF of Weibull as Equation 4,

$$F_{Weibull}(x_t, \beta, \eta) = \begin{cases} 1 - e^{-\left(\frac{x_t}{\eta}\right)^\beta}, & x_t \geq 0 \\ 0 & , x_t \leq \alpha \end{cases} \quad (4)$$

In the case where the parameter $\alpha = 0$ and $\beta = c$ (c is constant), the Weibull PDF in Equation 3 reduces to 1-parameter Weibull distribution in Equation 5,

$$f_{Weibull}(x_t, c, \eta) = \frac{c}{\eta} \left(\frac{x_t}{\eta}\right)^{c-1} e^{-\left(\frac{x_t}{\eta}\right)^c} \quad (5)$$

where only the scale parameter (η) is unknown in the distribution.

In this study we consider Equation 3, the two parameters Weibull distribution. The expectation of the Weibull PDF is presented as Equation 6,

$$\mu = E(x_t) = \int_0^{+\infty} x_t f(x_t) dx_t \quad (6)$$

The following Equations 7-12 has been derived by substituting $f(x_t)$ from Equation 3,

$$E(x_t) = \int_0^{+\infty} x_t \frac{\beta}{\eta} \left(\frac{x_t}{\eta}\right)^{\beta-1} e^{-\left(\frac{x_t}{\eta}\right)^\beta} dx_t \quad (7)$$

$$= \int_0^{+\infty} x_t e^{-\left(\frac{x_t}{\eta}\right)^\beta} d\left(\frac{x_t}{\eta}\right)^\beta \quad (8)$$

$$= \int_0^{+\infty} \eta \left(\frac{x_t}{\eta}\right) e^{-\left(\frac{x_t}{\eta}\right)^\beta} d\left(\frac{x_t}{\eta}\right) \tag{9}$$

$$= \int_0^{+\infty} \eta \left[\left(\frac{x_t}{\eta}\right)^\beta\right]^{\left(1+\frac{1}{\beta}\right)-1} e^{-\left(\frac{x_t}{\eta}\right)^\beta} d\left(\frac{x_t}{\eta}\right) \tag{10}$$

$$= \int_0^{+\infty} \eta \rho^{\left(1+\frac{1}{\beta}\right)-1} e^{-\rho} \tag{11}$$

$$= \eta \Gamma\left(1+\frac{1}{\beta}\right) \tag{12}$$

The variance of IRR Weibull PDF is as in Equation 13,

$$\sigma^2 = \text{var}(x_t) = E(x_t - E(x_t))^2 \tag{13}$$

$$= E(x_t^2) - [E(x_t)]^2$$

$$= \int_0^{+\infty} x_t^2 f(x_t) dx_t - \mu^2 \tag{14}$$

The following Equations 15-18 has been derived by substituting $f(x_t)$ from Equation 3,

$$= \int_0^{+\infty} x_t^2 \frac{\beta}{\eta} \left(\frac{x_t}{\eta}\right)^{\beta-1} e^{-\left(\frac{x_t}{\eta}\right)^\beta} dx_t - \mu^2 \tag{15}$$

$$= \int_0^{+\infty} x_t^2 e^{-\left(\frac{x_t}{\eta}\right)^\beta} d\left(\frac{x_t}{\eta}\right) - \mu^2 \tag{16}$$

$$= \int_0^{+\infty} \eta^2 \rho^{\left(1+\frac{2}{\beta}\right)-1} e^{-\rho} d\rho - \mu^2$$

$$= \eta^2 \Gamma\left(1+\frac{2}{\beta}\right) - \mu^2 \tag{17}$$

$$= \eta^2 \Gamma\left(1+\frac{2}{\beta}\right) - \eta^2 \Gamma^2\left(1+\frac{1}{\beta}\right) \tag{18}$$

where Γ is the Gamma function expression as Equation 19,

$$\Gamma(d) = \int_0^{+\infty} \rho^{d-1} e^{-\rho} d\rho, d > 0 \tag{19}$$

where $\Gamma(p+1) = p\Gamma(p), \Gamma(n+1) = n!$. The cumulative distribution function (CDF) of the

Weibull distribution can be obtained by integrating Equation 3 expressed as Equation 20,

$$F(x_t) = P(\rho \leq x_t) = \int_0^\beta f(\rho) d\rho = 1 - \exp\left[-\left(\frac{x_t}{\eta}\right)^\beta\right] \quad (20)$$

Weibull distribution interpolates between the standard exponential distribution when $\eta = 1$. It can be reduced to another special distribution called the Rayleigh distribution by setting the shape parameter $\beta = 2$. Several techniques have been used in estimating the unknown value of the Weibull distribution. In this study, a simulated annealing algorithm (SAA) incorporated in (MLE) has been utilised to maximise the Weibull distribution's fitness function. To the best of the author's knowledge, a simulated annealing algorithm (SAA) was not utilised to estimate the parameters of the modified version of Weibull distribution.

Mathematical Formulation of the Modified Internal Rate of Return Modelling

The investment strategy for holding the stock is allocating a level amount of contribution for K years at the beginning of the year. If we wish to hold the stock for the company chosen in the long term period, the stock valuation can also be seen by computing the (modified) internal rate of return (M)IRR). At the same time, if the company declares dividends yearly, the cash dividends are reinvested and together deposited with the level contribution to enlarging the share units. We let all our share units earn the share capital at the end of K years, indicating our investment profit. If our share capital is less than our total contribution, we may expect our MIRR to be in a negative form. The detailed procedure of the investment return was documented in Sabri and Sarsour (2019) is presented as Equations 21 and 22,

$$NPV = \left[S_k^{(2)} P_{u_{k+1,2}} + B_K + \delta_K \right] (1+r) - \frac{u_{K+1,1} - u_{1,1}}{365} - C \sum_{k=1}^{K+1} \mu_k (1+r) - \frac{u_{k+1,1} - u_{1,1}}{365} \quad (21)$$

$$\equiv F(K)(1+r) - \frac{u_{K+1,1} - u_{1,1}}{365} - \sum_{k=1}^{K+1} C_k^* (1+r) - \frac{u_{k+1,1} - u_{1,1}}{365} \quad (22)$$

where $k \in [1, 2, \dots, K]$ is defined as the Net Present Value (NPV) of stock investment, computed at time zero. $S_k^{(2)}$ is accumulated share unit after share issuance at the end of the year k , which can be computed as Equation 23,

$$S_k^{(2)} = \psi_k \times S_k^{(1)} \quad (23)$$

where ψ_k is the function of share issuance, k is the share units at the beginning of the year k , and $F(K)$ is the terminal value investment fund to be let at the end of the year K , which can be computed as Equation 24,

$$F(K) = S_K^{(2)} \times P_{u_{K+1,2}} + B_K + \delta_K \quad (24)$$

where $u_{k,1}$ represent the date of share purchased and sold, $u_{k,2}$, is the date of dividend and share issued based on the stock reported on year k , $P_{u_{k,2}}$ defined the stock price at the date $u_{k,2}$, B_k represents the cash balance at the year k , δ_k defined as a cash dividend at year k , r represents the modified internal rate of return (MIRR) of the Malaysian property development companies (MPDS), C is the yearly fixed contribution which can be computed as Equation 25,

$$C = \mu_k \frac{1}{C_k^*} \tag{25}$$

It is very important to choose the best potential stocks to hold in the long term (long term investment). Furthermore, holding a stock for a K -years period of the investment may vary in terms of MIRR. For example, some might choose the best time to start investing, but it is tough to identify it as the MIRR measure can only be observed yearly. Therefore, assuming the MIRR for all starting times to invest is common, we may define the MIRR, denoted as R_{tiK} , as a random variable having the mean and variance $E(R_k)$ and $Var(R_k)$ according to MIRR distribution.

Modified Internal Rate of Return on the assumption of Weibull Distribution

After acquiring the Weibull distribution parameters, a rate of return of the Malaysian property development sector (MPDS) can be observed for both short and long-term investment periods. In investment, we may obtain a positive value of profit (or even be greater than our capital investment) as well as poorly earn nothing. It indicates our capital of investment K could be infinite or even zero value. For some time K , our terminal investment $C(1 + R_k)^K$ is in between 0 to infinity Equation 26,

$$0 < C(1 + R_{ik})^K < \infty \rightarrow -1 < R_{ik} < \infty \tag{26}$$

since the rate of return is non-negative (*i.e* $R_{ik} > -1$), we transformed the rate of return, X_{tik} according to Equation 27 as follows,

$$X_{tik} = 1 + R_{tik} \tag{27}$$

The Weibull distribution (WD) is flexible and easily applied in modelling many different forms of data (Thomas, 1995). The MIRR data will be modelled on the modified Weibull distribution (WD) assumption but the shape and scale parameters are unknown. The transformed MIRR data (X_{tik}) is assumed to come from the Weibull distribution (WD) in this study. A continuous random variable X_{tik} is said to follow Weibull distribution with parameters $\alpha_k > 0, \beta_k > 0$ and $\eta_k > 0$ to be estimated as follows $X_{tik} \square Weibull(\alpha_k, \beta_k, \eta_k)$ if its PDF is given by Equation 28,

$$f_{X_{ik}}(X_{ik}, \alpha_k, \beta_k, \eta_k) = \begin{cases} \frac{\beta_k}{\eta_k} \left(\frac{X_{ik} - \alpha_k}{\eta_k} \right)^{\beta_k - 1} e^{-\left(\frac{X_{ik} - \alpha_k}{\eta_k} \right)^{\beta_k}} & , X_{ik} > \alpha \\ 0 & , X_{ik} \leq \alpha \end{cases} \quad (28)$$

From Equation (27), the mean of the three parameters WD is defined as Equation 29,

$$E(X_{ik}) = \eta_k \Gamma \left(1 + \frac{1}{\beta_k} \right) + \alpha_k \quad (29)$$

where Γ signifies a gamma function of the parenthetic expression, defined as Equation 30,

$$\Gamma(n) = \int_0^{\infty} e^{-x} x^{n-1} dx \quad (30)$$

The variance of the three parameters WD is a function of the shape (β_k) and scale parameters (η_k) deduced as Equation 31,

$$Var(X_{ik}) = \eta_k^2 \left[\Gamma \left(1 + \frac{2}{\beta_k} \right) - \Gamma^2 \left(1 + \frac{1}{\beta_k} \right) \right] \quad (31)$$

A higher variance would generally provide a lower investment return at the same point in time. If we wish to re-write the MIRR based on the Weibull distribution in Equation 28, we may have the following Equation 32,

$$f_{r_{ik}}(r_{ik}; \alpha_k, \beta_k, \eta_k) = \frac{\beta_k}{\eta_k} \left(\frac{(r_{ik} + 1) - \alpha_k}{\eta_k} \right)^{\beta_k - 1} e^{-\left(\frac{(r_{ik} + 1) - \alpha_k}{\eta_k} \right)^{\beta_k}} , r_{ik} > -1 \quad (32)$$

this will also indicate that mean and variance in Equations 29 and 31 can be re-written in terms of the transformed MIRR in Equations 33 and 34, respectively,

$$E(r_{ik}) = \eta_k \Gamma \left(1 + \frac{1}{\beta_k} \right) + \alpha_k \quad (33)$$

$$var(r_{ik}) = \eta_k^2 \left[\Gamma \left(1 + \frac{2}{\beta_k} \right) - \Gamma^2 \left(1 + \frac{1}{\beta_k} \right) \right] \quad (34)$$

Incorporating Growth Rate Parameter on Weibull distribution

The Internal rate of investment return (IRR) is usually used as a tool capable of evaluating

the behaviour of cash flows (Sabri & Sarsour, 2019; Sarsour & Sabri, 2020a; Sarsour & Sabri, 2020b). Investigating the behaviour of investment return can be a challenging task due to its non-linearity, non-stationary, and high uncertainty. The Weibull distribution model is flexible in estimating components exhibiting increasing, constant and decreasing failure rate functions; however, it cannot directly fit those products with bathtub shapes or other non-monotonic failure rates functions such as internal rate of return and insurance claims data (Tang et al. 2002; Boonta & Boonthiem, 2019). The importance of such an extension has been proved in recent years on various problems. Many standard distributions have been generalised (Pobočiková et al., 2018). A list of well-being indicators may include profit, risk and uncertainly and failure rate (Boonta & Boonthiem, 2019). Those indicators also represent essential aspects of the investment return. In this context, it is necessary to modify the existing Weibull distribution that takes those characteristics into account. Parameters are added as viable alternatives to deal with the complexity and the multiple objectives that financial decisions can possess. The model considers the dynamic nature and uncertainty involved in the rate of return in taken investment decision which is assumed to undergo growth or decay according to some rate of investment return over the investment period (Kellison, 2009). We imposed a growth rate (ω) for the investment period $K \geq 2$ that follows Equation 35,

$$X_{itK} = (1 + \omega)^{K-1} X_{it1} \quad (35)$$

For 2 year investment period, the value $K = 2$, we have Equation 36,

$$X_{it2} = (1 + \omega) X_{it1} \quad (36)$$

with the mean $E(X_{itK})$ and the variance $Var(X_{itK})$ in Equations 37 and 38, respectively as follows,

$$E(X_{itK}) = (1 + \omega)^{K-1} E(X_{it1}) \quad (37)$$

$$Var(X_{itK}) = \left((1 + \omega)^{K-1} Var(X_{it1}) \right)^2 \quad (38)$$

Substituting Equations 35 and 36 into Equations 37 and 38, respectively yields Equations 39 and 40,

$$E(X_{itK}) = (1 + \omega)^{K-1} \eta_K \Gamma \left(1 + \frac{1}{\beta_K} \right) + \alpha_K \quad (39)$$

$$Var(X_{itK}) = \left((1 + \omega)^{K-1} \eta_K^2 \left[\Gamma \left(1 + \frac{2}{\beta_K} \right) - \Gamma^2 \left(1 + \frac{1}{\beta_K} \right) \right] \right)^2 \quad (40)$$

For example, if $K = 5$, then the transformed MIRR of R_5 based on Weibull distribution with PDF of three parameters will be Equation 41,

$$f_{X_{i5}}(X_{i5}; \alpha_5, \beta_5, \eta_5, \omega) = \begin{cases} \frac{\beta_5}{\eta_5} \left(\frac{(r_{i5} + 1) - \alpha_5}{(1 + \omega)^4 \eta_5} \right)^{\beta_5 - 1} e^{-\left(\frac{(r_{i5} + 1) - \alpha_5}{(1 + \omega)^4 \eta_5} \right)^{\beta_5}}, & r_{i5} > -1 \\ 0 & \text{Otherwise} \end{cases} \quad (41)$$

According to Equation 32, the mean $E(X_{iK})$ and the variance $Var(X_{iK})$ of Equation 41 will be Equations 42 and 43,

$$E(X_{i5}) = (1 + \omega)^4 E(X_{i5}) \quad (42)$$

$$\text{var}(X_{i5}) = \left[(1 + \omega)^4 \eta_K^2 \left[\Gamma\left(1 + \frac{2}{\beta_K}\right) - \Gamma^2\left(1 + \frac{1}{\beta_K}\right) \right] \right]^2 \quad (43)$$

By setting $\alpha_K = 0$, Equation (41) is transformed into three-parameter Weibull distribution with ω a growth rate as Equation 44,

$$f_{X_{i5}}(X_{i5}; \beta_5, \eta_5, \omega) = \begin{cases} \frac{\beta_5}{\eta_5} \left(\frac{X_{i5}}{(1 + \omega)^4 \eta_5} \right)^{\beta_5 - 1} e^{-\left(\frac{X_{i5}}{(1 + \omega)^4 \eta_5} \right)^{\beta_5}}, & X_{i5} > 0 \\ 0 & \text{Otherwise} \end{cases} \quad (44)$$

If we consider the period of investment to be studied until K^* years, for the sample size n and the maximum of the years that the data has been collected is T . We re-write Equation 44 in general form as Equation 45,

$$f_{X_{iK}}(X_{iK}; \beta_K, \eta_K, \omega) = \begin{cases} \frac{\beta_K}{\eta_K} \left(\frac{X_{iK}}{(1 + \omega)^{K-1} \eta_K} \right)^{\beta_K - 1} e^{-\left(\frac{X_{iK}}{(1 + \omega)^{K-1} \eta_K} \right)^{\beta_K}}, & X_{iK} > 0 \\ 0 & \text{Otherwise} \end{cases} \quad (45)$$

For a period of investment, K , the ML of a random sample of $x_1, x_2, x_3, \dots, x_{K^*}$ size K^* , where $K^* \in K$ has been considered and the maximum investment period that MIRR data have been collected is T . The likelihood function of Weibull PDF in Equation 45 is presented as Equation 46,

$$L = \prod_{i=1}^n f_{R_{iK}}(X_{iK} | \beta_K, \eta_K, \omega) = \prod_{K=1}^{K^*} \frac{\beta_K}{\eta_K} \left(\frac{X_{iK}}{(1+\omega)^{K-1} \eta_K} \right)^{\beta_K-1} e^{-\left(\frac{X_{iK}}{(1+\omega)^{K-1} \eta_K} \right)^{\beta_K}} X_{iK} > 0 \tag{46}$$

The likelihood function of Weibull PDF in Equation 46 can be simplified to factor X_{iK} and η_K as Equation 47,

$$= \prod_{K=1}^{K^*} \frac{\beta_K}{\eta_K^{\beta_K}} \left(\frac{1}{(1+\omega)^{K-1}} \right)^{\beta_K-1} X_{iK}^{\beta_K-1} e^{-\left(\frac{X_{iK}}{(1+\omega)^{K-1} \eta_K} \right)^{\beta_K}} \tag{47}$$

The likelihood function of Weibull PDF is presented in Equation 47 can be simplified as Equation 48,

$$L\left[\left(X_{iK}; \bar{\xi} \right) \right] = \beta \eta^{-\sum_{K=1}^{K^*} \sum_{t=1}^{T-(K-1)} n\beta} \times (1+\omega)^{\sum_{K=1}^{K^*} \sum_{t=1}^{T-(K-1)} (\beta-1)(K-1)n} \times \prod_{T=1}^{K^*} \prod_{t=1}^{T-(K-1)} \prod_{i=1}^n X_{iK}^{\beta-1} \times e^{\sum_{K=1}^{K^*} \sum_{t=1}^{T-(K-1)} \sum_{i=1}^n \left(\frac{X_{iK}}{\eta(1+\omega)^{K-1}} \right)^\beta} \tag{48}$$

The Log-likelihood function of Equation 48 is presented as Equation 49,

$$\begin{aligned} \ln L(\bar{\xi} | X_{iK}) = & -n \left(K^*(T+1) - \frac{K^*(K^*+1)}{2} \right) \beta \ln(\eta) + \ln(\beta) - n \left(\sum_{K=1}^{K^*} (K-1)(T-(K-1)) \right) \\ & (\beta-1) \ln(1+\omega) + \left(\sum_{K=1}^{K^*} \sum_{t=1}^{T-(K-1)} \sum_{i=1}^n X_{iK} \right) (\beta-1) - \sum_{K=1}^{K^*} \sum_{t=1}^{T-(K-1)} \sum_{i=1}^n \left(\frac{X_{iK}}{\eta(1+\omega)^{K-1}} \right)^\beta \end{aligned} \tag{49}$$

where a vector $\bar{\xi} \in (\beta_K, \eta_K, \omega)$ is described as model parameters to be estimated. The vector $L(\bar{\xi})$ is considered as a non-linear objective function and $\bar{\xi}$ is taken as a decision variable, the problem can be taken as an unrestricted nonlinear optimisation problem that could then be computed by maximising the Weibull distribution based on the simulated annealing (SAA) procedure proposed by Abbasi et al. (2006) presented in the next section.

$$\begin{aligned} \ln L(\bar{\xi} | X_{iK}) = & -n \left(K^*(T+1) - \frac{K^*(T^*+1)}{2} \right) \beta \ln(\eta) + \ln(\beta) - n \left(\sum_{K=1}^{K^*} (K-1)(T-(K-1)) \right) \\ & (\beta-1) \ln(1+\omega) + \left(\sum_{K=1}^{K^*} \sum_{t=1}^{T-(K-1)} \sum_{i=1}^n X_{iK} \right) (\beta-1) - \sum_{K=1}^{K^*} \sum_{t=1}^{T-(K-1)} \sum_{i=1}^n \left(\frac{X_{iK}}{\eta(1+\omega)^{K-1}} \right)^\beta \end{aligned} \tag{50}$$

It is quite difficult and exhaustive to search the parameters of Equation 50 to attain the

complicated objectives function as observed by Abbasi et al. (2006), Abbasi et al. (2011), and Yonar and Pehlivan (2020). Metaheuristics algorithms have been incorporated to reduce the complication involved in estimating the parameters,

Simulated Annealing Algorithm (SAA)

Simulated annealing (SAA) is one of the first single-based stochastic metaheuristics optimisation algorithms. It is inspired by the simulated thermodynamic process used in metallurgic for solidification studied in statistical mechanics, in which a material changes state while reducing its energy state to the lowest level (Kirkpatrick et al., 1983). Simulated annealing is considered one of the most powerful computation methods applied in solving the optimisation problem in almost every area. This physical process occurs after the metal is removed from the heat source. When the molten material is physically rinsed, the temperatures are decreased very slowly as heat passes to the surrounding environment to crystallise into one large crystalline lattice structure, and metal becomes solid at this stage. The energy has reached its minimum level. The SAA can be slow in reaching the optimal solution because optimal results require a very slow lowering of the temperature with control from iteration to iteration (well organised and perfect structure). The resulting lattice structure is probably not ideal if the crystallisation is too fast (imperfect structure). The advantages SAA possessed over other metaheuristics include; easy implementation, finding a globally optimal solution that is feasible even after finding a locally optimal solution, and satisfactory results are guaranteed with a relatively low number of iterations.

Generally, the SAA algorithm is based on the stochastic search technique, which generates perturbation of the current state at a random instance that make up the solution area which later undertakes series of operations such as initialisation, measure the quality of the solution, and if it is better than the new one, accept the solution that could lead a better searching technique of the SAA, to escape from local optima and to be in close vicinity of the region where the optimal solution could be located quickly. Since its implementation, SAA has been updated and extended to many mathematical and engineering domains. In this work, a robust and powerful heuristics search technique known as SAA has been established for effectively searching the MLE fitness function for Weibull Distribution based on simulated data set mimicking the internal rate of return. In this regard, the steps of the SAA implementation is presented in the next section.

SAA Implementation

A simulated annealing algorithm (SAA) is a two-step search process that includes perturbing the solution and evaluating its quality. Usually, to decide about the acceptance of the new solution, the algorithm uses the solution error. It is a stochastic method design to solve

multidimensional global optimisation, i.e. problems with the following Equation 51,

$$f(\overline{\xi_{opt}}) = \min_{\xi_i \in X} f(\overline{\xi}) \text{ or } f(\overline{\xi_{opt}}) = \max_{\xi_i \in X} f(\overline{\xi}) \quad (51)$$

where the variable $\xi_i \in X$ is variable to be estimated via SAA. This representation is common to most optimisation algorithms. However, SAA is a temperature-dependent search procedure and the process temperature. Let τ_i be represented as the process temperature as Equation 52,

$$\tau_i = \lambda_T^{\min} + \tau_1 * (\lambda_T^{\max} - \lambda_T^{\min}) \quad (52)$$

where λ_T^{\min} and λ_T^{\max} are defined as the initial and final temperatures, N is the number of temperatures, and the values of $\tau_1 \in [0, N]$ are chosen based on a specific cooling schedule considered problem-dependent. It is advisable to repeat a fixed number of iterations at each temperature before the temperature drops to enhance the performance of SAA.

There are some specific criteria to accept a solution once it has been perturbed. One obvious requirement is to accept a solution whenever there is less error than the previous solution. The metropolis algorithm has been used in SAA to compute the probability of acceptance for a perturbed solution. During the annealing process, each new solution x_i was accepted with a temperature-dependent probability P_T given by Equation 53,

$$P_T = \begin{cases} 1 & \text{if } f(x_j) \leq f(x_i) \\ e^{-\frac{f(x_j) - f(x_i)}{k_T}} & \text{if } f(x_j) \geq f(x_i) \end{cases} \quad (53)$$

where T is the current temperature, and $f(x_i)$ and $f(x_j)$ are the fitness scores of the worst vertex x_i and new vertex of the simplex, respectively.

Performance Evaluation

Several tests were carried out to examine the suitability of the proposed modified Weibull distribution in describing the behaviour of investment return in terms of the accuracy and error accumulations during the parameter estimation process. The performance of the proposed model has been evaluated in terms of their R-square (R^2), mean absolute error (MAE), root means squared error (RMSE), Akaike's information criterion (AIC), and the Kolmogorov-Smirnov test (KS) to ascertain the difference between the true and estimated distribution functions. The formulation of the statistical test used is presented in Equations 54-58, respectively,

$$R^2 = \frac{\sum_{i=1}^n \left[\left(\hat{F}(X_{iK}) - \bar{F} \right)^2 \right]}{\sum_{i=1}^n \left[\left(\hat{F}(X_{iK}) - \bar{F} \right)^2 \right] + \left[\sum_{i=1}^n \left(F_n(X_{iK}) - \hat{F}(X_{iK}) \right)^2 \right]} \quad (54)$$

$$RMSE = \sqrt{\frac{1}{n} \sum_{i=1}^n \left[\left(\hat{F}(X_{iK}) - \bar{F} \right)^2 \right]} \quad (55)$$

$$MAE = \frac{1}{n} \sum_{i=1}^n \left| \hat{F}(X_{iK}) - \bar{F} \right| \quad (56)$$

$$AIC = 2k - 2 \ln L(\hat{\xi}) \quad (57)$$

$$KS = \max_{1 \leq i \leq n} \left| \hat{F}(X_{iK}) - F(X_{iK}) \right| = \max_{1 \leq i \leq n} \left| \hat{F}(X_{iK}) - P_i \right| \quad (58)$$

where $\hat{F}(X_{iK})$ and \bar{F} described the observed and the estimated parameters respectively, n defined as the total number.

Simulation Study

This section extends the two-parameters Weibull distribution to three Weibull distributions by imposing growth rate parameters on the existing Weibull model. The purpose is to investigate the long-term investment return that allows for identifying and forecasting company performance. Forecasting business return is necessary to properly analyse the business performance in either short-term or long-term periods. The analysis was conducted based on simulated data mimicking the internal rate of return (IRR). The parameters have been estimated for every sample size. We set the proposed Weibull distribution on the random variable X to mimic the simulation experiment's internal rate returns (IRR). The samples of different sizes $n \in [10, 100]$ were generated using Microsoft Excel 365. The parameters have been estimated via a programme executed on a Python programming language. Finally, the performance has been computed based on the goodness of fit using Microsoft Excel 365 for transparency.

Experimental Study

This section presents the experimental study used to analyse and compare the simulated data's fitness on the proposed model. First, the experimental methodology applied in this study, the definition of the algorithm and parameters are presented. Then, the experimental results and the statistical tests carried out to evaluate these results are outlined. Finally, a

discussion based on the performance of the proposed methodology is provided. A dataset randomly generated were used in conducting the statistical analysis and evaluating the proposed Weibull model performance. The following procedures are adopted to generate random samples on the assumption of both the proposed and the existing models;

- (i) choose starting values for the scale, shape, and growth rate parameters and determine the sample size n ;
- (ii) generate a random sample of size n from the proposed Weibull distribution;
- (iii) compute the estimates of the distribution parameters; and
- (iv) redo the steps (ii) and (iii) N times.

This study is carried out on a computer with Intel Core i3 CPUs and 8 GB RAM. The SA algorithm (Figure 1) has been developed using a Python programming language. Ten thousand independent runs of the SA algorithm are conducted to get several near-optimal solutions. The estimated parameters have been reported in Table 1, while Table 2 reported the goodness of fit of the proposed model based on simulated data. The source code file for the computational procedure on Excel 365 and a Python source is available on request from the authors.

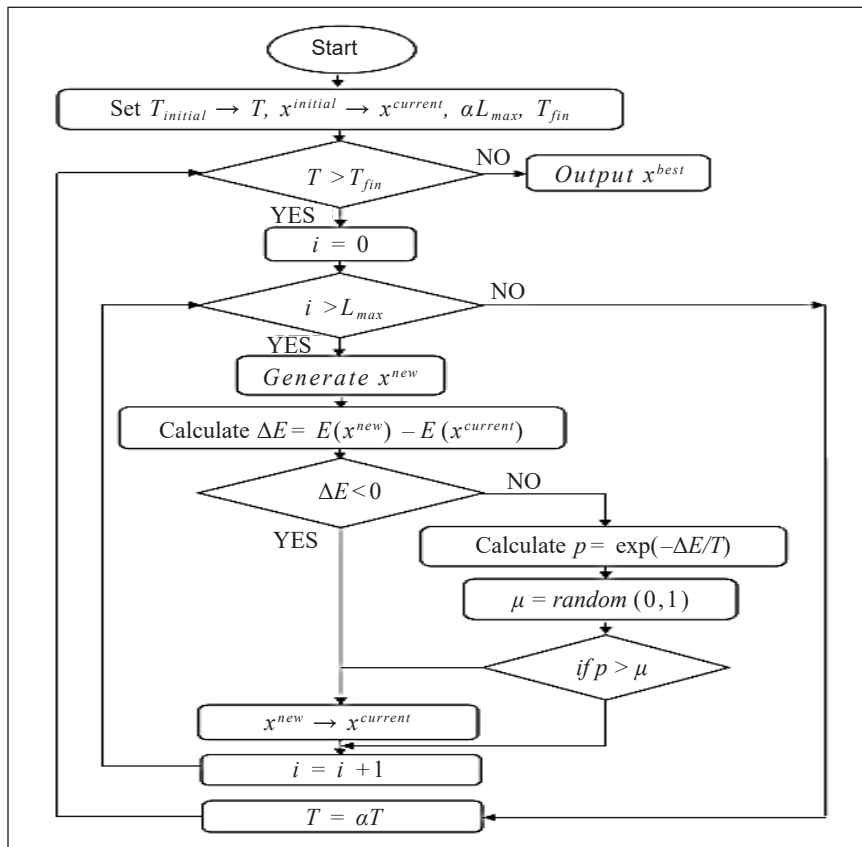


Figure 1. Flow diagram of SA algorithm

RESULTS AND DISCUSSION

The result of the estimates of unknown parameters of the proposed and the existing Weibull distributions are presented in Table 1. In addition, the goodness of fit test in terms of R^2 , MAE, RMSE, AIC, and K-S are listed in Table 2, while Figures 2 to 6 are the graphs displaying the results presented in Table 2 for easy analysis.

Table 1
Estimated parameter of Weibull distribution with Log-likelihood

n	Weibull Distributions	Parameter estimates	LogL
10	$W(\beta, \eta)$	2.9756, 1.4319	-13.7038
	$W(\beta, \eta, \omega)$	0.8647, 2.1491, -0.9832	-7.4251
20	$W(\beta, \eta)$	13.5808, 13.9272	-810.5536
	$W(\beta, \eta, \omega)$	1.3748, 1.4231, -0.7430	-15.5342
30	$W(\beta, \eta)$	7.644, 12.4506	-686.9850
	$W(\beta, \eta, \omega)$	-0.5301, 0.8923, -1.2423	-27.5219
40	$W(\beta, \eta)$	33.0149, 17.7373	-4749.5452
	$W(\beta, \eta, \omega)$	1.0475, 1.5442, -1.1191	-30.7496
50	$W(\beta, \eta)$	65.0825, 39.5618	-14997.9228
	$W(\beta, \eta, \omega)$	-0.2513, -11.1642, -1.2499	-82.6765
60	$W(\beta, \eta)$	14.2972, 16.3663	-2238.2231
	$W(\beta, \eta, \omega)$	1.0611, 1.5789, -1.4742	-25.5201
70	$W(\beta, \eta)$	66.8042, 65.6898	-23732.7831
	$W(\beta, \eta, \omega)$	0.9798, 2.1389, -0.7372	-69.3542
80	$W(\beta, \eta)$	48.3294, 22.6938	-15548.6651
	$W(\beta, \eta, \omega)$	0.8383, 46.8547, -0.9204	-260.8670
90	$W(\beta, \eta)$	159.9159, 79.6757	-78334.6861
	$W(\beta, \eta, \omega)$	0.9979, 1.9992, -0.5261	-84.0295
100	$W(\beta, \eta)$	11.2265, 7.4906	-2904.6339
	$W(\beta, \eta, \omega)$	0.92011, 2.6081, -1.4491	-112.6159

Table 2
Performance evaluation of modified Weibull distribution based on simulation data

n	Weibull Distribution	AIC	MAE	RMSE	R^2	KS
10	$W(\beta, \eta)$	-36.0919	0.4375	0.4815	0.9799	0.7466
	$W(\beta, \eta, \omega)$	-21.7737	0.4045	0.4486	0.8856	0.6785
20	$W(\beta, \eta)$	-76.1838	0.5250	0.5989	0.3214	1
	$W(\beta, \eta, \omega)$	-49.5474	0.3342	0.3718	0.9578	0.5631
30	$W(\beta, \eta)$	-1377.97	0.5167	0.7248	0.7077	0.9999
	$W(\beta, \eta, \omega)$	-61.0438	0.1443	0.2083	0.8400	0.3511
40	$W(\beta, \eta)$	-9503.09	0.5125	0.5882	NA	1
	$W(\beta, \eta, \omega)$	-67.4992	0.2624	0.2985	0.9820	0.5339

Table 2 (continue)

n	Weibull Distribution	AIC	MAE	RMSE	R^2	KS
50	$W(\beta, \eta)$	-19010.2	0.51000	0.5860	NA	1
	$W(\beta, \eta, \omega)$	-171.3530	0.2298	0.2838	0.8752	0.5802
60	$W(\beta, \eta)$	-4480.45	0.5083	0.5845	NA	1
	$W(\beta, \eta, \omega)$	-57.0402	0.2666	0.3100	0.9922	0.5472
70	$W(\beta, \eta)$	-47469.6	0.5071	0.5835	NA	1
	$W(\beta, \eta, \omega)$	-144.7083	0.2965	0.3508	0.9849	0.6222
80	$W(\beta, \eta)$	-31101.3	0.5062	0.5828	NA	1
	$W(\beta, \eta, \omega)$	-527.7340	0.4853	0.5590	0.9977	0.9615
90	$W(\beta, \eta)$	-62206.7	0.5055	0.5822	NA	1
	$W(\beta, \eta, \omega)$	-174.0589	0.2987	0.3451	0.9845	0.6076
100	$W(\beta, \eta)$	-124417	0.505	0.5082	0.5082	1
	$W(\beta, \eta, \omega)$	-231.2317	0.3052	0.3618	0.9831	0.6631

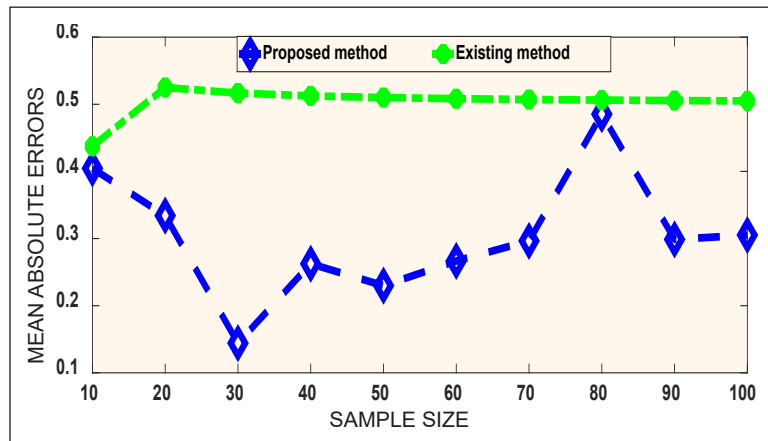


Figure 2. MEA Evaluation of models performance

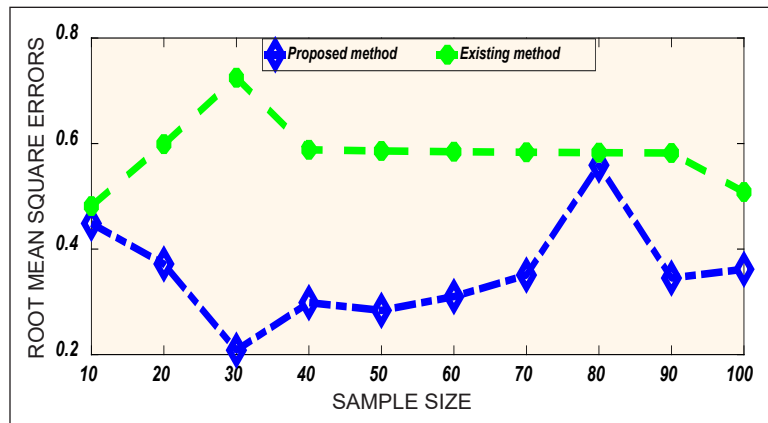


Figure 3. RMSE Evaluation of models performance

Weibull Distribution for Investment Return Modelling

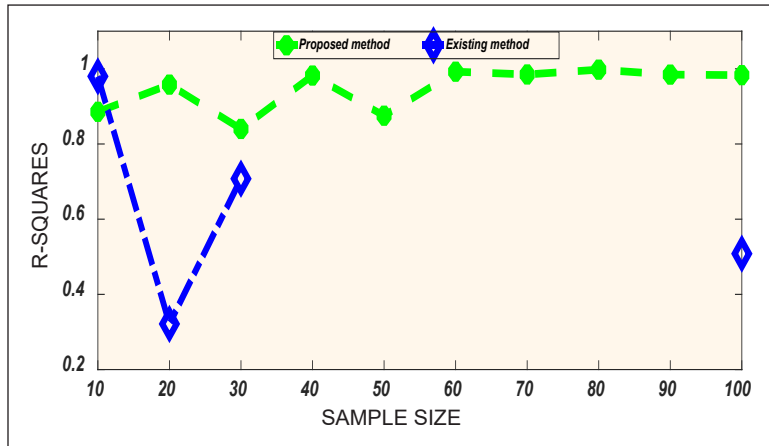


Figure 4. R-Square Evaluation of models performance

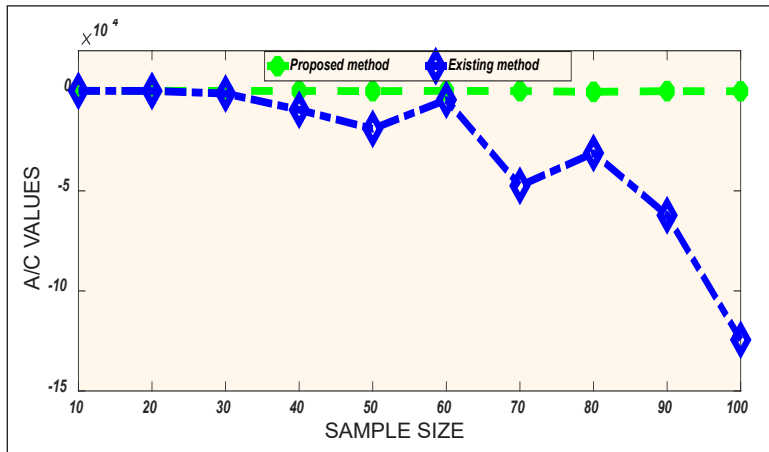


Figure 5. AIC Evaluation of models performance

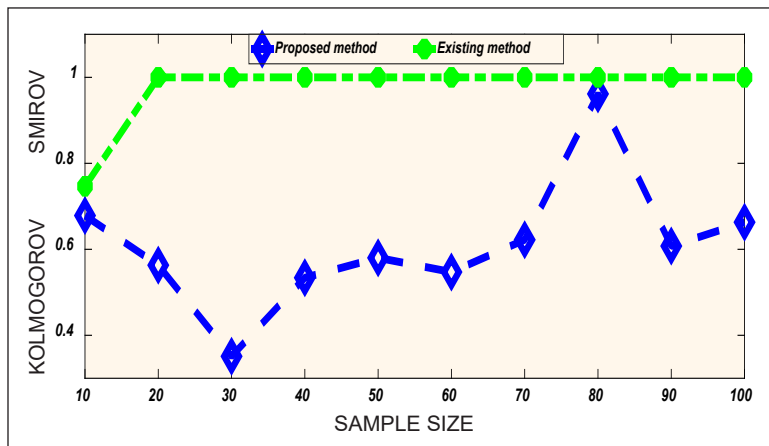


Figure 6. KS Test Evaluation of models performance

The estimated parameters and loglikelihood values of the proposed and the existing Weibull model have been reported in Table 1. It could be observed that all the estimated values showed a proper consistency based on the MAE and RMSE, which seem to decrease as the sample size increases in both models. Comparing the proposed model with the existing two parameters Weibull distribution, the results revealed that the proposed method produces the best-fit results in terms of MAE, RMSE, and R-square statistics in most of the cases. Therefore, according to the AIC value, the existing Weibull model is the better choice. The results in Table 2 have been displayed in Figures 1 to 5 for better analysis.

The results in Table 2 have been displayed in Figures 2-6 in evaluating the suitability of the proposed model in fitting the simulated data using MAE, RMSE, R-square, AIC, and KS test throughout the optimisation process. The best model was evaluated according to minimum MAE, RMSE, AIC, KS values, and high R-square values. Figures 2 and 3 displayed the MAE and RMSE of the simulated data from $n = 10$ to 100 sample size, mimicking IRR data on the assumption of the proposed model. It is observed that the error accumulation in the existing two-parameter Weibull distribution is constantly high with the increase in sample size for different values of the parameters. On the other hand, the errors decrease slightly with the increase in sample size. For example, at a sample of size 80, the MAE and RMSE increase but decrease as the sample size increases. In Figure 4, the R-square statistics have been displayed.

According to the R-square value of the Weibull models, the proposed model displayed high value through the simulation than the existing model. It is noticed that the existing Weibull model is found more complex in calculating the R-square value based on simulated data. It might be due to a large amount of error accumulation as the sample size increases. The R-square value cannot be computed when the sample size is high (*i.e* $n > 20$). R-square exceeds the threshold with the increase in sample size in the existing model. It reveals that the simulated data does not follow the model closely enough to make predictions confidently and that the data does not appear to follow a specific pattern. In Figure 4, Akaike's information criterion (AIC) has been displayed based on Table 3. According to AIC values, the existing model is the better choice. The "best" model will be the one that neither under-fits nor over-fits. Although the AIC will choose the best model from a set of models, it will not say anything about the absolute quality of the model.

However, the existing model is still as good as the proposed one according to the AIC value. It shows that the existing model is nearly as good as the proposed model. The KS result in Table 2 has been displayed in Figure 5, showing the KS test of the proposed model as was less than that of the existing methods throughout the simulations experiments. The KS test of the existing Weibull distribution is 1 in some instances, especially as the

sample size increases. It is an indication that the accumulation of the error is increasing as the sample size increases. It revealed that the CDF of the proposed model comes from the sample values that are equal to or less than x (i.e. sample data) (Dodge, 2008). Therefore, the proposed model is more accurate based on the simulated data used in this study. Consequently, the simulated data accepts the Weibull distribution at 95% confidence. The finding reveals that the existing two-parameter Weibull best fits a small sample size, while the accuracy of the proposed model increases as the sample size increases. The p-values are not that different for the smaller sample data. The proposed distribution model has the lowest values for all goodness-of-fit statistics among all fitted models. The analysis reveals that the proposed modified Weibull distribution provides a good fit to the simulated data sets by mimicking the internal rate of return (IRR).

CONCLUSION

A new distribution based on Weibull distributions has been proposed. Weibull distribution is used in modelling a wide variety of data, including wind speed, patient survival, and product lifetime. There has been an increasing interest in developing tractable lifetime models which fit financial data flexibly. This research proposed a new three-parameter Weibull distribution by imposing a growth rate parameter on the existing two parameters Weibull distribution model. Some of its characteristics include maximum likelihood function along with its characterisations. The estimation of the model parameters is obtained using the simulated annealing algorithm approach proposed by Abbasi et al. (2006). The experimental study was based on a simulated data set that mimicked the internal return rate for sample sizes 10 to 100. Based on the result presented in Tables 1 and 2, we presume that the proposed modified Weibull distribution will better fit IRR data when compared with the existing model. We have shown that the new modified Weibull distribution fits certain well-known data sets better than the existing Weibull distribution. Adding growth rate parameters by fixing one of the parameters still provides a better fit than existing models. Our future work is to extend the proposed model for the internal rate of return real-life data set. Statistical distributions such as gamma distribution, an exponentiated family of distribution, Pareto distribution and Rayleigh distribution can be modified to accommodate growth rate parameters to achieve better financial data fitting. Furthermore, the research will further explore various evolutionary computations and other metaheuristic algorithms to estimate the parameters of the proposed model.

ACKNOWLEDGEMENT

The authors would like to thank anonymous referees for their constructive comments on this manuscript. Special thanks to my humble supervisor for his helpful suggestions.

REFERENCES

- Abbasi, B., Jahromi, A. H. E., Arkat, J., & Hosseinkouchack, M. (2006). Estimating the parameters of Weibull distribution using a simulated annealing algorithm. *Applied Mathematics and Computation*, 183(1), 85-93. <https://doi.org/10.1016/j.amc.2006.05.063>
- Abbasi, B., Niaki, S. T. A., Khalife, M. A., & Faize, Y. (2011). A hybrid variable neighborhood search and simulated annealing algorithm to estimate the three parameters of the Weibull distribution. *Expert Systems with Applications*, 38(1), 700-708. <https://doi.org/10.1016/j.eswa.2010.07.022>
- Abubakar, H., & Danrimi, M. L. (2021). Hopfield type of artificial neural network via election algorithm as heuristic search method for random boolean ksatisfiability. *International Journal of Computing and Digital System*, 10(2), 660-673. <http://dx.doi.org/10.12785/ijcds/100163>
- Abubakar, H., Rijal, S., Sabri, S. R. M., Masanawa, S. A., & Yusuf, S. (2020a). Modified election algorithm in hopfield neural network for optimal random k satisfiability representation. *International Journal for Simulation and Multidisciplinary Design Optimization*, 16(11), 1-13. <https://doi.org/10.1051/smdo/2020008>
- Abubakar, H., M, S. A., Yusuf, S., & Abdurrahman, Y. (2020b). Discrete artificial dragonflies algorithm in agent based modelling for exact boolean k satisfiability problem. *Journal of Advances in Mathematics and Computer Science*, 35(4), 115-134. <https://doi.org/10.9734/JAMCS/2020/v35i430275>
- Abubakari, A. G., Kandza-Tadi, C. C., & Moyo, E. (2021). Modified Beta Inverse Flexible Weibull Extension Distribution. *Annals of Data Science*, 1-29. <https://doi.org/10.1007/s40745-021-00330-3>
- Almazah, M. M. A., Erbayram, T., Akdoğan, Y., AL Sobhi, M. M., & Afify, A. Z. (2021). A new extended geometric distribution: Properties, regression model, and actuarial applications. *Mathematics*, 9(12), 1336. <https://doi.org/10.3390/math9121336>
- Almetwally, E. M. (2021). Extended odd weibull inverse rayleigh distribution with application on carbon fibres. *Mathematical Sciences Letters*, 10(1), 5-14. <https://doi.org/10.18576/msl/100102>
- Alrashidi, M., Rahman, S., & Pipattanasomporn, M. (2020). Metaheuristic optimization algorithms to estimate statistical distribution parameters for characterizing wind speeds. *Renewable Energy*, 149, 664-681. <https://doi.org/10.1016/j.renene.2019.12.048>
- Alzaatreh, A., Lee, C., & Famoye, F. (2013). A new method for generating families of continuous distributions. *Metron*, 71(1), 63-79. <https://doi.org/10.1007/s40300-013-0007-y>
- Alzaeemi, S. A., & Sathasivam, S. (2020). Artificial immune system in doing 2-satisfiability based reverse analysis method via a radial basis function neural network. *Processes*, 8(10), Article 1295. <https://doi.org/10.3390/pr8101295>
- Bidrama, H., Behboodan, J., & Towhidib, M. (2013). The beta weibull-geometric distribution. *Journal of Statistical Computation and Simulation*, 83(1), 52-67. <https://doi.org/10.1080/00949655.2011.603089>
- Boonta, S., & Boonthiem, S. (2019). An approximation of minimum initial capital of investment discrete time surplus process with Weibull distribution in a reinsurance company. *Journal of Applied Mathematics*, 2019, Article 2191509. <https://doi.org/10.1155/2019/2191509>
- Chauhan, S. K., & Malik, S. C. (2017). Evaluation of reliability and MTSF of a parallel system with Weibull failure laws. *Journal of Reliability and Statistical Studies*, 10(1), 137-148.

- Datsiou, K. C., & Overend, M. (2018). Weibull parameter estimation and goodness-of-fit for glass strength data. *Structural Safety*, 73, 29-41. <https://doi.org/10.1016/j.strusafe.2018.02.002>
- Freitas de Andrade, C., dos Santos, L. F., Macedo, M. V. S., Rocha, P. A. C., & Gomes, F. F. (2019). Four heuristic optimization algorithms applied to wind energy: Determination of Weibull curve parameters for three Brazilian sites. *International Journal of Energy and Environmental Engineering*, 10, 1-12. <https://doi.org/10.1007/s40095-018-0285-5>
- Dodge, Y. (2008). Kolmogorov–Smirnov test. In *The concise encyclopedia of statistics* (pp. 283-287). Springer. https://doi.org/10.1007/978-0-387-32833-1_214
- Elmahdy, E. E., & Aboutahoun, A. W. (2013). A new approach for parameter estimation of finite Weibull mixture distributions for reliability modeling. *Applied Mathematical Modelling*, 37(4), 1800-1810. <http://doi.org/10.1016/j.apm.2012.04.023>
- Guedes, K. S., de Andrade, C. F., Rocha, P. A., Mangureira, R. D. S., & de Moura, E. P. (2020). Performance analysis of metaheuristic optimization algorithms in estimating the parameters of several wind speed distributions. *Applied Energy*, 268, Article 114952. <https://doi.org/10.1016/j.apenergy.2020.114952>
- Guerra, R. R., Peña-Ramírez, F. A., & Bourguignon, M. (2020). The unit extended Weibull families of distributions and its applications. *Journal of Applied Statistics*, 1-19. <https://doi.org/10.1080/02664763.2020.1796936>
- Hashmi, S., Ahsan, M., Haq, U., Muhammad, R., & Ozel, G. (2019). The Weibull-Moment Exponential Distribution: Properties, Characterizations & applications. *Journal of Reliability and Statistical Studies*, 12(1), 1-22.
- Hirose, H. (2002). Maximum likelihood parameter estimation in the extended Weibull distribution and its applications to breakdown voltage estimation. *IEEE Transactions on Dielectrics and Electrical Insulation*, 9(4), 524–536. <https://doi.org/10.1109/TDEI.2002.1024429>
- Kaba, A., & Suzer, A. E. (2021). Metaheuristic data fitting methods to estimate Weibull parameters for wind speed data: A case study of Hasan Polatkan Airport. *The Aeronautical Journal*, 125(1287), 916-948. <https://doi.org/10.1017/aer.2020.136>
- Kellison, S. G. (2009). *The theory of interest* (3rd Ed.). McGraw-Hill Education.
- Kirkpatrick, S., Gelatt, C. D., & Vecchi, M. P. (1983). Optimization by simulated annealing. *Science*, 220(4598), 671-680. <https://doi.org/10.1126/science.220.4598.671>
- Lee, C., Famoye, F., & Alzaatreh, A. Y. (2013). Methods for generating families of univariate continuous distributions in the recent decades. *Wiley Interdisciplinary Reviews: Computational Statistics*, 5(3), 219-238. <https://doi.org/10.1002/wics.1255>
- Liao, Q., Ahmad, Z., Mahmoudi, E., & Hamedani, G. G. (2020). A new flexible bathtub-shaped modification of the Weibull model: Properties and applications. *Mathematical Problems in Engineering*, 2020, Article 3206257. <https://doi.org/10.1155/2020/3206257>
- Okafor, E. G., Ezugwu, O. E., Jemitola, P. O., Sun, Y., & Lu, Z. (2018). Weibull parameter estimation using particle swarm optimization algorithm. *International Journal of Engineering and Technology (UAE)*, 7(3), 7-10. <https://doi.org/10.14419/ijet.v7i3.32.18380>

- Okasha, H. M., & Basheer, A. M. (2020). On marshall-olkin extended inverse weibull distribution: Properties and estimation using type-II censoring data. *Journal of Statistics Applications & Probability Letters*, 7(1), 9-21. <https://doi.org/10.18576/jsapl/070102>
- Phani, K.K. (1987). A New Modified Weibull Distribution. *Communications of the American Ceramic Society*, 184(August), 182-184. <https://doi.org/10.1111/j.1151-2916.1987.tb05719.x>
- Pobočíková, I., Sedliačková, Z., & Michalková, M. (2018). Transmuted Weibull distribution and its applications. *MATEC Web of Conferences*, 157, 1-11. <https://doi.org/10.1051/mateconf/201815708007>
- Sabri, S. R. M., & Sarsour, W. M. (2019). Modelling on stock investment valuation for long-term strategy. *Journal of Investment and Management*, 8(3), 60-66. <https://doi.org/10.11648/j.jim.20190803.11>
- Sarhan, A. M., & Zaindin, M. (2009). Modified Weibull distribution. *Applied Sciences*, 11(January 2000), 123-136. <https://doi.org/10.1051/mateconf/201815708007>
- Sarsour, W. M., & Sabri, S. R. M. (2020a). Evaluating the investment in the Malaysian construction sector in the long-run using the modified internal rate of return: A Markov chain approach. *The Journal of Asian Finance, Economics, and Business*, 7(8), 281–287. <https://doi.org/10.13106/jafeb.2020.vol7.no8.281>
- Sarsour, W. M., & Sabri, S. R. M. (2020b). Forecasting the long-run behavior of the stock price of some selected companies in the Malaysian construction sector: A Markov chain approach. *International Journal of Mathematical, Engineering and Management Sciences*, 5(2), 296-308. <https://doi.org/10.33889/IJMEMS.2020.5.2.024>
- Sathasivam, S., Mansor, M., Kasihmuddin, M. S. M., & Abubakar, H. (2020). Election algorithm for random k satisfiability in the Hopfield neural network. *Processes*, 8(5), Article 568. <https://doi.org/10.3390/pr8050568>
- Tang, Y., Xie, M., Lai, C. D., & Goh, T. N. (2002). Statistical analysis of a Weibull extension model, communications in statistics. *Theory and Methods*, 32(5), 913-928. <https://doi.org/10.1081/STA-120019952>
- Thomas, G. M. (1995). *Weibull parameter estimation using genetic algorithms and a heuristic approach to cut-set analysis* (Doctoral dissertation). Ohio University, USA.
- Wang, M., & Elbatal, I. (2015). The modified Weibull geometric distribution. *Metron*, 73(3), 303-315. <https://doi.org/10.1007/s40300-014-0052-1>
- Yonar, A., & Pehlivan, N. Y. (2020). Artificial bee colony with levy flights for parameter estimation of 3-p Weibull distribution. *Iranian Journal of Science and Technology, Transactions: Science*, 44, 851-864. <https://doi.org/10.1007/s40995-020-00886-4>

Analytical and Numerical Investigations of Mechanical Vibration in the Vertical Direction of a Human Body in a Driving Vehicle using Biomechanical Vibration Model

Maher Al-Baghdadi¹, Muhsin Jaber Jweeg² and Muhannad Al-Waily^{1*}

¹Mechanical Engineering Department, Faculty of Engineering, University of Kufa, Iraq

²College of Technical Engineering, Al-Farahidi University, Iraq

ABSTRACT

The main reason that affects the discomfort in a driving vehicle is the vibration response. The human body vibration leads to many malfunctions in both comfort and performance in human health. As a result, the human body's simulation in sitting posture in the driving vehicle has a strategic relationship for all Tires and vehicles manufacturers. The digital process simulation of the human body seat vehicle vibration shows two significant advantages. The first advantage is the prevention of the high-cost modifications in the construction stage of the vehicle, while the second one describes the stability test during the undesirable vibrations. This study modelled the human body's dynamic characterisations, natural frequency, and mechanical response when seated in the driving vehicle with vibration transmissibility in the vertical direction have been using the biomechanical vibration model. The vertical vibrations and the transmissibility of the human body dynamic response are presented in detail. Exciting results have been obtained, and they are significant for human health, which relates to sitting posture in the driving vehicle. It can assist in understanding the influences of low-frequency vibration on human health, comfort, and performance,

and therefore it could be applied for ride comfort evaluation. An analytical solution to derive the general equations of motion for the human system was developed. Then, using the vibration analysis technique and the corresponding equations, the accurate dynamic response of the selected mode is identified. Furthermore, the mathematical modelling for free vibration using the finite element analysis has been performed to

ARTICLE INFO

Article history:

Received: 11 April 2021

Accepted: 19 August 2021

Published: 18 October 2021

DOI: <https://doi.org/10.47836/pjst.29.4.30>

E-mail addresses:

mahirar.albaghdadi@uokufa.edu.iq (Maher Al-Baghdadi)

muhsin.jweeg@uofarahidi.edu.iq (Muhsin Jaber Jweeg)

muhanedl.alwaeli@uokufa.edu.iq (Muhannad Al-Waily)

* Corresponding author

determine the appropriate values and set its description. Then, the comparison results of the two techniques have been carried out.

Keywords: Apparent mass, biomechanical model, driving vehicle, human body vibration, mechanical response, model analysis

INTRODUCTION

A vibration problem in a driving vehicle is the main reason for discomfort for passengers. Human body vibration leads to many problems in human health, comfort feeling, and performance. The problems raised due to vibrations and their relations to the human body were investigated by many researchers. Most of the results obtained from these studies were the level of injury, and the discomfort can be estimated with this relationship (ISO 2631-1, 1997). The experiments on the human body's biodynamic responses in a driving vehicle to vertical vibration excitation have been measured and presented in International Standard 5982 (ISO 5982, 2001). The work also covered the investigation of the dynamic body response has different effects for different people, which is related to the inter-subject variability and within the person related to the intra-subject variability. Experimental work was presented and included investigating the factors that influence the human body mass, such as the ratio between the vertical force and the measured acceleration at the supporting seat. The vibration spectra, sitting posture, age, and vibration magnitude (Zheng et al., 2011), many forms of biodynamic models have been developed to represent the driving point apparent mass and the transmissibility of the human body.

The biodynamic models can be classified as lumped and multibody and finite element types. The lumped simulation is employed to predict the modulus and the inline vertical apparent mass phase. This modelling gives a reasonable agreement of the experimental measurement of the frequencies up to 20Hz in the case of one degree of freedom systems. It also gives an excellent correlation in modelling two degrees of freedom systems (Mohanty & Mahapatra, 2014). The movement of the human body segments during vertical excitation can be modelled using the combination of lumped-mass and rigid body dynamic response (Guo et al., 2016). The modelling does not take into considerations all the degrees of freedom of the body segments. It includes the pitching of the upper torso and the translational degrees of freedom of the lower body. For modelling the human body segments, they are represented by rigid bodies interconnected by joints that can be freely rotated (Nimmen et al., 2017).

The improvement of the spine's biomechanical vibration models and the torso opens the door to detect the harmful effects on the spine. The spinal load's effects have been analysed numerically using a multibody model of the human spine to calculate the compressive

forces at the trunk discs (Bayoglu et al., 2019). In addition, finite element biomechanical models have been used to simulate the human torso to evaluate the effectiveness of brace design in the context of adolescent idiopathic scoliosis on large cohorts of patients (Vergari et al., 2020).

The sensitivity and importance of the biomechanical vibration models have been recently focused on because of their importance in designing the seats of different modes of transport at a low cost and with high accuracy. Koutras et al. (2021) developed a comprehensive biomechanical vibration model of the torso, including soft tissue, ribcage and spine under typical loading conditions of scoliosis braces.

In this work, the dynamic behaviour of a whole human body in the driving vehicle is modelled using a biomechanical vibration model, analytically and numerically, to estimate the body's apparent mass and transmissibility and understand the effects of low-frequency vibration on human health, comfort, and performance. The analytical model is useful if quick calculations are required for simple systems to predict the human body's vibration without extensive calculations. Furthermore, analytical models are useful in that they may include a large portion of the relevant human body physics while at the same time having relatively short solution times. The analytical solution model is presented by driving the general equation of motion for the dynamic human body model and calculating the natural frequencies for each human part. In addition, the numerical technique uses the finite element method is also presented to calculate natural frequency and the dynamic response performed for the human body. When using the finite element method, the numerical biomechanical vibration models can study the effect of many properties and operating parameters and, therefore, much more computationally intensive, leading to longer solution times (Desai et al., 2018). However, these disadvantages are typically outweighed by the benefit of assessing the influence of more design parameters and their associated physical processes with high sensitivity and accuracy. Finally, the natural frequency results from both models, i.e. analytical and numerical, are compared with the available published experimental results.

ANALYTICAL TECHNIQUE

Biomechanical Vibration Model

In the case of the driving vehicle, the dynamic response of the human body can be obtained using the model shown in Figure 1. This biomedical model can be employed to simulate and design vibration isolators. In this work, the human body is positioned in a healthy posture and looks straight ahead without sideway movements with a relaxed upper body upright state. Also, it assumes that the hands were put on the lap and the foot is on the footplate. The biomechanical model of this human body consists of body parts such as the head, torso, thighs, pelvis, viscera, and legs, as shown in Figure 1.

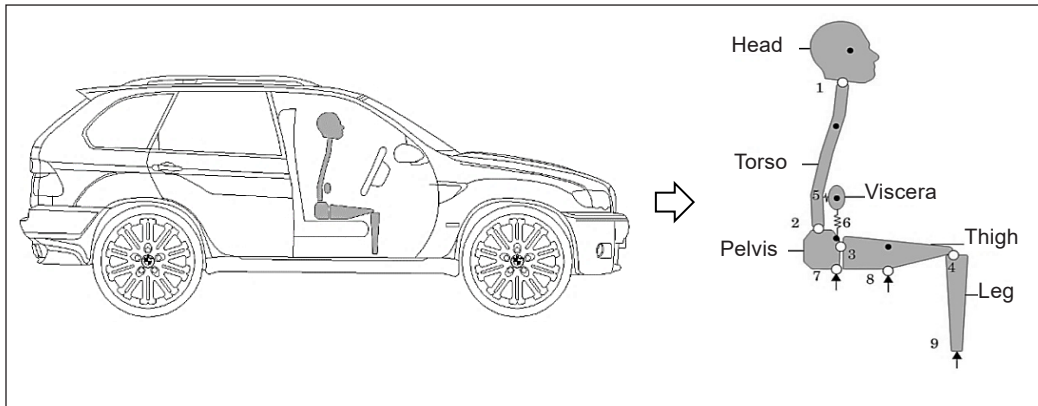


Figure 1. The geometry of the computational biomechanical model showing different parts of the human body and connections between them

The numbers refer to joints between two parts (white circles), and the centre of mass of each part of the body (black circles) and the vibration excitation locations (arrows) are also shown. Figure 1 shows that the primary vibration source in the desired biomechanical model is a seat in a vehicle found not modelled explicitly. Instead, a motion of the base node is used in the geometry of the computational model. Hence, the input excitation at three different locations in the vertical direction was employed. All the body parts in this model are treated as lumped masses, defined as rigid bodies. The viscera in this model are not allowed to turn, and the legs are also not allowed to translate as well rotate. The biomechanical model connections of the body parts are represented by translational and rotational springs and dashpot damper, which can predict the relative motion between the body segments. These types of joints are modelled using the elastic version of a fixed link. Once the flexible version of joints is used, the torsional stiffness and linear damper coefficient are assigned at the joints between the body parts will be provided. Therefore, the human biomechanical models for mechanical properties, motion description in an arbitrary position, and properties for inertia and geometry for a biomechanical model can be simulated in Figures 2 to 4, respectively (Griffin, 1990).

In the assumption of small deformation for individual vertebrae, the strain represents the rigid body rotation. Besides, the prediction of the spinal forces did not define; then, the human biomechanical joint modelling did not include the disks and the vertebrae. Also, it assumed no movements translational between the rigid bodies and its bodies connected by joints as pin joints. The linear spring and damper were considering modelling the shear and axial deformation for the thigh tissue and pelvis. The interface seat occupant friction force and the relative motion between the human body and the seat are neglected (Griffin, 1990). The human body parts directly in touch with the vibrating seat are legs, thighs, and pelvis. The connections between the human body and the vibrating seat are modelled using

a fixed joint. It is required to model the cushioning effect that the elastic behaviours on these joints are included everywhere of the seat. Also, the legs in this model are connected to the seat with the rigid version of fixed joint, and thus, it does not need to insert joint elasticity parameters. Table 1 presents the mechanical properties values such as mass and moment of inertia of each human body part about its centre of mass (Zheng et al., 2011), while the values of stiffness, damping coefficients, translational and rotational, for all the connections in the biomechanical model are listed in Table 2 (Zheng et al., 2011).

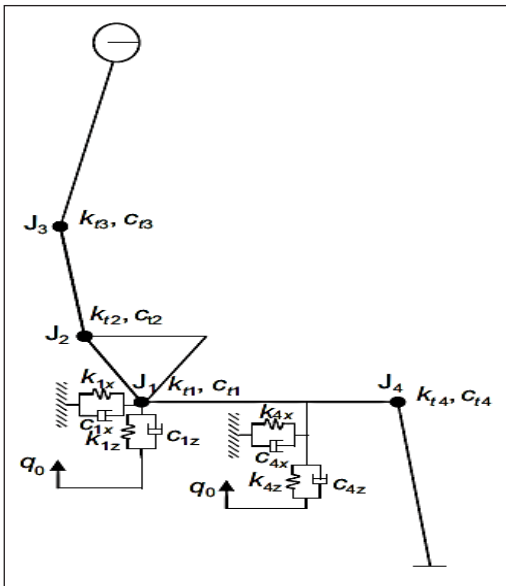


Figure 2. Mechanical properties modelling of the human biomechanical model

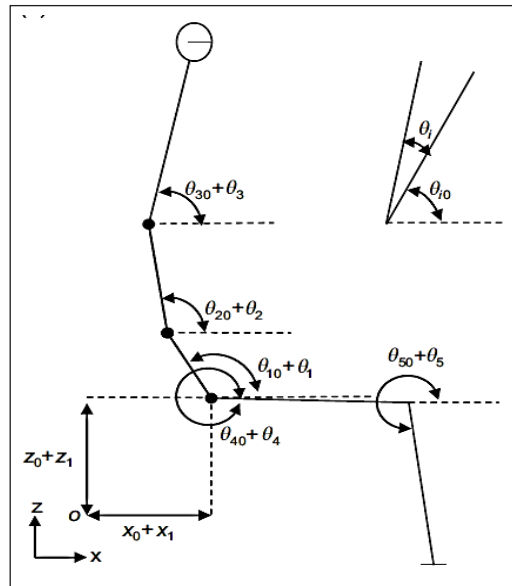


Figure 3. Description for motion in an arbitrary position of the biomechanical model

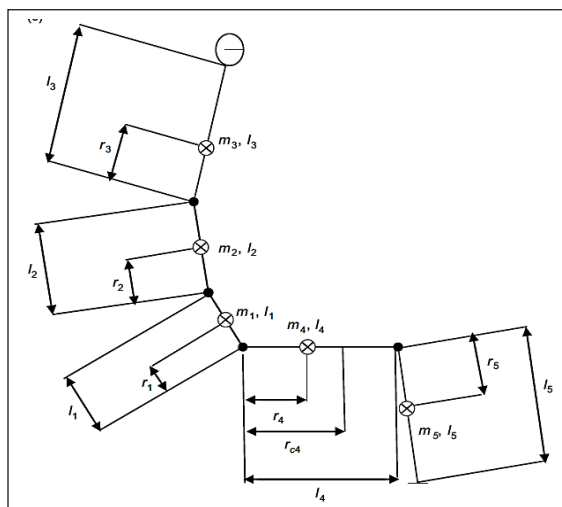


Figure 4. Properties for inertia and geometry for the biomechanical model

Table 1
Mass and moment of inertia of different human body parts

	Mass (kg)		Mass moment of inertia (kg.m ²)
m ₁	8.92	l ₁	0.0249
m ₂	10.97	l ₂	0.1186
m ₃	22.64	l ₃	1.28
m ₄	17.56	l ₄	0.45
m ₅	8.51	l ₅	0.13

Table 2
Joint elasticity details for human body parts of the biomechanical model

Joint	Fixed joint	Translational stiffness (kN/m)	Translational damping (kN.s/m)	Rotational stiffness (kN.m/Rad)	Rotational damping (kN.m.s/Rad)
1	Head-torso	113.7, 113.7	0.066, 0.066	0.915	0.340
2	Torso-pelvis	0.299, 0.299	1.79, 1.79	0.328	0.724
3	Pelvis-thigh	6.40, 6.40	0.061, 0.061	0.162	0.030
4	Thigh-leg	23.55, 23.55	0.154, 0.154	0.220	0.104
5	Viscera-torso	1.93, 0	0.079, 0	0	0
6	Viscera-pelvis	0, 18.37	0, 0.197	0	0
7	Seat-pelvis	0.905, 121.3	0.015, 0.047	0	0
8	Seat-thigh	0.614, 16.71	0.014, 8.01	0	0
9	Seat-leg	-	-	-	-

Biomechanical Vibration Analysis

The general equation of motion for the biomechanical model for the human body can be evaluated by assuming multi translational and rotational displacement on each mass. Therefore, the general coordinates can be considered small displacement with various time representations and be listed as Equation 1.

$$\{\delta\} = \{x_1 \quad z_1 \quad \theta_1 \quad \theta_2 \quad \theta_3 \quad \theta_4 \quad \theta_5\}^t \tag{1}$$

Therefore, by using the energy Lagrange technique can be derived the general equations of motion for the biomechanical model for vibration behaviour of the human body, for assuming small and linear vibration response for each human body part, as Equations 2-4,

$$T = \left(\begin{aligned} &\frac{1}{2}m_1(\dot{x}_1^2 + (\dot{z}_1 + r_1\dot{\theta}_1)^2) + \frac{1}{2}m_2(\dot{x}_1^2 + (\dot{z}_1 + l_1\dot{\theta}_1 + r_2\dot{\theta}_2)^2) + \\ &\frac{1}{2}m_3(\dot{x}_1^2 + (\dot{z}_1 + l_1\dot{\theta}_1 + l_2\dot{\theta}_2 + r_3\dot{\theta}_3)^2) + \frac{1}{2}m_4(\dot{x}_1^2 + (\dot{z}_1 + r_4\dot{\theta}_4)^2) + \\ &\frac{1}{2}m_5(\dot{x}_1^2 + (\dot{z}_1 + l_4\dot{\theta}_4 + r_5\dot{\theta}_5)^2) + \frac{1}{2}I_1\dot{\theta}_1^2 + \frac{1}{2}I_2\dot{\theta}_2^2 + \frac{1}{2}I_3\dot{\theta}_3^2 + \frac{1}{2}I_4\dot{\theta}_4^2 + \frac{1}{2}I_5\dot{\theta}_5^2 \end{aligned} \right) \tag{2}$$

$$U = \left(\frac{1}{2}(k_{1x} + k_{4x})x_1^2 + \frac{1}{2}k_{1z}(z_1 - q_o)^2 + \frac{1}{2}k_{4z}(z_1 + r_{c4}\theta_4 - q_o)^2 + \frac{1}{2}k_{t1}(\theta_1 + \theta_4)^2 + \frac{1}{2}k_{t2}(\theta_1 - \theta_2)^2 + \frac{1}{2}k_{t3}(\theta_2 - \theta_3)^2 + \frac{1}{2}k_{t4}(\theta_4 + \theta_5)^2 \right) \quad (3)$$

$$D = \left(\frac{1}{2}(c_{1x} + c_{4x})\dot{x}_1^2 + \frac{1}{2}c_{1z}(\dot{z}_1 - \dot{q}_o)^2 + \frac{1}{2}c_{4z}(\dot{z}_1 + r_{c4}\dot{\theta}_4 - \dot{q}_o)^2 + \frac{1}{2}c_{t1}(\dot{\theta}_1 + \dot{\theta}_4)^2 + \frac{1}{2}c_{t2}(\dot{\theta}_1 - \dot{\theta}_2)^2 + \frac{1}{2}c_{t3}(\dot{\theta}_2 - \dot{\theta}_3)^2 + \frac{1}{2}c_{t4}(\dot{\theta}_4 + \dot{\theta}_5)^2 \right) \quad (4)$$

Where, l_1 to l_5 and r_1 to r_5 are presenting in Table 3, the translational and rotational stiffness is shown in Table 4, and the translational and rotational damping coefficient are shown in Table 5, and r_4 used about (14.8) (Zheng et al., 2011).

Then, by using Lagrange’s equations to derive the general equations of motion for multi-degree of freedom, by using Equation 5,

$$\frac{d}{dt} \left(\frac{\partial T}{\partial \dot{\delta}_i} \right) - \left(\frac{\partial T}{\partial \delta_i} \right) + \left(\frac{\partial D}{\partial \dot{\delta}_i} \right) + \left(\frac{\partial U}{\partial \delta_i} \right) = F_i \quad (5)$$

Where, i number of degree of freedom, and F_i applied load.

Table 3
Dimensions for human body parts

Part length (cm)		Mass centre (cm)	
l_1	13.77	r_1	9.78
l_2	29.65	r_2	16.26
l_3	40.27	r_3	20.14
l_4	34.6	r_4	14.8
l_5	36.33	r_5	15.49

Table 4
Translational and rotational stiffness for biomechanical human body parts

Translational stiffness (kN/m)		Rotational stiffness (kN.m/rad)	
k_{1x}	0.905	k_{t1}	0.162
k_{4x}	0.614	k_{t2}	0.328
k_{1z}	121.3	k_{t3}	0.915
k_{4z}	16.71	k_{t4}	0.22

Table 5
Translational and rotational damping coefficient for the human body

Translational stiffness (kN.s/m)		Rotational stiffness (kN.m.s/rad)	
c_{1x}	0.015	c_{t1}	0.03
c_{4x}	0.014	c_{t2}	0.724
c_{1z}	0.047	c_{t3}	0.34
c_{4z}	8.01	c_{t4}	0.104

Then, by using Equations 2-4, can be evaluated using the general equation of motion of the system, as Equations 6-12,

For, $i = 1, \delta_1 = x_1,$

$$\frac{d}{dt} \left(\frac{\partial T}{\partial \dot{x}_1} \right) = ((m_1 + m_2 + m_3 + m_4 + m_5)\ddot{x}_1), \left(\frac{\partial T}{\partial x_1} \right) = 0$$

$$\left(\frac{\partial D}{\partial \dot{x}_1} \right) = ((c_{1x} + c_{4x})\dot{x}_1), \left(\frac{\partial U}{\partial x_1} \right) = ((k_{1x} + k_{4x})x_1)$$

Then,

$$(m_1 + m_2 + m_3 + m_4 + m_5)\ddot{x}_1 + (c_{1x} + c_{4x})\dot{x}_1 + (k_{1x} + k_{4x})x_1 = 0 \tag{6}$$

For, $i = 2, \delta_2 = z_1,$

$$\frac{d}{dt} \left(\frac{\partial T}{\partial \dot{z}_1} \right) = \left((m_1 + m_2 + m_3 + m_4 + m_5)\ddot{z}_1 + (m_1r_1 + m_2l_1 + m_3l_1)\ddot{\theta}_1 + (m_2r_2 + m_3l_2)\ddot{\theta}_2 + (m_3r_3)\ddot{\theta}_3 + (m_4r_4 + m_5l_4)\ddot{\theta}_4 + (m_5r_5)\ddot{\theta}_5 \right)$$

$$\left(\frac{\partial T}{\partial z_1} \right) = 0,$$

$$\left(\frac{\partial D}{\partial \dot{z}_1} \right) = ((c_{1z} + c_{4z})\dot{z}_1 + (c_{4z}r_{c4})\dot{\theta}_4 - (c_{1z} + c_{4z})\dot{q}_0), \left(\frac{\partial U}{\partial z_1} \right) = ((k_{1z} + k_{4z})z_1 + (k_{4z}r_{c4})\theta_4 - (k_{1z} + k_{4z})q_0)$$

Then,

$$\left((m_1 + m_2 + m_3 + m_4 + m_5)\ddot{z}_1 + (m_1r_1 + m_2l_1 + m_3l_1)\ddot{\theta}_1 + (m_2r_2 + m_3l_2)\ddot{\theta}_2 + (m_3r_3)\ddot{\theta}_3 + (m_4r_4 + m_5l_4)\ddot{\theta}_4 + (m_5r_5)\ddot{\theta}_5 + (c_{1z} + c_{4z})\dot{z}_1 + (c_{4z}r_{c4})\dot{\theta}_4 + (k_{1z} + k_{4z})z_1 + (k_{4z}r_{c4})\theta_4 \right) = \left((k_{1z} + k_{4z})q_0 + (c_{1z} + c_{4z})\dot{q}_0 \right) \tag{7}$$

For, $i = 3, \delta_3 = \theta_1,$

$$\frac{d}{dt} \left(\frac{\partial T}{\partial \dot{\theta}_1} \right) = \left((m_1r_1 + m_2l_1 + m_3l_1)\ddot{z}_1 + (m_1r_1^2 + m_2l_1^2 + m_3l_1^2 + I_1)\ddot{\theta}_1 + (m_2r_2l_1 + m_3l_2l_1)\ddot{\theta}_2 + (m_3r_3l_1)\ddot{\theta}_3 \right)$$

$$\left(\frac{\partial T}{\partial \theta_1} \right) = 0, \left(\frac{\partial D}{\partial \dot{\theta}_1} \right) = ((c_{t1} + c_{t2})\dot{\theta}_1 - (c_{t2})\dot{\theta}_2 + (c_{t1})\dot{\theta}_4), \left(\frac{\partial U}{\partial \theta_1} \right) = ((k_{t1} + k_{t2})\theta_1 - k_{t2}\theta_2 + (k_{t1})\theta_4)$$

Then,

$$\left((m_1r_1 + m_2l_1 + m_3l_1)\ddot{z}_1 + (m_1r_1^2 + m_2l_1^2 + m_3l_1^2 + I_1)\ddot{\theta}_1 + (m_2r_2l_1 + m_3l_2l_1)\ddot{\theta}_2 + (m_3r_3l_1)\ddot{\theta}_3 + (c_{t1} + c_{t2})\dot{\theta}_1 - (c_{t2})\dot{\theta}_2 + (c_{t1})\dot{\theta}_4 + (k_{t1} + k_{t2})\theta_1 - k_{t2}\theta_2 + (k_{t1})\theta_4 \right) = 0 \tag{8}$$

For, $i = 4, \delta_4 = \theta_2,$

$$\begin{aligned} \frac{d}{dt} \left(\frac{\partial T}{\partial \dot{\theta}_2} \right) &= ((m_2 r_2 + m_3 l_2) \ddot{z}_1 + (m_2 l_1 r_2 + m_3 l_1 l_2) \ddot{\theta}_1 + (m_2 r_2^2 + m_3 l_2^2 + I_2) \ddot{\theta}_2 + (m_3 r_3 l_2) \ddot{\theta}_3) \\ \left(\frac{\partial T}{\partial \theta_2} \right) &= 0, \left(\frac{\partial D}{\partial \dot{\theta}_2} \right) = ((c_{t2} + c_{t3}) \dot{\theta}_2 - (c_{t2}) \dot{\theta}_1 - (c_{t3}) \dot{\theta}_3), \left(\frac{\partial U}{\partial \theta_2} \right) = \left(\begin{matrix} (k_{t2} + k_{t3}) \theta_2 - \\ (k_{t2}) \theta_1 - (k_{t3}) \theta_3 \end{matrix} \right) \end{aligned}$$

Then,

$$\left(\begin{matrix} (m_2 r_2 + m_3 l_2) \ddot{z}_1 + (m_2 l_1 r_2 + m_3 l_1 l_2) \ddot{\theta}_1 + (m_2 r_2^2 + m_3 l_2^2 + I_2) \ddot{\theta}_2 + (m_3 r_3 l_2) \ddot{\theta}_3 + \\ (c_{t2} + c_{t3}) \dot{\theta}_2 - (c_{t2}) \dot{\theta}_1 - (c_{t3}) \dot{\theta}_3 + (k_{t2} + k_{t3}) \theta_2 - (k_{t2}) \theta_1 - (k_{t3}) \theta_3 \end{matrix} \right) = 0 \quad (9)$$

For, $i = 5, \delta_5 = \theta_3$,

$$\begin{aligned} \frac{d}{dt} \left(\frac{\partial T}{\partial \dot{\theta}_3} \right) &= ((m_3 r_3) \ddot{z}_1 + (m_3 l_1 r_3) \ddot{\theta}_1 + (m_3 l_2 r_3) \ddot{\theta}_2 + (m_3 r_3^2 + I_3) \ddot{\theta}_3) \\ \left(\frac{\partial T}{\partial \theta_3} \right) &= 0, \left(\frac{\partial D}{\partial \dot{\theta}_3} \right) = ((c_{t3}) \dot{\theta}_3 - (c_{t3}) \dot{\theta}_2), \left(\frac{\partial U}{\partial \theta_3} \right) = (k_{t3} \theta_3 - k_{t3} \theta_2) \end{aligned}$$

Then,

$$\left(\begin{matrix} (m_3 r_3) \ddot{z}_1 + (m_3 l_1 r_3) \ddot{\theta}_1 + (m_3 l_2 r_3) \ddot{\theta}_2 + (m_3 r_3^2 + I_3) \ddot{\theta}_3 + (c_{t3}) \dot{\theta}_3 - \\ (c_{t3}) \dot{\theta}_2 + k_{t3} \theta_3 - k_{t3} \theta_2 \end{matrix} \right) = 0 \quad (10)$$

For, $i = 6, \delta_6 = \theta_4$,

$$\begin{aligned} \frac{d}{dt} \left(\frac{\partial T}{\partial \dot{\theta}_4} \right) &= ((m_4 r_4 + m_5 l_4) \ddot{z}_1 + (m_5 r_5 l_4) \ddot{\theta}_5 + (m_4 r_4^2 + m_5 l_4^2 + I_4) \ddot{\theta}_4) \\ \left(\frac{\partial T}{\partial \theta_4} \right) &= 0 \\ \left(\frac{\partial D}{\partial \dot{\theta}_4} \right) &= ((c_{4z} r_{c4}) \dot{z}_1 + (c_{t1}) \dot{\theta}_1 + (c_{t4}) \dot{\theta}_5 + (c_{4z} r_{c4}^2 + c_{t1} + c_{t4}) \dot{\theta}_4 - (c_{4z} r_{c4}) \dot{q}_0) \\ \left(\frac{\partial U}{\partial \theta_4} \right) &= ((k_{4z} r_{c4}) z_1 + (k_{t1}) \theta_1 + k_{t4} \theta_5 + (k_{4z} r_{c4}^2 + k_{t1} + k_{t4}) \theta_4 - k_{4z} r_{c4} q_0) \end{aligned}$$

Then,

$$\left(\begin{matrix} (m_4 r_4 + m_5 l_4) \ddot{z}_1 + (m_5 r_5 l_4) \ddot{\theta}_5 + (m_4 r_4^2 + m_5 l_4^2 + I_4) \ddot{\theta}_4 + \\ (c_{4z} r_{c4}) \dot{z}_1 + (c_{t1}) \dot{\theta}_1 + (c_{t4}) \dot{\theta}_5 + (c_{4z} r_{c4}^2 + c_{t1} + c_{t4}) \dot{\theta}_4 + \\ (k_{4z} r_{c4}) z_1 + (k_{t1}) \theta_1 + k_{t4} \theta_5 + (k_{4z} r_{c4}^2 + k_{t1} + k_{t4}) \theta_4 \end{matrix} \right) = (k_{4z} r_{c4} q_0 + (c_{4z} r_{c4}) \dot{q}_0) \quad (11)$$

For, $i = 7, \delta_7 = \theta_5$,

$$\begin{aligned} \frac{d}{dt} \left(\frac{\partial T}{\partial \dot{\theta}_5} \right) &= ((m_5 r_5) \ddot{z}_1 + (m_5 l_4 r_5) \ddot{\theta}_4 + (m_5 r_5^2 + I_5) \ddot{\theta}_5) \\ \left(\frac{\partial T}{\partial \theta_5} \right) &= 0, \left(\frac{\partial D}{\partial \dot{\theta}_5} \right) = (c_{t4} \dot{\theta}_4 + c_{t4} \dot{\theta}_5), \left(\frac{\partial U}{\partial \theta_5} \right) = (k_{t4} \theta_4 + k_{t4} \theta_5) \end{aligned}$$

Then,

$$((m_5 r_5) \ddot{z}_1 + (m_5 l_4 r_5) \ddot{\theta}_4 + (m_5 r_5^2 + I_5) \ddot{\theta}_5 + c_{t4} \dot{\theta}_4 + c_{t4} \dot{\theta}_5 + k_{t4} \theta_4 + k_{t4} \theta_5) = 0 \quad (12)$$

Therefore, Equations 6-12, can be rewritten by using matrix form, as Equations 13 and 14,

$$[m]\{\ddot{\delta}\} + [c]\{\dot{\delta}\} + [k]\{\delta\} = \{F\} \quad (13)$$

Where,

$$[m] = \begin{bmatrix} m_{11} & \cdots & m_{17} \\ \vdots & \ddots & \vdots \\ m_{71} & \cdots & m_{77} \end{bmatrix}$$

For,

$$\begin{aligned} m_{11} &= (m_1 + m_2 + m_3 + m_4 + m_5), m_{12} = m_{13} = m_{14} = m_{15} = m_{16} = m_{17} = 0 \\ m_{22} &= (m_1 + m_2 + m_3 + m_4 + m_5), m_{23} = (m_1 r_1 + m_2 l_1 + m_3 l_1), m_{24} = (m_2 r_2 + m_3 l_2) \\ m_{25} &= (m_3 r_3), m_{26} = (m_4 r_4 + m_5 l_4), m_{27} = (m_5 r_5), m_{33} = (m_1 r_1^2 + m_2 l_1^2 + m_3 l_1^2 + I_1) \\ m_{34} &= (m_2 r_2 l_1 + m_3 l_2 l_1), m_{35} = (m_3 r_3 l_1), m_{36} = m_{37} = 0, m_{44} = (m_2 r_2^2 + m_3 l_2^2 + I_2) \\ m_{45} &= (m_3 r_3 l_2), m_{46} = m_{47} = 0, m_{55} = (m_3 r_3^2 + I_3), m_{56} = m_{57} = 0, \\ m_{66} &= (m_4 r_4^2 + m_5 l_4^2 + I_4) \\ m_{67} &= (m_5 r_5 l_4), m_{77} = (m_5 r_5^2 + I_5) \end{aligned}$$

And,

$$[c] = \begin{bmatrix} c_{11} & \cdots & c_{17} \\ \vdots & \ddots & \vdots \\ c_{71} & \cdots & c_{77} \end{bmatrix}$$

For,

$$\begin{aligned} c_{11} &= (c_{1x} + c_{4x}), c_{12} = c_{13} = c_{14} = c_{15} = c_{16} = c_{17} = 0, c_{22} = (c_{1z} + c_{4z}), c_{26} = (c_{4z} r_{c4}) \\ c_{23} &= c_{24} = c_{25} = c_{27} = 0, c_{33} = (c_{t1} + c_{t2}), c_{34} = -(c_{t2}), c_{36} = (c_{t1}), c_{35} = c_{37} = 0, c_{44} = \\ &= (c_{t2} + c_{t3}), c_{45} = -(c_{t3}), c_{46} = c_{47} = 0, c_{55} = (c_{t3}), c_{56} = c_{57} = 0, \\ c_{66} &= (c_{4z} r_{c4}^2 + c_{t1} + c_{t4}), c_{67} = (c_{t4}), c_{77} = (c_{t4}) \end{aligned}$$

Also,

$$[k] = \begin{bmatrix} k_{11} & \cdots & k_{17} \\ \vdots & \ddots & \vdots \\ k_{71} & \cdots & k_{77} \end{bmatrix}$$

For,

$$\begin{aligned} k_{11} &= (k_{1x} + k_{4x}), k_{12} = k_{13} = k_{14} = k_{15} = k_{16} = k_{17} = 0, k_{22} = (k_{1z} + k_{4z}), \\ k_{26} &= (k_{4z} r_{c4}) \end{aligned}$$

$$k_{23} = k_{24} = k_{25} = k_{27} = 0, k_{33} = (k_{t1} + k_{t2}), k_{34} = -(k_{t2}), k_{36} = (k_{t1}), k_{35} = k_{37} = 0, k_{44} = (k_{t2} + k_{t3}), k_{45} = -(k_{t3}), k_{46} = k_{47} = 0, k_{55} = k_{t3}, k_{56} = k_{57} = 0, k_{66} = (k_{4z}r_{c4}^2 + k_{t1} + k_{t4}), k_{67} = (k_{t4}), k_{77} = (k_{t4})$$

And,

$$\{\ddot{\delta}\} = \begin{Bmatrix} \ddot{x}_1 \\ \ddot{z}_1 \\ \ddot{\theta}_1 \\ \ddot{\theta}_2 \\ \ddot{\theta}_3 \\ \ddot{\theta}_4 \\ \ddot{\theta}_5 \end{Bmatrix}, \{\dot{\delta}\} = \begin{Bmatrix} \dot{x}_1 \\ \dot{z}_1 \\ \dot{\theta}_1 \\ \dot{\theta}_2 \\ \dot{\theta}_3 \\ \dot{\theta}_4 \\ \dot{\theta}_5 \end{Bmatrix}, \{\delta\} = \begin{Bmatrix} x_1 \\ z_1 \\ \theta_1 \\ \theta_2 \\ \theta_3 \\ \theta_4 \\ \theta_5 \end{Bmatrix}$$

$$\{F\} = \begin{Bmatrix} 0 \\ (k_{1z} + k_{4z})q_0 + (c_{1z} + c_{4z})\dot{q}_0 \\ 0 \\ 0 \\ 0 \\ ((k_{4z}r_{c4})q_0 + (c_{4z}r_{c4})\dot{q}_0) \\ 0 \end{Bmatrix} \tag{14}$$

Where, q_0 is the load-displacement, which can be assumed with a frequency range from 0.3 to 20 Hz (Zheng et al., 2011).

The mathematical modelling for vibration, translational and rotational motion for the biomechanical human body has been discussed to generate the eigenvalue problem. This analysis included solving for the equation of motion for, Equation 13 (Al-Waily, 2005; Rao, 2007; Rao, 2018; Abbas et al., 2019) to calculate natural frequencies for the human body, as Equation 15,

$$|[k] - \omega^2[m]||[X] = 0 \tag{15}$$

Where, $[k]$ and $[m]$ are stiffness and mass matrix for the human body, calculated from Equation 13, ω is the natural frequency for translational and rotational motion of the human body modelled as in Figure 3, and $[X]$ is the normal modes for translational and rotational motion.

BIOMECHANICAL FINITE ELEMENT MODEL

The finite element analysis with the help of the COMSOL Multi-Physics Multi-body Dynamics interfaces package software has been used to model and simulate the dynamic biomechanics of human body behaviour. The dynamic response under various frequencies applied load, and the natural frequency for each part's human body is calculated. The biomechanical model using finite element technique is divided into different roles,

first modelling for vibration behaviour for the human body, and secondly, meshes the human model with required element number by using mesh generation technique, and finally, solution vibration biomechanical human body model to evaluate the dynamic characterisations for modelling. The numerical results of the natural frequency, for each part of the human body, are found, comparison with analytical results calculating by using the analytical solution for biomechanical human body model, given in Equation 17, there is a good agreement between analytical and numerical results with a maximum error percentage (4.2%).

Human Body Vibration Model

The biomechanical model of the human body has been modelled using the finite element method to estimate the vertical vibration parameters natural frequencies of the human body vibration. The model consists of all body parts; torso, head, pelvis, legs, thighs, and viscera, as illustrated in the model geometry for different body parts, connections, mass centre's, and vibration excitation locations (Figure 1). All the human body parts in this model are defined as rigid bodies and lumped masses. The moment of inertia and mass values for each part of the body are listed in Table 1. The joints elasticity details for the human body parts in the model are shown in Table 2.

The fundamental governing equation for forced vibrations of a structure is written as Equation 16 (Rao, 2007; Rao, 2018),

$$[m]\{\ddot{\delta}\} + [c]\{\dot{\delta}\} + [k]\{\delta\} = \{F\} \quad (16)$$

Where, $[m]$, $[k]$, $[c]$, $\{\delta\}$, are the mass matrix, stiffness matrix, damping coefficient matrix, and displacement matrices, respectively, and is the external excitation force, as presented in Equation 14. Secondly, a frequency response analysis is modelled and carried out around the natural frequencies to determine the apparent mass and the two transmissibility. In sitting posture in vehicles, the vibration exciting the hip and thigh is transmitted to the human head through the entire body part. Therefore, the vibration transmissibility to the human head and driving point mechanical impedance or apparent mass of the human body are essential characteristics to express the vibration of a human body. The hip and human head vibration is also an important factor affecting ride comfort and visual disturbance. The vertical transmissibility (the ratio of vertical acceleration of the head to the input acceleration of the seat) is defined by Equation 17 (Kim et al., 2005),

$$H_{\text{vertical}} = \frac{(\ddot{y})_{\text{head}}}{(\ddot{y})_{\text{seat}}} \quad (17)$$

The rotational transmissibility (the ratio of the angular acceleration of the head to the input acceleration of the seat) is defined by Equation 18 (Kim et al., 2005),

$$H_{\text{rotational}} = \frac{(\ddot{\phi})_{\text{head}}}{(\ddot{y})_{\text{seat}}} \quad (18)$$

The apparent mass (the ratio of the force at the seat to the input acceleration of the seat) is defined by Equation 19 (Kim et al., 2005),

$$M_{\text{apparent}} = \frac{(F)_{\text{seat}}}{(\ddot{y})_{\text{seat}}} \quad (19)$$

The transmissibility's and apparent mass are directly related to the comfort feeling. Especially the vertical and rotational transmissibility affect ride comfort and vision.

Computational Grid

The biomechanical model's governing equations were discretised using a finite-element method and solved using the COMSOL Multi-Physics Multi-body Dynamics interface package to simulate the different parts in the model. The human body segments and the whole-body vibrations are studied. Three different positions of a vertical direction excitation of 1 m/s^2 are achieved. Numerical testing was applied for these models, and a quadratic elements mesh domain, with 598 boundary elements was found to provide sufficient spatial resolution (Figure 5). The coupled set of equations of the human body model was solved iteratively. The solution was considered convergent when the relative error was less than 1.0×10^{-6} in each field for two consecutive iterations.

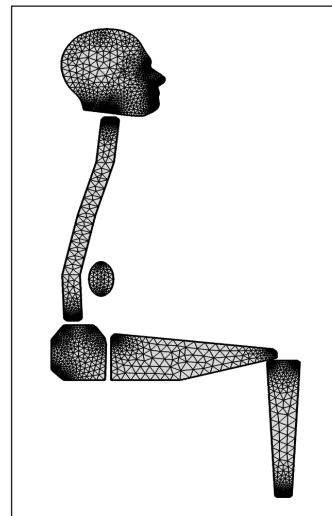


Figure 5. Computational quadratic mesh of the human body of the biomechanical model

RESULTS AND DISCUSSION

The biomechanical results included is employed to calculate the natural frequency for human body parts by using analytical and numerical techniques and then is compared the natural frequency results together, and after that, evaluating the vibration mode for human body parts with translational and rotational direction by using the numerical technique, by using finite element method.

Natural Frequency Results

The natural frequency for human body parts' translational and rotational biomechanical vibration is evaluated by an analytical solution for the general equation of motion for biomechanical modelling human body, Equation 15. Besides, the comparisons of the

numerical results with analytical results were calculated, as shown in Table 6. The comparison of analytical and numerical results give a functional discrepancy with maximum error did not exceed about (4.2%). Also, the results indicate that the maximum frequency occurs at a translational motion for the human body and the minimum frequency at rotational motion direction for the human body. So, these results can show the effect of applying load at the rotational human part more than the impact on the translational path. Furthermore, the results of the current work for both models were compared with the available published experimental results (Kim et al., 2005). The results showed that the maximum discrepancy did not exceed about (6%), as in the Head rotation.

Table 6
Natural frequency for biomechanical human model general coordinate

Human Model Coordinate	Natural Frequency (rad/sec)		Discrepancy (%)
	Analytically	Numerically	
x_1	16.02	15.56	2.87
z_1	126.4	121.24	4.08
θ_1	76.56	74.58	2.59
θ_2	3.07	2.93	4.56
θ_3	29.24	28.47	2.63
θ_4	37.09	35.96	3.05
θ_5	25.01	24.13	3.52

Numerical Results

The graphical representation of the rotational Eigen-modes of the un-damped biomechanical model of the human body is explained in Figure 6. In this figure, the vast rotational movement of the head and torso segments related to the other parts of the human body (legs, pelvis, viscera, and thighs) was presented. Figure 7 shows the translational Eigen-mode of the damped biomechanical model of the human body. It also shows the vast movement of the viscera, pelvis, and head compared to the other parts of the human body (torso, legs, and thighs). The vertical transmissibility for a range of excitation frequencies is drawn in Figure 8, while Figure 9 shows the vertical transmissibility of the biomechanical model for a variety of excitation frequencies. Figure 10 shows the rotational transmissibility (deg/m) of the excitation frequency values of the biomechanical model. The rotational transmissibility reduces the comfort level, and also it directly affects the vision. Therefore, it is not good when it is increasing, especially at a higher value. Figure 11 shows the biomechanical model’s apparent mass (kg) for a range of excitation frequency. The results clearly show that the visible mass transfers the driving point physical appearance, concerning the motion and force at the seat.

The present study results showed that the current two methodologies of the modelling and simulation of the human body using dynamic biomechanical vibration could sustain the design of vehicle seats. The mechanical response can be expected and predicted to respond to the human body using this biomechanical model in a vibratory environment as in a vehicle driving. It will help to stimulate the quality and design of vibration insulators such as seats, excitation frequency. The results clearly show that the visible mass transfers are associated with the driving point of physical appearance, the motion and the force at the seat.

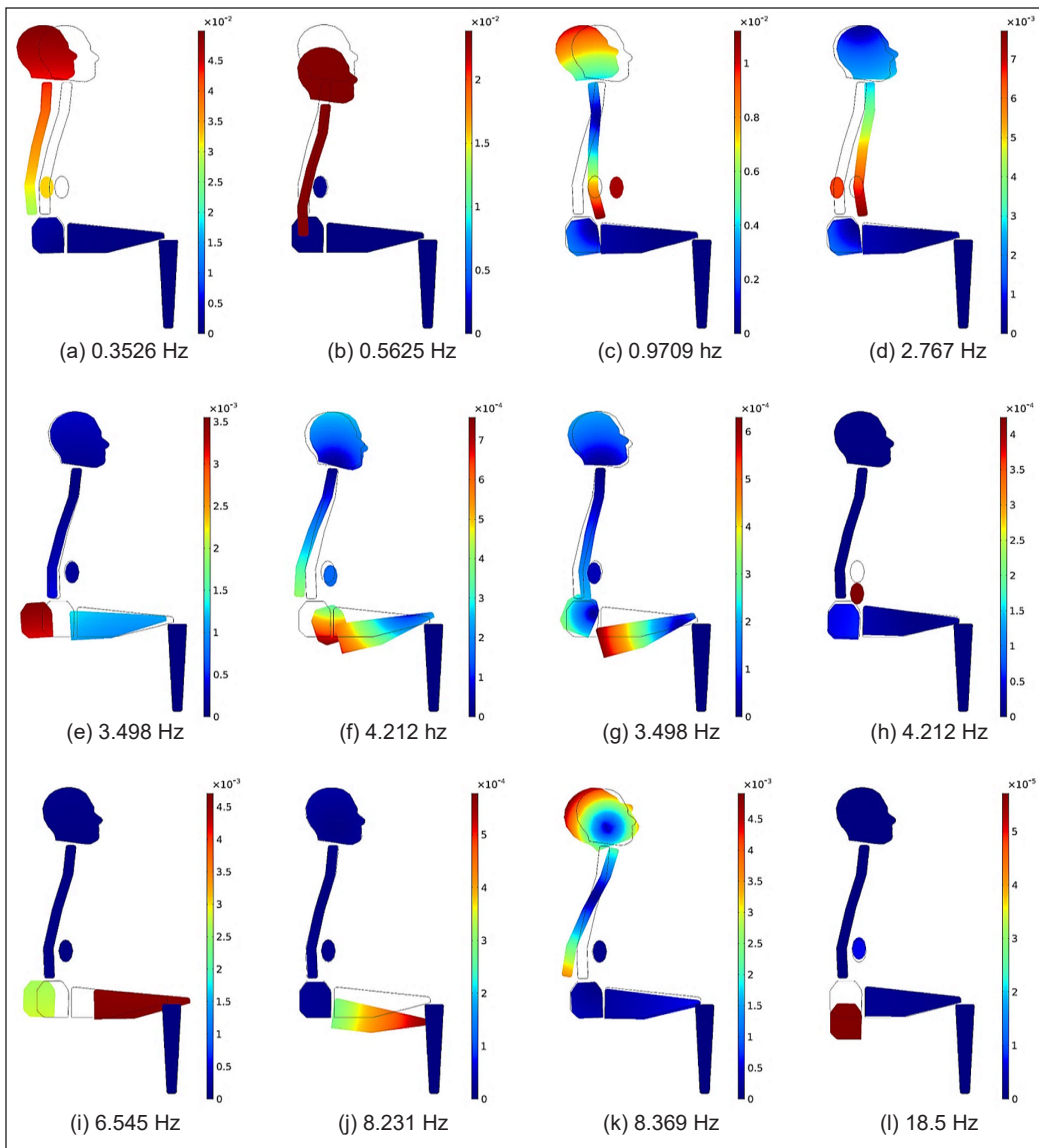


Figure 6. Rotational Eigen-Modes of the un-damped biomechanical model

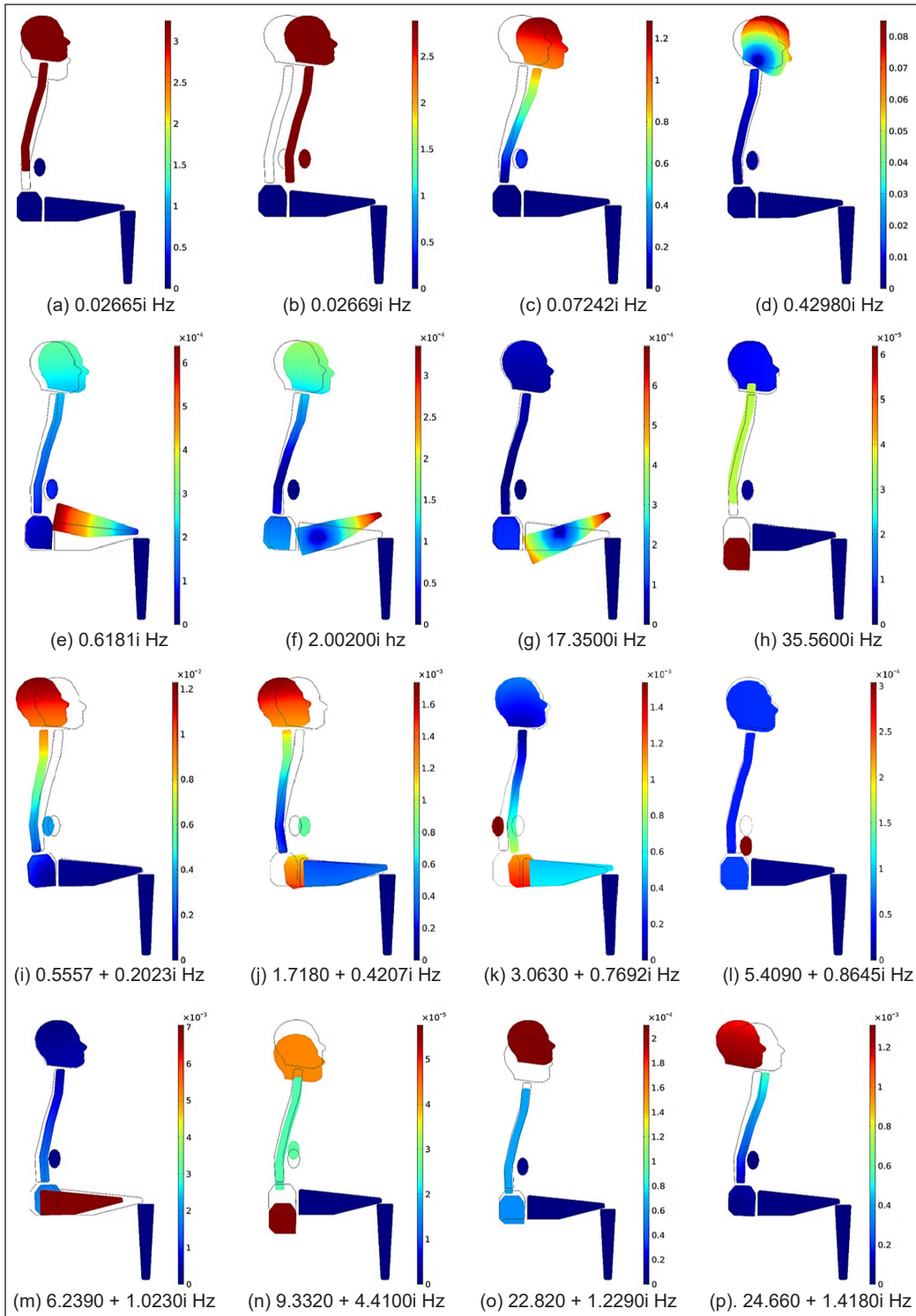


Figure 7. Translational Eigen-Mode of the damped biomechanical model

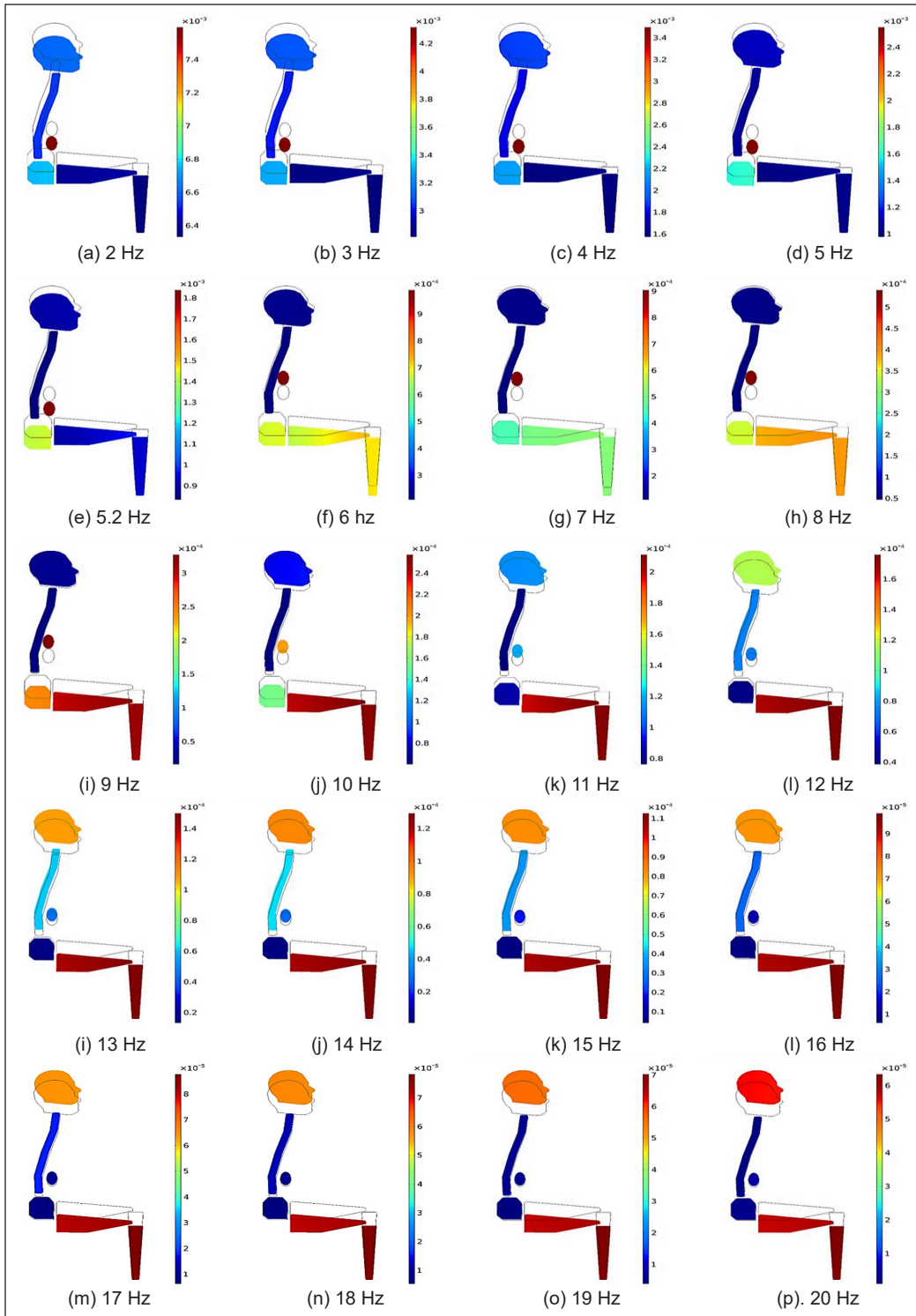


Figure 8. Vertical transmissibility for a range of excitation frequency

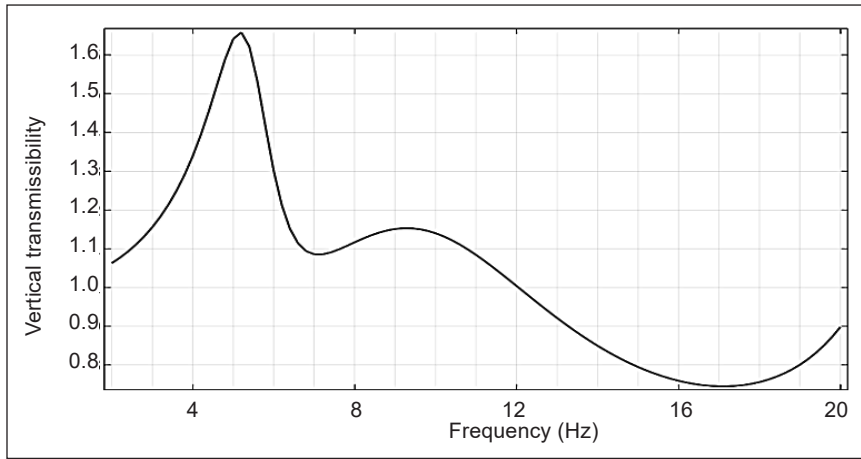


Figure 9. Vertical transmissibility of the biomechanical model for a range of excitation frequency

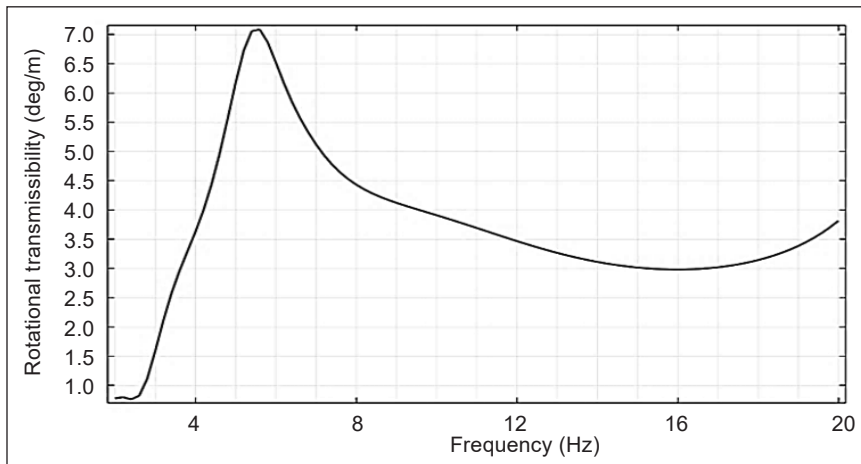


Figure 10. Rotational transmissibility of the biomechanical model for a range of excitation frequency

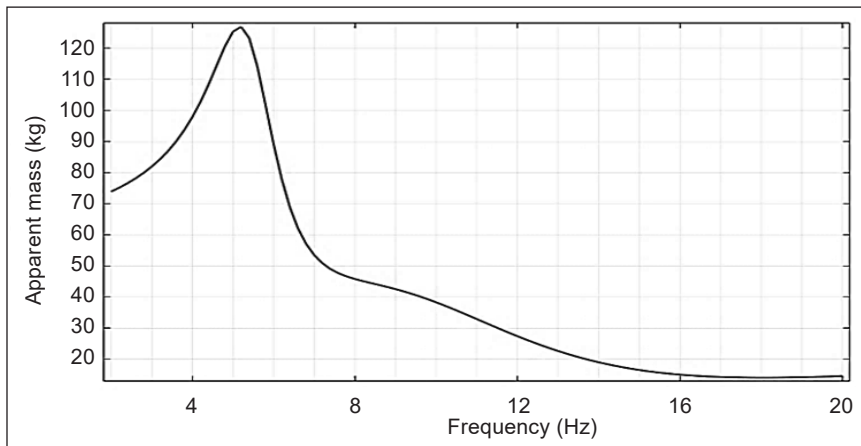


Figure 11. Apparent mass (kg) of the biomechanical model for a range of excitation frequency

CONCLUSION

In this study, analytical and numerical solutions for the dynamic biomechanical vibration model have been presented in detail to investigate and analyse the dynamic response of a human body when seated in a driving vehicle. The study included modelling the human body using a dynamic biomechanical vibration model and simulation with two methodologies. The first simulation was an analytical solution by deriving the general equations of the motion of the vibration behaviour for the human body to calculate the natural frequency for individual parts. The second simulation was a finite element technique to calculate natural frequency and vibration modes for the human body under different frequency loads. The simulation results show that the mechanical response expected and predicted to respond to the human body is perfect using this biomechanical model in a vibratory environment as in a vehicle driving, which will help stimulate the quality and design of vibration insulator such as a seat. Therefore, from this study can be concluded the following important points:

- The numerical vibration biomechanical human body model is a suitable technique and more sensitive that can be used to calculate the natural frequency for each part of the human body.
- Comparing human natural frequency results between analytical and numerical methods gives a good agreement results with maximum discrepancy not exceeding about (4.2%), and not exceeding (6%) compared with the available published experimental results.
- The maximum frequency occurs at a translational motion for the human body, and the minimum frequency at rotational motion direction for the human body occurs. Therefore, it can be shown that applying load on the rotational human parts is more than the effect of load on the translational human parts. So, the vibration response occurs at rotational human parts more than at translational human parts.
- The results are significant for human health in sitting position in the driving vehicle, which can assist understanding of the effects of low-frequency vibration on human health, comfort, and performance. Therefore it could be applied for ride comfort evaluation.

ACKNOWLEDGEMENT

The authors would like to thank the University of Kufa and the University of Al-Farahidi, Iraq, to support and fund this study.

REFERENCES

- Abbas, H. J., Jweeg, M. J., Al-Waily, M., & Diwan, A. A. (2019). Experimental testing and theoretical prediction of fiber optical cable for fault detection and identification. *Journal of Engineering and Applied Sciences*, 14(2), 430-438. <https://doi.org/10.36478/jeasci.2019.430.438>

- Al-Waily, M. (2005). *Analysis of stiffened and unstiffened composite plates subjected to time dependent loading* (MSc Thesis). University of Kufa, Iraq.
- Bayoglu, R., Galibarov, P. E., Verdonshot, N., Koopman, B., & Homminga, J. (2019). Twente spine model: A thorough investigation of the spinal loads in a complete and coherent musculoskeletal model of the human spine. *Medical Engineering & Physics*, 68, 35-45. <https://doi.org/10.1016/j.medengphy.2019.03.015>
- Desai, R., Guha, A., & Seshu, P. (2018). Multibody biomechanical modelling of human body response to direct and cross axis vibration. *Procedia Computer Science* 133, 494-501. <https://doi.org/10.1016/j.procs.2018.07.062>
- Griffin, M. J. (1990). *Handbook of human vibration*. Academic Press.
- Guo, L. X., Dong, R. C., & Zhang, M. (2016). Effect of lumbar support on seating comfort predicted by a whole human body-seat model. *International Journal of Industrial Ergonomics*, 53, 319-327. <https://doi.org/10.1016/j.ergon.2016.03.004>
- ISO 2631-1. (1997). *Mechanical vibration and shock - Evaluation of human exposure to whole-body vibration*. International Organizational for Standardization
- ISO 5982. (2001). *Mechanical vibration and shock - Range of idealized values to characterize seated-body biodynamic response under vertical vibration*. International Organizational for Standardization.
- Kim, T. H., Kim, Y. T., & Yoon, Y. S. (2005). Development of a biomechanical model of the human body in a sitting posture with vibration transmissibility in the vertical direction. *International Journal of Industrial Ergonomics*, 35, 817-829. <https://doi.org/10.1016/j.ergon.2005.01.013>
- Koutras, C., Pérez, J., Kardash, K., & Otaduy, M. A. (2021). A study of the sensitivity of biomechanical models of the spine for scoliosis brace design. *Computer Methods and Programs in Biomedicine* 207, Article 106125. <https://doi.org/10.1016/j.cmpb.2021.106125>
- Mohanty, P. P., & Mahapatra, S. S. (2014). A finite element approach for analyzing the effect of cushion type and thickness on pressure ulcer. *International Journal of Industrial Ergonomics*, 44, 499-509. <https://doi.org/10.1016/j.ergon.2014.03.003>
- Nimmen, K. V., Lombaert, G., Roeck, G. D., & den Broeck, P. V. (2017). The impact of vertical human-structure interaction on the response of footbridges to pedestrian excitation. *Journal of Sound and Vibration*, 402, 104-121. <https://doi.org/10.1016/j.jsv.2017.05.017>
- Rao, S. S. (2007). *Vibration of continuous systems*. John Wiley and Sons, Inc.
- Rao, S. S. (2018). *Mechanical vibrations*. Pearson Education, Inc.
- Vergari, C., Chen, Z., Robichon, L., Courtois, I., Ebermeyer, E., Vialle, R., Langlais, T., Pietton, R., & Skalli, W. (2020). Towards a predictive simulation of brace action in adolescent idiopathic scoliosis. *Computer Methods in Biomechanics and Biomedical Engineering*, 24(8), 874-882. <https://doi.org/10.1080/10255842.2020.1856373>
- Zheng, G., Qiu, Y., & Griffin, M. J. (2011). An analytic model of the inline and cross-axis apparent mass of the seated human body exposed to vertical vibration with and without a backrest. *Journal of Sound and Vibration*, 330, 6509-6525. <https://doi.org/10.1016/j.jsv.2011.06.026>

A Comparative Study on the Larvicidal Effects of *Piper sarmentosum* (Kaduk) Leaves Extracts against *Aedes aegypti*

Amelia Najiha Othman¹, Nur Farah Suryani Zainudin¹, Uswatun Hasanah Zaidan² and Suhaili Shamsi^{1*}

¹Laboratory for Animal Biochemistry and Biotechnology (ABBTech), Department of Biochemistry, Faculty of Biotechnology and Biomolecular Sciences, Universiti Putra Malaysia, 43400 UPM, Serdang, Selangor, Malaysia

²Food and Microbiome Technology Laboratory (FAMTech), Department of Biochemistry, Faculty of Biotechnology and Biomolecular Sciences, Universiti Putra Malaysia, 43400 UPM, Serdang, Selangor, Malaysia

ABSTRACT

Excessive use of synthetic larvicide has led to resistant strains of mosquito vectors and adverse ecological concerns globally. Hence, bioactive compounds from the plant have become a promising alternative to synthetic larvicide. Collectively, there is adequate evidence on the larvicidal effect of *Piper sarmentosum* (Kaduk). However, its leaves extract's larvicidal effects in different solvent systems are still recondite against *Aedes aegypti*. The present study aims to investigate the larvicidal activity of the leaves extracts of *P. sarmentosum* in methanol (ME), ethyl acetate (EE), dichloromethane (DE) and hexane (HE), towards the larvae of *A. aegypti*, following the laboratory guidelines provided by the World Health Organization (WHO). HE shows a significantly highest larvicidal activity followed by DE, EE and ME, with LC₅₀ and LC₉₀ values of 39.04 and 87.84, 62.78 and 134.73, 114.70 and 169.20, 156.10 and 182.10 µg/mL, respectively. The HE was also found to contain the highest total phenolic and total flavonoid content (TPC and TFC), with

various bioactive compounds at a higher percentage that exerts synergistic effects on the significantly improved larvicidal effect of HE compared to other solvent extracts. The morphological observation of *A. aegypti* larvae upon exposure to HE revealed a significant shrinkage of the internal structure of abdominal and siphon segments that indicates the acute toxicity effect of HE. The present study provides scientific-based

ARTICLE INFO

Article history:

Received: 13 April 2021

Accepted: 05 August 2021

Published: 18 October 2021

DOI: <https://doi.org/10.47836/pjst.29.4.31>

E-mail addresses:

amelianajiha66@gmail.com (Amelia Najiha Othman)

farahsuryanii@gmail.com (Nur Farah Suryani Zainudin)

uswatun@upm.edu.my (Uswatun Hasanah Zaidan)

sh_suhaili@upm.edu.my (Suhaili Shamsi)

* Corresponding author

evidence on the strongest larvicidal effect of HE from *P. sarmentosum* leaves extract towards *A. aegypti* for further development as a potential alternative for synthetic larvicide.

Keywords: *Aedes aegypti*, larvicidal activity, leaves extract, phytochemical content, *Piper sarmentosum*

INTRODUCTION

The World Health Organization (2021) claimed that the estimation of people at risk of contracting dengue was more than 3.9 billion in over 128 countries, with 96 million cases per year. In Malaysia alone, 88,845 dengue cases were recorded from January to December 2020, while in 2019, 127,407 cases were recorded within the same period. Selangor has recorded the highest number of dengue cases with 43,491 cases and 37 deaths, followed by Johor with 11,389 cases and 42 deaths in the Federal Territories of Kuala Lumpur and Putrajaya with 10,451 cases and seven deaths. Even though statistics show a decrease of 30.3% of dengue cases from 2019, the high number of cases recorded is still of concern (Ministry of Health Malaysia, 2020).

Mosquitoes are the primary known disease vectors able to transmit infectious diseases through the sucking of blood from the infected host (humans and animals) into a new host. There are more than 3,000 species of mosquitoes, but the common genera are *Aedes*, *Anopheles*, and also *Culex*. These mosquitoes serve as vector disease agents, including dengue fever, dengue haemorrhagic fever, Chikungunya, lymphatic filariasis, zika and malaria that are endemic and epidemic in many countries (Reiter, 2001).

Numerous approaches have been employed to hinder mosquito development, which largely involves vector control. Thus, vector control is often viewed as crucial. The mosquito larvae populations are usually controlled by the use of organophosphates, insect growth regulators, microbial agents, and residual spraying and insecticide-treated bed nets. While synthetic larvicides have supposedly become an effective means to control the mosquito larvae population, the excessive use of these synthetic larvicides has triggered the spread of resistant strains in the populations, as well as contributing to environmental pollution and mammalian toxicity (Mohiddin et al., 2016, Suratman et al., 2015). As a result, many non-targeted organisms, such as honey bees (Mahmood et al., 2014) and fish (Anadu et al., 1996, Wang et al., 2017), are at risk over the years. Hence, bioactive compounds isolated from the plant secondary metabolites have become potential alternatives to the present synthetic larvicides.

Consequently, this has become the centre of attention for researchers, specifically in screening potential bioactive compounds from botanical resources to produce biolarvicides. Biolarvicides can be an alternative to synthetic pesticides and have been proven to be more eco-friendly and safer for non-targeted organisms (Guleria & Tiku, 2009). In addition, chemicals derived from botanical sources have been discovered over decades to have a high potential in controlling mosquitoes (Sukumar et al., 1991).

The piper species are well-known herb species as they possess promising pharmacological activities along with pesticide and larvicidal activities. Genus *Piper*, the most abundant genera in the *Piperaceae* family, with 1000-2000 species are distributed worldwide, and over 400 species were recorded from the Malaysian region alone (Salleh et al., 2014). A previous study has reported on the insecticidal properties of *Piper sarmentosum* (*P. sarmentosum*), a wild plant usually grown in tropical countries including Malaysia, from the aerial part and root extracts (Hematpoor et al., 2016), but the data that supports the larvicidal effects of *P. sarmentosum* leaves extract against *Aedes aegypti* (*A. aegypti*) remain scarce. Furthermore, no published studies directly compare the effects of solvent extraction on *P. sarmentosum* leaves towards its larvicidal activity. Hence, the present study endeavours to evaluate and compare the larvicidal effects of *P. sarmentosum* (Kaduk) leaves extract in different solvents against *A. aegypti* and identify the potential bioactive components of the extract by using gas chromatography-mass spectrometry (GC-MS).

MATERIALS AND METHODS

Materials

All chemicals and reagents used were of analytical grade. Methanol, ethyl acetate, dichloromethane, hexane (R&M Chemicals, United Kingdom) and dimethyl sulfoxide (DMSO) (Merck, Germany) (PP: 99.8%, AR), Follin Ciocalteu reagent (Merck, Germany), gallic acid (Sigma Aldrich, Germany), quercetin hydrate (Acros Organics, United States), sodium carbonate (Merck, Germany), sodium nitrate (Merck, Germany), aluminium chloride (R&M Chemicals, United Kingdom), sodium hydroxide (Macron Fine Chemicals, United States), Abate 1.1® (BASF, Malaysia) were procured and used as purchased without further purification.

Methods

Plant Material. *Piper sarmentosum* leaves of similar sizes were collected from Taman Pertanian Universiti, Universiti Putra Malaysia and were further identified by a botanist (Dr Mohd Firdaus Ismail) from the Biodiversity Unit, Institute of Bioscience (IBS), Universiti Putra Malaysia. A specimen voucher (MFI 0149/20) was deposited in the Institute of Bioscience Herbarium. The leaves were then washed thoroughly minimise microbial contamination and remove debris and were spread onto trays and oven-dried at 50°C for three consecutive days. The leaves were ground into a fine powder using a food blender (Panasonic, Malaysia) and was kept in glass bottles, sealed and wrapped with aluminium foil for protection from sunlight and moisture at room temperature until further use.

Plant Extraction. The leaf extracts of *P. sarmentosum* were obtained by maceration using a shaking incubator (Sartorius, Germany) operating at 150 rpm at room temperature with

four different solvents, ethyl acetate, methanol, dichloromethane and hexane. Fifteen grams (15 g) of the dried leaf powder were dissolved in 150 mL of solvents for maceration. The mixture was macerated twice for three consecutive days at room temperature and stored in a dark condition to reduce sample degradation. It was followed by filtration of the crude extract using filter paper (Whatman, England). Finally, filtrates obtained from the maceration were pooled together and further concentrated using a rotary evaporator (Buchi, Switzerland). The dried crude extracts were stored in glass bottles at 4°C until further use.

Determination of Total Phenolic Content (TPC). The extract's total phenolic content (TPC) was determined by the Folin-Ciocalteu method as described previously (Ugusman et al., 2012) with modifications. The extracted sample (0.5 mL of 1 mg/mL of different solvent extracts) was mixed with Follin-Ciocalteu reagent (2.0 mL, 1:10 diluted with distilled water) for 5 minutes, and an aqueous solution of sodium carbonate (2.5 mL, 7.5% w/v) was then added. The mixture was allowed to stand for 90 minutes in a dark condition at room temperature, then estimated phenolic content by colourimetry at 760 nm (Spectrophotometer, Spectro 23, Labomed, USA). The standard curve ($y = 0.0046x - 0.063$, $R^2 = 0.998$) was prepared by using different concentrations (0-500 µg/mL) of gallic acid solution in aqueous methanol (10:90, v/v). The total phenolic content was expressed as a milligram of gallic acid equivalent per gram of the sample dry weight (mg GAE/g DW).

Determination of Total Flavonoid Content (TFC). The extract's total flavonoids content (TFC) was determined by the aluminium chloride colourimetric method as described previously with modifications (Ugusman et al., 2012). Each solvent extract (0.5 mL, 1 mg/mL) was mixed with 2 mL of distilled water and 0.15 mL of sodium nitrate (0.05 M). After a 5 minutes incubation at room temperature, 0.15 mL of aluminium chloride (0.1 M) and 1.0 mL of sodium hydroxide (1.0 M) were added. The test solution was filled up to 5.0 mL with distilled water, in which the absorbance was measured at 415 nm (Spectrophotometer, Spectro 23, Labomed, USA). The standard curve ($y = 0.0018x - 0.0087$, $R^2 = 0.9997$) was prepared by using different concentrations (0-300 µg/mL) of quercetin solutions in aqueous methanol (10:90, v/v). Total flavonoids content was expressed in milligrams of quercetin per gram of the sample dry weight (mg QE/g DW).

Collection of Mosquito Larvae. The mosquito eggs of susceptible *Aedes aegypti* (*A. aegypti*) strain were procured from the Vector Control Research Unit (VCRU), Universiti Sains Malaysia (USM), Penang. Upon arrival, the eggs were immediately transferred into 250 mL of distilled water containing 0.1 g of larvae food (fish food-BETTAS®; 45% crude protein, 5% crude fat, 2% crude fibre) to trigger the hatching process and provide a continuous supply of nutrients for the larvae growth. The larvae were allowed to grow until the late third instar following hatching prior to treatment. After that, the food was

replenished every day, and the larvae were maintained at room temperature with 14-h and 10-h dark/light cycles. The larvae were considered ready for treatment on day 7.

Larvicidal Activity. Each of the extracts representing different solvent extraction systems was tested for larvicidal activity at a concentration of 100 µg/mL against the mosquito larvae according to the laboratory guidelines of mosquito larvicide test, provided by the World Health Organization (2005) with several modifications. Four batches of 25 larvae (N=100) were isolated into a plastic cup for bioassay tests in 50 mL of the desired extract solution. The dried crude extracts of methanol and ethyl acetate were prepared in methanol, while the dichloromethane and hexane extracts were prepared in DMSO as the stock solutions. The concentration of methanol and DMSO was kept at 0.5% v/v throughout the experiment. Larvae treated with only 0.5% methanol or DMSO were considered as control. The bioassays were conducted at a temperature in the range of 25-28°C, with no food supply. Mortality of the larvae was recorded after 24 h of exposure, and the larvae were considered dead if they did not show any response or movement when the water was disturbed. The mortality percentage was calculated, and the mortality was corrected according to Abbott's formula (Equation 1)(Abbott, 1925). The survived adult mosquitoes were left to die without food supply for three days (De Almeida et al., 2010).

$$\text{Abbott's corrected mortality (\%)} = \frac{\% \text{ test mortality} - \% \text{ control mortality}}{100 - \% \text{ control mortality}} \times 100 \quad (1)$$

Concentration-Response Larvicidal Bioassay. In the concentration-response larvicidal bioassay, all extract solutions were serially diluted to obtain the concentrations in the range of 0-250 µg/mL of test solutions. The concentration of methanol and DMSO was kept at 0.5% v/v throughout the experiment. Each concentration of the test solution was treated on four batches of 25 larvae (N=100), and the mortality of the larvae was recorded following 24h of exposure. The effectiveness of the solvent extracts against the mosquito larvae was compared to a commercial synthetic larvicide, Abate 1.1[®], that contains temephos as the active ingredient at concentrations of 0-10 µg/L. Probit analysis was applied to acquire the LC₅₀ and LC₉₀ values (Finney, 1971).

Gas Chromatography-Mass Spectrometry (GC-MS) Analysis. All extracts were subjected to phytochemical analysis using the gas chromatography-mass spectrometry (GC-MS) method. The instrument consisted of a GC-MS QP2010 Plus SHIMADZU (Shimadzu, Japan) system. Compounds were separated on a ZB-5MS column (30 m × 0.25 mm ID × 0.25 µm) and a linear velocity column flow at 1 mL/min in a split mode. The column oven was kept at 50°C for 3 minutes and was gradually increased to 100°C (at 10°C/min) and to 250°C (at 20°C/min) for 5 minutes. All extracts were dissolved in

methanol at 5 µg/mL, and filtered through the 0.45 µm PTFE membrane filter (Millipore, USA) prior to analysis. The GC-MS injection volume was 0.5 µL and the analysis was conducted for 7 to 20 minutes. A mass spectrometer equipped with an ACQ detector, set at 240°C for ion source temperature and 300°C of interface temperature with m/z (mass scan) of 35–450 amu, was used to identify the compounds present. The compounds' names, molecular weight and structures were ascertained from the National Institute of Standards and Technology (NIST) 08 mass spectral data library.

Morphological Observation. The morphological abnormalities (head, thorax and abdominal segment) of the treated larvae (LC₉₀ value) were observed using an inverted microscope (TS100, Nikon, Japan) attached to the DinoLite microscope camera and controlled by the DinoCapture 2.0 software (DinoLite, USA), in comparison to the untreated larvae.

Data Analysis. Results for larvicidal activity, TPC and TFC were expressed as mean ± standard error of the mean (SEM). Statistical significance was determined by using a one-way analysis of variance (ANOVA) with Tukey's test applied post hoc for paired comparison of means. A *p*-value ≤ 0.05 was considered as statistically significant (GraphPad Prism 9 Software, United States).

RESULTS AND DISCUSSION

The methanol extract (ME) obtained the highest percentage yield of 14.73%, followed by ethyl acetate extract (EE), dichloromethane extract (DE), and hexane extract (HE) with percentage yields of 6.38, 5.50 and 2.23%, respectively. The percentage yield of HE was higher than a previous study (Hematpoor et al., 2016) that reported a percentage yield of only 0.97% for HE extracted from the roots of *P. sarmentosum*. The difference in the percentage yield obtained was due to the different parts of the plant used and the polarity of each solvent.

The Folin-Ciocalteu method used to determine the total phenolic content (TPC) depends largely on the electrons transfer from the hydroxyl group directly bonded to the aromatic hydrocarbon group in the phenolic compounds. It leads to forming of a blue chromophore constituted by a mixture of a heteropolyphosphotungstates-molybdates complex in an alkaline condition (Blainski et al., 2013), which results in a maximum absorption at a wavelength of 760 nm. The TPC values of ME, EE, DE and HE were calculated according to a constructed regression equation ($y = 0.0046x - 0.063$, $R^2 = 0.9980$), and the values were interpreted as mean ± SEM (mg GAE/g DW). HE exhibited the highest TPC value (26.68 ± 0.22) followed by DE (19.93 ± 0.13), EE (19.75 ± 0.10), and ME (17.25 ± 0.12) (Table 1). There is a significant difference in multiple comparisons between the extracts, except for EE and DE.

TFC was calculated from the regression equation ($y = 0.0018x - 0.0087$, $R^2 = 0.9997$) and was interpreted as mean \pm SEM (mg QE/g DW). The results obtained displayed that HE has the highest total flavonoids content of 18.99 ± 0.07 , followed by DE (13.33 ± 0.12), EE (10.04 ± 0.06), and ME (4.38 ± 0.05) (Table 1). The results indicate that flavonoids with higher molecular weight were able to be extracted in organic solvents (Zaidan et al., 2019), which is congruent with the previous studies by Lee et al. (2014) and Tuekaew et al. (2014). The flavonoid compounds in the extracts may be influenced by the part of the plant used, cultivation location, and most importantly, the solvent extraction system applied, which are the essential factors to be considered when comparing to previous studies (Zaidan et al., 2018, Altemimi et al., 2017, Anokwuru et al., 2011).

Table 1
Total phenolic and flavonoid contents of different solvent extracts of *P. sarmentosum* leaves

Solvent Extracts	Mean \pm SEM (n=3)	
	TPC (mg GAE/g DW) ¹	TFC (mg QE/g DW) ²
Methanol Extract (ME)*	17.25 \pm 0.12	4.38 \pm 0.05
Ethyl acetate Extract (EE)*	19.75 \pm 0.10	10.04 \pm 0.06
Dichloromethane Extract (DE)*	19.93 \pm 0.13	13.33 \pm 0.12
Hexane Extract (HE)	26.68 \pm 0.22	1.99 0.07

*Denotes significant difference to HE ($p \leq 0.05$). No significant difference was observed for EE and DE ($p > 0.05$)

The highest larvicidal activity of *P. sarmentosum* leaves extract was displayed by HE with a percentage mortality of 100%, followed by DE ($67.00 \pm 0.66\%$), EE ($24.00 \pm 0.80\%$), and ME ($18.00 \pm 0.40\%$) at 100 $\mu\text{g/mL}$ as shown in Table 2. The untreated larvae exposed to only 0.5% DMSO and methanol showed no significant mortality effect (Table 2). The highest larvicidal activity exhibited by HE was attributed to the presence of high phenolic and flavonoid compounds in the extract (Table 1). It was supported by a study conducted by Vimaladevi et al. (2012), which revealed that insoluble bound, soluble conjugated and free phenolic acid fractions of *Chaetomorpha antennina* had excellent larvicidal activity against *A. aegypti* with LC_{50} values of 23.4, 44.6 and 60.8 $\mu\text{g/L}$, respectively. In another study, there was a linear correlation between the total phenolic content of the selected Egyptian plants (aqueous and methanol extracts) and the larvicidal activity against *A. aegypti* (El-Hela et al., 2013).

The larvae of the *A. aegypti* were then exposed to different solvent extracts of *P. sarmentosum* at various concentrations of the test solutions (0-250 $\mu\text{g/mL}$). The mortality percentage was shown to be concentration-dependent (Figure 1). A significantly higher larvicidal activity of *P. sarmentosum* leaves extract was displayed by HE with LC_{50} and LC_{90} values of 39.04 and 87.84 $\mu\text{g/mL}$, followed by DE (62.78 and 134.73 $\mu\text{g/mL}$), EE (114.70 and 169.20 $\mu\text{g/mL}$), and ME (156.10 and 182.10 $\mu\text{g/mL}$), respectively as shown

in Figure 2. Abate 1.1® displayed superior efficacy of larvicidal activity with LC₅₀ and LC₉₀ values of 5.49 and 7.67 µg/L, respectively (Table 3). Abate 1.1® has been used extensively and intensively in controlling the *Aedes* mosquito larvae in Malaysia, which has contributed largely to the emergence of temephos resistance (Mohiddin et al., 2016). Moreover, the LC₅₀ value of *P. sarmentosum* leaves HE (39.04 µg/mL) was lower compared to the results from previous studies within the same species, 49.19 µg/mL (Intirach et al., 2016), which utilised essential oil extracted from *P. sarmentosum* against the larvae of *A. aegypti*. In another study by Hematpoor et al. (2016), the crude HE extracted from the roots of *P. sarmentosum* only exhibits 100% mortality towards *Aedes aegypti* at 250 µg/mL. Thus, it indicates a significantly improved larvicidal activity of *P. sarmentosum* from the leaves extract. Contrary to the HE used in the present study, the lower LC₅₀ value of 4.06 µg/mL reported by Chaithong et al. (2006) could be possibly contributed by more active compounds in the extract obtained from the whole plant of *P. sarmentosum*.

Table 2
Larvicidal activity of *P. sarmentosum* leaves extracts against *A. aegypti* at 100 µg/mL

Solvent Extracts	Mean mortality ± SEM (%) (N=100)
Methanol Extract (ME)*	18.00 ± 0.40
Ethyl acetate Extract (EE)*	24.00 ± 0.80
Dichloromethane Extract (DE)*	67.00 ± 0.66
Hexane Extract (HE)	100.00 ± 0.00
Control (0.5% Methanol)	2.00 ± 0.06
Control (0.5% DMSO)	0.00 ± 0.00

*Denotes significant difference to HE ($p \leq 0.05$).

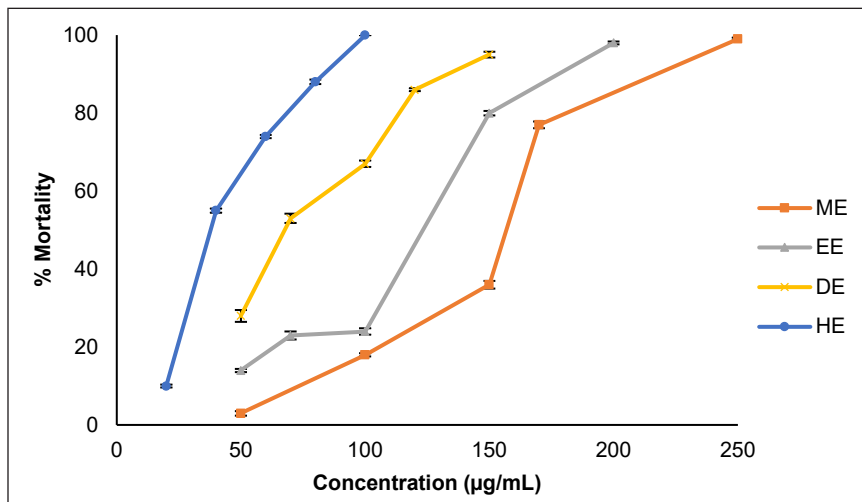


Figure 1. Concentration-response of the percentage of mortality of *P. sarmentosum* leaves extracts in hexane (HE), dichloromethane (DE), ethyl acetate (EE) and methanol (ME) against *A. aegypti* larvae at various concentrations of 0-250 µg/mL post-exposure (24 h). Data represent the value of mean ± SEM (N=100).

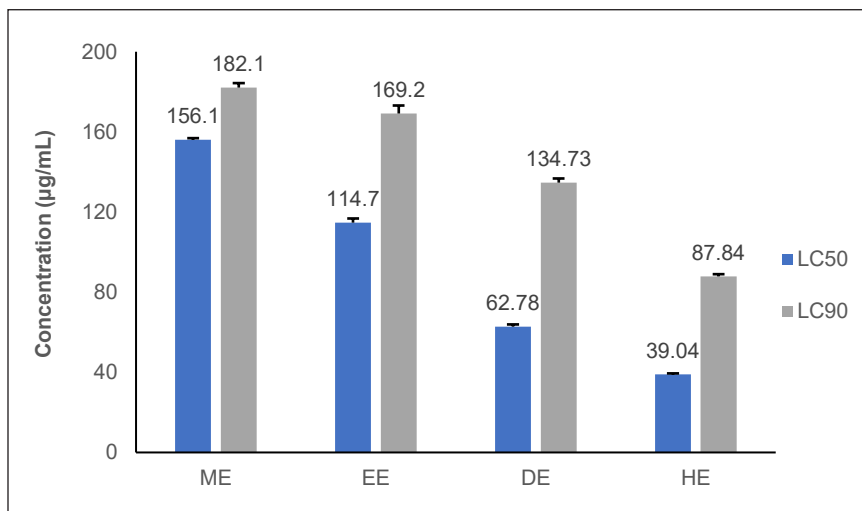


Figure 2. The larvicidal activity presented as LC₅₀ and LC₉₀ values of different solvent extracts of *P. sarmentosum* leaves; methanol extract (ME), ethyl acetate extract (EE), dichloromethane extract (DE) and hexane extract (HE) against *A. aegypti* larvae. Data presented as mean \pm SEM (N=100). * Indicates significant difference to HE at $p \leq 0.05$ of 95% confident interval (Tukey's Test).

Phytochemical profiling of *P. sarmentosum* leaves extracts was obtained by using the high-performance GC-MS method. The most prevailing phytochemicals in all extracts were found to be phenylpropanoids (*Z*-isoelemicin and asarone). ME contained (*Z*- isoelemicin (26.12%) and asarone (26.32%), EE; (*Z*- isoelemicin (27.10%) and asarone (29.91%), DE; (*Z*- isoelemicin (38.68%) and asarone (34.08%) and HE; (*Z*- isoelemicin (44.82%) and asarone (35.23%), respectively (Table 4). The higher efficacy of DE and HE compared to ME and EE are contributed to the additional compound of myristicin with a yield of 6.33% in DE and 9.03% in HE. Furthermore, the high yield of these phenylpropanoids was correlated with the larvicidal activity of *P. sarmentosum* leaves extracts against *A. aegypti*.

The current study's component proportions (isoelemicin, asarone, myristicin) of *P. sarmentosum* leaves extracts correspond to several previous studies within the same species (Abidin et al., 2020, Chanprapai & Chavasiri, 2017, Rahman et al., 2014, Qin et al. 2010). Isoelemicin was also found as the major composition in ethyl acetate extract of *P. solmsianum* leaves (Martins et al., 2000), (*Z*)-isoelemicin (21.5%) in *P. mikanianum* essential oil (Leal et al., 2005) and *E*-isoelemicin (40.81%) in *P. rivinoides* leaves essential oil (Leal et al., 2019). (*Z*)-Asarone (30.4%) appeared as the major constituent in the essential oil of *P. marginatum* leaves (Ribeiro et al., 2016). The presence of asarone and myristicin could be the main contributor to the potent larvicidal activity of HE compared to other extracts. Several studies have reported that different asarone stereoisomers exhibited different potential in larvicidal activity against *A. aegypti* larvae. β -asarone extracted from the root

Table 3

Comparative larvicidal activity of different solvent extracts of P. sarmentosum leaves and temephos (Abate 1.1) against A. aegypti larvae

Extract ($\mu\text{g/mL}$)	*Mean mortality \pm SEM (%)	LC values (95% CI, $\mu\text{g/mL}$)	
		LC ₅₀	LC ₉₀
Methanol Extract (ME)			
50	3.00 \pm 0.59		
100	18.00 \pm 0.40		
150	36.00 \pm 0.97	156.10 (155.30-156.90)	182.10 (179.8-184.40)
170	77.00 \pm 0.87		
250	99.00 \pm 0.35		
Ethyl acetate Extract (EE)			
50	14.00 \pm 0.40		
70	23.00 \pm 1.04		
100	24.00 \pm 0.80	114.70 (112.60-116.80)	169.20 (165.20-173.20)
150	80.00 \pm 0.57		
200	98.00 \pm 0.40		
Dichloromethane Extract (DE)			
50	28.00 \pm 1.50		
70	53.00 \pm 1.18		
100	67.00 \pm 0.66	66.32 (65.26-67.38)	131.83 (129.81-133.85)
120	86.00 \pm 0.40		
150	95.00 \pm 0.74		
Hexane Extract (HE)			
20	10.00 \pm 0.40		
40	55.00 \pm 0.52		
60	74.00 \pm 0.40	39.04 (38.59-39.49)	87.84 (86.65-89.04)
80	88.00 \pm 0.57		
100	100.00 \pm 0.00		
Control (0.5% MeOH)	2.00 \pm 0.40		
Control (0.5% DMSO)	-		
Larvicide ($\mu\text{g/L}$)	*Mean mortality \pm SEM (%)	LC values ($\mu\text{g/L}$)	
		LC ₅₀	LC ₉₀
Temephos (Abate 1.1[®])			
2	6.00 \pm 0.40		
4	23.00 \pm 0.11	5.49 (5.42-5.56)	7.67 (7.62-7.75)
6	52.00 \pm 0.86		
8	97.00 \pm 0.38		
10	100.00 \pm 0.00		
Control (distilled water)	-		

Note. *Mean value of four replicates, N=100

bark of *Cordia alliodora* has shown a minimal concentration of 25 µg/mL to kill all tested larvae (Ioset et al., 2000) and at LC₅₀ value of 26.99 µg/mL from *Asarum heterotropoides* roots (Perumalsamy et al., 2009). However, asarone isomers have demonstrated mammalian carcinogenic effects (Haupenthal et al., 2017, Uebel et al., 2020). On the other hand, myristicin was found to be one of the major components in *P. permucronatum* (25.61%) and *P. hostmanianum* (20.26%) (de Morais et al., 2007). Myristicin previously has been reported to possess insecticidal effect against *Spilarctia obliqua* (Srivastava et al., 2001). A study by Seo et al. (2015) has revealed a significant efficacy of myristicin from the essential oil of *Illicium difengpi* against *A. aegypti* larvae with an LC₅₀ value of 15.26 µg/mL. At 50 µg/mL of myristicin treatment, 92.5% mortality resulted against *Ae. albopictus* larvae (Seo et al., 2015). According to Hematpoor et al. (2016), three active phenylpropanoids: asaricin, isoasarone and trans-asarone were identified and isolated by hexane extraction from the roots of *P. sarmentosum*. Asaricin and isoasarone were highly potent against *Aedes aegypti*, *Aedes albopictus* and *Culex quinquefasciatus* larvae causing up to 100% mortality at ≤ 15 µg/mL of concentration. These findings coupled with the high acetylcholinesterase (AChE) inhibition suggest that asaricin and isoasarone are neurotoxic compounds towards *Aedes aegypti*, *Aedes albopictus*, and *Culex quinquefasciatus*. The variations in the type of phytochemicals present in *P. sarmentosum* extracts were contributed by plant species, plant parts used, age of plant parts, geographical origin of the plant and solvent used for extraction (Ghosh et al., 2012). Solvents with different polarities could cause different compounds to be extracted (Ugusman et al., 2012, Shaalan et al., 2005).

After several hours of treatment, the larvae lost their mobility when exposed to the test solutions. After 24 h of exposure to HE (LC₉₀ value), the dead larvae were observed for morphological changes under an inverted microscope. The observation displayed alterations in the internal structure of the abdominal segment and the siphon (Figures 3a & 3b), compared to the untreated larvae with no abnormal alteration and normal appearance of the siphon structure (Figures 3c & 3d).

The present study's findings agree with the previous study of Chaithong et al. (2006), in which the pepper-treated larvae displayed remarkable shrinkage of anal papillae. However, HE clearly showed delayed toxicity when a few moribund larvae (do not respond when disturbed) still displayed pounding heartbeats upon 24 h of exposure. Thus, it indicates a slower action of HE in larvae killing and was probably only targeting the neuromuscular system (Sakthivadivel & Thilagavathy, 2003), as the moribund larvae showed partial paralysis after treatment. In addition, the structural alterations of the internal tracheal tube and abdomen segment may demonstrate respiratory and gastrointestinal tract failure, leading to the larvae's dysfunction and death.

Table 4

Chemical composition of methanol extract (ME), ethyl acetate extract (EE), dichloromethane extract and hexane extract (HE) of P. sarmentosum leaves

Compounds	MW	RI	Peak area (%)			
			ME	EE	DE	HE
4,8-dimethylnonanol	172	1229	-	-	0.25	-
2-Butyloctanol	186	1393	1.12	-	-	-
1-Tetradecene	196	1403	2.47	-	-	-
1,6-heptadiene-2-methyl-6-phenyl-	186	1424	2.64	1.76	-	-
Decane-1-iodo	268	1430	1.60	-	-	-
Cyclopentanecarboxylic acid	208	1456	1.51	-	-	-
Caryophyllene	204	1494	1.20	1.55	3.28	0.59
Bicyclogermacrene	204	1497	-	0.08	-	-
1,3-Benzodioxole-4-methoxy-6-(2-propenyl)	192	1516	2.80	-	-	-
δ -Cadinene	204	1518	-	0.61	0.32	-
Myristicin	192	1520	-	3.23	6.33	9.03
Cyclohexanemethanol	222	1522	-	0.25	0.33	-
Elemicin	208	1551	0.39	0.32	0.30	0.59
Phenol-2,4-bis(1,1-dimethylethyl)	206	1555	3.29	2.21	0.30	-
1-Dodecanol-3,7,11-trimethyl	228	1563	-	0.42	-	-
(Z)-Isoelemicin	208	1565	26.12	27.10	38.68	44.82
Asarone	208	1568	26.32	29.91	34.08	35.23
(Z)- β -Asarone	208	1568	0.49	0.47	-	-
1-naphthalenol	222	1580	0.72	-	-	-
Dillapiole	210	1621	-	1.43	-	-
α -Muurolol	222	1651	-	0.62	0.63	0.96
Apiole	222	1683	-	0.94	1.61	2.10
Apiol	222	1705	0.84	-	1.12	2.09
2-Propenoic acid, 3-(3,4-dimethoxyphenyl)	208	1735	-	-	-	0.89
Hexahydrofarnesyl acetone	268	1754	0.66	-	-	0.69
Neophytadiene	278	1836	4.69	8.55	6.78	2.17
1,5-diphenyl-2-pentene	222	1872	1.35	-	-	-
Palmitic acid	270	1878	4.21	5.14	-	-
3-methyl-2-(3,7,11-trimethyldodecyl) furan	292	1931	0.37	-	-	-
Methyl isostearate	298	2013	-	3.52	-	-
Phytol	296	2045	4.70	7.87	5.99	0.84
3-Methyl-2-(3,7,11-trimethyldodecyl)	392	2045	-	0.45	-	-
Octadecanoic acid, methyl ester	298	2077	4.53	-	-	-
(Z)-6-Octadecenoic acid, methyl ester	296	2085	3.10	2.80	-	-
Benzenepropanoic acid, 3,5-bis(1,1-dimethylethyl)-4-hydroxy	292	2134	4.88	-	-	-
Piperidine	281	2366	-	0.77	-	-
Total identified (%)			100	100	100	100

Note. MW: Molecular Weight; RI: Retention Index

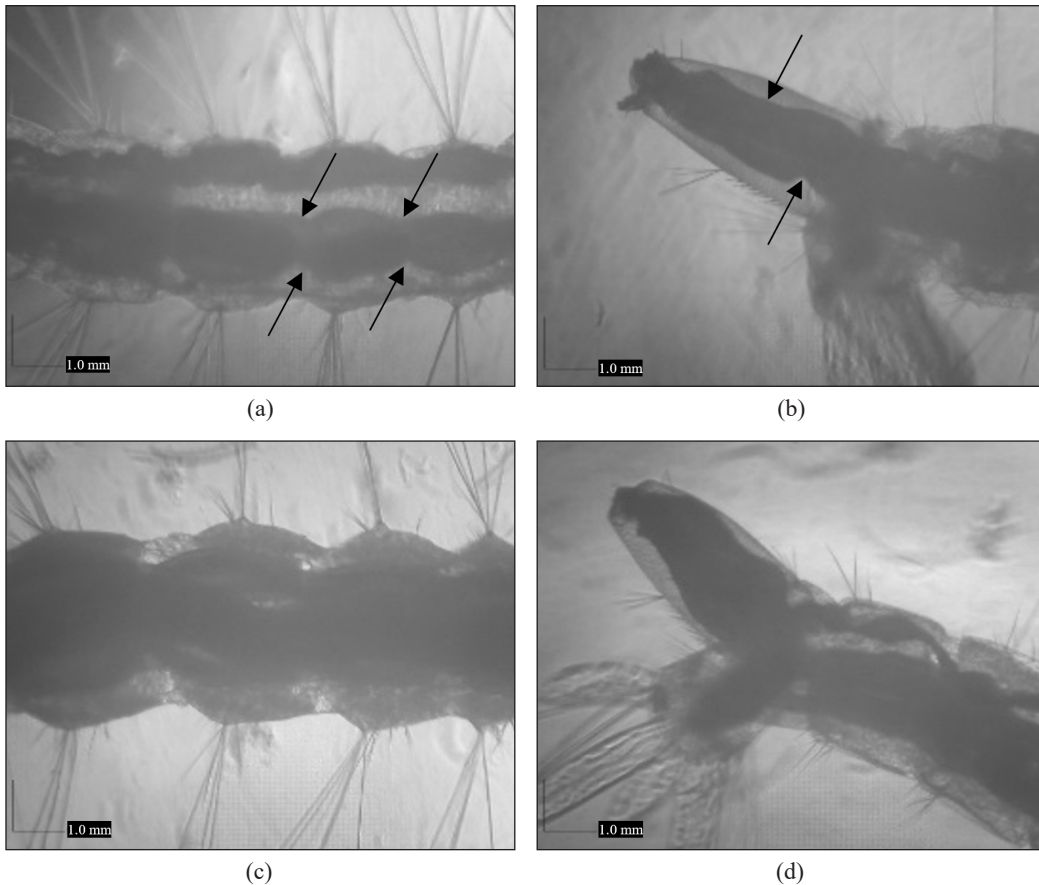


Figure 3. Morphological alterations in the treated larvae (LC₉₀ of HE) with significant shrinkage of the internal structure of (a) abdominal segment and the (b) siphon as indicated by arrows. No alterations were observed on untreated larvae of the (c) internal structure of the abdominal segment and (d) the internal structure of the siphon. Scale bar represents 1.0 mm at 40× magnification.

CONCLUSION

Botanical resources can be an alternative to the problematic synthetic larvicides in controlling the mosquito vector population. In this study, HE of *P. sarmentosum* leaves exhibited the highest potential of larvicidal activity with an LC₅₀ value of 39.04 µg/mL and LC₉₀ value of 87.84 µg/mL, compared to other solvent extracts. Morphological alterations of the internal abdominal segment and siphon of the treated larvae indicate acute toxicity of HE. It is suggested that the presence of various bioactive compounds at a higher percentage in HE exert synergistic effects on the significantly improved larvicidal activity of HE compared to other solvent extracts. However, further research that focuses on the larvicidal mechanism of the HE, susceptibility, stability and toxicity of the HE towards non-targeted organisms is warranted for the HE to be developed as a potential alternative for synthetic larvicides.

ACKNOWLEDGMENTS

The research was financially supported by a research grant provided by the Ministry of Higher Education of Malaysia, namely the Fundamental Research Grant Scheme (FRGSFRGS/1/2018/SKK11/UPM/02/1). In addition, the authors acknowledge the facilities and technical assistance provided by the Institute of Biosciences (IBS) at Universiti Putra Malaysia.

REFERENCES

- Abbott, W. S. (1925). A method of computing the effectiveness of an insecticide. *Journal of Economic Entomology*, 18(2), 265-267.
- Abidin, I. Z. Z., Fazry, S., Jamar, N. H., Dyari, H. R. E., Ariffin, Z. Z., Johari, A. N., Ashaari, N. S., Johari, N. A., Wahab, R. M. A., & Ariffin, S. H. Z. (2020). The effects of *Piper sarmentosum* aqueous extracts on zebrafish (*Danio rerio*) embryos and caudal fin tissue regeneration. *Scientific Reports*, 10(1), Article 14165. <https://doi.org/10.1038/s41598-020-70962-7>
- Altemimi, A., Lakhssassi, N., Baharlouei, A., Watson, D., & Lightfoot, D. (2017). Phytochemicals: Extraction, isolation, and identification of bioactive compounds from plant extracts. *Plants*, 6(4), Article 42. <https://doi.org/10.3390/plants6040042>
- Anadu, D. I., Aanaso, H. U., & Onyeka, O. N. D. (1996). Acute toxicity of the insect larvicide abate® (temephos) on the fish *Tilapia melanopleura* and the dragonfly larvae *Neurocordelia virginensis*. *Journal of Environmental Science and Health*, 31(6), 1363-1375. <https://doi.org/10.1080/03601239609373072>
- Anokwuru, C. P., Anyasor, G. N., Ajibaye, O., Fakoya, O., & Okebugwu, P. (2011). Effect of extraction solvents on phenolic, flavonoid and antioxidant activities of three Nigerian medicinal plants. *Nature and Science*, 9(7), 53-61.
- Blainski, A., Lopes, G., & de Mello, J. (2013). Application and analysis of the folin ciocalteu method for the determination of the total phenolic content from *Limonium Brasiliense* L. *Molecules*, 18(6), 6852-6865. <https://doi.org/10.3390/molecules18066852>
- Chaihong, U., Choochote, W., Kamsuk, K., Jitpakdi, A., Chaiyasit, D., Champakaew, D., Tuetun, B., Pitasawat, B., & Tippawangkosol, P. (2006). Larvicidal effect of pepper plants on *Aedes aegypti* (L.) (Diptera: Culicidae). *Journal of Vector Ecology*, 31(1), 138-144. [https://doi.org/10.3376/1081-1710\(2006\)31\[138:LEOPPO\]2.0.CO;2](https://doi.org/10.3376/1081-1710(2006)31[138:LEOPPO]2.0.CO;2)
- Chanprapai, P., & Chavasiri, W. (2017). Antimicrobial activity from *Piper sarmentosum* Roxb. against rice pathogenic bacteria and fungi. *Journal of Integrative Agriculture*, 16(11), 2513-2524. [https://doi.org/10.1016/S2095-3119\(17\)61693-9](https://doi.org/10.1016/S2095-3119(17)61693-9)
- De Almeida, S. J., Ferreira, R. P. M., Eiras, Á. E., Obermayr, R. P., & Geier, M. (2010). Multi-agent modeling and simulation of an *Aedes aegypti* mosquito population. *Environmental Modelling & Software*, 25(12), 1490-1507. <https://doi.org/10.1016/j.envsoft.2010.04.021>
- de Moraes, S. M., Facundo, V. A., Bertini, L. M., Cavalcanti, E. S. B., dos Anjos Júnior, J. F., Ferreira, S. A., de Brito, E. S., & de Souza Neto, M. A. (2007). Chemical composition and larvicidal activity of essential

- oils from Piper species. *Biochemical Systematics and Ecology*, 35(10), 670-675. <https://doi.org/10.1016/j.bse.2007.05.002>
- El-Hela, A. A., Abdel-Hady, N. M., & Dawoud, G. T. M. (2013). Phenolic content, antioxidant potential and *Aedes aegyptii* ecological friend larvicidal activity of some selected Egyptian plants. *Journal of the Egyptian Society of Parasitology*, 43(1), 215-234. <https://doi.org/10.12816/0006379>
- Finney, D. J. (1971). *Probit analysis* (3rd ed.). Cambridge University Press.
- Ghosh, A., Chowdhury, N., & Chandra, G. (2012). Plant extracts as potential mosquito larvicides. *Indian Journal of Medical Research*, 135(5), 581-598. [/pmc/articles/PMC3401688/](https://pubmed.ncbi.nlm.nih.gov/23401688/)
- Guleria, S., & Tiku, A. K. (2009). Botanicals in pest management: Current status and future perspectives. In *Integrated Pest Management: Innovation-Development Process* (pp. 317-329). Springer. https://doi.org/10.1007/978-1-4020-8992-3_12
- Hauptenthal, S., Berg, K., Gründken, M., Vallicotti, S., Hemgesberg, M., Sak, K., Schrenk, D., & Esselen, M. (2017). In vitro genotoxicity of carcinogenic asarone isomers. *Food and Function*, 8(3), 1227-1234. <https://doi.org/10.1039/c6fo01701k>
- Hematpoor, A., Liew, S. Y., Chong, W. L., Azirun, M. S., Lee, V. S., & Awang, K. (2016). Inhibition and larvicidal activity of phenylpropanoids from *Piper sarmentosum* on acetylcholinesterase against mosquito vectors and their binding mode of interaction. *PLoS ONE*, 11(5), 1-27. <https://doi.org/10.1371/journal.pone.0155265>
- Intirach, J., Junkum, A., Lumjuan, N., Chaithong, U., Jitpakdi, A., Riyong, D., Wannasan, A., Champakaew, D., Muangmoon, R., Chansang, A., & Pitasawat, B. (2016). Antimosquito property of *Petroselinum crispum* (Umbelliferae) against the pyrethroid resistant and susceptible strains of *Aedes aegypti* (Diptera: Culicidae). *Environmental Science and Pollution Research*, 23(23), 23994-24008. <https://doi.org/10.1007/s11356-016-7651-8>
- Ioset, J. R., Marston, A., Gupta, M. P., & Hostettmann, K. (2000). Antifungal and larvicidal compounds from the root bark of *Cordia alliodora*. *Journal of Natural Products*, 63(3), 424-426. <https://doi.org/10.1021/np990393j>
- Leal, A. L. A. B., Machado, A. J. T., Bezerra, C. F., Inácio, C. E. S., Rocha, J. E., Sales, D. L., de Freitas, T. S., de Oliveira Almeida, W., do Amaral, W., da Silva, L. E., Ferriani, A. P., de Noronha Sales Maia, B. H. L., Morais-Braga, M. F. B., Barreto, H. M., & Coutinho, H. D. M. (2019). Chemical identification and antimicrobial potential of essential oil of *Piper rivinoides* kunth (BETIS-WHITE). *Food and Chemical Toxicology*, 131, Article 110559. <https://doi.org/10.1016/j.fct.2019.06.006>
- Leal, L. F., Miguel, O. G., Silva, R. Z., Yunes, R. A., Santos, A. S., & Miguel, O. G. (2005). Chemical composition of *Piper mikanianum* essential oil. *Journal of Essential Oil Research*, 17(3), 316-317. <https://doi.org/10.1080/10412905.2005.9698916>
- Lee, J. H., Cho, S., Paik, H. D., Choi, C. W., Nam, K. T., Hwang, S. G., & Kim, S. K. (2014). Investigation on antibacterial and antioxidant activities, phenolic and flavonoid contents of some Thai edible plants as an alternative for antibiotics. *Asian-Australasian Journal of Animal Sciences*, 27(10), 1461-1468. <https://doi.org/10.5713/ajas.2013.13629>

- Mahmood, Q., Bilal, M., & Jan, S. (2014). Herbicides, pesticides, and plant tolerance: An overview. *Emerging Technologies and Management of Crop Stress Tolerance, 1*, 423-448. <https://doi.org/10.1016/B978-0-12-800876-8.00017-5>
- Martins, R. C. C., Latorre, L. R., Sartorelli, P., & Kato, M. J. (2000). Phenylpropanoids and tetrahydrofuran lignans from *Piper solmsianum*. *Phytochemistry, 55*(7), 843-846. [https://doi.org/10.1016/S0031-9422\(00\)00295-8](https://doi.org/10.1016/S0031-9422(00)00295-8)
- Ministry of Health Malaysia. (2020). *Kenyataan Akhbar Ketua Pengarah Kesihatan Malaysia Situasi Semasa Demam Denggi, Zika dan Chikungunya Di Malaysia- ME 48 2020* [Press statement of the director general of health Malaysia: Current situation of Dengue Fever, Zika and Chikungunya in Malaysia- ME 48 2020]. Portal Rasmi Kementerian Kesihatan Malaysia.
- Mohiddin, A., Lasim, A. M., & Zuharah, W. F. (2016). Susceptibility of *Aedes albopictus* from dengue outbreak areas to temephos and *Bacillus thuringiensis* subsp. *israelensis*. *Asian Pacific Journal of Tropical Biomedicine, 6*(4), 295-300. <https://doi.org/10.1016/j.apjtb.2016.01.006>
- Perumalsamy, H., Kim, N. J., & Ahn, Y. J. (2009). Larvicidal activity of compounds isolated from *Asarum heterotropoides* against *Culex pipiens pallens*, *Aedes aegypti*, and *Ochlerotatus togoi* (Diptera: Culicidae). *Journal of Medical Entomology, 46*(6), 1420-1423. <https://doi.org/10.1603/033.046.0624>
- Qin, W., Huang, S., Li, C., Chen, S., & Peng, Z. (2010). Biological activity of the essential oil from the leaves of *Piper sarmentosum* Roxb. (Piperaceae) and its chemical constituents on *Brontispa longissima* (Gestro) (Coleoptera: Hispididae). *Pesticide Biochemistry and Physiology, 96*(3), 132-139. <https://doi.org/10.1016/J.PESTBP.2009.10.006>
- Rahman, S. F. S. A., Sijam, K., & Omar, D. (2014). Chemical composition of *Piper sarmentosum* extracts and antibacterial activity against the plant pathogenic bacteria *Pseudomonas fuscovaginae* and *Xanthomonas oryzae* pv. *oryzae*. *Journal of Plant Diseases and Protection, 121*(6), 237-242. <https://doi.org/10.1007/BF03356518>
- Reiter, P. (2001). Climate change and mosquito-borne disease. *Environmental Health Perspectives, 109*(1), 141-161. <https://doi.org/10.1289/ehp.01109s1141>
- Ribeiro, N., Camara, C., & Ramos, C. (2016). Toxicity of essential oils of *Piper marginatum* Jacq. against *Tetranychus urticae* Koch and *Neoseiulus Californicus* (McGregor). *Chilean Journal of Agricultural Research, 76*(1), 71-76. <https://doi.org/10.4067/S0718-58392016000100010>
- Sakthivadivel, M., & Thilagavathy, D. (2003). Larvicidal and chemosterilant activity of the acetone fraction of petroleum ether extract from *Argemone mexicana* L. seed. *Bioresource Technology, 89*(2), 213-216. [https://doi.org/10.1016/S0960-8524\(03\)00038-5](https://doi.org/10.1016/S0960-8524(03)00038-5)
- Salleh, W. M. N. H. W., Hashim, N. A., Ahmad, F., & Heng Yen, K. (2014). Anticholinesterase and antityrosinase activities of ten piper species from malaysia. *Advanced Pharmaceutical Bulletin, 4*(Suppl 2), 527-531. <https://doi.org/10.5681/apb.2014.078>
- Seo, S. M., Jung, C. S., Kang, J., Lee, H. R., Kim, S. W., Hyun, J., & Park, I. K. (2015). Larvicidal and acetylcholinesterase inhibitory activities of apiaceae plant essential oils and their constituents against *Aedes albopictus* and formulation development. *Journal of Agricultural and Food Chemistry, 63*(45), 9977-9986. <https://doi.org/10.1021/acs.jafc.5b03586>

- Shaalán, E. A. S., Canyon, D., Younes, M. W. F., Abdel-Wahab, H., & Mansour, A. H. (2005). A review of botanical phytochemicals with mosquitocidal potential. In *Environment International* (Vol. 31, Issue 8, pp. 1149-1166). Elsevier Ltd. <https://doi.org/10.1016/j.envint.2005.03.003>
- Srivastava, S., Gupta, M. M., Prajapati, V., Tripathi, A. K., & Kumar, S. (2001). Insecticidal activity of myristicin from *Piper mullesua*. *Pharmaceutical Biology*, 39(3), 226-229. <https://doi.org/10.1076/phbi.39.3.226.5933>
- Sukumar, K., Perich, M. J., & Boobar, L. R. (1991). Botanical derivatives in mosquito control: A review. *Journal of the American Mosquito Control Association*, 7(2), 210-237.
- Suratman, S., Edwards, J. W., & Babina, K. (2015). Organophosphate pesticides exposure among farmworkers: Pathways and risk of adverse health effects. *Reviews on Environmental Health*, 30(1), 65-79. <https://doi.org/10.1515/REVEH-2014-0072>
- Tuekaew, J., Siriwatanametanon, N., Wongkrajang, Y., Temsiririrkkul, R., & Jantan, I. (2014). Evaluation of the antioxidant activities of Ya-hom Intajak, a Thai herbal formulation, and its component plants. *Tropical Journal of Pharmaceutical Research*, 13(9), 1477-1485. <https://doi.org/10.4314/tjpr.v13i9.14>
- Uebel, T., Hermes, L., Hauptenthal, S., Müller, L., & Esselen, M. (2020). α -Asarone, β -asarone, and γ -asarone: Current status of toxicological evaluation. *Journal of Applied Toxicology*, 41(8), 1166-1179. <https://doi.org/10.1002/jat.4112>
- Ugusman, A., Zakaria, Z., Hui, C. K., Nordin, N. A. M. M., & Mahdy, Z. A. (2012). Flavonoids of *Piper sarmentosum* and its cytoprotective effects against oxidative stress. *EXCLI Journal*, 11, 705-714. <https://doi.org/10.17877/DE290R-10356>
- Vimaladevi, S., Mahesh, A., Dhayanithi, B., & Karthikeyan, N. (2012). Mosquito larvicidal efficacy of phenolic acids of seaweed *Chaetomorpha antennina* (Bory) Kuetz. against *Aedes aegypti*. *Biologia*, 67(1), 212-216. <https://doi.org/10.2478/s11756-011-0152-9>
- Wang, Y., Lv, L., Yu, Y., Yang, G., Xu, Z., Wang, Q., & Cai, L. (2017). Single and joint toxic effects of five selected pesticides on the early life stages of zebrafish (*Denio rerio*). *Chemosphere*, 170, 61-67. <https://doi.org/10.1016/j.chemosphere.2016.12.025>
- World Health Organization. (2005). *Guidelines for laboratory and field testing of mosquito larvicides*. World Health Organization.
- World Health Organization. (2021). *Dengue and severe dengue*. World Health Organization.
- Zaidan, U. H., Hamid, S. N. M., Yusof, M. F. M., Ahmad, S., Gani, S. S. A., & Shamsi, S. (2018). Chemical evaluation and antioxidant properties of extracts and essential oil from *Stevia rebaudiana* leaves. *Malaysia Applied Biology*, 47(2), 15-23.
- Zaidan, U. H., Zen, N. I. M., Amran, N. A., Shamsi, S., & Gani, S. S. A. (2019). Biochemical evaluation of phenolic compounds and steviol glycoside from *Stevia rebaudiana* extracts associated with in vitro antidiabetic potential. *Biocatalysis and Agricultural Biotechnology*, 18, Article 101049. <https://doi.org/10.1016/j.bcab.2019.101049>



The Estimation of Iron Oxide Content in Soil based on Landsat 8 OLI TIRS Imagery in Wetland Areas

Deasy Arisanty^{1*}, Aswin Nur Saputra¹, Akhmad Munaya Rahman¹,
Karunia Puji Hastuti¹ and Dedi Rosadi²

¹Department of Geography Education, Faculty of Teacher Training and Education, Lambung Mangkurat University, Brigjend H. Hasan Basry Street, 70123 Banjarmasin, Indonesia

²Department of Mathematics, Faculty of Mathematics and Natural Sciences, Gadjah Mada University, Sekip Utara, 55281 Yogyakarta, Indonesia

ABSTRACT

Wetland areas are volatile and have high iron content. In this study, through a remote sensing approach, especially using Landsat Operational Land Imager (OLI) and Thermal Infrared Sensor (TIRS) imagery, we discussed the method to estimate the presence of iron oxide in the wetlands of South Kalimantan in 2018, 2019, and 2020. Interpretation of the Landsat OLI TIRS was employed in April 2018, August 2018, February 2019, August 2019, March 2020, and August 2020. The band ratio method was used to determine the distribution of samples in this study. The results of the iron oxide index from the image were performed regression and correlation analysis with field measurement and laboratory test results to validate the oxide index values. The results showed that the iron oxide index value in the dry season was higher than in the rainy season. Iron oxide index value in open land was higher than in vegetation cover. The wetland was in dry condition during the dry season, making it easier to detect iron oxide values. Vegetation cover could reduce the iron oxide index value on the soil surface so that the iron oxide value was more easily identified in open land. The results of linear regression testing for the wet season sample

obtained a coefficient of determination $R^2 = 0.413$, while the results of linear regression testing for the dry season sample obtained a coefficient of determination $R^2 = 0.667$. Thus, the Landsat image has strong enough to estimate the iron oxide index in the wetland area of Kalimantan.

Keywords: Iron oxide, Landsat 8 OLI TIRS, wetland

ARTICLE INFO

Article history:

Received: 23 April 2021

Accepted: 28 July 2021

Published: 22 October 2021

DOI: <https://doi.org/10.47836/pjst.29.4.32>

E-mail addresses:

deasyarisanty@ulm.ac.id (Deasy Arisanty)

aswin.saputra@ulm.ac.id (Aswin Nur Saputra)

munaya.rahman@ulm.ac.id (Akhmad Munaya Rahman)

karunia.puji@ulm.ac.id (Karunia Puji Hastuti)

dedirosadi@ugm.ac.id (Dedi Rosadi)

* Corresponding author

INTRODUCTION

Natural wetlands play an essential role in increasing the total dissolved Fe concentration (Guan et al., 2020). Iron (Fe) oxide is the most common metal oxide found in the soil. The Fe oxide surface is mainly covered with complex organic compounds that determine its reactivity and retention to the ions dissolved in the soil (Xing & Niu, 2019). The reactivity of Fe is significantly increased in wetland soils (Davranche et al., 2013). Fe₂O₃ is formed by reacting oxygen in the atmosphere and the main Fe²⁺ mineral in the soil (Guo et al., 2020). The reduction and oxidation of iron in wetlands occur due to tidal fluctuations, especially in tidal swamps (Arisanty, 2017).

Data obtained through remote sensing can be used to investigate the components of the wetland ecosystem, one of which is soil data (Guo et al., 2017; Radeva et al., 2019; Sulaeman et al., 2020). Remote sensing allows identifying soil conditions by comparing the remote sensing data to the soil conditions in the field (Zhai, 2019). Remote sensing has been widely used for estimating soil characteristics based on sensors and different remote sensing techniques (Zribi et al., 2011). Soil data that can be identified through remote sensing is the iron content in the soil surface (Govil et al., 2018; Qing et al., 2019).

Landsat 8 OLI TIRS is a useful tool for researchers to collect research data (Ridwan et al., 2018). Landsat 8 OLI TIRS can be administered in soil mapping and is a crucial tool for soil observation, land planning, management, and precision agriculture (Meng et al., 2016; Silvero et al., 2021). Landsat imaging has been widely used in observing iron oxide content. The spectral response toward iron oxide content in the soil is the basis for estimating the distribution of iron oxide content used in estimating the iron oxide content in the Gunungsewu Karst area instead of using ALOS (Advanced Land Observing Satellite) AVNIR-2 (Advanced Visible and Near Infrared Radiometer type 2) (Nugroho & Purwanto, 2013). In addition to determining the distribution of iron oxide content in the soil, Landsat TM has been found effective in carrying out detections than ALOS AVNIR-2.

Landsat 8 OLI TIRS can be used to calculate the correlation between iron oxide content in the soil and the possibility of hydrothermal alteration (Aisabokhae & Oresajo, 2018; Putra et al., 2017). Red/blue band probes 6/7, 5/6 were performed to identify iron oxide minerals, clay minerals, carbonate minerals, and ferromagnesian (Pour & Hashim, 2015). The Landsat 8 OLI TIRS can determine the distribution of iron oxide and hydroxide minerals that dominate the alluvium and ophiolite rocky areas (Darmawan et al., 2020). The spectral reference, which involves thermal sensors, can also be used in iron oxide identification (Haq, 2017). The combination of band ratio and land surface temperature method results in sound accuracy in iron oxide identification. Landsat 8 image processing methods such as band combination, band ratio, and principal component analysis proved accurate for identifying iron oxides (Frutuoso et al., 2021). Landsat data can be used for preliminary mapping of iron oxide before detailed fieldwork and before selecting sampling sites (D'Arcy et al., 2018).

The iron oxide content in wetland areas can be analysed using remote sensing technology using Landsat 8 OLI TIRS. Landsat 8 OLI TIRS offers an easier way to identify the iron oxide content in the soil. The spectral value in the image can determine the iron oxide value in wetlands (Demattê et al., 2017). Iron oxide research using remote sensing is mostly carried out in dryland with low vegetation cover and mining areas. In contrast, in wetlands, especially in the Kalimantan area, it is still limited. Wetlands in the Kalimantan region have high vegetation cover and a significant seasonal effect on the land. Landsat imagery is easily accessible, available in a short time, temporal support, and the combination of band ratio can detect multi-temporal iron oxide, so this study uses Landsat 8 OLI TIRS imagery. This study estimated iron oxide content in wetlands in two seasons (dry and rainy) and different vegetation cover conditions (open and vegetated). Thus, the use of this image can be identified in seasonal variations and variations in vegetation cover conditions. This study aims to estimate the presence of iron oxide in the wetlands of South Kalimantan in 2018, 2019, and 2020.

METHODS

Research Location

This research was conducted in Banjarbaru, South Kalimantan Province, Indonesia. Banjarbaru is located on 3°25'40"S-3°28'37"S and 114°41'22"E-114°54'25"E. Wetlands in South Kalimantan, as the research area, especially in Banjarbaru, are usually dry in the dry season and flooding in the rainy season (Arisanty et al., 2019; Arisanty et al., 2020). The map of the research location is presented in Figure 1.

Data

The Landsat 8 OLI TIRS data used was in 2018, 2019, and 2020. The selected satellite imagery was in April 2018 in the rainy season, August 2018 in the dry season, February 2019 in the rainy season, August 2019 in the dry season, and land fires occur, March 2020 in the wet season, and August 2020 in the dry season. The consideration in choosing this image is that the image condition is relatively clear from cloud cover because Kalimantan is often covered by clouds, especially during the rainy season. The study site is usually dry in the dry season and inundated in the rainy season. Therefore, two different conditions caused the image used to predict iron oxide also in two seasons. The description of the dataset is presented in Table 1. The research location is presented in Figure 2.

The number of samples taken in this study was 12 samples. Samples were taken randomly to represent open land and vegetation coverage. Sample 1-4 illustrate the value of iron oxide on open land, while samples 5-12 are the iron oxide values in the vegetation-covered sample. The results of the oxide index were performed correlation and regression

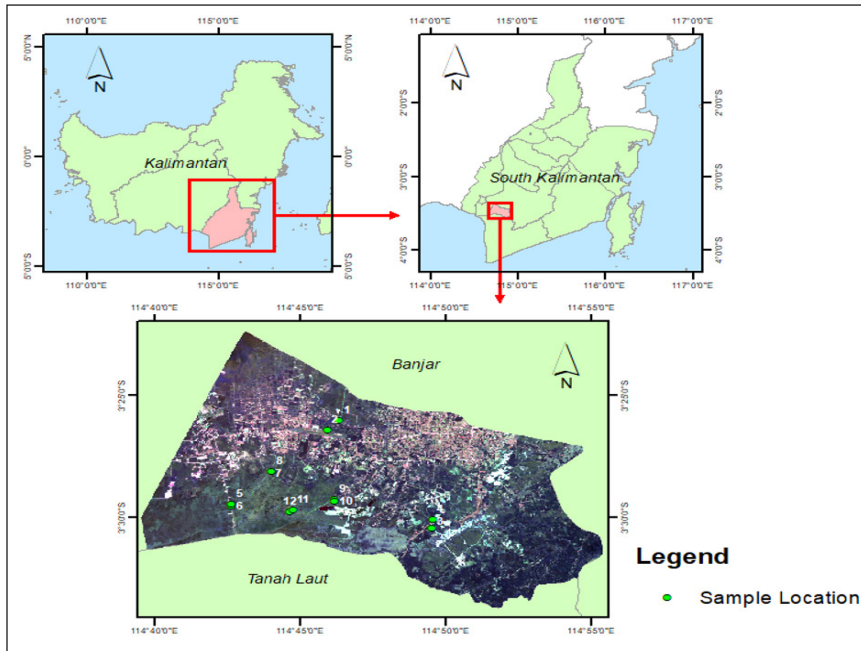


Figure 1. Map of research location in Banjarbaru

Table 1
The Description of the dataset

Acquisition time	Satellite	Sensor	Sources
2018.04.30	Landsat 8	OLI/TIRS	USGS
2018.08.20	Landsat 8	OLI/TIRS	USGS
2019.02.28	Landsat 8	OLI/TIRS	USGS
2019.08.23	Landsat 8	OLI/TIRS	USGS
2020.03.02	Landsat 8	OLI/TIRS	USGS
2020.08.09	Landsat 8	OLI/TIRS	USGS

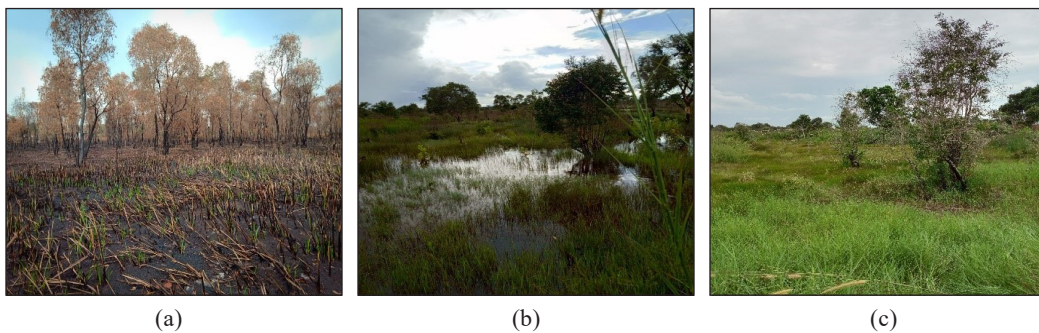


Figure 2. Research location: (a) August 2018 (Dry season); (b) February 2019 (Rainy season); and (c) August 2020 (Dry season).

analysis with field measurement and laboratory test results to validate the oxide index values. The field sampling uses the hand bore to collect the soil sample. Analysis of Fe content using analysis of Ammonium Acetate (NH₄OAc) extract.

Imaging Correction

The imaging correction process allows images to be refined before use. This correction improves image quality. The most common correction is a radiometric correction. The 1T level data had been corrected geometrically and automatically, while atmospheric disturbances had been removed. The conversion was carried out based on an algorithm proposed by the United States Geological Survey (USGS) (Ihlen, 2019) using the Envi 4.5 software.

The algorithm used to convert the DN image into a reflectance value is presented as Equation 1:

$$\rho_{\lambda}' = M_{\rho} * Q_{cal} + A_{\rho} \quad (1)$$

Remarks:

ρ_{λ}' = Spectral reflectance, without concerning the sun angle

M_{ρ} = Multiplicative reflectance-related factors in every band (REFLECTANCE_MULT_BAND_n on metadata)

A_{ρ} = Additive reflectance-related factors in every band (REFLECTANCE_ADD_BAND_n on metadata)

Q_{cal} = Image pixel score (DN)

After the image pixel score was converted into a reflectance value, solar angle correction was performed based on the equation proposed by USGS as Equation 2.

$$\rho_{\lambda} = \frac{\rho_{\lambda}'}{\sin(\theta)} \quad (2)$$

Remarks:

ρ_{λ} = Reflectant score after solar angle correction

θ = Sun elevation angle (SUN_ELEVATION from metadata)

The relative atmospheric correction using the dark object subtraction (DOS) method was then performed to produce an image with a surface reflectance value using ENVI 4.5 software (Kamal et al., 2012).

Data Extraction Process

In the data extraction stage, the information of remote sensing images was collected. Data extraction was carried out through digital image processing using spectral transformation in

the band ratio method. In addition, the band ratio method employed an algorithm proposed in previous research, arranged, and used as a research mapping unit. The band ratio method determined the distribution of the samples of this study.

Strong reflection in the red spectrum, as opposed to strong absorption in the blue spectrum, should be highlighted concerning iron fraction minerals using the following ratio index (Equation 3).

$$\text{Iron Oxidation} = \frac{BV_{red}}{BV_{blue}} \quad (3)$$

Given that both the red and blue bands were subject to interference in the form of scatters in the atmosphere, where the minimum value that supposed to be zero become > 0 , the following formula for the iron fraction index was used (Equation 4) (Liu & Mason, 2009):

$$\text{Iron Oxidation Index} = \frac{BV_{red} - \min(BV_{red})}{BV_{blue} - \min(BV_{blue})} \quad (4)$$

RESULTS

The Estimation of Iron Oxide Content at Different Seasons

Table 2 and Figure 3 show the iron oxide content in 2018, 2019, and 2020. The mean value of the iron oxide index on April 30, 2018, was 0.980, and the iron oxide index on August 20, 2018, was 1.072. On February 28, 2019, the iron oxide index value was 0.952, and the iron oxide index value on August 23, 2019, was 1.012. On March 02, 2020, the iron oxide index value was 0.953, and on August 09, 2020, the iron oxide index value was 0.977. Based on the data, identifying iron oxide levels is better done in the dry season than in the rainy season because the iron oxide index value is high. In the rainy season, the land is inundated, while in the dry season, the land is dry. Therefore, iron oxide values are more predictable in the dry season in wetland areas than in a rainy season based on index value due to the value of iron oxide in dry season more than rainy season.

The image in the dry season is clearer from cloud cover than the image in the rainy season. The Kalimantan region is on the equator so that the cloud cover is very thick during the rainy season. The cloud masking process affects the iron oxide index value, which is difficult to remove, especially thin clouds. Analysis of iron oxide should be able to use images of the month entering the dry season. The clarity of the image coverage from the cloud cover also affected the image collection within a specific time. It was challenging to obtain clear image coverage without being influenced by the vast cloud cover at the beginning of the rainy season. The rainy season usually takes place from October to March.

Corrections are applied in the image to the surface reflectance level to interpret better the appearance of object values on the earth's surface. The corrected image is then subjected

Table 2
Iron oxide index value

No	Coordinate		Iron Oxide Index											
	X	Y	30-April-18		20-Aug-18		28-Feb-19		23-Aug-19		2-March-20		09-Aug-20	
			Wet Season	Dry Season	Wet Season	Dry Season	Wet Season	Dry Season	Wet Season	Dry Season	Wet Season	Dry Season	Wet Season	Dry Season
1	252501.147	9620134.782	1.195	1.530	1.181	1.277	1.200	1.254	1.181	1.279	1.245	1.188	1.101	1.101
2	251710.588	9619459.677	1.291	1.420	1.279	1.245	1.176	1.555	1.166	1.312	1.176	1.208	1.660	1.660
3	258442.151	9612049.356	1.063	1.369	1.166	1.312	0.829	0.729	1.242	0.852	0.829	0.814	0.723	0.723
4	258455.388	9612673.802	1.346	1.420	1.217	1.242	0.865	0.865	0.808	0.852	0.829	0.814	0.723	0.723
5	245603.062	9613802.556	0.819	0.865	0.808	0.852	0.864	0.864	0.814	0.845	0.814	0.866	0.788	0.788
6	245632.264	9613699.203	0.808	0.864	0.814	0.845	0.902	0.902	0.842	0.910	0.866	0.845	0.791	0.791
7	248142.707	9616326.060	0.853	0.902	0.842	0.910	0.897	0.897	0.823	0.907	0.845	0.826	0.703	0.703
8	248157.958	9616292.580	0.876	0.897	0.823	0.907	0.881	0.881	0.812	0.857	0.826	0.854	0.758	0.758
9	252220.058	9614166.764	0.863	0.881	0.812	0.857	0.946	0.946	0.859	0.875	0.854	0.821	0.830	0.830
10	252192.490	9614080.733	0.946	0.878	0.859	0.875	0.901	0.901	0.820	0.891	0.821	0.809	0.832	0.832
11	249546.925	9613385.539	0.856	0.901	0.820	0.891	0.940	0.940	0.800	0.926	0.809	0.832	0.832	0.832
12	249345.091	9613270.896	0.836	0.940	0.800	0.926	1.072	1.072	0.952	1.012	0.953	0.977	0.977	0.977
Mean			0.980	1.072	0.952	1.012	0.953	0.977	0.952	1.012	0.953	0.977	0.977	0.977

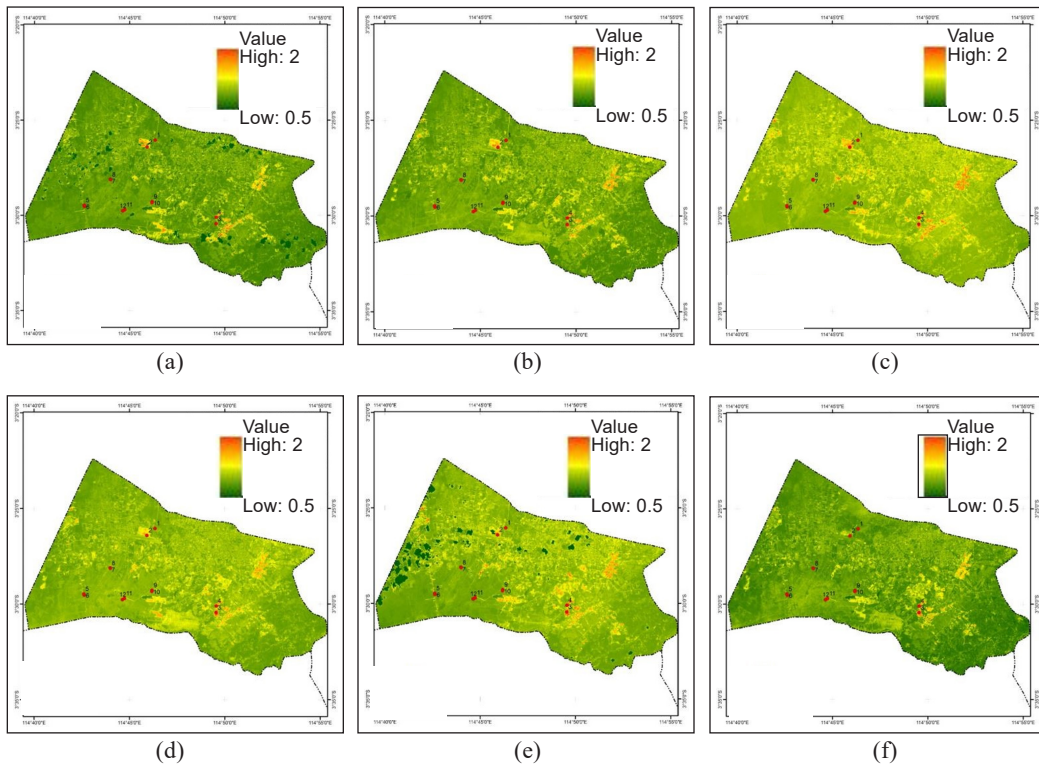


Figure 3. Iron oxide content map.: (a) April 30, 2018; (b) August 20, 2018; (c) February 28, 2019; (d) August 23, 2019, (e) March 2, 2020; (f) August 09, 2020

to spectral transformation using iron oxide index to highlight further the appearance of an iron oxide content on the soil surface.

The Estimation of Iron Oxide Content based on Vegetation-Covered Condition

The value of iron oxide on open land was higher than the value of iron oxide on land covered with vegetation. In Table 2, samples 1-4 illustrate the iron oxide value on open land, while samples 5-12 are the iron oxide values in the vegetation-covered sample. The value of iron oxide on the open land is more than 1, while on the land covered with vegetation, the value is less than 1.

The vegetation cover on the soil surface also influences the detection of soil oxide content. Based on the observations of the band material, the index value of the oxide content is influenced by the vegetation cover in the area. Most high index values were mainly found in extremely low vegetation cover areas and those with no vegetation cover. The high vegetation cover will block the electromagnetic waves from touching the ground. If the waves reach the bottom, it will not be easy to reflect electromagnetic waves through the vegetation cover. Therefore, the vegetation cover has an effect on the value of iron oxide

in the soil. In open land, iron content is more exposed than vegetated land. Moreover, the image interpretation value and the value of the iron content test in open land are higher than vegetation covered. Figures 4 and 5 describe the comparison of iron oxide values in various seasons and vegetation cover.

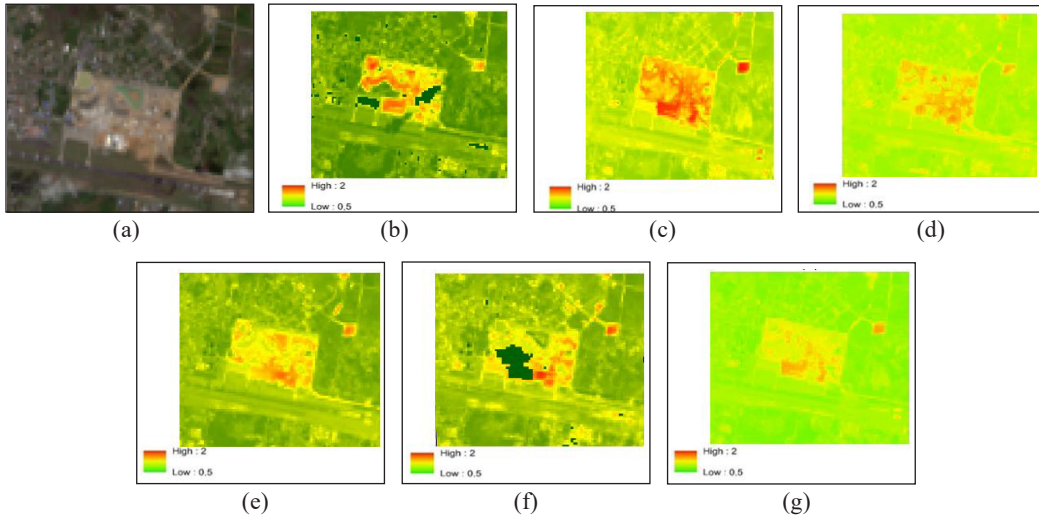


Figure 4. (a) Database Arcmap images; (b) Iron oxide transformation images on April 30, 2018; (c) Iron oxide transformation images on August 20, 2018; (d) Iron oxide transformation images on February 28, 2019; (e) Iron oxide transformation images on August 23, 2019; (f) Iron oxide transformation images on March 02, 2020; (g) Iron oxide transformation images on August 9, 2020. Comparison between the effects of open land and vegetated land on the spectral transformation of iron oxides.

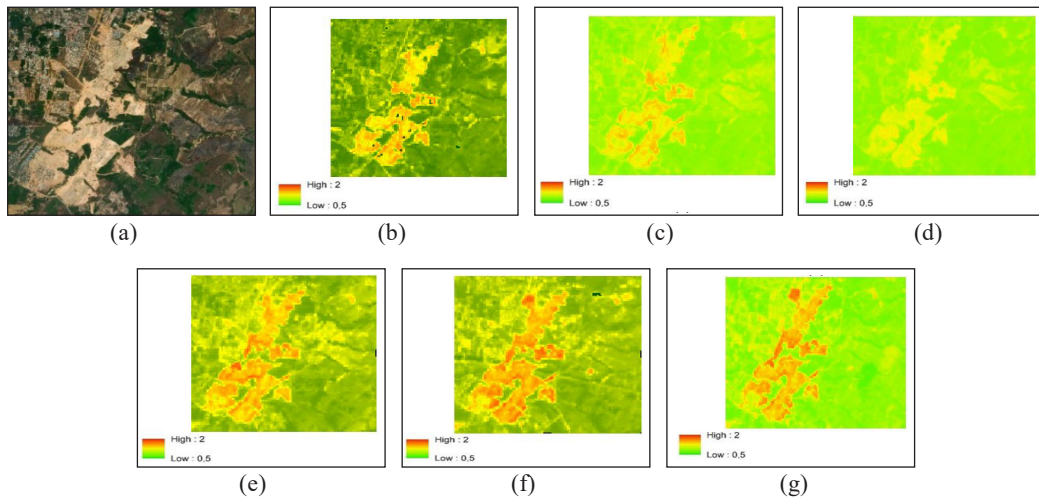


Figure 5. (a) Image true colour composite; (b) Iron oxide transformation images on April 30, 2018; (c) Iron oxide transformation images on August 20, 2018; (d) Iron oxide transformation images on February 28, 2019; (e) Iron oxide transformation images on August 23, 2019; (f) Iron oxide transformation images on March 02, 2020; (g) Iron oxide transformation images on August 9, 2020. Comparison between the effects of open land and vegetated land on the spectral transformation of iron oxides.

As shown in Figures 4 and 5, the land cover in open land detected iron oxide content in the soil easier, the season when the coverage for the images was very influential on changes in the index value. Figures 4 and 5 illustrate the land covered in August, which coincided with the dry season (Figures 4c, 4e, 4g, 5c, 5e, & 5g), in which the iron oxide was more clearly seen in open land areas with no vegetation cover. As a result, the colour of the open land becomes yellow-red, which indicates a high index value. Meanwhile, on vegetated land, the colour is green, which indicates a lower index value. In addition, the coverage image during the rainy season (Figures 4b, 4d, 4f, 5b, 5d, & 5f) was correlated to the lower index value compared to the other images in the dry season. Based on those insights, it is highly recommended to conduct studies on iron oxide content through images during the dry season and open land. However, several factors should be considered in detecting the iron oxide content in the soil.

The Validation of Iron Oxide Index Value

The results of regression and correlation analysis were carried out on the samples from the iron content test. The samples tested were field samples in February 2019 and in August 2020. The data are tested for regression and correlation with the Landsat 8 image coverage in February 2019 and in August 2020. The Landsat 8 image was previously carried out by a spectral transformation process using the iron oxide index to highlight the appearance of iron oxide on the soil surface. The validation of the iron oxide index is presented in Table 3.

The results of linear regression testing for the February 2019 sample obtained a coefficient of determination $R^2 = 0.413$ with a correlation of $r = 0.565$ and P-value 0.0178.

Table 3

The validation of the iron oxide index

No.	February 2019 (Wet season)		August 2020 (Dry season)	
	Field Survey (ppm)	Images	Field Survey (ppm)	Images
1	2200.74	1.181	6394.23	1.254
2	105.36	1.279	3822.12	1.101
3	150.11	1.166	2826.92	1.555
4	2200.74	1.217	1971.15	1.660
5	265.45	0.808	1793.27	0.729
6	305.89	0.814	1514.42	0.723
7	332.53	0.842	1471.15	0.788
8	344.78	0.823	1250.00	0.791
9	30.39	0.812	967.31	0.703
10	105.36	0.859	279.81	0.758
11	150.11	0.820	231.73	0.830
12	30.39	0.800	153.37	0.832

Source: Laboratory test and interpretation Landsat 8 OLI TIRS (2021); (Arisanty et al., 2020)

The P-value $< \alpha$, $0.0178 < 0.05$, means that image interpretation results can be used to predict the value of iron oxide in the wet season. The results of linear regression testing for the August 2020 sample obtained a coefficient of determination $R^2 = 0.667$ with a correlation of $r = 0.530$ and P-value 0.00066 . The P-value $< \alpha$, $0.00066 < 0.05$, means that the image interpretation results can be used to predict the value of iron oxide in the dry season. The regression value of iron oxide content is presented in Table 4.

Based on the test results, the sample in February 2019 and August 2020 has a strong enough influence and relationship with the image of the iron oxide index. It shows that the Landsat 8 image with the iron oxide index spectral transformation process can match the iron oxide content test results, especially the image in the dry season. Some things that must be considered in applying the image are the condition of cloud cover during image coverage, especially when entering the rainy season. In addition, the level of vegetation cover when determining the sample needs to be considered so as not to obstruct the monitoring of the iron oxide content found on the soil surface.

Table 4
Regression value of iron oxide content

Regression Statistics (February 2019/Wet Season)		Regression Statistics (August 2020/Dry Season)	
Multiple R	0.642	Multiple R	0.816
R Square	0.413	R Square	0.667
Adjusted R Square	0.322	Adjusted R Square	0.575
Standard Error	0.775	Standard Error	0.620
Observations	12	Observations	12

DISCUSSIONS

Landsat 8 OLI TIRS image can detect erroneous mineral clusters, especially in seasonally dry areas (Rockwell, 2013). Therefore, field testing is necessary to improve detection quality. Nonetheless, Landsat 8 OLI TIRS images showed good performance for iron oxide exploration, even in crowded vegetation areas (Ducart et al., 2016; Zabloskii, 2019). Besides, the Landsat 8 OLI TIRS is highly useful for low-cost mapping purposes and use in remote areas (Traore et al., 2020).

The reflection of electromagnetic waves was the basis for oxide content detection in the soil. On the surface, soil surfaces containing oxides will show higher reflection values in the blue band (400 nm to 500 nm) and the red band (600 nm to 700 nm). Therefore, during the field checks, metal roofs were detected to have a high index value in the transformed image. Hence, it is necessary to further study the image transformation results from open land to be used as the basis for the determination of correlation between index value and the soil oxide content.

The variation in the value of the spectral response shown in the open ground is also possible due to moisture content, organic matter, and particle size (Cardoso et al., 2014). Other vital variables are organic carbon content, particle size, and mineralogical composition (Demattê et al., 2017). The use of band 4 (600 nm to 700 nm) and band 2 (400 nm to 500 nm) appears to be quite effective in identifying iron oxide content in open ground.

Iron oxide and vegetation have a similar reflection spectrum in the wavelength region of bands 1 and 2 in the Landsat 8 OLI TIRS image and a slight difference in band 3. The peak values of vegetation have similar values to goethite minerals in band 3 (Traore et al., 2020). In contrast, in band 3, the reflectance value of hematite minerals was lower than that of goethite and vegetation. Therefore, the three bands are not suitable for identifying iron oxide with high vegetation cover in the land. Band 4 in the Landsat 8 OLI TIRS image, iron oxide and clay minerals have high reflectance and, conversely, chlorophyll from green plants absorbs intense radiation at red wavelengths (band 4). Moist vegetation has more radiation absorption in band 7, and high reflectance by plant tissues at near-infrared wavelengths (band 5). In the spectral scope of band 5 in the Landsat 8 OLI image, the dominant iron oxide shows more radiation absorption. The high value in the 4/2 band ratio helps detect the absorption of radiation values for iron oxide in the blue wavelength range. The band 4 and band 2 band ratios provide greater sensitivity to iron content even in low concentrations. However, the high value of this band ratio only highlights the iron oxide associated with the mafic regolith layer, not including the higher quality iron ore content (Ducart et al., 2016).

Mapping of this iron oxide both in open areas and under vegetation cover plays a crucial role. The role of iron oxide mapping can estimate the iron oxide deposits in the wetlands. Landsat utilisation for iron oxide estimation in wetlands has the highest R^2 value (Guo et al., 2020). Spectrum values can identify wetland soil pedogenetic associated with variations in iron oxide (Demattê et al., 2017). The method can be an alternative for mineral mapping, saving costs, risks, and time. Spatial information determines the quality of data in a study. Spatial data can make it easier to research at a low cost (Rozpondek et al., 2016).

CONCLUSIONS

The iron oxide index value in wetlands can be estimated using Landsat OLI TIRS imagery. The results of this study have proven that this image can estimate the value of iron oxide in the wetlands. Estimation of iron oxide in wetland is better done in the dry season image because the land is in dry condition, and cloud cover can affect the value of the iron oxide index. Besides, areas covered with vegetation also have a lower value than open land, so it is better to identify them on open land than under vegetation cover. The recommendation is to use this Landsat OLI TIRS with different land conditions and with various land covers to determine the ability of Landsat OLI TIRS imagery to estimate the iron oxide under multiple conditions.

ACKNOWLEDGMENTS

This research is funded by Lambung Mangkurat University, Research Grand Number 212.38/UN8.2/PL/2020.

REFERENCES

- Aisabokhae, J. E., & Oresajo, S. B. (2018). Supervised classification of Landsat-8 band ratio images for geological interpretation of Sokoto, Nigeria. *South African Journal of Geomatics*, 7(3), 360-371.
- Arisanty, D. (2017). The influence of tide on suspended sediment transport in barito delta, Southern Kalimantan, Indonesia. *Ecology, Environment and Conservation*, 23(2), 696-703.
- Arisanty, D., Adyatma, S., Muhaimin, M., & Nursaputra, A. (2019). Landsat 8 OLI TIRS imagery ability for monitoring post forest fire changes. *Pertanika Journal of Science & Technology*, 27(3), 1105-1120.
- Arisanty, D., Jędrasiak, K., Rajiani, I., & Grabara, J. (2020). The destructive impact of burned peatlands to physical and chemical properties of soil. *Acta Montanistica Slovaca*, 25(2), 213-223. <https://doi.org/10.46544/AMS.v25i2.8>
- Cardoso, G. F., Souza, C., & Souza-Filho, P. W. M. (2014). Using spectral analysis of Landsat-5 TM images to map coastal wetlands in the Amazon River mouth, Brazil. *Wetlands Ecology and Management*, 22(1), 79-92. <https://doi.org/10.1007/s11273-013-9324-4>
- D'Arcy, M., Mason, P. J., Roda-Boluda, D. C., Whittaker, A. C., Lewis, J. M. T., & Najorka, J. (2018). Alluvial fan surface ages recorded by Landsat-8 imagery in Owens Valley, California. *Remote Sensing of Environment*, 216, 401-414. <https://doi.org/10.1016/j.rse.2018.07.013>
- Darmawan, I. G. B., Yassar, M. F., Elvarani, A. Y., Vira, B. A., & Damayanti, L. (2020). Preliminary study of mining material prospects based on hydrothermal alteration distribution using composite and density slicing of Landsat 8 image in Ulubongka Regency, Central Sulawesi. *PROMINE*, 8(1), 1-7. <https://doi.org/10.33019/promine.v8i1.1799>
- Davranche, M., Dia, A., Fakhri, M., Nowack, B., Gruau, G., Ona-nguema, G., Petitjean, P., Martin, S., & Hochreutener, R. (2013). Organic matter control on the reactivity of Fe (III)-oxyhydroxides and associated As in wetland soils: A kinetic modeling study. *Chemical Geology*, 335, 24-35. <https://doi.org/10.1016/j.chemgeo.2012.10.040>
- Demattê, J. A. M., Horák-Terra, I., Beirigo, R. M., da Silva Terra, F., Marques, K. P. P., Fongaro, C. T., Silva, A. C., & Vidal-Torrado, P. (2017). Genesis and properties of wetland soils by VIS-NIR-SWIR as a technique for environmental monitoring. *Journal of Environmental Management*, 197, 50-62. <https://doi.org/10.1016/j.jenvman.2017.03.014>
- Ducart, D. F., Silva, A. M., Toledo, C. L. B., & de Assis, L. M. (2016). Mapping iron oxides with Landsat-8/OLI and EO-1/Hyperion imagery from the Serra Norte iron deposits in the Carajás Mineral Province, Brazil. *Brazilian Journal of Geology*, 46(3), 331-349. <https://doi.org/10.1590/2317-4889201620160023>
- Frutuoso, R., Lima, A., & Teodoro, A. C. (2021). Application of remote sensing data in gold exploration: Targeting hydrothermal alteration using Landsat 8 imagery in northern Portugal. *Arabian Journal of Geosciences*, 14(6), 1-18. <https://doi.org/10.14419/ijbas.v3i3.2821>

- Govil, H., Tripathi, M. K., Diwan, P., & Guha, S. (2018). Identification of iron oxides minerals in Western Jahajpur Region, India using aviris-ng hyperspectral remote sensing. *International Archives of the Photogrammetry, Remote Sensing & Spatial Information Sciences*, 43(5), 233237. <https://doi.org/10.5194/isprs-archives-XLII-5-233-2018>
- Guan, J., Qi, K., Wang, J., Zhuang, J., Yuan, X., Yan, B., Lu, N., & Qu, J. (2020). Effects of conversion from boreal natural wetlands to rice paddy fields on the dynamics of total dissolved iron during extreme precipitation events. *Chemosphere*, 242, Article 125153. <https://doi.org/10.1016/j.chemosphere.2019.125153>
- Guo, B., Zang, W., Luo, W., Wen, Y., Yang, F., Han, B., Fan, Y., Chen, X., Qi, Z., & Wang, Z. (2020). Detection model of soil salinization information in the Yellow River Delta based on feature space models with typical surface parameters derived from Landsat 8 OLI image. *Geomatics, Natural Hazards and Risk*, 11(1), 288-300. <https://doi.org/10.1080/19475705.2020.1721573>
- Guo, M., Li, J., Sheng, C., Xu, J., & Wu, L. (2017). A review of wetland remote sensing. *Sensors*, 17(4), Article 777. <https://doi.org/10.3390/s17040777>
- Haq, M. A. (2017). Analysis of land surface temperature, distribution of clay minerals and fault fracture density using Landsat 8 imagery in the Dieng geothermal system and its surroundings, Central Java Province, Indonesia (Doctoral dissertation). Faculty of Engineering, Diponegoro University, Semarang, Indonesia.
- Ihlen, V. (2019). Landsat 8 data users handbook. U.S. Geological Survey. USGS Publication.
- Kamal, M., Adi, N. S., & Arjasakusuma, S. (2012). Jaz EL-350 VIS NIR portable spectrometer: Panduan operasional pengukuran dan pengelolaan data pantulan spektral obyek (Versi 1 2012) [Jaz EL-350 VIS NIR portable spectrometer: Operational guide for spectral object data measuring and managing (Version 1/2012)]. Universitas Gadjah Mada.
- Liu, J. G., & Mason, P. J. (2009). *Essential image processing and GIS for remote sensing* (1st Edit). Wiley Online Library. <https://doi.org/10.1002/9781118687963>
- Meng, L., Zhou, S., Zhang, H., & Bi, X. (2016). Estimating soil salinity in different landscapes of the Yellow River Delta through Landsat OLI/TIRS and ETM+ Data. *Journal of Coastal Conservation*, 20(4), 271-279. <https://doi.org/10.1007/s11852-016-0437-9>
- Nugroho, Y. A., & Purwanto, T. H. (2013). Study of estimation iron oxide content using mutispectral medium resolution imagery. *Jurnal Bumi Indonesia*, 2(3), 117-126.
- Pour, A. B., & Hashim, M. (2015). Hydrothermal alteration mapping from Landsat-8 data, Sar Cheshmeh copper mining district, south-eastern Islamic Republic of Iran. *Journal of Taibah University for Science*, 9(2), 155-166. <https://doi.org/10.1016/j.jtusci.2014.11.008>
- Putra, I. D., Nasution, R. A. F., & Harijoko, A. (2017). Aplikasi Landsat 8 OLI/TIRS dalam mengidentifikasi alterasi hidrotermal skala regional: studi kasus Daerah Rejang Lebong dan sekitarnya, Provinsi Bengkulu [Landsat 8 OLI/TIRS application in identifying regional scale hydrothermal alterations: A case study]. *Proseding Seminar Nasional Kebumian*, 10, 1812-1826.
- Qing, K., Zhao, Y. J., & Cui, X. (2019). Research on information extraction technology of iron oxide based on airborne hyperspectral data. In *IGARSS 2019-2019 IEEE International Geoscience and Remote Sensing Symposium* (pp. 6764-6767). IEEE Publishing. <https://doi.org/10.1109/IGARSS.2019.8900647>

- Radeva, K., Velizarova, E., & Dancheva, A. (2019). Land cover monitoring as part of a survey on wetland ecosystem conservation in the Negovan village area using remote sensing tools. *Glasnik Sumarskog Fakulteta*, 119, 175-188. <https://doi.org/10.2298/GSF1919175R>
- Ridwan, M. A., Radzi, N. A. M., Ahmad, W., Mustafa, I. S., Din, N. M., Jalil, Y. E., Isa, A. M., Othman, N. S., & Zaki, W. (2018). Applications of landsat-8 data: A Survey. *International Journal of Engineering & Technology*, 7(4), 436-441. <https://doi.org/10.14419/ijet.v7i4.35.22858>
- Rockwell, B. W. (2013). Automated mapping of mineral groups and green vegetation from Landsat Thematic Mapper imagery with an example from the San Juan Mountains, Colorado. US Geological Survey Scientific Investigations Map.
- Rozpondek, R., Wancisiewicz, K., & Kacprzak, M. (2016). GIS in the studies of soil and water environment. *Journal of Ecological Engineering*, 17(3), 134-142. <https://doi.org/10.12911/22998993/63476>
- Silvero, N. E. Q., Demattê, J. A. M., Amorim, M. T. A., dos Santos, N. V., Rizzo, R., Safaneli, J. L., Poppiel, R. R., de Sousa Mendes, W., & Bonfatti, B. R. (2021). Soil variability and quantification based on Sentinel-2 and Landsat-8 bare soil images: A comparison. *Remote Sensing of Environment*, 252, Article 112117. <https://doi.org/10.1016/j.rse.2020.112117>
- Sulaeman, Y., Poggio, L., Minasny, B., & Nursyamsi, D. (2020). Tropical wetlands-innovation in mapping and management. *International Workshop on Tropical Wetlands: Innovation in Mapping and Management*, 2018, Article 197. <https://doi.org/10.1201/9780429264467>
- Traore, M., Wambo, J. D. T., Ndepete, C. P., Tekin, S., Pour, A. B., & Muslim, A. M. (2020). Lithological and alteration mineral mapping for alluvial gold exploration in the south east of Birao area, Central African Republic using Landsat-8 Operational Land Imager (OLI) data. *Journal of African Earth Sciences*, 170, Article 103933. <https://doi.org/10.1016/j.jafrearsci.2020.103933>
- Xing, L., & Niu, Z. (2019). Mapping and analyzing China's wetlands using MODIS time series data. *Wetlands Ecology and Management*, 27(5), 693-710. <https://doi.org/10.1007/s11273-019-09687-y>
- Zabloskii, V. R. (2019). The method of detection of clay minerals and iron oxide based on landsat multispectral images (as exemplified in the Territory of Thai Nguyen Province, Vietnam). *Mining Science and Technology*, 4(1), 65-75. <https://doi.org/10.17073/2500-0632-2019-1-65-75>
- Zhai, M. (2019). Inversion of organic matter content in wetland soil based on Landsat 8 remote sensing image. *Journal of Visual Communication and Image Representation*, 64, Article 102645. <https://doi.org/10.1016/j.jvcir.2019.102645>
- Zribi, M., Baghdadi, N., & Nolin, M. (2011). Remote Sensing of Soil. *Applied and Environmental Soil Science*, 2011, 1-2. <https://doi.org/10.1155/2011/904561>



Mathematical Modelling of Infra-Red Evaporation Characteristics of Wheat Straw Black Liquor

Surendra Pratap Singh¹, Mohammad Jawaid^{2*}, Bhoomika Yadav³ and Mohd Supian Abu Bakar²

¹*Pulp & Paper Research Institute, Rayagada, Odisha, 765001, India*

²*Laboratory of Biocomposite Technology, Institute of Tropical Forestry and Forest Products (INTROP) Universiti Putra Malaysia, 43400 UPM, Serdang, Selangor, Malaysia*

³*Department of Material Science and Metallurgical Engineering, University Institute of Engineering and Technology, CSJM University, Kanpur, 208024, India*

ABSTRACT

Infrared (IR) evaporation characteristics of Weak Soda Black Liquor (WSBL) were determined at five different temperatures of 80, 90, 100, 110 and 120°C. The effect of constant temperature on evaporation rate and moisture content (on a dry basis) of 1.5 gm approx. WSBL tests were contemplated and required a careful time frame of IR dissipation to vanish the dampness content at a different consistent temperature. The dissipation rate expanded with expanding infrared temperature. Therefore, different numerical models, such as Page and Logarithmic, Henderson, Pabis and Lewis, were utilised to fit the experimental data properly. A Gaussian model equation was developed for evaporation rate and moisture fraction of black liquor. The probable empirical parameters, along with the relating of reduced chi-square (X^2), Residual Sum of Square (RSS), and coefficients of determination (adjusted R^2) from non-linear regression analysis of all the numerical model equations, were examined. In addition, the effect of evaporation temperature on the water removal rate, the effective diffusion coefficient and activation energy were also estimated. The effective diffusion coefficient ranges from 2.67×10^{-10} m²/s to 10.4×10^{-10} m²/s, and the activation energy was 39.19 kJ/mol. The statistical indicators (chi-square and determination coefficient) showed that the Decay model equation and Gaussian equation are the most suitable models for describing the evaporation process of WSBL.

ARTICLE INFO

Article history:

Received: 16 April 2021

Accepted: 28 July 2021

Published: 22 October 2021

DOI: <https://doi.org/10.47836/pjst.29.4.33>

E-mail addresses:

spinghbh@gmail.com (Surendra Pratap Singh)

jawaid@upm.edu.my (Mohammad Jawaid)

bhoomika@iitk.ac.in (Bhoomika Yadav)

supian7779@gmail.com (Mohd Supian Abu Bakar)

* Corresponding author

Keywords: Biomass, black liquor, evaporation, viscosity, wheat straw

INTRODUCTION

In the soda pulping process, the fibres are separated from the agricultural residue. Lignin, hemicelluloses, and low molecular weight carbohydrates are removed by agricultural pulping residue in the cooking chemical solution, which contains active chemicals and caustic soda at high temperature and pressure (approximately 165 to 170°C and 6 to 8 kg/cm²) in the digester. The digested material coming out from the blow tank contains both the spent cooking liquor and the fibres. The spent liquor of dark brownish colour is called black liquor (Do et al., 2020). The black liquor contains a mixture of inorganic chemicals (NaOH) and a large proportion of organic chemicals, mainly lignin (Alriols et al., 2009; Hurter, 1991). The weak black liquor normally has dry solids content of 14% to 18% (approximately) and is not suitable for direct use in the chemical recovery furnace as fuel (Bajpai, 2017). The main purpose of evaporation of black liquor is to increase the dry solids content by evaporating excess water until reaching a solids content that is suitable for burning in the chemical recovery furnace (Goodell & Point, 1933). Since there is probable danger of smelt explosions, the dry solids content of heavy black liquor (HBL) should be a minimum of 58%. Nowadays, the dry solids content of 70% to 75% is normal, and even 80% to 85% is the target value for the dry solids content with wood to increase the chemical recovery furnace thermal efficiency (Naqvi et al., 2010; Nasir et al., 2020; Low & Ong, 2020), with agricultural residues black liquor, is normally in the range of 60% to 65 %.

In conventional evaporation of black liquor displays two distinct stages of evaporation. The preliminary stage of the evaporation process is similar to the evaporation of water from the free surface. The evaporation rate is not dependent on the water content of the black liquor. This evaporation stage is known as the “Constant Rate Period (CRP)” in the evaporation of black liquor. However, through the removal of freely available water from black liquor, the evaporation rate decreases, then this stage of evaporation is known as the “Falling Rate Period (FRP)”. The water quantity removed during this interval is comparatively small compared to the initial stage and the time engaged was extensive. The longer time interval required during the falling rate period in conventional evaporation means excess consumption of energy (Mujumdar, 2007; Nasir et al., 2020). Generally, the usual evaporators used in the paper industry are falling film, rising film and forced circulation evaporators (Haghsheno & Kouhikamali, 2020).

Evaporation is a complex thermal process in which unsteady heat and moisture transfer co-occur. From an engineering point of view, it is better to understand this complex process's controlling parameters. Mathematical models of the drying processes are used to design new or improving existing evaporation systems or even control the evaporation process. The major disadvantages of these evaporators are the long evaporation time during the evaporation and low energy efficiency. In recent years, infra-red and microwave evaporation has gained attention as an optional evaporation/drying method in the food and

beverages industries (Darvishi et al., 2013; Datta & Anantheswaran, 2001; Hatibaruah et al., 2013; Sandu, 1986). However, there has been not much information available on infra-red evaporation characteristics of soda black liquor, which is a by-product of the agricultural residues-based pulp and paper industry. The infra-red heating process may extensively improve the evaporation quality of black liquor. Reducing energy consumption and period using infra-red in black liquor evaporation may significantly contribute to the pulp and paper industry. Thus, this present study aims to explore the influence of infra-red temperature levels on evaporation kinetics and establish an appropriate model for infra-red evaporation of weak soda black liquor. It is also helps to design an evaporator equipped with an infrared heating facility to enhance process and energy efficiency for the pulp and paper industry.

MATERIALS AND METHODS

Analysis of Black Liquor

From Table 1, the TAPPI methods (TAPPI, Atlanta, USA) and provisional methods have described the physico-chemical properties from black liquor, where the pH value and total dissolved solids in black liquor have been measured after constant weight condition has obtained at 24 hours preservation. The inorganic matter was shown at a combustion temperature of $525 \pm 3^\circ\text{C}$, while the organic matter was figured out as the distinction between

Table 1
Characterisation of soda black liquor

Particulars	Quantity	Test Methods
Chemical compositions		
pH at room temp.	11.9	-
Specific gravity/20°C	1.04	TAPPI T-625 CM-85
Total solids, %w/w	8.1	TAPPI T-625 CM-85
Residual Active Alkali, g/L as NaOH	7.32	TAPPI T-625 CM-85
Total alkali, g/L as NaOH	18.5	TAPPI T-625 CM-85
Silica, as SiO ₂ , % w/w	3.76	TAPPI T-625 CM-85
Inorganics, %w/w	32.35	TAPPI T211 om-93
Elemental composition		
Carbon, % w/w	30.1	CHNS Analyser (Instrumental method)
Hydrogen, %w/w	4.15	CHNS Analyser (Instrumental method)
Oxygen, %w/w	36.85	By difference
Nitrogen, %w/w	1.11	CHNS Analyser (Instrumental method)
Sodium, %w/w	19.5	AAS (Instrumental method)
Calcium, %w/w	3.46	AAS (Instrumental method)
Potassium, %w/w	3.08	AAS (Instrumental method)
CV (MJ/kg)	11.63	Bomb calorimeter

inorganic matter and total dissolved solids. Furthermore, the analyses of Carbon, Hydrogen, Nitrogen, and Sulphur (CHNS) was performed with CHNS analyser (Vario, Model: E III). The elemental analysis was performed by Atomic Absorption Spectra (AAS) (Perkin Elemer, Model: 800) after alkaline fusion by ASTM D368296. The calorific value analyses of oxygen content in the black liquor solids were determined using a bomb calorimeter (Toshniwal Technologies Pvt. Ltd., New Delhi, India). The characteristics of the soda black liquor sample are summarised in Table1.

Infrared Drying Experiments

Weak black liquor samples of 12 to 14% solids content used in the evaporation experiments were collected from M/S Mohit Paper Mills Ltd., Bijnor (U.P), India. An IR moisture analyser (Model no. XM-120, Precisa Gravimetrics AG, 8953 Dietikon, Switzerland) was used for the present study. The IR moisture analyser is equipped with the facility to adjust temperature levels at 90, 100, 110 and 120°C. The dimensions of the IR moisture analyser (Instrument housing, W×H×D mm) used for drying were 210 mm (W) × 340 mm (D) × 170mm (H).

The evaporation trial was carried out for a 1.2 gm (approx.) sample at four different infra-red temperature levels *viz.*, 90, 100, 110 and 120°C. During experiments, each sample was put on the stationary sample pan filled with 2mm sand to avoid skin formation during evaporation. The pan was placed in the centre of the moisture analyser. The XM-120 infra-red (IR) moisture analyser can be used for reliable and quick determination of the moisture content of liquid, semisolid and solid substances according to the thermo-gravimetry method. The moisture content of the black liquor sample was calculated according to the early moisture content and the mass loss during evaporation. The moisture loss was determined by thermo-gravimetric analysis of the sample at one-minute intervals. For better quality, evaporation was resumed until the moisture content of the black liquor sample concentrated to about 2.5 to 3%. The TAPPI standards obtained the moisture content of the completely dry black liquor samples. Experiments were carried out in triplicate to minimise the possible errors.

In the present investigation, a radiator is used as drying equipment to transmit electromagnetic radiation in short to medium frequency wave IR radiation (wavelength in the range of 2 to 3.5 nm, as specified in the

Table 2
The technical specification of the IR moisture analyser apparatus

Properties	Range
Power consumption max (VA)	470 VA
Frequency (Hz)	50 Hz
Temperature range/steps(°C)	30-230°C /1°C
Graduation	1 °C
Time switch (range)	240 min
Weighing range (g)	124 g
Smallest sample weight (g)	0.2 g
Pan Size [Ø mm]	100
Readability (g)	0.001g
Moisture Analysis Readability (%)	0.001

equipment manual). The technical specification of the IR moisture analyser apparatus (PRECISA, Series 330 XM - Model XM60, Switzerland) was displayed in Table 2.

Determination of Evaporation Rate and Diffusion Co-efficient

In the present investigation, the variables on the moisture fraction effect of black liquor and the evaporation rate were studied (Thakor et al., 1999). The moisture fraction (X) of black liquor samples was calculated using Equation 1.

$$x = \frac{M_t - M_e}{M_o - M_e} \approx \frac{M_t}{M_o} \quad (1)$$

Equation 1 x is the moisture fraction of black liquor and dimensionless term: the initial moisture content, M_o of the black liquor (gm water/gm solids content). Meanwhile, the moisture content of black liquor at any time (t), (gm water/gm solids content) was indicated as M_t and M_e are balanced in the moisture content of black liquor sample (gm water/g solids content). The value of M_e is negligible compared with M_t or M_o specifically for IR evaporation. Thus, M_e was neglected and is assumed as zero. The overall evaporation rate (ER) was characterised as the variation of moisture fraction in a unit time (t), using Equation 2.

$$ER = \frac{dx}{dt} \quad (2)$$

The general Gaussian model equation is given by Equation 3,

$$y = ER = \sum_{i=1}^n a_i e^{\left[-\left(\frac{x-b_i}{c_i}\right)^2\right]} \quad (3)$$

Where, a is the amplitude, b is the centroid (location), c is related to the peak width, n is the number of peaks to fit, and $1 \leq n \leq 8$ (Guo 2011).

The determination of effective diffusivity of the evaporation of weak black liquor has occurred in both the Constant Rate Period (CRP) and Falling Rate Period (FRP). Therefore, Fick's second law of diffusion displayed in Equation 4,

$$\frac{\partial x}{\partial t} = \nabla [D_{eff}(\nabla x)] \quad (4)$$

Subsequently, the internal mass transfer element has controlled the evaporation process. Therefore, Equation 4 defined the evaporation process and determined the experimental data during the Falling Rate Period (FRP). Assuming that the moisture migrates barely by diffusion and no shrinkage occurred. Therefore, the actual diffusion co-efficient is constant,

and the water evaporation is only from the free surface of the black liquor sample, then the empirical solution for the Ficks second law of diffusion can be described as Equation 5 (Crank, 1975),

$$X = \frac{8}{\pi^2} \sum_{n=0}^{\infty} \frac{1}{(2n+1)^2} \exp\left[-(2n+1)^2 \pi^2 \frac{D_{eff} t}{r^2}\right] \quad (5)$$

Where D_{eff} is moisture diffusivity (m^2/s), r is the average radius of the sand particles (m), and t is time (sec). Equation 6 could be additionally streamlined by taking the initial term of the arrangement as (Tütüncü & Labuza, 1996).

$$X = \frac{8}{\pi^2} \exp\left[-\pi^2 \frac{D_{eff} t}{r^2}\right] \quad (6)$$

Taking natural logarithm both sides, Equation 6 becomes Equation 7,

$$\ln(X) = \ln\left(\frac{8}{\pi^2}\right) - \left(\frac{\pi^2 D_{eff}}{4r^2} t\right) \quad (7)$$

The effective moisture diffusivity D_{eff} was analysed by plotting experiential evaporation data in $\ln(X)$ versus time (t). From Equation 7, a plot of $\ln(X)$ versus time (t) gives a straight line with a slope k_0 as Equation 8,

$$k_0 = \frac{\pi^2 D_{eff}}{4r^2} \quad (8)$$

In addition, the influence of temperature on effective diffusivity (D_{eff}) can be illustrated by Arrhenius Equation 9 (Madamba et al., 1996; Sanjuán et al., 2003),

$$D_{eff} = D_0 \exp\left(-\frac{E_a}{RT}\right) \quad (9)$$

Therefore, from Equation 9, E_a is activation energy (kJ/mol). Meanwhile, D_0 is the pre-exponential factor of the Arrhenius equation (m^2/s), R is the ideal gas constant (kJ/mol K), and T is the evaporation temperature (K). Further, the value E_a/R was obtained by plotting $\ln(D_{eff})$ versus the mutual of temperature ($1/T$).

Statistical and Mathematical Modelling of the Evaporation Curve

The experimental evaporation data were tested to find the most appropriate model among seven different models defining evaporation/drying process put forward by several authors. Furthermore, the seven mathematical model equations effectively utilised in other

exploration were utilised to assess the relationship between evaporation time (evaporation curve) and moisture fraction (X) of black liquor using a non-linear regression procedure (Table 3).

The test data in this present study was additionally fitted with other regression equations and has indicated a high degree of fitting at the non-linear regression method. The non-linear regression method, was constructed by the Levenberg–Marquardt (LM) algorithm, where it has extensively used algorithm in non-linear least square fitting. The Levenberg–Marquardt algorithm, starting with some initial parameter values, minimises RSS by presenting a series of repetitions on the parameter values and computing RSS at every stage. Therefore, to perform this method, the initial partial derivatives were analysed for all values of the input parameters (Ranganathan, 2004).

The coefficients were estimated using OriginPro 9 software (The OriginLab Corporation, USA) according to the non-linear least square method. The three parameters reduced chi-square (X^2), residual sum of square (RSS), and determination coefficient (R^2) were used to evaluate the deviation between the predicted values and the experimental data for the dependent variable. These can be used for comparing various models representing the same dependent variable. The fitness parameters among distinct models were performed at $p < 0.05$ of variance (ANOVA) analysis (Table 4). Thus, the best model used for defining the evaporation characteristics of black liquor samples under infra-red (IR) radiation heating was preferred with the lowest reduced data of chi-square (X^2), residual sum of square (RSS) and highest coefficient of the determinant (R^2) or adjusted R -squared (R^2_{adj}). The statistical values were calculated with below Equations 10-13 as,

$$X^2 = \sum_{i=1}^n \frac{(X_{i_{exp}} - X_{i_{pred}})^2}{X_{i_{exp}}} \quad (10)$$

$$RSS = \sum_{i=1}^n (X_{i_{exp}} - X_{i_{pred}})^2 \quad (11)$$

Table 3
Mathematical models of the evaporation curves of black liquor sample

No.	Equations	Model name	References
1.	$X = \exp(-kt)$	Lewis	(Bruce, 1985)
2.	$X = \exp(-kt^n)$	Page	(Chen, 2009)
3.	$X = \exp(-(kt)^n)$	Modified Page-I	(Overhults et al., 1973)
4.	$X = a \exp(-kt)$	Henderson and Pebis	(Bhargava, 1966)
5.	$X = 1 + at + bt^2$	Wang and Singh	(Ahou et al., 2014)
6.	$X = a \exp(-kt) + c$	Logarithmic	(Yagcioglu et al., 1999)
7.	$X = a + b + (0.25c^2t^2) - (a^{0.5}ct)$	Decay	Present study

$$R^2 = 1 - \frac{\sum_{i=1}^n (X_{i_{exp}} - X_{i_{pred}})^2}{\sum_{i=1}^n (X_{i_{exp}} - \bar{X})^2} \quad (12)$$

$$R_{adj}^2 = 1 - \frac{(1 - R^2)(n - 1)}{n - p} \quad (13)$$

Where, \bar{X} is the average value of the experimental moisture ratio, $X_{i_{pred}}$ and $X_{i_{exp}}$ are predicted, and experimental moisture ratios, respectively, p is the number of evaporation constants, and n is the number of observations.

RESULTS AND DISCUSSION

Analysis of Evaporation Curves and Model Fitting

The changing of the moisture fraction versus evaporation time for black liquor samples is shown in Figure 1. It was shown that the moisture fraction is affected by the isothermal temperature and evaporation time of black liquor. Moreover, from Figure 1, the evaporation time was significantly reduced from 9.5 to 4 minutes as the temperature increases; besides, an increase of the temperature has shortened the evaporation duration up to 55%. From the observation from the Figure 1 curve, the moisture fraction constantly decreases with evaporation time, and no constant evaporation rate period exists.

These observations are validated with previous literature studies on the evaporation/drying of organic compounds (Gögüs & Maskan, 2001; Meziane et al., 2006; Amin et al., 2019). As shown in Figure 2, the rate of moisture loss of black liquor was high at the initial

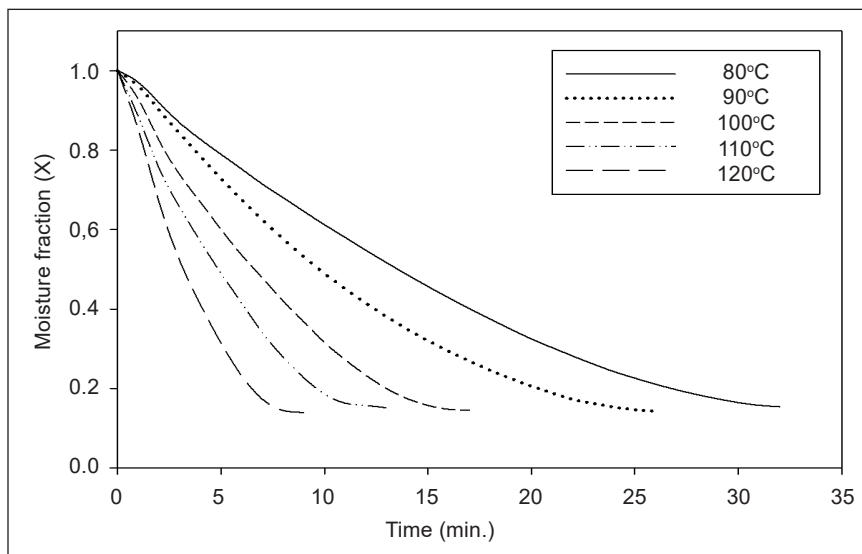


Figure 1. Evaporation curves of soda black liquor at different temperatures

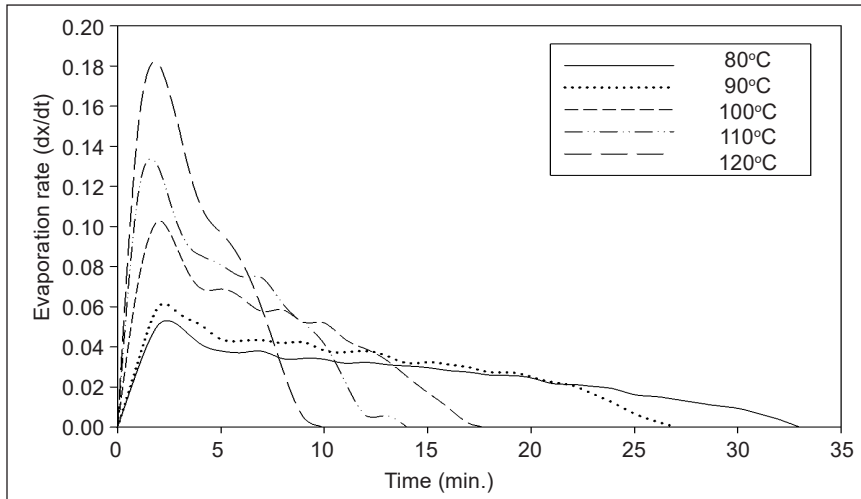


Figure 2. Variation of evaporation rate with evaporation time of black liquor

stage. In contrast, equally two-thirds of the time has been spent removing the last one-third of the moisture content due to the slow diffusion process. However, the black liquor evaporation at a higher temperature is significantly less. Thus, the overall evaporation time of the black liquor was reduced significantly with the increase in temperature. Thus, the physical mechanism prevailing in moisture transfer of the black liquor sample has resulted in a falling rate period (FRP) and internal diffusion throughout the evaporation process. Moreover, other studies also have reported similar behaviour (Karlsson, 2020).

From Figure 2, every plot has two stages in which evaporation progresses, where the evaporation rate rapidly increases and then slowly decreases. Otherwise, from this present study, it has been found that the evaporation rate will decrease corresponding to the period or with the reduction of the moisture fraction. Furthermore, the moisture fraction of the black liquor is high in the initial phase of evaporation, which has resulted in greater absorption of IR radiation and a higher evaporation rate due to the higher moisture diffusion. As the evaporation progresses, the reduction in moisture fraction in the black liquor causes a decrease in the absorption of IR radiation, and the results of evaporation rate fall tremendously. A higher evaporation rate was obtained at higher Infrared output temperature. Thus, the infrared output temperature had a significant consequence on the evaporation rate of black liquor. In comparison, the total evaporation times required to reach the final moisture content were 33, 27, 18, 14, and 10 minutes at 80, 90, 100, 110, and 120°C, respectively, as shown in Figure 1. Meanwhile, the evaporation time until moisture fraction up to 0.5 was 3.3, 4.8, 6.6, 9.6, and 15.5 minutes at 120, 110, 100, 90, and 80°C, respectively. The evaporation rates were more at the beginning of the evaporation process due to the evaporation of moisture from black liquor and then reduced with reducing moisture content (Figure 2).

The thin layer evaporation model equation of the infra-red evaporation process was suitable for the preliminary evaluation and constant evaporation stages. It can convey the important equation characteristic parameters such as heat, thermal diffusivity, moisture diffusivity, and mass transfer coefficients. Moreover, various models have been advised to depict the rate of moisture loss throughout the thin layer drying process of organic materials. Therefore, this present study has nominated seven mathematical models (Table 3) of the evaporation curves used in previous studies. Besides, the non-dimensional in Equation 1 has been used to compile data in experimental of moisture fraction. Meanwhile, the regression analysis was prepared for seven distinct thin layer drying models by correlating the dimensionless moisture fraction (X) for 80, 90, 100, 110, and 120°C temperatures and evaporation time. The statistical analysis values obtained from fitting the experimental data to the widely used semi-theoretical thin layer models (Table 3) are presented in Table 4.

Table 4
Fitness of different models for IR evaporation of black liquor

Equation	Temp.(K)			Reduced, X^2	RSS	Adj. R^2
Lewis		k				
	353K	0.05452		6.47E-04	0.02005	0.99062
	363K	0.07387		5.11E-04	0.01328	0.9932
	373K	0.11233		6.35E-04	0.01079	0.99203
	383K	0.15209		4.39E-04	0.0057	0.99463
	393K	0.22638		7.20E-04	0.00648	0.99239
Page		k	n			
	353K	0.03414	1.16567	5.27E-05	0.00158	0.99924
	363K	0.05136	1.14043	4.28E-05	0.00107	0.99943
	373K	0.08077	1.15162	9.67E-05	0.00155	0.99879
	383K	0.12537	1.10208	1.97E-04	0.00236	0.99759
	393K	0.18174	1.14522	2.25E-04	1.80E-03	9.99E-01
Modified Page		k	n			
	353K	0.05518	1.16599	5.27E-05	0.00158	0.99924
	363K	0.07403	1.14002	4.28E-05	0.00107	0.99943
	373K	0.11249	1.15155	9.67E-05	0.00155	0.99879
	383K	0.15196	1.10195	1.97E-04	0.00236	0.99759
	393K	0.22562	1.14479	2.25E-04	0.0018	0.99762
Henderson and Pebis		a	k			
	353K	1.04392	0.0575	3.87E-04	0.0116	0.99439
	363K	1.04645	0.07788	2.31E-04	0.00577	0.99693
	373K	1.04138	0.11771	4.07E-04	0.0065	0.9949
	383K	1.02584	0.15658	3.63E-04	0.00435	0.99556
	393K	1.03465	0.23501	5.72E-04	0.00457	0.99396

Table 4 (continue)

Equation	Temp.(K)				Reduced, X^2	RSS	Adj. R^2
Singh and Wang		a	b				
	353K	-0.04468	5.56E-04		2.05E-05	6.16E-04	0.9997
	363K	-0.06154	0.00109		5.04E-05	0.00126	0.99933
	373K	-0.0927	0.00245		6.38E-05	0.00102	0.9992
	383K	-0.12789	0.00476		6.13E-05	7.35E-04	0.99925
	393K	-0.1884	0.0102		1.33E-04	0.00106	0.99859
Logarithmic		a	k	c			
	353K	1.21969	0.04085	-0.20557	5.94E-05	0.00172	0.99914
	363K	1.10363	0.06741	-0.07277	1.36E-04	0.00326	0.99819
	373K	1.1294	0.09592	-0.10766	2.11E-04	0.00316	0.99735
	383K	1.07066	0.13986	-0.05545	3.12E-04	0.00344	0.99618
	393K	1.08303	0.20869	-0.05849	5.23E-04	0.00366	0.99447
Decay		a	b	c			
	353K	0.89654	0.11	0.05	1.68E-05	4.86E-04	0.99976
	363K	0.87489	0.14	0.07	2.05E-05	4.91E-04	0.99973
	373K	0.88186	0.13	0.10	5.08E-05	7.63E-04	0.99936
	383K	0.86006	0.14	0.14	6.56E-05	7.22E-04	0.9992
	393K	0.87696	0.13	0.21	5.91E-05	4.13E-04	0.99937

The capability of the model is based on the value of X^2 , RSS and adjusted R^2 . The absolute mathematical model has indicated the highest value in R^2 , lowest reduced X^2 and lowest RSS. The regression coefficients and standard deviations of single-layer drying models for black liquor during infra-red evaporation under the infra-red temperature range of 80-120°C are shown in Table 4. The modified Page and Page equation model was an exponent 'n' added to the drying constant 'k', which contributes to the evaporation constant of distinct magnitude. All the models exhibited great concurrence with the IR evaporation data of black liquor. The experimental data of the Decay model in Equation 14 has illustrated the closest fit to the black liquor evaporation for all the infra-red temperature range tested.

$$X = a + b + (0.25c^2t^2) - (a^{0.5}ct) \quad (14)$$

From Equation 14 above, X indicates the moisture fraction and t was signified the evaporation time, respectively. The valued parameters of this model (a , b , and c) and values of reduced X^2 , RSS and adjusted R^2 are emphasised in Table 4. The Decay model has been stated as the improved fitting evaporation model, which features the highest R^2 , lowest reduced X^2 and RSS values for the entire infra-red temperature range of 80 to 90°C. The adjusted R^2 values were higher than 0.9992, and reduced X^2 and RSS values were lower than 6.56×10^{-5} & 7.63×10^{-4} , respectively, for the entire infra-red evaporation conditions.

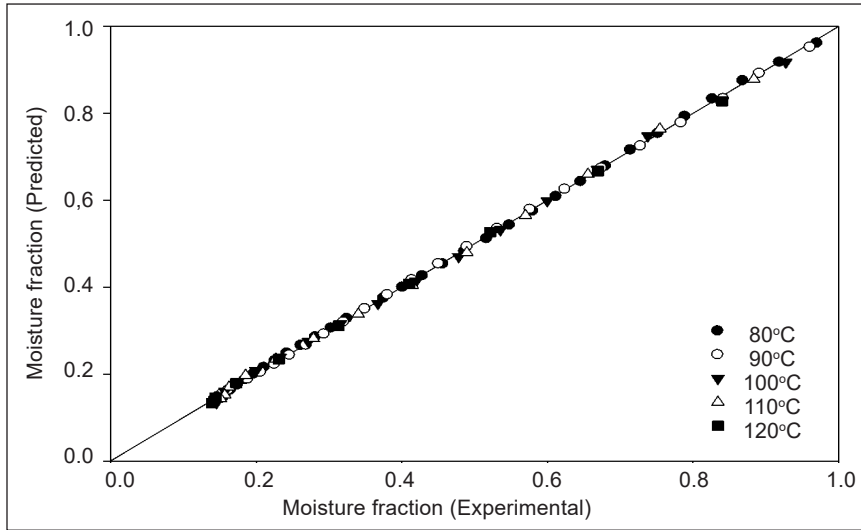


Figure 3. Experimentally determined and predicted moisture fraction of black liquor from Decay model Equation 14.

Although, the fitted evaporation curves based on the Decay model initiated to deliver outstanding fits of the test temperatures of 80, 90, 100, 110, and 120°C shown in Figure 3.

The parameter of the evaporation constants (a, b, and c) in the Decay model indicates that the relative magnitude of the parameter accurately reflects the evaporation behaviour. Meanwhile, the values of the evaporation constants “a” and “b” were in the range of 0.89654-0.86006 and 0.11-0.14 under the infra-red (IR) temperature range of 80-120°C, respectively (Table 4). Moreover, the value of the evaporation constant “c” increased with the increase in infra-red (IR) temperature. Besides, the higher “c” values demonstrate higher moisture removal rates and improve evaporation potential. Thus, though the Decay model could function to simulate the evaporation curves of black liquor with satisfactory test results, in spite the parameters of these models should improvise due to lack of physical sense.

Mathematical Modelling of Evaporation Rate

The variations of the drying rates versus moisture content are shown in Figure 4. The evaporation rate for black liquor at different temperatures based on Gaussian law Equation 3 was derived from the plot of evaporation rate (dx/dt) versus moisture fraction (X) in Figure 4.

General model Gaussian 3 given by Equation 15,

$$ER = \frac{dx}{dt} = a_1 e^{\left(\frac{x-b_1}{c_1}\right)^2} + a_2 e^{\left(\frac{x-b_2}{c_2}\right)^2} + a_3 e^{\left(\frac{x-b_3}{c_3}\right)^2} \quad (15)$$

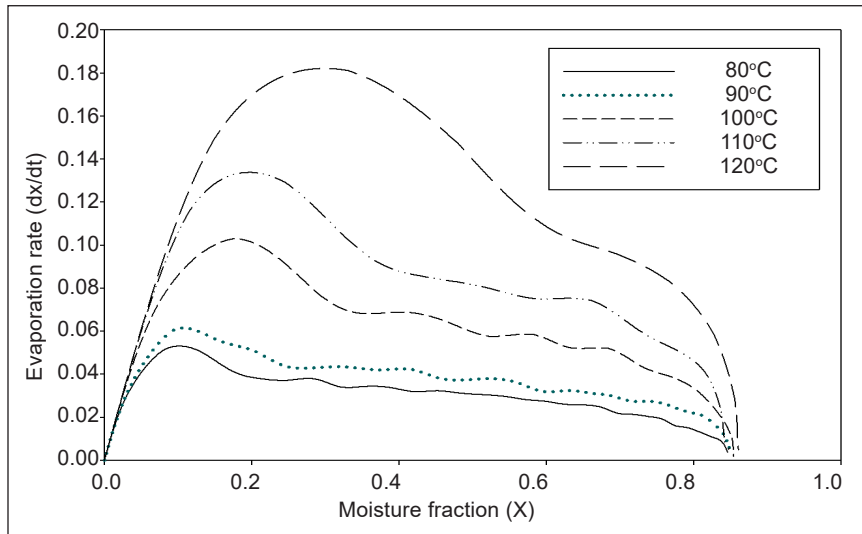


Figure 4. A variance of evaporation rate with a moisture content of black liquor

Table 5

Regression coefficients of black liquor through infra-red evaporation

Temperature (°C)	a1	b1	c1	a2	b2	c2	a3	b3	c3
80	0.0369	2.388	1.481	0.02291	6.206	4.277	0.02881	15.99	11.91
90	0.06368	1.374	2.734	-0.08997	-1.54	3.584	0.04065	9.36	13.27
100	0.08122	1.814	1.227	0.04908	4.199	2.434	0.05342	9.258	5.08
110	-0.4649	0.3825	0.4103	-0.7202	2.446	4.471	0.842	1.97	5.188
120	-2.77E+13	-26.42	4.711	0.2282	-1.275	6.724	-	-	-

Coefficients (with 95% confidence bounds)

Table 6

Standard deviations of goodness on fit of Gaussian model for black liquor

Temperature(°C)	SSE	R ²	Adjusted R ²	RMSE
80	0.000216	0.9614	0.949	0.002939
90	0.000242	0.9649	0.9501	0.003567
100	0.000361	0.9778	0.9601	0.006011
110	0.000117	0.9954	0.9893	0.004421
120	4.23E-05	0.9731	0.9462	0.002908

The regression coefficient of the Gaussian model Equation 3 is shown in Table 5. The statistical analysis values obtained from fitting the experimental data to the Gaussian model equation is presented in Table 6. The R^2 , SSE and RMSE values ranged from 0.9614-0.9954, 0.0000423-0.000361 and 0.002908-0.006011 for black liquor, respectively (Table 6).

Calculation of Effective Diffusivity and Activation Energy

The effective moisture diffusivity is an important transport property in food and other materials drying processes modelling, being a function of temperature and moisture content in material (Liu et al., 2009). The effective diffusivity and activation energy calculation has indicated that the isothermal condition was founded instantaneously and sustained throughout the evaporation of the black liquor process. In this method, with negligible sample shrinkage and uniform initial moisture distribution assumptions, the D_{eff} can be defined with an appropriate mathematical solution of Fick’s second law for diffusion in Equation 5. Meanwhile, Figure 5 has displayed the plots of the experimental results as $\ln(X)$ versus time, corresponding with different temperatures. The values of the effective moisture diffusivity were calculated using Equation 9 and are shown in Table 5 and Figure 5.

The D_{eff} values were varied in the range of $2.67 \times 10^{-10} \text{ m}^2/\text{s}$ to $10.4 \times 10^{-10} \text{ m}^2/\text{s}$ (Table 7). It was noted that D_{eff} values increased greatly with increasing drying temperature. When samples were dried at a higher temperature, increased heating energy would increase the activity of water molecules leading to higher moisture diffusivity.

Arrhenius plot, $\ln D_{eff}$ versus $1/(T + 273.15)$ Equation 9. The $\ln D_{eff}$ as a function of the reciprocal of absolute temperature was plotted in Figure 6. The slope of the line is $(-E_a/R)$, and the intercept equals to $\ln(D_o)$. The activation energy data achieve with formulation from Equation 8. Therefore, the results have displayed with linear relationship shown in Figure 6 due to the Arrhenius-type dependence ($R^2= 0.9651$). Therefore, the linear slope

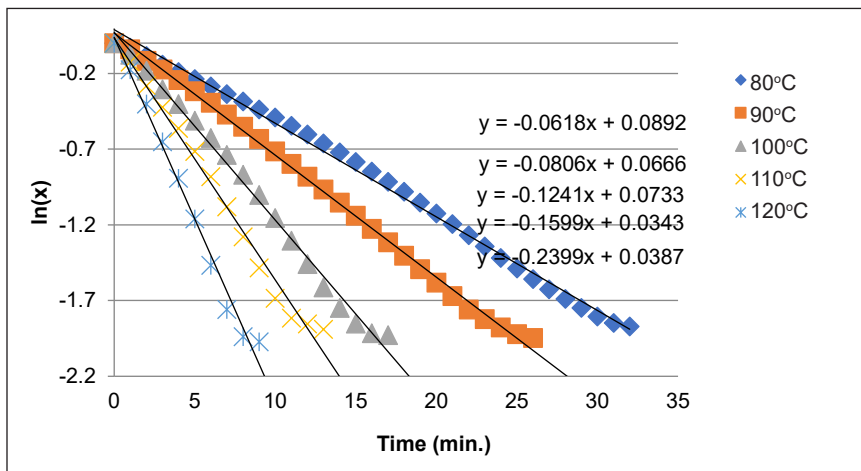


Figure 5. The plot of $\ln X$ versus time for infra-red evaporation of weak black liquor at different temperatures

Table 7
Effective diffusivities of black liquor under the infrared temperature range of 80-120°C

Temperature (°C)	80	90	100	110	120
D_{eff} (m^2/s)	2.67×10^{-10}	3.48×10^{-10}	5.37×10^{-10}	6.93×10^{-10}	10.4×10^{-10}

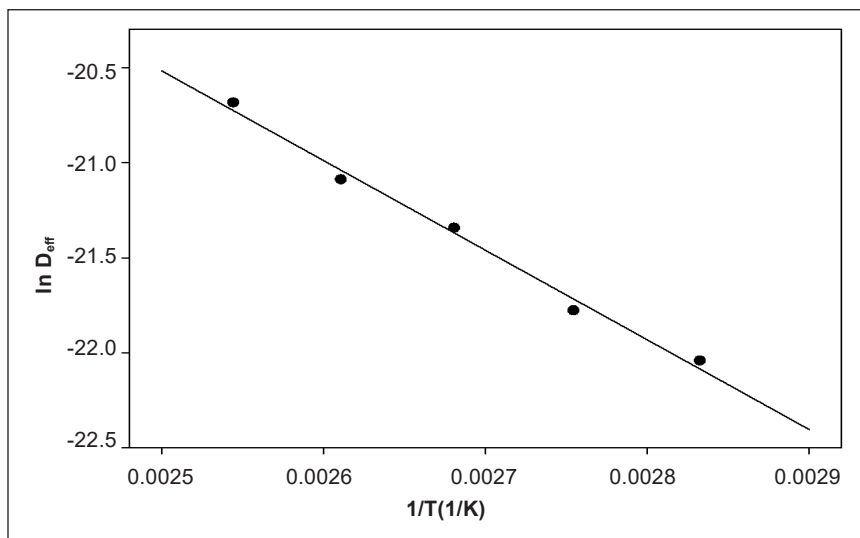


Figure 6. Arrhenius type correlation for temperature and effective diffusivity of black liquor

from the graph has denoted 39.19 kJ/mol of activation energy value, and pre-exponential factor $1.6 \times 10^{-4} \text{ m}^2/\text{s}$ was determined for evaporation of black liquor. The activation energy values were within the general range of 12.7 to 110 kJ/mol for various food materials (Zogzas et al., 1996).

CONCLUSIONS

The effect of infra-red evaporation temperature on moisture fraction, evaporation rate and effective diffusivity of soda black liquor was studied. Soda black liquor with an initial solids content of 13.5 to 15 % was evaporated to the final moisture fraction approx. 0.025 in 33 minutes at 80°C, and it is performed within 10 minutes at 120°C. Increasing the infrared (IR) temperature increased the evaporation rate and consequently decreased the evaporation duration within a certain infrared (IR) temperature range (80-120°C in the present investigation). Major evaporation occurred in the falling rate period (FRP). The decay empirical model showed a good fit for all the conditions than the other six thin layer evaporation models for describing soda black liquor's infra-red (IR) evaporation behaviour. The adjusted R^2 values were higher than 0.9992, and reduced R^2 and RSS values were lower than 6.56×10^{-5} and 7.63×10^{-4} , respectively, for the entire infra-red evaporation conditions.

The values of evaporation constant "a" and constant "b" were in the range of 0.89654 to 0.86006 and 0.11 to 0.14 under the infra-red (IR) temperature range of 80 to 120°C, respectively. The effective moisture diffusivity of black liquor under an infrared temperature range of 80-120°C was in the range of $2.6 \times 10^{-10} \text{ m}^2/\text{s}$ to $10.4 \times 10^{-10} \text{ m}^2/\text{s}$. The experimental results have shown that the moisture diffusivity of black liquor is lower than other organic materials, which could be discovered in the literature under similar evaporation conditions.

ACKNOWLEDGMENT

First author thankful to Department of Paper Technology, IIT Roorkee, India, for providing facility to conduct research work.

REFERENCES

- Ahou, K., Emmanuel, A. N., Patrice, K., & Benjamin, Y. (2014). Modelling of rough rice solar drying under natural convection. *European Scientific Journal*, 10(3), 141-156.
- Alriols, M. G., Tejado, A., Blanco, M., Mondragon, I., & Labidi, J. (2009). Agricultural palm oil tree residues as raw material for cellulose, lignin and hemicelluloses production by ethylene glycol pulping process. *Chemical Engineering Journal*, 148(1), 106-114. <https://doi.org/10.1016/j.cej.2008.08.008>
- Amin, N., Sabli, N., Izhar, S., & Yoshida, H. (2019). Sago wastes and its applications. *Pertanika Journal of Science and Technology*, 27(4), 1841-1862.
- Bajpai, P. (2017). Evaporation of black liquor. In *Pulp and Paper Industry* (pp. 39-66). Elsevier. <https://doi.org/10.1016/b978-0-12-811103-1.00003-6>
- Bhargava, V. K. (1966). *Drying of wheat grain in thin layers* (Doctoral dissertation). University of British Columbia, Canada.
- Bruce, D. M. (1985). Exposed-layer barley drying: Three models fitted to new data up to 150°C. *Journal of Agricultural Engineering Research*, 32(4), 337-348. [https://doi.org/10.1016/0021-8634\(85\)90098-8](https://doi.org/10.1016/0021-8634(85)90098-8)
- Chen, X. D. (2009). On a relationship proposed for thin layer drying of porous materials. *Chemical Engineering and Processing: Process Intensification*, 48(11-12), 1583-1584. <https://doi.org/10.1016/j.cep.2009.10.001>
- Crank, J. (1975). *The mathematics of diffusion*. Oxford University Press. <https://doi.org/10.1021/ja01562a072>
- Darvishi, H., Azadbakht, M., Rezaeiasl, A., & Farhang, A. (2013). Drying characteristics of sardine fish dried with microwave heating. *Journal of the Saudi Society of Agricultural Sciences*, 12(2), 121-127. <https://doi.org/10.1016/j.jssas.2012.09.002>
- Datta, A. K., & Anantheswaran, R. C. (2001). Handbook of microwave technology for food applications. In A. K. Datta & R. C. Anantheswaran (Eds.), *Marcel Dekker, Inc. All Rights Reserved* (1st Ed.). Taylor & Francis. <https://doi.org/https://doi.org/10.1201/9781482270778>
- Do, N. H., Pham, H. H., Le, T. M., Lauwaert, J., Diels, L., Verberckmoes, A., Do, N. H. N., Tran, V. T., & Le, P. K. (2020). The novel method to reduce the silica content in lignin recovered from black liquor originating from rice straw. *Scientific Reports*, 10(1), 1-11. <https://doi.org/10.1038/s41598-020-77867-5>
- Gögüs, F., & Maskan, M. (2001). Drying of olive pomace by a combined microwave-fan assisted convection oven. *Nahrung - Food*, 45(2), 129-132. [https://doi.org/10.1002/1521-3803\(20010401\)45:2<129::AID-FOOD129>3.0.CO;2-T](https://doi.org/10.1002/1521-3803(20010401)45:2<129::AID-FOOD129>3.0.CO;2-T)
- Goodell, E. G., & Point, S. (1933). *Black liquor recovery process and apparatus* (Patent No. US1931536A). Patented Oct 31, 1933.
- Guo, H. (2011). A simple algorithm for fitting a Gaussian function [DSP tips and tricks]. *IEEE Signal Processing Magazine*, 28(5), 134-137.

- Haghsheno, M., & Kouhikamali, R. (2020). Numerical investigation of effective parameters of falling film evaporation in a vertical-tube evaporator. *Heat Transfer*, 50(3), 2764-2792. <https://doi.org/10.1002/hjt.22004>
- Hatibaruah, D., Baruah, D. C., & Sanyal, S. (2013). Microwave drying characteristics of assam ctc tea (*Camellia assamica*). *Journal of Food Processing and Preservation*, 37(4), 366-370. <https://doi.org/10.1111/j.1745-4549.2011.00656.x>
- Hurter, R. W. (1991). *Nonwood plant fiber characteristics*. Tappi Press.
- Karlsson, E. (2020). Evaluation of sodium salt scaling in black liquor evaporators using existing process data. *Nordic Pulp and Paper Research Journal*, 35(4), 516-532. <https://doi.org/10.1515/npprj-2020-0038>
- Liu, X., Qiu, Z., Wang, L., Cheng, Y., Qu, H., & Chen, Y. (2009). Mathematical modeling for thin layer vacuum belt drying of panax notoginseng extract. *Energy Conversion and Management*, 50(4), 928-932.
- Low, E. S., & Ong, P. (2020). On the formulation of metaheuristic algorithm-based approximation approach for non-linear ordinary differential equations with application to heat exchanger problem. *Pertanika Journal of Science and Technology*, 28(4), 1221-1265. <https://doi.org/10.47836/pjst.28.4.06>
- Madamba, P. S., Driscoll, R. H., & Buckle, K. A. (1996). The thin-layer drying characteristics of garlic slices. *Journal of Food Engineering*, 29(1), 75-97. [https://doi.org/10.1016/0260-8774\(95\)00062-3](https://doi.org/10.1016/0260-8774(95)00062-3)
- Meziane, S., Kadi, H., & Lamrous, O. (2006). Kinetic study of oil extraction from olive foot cake. *Grasas y Aceites*, 57(2), 175-179. <https://doi.org/10.3989/gya.2006.v57.i2.34>
- Mujumdar, A. S. (2007). Book review: Handbook of industrial drying (3rd Ed.). *Drying Technology*, 25(6), 1133-1134. <https://doi.org/10.1080/07373930701399224>
- Naqvi, M., Yan, J., & Dahlquist, E. (2010). Black liquor gasification integrated in pulp and paper mills: A critical review. *Bioresource Technology*, 101(21), 8001-8015. <https://doi.org/10.1016/j.biortech.2010.05.013>
- Nasir, N. A. F. M., Jamaluddin, J., Zainudin, Z., Busheri, M. M., Adrus, N., Azim, F. S. S., & Hasham, R. (2020). The effect of alkaline treatment onto physical, thermal, mechanical and chemical properties of Lemba leaves fibres as new resources of biomass. *Pertanika Journal of Science and Technology*, 28(4), 1531-1547. <https://doi.org/10.47836/pjst.28.4.21>
- Overhults, D. G., White, G. M., Hamilton, H. E., & Ross, I. J. (1973). Drying soybeans with heated air. *Transactions of the American Society of Agricultural Engineers*, 16(1), 112-113. <https://doi.org/10.13031/2013.37459>
- Ranganathan, A. (2004). The levenberg-marquardt algorithm. *Tutorial on LM algorithm*, 11(1), 101-110.
- Sandu, C. (1986). Infrared radiative drying in food engineering: A process analysis. *Biotechnology Progress*, 2(3), 109-119. <https://doi.org/10.1002/btpr.5420020305>
- Sanjuán, N., Lozano, M., García-Pascual, P., & Mulet, A. (2003). Dehydration kinetics of red pepper (*Capsicum annuum* L var Jaranda). *Journal of the Science of Food and Agriculture*, 83(7), 697-701. <https://doi.org/10.1002/jsfa.1334>
- Thakor, N. J., Sokhansanj, S., Sosulski, F. W., & Yannacopoulos, S. (1999). Mass and dimensional changes of single canola kernels during drying. *Journal of Food Engineering*, 40(3), 153-160. [https://doi.org/10.1016/S0260-8774\(99\)00042-4](https://doi.org/10.1016/S0260-8774(99)00042-4)

- Tütüncü, M. A., & Labuza, T. P. (1996). Effect of geometry on the effective moisture transfer diffusion coefficient. *Journal of Food Engineering*, 30(3-4), 433-447. [https://doi.org/10.1016/s0260-8774\(96\)00028-3](https://doi.org/10.1016/s0260-8774(96)00028-3)
- Yagcioglu, A. K., Degirmencioglu, A., & Cagatay, F. (1999, May 26). Drying characteristics of laurel leaves under different drying conditions. In *7th International Congress on Agricultural Mechanization and Energy* (pp. 565-569). Adana, Turkey.
- Zogzas, N. P., Maroulis, Z. B., & Marinos-Kouris, D. (1996). Moisture diffusivity data compilation in foodstuffs. *Drying Technology* 14(10), 2225-2253. <https://doi.org/10.1080/07373939608917205>

Enhanced IoT-Based Climate Control for Oyster Mushroom Cultivation Using Fuzzy Logic Approach and NodeMCU Microcontroller

Muhammad Azizi Mohd Ariffin^{1*}, Muhammad Izzad Ramli¹, Zarina Zainol¹, Mohd Nazrul Mohd Amin¹, Marina Ismail¹, Rosanita Adnan¹, Nor Diana Ahmad¹, Norhasiah Husain² and Nursuriati Jamil¹

¹National Autism Resource Centre, Faculty of Computer and Mathematical Sciences, UiTM, Shah Alam, 40450, Malaysia

²The National Autism Society of Malaysia, Pacific Place Commercial Centre, Unit B-2-3, B-3-3, Jalan PJU 1A/4, Ara Damansara, 47301, Petaling Jaya, Selangor, Malaysia

ABSTRACT

Urban farming has the potential to utilise unused space in the community to alleviate food shortages and increase the community's income through local food production. When Internet of Things (IoT) technology is integrated with urban farming, it can further improve its efficiencies and yield. The work in this paper improved our previous work of using an IoT-based climate control system to regulate the cultivation environment of oyster mushrooms automatically. Even though the climate control system could produce two batches of mushroom yields, there were several limitations, such as less efficient climate control due to threshold-based corrective action, water wastage, and system instability. This paper aims to address these stated limitations by implementing a fuzzy logic

algorithm and redesigned the climate control system. Two crisp input variables from DHT22 sensors representing temperature and humidity were fed into the Node MCU microcontroller's fuzzy logic coded in C language. The temperature and humidity conditions were divided into five fuzzy trapezoidal membership functions resulting in 25 fuzzy rules to control the duration of running the water pump and ventilation fan. An internal, lightweight web server were managed all HTTP client requests. The enhanced system also included a safety

ARTICLE INFO

Article history:

Received: 16 April 2021

Accepted: 13 August 2021

Published: 22 October 2021

DOI: <https://doi.org/10.47836/pjst.29.4.34>

E-mail addresses:

mazizi@fskm.uitm.edu.my (Muhammad Azizi Mohd Ariffin)

izzad@fskm.uitm.edu.my (Muhammad Izzad Ramli)

zarina@fskm.uitm.edu.my (Zarina Zainol)

nazrul@fskm.uitm.edu.my (Mohd Nazrul Mohd Amin)

marina@fskm.uitm.edu.my (Marina Ismail)

rosanita@fskm.uitm.edu.my (Rosanita Adnan)

nordiana@fskm.uitm.edu.my (Nor Diana Ahmad)

norhasiah.husain@nasom.org.my (Norhasiah Husain)

lizajamil@computer.org (Nursuriati Jamil)

* Corresponding author

measurement to avoid overheating the microcontroller and causing water wastage. Upon analysis of the data captured in two months, the result showed a decrease of 40% in water utilisation and an increase of mushrooms yield up to 226%. The enhanced climate control system also facilitated maintaining and controlling the temperature and humidity conducive for optimal mushroom cultivation.

Keyword: Fuzzy logic, Internet of Things (IoT), node MCU microcontroller, oyster mushroom cultivation, urban farming

INTRODUCTION

Research of IoT utilisation in smart farming has increased tremendously, and this fact is reflected in the number of publications which has increased by 278% in 2017/2018 compared to 2016 (Navarro et al., 2020). In crop monitoring, big data analytics and machine learning techniques were largely used to predict environmental conditions (Adenugba et al., 2019), identify growth stages (Xia et al., 2018), and the health of plantations (Li et al., 2018). However, these technologies require massive resources and are more cost-benefitting for large plantations. In small-scale farming, particularly urban farming, IoTs are used mainly for crop monitoring and environment control. Urban farming can utilise unused space in the community to alleviate food shortages and increase the community's income through local food production (Poulsen et al., 2017). Oyster mushroom cultivation is among the top choice of crops for urban farming as it requires small space, has high nutritional and medicinal values and takes a shorter time to harvest (Nongthombam et al., 2021).

This paper presented an enhanced IoT-based climate control system for oyster mushroom cultivation, initially presented in the 10th Conference on System Engineering and Technology (ICSET) (Ariffin et al., 2020). In the previous IoT-based climate control system, fixed thresholds were used to automatically regulate the cultivation environment of oyster mushrooms in a mushroom house. Even though the IoT system alleviated the manual cultivation of oyster mushrooms at NASOM's (National Autism Society of Malaysia) Autism Care Centre in Bandar Puteri Klang, there were two limitations. The first limitation was the inability to regulate the mushroom house's environment to adapt to the weather changes during the wet and dry seasons. Malaysia experiences an equatorial climate with hot and humid weather for the whole year and two monsoon seasons from late May to September and October to March, respectively (Tang, 2019). The average temperature is 25.8°C, with the highest at 30.3°C and the lowest at 21.9°C (Climate-Data.org., 2021). Malaysia also has a relatively high humidity with an average of 250cm yearly rainfall (Saw, 2007). The rainy season occurs from November to January, while the drier season occurs from May to July (Wong et al., 2016). Ideally, the IoT system should perform a corrective action by turning on/off the ventilation fan and water pump on/off depending on the humidity and temperature changes due to the weather. Thus, the IoT system should

automatically water the mushroom house during the dry season more frequently than the rainy season. However, since the control of the water pump and ventilation fan depended on pre-determined fixed thresholds, the same threshold values were used to control the climate of the mushroom house throughout the year. As a result, it has led to a less conducive environment for the cultivation of oyster mushrooms.

The second limitation is the wastage of water resources, again due to fixed thresholds and time intervals in controlling the water pump. For example, even though the relative humidity was high during the rainy season, the misting sprinkler was turned on according to the fixed intervals causing wastage of precious water resources. Therefore, it will contribute to the unsustainable use of water resources for agriculture (Al-Saidi & Elagib, 2017). Moreover, the previous IoT system also frequently experienced system instability due to an unstable power source. The microcontroller and all the electronic components were placed together on a single breadboard (Figure 1).

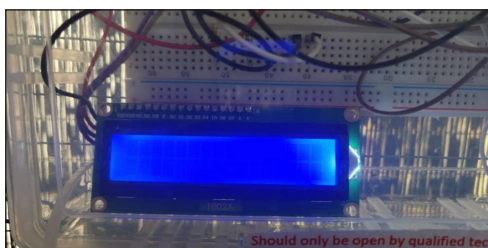


Figure 1. Blank LCD due to system error

Therefore, this paper proposed to overcome the limitation of using fixed thresholds to automatically control the climate of a mushroom house using a fuzzy logic approach and revised the system hardware specification to improve the system stability due to the power supply issues. The contribution of this paper is twofold: 1) This paper demonstrates the execution of an IoT climate control system in a mushroom house located in Bandar Puteri, Klang, Malaysia; and 2) This paper proved that the implementation of the fuzzy logic for IoT controller was able to provide better environmental management as required for mushroom cultivation and reduced the water usage resulted in a higher yield of harvested mushroom.

RELATED WORK

Machine learning and big data analytics were, and machine learning techniques were mainly used in large plantations for crop monitoring and by predicting the environmental conditions. Fuzzy logic is another option of crop monitoring and is commonly used to monitor multiple variables such as temperature and humidity in greenhouses and urban farming. Therefore, it is suitable for implementing a complex IoT system with multiple inputs and granular and dynamic action as an output (Krishnan et al., 2020). In Algarín et al. (2017) and Revathi and Sivakumaran (2016), a greenhouse's cooling and irrigation system was controlled using fuzzy logic. A heat loss gain method was used to compare the proposed system with the conventional manual method of controlling the light, temperature, humidity, and water supplied to the greenhouse. The results showed that the fuzzy logic control system needed approximately 25% less energy to heat the greenhouse.

The authors further claimed that their proposed system contained more new technologies than previous similar work and allowed the crop to grow at the optimum level. However, the crop yields were not made available in the paper. Similarly, Alpay and Erdem (2018) used fuzzy logic to optimise the sensors' operations to monitor soil moisture, temperature, lighting, and relative humidity in a greenhouse. A greenhouse prototype using acrylic and aluminium was built for the sensors and fuzzy logic control system. When tested in real-time, the proposed fuzzy logic control system showed good stabilisation times (i.e., 4-10 mins) and average tolerances of 5% for relative humidity, 2% for temperature, and 6% for soil moisture under different environmental conditions. However, the control system was tested in a controlled greenhouse prototype.

Implementation of IoT technology in mushroom cultivation was also commonly done, especially in Southeast ASEAN countries. Kassim et al. (2019) and Mat et al. (2019) developed a wireless sensor network system with a real-time embedded system to control temperature, humidity, and CO₂ parameters to grow shiitake mushrooms in a controlled room of a building. Based on these parameters, the system provided feedback based on pre-defined thresholds to control the actuators attached to the exhaust fan, humidifier, circulation fan, and mist sprinkler. Even though the results showed 192.9% of mushroom yields, the system was not implemented in a real environment. Ibrahim et al. (2018) monitored temperature, humidity, and CO₂ in a smart mushroom house for three days and captured the sensor data in 3 minutes intervals. When the humidity in the mushroom house dropped below 75%, a humidifier was activated until the humidity reached 85%.

Meanwhile, the CO₂ values were kept under 500ppm by turning on an exhaust fan whenever CO₂ readings went over 600ppm. The authors also showed that the average thickness per mushroom increased from 2.3cm to 2.6cm, and its average weight attained 40gm compared to 35gm when using the conventional method. Najmurokhman et al. (2020) implemented a similar IoT-based system using a closed box made of plastic to grow oyster mushrooms by monitoring the level of humidity and temperature. When the temperature and humidity reached above or under a set threshold, the lamp, fan, and mist sprinkler were turned on to reset the temperature and humidity to their respective fixed values. A further related literature search was done, and the summary is presented in Table 1. Based on Table 1, temperature and humidity are the two important parameters in mushroom cultivation. At the same time, CO₂ is recommended for shiitake mushrooms identified by Mat et al. (2019) and Ibrahim et al. (2018), especially in an enclosed room in a building where air circulation is stagnant (Mat et al., 2019; Shakir et al., 2019). In their control setup, Shakir et al. (2019) also added a light intensity parameter to light up the enclosed room after 6.00 pm. They observed the increase of CO₂ level in the presence of artificial light, indicating the mushrooms produced more CO₂ when the light was turned on. Therefore, our study omitted CO₂ as the observed parameter as the focus is oyster mushroom cultivation, and the mushroom house has good air circulation.

Table 1 also showed that while the use of fuzzy logic control systems was beginning to be implemented in recent years, most mushroom cultivations still relied on utilising fixed thresholds to monitor temperature and humidity. Even though Chieochan et al. (2017) and Boonchieng et al. (2018) reported a ten times reduction in labour costs of mushroom cultivation when they implemented an IoT-based monitoring system using fixed thresholds in a mushroom hut, they did not report on the mushroom yields. Cruz-Del Amen and Villaverde (2019) and Hendrawan et al. (2019) used fuzzy logic to control temperature and humidity in their oyster mushroom cultivations. While Cruz-Del Amen and Villaverde (2019) conducted their experiments in a controlled enclosed space, the latter implemented the testing using a plastic container box.

Table 1

Summary of selected IoT-based mushroom cultivations work

Authors	Controlled parameters			Cultivation setup	Monitoring technique
	Temperature	Humidity	CO ₂		
Ibrahim et al. (2018)	√	√	√	Mushroom house	Fixed threshold
Kassim et al. (2019)	√	√	√	Building room	Fixed threshold
Mat et al. (2019)					
Najmurokhman et al. (2020)	√	√		Mocked prototype	Fixed threshold
Chieochan et al. (2017)	√	√		Mushroom hut	Fixed threshold
Boonchieng et al. (2018)					
Shakir et al. (2019)	√	√	√	Building room	Fixed threshold
Cruz-Del Amen and Villaverde (2019)	√	√		Controlled enclosed space	Fuzzy logic
Hendrawan et al. (2019)	√	√		Plastic container box	Fuzzy logic

This paper differs from work in the literature where the mushroom cultivation was done in a real mushroom house exposed to pest threats, unpredictable weather, and noisy environments from car traffic. This paper reports on the experiences, challenges, and limitations of implementing a fuzzy control climate system for cultivating oyster mushrooms within two months.

METHODOLOGY

The IoT-Based climate control system was implemented in a mushroom house at NASOM's Autism Care Centre in Bandar Puteri Klang, Malaysia. First, the primary data from the sensors were captured. The captured data were average temperature, humidity, mushroom yield, and water usage. The data analysis was then conducted and compared with our first IoT-based system that used fixed thresholds.

System Design

The improved IoT-based climate control design was divided into three sections: Oyster Mushroom Cultivation Environment, IoT-Based Climate Control System, Fuzzy Logic Algorithm, and Web Interface.

Oyster Mushroom Cultivation Environment

Oyster mushroom has a specific growing environment to ensure healthy and productive yield. It needs to grow in a temperature range of 22-28°C and humidity range of 60-80% (Adhitya et al., 2017). Thus, a farmer would manually spray water to the floor to control the temperature and humidity level in the conventional cultivation method. However, the mushrooms cannot contact directly with the water as a wet growing medium will damage the mushroom with bacterial or fungal infection (Hamidizade et al., 2020). Moreover, the mushroom also needs to be protected from insects, pests, or bad odour to ensure quality yield. Therefore, to grow and cultivate oyster mushrooms in a controlled environment, farmers grow oyster mushrooms inside a mushroom house. However, maintaining a conventional mushroom house is tedious as a farmer needs to control the climate inside the mushroom house manually. Thus, this paper proposed a smart mushroom powered by an enhanced IoT-based climate control using the fuzzy logic system. Figure 2 shows the physical arrangement of the smart mushroom house.

The size of the smart mushroom house is 547 × 347 cm, and it consists of several components such as the IoT Control Box, Access Point, Water Pump, Exhaust Fan, Sensors, and Rack. The mushroom house can fit ten racks for holding up to 2,000 blocks of oyster

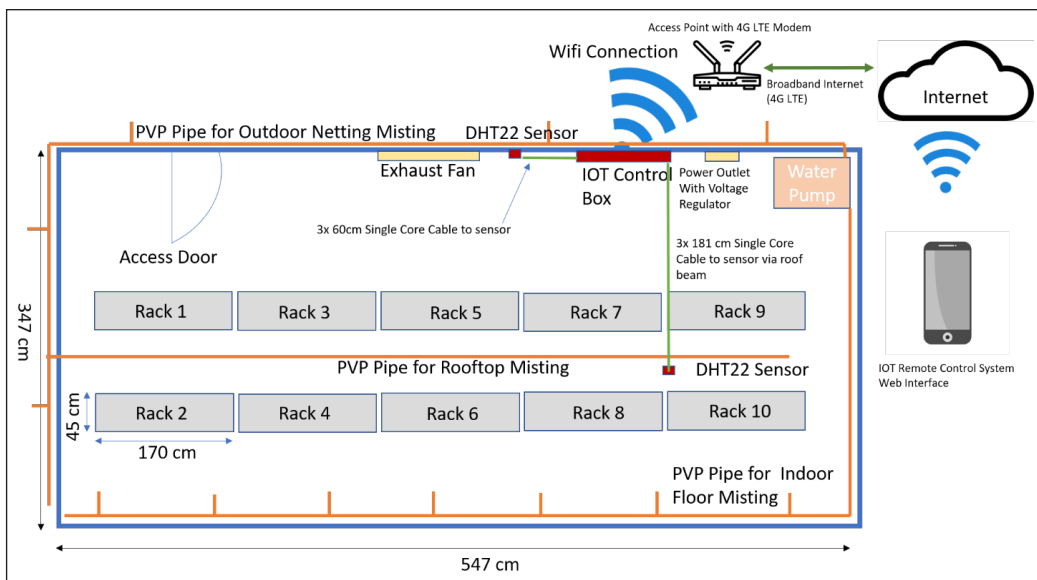


Figure 2. Mushroom house with IoT-based climate control physical arrangement

mushroom growing medium. The racks holding the growing medium were rearranged to improve the air circulation. Based on our earlier experiences, the vertical arrangement of the racks did not allow optimal airflow, and the mushroom blocks got easily wet during heavy rains. Therefore, the racks were subsequently horizontally rearranged, as shown in Figure 2, to ensure optimal air circulation and easy access to the growing medium. The IoT control box hosted the Node MCU Microcontroller, which contained the fuzzy logic to control the ventilation fan and water pump automatically. Two DHT22 sensors were placed at the ceiling and connected to the Node MCU for capturing temperature and humidity inside the mushroom house. The connection between the microcontroller and the sensor was via three single-core wires of size 0.5×0.25 mm. The length of the connection wire to the first sensor was 60 cm, while the second sensor was located 180 cm from the IoT box, and the wire was placed along the roof beam. The power for the IoT control box was supplied by a power outlet equipped with a voltage regulator to ensure a stable supply of 5V 2A DC electricity. The mushroom house was also equipped with an access point with a built-in 4G LTE Modem to connect the IoT control box. Internet connectivity was used to display the climate data to the end-user via a web interface and enabled the end-user to control the IoT system remotely.

The purpose of the ventilation fan was to pump out hot air from inside the mushroom house and ensure optimal air circulation, which was vital for oyster mushroom cultivation (Wahab et al., 2019). On the other hand, the water pump was connected to the PVC pipes to supply water to the misting head to spray the floor and the roof to regulate the temperature inside the mushroom house. Unfortunately, the climate control system was not equipped with a nozzle head to spray the roof in our initial work. Thus, the enhanced climate control system added water nozzles on top of the roof to further improve temperature regulation in the mushroom house. Furthermore, since the mushroom house is located on a busy road in an urban area, the heat from the traffic contributed to the high-temperature occurrence. Lastly, the bottom half of the mushroom house wall was built using bricks. At the same time, the upper part was installed with steel netting and agriculture grade black netting to protect the mushroom house from pest invasions and ensure proper air circulation.

IoT-Based Climate Control System

The system's intelligence to control climate and regulate the environment was in the fuzzy logic algorithm running in the Node MCU microcontroller. Figure 3 shows the logical diagram of the IoT-based climate control system. First, the temperature and humidity crisp values are inputs to the system. The crisp values were converted to a fuzzy value using a trapezoidal fuzzifier function. At the same time, the crisp values were also sent to a light web server so that they can be displayed to LCD via GPIO and web interface via network communication. After the crisp values were converted, they were fed to the fuzzy logic function for further processing.

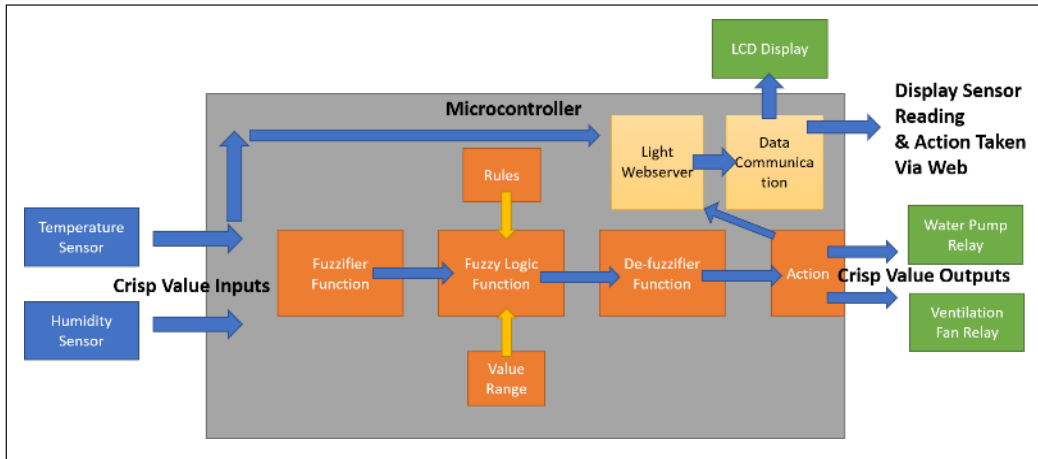


Figure 3. System logical diagram

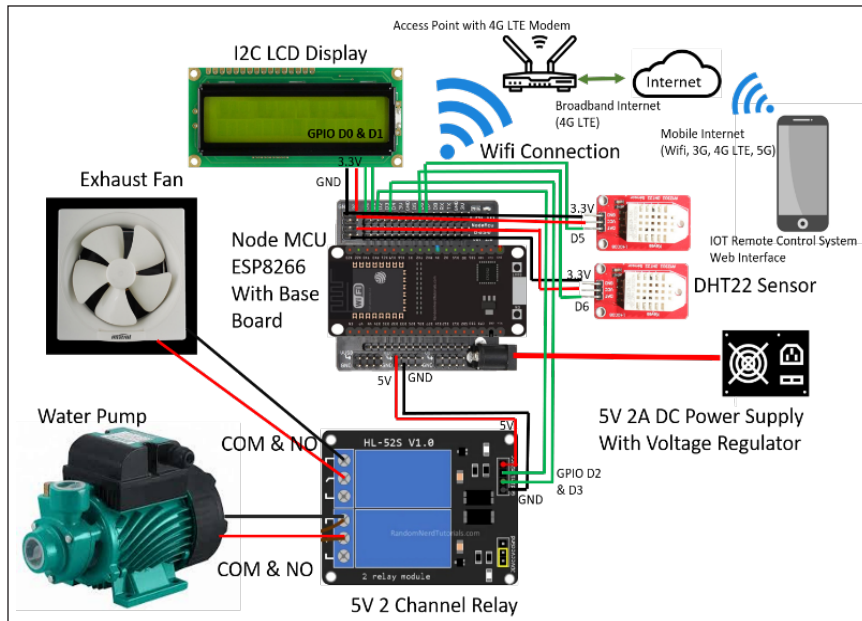


Figure 4. IoT based climate control hardware schematic.

The fuzzy logic algorithm checked the fuzzy rules and depending on the fuzzy input. Then, the algorithm inferred a suitable value range for the fuzzy output. After that, the fuzzy output was sent to the defuzzifier function to be converted back to the crisp value. The crisp value determined the action taken by the system to regulate the mushroom house. An example of such action was turning on the water pump for 30 seconds and the ventilation fan for 40 seconds due to Hot Temperature. The hardware schematic for implementing the enhanced IoT system is shown in Figure 4.

The system used Node MCU Microcontroller equipped with an ESP8266 chip Base Board to run the fuzzy logic and connect with the sensors and relays. Node MCU was used extensively by various IoT and Wireless sensor network projects due to its capability to connect to the Internet via Wi-Fi using very low power and miniature configuration (Kashyap et al., 2018). The width of the Node MCU board is only 30 mm and equipped with integrated GPIO, PWM, IIC, 1-Wire, and ADC all in one board. The Node MCU board provided an easy connection with the sensors, relay, and I2C LCD. Furthermore, it also ensured stable power input with an onboard 5V voltage regulator capable of the maximum voltage output of 1A. In our initial climate control system, the microcontroller was only connected to the breadboard without any baseboard. It has caused instability to the system due to a lack of voltage regulators and proper pin connection. The DHT22 sensor module measured temperature in -40°C to 80°C and humidity range of 0 to 100%. It has $\pm 2\%$ RH accuracy, ± 0.5 degrees $^{\circ}\text{C}$ accuracy, and the ability to read data every 2 seconds (CircuitSchools Staff, 2020). The ventilation fan and the 240V AC water pump were controlled by the control climate system using 5V 2 Channel relay. Meanwhile, the I2C LCD displayed current sensor reading, action, and any error logs. A stable power supply was ensured by a power outlet equipped with a voltage regulator to ensure a stable supply of 5V 2A DC electricity.

Fuzzy Logic Algorithm

The first stage in constructing the fuzzy logic algorithm involved defining the linguistic variables and terms for the input and output; constructing the fuzzy logic membership functions and the rule base. The input variables were temperature and humidity; the linguistic terms for temperature were {Too cold, Cold, Normal, Hot, Too hot} and the trapezoidal membership function simulated in MATLAB was constructed as shown in Figure 5. The 'Normal' temperature ranges from 22 to 29°C , which is the desirable state of temperature for the best yield of the mushrooms.

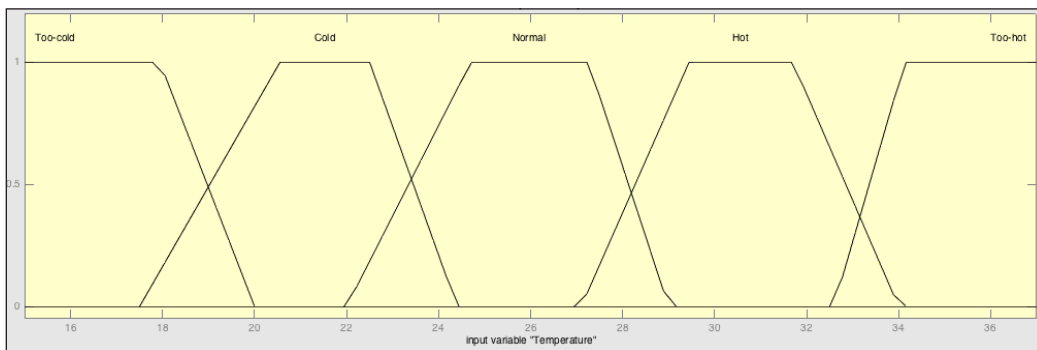


Figure 5. Trapezoidal membership function with fuzzy sets for temperature

Humidity was defined as {Too humid, Humid, Normal, Dry, Too Dry}, and its trapezoidal membership function can be seen in Figure 6. The fuzzy set for ideal humidity of the mushrooms ranges from 71 to 84%, and the climate control system commanded the ventilation fan and water pump accordingly to maintain the humidity.

Duration of the ventilation fan and water pump were the output variables, and the linguistic terms for the duration were {Slow, Medium, Long}. The trapezoidal membership functions for the ventilation fan and water pump duration are shown in Figures 7 and 8, respectively. The fuzzy data sets for the ventilation fan and water pump are shown in Table 2.

Table 2
Membership functions with fuzzy sets for the duration of ventilation fan and water pump

Output	Ventilation fan (sec)	Water pump (sec)
Short	0 – 93	0 – 93
Medium	80 – 173	66 – 173
Long	165 – 250	146 – 250

The knowledge base rules are shown as a matrix in Table 3 containing 25 rules according to the Mamdani fuzzy inference system. The rules were used to decide the duration of the ventilation fan and water pump in 3 membership degrees of Short, Medium, and Long. Three examples of the rules in the knowledge base were:

Rule 1: IF Temperature is (Too Cold OR Cold) AND Humidity is Too Humid THEN Action is Long Duration (Fan)

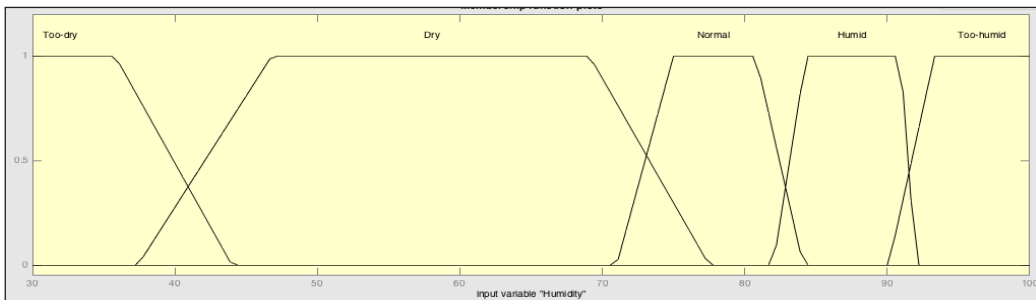


Figure 6. Trapezoidal membership function with fuzzy sets for humidity

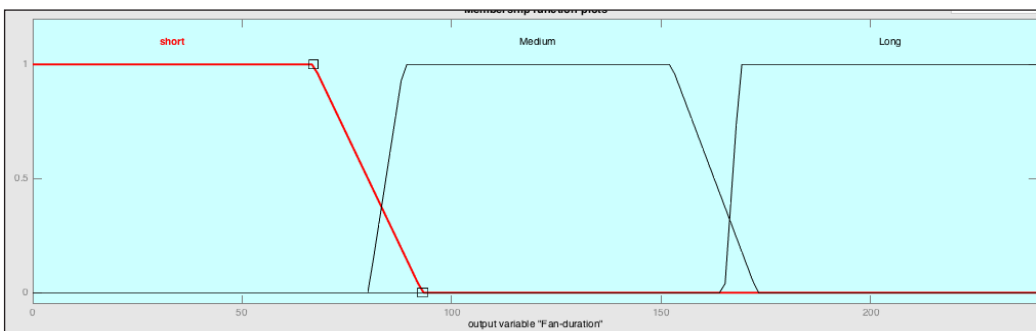


Figure 7. Trapezoidal membership function with fuzzy sets of the duration for ventilation fan

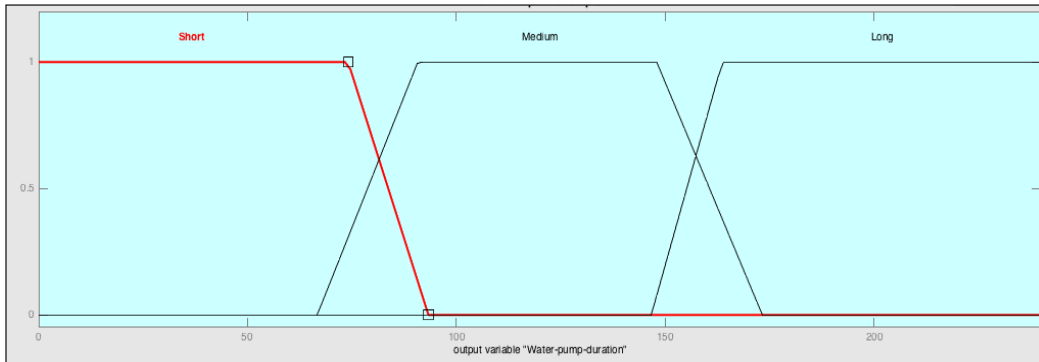


Figure 8. Trapezoidal membership function with fuzzy sets of the duration for water pump

Table 3
Fuzzy rules and action taken using rules based on Mamdani fuzzy inference system

Temperature / Humidity	Too Humid	Humid	Normal	Dry	Too Dry
Too Cold	Long duration (fan)	Long duration (fan)	Medium duration (fan) and short duration (water pump)	Short duration (fan) and medium duration (water pump)	Short duration (fan) and long duration (water pump)
Cold	Long duration (fan)	Medium duration (fan)	Short duration (fan) and (water pump)	Short duration (fan) and medium duration (water pump)	Short duration (fan) and long duration (water pump)
Normal	Short duration (fan)	Short duration (fan)	Short duration (fan) and (water pump)	Short duration (fan) and medium duration (water pump)	Short duration (fan) and long duration (water pump)
Hot	Medium duration (fan) and (water pump)	Medium duration (fan) and (water pump)	Long duration (fan) and (water pump)	Long duration (fan) and (water pump)	Long duration (fan) and (water pump)
Too Hot	Long duration (fan) and (water pump)	Long duration (fan) and (water pump)	Long duration (fan) and (water pump)	Long duration (fan) and (water pump)	Long duration (fan) and (water pump)

Rule 2: IF Temperature is (Hot OR Too Hot) AND Humidity is Too Dry THEN (Action is Long Duration (Fan) AND Long Duration (Water Pump))

Rule 3: IF Temperature is Too Cold AND Humidity is Normal THEN (Action is Medium Duration (Fan) AND Short Duration (Water Pump))

In the fuzzification stage, the crisp input values of humidity and temperature were converted to fuzzy values using the constructed trapezoidal membership functions.

The graphical user interface to design the fuzzy logic is shown in Figure 9, while the defuzzification is described in Figures 10 and 11, respectively. The fuzzification used Max and Min for Boolean operations OR and AND, respectively. The results were fuzzy values for the duration of the ventilation fan and water pump. The defuzzification stage was then performed according to the respective membership functions using the centre of gravity ('centroid') algorithm to obtain the crisp output value for durations.

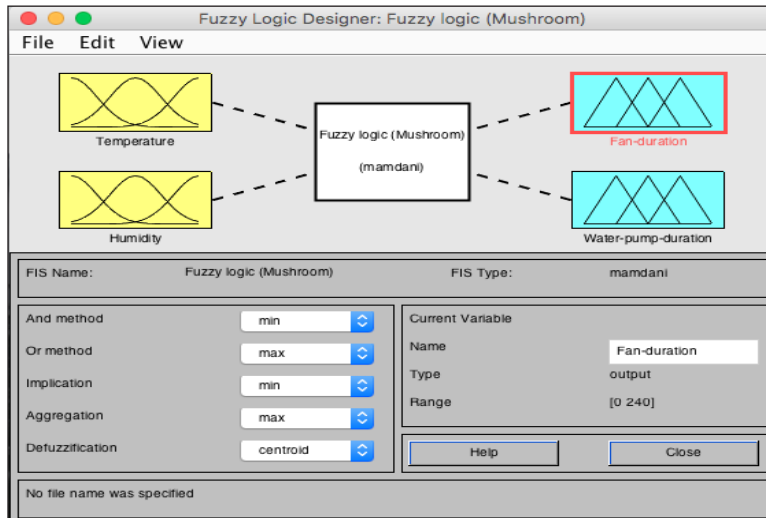


Figure 9. The graphical user interface of the enhanced fuzzy logic-based system by using the Mamdani fuzzy inference system

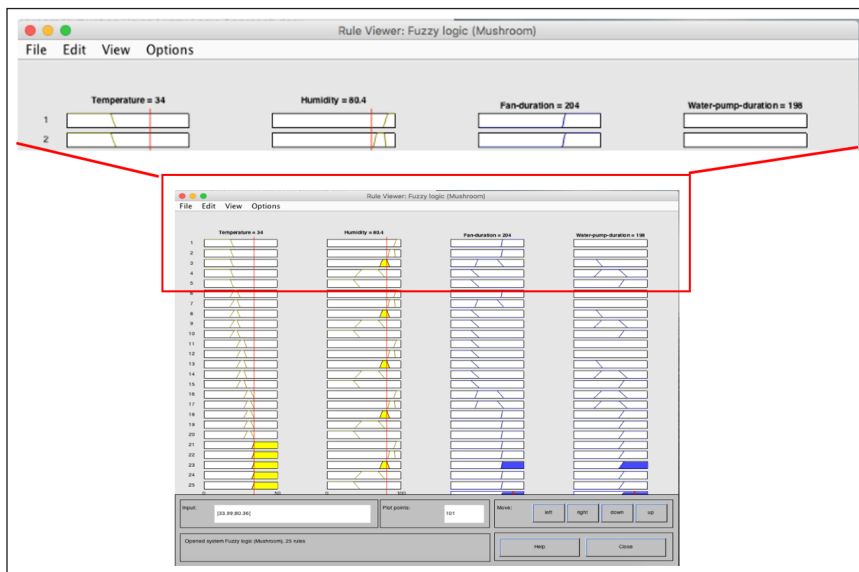


Figure 10. Simulation result for input variables with the temperature value equals to 34°C and the humidity value is equal to 80.4 %

In Figure 10, the crisp input values for temperature and humidity were 34°C and 80.4 %, respectively. The fuzzy logic then executed the rule “IF Temperature is (Hot OR Too Hot) AND Humidity is Normal THEN (Action is Long Duration (Fan) AND Long Duration (Water Pump))” and resulted in turning on the ventilation fan for 204 seconds and the water pump running for 198 seconds.

Figure 11 demonstrates another example of the fuzzy logic system with an input temperature of 16.4°C and a humidity value of 38.9 %. The fuzzy rule “IF Temperature is (Too Cold OR Cold) AND Humidity is Too Dry THEN (Action is Short Duration (Fan) AND Long Duration (Water Pump))” was initiated, and the output resulted in turning on the ventilation fan for 42 seconds and the duration of the water pump for 180 seconds.

The simulated fuzzy logic algorithm was tested based on actual data collected from the sensors, and the actions taken were validated based on the input variables. Finally, the fuzzy logic algorithm was coded in C language and implemented in the NodeMCU controller for the proposed enhanced IoT-based climate control system.

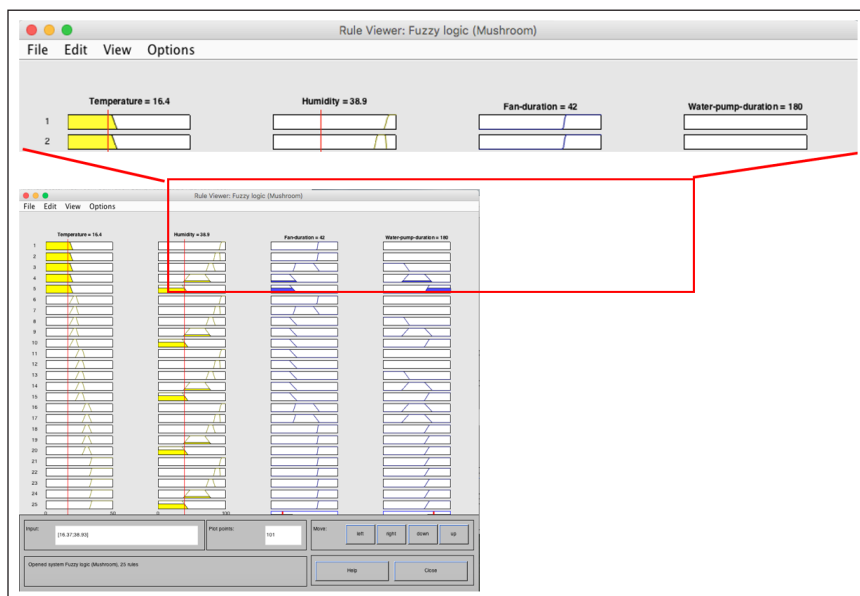


Figure 11. Simulation result for input variables with the temperature value equals 16.4°C and the humidity value is equal to 38.9 %

Web Interface

The IoT system has a web interface that displays the end-users sensor reading, action is taken, and system uptime. It was connected to the Internet, which enabled the end-users to access the web interface remotely via a web browser with Internet access availability. The NodeMCU microcontroller has adequate processing power to run a lightweight web server inside its system. The web server was implemented using built-in Arduino’s ESP8266

Web server function to listen to HTTP client requests. Simple HTML code was written to display the sensor reading. This project retained the same web interface layout as our previous work, as illustrated in Figure 12.

Summary of System Design

As this paper improves the IoT-based climate control system proposed in Ariffin et al. (2020), comparisons of features and specifications are presented in Table 4.



Figure 12. System web interface

Table 4
Summary of improved features and specifications compared to Ariffin et al. (2020)

No	Features / Specification	Ariffin et al. (2020)	Enhanced System Design
1.	Microcontroller Logic	Threshold-based Logic	Fuzzy Logic
2.	Power & Connection	Two 5V External power sources and connection was via Breadboard	Single External power source powering the NodeMCU Baseboard with 5V voltage regulator
3.	Rack Arrangement	Vertical arrangement	Horizontal arrangement to allow optimal airflow and to avoid wetting the mushroom block during rainfall
4.	Water Nozzle Placement	Nozzle was not installed to spray the roof	Installed nozzle to spray water on the roof

System Implementation

This section discusses how the enhanced IOT-based climate control system was implemented in the real-world setup as a proof of concept.

The Mushroom House Setup

The IoT-based climate control system was implemented in a real-world mushroom house located at NASOM Centre in Bandar Puteri, Klang, Malaysia. Thus, the result collected in this paper is based on real-world results. The mushroom house utilised the unused community space at the NASOM Centre to generate income for the autism centre. The mushroom house was built on a brick structure at the bottom and wired fencing reaching the roof to ensure better air circulation. These wired fences were covered with black netting to prevent direct sunlight that is not conducive for oyster mushroom growth. In addition, the water mist spraying system surrounded the floor and roof of the mushroom house to reduce the house's temperature. Figure 13 shows the implementation of the mushroom house with black netting and water mist spraying surrounding the structure. Figure 14 depicts the racks inside the mushroom house that are partially stocked with 500 growing mediums. In Figure 15, the IoT control box that automatically controls the climate inside



Figure 13. Smart Mushroom house situated on the unused community space



Figure 14. Setup of the racks inside the mushroom house

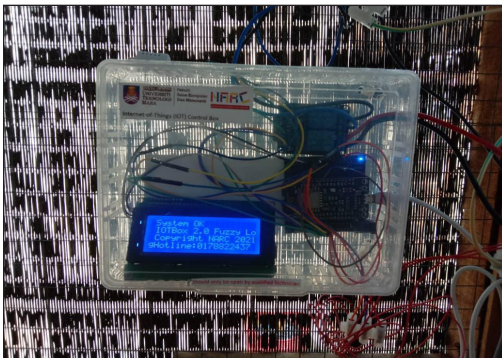


Figure 15. IoT control box for the system



Figure 16. Ventilation fan to cool down the temperature and for air circulation

the mushroom house is displayed. Finally, Figure 16 shows the ventilation fan mounted on the wall to cool down the internal temperature and ensure good air circulation.

Deployment of IoT-Based Climate Control System

The IoT control box was deployed in the house and connected to a relay. Figure 17 shows the flow chart of the system. Upon booting up, the system waited for 5s to ensure the DHT22 sensor could provide a reading for temperature and humidity. If the reading was not NULL, the system calculated the average value for temperature and humidity from the two sensors and displayed it on the LCD and the web interface. Next, the system converted the average temperature and crisp humidity values into fuzzy values and processed them into crisp output based on the fuzzy logic algorithm. The inference made by the fuzzy rules determined whether to turn the water pump and ventilation fan on or off. The result of the inference was displayed on the LCD and the web interface. The system also implemented a safety measure by using an increment to a program counter. If the counter reached above the value of 3, the system paused for an hour to ensure that it did not repeat too many

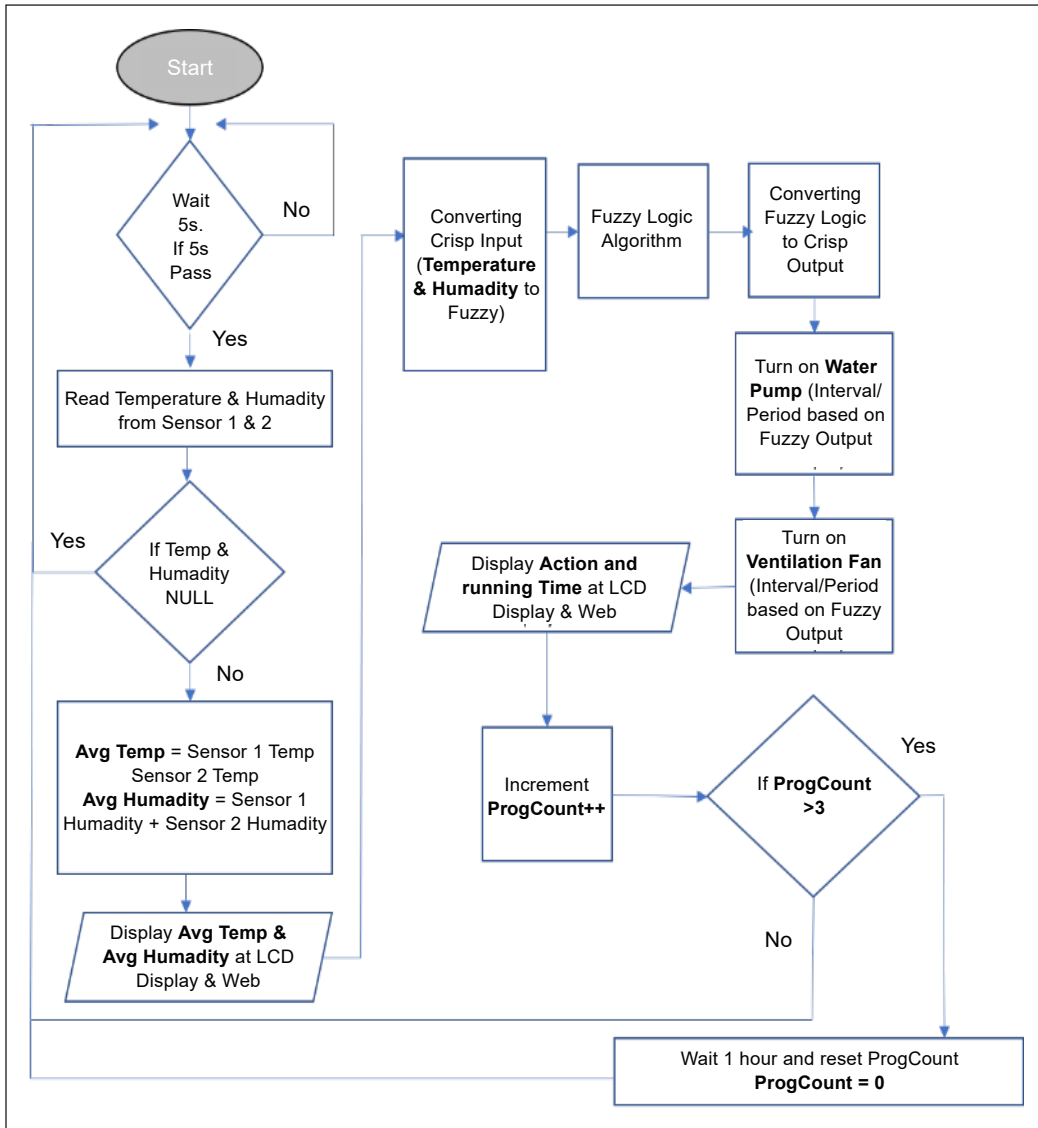


Figure 17. Flowchart of the climate control system

actions. Too many repeated actions may overheat the controller, and continuous running of the water pump will cause water wastage.

The fuzzy logic algorithm implemented 25 fuzzy rules derived from the simulation conducted in MATLAB to determine the duration of operating the water pump and ventilation fan. All the rules were coded using C language using Arduino IDE into the Arduino compatible microcontroller, NodeMCU. The snippet of the code is shown as Algorithm 1. The fuzzy logic was encapsulated in a function that can be invoked every time the microcontroller obtained the crisp temperature and humidity readings.

Algorithm 1: Fuzzy Logic Algorithm Implementation**Input:** *avgt*, *avgh* average temperature and humidity reading from two sensor

```

void fuzzyCalculator(float avgt, float avgh){
if(avgt >= 0 && avgt <=20.0{
  // Long Duration (fan) Rules
  if (avgh >= 90.0 && avgh <= 100.0 ) {
    FanDuration = 250 //seconds
  }
  else if (avgh >= 82.0 && avgh <= 92.0 ) {
    FanDuration = 230 //seconds
  }
  else if (avgh >= 70.0 && avgh <= 85.0 ) {
    FanDuration = 200 //seconds
  }
  else if (avgh >= 38.0 && avgh <= 78.0 ) {
    FanDuration = 180 //seconds
  }
  else if (avgh >= 30.0 && avgh <= 44.0 ) {
    FanDuration = 170 //seconds
  }
  WaterDuration = 0
  indicator = 1;
}
//.....omitting some codes.....

else if(avgt >= 17.0 && avgt <= 24.50){
  // Short Duration (fan) and (Water Pump) Rules
  if (avgh >= 90.0 && avgh <= 100.0) {
    FanDuration = 90 //seconds
    WaterDuration = 90 //seconds
  }
  else if (avgh >= 82.0 && avgh <= 92.0 ) {
    FanDuration = 70 //seconds
    WaterDuration = 70 //seconds
  }
  else if (avgh >= 70.0 && avgh <= 85.0 ) {
    FanDuration = 50 //seconds
    WaterDuration = 50 //seconds
  }
  else if (avgh >= 38.0 && avgh <= 78.0 ) {
    FanDuration = 30 //seconds
    WaterDuration = 30 //seconds
  }
  else if (avgh >= 30.0 && avgh <= 44.0 ) {
    FanDuration = 10 //seconds
    WaterDuration = 10 //seconds
  }
  indicator = 8;
}
//.....Only showing 2 rules out of 25 rules.....
}

```

Output: *FanDuration* and *WaterDuration* value (sec) updated a global variable

RESULTS AND DISCUSSION

The previous IoT-based climate control system using a fixed threshold started in late November 2020, and the enhanced climate control system using fuzzy logic began in January 2021 (Ariffin et al., 2020). This section presents the data captured before and after implementing the enhanced IoT-based climate control system using fuzzy logic. The findings are discussed according to the following criteria:

- i. Water utilisation.
- ii. Temperature.
- iii. Humidity.
- iv. Mushroom harvest per month.

Water Utilisation

The water utilisation for December 2020 and January 2021 were recorded based on the utility bill generated from the Air Selangor customer portal. The bill reflected the total water usage for both the mushroom house and the daycare centre. Since there was no student's activity since November 2020 due to the movement control order as stipulated by the government and the number of households remained the same in the daycare centre, it can be concluded that the decrease in water utilisation was due to the implementation of the enhanced climate control system in the mushroom house.

From November 2020 until December 2020, the system is still running the current IoT system with threshold-based logic. In January 2021, the system has replaced with the newly enhanced system with fuzzy logic. Figure 18 shows a significant decrease in water consumption from 20.0m³ in December 2020 to 12.0m³ in January 2021, indicating that the enhanced climate control system can reduce water consumption. In Table 5, a substantial 40% saving of both water utilisation and total bills in January 2021 can be seen.



Figure 18. Water usage and bill amount for December 2020 and January 2021

Table 5
Percentage of savings after the implementation of the Fuzzy Logic approach

	Month		Differences	Savings (%)
	December 2020	January 2021		
Water Usage (m ³)	20.0	12.0	8.0	40
Bill Amount (RM)	11.4	6.84	4.56	40

Temperature and Humidity Control

In addition to water utilisation, temperature and humidity were also recorded. Thus, we performed a comparative analysis before and after the fuzzy logic algorithm was embedded in the enhanced climate control system. The ‘before’ readings were extracted from (Ariffin et al., 2020). Figures 19 and 20 show the results of average temperature and humidity monitored for six days, respectively. The temperature and humidity readings were taken three times a day, specifically at 10.00 am, 12.00 noon, and 2.00 pm. Then the average was calculated.

The graph in Figure 19 shows that the average temperature was lower most of the days after implementing the fuzzy logic algorithm in the enhanced system. It indicated that the ideal temperature for mushroom cultivation was achieved with the enhanced climate control system. The temperature on day 2 was slightly higher than the day before. However, the average reading for all six days proved that the fuzzy logic embedded in the enhanced

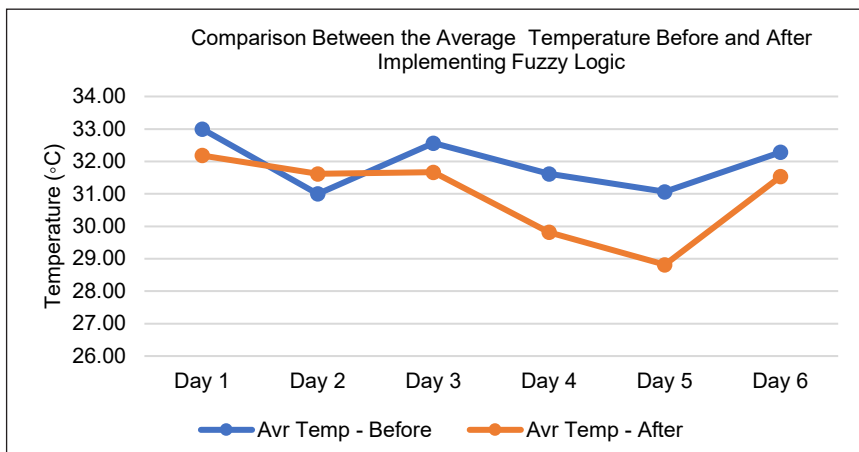


Figure 19. Average temperature before and after implementing Fuzzy Logic

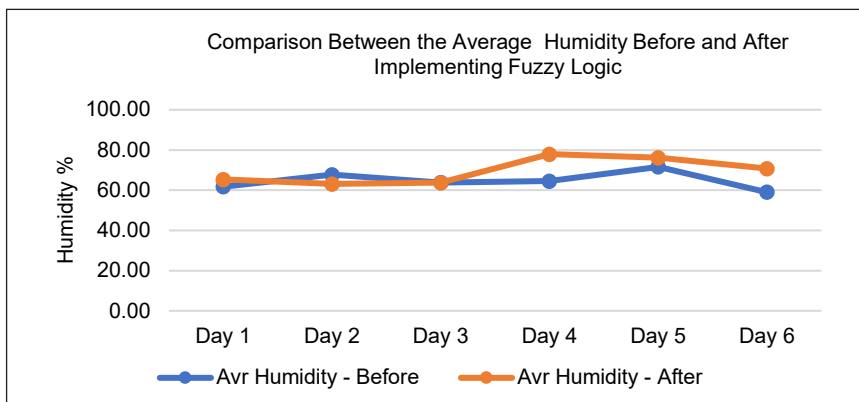


Figure 20. Average humidity before and after implementing Fuzzy Logic

climate control system assisted the temperature management in the mushroom house. The same result appeared in the average humidity graph in Figure 20. Except for day 2, the average humidity was equal to or higher after implementing the fuzzy logic algorithm. These results proved that embedding fuzzy logic in the enhanced climate control system facilitated maintaining and controlling the ideal humidity for mushroom cultivation.

Mushroom Harvest or Yield

A full month mushroom yield was recorded for December 2020 and February 2021. However, due to replacing the previous climate control system with the enhanced system, we omitted the yield for January 2021. As a result, the production of mushrooms increased dramatically from 4.260 kg in December to 10.470 kg in February 2021, as shown in Table 6. The 226% increase of mushroom yield proved that the success of environmental management after implementing the fuzzy logic algorithm had promoted mushroom growth to the optimum.

Table 6
Total mushroom harvested before and after the implementation of the Fuzzy Logic approach

	Month		Differences	Increase of harvest (%)
	December 2020	February 2021		
Total Harvest (kg)	4.620	10.470	6.210	226

CONCLUSION

The cultivation of oyster mushrooms was successfully implemented at NASOM's Autism Care Centre in Bandar Puteri Klang, Malaysia. It has helped the centre generate sustainable income via urban farming. Using a fuzzy logic algorithm and improving both the climate control system and physical internal design of the mushroom house has shown promising results based on the mushroom yield and water saving. The enhanced IoT-based climate control system has been running successfully for more than six months and has produced cumulatively 43.460 kg. On the other hand, there is still room for improvement. Since the IoT-based climate control system was deployed in the real environment, many unexpected, unforeseen circumstances have occurred. For example, the mushroom house is located near a busy road, emissions from vehicles may cause an increase in air pollutants. Our next step is to investigate further the level of carbon dioxide, carbon monoxide or other chemical matters and recommend different technologies to be implemented.

ACKNOWLEDGEMENT

The authors would like to extend appreciation to National Autism Resource Center (NARC) and the Faculty of Computer and Mathematical Sciences, UiTM Shah Alam, for supporting this project by providing a research grant (600-TNCPI/PBT 5/3 (017/2020)).

REFERENCES

- Adenugba, F., Misra, S., Maskeliūnas, R., Damaševičius, R., & Kazanavičius, E. (2019). Smart irrigation system for environmental sustainability in Africa: An internet of everything (IoE) approach. *Mathematical Biosciences and Engineering*, 16(5), 5490-5503. <https://doi.org/10.3934/mbe.2019273>
- Adhitya, R. Y., Ramadhan, M. A., Kautsar, S., Rinanto, N., Sarena, S. T., Munadhif, I., Syai'In, M., Soelistijono, R. T., & Soeprijanto, A. (2017). Comparison methods of fuzzy logic control and feed forward neural network in automatic operating temperature and humidity control system (Oyster mushroom farm house) using microcontroller. In *2016 International Symposium on Electronics and Smart Devices (ISESD)* (pp. 168-173). IEEE Publishing. <https://doi.org/10.1109/ISESD.2016.7886713>
- Algarín, C. R., Cabarcas, J. C., & Llanos, A. P. (2017). Low-cost fuzzy logic control for greenhouse environments with web monitoring. *Electronics*, 6(4), Article 71. <https://doi.org/10.3390/electronics6040071>
- Alpay, Ö., & Erdem, E. (2018). The control of greenhouses based on fuzzy logic using wireless sensor networks. *International Journal of Computational Intelligence Systems*, 12(1), 190-203. <https://doi.org/10.2991/ijcis.2018.125905641>
- Al-Saidi, M., & Elagib, N. A. (2017). Towards understanding the integrative approach of the water, energy and food nexus. In *Science of the Total Environment* (Vol. 574, pp. 1131-1139). Elsevier. <https://doi.org/10.1016/j.scitotenv.2016.09.046>
- Ariffin, M. A. M., Ramli, M. I., Amin, M. N. M., Ismail, M., Zainol, Z., Ahmad, N. D., & Jamil, N. (2020). Automatic climate control for mushroom cultivation using IoT approach. In *2020 IEEE 10th International Conference on System Engineering and Technology (ICSET)* (pp. 123-128). IEEE Publishing. <https://doi.org/10.1109/ICSET51301.2020.9265383>
- Boonchieng, E., Chiochan, O., & Saokaew, A. (2018). Smart farm: Applying the use of NodeMCU, IOT, NETPIE and LINE API for a Lingzhi mushroom farm in Thailand. *IEICE Transactions on Communications*, E101B(1), 16-23. <https://doi.org/10.1587/transcom.2017ITI0002>
- Chiochan, O., Saokaew, A., & Boonchieng, E. (2017). IOT for smart farm: A case study of the Lingzhi mushroom farm at Maejo University. In *2017 14th International Joint Conference on Computer Science and Software Engineering (JCSSE)* (pp. 1-6). IEEE Publishing. <https://doi.org/10.1109/JCSSE.2017.8025904>
- CircuitSchools Staff. (2020). *DHT22 temperature and humidity sensor*. Retrieved June 29, 2021, from <https://www.circuitschools.com/dht22-temperature-and-humidity-sensor/>
- Climate-Data.org. (2021). *Kuala Lumpur climate: Average temperature, weather by month, Kuala Lumpur weather averages*. Retrieved February 28, 2021, from <https://en.climate-data.org/asia/malaysia/kuala-lumpur/kuala-lumpur-715107/#climate-graph>
- Cruz-Del Amen, J. D., & Villaverde, J. F. (2019). Fuzzy logic-based controlled environment for the production of oyster mushroom. In *2019 IEEE 11th International Conference on Humanoid, Nanotechnology, Information Technology, Communication and Control, Environment, and Management (HNICEM)* (pp. 1-5). IEEE Publishing. <https://doi.org/10.1109/HNICEM48295.2019.9072902>
- Hamidzade, M., Taghavi, S. M., Martins, S. J., Herschlag, R. A., Hockett, K. L., Bull, C. T., & Osdaghi, E. (2020). Bacterial brown pit, a new disease of edible mushrooms caused by mycetocola sp. *Plant Disease*, 104(5), 1445-1454. <https://doi.org/10.1094/PDIS-10-19-2176-RE>

- Hendrawan, Y., Anta, D. K., Ahmad, A. M., & Sutan, S. M. (2019). Development of fuzzy control systems in portable cultivation chambers to improve the quality of oyster mushrooms. *IOP Conference Series: Materials Science and Engineering*, 546(3), Article 032013. <https://doi.org/10.1088/1757-899X/546/3/032013>
- Ibrahim, N. H. N., Brahim, A. R., Mat, I., Harun, A. N., & Witjaksono, G. (2018). IR 4.0 using IoT and LORAWAN to accelerate *Lentinula Edodes* growth. In *2018 2nd International Conference on Smart Sensors and Application (ICSSA)* (pp. 28-32). IEEE Publishing. <https://doi.org/10.1109/ICSSA.2018.8535954>
- Kashyap, M., Sharma, V., & Gupta, N. (2018). Taking MQTT and NodeMcu to IOT: Communication in internet of things. *Procedia Computer Science*, 132, 1611-1618. <https://doi.org/10.1016/j.procs.2018.05.126>
- Kassim, M. R. M., Mat, I., & Yusoff, I. M. (2019). Applications of internet of things in mushroom farm management. In *2019 13th International Conference on Sensing Technology (ICST)* (pp. 1-6). IEEE Publishing. <https://doi.org/10.1109/ICST46873.2019.9047702>
- Krishnan, R. S., Julie, E. G., Robinson, Y. H., Raja, S., Kumar, R., Thong, P. H., & Son, L. H. (2020). Fuzzy logic based Smart Irrigation System using Internet of Things. *Journal of Cleaner Production*, 252, Article 119902. <https://doi.org/10.1016/j.jclepro.2019.119902>
- Li, S., Ding, X., Kuang, Q., Ata-UI-Karim, S. T., Cheng, T., Liu, X., Tian, Y., Zhu, Y., Cao, W., & Cao, Q. (2018). Potential of UAV-based active sensing for monitoring rice leaf nitrogen status. *Frontiers in Plant Science*, 9, Article 1834. <https://doi.org/10.3389/fpls.2018.01834>
- Mat, I., Kassim, M. R. K., Harun, A. N., & Yusoff, I. M. (2019). Smart agriculture using internet of things. In *2018 IEEE conference on open systems (ICOS)* (pp. 54-59). IEEE Publishing. <https://doi.org/10.1109/ICOS.2018.8632817>
- Najmurokhman, A., Kusnandar, Daelami, A., Nurlina, E., Komarudin, U., & Ridhatama, H. (2020). Development of temperature and humidity control system in Internet-of-Things based oyster mushroom cultivation. In *2020 3rd International Seminar on Research of Information Technology and Intelligent Systems (ISRITI)* (pp. 551-555). IEEE Publishing. <https://doi.org/10.1109/ISRITI51436.2020.9315426>
- Navarro, E., Costa, N., & Pereira, A. (2020). A systematic review of IoT solutions for smart farming. *Sensors*, 20(15), Article 4231. <https://doi.org/10.3390/s20154231>
- Nongthombam, J., Kumar, A., Ladli, B., Madhushekar, M., & Patidar, S. (2021). A review on study of growth and cultivation of oyster mushroom. *Plant Cell Biotechnology and Molecular Biology*, 22(5&6), 55-65.
- Poulsen, M. N., Neff, R. A., & Winch, P. J. (2017). The multifunctionality of urban farming: Perceived benefits for neighbourhood improvement. *Local Environment*, 22(11), 1411-1427. <https://doi.org/10.1080/13549839.2017.1357686>
- Revathi, S., & Sivakumaran, N. (2016). Fuzzy based temperature control of greenhouse. *IFAC-PapersOnLine*, 49(1), 549-554. <https://doi.org/10.1016/j.ifacol.2016.03.112>
- Saw S. H. (2007). *The population of Peninsular Malaysia*. Institute of Southeast Asian Studies.
- Shakir, A. A., Hakim, F., Rasheduzzaman, M., Chakraborty, S., Ahmed, T. U., & Hossain, S. (2019). Design and implementation of SENSEP ACK: An IoT based mushroom cultivation monitoring system. In *2019*

- International Conference on Electrical, Computer and Communication Engineering (ECCE)* (pp. 1-6). IEEE Publishing. <https://doi.org/10.1109/ECACE.2019.8679183>
- Tang, K. H. D. (2019). Climate change in Malaysia: Trends, contributors, impacts, mitigation and adaptations. In *Science of the Total Environment* (Vol. 650, pp. 1858-1871). Elsevier. <https://doi.org/10.1016/j.scitotenv.2018.09.316>
- Wahab, H. A., Manap, M. Z. I. A., Ismail, A. E., Ong, P., Ismon, M., Zainulabidin, M. H., Noor, F. M., & Mohamad, Z. (2019). Investigation of temperature and humidity control system for mushroom house. *International Journal of Integrated Engineering*, 11(6), 27-37. <https://doi.org/10.30880/ijie.2019.11.06.004>
- Wong, C. L., Liew, J., Yusop, Z., Ismail, T., Venneker, R., & Uhlenbrook, S. (2016). Rainfall characteristics and regionalization in Peninsular Malaysia based on a high resolution gridded data set. *Water*, 8(11), Article 500. <https://doi.org/10.3390/w8110500>
- Xia, J., Yang, Y., Cao, H., Zhang, W., Xu, L., Wang, Q., Ke, Y., Zhang, W., Ge, D., & Huang, B. (2018). Hyperspectral identification and classification of oilseed rape waterlogging stress levels using parallel computing. *IEEE Access*, 6, 57663-57675. <https://doi.org/10.1109/ACCESS.2018.2873689>



Participatory Design: Apps from The Older Adults to The Older Adults

Zaidatol Haslinda Abdullah Sani*, Dinna@Ninna Mohd Nizam and Aslina Baharum

Faculty of Computing and Informatics, Universiti Malaysia Sabah, Labuan International Campus, 87000 Labuan FT, Malaysia

ABSTRACT

The use of technology to address health issues among older adults is becoming popular nowadays, but, in practice, there is very little systematic work on how to design and develop for older adults. This paper investigated participatory design in designing and developing two mobile apps to support community-living older adults to maintain their health. We examine 1) three older adults to individually participate in designing an app to self-monitor their fruit, vegetable and liquid intakes and 2) a group of four older adults participate in designing an app to address loneliness. In this paper, we present methodological insights of conducting participatory design with older adults. We focus more on the mutual learning between the researcher and the older adults as “designers”. We found that both methods provide rich data for developing the apps. However, when having a group of older adults together was found to stimulate the discussion among them easily, the participants were more open to critique the design suggestions, the moderator did not have to provoke often to guide the discussion, and in terms of time, although the session was slightly longer, it generates more data per participant. We acknowledge that the topic between the two groups

was different, and each topic’s privacy was also a concern. We also acknowledge that the number of participants is low, and the participant’s technology background can be a concern. Either way, we recommend continuing to involve older adults in the technology design and development phase.

ARTICLE INFO

Article history:

Received: 13 May 2021

Accepted: 19 August 2021

Published: 22 October 2021

DOI: <https://doi.org/10.47836/pjst.29.4.35>

E-mail addresses:

linda.sani@ums.edu.my (Zaidatol Haslinda Abdullah Sani)

dinna@ums.edu.my (Dinna@Ninna Mohd Nizam)

aslina@ums.edu.my (Aslina Baharum)

* Corresponding author

Keywords: Evaluation, participatory design, user experience

INTRODUCTION

Defining when one becomes old is difficult. The chronological age of 65 years or over is often the definition of older adults, as this has become the retirement age in most countries. However, not all countries have the same retirement age. Develop countries, for example, the United States, currently retires at age 66. In developing countries, such as Malaysia, the retirement age is slightly lower, which is either 55, 56, 58, or 60, depends solely on the employee themselves when they want to retire. Moreover, in some countries, the retirement age differs between genders. For example, in China, the men retire at age 60 years, and the women retire at age 50 to 55 years. Thus, with respect to all nations, the World Health Organization (WHO) and the United Nations (UN) use 60 years and above to define older adults in their reports. The population of older adults aged 60 years and above worldwide is multiplying (WHO, 2021). It is predicted that by 2050, the older adult population will double the current amount (WHO, 2021).

In Malaysia, however, the Department of Statistics Malaysia (DOSM) refers to an older adult as one age 65 years and above. Older adults increased from 1.75 million (5%) in 2010 to 2.3 million (7%) in 2020. The number is estimated to increase to 3.49 million (14.5%) in 2040 (DOSM, 2020). The DOSM has also projected that in 2040 the younger population age below 14 years old to decrease from 27.4% in 2010 to 18.6% in 2040. DOSM also predicted that the old-age support ratio, the number of working adults aged 15 to 64 years to older adults, will triple from 7.4 in 2010 to 21.7 in 2040 (DOSM, 2020). It shows a growing need to support older adults to remain independent in their later life.

The rising of the older adult population has raised concerns regarding their health conditions as their health tends to decline easily. Common health issues among older adults are malnutrition, dehydration and loneliness (BDA, 2021). It is known that the solution to treat any health issues is through healthy eating with well-balanced nutrition. In regard to loneliness, bereavement or children moving away from the family home are the most common reasons why older adults feel lonely in their later age. Moreover, older adults would not want to have health issues as these feelings are private and personal (Sani et al., 2020).

The rising of the older adult population and the low number of younger adults raised concerns that we need to ensure that the older adults will have enough support to live on their own in their later life. In regard to this, technology has become a promising tool to promote healthy living among older adults. There is a growth of gerontology studies to assist older adults to promote healthy attitudes and behaviour among older adults. Several technologies have been developed to assist older adult's health issues apart from taking medicines. For example, Tulu et al. (2016) developed an app for diabetic older adults to self-manage their daily life. Hakobyan et al. (2016) designed and developed a diet diary app for older adults with age-related macular degeneration. Sani and Petrie (2017) designed

and developed an app for the community living older adults to self-monitor their food and liquid intakes. Mehra et al. (2018) developed an app to guide and monitor older adults exercising from afar. All of these examples have the same aim, which is to assist older adults to self-monitor themselves.

Participatory Design

Designing an app for older adults is not an easy task. This population group needs specific skills and guidelines prior to designing such technology for them. Participatory design is one method that engages all users of such technology to raise concerns, provide ideas and suggestions in designing such technology (DiSalvo et al., 2017). The thought of bringing users as close to the project development tends to bring them joy as they deem the technology is then developed based on all their requirements, concerns, ideas and suggestions. Participatory design occurs in the early stage of the software development cycle. The process of conducting participatory design is considered cheap as no coding is involved. Thus the overall project cost can be reduced by only paying programmers to develop only after the design of the technology is secure.

The aim of participatory design is evaluation. That said, the prototype or concept design was iteratively designed and evaluated to improve problems found in the original design. Therefore, the shared views and concerns raised during the participatory design sessions are essential, especially during design. Human-Computer Interaction (HCI) studies conducting participatory design has proven that by incorporating users as the “designers” during the design stage, the usability of the technology is often positive.

For example, a study by Razak et al. (2013) shows that including a number of older adults in a participatory design to develop a medicine reminder system brings positive outcomes during the field study. Fewer usability problems have been found in each stage of the design and development. Lee et al. (2017) conducted a participatory design to design a robotic technology with older adults with depressions. They conducted a few stages of participatory design involving all stakeholders, including many older adults, clinicians and caretakers. Rich data have been gathered to design the robotic technology, including the methodological aspect of conducting participatory design. Another participatory design by Ahmed et al. (2019) found that the method works perfectly in order for the researcher to develop a dashboard system for the cardiac patient. Similarly, this study conducted participatory design sessions with new numbers of older adults and clinicians.

Number of Participants per Participatory Design

There are mixed views in the literature about the optimal number of participants in a participatory design. In the Handbook of Participatory Design, the authors highlighted having several people join a participatory design to get a broader view or ideas of evaluating

such a product (Simonsen & Robertson, 2012). Fewer participants may influence the number of data gathered compared to having a large number of participants. However, no exact figure was given. A survey paper by Bossen et al. (2016) also did not highlight the optimum number of participants in the 17 participatory design studies they reviewed. The authors focused more on the result and the process to run the participatory design study.

In the early days, taken nearly a decade back, in Razak et al. (2013) study, as stated above, they recruited six older adults in six different sessions to achieve the paper's objective. That being said, they had one older adult per one participatory design session. However, just a year later, in a study by Wilkinson and De Angeli (2014), they recruited 25 participants (16 males, 9 females) in one session to investigate designing a walking-aid intelligent mobility device to assist in daily activities, for example, shopping in a shopping complex. The session includes discussing how shopping means for them and how technology can assist them in shopping effectively.

In Van Vensen et al. (2015), they recruited seven participants (no gender given) in one session to discuss a technology design concept for detecting and preventing frailty among older adults. However, in a study by Šabanović et al. (2015) to design socially assistive robots for older adults, they conducted two workshops to 1) learn what older adults think about technology and 2) design technology that suits them. In the first workshop, the authors had four participants (3 males, 1 female). In the second workshop, they had three participants (2 males, 1 female).

In recent studies of engaging older adults in participatory design by Ahmed et al. (2019), the authors recruited seven older adults in one participatory design session to design a dashboard system for the cardiac patient. In LaMonica et al. (2021) study, they had 21 older adults in four participatory design sessions. Unfortunately, no breakdown of the number of participants in each session was given.

To the best of our knowledge, after reviewing the literature, although all papers succeeded in using participatory design to achieve their objectives, no specific reason was given as to why the authors had this number of participants. The numbers varied from having one participant per participatory design study to 25 per session. There is also no definite number of participants for participatory design concerning the age group of the participants, especially with older adults. It shows that limited participatory design studies investigated the number of participants that suits a participatory design session. The mixed views on the optimal number of participants per participatory design prompt us to explore more in this area and how this affects the quality of the evaluation elicited. We also hoped to provide reflections on how best to conduct participatory design with older adults.

We are interested in designing and developing apps for older adults to address malnutrition, dehydration, and loneliness. Unfortunately, these health areas are too private and personal for a community of older adults to admit that they are malnourished or lonely.

Thus, we are interested in investigating the use of two participatory designs to design two apps. The first participatory design is to be conducted individually between one older adult and the moderator, following what was practised by Razak et al. (2013) to address malnourishment. The second participatory design to address loneliness to be conducted in groups, following what was practised by Šabanović et al. (2015).

This paper is organised as a section of the methodology, followed by the results and discussions, and lastly, conclusion of the paper.

METHODOLOGY

Design

Two participatory design studies were conducted to achieve this. These two app suggestions derive from our previous study, which can be found in Sani et al. (2020). One participatory design (hereafter “PD1”) with three older adults was to individually design a web app to self-monitor their fruit, vegetable and liquid intakes. The second participatory design (hereafter “PD2”) was with a group of four older adults to design a smartphone app to address loneliness.

For both studies, a concept design storyboard of how the app might work was illustrated to the participant. That said, for PD1, a concept design to self-monitor fruit and vegetable intakes were provided and for PD2, a concept design to address loneliness was presented. The concept design was created following heuristics and guidelines for developing applications for older adults (e.g. Silva et al., 2015; Baharum et al., 2018; Sani & Petrie, 2019). The concept designs were then evaluated for usability with experts prior to the study with the older adults. It makes sense to allow the experts to identify potential usability problems before evaluating the system to the older adults.

This study evaluated the concept design in three sessions to the participants in PD1 and one session for PD2. Both studies were moderated by the same moderator who has experience in research with older adults.

Participants

The inclusion criteria were to be 55 years or over, as this is still a choice of retirement age in Malaysia, and to live independently, either alone or with family members. That being said, we did not recruit older adults who have a carer or one who cannot manage to take care of themselves. Participants did not have to have any technology experiences. Participants were recruited from Pusat Aktiviti Warga Emas (PAWE), a social centre for older adults in Malaysia. In addition, participants were recruited from PAWE Labuan and PAWE Kota Kinabalu. All participants own and use smartphones. None of the participants was related to one another. Table 1 summarises the participants demographic.

Table 1
Demographic of the participants

Characteristic	PD1	PD2
Gender	2 women, 1 man	2 women, 2 men
Age	60 – 63 years	62 – 65 years
Living Arrangement	All living with partner / family	All living with partner / family
Employment Status	All retired	All retired

Procedure

The procedure was the same for both studies. Malay and English languages were used to ease the participants. For PD1, the session started one by one with 10 minutes gap in between. Each session lasted approximately 45 mins. For PD2, one session was conducted with all four participants discussing together. The session was approximately 110 mins. During the studies, there were no other activities at PAWE.

The moderator started the study by introducing the objectives and procedures of the study. Participants were welcome to ask any questions prior to the study if they had any confusion. The moderator then displayed the concept design of the app. The participants were then asked to think aloud their thoughts and concerns about the design. The participants were also asked to give design suggestions and improvements if they deemed needed to motivate them to use the app in the future.

At the end of the study, the moderator highlighted all the key points reported by the participants. The participants were also debriefed. Finally, pack lunch meals and a monetary reward was given to each participant to thank them for their time and efforts.

Materials and Equipment

Two concept design storyboards were printed screen by screen on A4 papers. Sample of the concept design for PD1 and PD2 is as shown in Figures 1 and 2, respectively. In addition, each participant was given a copy of the concept design storyboard for both sessions to stimulate the discussion.

Participants were also provided with A4 papers for them to scribble their design suggestions and concerns. In addition, pens and markers were scattered around the table to reach them when needed easily.

The studies were audio-recorded using the Voice Recorder application on Samsung Note 9, running on Android 10.

Data Analysis

The audio recordings were transferred to iTunes for transcriptions and analysis of data. The transcriptions were translated to English by a translator.

Participatory Design: Apps from Older Adults to Older Adults

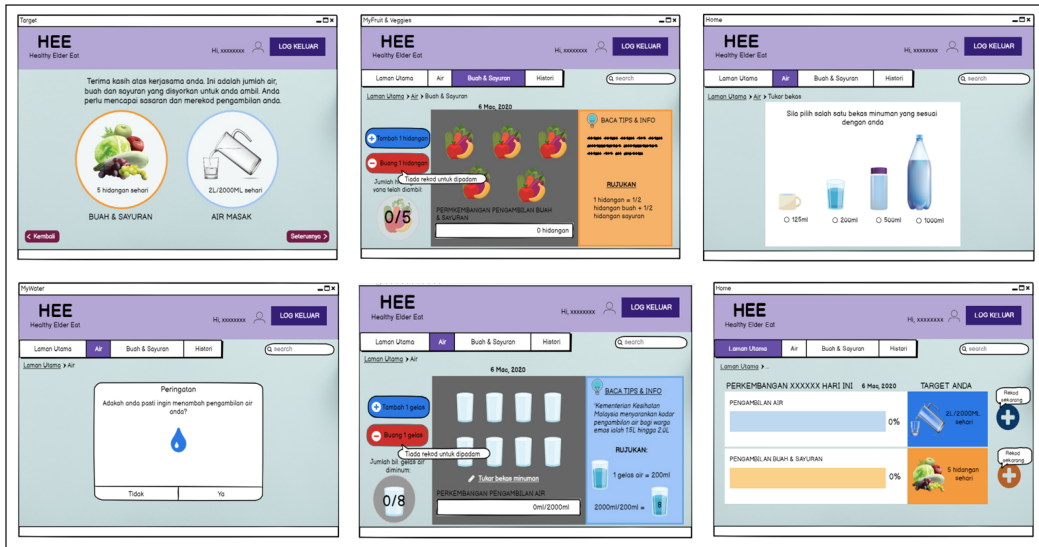


Figure 1. Sample of the concept design for PD1; an app to self-monitor fruit, vegetable and liquid intakes

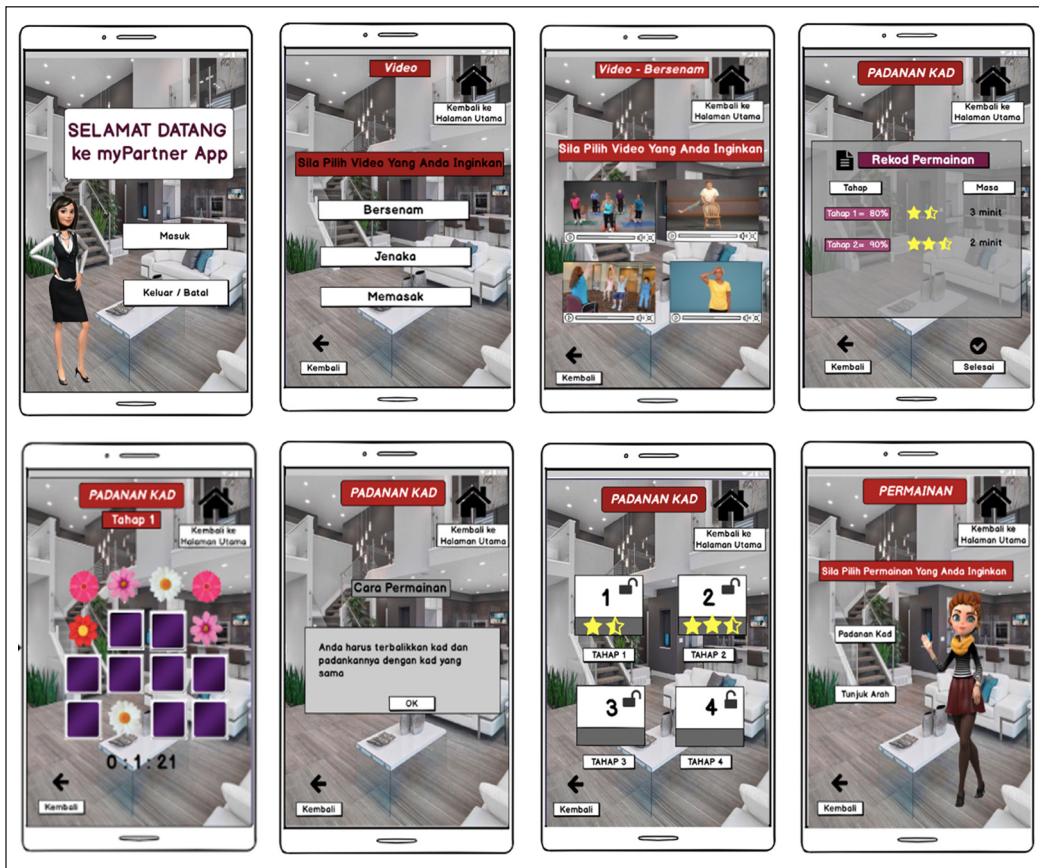


Figure 2. Sample of the concept design for PD2; an app to address loneliness

Thematic analysis was conducted on the transcripts (Terry et al., 2017). It was to identify all suggestions, ideas, and concerns related to older adults in using the apps. First, an open coding technique was done until refined themes were found (Williams & Moser, 2019). Then, to ensure the inter-coder reliability of the themes, a second coder went through all of the suggestions, ideas, and concerns and any disagreements were resolved.

RESULT

The studies provided insights that older adults can articulate their wants and needs in designing technology. For example, in both PD1 and PD2, we repeatedly found similar themes across both studies regarding having a technology that suits this particular group.

Awareness of Personal Limitation

Older adults have a certain ability to remember as their cognitive ability tends to decline as they get old. The older adults in this study were aware of their limitations in achieving a certain goal. It was repeatedly said in both PD1 and PD2. Some of the comments were:

- “I do not think I can remember all those steps” *PD1.p1*
- “The memory game requires a lot of attention I need time to learn that” *PD2.p3*
- “The exercise should be suitable for us we are sixty plus we cannot do like the younger people do” *PD2.p1*
- “That message was good it is needed so we know what we just did you know sometimes we tend to forget” *PD1.p1*

Self-doubt and Concerns

Literature has shown that older adults have positive and negative attitudes towards technology (e.g. Anderson & Perrin, 2107; Elueze & Quan-Haase, 2018). Similar to the findings in the literature, some older adults in this study also doubt certain features of the app and their capability to use it. Some of the comments were:

- “well I guess you know that we are not well adapt to using technology changes can be made but I think to get everyone to like using it is a different story” *PD1.p3*
- “you were born in a different era than us we grew up with no technology whatsoever I only started seeing this when I work I mean a few years working already then only we had computers the big ones so what I am trying to say is this changes it takes time maybe for me maybe not for me” *PD2.p2*

Encouraging Interactions

Literature has shown that older adults are prone to using such technologies if given sufficient and not burden instructions (Betts et al., 2019). The older adults in this study reported

needing encouraging interactions that can assist them when required, especially if they feel lost upon using the technology. Some of the comments were:

- “I was a bit lost just now maybe you can have a little note to tell us where are we now” *PD2.p2*
- “so now what will happen how can I see what I just drank maybe you can direct me to that page or at least give me a message” *PD1.p1*
- “this is useful when you keep on giving us those messages I can see it helps us I like them” *PD1.p2*

Learnability

The older adults in this study prefer to use technology that does not require them to learn a lot. Instead, they suggest having features that are similar or familiar to them. It can be seen to reduce their mental workload to learn something new. Some of the comments were:

- “The overall flow of adding intakes should be made easy” *PD1.p3*
- “Why not you do something that is familiar to us but in a technology way I mean for example the ” *PD1.p1*
- “The layout should be consistent and similar among all pages if a button is there at this page it should be there at the next page with the same size same location as an older person it will be easier for us to remember if there is not a lot of changes between the pages” *PD2.p3*
- “limit the amount of features to do per page please I cannot remember what to do if you give me all of those in one go” *PD1.p2*

Privacy and Personal Matters

We are aware that the topics between the two studies are different. We noticed that the older adults in PD1 are more open to discussing from their perspective. However, in PD2, the older adults often discuss by referring themselves to a friend or partner. Some of the comments were:

- “I want to use it cause I want to know my daily intakes I can also compare my whole week or months right” *PD1.p3*
- “I cannot lie I do not really drink water but I think this can help me to monitor my intake” *PD1.p2*
- “if you ask me know I can only say from the perspective of other older adults because I do not think that I am lonely” *PD2.p3*
- “Like my friend she lives alone she never says she is lonely but I think she is especially at night her children lives far away and she lost her husband I think this app can be useful for her she can spend time using it” *PD2.p1*

- “for example my husband he is a lot older than me he likes to stay at home I sometimes go out with my girl friends we go mengaji like that so I think like my husband he can use this to fill in his free time rather than just watching tv right when I am not around” *PD2.p4*
- “maybe you can include a chatting section or video call features like whatsapp right I am not that lonely but I do think communication is important to reduce loneliness my sister living far in our village might need this app she can play the game or do some exercise to spend some time alone right” *PD2.p3*

Older Adults as Designers

Both PD1 and PD2 were discussing health app designs that might help older adults in their daily life. We acknowledge that both topics were significant health issues among older adults (BDA, 2021).

In PD1, the moderator had to provoke the session more to encourage the design suggestions, which was not a surprise as this was a one-to-one discussion. In PD2, the participants built up the discussion and suggestions but were closely monitored by the moderator to avoid the discussion going out of topic or one participant conquering the discussion.

In PD1, we noticed that involving the moderator directly with the participants, allows them to articulate their design concerns and needs eagerly. Unfortunately, compared to PD2, some design suggestions or concerns were supported or rejected by the participants. However, the moderator resolved it by reminding us that all suggestions or concerns were welcome in the discussion.

In regards to time, four sessions of PD1 were approximately 60mins per participant. For PD2, the session lasted for 110mins. Therefore, it can be said as 27.5mins per participant to articulate their thoughts and concerns on the discussion. We did not count the number of contributions per participant as it was not in the interest of this paper.

DISCUSSIONS AND CONCLUSION

This paper investigated the use of two methods on participatory design for working with older adults to design and evaluate technologies to support independent living. That being said, our study focuses on the mutual learning concept between researchers and the older adults as users.

For PD1, we asked about an app to self-monitor fruits, vegetables and liquid intake. For PD2, we asked about an app to address loneliness. We found that both PDs brings rich data to our research. However, in PD1, the moderator may need to put effort to encourage the

discussion. It is not a big issue as participants need time to warm up prior to the discussion. In PD2, although the participants did not know each other, they managed to sit down and discuss the topic together. No major issue was raised during PD2. All participants were given time to speak, raised concerns and gave suggestions to design the app.

We acknowledged that the topic of discussions might be too personal or private. However, the participants in both PDs did not claim that they were lonely or malnourished. Their health condition is also not in the interest of the PDs. In PD2, the participants refer to loneliness by referring to themselves from a friend or partner's point of view. In PD1, by just having the moderator and the participant in each session, the participants seem to be more open and gave concerns from their point of view. It is, however, not the interest of this paper to compare the amount of contribution per participant in regards to the same topic, individually or in a group.

We understand the fact that older adults are less experienced in using technology as compared to younger adults. Thus, we recommend that the moderator be well adept and experienced in research with older adults. Although there was no issue in the study, moderators may need to explain more, especially in the designs and interfaces that are not familiar with the older adults. In particular, we found that the older adults in PD2 did not like the interactions with humour videos, which further investigation can be done. We also acknowledge that the participants in this study have a socio-economic of the somewhere middle class. Thus, the results might differ if we had a range of participants.

We are also aware of the limitations relating to the methodology, and the conclusion drawn from this paper should be taken with these in mind. Finally, we acknowledge that although this current study produced enough data for us to develop the apps, this study has a very minimal number of participants that are unable to represent the whole targeted population.

Overall, either alone or in a group, both methods show that older adults can articulate their wants and needs in designing technology. Therefore, we recommend using this method in regard to designing technologies for older adults. Future work can perhaps investigate preference PD based on the topic to be discussed. It is unclear from this study if the topics in both PDs interfere with the contribution per discussion.

ACKNOWLEDGEMENTS

University Malaysia Sabah funds this research under the grant SPLB0180-2018 led by the first author. We want to thank all participants in this study for their time and effort. We would also like to thank the first author's Final Year students for assisting in designing and developing the apps.

REFERENCES

- Ahmed, R., Toscos, T., Ghahari, R. R., Holden, R. J., Martin, E., Wagner, S., & Mirro, M. (2019). Visualization of cardiac implantable electronic device data for older adults using participatory design. *Applied Clinical Informatics*, 10(4), 707-718. <https://doi.org/10.1055/s-0039-1695794>
- Anderson, M., & Perrin, A. (2017). *Technology use among seniors*. Pew Research Center for Internet & Technology.
- Baharum, A., Ismail, R., Saad, N., Daruis, D. D. I., Noh, N. A. M., & Noor, N. A. M. (2018). Development of elderly reminder mobile application using mental model. In *Proceedings of the 2018 International Conference on Artificial Intelligence and Virtual Reality* (pp. 131-136). ACM Publishing. <https://doi.org/10.1145/3293663.3293665>
- Betts, L. R., Hill, R., & Gardner, S. E. (2019). "There's not enough knowledge out there": Examining older adults' perceptions of digital technology use and digital inclusion classes. *Journal of Applied Gerontology*, 38(8), 1147-1166. <https://doi.org/10.1177/0733464817737621>
- Bossen, C., Dindler, C., & Iversen, O. S. (2016). Evaluation in participatory design: A literature survey. In *Proceedings of the 14th Participatory Design Conference: Full papers-Volume 1* (pp. 151-160). ACM Publishing. <https://doi.org/10.1145/2940299.2940303>
- BDA. (2021). *Loneliness and malnutrition*. The Association of UK Dietitians
- DOSM. (2020). *Current population estimates, Malaysia, 2018-2019*. Department of Statistics Malaysia.
- DiSalvo, B., Yip, J., Bonsignore, E., & DiSalvo, C. (Eds.). (2017). *Participatory design for learning: Perspectives from practice and research*. Taylor & Francis.
- Elueze, I., & Quan-Haase, A. (2018). Privacy attitudes and concerns in the digital lives of older adults: Westin's privacy attitude typology revisited. *American Behavioral Scientist*, 62(10), 1372-1391. <https://doi.org/10.1177/0002764218787026>
- Hakobyan, L., Lumsden, J., Shaw, R., & O'Sullivan, D. (2016). A longitudinal evaluation of the acceptability and impact of a diet diary app for older adults with age-related macular degeneration. In *Proceedings of the 18th International Conference on Human-Computer Interaction with Mobile Devices and Services* (pp. 124-134). ACM Publishing. <https://doi.org/10.1145/2935334.2935356>
- LaMonica, H. M., Davenport, T. A., Roberts, A. E., & Hickie, I. B. (2021). Understanding technology preferences and requirements for health information technologies designed to improve and maintain the mental health and well-being of older adults: Participatory design study. *JMIR Aging*, 4(1), Article e21461. <https://doi.org/10.2196/21461>
- Lee, H. R., Šabanović, S., Chang, W. L., Nagata, S., Piatt, J., Bennett, C., & Hakken, D. (2017). Steps toward participatory design of social robots: Mutual learning with older adults with depression. In *Proceedings of the 2017 ACM/IEEE international conference on human-robot interaction* (pp. 244-253). ACM Publishing. <https://doi.org/10.1145/2909824.3020237>
- Mehra, S., Visser, B., Dadema, T., Van Den Helder, J., Engelbert, R. H., Weijs, P. J., & Kröse, B. J. (2018). Translating behavior change principles into a blended exercise intervention for older adults: Design study. *JMIR Research Protocols*, 7(5), Article e117. <https://doi.org/10.2196/resprot.9244>

- Razak, F. H. A., Razak, N. A., Adnan, W. A. W., & Ahmad, N. A. (2013). How simple is simple: Our experience with older adult users. In *Proceedings of the 11th Asia Pacific Conference on Computer Human Interaction* (pp. 379-387). ACM Publishing. <https://doi.org/10.1145/2525194.2525307>
- Šabanović, S., Chang, W. L., Bennett, C. C., Piatt, J. A., & Hakken, D. (2015). A robot of my own: Participatory design of socially assistive robots for independently living older adults diagnosed with depression. In *International conference on human aspects of it for the aged population*(pp. 104-114). Springer. https://doi.org/10.1007/978-3-319-20892-3_11
- Sani, Z. H. A., & Petrie, H. (2017). Evaluation of an app to support healthy living by older adults. *Electronic Visualisation and the Arts (EVA 2017)*, 1-14. <https://doi.org/10.14236/ewic/HCI2017.42>
- Sani, Z. H. A., & Petrie, H. (2019). Older adults' number entry using touchscreen and keyboard-mouse computers. In *International Visual Informatics Conference* (pp. 353-367). Springer. https://doi.org/10.1007/978-3-030-34032-2_32
- Sani, Z. H. A., Nizam, D. N. M., Baharum, A., & Tanalol, S. H. (2020). Older adults' needs and worries about healthy living and mobile technology: A focus group study. *International Journal of Advanced Science and Technology*, 29(9s), 1127-1136.
- Silva, P. A., Holden, K., & Jordan, P. (2015). Towards a list of heuristics to evaluate smartphone apps targeted at older adults: a study with apps that aim at promoting health and well-being. In *2015 48th Hawaii International Conference on System Sciences* (pp. 3237-3246). IEEE Publishing. <https://doi.org/10.1109/HICSS.2015.390>
- Simonsen, J., & Robertson, T. (Eds.). (2012). *Routledge international handbook of participatory design*. Routledge.
- Terry, G., Hayfield, N., Clarke, V., & Braun, V. (2017). *Thematic analysis*. In C. Willig & W. Stainton-Rogers (Eds.), *The Sage handbook of qualitative research in psychology* (pp. 17-37). Sage Publication Ltd.
- Tulu, B., Strong, D., Wang, L., He, Q., Agu, E., Pedersen, P., & Djamasbi, S. (2016). Design implications of user experience studies: the case of a diabetes wellness app. In *2016 49th Hawaii International Conference on System Sciences (HICSS)* (pp. 3473-3482). IEEE Publishing. <https://doi.org/10.1109/HICSS.2016.434>
- Van Velsen, L., Illario, M., Jansen-Kosterink, S., Crola, C., Di Somma, C., Colao, A., & Vollenbroek-Hutten, M. (2015). A community-based, technology-supported health service for detecting and preventing frailty among older adults: a participatory design development process. *Journal of Aging Research*, 2015, Article 216084. <https://doi.org/10.1155/2015/216084>.
- Wilkinson, C. R., & De Angeli, A. (2014). Applying user centred and participatory design approaches to commercial product development. *Design Studies*, 35(6), 614-631. <https://doi.org/10.1016/j.destud.2014.06.001>
- Williams, M., & Moser, T. (2019). The art of coding and thematic exploration in qualitative research. *International Management Review*, 15(1), 45-55.
- WHO. (2021). *Ageing and health*. World Health Organization.



Development of Pulp Moulded Packaging Samples from Empty Fruit Bunch Fibre

Qiuyun Liu^{1*}, Ceri Loxton¹, Amir Alzahari Mohamed², Mohammad Jawaid³, Radek Braganca¹ and Robert Elias¹

¹The Biocomposites Centre, Bangor University, Bangor, Gwynedd, LL57 2UW, UK

²Eco Premium Packaging, 71800 Nilai, Negeri Sembilan, Malaysia

³Laboratory of Biocomposite Technology, INTROP, Universiti Putra Malaysia, 43400 UPM Serdang, Selangor, Malaysia

ABSTRACT

Single-use plastic packaging is a cause of rising environmental concerns due to high production volumes, short usage time, and problems related to end of life management and release into the environment. As a result, there is an increased demand to develop alternative non-plastic packaging from agricultural waste materials. This paper reported findings for converting, via atmospheric refining, waste oil palm empty fruit bunch (EFB) fibres into a fibrous pulp which can then be used to produce three-dimensional pulp moulded products. By optimising the mould design, the efficiency of vacuum suction was improved, which in turn helped to improve fibre distribution and the quality of moulded trays; such moulded trays are suitable for the containment of food items such as fruit and vegetables. Furthermore, when combined with compostable barrier treatments, lidding and adhesive films currently under development, there is an opportunity to provide a complete biocompostable packaging solution for some food items. Furthermore, as these pulp moulded packaging products are made from agricultural fibre wastes rather than plastics, the pulp moulded trays are recyclable or compostable at the end of life. Therefore, if a release does occur into the environment, it would not persist.

Keywords: Empty fruit bunch, packaging, pulp moulding, trays

ARTICLE INFO

Article history:

Received: 11 May 2021

Accepted: 27 July 2021

Published: 22 October 2021

DOI: <https://doi.org/10.47836/pjst.29.4.36>

E-mail addresses:

q.liu@bangor.ac.uk (Qiuyun Liu)

c.loxton@bangor.ac.uk (Ceri Loxton)

amiralzahari@gmail.com (Amir Alzahari Mohamed)

jawaid@upm.edu.my (Mohammad Jawaid)

r.braganca@bangor.ac.uk (Radek Braganca)

r.m.elias@bangor.ac.uk (Robert Elias)

* Corresponding author

INTRODUCTION

Plastic packaging represented 36% of global plastic production in 2015 (Geyer et al., 2017). However, Geyer et al. (2017)

estimate that just 9% of all plastic ever produced has been recycled, 12% has been incinerated, but the remaining 79% has either been landfill, dumped or ended up as litter in the environment.

Growing public and governmental concerns around plastic packaging, particularly single-use plastics, have led to more than 60 countries introducing regulations to limit the use of plastic bags and Styrofoam products (UNEP, 2018). In Europe, there has been increased interest in alternatives to single-use plastic packaging following various high profile news items about the ‘ocean of plastic’ and the banning of waste plastic imports by China (Cole, 2017). In the UK, a number of supermarkets have announced that they are phasing out plastic from their packaging (Laville & Smithers, 2018), while the world’s first plastic-free shopping aisle opened in the Netherlands in 2018 (Taylor, 2018).

These measures are predicted to be a step towards other policies aimed at reducing plastic waste by replacement with more sustainable, environmentally friendly alternatives. Furthermore, bans on the use of plastic and growing governmental and customer concerns around single-use plastics are resulting in opportunities for the introduction of marketing innovative, environmentally sound alternatives (UNEP, 2018) and have led to a growing interest in packaging alternatives (Porter, 2018).

In Europe, demand for paper-based packaging now represents more than half of European packaging production. Pulp moulded products (PMPs) are one such alternative to plastic packaging. They have been gaining rapid commercial importance over recent years as companies look for alternatives to plastic-based packing; the demand increases due to their sustainability qualities (Wever & Twede, 2007). Initially, PMPs were associated with egg packaging and fruit trays (dry foods). However, they are now finding applications as “food containers, clinical waste healthcare products, and packaging for electronic goods” (Didone et al., 2017). PMPs are usually made from a wood fibre-based raw material, often derived from recycled paper/card. Depending on the source of that recycled material the resulting pulp may or may not be suitable for packaging material that will come into contact with food.

Different grades of recovered/recycled paper and board are available. More than 50 grades are defined in the European List of Standard Grades of Recovered Paper and Board as per EN643. These grades can be categorised (Didone et al., 2017) into three principal groups: low grades, de-inking grades and high grades. The high grades originate mainly from within manufacturing environments—so offcuts from sheets or print run. The de-inking grade originates primarily from newspaper and magazine material and is not suitable for direct contact with food. This grade is also considered to be a low grade because of the extensive deinking that is required. The bulk of recovered paper falls into the ‘low’ grade category and comprises mixed papers, old corrugated containers and boxes. This low grade recycled material is mainly destined for secondary packaging applications.

Unfortunately, only some grades of recycled paper are considered suitable for use as food packaging. The majority are not due to possible contamination. The principal contaminants in paper and board products are derived from dyes, printing inks and lacquers, adhesives, sizing and coating agents; however, there may also be dispersants used at the de-inking stage during recycling (Bengström, 2014). Mineral oil hydrocarbons, derived from printing inks, were of particular concern in the 1990s and onwards, leading to new legislation to minimise migration of mineral oils from boxes of recycled paperboard to dry food. However, this legislation is still to be fully enforced (Grob, 2018). Nevertheless, it is one reason for interest in finding alternative fibre sources from which to make PMPs. 'Waste' agricultural fibres may be able to provide suitable quality fibre that has not been contaminated with dyes and inks from recycled papers.

Once the pulp has been prepared, the next step in the manufacturing process of pulp moulded products involves vacuum-forming the pulp slurry (fibres mixed with water) over a wire forming mesh into the desired shape. Water drains from the pulp through the wire mesh, leaving a wet formed shape from which additional water is then removed by the application of pressure and or heat and pressure. The resulting three-dimensional product can be classified in a number of different ways according to density and fabrication method. The classification that has been accepted by the International Moulded Fibre Association (National Agricultural Library, 2014) lists four main categories of PMPs, these being thick-walled (5 to 10mm), transfer moulded (3 to 5mm wall thickness), thermoformed (with hot-pressed, densified walls of 0.8 to 1.2mm in thickness). The fourth general category is 'processed'. The processed category covers any moulded product that has undergone further treatment, such as the addition of paint, coatings, or additives.

Non-wood fibres such as sugar cane, bagasse and various cereal straws, flax and hemp are being used to manufacture paper (Zhaohua et al., 1998; Hammet et al. 2001) and thus are likely to find their way into recycled paper streams and so into pulp moulded products. However, to date, little work has been published in the area of directly substituting wood-based pulps for non-wood fibre pulps in pulp moulded products. Curling et al. (2017) looked at the feasibility of substituting pure Kraft pulp, which is relatively expensive, with cereal straw and successfully up to 80% substitution. However, they could not make a product from 100% wheat straw (*Triticum aestivum* cv Solstice) due to poor wet strength preventing removal of the product from the mould. Kim et al. (2016) reported an addition of empty fruit bunch fibres to pulp made from old newspaper to help improve properties with changes to bulk density improving drainage. Hamouda et al. (2019) reported fabricating hybrid composite materials using Tetra Pak package waste reinforced with waste wool fibres for packaging applications.

While the pulp moulding industry is generally well established around recycled paper and existing supply chains (mainly wood-based raw materials), there is a growing interest in

looking at alternative fibre sources. There are a number of traditional drivers for looking at non-wood pulps, supply, cost, availability, fibre characteristics, sustainability and increased interest in the circular economy (Geueke et al., 2018).

The oil palm (*Elaeis guineensis*) industry in Malaysia generates much waste; for every 5.5, tonnes of oil produced 55 tonnes of dry fibrous biomass is left behind (Or et al., 2017). Among the various dry fibrous biomass from an oil palm tree, empty fruit bunch account for up to 73% of this fibrous biomass. Hamzah et al. (2019) reported that in 2017, 22.2 million tonnes of EFB was produced—which normally ends up being incinerated or applied to fields. This research project aimed to establish if EFB would be a suitable raw material for pulp moulded products.

Empty fruit bunch fibre can be pulped using various chemical, semi-chemical or thermomechanical pulping methods (Ferrer et al., 2011). Chemical and semi-chemical processing are preferable where high-quality pulp is required. Ibrahim et al. (2007) reported on the successful production, at a commercial scale, of paper from EFB using soda pulping. This paper will report findings for converting, via atmospheric refining, the waste material of EFB fibres into a fibrous pulp which was then used to produce pulp moulded product samples in the development of compostable barrier treatments lidding and adhesive films.

MATERIALS AND METHODS

Raw Materials

Empty fruit bunch fibre (EFB) was supplied by Eco Premium Packaging from Malaysia and sent to The BioComposites Centre at Bangor University in the UK. The control material was recycled cardboard (without ink) collected in the UK.

Atmospheric Refining of EFB Fibres

The length of EFB fibre was reduced by first chopping the long fibre bundles to approximately 5cm in length using a Pierret B6838 Corbion. The fibre length is achieved by adjusting the speed of the feed rollers. It was required to ensure that the material would transfer through the screw feeder to the refining zone of the laboratory 12” Sprout Waldron single atmospheric disc refiner. The diameter of the screw feeder was 100mm. The chopped EFB fibres were soaked overnight in water at room temperature prior to refining, as shown in Figure 1(a).

The EFB/water mix was poured into the feed hopper of the atmospheric refiner. Care was needed to distribute the EFB evenly to avoid clumping the material as it entered the screw feeder, as this could lead to blockages. Target consistency for this stage was 4%. Two experimental pulps were produced, one from material that had passed through the refining zone three times (“3 Pass”), with the plate gap being reduced on each subsequent

pass. The starting plate gap was 25/1000, followed by plate gaps of 10 and 5/1000". This pulp was then split into half and one portion was passed through the refiner for a fourth time ("4 Pass") at a smaller plate gap of 3/1000". Refined EFB after 3 passes is shown in Figure 1(b). A reduction in fibre length (3 to 5mm) was visible by the eye.

Hand Sheets

Information gathered from test handsheets is widely used in the paper industry as an indication of pulp quality and a measure of the potential contribution of the pulp to the strength of the finished paper product (Kibblewhite et al., 2000). Whilst not strictly designed for pulp moulded products, the same approach can be used to assess the properties of the pulps and products. In this case, the handsheet making procedure was based on TAPPI Method T 205 (TAPPI TEST Methods, 1994a). The method involved disintegration at a consistency of 2.5% (corresponding to 50 g of material in a total volume of 2 litres); sheet making at a consistency of 1.5%; couching (standard couch roll and plate), and laying in a press (first and second pressing) and finally drying (using mirror-polished discs in 160mm diameter with rubber seatings for holding the sheets to the polished discs during drying). Ten standard sheets (159mm in diameter) from the 4 refiner passes formulation and recycled cardboard was made successfully with a target weight of 1.2g (oven-dry weight) per sheet and tested. However, handsheets from 3 refiner passes EFB fibres could not be removed from the couching plate. Therefore, no handsheets were made from this formulation.

Handsheet Testing

The physical properties of handsheets made from the 4 passes formulation and recycled cardboard were tested as per TAPPI Method T 220 with a sample cutting pattern shown in Figure 2. All samples were conditioned and tested at room conditions. From TAPPI Method T220 (TAPPI TEST Methods, 1994b), physical testing of pulp handsheets should include mass per unit area (grammage), specific volume, apparent density, tensile strength, stretch, bursting strength, tearing resistance, and MIT folding endurance. Test results are summarised in Table 1.



(a)



(b)

Figure 1. EFB fibres before the refining with fibre length at 5cm (a) and fibre length reduced to 3 to 5mm after the refining (b)

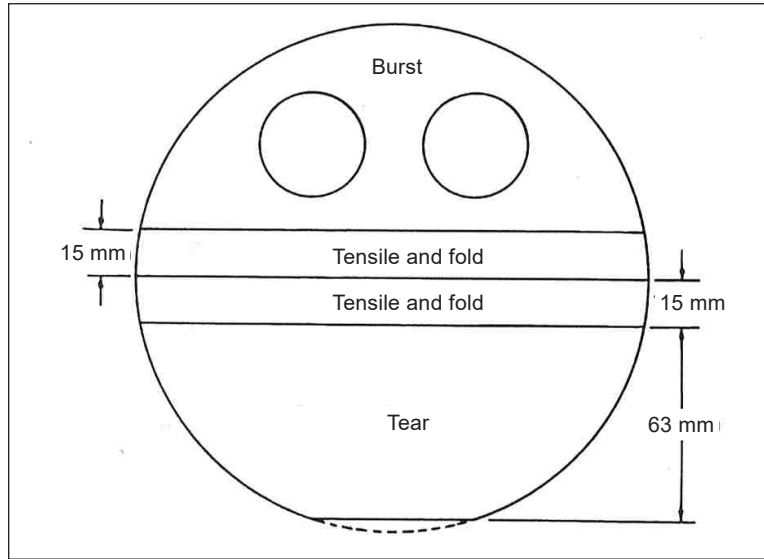


Figure 2. Handsheet cutting pattern

Table 1
Handsheet properties of EFB atmospherically refined

Property	100% EFB 3 Passes	100% EFB 4 Passes	100% Cardboard*
Freeness (CSF)	560	420	485
Apparent bulk density		0.25	0.49
Specific volume (bulk)		4.02	2.04
Tensile Index		10.0	35.7
Tensile (Breaking Length) m		1019	3637
T.E.A. Index		131	372
Tear Index		5.3	10.4
Burst Index		0.00	1.37
Moisture (% oven dry weight)		7.6	6.9
Grammage (air dry) g/m ²		63.6	62.5
Grammage (oven dry) g/m ²		58.8	58.2

*Handsheet made from 100% recycled cardboard

Freeness of Pulp

The freeness of pulp is designed to measure the rate at which a dilute suspension of pulp (3g of pulp in 1 L of water) may be drained.

The freeness of atmospherically refined EFB fibres and recycled cardboard was tested using the standard Canadian method as per TAPPI Method T227 (TAPPI TEST Methods, 1994c), results were included in Table 1.

Pulp Moulding

Pulp moulding product trials were performed using a specially designed laboratory-scale pulp moulding machine. The machine is composed of a control panel, a pulp tank, a set of wet forming moulds, and press moulds. Mould dimensions were approximately 55 mm deep, 170 mm long by 140 mm wide. The process includes wet forming followed by de-watering and drying under elevated temperatures. By controlling the consistency in the pulp tank and the forming/drainage time, the thickness of the resulting punnet can be adjusted. A consistency of between 0.4% and 0.6% was used during these trials, and the drying temperature and time adjusted depending on the material, thickness and drainage properties.

RESULTS AND DISCUSSION

Freeness of Atmospheric Refined EFB

Empty fruit bunch fibre was successfully refined using a 12" laboratory atmospheric refiner. Throughput became successively smoother with each pass as the material became finer and more consistent and thus reduced the tendency to block and clump in the feed screw. Freeness (Canadian standard freeness) was measured after 3 and 4 passes through the refiner and were recorded as 560 and 420, respectively, as shown in Table 1. Freeness is related to the surface conditions and swelling of the fibres (TAPPI method T227, 1994). The higher value of 560 for 3 passes EFB indicated that the pulp is coarser than that of 4 passes EFB at 420.

Properties of Handsheets from Atmospherically Refined EFB

Handsheets were successfully made from the control sample (100% recycled cardboard) and EFB pulp with 4 passes in the atmospheric refiner. The freeness of the EFB pulp that had received 3 passes was 560 CSF compared to 485 CSF for the control pulp made from recycled cardboard. It proved difficult to make a handsheet from the 3 pass EFB pulp due to its coarse nature. Physical properties of handsheets are summarised in Table 1. It could be seen that the apparent bulk density of 4 passes EFB fibres was 0.25, which was about half of the value of the control sample. The low bulk density of EFB fibres resulted in the low values in mechanical properties, for example, Tensile Index at 10 and Tear Index of 5.3; both are much lower than that of control.

Pulp Moulding Trials and Mould Modification

Initial Pulp Moulding Trial. Trials were carried out on the pulp moulder to make punnets from atmospherically refined EFB fibre. Initial trials with the 4 pass pulp were not satisfactory due to difficulties controlling thickness, fibre distribution and moisture content

prior to hot pressing. The 3 pass pulp was then blended with the 4 pass pulp at a ratio of 3:7, and with some adjustments to absorbing time, consistency and drainage times, punnets were successfully manufactured. Figure 3 shows the inside and outside of six punnets manufactured from atmospherically refined EFB. The punnet had 12.5cm in width, 17cm in length and 4cm in depth. The appearances of the inside and outside punnet were different due to the setup of the drying process. The inside was smooth, whereas the outside showed the impression of the meshed wire structure.



Figure 3. Punnets made from atmospherically refined EFB fibre

Colour differences can be seen in Figure 3. Watermarks caused these due to poor fibre distribution and weak vacuum suction resulting in uneven and excessive water in the punnets prior to hot pressing. If the punnets were too wet going into the hot press, long press times were required to reduce the punnets' tendency to blow apart on the release of the press at the end of the pressing cycle. Pre-drying the punnets (placing them in an oven at 50°C overnight) prior to hot pressing significantly reduce the punnets' tendency of to 'blow' apart. However, it did not solve the problem of uneven fibre distribution, which resulted in some punnets having very thin walls—often resulting in holes forming in the punnets on removal from the hot press.

Mould Modification. The initial trials indicated that empty fruit bunch fibre could be refined and pulp moulded into a three-dimensional product. However, the trials brought to light some limitations of the existing laboratory setup and mould configuration. In addition to problems with poor fibre distribution, the mould configuration limitations included: the lack of a rolled and self-trimming lip—important for reducing production time and costs, a lip of suitable dimensions to accept the application of a top seal and a design that would ensure that when the trays are stacked prior to use they can be “de-nested” quickly and do not stick together which is important for production throughput. Therefore, a new mould design with the required features was proposed to solve these issues, as shown in Figure 4 with a digital 3D projection of the expected tray. A new set of moulds were then manufactured and installed (Eco Premium Packaging, Malaysia) onto the existing pulp moulding machine at Bangor University.

With the new design, the mould orientation was changed from the initial concave mould to convex. As shown in Figure 5, the orientation changes were made to improve

the efficiency of the vacuum suction system, which in turn would help improve the fibre distribution. The addition of a turned edge (rim/flange) means that trimming could be avoided, and the rim should allow for the application of a top seal if required.

Trials were performed using the same formulation and method as described above on the new mould. Punnets were produced successfully without any fibre distribution issues, watermarks also disappeared, and the edges did not require trimming. As shown in Figures 6(a) and (b), smooth surfaces were obtained inside and outside. Punnets were successfully and repeatedly produced, which demonstrated the success of the new moulds in improving the vacuum suction efficiency. Top seal trials were performed within the consortium, and no

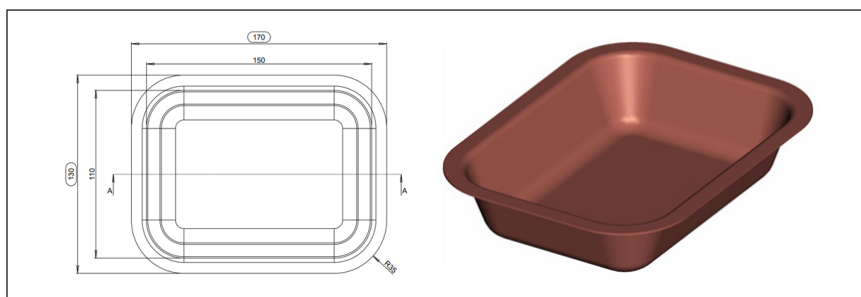


Figure 4. New mould drawing and expected trays



Figure 5. Current concave forming mould (a) and the new convex forming mould (b)

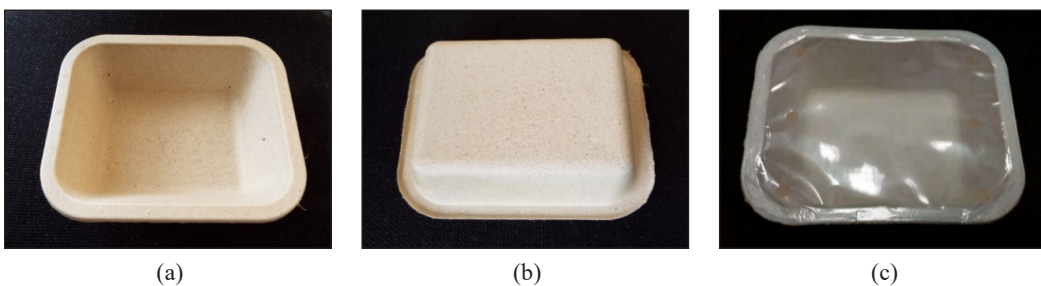


Figure 6. Punnets made from new mould: (a) Inside; (b) Outside; and (c) Top sealed

issues were identified when sealing such trays with both fossil-based and bio-compostable lidding films, as shown in Figure 6(c). The results confirmed that it is possible to produce a pulp suitable for making a moulded product by atmospheric refining empty fruit bunch fibre. As atmospheric refining is a mechanical method to break down fibres, no chemicals were needed over the whole pulping processing. The water used in pulp moulding can be easily recycled and reused.

Food interacts with the packaging used to contain it (Munro et al., 2009), so it is important to select packaging that best meets the needs of particular foods (Marsh & Bugusu, 2007). Further food fill-in testing will be required to understand the interaction between food and EFB pulp moulded trays to bring pulp moulded packaging to the market. Once the food type has been matched to the packaging, marketing is important. Customers are looking for plastic alternatives to food packaging (Guillard et al., 2018) with improved environmental characteristics. Life cycle analysis (to be reported in a further paper) will help provide information on the environmental impact of this package and provide data for marketing.

Importantly food packaging must maintain the quality and safety of food (Geueke et al., 2018) over time and balance different priorities not only for the consumer but also for the pre-consumer (food producer, packaging and distribution) and postconsumer (waste recycling/disposal). Therefore, further testing on pulp moulded EFB fibres will demonstrate the suitability and benefits of moulded trays as food packaging. Findings will be reported in the following papers.

CONCLUSION

The work concluded that, with careful design on moulds, it is possible to produce a pulp suitable for making a pulp moulded product by atmospheric refining empty fruit bunch fibre. As atmospheric refining is a mechanical method to break down fibres, no chemicals were needed over the whole pulping processing. The water used in pulp moulding can be easily recycled and reused. There are obvious environmental benefits to use such refining techniques and agricultural wastes such as EFB for pulp moulding.

While this paper has reported on a method that demonstrates that using a non-wood raw material to make a pulp moulded product is possible, more work is needed before such products find their way into the market. Therefore, the next stage of this project should be to align the properties of this type of packaging material with a food type and then carry out packaging and consumer-based tests and assessments.

ACKNOWLEDGEMENTS

The authors would like to acknowledge the project funding of Newton-Ungku Omar Coordination Fund: UK-Malaysia Research & Innovation Bridges Competition 2015

specific project SafeBioPack (102722). The authors also want to thank all the project partners for their technical support.

REFERENCES

- Bengtström, L. (2014). *Chemical identification of contaminants in paper and board food contact materials* (PhD Thesis). Technical University of Denmark, Denmark.
- Cole, C. (2017, October 20). China bans foreign waste - but what will happen to the world's recycling? *The Conversation*. <https://theconversation.com/china-bans-foreign-waste-but-what-will-happen-to-the-worlds-recycling-85924>
- Curling, S., Laffin, N., Davies, G., Ormondroyd, G., & Elias, R. (2017). Feasibility of using straw in a strong, thin, pulp moulded packaging material. *Industrial Crops and Products*, 97, 395-400. <https://doi.org/10.1016/j.indcrop.2016.12.042>
- Didone, M., Saxena, P., Meijer, E. B., Tosello, G., Bissacco, G., McAloone, T. C., & Howard, T. J. (2017). Moulded pulp manufacturing: Overview and prospects for the process technology. *Packaging Technology and Science*, 30(6), 231-249. <https://doi.org/10.1002/pts.2289>
- Ferrer, A., de Vega, A., Ligerio, P., & Rodríguez A. (2011). Pulping of empty fruit bunches (EFB) from the palm oil industry by formic acid. *Bioresources*, 6(4), 4282-4301.
- Geueke, B., Groh, K., & Muncke, J. (2018). Food packaging in the circular economy: Overview of chemical safety aspects for commonly used materials. *Journal of Cleaner Production*, 193, 491-505. <https://doi.org/10.1016/j.jclepro.2018.05.005>
- Geyer, R., Jambeck, J. R., & Law, K. L. (2017). Production, use and fate of all plastics ever made. *Science Advance*, 3(7), Article e1700782. <https://doi.org/10.1126/sciadv.1700782>
- Grob, K. (2018). Mineral oil hydrocarbons in food: A review. *Food Additives & Contamination: Part A*, 35(9), 1845-1860. <https://doi.org/10.1080/19440049.2018.1488185>
- Guillard, V., Gaucel, S., Fornaciari, C., Angellier-Coussy, H., Buche, P., & Gontard, N. (2018). The next generation of sustainable food packaging to preserve our environment in a circular economy context. *Frontiers in Nutrition*, 5, Article 121. <https://doi.org/10.3389/fnut.2018.00121>
- Hammett, A. L., Youngs, R. L., Sun, X., & Chandra, M. (2001). Non-wood fiber as an alternative to wood fiber in chinas pulp and paper industry. *Holzforschung*, 55(2), 219-224. <https://doi.org/10.1515/HF.2001.036>
- Hamouda, T., Hassanin, A. H., Saba, N., Kilic, M. D. A., Candan, Z., & Jawaid, M. (2019). Evaluation of mechanical and physical properties of hybrid composites from food packaging and textiles wastes. *Journal of Polymers and the Environment*, 27, 489-497. <https://doi.org/10.1007/s10924-019-01369-3>
- Hamzah, N., Tokimatsu, K., & Yoshikama K. (2019). Solid fuel from oil palm biomass residues and municipal solid waste by hydrothermal treatment for electrical power generation in Malaysia: A review. *Sustainability*, 11(4), 1-23. <https://doi.org/10.3390/su11041060>
- Ibrahim, R., Jasmani, L., Kong, H. W., & Yusoff, M. N. H. (2007). Commercial-scale production of soda pulp and medium paper from oil palm empty fruit bunches. *Journal of Tropical Forest Science*, 19(3), 121-126.

- Kibblewhite, R. P., Riddell, M. J. C., & Shelbourne, C. J. A. (2000). Variation in wood, kraft fibre, and handsheet properties among 29 trees of *Eucalyptus regnans*, and comparison with *E. Nitens* and *E. Fastigata*. *New Zealand Journal of Forestry Science*, 30(3), 458-474.
- Kim, D. S., Sung, Y. J., Kim, C. H., & Kim, S. B. (2016). Changes in the process efficiency and product properties of pulp mold by application of oil palm efb. Palpu Chongi Gisul. *Journal of Korea Technical Association of the Pulp and Paper Industry*, 48(1), 67-74. <https://doi.org/10.7584/ktappi.2016.48.1.067>
- Laville, S., & Smithers, R. (2018, April 26). UK supermarkets launch voluntary pledge to cut plastic packaging. *The Guardian*. <https://www.theguardian.com/environment/2018/apr/26/uk-supermarkets-launch-voluntary-pledge-to-cut-plastic-packaging>
- Marsh, K., & Bugusu, B. (2007). Food packaging - Roles, materials, and environment issues. *Journal of Food Science*, 72, 39-55
- Munro, I. C., Haighton, L. A., Lynch, B. S., & Tafazoli, S. (2009). Technological challenges of addressing new and more complex migration products from novel food packaging materials. *Good Addit Contam Part A Chem Anal Control Expo Risk Assess*, 12, 1534-1546.
- National Agricultural Library. (2014). *Develop a post-market test for recycled food contact materials* (Final report: FS241007). U.S. Department of Agriculture.
- Or, K. H., Putra, A., & Selamat, M. Z. (2017). Oil palm empty fruit bunch fibres as sustainable acoustic absorber. *Applied Acoustics*, 119, 9-15.
- Porter, J. (2018, August 12). Wrapper's delight: eco-friendly plastic alternatives. *The Caterer*. <https://www.thecaterer.com/articles/534918/wrappers-delight-eco-friendly-plastic-alternatives>
- TAPPI TEST Methods. (1994a). *Forming handsheets for physical tests of pulp*. TAPPI Press.
- TAPPI TEST Methods. (1994b). *Physical testing of pulp handsheets*. TAPPI Press.
- TAPPI TEST Methods. (1994c). *Freeness of pulp (Canadian standard method)*. TAPPI Press.
- Taylor, M. (2018, February 28). World's first plastic-free aisle opens in Netherlands supermarket. *The Guardian*. <https://www.theguardian.com/environment/2018/feb/28/worlds-first-plastic-free-aisle-opens-in-netherlands-supermarket>
- UNEP. (2018). *Single-use plastics: A roadmap for sustainability*. United Nations Environment Programme.
- Wever R., & Twede D. (2007). The history of molded fiber packaging: A 20th century pulp story. In *Proceedings of the 23rd IAPRI symposium on packaging* (pp. 1-8). Pira International.
- Zhaohua, Z., Chunqian, J., Maogong, Z., & Huafu, W. (1998). *Status, trends and prospects for non-wood and recycled fibre in China. Asia-pacific forestry towards 2010*. Asia-Pacific Forestry Sector Outlook Study Working Paper Series (FAO).

Empirical Model of Ground-Borne Vibration Induced by Commuter Railway Traffic

Mohd Khairul Afzan Mohd Lazi^{1*}, Muhammad Akram Adnan² and Norliana Sulaiman³

School of Civil Engineering, College of Engineering, University of Technology MARA (UiTM), 40450 Shah Alam, Selangor, Malaysia

ABSTRACT

Train-induced ground-borne vibration has a negative effect on residential areas near railway tracks. Residents who are regularly exposed to ground-borne vibration can experience sleep disturbances and more serious health problems in the long run. In addition, it concerns the mental health of those who live nearby. Residents' productivity and quality of life can be harmed as a result of direct exposure to train-induced ground-borne vibration. The relevant authorities must record a few precise measurements using technically sophisticated instruments and equipment to research further the impact of ground-borne vibrations induced by train traffic. However, the equipment is usually costly, and it has become one of the main stumbling blocks to achieving the desired results. This paper aimed to propose an alternative to the authority's current guidelines and standards for vibration limits and environmental control. This research established a regression prediction model to forecast the peak particle velocity of commuter train ground-borne vibration. The established model considered a few parameters obtained from site surveys with limited or no tools at all.

The data collected was measured along the ground rail tracks involving human-operated trains. Residents living in landed residential areas near railway tracks were selected as the recipients. Finally, the peak particle velocity models were established, validated, and a sensitivity analysis was carried out.

ARTICLE INFO

Article history:

Received: 09 May 2021

Accepted: 21 July 2021

Published: 22 October 2021

DOI: <https://doi.org/10.47836/pjst.29.4.37>

E-mail addresses:

tmm_afzan@yahoo.com (Mohd Khairul Afzan Mohd Lazi)

akram@uitm.edu.my (Muhammad Akram Adnan)

norliana545@uitm.edu.my (Norliana Sulaiman)

* Corresponding author

Keywords: Commuter train, empirical model, ground-borne vibration, peak particle velocity

INTRODUCTION

It is important for businesses or companies involved in constructing of a new railway system to develop a predictive method that allows for the prediction of vibration levels in the early planning stages of new railways, which may be in the form of cost-effective vibration countermeasures. However, while designing a new railway line or increasing the capacity of an existing one, the designers are constantly concerned about how far from the railway would be disturbed beyond regulation, resulting in how many residences would have to be relocated. Many prediction models, such as the analytical, numerical, and scope models, have been established in recent years. Despite the widespread use of numerical methods in recent studies, field test analysis is still essential to give direct evidence to validate various prediction models. Meanwhile, research is being carried out to reduce vibration caused by railways (Hu et al., 2018).

Because of its potential consequences on the comfort of local citizens, the long-term preservation of historic buildings, and the operation of precision instruments, the problem of train-induced vibrations is receiving more attention (Ma et al., 2020). Furthermore, as residents' living standards rise, the demand for and emphasis on environmental quality is becoming more important. Vibration pollution refers to ground vibrations caused by railway and other traffic vehicles, and human activities that have a negative impact on human comfort and the psychological health of those living near the source of the vibration. The ground-borne vibrations will also impact the protection of buildings, the functioning of sensitive machinery and instruments, and the working conditions in the affected areas.

This research sought an alternative to the local authority guidelines on vibration limits and control based on the local environment and conditions. This study combined Malaysian railway traffic, environment, and geological conditions to establish an empirical model for ground-borne vibration prediction. The developed empirical model should to predict the ground-borne vibration induced by railway traffic operating on a railway system, particularly during the planning phase of projects and mitigation measures. This research is fundamental in constructing high-speed railway systems since high-speed train service is expected to cause greater ground vibrations. The operation of a high-speed railway system in Malaysia is currently in the planning stages. The established model is expected to aid the authority in addressing ground-borne vibrations if the railway system is built.

This research project is intended to fill a knowledge gap in the fundamental understanding of ground-borne vibration, which comprises many branches of knowledge about local rail traffic conditions. The study was motivated by limited findings regarding the degree of perceived irritability and annoyance experienced by affected people living near the source of the vibrations, especially in Malaysia. Therefore, this thesis attempted to collect empirical data by installing a few basic instruments at the study site to test the vibrations caused by railway traffic.

LITERATURE REVIEW

Propagation

After ground-borne vibrations are produced in the railway, vibrations typically spread to the surrounding area through the soil media. Propagation characteristics are influenced by soil properties, parameters, and distance from the source. The type of soil has a significant impact on ground vibration; the stiffer the soil, the lower the ground vibration attenuation effect (Kuo et al., 2017). Ground vibration will be quickly attenuated as the distance along with the ground transmission path increases. Ground vibration in stiff or hard soil could be attenuated and absorbed considerably faster over time than in soft soil. The frequency of soft ground is lower than that of rigid or hard ground. In the soft ground profile zone, the ground vibration frequency ranges from 5 to 10 Hz. Vibrations in the ground at these low frequencies may travel further away from their source. The main factor that affects substantial ground vibration that can cause discomfort to people who live 100 to 200 meters away from the rail tracks is soft soil formation, such as silt or soft clay (Madshus et al., 1996).

The most well-known and widely used vibration measurement is the peak particle velocity (PPV), which measures the rate of vibration. The majority of guidelines and regulations use PPV to determine vibration thresholds. The peak particle velocity for each observed waveform is defined as the maximum particle velocity over the total recorded time. Thus, the PPV is the maximum instantaneous velocity at a point in a given time interval. As a disturbance from a source of waves propagates outward from the source with a certain amount of wave velocity, ground particles vibrate with varying particle velocity. The motion is represented in three perpendicular components (usually transverse, vertical, and radial or longitudinal). All three components must be calibrated at the same time to ensure that the PPV is determined correctly (Avellan et al., 2017).

The Impact of Speed on Ground Borne Vibrations

One of the variables that influence the level of the ground-borne is train speed. As expected, increasing train speeds will result in higher ground-borne vibrations (Shih et al., 2018). The vibration frequency normally increases by 4 to 6 dB as the train's speed is raised. Fesharaki and Hamedi (2016) have demonstrated that the vibration level rises as the speed rises. They also demonstrated that when train speeds reach 200 km/h, vibrations increase dramatically. The relationship between train speed and ground-borne vibrations was also discovered by Connolly et al. (2014). The study was able to show that, despite the fact that the vibration receivers are located at different locations, the relationship between train speed and vibration levels is the same, with vibration levels predicted to rise as train speed increases.

The Impact of Distance on Ground Borne Vibrations

The distance between the receivers and the source of vibrations significantly impacts the level of ground-borne vibrations (Ibrahim et al., 2018). Theoretically, as the distance between the vibration sources and the receiver decreases, the ground vibration will increase. Regardless of the form of soil, Fesharaki and Hamed (2016) demonstrated that the longer the distance between sources and receiver, the lower the vibrations. Based on field analysis, Connolly et al. (2014) found that vibration detected near the rail track was higher than vibration detected further away from the rail track.

Established Standard and Guidelines on Human Annoyance

The magnitude of a vibration can be determined in several ways. Velocity (mm/s), displacement (mm), and acceleration (mm/s²) are the three most used methods for determining vibrations (Eitzenberger, 2008). The velocity (mm/s) was employed in this investigation since the data were compared to the values recommended by the standard Malaysian guidelines. The magnitude of vibrations is measured using velocity in the standard guidelines. The International Standards Organization (ISO) published the *Guide to the Evaluation of Human Exposure to Vibration and Shock in Buildings (1 Hz to 80 Hz)* (ISO, 1997). The ISO stated that 0.2032 mm/s is the allowable response of a human to continuous vibration from traffic for the residence area. Most countries throughout the world utilise this ISO standard as a reference for developing their standards. Therefore, vibrations have varying limits in different countries based on local conditions. Table 1 summarises the different limits of vibrations for residential among the countries.

Table 1
Different limits of vibrations for residential among the countries

Country/Standard	Vibration limits (mm/s)
United State (Bahrekazemi, 2004)	0.2540
Norway (David et al, 2015)	0.6000
Sweden (David et al, 2015)	0.4000
California (California Department of Transportation, 2013)	0.3048
The Netherlands (Patrick & Michel, 2012)	0.8000
Malaysia (Department of Environment Malaysia, 2007)	0.5670

According to most countries' guidelines, the highest vibrations limit for human response and annoyance is valued below 0.8 mm/s. However, in Malaysia, the suggested limits for human response and annoyance in commercial areas are 1.176 mm/s, greater than the 0.567 mm/s in residential zones.

Review of Prediction Model from Railway Traffic

Model development aims to either describe or estimate and forecast the ground vibration phenomenon. If the established models can solve problems and make accurate predictions of ground-borne vibration in real-world conditions, they are important and useful. Ground-borne vibration prediction models are expected to include at least three basic elements: the receiver, the source, and the propagation direction.

Despite the fact that there are numerous ground vibration prediction models available, unique models for predicting ground vibrations in Malaysia have yet to be created. Therefore, many other researchers have used Madshus et al. (1996) model as a primary reference when developing new vibration prediction models.

$$V = F_V F_R F_B = [V_T F_S F_D] F_R F_B \quad [1]$$

Equation 1 shows the formula for the created by, where F_V is the basic vibration function, F_R is the track quality factor, and F_B is the building amplification factor. The basic vibration feature comprises three-element: the specific type of train vibration level, V_T , the reference distance D_0 of 15 m, and the reference speed, S_0 is 70 km/h on a standard track and embankment. A reference distance of 15 m was determined to prevent the influence of nearby field waves. F_S is a speed factor that considers the impact of the train's speed, S . $F_S = \left(\frac{S}{S_0}\right)^A$ is how the F_S is represented. A , where A denotes the train's speed exponent. F_D is a distance factor, with the expression of $F_D = \left(\frac{D}{D_0}\right)$. D is the distance of the embankment or track's core to the recipient, and B is the distance exponential value. Based on vibration measurements, it has been determined that ground conditions, train type, line quality and embankment design, train speed, distance from track to building, and building condition are the most important factors for low-frequency railway induced vibration on soft ground and its effect on neighbouring houses. The model assumes that the impacts of components of train type, line quality and embankment design, train speed, distance from track to building, and building condition are separable and that the factors, in principle, fluctuate with the ground conditions. Ground conditions, type of train, line quality, and type of buildings have been divided into small groups to make the model a convenient planning tool. Suhairy (2000) also developed a prediction model based on Madshus et al. (1996) model. Equation 2 shows the formula established by Suhairy (2000).

$$V = V_T * \left(\frac{D}{D_0}\right)^B * \left(\frac{S}{S_0}\right)^A * F_R * F_B \quad [2]$$

This formula can calculate vibration velocities for various train types and distances between the source and receiver. V_T represents the vibration levels caused by trains at 20m

and 70 km/h, D represents the distance from the track's middle, and D_0 is set to 20m to avoid the effects of nearby field waves. B is distance-based, with different values depending on the train type. S stands for train speed, and S_0 is set to 70 km/h for all types of trains. Madshus et al. (1996) assume that A is the speed-dependent exponential and that it is 0.9. The efficiency factor, F_R , is believed to be 0.8, and the building amplification factor, F_B , is set to 2. The essential parameter has been identified using Madshus et al. (1996) formula, and the information that has been measured can be expressed in a generic form using Suhairy (2000) equation for the acquired results for F_R , F_B , F_D and F_S . This equation can be used to calculate the vibration velocities for a variety of train types and distances.

Rossi (2003) developed a simple model to predict the vibrations caused by trains as part of his research. The absolute value of the particle vibration velocity, U , can be calculated using longitudinal and transversal velocities, as shown in Equation 3.

$$U = \sqrt{u_T^2 + u_L^2} \tag{3}$$

where u_T is the particle's root mean square ,r.m.s of the transversal velocity, while u_L is the r.m.s for the longitudinal velocity. Equations 4, 5, and 6 give the formulas for obtaining u_T and u_{TL} .

$$u_T = \sqrt{\frac{J_T}{z_T}} \tag{4}$$

and

$$u_L = \sqrt{\frac{J_L}{z_L}} \tag{5}$$

where:

$$z_T = \sqrt{\rho \cdot G} \quad \text{where } G = \frac{E}{2(1+\nu)}$$

$$z_L = \sqrt{\rho \cdot D} \quad \text{where } D = \frac{E(1-\nu)}{(1+\nu)(1-2\nu)} \tag{6}$$

Rossi's prediction formula takes into account z_T and z_L mechanical impedances, the soil Poisson's ratio, ν , soil density, ρ , soil torsional elasticity module, G , and soil longitudinal rigidity, D . Rossi (2003) proposed the model for train-induced soil vibration prediction furnishes velocities (longitudinal and transversal) and global vibration level. A measuring campaign along an Italian high-speed train was used to calibrate the model. Paneiro et al. (2015) also predicted the amplitudes of ground vibrations generated by rail traffic. Equation 7 defines the peak vector sum (PVS) in mm/s, calculated using mathematical relationships between the dependent variable and the predictors.

$$PVS = f(D, V, T, B, G) \quad (7)$$

The distance between the source and the receiver is denoted by D , the train speed in kilometres per hour is denoted by V , T predictors for track type, B predictors for building type, and G qualitative predictors for the dominant geology are denoted by G . If energy is taken into account, the train speed from Equation 7 is replaced with W , the kinetic energy. According to the suggested regression model by Rossi (2003), for the investigation of qualitative predictors, all building types evaluated have varied responses to railway traffic vibrations. From another researcher, as shown in Equation 8, Bahrekazemi (2004) summarised a semi-empirical model to predict particle velocity, V .

$$V = (a \cdot speed + b) \left[\frac{r}{r_0} \right]^{-n} \quad (8)$$

r is the source-to-receiver distance, while r_0 is the reference distance, according to this model. Fitting the calculated data with the equation in at least a square sense is needed to determine the distribution of attenuation, n . The two parameters known as functions of a wheel force are a and b , while $speed$ is the train speed in kilometres per hour. This prediction unit is measured in millimetres per second. The majority of the train vibration prediction models in this literature have taken into account different factors such as track efficiency, sleeper vibration, building amplification factor, and wheel power. Analysing these factors often necessitates permission from the appropriate authority, which can be viewed as a research gap. By introducing a simplified method of in-situ data collection, this study aimed to bridge the research gap. This study suggested using basic and minimal measurement instruments, or even without specialised equipment, to predict the vibrations caused by railways. The distance between the source and the receiver can be determined with a meter tape or a manual step count, and train speed can be estimated by dividing the distance travelled by trains by the time it takes to run. A standard stopwatch may be used to monitor the time. The values of these parameters can then be used in the models that have been developed. Previous researchers' prediction models differed depending on the geological and environmental conditions of the countries. This study also looked at the geological factors and conditions in the region. The factors or elements that had previously been used in other researchers' developed models were simplified in this study to reduce the reliance on advanced equipment when collecting data to predict ground-borne vibrations using the developed models.

MATERIALS AND METHODS

Case Study

This study was carried out along the Kereta Api Tanah Melayu Berhad (KTMB) railway route, which runs from Padang Jawa in Shah Alam to Klang in Selangor. The railway is a

two-way track with two train routes: Kuala Lumpur and Pelabuhan Klang, Selangor. These sites were chosen to distinguish the various vibration magnitudes caused by trains on the railway track. In addition, the locations were chosen because of their strategic locations, as many residential areas along the track were endangered by ground-borne vibration caused by trains. This study also concentrated on areas with landed type residential buildings.

Because of landed residential buildings in the areas adjacent to the railway track, the route was chosen. There are no vibration barriers in the vicinity of the case study sites. For this analysis, the distance between the residential area and the rail track is less than 30 meters. Train parameters, such as train speed, were collected in the field during the

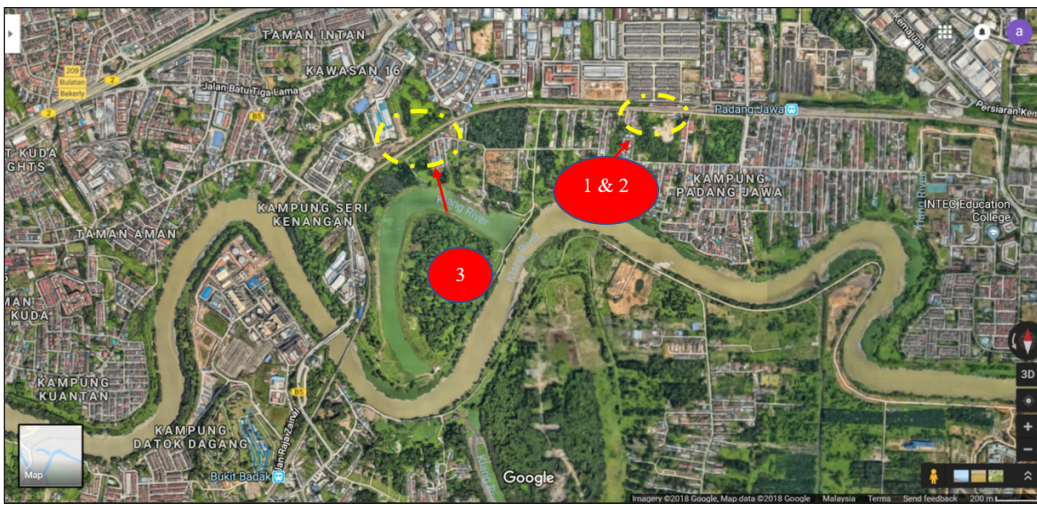


Figure 1. Aerial view of site location for the lane of Padang Jawa Station to Bukit Badak Station consists of site 1, site 2 and site 3

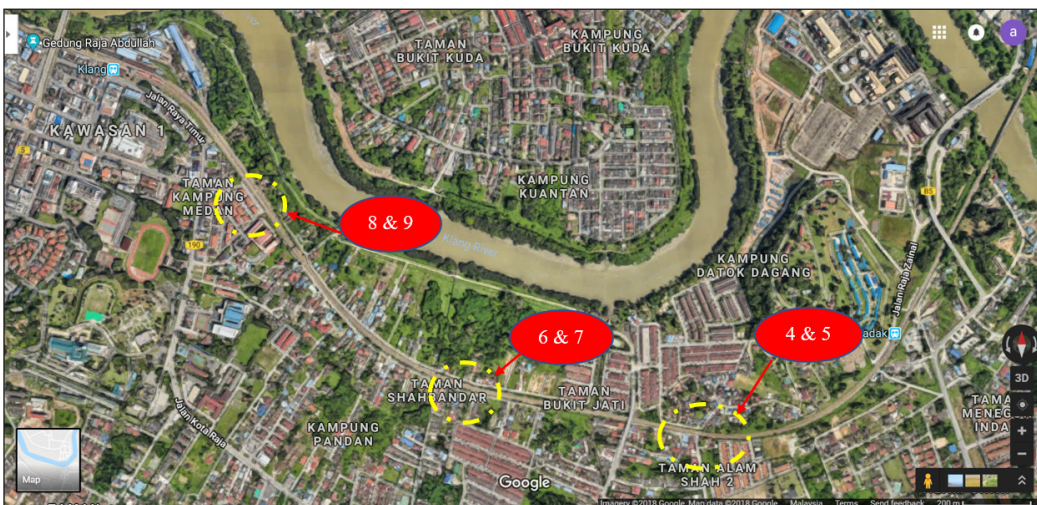


Figure 2. Aerial view for site 4 until site 9 located along the lane of Bukit Badak Station to Klang Station

site survey. Radial vertical and horizontal wave vibrations make up the ground-borne vibration velocity measurements. The data was collected using a seismograph mounted at the locations. Three sites were selected, ranging from Padang Jawa station to Bukit Badak station. The remaining six sites are in the vicinity of Bukit Badak Station and Klang Station. As a result, a total of nine (9) stations were selected. The locations were selected to be as close between the track to the landed residential areas as possible. Different sites were chosen to achieve different train speeds and distances from the residential areas to the sources. Part of the most populated areas in Malaysia is Shah Alam and Klang, which have one of the highest populations. Figures 1 and 2 depict aerial views of the site positions between Padang Jawa Station in Shah Alam and Klang Station in Klang, from Site 1 to Site 9.

Instrumentation and Equipment Strategy Setting Up

The measurement equipment consists of the following parts to collect valuable data to study the ground vibrations: a pick-up sensor or transducer, an amplifier, a level indicator or amplitude or a recorder with a signal analyser. Filters (low pass, high pass) should be used to restrict the equipment's frequency spectrum and add the necessary

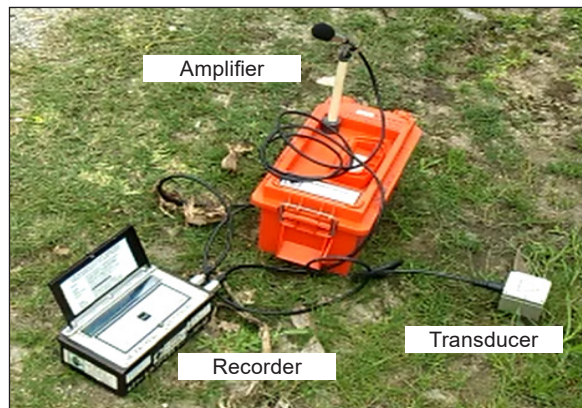


Figure 3. Components of vibration measurement

filters to the input signal, where applicable. The vibration transducer, the auxiliary equipment, including amplifiers, variable frequency equipment and carrier systems, must comply with the standards (Department of Environment Malaysia, 2007). Figure 3 shows an example of the vibration measurement system. The transducer is used to measure vibration by translating one form of energy to another. The magnitude of the ground-borne vibration can be measured in velocity, displacement and acceleration at the site.

The relationship between the parameters for the ground vibration's magnitude is shown in Equations 9 and 10 (California Department of Transportation, 2019).

$$D = V / 2\pi f \quad [9]$$

and

$$a = 2\pi f V \quad [10]$$

where:

D = displacement (amplitude) (mm)

V = particle velocity (mm/s)

f = frequency (Hz)

a = acceleration (mm/s²)

Vibration transducers that are normally used comprise the geophone and the accelerometer. The accelerometer normally detects measurement of strong ground motion, and weaker ground motion is normally measured using the geophone. It is due to an accelerometer's larger amplitude detection than a geophone (Hons et al., 2008). Figure 4 shows the geophone installation at a railway track to measure the vibrations induced by trains conducted by Crespo-Chacón et al. (2016). In vibration measurement, a geophone detects three orthogonal axes of vibration, which are in the radial, vertical and transverse direction

The range of measurement using a geophone can start from the value as low as 0.063 mm/s up to 30.5 mm/s (Sulaiman, 2018). Zhang et al. (2016), Adnan et al. (2012) and Bahrekazemi (2004) were among the researchers who measured and recorded the ground vibration using accelerometers. Figure 5 shows an accelerometer installation at the site conducted by Zhang et al. (2016).

For measuring excessive ground-borne vibration from high-speed trains, several types of accelerometers are available. The dynamic limit of measurement by accelerometers for ground-borne vibrations varies from the value of 0.01 mm/s² to more than 50 000 m/s².



Figure 4. Geophone was installed at the study site by Crespo-Chacón et al. (2016)



Figure 5. Example of accelerometer installation by Zhang et al. (2016) on railway-induced building vibrations experiment

Based on the local guideline by Malaysian authorities, the analysis for vibration frequencies within the range of 1 to 100 Hz should utilise analysers or signal analysers with one-third octave-filter sets or narrowband FFT (fast Fourier transform). These can either be instrumentation hardware or digital signal processor software. This usage of the equipment must be according to the manufacturer’s instructions (Department of Environment Malaysia, 2007). The suitability of the measurement equipment, namely the geophone, accelerometer or strain gauge, depending on the vibration amplitude and frequency required in the study. As for this research, due to its accuracy aspect and the availability of the equipment, a seismograph was chosen to calculate the low ground vibration magnitude near the railway tracks.

A seismograph meter, also known as the Mini-SEIS, was used to perform four repetitions of data reading and measurements for each site position for this analysis. A Mini-SEIS is made up of a microphone, a geophone transducer, and a data logger display (White Industrial Seismology Inc., 2009). The data was collected and categorised into two groups: peak and non-peak hours at two different distances at each site location. It was done because it was assumed that the load borne by the trains would vary between peak and non-peak hours. After all, peak hour passenger numbers were projected to be higher. Figures 6 and 7 provide a detailed diagram of where the Mini-SEIS should be mounted. Two data collection sessions were performed in the morning for the experiments, with each session

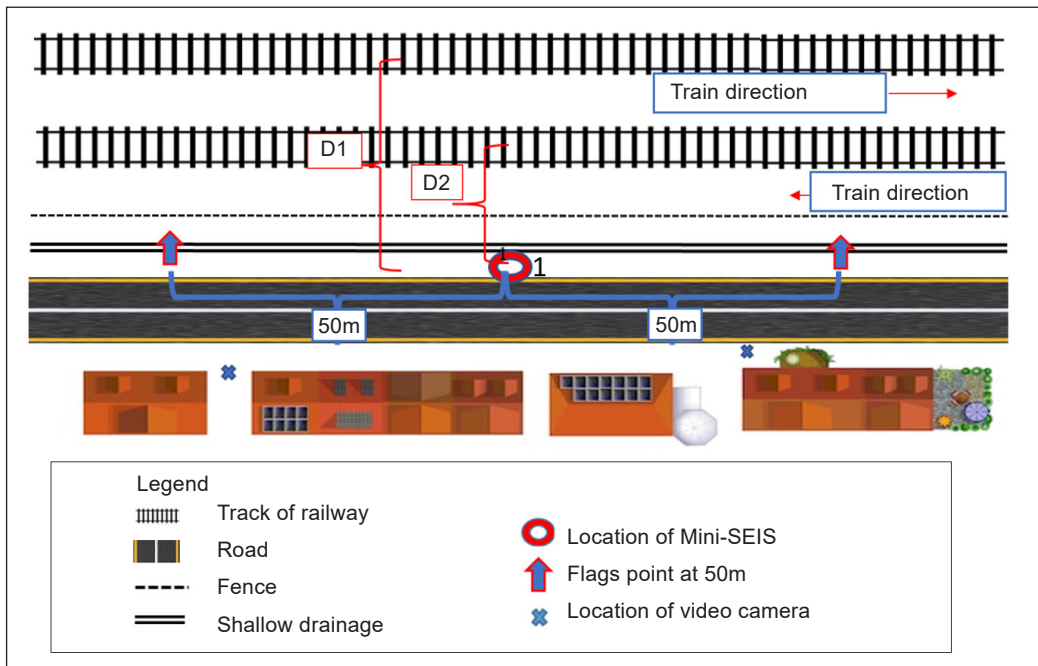


Figure 6. The location of Mini-SEIS at location 1 for morning session and midnight session of each site locations

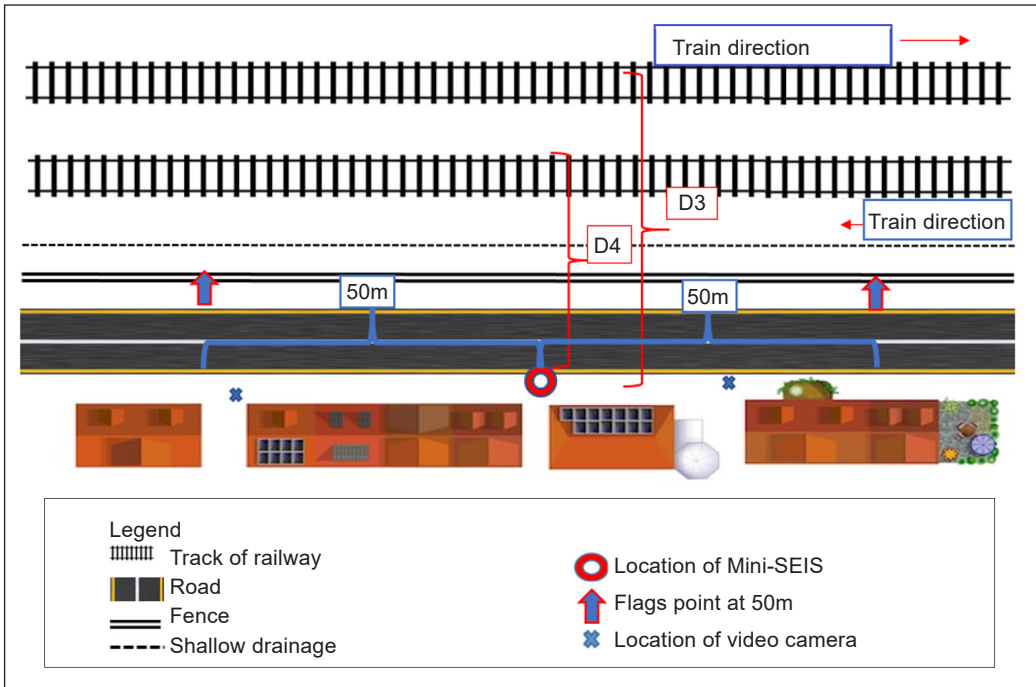


Figure 7. The location of Mini-SEIS at location 2 during the evening session of each site location

consisting of a two-hour experiment. First, it was done to gather data on peak and non-peak hour sessions. Then, two sessions were performed in the evening to collect peak and non-peak hour data from the Mini-SEIS sources at different distances. The data collection timeline is shown in Table 2: Figures 6 and 7 show where the Mini-SEIS is located.

Table 2
The timeline of data collection is based on the location of Mini-SEIS

Time		Location of mini-SEIS and distance taken	Type of Train
Peak Hour	Non-peak Hour		
6.30am – 8.30am	9.00am – 11.00am	1 = d1 & d2	Commuter
5.30pm – 7.30pm	3.00pm – 5.00pm	2 = d3 & d4	Commuter

Note: Location of mini-SEIS 1 & 2 and distance d1,d2,d3 and d4 refer to Figure 5 and Figure 6

A Mini-SEIS digital seismograph was used to measure ground vibrations in this analysis. As shown in Figure 8, the microphone and geophone transducer were mounted on residential areas and connected to a Mini-SEIS display. A GPS meter was used to calculate the Mini-SEIS’s coordinates. The times shown by the Mini-SEIS were recorded to match the actual time of the trains passing by the designated points to denote the data during data processing. The Mini-SEIS was installed outside the KTMB fencing gate on the railway tracks.

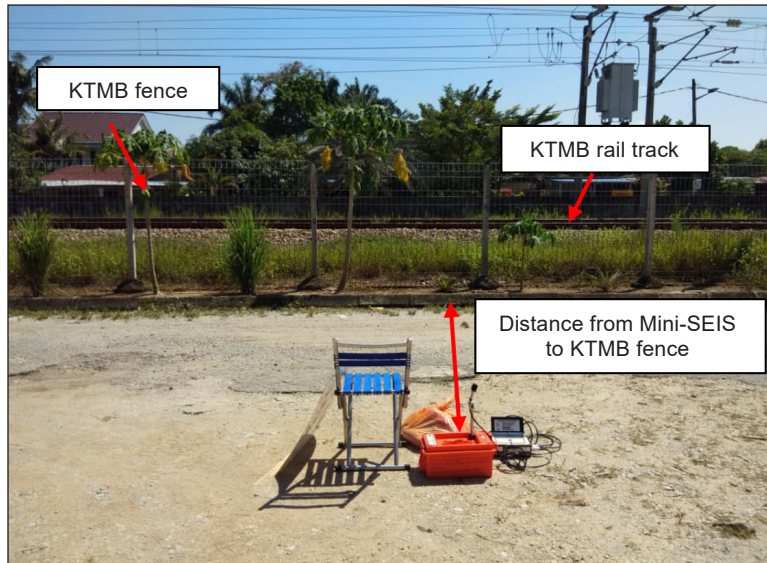


Figure 8. Installation of Mini-SEIS at the study area

The Mini-SEIS was installed within a 25 meters radius of the rail track. This distance was deemed adequate for this analysis because houses within this range allow for assessing human discomfort induced by the vibration.

RESULTS AND DISCUSSION

Threshold Limit for Allowable Limit Based on Malaysian Standard

Figure 9 shows the scatterplot of the peak particle velocity induced by the railway traffic in comparison with the allowable limit of vibration based on the guideline fixed by the Malaysian Department of Environment (DOE).

The recommended limit for human annoyance set by the authority guideline with regard to the steady-state vibrations is 0.567 mm/s for residential areas. The result in Figure 9 shows that most of the vibration induced by the train travelling along with the sites under study were more than the allowable vibration limit stated in the guideline for human annoyance. The vibration values obtained were even higher than the recommended vibration limit for commercial areas taken from the similar guideline, 1.176 mm/s. All other international standards state that the allowable vibrations limit with regard to human annoyance is not more than 0.8 mm/s. The results from this study revealed that the vibration values induced by the trains were way above the allowable limits.

Moreover, the results also showed that the vibrations induced along the study sites exceeded the recommended limit for commercial areas despite being residential. Therefore, it contributed to a higher perception of annoyance among the residents of the affected areas. A similar trend of results was also obtained by most of the researchers such as Zapfe et

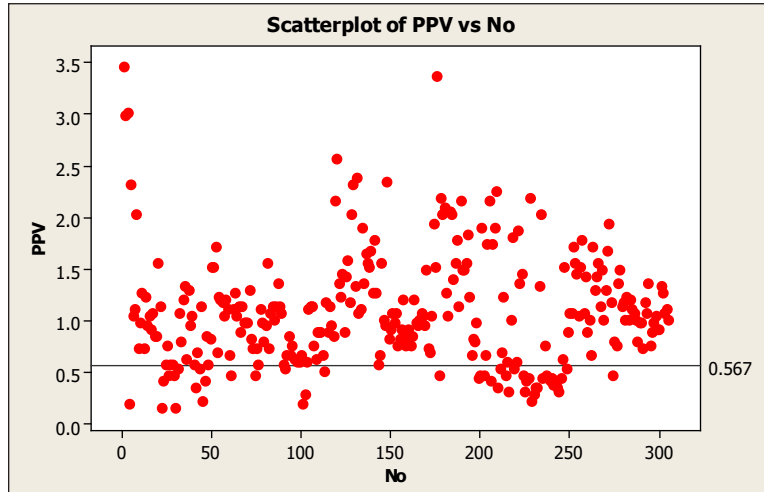


Figure 9. Scatterplot of PPV comparison with the allowable limit set by the authority guideline
 Note. The red line (0.567 mm/s) is the allowable vibration limit with regard to the human annoyance level set by the Malaysian authority in residential areas. The green line (0.8 mm/s) is the average allowable vibration limit of human annoyance in other countries. The black line (1.176 mm/s) is the allowable vibration limit of the human annoyance level set by Malaysian authorities in commercial areas.

al. (2012) from the United States and Maclachlan et al. (2018) from Sweden, whereby in their research, vibrations induced by trains had exceeded the allowable limit of perceived annoyance by humans when they comparisons were made against their countries’ guideline set by the local authorities. Therefore, the finding of the results that shows on the human annoyance towards ground-borne vibration induced by train is exceeding allowable limit from the standards and give motivation to this paper produce a model to predict the vibration value from the trains.

Descriptive Statistic of the Empirical Peak Particle Velocity Data

The descriptive statistics encapsulated the empirical peak particle velocity data analysis, which included all variables such as mean, maximum, minimum, median, skewness, kurtosis value, and standard deviation. Therefore, extreme values may be identified throughout the screening phase using the descriptive statistic’s performance. Table 3 shows the empirical peak particle velocity data after the screening, in which the extreme values

Table 3
 Descriptive statistic for the commuter PPV

Variable	Mean	StDev	Minimum	Median	Maximum	Skewness	Kurtosis
PPV	1.0405	0.4762	0.1588	1.0160	2.3813	0.59	0.04
s	41.67	17.05	16.00	40.00	83.00	0.33	-1.12
d	12.10	5.16	4.23	11.71	25.70	0.85	0.55

PPV = peak particle velocity (mm/s); s = speed (km/h); d = distance (m)

for commuter train engineering parameters were identified. The extreme values were identified as errors during the peak particle velocity data inspection during the data input phase. An error should be eliminated to prevent more comprehensive mistakes during the model development process.

Correlation Analysis for the Commuter Peak Particle Velocity Parameters

The method of diagnosing the possible relationship between the dependent and independent variables used in developing regression models is correlation analysis. The following is the correlation research hypothesis:

H_0 = There is no correlation between two variables

H_1 = There is a correlation between two variables

Correlation analysis was used to test all possible variable combinations, and the results for the overall variables are shown in the Table 4 correlation matrix. The r-value and p-value are in each column. Thus, the r-values are at the top of each row, and the p-values are at the bottom of each row.

Table 4
The correlation matrix among variables

	Peak Particle Velocity (mm/s)	<i>s</i>
Speed of train (km/h)	0.502 0.000	- -
Distance (m)	-0.626 0.000	-0.239 0.000

For the empirical data obtained from the site, Table 4 shows the correlation values between the variables PPV, *s*, and *d*. *d* was found to have a stronger relationship with PPV (r-value > 0.5). However, since the p-values were less than 0.05, both variables were assumed to impact the PPV significantly.

Multiple Linear Regressions

The commuter peak particle velocity (PPV) was used as the response in the multiple linear regressions, while the train speed (*s*) and distance (*d*) were used as predictors. The constant values and predictors are shown in Table 5.

Table 5
Multi linear regression model for commuter PPV

Predictor	Coef	SE Coef	T	P	S	R-Sq
Constant	1.20601	0.0807538	14.9344	0.000		
Speed	0.01043	0.0012165	8.5755	0.000	0.329780	52.4%
Distance	-0.04960	-0.040217	-12.3319	0.000		

The hypothesis for the final estimating mode is declared as follows:

H₀ = The predictor cannot be used for estimation in the PPV model

H₁ = The predictor can be used for estimating in the PPV model

Table 5 lists the variables for the commuter train model that were significant with the independent variables for estimating the PPV and had p-values of less than 0.05 in the multiple linear regression. The null hypothesis (H₀) was rejected, while the alternative hypothesis (H₁) was accepted. As a result, these predictors may be used in the model to estimate commuter PPV. The constant value's standard error coefficient was 1.20601. In the meantime, the speed was 0.01043, and the distance was -0.04960. As a result, each variable's standard error was small values, meaning that it was dependable in predicting the population parameter. The R-squared (R²) value indicates how well the model fits the results (Minitab, 2010). In the linear relationship between the predictor and the response, the S value was 0.329780, which reflected the prediction of the variance of the results. Thus, the linear relationship between the predictor and the response is regulated by R². The R² value used in the model's development was 52.4 per cent of the variances.

The analysis of variance (ANOVA) allocation of the output is shown in Table 6. Therefore, this test's hypothesis can be determined as follows:

H₀ = The PPV model cannot be used for estimation

H₁ = The PPV model can be used for estimation

Table 6
Analysis of variance for Commuter model

Source	DF	SS	MS	F	P
Regression	2	31.850	15.925	146.43	0.000
Residual Error	266	28.929	0.109	-	-
Total	268	60.779	-	-	-

Table 6 shows that the p-value was less than the 0.05 α-level, indicating that H₁ was accepted and H₀ was refused. As a result, if empirical speed and distance data were used, the regression model was significant and could elaborate or forecast commuter PPV. Finally, the model for estimation was developed as shown in Equation 11 as the commuter PPV regression equation.

$$PPV_{Commuter} = 1.21 + 0.0104s - 0.0496d \quad [11]$$

Where:

PPV_{Commuter} = Peak Particle Velocity (mm/s) for commuter train

s = Speed of train (km/h)

d = distance (m) from receiver to sources

The coefficients for the essential variables in this model are shown in the equation. The positive sign of speed indicates that increasing speed will increase the PPV while decreasing the distance between the source and the receiver will increase the PPV. The model's parameter considerations were similar to those found in a study by Paneiro et al. (2015), who discovered that only speed and distance significantly impact the magnitude of ground-borne vibrations.

Justification of the Regression Model Assumptions

The following process in the analysis was to check the residual plots to see if the model was acceptable and if the regression forecast had been identified. The residual plots show the characteristics of the fitted and observed response values. For example, the residuals versus suits value plot for commuter PPV is shown in Figure 10. The residual plots are dispersed randomly in the diagram, and the plot scattered close to the horizontal line has nearly zero residuals. As a result, there was no proof of missing terms or non-constant variation (Minitab, 2010).

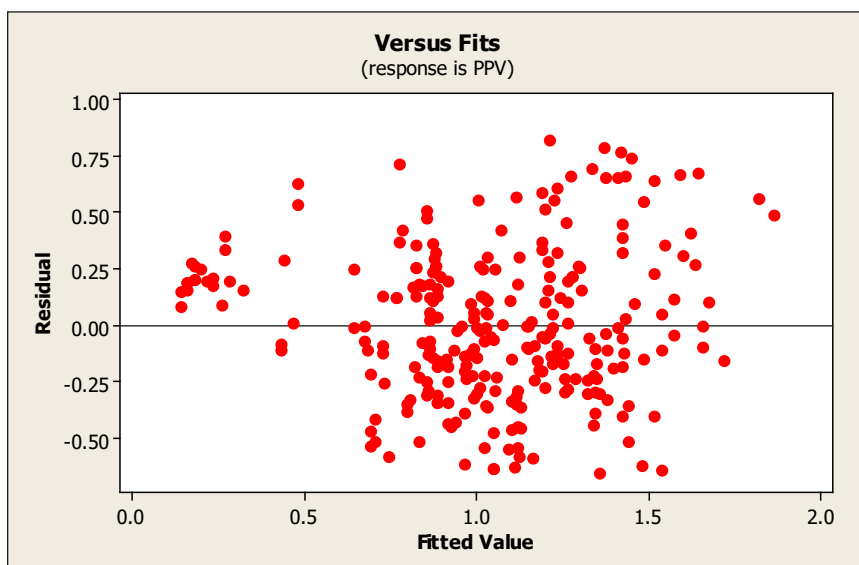


Figure 10. Graph of residuals versus fitted values for commuter PPV prediction model

Normality Test for Residuals of Commuter PPV Prediction Model

The goodness-of-fit test and probability plots such as the Kolmogorov Smirnov and Anderson Darling normality tests are used to decide if the residuals are normally distributed. The points are scattered closely along the straight line in Figures 11 and 12, indicating that the residual was normally distributed.

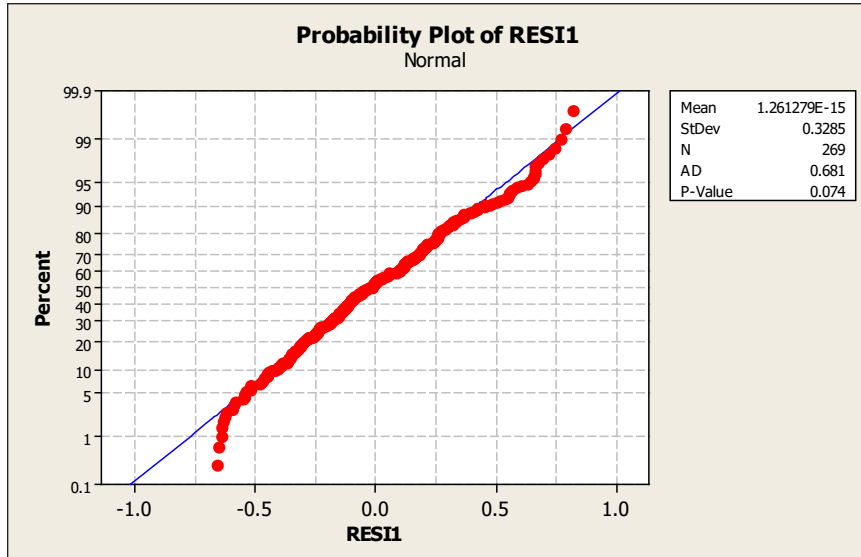


Figure 11. Anderson Darling normality test for commuter PPV prediction model

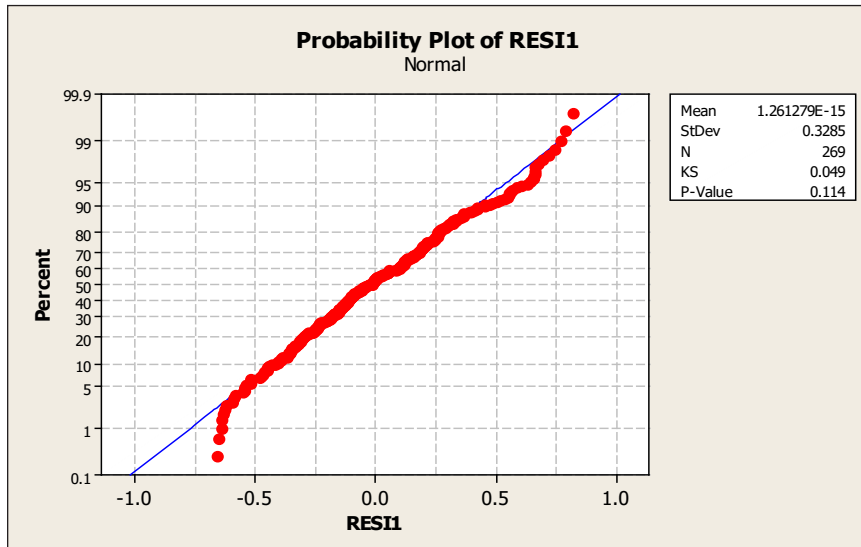


Figure 12. Kolmogorov Smirnov normality test for commuter PPV prediction model

The following are the hypothesis tests for the Kolmogorov Smirnov and Anderson Darling normality tests:

H_0 = The residuals for the predicted model are normal.

H_1 = The residuals for the predicted model are not normal.

The H_0 hypothesis was accepted because the residuals followed a normal distribution curve, and the p-values of the Anderson Darling and Kolmogorov Smirnov normality tests were greater than 0.05.

VALIDATION OF THE COMMUTER MODEL

The developed PPV model for commuter trains must be tested to determine if it can accurately reflect the real-world situation and condition to explain variability in a sample other than the one used to create the model.

Scatterplot of the Commuter Model

Figure 13 depicts the relationship between the empirical PPV and the predicted PPV established in this study for commuter trains.

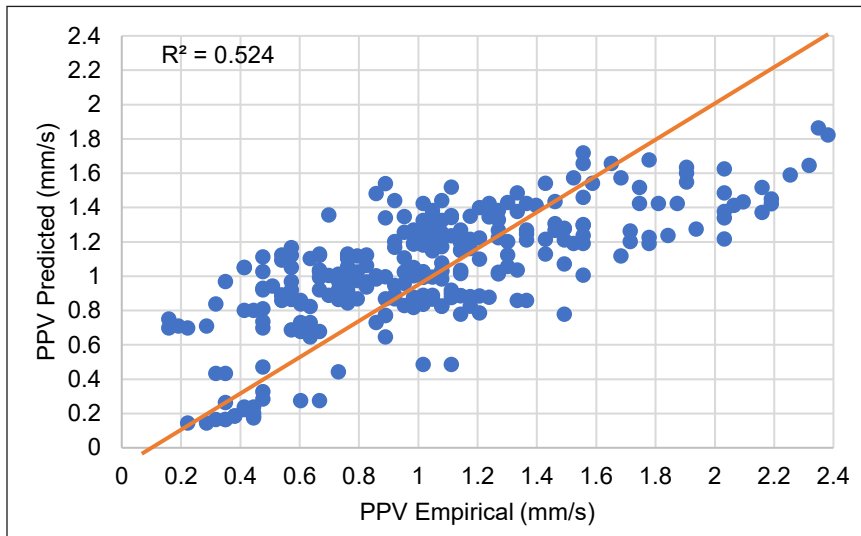


Figure 13. Predicted PPV versus empirical PPV [PPV empirical is denoted as PPV empirical (mm/s) and PPV predicted using Equation 11 is denoted as PPV predicted (mm/s)]

RMSE, MAE and MAPE of PPV Model

The RMSE, MAE, and MAPE of the PPV for the predicted commuter train model are compared in Table 7.

Table 7
RMSE, MAE and MAPE for PPV commuter

MODEL	RMSE (mm/s)	MAE (mm/s)	MAPE (%)
PPV Commuter	0.32795	0.2673	26.8211

The RMSE deviation from the empirical value of PPV was 0.328 mm/s, as shown in Table 6. The PPV’s MAE deviation from the empirical value was 0.267 mm/s. The MAPE for PPV calculated from the empirical value was 26.8%. As a result of the small discrepancy values from the RMSE, MAE, and MAPE, the PPV model for commuters can be considered acceptable for predicting the peak particle velocity caused by the commuter train.

Comparing the Mean for PPV Empirical with PPV Predicted using Paired T-test

Mean comparison was made between predicted PPV and PPV from observed data using the validation data set shown in Table 8. The following alternative and null hypotheses were used to form the hypothesis:

H_0 = the difference mean for the model is equal to zero

H_1 = the difference mean for the model does not equal to zero

Table 8 shows that the null hypothesis (H_0) was not dismissed at the 5% significance level since the p-value was 0.897, which was greater than 0.05. Thus, the PPV model expected for commuter trains did not differ much from the empirical PPV values.

Table 8
Validation analysis result for PPV from commuter model

Test	Vab
t-statistic	-0.13
p-value	0.897

CONCLUSION

The peak particle velocity of ground-borne vibrations could be determined using the train speed and the distance from the receiver to the sources, according to the equation models developed in multiple linear regressions. The result from human annoyance towards ground-borne vibrations induced by commuter trains at the case study motivates prediction model development. The data show that the vibration levels from the train exceeded the allowable limit from the Malaysian standard, which is 0.567 mm/s. The prediction formula was developed as $PPV_{Commuter} = 1.21 + 0.0104s - 0.0496d$, whereas PPV is the peak particle velocity of the train, s is the train speeds, and d is the distance from the track to the residential area. For the commuter type of trains, the peak particle velocity of the ground-borne vibration increased almost linearly as the train speed increased. According to the regression model, the distance between the receivers (residential areas) and the sources (train tracks) had a reverse effect on the peak particle velocity of the ground-borne caused by commuter trains. The peak particle velocity of ground-borne vibration decreases as the distance increases, as shown by the equation model. Residents can feel the ground-borne vibrations more strongly the closer their homes are to the tracks. The formula can be implemented to predict the ground-borne vibrations based on the limitation of local condition since the formula achieve the multiple linear regression analysis.

ACKNOWLEDGEMENT

The authors would like to thank the Faculty of Civil Engineering authorities, Universiti Teknologi MARA (UiTM), for their constant support and encouragement. In addition, appreciation goes to the Research Management Institute (RMI, UiTM) and Ministry of Higher Education Malaysia (MOHE) for the financial supports FRGS Grant scheme: RMI File No: 600-IRMI/FRGS 5/3 (008/2019), Sponsorship File No: FRGS/1/2018/SKK06/UITM/02/5.

REFERENCES

- Adnan, M. A., Adnan, N. H., & Sulaiman, N. (2012). Visual field monitoring of road defect and modeling of pavement road vibration from moving truck traffic. In *IEEE Colloquium on Humanities, Science and Engineering (CHUSER)* (pp. 826-831). IEEE Publishing. <https://doi.org/10.1109/CHUSER.2012.6504428>.
- Avellan, K., Belopotocanova, E., & Puurunen, M. (2017). Measuring, monitoring and prediction of vibration effects in rock masses in near-structure blasting. *Procedia Engineering*, *191*, 504-511. <https://doi.org/10.1016/j.proeng.2017.05.210>
- Bahrekazemi, M. (2004). *Train-induced ground vibration and its prediction* (PhD thesis). Royal Institute of Technology, Stockholm, Sweden.
- California Department of Transportation. (2013). *Transportation and construction vibration guidance manual*. Retrieved September 19, 2019, from <https://www.contracosta.ca.gov/DocumentCenter/View/34120/Caltrans-2013-construction-vibration-PDF>
- California Department of Transportation. (2019). *Caltrans seismic design criteria: Version 2.0*. Retrieved September 2019, 2019, from <https://dot.ca.gov/-/media/dot-media/programs/engineering/documents/seismicdesigncriteria-sdc/sdc20april2019final.pdf>
- Connolly, D., Kouroussis, G., Woodward, P., Costa, P. A., Verlinden, O., & Forde, M. (2014). Field testing and analysis of high speed rail vibrations. *Soil Dynamis and Earthquake Engineering*, *67*, 102-118. <https://doi.org/10.1016/j.soildyn.2014.08.013>.
- Crespo-Chacón, I., García-De-La-Oliva, J. L., & Santiago-Recuerda, E. (2016). On the use of geophones in the low-frequency regime to study rail vibrations. In *Procedia Engineering* (Vol. 143, pp. 782-794). Elsevier Ltd. <https://doi.org/10.1016/j.proeng.2016.06.126>
- David, W., James, W., Michael, G. S., Sabine, J., & Kerstin, P. W. (2015) Cargovibes: Human response to vibration due to freight rail traffic. *International Journal of Rail Transportation*, *3*(4), 233-248. <https://doi.org/10.1080/23248378.2015.1076623>.
- Department of Environment Malaysia. (2007). *The planning guidelines for vibration limits and control in the environment*. Ministry of Natural Resources and Environment. Retrieved October 2, 2018, from <https://environment.com.my/wp-content/uploads/2016/05/Vibration.pdf>
- Eitzenberger, A. (2008). *Train-induced vibrations in tunnels - A review, division of mining and geotechnical engineering* (Technical Report). Department of Civil, Mining and Environmental Engineering, Luleå University of Technology.
- Fersharaki, M., & Hamedi, A. (2016). Effects of high-speed rail substructure on ground-borne vibrations. *Florida Civil Engineering Journal*, *2*, 38-47. Retrieved February 02, 2019, from <https://myweb.fiu.edu/wp-content/uploads/sites/395/2016/09/Effects-of-High-Speed-Rail-substructure-on-ground-borne-vibrations.pdf>.
- Hons, M. S., Stewart, R. R., Lawton, D. C., & Bertram, M. (2008). Accelerometer vs. geophone response: A field case history. In *70th EAGE Conference and Exhibition Incorporating SPE EUROPEC 2008* (pp. cp-40). European Association of Geoscientists & Engineers. <https://doi.org/10.3997/2214-4609.20148091>
- Hu, J., Luo, Y., Ke, Z., Liu, P., & Xu, J. (2018) Experimental study on ground vibration attenuation induced by heavy freight wagons on a railway viaduct. *Journal of Low Frequency Noise, Vibration and Active Control*, *37*(4), 881-895. <https://doi.org/10.1177/1461348418765949>

- Ibrahim, H., Aliyu, D. S., Ma'aruf, A., & Farouq, M. (2018). Ground-borne vibration transmission on structure (effect and control): A review. *International Journal of Engineering and Science Research*, 1(Special Issue), 1-7.
- ISO. (1997). ISO 2631-1:1997(en) *Mechanical vibration and shock - Evaluation of human exposure to whole-body vibration - Part 1: General requirements*. International Organization for Standardization.
- Kuo, K. A., Lombaert, G., & Degrande G., (2017). Quantifying dynamic soil-structure interaction for railway induced vibrations. *Procedia Engineering*, 199, 2372-2377. <https://doi.org/10.1016/j.proeng.2017.09.256>
- Ma, M., Jiang, B., Liu, W., & Liu, K. (2020). Control of Metro train-induced vibrations in a laboratory using periodic piles. *Sustainability*, 12(14), Article 5871. <https://doi.org/10.3390/su12145871>
- Maclachlan, L., Orgen, M., Kempen, E. V., Alkhateeb, L. H., & Wayne, K. P. (2018). Annoyance in response to vibrations from railways. *International Journal of Environmet Research and Public Health* 15(9), Article 1887. <https://doi.org/10.3390/ijerph15091887>
- Madshus, C., Bessason, B., & Hårvik, L. (1996). Prediction model for low frequency vibration from high speed railways on soft ground. *Journal of Sound and Vibration*, 193(1), 195-203. <https://doi.org/10.1006/jsvi.1996.0259>
- Minitab. (2010). *Minitab statistical software, release 16 for windows, State College, Pennysylvania*. Retrieved February 15, 2019, from <https://www.minitab.com/enus/products/minitab/>
- Paneiro, G., Durão, F. O., de Silva, M. C., & Neves, P. F. (2015). Prediction of ground vibrationv amplitudes due to urban railway traffic using quantitative and qualitative field data. *Transportation Research Part D: Transport and Environment*, 40, 1-13. <https://doi.org/10.1016/j.trd.2015.07.006>
- Patrick, E., & Michel, V. (2012). *Review of existing standards, regulations and guidelines, as well as laboratory and field studies concerning human exposure to vibration*. Railway-Induced Vibration Abatement Solutions Collaborative project: International Union of Railways (UIC). Retrieved September 19, 2019, from http://www.rivas-project.eu/fileadmin/documents/rivas_cstb_wp1_d1_4_v03_assesment_human_response.pdf
- Rossi, F. (2003). A simple model to predict train-induced vibration: theoretical formulation and experimental validation. *Environmental Impact Assessment Review*, 23(3), 305-322. [https://doi.org/10.1016/S0195-9255\(03\)00005-2](https://doi.org/10.1016/S0195-9255(03)00005-2)
- Shih, J. Y., Thompson, D. J., & Zervos, A. (2018). Modelling of ground-borne vibration when the train speed approaches the critical speed. In *Noise and Vibration Mitigation for Rail Transportation Systems* (pp. 497-508). Springer. https://doi.org/10.1007/978-3-319-73411-8_39
- Suhairy, S. A. (2000). *Prediction of ground vibration from railways*. SP Swedish National Testing and Research Institute. Retrieved January 10, 2019, from <http://doutoramento.schiu.com/referencias/outras/Suhairy,%20Sinan%20al.pdf>
- Sulaiman, N. (2018). *Empirical modelling of ground-borne vibration from road traffic*. (Unpublished Doctoral dissertation). University Putra Malaysia, Malaysia.
- White Industrial Seismology Inc. (2009). *Mini-seis digital seismograph: Operating manual*. Retrieved October 20, 2019, from <https://whiteseis.com/MemberPages/docspecs/Mini-Seis%20Manual.pdf>

- Zapfe, J. A., Saurenman, H., & Fidell, S. (2012). Human response to groundborne noise and vibration in buildings caused by rail transit: Summary of the TCRP D-12 study. In *Noise and vibration mitigation for rail transportation systems* (pp. 25-32). Springer. https://doi.org/10.1007/978-4-431-53927-8_4.
- Zhang, Y., Zhang, N., Cao, Y., & Yu, Y. (2016). A prediction model and its validation of railway-induced building vibrations. *Advances in Mechanical Engineering*, 8(10). <http://doi:10.1177/1687814016672366>



Review article

Impact of Climate Change on Migratory Birds in Asia

Nurhafizul Abu Seri and Azimah Abd Rahman*

Geoinformatic Unit, Geography Section, School of Humanities, Universiti Sains Malaysia, 11800 USM, Pulau Pinang, Malaysia

ABSTRACT

Climate change is not something that has never happened before. However, it has recently been reported that climate change has affected living things such as humans, animals and plants. Among the animals that may be vulnerable to the effects of climate change are migratory bird species. Therefore, this review paper will emphasise the checklist of migratory bird species found to be affected by climate change. Data for bird migration species in Asia are obtained from the Birdlife Data Zone. At the same time, the data for Global land surface temperature (1910-2020) and Asia land surface temperature (1910-2020) were taken from National Oceanic and Atmospheric Administration for Environmental information. These papers showed that climate warming could affect species differently, but there are still species from certain populations not affected at all. This paper also reviewed that approximately 169 species of migratory birds in Asia are affected by climate change and severe weather. Of the total, 5 species (2.96%) are critically endangered, 8 (4.73%) endangered, 21 (12.43%) vulnerable, 27 (15.98%) near threatened and 123 (63.91%) least concern.

Keywords: Asia, climate change, migratory birds, species, temperature

ARTICLE INFO

Article history:

Received: 27 April 2021

Accepted: 30 July 2021

Published: 28 October 2021

DOI: <https://doi.org/10.47836/pjst.29.4.38>

E-mail addresses:

nurhafizul.abuseri97@gmail.com (Nurhafizul Abu Seri)

azimahrahman@usm.my (Azimah Abd Rahman)

* Corresponding author

INTRODUCTION

Overharvesting may be one of the most persistent threats to migratory birds because of human exploitation of their biology, including predictable spatiotemporal peaks in large quantities at various scales (Shuter et al., 2011). Nevertheless, today, overharvesting is no longer the only major threat to migratory birds because of the

emergence of a new threat that may have occurred over a long period. However, it has not been realised at that time that is climate change. Turrin and Watts (2016) assessed and calculated the sustainable harvest threshold for Asia-Pacific migratory shorebirds. Global climate change has a significant effect on the phenology of seasonal events (Lehikoinen et al., 2004; Ahas & Aasa, 2006; Menzel et al., 2006), and it has the potential to alter migration phenology (Both & te Marvelde, 2007; Rubolini et al., 2007).

Climate change can cause specific problems for migratory birds living in different parts of the annual cycle in other world regions (Silllett et al., 2000). One of the most crucial concerns is climate change when global surface temperatures have warmed at an average of 0.16°C to 0.18°C per decade since the 1970s (Solomon et al., 2007). The 2013 Intergovernmental Panel on Climate Change predicts that if the present pattern in emissions continues, global temperatures are expected to rise by 2°C or as much as 4.8°C by 2100 (Collins et al., 2013; Pachauri et al., 2014).

One of the most interesting facets of birdlife is migration. They get the ability to migrate hundreds or thousands of kilometres across geographical boundaries to other parts of the globe in response to changes in habitat, food availability, climate, and other factors. For example, there are almost 828 species of migratory birds in Asia, while in Europe, there are 429 species. However, many migration birds, mammals, fish, and invertebrates have experienced population loss in previous centuries (Wilcove & Wikelski, 2008; Gilroy et al., 2016). Therefore, a large number of migratory birds use flyways as their flight path. A flyway is a biological system consisting of entire types of migratory bird species, related communities of species, or different populations of one species that migrate annually from breeding areas to non-breeding areas, including a stopover and feeding areas as well as migration areas (Bridge et al., 2007).

The Eastly-Australasian Flyway (EAAF) is an important flyway in Asia that is also one of the nine major routes used by migratory birds. This EAAF flyway, which crosses three continents and 22 countries, is one of the world's biggest and most species-rich migration corridors (Turrin & Watts, 2016). Apart from the EAAF, the West Pacific Flyway and West Asian Flyway are two of the three flyways available in Asia. As a consequence, determining the migration paths and stopovers of migratory animals is important for effective population management and habitat conservation (Hutto, 2000; Faaborg et al., 2010). However, this review will not concentrate on a single migratory bird route in Asia but the total migratory birds observed in Asia from different flyways. First, the purpose of this study is to identify and list the species of avian (migratory birds) found in Asia that affected reference to previous studies that analysed the relationship between climate change and migratory birds. Second, the goal of this study was to identify migratory bird species in Asia that are sensitive to the impact of climate change, which may contribute to species loss. This information is essential for designing new conservation strategies and prioritising the endangered species and critically endangered species.

THE CLIMATE-CHANGING SINCE 1910-2020

The primary data sources for migration bird checklists found in Asia used in this article are obtained from the Birdlife Data Zone. Species threat data on climate change and extreme weather for birds migrating in Asia were also collected from the Birdlife Data Zone. All data observed are the latest updated until 23 February 2021. Meanwhile, data for Global land surface temperature (1910-2020), Asia land surface temperature (1910-2020) were taken from NOAA National Centers for Environmental information (2021). According to the International Union for Conservation of Nature (IUCN), the conservation status of migratory bird species was identified.

The earth's climate has changed over a long period until now, which has seen a very significant change. The tropopause, the border between the stratosphere and the troposphere, has climbed several hundred metres in height since 1979. Human-induced increases in ozone and mixed greenhouse gases account for approximately 80% of the simulated tropopause height increase from 1979 to 1999 (Santer et al., 2003). One of the most commonly used measures of global climate change is the global average temperature, and it has shown a series of increases since the early twentieth century. Natural processes, as well as certain impacts from human activity, lead to year-to-year temperature changes.

Figures 1 and 2 show the global land temperature anomalies from January to December for 1910 to 2020. Based on Figure 1, the negative anomaly (colder than normal) occurred around 1910 to 1937 before it fell to a positive anomaly (warmer than normal) in 1938 to 1944. The decline from negative anomalies in 1910 to 1937 to positive anomalies in a subsequent year shows evidence that there had been changes in terms of global climate around the 90s. Since then, annual anomalies for global surface temperatures have been seen as erratic and often change almost every year. For example, several other negative anomalies have occurred before 2000, namely in 1945 to 1946, 1949 to 1952, 1954 to 1957, 1960, 1964 to 1966, 1968 to 1969, 1971 to 1972 and 1974 to 1976. While the positive anomalies that occurred before the year 2000 were in 1947 to 1948, 1953, 1958 to 1959, 1961 to 1963, 1967, 1970, 1973, 1975, 1977 to 1999. Then, from 2000 to 2020, all those years recorded only positive anomalies marked since the beginning of the 20s era of global surface temperature conditions were warming. Therefore, based on all the data shown and proved from 1910 to 2020, there has been a change in global climate. In conclusion, climate change has occurred globally, increasing land temperature anomaly from -0.36°C (cold) in 1910 to 1.59°C (hot) in 2020.

Figure 2 shows the Asia land temperature anomalies from January to December for the years 1910-2020. In Asia, around 1910 to 1976 (66 years), the majority of those years were to record the negative land temperature anomaly. However, there were still some years that showed warmer than normal conditions (positive anomaly). The hot years were 1914, 1925, 1932, 1938 to 1939, 1943 to 1944, 1948, 1951, 1953, 1959, 1961 to 1963, 1967, 1971,

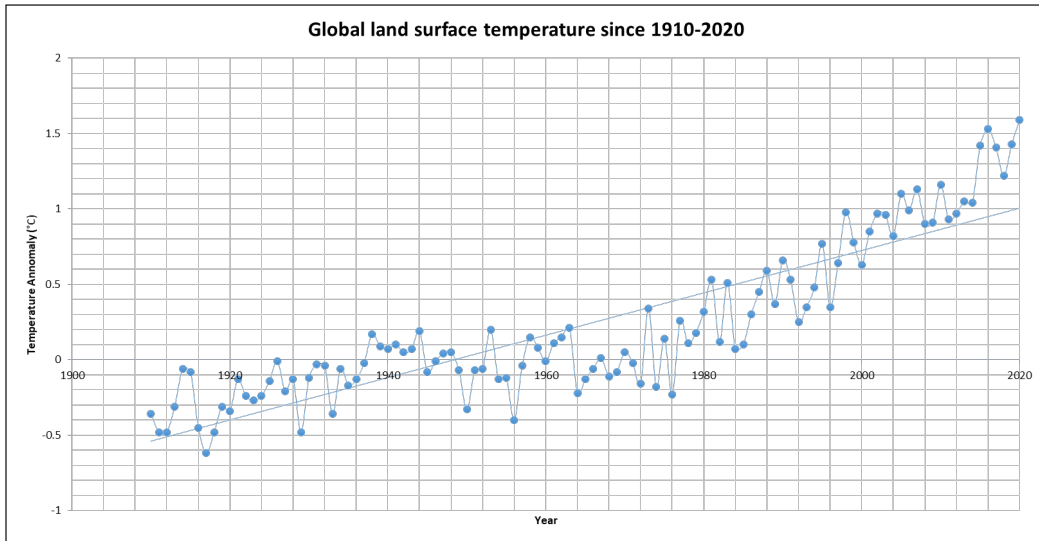


Figure 1. Global land surface temperature anomalies from 1910 to 2020

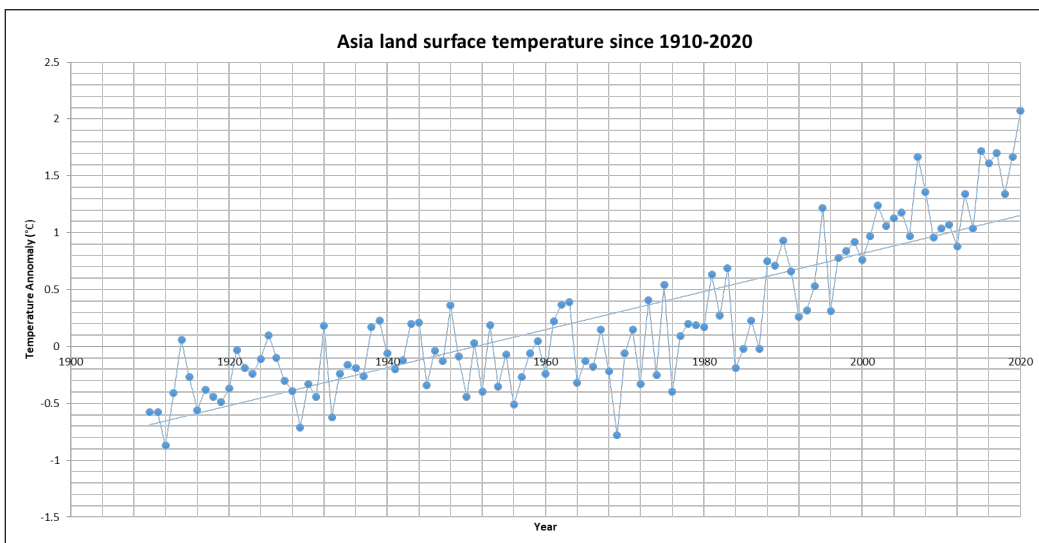


Figure 2. Asia's land surface temperature anomalies from 1910 to 2020

1973 and 1975. Later in the year, 1977 to 1983 also showed positive anomalies before the next two years recorded negative anomalies in 1984 to 1985. From 1988 to 2020, all these years recorded a positive anomaly which means that the land surface temperature in Asia is warming up in the 20s. It can be concluded here that there has been climate change in Asia when there was an increase in land temperature anomaly from -0.58°C (cold) in 1910 to 2.07°C (hot) in 2020. Land temperature anomaly in 2020 is quite high if compared to previous years because it has exceeded 2°C .

THE CATASTROPHE OF CLIMATE CHANGE ON MIGRATORY BIRDS- THE EVIDENCE

For decades, researchers have studied the impact of daily weather variations on the number of birds that have avoided migration. During the 1960s and 1970s, when some radar and visual experiments on migration were performed, the research was particularly active (Richardson, 1990). Rising temperatures are the most significant factor affecting bird migration trends, forcing birds to migrate a little early each spring and change the return journey by less than two days per decade (Richardson, 1990; Horton et al., 2020). As a result, migratory species may need to adapt their seasonal and annual migration patterns to avoid entering areas with extreme climates such as too cold, too hot, too low humidity, too high humidity, and to use new habitats in areas with previously low temperatures and humidity. In response, the distribution of species may vary (Langham et al., 2015). For example, it has been found that large bustard migration patterns of males (but not females) are closely related to extreme temperatures during the summer breeding season (Alonso et al., 2009).

In addition to forcing birds to migrate a little earlier, changes in temperature associated with climate change are expected to result in a reduction in body size, a primary determinant of animal physiology and ecology (Weeks et al., 2019). Thus, climate change, regarded as one of the most serious threats to biodiversity and ecosystems, may impact migratory bird distribution and survival (Liang et al., 2018). Additionally, a number of additional studies have forecasted changes in species richness or distribution in China as a result of climate change scenarios (Hu et al., 2017; Liang et al., 2018). It may also be concluded that animals have evolved to withstand extreme temperatures, and climate change has had a significant effect on species physiology, including increases in exposure to elevated temperatures, differences in sex ratios in species with temperature-dependent sex, and increased metabolic costs associated with living in a warmer environment (Scheffers et al., 2016).

However, trying to forecast which components of climate have the most influence on species distribution is one of the issues confronted by ecologists and conservation biologists (Bateman et al., 2015). Furthermore, the potential consequences of climate change on bird distribution have been explored extensively today, such as polar or short-range winter breeding distances by La Sorte et al. (2017) and Wauchope et al. (2017). The influence of climate change on food sources and the habitat of migratory bird species has been highlighted as one of the most critical components in migratory bird research (Walther et al., 2002). It is proven that the consequences of recent climate change have been discovered to affect migratory bird migration patterns (Both et al., 2006; Harris et al., 2013). According to Harris et al. (2013), climate change causes a shift in migration time for some birds in Southeast Asia. The reason for this delay of long-distance migrants is that warmer temperatures allow species to stay in northern breeding sites longer. Delayed arrivals in winter places may have a tiering influence on migratory species' yearly cycles,

such as changing the arrival date in breeding places, which can influence fitness. Harries et al. (2013) discovered a 1 to 3 days arrival delay in the Japanese sparrowhawk *Accipiter gularis* and the sandpiper curlew *Calidris ferruginea*, but no change in the arrival date for the other species.

As a result, the timing of bird migration has served as a useful framework for researching how natural processes react to climate change (Hurlbert & Liang, 2012; Jonzen, 2006). It was discovered that animals arriving late in the migration phase might have difficulty developing breeding areas or finding compatible partners (Møller, 2001; Pulido, 2007; Faaborg et al., 2010). According to a number of surveys have been done by Hughes (2000), McCarty (2001), Ottersen et al. (2001), and Wuethrich (2000), the current climate change has affected a diverse range of animals with geographically distributed regional ranges. Pacifici et al. (2017) showed that climate change has already impacted a significant number of endangered species populations by modelling the interaction between observed and inherent responses and spatial properties. Climate change could have harmed at least 47% of non-terrestrial endangered mammals (873 species) and 23.4% of endangered birds (1,272 species) in at least part of their range, according to the study's findings (Pacifici et al., 2017).

According to atmospheric conditions in the 21st century, the ideal migration site between Japan and China occurred in the East China Sea (2006-2013) (Figure 3) (Nourani et al., 2017). According to their findings, the expected changes in atmospheric conditions

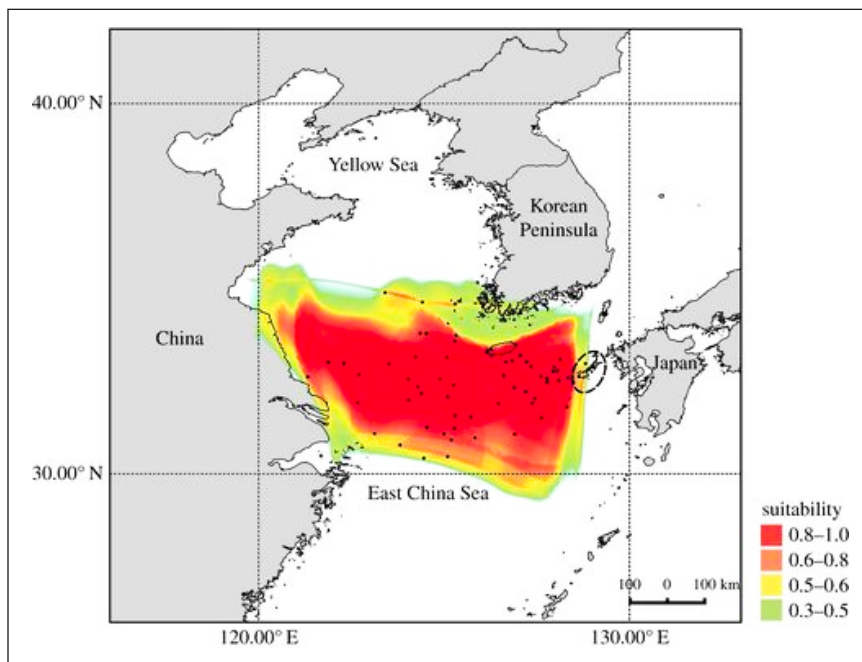


Figure 3. Ensemble model projections for suitable atmospheric conditions for the fall migration of Oriental honeybuzzards (2006–2013) (Nourani et al., 2017)

caused by climate change may have a negative impact on the suitability of traditional bird migration routes. Under the RCP4.5 scenario, suitable areas will move northward in the middle of this century. Highly suitable areas' scope and connectivity will suffer greater loss (Figures 4a & 4b), resulting in more severe conditions. However, by the turn of the century, the model identified a suitable area in the eastern part of the Korean Peninsula under RCP4.5 (Figure 4c) and a moderately small area under RCP8.5 (Figure 4d). Both deviate from the traditional route and cannot provide a complete route from Japan to China. Thus, it can be said that climate change has changed the best wind-dependent flight routes for bird migration.

Warren et al. (2013) undertook a global study of potential climate range transitions from common and prevalent species. They found that, there would be $57 \pm 6\%$ of plants without mitigation, and $34 \pm 7\%$ of animals would lose 50% of their climate range by the 2080s. However, if emissions plateau in 2016, losses are reduced by 60%, and if emissions peak

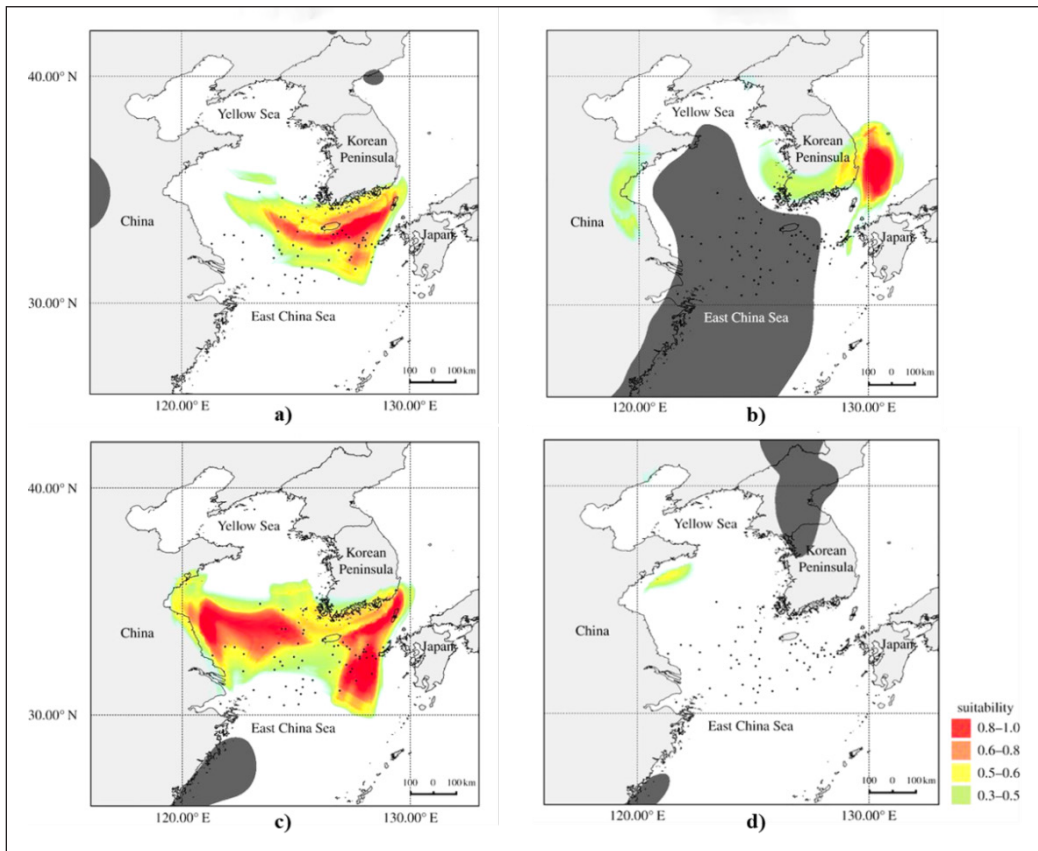


Figure 4. Ensemble model projections for suitable atmospheric conditions for the fall migration of Oriental honeybuzzards: (a) mid-century (2046 to 2055; RCP4.5 scenario), (b) mid-century (2046 to 2055; RCP8.5 scenario), (c) late century (2091 to 2100; RCP4.5 scenario), and (d) late century (2091 to 2100; RCP8.5 scenario) (Nourani et al., 2017)

in 2030, losses are reduced by 40%. With the influence of rising temperatures on animal species due to climate change, it can be projected that migratory birds are also likely to suffer the same fate or even worse. Because migratory birds are not a species in the areas they visit, they will face problems adapting to places other than their area of origin. Thus, it can be argued that migratory birds found in Asia may need help adapting to climate change to survive or live in an area. Table 1 shows the impact of climate change on different animal species that have occurred. Other animals such as turtles, whales, sharks, dolphins, and avian species are also affected by this climate change. Each animal was found to be affected by different climatic factors (Table 1).

Table 1
Climate change's effect on certain animal species (Trouwborst, 2012)

Climate Impact	Impact on Animal Species	Animal Species
Temperatures are rising	a) Melting sea ice has resulted in habitat destruction; b) Zooplankton density has changed; and c) Sex ratios have changed.	a) <i>Balaena Mysticetus</i> b) <i>Cetorhinus Maximus</i> c) <i>Dermodochelys Coriacea</i>
Changes in Precipitation	a) Wetland habitat for breeding and feeding is vanishing; b) Grazing habitat for terrestrial mammals is vanishing; and c) Rainfall changes affect breeding performance.	a) <i>Calidris Canutus Rufa</i> b) <i>Addax Nasomaculatus</i> c) <i>Gavialis Gangeticus</i>
Weather Extremes	a) Extremes of temperature; b) Storm frequency and severity have increased; and c) Precipitation extremes have increased.	a) <i>Platanista Gangetica</i> b) <i>Tadarida Brasiliensis</i> c) <i>Trichechus Senegalensis</i>
Increasing Sea Levels	a) The loss of low-lying marine habitat; and b) The disappearance of nesting areas.	a) <i>Anser Cygnoides</i> b) <i>Chelonia Mydas</i>
Acidification of the Oceans	a) Food web affected; and b) Habitat degradation.	a) <i>Eubalaena Japonica</i> b) <i>Eretmochelys Imbricata</i>
Ocean Circulation Changes	a) Shifts in food distribution and abundance; and b) Migration-related impact.	a) <i>M e g a p t e r a Novaeangliae</i> b) Hawksbill Turtle
Spatial and Temporal Responses	a) Biome shifts; b) Phenological shifts; and c) Destruction of habitat.	a) <i>Puffinus Mauretanicus</i> b) <i>Caretta Caretta</i> c) <i>Grus Leucogeranus</i>
Existing Threats are Getting Worse	-	a) <i>Acrocephalus Griseldis</i>

The highest number of endangered migratory bird species has been identified in many locations. For example, the East Asia-Australasia Region has the highest percentage of endangered migratory waterbirds, which is 20%. Although Africa, Eurasia, Central Asia, and East Asia-Australasia have the highest percentage of endangered birds (roughly 30% each), America, Africa, Eurasia, and East Asia-Australasia have the highest percentage of endangered seabirds (roughly 30% each). The East Asia-Australasia flyway has the highest

number of endangered migratory waterbirds (19%) when it comes to flyways. Though the Black Sea-Mediterranean, East Asia-East Africa, Central Asia, and East Asia-Australasia have the highest percentages of vulnerable soaring birds (between 24 and 34%), the Black Sea-Mediterranean, East Asia-East Africa, Central Asia, and East Asia-Australasia have the lowest (Galbraith et al., 2014). Globally, 317 (14%) migratory bird species are classified as endangered or near-threatened. According to the 2010 IUCN Red List, there are 17 critically endangered migratory bird species, 50 threatened migratory bird species, vulnerable migratory bird species, and near-threatened migratory bird species out of 317 migratory bird species (122). According to an overview of the number of species moving between Red List categories since 1988, 53 species have decreased in status, and only nine have improved (Galbraith et al., 2014).

Then, Hu et al. (2010) found that the black-faced spoonbill (*Platalea minor*) is an endangered migratory species confined to East Asia due to climate change. They also predicted that by 2080, the population of black-faced spoonbills in various regions in Asia, including northeastern Vietnam, Taiwan, and coastal areas around the South China Sea, might be drastically reduced. They also indicated that the centre of the expected spoonbill range will migrate northwards by as much as 240 km by 2020, 450 km by 2050, and 600 km by (2080). Finally, Liang et al. (2018) utilised species distribution models (SDM) and climate data to forecast future changes in migratory birds species distribution and how the geographical expansion of these endangered birds may adapt to changing climates by 2050 under current and future climate scenarios in China. The findings suggest that migratory bird hotspots would likely remain downstream and in the centre of China's Yangtze River. At the same time, more species will likely dwell in the coastal areas of Bohai Bay and the Yellow Sea in the future. Also, according to the findings, the proportion of all migratory bird species distribution or hotspots for all endangered migratory bird species protected by national nature reserves (NNRs) in China is still low in 2050.

Besides that, Runge et al. (2015) found that only a small fraction of migratory birds receive appropriate protection across their breeding and wintering ranges throughout the world. Given that over half of the world's migratory bird populations are dropping, these findings, according to them, highlight the urgency with which we must work to protect migratory birds during their entire migratory cycle. According to the study, only 9% of 1451 migratory birds are sufficiently protected by sheltered locations at all phases of their yearly cycle, compared to 45% of non-migratory species (Runge et al., 2015). The long-distance migrating birds, which rely on an endogenous circannual rhythm to trigger their migration, face unique hurdles in reacting to changes due to their extensive seasonal movements (Briedis et al., 2017).

Climate change has been shown to alter morphology in butterflies, dragonflies, and birds, which results in colour changes (Karell et al., 2011; Kingsolver & Buckley, 2015; Roulin, 2014; Zeuss et al., 2014). In addition, climate change can influence the timing of

migratory species' arrival on breeding grounds or the initiation of breeding activities, as well as the availability of resources required for successful reproduction (Burgess et al., 2018; Franks et al., 2017; Møller et al., 2008; Mayor et al., 2017). When all of those phenological incompatibilities exist, it may result in lower reproductive success and population decline (Møller et al., 2008; Miller-Rushing et al., 2010; Dunn & Møller, 2013). However, Mayor et al. (2017) suggest that migratory birds could be among the species most readily suited to climate change because of their ability to migrate fast over long distances. Again, Mayor et al. (2017) argue that migration responds to annual climate change, so additional annual climate change is unlikely to pose a challenge in terms of adaptation.

Perhaps climate change might not be the only factor affecting these migratory birds; human actions such as economic activities also play a role in migratory bird species disruption. For example, considering China as a case study, which is a country with fast-rising economic activity, it has a significant impact on migratory bird stopover habitat (Ma et al., 2014; Kamp et al., 2015), resulting in dropping migratory bird populations (Runge et al., 2015). However, generally speaking, that economic activities are happening in China, and other countries in the world may also be among those contributing to climate change. Therefore, it suggests that indirectly the economic activities that have contributed to climate change will likely also contribute to the disruption of the stopover of migratory birds, their food and so on. The situation may worsen when the area that should be used as a stopover has lost the characteristics and to needs these migratory birds need while living in the areas even if only for a while.

According to Kamp et al. (2015), persecution and over-exploitation by humans are also one of the major causes of species extinction. Between 1980 and 2013, the Yellow-breasted Buntings (*Emberiza aureola*) population dropped by 84.3% to 94.7%, and the species' range shrank by 5000 kilometres. Quantitative data gathered during police raids revealed that the species was illegally trapped along its East Asian flyway in China. As the consumption of Yellow-breasted Bunting and other songbirds has grown, it is once again suggested that causes of economic development and prosperity in East Asia are the reason for the decline (Kamp et al., 2015). It has been proven that climate change is not the only cause of the current disturbance and reduction in the population of migratory bird species; other causes may also be at play.

The Condition of Asia Migratory Bird Affected by Climate Change and Severe Weather- Birdlife Data Zone and IUCN Lists

The latest data from the Birdlife Data Zone shows that approximately 169 migratory birds in Asia are affected by climate change and severe weather. Of the total, five species (2.96%) of migratory birds occupy the critically endangered category in the Global IUCN Red List, namely Siberian Crane (*Leucogeranus leucogeranus*) from the family Gruidae (Cranes), Christmas Frigatebird (*Fregata andrewsi*) from the family Fregatidae (Frigatebirds),

Sociable Lapwing (*Vanellus gregarius*) from the family Charadriidae (Plovers), Spoon-billed Sandpiper (*Calidris pygmaea*) from the family Scolopacidae (Sandpipers, Snipes, Phalaropes) and Chinese Crested Tern (*Thalasseus bernsteini*) from the family Laridae (Gulls, Terns, Skimmers). In addition, there are eight species (4.73%) in the endangered category, such as White-headed Duck, Lesser Frigatebird, Barau's Petrel, Abbott's Booby, Great Knot, Far Eastern Curlew, Rufous-headed Robin and Pallas's Fish-eagle. While there are 21 species (12.43%) that fall in the vulnerable category, 27 species (15.98%) are near threatened, and 123 species (63.91%) are in the least concerned category (BirdLife International, 2021).

Critically Endangered Species. Referring to Table 2, the Siberian Crane or Siberian White Crane or Snow Crane (*Grus leucogeranus*) is one of the critically endangered migratory species. According to the IUCN Red List, the Siberian Crane was classified as threatened in 1988, endangered in 1994 and 1996, and critically endangered from 2000 to 2018 (BirdLife International, 2021). According to research by Ming-Qin & Hong (2014), low water levels in spring and early summer in Lake Poyang have reduced food availability for many water birds that have migrated to the area in recent years. They also discovered that the Siberian Cranes' distribution pattern was impacted by a lack of food availability that could feed all of the cranes in Banghu. Meanwhile, the Siberian Crane's departure time from Lake Poyang was reported as being slower, which might be attributed to a delay in the winter season as a result of climate change. Therefore, it is essential to study and focus on this species in the Poyang lake area, where more than 98% of their population overwinters in the lake.

Table 2

Asia migratory birds affected by climate change and severe weather (BirdLife International, 2021)

Species	Global (IUCN) status
<i>Leucogeranus leucogeranus</i>	Critically Endangered
<i>Fregata andrewsi</i>	Critically Endangered
<i>Vanellus gregarius</i>	Critically Endangered
<i>Calidris pygmaea</i>	Critically Endangered
<i>Thalasseus bernsteini</i>	Critically Endangered
<i>Oxyura leucocephala</i>	Endangered
<i>Sypheotides indicus</i>	Endangered
<i>Pterodroma barau</i>	Endangered
<i>Papasula abbotti</i>	Endangered
<i>Numenius madagascariensis</i>	Endangered
<i>Calidris tenuirostris</i>	Endangered
<i>Haliaeetus leucorhynchus</i>	Endangered
<i>Larvivora ruficeps</i>	Endangered

It has been proven that the Poyang lake area is the most important wintering ground for the globally critically endangered Siberian crane (Chen et al., 2016). In 2011–2012, the total population of Siberian Cranes in the Poyang Lake basin was projected to be 3,500–4,000 individuals. In December 2011, there were 4577 Siberian Cranes (*Grus leucogeranus*), 302 Hooded Cranes (*Grus monacha*), 885 White-naped Cranes (*Grus vipio*), and 8408 Eurasian Cranes (*G. grus*). In February 2012, there were 3335 Siberian Cranes, 110 (Hooded Cranes), 283 (White-naped Cranes), and 2205 (Eurasian Cranes). Thus, the number of Siberian Cranes counted had fallen by 1242 in February 2012. Similarly, Hooded Cranes declined by 192, White-naped Cranes (602) and Eurasian Cranes (6203) (Li et al., 2012).

The effective population size for Christmas Island frigatebirds (*Fregata andrewsi*) is around 5,000 (Morris-Pocock et al., 2012), and this species is listed as Critically Endangered by the IUCN (Birdlife International, 2021). For a long time, the status of the Christmas Island Frigatebird in India was unclear until Praveen et al. (2013) discovered few previous reports of Great or Lesser Frigatebird misidentification. It indicates a flaw in earlier researchers' documentation, which resulted in a paucity of data for this bird species. The first record of Christmas Island Frigatebird *Fregata Andrewsi* in Timor was in 1986, which was found flying along the coast near Kupang, Timor (McKean, 2011). *Fregata andrewsi* has also been discovered in southern New Guinea (Simpson, 1990). In July 2012, there were 209 individuals of this species in Indonesia. In contrast, in May 2013, 113 individuals of this species were discovered using the Jakarta Bay to obtain food, relax in Sero, and Pulau Rambut at night (Tirtaningtyas & Yordan, 2017). McMaster et al. (2015) in 2014 found an adult female Christmas Frigatebird and an unconfirmed juvenile Christmas Frigatebird in the Nightcliff foreshore, Darwin, Australia.

Several anthropogenic threats to Christmas Island Frigatebirds have been identified in Jakarta Bay, Indonesia, including the unintentional involvement of fishing gear, as well as capture, poisoning, and shooting (Tirtaningtyas & Hennicke, 2015). It has also been revealed that climate change can impact the population of this species, with severe storms likely to cause fatality in juveniles and adults (Hill et al., 2004). The situation is anticipated to deteriorate if severe storms become more common as a result of climate change (Harley et al., 2006). This catastrophic storm occurrence will almost certainly increase storm-related fatalities of this species. In addition, higher sea surface temperatures linked with climate change have been shown to impact marine productivity (Harley et al., 2006), which is thought to affect food availability for Christmas Island frigatebirds.

According to Watson et al. (2006), the *Sociable Lapwing Vanellus gregarius* is a critically endangered species likely to experience a decline in its total population, i.e. from 5000 pairs to 500 pairs, within 11 years. The decline of this species is likely due to climatic and societal changes that cause nesting habitat for the *Sociable Lapwing Vanellus gregarius* to be more extensively grazed (Shevchenko, 1998). In 1988 this species was

listed as threatened, vulnerable from 1994 to 2000, and critically endangered from 2004 to 2018 (BirdLife International, 2021). The number of nests of *Sociable Lapwing Vanellus gregarius* discovered in the 14 core colonies of the Korgalzhyn region, in the other colonies of the Korgalzhyn region, and in the other colonies of the Pavlodar region increased from 2005 to 2007, but then declined from 2008 to 2012. The 330 *Sociable Lapwing Vanellus gregarius* nests discovered in 2007 were reduced to 137 in 2008, 122 in 2009, 131 in 2010, 105 in 2011, and 44 in 2012 (Sheldon et al., 2012). Watson et al. (2006) expressed worry about the increasingly dry climate in breeding and wintering ranges, which might endanger semi-desert species. The drier climate in its breeding and wintering areas may influence this species, although it is uncertain whether this benefits or harms this semi-desert species (Watson et al., 2006). So, additional research on the link between climate, breeding size, and population size for this species is required. However, contrary to the findings of Jayendra et al. (2014), low rainfall attracts more birds to winter in Gujarat.

Since 1977 and 2000, the breeding population of the critically endangered Spoon-billed Sandpiper *Calidris pygmaeus* has declined dramatically (Tomkovich et al., 2002). The decrease has indeed continued, with the rate of decline estimated to be 25% per year (Zöckler et al., 2010a; Zöckler et al., 2010b). This species has declined rapidly throughout the winter range from 2005 to 2013 with current estimates putting the breeding population at less than 120 pairs (242 to 378 individuals) (Zöckler et al., 2016). At the same time, Clark et al. (2018) estimated the spoon-billed sandpiper breeding population in 2014 to be 210 to 288 pairs, with a total post-breeding population of 661 to 718 individuals. Waterbird surveys in early 2018 yielded no Spoon-billed Sandpiper sightings throughout a 243.8 kilometre stretch of coast in North Sumatra Province, from Langkat District to Asahan District (Putra & Hikmatullah, 2018). Meanwhile, one Spoon-billed Sandpiper was discovered at the end of 2018 (2-4 November) in Seunodon Sub-district, North Aceh District, Aceh Province, Sumatra, Indonesia. It demonstrates that the Spoon-billed Sandpiper is highly endangered and has lacked protection status in Indonesia (Putra et al., 2019). The spoon-billed sandpiper population in China has declined from 2,000 to 2,800 breeding pairs in the 1970s to around 220 in 2010 (Yang et al., 2017). In 1988 this species was listed as threatened, vulnerable from 1994 to 2000, endangered in 2004 and critically endangered from 2008 to 2018 (BirdLife International, 2021). Climate change in their breeding locations has produced soil moisture and vegetation changes in breeding grounds (Tomkovich et al., 2002; Zöckler et al., 2003). This species' population is declining due to hunting and loss of appropriate habitat in trail and winter locations, as well as disturbance, pollution, and the impacts of climate change (Clark et al., 2018; Syroechkovskiy et al., 2010; Tomkovich et al., 2002; Zöckler et al., 2016).

The Chinese Crested Tern *Thalasseus bernsteini* has less than 50 individuals (Chen et al., 2015) and is the most critically endangered seabird species in Asia (Hung et al.,

2018). This species is not just one of Asia's most endangered species, but it is also one of the world's most endangered seabird species, with only a small breeding population of approximately 100 individuals (Gu et al., 2021; Lu et al., 2020). In their study, Lu et al. (2020) discovered a worldwide population of this species that exceeded 100 for the first time in history, with breeding grounds restricted to East China and the Yellow Seas. In 1988 this species was listed as threatened and critically endangered from 1994 to 2018 (BirdLife International, 2021). It is unclear which causes, such as habitat loss, overexploitation, marine pollution, egg harvesting, climate change, restricted biological niches, or even inherent rarity, are causing the reduction in the population of Chinese Crested Tern species (Brook et al., 2008; Chen et al., 2009; Davies et al., 2004; Liu et al., 2009). Another major factor that may contribute to the near extinction of the endangered Chinese Crested Tern is poachers in the market selling seagull eggs and terns during the breeding season (Chen et al., 2015). Additionally, natural calamities pose a threat to the population of this species since summer hurricanes in coastal areas frequently cause Chinese Crested Tern breeding failure (Chen et al., 2015).

Endangered Species. In 1988, White-headed Duck (*Oxyura leucocephala*) was listed as threatened, Vulnerable in 1994 & 1996, and endangered from 2000 to 2017 (BirdLife International, 2021). At the turn of the 21st century, the global population of the White-headed Duck was estimated to be approximately 8,000 to 13,000 individuals (Li et al., 2003). In 2016, more than 20 000 individuals were recorded, while in 2017, around 7500 individuals (Koshkina et al., 2019). In Turkey, the breeding population of the White-headed Duck was estimated to be 200 to 250 pairs from 1996 to 2001, but current observations suggest that the number of such species presently does not surpass 80 to 125 pairs, representing a 50% drop in two decades. Meanwhile, the non-breeding winter population ranges from 8,500 to 10,000 individuals, with Burdur Lake once housing more than 90% of the population but no longer serving as a prominent resting site. From more than 10,000 birds in the early 1990s to a few hundred in the early 2000s, this number began to fall (Gürsoy-Ergen, 2019). In addition, climate change has caused the wetlands that once housed White-headed Ducks to dry up in 2018 and 2019. White-headed Ducks, for example, are among the species most impacted when wetlands in Çavuşlu ponds or parts of Lake Mogan, Turkey, begin to dry up early as a result of climate change (Özgencil & Uslu, 2021).

For at least 50 to 60 years, Lesser Florican *Sypheotides indicus* has been declining. From 1982 to 1989, its population declined by approximately 60%, but by 1994, it had recovered by 32% to 2,206 individuals (Kasambe & Gahale, 2010). Raghavendra (2011) found the first record of the Lesser Florican *Sypheotides indicus* female at dry Lake Bed, Hesarghatta, Bangalore in 2011; and this species is an endangered endemic group in the Indian subcontinent. India is said to have 90% of the world's population of the Lesser

Florican and therefore plays an important role in its protection and conservation (Sankaran et al., 1992). Dutta et al. (2018) stated that threats to this species include the presence of unpredictable and changing rainfall patterns as a result of climate change. Perhaps the consequences of climate change are unproven but probable to happen in the future. The evidence in Dutta et al. (2018) indicates that the lesser florican will become extinct in the world within the next 20 years, and conservation is needed to protect this species. Apte et al. (2020) also argue that the impacts of climate change, particularly erratic rainfall, pose an indirect risk to this species. This Lesser Florican is a monsoon breeder. It changes its breeding sites depending on the monsoon conditions, making conservation challenging. Climate changes and unpredictable rainfall in several areas of its distribution range have resulted in its extinction, or irregular presence in typically frequented sites.

Barau's petrel (*Pterodroma barau*) is an endangered tropical seabird (Pinet et al., 2011). The Barau's petrel is an endemic species on Reunion Island that has been listed as endangered by IUCN since 2008, and its population is believed to be declining (Dufour et al., 2016). According to Pinet et al. (2009), the extinction of the Barau petrel happened in less than 100 years owing to the unavailability of cat predation control in this species' temporary breeding colonies. Meanwhile, Le Corre et al. (2002) reported that metropolitan illumination has resulted in large and seasonal light-induced mortality of Barau's petrel fledglings. According to Le Corre et al. (2002), projections concerning population decrease were erroneous due to a lack of precise data on this species' life history. One study shows, because the Petrel Barau species is endemic and strongly philopathic the existing Petrel Barau winter habitat may become less suitable in the future (Pinet et al., 2009). According to Legrand et al. (2016), a large number of Barau petals may have difficulties altering their migratory routes and tactics in a fast-changing world (including climate change). Furthermore, most Intergovernmental Panel on Climate Change (IPCC) models predict that appropriate habitat size will be reduced by the end of the twenty-first century.

Then, the winter area's carrying capacity is diminished, which might lead to increased intra and inter-specific competition for prey. Legrand et al. (2016) undertook one of the first studies to utilise current detection data and habitat modelling to anticipate the long-term impacts of climate change on seabirds (Petrel Barau). Figure 5a depicts how climate change scenarios RCP 2.6, RCP 4.5, and RCP 8.5 forecast a 33%, 19%, and 5% decline in suitable habitat size, respectively. Figure 5b depicts all of the scenarios indicating the westward shift, including RCP 2.6 (5°), RCP 4.5 (7°), RCP 6.0 (11°), and RCP 8.5 (9°). Meanwhile, RCP 4.5, RCP 6.0, and RCP 8.5 forecast a 3°, 5°, and 7° southerly shift, respectively (Figure 5c). Based on the graph in Figure 5c, the most optimistic climatic scenario is (RCP 2.6), which anticipated a 2° northward shift until 2020, followed by stagnation until 2100. Based on this data, Legrand et al. (2016) determined that suitable habitats are expected to decline and move westward and southward by the end of the twenty-first century.

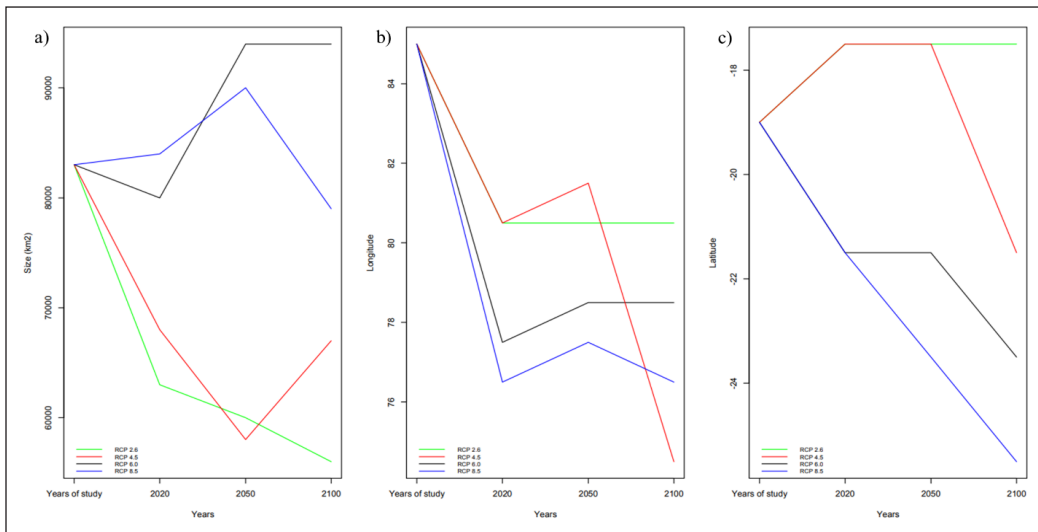


Figure 5. The evolution through time of (a) the size, (b) longitude, and (c) latitude of suitable wintering areas for Barau's petrels under climate change scenarios; Representative Concentration Pathway (RCP 2.6, RCP 4.5, RCP 6.0, RCP 8.5) (Legrand et al., 2016)

Records suggest that between 1970 and 1983, at least 400 couples of Abbott's Booby vanished from the reproductive population (Yorkston & Green, 1997). In 1988 this species was listed as threatened, Vulnerable in 1994 & 1996, critically endangered in 2000 and 2004. Then this species came back out of the critical situation from critically endangered to endangered from 2005 to 2019 (BirdLife International, 2021). Christmas Island was the only breeding colony location of Abbott's Booby until 1991, with an estimated population of 2,500 pairs (Yorkston & Green, 1997). Now, the effective population size for Abbott's Booby is likewise approximately 2,100 individuals on Christmas Island (Morris-Pocock et al., 2012). Rising sea surface temperatures (due to anthropogenic greenhouse gas emissions), stochastic events (storms and hurricanes), and global warming are all potential threats to Abbott's booby (Department of the Environment and Heritage, 2004). This situation likely will cause declination in the population. In addition, climate change, especially rising sea surface temperatures, has reduced marine productivity in Abbott's Boobies foraging near Christmas Island. As a result, it may be claimed that climate change is already impacting the seabird food chain in the Christmas Frigatebird nesting region (Hennicke & Weimerskirch, 2014).

In 1988, the Far Eastern Curlew (*Numenius madagascariensis*) was listed as lower risk/least concern, lower risk/near threatened in 1994 & 2000, least concern in 2004 to 2009, vulnerable in 2010 & 2012 and endangered in 2015 & 2016 (BirdLife International, 2021). In 1992 and 2008, the Far Eastern Curlew was reported to decline steadily in Australia, at 2.4% each year in Moreton Bay (Wilson et al., 2011). Meanwhile, in Tasmania since

the 1950s, this species has declined by more than 65% (Reid & Park, 2003). Hunting, pollution, changes in water regimes, disturbances, and the influence of climate change on breeding sites all pose threats to the species (Harding et al., 2007). In Australia, the species was recently classified as endangered under Australian Government law because of its ongoing population reduction due to its breeding grounds. Decreases in the species have been documented from almost every place monitored along the Australian coast, and local extinction is projected in certain areas over the next thirty years (Lilleyman et al., 2016).

Nearly 425,000 Great Knot individuals are currently known to exist (Hansen et al., 2016). However, the research done by Rogers et al. (2006) and Clemens et al. (2016) revealed that the species' total population in Australia has declined since it was found that this species may have had a greater total population a few decades ago. The same total population loss of 1.8% each year was seen across the continent (Clemens et al., 2016). Since 2015 and 2016, this species has been categorised by the IUCN as an endangered species (Bird Life International, 2021). According to Piersma et al. (2016), survival during the migration and breeding seasons of red knot *Calidris canutus piersmai*, great knot *Calidris tenuirostris*, and bar-tailed godwit *Limosa lapponica menzbieri* began to fall in 2011. According to them, the three species will suffer an annual loss of 20%. By 2012, actual survival for the bar-tailed godwit was as low as 0.71, 0.68 for the great knot, and 0.67 for the red knot. According to Clemens et al. (2016), the reduction in migratory shorebird populations (including the Great Knot) along the East Asian – Australasian Flyway (EAAF) was most probably triggered by factors outside of Australia. There is also has a strong relationship between the decrease bird species that use wetlands on the land continent and unsuitable water levels, a hazard that tends to rise with climate change (Finlayson, 2013).

In 1988 Pallas's Fish Eagle (*Haliaeetus leucoryphus*) was listed as threatened, Vulnerable in 1994 to 2016, and critically endangered from 2017 and 2018 (BirdLife International, 2021). In addition, several migratory bird species and subspecies have been identified as endangered in China, including Long-Tailed Duck (*Clangula hyemalis*), Black-Winged Kite (*Elanus caeruleus vociferus*), Pallas's Fish Eagle (*Haliaeetus leucoryphus*), Himalayan Griffon (*Gyps himalayensis*), Demoiselle Crane (*Anthropoides virgo*), White-Breasted Waterhen (*Amaurornis phoenicurus phoenicurus*), Eurasian Collared Dove (*Streptopelia decaocto decaocto*, *Streptopelia decaocto xanthocyclus*), Chestnut-Winged Cuckoo (*Clamator coromandus*), Barn Owl (*Tyto alba javanica*, *Tyto alba stertens*), and Light-Vented Bulbul (*Pycnonotus sinensis sinensis*, *Pycnonotus sinensis formosae*, *Pycnonotus sinensis hainanus*) (Wu & Shi, 2016). According to them, the species or subspecies is categorised as endangered as a consequence of climate change, as evidenced by changes in the distribution centre's latitude and longitude, as well as the southern, northwestern, and eastern boundaries of migrating birds (Wu & Shi, 2016). Pallas's Fish Eagle populations also reported decreased in Bangladesh, and it is now seldom seen outside of the haors (Sourav et al., 2011).

While field surveys conducted between 2013 and 2016, as well as data from earlier observers in Rajiv Gandhi Orang National Park, India, suggest that Pallas's Fish-eagle is one of the five endangered species (Chakdar et al., 2019). Comprehensive research was conducted in the Bundelkhand region of India between 2006 and 2010. *Haliaeetus leucoryphus*, *Ichthyophaga ichthyaetus*, *Aquila helica*, *Ictinaetus malayensis*, and *Aquila chrysaetos* were determined as migratory species to be the rarest in Panna National Park (Gupta & Kanaujia, 2012). Based on a study done by Gupta and Kanaujia (2012), climatic conditions are one of the greatest risks to eagles in the Bundelkhand Province. Extreme temperatures define the Bundelkhand area, with temperatures ranging from mid to over 40°C in the summer and as low as 1°C in the winter. As a result, there are documented deaths over the summer. It was also discovered that *Haliaeetus leucoryphus* in Mongolia is small, and there is evidence of decreasing occupancy. The fall in the population of these species might also be attributed to a long-term decline in accessible surface water, which has resulted in lower water levels in many lakes and the drying up of several major rivers drains for *Haliaeetus leucoryphus* in Mongolia (Sternberg, 2008; Sukh, 2011). Long-term climate models suggest that this trend will likely continue, potentially leading to habitat loss for this species in the future (Simonov & Dahmer, 2008).

The Rufous-headed Robin *Larvivora ruficeps* is one of the world's rarest and least-studied birds. For the first time in many years, no singing males of *Larvivora ruficeps* were recorded at Jiuzhaigou, China, in 2016 (Zhao et al., 2016). Rufous-headed Robin *Luscinia ruficeps* is only known to breed in the Min Shan region of northern Sichuan province and the Qinling Shan range in southern Shaanxi province of China but has not been observed in the latter since 1905. On November 16, 2012, a brown-coloured *Luscinia* was discovered in an urban garden in central Phnom Penh, Cambodia, the second record outside its breeding range (Mahood et al., 2013). There is very little information on this species' population, although it is likely to exist at very high densities in suitable habitats; nevertheless, a dearth of records implies that it may be relatively limited in distribution and may have a tiny population (Mackinnon, 2001). However, this species was classified as endangered on the IUCN list in 2013 and 2016 and as a migratory bird threatened by climate change (BirdLife International, 2021) No research has been conducted to demonstrate a link between these species and climate change effects. It is most likely owing to the scarcity of data on the population and existence of this species.

CONCLUSION

Migratory birds are particularly vulnerable to environmental changes such as climate change because they are susceptible to ongoing changes that may be adversely correlated. Conservation measures for maintaining the survival of migratory bird populations are crucial as they are key to good ecosystem health (Bauer & Hoye, 2014). Relevant parties

and world leaders need to be more sensitive to climate change that has disrupted the lives of these migratory birds to ensure that they do not become extinct. Based on the literature review results, researchers can conclude that migratory birds are currently stressed by environmental changes, especially climate change that has changed the temperature of the earth's surface. Therefore, it is important to understand how these migratory bird species adapt to ongoing climate change and its impact on the bird itself.

ACKNOWLEDGEMENT

This research was financed by Short Term Grant (USM) and got cooperation from the Department of Wildlife and National Parks Peninsular Malaysia regarding information and data needed.

REFERENCES

- Ahas, R., & Aasa, A. (2006). The effects of climate change on the phenology of selected Estonian plant, bird and fish populations. *International Journal of Biometeorology*, 51(1), 17-26. <https://doi.org/10.1007/s00484-006-0041-z>
- Alonso, J. C., Palacin, C., Alonso, J. A., & Martín, C. A. (2009). Post-breeding migration in male great bustards: Low tolerance of the heaviest Palaearctic bird to summer heat. *Behavioral Ecology and Sociobiology*, 63(12), 1705-1715. <https://doi.org/10.1007/s00265-009-0783-9>
- Apte, D., Narwade, S., Bora, N., Pansare, P., Prajapat, C., Hinonia, V. K., Panwar, A. S., Sahu, H., Mathur, P., & Rathore, R. S. (2020). *Status survey of Lesser Florican *Sypheotides indicus* for developing a conservation plan for Shokaliya landscape, Ajmer, Rajasthan* (Final Report). BNHS.
- Bateman, B. L., Pidgeon, A. M., Radeloff, V. C., VanDerWal, J., Thogmartin, W. E., Vavrus, S. J., & Heglund, P. J. (2015). The pace of past climate change vs. potential bird distributions and land use in the United States. *Global Change Biology*, 22(3), 1130-1144. <https://doi.org/10.1111/gcb.13154>
- Bauer, S., & Hoyer, B. J. (2014). Migratory animals couple biodiversity and ecosystem functioning worldwide. *Science*, 344(6179), Article 1242552. <https://doi.org/10.1126/science.1242552>
- BirdLife International. (2021). *Introducing the IUCN red list*. BirdLife.
- Both, C., & te Marvelde, L. (2007). Climate change and timing of avian breeding and migration throughout Europe. *Climate Research*, 35(1-2), 93-105. <https://doi.org/10.3354/cr00716>
- Both, C., Bouwhuis, S., Lessells, C. M., & Visser, M. E. (2006). Climate change and population declines in a long-distance migratory bird. *Nature*, 441(7089), 81-83. <https://doi.org/10.1038/nature04539>
- Bridge, L. K., Stroud, D., Galbraith, C. A., & Boere, G. (2007). *Waterbirds around the world: A global overview of the conservation, management and research of the world's waterbird flyways*. The Stationary Office Books.
- Briedis, M., Hahn, S., & Adamík, P. (2017). Cold spell en route delays spring arrival and decreases apparent survival in a long-distance migratory songbird. *BMC Ecology*, 17(1), 1-8. <https://doi.org/10.1186/s12898-017-0121-4>

- Brook, B. W., Sodhi, N. S., & Bradshaw, C. J. (2008). Synergies among extinction drivers under global change. *Trends in Ecology & Evolution*, 23(8), 453-460. <https://doi.org/10.1016/j.tree.2008.03.011>
- Burgess, M. D., Smith, K. W., Evans, K. L., Leech, D., Pearce-Higgins, J. W., Branston, C. J., Briggs, K., Clark, J. R., du Feu, C. R., Lewthwaite, K., Nager, R. G., Sheldon, B. C., Smith, J. A., Whytock, R. C., Willis, S. G., & Phillimore, A. B. (2018). Tritrophic phenological match-mismatch in space and time. *Nature Ecology & Evolution*, 2(6), 970-975. <https://doi.org/10.1038/s41559-018-0543-1>
- Chakdar, B., Singha, H., & Choudhury, M. R. (2019). Bird community of Rajiv Gandhi Orang National Park, Assam. *Journal of Asia-Pacific Biodiversity*, 12(4), 498-507. <https://doi.org/10.1016/j.japb.2019.07.003>
- Chen, B., Cui, P., Xu, H., Lu, X., Lei, J., Wu, Y., Shao, M., Ding, H., Wu, J., Cao, M., & Liu, G. (2016). Assessing the suitability of habitat for wintering Siberian cranes (*Leucogeranus leucogeranus*) at different water levels in Poyang Lake area, China. *Polish Journal of Ecology*, 64(1), 84-97. <https://doi.org/10.3161/15052249PJE2016.64.1.008>
- Chen, S., Chang, S. H., Liu, Y., Chan, S., Fan, Z., Chen, C., Yen, C. W., & Guo, D. (2009). A small population and severe threats: Status of the critically endangered Chinese crested tern *Sterna bernsteini*. *Oryx*, 43(2), 209-212. <https://doi.org/10.1017/S0030605308001142>
- Chen, S., Fan, Z., Roby, D. D., Lu, Y., Chen, C., Huang, Q., Cheng, L., & Zhu, J. (2015). Human harvest, climate change and their synergistic effects drove the Chinese crested tern to the brink of extinction. *Global Ecology and Conservation*, 4, 137-145. <https://doi.org/10.1016/j.gecco.2015.06.006>
- Clark, N. A., Anderson, G. Q. A., Li, J., Syroechkovskiy, E. E., Tomkovich, P. S., Zöckler, C., Lee, R., & Green, R. E. (2018). First formal estimate of the world population of the critically endangered spoon-billed sandpiper *Calidris pygmaea*. *Oryx*, 52(1), 137-146. <https://doi.org/10.1017/S0030605316000806>
- Clemens, R., Rogers, D. I., Hansen, B. D., Gosbell, K., Minton, C. D. T., Straw, P., Bamford, M., Woehler, E. J., Milton, D. A., Weston, M. A., Venables, B., Wellet, D., Rutherford, B., Onton, K., Herrod, A., Studds, C. E., Choi, C. Y., Dhanjal-Adams, K. L., Murray, N. J., ... & Fuller, R. A. (2016). Continental-scale decreases in shorebird populations in Australia. *Emu-Austral Ornithology*, 116(2), 119-135. <https://doi.org/10.1071/MU15056>
- Collins, M., Knutti, R., Arblaster, J., Dufresne, J. L., Fichefet, T., Friedlingstein, P., Gao, X., Gutowski, W. J., Johns, T., Krinner, G., Shongwe, M., Tebaldi, C., Weaver, A. J., Wehner, M. F., Allen, M. R., Andrews, T., Beyerle, U., Bitz, C. M., Bony, S., & Booth, B. B. B. (2013). Long-term climate change: Projections, commitments and irreversibility. In *Climate Change 2013-The Physical Science Basis: Contribution of Working Group I to the Fifth Assessment Report of the Intergovernmental Panel on Climate Change* (pp. 1029-1136). Cambridge University Press.
- Davies, K. F., Margules, C. R., & Lawrence, J. F. (2004). A synergistic effect puts rare, specialized species at greater risk of extinction. *Ecology*, 85(1), 265-271. <https://doi.org/10.1890/03-0110>
- Department of the Environment and Heritage. (2004). *National recovery plan for the Abbott's Booby (Papasula abbotti)*. Department of the Environment and Heritage
- Dufour, O., Gineste, B., Bas, Y., Le Corre, M., & Artières, T. (2016). First automatic passive acoustic tool for monitoring two species of procellariids (*Pterodroma barau* and *Puffinus bailloni*) on Reunion Island, Indian Ocean. *Ecological Informatics*, 35, 55-60. <https://doi.org/10.1016/j.ecoinf.2016.08.004>

- Dunn, P. O., & Møller, A. P. (2013). Changes in breeding phenology and population size of birds. *Journal of Animal Ecology*, 83(3), 729-739. <https://doi.org/10.1111/1365-2656.12162>
- Dutta, S., Narwade, S., Bipin, C. M., Gadhavi, D., Uddin, M., Mhaskar, M., Pandey, D., Mohan, A., Sharma, H., Iyer, S., Tripathi, R., Verma, V., Varma, V., Jangid, A., Chakdar, B., Karulkar, A., Lambture, B., Khongsai, N., Kumar, S., ... & Jhala, Y. V. (2018). *Status of the lesser florican *Sypheotides indicus* and implications for its conservation*. Wildlife Institute of India.
- Faarborg, J., Holmes, R. T., Anders, A. D., Bildstein, K. L., Dugger, K. M., Gauthreaux, S. A., Heglund, P., Hobson, K. A., Jahn, A. E., Johnson, D. H., Latta, S. C., Levey, D. J., Marra, P. P., Merkord, C. L., Nol, E., Rothstein, S. I., Sherry, T. W., Sillett, T. S., Thompson, F. R., & Warnock, N. (2010). Recent advances in understanding migration systems of New World land birds. *Ecological Monographs*, 80(1), 3-48. <https://doi.org/10.1890/09-0395.1>
- Finlayson, C. M. (2013). Climate change and the wise use of wetlands: Information from Australian wetlands. *Hydrobiologia*, 708(1), 145-152. <https://doi.org/10.1007/s10750-013-1474-0>
- Franks, S. E., Pearce-Higgins, J. W., Atkinson, S., Bell, J. R., Botham, M. S., Brereton, T. M., Harrington, R., & Leech, D. I. (2017). The sensitivity of breeding songbirds to changes in seasonal timing is linked to population change but cannot be directly attributed to the effects of trophic asynchrony on productivity. *Global Change Biology*, 24(3), 957-971. <https://doi.org/10.1111/gcb.13960>
- Galbraith, C., Jones, T., Kirby, J., & Mundkur, T. (2014). *A review of migratory bird flyways and priorities for management* (CMS Technical Series Publication No. 27). Secretariat of the Convention on the Conservation of Migratory Species of Wild Animals.
- Gilroy, J. J., Gill, J. A., Butchart, S. H. M., Jones, V. R., & Franco, A. M. A. (2016). Migratory diversity predicts population declines in birds. *Ecology Letters*, 19(3), 308-317. <https://doi.org/10.1111/ele.12569>
- Gu, N., Chen, G., Yang, J., Zheng, C., Gao, X., Yuan, L., Wang, S., Fan, Z., Lu, Y., Song, G., Chen, S., & Liu, Y. (2021). Novel microsatellite markers reveal low genetic diversity and evidence of heterospecific introgression in the critically endangered Chinese crested tern (*Thalasseus bernsteini*). *Global Ecology and Conservation*, 28, Article e01629. <https://doi.org/10.1016/j.gecco.2021.e01629>
- Gupta, R., & Kanaujia, A. (2012). Ecology of eagles in Bundelkhand Region, India. *Veterinary World*, 5(1), 31-35. <https://doi.org/10.5455/vetworld.2012.31-35>
- Gürsoy-Ergen, A. (2019). Hope for the white-headed duck, *Oxyura leucocephala* (Aves: Anatidae) in Turkey despite a declining breeding population and abandonment of its traditional wintering area? *Zoology in the Middle East*, 65(2), 116-127. <https://doi.org/10.1080/09397140.2019.1580930>
- Hansen, B. D., Fuller, R. A., Watkins, D., Rogers, D. I., Clemens, R. S., Newman, M., Woehler, E. J., & Weller, D. R. (2016). *Revision of the East Asian-Australasian Flyway population estimates for 37 listed migratory shorebird species* (Unpublished report). Department of the Environment, BirdLife Australia, Melbourne.
- Harding, S. B., Wilson, J. R., & Geering, A. D. W. (2007). Threats to shorebirds and conservation actions. In A. D. W. Geering, L. Agnew, & S. Harding (Eds.), *Shorebirds of Australia* (pp. 197-213). CSIRO Publishing.
- Harley, C. D. G., Hughes, A. R., Hultgren, K. M., Miner, B. G., Sorte, C. J. B., Thornber, C. S., Rodriguez, L. F., Tomanek, L., & Williams, S. L. (2006). The impacts of climate change in coastal marine systems. *Ecology letters*, 9(2), 228-241. <https://doi.org/10.1111/j.1461-0248.2005.00871.x>

- Harris, J., Yong, D., Sodhi, N., Subaraj, R., Fordham, D., & Brook, B. (2013). Changes in autumn arrival of long-distance migratory birds in Southeast Asia. *Climate Research*, 57(2), 133-141. <https://doi.org/10.3354/cr01172>
- Hennicke, J. C., & Weimerskirch, H. (2014). Coping with variable and oligotrophic tropical waters: Foraging behaviour and flexibility of the Abbott's booby *Papadula abbotti*. *Marine Ecology Progress Series*, 499, 259-273. <https://doi.org/10.3354/meps10664>
- Hill, R., Dunn, A., & Australia, B. (2004). *National recovery plan for the Christmas Island Frigatebird (Fregata andrewsi)*. Commonwealth of Australia, Canberra.
- Horton, K. G., La Sorte, F. A., Sheldon, D., Lin, T. Y., Winner, K., Bernstein, G., Maji, S., Hochachka, W. M., & Farnsworth, A. (2020). Phenology of nocturnal avian migration has shifted at the continental scale. *Nature Climate Change*, 10(1), 63-68. <https://doi.org/10.1038/s41558-019-0648-9>
- Hu, J., Hu, H., & Jiang, Z. (2010). The impacts of climate change on the wintering distribution of an endangered migratory bird. *Oecologia*, 164(2), 555-565. <https://doi.org/10.1007/s00442-010-1732-z>
- Hu, R., Wen, C., Gu, Y., Wang, H., Gu, L., Shi, X., Zhong, J., Wei, M., He, F., & Lu, Z. (2017). A bird's view of new conservation hotspots in China. *Biological Conservation*, 211, 47-55. <https://doi.org/10.1016/j.biocon.2017.03.033>
- Hughes, L. (2000). Biological consequences of global warming: is the signal already apparent? *Trends in Ecology & Evolution*, 15(2), 56-61. [https://doi.org/10.1016/s0169-5347\(99\)01764-4](https://doi.org/10.1016/s0169-5347(99)01764-4)
- Hung, C. H., Chang, L. N., Chiang, K. K., & Yuan, H. W. (2018). Trends in numbers of the critically endangered Chinese crested tern *Thalasseus bernsteini* and sympatrically nesting greater crested Tern *T. bergii* in the Matsu archipelago, Taiwan. *Bird Conservation International*, 29(3), 386-399. <https://doi.org/10.1017/S0959270918000369>
- Hurlbert, A. H., & Liang, Z. (2012). Spatiotemporal variation in avian migration phenology: Citizen science reveals effects of climate change. *PLoS ONE*, 7(2), Article e31662. <https://doi.org/10.1371/journal.pone.0031662>
- Hutto, R. L. (2000). On the importance of en route period to the conservation of migratory landbirds. *Studies in Avian Biology*, 20, 109-114. <https://sora.unm.edu/node/139385>
- Jayendra, L., Gavali, D., Deshkar, S., & Rathod, J. (2014). Migration pattern of sociable lapwing (*Valenus Gregarious*) in wintering grounds of Gujarat, India. *International Journal of Research in Zoology*, 4(2), 29-31.
- Jonzen, N. (2006). Rapid advance of spring arrival dates in long-distance migratory birds. *Science*, 312(5782), 1959-1961. <https://doi.org/10.1126/science.1126119>
- Kamp, J., Oppel, S., Ananin, A. A., Durnev, Y. A., Gashev, S. N., Hölzel, N., Mishchenko, A. L., Pessa, J., Smirenski, S. M., Strelnikov, E. G., Timonen, S., Wolanska, K., & Chan, S. (2015). Global population collapse in a superabundant migratory bird and illegal trapping in China. *Conservation Biology*, 29(6), 1684-1694. <https://doi.org/10.1111/cobi.12537>
- Karell, P., Ahola, K., Karstinen, T., Valkama, J., & Brommer, J. E. (2011). Climate change drives microevolution in a wild bird. *Nature Communications*, 2(1), 1-7. <https://doi.org/10.1038/ncomms1213>

- Kasambe, R., & Gahale, P. (2010). Status survey and sighting records of Lesser Florican in Maharashtra. *Mistnet*, 11(2), 7-9.
- Kingsolver, J. G., & Buckley, L. B. (2015). Climate variability slows evolutionary responses of *Colias* butterflies to recent climate change. *Proceedings of the Royal Society B: Biological Sciences*, 282(1802), Article 20142470. <https://doi.org/10.1098/rspb.2014.2470>
- Koshkina, A. I., Koshkin, A. V., Timoshenko, A. Y., Koshkin, A. A., & Schielzeth, H. (2019). A population survey of the endangered white-headed duck *Oxyura leucocephala* in Kazakhstan shows an apparently increasing Eastern population. *Bird Study*, 66(1), 111-120. <https://doi.org/10.1080/00063657.2019.1618239>
- La Sorte, F. A., Fink, D., Blancher, P. J., Rodewald, A. D., Ruiz-Gutierrez, V., Rosenberg, K. V., Hochachka, W. M., Verburg, P. H., & Kelling, S. (2017). Global change and the distributional dynamics of migratory bird populations wintering in Central America. *Global Change Biology*, 23(12), 5284-5296. <https://doi.org/10.1111/gcb.13794>
- Langham, G. M., Schuetz, J. G., Distler, T., Soykan, C. U., & Wilsey, C. (2015). Conservation status of North American birds in the face of future climate change. *PLoS ONE*, 10(9), Article e0135350. <https://doi.org/10.1371/journal.pone.0135350>
- Le Corre, M., Ollivier, A., Ribes, S., & Jouventin, P. (2002). Light-induced mortality of petrels: A 4-year study from Réunion Island (Indian Ocean). *Biological Conservation*, 105(1), 93-102. [https://doi.org/10.1016/S0006-3207\(01\)00207-5](https://doi.org/10.1016/S0006-3207(01)00207-5)
- Legrand, B., Benneveau, A., Jaeger, A., Pinet, P., Potin, G., Jaquemet, S., & Le Corre, M. (2016). Current wintering habitat of an endemic seabird of Réunion Island, Barau's petrel *Pterodroma baraui*, and predicted changes induced by global warming. *Marine Ecology Progress Series*, 550, 235-248. <https://doi.org/10.3354/meps11710>
- Lehikoinen, E., Sparks, T. H., & Zalakevicius, M. (2004). Arrival and departure dates. *Birds and Climate Change*, 35, 1-31. [https://doi.org/10.1016/s0065-2504\(04\)35001-4](https://doi.org/10.1016/s0065-2504(04)35001-4)
- Li, D., Wei, Z., & Mundkur, T. (2003). *Status overview and recommendations for conservation of the white-headed duck Oxyura leucocephala in Central Asia*. Convention on Conservation of Migratory Species of Wild Animals.
- Li, F., Wu, J., Harris, J., & Burnham, J. (2012). Number and distribution of cranes wintering at Poyang Lake, China during 2011-2012. *Chinese Birds*, 3(3), 180-190. <https://doi.org/10.5122/cbirds.2012.0027>
- Liang, J., Gao, X., Zeng, G., Hua, S., Zhong, M., Li, X., & Li, X. (2018). Coupling modern portfolio theory and Marxan enhances the efficiency of lesser white-fronted goose's (*Anser erythropus*) habitat conservation. *Scientific Reports*, 8(1), 1-8. <https://doi.org/10.1038/s41598-017-18594-2>
- Liang, J., Xing, W., Zeng, G., Li, X., Peng, Y., Li, X., Gao, X., & He, X. (2018). Where will threatened migratory birds go under climate change? Implications for China's national nature reserves. *Science of the Total Environment*, 645, 1040-1047. <https://doi.org/10.1016/j.scitotenv.2018.07.196>
- Lilleyman, A. M. A. N. D. A., Garnett, S. T., Rogers, D. I., & Lawes, M. J. (2016). Trends in relative abundance of the Eastern Curlew (*Numenius madagascariensis*) in Darwin, Northern Territory. *Stilt*, 68, 25-30.

- Liu, Y., Guo, D. S., Qiao, Y. L., Zhang, E., & Cai, B. (2009). Regional extirpation of the critically endangered Chinese Crested Tern (*Thalasseus bernsteini*) from the Shandong coast, China. *Waterbirds*, 32(4), 597-599. <https://doi.org/10.1675/063.032.0414>
- Lu, Y., Roby, D. D., Fan, Z., Chan, S., Lyons, D. E., Hong, C. H., Wang, S., Yang, J., Zhou, X., Chen, D., Yuan, H. W., & Chen, S. (2020). Creating a conservation network: Restoration of the critically endangered Chinese crested tern using social attraction. *Biological Conservation*, 248, Article 108694. <https://doi.org/10.1016/j.biocon.2020.108694>
- Ma, Z., Melville, D. S., Liu, J., Chen, Y., Yang, H., Ren, W., Zhang, Z., Piersma, T., & Li, B. (2014). Rethinking China's new great wall. *Science*, 346(6212), 912-914. <https://doi.org/10.1126/science.1257258>
- Mackinnon, J. (2001). Threatened birds of Asia: The BirdLife International Red Data Book. Collar, N.J., (Editor-in-chief), Andreev, A.V., Chan, S., Crosby, M.J., Subramanya, S. and Tobias, J.A. Maps by Rudyanto and M. J. Crosby. BirdLife International, Cambridge. 3,038 pages, in two volumes, £55.00. *Bird Conservation International*, 11(4), 325-328. <https://doi.org/10.1017/S0959270901210375>
- Mahood, S. P., Eaton, J. A., & Leader, P. J. (2013). Second record of Rufous-headed Robin *Luscinia ruficeps* outside its breeding range and a description of its first-winter plumage. *BirdingAsia*, 19, 43-47.
- Mayor, S. J., Guralnick, R. P., Tingley, M. W., Otegui, J., Withey, J. C., Elmendorf, S. C., Andrew, M. E., Leyk, S., Pearse, I. S., & Schneider, D. C. (2017). Increasing phenological asynchrony between spring green-up and arrival of migratory birds. *Scientific Reports*, 7(1), 1-10. <https://doi.org/10.1038/s41598-017-02045-z>
- McCarty, J. P. (2001). Ecological consequences of recent climate change. *Conservation Biology*, 15(2), 320-331. <https://doi.org/10.1046/j.1523-1739.2001.015002320.x>
- McKean, J. L. (2011). A first record of Christmas Island Frigatebird *Fregata andrewsi* on Timor. *Kukila*, 3(1-2), 48.
- McMaster, D., Rayner, T. S., & McMaster, C. A. (2015). Additional records of Christmas Frigatebird 'Fregata andrewsi' in the Northern Territory, Australia. *Australian Field Ornithology*, 32(3), 113-117.
- Menzel, A., Sparks, T. H., Estrella, N., Koch, E., Aasa, A., Ahas, R., Alm-Kübler, K., Bissolli, P., Braslavská, O., Briede, A., Chmielewski, F. M., Crepinsek, Z., Curnel, Y., Dahl, Å., Defila, C., Donnelly, A., Filella, Y., Jatczak, K., Måge, F., & Mestre, A. (2006). European phenological response to climate change matches the warming pattern. *Global Change Biology*, 12(10), 1969-1976. <https://doi.org/10.1111/j.1365-2486.2006.01193.x>
- Miller-Rushing, A. J., Høye, T. T., Inouye, D. W., & Post, E. (2010). The effects of phenological mismatches on demography. *Philosophical Transactions of the Royal Society B: Biological Sciences*, 365(1555), 3177-3186. <https://doi.org/10.1098/rstb.2010.0148>
- Ming-Qin, S. H. A. O., & Hong, G. U. O. (2014). Population sizes and group characteristics of Siberian crane (*Leucogeranus leucogeranus*) and hooded crane (*Grus monacha*) in Poyang Lake Wetland. *Zoological Research*, 35(5), 373-379. <https://dx.doi.org/10.13918%2Fj.issn.2095-8137.2014.5.373>
- Møller, A. P. (2001). Heritability of arrival date in a migratory bird. *Proceedings of the Royal Society of London. Series B: Biological Sciences*, 268(1463), 203-206. <https://doi.org/10.1098/rspb.2000.1351>

- Møller, A. P., Rubolini, D., & Lehikoinen, E. (2008). Populations of migratory bird species that did not show a phenological response to climate change are declining. *Proceedings of the National Academy of Sciences*, 105(42), 16195-16200.
- Morris-Pocock, J. A., Hennicke, J. C., & Friesen, V. L. (2012). Effects of long-term isolation on genetic variation and within-island population genetic structure in Christmas Island (Indian Ocean) seabirds. *Conservation Genetics*, 13(6), 1469-1481. <https://doi.org/10.1007/s10592-012-0390-6>
- NOAA National Centers for Environmental Information. (2021). *Climate at a Glance: Global Mapping*. National Oceanic and Atmospheric Administration.
- Nourani, E., Yamaguchi, N. M., & Higuchi, H. (2017). Climate change alters the optimal wind-dependent flight routes of an avian migrant. *Proceedings of the Royal Society B: Biological Sciences*, 284(1854), Article 20170149. <https://doi.org/10.1098/rspb.2017.0149>
- Ottersen, G., Planque, B., Belgrano, A., Post, E., Reid, P. C., & Stenseth, N. C. (2001). Ecological effects of the North Atlantic Oscillation. *Oecologia*, 128(1), 1-14. <https://doi.org/10.1007/s004420100655>
- Özgentil, İ. K., & Uslu, A. (2021). Update on the status of white-headed duck *Oxyura leucocephala* and its breeding phenology in Central Anatolia, Turkey. *Sandgrouse*, 43, 112-122.
- Pachauri, R. K., Allen, M. R., Barros, V. R., Broome, J., Cramer, W., Christ, R., Church, J. A., Clarke, L., Dahe, Q., Dasgupta, P., Dubash, N. K., Edenhofer, O., Elgizouli, I., Field, C. B., Forster, P., Friedlingstein, P., Fuglestedt, J., Gomez-Echeverri, L., Hallegatte, S., ... & van Ypersele, J. P. (2014). *Climate change 2014: Synthesis Report. Contribution of Working Groups I, II and III to the Fifth Assessment Report of the Intergovernmental Panel on Climate Change*. IPCC.
- Pacifici, M., Visconti, P., Butchart, S. H. M., Watson, J. E. M., Cassola, F. M., & Rondinini, C. (2017). Species' traits influenced their response to recent climate change. *Nature Climate Change*, 7(3), 205-208. <https://doi.org/10.1038/nclimate3223>
- Piersma, T., Lok, T., Chen, Y., Hassell, C. J., Yang, H. Y., Boyle, A., Slaymaker, M., Chan, Y. C., Melville, D. S., Zhang, Z. W., & Ma, Z. (2016). Simultaneous declines in summer survival of three shorebird species signals a flyway at risk. *Journal of Applied Ecology*, 53(2), 479-490. <https://doi.org/10.1111/1365-2664.12582>
- Pinet, P., Jaquemet, S., Pinaud, D., Weimerskirch, H., Phillips, R., & Le Corre, M. (2011). Migration, wintering distribution and habitat use of an endangered tropical seabird, Barau's petrel *Pterodroma baraui*. *Marine Ecology Progress Series*, 423, 291-302. <https://doi.org/10.3354/meps08971>
- Pinet, P., Salamolard, M., Probst, J. M., Russell, J., Jaquemet, S., & Le Corre, M. (2009). Barau's Petrel *Pterodroma baraui*: History, biology and conservation of an endangered endemic petrel. *Marine Ornithology*, 37(2), 107-113.
- Praveen, J., Jayapal, R., & Pittie, A. (2013). Notes on Indian rarities-1: Seabirds. *Indian Birds*, 8(5), 113-125.
- Pulido, F. (2007). Phenotypic changes in spring arrival: Evolution, phenotypic plasticity, effects of weather and condition. *Climate Research*, 35(1-2), 5-23. <https://doi.org/10.3354/cr00711>
- Putra, C. A., & Hikmatullah, D. (2018). *Survey of waterbird and waterbird hunting problem on the Eastern Coastline of North Sumatra, Indonesia (January-April 2018)* (Unpublished report). The Manfred-Hermesen Stiftung Foundation, Birding Sumatra/Sumatra Wild Heritage Foundation, North Sumatra, Indonesia.

- Putra, C. A., Hikmatullah, D., Zöckler, C., Syroechkovskiy, E. E., & Hughes, B. (2019). Spoon-billed Sandpiper: A new species for Indonesia. *Wader Study*, 126(1), 60-63. <https://doi.org/10.18194/ws.00135>
- Raghavendra, M. (2011). Occurrence of Lesser Florican *Sypheotides indicus* in Bangalore, Karnataka, India. *Indian BIRDS*, 7(5), 140-142.
- Reid, T., & Park, P. (2003). Continuing decline of Eastern Curlew, *Numenius madagascariensis*, in Tasmania. *Emu - Austral Ornithology*, 103(3), 279-283. <https://doi.org/10.1071/mu00079>
- Richardson, W. J. (1990). Timing of bird migration in relation to weather: Updated review. In E. Gwinner (Ed.), *Bird Migration* (pp. 78-101). Springer. https://doi.org/10.1007/978-3-642-74542-3_6
- Rogers, D. I., Rogers, K. G., Gosbell, K. B., & Hassell, C. J. (2006). Causes of variation in population monitoring surveys: Insights from non-breeding counts in north-western Australia, 2004-2005. *Stilt*, 50, 176-193.
- Roulin, A. (2014). Melanin-based colour polymorphism responding to climate change. *Global Change Biology*, 20(11), 3344-3350. <https://doi.org/10.1111/gcb.12594>
- Rubolini, D., Møller, A., Rainio, K., & Lehikoinen, E. (2007). Intraspecific consistency and geographic variability in temporal trends of spring migration phenology among European bird species. *Climate Research*, 35(1-2), 135-146. <https://doi.org/10.3354/cr00720>
- Runge, C. A., Watson, J. E. M., Butchart, S. H. M., Hanson, J. O., Possingham, H. P., & Fuller, R. A. (2015). Protected areas and global conservation of migratory birds. *Science*, 350(6265), 1255-1258. <https://doi.org/10.1126/science.aac9180>
- Sankaran, R., Rahmani, A. R., & Ganguli-Lachungpa, U. (1992). The distribution and status of the Lesser Florican *Sypheotides indica* (JF Miller) in the Indian subcontinent. *Journal of the Bombay Natural History Society*, 89(2), 156-179.
- Santer, B. D., Wehner, M. F., Wigley, T. M. L., Sausen, R., Meehl, G. A., Taylor, K. E., Ammann, C., Arblaster, J., Washington, W. M., Boyle, J. S., & Brüggemann, W. (2003). Contributions of anthropogenic and natural forcing to recent tropopause height changes. *Science*, 301(5632), 479-483. <https://www.jstor.org/stable/3834678?seq=1>
- Scheffers, B. R., De Meester, L., Bridge, T. C. L., Hoffmann, A. A., Pandolfi, J. M., Corlett, R. T., Butchart, S. H. M., Pearce-Kelly, P., Kovacs, K. M., Dudgeon, D., Pacifici, M., Rondinini, C., Foden, W. B., Martin, T. G., Mora, C., Bickford, D., & Watson, J. E. M. (2016). The broad footprint of climate change from genes to biomes to people. *Science*, 354(6313), aaf7671-1-aaf7671-11. <https://doi.org/10.1126/science.aaf7671>
- Sheldon, R. D., Kamp, J., Koshkin, M. A., Urazaliev, R. S., Isakov, T. K., Field, R. H., Salemgareev, A. R., Khrokov, V. V., Zhuly, V. A., Sklyarenko, S. L., & Donald, P. F. (2012). Breeding ecology of the globally threatened sociable lapwing *Vanellus gregarius* and the demographic drivers of recent declines. *Journal of Ornithology*, 154(2), 501-516. <https://doi.org/10.1007/s10336-012-0921-4>
- Shevchenko, V. L. (1998). The sociable plover *Chettusia gregaria* north of the Caspian Sea. *Bulletin-Wader Study Group*, 87, 48-50.
- Shuter, J. L., Broderick, A. C., Agnew, D. J., Jonzén, N., Godley, B. J., Milner-Gulland, E. J., & Thirgood, S. (2011). Conservation and management of migratory species. In E. J. Milner-Gulland, J. M. Fryxell & A. R. E. Sinclair (Eds.), *Animal migration: A synthesis* (pp. 172-206). Oxford University Press.

- Sillett, T. S., Holmes, R. T., & Sherry, T. W. (2000). Impacts of a global climate cycle on population dynamics of a migratory Songbird. *Science*, 288(5473), 2040-2042. <https://doi.org/10.1126/science.288.5473.2040>
- Simonov, E. A., & Dahmer, T. D. (Eds.). (2008). *Amur-Heilong river basin reader* (p. 426). Ecosystems.
- Simpson, D. M. (1990). Paradise lost? Birdwatching along the Fly River, Papua New Guinea. *Sea Swallow*, 39, 53-57.
- Solomon, S., Manning, M., Marquis, M., & Qin, D. (2007). *Climate change 2007-the physical science basis: Working group I contribution to the fourth assessment report of the IPCC (Vol. 4)*. Cambridge University Press.
- Sourav, S. H., Ahmed, B. A. S. H. I. R., & Thompson, P. A. U. L. (2011). Pallas's fish eagle *Haliaeetus leucoryphus* in Bangladesh. *Birding ASIA*, 16, 101-105.
- Sternberg, T. (2008). Environmental challenges in Mongolia's dryland pastoral landscape. *Journal of Arid Environments*, 72(7), 1294-1304. <https://doi.org/10.1016/j.jaridenv.2007.12.016>
- Sukh, T. (2011). *Local understanding of hydro-climate changes in Mongolia* (MSc Thesis). Colorado State University, USA.
- Syroechkovski, E. E., Tomkovich, P. S., Kashiwagi, M., Taldenkov, I. A., Buzin, V. A., Lappo, E. G., & Zöckler, C. (2010). Population decline in the spoon-billed sandpiper (*Eurynorhynchus pygmeus*) in northern Chukotka based on monitoring on breeding grounds. *Biology Bulletin*, 37(9), 941-951. <https://doi.org/10.1134/s1062359010090074>
- Tirtaningtyas, F. N., & Henniecke, J. C. (2015). Threats to the critically endangered Christmas Island Frigatebird *Fregata andrewsi* in Jakarta Bay, Indonesia, and implications for reconsidering conservation priorities. *Marine Ornithology*, 43, 137-140.
- Tirtaningtyas, F. N., & Jordan, K. (2017). Updating the seabird fauna of Jakarta Bay, Indonesia. *Marine Ornithology*, 45, 11-16.
- Tomkovich, P. S., Syroechkovski Jr, E. E., Lappo, E. G., & Zöckler, C. (2002). First indications of a sharp population decline in the globally threatened Spoon-billed Sandpiper *Eurynorhynchus pygmeus*. *Bird Conservation International*, 12(1), 1-18. <https://doi.org/10.1017/s0959270902002010>
- Trouwborst, A. (2012). Transboundary wildlife conservation in a changing climate: Adaptation of the Bonn convention on migratory species and its daughter instruments to climate change. *Diversity*, 4(3), 258-300. <https://doi.org/10.3390/d4030258>
- Turrin, C. O. U. R. T. N. E. Y., & Watts, B. D. (2016). Sustainable mortality limits for migratory shorebird populations within the East Asian-Australian Flyway. *Stilt*, 68, 2-17.
- Walther, G. R., Post, E., Convey, P., Menzel, A., Parmesan, C., Beebee, T. J. C., Fromentin, J. M., Hoegh-Guldberg, O., & Bairlein, F. (2002). Ecological responses to recent climate change. *Nature*, 416(6879), 389-395. <https://doi.org/10.1038/416389a>
- Warren, R., VanDerWal, J., Price, J., Welbergen, J. A., Atkinson, I., Ramirez-Villegas, J., Osborn, T. J., Jarvis, A., Shoo, L. P., Williams, S. E., & Lowe, J. (2013). Quantifying the benefit of early climate change mitigation in avoiding biodiversity loss. *Nature Climate Change*, 3(7), 678-682. <https://doi.org/10.1038/nclimate1887>

- Watson, M., Wilson, J. M., Koshkin, M., Sherbakov, B., Karpov, F., Gavrilov, A., Schielzeth, H., Brombacher, M., Collar, N. J., & Cresswell, W. (2006). Nest survival and productivity of the critically endangered sociable lapwing *Vanellus gregarius*. *Ibis*, *148*(3), 489-502. <https://doi.org/10.1111/j.1474-919x.2006.00555.x>
- Wauchope, H. S., Shaw, J. D., Varpe, Ø., Lappo, E. G., Boertmann, D., Lanctot, R. B., & Fuller, R. A. (2017). Rapid climate-driven loss of breeding habitat for Arctic migratory birds. *Global Change Biology*, *23*(3), 1085-1094. <https://doi.org/10.1111/gcb.13404>
- Weeks, B. C., Willard, D. E., Zimova, M., Ellis, A. A., Witynski, M. L., Hennen, M., & Winger, B. M. (2019). Shared morphological consequences of global warming in North American migratory birds. *Ecology Letters*, *23*(2), 316-325. <https://doi.org/10.1111/ele.13434>
- Wilcove, D. S., & Wikelski, M. (2008). Going, going, gone: Is animal migration disappearing. *PLoS Biology*, *6*(7), Article e188. <https://doi.org/10.1371/journal.pbio.0060188>
- Wilson, H. B., Kendall, B. E., Fuller, R. A., Milton, D. A., & Possingham, H. P. (2011). Analyzing variability and the rate of decline of migratory shorebirds in Moreton Bay, Australia. *Conservation Biology*, *25*(4), 758-766. <https://doi.org/10.1111/j.1523-1739.2011.01670.x>
- Wu, J., & Shi, Y. (2016). Attribution index for changes in migratory bird distributions: The role of climate change over the past 50 years in China. *Ecological Informatics*, *31*, 147-155. <https://doi.org/10.1016/j.ecoinf.2015.11.013>
- Wuethrich, B. (2000). ECOLOGY: How Climate Change Alters Rhythms of the Wild? *Science*, *287*(5454), 793-795. <https://doi.org/10.1126/science.287.5454.793>
- Yang, H., Ma, M., Thompson, J. R., & Flower, R. J. (2017). Protect coastal wetlands in China to save endangered migratory birds. *Proceedings of the National Academy of Sciences*, *114*(28), E5491-E5492. <https://www.pnas.org/content/114/28/E5491>
- Yorkston, H. D., & Green, P. T. (1997). The breeding distribution and status of Abbott's booby (*Sulidae: Papasula abbotti*) on Christmas Island, Indian Ocean. *Biological Conservation*, *79*(2-3), 293-301. [https://doi.org/10.1016/s0006-3207\(96\)00088-2](https://doi.org/10.1016/s0006-3207(96)00088-2)
- Zeuss, D., Brandl, R., Brändle, M., Rahbek, C., & Brunzel, S. (2014). Global warming favours light-coloured insects in Europe. *Nature Communications*, *5*(1), 1-9. <https://doi.org/10.1038/ncomms4874>
- Zhao, M., Alström, P., Hu, R., Zhao, C., Hao, Y., Lei, F., & Qu, Y. (2016). Phylogenetic relationships, song and distribution of the endangered Rufous-headed Robin *Larvivora ruficeps*. *Ibis*, *159*(1), 204-216. <https://doi.org/10.1111/ibi.12426>
- Zöckler, C., Delany, S., & Hagemeyer, W. (2003). Wader populations are declining-how will we elucidate the reasons? *Wader Study Group Bulletin*, *100*, 202-211.
- Zöckler, C., Beresford, A. E., Bunting, G., Chowdhury, S. U., Clark, N. A., Fu, V. W. K., Htin Hla, T., Morozov, V. V., Syroechkovskiy, E. E., Kashiwagi, M., Lappo, E. G., Tong, M., Long, T. L., Yu, Y. T., Huettmann, F., Akasofu, H. K., Tomida, H., & Buchanan, G. M. (2016). The winter distribution of the Spoon-billed Sandpiper *Calidris pygmaeus*. *Bird Conservation International*, *26*(4), 476-489. <https://doi.org/10.1017/s0959270915000295>

- Zöckler, C., Hla, T., Clark, N., Syroechkovskiy, E., Yakushev, N., Daengphayon, S., & Robinson, R. (2010a). Hunting in Myanmar is probably the main cause of the decline of the Spoon-billed Sandpiper *Calidris pygmeus*. *Wader Study Group Bulletin*, 117(1), 1-8.
- Zöckler, C., Syroechkovskiy, E. E., & Atkinson, P. W. (2010b). Rapid and continued population decline in the Spoon-billed Sandpiper *Eurynorhynchus pygmeus* indicates imminent extinction unless conservation action is taken. *Bird Conservation International*, 20(2), 95-111. <https://doi.org/10.1017/s0959270910000316>



Enhanced Deep Hierarchical Long Short-Term Memory and Bidirectional Long Short-Term Memory for Tamil Emotional Speech Recognition using Data Augmentation and Spatial Features

Bennilo Fernandes* and Kasiprasad Mannepalli

Department of ECE, Koneru Lakshmaiah Education Foundation, Guntur, Andhra Pradesh, 520002 India

ABSTRACT

Neural networks have become increasingly popular for language modelling and within these large and deep models, overfitting, and gradient remains an important problem that heavily influences the model performance. As long short-term memory (LSTM) and bidirectional long short-term memory (BILSTM) individually solve long-term dependencies in sequential data, the combination of both LSTM and BILSTM in hierarchical gives added reliability to minimise the gradient, overfitting, and long learning issues. Hence, this paper presents four different architectures such as the Enhanced Deep Hierarchical LSTM & BILSTM (EDHLB), EDHBL, EDHLL & EDHBB has been developed. The experimental evaluation of a deep hierarchical network with spatial and temporal features selects good results for four different models. The average accuracy of EDHLB is 92.12%, EDHBL is 93.13, EDHLL is 94.14% & EDHBB is 93.19% and the accuracy level obtained for the basic models such as the LSTM, which is 74% and BILSTM, which is 77%. By evaluating all the models, EDHBL performs better than other models, with an average efficiency of 94.14% and a good accuracy rate of 95.7%. Moreover, the accuracy for the collected Tamil emotional dataset, such as happiness, fear, anger, sadness, and neutral emotions indicates 100% accuracy in a cross-fold matrix. Emotions such as disgust show around 80% efficiency. Lastly, boredom shows 75% accuracy. Moreover, the training time and evaluation time utilised by EDHBL is less when compared with the other models. Therefore, the experimental analysis shows

EDHBL as superior to the other models on the collected Tamil emotional dataset. When compared with the basic models, it has attained 20% more efficiency.

Keywords: BILSTM, data augmentation, emotional recognition, LSTM

ARTICLE INFO

Article history:

Received: 07 May 2021

Accepted: 30 July 2021

Published: 28 October 2021

DOI: <https://doi.org/10.47836/pjst.29.4.39>

E-mail addresses:

bennij05@gmail.com (Bennilo Fernandes)

mkasiprasad@gmail.com (Kasiprasad Mannepalli)

* Corresponding author

INTRODUCTION

A majority of natural speech processing strategies, such as voice-activated methods and chatbots, call for speech to be considered suggestions. Usually, the basic treatment is to initially transform this speech type into textual content by using Automatic Speech Recognition (ASR) methods and next run other learning operations or classification followed by the ASR content paper. Convolutional neural network (CNN), in addition to the pre-trained phrase vectors for sentence-level distinction and also accomplish state-of-the-art outcomes on several benchmarks. CNNs are used for text groups, and it has proved similar outcomes towards standard versions as bag full of words, n-grams and their term frequency-inverse document frequency (TF IDF) versions, ConvNets based on the words, and Recurrent Neural Networks (RNN).

Human-computer interactions are used to acquire additional active and personalised as computer systems develop as part of predicting the present mental status of the man speaker, aiding them in distinguishing various contextual meanings of the identical terms. ASR resolves variants in a speech from diverse people using probabilistic acoustic plus words designs, which results in speech transcriptions and makes the speaker impartial. This approach will be acceptable enough for many programs but has an undesired consequence for methods that depend on understanding the planned emotion in the speech to operate properly.

State-of-the-art ASR methods create outputs with good precision but shed a considerable quantity of information that hinted at emotions offered by speech. This specific gap has led Speech-based Emotion Recognition (SER) devices to turn into a location of fascinating exploration for several decades. Speech is among the organic methods for people to convey individual emotions.

The features of Long short-term memory (LSTM) and Bidirectional LSTM (BiLSTM) have been investigated in this study for emotional voice recognition using a Tamil emotional information collection and an appropriate clustering technique. Different user-defined classification techniques are used end-to-end to identify data sets using Connectionist temporal classification (CTC). The group in emotional voice recognition and machine learning collaborated for this project. The technique provides a concise overview of RNN and its layers and the function extraction variables used. The dataset array and its specifics were then briefly identified. Finally, the analysis output and results were recorded using five different testing datasets, followed by a hypothesis and analysis compared with the other designs.

MATERIALS AND METHODS

A common SER structure operates on removing options such as spectral characteristics, pitch frequency functions, formant characteristics and effort associated capabilities coming

from speech (Hochreiter & Schmidhuber, 1997; Zhou et al., 2016; Krizhevsky et al., 2012; Graves et al., 2013; Sak et al., 2014). These were observed using a distinction process to forecast a variety of instructional classes of emotion such as Bayesian Network Model (BNM), Hidden Markov Model (HMM), Support Vector Machines (SVM), Gaussian Mixture Model and the Multi Classifier Fusion. In addition, there are several methods utilised in conventional category projects (Liu et al., 2018; Cummins et al., 2017; Mustaqeem & Kwon, 2020; Mannepalli et al., 2016a; Hussain et al., 2020). Studying powerful RNN models and their novelty within the machine learning group is an extremely energetic analysis issue. RNNs resemble LSTMs and are presented as topics for some experiments and alterations during the earlier decade (Huang et al., 2019; Khan et al., 2019; Karim et al., 2019).

This specific evolution has very recently resulted in a novel structure known as Gated Recurrent Unit (GRU), which simplifies the complicated LSTM mobile layout. In addition, the Deep Learning methods used in earlier years have contributed breakthroughs in natural speech understanding (NLU) (Alías et al., 2016; Sastry et al., 2016; Mannepalli et al., 2016b). Nevertheless, the applicability of RNN is minimal based on two factors. First, the CTC technique has become beneficial in positioning among feedback and the resulting labelling that is unfamiliar (Zhang et al., 2016; Kumar et al., 2017; Li et al., 2014; Rao et al., 2018).

For any long-term dependencies in information where the gap involves the pertinent information and the location exactly where it is required is large, and RNNs have minimal consumption (Srivastava et al., 2014; Ioffe & Szegedy, 2015; Park et al., 2019). As a result, a specific criterion in RNN, the LSTM architecture networks, are released. LSTMs are usually created to focus on long-term dependencies on collected datasets. LSTM has proved in many situations to be good at speech identification responsibilities in which the specific recollection of LSTMs cells is utilised to determine longer dependencies. GRUs can also be created for long-range dependencies as it works well with sequential details as do LSTMs (Liu et al., 2014; Rao & Kishore, 2016; Schwarz et al., 2015). Deep Belief Networks (DBN) for emotional speech recognition has displayed a tremendous enhancement above basic designs which do not make use of deep learning, and that implies nonlinear with high order associations, which were much more effective when prepared for emotion speech recognition (Ravanelli et al., 2016; Kishore & Prasad, 2016; Ravanelli et al., 2017). Deep neural network extreme learning machine (DNN ELM) uses utterance level features from segment level chances distributions plus an individual hidden level neural net to recognise utterance amount feelings. However, enhancement of accuracies had been restricted. Bidirectional LSTM designs are meant to instruct the characteristic sequences. They have also accomplished an emotion recognition precision of 62.8% within the interactive emotional dyadic motion capture (IEMOCAP) dataset, a tremendous enhancement across

DNN ELM. CNNs in deep conjunction with LSTMs managed to attain good outcomes within the IEMOCAP dataset. Recently, scientists have already commenced exploring the usage of multimodal functions for emotion recognition.

Data Augmentation

In order to procedure information, waveform sound changes to spectrogram and nourishes neural networking to produce output. The standard way to do data augmentation is generally given waveform and other strategies that adjust spectrogram (Park et al., 2019). It presented a spectrogram, which can see it as a picture in which the x-axis is normally the period while the y-axis is considered the frequency. Understandably, it obtains a better training rate as it conveys information transformation among waveform information to spectrogram information and augments spectrogram information. Later SpecAugment for information augmentation were found in speech recognition (Park et al., 2019). There are three standard methods to augment information.

First, Time Warping is a unique factor that will likely be identified and warping to either right or left with a distance chosen from consistent distribution from zero on the moment warp parameter W of that particular series.

Second, Frequency Masking is where the frequency stations $[f_0, f_0 + f)$ will be masked and f can be selected using a consistent division by zero on the frequency conceal parameter F , and also f_0 might be selected through $(0, v \cdot f)$ wherein v is the number of frequency networks.

Third, Moment Masking with t consecutive period measures $[t_0, t_0 + t)$ will be masked, and t can be selected from a consistent division from zero on the moment mask parameter T , and t_0 is selected from $[0, \tau \cdot t)$.

Feature Extraction

Mel Frequency Cepstral Coefficients (MFCCs). These are a parametric representation of the speech signal, widely used around automated speech recognition, though they have turned out to achieve success for remaining functions too; some of them are speaker identification and emotion recognition (Manneppalli et al., 2016a). It is recognised for being robust to all of the features for virtually any kind of speech activity. A Mel will be a product of measuring recognised frequency or pitch associated with an overall tone. Mapping upon the Mel-scale, which can be an adaptation on the Hertz scale for frequency to the man's feeling of hearing, MFCCs identify a signal characterisation closer to man's belief. They are estimated using a Mel scale filtration bank on the Fourier transform associated with a windowed signal. As a result, a Discrete Cosine Transform (DCT) converts the logarithmical spectrum directly into a cepstrum using Equation 1 given as follows:

$$c[n] = \sum_{m=1}^M s[n] \cdot e^{-\frac{j2\pi nk}{N}}, 0 \leq k \leq N - 1 \quad [1]$$

Mel filtering banks are composed of overlapping triangular screens from the cut of wavelengths based on the middle wavelengths of the two adjacent filters. The air filters have been arranged linearly with spaced middle wavelengths and restored band breadth over the Mel dimensions. The logarithms have the impact of modifying multiplication to the inclusion of addition.

Spectral Centroid. The spectral centroid is a degree utilised within electronic signal processing to represent a spectrum. It recommends where the centre of mass on the spectrum is located. Perceptually, it has a strong relationship which gives a feeling of enhancement of a noise. It is used to relate the median on the spectrum, where it represents another statistic, and the gap between them is the same as the real difference between the unweighted median and mean reports. Since each of these tends to be actions of main inclination, the addition of certain circumstances that exhibit some identical behaviour. However, the regular acoustic spectra are randomly distributed, and the two parameters usually provide strong and distinct values. The analysis reveals that the mean will be a greater match compared to the median. It is estimated that since the weighted hostile is estimated with the help of Fourier transform, with the magnitudes of their weights (Equation 2):

$$Centroid = \frac{\sum_{n=0}^{N-1} f(n) x(n)}{\sum_{n=0}^{N-1} x(n)} \quad [2]$$

Here $x(n)$ belongs to the weighted frequency level or maybe magnitude of bin quantity n , and then $f(n)$ belongs to the middle frequency of that bin.

Spectral Crest. The crest element is a variable of any wave function, such as alternating sound or current, which displays good standards' correlation with the actual value. The crest element signifies precisely how severely the peaks are represented in a waveform. Crest point one specifies the number of peaks, such as immediate current or even a square wave. Greater crest variables suggest peaks, such as audio waves generally, which have higher crest elements. The Crest factor may be the highest amplitude on the waveform split through the RMS benefit of the waveform (Alías et al., 2016). It corresponds to the ratio on the L_∞ standard on the L_2 norm on the parameters within the waveform (Equation 3):

$$C = \frac{|x_{peak}|}{x_{rms}} = \frac{\|x\|_\infty}{\|x\|_2} \quad [3]$$

Spectral Entropy (SEN). It is a distributive type of Shannon's entropy, and it has the energy spectrum amplitude parts on the time frame sequence required for entropy analysis. It quantifies the spectral intricacy of the EEG signal. Shannon's Entropy (ShEn) would measure the collection of relational variables that change linearly, together with the logarithm belonging to the number of options. It is also a degree of information spread and is most often accustomed to evaluating the dynamic purchase. SEN is normally acquired by multiplying the strength in every frequency by the logarithm of the very same energy, so the item is multiplied by one. The SEN is provided by Equation 4,

$$SEN = \sum_f p_f \log \left(\frac{1}{p_f} \right) \quad [4]$$

Spectral Flatness. It is a degree utilised majorly in electronic signal processing to analyse a sound spectrum, and it is measured in decibels. It also provides the means to identify just how to tone such a sound instead of becoming noise-like parameters. The significance of the tonal within this context is within the experience of volume in peaks or maybe a resonant framework on a strength spectrum instead of the dull spectrum associated with white noise. A substantial spectral flatness suggests the spectrum has a comparable quantity of energy in most spectral bands, and this also would seem much like white noise. Therefore, the graph on the spectrum would seem to be at a perfect level and sleek. A reduced spectral flatness suggests that the spectral strength is concentrated in essentially a few of the bands, and this will usually seem like a blend of sine waves. The spectrum would seem sharply spiked. The spectral flatness is estimated by getting a ratio of the geometric norm of the power spectrum through the arithmetic median on the power spectrum (Equation 5), i.e.

$$Flatness = \frac{\exp \left(\left(\frac{1}{N} \right) \sum_{n=0}^{N-1} \ln x(n) \right)}{\left(\frac{1}{N} \right) \sum_{n=0}^{N-1} \ln x(n)} \quad [5]$$

Here $x(n)$ belongs to the magnitude of bin quantity n . It is necessary to be aware that when an individual (or more) cleans out a bin will yield a flatness of zero, and therefore the measure is most helpful when receptacles are not null.

Spectral Flux. It is the method for spectral modification among two successive frames. First, the squared distinction between the normalised magnitudes and the spectra on the two successive short-term windows is calculated: the 'ith' normalised DFT coefficient in the 'ith' frame. Then, the spectral flux will continue to be applied within the following Equation 6:

$$Fl_{(i,i-1)} = \sum_{k=1}^{Wfl} (EN_i(k) - EN_{i-1}(k))^2 \quad [6]$$

The histograms represent the mean valuation of spectral flux progression of segments through two classes: i) speech and ii) music. It may be observed that the values of spectral flux are bigger with the speech type. It is anticipated that the local spectral adjustments are more regular using speech data due to the fast conversion with phonemes, and several of them are quasi-periodic. However, others are associated with a loud nature.

Spectral Skewness. The level of asymmetry of the frequency division of band energy talks about the spectrum skewness. A skewness worth zero will show that the spectrum band power is equally dispersed earlier and beneath the spectrum centroid frequency. Adverse skewness suggests that much more band power will occur over the centroid. Excellent skewness suggests that much more band power occurs beneath the centroid (Equation 7).

$$\tilde{\mu}_3 = \frac{[(X - \mu)^3]}{(E[X - \mu]^2)^{3/2}} \quad [7]$$

Where μ represent the mean, the standard deviation as σ , the μ_3 moment of the third centroid, and E is the expected operator.

Spectral Slope. It is a degree of dependency on the reflectance over the wavelength. Several organic acoustic impulses hold the inclination of a lot less power during the fact and high frequencies, which this particular pitch has and is connected to the dynamics of an audio source of energy. One method is to quantify the use of linear regression on the Fourier magnitude spectrum on the signal. That will create a single amount indicating the incline on the line-of-best-fit from the spectral information. In signal processing, it is a degree of just how efficiently the spectrum of an audio sound tail from towards the high wavelengths, estimated utilising a linear regression (Equation 8).

$$S = \frac{R_{F1} - R_{F0}}{\lambda_1 - \lambda_0} \quad [8]$$

It is where R_{F1} , R_{F0} gives the reflectance value and filters F_0 , F_1 and λ_0 , λ_1 as central wavelength.

Dataset Collection

Mobile applications are used to monitor psychological speech signals for research and training. Both signals are mono signals with a 44KHz frequency. The data recorded has

been used to achieve the prediction goal. The speech data comes from ten different male and female speakers. Every performer must repeat each expression ten times in various emotions such as anger, disgust, fear, sorrow, happiness, normal and boredom. Female and male speakers claim a sample of 1400 cognitive speech data sets. As it is the concept flow study, these samples were analysed. In addition, learners of skills have taken samples based on sentences. The samples were obtained with co-working spaces staff to assess their feelings throughout the therapy period to obtain the research objective.

A total of 350 samples were collected, and five datasets were made randomly with fifty samples in each dataset with about the same 44KHz that use the same mobile apps. As a result, these five datasets with fifty samples in each dataset were used to try and figure out how faculty members felt about functioning together. Since professional actors gathered the coaching knowledge base, the emotional appraisal database could be identified with great sensitivity and efficiency using Tamil emotional specifics as a base.

LSTM & BILSTM Network Architecture

A standard recurrent neural community (RNN) iterates the following formulae from $t = 1$ to T to compute the hidden vector sequence $h = (h_1, \dots, h_T)$ and the paper vector sequence $y = (y_1, \dots, y_T)$ given an input sequence $x = (x_1, \dots, x_T)$ (Equations 9 & 10) (Mustaqeem et al. 2020).

$$h_t = H(W_{xh}x_t + W_{hh}h_{t-1} + b_h), \tag{9}$$

$$y_t = W_{hy}h_t + b_y \tag{10}$$

The W requirements signify weights matrix multiplication (for example, W_{xh} is the input hidden weight matrix). At the same time, the b conditions denote bias vectors (for example, b_h is the main bias vector H) and could be the embedded level feature (Chen et al., 2015; Weninger et al., 2015; Erdogan et al., 2015; Eyben et al., 2013; Pascanu et al., 2013).

In most cases, H is an elementwise program with a hidden layer. It was learned that its Long Short-Term Memory (LSTM) architecture stores information in purpose-built

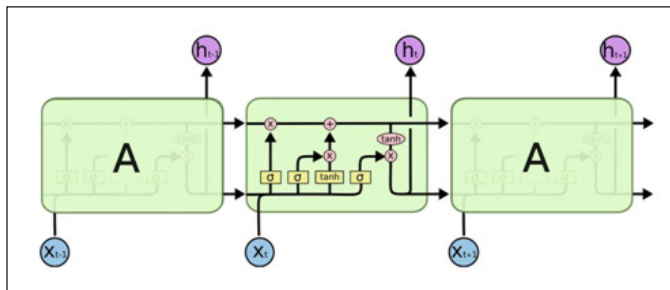


Figure 1. Sequential LSTM layer internal architecture

memory cells, which are good to find and exploit for longer range meaning. Figure 1 displays a one-of-a-kind LSTM memory cell. The subsequent recursive method is used to apply [twelve] H to the LSTM version added to this paper (Equations 11-15).

$$i_t = \sigma (W_{xi}x_t + W_{hi}h_{t-1} + W_{ci}c_{t-1} + b_i) \tag{11}$$

$$f_t = \sigma (W_{xf}x_t + W_{hf}h_{t-1} + W_{cf}c_{t-1} + b_f) \tag{12}$$

$$c_t = f_t c_{t-1} + i_t \tanh (W_{xc}x_t + W_{hc}h_{t-1} + b_c) \tag{13}$$

$$o_t = \sigma (W_{xo}x_t + W_{ho}h_{t-1} + W_{co}c_t + b_o) \tag{14}$$

$$h_t = o_t \tanh(c_t) \tag{15}$$

Where σ is the logistic sigmoid function, and i, f, o and c are the forms for the *input gate*, *forget gate*, *output gate* and *cell* activation in the vectors, are nearly the same measurements as the hidden parameter h . Since the weight matrices from modular to gate functions (e.g. W_{si}) are diagonal, each gate vector's component m only takes messages from object m , mostly on the cell vector.

Modern RNNs have the disadvantage of being unable to use past meaning. However, there is no excuse not to use potential meaning in speech recognition, where full statements are compiled simultaneously. Bidirectional RNNs (BRNNs) [thirteen] do this by storing data in one direction with two separate hidden rates and then feeding it forward on the same paper sheet. For example, a BRNN evaluates the *forward* concealed sequence \vec{h} , the *backward* hidden sequence \overleftarrow{h} , and the document variable y by repeating the reversible level from $t = T$ to 1, the forward rate from $t = 1$ to T , and afterwards modifying the performance sheet, as shown in Figure 2 (Equations 16-18):

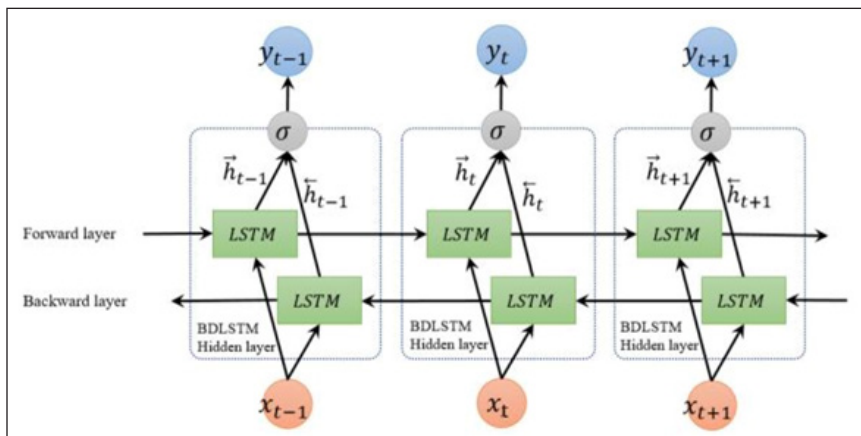


Figure 2. BiLSTM layer internal architecture

$$\vec{h} = H (W_{x\vec{h}}x_t + W_{\vec{h}\vec{h}}\vec{h}_{t-1} + b_{\vec{h}}) \quad [16]$$

$$\overleftarrow{h} = H (W_{x\overleftarrow{h}}x_t + W_{\overleftarrow{h}\overleftarrow{h}}\overleftarrow{h}_{t+1} + b_{\overleftarrow{h}}) \quad [17]$$

$$y_t = W_{\overleftarrow{h}y}\overleftarrow{h}_t + W_{\vec{h}y}\vec{h}_t + b_y \quad [18]$$

When BRNNs are combined with LSTM, bidirectional LSTM is formed, using a long-range background for both entryways. The use of serious structures, capable of building gradually better level depictions of acoustic knowledge, is a key element of the most recent hybrid approach. Deep RNNs can be created by piling several RNN hidden stages on top of each other, with such a single-level text series that serves as the time step only for the arriving, as shown in Figure 3. Assume that the very same hidden state feature is used in almost all N instances in the memory, $n = 1$ to N and $t = 1$ to T were used to compute the sequence of hidden vectors (Equation 19).

$$h_t^n = H (W_{h^{n-1}h^n}h_t^{n-1} + W_{h^n h^n}h_{t-1}^n + b_h^n) \quad [19]$$

Then we calculate $h^0 = x$. The y_t machine output is in Equation 20.

$$y_t = W_{h^N y}h_t^N + b_y \quad [20]$$

Proposed Enhanced Deep Hierarchal Architecture

The dataset includes 1400 utterances delivered by ten male and ten female performers. All of them are intended to express various emotions such as neutral tone, happiness, sadness, anger, boredom, fear and disgust. The input speech data is given to data augmentation, and its value is fixed as 10 so that single data is converted into ten samples. Additionally, this evaluation value takes a long time, and its space occupancy is very high. Therefore, the feature extractions were selected among many spatial features such as Spectral Centroid, Spectral Crest, Spectral Entropy, Spectral Flatness, Spectral Flux, Spectral Skewness, Spectral Slope and Temporal Feature MFCC were utilised to extract the features from augmented data.

Then the data from feature extraction were converted into sequential data and passed into LSTM or BiLSTM (where one will be selected—either LSTM or BiLSTM). The layers and features were analysed, and then it is passed to the next LSTM layer with the introduction of the dropout layer, where gradient and overfitting of feature extraction can be minimised. Again, the features were analysed in LSTM or BiLSTM (where one will be selected) and the layers and will be passed on to a fully connected layer with the addition of a second dropout layer, as shown in Figure 3. Thus, the fully connected layer connects all the nodes and passes the data to the soft matrix and classification layers to classify the types of emotions for the testing data.

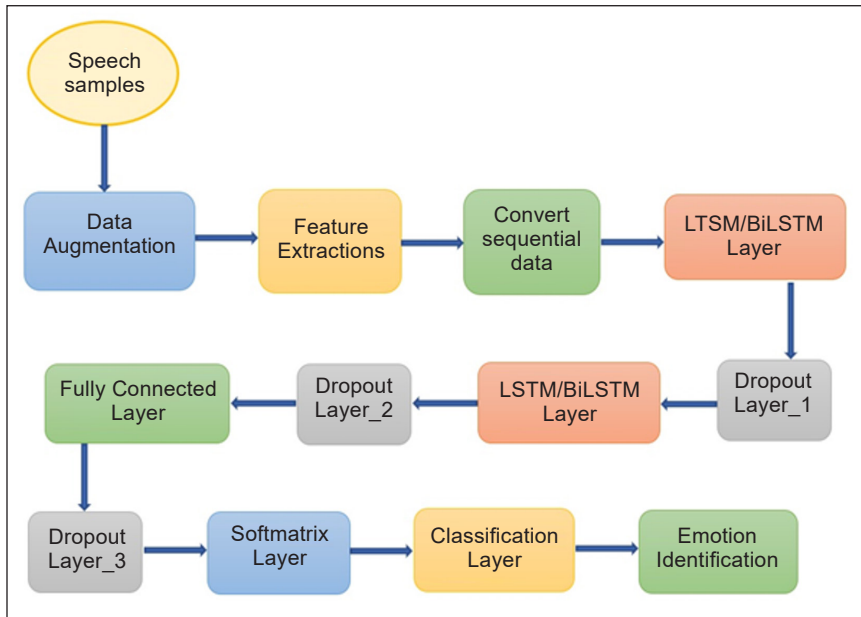


Figure 3. Proposed design flow architecture

Among other spectral features, these features were examined individually and finally concatenated by normalising the features. Then the mean and standard deviations were identified for the entire data samples according to each emotion. Even though augmentation gives a better result of overfitting, the dropout layer is also used to enhance the efficiency of emotional speech recognition. Thus, the overfitting can be reduced at the maximum level. Three dropout layers are used for the analysis dropout. Layer 1 is fixed with 0.5, Layer 2 is 0.6, and Layer 3 is 0.8. The range lies between 0 to 1, and where the standard level for dropout is 0.5, and by increasing the level to 0.8, overfitting will be reduced in the higher range.

The number of units for each LSTM and BiLSTM is 250, with a total of 500 units utilised for this design architecture with an initial learning rate of 0.03. For the training optimisation, all three techniques were taken into consideration for better efficiency. From the analysis of Whale Optimization Algorithm (WOA), ADAM, SGDM and RMSPROP with minibatch size as 250, the drop period of learning rate is fixed as two and max epochs is taken as 10, so that WOA optimisation shows better performance more than other techniques. Thus, as shown in Figure 3, all four-design architecture experimented with these parameters for the Tamil emotional dataset. The other properties which were analysed by fixing the values for the audio dataset are follows. The pitch shifting probability is given as 0.5, with the time-shifting probability as 1, the volume control probability as 0.7, the volume gain range is -6 to 6, the time stretch probability as 0.5 and the range lies between 0 to 1, with the noise add probability as 1 and SNR range between -30 to 50.

RESULTS AND DISCUSSION

Enhanced Deep Hierarchical LSTM & LSTM (EDHLL) Architecture

As stated, within the layout flow and with the parameters for the input, emotional speech signals are prepared with the inclusion of spectral features, concatenation, and data augmentation with dropout level. The functionality of the EDHLL designs is examined to attain a conclusion that EDHLL design makes a confusion matrix with ten-fold cross-validation. Since cross folding is arbitrary, each evaluation result exhibits different precision amounts for a different dataset with a mean of five assessments viewed for precision rate.

In the assessment stage, a total of 250 emotional samples were clustered into five datasets, and 50 samples for each dataset were randomly taken in order to analyse the maximum efficiency of this architecture, such that a mean of five dataset accuracy was considered as the overall efficiency for the designed deep learning architecture.

From the five datasets analysis of ten folds cross valuation, an average value was grabbed for every fold and general accuracy, as shown in Figure 4. Thus, Fold four, nine and ten show 97.2% of reliability, Fold five, seven and eight show 93.7% of reliability.

It is shown in Figure 5, where some folds likewise show much better overall accuracy performance with around 80%, and the typical total accuracy rate obtained for the entire five datasets is 92.12%. By examining the private functionality of five datasets, the fourth dataset shows a much better recognition rate of 92.9%.

By studying the time factor, among the five datasets, the time taken for evaluation and classification training were considered and shown in Figure 5. While shooting the mean worth, it is apparent that for the instruction of EDHLL, the requirement was around 0.50 seconds of evaluation time and 4.59 minutes of training time.

By thinking about the unique performance of training and evaluation time as captured in different dataset collections, the time taken in the fourth dataset is less than 0.51 minutes and 4.4 minutes for evaluation and training.

From Figure 6, it can be understood that the accuracy level of all five datasets simulation has been established. As the cross-validation folds are arbitrary, the accuracy amount changes randomly according to the fifth dataset execution. However, in each execution, it lies in the range between 91.15% to 92.9%. Among the simulation of the fifth dataset, the fourth dataset shows greater precision and efficiency rate of 92.9% more than the outcome of another dataset.

Finally, in thinking about the precision amount of each feeling as revealed in Figure 7, it is apparent that for the fourth dataset of Tamil emotional samples, the EDHLL design provides 92.9% effectiveness. However, in the confusion matrix, emotions such as anger and fear give a higher rate of 100%.

Emotions, such as happiness and neutral tone show, 98% accuracy. Also, this model lags in other emotional states. For example, emotions of boredom and disgust lag in the

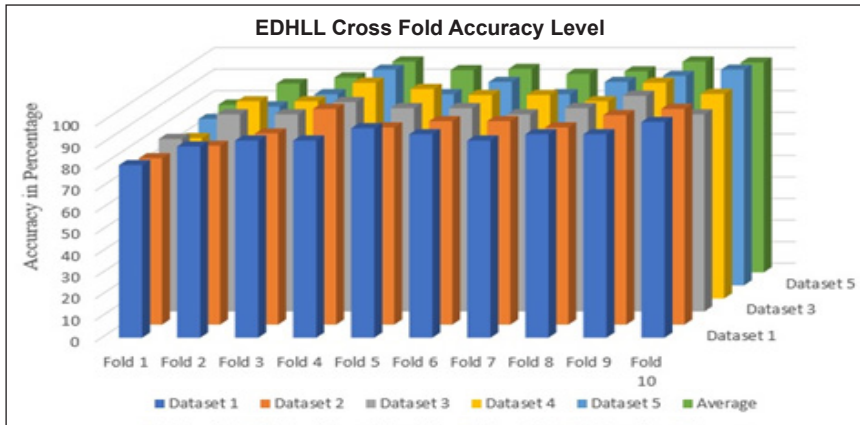


Figure 4. EDHLL cross fold output for five datasets

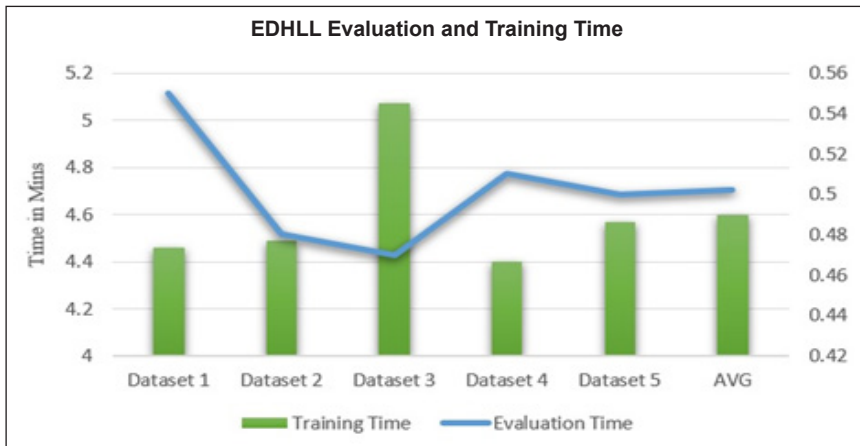


Figure 5. EDHLL evaluation time and training time for five datasets

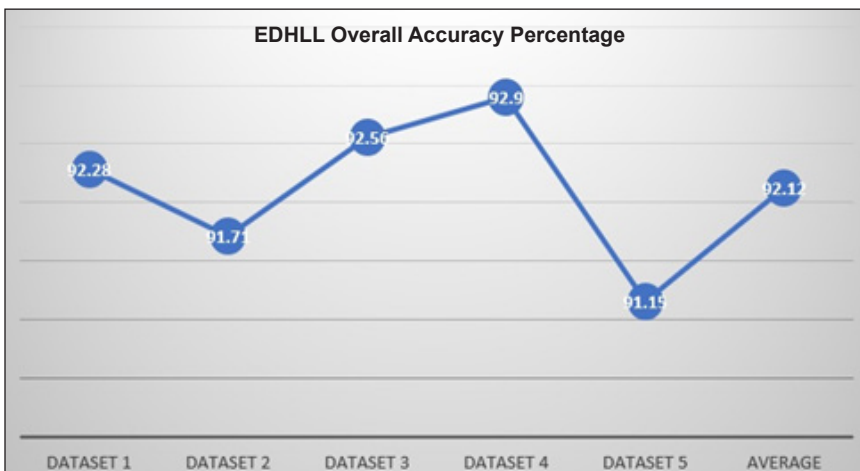


Figure 6. EDHLL overall accuracy rate for five datasets

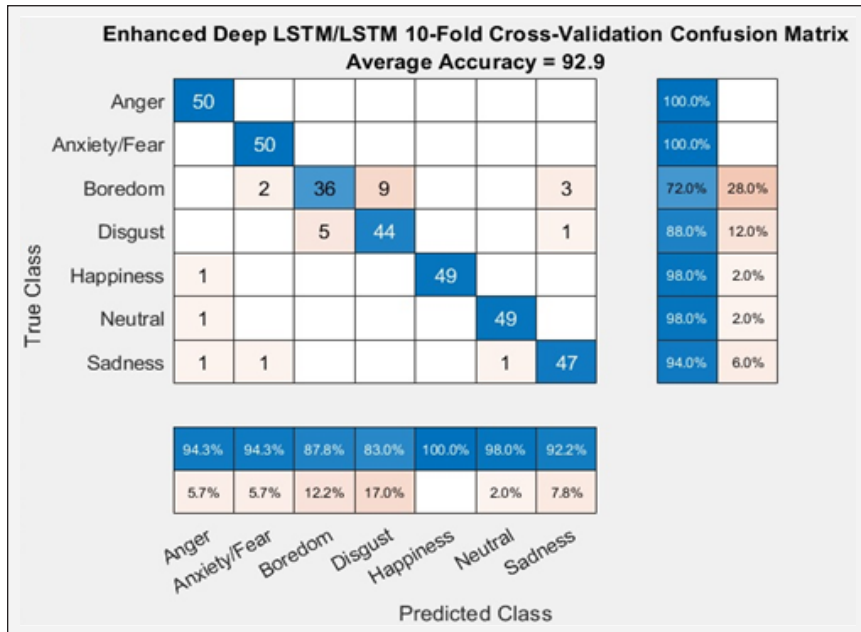


Figure 7. Cross fold confusion matrix for EDHLL

EDHLL model. About 72% and 88% of accuracy has been obtained in both states, and it shows the lowest efficiency rate on all emotions. Overall, the accuracy rate is better than DHLL design architecture.

Enhanced Deep Hierarchical LSTM & BILSTM (EDHLB) Architecture

The functionality of the EDHLB designs was examined to attain a conclusion that EDHLB design makes a confusion matrix with ten-fold cross-validation. Since cross folding is arbitrary and each evaluation result exhibits a different precision amount for a different dataset with a mean of five assessments, this was viewed for precision rate. Again, the same five datasets used in the earlier model are used to evaluate the EDHLB design architecture in the assessment stage. Fifty samples for each dataset are randomly taken to analyse the maximum efficiency of this architecture. A mean of five dataset accuracies was considered as the overall efficiency for the designed deep learning architecture.

From the 5-dataset analysis of ten folds cross valuation, an average value was grabbed for every fold and general accuracy. Thus, fold ten shows 98.2% of reliability and also fold five, eight and nine shows 96.56% of reliability as shown in Figure 8, where other folds likewise show a better overall performance of accuracy, which stands around 80% to 93% and also the typical total accuracy rate obtained for the entire five dataset is 92.44%. By examining the private functionality of the fifth datasets, the fourth dataset shows a better recognition rate of 93.13%.

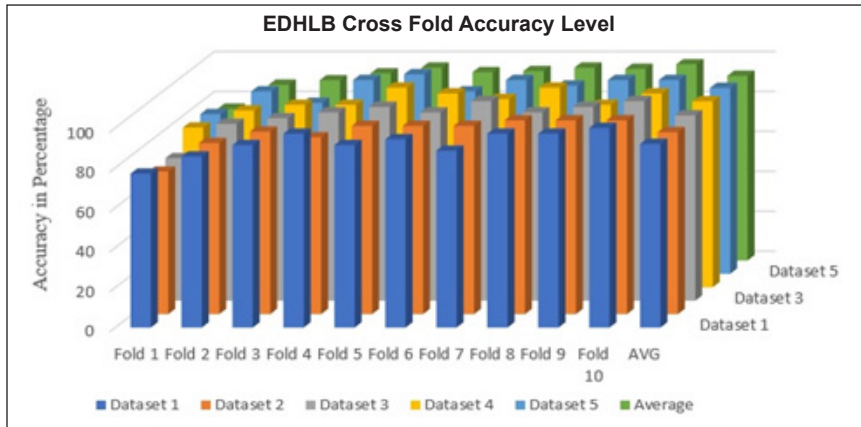


Figure 8. EDHLB cross fold output for five datasets

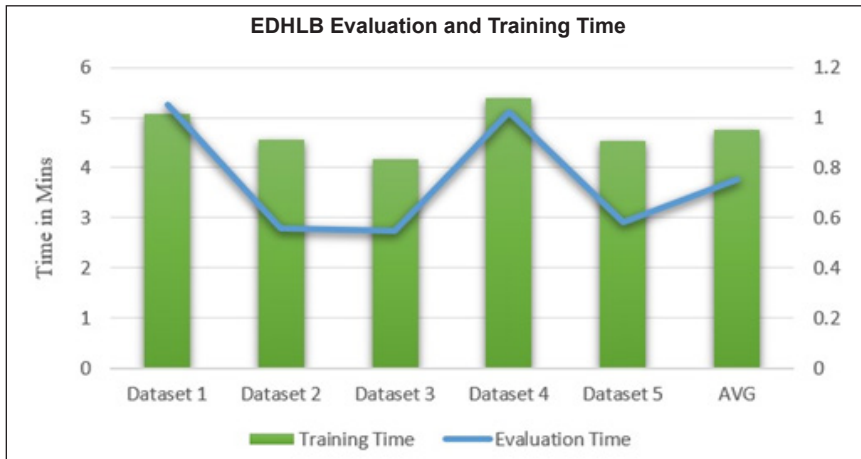


Figure 9. EDHLB evaluation time and training time for five datasets

By studying the time factor, among the five datasets, the time taken for evaluation and classification training were considered and shown in Figure 9. While shooting, the mean worth it is apparent that the instruction of EDHLB requires around 1.05 minutes of evaluation time and 5.14 minutes of training time.

Thinking of the unique performance of training and evaluation time captured in different dataset collection, the time taken for the third dataset is less than 0.55 minutes with 4.18 minutes for evaluation and training.

Figure 10 indicates that the accuracy level of all five-dataset simulations has been established. As the cross-validation folds are arbitrary, the accuracy amount changes randomly according to the dataset in five executions, but it lies between 91.13% to 93.13% in each execution. Thus, among the simulation of the fifth dataset, the fourth dataset shows greater precision and efficiency rate of 93.13% and more than the outcome of another dataset.

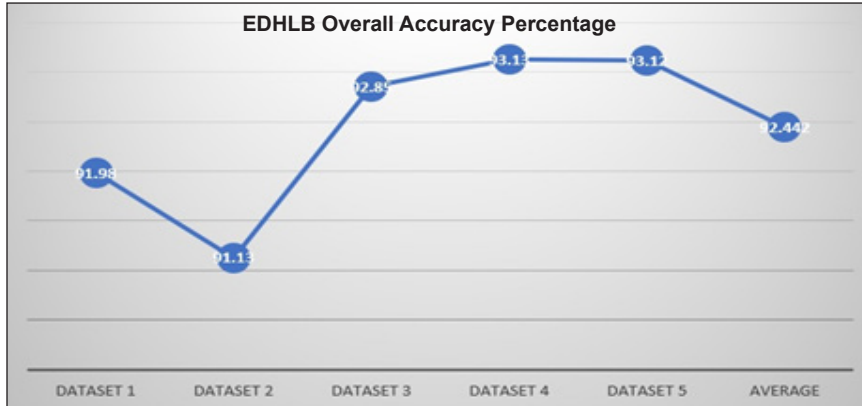


Figure 10. EDHLB overall accuracy rate for five datasets

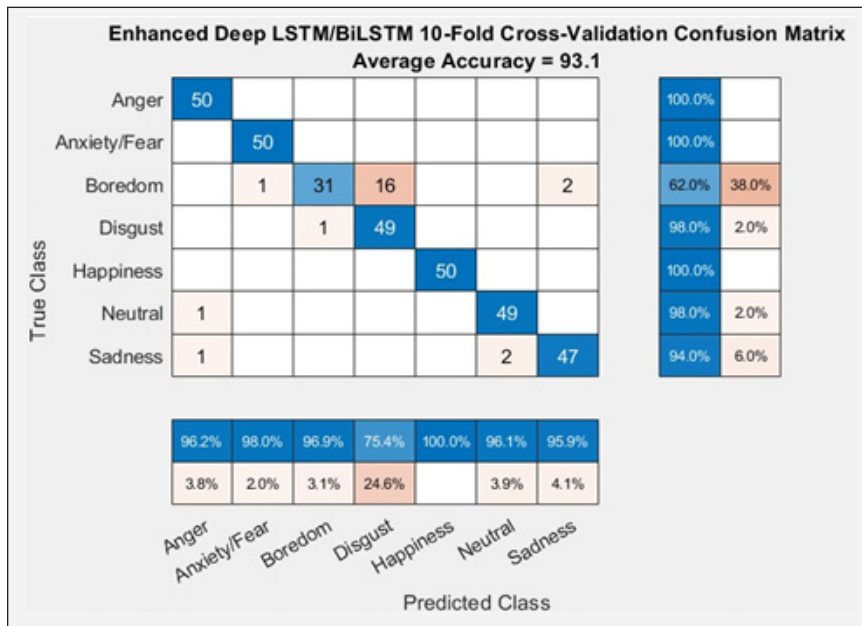


Figure 11. Cross fold confusion matrix for EDHLB

Finally, by thinking about the precision amount of each feeling as revealed in Figure 11, it is apparent that for the fourth dataset of Tamil emotional samples, the EDHLB design provides 93.1% effectiveness. In the confusion matrix, emotions such as happiness, anger and fear give a higher rate of 100%, and emotions such as disgust and neutral tone show 98% accuracy.

This model too lags with regard to other emotional states. The emotions of boredom and sadness lag in the EDHLB model, and only 62% and 94% of accuracy have been obtained in both states, and it shows the lowest efficiency rate of all emotions. Overall, the accuracy rate is better than the DHLB design architecture.

Enhanced Deep Hierarchical BILSTM & LSTM (EDHBL) Architecture

The functionality of the EDHBL designs is examined to attain a conclusion that EDHBL design makes a confusion matrix with ten-fold cross-validation. Since cross folding is arbitrary, each evaluation result exhibits different precision amounts for different datasets with a mean of five assessments, which were viewed for precision rate. Again, the same five datasets used in previous models are used to evaluate EDHBL design architecture in the assessment stage. Fifty samples for each dataset were randomly taken to analyse the maximum efficiency of this architecture. A mean of five dataset accuracy was considered the overall efficiency for the designed deep learning architecture.

From the 5-dataset analysis of ten folds cross valuation, an average value was grabbed for every fold for general accuracy. Thus, fold five, eight, nine and ten shows 98.2% of reliability and folds two, three, four and six show 94.26% of reliability as in Figure 12, where some folds likewise show a much better overall performance of accuracy around 80% to 93% and also the typical total mean accuracy rate obtained for entire five datasets is 94.15%. By examining the private functionality of the fifth dataset, the fourth datasets show a much better recognition rate of 95.7%.

In studying the time factor, among the five datasets, the time taken for evaluation and classification training was considered in Figure 13. While shooting, the mean worth it becomes apparent that the instruction of EDHBL requires around 1.38 minutes of evaluation time and 4.32 minutes of training time.

In thinking about the unique performance of training and evaluation time captured in different dataset collections, the time taken for the third dataset is as little as 1.12 minutes and 4.25 minutes for evaluation and training.

From Figure 14, there is evidence that the accuracy level of all five-dataset simulations has been established. As the cross-validation folds are arbitrary, the accuracy amount changes randomly according to the dataset in five executions. In each execution, the range is between 93.41% to 95.7%. For example, among the simulation of the fifth dataset, the fourth dataset shows a greater precision and efficiency rate of 95.7% than the outcome of the other dataset.

Finally, considering the precision amount of each feeling as revealed in Figure 15, it becomes apparent that for the fourth dataset of Tamil emotional samples, EDHBL design provides 93.1% of effectiveness. In the confusion matrix, emotions such as happiness, anger and neutral tone give a higher rate of 100%. Emotions such as fear and sadness show 98% and 94% of accuracy.

Also, this model lags in other emotional states and emotions such as boredom and disgust lag in the EDHBL model, and only 90% & 88% of accuracy is obtained in both states. It shows the lowest efficiency rate of all emotions. Overall, the accuracy rate is better than DHBL design architecture.

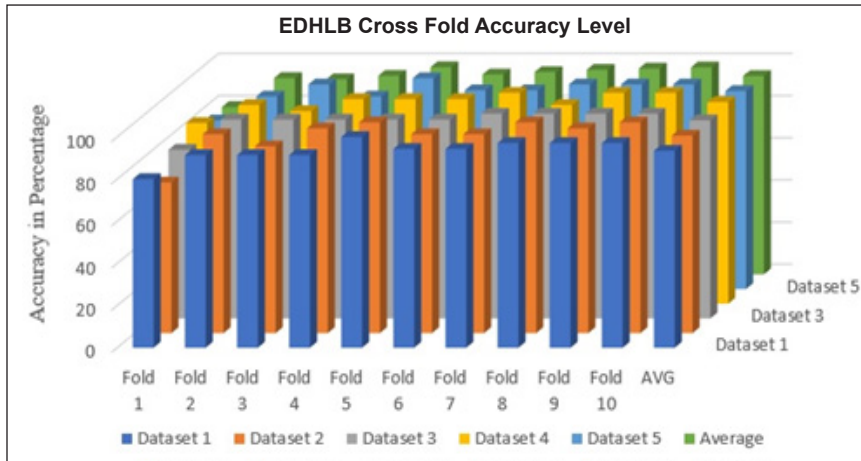


Figure 12. EDHLB cross fold output for five datasets

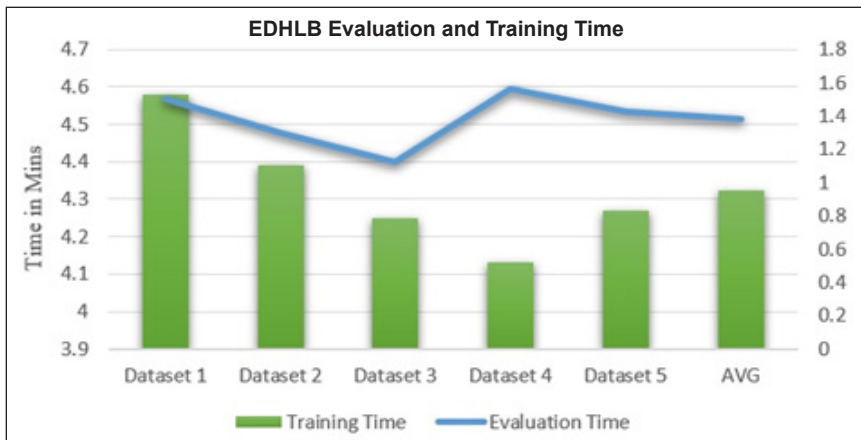


Figure 13. EDHBL evaluation time and training time for five datasets

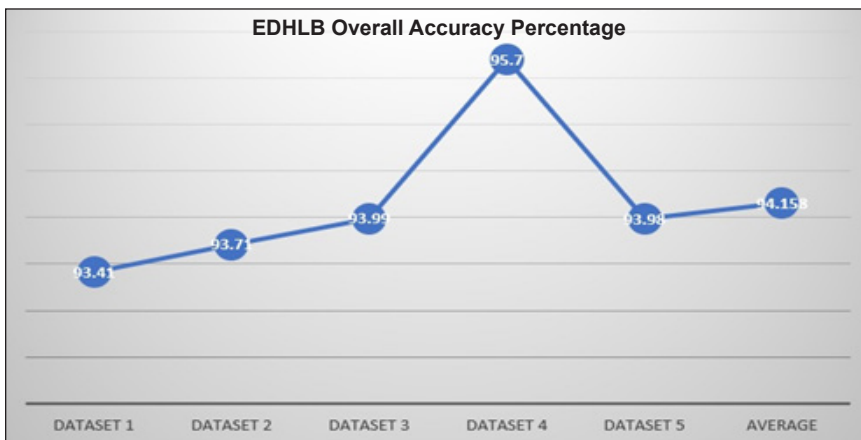


Figure 14. EDHBL overall accuracy rate for five datasets

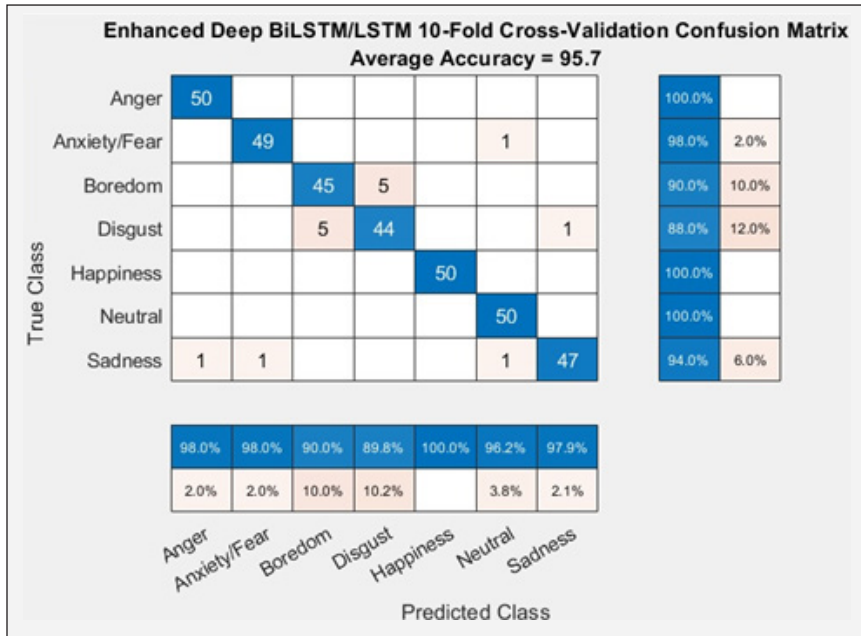


Figure 15. Cross fold confusion matrix for EDHBL

Enhanced Deep Hierarchical BiLSTM & BiLSTM (EDHBB) Architecture

The functionality of EDHBB designs was examined to conclude that EDHBB designs make a confusion matrix with ten-fold cross-validation. Since cross folding is arbitrary, each evaluation result exhibits different precision amounts for different datasets, a mean of five assessments was viewed for precision rate. Again, the same five datasets were used as in the previous model to evaluate EDHBB design architecture in the assessment stage. Fifty samples for each dataset were randomly taken in order to analyse the maximum efficiency of this architecture. A mean of five dataset accuracy was considered as the overall efficiency for the designed deep learning architecture.

From the 5-dataset analysis of ten folds cross valuation, an average value was grabbed for every fold and general accuracy. Thus, fold five and nine show 99.42% reliability and also folds four, seven, eight and ten show 95.4% reliability as shown in Figure 16, where some folds likewise show a better overall performance of accuracy of around 80% to 93% and also the typical total mean accuracy rate obtained for the entire five datasets is 93.19%. By examining the private functionality of the fifth dataset, the fourth dataset shows a better recognition rate of 94%.

In studying the time factor, among the five datasets, the time taken for evaluation and classification training was considered in Figure 17. While shooting, the mean worth, it is apparent that the instruction of EDHBB requires around 2.06 minutes of evaluation time and 5.17 minutes of training time.

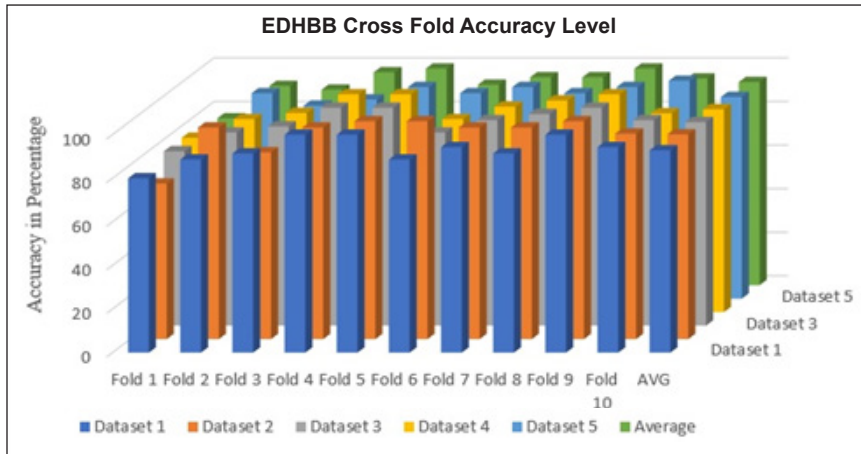


Figure 16. EDHBB cross fold output for five datasets

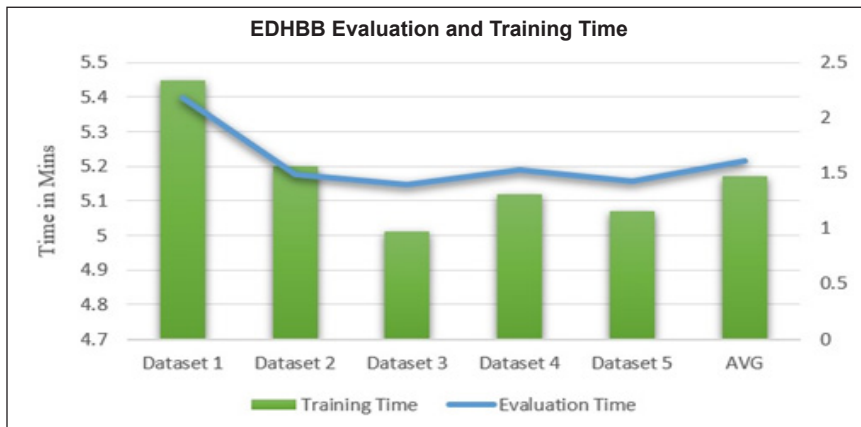


Figure 17. EDHBB evaluation time and training time for five datasets

In thinking about the unique performance of training and evaluation, the time captured in different dataset collections, the time is taken for the third dataset is as little as 1.04 minutes and 5.01 minutes for evaluation and training.

Figure 18 indicates that the accuracy level of all five-dataset simulations has been established. As the cross-validation, the folds are arbitrary; the accuracy amount changes randomly according to the dataset in 5 executions. In each execution, it lies in the range of 92.56% to 93.98%. Among the simulation of five datasets, the second dataset shows greater precision and efficiency rate of 93.98% more than the outcome of the other datasets.

Finally, thinking about the precision amount of each feeling, as revealed in Figure 19, it is apparent that for the second dataset of Tamil emotional samples, the EDHBB design provides 93.98% effectiveness. In the confusion matrix, emotions such as happiness, anger and fear give a higher rate of 100%. Moreover, emotions such as neutral tone and disgust show 96% and 94% accuracy.

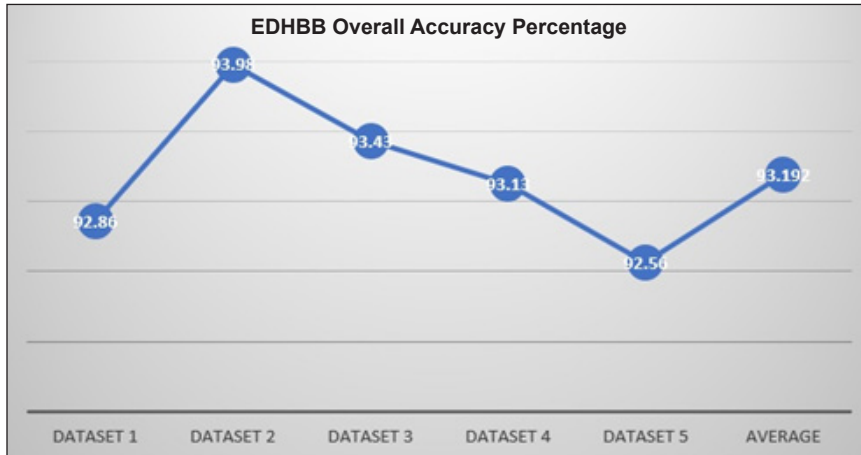


Figure 18. EDHBB overall accuracy rate for five datasets

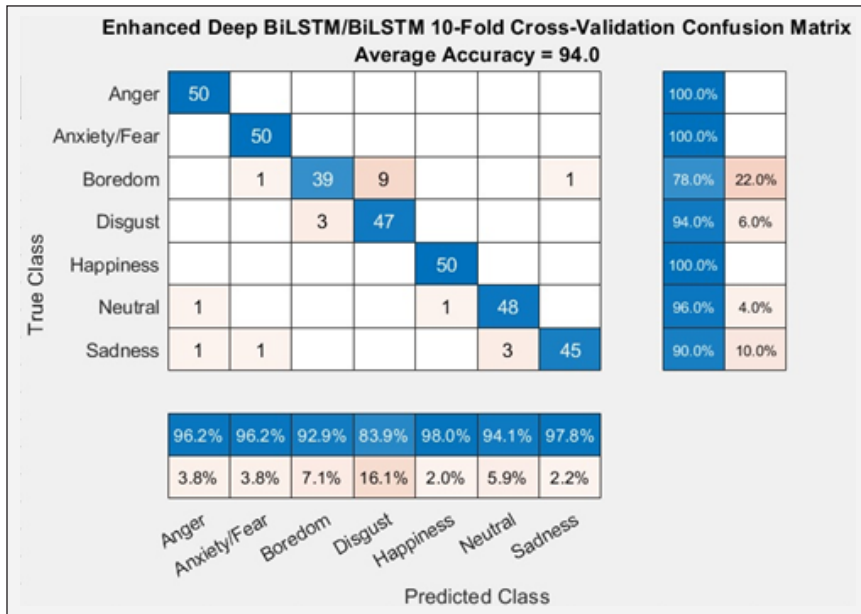


Figure 19. Cross fold confusion matrix for EDHBB

Also, this model lags in other emotional states. Emotions such as boredom and sadness lag in the EDHBL model. Only 78% and 90% of accuracy is obtained in both states and shows the lowest efficiency of all emotions. Overall, the accuracy rate is better than the DHBB design architecture.

Tables 1 and 2 show the overall performance of the complete designs. When comparing the base models of LSTM and BiLSTM, EDHBL shows better performance than the other models. The EDHBB achieves comparable performance to EDHBL, and both models give average accuracy of 95.7% and 94% for the collected Tamil emotional database.

Table 1
Cross fold accuracy of EDH LL/LB/BL/BB Layers

Fold Accuracy/ Methodology	LSTM	BILSTM	EDHLL	EDHLB	EDHBL	EDHBB
Fold 1	69.2	71.4	74.3	80	85.7	71.4
Fold 2	72.1	74.9	91.4	88.6	94.3	97.1
Fold 3	72.1	74.7	91.4	91.4	91.4	85.7
Fold 4	75.5	73.8	100	91.4	97.1	97.1
Fold 5	73.9	79.6	97.1	100	97.1	100
Fold 6	72.1	74.9	94.3	97.1	97.1	100
Fold 7	73.9	79.6	94.3	94.3	100	97.1
Fold 8	75.5	79.2	91.4	100	94.3	97.1
Fold 9	75.5	76.1	100	91.4	100	100
Fold 10	76.8	79.6	94.8	97.1	100	94.3

Table 2
Overall performance of EDH LL/LB/BL/BB Layers

Overall Performance (Among 5 dataset)	LSTM	BILSTM	EDHLL	EDHLB	EDHBL	EDHBB
Best Accuracy	74	77	92.9	93.13	95.7	94
Average accuracy	73	76	92.12	92.44	94.1	93.19
Best Evaluation Time	0.45	0.51	0.47	0.55	1.12	1.4
Average Evaluation Time	0.56	0.59	0.5	1.05	1.38	2.06
Best Training Time	4.5	5.11	4.4	4.18	4.13	5.01
Average Training Time	5.08	5.27	4.59	5.04	4.32	5.17

When comparing the training time to identify the different emotional classifications for the input of 50 samples, it was learnt that the training time and the evaluation time also varied in each dataset. However, only seconds of variation can be identified. EDHBL shows a lower training time than the other models in the testing phase, and it takes only 4.13 minutes to complete the training. The other models have a lag in time for the training process. The average training time taken by the EDHBL model is 4.32 minutes, where other models take more than 30 seconds slightly to complete the training.

After training, the evaluation time for all models EDHBL lag when compared with the other models. Even though EDHBB shows comparable performance towards EDHLL and EDHBB, it takes additional to evaluate the testing database. The time is reduced by 50% in EDHLL. Around 1.12 minutes were taken to evaluate the database in the EDHBL model with an average time of 1.38 minutes. In contrast, EDHBB took around 1.4 minutes to complete the evaluation, and EDHLB took 0.55 minutes for evaluating the dataset. Though it lags in training time, it shows better results in training time.

Most efficiently, Enhanced Deep Hierarchical BILSTM and LSTM give better performance than the basic models of LSTM and BILSTM. For example, when comparing the cross folds from the above table in EDHBL folds 7, 9 and 10, it gives an accuracy rate of 100%, and in EDHBB also folds 5, 6 and 9 yield an accuracy of 100%. However, the EDHBL model takes slightly more time for training and is best in evaluation, whereas other techniques take a few more seconds to complete the evaluation. The results obtained from different models have been generated and presented effectively in this paper. Thus, further design layers can enhance this model and optimise its use with added computation and data.

CONCLUSION

Since the ordinary feedforward neural networks cannot deal with speech information for the maximum accuracy rate, the RNNs were exposed to grab the temporal dependencies of speech information were taken into account. RNNs cannot take care of the extended dependencies of gradient vanishing issues and also with regard to overfitting. Therefore, LSTMs and BILSTM were introduced to overcome the shortcomings of RNNs. In this study, the limitations of gradient vanishing, long term dependencies and overfitting problems have been reduced with an augmented data approach for SER. It improves the recognition accuracy and reduces the limitations when the overall model cost computation and processing time are considered.

In this paper, four new architecture designs were developed to select an efficient sequence for Tamil emotional speech: Enhanced Deep Hierarchical LSTM & BILSTM (EDHLB), Enhanced Deep Hierarchical BILSTM & LSTM (EDHBL), EDHLL and EDHBB. In enhancing the DHLL, DHLB, DHBL, and DHBB models with data augmentation and concatenation of MFCC & Spectral Feature problems such as overfitting, gradient exploding, and long-term dependencies were reduced to the maximum rate. Furthermore, training time and evaluation time were considered for experimental analysis properties such as the average accuracy rate. From the analysis, EDHBL shows better performance when compared to all other modes. The best accuracy rate is approximately 95.7%, with a minimal training time of 4.13 minutes, and the evaluation time of 1.12 minutes was obtained from EDHBL architecture. Therefore, for the collected Tamil emotional database, emotions such as anger, sadness, neutral tone, happiness, and fear show an efficiency rate of 100%. On the other hand, motions such as disgust and boredom still lag in the accuracy rate. Also, the EDHBB model indicates a result of 94%. Hence for the collected Tamil emotional dataset, the EDHBL model was considered to perform better when compared with other models with an average computation of accuracy rate of 94.1%, evaluation time of 1.38 minutes and training time of 4.32 minutes.

ACKNOWLEDGEMENT

The author thanks KL University, AP, India, for supporting this work and the faculty members who assisted in providing the data for this research.

REFERENCES

- Alías, F., Socoró, J. C., & Sevillano, X. (2016). A review of physical and perceptual feature extraction techniques for speech, music and environmental sounds. *Applied Sciences*, 6(5), Article 143. <https://doi.org/10.3390/app6050143>.
- Chen, Z., Watanabe, S., Erdogan, H., & Hershey, J. (2015). Speech enhancement and recognition using multi-task learning of long short-term memory recurrent neural networks. In *Sixteenth Annual Conference of the International Speech Communication Association* (pp. 3274-3278). IEEE Publishing. <https://doi.org/10.1109/SLT.2016.7846281>
- Cummins, N., Amiriparian, S., Hagerer, G., Batliner, A., Steidl, S., & Schuller, B. W. (2017). An image-based deep spectrum feature representation for the recognition of emotional speech. In *Proceedings of the 25th ACM international Conference on Multimedia* (pp. 478-484). ACM Publishing. <https://doi.org/10.1145/3123266.3123371>
- Erdogan, H., Hershey, J. R., Watanabe, S., & Roux, J. L. (2015). Phase-sensitive and recognition-boosted speech separation using deep recurrent neural networks. In *2015 IEEE International Conference on Acoustics, Speech and Signal Processing (ICASSP)* (pp. 708-712). IEEE Publishing. <https://doi.org/10.1109/ICASSP.2015.7178061>.
- Eyben, F., Weninger, F., Squartini, S., & Schuller, B. (2013). Real-life voice activity detection with LSTM recurrent neural networks and an application to Hollywood movies. In *2013 IEEE International Conference on Acoustics, Speech and Signal Processing* (pp. 483-487). IEEE Publishing. <https://doi.org/10.1109/ICASSP.2015.7178061>.
- Graves, A., Jaitly, N., & Mohamed, A. (2013). Hybrid speech recognition with deep bidirectional LSTM. In *2013 IEEE Workshop on Automatic Speech Recognition and Understanding* (pp. 273-278). IEEE Publishing. <https://doi.org/10.1109/ASRU.2013.6707742>.
- Hochreiter, S., & Schmidhuber, J. (1997). Long short-term memory. *Neural Computation*, 9(8), 1735-1780. <https://doi.org/10.1162/neco.1997.9.8.1735>.
- Huang, J., Chen, B., Yao, B., & He, W. (2019). ECG arrhythmia classification using STFT-based spectrogram and convolutional neural network. *IEEE Access*, 7, 92871-92880. <https://doi.org/10.1109/ACCESS.2019.2928017>
- Hussain, T., Muhammad, K., Ullah, A., Cao, Z., Baik, S. W., & de Albuquerque, V. H. C. (2019). Cloud-assisted multiview video summarization using CNN and bidirectional LSTM. *IEEE Transactions on Industrial Informatics*, 16(1), 77-86. <https://doi.org/10.1109/TII.2019.2929228>
- Ioffe, S., & Szegedy, C. (2015). Batch normalization: Accelerating deep network training by reducing internal covariate shift. In *International Conference on Machine Learning* (pp. 448-456). MLResearchPress. <https://doi.org/10.5555/3045118.3045167>.

- Karim, F., Majumdar, S., & Darabi, H. (2019). Insights into LSTM fully convolutional networks for time series classification. *IEEE Access*, 7, 67718-67725. <https://doi.org/10.1109/ACCESS.2019.2916828>
- Khan, S. U., Haq, I. U., Rho, S., Baik, S. W., & Lee, M. Y. (2019). Cover the violence: A novel Deep-Learning-Based approach towards violence-detection in movies. *Applied Sciences*, 9(22), Article 4963. <https://doi.org/10.3390/app9224963>
- Kishore, P. V. V., & Prasad, M. V. D. (2016). Optical flow hand tracking and active contour hand shape features for continuous sign language recognition with artificial neural network. *International Journal of Software Engineering and its Applications*, 10(2), 149-170. <https://doi.org/10.1109/IACC.2016.71>
- Krizhevsky, A., Sutskever, I., & Hinton, G. E. (2012). Imagenet classification with deep convolutional neural networks. *Advances in neural information processing systems*, 25, 1097-1105. <https://doi.org/10.1145/3065386>.
- Kumar, K. V. V., Kishore, P. V. V., & Kumar, D. A. (2017). Indian classical dance classification with adaboost multiclass classifier on multi feature fusion. *Mathematical Problems in Engineering*, 20(5), 126-139. <https://doi.org/10.1155/2017/6204742>.
- Li, J., Deng, L., Gong, Y., & Haeb-Umbach, R. (2014). An overview of noise-robust automatic speech recognition. *IEEE/ACM Transactions on Audio, Speech and Language Processing*, 22(4), 745-777. <https://doi.org/10.1109/TASLP.2014.2304637>
- Liu, B., Qin, H., Gong, Y., Ge, W., Xia, M., & Shi, L. (2018). EERA-ASR: An energy-efficient reconfigurable architecture for automatic speech recognition with hybrid DNN and approximate computing. *IEEE Access*, 6, 52227-52237. <https://doi.org/10.1109/ACCESS.2018.2870273>
- Liu, Y., Zhang, P., & Hain, T. (2014). Using neural network front-ends on far field multiple microphones based speech recognition. In *2014 IEEE International Conference on Acoustics, Speech and Signal Processing (ICASSP)* (pp. 5542-5546). IEEE. <https://doi.org/10.1109/ICASSP.2014.6854663>.
- Mannepalli, K., Sastry, P. N., & Suman, M. (2016a). MFCC-GMM based accent recognition system for Telugu speech signals. *International Journal of Speech Technology*, 19(1), 87-93. <https://doi.org/abs/10.1007/s10772-015-9328-y>
- Mannepalli, K., Sastry, P. N., & Suman, M. (2016b). FDBN: Design and development of fractional deep belief networks for speaker emotion recognition. *International Journal of Speech Technology*, 19(4), 779-790. <https://doi.org/10.1007/s10772-016-9368-y>
- Mustaqeem, & Kwon, S. (2020). A CNN-assisted enhanced audio signal processing for speech emotion recognition. *Sensors*, 20(1), Article 183. <https://doi.org/10.3390/s20010183>
- Park, D. S., Chan, W., Zhang, Y., Chiu, C., Zoph, B., Cubuk, E. D., & Le, Q. V. (2019). *SpecAugment: A simple data augmentation method for automatic speech recognition*. ArXiv Publishing.
- Pascanu, R., Mikolov, T., & Bengio, Y. (2013). On the difficulty of training recurrent neural networks. In *International conference on machine learning* (pp. 1310-1318). MLResearchPress. <https://doi.org/10.5555/3042817.3043083>.

- Rao, G. A., & Kishore, P. V. V. (2016). Sign language recognition system simulated for video captured with smart phone front camera. *International Journal of Electrical and Computer Engineering*, 6(5), 2176-2187. <https://doi.org/10.11591/ijece.v6i5.11384>
- Rao, G. A., Syamala, K., Kishore, P. V. V., & Sastry, A. S. C. S. (2018). Deep convolutional neural networks for sign language recognition. *International Journal of Engineering and Technology (UAE)*, 7(Special Issue 5), 62-70. <https://doi.org/10.1109/SPACES.2018.8316344>
- Ravanelli, M., Brakel, P., Omologo, M., & Bengio, Y. (2016). Batch-normalized joint training for dnn-based distant speech recognition. In *2016 IEEE Spoken Language Technology Workshop (SLT)* (pp. 28-34). IEEE Publishing. <https://doi.org/10.1109/SLT.2016.7846241>.
- Ravanelli, M., Brakel, P., Omologo, M., & Bengio, Y. (2017). A network of deep neural networks for distant speech recognition. In *2017 IEEE International Conference on Acoustics, Speech and Signal Processing (ICASSP)* (pp. 4880-4884). IEEE Publishing. <https://doi.org/10.1109/ICASSP.2017.7953084>.
- Sak, H., Senior, A. W., & Beaufays, F. (2014, September 14-18). Long short-term memory recurrent neural network architectures for large scale acoustic modeling. In *Fifteenth Annual Conference of the International Speech Communication Association* (pp. 338-342). Singapore.
- Sastry, A. S. C. S., Kishore, P. V. V., Prasad, C. R., & Prasad, M. V. D. (2016). Denoising ultrasound medical images: A block based hard and soft thresholding in wavelet domain. *Medical Imaging: Concepts, Methodologies, Tools, and Applications*, 761-775. <https://doi.org/10.1016/j.procs.2015.08.040>
- Schwarz, A., Huemmer, C., Maas, R., & Kellermann, W. (2015). Spatial diffuseness features for DNN-based speech recognition in noisy and reverberant environments. In *2015 IEEE International Conference on Acoustics, Speech and Signal Processing (ICASSP)* (pp. 4380-4384). IEEE Publishing. <https://doi.org/10.1109/ICASSP.2015.7178798>.
- Srivastava, N., Hinton, G., Krizhevsky, A., Sutskever, I., & Salakhutdinov, R. (2014). Dropout: A simple way to prevent neural networks from overfitting. *Journal of Machine Learning Research*, 15, 1929-1958. <https://doi.org/10.5555/2627435.2670313>.
- Weninger, F., Erdogan, H., Watanabe, S., Vincent, E., Roux, J. L., Hershey, J. R., & Schuller, B. W. (2015). Speech enhancement with LSTM recurrent neural networks and its application to noise-robust ASR. In *International conference on latent variable analysis and signal separation* (pp. 91-99). Springer. https://doi.org/10.1007/978-3-319-22482-4_11
- Zhang, Y., Chen, G., Yu, D., Yao, K., Khudanpur, S., & Glass, J. R. (2016). Highway long short-term memory RNNs for distant speech recognition. In *2016 IEEE International Conference on Acoustics, Speech and Signal Processing (ICASSP)* (pp. 5755-5759). IEEE Publishing. <https://doi.org/10.1109/ICASSP.2016.7472780>
- Zhou, G., Wu, J., Zhang, C., & Zhou, Z. (2016). Minimal gated unit for recurrent neural networks. *International Journal of Automation and Computing*, 13(3), 226-234. <https://doi.org/10.1007/s11633-016-1006-2>.

Proposed Methodology for End-of-Life Option using Multi Criteria Decision Analysis: A Study for General Paper Product

Salwa Mahmood^{1*}, Muhammad Aizrul Ezuan Edirudzin¹ and Nur Syamimi Jiran²

¹*Department of Mechanical Engineering Technology, Faculty of Engineering Technology, Universiti Tun Hussein Onn Malaysia, Pagoh Campus, KM 1 Jalan Panchor, 84600 Pagoh, Johor, Malaysia*

²*School of Mechanical Engineering, Faculty of Engineering, Universiti Teknologi Malaysia, 81310 Skudai, Johor Bahru, Johor, Malaysia*

ABSTRACT

Over the years, the world population has been growing exponentially. This population growth affects the number of waste products due to the increased production, which leads to greater environmental impact and other problems. There are different numbers of product end-of-life (EOL) options to handle waste based on product characteristics. This research is designed to develop a methodology to determine the best EOL option for a paper product using the analytical hierarchy process (AHP). AHP is one of the multi-criteria decision analysis (MCDA) methods employed to select the best option by considering the user's preferences and output of competing EOL options related to different product criteria. A graphical user interface (GUI) called AHP-based software was developed using Microsoft Excel through the programming function of Visual Basic for Applications as a user facilitating tool when conducting the analysis. The case study technique is applied to five different types of paper products to assess the capability of the proposed AHP-based software. Results from the AHP-based software reveal that recycling is the most suitable EOL technique for most paper products compared to other techniques. However, polluted products with ink or food waste and coating may not be suitable for this method. The research assists the users to identify the most sustainable ways to handle paper product waste based on the product condition.

ARTICLE INFO

Article history:

Received: 05 May 2021

Accepted: 05 August 2021

Published: 28 October 2021

DOI: <https://doi.org/10.47836/pjst.29.4.40>

E-mail addresses:

msalwa@uthm.edu.my (Salwa Mahmood) aizrule@gmail.com

(Muhammad Aizrul Ezuan Edirudzin)

syamimi.jiran@gmail.com (Nur Syamimi Jiran)

* Corresponding author

Keywords: Analytical hierarchy process, end-of-life, multi-criteria decision analysis, paper product

INTRODUCTION

The increase in the human population indirectly causes the demand for products to continue rising (Jiran et al., 2019).

However, products lifespan is declining to cope with the recent technologies and trends. Rapid production and advanced manufacturing technology to meet consumer demand indirectly affect the environment and produce much solid waste. In addition, unsustainable consumption and production patterns have resulted in increased waste generation over many decades (Vlachokostas et al., 2021). The impact of a high production process can lead to the environmental effect of products through their entire life cycle (Gehin et al., 2008). Solid Waste Management (SWM) is a global problem, particularly in emerging industrial countries, including Malaysia (Badgie et al., 2012). According to the UN, global waste generation is projected to double between 2016 and 2050 (Nation, 2019). Although increased waste generation is indirectly caused by urbanisation and rising living standards (Arikan et al., 2017; Ibrahim et al., 2017) developed countries generate more solid waste than developing countries (Sekhon & Karthigesu, 2017). For example, Malaysia's waste generation is estimated at 38,000 metric tons per day (Lim, 2018) and is predicted to increase by 3% annually (Badgie et al., 2012).

Due to inadequate suitable technology, manpower, land scarcity and waste facilities in Malaysia (Badgie et al., 2012; Zainu & Songip, 2017), SWM is becoming one of the most critical environmental issues (Kharat et al., 2019) and also requiring a major commitment (Rahman et al., 2020) to deal with the rapid increase in waste generation in line with human population growth (Ibrahim et al., 2017). More than 80% of solid waste is disposed of in landfills and open dumps (Liu et al., 2017; Rahman et al., 2020), while only 20% is recycled (Jereme et al., 2015). The low recycling percentage is due to low cooperation in the recycling activity and solid waste separation at the source (Moh & Manaf, 2017). The Malaysian Recycle Program was first launched in 1993 (Rahman et al., 2020) and then launched second in the 8th Malaysian Plan (2001-2005) by the Government with elements for minimising waste, promoting re-use activities and developing several pilot projects for the recycling program (Zainu & Songip, 2017). The 3R (i.e. reuse, reduce, recycle) campaign is part of this plan and was introduced in 2005 through the National Strategic Plan for Solid Waste Management (Rahman et al., 2020).

The European Union has established a waste management hierarchy as a guideline for waste management, consisting of 5 steps (Commission, 2008), i.e. prevention, reuse, recycle, recovery and disposal. Prevention is the first step and the best option for waste management (Ismail & Hanafiah, 2017), starting with the product before it is converted into waste. Prevention refers to reducing and restricting several hazardous materials and shifting the use to a safer material option (Ongondo et al., 2011). In addition, it may also refer to the reduction of total waste generation as early as during the product fabrication (Ahmadi, 2017; Rahman et al., 2020). Manufacturers are responsible for producing products from environmentally friendly materials and are encouraged to dispose of the products safely and properly (Ismail & Hanafiah, 2017; Rahman et al., 2020). Reuse is the best option

for EOL (Ahmadi, 2017) in which it refers to continuous usage of the product multiple times before it can be disposed of, such as the use of a bio-bag or a recycling bag while shopping, rather than a single-use of plastic bag (Ahmadi, 2017). Reuse can also be applied by selling, donating or repairing the product for it to be used by others, thus extending the product's life and reducing the generation of waste (T'ing et al., 2020). Recycle is the activity of collecting, separating and processing waste (paper, plastic metal and glass) into a new valuable product (T'ing et al., 2020; Rahman et al., 2020). Disposal at the landfill site is the last option in the waste management hierarchy, and the use should be minimised.

Disposal at the landfill sites continues to be the main option for SWM in Malaysia (Arifin et al., 2021; Ibrahim et al., 2017; Rahman et al., 2020; Samad et al., 2017). Unfortunately, improper SWM sites directly harm biodiversity, contributing to pollution, loss of eco-tourism amenities, loss of aesthetic scenery, and cause explosion hazards (Ahmadi, 2017; Arifin et al., 2021; Badgie et al., 2012). Moreover, numerous illegal dumping sites throughout Malaysia worsens the situation as SWM in Malaysia is driven by profit and economic incentives with low dumping costs while ignoring environmental impacts (Mah et al., 2018). Improper and unsanitary SWM sites, as well as illegal dumpsites, cause visual pollution, which has an indirect impact on the quality of life in the community, as well as the economic, health and wellness of human beings (Ibrahim et al., 2017; Jayaraman et al., 2019; Matsakas et al., 2017; Samad et al., 2017). In addition, incineration or waste-to-energy is a waste-handling technology commonly used in developed countries to dispose of hazardous waste (Kumar & Samadder, 2017). In Malaysia, this technology is used in the islands of Langkawi, Pangkor, Tioman, and Labuan (Rahman et al., 2020) to reduce waste transport costs to the mainland and handle clinical waste only in specific states. However, this technology is still being developed, and the operation is prohibitively expensive (Rahman et al., 2020). Compost is a common EOL option used by Malaysians, but it is still underutilised. Gathered leaves, yard waste, and food waste will be separated by compost microorganisms (Arifin et al., 2017) to improve the structure and pH of the soil and provide nutrients to the soil (Rahman et al., 2020).

A poor SWM system may also contribute to the depletion of natural resources (Rahman et al., 2020). Furthermore, due to the lack of available space for a new landfill site, the landfill cannot be the primary option for product EOL (Arifin et al., 2017; Ibrahim et al., 2017; Randazzo et al., 2018). As a result, an effective SWM system is vital for maintaining the ecosystem and giving other benefits to the community, as well as lowering the waste management cost (Kharat et al., 2019; Rahman et al., 2020). Aside from that, implementing the 3R concept may help improve the SWM system and reduce the total waste generation in Malaysia, paving the way for sustainable SWM (Ahmadi, 2017; Badgie et al., 2012; Jayaraman et al., 2019; Jereme et al., 2015). A sustainable SWM should be environmentally friendly, economically feasible, and socially acceptable (Kharat et al., 2019). Another

advantage of the 3R concept is that it reduces the greenhouse effect, reduces air, water, and land pollution, and increases natural resources. It is consistent with the goal of sustainable SWM, which is to balance the ecological system by recovering more products from waste with less energy usage and more positive environmental impacts (Badgie et al., 2012; Kharat et al., 2019; Sarigiannis et al., 2021). Education and awareness campaigns, particularly at the early age of education, can help to reduce waste generation (Zainu & Songip, 2017). According to a study conducted by Ting et al. (2020), attitude, facility, and habit contribute to the success of a recycling campaign among Malaysians.

Malaysia is one of the developing countries that is still trying to find the best way to manage and dispose of waste (Sekhon & Karthigesu, 2017). Multi-criteria Decision Analysis (MCDA) has become critical because the problem is currently complex but must be resolved quickly and effectively (Mamat et al., 2018), including to solve SWM problems (Coban et al., 2018). MCDA is a versatile method for determining optimal outcomes (Kumar & Samadder, 2017) that explicitly reflect numerous, multiple priorities while aggregating incomparable value (Coelho et al., 2017), and it can be combined with other tools such as life cycle assessment (LCA) (Vlachokostas et al., 2021). Moreover, compared to other decision-making support systems, it provides more robust decisions (Vlachokostas et al., 2021).

MCDA can be used to recognise among the most preferred options, rank options, short-list a limited number of options for further consideration, or distinguish acceptable options from unacceptable options (Achillas et al., 2013). As a result, it may be useful in assisting the strategy teams in planning and identifying high-value strategic options (Coelho et al., 2017). There are many different types of MCDA procedures, and each method has its characteristics. Some MCDA procedures are better suited for specific situations than others (Coelho et al., 2017). The methods are shown as follows:

- Weighted sum model (WSM)
- Weighted product model (WPM)
- Analytical hierarchy process (AHP)
- Preference ranking organisation method for enrichment evaluation (PROMETHEE)
- Elimination and choice translating reality (ELECTRE)
- Technique for order preference by similarity to ideal solution (TOPSIS)
- Compromise programming (CP)
- Multi-attribute utility theory (MAUT)

AHP is a type of MCDA method proposed by Prof Thomas Saaty in the 1970s (Dos Santos et al., 2019; Qazi et al., 2018) for solving complex and irregular decision-making problems using a hierarchical structure of criteria and alternatives (Abadi et al., 2018). AHP is the most commonly used MCDA technique (Badi et al., 2019; Coelho et al., 2017; Qazi et al., 2018; Vlachokostas et al., 2021) because it is an efficient approach for resolving

a complex problem and is able to assist decision-makers in setting priorities and making the best decision (Qazi et al., 2018). AHP is an approach that evaluates alternatives using pairwise comparisons (Coelho et al., 2017) to determine a result based on the hierarchical relationship between factors, attributes, characteristics, or alternatives in the decision-making environment (Abadi et al., 2018). However, judging pairwise scales is a difficult part (Torkayesh et al., 2021), so it must be done under the supervision of an expert (Qazi et al., 2018). According to Subramanian and Ramanathan (2012), most of the previous AHP studies is an application and case-study basis before the proposed AHP model being used in the real-life problem. AHP-model had used in various problems such as selecting notebook (Abadi et al., 2018), identify solid waste treatment (Badi et al., 2019), an evaluation tool for end-of-life vehicles (Mamat et al., 2018), selection of MSW treatment and disposal technology (Kharat et al., 2019) and many more. AHP-model can be used for decision-making of various life problems from simple with multiple alternatives up to complex criteria and many choices of alternatives.

Several studies on EOL have been conducted in recent years, using various techniques such as AHP (Badi et al., 2019; Ghazalli & Murata, 2011; Mamat et al., 2018), LCA (Ismail & Hanafiah, 2017; Mah et al., 2018; Sarigiannis et al., 2021), MCDA (Achillas et al., 2013; Coelho et al., 2017; Qazi et al., 2018; Schwenk et al., 2012), TOPSIS (Büyüközkan & Gocer, 2017; Yadav et al., 2020), and combining several methods (Coban et al., 2018; Torkayesh et al., 2020). However, most EOL studies in Malaysia focus on vehicle EOL (Ahmed et al., 2016; Mamat et al., 2018; Wong et al., 2018), e-waste (Ismail & Hanafiah, 2017; Jayaraman et al., 2019; Kalana, 2010) and a review of the current state of EOL activity in Malaysia, with several recommendations for successful EOL SWM in Malaysia (Badgie et al., 2012; Ismail & Hanafiah, 2017; Rahman et al., 2020; Zainu & Songip, 2017). Paper product production and consumption are declining, but because their lifespan is short, they have become one of the major components of solid waste generation (Vukoje & Rožić, 2018). It contributes to 7% of Malaysian total waste generation (Manaf et al., 2009; Zainu & Songip, 2017) apart from food, plastic, iron and glass that weighed up to 80% of total waste weight (Badgie et al., 2012; Kathirvale et al., 2004).

There are many different types of paper available, and for a variety of reasons, some of them can be recycled while others cannot. Normally, the EOL option for the paper product is incineration, non-recovery, landfill and boiler ash for industrial paper waste (van Ewijk et al., 2017). Choosing the best EOL option is difficult because there are many options and multiple criteria to consider (Kharat et al., 2019). Several researchers investigated the EOL option for paper products using various methods, but only a few used the MCDA method. Mostly developed methodologies do not consider the material, ecological, economic and social parameters to decide product EOL. Failure to select the best waste EOL option may exacerbate the SWM scenario (Torkayesh et al., 2021). Therefore, the

goal of this research is to develop a graphical user interface (GUI) of the methodology for determining product paper EOL options using the AHP method while considering resources, environmental impacts, economic benefit and legislative significance, which are the three pillars of sustainability (Ahmad et al., 2018; Coelho et al., 2017; Colapinto et al., 2019). These include both quantitative and qualitative measures. The proposed methodology will also be validated using a case study of a paper product to demonstrate the capability and applicability of the GUI in providing end-users with guidelines for paper EOL options.

MATERIAL AND METHOD

Proposed Methodology

The proposed methodology employs the AHP method to determine the best EOL option for different paper products based on several criteria. Figure 1 shows the proposed methodology of this study. Firstly, set the goal to achieve, criteria as a boundary or requirement that need to fulfil and lastly listed the alternative options to be chosen. Next, identify any sub-criteria that may exist. Finally, draw the structural hierarchy and list all elements (options) and criteria for comparing all alternatives to mapping the problem. This study’s AHP structure consists of four criteria: resource, environmental impact, economic value, and legislative priority, and five options: recycle, remanufacturing, reuse, incineration, and landfill. Table 1 lists the components of the AHP steps.

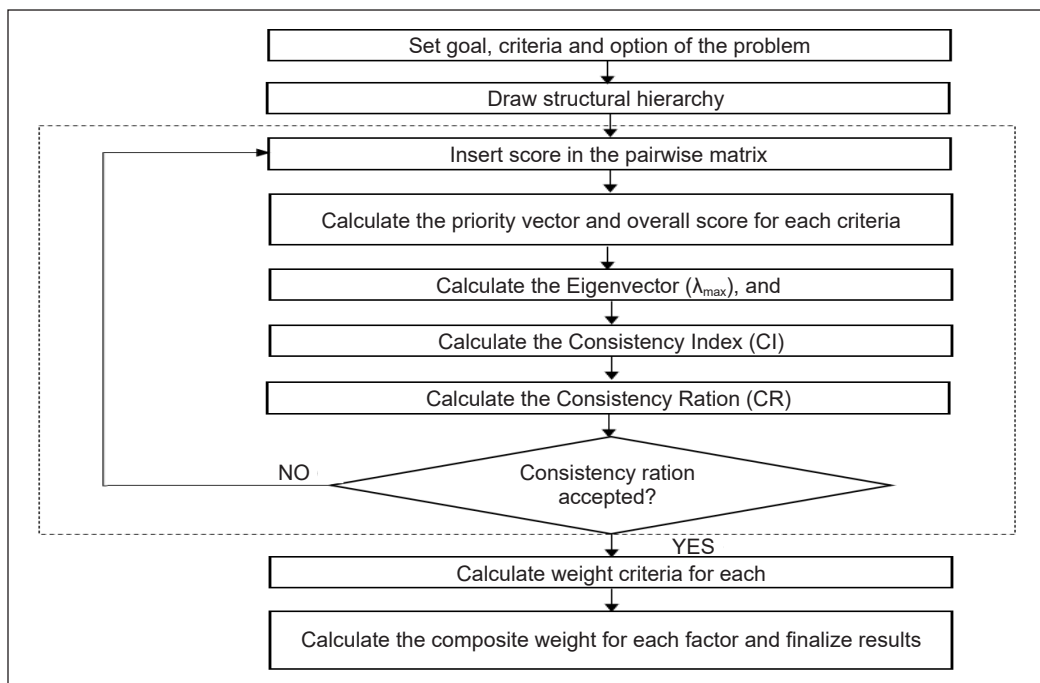


Figure 1. Flowchart of the proposed methodology of the study

Table 1
AHP conceptual reference of alternatives selection criteria

Step	Dimension of Ranking
Objective	The vision or mission to do and develop.
Alternative	The types of vision or mission.
Criteria	The explanation of reason to choose that alternative.

The following steps are involved the AHP method. The basic steps for conducting AHP are defining the objective into a hierarchical model, determining weights for each criterion, calculating the score of each criterion's alternatives, and finally calculating each alternative's overall score (Kumar & Samadder, 2017). AHP fulfils the SWM assessment requirements because, in the waste management context, criterion weights are frequently defined by the researcher's judgment (Coelho et al., 2017) while ignoring other factors. Since comparing elements in the evaluation is one of the most critical steps in AHP, it has become one of the most common and commonly used decision-making methods (Mamat et al., 2018). The AHP method usually applies numerical analysis to the pairwise comparison matrix in two steps, as stated below:

- Scoring: a numerical score on the strength of the preference scale for each option for each criterion is allocated to the predicted consequences of each option.
- Weighting: numerical weights are allocated to describe the relative values of a change between the top and bottom of the selected scale for each criterion.

The next step is to determine the pairwise score, which compares alternatives or variables depending on the analysis's target (Qazi et al., 2018; Randazzo et al., 2018). A pairwise comparison matrix is formed on the basis of the scores given for each of the components as input for the qualitative information. Pairwise comparisons on a scale of 1-9 are shown in Table 2. The decision maker's correlations are set in reciprocal matrices in pairwise comparison (Ahmadi, 2017). The diagonal elements of the matrix are 1. For example, a basic AHP application involving a number of I alternatives assessed by a total of J criteria can be represented by a comparison matrix of I rows and J columns, where A_{ij} corresponds to the score of the jth criteria for the ith alternative evaluated (Coelho et al., 2017). The value in the proportional (A_{ji}) can be calculated using the following formula in Equation 1. For example, the value of A_{ij} is 5, so the value for A_{ji} is 1/5 based on Equation 1.

$$A_{ij} = 1/A_{ji} \quad (1)$$

Then, for each criterion, the priority vector and summation are computed. The Eigenvector (λ_{\max}) will be calculated using both elements. The maximum Eigenvector is equal to the number of correlations for a consistent reciprocal matrix that can be calculated using Equation 2:

$$\lambda_{\max} = \sum (\text{priority vector} \times \text{sum of criteria}) \tag{2}$$

The Consistency Index (CI) is a metric of consistency used as a variance or degree of consistency using the formula shown in Equation 3. CI is used to calculate the Consistency Ratio (CR) as CR is a comparison between CI and random consistency index (RI) as tabulated in Table 3. CR can be calculated using Equation 4. It is necessary to determine the CR for which the appropriate value should be less than 10% or else, judgments of pairwise score need to be revised (Saaty, 2008). The accuracy ratio indicates how accurate the user’s judgments are. The CR value will be close to zero if the decisions are close to each other. Option comparison is chosen based on the result of the weight ratio scale of each criterion comparison. The highest result will be the best option compared to other options.

$$\text{Consistency Index (CI)} = \frac{(\lambda_{\max}) - n}{n - 1} \tag{3}$$

$$\text{Consistency Ratio (CR)} = \frac{\text{Consistency Index (CI)}}{\text{Random Consistency Index (RI)}} \tag{4}$$

Repeat the AHP steps for each different type of product. Next, calculate the adjusted weight criteria (in ratio 1) for each criterion if the value of priority vector of any criterion

Table 2
Evaluation scales of pairwise comparison

Intensity of Importance	Definition	Explanation
1	Equal Importance	Two activities contribute equally to the objective
2	Weak or slight	N/A
3	Moderate importance	Experience and judgment slightly favor one activity over another
4	Moderate plus	N/A
5	Strong importance	Experience and judgment strongly favor one activity over another
6	Strong plus	N/A
7	Very strong or demonstrated importance	An activity is favored very strongly over another; its dominance demonstrated in practice
8	Very, very strong	N/A
9	Extreme importance	The evidence favoring one activity over another is of the highest possible order of affirmation

Table 3
Random consistency index (Adopted from Saaty, 2008)

Size of matrix (n)	1	2	3	4	5	6	7	8	9
Random consistency index (RI)	0	0	0.58	0.90	1.12	1.24	1.32	1.41	1.45

is small, or use the priority vector as the adjusted weight. Lastly, calculate the composite weight of each option by using Equation 5. The final results of the proposed methodology are in the form of a weight ratio preference scale. For example, the result for X is 38%, Y is 49%, and Z is 13%. It indicates that Y weights 3.8 times more preference than Z. meanwhile, Z has 1.3 times more preferable than X.

$$\text{Composite weight} = \sum (\text{scale} \times \text{adjusted weight criteria}) \quad (5)$$

Graphical User Interface

A graphical user interface (GUI) is a user interface functionality with electronic devices that visually represent the necessary commands and operating system or software device functions. For this project, GUI was developed using Microsoft Excel that employed a programming function of Visual Basic for Applications (VBA) based on the process of the AHP method. The developed software allows users to use various computational techniques and send the results back to the datasheet. VBA is an adaption of the event-driven programming language in Microsoft Visual Basic. In this research, the user must click on the CALCULATE cell to generate the results for each option developed using the proposed methodology. In addition, AHP-based software was developed to evaluate the EOL options for the paper product that enabled the general public to access all kinds of systems for everyday use, regardless of their experience or knowledge.

The first step in developing the proposed GUI is to define the user and its requirement. The users of the proposed GUI are OEMs, remanufacturers, recyclers or government specialists, as a result of which there will be different inclinations to make a judgment. For example, manufacturers and recyclers may be more interested in optimising the resource and environmental impact as their main criteria when determining EOL products. As for government specialists, they may prefer the legislative priority and economic value as their main criteria.

Next, identify the problem that needs to be solved. Then, list the input, output and processing of the proposed software. Input is the list of source data supplied to the problem. Output is the list of required outcomes from the software. Meanwhile, the processing is the list of actions required to produce the required output. The list of input, processing and output of proposed AHP-based software is presented in Table 4.

After identifying the problem and expected outcome, the outline of the solution is presented, i.e. the developed methodology. As for this research, the steps in the proposed software are computation of pairwise matrix, computation of consistency ratio, and finalising the EOL option. The GUI will visually and numerically display the percentage of components of a particular EOL. Once the user is satisfied with the result, they can save the results by saving the Excel folder.

Table 4
List of input, processing and output of the proposed AHP-based software

Input	Processing	Output
<ul style="list-style-type: none"> • Weightage of main criteria (Resource, environmental impact, economic value, legislative priority). • Judgments of performance of 5 EOL option within each criteria. 	<ul style="list-style-type: none"> • Computation of pairwise matrix. • Computation of consistency ratio (CR). • Computation of global priority of each EOL option for each component of the product. • Computation of the percentage usage of each EOL option based on number of parts. 	<ul style="list-style-type: none"> • Preferred EOL option for a component. • Consistency and acceptability of the user's judgments. • Important ratings of EOL options based on their percentage.

Algorithm Testing for Correctness

After developing the AHP-based software, the following step is to perform algorithm testing for correctness. The main aim of this phase is the early detection of major logical errors to be easily corrected. Test data must be walked through each step in the algorithm to ensure that the instruction defined in the algorithm does what it is supposed to do. For example, the data used to test the algorithm for calculating the pairwise matrix was a matrix of 4x4. The matrix values are shown in Table 5, with the resulting priority value and CR value in Table 6.

Table 5
Pre-defined data for testing (Adopted from Saaty, 2008)

	A	B	C	D
A	1.00	4.00	2.00	5.00
B	0.25	1.00	0.33	4.00
C	0.50	3.00	1.00	4.00
D	0.20	0.25	0.25	1.00

Table 6
Priorities of pre-defined data

A	B	C	D
47.82%	15.70%	29.62%	6.85%

CR= 9.21%

After checking with the developed algorithm, the results were found to match the desired results, as shown above, thus verifying that the algorithm developed is working as desired. The value was used for the main criteria in the program.

Case Study Description

A case study is used to demonstrate the efficacy of the proposed software, which uses the AHP as the optimisation method to find the best EOL option for paper products. It aids in the selecting the best EOL option for various types of paper products based on the user's criteria. The five types of paper products used in this study are offset, coated, newsprint, cardboard, and paperboard. All of this is common paper waste found in Malaysia. The criteria for determining the best EOL for each type of paper product are a resource, environmental impact, economic value, and legislative priority. Resources refer to the effects of the EOL alternative on the resource. Products made from scarce resources that are difficult to manufacture can necessitate alternatives to landfilling and incineration to ensure the best use

of the resources. The environmental impact factor includes the effect on the environment, whether negative or positive, of human behaviour, commodity production, or operation in the plant. An economic benefit is a monetary indicator of a business person’s benefit from a good or service. There are various waste management solutions available today, but the cost-benefit analysis of those technologies remains a major problem (Sarigiannis et al., 2021). The factor of legislative priority refers to the waste hierarchy framework, as previously stated. Waste should be reduced as early as in the product production process as possible. When a product becomes waste, landfill disposal should be the last alternative after exhausted all solutions such as recycling and minimising. In the meantime, the EOL options in this study are recycling, remanufacturing, reusing, incineration, and landfill.

RESULTS AND DATA ANALYSIS

Proposed Methodology

The proposed methodology was developed by using a computer datasheet in Microsoft Excel. This model consists of 5 layers of Excel worksheets consists of Main Criteria, Factor A Resource, Factor B Environmental Impact, Factor C Economic Value, Factor D Legislative Priority and Composite Weight. The following section will explain the features of the developed software that employed AHP as an optimisation method and the results generated from the developed software.

AHP-based Software

All calculation to determine the suitable option for a paper product that employed AHP analysis was developed using Microsoft Excel. Users are only required to key in the value for each criterion and the EOL option before clicking the CALCULATE button, and the result for the EOL option will appear. In this analysis, the criteria or factors considered are resources, environmental impact, economic value and legislative priority, as shown in Figure 2. Each factor would compute the λ_{max} , CI and CR. Figure 3 shows an example of

Product Name					
Main Criteria	Resource	Environmental Impact	Economic Value	Legislative Priority	Priority
Resource	1.00				
Environmental Impact		1.00			
Economic Value			1.00		
Legislative Priority				1.00	
Sum					100%
λ_{max}					
CI					
CR					

Figure 2. Main criteria

Factor A	Resource					
Choice	Recycle	Remanufacture	Reuse	Incinerate	Landfill	Priority
Recycle	1.00					
Remanufacture		1.00				
Reuse			1.00			
Incinerate				1.00		
Landfill					1.00	
Sum						100%
λ_{max}						
CI						
CR						

Figure 3. Resource

	Factor A	Factor B	Factor C	Factor D	Composite Weight
Adjusted Weight					
Recycle					
Remanufacture					
Reuse					
Incinerate					
Landfill					
	Calculate				

Figure 4. Composite weight

GUI for factor resource. The most suitable option for EOL product paper is illustrated in the composite weight as in Figure 4 in percentages. The highest percentage shows that it is the best solution as compared to other options.

Results Analysis

Offset, coated, newsprint, cardboard, and paperboard were chosen as case studies to test the capability of the established methodology in determining the most suitable EOL option. After judging all products, a list of composite weights for all products was generated, as shown in Table 7. The results show that, except for coated paper, the rest of the paper items can be recycled. The recycling option has a composite weight of 36.5% for offset, 35.48% for newsprint, 36.51% for cardboard and 38.38% for paperboard. Meanwhile, incineration has the maximum composite weight for coated paper at 32.68%. It indicates that recycling offset paper is 0.365 times more preferable than reusing. Meanwhile, incineration is 0.3268 times more superior to a landfill for coated paper. For newsprint, recycle weights are 0.3548 times more preferable compared to incineration. When it comes to cardboard, recycling is 0.3651 times more preferable than remanufacturing. Finally, for paperboard, recycling is 0.3838 times more preferable than reusing.

Table 7
Composite weight of paper product

No	Product	Recycle	Remanufacture	Reuse	Incinerate	Landfill
1	Offset	36.50%	25.97%	29.22%	3.52%	4.78%
2	Coated	18.46%	8.47%	13.47%	32.68%	26.91%
3	Newsprint	35.48%	23.01%	13.24%	24.65%	3.62%
4	Cardboard	36.51%	32.68%	21.31%	5.54%	3.97%
5	Paperboard	38.38%	20.87%	29.65%	6.72%	4.37%

DISCUSSION

The effective method of EOL for paper products is directly dependent on the relationship of papers and printing inks (Vukoje & Rožić, 2018). According to the findings of the AHP-based software, most forms of paper products can be recycled during the EOL stage. Recycling is the method of storing and processing waste according to its type before producing a new product or reusing it for other purposes in the form of recycled materials or cardboard items (Jereme et al., 2015; Vukoje & Rožić, 2018). However, coated paper is more likely to be incinerated or landfilled because it contains toxic materials that endanger human health and wellbeing (Vukoje & Rožić, 2018). Aside from that, the manufacturer must take extra steps to strip the coating before it can be recycled. Therefore, it will increase the time required to recycle or remanufacture as well increasing the cost that has to be borne by the manufacturer.

Furthermore, if the paper has been covered with polyethene, the quality of recycling is poor. As a result, it is preferable to be incinerated to provide more energy (Vukoje & Rožić, 2018). Recycling paper waste is a beneficial action (Vukoje & Rožić, 2018) because it reduces the waste capacity for disposal at landfills or incineration, all of which cause pollution (Badgie et al., 2012; Joshi et al., 2017). In addition, the use of recycled materials in the manufacturing industry may minimise the amount of energy and resources required to create a new product (Vukoje & Rožić, 2018), hence lowering the environmental effect on the ecosystem (Badgie et al., 2012; Jereme et al., 2015; Mah et al., 2018). Furthermore, recycling can be a secondary source of revenue for low-income people (Badgie et al., 2012; Rahman et al., 2020). However, recycling activity must be handled properly to prevent any negative consequences for the environment and the staff who handle the operation (Ismail & Hanafiah, 2017; Mahmood et al., 2019; Sekhon & Karthigesu, 2017; Vukoje & Rožić, 2018).

On the other hand, papers that have been contaminated with other products, such as food juice or oil, should be disposed of or incinerated (Saraiva et al., 2016). Landfilling is still the most popular EOL solution in most developing countries, including Malaysia (Kumar & Samadder, 2017), since it can handle almost any form of waste (Badgie et al.,

2012; Zainu & Songip, 2017). Inefficient SWM in unsanitary landfills, on the other hand, can lead to other problems and different forms of pollution in the short and long term, in addition to the effects on human health and the environment (Assi et al., 2020; Das et al., 2019; Kumar & Samadder, 2017; Rahman et al., 2020; Zainu & Songip, 2017). Therefore, aside from landfills, incineration has become the most common EOL alternative among Malaysians (Badgie et al., 2012), as it can minimise waste volume by up to tenfold (Badgie et al., 2012). In practice, incineration is one of the most commonly used waste-to-energy technologies when dealing with waste that cannot be recycled (Vukoje & Rožić, 2018), particularly in developed countries (Dong et al., 2018; Kumar & Samadder, 2017), because it has very low operating costs when compared to other technologies (Almanaseer et al., 2020).

However, poor controls in incineration operations result in toxic chemicals such as dioxins being released into the air, soil, and water, which may have an impact on human health and the ecosystem (Randazzo et al., 2018; Sarigiannis et al., 2021; Zainu & Songip, 2017). Nevertheless, the disadvantages of the incineration process such, as GHG emissions and environmental harm, can be overcome if the bottom ash is treated properly (Almanaseer et al., 2020). However, composting is more environmentally sustainable than incineration (Arikan et al., 2017). According to Das et al. (2019) and Qazi et al. (2018), composting reduces GHG emissions up to 47% compared to incineration. Furthermore, composting through organic recycling is appropriate for polluted paper products that cannot be recycled conventionally (Vukoje & Rožić, 2018).

Rapid urban global growth leads to change in the human population and, as a result, causing a hike in waste production (Manaf et al., 2009; Samad et al., 2017). Therefore, it is essential to develop a sustainable SWM that creates a 'closed loop' waste cycle that focuses on reducing waste in order to conserve natural resources for future generations (Manaf et al., 2009) is needed. Waste generation must be treated and disposed of properly (Torkayesh et al., 2021), and one approach is through waste recycling. Waste recycling in Malaysia seems unsuccessful (T'ing et al., 2020) within the first two years since it was implemented and is still developing. However, the percentage of waste recycled has risen and has reached the 2019 recycling goal (Rahman et al., 2020). Furthermore, educating the public about environmental consciousness, including proper recycling operation and waste separation at the source, enforcing waste regulations, designing an intelligent mechanism for managing the composition, and receiving support from the private waste management industry all lead to the effective adoption of sustainable SWM in Malaysia (Badgie et al., 2012; Jayaraman et al., 2019; T'ing et al., 2020; Manaf et al., 2009; Sarigiannis et al., 2021). Overall, customers must adjust their attitudes towards waste management at home and adapting it as a new social practice (Jayaraman et al., 2019).

CONCLUSION AND RECOMMENDATION

In conclusion, the aim of the research, which is to develop an effective methodology for MCDA towards finding the best suitable alternative to treat EOL of the paper product, has been accomplished. The developed methodology focuses on evaluating and choosing the EOL options based on their compliance with all applicable criteria and considering the decision-maker's preferences. The methodology and AHP-based software were successfully developed using Microsoft Excel, and the AHP method is employed as the MCDA method of choice. This methodology had been validated by using a case study technique with various types of paper products. The judgments were delivered as a single decision-maker result, reflecting the OEM because of the easy nature of the product. The findings of the developed methodology indicate that recycling is the most preferred choice for almost all types of paper products due to the type of raw material used to manufacture the product.

However, some other products, especially polluted paper, may only be suitable for other techniques, including incineration. Nevertheless, to enhance the developed methodology, it is proposed that a group of decision-makers analyses the software to provide wider acceptability of decisions based on their preferences, and the outcome of the assessment will be more reliable. Furthermore, the software should be improved by removing values by adding the coding for the delete button to make it more user-friendly. Moreover, certain complex items require more parameters to be analysed, so it is crucial to enhance the coding to provide more than four criteria. Lastly, it can be seen that the major improvements involve the coding in Excel, which indicates that the improvement of GUI was needed to make the GUI easier and more user-friendly.

ACKNOWLEDGEMENT

The authors would like to thank the Ministry of Higher Education (MoHE), Universiti Tun Hussein Onn Malaysia and Universiti Teknologi Malaysia for funding this research work through the Collaborative Research Grant funding number K263.

REFERENCE

- Abadi, S., Huda, M., Basiron, B., Ihwani, S. S., Jasmi, K. A., Hehsan, A., Safar, J., Mohamed, A. K., Embong, W. H. W., Mohamad, A. M., Noor, S. S. M., Novita, D., Maselena, A., Irviani, R., Idris, M., & Muslihudin, M. (2018). Implementation of fuzzy analytical hierarchy process on notebook selection. *International Journal of Engineering and Technology*, 7(1), 238-243. <https://doi.org/10.14419/IJET.V7I2.27.12047>
- Achillas, C., Moussiopoulos, N., Karagiannidis, A., Baniyas, G., & Perkoulidis, G. (2013). The use of multi-criteria decision analysis to tackle waste management problems: A literature review. *Waste Management & Research*, 31(2), 115-129.

- Ahmad, S., Wong, K. Y., Tseng, M. L., & Wong, W. P. (2018). Sustainable product design and development: A review of tools, applications and research prospects. *Resources, Conservation and Recycling*, 132, 49-61. <https://doi.org/10.1016/j.resconrec.2018.01.020>
- Ahmadi, M. (2017). Evaluating the performance of 3Rs waste practices: Case study-region one municipality of Tehran. *Advances in Recycling and Waste Management*, 2(130), 1-6. <https://doi.org/10.4172/2475-7675.1000130>
- Ahmed, S., Ahmed, S., Shumon, M. R. H., Falatoonitoosi, E., & Quader, M. A. (2016). A comparative decision-making model for sustainable end-of-life vehicle management alternative selection using AHP and extent analysis method on fuzzy AHP. *International Journal of Sustainable Development & World Ecology*, 23(1), 83-97. <https://doi.org/10.1080/13504509.2015.1062814>
- Almanaseer, N., Abbassi, B., Dunlop, C., Friesen, K., & Nestico-Semianiw, E. (2020). Multi-criteria analysis of waste-to-energy technologies in developed and developing countries. *Environmental Research, Engineering and Management*, 76(1), 32-43. <https://doi.org/10.5755/j01.erem.76.1.25254>
- Arifin, M. H., Kayode, J. S., Ismail, M. K. I., Abdullah, A. M., Embrandiri, A., Nazer, N. S. M., & Azmi, A. (2021). Environmental hazard assessment of industrial and municipal waste materials with the applications of RES2-D method and 3-D Oasis Montaj modeling: A case study at Kepong, Kuala Lumpur, Peninsula Malaysia. *Journal of Hazardous Materials*, 406, Article 124282. <https://doi.org/10.1016/j.jhazmat.2020.124282>
- Arikan, E., Şimşit-Kalender, Z. T., & Vayvay, Ö. (2017). Solid waste disposal methodology selection using multi-criteria decision making methods and an application in Turkey. *Journal of Cleaner Production*, 142, 403-412. <https://doi.org/10.1016/j.jclepro.2015.10.054>
- Assi, A., Bilo, F., Zanoletti, A., Ponti, J., Valsesia, A., La Spina, R., Zacco, A., & Bontempi, E. (2020). Zero-waste approach in municipal solid waste incineration: Reuse of bottom ash to stabilize fly ash. *Journal of Cleaner Production*, 245, Article 118779. <https://doi.org/10.1016/j.jclepro.2019.118779>
- Badgie, D., Samah, M. A. A., Manaf, L. A., & Muda, A. (2012). Assessment of municipal solid waste composition in Malaysia: Management, practice, and challenges. *Polish Journal of Environmental Studies*, 21(3), 539-547.
- Badi, I., Abdulshahed, A., Shetwan, A., & Eltayeb, W. (2019). Evaluation of solid waste treatment methods in Libya by using the analytic hierarchy process. *Decision Making: Applications in Management and Engineering*, 2(2), 19-35. <https://doi.org/10.31181/dmame1902038b>
- Büyüközkan, G., & Gocer, F. (2017). An intuitionistic fuzzy MCDM approach for effective hazardous waste management. In *Intelligence systems in environmental management: Theory and applications* (pp. 21-40). Springer.
- Coban, A., Ertis, I. F., & Cavdaroglu, N. A. (2018). Municipal solid waste management via multi-criteria decision making methods: A case study in Istanbul, Turkey. *Journal of Cleaner Production*, 180, 159-167. <https://doi.org/10.1016/j.jclepro.2018.01.130>
- Coelho, L. M. G., Lange, L. C., & Coelho, H. M. (2017). Multi-criteria decision making to support waste management: A critical review of current practices and methods. *Waste Management & Research*, 35(1), 3-28.

- Colapinto, C., Jayaraman, R., Abdelaziz, F. B., & La Torre, D. (2019). Environmental sustainability and multifaceted development: Multi-criteria decision models with applications. *Annals of Operations Research*, 293, 405-432. <https://doi.org/10.1007/s10479-019-03403-y>
- Commission, E. (2008). *Directive 2008/98/EC on waste (Waste Framework Directive)*. European Commission.
- Das, S., Lee, S. H., Kumar, P., Kim, K. H., Lee, S. S., & Bhattacharya, S. S. (2019). Solid waste management: Scope and the challenge of sustainability. *Journal of Cleaner Production*, 228, 658-678. <https://doi.org/10.1016/j.jclepro.2019.04.323>
- Dong, J., Tang, Y., Nzihou, A., Chi, Y., Weiss-Hortala, E., Ni, M., & Zhou, Z. (2018). Comparison of waste-to-energy technologies of gasification and incineration using life cycle assessment: Case studies in Finland, France and China. *Journal of Cleaner Production*, 203, 287-300. <https://doi.org/10.1016/j.jclepro.2018.08.139>
- Dos Santos, P. H., Neves, S. M., Sant'Anna, D. O., Oliveira, C. H. d., & Carvalho, H. D. (2019). The analytic hierarchy process supporting decision making for sustainable development: An overview of applications. *Journal of Cleaner Production*, 212, 119-138. <https://doi.org/10.1016/j.jclepro.2018.11.270>
- Gehin, A., Zwolinski, P., & Brissaud, D. (2008). A tool to implement sustainable end-of-life strategies in the product development phase. *Journal of Cleaner Production*, 16(5), 566-576. <https://doi.org/10.1016/j.jclepro.2007.02.012>
- Ghazalli, Z., & Murata, A. (2011). Development of an AHP-CBR evaluation system for remanufacturing: End-of-life selection strategy. *International Journal of Sustainable Engineering*, 4(01), 2-15. <https://doi.org/10.1080/19397038.2010.528848>
- Ibrahim, T. N. T., Mahmood, N. Z., & Othman, F. (2017). Estimation of leachate generation from MSW landfills in Selangor. *Environmental Science*, 19(1), 43-48.
- Ismail, H., & Hanafiah, M. M. (2017). Management of end-of-life electrical and electronic products: The challenges and the potential solutions for management enhancement in developing countries context. *Acta Scientifica Malaysia (ASM)*, 1(2), 5-8. <https://doi.org/10.26480/asm.02.2017.05.08>
- Jayaraman, K., Vejayon, S., Raman, S., & Mostafiz, I. (2019). The proposed e-waste management model from the conviction of individual laptop disposal practices-An empirical study in Malaysia. *Journal of Cleaner Production*, 208, 688-696. <https://doi.org/10.1016/j.jclepro.2018.10.125>
- Jereme, I. A., Alam, M. M., & Siwar, C. (2015). Waste recycling in Malaysia: Transition from developing to developed country. *Indian Journal of Education and Information Management*, 4(1), 1-14.
- Jiran, N. S., Gholami, H., Mahmood, S., Mat Saman, M. Z., Yusof, N. M., Draskovic, V., & Jovovic, R. (2019). Application of activity-based costing in estimating the costs of manufacturing process. *Transformations in Business & Economics*, 18(2B), 839-860.
- Joshi, G., Naithani, S., Varshney, V. K., Bisht, S. S., & Rana, V. (2017). Potential use of waste paper for the synthesis of cyanoethyl cellulose: A cleaner production approach towards sustainable environment management. *Journal of Cleaner Production*, 142, 3759-3768. <https://doi.org/10.1016/j.jclepro.2016.10.089>

- Kalana, J. A. (2010). Electrical and electronic waste management practice by households in Shah Alam, Selangor, Malaysia. *International Journal of Environmental Sciences*, 1(2), 63-75.
- Kathirvale, S., Yunus, M. N. M., Sopian, K., & Samsuddin, A. H. (2004). Energy potential from municipal solid waste in Malaysia. *Renewable Energy*, 29(4), 559-567. <https://doi.org/10.1016/J.RENENE.2003.09.003>
- Kharat, M. G., Murthy, S., Kamble, S. J., Raut, R. D., Kamble, S. S., & Kharat, M. G. (2019). Fuzzy multi-criteria decision analysis for environmentally conscious solid waste treatment and disposal technology selection. *Technology in Society*, 57, 20-29. <https://doi.org/10.1016/j.techsoc.2018.12.005>
- Kumar, A., & Samadder, S. R. (2017). A review on technological options of waste to energy for effective management of municipal solid waste. *Waste Management*, 69, 407-422. <https://doi.org/10.1016/j.wasman.2017.08.046>
- Lim, R. (2018, September 9). Green way to manage waste. *The Star*. <https://www.thestar.com.my/news/nation/2018/09/09/green-ways-to-manage-wasteswcorp-goes-for-green-technology-and-educating-the-young/>.
- Liu, C., Hotta, Y., & Totoki, Y. (2017). *State of 3Rs in Asia and the Pacific country report: Malaysia*. United Nations Centre for Regional Development
- Mah, C. M., Fujiwara, T., & Ho, C. S. (2018). Life cycle assessment and life cycle costing toward eco-efficiency concrete waste management in Malaysia. *Journal of Cleaner Production*, 172, 3415-3427. <https://doi.org/10.1016/j.jclepro.2017.11.200>
- Mahmood, S., Hardan, M. N., Samat, M. K., Jiran, N. S., & Shaari, M. F. (2019). Ergonomic posture assessment of butchers: A small enterprise study in malaysia food industry. *Jurnal Teknologi*, 81(6), 89-102. <https://doi.org/10.11113/JT.V81.13615>
- Mamat, T. N. A., Saman, M. Z. M., Sharif, S., Simic, V., & Wahab, D. A. (2018). Development of a performance evaluation tool for end-of-life vehicle management system implementation using the analytic hierarchy process. *Waste Management & Research*, 36(12), 1210-1222.
- Manaf, L. A., Samah, M. A. A., & Zukki, N. I. M. (2009). Municipal solid waste management in Malaysia: Practices and challenges. *Waste Management*, 29(11), 2902-2906. <https://doi.org/10.1016/j.wasman.2008.07.015>
- Matsakas, L., Gao, Q., Jansson, S., Rova, U., & Christakopoulos, P. (2017). Green conversion of municipal solid wastes into fuels and chemicals. *Electronic Journal of Biotechnology*, 26, 69-83. <https://doi.org/10.1016/j.ejbt.2017.01.004>
- Moh, Y., & Manaf, L. A. (2017). Solid waste management transformation and future challenges of source separation and recycling practice in Malaysia. *Resources, Conservation and Recycling*, 116, 1-14. <https://doi.org/10.1016/j.resconrec.2016.09.012>
- Nation, U. (2019). *The Sustainable Development Goals Report 2019*. United Nations.
- Ongondo, F. O., Williams, I. D., & Cherrett, T. J. (2011). How are WEEE doing? A global review of the management of electrical and electronic wastes. *Waste Management*, 31(4), 714-730. <https://doi.org/10.1016/j.wasman.2010.10.023>

- Qazi, W. A., Abushammala, M. F., & Azam, M. H. (2018). Multi-criteria decision analysis of waste-to-energy technologies for municipal solid waste management in Sultanate of Oman. *Waste Management & Research*, 36(7), 594-605. <https://doi.org/10.1177/0734242X18777800>
- Rahman, N. I. A., Khoiry, M. A., Rahim, S., & Basri, N. E. A. (2020). Review on current municipal solid waste management in Malaysia. *International Journal of Disaster Recovery and Business Continuity*, 11(1), 2229-2242.
- Randazzo, L., Cusumano, A., Oliveri, G., Di Stefano, P., Renda, P., Perricone, M., & Zarcone, G. (2018). Landfill site selection for municipal solid waste by using AHP method in GIS environment: Waste management decision-support in Sicily (Italy). *Detritus*, 2(1), 78-88. <https://doi.org/10.31025/2611-4135/2018.13656>
- Saaty, T. L. (2008). Decision making with the analytic hierarchy process. *International Journal of Services Sciences*, 1(1), 83-98. <https://doi.org/10.1504/IJSSCI.2008.017590>
- Samad, N. A. F. A., Jamin, N. A., & Saleh, S. (2017). Torrefaction of municipal solid waste in Malaysia. *Energy Procedia*, 138, 313-318. <https://doi.org/https://doi.org/10.1016/j.egypro.2017.10.106>
- Saraiva, A. B., Pacheco, E. B., Gomes, G. M., Visconte, L. L., Bernardo, C., Simões, C. L., & Soares, A. G. (2016). Comparative lifecycle assessment of mango packaging made from a polyethylene/natural fiber-composite and from cardboard material. *Journal of Cleaner Production*, 139, 1168-1180. <https://doi.org/10.1016/J.JCLEPRO.2016.08.135>
- Sarigiannis, D. A., Handakas, E. J., Karakitsios, S. P., & Gotti, A. (2021). Life cycle assessment of municipal waste management options. *Environmental Research*, 193, Article 110307. <https://doi.org/10.1016/j.envres.2020.110307>
- Schwenk, W. S., Donovan, T. M., Keeton, W. S., & Nunery, J. S. (2012). Carbon storage, timber production, and biodiversity: Comparing ecosystem services with multi-criteria decision analysis. *Ecological Applications*, 22(5), 1612-1627.
- Sekhon, P. S., & Karthigesu, I. T. (2017). Awareness on health and safety among municipal workers on solid waste collections: A case study in Malaysia. *Malaysian Journal of Public Health Medicine*, 9, 19-27.
- Subramanian, N., & Ramanathan, R. (2012). A review of applications of analytic hierarchy process in operations management. *International Journal of Production Economics*, 138(2), 215-241. <https://doi.org/https://doi.org/10.1016/j.ijpe.2012.03.036>
- T'ing, L. C., Moorthy, K., Mei, C. Y., Yin, F. P., Ying, W. Z., Khong, C. W., Chern, G. Z., & Lin, T. Z. (2020). Determinants of 3Rs behaviour in plastic usage: A study among Malaysians. *Heliyon*, 6(12), 1-11. <https://doi.org/10.1016/j.heliyon.2020.e05805>
- Torkayesh, A. E., Malmir, B., & Asadabadi, M. R. (2021). Sustainable waste disposal technology selection: The stratified best-worst multi-criteria decision-making method. *Waste Management*, 122, 100-112. <https://doi.org/10.1016/j.wasman.2020.12.040>
- Torkayesh, S. E., Amiri, A., Iranizad, A., & Torkayesh, A. E. (2020). Entropy based EDAS decision making model for neighborhood selection: A case study in Istanbul. *Journal of Industrial Engineering and Decision Making*, 1(1), 1-11. <https://doi.org/10.31181/jiedm200101001t>

- van Ewijk, S., Stegemann, J. A., & Ekins, P. (2017). Global life cycle paper flows, recycling metrics, and material efficiency. *Journal of Industrial Ecology*, 22(4), 686-693. <https://doi.org/10.1111/jiec.12613>
- Vlachokostas, C., Michailidou, A. V., & Achillas, C. (2021). Multi-criteria decision analysis towards promoting waste-to-energy management strategies: A critical review. *Renewable and Sustainable Energy Reviews*, 138, Article 110563. <https://doi.org/10.1016/j.rser.2020.110563>
- Vukoje, M., & Rožić, M. (2018). Various valorisation routes of paper intended for recycling - A Review. *Cellulose Chemistry and Technology*, 52(7-8), 515-541.
- Wong, Y. C., Al-Obaidi, K. M., & Mahyuddin, N. (2018). Recycling of end-of-life vehicles (ELVs) for building products: Concept of processing framework from automotive to construction industries in Malaysia. *Journal of Cleaner Production*, 190, 285-302. <https://doi.org/10.1016/j.jclepro.2018.04.145>
- Yadav, V., Kalbar, P. P., Karmakar, S., & Dikshit, A. (2020). A two-stage multi-attribute decision-making model for selecting appropriate locations of waste transfer stations in urban centers. *Waste Management*, 114, 80-88. <https://doi.org/10.1016/j.wasman.2020.05.024>
- Zainu, Z. A., & Songip, A. R. (2017). Policies, challenges and strategies for municipal waste management in Malaysia. *Journal of Science, Technology and Innovation Policy*, 3(1), 10-14. <https://doi.org/10.11113/jostip.v3n1.18>

Reduction of the Backing Gas Sequence as a Facile Method to Improve Corrosion Resistance in Duplex Stainless Steel (DSS) Weldment

Basuki Tri Laksono¹, Hendri Budi Kurniyanto^{2*}, Purwa Sadewa² and Riza Wirawan¹

¹Faculty of Mechanical and Aerospace Engineering, Institut Teknologi Bandung, Jalan Ganesa No. 10 Bandung 40132, Indonesia

²Welding Engineering Department, Shipbuilding Institute of Polytechnic Surabaya, Jalan Teknik Kimia ITS Sukolilo Surabaya 60111, Indonesia

ABSTRACT

Duplex stainless steel (DSS) is an important material used for corrosion resistance in various harsh environment plants such as petrochemical, offshore subsea component, and other chemical industries. An approximately equal amount of austenite and ferrite (A/F) ratio grants good mechanical properties and rust protection on. The detrimental intermetallic phase frequently occurs due to an unbalanced A/F ratio caused by the welding's thermal cycle. Backing gas is commonly applicable in the field combined Gas Tungsten Arc Welding (GTAW) process. However, the use of backing gas to complete a single weld from root to cap joint required huge additional costs for consumables. Maintaining the thermal cycle in the welding parameter and GTAW process with ER2209 filler metal for DSS below 10 mm thick can reduce the backing gas sequence. The research aims to efficiently substitute full backing gas consumption, which meets a desirable quality in terms of corrosion resistance. The effect of backing gas reduction was studied. All specimens

were tested by visual, Vickers microhardness, metallography, ferrite content measurement, and electrochemical corrosion test. The visual test shows no defects beyond the range of the ASME IX acceptance and criteria. The evaluation comes from the ferrite scope and electrochemical corrosion test. The backing gas on the root weld shows a balance A/F ratio of around 38% ferrite content accepted in various standards. The

ARTICLE INFO

Article history:

Received: 07 May 2021

Accepted: 22 August 2021

Published: 28 October 2021

DOI: <https://doi.org/10.47836/pjst.29.4.41>

E-mail addresses:

basukitriaksono@gmail.com (Basuki Tri Laksono)

hendribudi@ppns.ac.id (Hendri Budi Kurniyanto)

purwasdw@gmail.com (Purwa Sadewa)

riza.wirawan@itb.ac.id (Riza Wirawan)

* Corresponding author

backing gas sequence on the root until filler-pass obtained 0.04 mm/year, which is the desirable corrosion resistance and met the requirement of ASTM A932.

Keywords: Backing gas, corrosion resistance, detrimental intermetallic phase, duplex stainless steel, GTAW

INTRODUCTION

Due to their lightweight and long life-cycle, Duplex Stainless Steel is commonly used in oil and gas plants, construction, petrochemical, and others chemical industries. The local microstructure of DSS is heavily influenced by the fabrication process, especially the welding process (Bhattacharya & Singh, 2007; Chen & Yang, 2002). During multipass welding, the microstructure of DSS can transform to the detrimental phase, such as chromium nitride precipitation and secondary austenite formation, leading to significant unbalanced the austenite-to-ferrite (A/F) ratios (Badji et al., 2008; Chan & Tjong, 2014; Liou et al., 2002; Varbai et al., 2019; Zhang et al., 2016). As a result, the DSS acquires a dual microstructure consisting of an approximately equal volume fraction of α -ferrite and γ -austenite phases. However, the unequal A/F ratio is frequently encountered due to heat input and reheat cycles, decreasing ductility, toughness, and corrosion resistance (Varbai et al., 2019; Verma & Taiwade, 2017; Wang et al., 2011). Moreover, the DSS may become more prone to stress corrosion cracking in the presence of high temperature, tensile stress, and an aggressive environment (Bhattacharya & Singh, 2007; Verma & Taiwade, 2017).

The A/F ratio is an important factor in the welding of DSS. Several studies have been performed to mitigate the excessive contraction of austenite content in the weld metal. For example, Verma *et al.* (2017) reported that higher austenite composition was obtained during quenching if the welding filler metal had 2% to 4 % more Ni than the base metal. However, researchers tried to replace the filler metal of Ni-based alloy over ER 2209 due to the fluctuation of Ni-based alloy, which can be ten times more expensive (Lippold et al., 1988; Nana & Cortie, 1993). The effect of mixing 2% nitrogen added 98% argon as backing gas for greater than 10 mm thickness, improving the corrosion resistance (Sales et al., 2016). Furthermore, several authors reported utilising nitrogen in the shielding and backing gas, leading to an increase of the austenite formation and lower chromium nitrides in the weld metal microstructure (Baghdadchi et al., 2020; Betini et al., 2019; Gozarganji et al., 2021; Liu et al., 2020; Matsunaga et al., 2013; Muthupandi et al., 2005). In contrast, the unbalance A/F transformation still occurred even with mixing a small percentage of nitrogen in argon for shielding gas or backing gas because the solubility and diffusion kinetics of atomic nitrogen in the solid-state is not in the liquid phase. Thus, the solution to obtain the balance A/F phase transformation governed by thermal exposures can control the welding parameters such as the subsequent cooling rate, proper filler metal selection, and maintaining heat input (Varbai et al., 2019). The correct thermal setting of duplex stainless

steel eliminates these detrimental phases. Rapid cooling during the thermal exposures in the temperature range 320 to 955°C provides the maximum resistance to the formation of detrimental phases by subsequent thermal exposures (Geng et al., 2015; Ramkumar et al., 2015).

Although many studies on the detrimental phases such as chromium nitride and austenite precipitation in DSS while welding process has been reported (Baghdadchi et al., 2020; Betini et al., 2019; Gozarganji et al., 2021; Karlsson et al., 1995; Lippold & Kotecki, 2005; Liu et al., 2020; Matsunaga et al., 2013; Muthupandi et al., 2005; Ramirez et al., 2003), not much work has been done to simplify the DSS's welding method by reducing backing gas consumption. In this research, the authors simplified its method by varying sequences of backing gas. Generally, the backing gas is served from the start to the end of the welding process, requires much shielding gas consumption (Sales et al., 2016). GTAW is one of the most popular technologies for welding DSS because it produces soundness welds that meet service requirements (Chern et al., 2011; Zhang et al., 2016). Soundness weld means the degree of freedom from defects in the weld, which is found by visual inspection of any exposed welding surface. Geng et al. (2015) found E/ER 2209 with different processes for joining similar and dissimilar DSSs shows better corrosion resistance and mechanical properties. Therefore, the research aimed to use the combination of GTAW and the E/ER 2209 for DSS below 10 mm thick. Reducing the backing gas sequence method can optimally and efficiently substitute full backing gas consumption, costing a desirable quality corrosion resistance standard.

In the present work, the influence of each reduction of the backing gas sequence was further investigated. Special attention was given to the influence of the R-F joint and the R joint on the corrosion resistance and ferrite content. The ferrite content was measured by ferrite-scope, while a light microscope analysed the microstructure of its varying joint. Also, the corrosion rate of the varying joint was evaluated by utilising the electrochemical test.

MATERIAL AND METHODS

The base metal studied in this research was the DSS type 2205; according to ASME section II part C and section IX QW/QB-422, the material can be categorised as SA 240 type 2205 UNS No. S31803, P-No = 10H, Group No = 1.

Table 1
Chemical composition of the DSS type 2205 and ER2209

Type	wt %								
	C	Mn	P	S	Si	Cr	Ni	Mo	N
2205	0.02	0.95	0.02	0.01	0.95	22.00	5.00	3.00	0.18
ER2209	0.013	1.54	0.018	0.007	0.49	22.92	8.61	3.18	0.17

The base metal was machined to 300 mm x 300 mm x 6 mm to form a single V-groove of 60°. The joints were carried out by filler metal of Ø 2.4 mm ER2209. The chemical composition of DSS type 2205 plates and ER2209 were analyzed as given in Table 1.

These specimens were welded using GTAW. The welding was conducted manually on the 1G (flat) welding position with direct current straight polarity and maintained interpass temperature at approximately 150°C. The Ultra-High Purity (UHP) of 99.99% Argon gas served as a shielding gas and backing gas. The backing gas flow path installation of was commenced by sticking aluminium foil and tacked welds, as shown in Figure 1. Once the utilisation sequence of backing gas eliminates each welding layer, it will affect the cooling rate during welding. For example, the R-C joint also accelerates the interpass temperature because backing gas is served to protect the weld pool during welding from the other atom

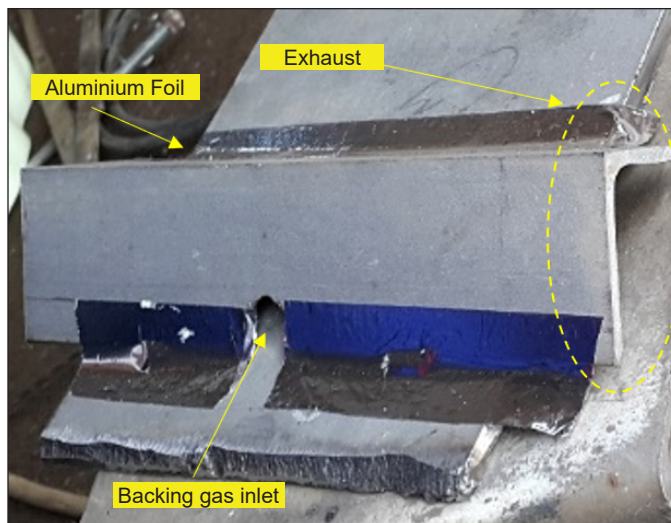


Figure 1. Configuration of backing gas flow path

Table 2
Welding parameter

ID	Weld pass	Weld run	Current (A)	Voltage (V)	Travel speed (mm/min)	Heat input (kJ/mm)	Flow rate (l/min)	
							Backing gas	Shielding gas
R-C	1	Root	95 - 110	9 - 10	65 - 75	0.9 - 1.0	10 - 15	10 - 15
	2	Fill	110 - 120	11 - 12	75 - 90	0.9 - 1.0	10 - 15	10 - 15
	3	Cap	120 - 130	11 - 12	65 - 75	1.0 - 1.3	10 - 15	10 - 15
R-F	1	Root	95 - 110	9 - 10	65 - 75	0.9 - 1.0	10 - 15	10 - 15
	2	Fill	110 - 120	11 - 12	75 - 90	0.9 - 1.0	10 - 15	10 - 15
	3	Cap	120 - 130	11 - 12	65 - 75	1.0 - 1.3	-	10 - 15
R	1	Root	95 - 110	9 - 10	65 - 75	0.9 - 1.0	10 - 15	10 - 15
	2	Fill	110 - 120	11 - 12	75 - 90	0.9 - 1.0	-	10 - 15
	3	Cap	120 - 130	11 - 12	65 - 75	1.0 - 1.3	-	10 - 15

being dissolved and contributes to relieving the specimen’s heat energy during welding.

As shown in Figure 2, the research variable was commenced by the varying sequence of backing gas. First, the R-C joint (root pass – capping) entirely served backing gas. Furthermore, the R-F joint (root pass–fill pass) defined backing gas limited from root pass until fill pass. Lastly, the R joint was only applying backing gas at the root pass. The welding parameter shows in Table 2.

All welds were inspected by non-destructive visual examination by following the criteria of ASME section IX QW-144 and QW-194. The visual inspection equipment was a welding gauge type Cambridge and digital vinier calliper to measure the dimension of weldment profile. Visual was only using a naked eye with a flashlight with minimum 1000 lux light intensity. According to the interpretation and evaluation of visual testing, there was no discontinuity exceeding the applicable code. All specimens were cut and prepared into the cross-section of the welds. Hereinafter, the cross-section degreased in chlorinated solvents abrades with SiC paper 180 grits to removed burrs. After that, the cross-section of welds was ground to 240, 320, 500, 800, 1000, 1500, 2000, and 5000 grit by SiC paper usage. Once grinding was completed, specimens were polished using 0.05 µm sol-gel alumina suspension according to the standard metallographic technique for

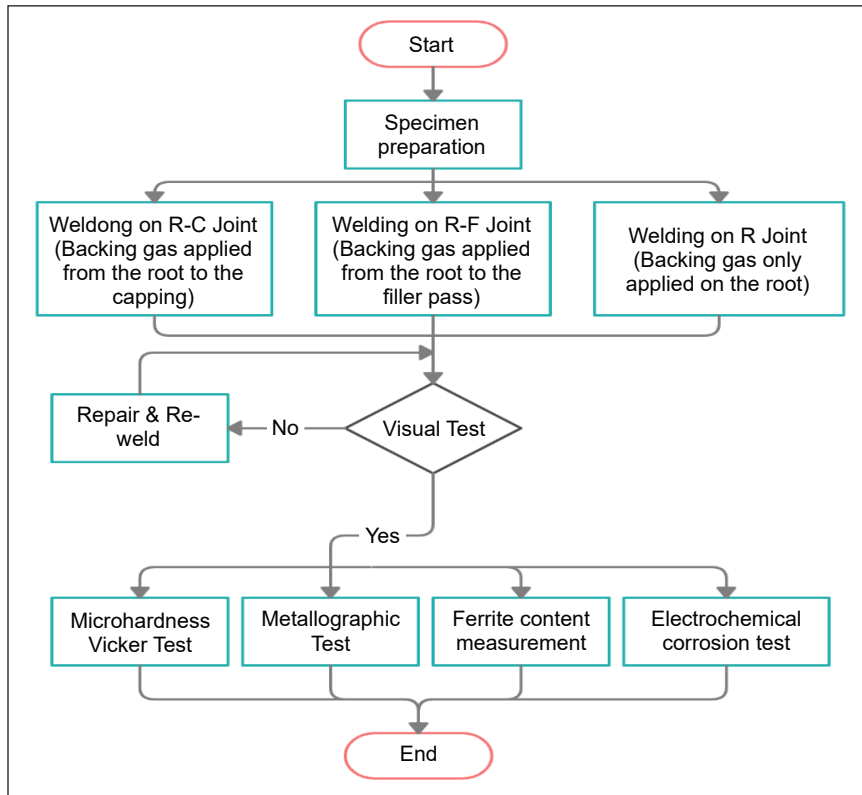


Figure 2. Research flowchart

etched conditions. The electrolytic etching was performed by creating a solution of 100 ml H₂O, added 10-gram C₂H₂O₄ (*Oxalic Acid*). Hereinafter, the cross-section of weld joints was electrised 12 *Voltage 3 Ampere* using the direct current power supply for detecting detrimental intermetallic phases.

The metallographic examination of crystal structure was executed in the light microscope with 200x magnification. The ferrite content measurement was performed by ferrite scope, which took a sample from the capping layer, filler pass, and root pass of the varying weld joints. The Hardness Vickers (HV) testing with a load of 5 *kgf* was examined on the cross-section of the weldment, which took 18 of HV's indentation per the varying joints. The HV's indentation was taken from Heat Affected Zone (HAZ), Base Metal (BM), and Weld Metal (WM). The corrosion rates of the research experiment were determined in the electrochemical measurement according to ASTM G102, which was performed by three cell electro system at the scanning rate of 1 mV/s with a mixed solution of 5 *Liter* water and 3.5% HCL. Autolab PGSTAT302N was the instrument being used to conduct linear polarisation. The electrodes include work electrode, which is made from all variants of weldment; reference electrode made from Silver/ Silver Chloride (Ag/AgCl); and counter electrode from Platinum (Pt). According to the ASTM G102 standard (ASTM G102-89(2015)e1, 2015), this research use Faraday's law to calculate the corrosion rate the form Penetration Rate (CR) in units of (mm/year), as expressed in Equation 1:

$$CR = K_1 \left(\frac{i_{corr}}{\rho} \right) EW \quad (1)$$

Where,

CR define *Corrosion Rate* in (mm/year)

I_{corr} is density of the corrosion current ($\mu\text{A}/\text{cm}^2$)

$K_1 = 3.27 \times 10^{-3}$, (mm g/ μA cm year)

ρ is density of the material in (g/cm^3)

Furthermore, EW means equivalent weight or the amount of metal mass that will be oxidised when getting an electric charge of one Faraday. Therefore, EW can be expressed in Equation 2:

$$EW = \frac{1}{Q} \quad (2)$$

The Q value for a material consisting of several elements is calculated based on the formula as shown in Equation 3:

$$Q = \sum \frac{n_i f_i}{W_i} \quad (3)$$

Where,

n is the number of valence electrons of the constituent elements of the metal alloy

f is the mass fraction of the constituent elements of the metal alloy

W is the atomic weight of the alloying elements

The metal constituents used to calculate Q are elements with a mass fraction greater than 1%. Therefore, in accordance with the test results of the DSS type 2205 specimen's material composition, we only use the element Fe to calculate Q .

The calculation of corrosion rate was conducted automatically by NOVA software. The parameters were density of Fe at 7.8 gram/cm³ and EW valued at 55.84 gram/mol. The execution of the electrochemical test began with the dimensional measurement of the sample using a vernier calliper and calculated the area, and then connected the instrument to the electrodes. Hereinafter, created the mixing solution and soaked the electrodes in this mixing solution for 55 minutes. Next, measure the potential value using the AVO meter toward the reference electrode. The value indicates the free corrosion potential (E_{corr}). Then, they turned on the instrument, adjusted the voltage until the potential metal value was shown 50mV below E_{corr} . Finally, NOVA software will automatically calculate the corrosion rate. Repeat all the steps for all variants of a specimen.

RESULT AND DISCUSSION

Effect of Reduction of Backing Gas Sequence on Microstructure

The etching process is applied to the cross-section of weldments that will emerge from the weld zone. Hereinafter, examination conducts in the light microscope with 200x magnification. The microstructure of the 2205 base metal observed that morphology consists of two phases: the ferrite in dark grey colour and the austenite in white grey, as presented in Figure 3.

According to the Fe-Cr-Ni ternary alloy phase diagrams, the 2205 DSS comprises δ -ferrite when cooled from the solidification point to 1200°C. Following a high cooling rate from 1200 to 800°C, austenite (γ -phase) is precipitated from the ferrite's grain boundary (δ -phase). The nucleated austenite evolves into flakes and grows as Widmanstätten plates into the δ -ferrite grains (Kordatos et al., 2001; Wu et al., 2017). The morphology appearance of 2205 base metal is a clear boundary in the elongated and white-grey austenite distributed into the ferrite matrix. The phase fraction is composed in equal amounts and distributed uniformly along the rolling direction. All of the varying weld joints indicated no influence on the excessive evolution of austenite to ferrite fraction in the base metal during the welding process caused by the reduction of backing gas.

The microstructure of the fusion zone presents the coarser microstructure and columnar grains, as shown in Figure 4. The DSS weld's epitaxial and competitive ferrite grain growth promotes a coarse and columnar ferrite grain structure (Lippold & Kotecki, 2005). The ferrite phase in Figures 4 (a) and 4(b) is presented in columnar grains. The austenite phase

nucleated at the ferrite grain boundaries and formed a continuous distributed network. A fraction of this newly transformed ferrite is retained upon rapid cooling triggered by full backing gas usage. Thus, the ferrite-to-austenite transformation is incomplete—a smaller austenite fraction results in the R-C weld pass deposit area. Since a portion of the original austenite fraction has transformed and retained as ferrite fraction, the austenite fraction in the R-C weld pass was decreased, as shown in Figures 4(a) and 4(b). However, the high

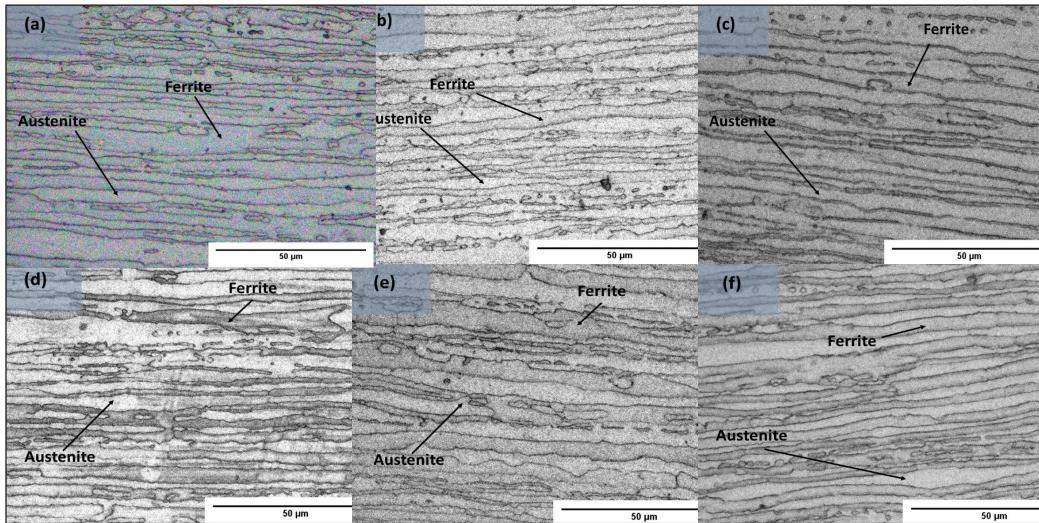


Figure 3. Base metal microstructure of weld joints #1 and #2: (a) (b) represent an R-C joint, (c) (d) define an R-F joint, and (e) (f) is an R joint. The ferrite phase is in dark-grey, and austenite is in white-grey

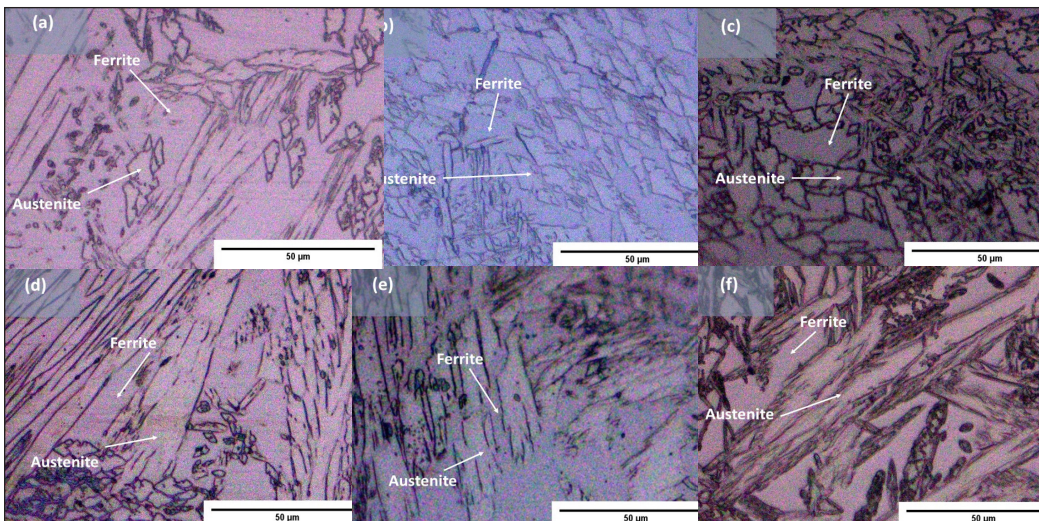


Figure 4. Weld microstructure of weld joints #1 and #2: (a) (b) represent an R-C joint, (c) (d) define an R-F joint, and (e) (f) is an R joint. The ferrite phase is in dark grey, and austenite is in white grey

austenite microstructure obtained in Figures 4(c), 4(d), 4(e), and 4(f) while backing gas sequence being reduced. Due to the effect on the weld thermal cycle, the weld heat input has been shown to have a significant influence on the microstructure. In contrast, high heat input (low cooling rate) prevents excessive ferrite grain growth in these weld regions. The multipass welding simulations in this experiment showed that solid-state reheating of as-welded microstructures would increase austenite fraction in the weld metal. Thus, using reduction of the backing gas sequence shows the lower cooling rate, which is resulted in an increasing austenite fraction in the HAZ because there was more time for nitrogen diffusion during the solid-state ferrite-to-austenite phase transformations (Gozarganji et al., 2021; Kordatos et al., 2001; Varbai et al., 2019).

Effect of Controlling Thermal Cycle on Austenite/ Ferrite Ratio

The emergence of the weld zone due to the etching process will aid to determine the ferrite content measurement spot. The ferrite scope measures six spots per weld joint variation, which spread on the capping, the side weld, and the root. As indicated in the previous microstructure sub-section, the A/F ratio balance in fusion zone microstructures is influenced by the local weld thermal cycle and compositional effects. The weld thermal cycle depends on the cooling rate in the specific transformation temperature range. On the other hand, a good compositional effect relays on the base alloy composition, filler metal composition, and shielding gas composition. Interestingly, Zhang et al. (2016) found that using filler metal ER2209 combined GTAW in the DSS weldment can be an austenite stabiliser, which promotes face-centred cubic structure, resulting in good toughness and pitting resistance. Figure 5 shows the value of ferrite content measurement using the ferrite scope.

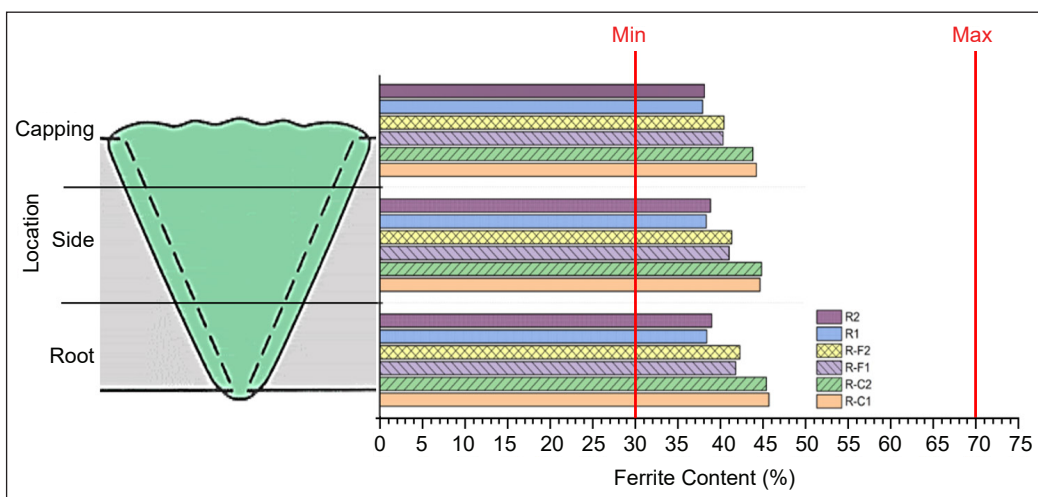


Figure 5. Ferrite content measured in all varying of the weld joint #1 and #2

The R-C weld joint obtains the highest ferrite content than other varying weld joints because a higher cooling rate influenced by utilising backing gas will be decreasing the austenite fraction. In Figure 5 can be understood that reducing of backing gas sequence is significantly affected by ferrite fraction. According to ISO 15156-3, the ferrite content in the fusion welded joint should be within the range of 30% to 70% (ISO 15156-3, 2015). Therefore, ferrite content on all varying weld joints is approximately 38% to 45% which means within in range acceptable standard.

Effect of Cooling Rate on Hardness

HV's indentation has 18 spots per the varying joint with a load of 5 kgf, which spreads the BM, the HAZ, and the WM. Figure 6 presents the microhardness Vickers of weld joint #1 and weld joint #2. Figures 6(a) and 6(b) shows that the microhardness value on the weld metal (WM) of the R-C weld joints is the highest value than of the R-F weld joint and the R weld joint. Varbai et al. (2019) found that the high cooling rate increases the ferrite fraction, which provides a high microhardness value. Due to the utilising of backing gas,

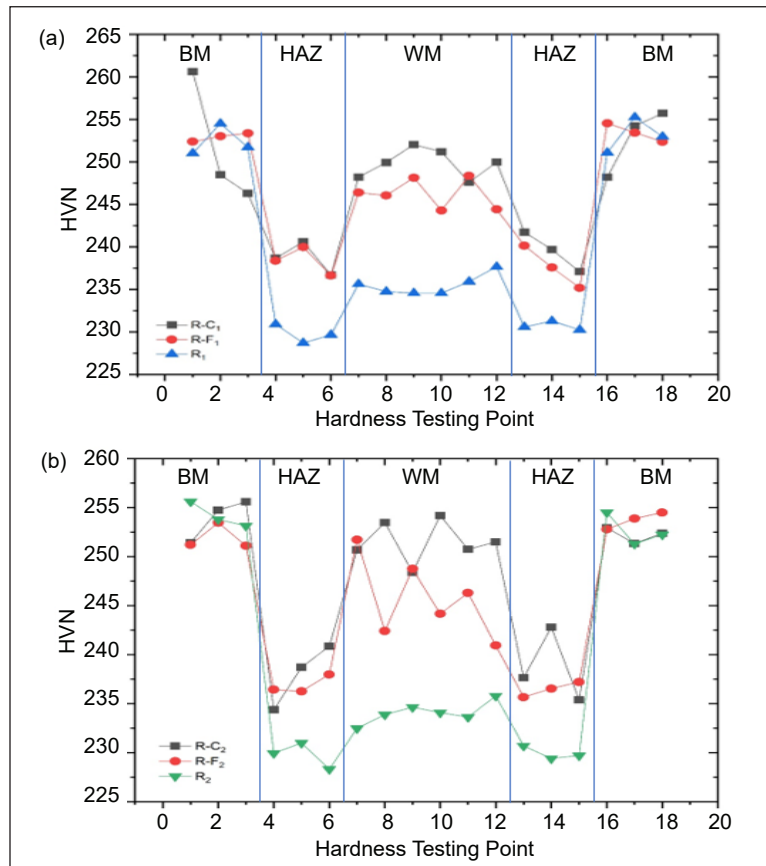


Figure 6. Microhardness Vickers of (a) weld joint #1; (b) weld joint #2

a high cooling rate was obtained, whereas the R-F weld joint and the R weld joint are slightly lower hardness values upon backing gas sequence being reduced. However, the mechanical property of welded 2205 DSS does not vary considerably for normal heat input (0.3 to 2.0 kJ/mm) or a weld metal of ferrite level between 23% and 53% (Giridharan & Murugan, 2009; Hertzman, 2001; Verma & Taiwade, 2017). Accordingly, heat input being applied is around 0.9 to 1.3 kJ/mm in Table 2, and ferrite level acquired about 38% to 45%. As shown in Figure 6, there is no significant effect on microhardness by reducing the backing gas sequence.

Electrochemical Corrosion Resistance

Based on the result of linear polarisation using the Autolab PGSTAT302N and calculated by NOVA software in electrochemical using three cell electrodes, obtains corrosion rate of welded joint with all varying backing gas on the DSS weldment is presented in Table 3.

The highest corrosion resistance value was found in the R-C₂ specimen at 0.012 mm/year, while the lowest was found in the R₁ specimen at 0.062 mm/year. In Figure 5, the R-C weld joint has about 45% of ferrite level, which indicates the highest value over another varying weld joint. The huge amount of ferrite fraction in weldment contributes to better corrosion resistance toward the DSS weldment. The high cooling rate influenced by the backing gas utilisation lets ferrite fraction grow widely, as shown in the R-C weld joint. Consequently, reducing of backing gas sequence gives a slightly decreasing ferrite level in weldment, as shown in Figure 5. In many industrial applications, a ferrite content of 35% to 65% is recommended for optimum corrosion resistance (Lippold & Kotecki, 2005; ISO 15156-3, 2015; Varol et al., 1992; Verma & Taiwade, 2017). According to ASTM A 923, the maximum acceptable corrosion rate is 10 mdd (ASTM A923-14, 2014). The equivalency of 1 mm/year is 250 mdd which means 10 mdd equal to 0.040 mm/year (Charles, 2013). The average corrosion rate of the R weld joint does not pass the maximum acceptable in ASTM A 923. Despite the corrosion rate of the R weld joint is slightly exceeding the maximum value, its ferrite content is about 38% within the recommended range for optimum corrosion

Table 3
Experimental results of electrochemistry

No	Specimen ID	E_{corr} (mV)	i_{corr} ($\mu\text{A}/\text{cm}^2$)	Polarisation resistant ($\text{k}\Omega$)	Corrosion Rate (mm/years)	Average Corrosion Rate (mm/years)
1	R - C ₁	-40.42	3.07	9.02	0.017	0.014
	R - C ₂	29.24	113.03	99.56	0.012	
2	R - F ₁	-2.23	497.09	7.29	0.046	0.040
	R - F ₂	94.13	747.07	36.77	0.034	
3	R ₁	154.85	283.64	133.89	0.062	0.054
	R ₂	-194.78	19.17	4.15	0.047	

resistance. The R weld joint can be applied as long as not in an aggressive environment, but further corrosion protection is needed. Additionally, Conradi et al. (2012) stated that the application of DSS 2205 in many aggressive environments, such as a chloride-ion environment, required to spray a thin polymer coating synthesized from 30-nm and 600-nm silica particles dispersed in polyvinyl chloride (PVC), which is improving corrosion resistance. Reducing the backing gas sequence method can substitute full backing gas consumption in the R-F weld joint because it has approximately 40% ferrite level and corrosion rate acquired 0.040 mm/year.

CONCLUSION

In this paper, the reduction of the backing gas sequence in the 2205 DSS weldment was studied. The influence of the thermal cycle due to the reduction of the backing gas sequence will affect the microstructure, microhardness, and corrosion resistance. The effect of various reductions of the backing gas sequence has been investigated for below 10-mm thick. Combining the GTAW process and ER2209 filler metal provides the soundness welds as represented in the microstructure. Even using the R weld joint was not affected the hardness value because the heat input was applied around 0.9 to 1.3 kJ/mm. By controlling heat input will lead to the balance A/F ratio. Ferrite content acquired about 38% to 45%, which is accepted within the various applicable industrial standard. The R weld joint showed slightly improper corrosion resistance and did not pass ASTM A932 acceptance criteria. However, the R-F weld joint's use improved the sufficient corrosion resistance at 0.04 mm/year, which reached the requirement of ASTM A932. Thus, reducing the backing sequence affects backing gas consumption and costs a desirable quality corrosion resistance with a lower deviation standard.

ACKNOWLEDGEMENT

The authors would like to express their special thanks to Lembaga Pengelola Dana Pendidikan (LPDP) Republik Indonesia, who sponsored this work.

REFERENCES

- ASTM A923-14. (2014). *Standard test methods for detecting detrimental intermetallic phase in duplex austenitic/ferritic stainless steels*. ASTM Internasional.
- ASTM G102-89(2015)e1. (2015). *Standard practice for calculation of corrosion rates and related information from electrochemical measurements*. ASTM Internasional.
- Badji, R., Bouabdallah, M., Bacroix, B., Kahloun, C., Belkessa, B., & Maza, H. (2008). Phase transformation and mechanical behavior in annealed 2205 duplex stainless steel welds. *Materials Characterization*, 59(4), 447-453. <https://doi.org/10.1016/j.matchar.2007.03.004>

- Baghdadchi, A., Hosseini, V. A., Hurtig, K., & Karlsson, L. (2020). Promoting austenite formation in laser welding of duplex stainless steel - Impact of shielding gas and laser reheating. *Welding in the World*, 65, 499-511. <https://doi.org/10.1007/s40194-020-01026-7>
- Betini, E. G., Gomes, M. P., Mucsi, C. S., Orlando, M. T. D. A., Luz, T. D. S., Avettand-Fènoël, M. N., & Rossi, J. L. J. M. R. (2019). Effect of nitrogen addition to shielding gas on cooling rates and in the microstructure of thin sheets of duplex stainless steel welded by pulsed gas tungsten arc welding process. *Materials Research*, 22(Suppl 1), Article e20190247. <https://doi.org/10.1590/1980-5373-mr-2019-0247>
- Bhattacharya, A., & Singh, P. M. (2007). Stress corrosion cracking of welded 2205 duplex stainless steel in sulfide-containing caustic solution. *Journal of Failure Analysis and Prevention*, 7(5), 371-377. <https://doi.org/10.1007/s11668-007-9069-6>
- Chan, K. W., & Tjong, S. C. J. M. (2014). Effect of secondary phase precipitation on the corrosion behavior of duplex stainless steels. *Materials*, 7(7), 5268-5304. <https://doi.org/10.3390/ma7075268>
- Charles, J. (2013). Corrosion resistance properties. In I. Alvarez-Armas & S. Degallaix-Moreuil (Eds.), *Duplex Stainless Steels* (pp. 47-114). John Wiley & Sons, Inc. <https://doi.org/10.1002/9781118557990.ch2>
- Chen, T. H., & Yang, J. R. (2002). Microstructural characterization of simulated heat affected zone in a nitrogen-containing 2205 duplex stainless steel. *Materials Science and Engineering: A*, 338(1-2), 166-181. [https://doi.org/10.1016/S0921-5093\(02\)00065-5](https://doi.org/10.1016/S0921-5093(02)00065-5)
- Chern, T. S., Tseng, K. H., & Tsai, H. L. (2011). Study of the characteristics of duplex stainless steel activated tungsten inert gas welds. *Materials & Design*, 32(1), 255-263. <https://doi.org/10.1016/j.matdes.2010.05.056>
- Conradi, M., Kocijan, A., Zorko, M., & Jerman, I. J. P. i. O. C. (2012). Effect of silica/PVC composite coatings on steel-substrate corrosion protection. *Progress in Organic Coatings*, 75(4), 392-397. <https://doi.org/10.1016/j.porgcoat.2012.07.008>
- Geng, S., Sun, J., Guo, L., & Wang, H. (2015). Evolution of microstructure and corrosion behavior in 2205 duplex stainless steel GTA-welding joint. *Journal of Manufacturing Processes*, 19, 32-37. <https://doi.org/10.1016/j.jmapro.2015.03.009>
- Giridharan, P. K., & Murugan, N. (2009). Optimization of pulsed GTA welding process parameters for the welding of AISI 304L stainless steel sheets. *The International Journal of Advanced Manufacturing Technology*, 40, 478-489. <https://doi.org/10.1007/s00170-008-1373-0>
- Gozarganji, E. H., Farnia, A., & Ebrahimmia, M. (2021). Effect of shielding gas composition on geometry and austenite formation in low power pulsed Nd: YAG laser welded 2205 duplex stainless steel. *Archives of Metallurgy and Materials*, 66, 187-195. <https://doi.org/10.24425/amm.2021.134775>
- Hertzman, S. (2001). The influence of nitrogen on microstructure and properties of highly alloyed stainless steel welds. *ISIJ International*, 41(6), 580-589. <https://doi.org/10.2355/isijinternational.41.580>
- ISO 15156-3. (2015). *Petroleum and natural gas industries - Materials for use in H₂S-containing environments in oil and gas production - Part 3: Cracking-resistant CRAs (corrosion resistant alloys) and other alloys*. ISO.
- Karlsson, L., Pak, S., & Ryen, L. (1995). Precipitation of intermetallic phases in 22% Cr duplex stainless weld metals. *Welding Journal*, 74(1), 28-38.

- Kordatos, J., Fournalaris, G., & Papadimitriou, G. (2001). The effect of cooling rate on the mechanical and corrosion properties of SAF 2205 (UNS 31803) duplex stainless steel welds. *Scripta Materialia*, 44(3), 401-408. [https://doi.org/10.1016/S1359-6462\(00\)00613-8](https://doi.org/10.1016/S1359-6462(00)00613-8)
- Liou, H. Y., Hsieh, R. I., & Tsai, W. T. (2002). Microstructure and pitting corrosion in simulated heat-affected zones of duplex stainless steels. *Materials Chemistry and Physics*, 74(1), 33-42. [https://doi.org/10.1016/S0254-0584\(01\)00409-6](https://doi.org/10.1016/S0254-0584(01)00409-6)
- Lippold, J. C., Baeslack III, W. A., & Varol, I. (1988). Heat-affected zone liquation cracking in austenitic and duplex stainless steels. *Welding Journal*, 71(1), 1s-14s.
- Lippold, J. C., & Kotecki, D. J. (2005). *Welding metallurgy and weldability of stainless steels*. Wiley-VCH.
- Liu, Z., Fan, C. L., Ming, Z., Chen, C., Liu, A., Yang, C. L., Lin, S. B., & Wang, L. P. (2020). Gas metal arc welding of high nitrogen stainless steel with Ar-N₂-O₂ ternary shielding gas. *Defence Technology*, 17(3), 923-931. <https://doi.org/10.1016/j.dt.2020.05.021>
- Matsunaga, H., Sato, Y. S., Kokawa, H., & Kuwana, T. (2013). Effect of nitrogen on corrosion of duplex stainless steel weld metal. *Science and Technology of Welding and Joining*, 3(5), 225-232. <https://doi.org/10.1179/stw.1998.3.5.225>
- Muthupandi, V., Srinivasan, P. B., Shankar, V., Seshadri, S. K., & Sundaresan, S. (2005). Effect of nickel and nitrogen addition on the microstructure and mechanical properties of power beam processed duplex stainless steel (UNS 31803) weld metals. *Materials Letters*, 59(18), 2305-2309. <https://doi.org/10.1016/j.matlet.2005.03.010>
- Nana, S., & Cortie, M. B. (1993). Microstructure and corrosion resistance of experimental low-nickel duplex stainless steels. *Journal of the Southern African Institute of Mining and Metallurgy*, 93(11), 307-315.
- Ramirez, A. J., Lippold, J. C., & Brandi, S. D. (2003). The relationship between chromium nitride and secondary austenite precipitation in duplex stainless steels. *Metallurgical and Materials Transactions A*, 34(8), 1575-1597. <https://doi.org/10.1007/s11661-003-0304-9>
- Ramkumar, K. D., Mishra, D., Raj, B. G., Vignesh, M. K., Thiruvengatam, G., Sudharshan, S. P., Arivazhagan, N., Sivashanmugam, N., & Rabel, A. M. (2015). Effect of optimal weld parameters in the microstructure and mechanical properties of autogeneous gas tungsten arc weldments of super-duplex stainless steel UNS S32750. *Materials & Design (1980-2015)*, 66, 356-365. <https://doi.org/10.1016/j.matdes.2014.10.084>
- Sales, A. M., Westin, E. M., & Colegrove, P. (2016). Effect of nitrogen in backing gas on duplex root weld properties of heavy-walled pipe. *Welding in the World*, 60(5), 877-882. <https://doi.org/10.1007/s40194-016-0347-3>
- Varbai, B., Adonyi, Y., Baumer, R., Pickle, T., Dobranszky, J., & Majlinger, K. (2019). Weldability of duplex stainless steels - Thermal cycle and nitrogen effects. *Welding Journal*, 98(3), 78-87. <https://doi.org/10.29391/2019.98.006>
- Varol, I., Lippold, J. C., & Baeslack, W. A. (1992). Welding of duplex stainless steels. In D. L. Olson & T. H. North (Eds.), *Key Engineering Materials* (Vol. 69, pp. 217-252). Trans Tech Publications Ltd. <https://doi.org/10.4028/www.scientific.net/KEM.69-70.217>

- Verma, J., & Taiwade, R. V. (2017). Effect of welding processes and conditions on the microstructure, mechanical properties and corrosion resistance of duplex stainless steel weldments - A review. *Journal of Manufacturing Processes*, 25, 134-152. <https://doi.org/10.1016/j.jmapro.2016.11.003>
- Wang, S., Ma, Q., & Li, Y. (2011). Characterization of microstructure, mechanical properties and corrosion resistance of dissimilar welded joint between 2205 duplex stainless steel and 16MnR. *Materials & Design*, 32(2), 831-837. <https://doi.org/10.1016/j.matdes.2010.07.012>
- Wu, M., Liu, F., Pu, J., Anderson, N. E., Li, L., & Liu, D. (2017). The microstructure and pitting resistance of weld joints of 2205 duplex stainless steel. *Journal of Materials Engineering and Performance*, 26(11), 5341-5347. <https://doi.org/10.1007/s11665-017-2976-0>
- Zhang, Z., Jing, H., Xu, L., Han, Y., & Zhao, L. (2016). Investigation on microstructure evolution and properties of duplex stainless steel joint multi-pass welded by using different methods. *Materials & Design*, 109, 670-685. <https://doi.org/10.1016/j.matdes.2016.07.110>



Failure Rate Estimation for Transformer Population based on Health Index through Markov Model Approach

Nor Shafiqin Shariffuddin^{1,2}, Norhafiz Azis^{1,3*}, Amran Mohd Selva¹,
Muhammad Sharil Yahaya⁴, Jasronita Jasni¹, Mohd Zainal Abidin Ab Kadir¹
and Mohd Aizam Talib⁵

¹Advanced Lightning, Power and Energy Research Centre (ALPER), Faculty of Engineering, Universiti Putra Malaysia, 43400 UPM, Serdang, Selangor, Malaysia

²Electrical Technology Section, Universiti Kuala Lumpur British Malaysian Institute, 53100 Gombak, Selangor Malaysia

³Institute of Advanced Technology (ITMA), Universiti Putra Malaysia, 43400 UPM, Serdang, Selangor, Malaysia

⁴Faculty of Electrical and Electronic Engineering Technology, Universiti Teknikal Malaysia Melaka, Hang Tuah Jaya, 76100 Durian Tunggal, Melaka, Malaysia

⁵TNB Research Sdn. Bhd., No. 1, Lorong Ayer Itam, Kawasan Institut Penyelidikan, 43000 Kajang, Selangor, Malaysia

ABSTRACT

This work examines the failure rate of the transformer population through the application of the Markov Model (MM) and Health Index (HI). Overall, the condition parameters data extracted from 3,192 oil samples were analysed in this study. The samples were from 370 transformers with the age range between 1 and 25 years. First, both HIs and failure rates of transformers were determined based on the condition parameters data of the oil samples known as Oil Quality Analysis (OQA), Dissolved Gas Analysis (DGA), Furanic Compounds Analysis (FCA) and age. A two-parameter exponential function model was applied to represent the relationship between the HI and failure rate. Once the failure rate state was

obtained, the non-linear optimisation was used to determine the transition probability for each age band. Next, the future failure rate of the transformer population was computed through the MM prediction model. The goodness-of-fit test and Mean Absolute Percentage Error (MAPE) were utilised to determine the performance of the predicted failure rate. The current study reveals that the future state of the transformer population and failure rate could

ARTICLE INFO

Article history:

Received: 09 May 2021

Accepted: 13 August 2021

Published: 28 October 2021

DOI: <https://doi.org/10.47836/pjst.29.4.42>

E-mail addresses:

snorshafiqin@gmail.com (Nor Shafiqin Shariffuddin)

norhafiz@upm.edu.my (Norhafiz Azis)

amranms.88@gmail.com (Amran Mohd Selva)

sharil@utem.edu.my (Muhammad Sharil Yahaya)

jas@upm.edu.my (Jasronita Jasni)

mzk@upm.edu.my (Mohd Zainal Abidin Ab Kadir)

aizam.talib@tnb.com.my (Mohd Aizam Talib)

* Corresponding author

be predicted through MM based on updated transition probabilities. It is observed that the MAPE between predicted and computed failure rates is 7.3%.

Keywords: Condition parameters data, failure rate, health index, Markov model, transformer

INTRODUCTION

One of the most crucial components in the electrical power network is a transformer. It can be subjected to various types of stresses during its operational lifetime. These events could lead to degradation, whereby without mitigation, it could lead to irreparable damages. As the population of in-service transformers are getting old, much attention should be highlighted to its reliability (CIGRE WG A2.18, 2003; Emsley et al., 2000; Lundgaard et al., 2004). Condition assessment is essential to optimise the transformer lifetime by an active maintenance and replacement strategies.

Most utilities have implemented Condition-based management to evaluate the health of transformers. This approach could increase the efficiency of asset management practices, which subsequently reduces the related costs through advanced analysis that acts as a preventive measure against underlying failures (Jahromi et al., 2009). Health Index (HI) is a concept under condition-based management whereby a single measurable index is proposed to classify the condition of a transformer. HI considers multiple condition parameters data and utilises various criteria to determine the ageing condition of transformers, which may not be assessable through individual measurement techniques. HI is computed through a scoring method whereby the condition parameters data are classified through weighting and ranking approaches. Based on HI, the condition is graded into several categories defined by Naderian et al. (2008).

Apart from HI, the failure rate is also one of the important aspects that can be used to analyse the reliability, which can be used to drive the optimal maintenance planning (Jürgensen et al., 2016a). Conventionally, the failure rate can be used to evaluate the effectiveness of maintenance strategies (Jürgensen, 2018). However, due to the long lifetimes of transformers, in-service failures data are quite difficult to be obtained (Zaidey et al., 2015). Many studies such as the proportional hazard model, Bayesian updating scheme and linear interpolation between different inspections outcomes are proposed to estimate the failures data based on the available information (Brown et al., 2018; Jürgensen et al., 2016a; Lindquist et al., 2005). Among the difficulties for failure rate modelling is the limitation of historical failures record (Jürgensen et al., 2018; Lindquist et al., 2005). One of the unique approaches to determine failure rate can be carried out based on the condition of the assets (Jürgensen, 2016). Currently, the study to predict the failure rate of the transformers is still limited. Other studies by Jürgensen (2016) and Jürgensen et al. (2016b) mainly focus on

single time condition parameters data whereby statistical data-driven approaches are used to model the failure rate. Markov model (MM) has been identified as one of the methods used to predict the failure rate of transformers.

MM is a stochastic model whereby the conditional distribution of future states of the process given present and previous states depends only on the present state (memoryless property) (Chatfield, 1973). In principle, MM is used as a model to predict the performance of assets by identifying discrete conditions through utilisation of transition state probability over multiple discrete time intervals, where P_{ij} is the probability of a failure rate to transit from state i to state j within a certain year of interval (McDonald, 2004; Borovkov, 2003). MM is widely implemented in civil engineering for various applications (Edirisinghe et al., 2015; Setunge & Hasan, 2011; Agrawal et al., 2006; Camahan et al., 1987; Micevski et al., 2002). It is also utilised in electrical equipment such as switchgear and transformers (Hoskins et al., 1999; Hamoud, 2011; Hamoud, 2012). Recently, many studies have been carried out to employ the MM to determine the transition probabilities of the transformer population for condition state prediction (Selva et al., 2018; Yahaya et al., 2017).

In this paper, the estimation of the future failure rate for the transformer population-based on HI is carried out by MM. The contribution of this work is the utilisation of MM and HI to predict the future failure rate of the transformer population. First, the HIs and failure rates are computed. Next, the transition probability is obtained, and subsequently, the failure rate prediction is carried out. Finally, the predicted failure rate is compared with the computed failure rate.

METHODS

The model was developed based on oil samples data of 33/11 kV distribution transformers with ages ranging from 1 to 25 years retrieval from one of Malaysia's utilities (Company A, personal communication, November 13, 2016). Oil Quality Analysis (OQA) parameters used in the current study were AC breakdown voltage, acidity, moisture in oil, colour and interfacial tension. The Dissolved Gas Analysis (DGA) included hydrogen (H_2), carbon monoxide (CO), carbon dioxide (CO_2), methane (CH_4), ethane (C_2H_6), ethylene (C_2H_4) and acetylene (C_2H_2). The Furanic Compound Analysis (FCA) consisted of 2-furaldehyde (2FAL), while age was also considered in this case study. The condition parameters data were used to calculate both HI and Individual Failure Rate (IFR). The workflow of this study can be seen in Figure 1.

The HI was computed through the scoring and weighting method utilising the corresponding scales given by Jahromi et al. (2009) and Naderian et al. (2008). Both oil quality and dissolved gasses factors were determined based on Equation 1 (Jahromi et al., 2009; Naderian et al., 2008):

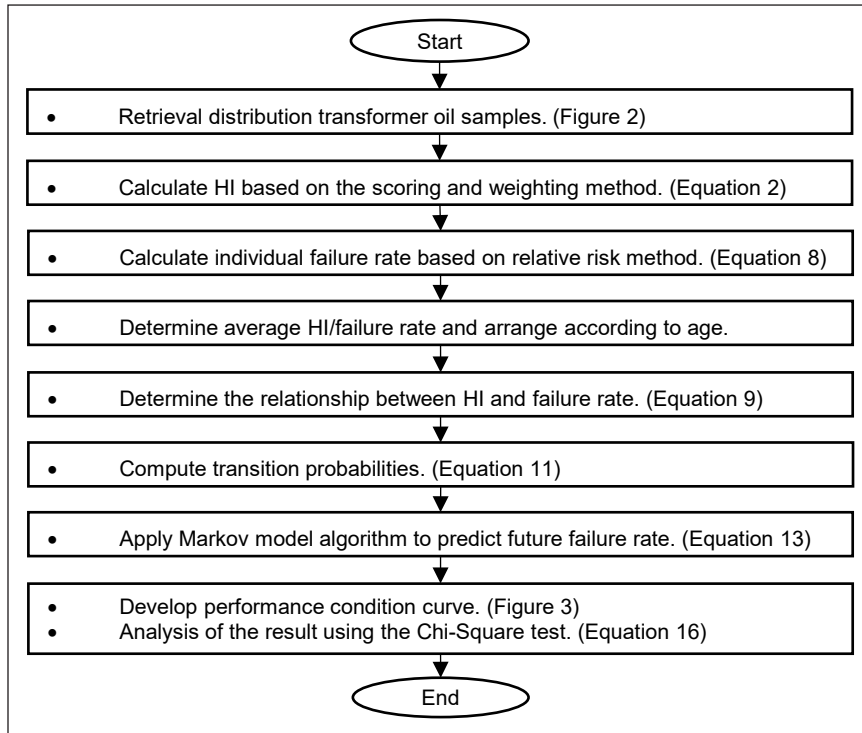


Figure 1. Workflow of the research

$$DGF = OQA = \frac{\sum_{i=1}^n S_j \times W_j}{\sum_{i=1}^n W_j} \quad [1]$$

where W_j represents the parameter's weighting factor, n represents the number of parameters in each factor, and S_j represents the parameter's score. All parameters rating codes were identified based on Jahromi et al. (2009); Naderian et al. (2008). The final HI was determined based on Equation 2 (Yahaya et al., 2017):

$$HI = \frac{K_{DGA}HIF_{DGA} + K_{OQA}HIF_{OQA} + K_{FCA}HIF_{FCA} + K_{AG}HIF_{AG}}{4K_{DGA} + 4K_{OQA} + 4K_{FCA} + 4K_{AG}} \quad [2]$$

where K represents the rating assigned to each factor, and HIF represents each factor's score.

The failure rate of the individual transformer was determined based on the relative risk method (Jürgensen et al., 2016b). The average failure rate, failure location and confidence level were determined as per Jürgensen et al. (2016b). Based on the condition parameters data of the transformer population, the average condition parameter was computed according to Equation 3 (Jürgensen et al., 2016b):

$$\theta_{j,N} = \frac{1}{m} \sum_{k=1}^m \theta_{j,k} \quad [3]$$

where m represents the number of transformer population, $\theta_{j,N}$ represents the average of all obtained values $\theta_{j,k}$ in each parameter. In this study, all condition parameters data were assumed to correspond to winding failures (Jürgensen et al., 2016b). Therefore, when multiple condition parameters data was associated with winding failures, each parameters' weighting was required to demonstrate its significance to indicate the condition in one failure location. The assigned scores and weights of all condition parameters data were determined based on Equation 4 (Jahromi et al., 2009; Jürgensen et al., 2016b):

$$W_{jp} = \frac{C_p}{\sum_{i=1}^n C_i} \tag{4}$$

where C_p represents the weight score assigned to each parameter, the 2FAL and age scores were obtained based on Jahromi et al. (2009). Next, the condition parameter factor, $S_{j,k}$ was identified as either a positive or negative linear function (Jürgensen et al., 2016b). Finally, the positive or negative linear function was determined based on Equations 5 and 6 (Jürgensen et al., 2016b):

$$S_{j,k} = \frac{1}{\theta_{j,N}} \theta_{j,k} \tag{5}$$

$$S_{j,k} = \frac{\theta_{pc,j} - \theta_{j,k}}{\theta_{pc,j} - \theta_{j,N}} \tag{6}$$

where $\theta_{pc,j}$ is described as a perfect condition or as a new condition. Next, the condition parameter factors of all condition parameters for each of the transformers were computed by Equation 7 (Jürgensen et al., 2016b):

$$S_{j,k} = W_j^T S_{jp,k} \tag{7}$$

Finally, the IFR of the transformer was determined based on Equation 8 (Jürgensen et al., 2016b):

$$\lambda_{IFR,k} = \lambda_N \sum_{j=i=1}^n (S_{j,k} \rho_j \alpha_i + (1 - \rho_j) \alpha_i) \tag{8}$$

where λ_N represents the average failure rate, $S_{j,k}$ represents the condition parameter factor for each transformer, α_i represents failure location, and ρ_j represents the probability of condition parameters.

Once the average HI and failure rate of the individual transformer was obtained, the corresponding relationship was modelled based on a two-parameter exponential function model as shown in Equation 9:

$$y = ab^x \tag{9}$$

where y is the failure rate, a is the initial failure rate, b is the accumulation factor, and x is the HI. Based on Equation 9, the failure rate indicator scales and states were determined with reference to the condition of HI from 100% - 0%, corresponding to very good until very poor as defined by Jahromi et al. (2009); Naderian et al. (2008). The failure rate scales and states used for the MM are shown in Table 1.

Table 1
Relationship among the state, health index, failure rate and condition based on two-parameter exponential function model

State	Health Index (%)	Failure Rate (%)	Condition
1	85 – 100	1.27 – 1.59	Very Good
2	70 – 84	1.60 – 1.99	Good
3	50 – 69	2.00 – 2.69	Fair
4	30 – 49	2.70 – 3.59	Poor
5	0 – 29	3.60 – 5.60	Very Poor

MM was implemented to predict the future failure rate of the transformer population. Two assumptions were made to simplify the model in this study. Firstly, natural and monotonic distributions were considered for the future failure rate model. Secondly, the probability summation in each of the rows for the MM transition matrix was set to one. In total, five P_{ij} terms were required to formulate the transition matrix of the MM as seen in Equation 10:

$$P = \begin{bmatrix} P_{11} & 1 - P_{11} & 0 & 0 & 0 \\ 0 & P_{22} & 1 - P_{22} & 0 & 0 \\ 0 & 0 & P_{33} & 1 - P_{33} & 0 \\ 0 & 0 & 0 & P_{44} & 1 - P_{44} \\ 0 & 0 & 0 & 0 & 1 \end{bmatrix} \quad [10]$$

The final state, P_{55} , was set to 1 to simplify the MM process, assuming that all transformers would reach a deplorable state. As represented in Equation 11, the nonlinear optimisation technique was implemented to determine the transition probabilities matrix, which could minimise the overall difference between computed and predicted failure rates for every age zone (Selva et al., 2018; Yahaya et al., 2017).

$$\min \sum_{t=1}^N |A(t) - B(t, P)| \quad [11]$$

where N represents the number of years in each zone, P represents the transition probabilities, P_{11} , P_{22} , P_{33} , P_{44} , $A(t)$ represents the computed failure rate at time t , and $B(t, P)$ represents the predicted failure rate by MM at time t . Next, the prediction of the future failure rate state in a year, t can be represented by Equation 12:

$$F_t = F_0 \times P^t \quad [12]$$

where t represents the interval number, F_0 represents the initial state, and P represents the transition probability matrix. In this study, the F_0 was set as $F_0 = [10000]$ based on the

assumption for an initial state for a newly installed transformer. Finally, the future failure rate of the transformer population at n year was computed based on Equation 13:

$$F_{n+1} = F_n \times P \times R^T \tag{13}$$

where F_{n+1} is the next failure rate at the specific interval, F_n is the current failure rate, and R^T is the matrix transform of the failure rate state scales where $R = [1.59 \ 1.99 \ 2.69 \ 3.59 \ 5.60]$ is obtained from Table 1.

RESULTS AND DISCUSSION

The distribution of the number of oil samples between 1 and 25 years is shown in Figure 2. It is observed that the highest and lowest numbers of oil samples are distributed at the age of 14 and 25 years, respectively. The computed failure rate of the transformers according to the zone and age is shown in Table 2. It is found that the failure rate increases with age. Once the transformer population reaches 6 years, the failure rate slightly exceeds the global average failure rate, which is 2%, as reported in Bossi et al. (1983). However, as the age increases from 7 to 13 years, the transformer population failure rate decreases slightly than the global average failure rate. Finally, at the age between 14 and 25 years, the transformer population failure rate once again exceeds the global average failure rate.

Next, based on computed failure rate values, the transition probabilities were determined by minimising the summation of absolute differences between the computed and predicted failure rates for each year based on Equation 11. The computed failure rates for zones 1 and 2 were utilised to determine the transition probability matrix for training and application. For zones 3 to 5, the computed failure rates data were used to verify the

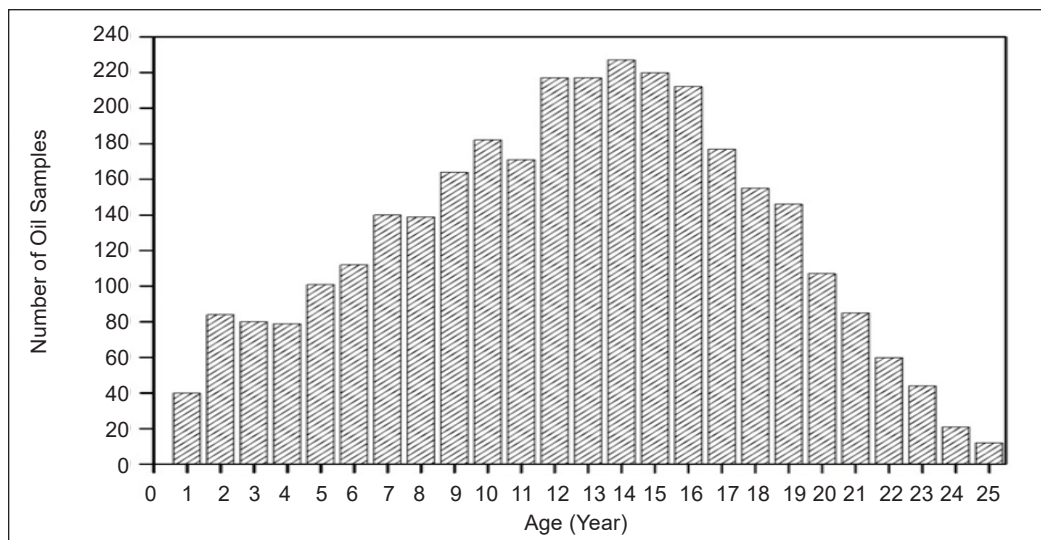


Figure 2. Distribution of oil sample data versus age

Table 2
Computed failure rate by ages and zones

Zone	Transformer Age (Year)	Number of Sample	Computed Failure Rate (%)
1	1	40	1.54
	2	84	1.67
	3	80	1.64
	4	79	1.80
	5	101	1.70
2	6	112	2.05
	7	140	1.93
	8	139	1.74
	9	164	1.91
	10	182	1.80
3	11	171	1.90
	12	217	1.92
	13	217	1.90
	14	227	2.04
	15	220	2.01
4	16	212	2.07
	17	177	2.18
	18	155	2.47
	19	146	2.23
	20	107	2.51
5	21	85	2.43
	22	60	2.92
	23	44	2.16
	24	21	2.31
	25	12	2.59

predicted failure rate computed by the MM approach. Based on Equation 11 and Table 2, the transition probability matrix for zone 1 was computed as seen in Equation 14:

$$P = \begin{bmatrix} 0.9348 & 0.0652 & 0 & 0 & 0 \\ 0 & 0.9900 & 0.0100 & 0 & 0 \\ 0 & 0 & 0.5493 & 0.4507 & 0 \\ 0 & 0 & 0 & 0.9900 & 0.0100 \\ 0 & 0 & 0 & 0 & 1 \end{bmatrix} \quad [14]$$

Next, the failure rate state probability for years 1 to 5 was determined based on Equation 14 based on the product of the initial state and transition probability matrix. The computational process of failure rate state probability for each year can be seen in Table 3.

The last failure rate state probability computed for year 5 from Table 3 was used as the initial state for zone 2. The computed transition probability matrix for zone 2 is shown in Equation 15:

Table 3
Failure rate state for years 1 to 5

Year	MM Process	Failure Rate State Probability
1	$F_0 \times P^1$	[0.9348, 0.0652, 0.0000, 0.0000, 0.0000]
2	$F_0 \times P^2$	[0.8739, 0.1254, 0.0007, 0.0000, 0.0000]
3	$F_0 \times P^3$	[0.8170, 0.1811, 0.0016, 0.0003, 0.0000]
4	$F_0 \times P^4$	[0.7637, 0.2326, 0.0027, 0.0007, 0.0003]
5	$F_0 \times P^5$	[0.7139, 0.2800, 0.0038, 0.0012, 0.0010]

$$P = \begin{bmatrix} 0.7515 & 0.2485 & 0 & 0 & 0 \\ 0 & 0.9900 & 0.0100 & 0 & 0 \\ 0 & 0 & 0.9900 & 0.0100 & 0 \\ 0 & 0 & 0 & 0.5003 & 0.4997 \\ 0 & 0 & 0 & 0 & 1 \end{bmatrix} \quad [15]$$

The computed transition probability matrix for zone 2 was used to calculate the failure rate state probability for years 6 to 10 as in Table 4.

Table 4
Failure rate state for years 6 to 10

Year	MM Process	Failure Rate State Probability
6	$F_0 \times P^6$	[0.5365, 0.4546, 0.0066, 0.0006, 0.0016]
7	$F_0 \times P^7$	[0.4032, 0.5834, 0.0111, 0.0004, 0.0020]
8	$F_0 \times P^8$	[0.3030, 0.6778, 0.0168, 0.0003, 0.0021]
9	$F_0 \times P^9$	[0.2277, 0.7463, 0.0234, 0.0003, 0.0023]
10	$F_0 \times P^{10}$	[0.1711, 0.7954, 0.0306, 0.0004, 0.0025]

These steps were repeated to determine the future failure rate state probability for zones 3 to 5, where the last failure rate state probability from the previous zone was used as the initial state for the next zone. The initial state for zones 1 to 8 are shown in Table 5.

Table 5
Initial state for zone 1 to 8

Zone	Initial State				
1	1.0000	0.0000	0.0000	0.0000	0.0000
2	0.7139	0.2800	0.0038	0.0012	0.0010
3	0.1711	0.7954	0.0306	0.0004	0.0025
4	0.1627	0.7639	0.0517	0.0087	0.0130
5	0.0000	0.6703	0.1814	0.0625	0.0858
6	0.0000	0.4780	0.1768	0.0772	0.2681
7	0.0000	0.3408	0.1403	0.0654	0.4535
8	0.0000	0.2430	0.1044	0.0498	0.6029

Figure 3 shows the predicted failure rate computed by MM based on Equation 13 and Table 2 within 40 years. Most of the predicted failure rates are quite close to the computed failure rates, as illustrated in Table 2. The predicted failure rates exhibit slight differences from computed failure rates at 6, 23, 24 and 25 years. The predicted failure rate of the transformer population is quite low during the first 13 years of service, and it is lower than the global average failure rate, which is 2%. The predicted failure rate of the transformer population begins to exceed the global average failure rate at the age of 14 years and remains high until 40 years. Based on the prediction, the high increment failure rate occurs at 23 to 40 years.

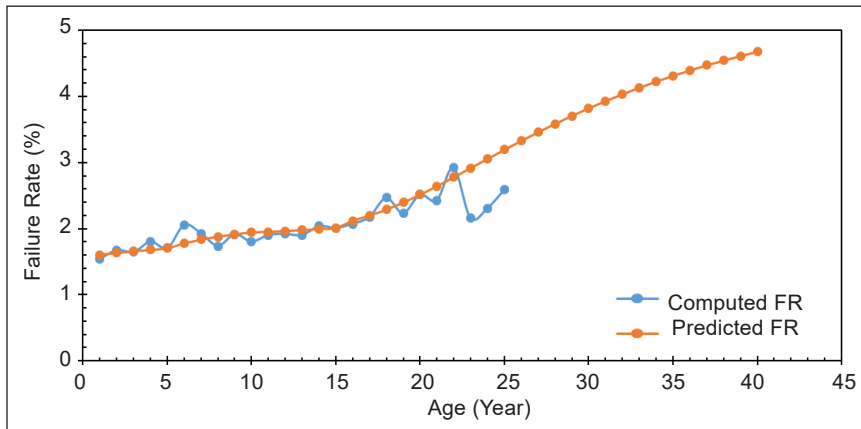


Figure 3. Comparison between computed and predicted failure rates

The Chi-squared test based on Equation 16 was used to evaluate the goodness-of-fit between the predicted and computed failure rates:

$$X^2 = \sum_{i=1}^k \frac{(R_i - E_i)^2}{E_i} \quad [16]$$

where k represents the observation number, E_i represents the computed value at i year, R_i represents the predicted value of the i , year and X^2 represents a Chi-squared distribution coefficient with $k - 1$ degree of freedom. The coefficient X^2 is 0.79 where it is lower than the significance value at the region of 0.05 with 24 degrees of freedom which is 36.42 based on the Chi-Square distribution table (Onchiri, 2013). This result indicates that there is no significant difference between the predicted and computed failure rates.

Mean absolute percentage error (MAPE) was used to calculate the difference between computed and predicted failure rates according to Equation 17:

$$MAPE (\%) = \frac{\sum_{t=1}^{25} \left(\frac{|Y_t - X_t|}{|Y_t|} \times 100\% \right)}{25} \quad [17]$$

where Y_t represents the computed failure rates, X_t represents the predicted failure rates, and t represents the age of the transformer. The MAPE and accuracy level are tabulated in Table 6. The absolute errors between computed and predicted failure rates for each zone are shown in Figure 4. It is found that the highest and lowest percentage of errors in zone 1 is at the age of 4 and 5 years, respectively. For zone 2, the highest and lowest percentage of errors are between 6 and 9 years. The highest and lowest percentage of errors in zone 3 is at 13 and 15 years, respectively. Zone 4 has the highest and lowest percentage of errors at the age of 19 and 20 years. Finally, the highest and lowest percentage of errors in zone 5 is 23 and 22 years. A significant difference in the percentage of errors between computed and predicted failure rates are observed at the age of 23 to 25 years due to the low distribution of oil samples data used in failure rates computation for this zone.

Table 6
Mean absolute percentage error and accuracy level for failure rate

Zone	MAPE (%)	Level of accuracy (%)
Zone 1 – 5	7.27	92.73
Zone 3 - 5	8.91	91.09

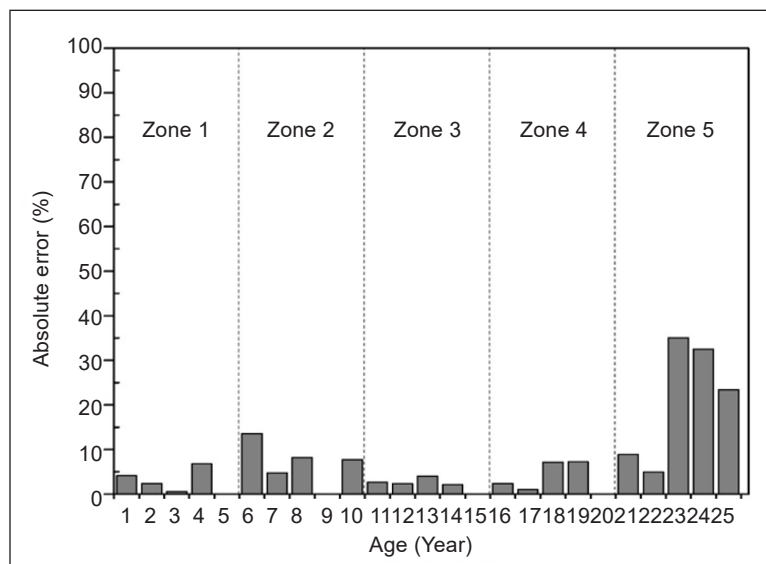


Figure 4. Absolute error between computed and predicted failure rates for each of the zones

CONCLUSION

It is found that the MM can be utilised to predict future failure rates based on HI. The majority of the predicted failure rates are quite close to the computed failure rates, with an accuracy level of 91.10%. Notwithstanding, higher discrepancies between the computed and predicted failure rates in Zone 5 are observed due to insufficient oil samples data to compute the failure rates in the respective zone. Based on the MM prediction, the failure rate of the transformer population increases as the transformer’s age increases, and it begins

to exceed the global average failure rates at 14 years. Overall, MM can be considered a viable approach to predict transformer failure rates, and it can be used as an alternative option to determine the forecasted failure data.

ACKNOWLEDGEMENTS

The authors would like to express sincere gratitude to the Ministry of Higher Education for the funding provided for this study under the FRGS scheme of FRGS/1/2019/TK07/UPM/02/3 (03-01-19-2071FR).

REFERENCES

- Agrawal, A. K., Qian, G., Kawaguchi, A., Lagace, S., Delisle, R., Kelly, B., Weykamp, P., Conway, T., & Dubin, E. (2006). Deterioration rates of typical bridge elements in New York. In *Proceedings of the Structures Congress and Exposition* (pp. 1-10). ASCE Library. [https://doi.org/10.1061/40889\(201\)128](https://doi.org/10.1061/40889(201)128)
- Borovkov, K. (2003). Markov chains. In *Elements of Stochastic Modelling* (pp. 75-128). World Scientific. https://doi.org/10.1142/9789812779199_0003
- Bossi, A., Dind, J. E., Frisson, J. M., Khoudiakov, U., Light, H. F., & Al., E. (1983). An international survey of failures in large power transformers in service. In *Final report of the CIGRE Working Group 12.05* (pp. 20-48). *Electra*.
- Brown, R. E., Member, S., Frimpong, G., Member, S., & Willis, H. L. (2018). *Failure rate modeling using equipment inspection data*. In *IEEE Power Engineering Society General Meeting, 2004* (pp. 693-700). IEEE Publishing. <https://doi.org/10.1109/TPWRS.2004.825824>
- Camahan, J. V., Davis, W. J., Shahin, M. Y., Keane, P. L., & Wu, M. I. (1987). Optimal maintenance decisions for pavement management. *Journal of Transportation Engineering*, 113(5), 554-572. [https://doi.org/10.1061/\(ASCE\)0733-947X\(1987\)113:5\(554\)](https://doi.org/10.1061/(ASCE)0733-947X(1987)113:5(554))
- Chatfield, C. (1973). Statistical inference regarding Markov chain models. *Applied Statistics*, 22(1), 7-20. <https://doi.org/10.2307/2346299>
- CIGRE WG A2.18. (2003). *Life management techniques for power transformer*. CIGRE Publication.
- Edirisinghe, R., Setunge, S., & Zhang, G. (2015). Markov model-based building deterioration prediction and ISO factor analysis for building management. *Journal of Management in Engineering*, 31(6), Article 04015009. [https://doi.org/10.1061/\(asce\)me.1943-5479.0000359](https://doi.org/10.1061/(asce)me.1943-5479.0000359)
- Emsley, A. M., Xiao, X., Heywood, R. J., & Ali, M. (2000). Degradation of cellulosic insulation in power transformers. Part 3: Effects of oxygen and water on ageing in oil. *IEE Proceedings: Science, Measurement and Technology*, 147(3), 115-119. <https://doi.org/10.1049/ip-smt:20000021>
- Hamoud, G. A. (2011). Assessment of spare transformer requirements for distribution stations. *IEEE Transactions on Power Systems*, 26(1), 174-180. <https://doi.org/10.1109/TPWRS.2010.2046429>
- Hamoud, G. A. (2012). Use of Markov models in assessing spare transformer requirements for distribution stations. *IEEE Transactions on Power Systems*, 27(2), 1098-1105. <https://doi.org/10.1109/TPWRS.2011.2177999>

- Hoskins, R. P., Strbac, G., & Brint, A. T. (1999). Modelling the degradation of condition indices. *IEEE Proceedings: Generation, Transmission and Distribution*, 146(4), 386-392. <https://doi.org/10.1049/ip-gtd:19990063>
- Jahromi, A., Piercy, R., Cress, S., Service, J., & Fan, W. (2009). An approach to power transformer asset management using health index. *IEEE Electrical Insulation Magazine*, 25(2), 20-34. <https://doi.org/10.1109/MEI.2009.4802595>
- Jürgensen, J. H., Nordstrom, L., & Hilber, P. (2016a). A review and discussion of failure rate heterogeneity in power system reliability assessment. In *2016 International Conference on Probabilistic Methods Applied to Power Systems (PMAPS)* (pp. 1-8). IEEE Publishing. <https://doi.org/10.1109/PMAPS.2016.7764078>
- Jürgensen, J. H., Nordström, L., & Hilber, P. (2016b). Individual failure rates for transformers within a population based on diagnostic measures. *Electric Power Systems Research*, 141, 354-362. <https://doi.org/10.1016/j.epsr.2016.08.015>
- Jürgensen, J. H. (2016). *Condition-based failure rate modelling for individual components in the power system* (Licentiate dissertation). KTH Royal Institute of Technology, Sweden.
- Jürgensen, J. H. (2018). *Individual Failure Rate Modelling and Exploratory Failure Data Analysis for Power System Components* (PhD dissertation). KTH Royal Institute of Technology, Sweden.
- Jürgensen, J. H., Brodersson, A. L., Nordstrom, L., & Hilber, P. (2018). Impact assessment of remote control and preventive maintenance on the failure rate of a disconnector population. *IEEE Transactions on Power Delivery*, 33(4), 1501-1509. <https://doi.org/10.1109/TPWRD.2017.2710482>
- Lindquist, T. M., Bertling, L., & Eriksson, R. (2005). Estimation of disconnector contact condition for modelling the effect of maintenance and ageing. In *2005 IEEE Russia Power Tech* (pp. 1-7). IEEE Publishing. <https://doi.org/10.1109/PTC.2005.4524406>
- Lundgaard, L. E., Hansen, W., Linhjell, D., & Painter, T. J. (2004). Aging of oil-impregnated paper in power transformers. *IEEE Transactions on Power Delivery*, 19(1), 230-239. <https://doi.org/10.1109/TPWRD.2003.820175>
- McDonald, D. (2004). *Elements of applied probability for engineering, mathematics and systems science*. World Scientific. <https://doi.org/10.1142/5456>
- Micevski, T., Kuczera, G., & Coombes, P. (2002). Markov model for storm water pipe deterioration. *Journal of Infrastructure Systems*, 8(2), 49-56. [https://doi.org/10.1061/\(asce\)1076-0342\(2002\)8:2\(49\)](https://doi.org/10.1061/(asce)1076-0342(2002)8:2(49))
- Naderian, A., Cress, S., Piercy, R., Wang, F., & Service, J. (2008). An approach to determine the health index of power transformers. In *Conference Record of the 2008 IEEE International Symposium on Electrical Insulation* (pp. 192-196). IEEE Publishing. <https://doi.org/10.1109/ELINSL.2008.4570308>
- Onchiri, S. (2013). Conceptual model on application of chi-square test in education and social sciences. *Educational Research and Reviews*, 8(15), 1231-1241. <https://doi.org/10.5897/ERR11.305>
- Selva, A. M., Azis, N., Yahaya, M. S., Kadir, M. Z. A. A., Jasni, J., Ghazali, Y. Z. Y., & Talib, M. A. (2018). Application of markov model to estimate individual condition parameters for transformers. *Energies*, 11(8), Article 2114. <https://doi.org/10.3390/en11082114>

Nor Shafiqin Shariffuddin, Norhafiz Azis, Amran Mohd Selva, Muhammad Sharil Yahaya,
Jasronita Jasni, Mohd Zainal Abidin Ab Kadir and Mohd Aizam Talib

- Setunge, S., & Hasan, M. S. (2011, December 16-18). Concrete bridge deterioration prediction using Markov chain approach. In *Proceedings of the International Conference on Structural Engineering, Construction and Management (ICSECM)* (pp. 1-14). Earl's Regency Kandy, Sri Lanka.
- Yahaya, M. S., Azis, N., Kadir, M. Z. A. A., Jasni, J., Hairi, M. H., & Talib, M. A. (2017). Estimation of transformers health index based on the markov chain. *Energies*, *10*(11), 1-11. <https://doi.org/10.3390/en10111824>
- Zaidey, Y., Ghazali, Y., & Soosai, A. M. (2015, June 15-18). TNB Approach on managing asset retirement for distribution. In *23rd International Conference on Electricity Distribution* (pp. 1-5). Lyon, France.

Morphological Characteristics and Plant Species for Noise Reducer and Pb Metal Absorbers at Adisucipto Airport: Yogyakarta, Indonesia

Chales Torang Pandapotan, Siti Nurul Rofiqo Irwan* and Eka Tarwaca Susila Putra

Department of Agronomy, Faculty of Agriculture, Universitas Gadjah Mada, St Flora, Bulaksumur, 55281, Yogyakarta, Indonesia

ABSTRACT

The dense activity of aircraft at the airport leads to a strong mobilisation of transportation, generating noise. Meanwhile, increased aviation mobilisation has the potential to produce Pb metal since the utilisation of landscape plants is an effort to reduce noise and Pb. Therefore, this study aims to determine the ability of three species of landscape plants to absorb noise and Pb at Adisucipto airport, Yogyakarta in Indonesia. The study was conducted from August 2019 to September 2020, and the survey and the laboratory method were used with nested design data analysis followed by the Tukey HSD 5% test. The results showed that fan pine had a higher ability to absorb noise. On the contrary, croton had a higher ability to absorb Pb metal.

Keywords: Absorbers, airport, landscape plants, noise, Pb metal, reducer

INTRODUCTION

An airport is an area with certain boundaries used to land and takes off aeroplanes (Setiawan et al., 2013; Sumathi & Parthasarathi, 2018). The dense activity of aircraft at the airport results in the high mobilisation of transportation, which can trigger noise, a form of environmental pollution (noise pollution) that can disturb comfort and damage human hearing (Clark et al., 2013). The noise level is influenced by the frequency of flights and jet aircraft engines. It causes disturbance to airport workers (*ground handling*) and residents outside the area with a 1-5 km radius.

Furthermore, the noise level can disturb the surrounding residential areas (Herawati,

ARTICLE INFO

Article history:

Received: 24 May 2021

Accepted: 19 July 2021

Published: 28 October 2021

DOI: <https://doi.org/10.47836/pjst.29.4.43>

E-mail addresses:

chalezma@gmail.com (Chales Torang Pandapotan)

rofiqoirwan@ugm.ac.id (Siti Nurul Rofiqo Irwan)

eka.tarwaca.s@ugm.ac.id (Eka Tarwaca Susila Putra)

* Corresponding author

2016), negatively impact human health and environmental comfort. This effect is determined by ear sensitivity and *sound pressure level* (SPL). Continuous noise results in heart disease, physical and mental fatigue, and hearing loss (Black et al., 2007). In addition, an increase in the number of flight frequencies also has the potential to produce pollutants that are released into the air polluting the environment. They come from aircraft fuel, in-plane air controllers (AC), and air fresheners in aircraft. Avtur and kerosene as aircraft fuel produce carbon dioxide (CO₂), methane (CH₄), NO_x, CO, and SO₂ emissions, and contrails (pollutant materials that effectively absorb heat and have an impact on global warming). In addition, chlorofluorocarbon (CFC) in air conditioning, air freshener in aircraft, and NO_x damages the ozone layer in the stratosphere (Ashford et al., 2011). Furthermore, pollutants have a negative impact on human health (Corbitt, 2004; Andersen et al., 2011), and one of the efforts to minimise the number is by creating a noise barrier using landscape plants.

Apart from functioning as greenery and beauty, these plants are used as a noise barrier and function as a living filter. It reduces pollution levels by absorbing, detoxifying, accumulating, and or regulating metabolism in the air. Therefore, air quality can be increased by releasing oxygen (Shannigrahi et al., 2010), and the ability of plants to reduce noise is seen from the texture of the leaves and plant growth (plant canopy density). The broad, coarse leaf texture and dense leaf are the most effective plant characteristics in reducing noise. Plants have the ability to absorb and accumulate pollutants and capture lead particles and other pollutants released by public transportation through their leaves (Hendrasarie, 2007). According to Koeppel and Miller (1970), the ability to absorb pollutants is strongly influenced by the surface conditions of plant leaves. Plants with hair (pubescent) or rough surfaces (wrinkles) have a higher ability to absorb pollutants than those with smoother and flatter surfaces. Similarly, Megia et al. (2015) reported that the ability of plant leaves to absorb pollutants is influenced by morphological characteristics, such as leaf size and shape, the presence of hair on the surface, and texture.

MATERIALS AND METHODS

Time, Location, and Sample Collection

The study was conducted from August 2019 to April 2020 at Adisucipto Airport, Yogyakarta Special Region, Indonesia (Figure 1). Furthermore, analysis of samples was conducted at the Yogyakarta Agricultural Technology Research Center Laboratory, the Plant Production Management Laboratory, Faculty of Agriculture, and the Plant Structure and Development Laboratory, Faculty of Biology, Gadjah Mada University using survey methods and laboratory analysis. The selected plants used had the highest dominance based on the results of pre-observations. Initial observations showed that the dominant plant species were fan pine (*Platyclusus Orientalis*), red shoots (*Syzygium myrtifolium*), and croton (*Codiaeum variegatum*).

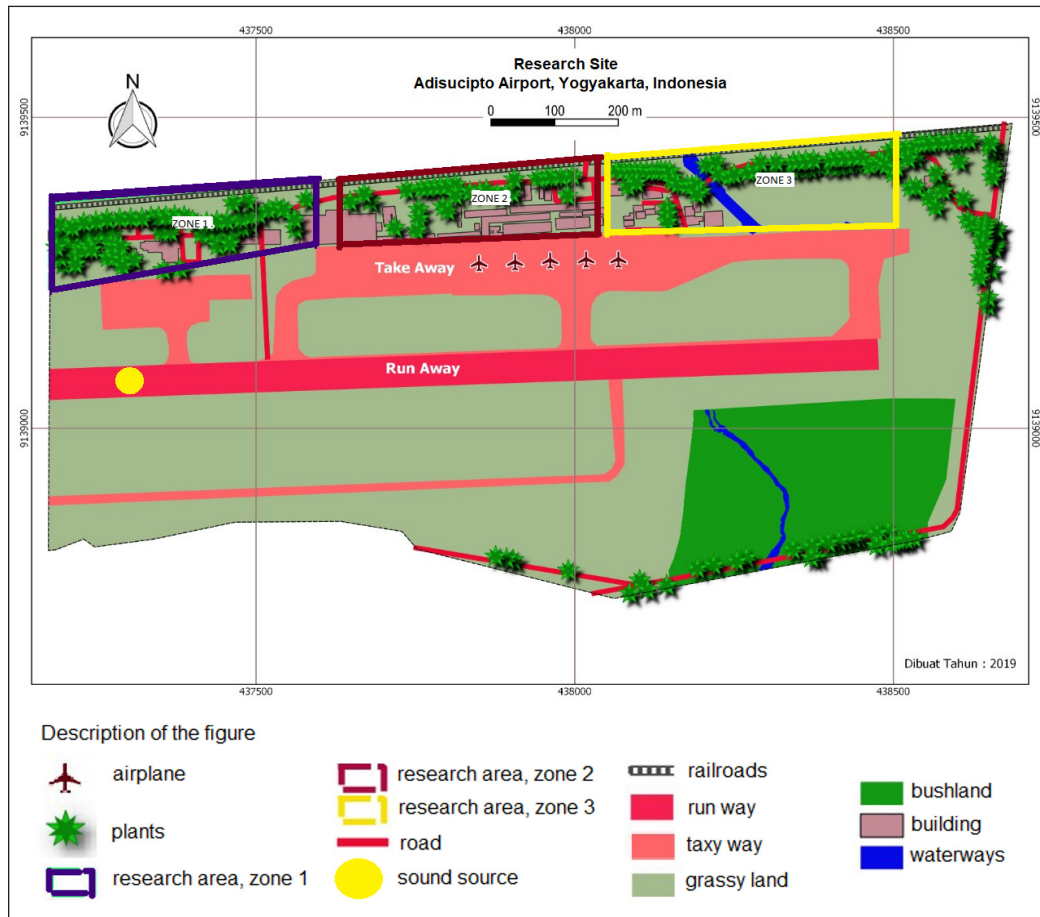


Figure 1. Research Site at Yogyakarta Adisucipto Airport, Indonesia

Analytical Method

The results of preliminary observations showed that the Adisucipto airport landscape area was divided into three zones, namely 1) the difference in the distance between the observation zone and the sound source was 0.5 km located in the airport park area of terminal A, 2) the difference in the distance between the observation zone and the sound source was 1 km located in the terminal area B, and 3) the difference in distance between the observation zone and the sound was 1.5 km located in the airport parking area. These three zones showed that the environmental design used was a nested type. In each zone, there were three species of landscape plants to be studied, namely *P. Orientalis* (fan pine), *S. myrtifolium* (red shoot), and *C. variegatum* (croton). The number of samples was four stands per species/zone as replicates in blocks. The study was conducted with a survey method and divided into ten stages of activity, namely: 1) planning, 2) licensing, 3) sample organisation, 4) field preparation, 5) observation and data collection, 6) sampling, 7) sample

testing in the laboratory, 8) data analysis, 9) data interpretation, and 10) preparation of research reports.

Noise Measurement

Two points measured noise measurement. The first point was outside the canopy (A1), and the second was inside (A2) (Figure 3). This noise measurement was conducted because the area of the airport environment was very heterogeneous. Thus, to find out that plants reduced the noise, the total decibels outside the canopy should be subtracted by the total decibels inside the canopy. This measurement was conducted eight times on 12 experimental plant sample points.

Noise measurement in the area was consistent with KEP-48 / MENLH / 11/1996, a 10-minute measurement of every five seconds reading with the sound level meter's minimum and maximum decibel values. The measurement of the noise level was divided into several time intervals, including morning: 07.00-10.59 WIT, afternoon: 11.00-14.59 WIT, and night : 15.00-18.00 WIT. (noted : WIT = West Indonesia Time).

Identification of Pb Metal

The observation of Pb heavy metal analysis was conducted in 3 stages: preparation and sampling, diluents and standard solutions, and preparation for testing and metal analysis in landscape plants. One hundred grams of the sample were taken, put in a clean plastic container and checked for Pb content using Atomic Absorption Spectrophotometry (AAS). The dilution solution for metal was conducted based on SNI 06-6989-.4-2004 standards. The procedure used was nitric acid (HNO₃) plus aqua dest to pH 2. In addition, landscape plant samples were cleaned with running tap water, dried at room temperature. Also, 100 grams of the sample was weighed and dried in an oven at a temperature (50 to 100°C) for three hours. Then, That sample was cooled in a closed desiccator, weighed again as dry weight, and pounded until smooth using a stamper mortar. It was weighed as much as 0.5 g, plus 100 ml of aqua dest and the addition of 5 ml of concentrated nitric acid and deconstruction using hotplate tool until the solution was approximately 20 ml clear. Also, it was filtered using Whatman filter paper, and distilled water was added to the filtrate until the solution became 100 ml. Furthermore, it was read by atomic absorption spectrophotometry with a wavelength and a cathode lamp of Pb 217 nm. Finally, the prepared samples were analysed using Atomic Absorption Spectrophotometry (AAS).

Pb Metal Absorption

Pb absorption was carried out by comparing the uptake or total Pb content in plants in the airport area with the home garden. In addition, the ability of plants to absorb Pb was calculated by reduced airport Pb metal with Pb metal in home gardens.

RESULTS AND DISCUSSION

Morphological Characteristics of Plants

Plant observations, including morphological components in several types of landscape, can be seen in Table 1.

Table 1

Leaf description observation of landscape plants at Adisucipto airport

Plant Species	Leaf Shape	Leaf Edge Shape	Leaf Surface
<i>P. orientalis</i> (Fan Pine)	needle	flat	coarse
<i>S. myrtifolium</i> (Red Shoot)	oval	flat	smooth and slippery
<i>C. variegatum</i> (Croton)	round wavy	flat	smooth

The results showed that the three landscape plants had different leaf shapes and surfaces, while the edges had the same shape. Furthermore, the leaf arrangement on the stem and angle for each of the three landscape plants were presented in tabular form below.

Table 2

Leaf arrangement observation, leaf arrangement on a stem, and leaf angle

Plant Species	Leaf Arrangement	Stem Leaf Arrangement	Corner of the Leaf
<i>P. orientalis</i> (Fan Pine)	dichotom	spread	blunt
<i>S. myrtifolium</i> (Red Shoot)	pinnate	spread	flat
<i>C. variegatum</i> (Croton)	curved	spread	pointed

Table 2 showed that *P. orientalis* (fan pine), *S. myrtifolium* (red shoot), and *C. variegatum* (croton) in all zones had the same leaf stem arrangement, which is scattered. This include arrangement of *P. orientalis* (fan pine) was dichotomous, *S. myrtifolium* (red shoot) pinnate, and curved *C. variegatum* (croton). In addition, the leaf angles in *P. orientalis* (fan pine) were blunt, *S. myrtifolium* (red shoot) flat, and *C. variegatum* (croton) had pointed corners.

The measurements of the physical character of landscape plants for each airport zone are presented in Table 3. It indicated that the three landscape plants have different canopy shapes: *P. orientalis* (fan pine), *S. myrtifolium* (red shoot), and *C. variegatum* (croton) with a conical, globular and cylindrical shape, respectively. In addition, Table 3 showed the largest to the smallest area of plant crown projections, namely *P. orientalis* (fan pine), *S. myrtifolium* (red shoot), and *C. variegatum* (croton). The results showed that *P. orientalis* (fan pine) had a larger crown area than *S. myrtifolium* (red shoot) and *C. variegatum* (croton). Therefore *P. orientalis* (fan pine) had a higher average ability to reduce noise than *S. myrtifolium* (red shoot) and *C. variegatum* (croton).

Table 3

Observation of canopy shape, canopy projection area, leaf area index, and area of landscape plant canopy at Adisucipto airport

Plant Species	Zone	Canopy Shape	Canopy Projection Area (m ²)	Leaf Area Index (LAI)	Canopy Area (m ²)
<i>P. orientalis</i> (Fan Pine)	1	conus	5652,00	5,63	31792,50
	2		4083,57	6,28	25658,43
	3		4003,89	5,38	21520,92
<i>S. myrtifolium</i> (Red Shoot)	1	globular	2802,55	5,73	16070,86
	2		1814,92	7,25	13158,17
	3		1739,30	8,18	14227,47
<i>C. variegatum</i> (Croton)	1	cylinder	1533,20	0,84	1287,35
	2		1430,88	0,71	1015,92
	3		1978,59	0,91	1797,22

Zone Noise Level

The results of noise level measurements conducted during the study can be seen in Figure 2. Figure 2 showed that the noise level in all zones was different. The level in one and two was higher than in zone three. Therefore, the highest noise occurs in zone one, namely 76.13 db, followed by two 74.45 db and three 73.45 db. It was due to differences in the distance from the sound source to the zone area. The distance from the sound source to zone one was 0.5 km, two was 1 km, and three was 1.5 km. Apart from differences in distance, noise levels are also influenced by other factors, such as a very heterogeneous environment. The noise state was determined by many factors, namely heterogeneous environmental conditions and distance from sound sources. Environmental differences that are very heterogeneous are one of the factors causing noise in the airport area.

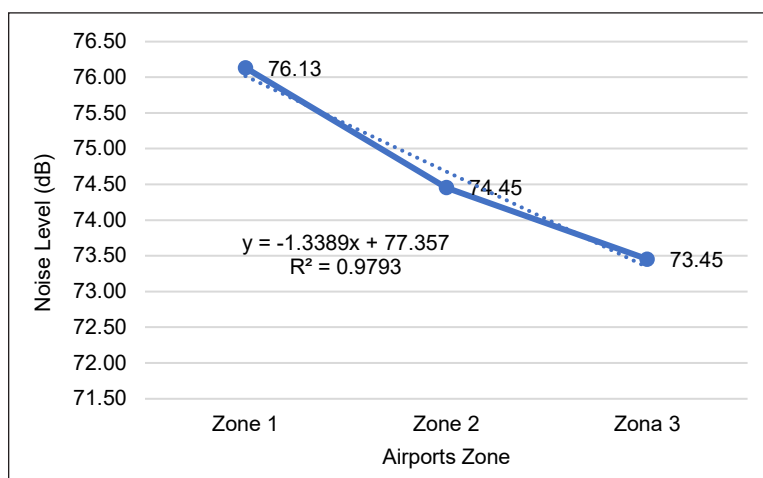


Figure 2. Noise levels in all airport zones

Noise Reduction Function

The noise reduction results outside and in the canopy of morning landscape plants (Table 4) showed a significant difference. Variation in zones have a different effect on noise between the outer and inner plant canopy, and the greatest reduction capability was in zone one.

Table 4

The result of noise reduction outside the canopy within the canopy of landscape plants in the morning

Plant Species	Average ability (db)			
	Zone1	Zone2	Zone3	Average
<i>P. orientalis</i> (Fan Pine)	11.38a	4.29c	3.95c	6.54
<i>S. myrtifolium</i> (Red Shoot)	6.19b	2.96cde	3.25cde	4.13
<i>C. variegatum</i> (Croton)	3.36cde	2.61d	2.42e	2.80
Average	6.98	3.29	3.21	4.49
Coefisien Variansi (%)				13.65

Note. Numbers followed by the same letter in the same column or row are not significantly different according to the Tukey HSD test; ns means not significantly different, * at the 5% significance level

The analysis showed that the greatest reduction results to the lowest in the morning were fan pine, red shoots, and croton. The average ability of landscape plants as noise reducers in the morning against the differences outside and inside the canopy was 6.54 db of pine cones, 4.13 db of red shoots, and 2.80 db of croton. The reduction of landscape plants in the three zones was 4.49 db.

Furthermore, the average noise reduction of landscape plants at the difference between the outer and inner canopy noise levels observed during the day are presented in Table 5.

Table 5

The result of noise reduction outside the canopy within the canopy of landscape plants during the day

Plant Species	Average ability (db)			
	Zone 1	Zone2	Zone3	Average
<i>P. orientalis</i> (Fan Pine)	6.17a	3.84bc	4.16b	4.72
<i>S. myrtifolium</i> (Red Shoot)	4.24b	2.92cd	3.24bcd	3.47
<i>C. variegatum</i> (Croton)	2.72d	2.46d	2.58d	2.59
Average	4.38	3.07	3.33	3.59
Coefisien Variansi (%)				11.74

Note. Numbers followed by the same letter in the same column or row are not significantly different according to the Tukey HSD test; ns means not significantly different, * at the 5% significance level

Table 5 showed a significant difference in the ability of the three species of landscape plants. In Table 5, it can be concluded that the distance (zone) has a significant effect on the ability of plants to reduce noise. The average ability of landscape plants to reduce noise during the day showed a significant difference. *Platycladus orientalis* (fan pine) was more

effective at reducing noise than *C. variegatum* (croton) and was not significantly different in *S. myrtifolium* (red shoot).

Table 6
The result of noise reduction outside the canopy within the canopy of landscape plants in the afternoon

Plant Species	Average ability (db)			
	Zone 1	Zone 2	Zone 3	Average
<i>P. orientalis</i> (Fan Pine)	5,93a	4,12abc	4,01abc	4,69
<i>S. myrtifolium</i> (Red Shoot)	5,11ab	3,20dc	3,15d	3,82
<i>C. variegatum</i> (Croton)	3,62bcd	2,60d	2,57cd	2,93
Average	4,88	3,31	3,24	3,81
Coeffisien Variansi (%)				5,82

Note. Numbers followed by the same letter in the same column or row are not significantly different according to the Tukey HSD test; ns means not significantly different, * at the 5% significance level. * Data converted in ancient sine form $\sqrt{\log_{10}(y)/100}$.

Table 6 above showed that the zones significantly affect the noise reduction results of the three landscape plants in the afternoon, and the highest results are in zone one. *Platyclusus orientalis* (fan pine) was a landscape plant with the largest reduction results with a reduction of 5,93 db, while red shoots are 5,11 db and croton 3.62 db. In addition, the noise reduction of *P. orientalis* (fan pine) in zone two was not significantly different from the red shoots and significantly different from the croton, with the value of *P. orientalis* (fan pine) 4.69 db, *S. myrtifolium* (red shoots) 3.82 db, and *C. variegatum* (croton) 2.93 db. In zone three, the results from the three landscape plant species have no significant differences.

The results of noise reduction showed that landscape plants are used as noise absorbers. When sound waves spread into the air, the lower frequencies result in clearer diffraction (Yang et al., 2013). Furthermore, Yang et al. (2013) also explained that this resulted in large and dense plant arrangements with high noise attenuation values. Sound waves propagate through the air and leaves, while the energy causes leaf molecules to resonate. Therefore, *P. orientalis* (fan pine) and *S. myrtifolium* (red shoot) are better at reducing noise than *C. variegatum* (croton). It was because the arrangement of plants, which became a noise barrier, was quite thick. It makes it quite difficult for sound waves to pass through the barrier of the landscape plants. According to Hidayat (2010), plants reduce noise even though they do not eliminate it. It was possible when the planting pattern was with a high density resembling a wall or building barrier.

Price (1988) explained that leaves have an important role in reducing noise. Plants with large number of leaves are better at reducing noise than those with a small number. Maleki and Hosseini (2011) results also showed that plants with leaf thickness are more effective at reducing noise.

The results showed that the *P. orientalis* (fan pine) has the highest ability to reduce noise with a large header. According to Carpenter et al. (1975) explanation, the noise suppression capacity of vegetation was highly dependent on the plant canopy. Fitriyati and Nasrullah (2005) reported that the capacity to reduce noise by vegetation depends on the type, density, and denseness. Putra et al. (2018) stated that trees reduce sound by absorbing waves from leaves, branches, and twigs. The plant species that are most effective at reducing sound have a thick canopy with dark leaves. Plant foliage absorbs up to 95% noise (Putra et al., 2018) and causes the reduction ability of *P. orientalis* (fan pine) better than *S. myrtifolium* (red shoot) and *C. variegatum* (croton) (Table 3).

Heavy Metal (Pb) Absorption

The content of heavy metal Pb in the three types of landscape plants (Table 7) showed a significant difference. *C. variegatum* (croton) has the highest ability in absorbing Pb metal, and the highest to lowest plants ability to absorb Pb were *C. variegatum* (croton), *S. myrtifolium* (red shoot), and *P. orientalis* (fan pine).

Table 7
Pb level in these three species of landscape plants at the Adisucipto airport area

Plant Species	Pollutant Pb (ppm)			
	Zone 1	Zone 2	Zone 3	Average
<i>P. orientalis</i> (Fan Pine)	5.56f	2.02h	1.70h	3.09
<i>S. myrtifolium</i> (Red Shoot)	17.18c	11.76e	4.30g	11.08
<i>C. variegatum</i> (Croton)	22.35a	19.59b	13.09d	18.34
Average	15.03x	11.12y	6.36z	10.84
Coefisien Variansi (%)				2.48

Note. Numbers followed by the same letter in the same column or row are not significantly different according to the Tukey HSD test; ns means not significantly different, * at the significance level of 5%

The levels of heavy metal Pb in Table 7 above showed that *C. variegatum* (croton) has a higher ability than *S. myrtifolium* (red shoot) and *P. orientalis* (fan pine) in the three zones. The ability of *C. variegatum* (croton) to absorb Pb was because this was a biosorption plant or the ability to reduce heavy metals from water bodies (Kurniawati et al., 2016). In zone one, plants with the highest to low Pb absorption were *C. variegatum* (croton) at 22.35 ppm, *S. myrtifolium* (red shoot) at 17.18 ppm, and *P. orientalis* (fan pine) at 5,56 ppm. In zone two, the highest to lowest adsorptions were also similar to one, namely *C. variegatum* (croton) 19.59 ppm, *S. myrtifolium* (red shoot) 11.76 ppm, and *P. orientalis* (fan pine) 2.02 ppm. In zone three, metal absorption has decreased slightly compared to zones one and two. The highest Pb metal adsorptions of the three species were *C. variegatum* (croton) 13.09 ppm, *S. myrtifolium* (red shoot) 4.30 ppm, and *P. orientalis* (fan pine) 1.70 ppm.

The results of Pb adsorptions by plants in all zones were then compared with the Pb content of those in home gardens (Table 8).

Table 8

The differences between Pb pollutant content with control on three species of landscape plants in the Adisucipto airport area and home gardens

Plant Species	Pb (ppm)		
	Airport Area	Home Garden	Average
<i>P. orientalis</i> (Fan Pine)	3,09c	0,22e	1,66
<i>S. myrtifolium</i> (Red Shoot)	11,08b	0,44de	5,76
<i>C. variegatum</i> (Croton)	18,34a	0,64d	8,85
Average	10,84x	0,44y	5,64
Coefisien Variansi (%)			1,24

Note. Numbers followed by the same letter in the same column or row are not significantly different according to the Tukey HSD test; ns means not significantly different, * at the significance level of 5%

Table 8 above showed that the Pb content of the three landscape plants in the airport area was higher than that of home gardens. It showed that the airport area has a Pb heavy metal content. Plants in the zone area have a high Pb content, with a level of 10.84 ppm. These results showed that the three landscape plants absorb heavy metal contents and can be used as landscape plants to fulfil ecological functions.

Based on the description above, it was explained that the binding of Pb metal varies. *C. variegatum* (croton) was relatively better in accumulating heavy metals in plant leaves, and this ability was different for each vegetation type. Dudka et al. (1996) compared the concentrations of Pb and Cd metals in potato, banana, and wheat crops. The results obtained showed that the concentrations of Pb and Cd were different in plant parts and species. It was consistent with (Fergusson, 1990), where it was reported that many factors influence heavy metal levels in vegetation, including the type of vegetation, the content and availability of these heavy metals in the soil.

DISCUSSION

Plants in the very suitable category have physical characteristics and proper planting following the criteria of gas pollutants adsorbent. Observation showed that the three landscape plants are tolerant and capable of absorbing air pollution and cleaning dirty air more effectively through the tree canopy. In addition, the three landscape plants have great potential to absorb gaseous pollutants since they are expected to be preserved.

Azzahro et al. (2019) reported that a canopy reduces the pollutants released in the environment by diverting wind gusts into a wider atmosphere, and it absorbs pollutants on the surface of the leaves, stems, and twigs. Therefore, the plant selection to increase the ability of green open spaces to absorb pollutants should follow the physical criteria of

plants that can absorb gaseous pollutants. It includes having a dense canopy and a large number of leaves. Increasing the absorption of gaseous pollutants was conducted by adding a combination of shrubs, bushes, and ground cover crops to each tree. This combination increases the filtering of gaseous pollutants. In the Adisucipto airport area, plants were found to absorb tolerant pollutants.

Landscape plants are one of the most promising solutions to tackle air pollution, reducing noise and absorbing heavy metal particles. Therefore, the planning and selection for urban areas, such as airports, should be conducted since air pollution does not worsen. Apart from functioning as a chemical pollutant absorbent, landscape plants also reduce qualitatively and quantitatively noise (Nugraheni et al., 2018). Furthermore, it was explained that landscape plants as a metal binder or bioaccumulator absorb and accumulate heavy metals in plant parts and reduce noise.

In the previous study related to noise reduction, *P. orientalis* (fan pine) was the plant species with the best ability, followed by *S. myrtifolium* (red shoot) and *C. variegatum* (croton). Meanwhile, from the aspect of its ability to absorb Pb metal pollutants, it was reversed because *C. variegatum* (croton) has the best ability to absorb Pb, followed by *S. myrtifolium* and *P. orientalis* (fan pine). There are at least two kinds of pollutants, namely noise and heavy metals. It includes a combination of several species, namely *P. orientalis* (fan pine), *C. variegatum* (croton), and *S. myrtifolium* (red shoot). The landscape function was perfect in reducing these two pollutants. The composition of the three species needs to be regulated in a balanced proportion considering that each of them has a specific optimal function. Therefore, in arranging the landscape, a mixed crop was the best choice to optimise its function. Besides functioning as a chemical pollutant absorbent, they also reduce qualitatively and quantitatively noise (Martuti, 2013).

This study examined three dominant landscape plants in the Adisucipto area. The selection of the dominant plants was carried out during pre-observation. They were *P. orientalis* (fan pine), *S. myrtifolium* (red shoot), and *C. variegatum* (croton), and the study was conducted in the airport area using the zoning method. The area was divided into three zones of 1, 2 and 3 with a distance of 0.5 km, 2 km, and 1 km from the sound source, respectively.

The average noise level in each zone was different (Figure 2), occurring in zone 1 at 76.13 db, the average noise in zone 2 was 74.45 dB, and the average noise in zone 3 was 73.45 db. These differences indicated that the amount of sound produced by each zone was different. Therefore, the closer to the sound source, the higher the noise level. Furthermore, high pollutants were also due to heterogeneous environmental conditions.

The experimental results showed that zoning the airport area did not affect the scope of human activity. Based on the Minister of Environment Decree No. KEP-48 / MENLH / 11/1996, the noise standard for residential areas was 55 db (State Minister of the

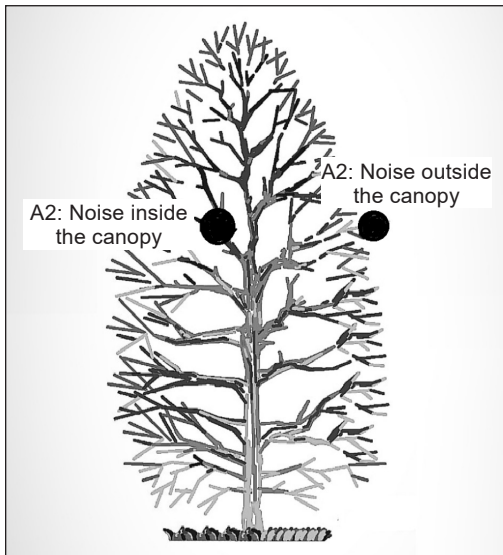


Figure 3. Noise measurement

Environment, 1996). Therefore, the noise has not had a real effect in reducing the sound for the space needs of human activities.

Landscape plants with different morphological characteristics have different abilities to reduce noise. Differences in the absorption of Pb metal occurred in the three species. Meanwhile, differences in reduction and absorption also happened in the zoning area. The highest noise reduction ability in each zone (zone 1,2,3) was *P. orientalis* (fan pine) plants. It reduces noise up to 6.54 db, while the highest ability to absorb heavy metals was by *C. variegatum* (croton) with the absorption of 17,77 ppm by the

difference between the Pb content of the airport area (18,34 ppm) and home garden (0,64 ppm). Therefore, the dominant abilities of landscape plants were different.

The morphological characteristics of needle-shaped *P. orientalis* (fan pine) leaves (Table 3) had a high noise reduction value. Furthermore, it has a fast photosynthetic rate compared to *S. myrtifolium* (red shoot) and *C. variegatum* (croton). Therefore, needle-shaped plants with a fast photosynthesis rate can be used for effective noise reduction.

The noise condition at zone 1 of the airport was 76.13 db, which was expected to be reduced to 6.54 db. In high noise conditions, zone 1 had high pollutant levels. Therefore, it was necessary to have a proportional composition of planting in the airport landscape area. Therefore, recommendations for the arrangement in the first layer of zone one was *P. orientalis* (fan pine) with a larger proportion. In contrast, the second and third layers were *C. variegatum* (croton) and *S. myrtifolium* (red shoot). The selection of *P. orientalis* (fan pine) in layer one of zone 1 was because the plant absorbs air pollution and does not reach areas outside the airport.

The percentage of plant composition in zone one for *P. orientalis* (fan pine) was 50%. Furthermore, *C. variegatum* (croton) in the second layer with a total percentage of 25% was expected to absorb pollutants where the highest source was in zone 1. The *S. myrtifolium* (red shoot) plant in the third layer with a composition of 25% was expected to be a noise reduction plant. It was because the sound not obstructed by *P. orientalis* (fan pine) can be suppressed. Moreover, the proportional planting of *S. myrtifolium* (red shoot) in layer three should absorb pollutants in areas outside the airport since three species of landscape plants can filter ecologists.

Furthermore, in the second zone, with a noise level of 74.45 db and high metal pollutants, landscape plants should minimise ecological conditions at the airport. The planting proportion in zone two was *C. variegatum* 50% (croton), *P. orientalis* (fan pine) 30%, and *S. myrtifolium* (red shoot) 20%. *C. variegatum* (croton) on the first layer absorbs pollutants from planes and other airport activities. In the second layer, planting a *P. orientalis* (fan pine) reduces the sound source from planes and other activities. Finally, *S. myrtifolium* (red shoot) with moderate metal reduction and absorption capabilities neutralises the second zoning area in the third layer.

In zone three, the proportions of landscape plants were 40% *S. myrtifolium* (red shoot), 30% *C. variegatum* (croton), and 30% *P. orientalis* (fan pine). In layer one, the arrangement of *S. myrtifolium* (red shoot) plants reduces noise from pressure at sound sources of the airport. In addition, the plant suppresses pollutants from the airport area to the residential zone. *C. variegatum* (croton) was planted in the second layer to expect the pollutant absorption to be more optimal since it does not reach the residential area. Finally, in the third layer, *P. orientalis* (fan pine) was planted at a percentage of 20% since open sound sources can be absorbed to prevent them from reaching the houses in the airport area.

The significance of the urgency in selecting *P. orientalis* (fan pine) plants becomes the input for planting vegetation in the airport area. Furthermore, plant species in the same family as *P. orientalis* (fan pine), such as Cupresaceae and needle-shaped leaves, were used to combine plant selection in green open space arrangement. The selection of plant species, such as *S. myrtifolium* (red shoot), was used as an alternative for planting in airport landscapes. Moreover, shrubs may also be used as input or recommendations for selecting vegetation planting in the airport landscape. Besides *P. orientalis* (fan pine) and *S. myrtifolium* (red shoot), *C. variegatum* (croton) species with high canopy characteristics were used as input as one of the available vegetation in the airport layout.

The morphological characteristics of *P. orientalis* (fan pine), *S. myrtifolium* (red shoot), and *C. variegatum* (croton) were used as input for selecting the airport landscape. Planting a mixed crop with the input of various plant species may be perfect in utilising the function of landscape plants as an air filter, especially in reducing noise and absorbing air pollution.

CONCLUSION

P. orientalis (fan pine) was a landscape plant with an increased noise reduction ability of 6.54 db. This study reported that the plant with the most potential as a Pb absorbent was *C. variegatum* (croton), with absorption of 17,77 ppm. Furthermore, a mixed crop was recommended because landscape arrangement provides an optimal function. Besides functioning as a chemical pollutant absorbent, landscape plants also act as noise reduction, qualitative and quantitative.

ACKNOWLEDGMENTS

The author is grateful to the LPDP (Educational Fund Management Institution), Indonesian Ministry of Finance, for providing financial support during research and studies at Gadjah Mada University.

REFERENCES

- Andersen, Z. J., Hvidberg, M., Jensen, S. S., Ketzel, M., Loft, S., Sørensen, M., Tjønneland, A., Overvad, K., & Nielsen, O. R. (2011). Chronic obstructive pulmonary disease and long-term exposure to traffic-related air pollution. *American Journal of Respiratory and Critical Care Medicine*, 183(4), 455-461. <https://doi.org/10.1164/rccm.201006-0937OC>
- Ashford, N. J., Mumayiz, S., & Wright, P. H. (2011). *Airport engineering planning, design and development of 21st century airports fourth edition*. John Wiley & Sons, Inc. <https://doi.org/10.1002/9780470950074>
- Azzahro, F., Yulfiah., & Anjarwati. (2019). Penentuan hasil evaluasi pemilihan spesies pohon dalam pengendalian polusi udara pabrik semen berdasarkan karakteristik morfologi [Determining the results of the evaluation of tree species selection in air pollution control of cement factories based on morphological characteristics]. *Journal of Research and Technology*, 5(2), 89-98.
- Black, D. A., Black, J. A., Issarayangyun, T., & Samuels, S. E. (2007). Aircraft noise exposure and resident's stress and hypertension: A public health perspective for airport environmental management. *Journal of Air Transport Management*, 13(5), 264-276. <https://doi.org/10.1016/j.jairtraman.2007.04.003>
- Carpenter, P. L., Walker T. D., & Lanphear F. O. (1975). *Plant in the landscape*. W.H. Freeman and Co.
- Clark, C., Head, J., & Stansfeld, S. A. (2013). Longitudinal effects of aircraft noise exposure on children's health and cognition: A six-year follow-up of the UK RANCH cohort. *Journal of Environmental Psychology*, 35, 1-9. <https://doi.org/10.1016/j.jenvp.2013.03.002>
- Corbitt, R. A. (Ed). (2004). *Air pollution in standard handbook of environmental engineering second edition*. McGraw-Hill.
- Dudka, S., Piotrowska, M., & Terelak, H. (1996). Transfer of cadmium, lead, and zinc from industrially contaminated soil to crop plants: A field study. *Environmental Pollution*, 94(2), 181-188. [https://doi.org/10.1016/S0269-7491\(96\)00069-3](https://doi.org/10.1016/S0269-7491(96)00069-3)
- Ferguson, J. E. (1990). *The heavy elements: Chemistry, environmental impact and health effects*. Pergamon Press.
- Fitriyati, N., & Nasrullah, N. (2005). The role of vegetation canopy as noise barrier. *Jurnal Lanskap Indonesia*, 1(1), 4-6.
- Hendrasarie, N. (2007). Kajian efektifitas tanaman dalam menyerap kandungan pb di udara [Study of the effectiveness of plants in absorbing lead content in air]. *Jurnal Rekayasa Perencanaan*, 3(2), 1-15.
- Herawati, P. (2016). Dampak kebisingan dari aktifitas bandara sultan thaha Jambi terhadap pemukiman sekitar bandara [Impact of noise from Sultan Thaha Airport activities Jambi towards settlements around the airport.]. *Jurnal Ilmiah Universitas Batanghari Jambi*, 16(1), 104-108.

- Hidayat, I. W. (2010). Study of the ecological function of roadside greenery as environmental bulfer on jagorawi highway. *Jurnal Manusia dan Lingkungan*, 17(2), 124-133.
- Koeppel, D. E., & Miller, R. J. (1970). Lead effect on corn mitochondrial respiration. *Science*, 167(3923), 1376-1378. <https://doi.org/10.1126/science.167.3923.1376>
- Kurniawati, L., Syamsidar, H. S., & Kurnia, R. (2016). Fitoremediasi logam kadmium (Cd) dari asap rokok menggunakan tanaman puring [Phytoremediation of cadmium metal (Cd) from cigarette smoke using croton (*Codiaeum variegatum*)]. *Jurnal Al- Kimia*, 4(1), 62-67. <https://doi.org/10.24252/al-kimia.v4i1.1457>
- Maleki, K., & Hosseini, S. M. (2011). Investigation of the effects of leaves, branches and canopies of trees on noise pollution reduction. *Annals of Environmental Science*, 5, 13-21.
- Martuti, N. K. T. (2013). The role of plants against air pollution in the protocol street of Semarang city. *Journal Biosantifika*, 5(1), 36-42.
- Megia, R., Ratnasari., & Hadisunarso. (2015). Karakteristik morfologi dan anatomi, serta kandungan klorofil lima kultivar tanaman penyerap polusi udara sansevieria trifasciata [Morphological and anatomical characteristics, as well as chlorophyll content of five cultivars of air pollution-absorbing *Sansevieria tripasciata*]. *Jurnal Sumberdaya Hayati*, 1(2), 34-40.
- Menteri Negara Lingkungan Hidup. (1996). *Baku tingkat kebisingan* [Standard noise level]. Surat Keputusan Menteri Negara Lingkungan Hidup Nomor: Kep 48/MENLH/1996/25 November 1996. Jakarta.
- Nugraheni, D. S., Putri, R. A., & Rini, E. F. (2018). The capability of vegetation cover of rth in absorbing co₂ emission of transportation sector in Surakarta city. *Jurnal Pembangunan Wilayah dan Perencanaan Partisipatif*, 12(2), 182-198.
- Price, M. A. (1988). Sound attenuation through trees: Measurement and models. *Journal of Acoustical Society of America*, 84(5), 1836-1844. <https://doi.org/10.1121/1.397150>
- Putra, I. S., Rombang, J. A., & Nurmawan, W. (2018). Analisis kemampuan vegetasi dalam meredam kebisingan [Analysis of vegetation capability to reduce noise]. *Eugenia*, 24(3), 105-115. <https://doi.org/10.35791/eug.24.3.2018.22660>
- Setiawan, I., Majid, S. A., & Yuliantini, Y. (2013). Airport factor in flight delays in Indonesia. *Jurnal Manajemen Transportasi & Logistik*, 2(3), 365-384. <http://dx.doi.org/10.25292/j.mtl.v2i3.115>
- Shannigrahi, A. S., Sharma, R., & Fukushima, T. (2010). Air pollution control by optimal green belt development around the victoria memorial monument, Kolkata (India). *International Journal of Environmental Studies*, 60(3), 241-249. <https://doi.org/10.1080/0020723022000008202>
- Sumathi, N., & Parthasarathi, A. (2018). Analysis of airport operations. *International Journal of Latest Technology in Engineering, Management & Applied Science (IJLTEMAS)*, 7(3), 119-123.
- Yang, H. S., Kang, J., & Cheal, C. (2013). Quantifying scattered sound energy from a single tree by means of reverberation time. *The Journal of the Acoustical Society of America*, 134(1), 264-274. <https://doi.org/10.1121/1.4808175>



Crack Behaviour of Self-Compacting Concrete (SCC) Beams Containing Eggshell in Flexural

Mohd Raizamzamani Md Zain^{1*}, Oh Chai Lian¹, Lee Siong Wee², Norrul Azmi Yahya¹ and Anizahyati Alisibramulisi¹

¹School of Civil Engineering, College of Engineering, Universiti Teknologi MARA, 40450, Shah Alam, Selangor Darul Ehsan, Malaysia

²School of Civil Engineering, College of Engineering, Universiti Teknologi MARA Johor, Pasir Gudang Campus, 81750, Masai, Johor, Malaysia

ABSTRACT

Rapid innovations in the ever-expanding area of the construction sector have turned into such a self-compacting concrete investigation (SCC). As a result of the effect on financial and ecological values, the importance of such innovation is expanding quickly. Many researchers have improved the efficiency of the present SCC using industrial materials. Pertinently, substituting cement with surplus material in the manufacture of concrete is environmentally sustainable. Eggshell has become one of the possible alternatives for cementitious material because it encompasses a compound of calcium. Such endeavour is primarily driven by the restriction of landfill sites and the desire to decrease the warming effect. This study describes the failure behaviour and cracks characteristics of SCC beams comprising eggshells under flexural assessment. In order to measure its compressive

strength, an SCC mixture encompassing eggshells was developed and evaluated. The ultimate flexural strength and propagation of cracks were discussed for SCC beams tested under flexural using a various a/d (shear span to an effective depth) ratio. The SCC beams crack widths were also validated with Eurocode2. When loads are placed close to supports (lower a/d ratio), the results show that SCC beams can sustain a higher load with improved deflection control. The finding among all SCC beam assessments

ARTICLE INFO

Article history:

Received: 26 May 2021

Accepted: 4 August 2021

Published: 28 October 2021

DOI: <https://doi.org/10.47836/pjst.29.4.44>

E-mail addresses:

raizam@uitm.edu.my (Mohd Raizamzamani Md Zain)

chailian@uitm.edu.my (Oh Chai Lian)

leesiongwee@uitm.edu.my (Lee Siong Wee)

norrulazmi@uitm.edu.my (Norrul Azmi Yahya)

aniza659@uitm.edu.my (Anizahyati Alisibramulisi)

*Corresponding author

unveiled that the initial value of experimental crack width was significantly less than the 0.3mm maximum crack control limit delineated by Eurocode2 (EN 1992-1-1, 2004). Various kinds of crack characteristics have also been detected in SCC beam specimens marked as flexural, shear, and combination of shear-flexural cracks.

Keywords: Crack patterns, eggshell, flexural strength, SCC beams, self-compacting concrete

INTRODUCTION

Concrete has figured prominently and is also the most widely used construction material for hundreds of years, particularly in building applications. Now, a considerable effort is being made to improvise the properties of concrete, whether through its shear and flexural strength, tensile strength, compressive strength, aesthetic appearance or compaction properties. Nowadays, numerous types of recycled materials have been used in the building industry. Waste materials, including fly ash, bottom ash, sludge, palm oil and eggshells, have been used to manufacture concrete and have become a common alternative to well-functioning concrete technology. These helped increase profits in addition to reducing the number of waste products. Furthermore, incorporating mineral admixtures in the concrete mixture has resulted in SCC produced cheaply while not undermining the other features of the concrete concurrently.

Self-compacting concrete (SCC) could also be defined as concrete that does not necessitate compaction and spreads through its weight even without bleeding and segregation to enable greater compactness and placement. SCC had first been initially developed in 1983 to address the resilience of concrete buildings in Japan due to the deficiency of qualified workers (Okamura & Ouchi, 2003; Akinpelu et al., 2019; Siddique, 2011). Adequate compaction via qualified labour is necessary to create long-lasting concrete buildings. Nevertheless, the steady drop in the number of qualified construction workers has resulted in a corresponding decline in the quality of construction activities. Therefore, the utilisation of SCC, which could be compacted into every section of a formwork, became one alternative for achieving long-lasting concrete buildings, regardless of the quality of construction activities. SCC has numerous benefits, including the avoidance of expensive labour activities, which improves the construction site's productivity from the contractor's perspective. Furthermore, as vibration is excluded during casting processes, workers have few intensive tasks with substantially less noise. It is indeed a revolutionary concrete capable of flowing under its weight, entirely covering the formwork and thus maximising compaction (Okamura & Ouchi, 2003; Akinpelu et al., 2019).

However, the only concern with self-compacting concrete was its cost. It contributes to the massive amount of Portland cement and preserving the needed freshness and durability of the SCC. As demonstrates by EPG (2015), Challagalli and Hiremath (2017), Dinakar

et al. (2008), Dinakar et al. (2013), Safi et al. (2013), Siddique (2011), and Faraj et al. (2020), the approach to attain the performance and intended freshness of the SCC via the utilisation of mineral mixtures such as fly ash, silica fumes, plastic waste, tyre rubber waste and fibre, which finely granulated and blended into a concrete mixture. It indicates that it is possible to obtain a multitude of SCC strengths utilising waste materials. SCC typically uses lesser volumes and smaller amounts of coarse aggregates relative to conventional concrete, which greatly influences the mechanical properties (Yerramala, 2014; Oh et al., 2019; Olowofoyeku et al., 2019).

Furthermore, apart from examining the rheological features of SCC incorporating waste materials, many researchers also have explored the hardened properties, shear and flexural characteristics of SCC (Domone, 2007; Tang et al., 2016; Panda & Bal, 2013; Karthick et al., 2014; Parthasarathi et al., 2017). Domone (2007) reviewed and correlated over 70 research findings on the hardened features of SCC in order to generate comparative analysis with the characteristics of similar strength of ordinarily or normally vibrated concrete (NVC). Tang et al. (2016) and Panda and Bal (2013) evaluated the hardened properties of SCCs comprising recycled coarse aggregates. Concrete reuse such as recycled coarse aggregates not just preserves virgin resources of concrete but also decreases environmental impacts and directly eliminates carbon dioxide from the atmosphere. Nevertheless, according to Panda and Bal (2013), the results of split tensile, compressive and flexural strengths of the SCC encompassing the natural aggregate is more than the SCC comprising the recycled concrete aggregate (RCA). As a result, multiple substitutes were adopted, including agricultural by-products such as eggshells as a partial substitute for sand or cement.

Karthick et al. (2014) performed an experimental study to evaluate the influence of eggshells as a partial substitution of sand in concrete, having undergone split tensile, compressive and flexural strength tests. The researchers discovered that the concrete compressive strength fulfilled the desired strength with an optimal proportion of 20 per cent of eggshells as a substitute for sand in the mixture of concrete. The use of eggshell and silica fume as partial substitutes of cement was also being investigated by Parthasarathi et al. (2017). The tests demonstrated that the inclusion of waste products such as silica fume improves strength. However, the substitution of eggshell powder (ESP) seems more cost-effective and produces the predicted strength. This research investigation has shown that the ESP alone can serve as a substitute for cement, enhancing the concrete strength parameters and reducing the need for cement.

Numerous studies have been carried out to examine the behaviour of self-compacting concrete beams (Sonebi et al., 2003; Tošić et al., 2016; Boel et al., 2010; Hassan et al., 2008; Mahmud et al., 2018; Sharifi, 2012; Harkouss & Hamad, 2015; Odaa et al., 2021). In terms of shear and flexural characteristics, Tošić et al. (2016) provided a comprehensive study on shear and flexural characteristics of beams utilising RCA with and without

stirrup. The results have shown that the shear and flexural strength of the concrete beam specimens without stirrups seem to be in close agreement with Eurocode2 (EN 1992-1-1, 2004). Boel et al. (2010) explored the shear strength of normal vibrated and SCC beam samples. The aggregate content in the SCC sample was 43 per cent lower. The findings demonstrate that the shear capacity of a normal vibrated concrete (NVC) beam sample is significantly higher than that of an SCC beam sample, which could be attributed to higher aggregate interlock triggered by higher coarse aggregates (Boel et al., 2010). Hassan et al. (2008) also investigated the strength properties (shear capacity) and cracking behaviour patterns of full-scale concrete beams of SCC and NVC. Compared to NVC beams, SCC beam samples had a reduced maximum shear strength due to fewer coarse aggregates in SCC beams than in NVC samples.

Mahmod et al. (2018) examined the flexural strength of 14 reinforced SCC beams comprising varying percentages of steel fibre. The results have been compared to the international standard (ACI CODE-318-14, 2014). Flexural strength in beams has been found to upsurge with increasing compressive strength of concrete, the ratio of longitudinal steel rebar, and fibre content. Sharifi (2012) investigated and compared the mechanical characteristics of reinforced SCC beams to the anticipated provisions code for NVC. The findings suggest that theoretical estimations for reinforced concrete beams are reliable enough to be applied in assessing SCC beam capacities (Sharifi, 2012). Although a great deal of work was undertaken on reinforced concrete beams containing additives or waste, specific information of the failure behaviour and crack patterns of SCC beams containing eggshells in flexural are minimal, and the subject remains open.

Based on the preceding literature search, the ESP has demonstrated to be an excellent catalyst for cement-bound material due to several advantages, including being rich in calcium composition, quite similar to the limestone used to make cement. The eggshell thus becomes beneficial for lessening the need for cement in concrete casting and seems to be useful for recycling waste materials. Thereby, in consideration of these and taking into account the benefit of the use of ESP in the manufacture of SCC beams, a series of laboratory testing were employed to examine the flexural strength and analyse the characteristics of the crack of SCC beams encompassing ESP under bending assessment.

METHOD

For this research, an experimental study was conducted on SCC beams comprising eggshells as a cement substitute. The preparation of the production of the SCC beams was separated into two (2) stages. The first stage necessitates establishing the SCC mixture. The second stage entails the testing process of SCC beams under flexural to evaluate their structural strengths and assess crack patterns, as illustrated in Figure 1. Particulars upon this preparation of specimens, the set-up of the test and the laboratory tests were presented and explained in the subsequent sub-topics.

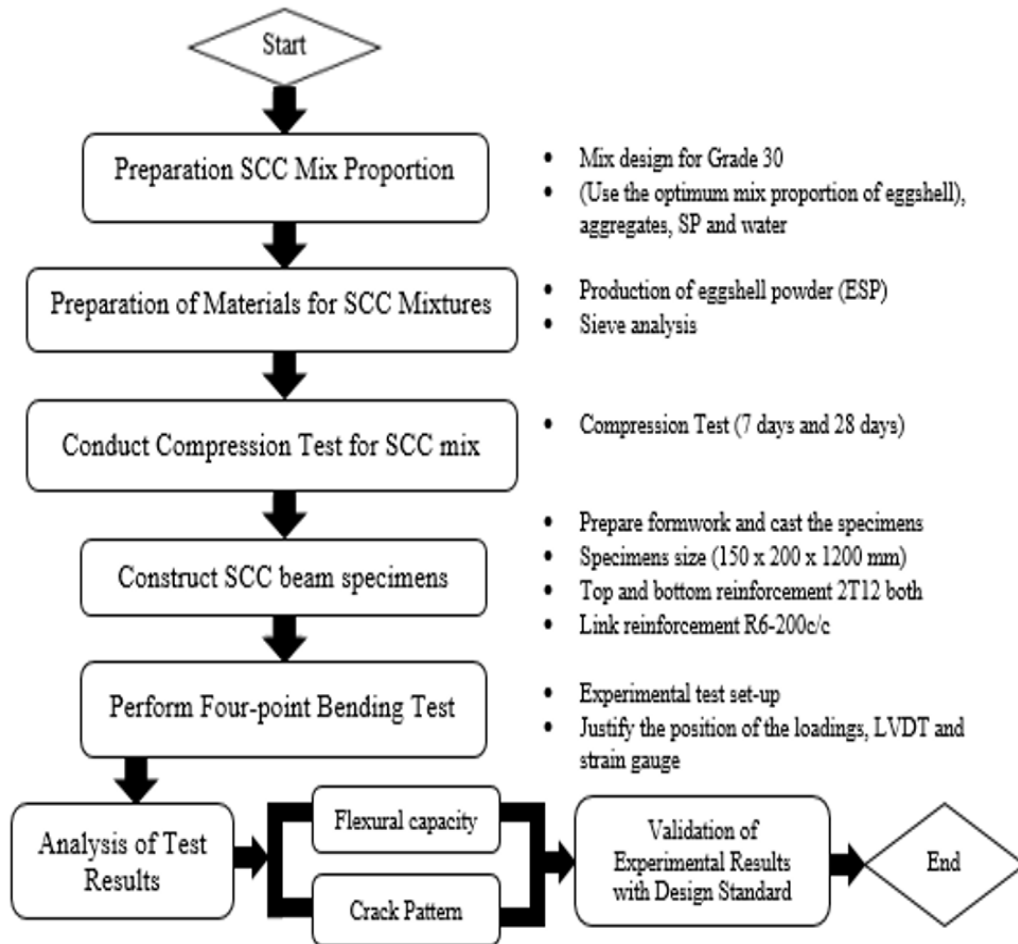


Figure 1. A research flow chart that summarises the process of preparing and testing beam specimens

Materials and Mixture Proportions

The key materials involved in this laboratory study encompass Portland cement, coarse aggregate, water, eggshell, fine aggregate and superplasticiser, as depicted in Figure 2. In this SCC mixture, the ESP and ordinary Portland cement have been employed as binders. Also, the coarse aggregate (CA) size used was less than 10 mm for the mixture of SCC, as anticipated in the mix design. In order to accomplish the preferred aggregate size, it was sieved before being employed in the concrete mix. While, for fine aggregates (FA), the natural sand, with the size around 0.3mm to 0.8mm, was used. The ratio of fine-coarse aggregates and water-cement was 0.6 and 0.4, respectively. Besides that, type of superplasticiser (SP) used was BASF MasterGlenium8784 obtained from BASF (Malaysia) Sdn Bhd situated in Selangor, as shown in Figure 2(d). The quantity of superplasticiser applied to the mixture was 1% of the amount of cement content. Besides that, eggshells

gathered from different sources were crushed via grinders and sieved by sieving machines to attain 0.6 μm of fine eggshell powder (ESP), as displayed in Figure 2(e).

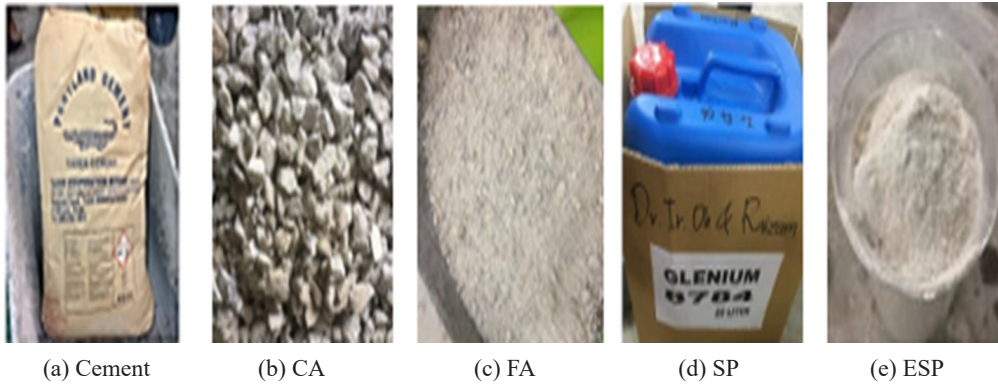


Figure 2. SCC constituent materials

The mixing design process was undertaken in compliance with BS 1881-125:2013 (2013) (standard design procedure). The number of constituent materials employed for all SCC mixtures encompassing 0.6 μm eggshell as cement substitute is indicated in Table 1. Meanwhile, the chemical properties of cement and eggshell are demonstrated in Table 2.

Table 1

Quantity of constituent materials used for the SCC mixture

Cement (kg/m ³)	FA (kg/m ³)	CA (kg/m ³)	Water (litre/m ³)	SP (litre/kg/m ³)	ESP (kg/m ³)
463.5	644	966	215	5.15	51.5

Table 2

Elemental composition of cement and eggshell powder

Elemental composition of cement		Elemental composition of eggshell powder	
Compositions	Percentage	Compositions	Percentage (%)
CaO	64.64	CaO	71.77
SiO ₂	21.28	SiO ₂	16.28
Fe ₂ O ₃	3.36	Fe ₂ O ₃	4.37
Al ₂ O ₃	5.60	Al ₂ O ₃	2.92
MgO	2.06	SO ₃	2.60
SO ₃	2.14		
Loss on Ignition	0.64		
Insoluble Residue	0.22		
Total Alkalis	0.05		

Details of Test for SCC Beam Specimens

In this study, SCC cubes and SCC beam specimens were prepared and tested for failure. A total of six SCC cubes (150mm x 150 mm in cross-sectional dimension with 150 mm in height) have been cast and tested for assessing their compressive strength (f_{cu}). In addition, SCC cube specimens were checked and tested for failure under axially compression loading after 7 days and 28 days of curing age to examine the hardened state of the mixture as shown in Figure 3, and the outcome is presented in Figure 4.



Figure 3. SCC cube under axially compressive loading

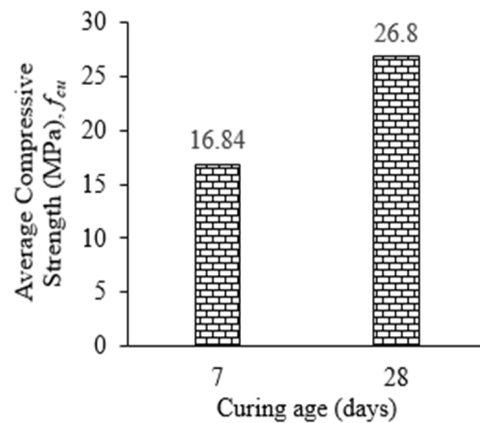


Figure 4. Hardened properties of the SCC mixture

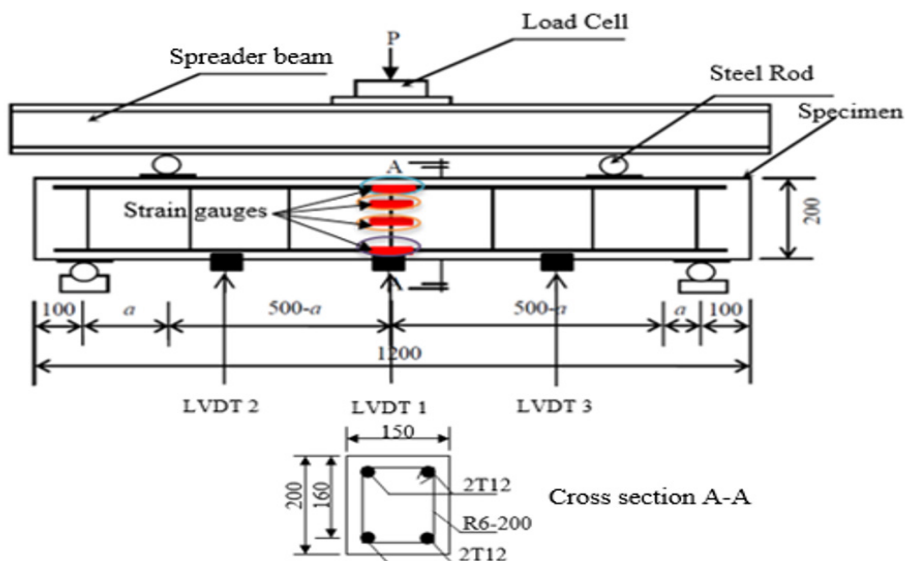
Three (3) numbers of SCC beam specimens (150mm x 200mm in cross-section and 1200mm length) comprising ESP labelled as SCCBESP1.0, SCCBESP2.0 and SCCBESP3.0 were constructed with 10 mm diameter of both upper and lower rebars. The nominal cover and effective depth of the SCC beams are 25mm and 160mm, respectively. Its high yield deformed longitudinal rebar, and the link of 6mm diameter have the characteristics strength of 460 N/mm² and 250 N/mm², respectively. The link was installed at 200mm spacing across the beam. All specimens of SCC beams were cast and tested for failure under flexural test after 28 days of their designated age.

Instrumentation, Procedure and Test Set-up

Under flexural inspection, all specimens of the SCC beam delineated as SCCBESP1.0, SCCBESP1.5 and SCCESP2.0 were tested up to failure utilising Universal Testing Machine (UTM). Also, every SCC beam specimen has been tested for failure under bending test (4-point flexural test) at a/d (shear span to effective depth) ratio of 1.0 ($a=160$ mm), 1.5 ($a=240$ mm) and 2.0 ($a=320$ mm), respectively, as depicted in Figure 5. The values of varying shear spans (a) were 320 mm, 240 mm and 160 mm. Linear variable differential

transformers (LVDTs) were positioned at one-third of the beam span from each support (lower part of the beams) and at the central part of the beam soffit to evaluate cross-head deformation under the applied load. The load applied was increased continuously till failure at a displacement rate of 0.01 mm/s.

All measurements were recorded automatically via an automated data acquisition system. The formation of cracks was observed and marked as shown in Figure 6(a). Assessment of the behaviour of cracks was visually conducted, whereas the crack patterns and propagation were hand-marked. Optical magnification X10 microscope (reading up to 0.02 mm) were used to measure the crack widths, as shown in Figure 6(b). Formation and spread of both shear and flexural cracks were recorded toward respectively applied loads.



(a) Load test schematic diagram (beam reinforcement arrangement)



(b) Universal Testing Machine (UTM) was used to conduct the beam load test

Figure 5. Experimental set-up of beam specimen and load test



(a) Cracks formation on SCC beam

(b) Measurement of crack widths via optical magnification X10 microscope

Figure 6. Observation and measurement of cracks on SCC beam specimen

RESULTS AND DISCUSSION

Under the flexural test, three SCC beam specimens containing eggshells as partial cement substitutes were prepared and tested for failure. In addition, measurements on the optimal flexural strength were reported for SCC beam specimens, and the observation on cracking features was deliberated on the subsequent sub-topics.

Flexural Strength

The flexural test performed on SCC beam specimens was used to assess the load-deflections curve relationship, types and patterns of cracks on beam specimens, and the initial beams crack width diameter. The result of the load versus deflection relationship of SCC beam specimens was depicted in Figures 7 to 9.

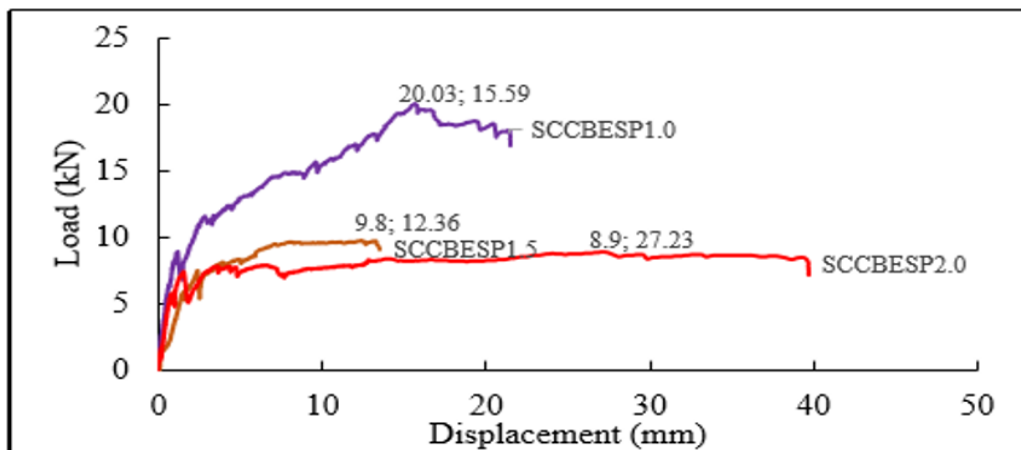


Figure 7. Applied load-mid-span deflection curves of SCC beam specimens (LVDT 1)

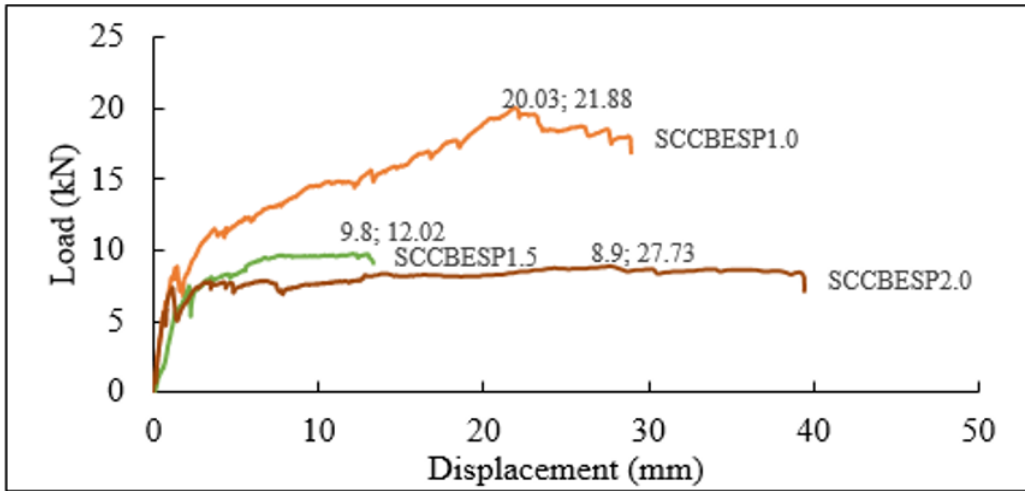


Figure 8. Applied load-mid-span deflection curves of SCC beam specimens (LVDT 2)

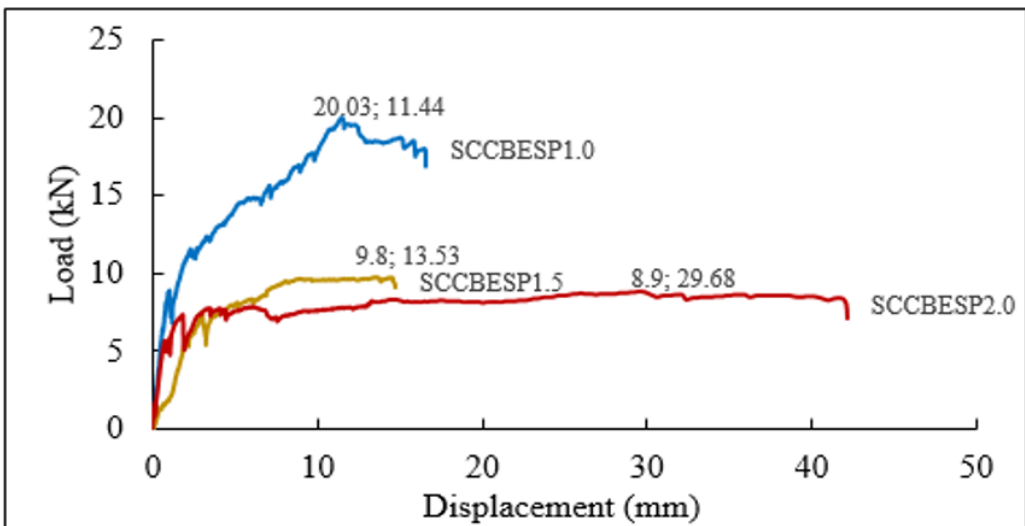


Figure 9. Applied load-mid-span deflection curves of SCC beam specimens (LVDT 3)

The relationship between load and deflection for SCCBESP1.0, SCCBESP1.5 and SCCESP2.0 of LVDT 1 (mid-span), LVDT 2 and LVDT 3 are presented in Figures 7 to 9, respectively. Typically, all load-deflection curves display a linear elastic pattern before switching to plastic. Nevertheless, the SCCBESP1.0 beam displayed higher failure loads (20.03kN) contrasted with SCCBESP1.5 (9.8kN) and SCCBECSP2.0 (8.9 kN). Pertinently, the load-deflection curves for SCCBESP1.0 signify a nonlinear rise, while for SCCBESP1.5 and SCCBESP2.0, the curves seem to be almost flat in the plastic area before the beams have failed. It is noticed that with a lower a/d ratio (or when loads have been put close to

supports), the beam can retain a higher load with improved deflection control compared to SCCBESP2.0.

Failure and Crack Behaviour

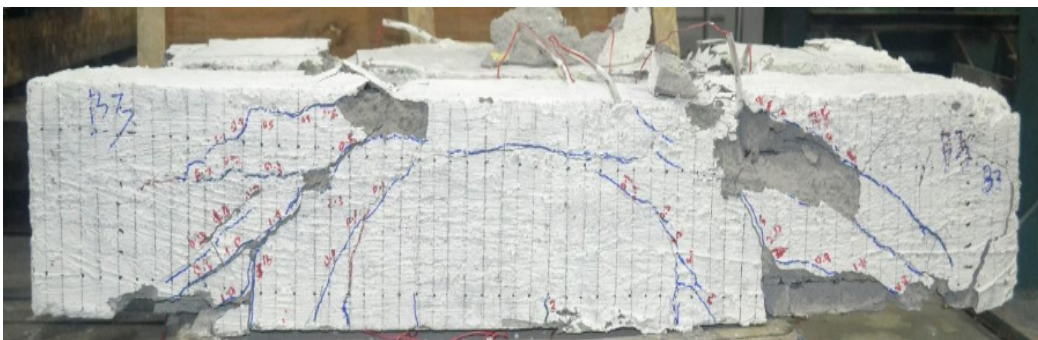
The characteristics of the crack were delineated in Figure 10 (a, b and c) with regards to the results gained through experimental observations for three (3) SCC beams, namely SCCBESP1.0, SCCBESP2.0 and SCCBESP3.0.



(a) SCCBESP1.0 (a=160mm)



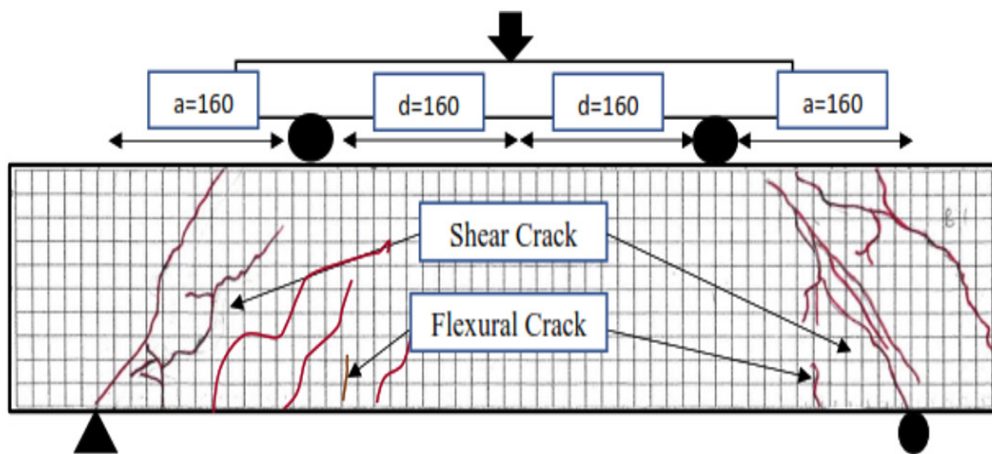
(b) SCCBESP2.0 (a=240mm)



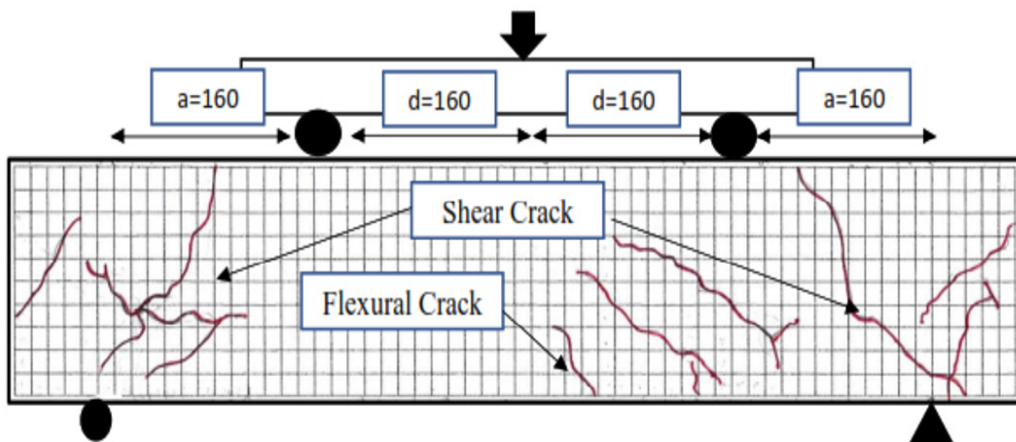
(c) SCCBESP3.0 (a=320mm)

Figure 10. SCC beams crack features in flexural

SCC beams with a wider range of cracks and cracks widths appeared to have emerged and were spotted at the support, and then spreads to the medium beam span as the a/d ratio upsurges from 1.0 to 2.0, as presented in Figure 10. It may be because the SCC beam comprising ESP suffered significant deformations prior to failure, which led to the establishment of more and broader cracks. Therefore, each of the developed cracks in the SCC beams was examined to assess the characteristics and patterns of cracks. The SCC beams cracking behaviour are depicted in Figures 11 to 13.

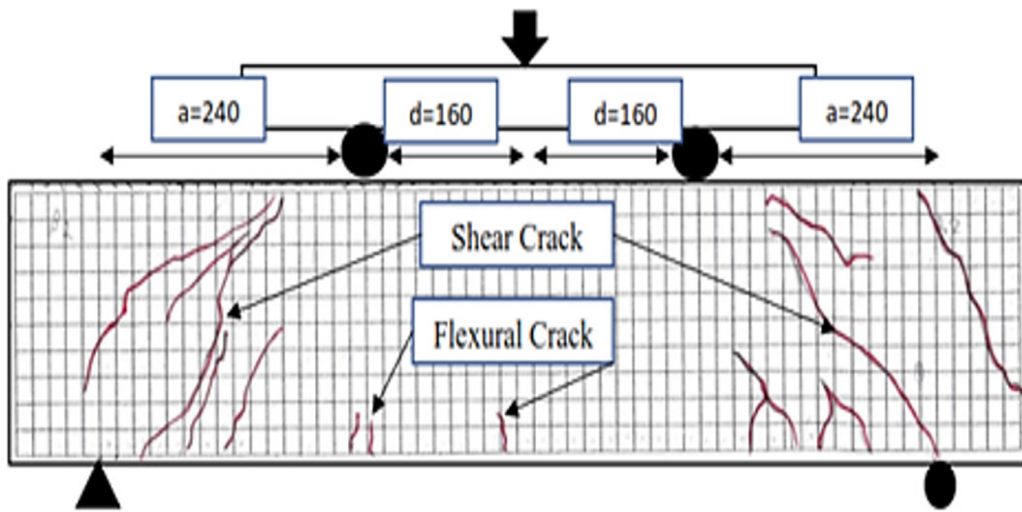


(a) Front observation

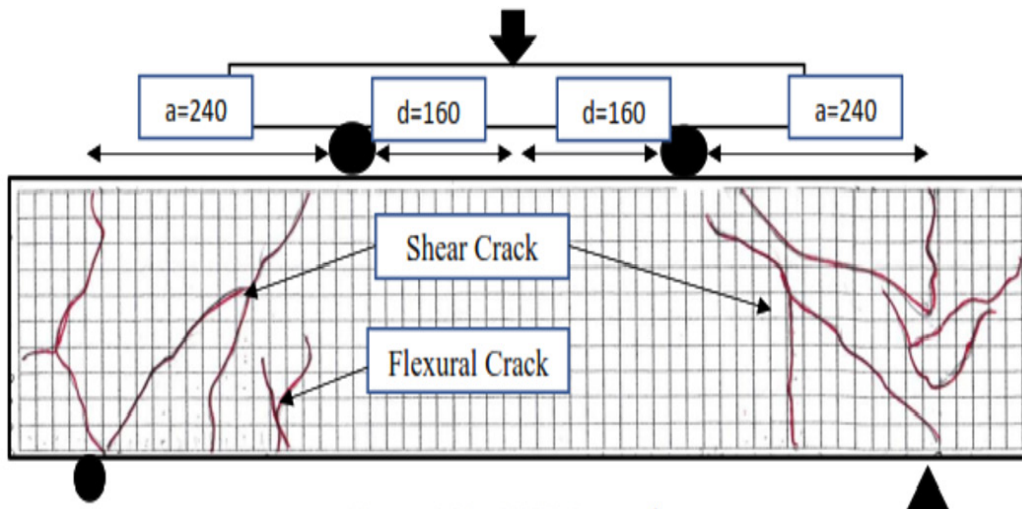


(b) Rear observation

Figure 11. Characteristics of cracks on SCC beams under flexural test ($a=160\text{mm}$)



(a) Front observation



(b) Rear observation

Figure 12. Characteristics of cracks on SCC beams under flexural test ($a=240\text{mm}$)

Shear cracks, flexural cracks, and shear-flexural cracks combination, as depicted in Figures 11 to 13, are the varieties of cracks observed for SCC beams. Shear cracks were found mostly at the support, while flexural cracks were noticed at the central part of the SCC beam span length. At quarter points along the SCC beam, shear cracks were detected (diagonal cracks). Afterwards, flexural fractures were formed vertically by enhancing the load, and cracks in the pattern of flexure-shear (inclined) started to emerge. Table 3 provides a comparative analysis of crack widths for all beam specimens tested

with international standard Eurocode2. The present result revealed that the initial crack width for SCCBESP1.0 was recorded as 0.1mm. Meanwhile, for specimens designates as SCCBESP2.0 and SCCBESP3.0, the initial crack width was recorded as 0.1mm and 0.1mm, respectively. Moreover, the ratio between both the experiments crack widths w_E and theoretical crack control width w_T (Eurocode2 (EN 1992-1-1, 2004)) for all beam specimens (SCCBESP1.0, SCCBESP2.0 and SCCBESP3.0) was recorded as 0.67, 0.33 and 0.33, respectively.

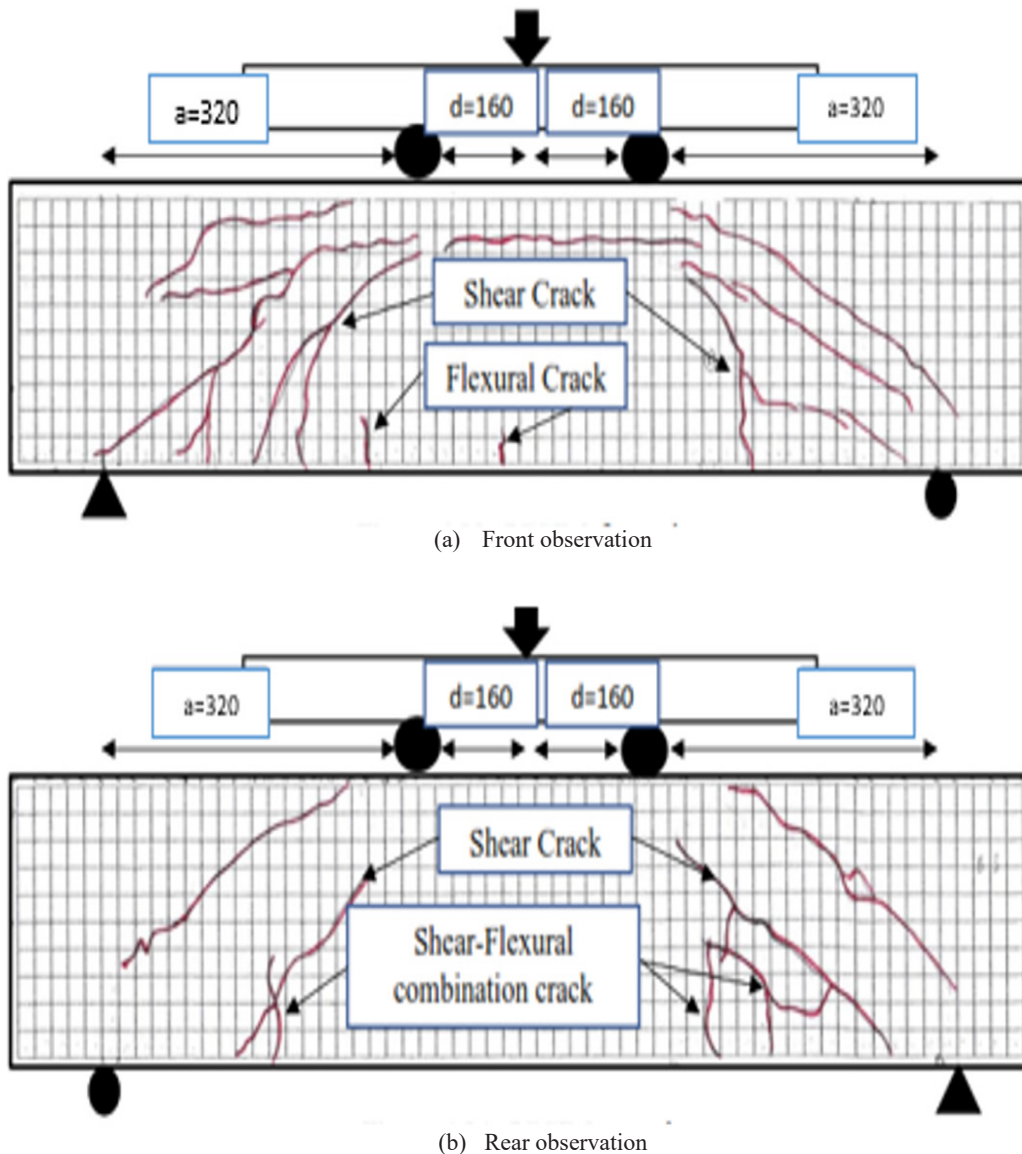


Figure 13. Characteristics of cracks on SCC beams under flexural test ($a=320$ mm)

Table 3

Comparative analysis of the experimental and theoretical crack widths (Eurocode2)

Mixture ID	* w_E	* w_T	w_E / w_T
SCCBESP1.0 ($a/d=1.0$)	0.2	0.3 – 0.4	0.67
SCCBESP2.0 ($a/d=1.5$)	0.1	0.3 – 0.4	0.33
SCCBESP3.0 ($a/d=2.0$)	0.1	0.3 – 0.4	0.33

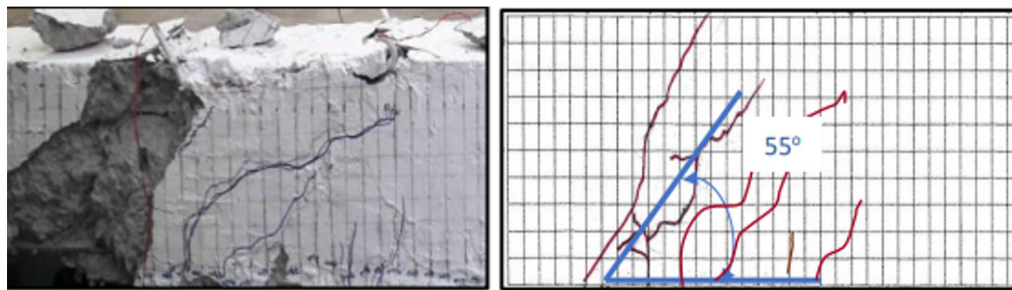
* w_E denotes the experimental crack width (mm)

w_T denotes the theoretical crack width (mm)

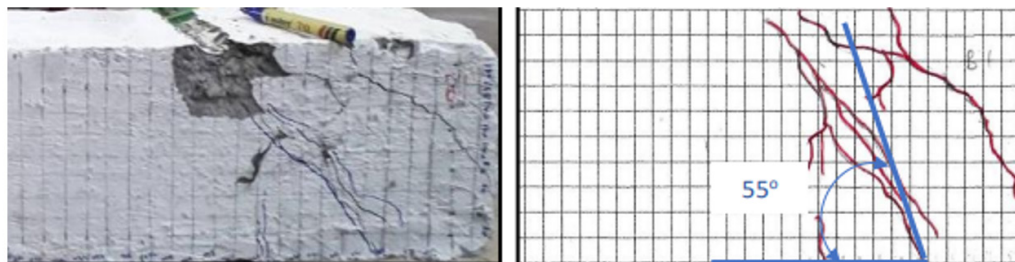
As portrayed in Table 3, the experimental crack widths w_E fulfilled the maximum theoretical crack width w_T (0.3mm–0.4mm) quantified by Eurocode2.

Correlation Among a/d Ratio and Critical Crack Width (CDC)

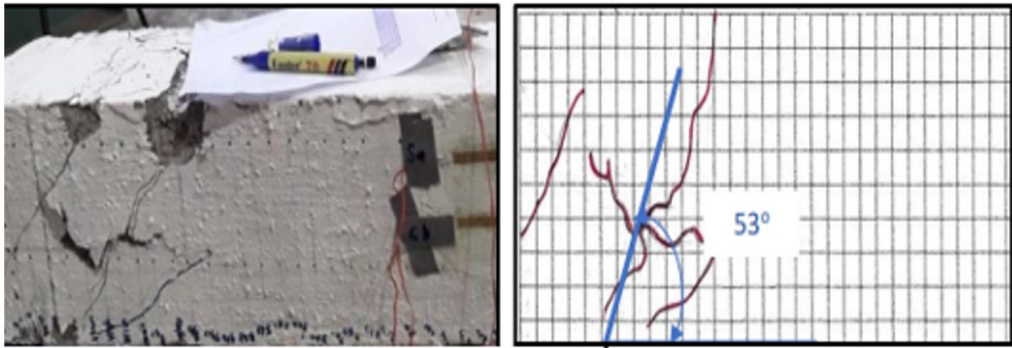
The critical diagonal crack, or delineated as CDC, was the significant crack that appeared when the beams underwent the load test and failed. Essentially, CDC occurred at the shear crack in which the initial crack took place. Therefore, the inclination angle of CDC regarding beam specimens longitudinal axis denotes as SCCBESP1.0, SCCBESP2.0, and SCCBESP3.0 was drawn as depicted in Figures 14 to 16.



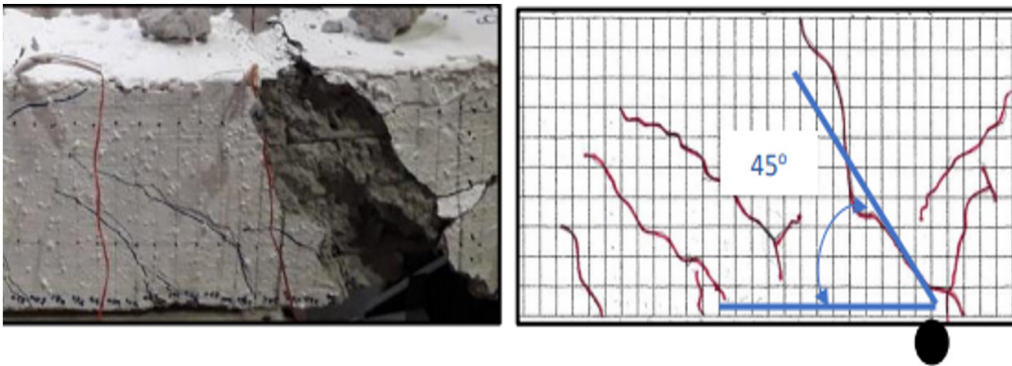
(a) Front view (Left)



(b) Front view (Right)

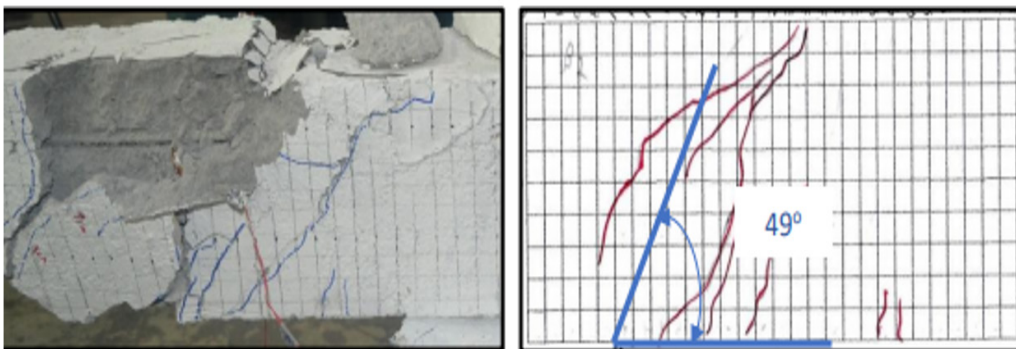


(c) Rear view (Left)

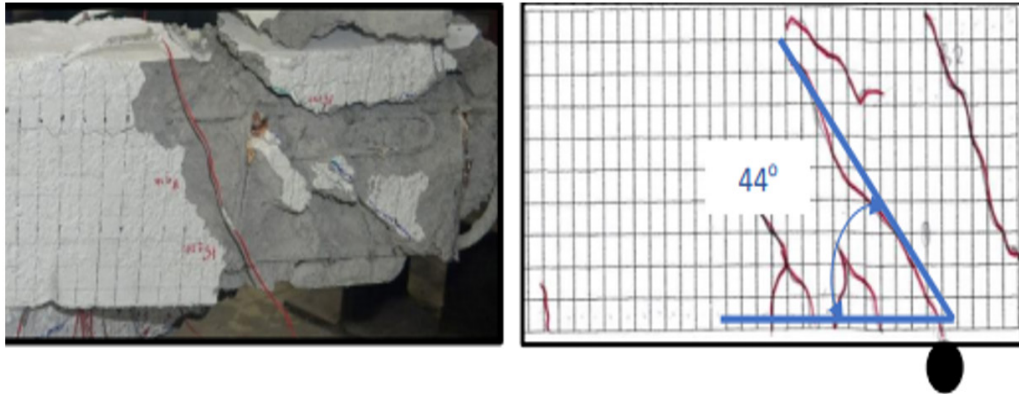


(d) Rear view (Right)

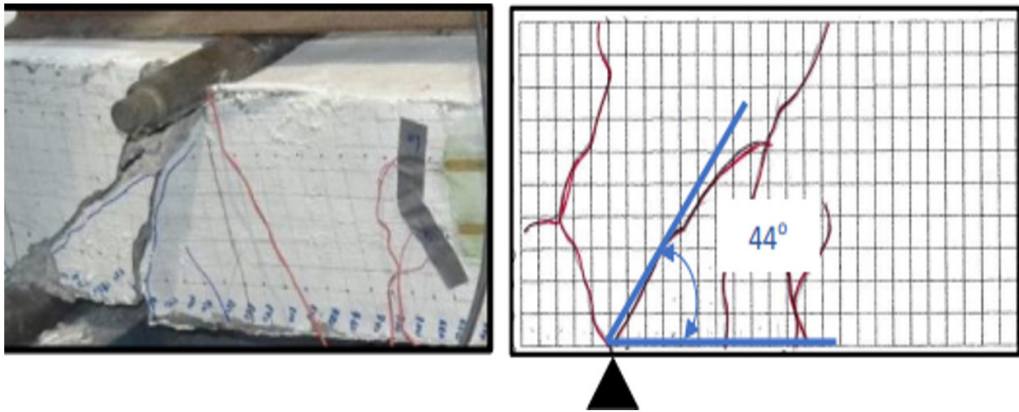
Figure 14. Critical crack width (CDC) of beam specimen (SCCBESP1.0)



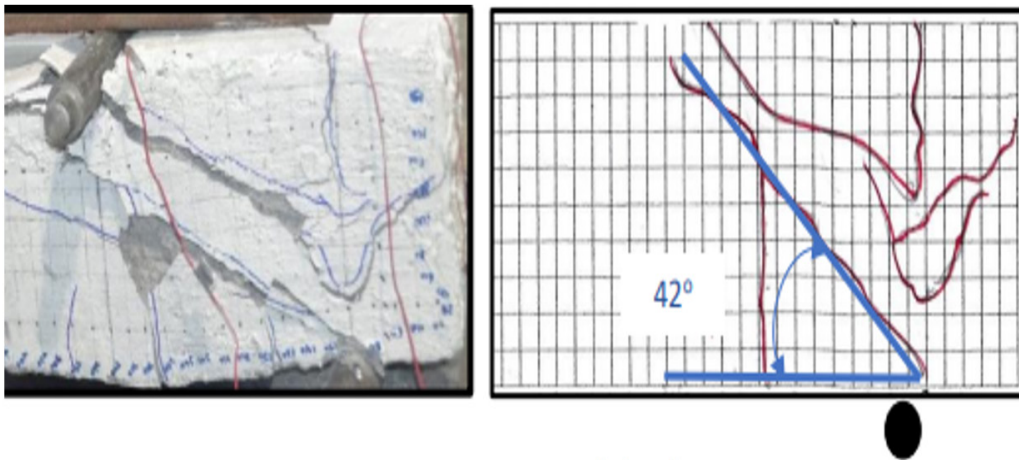
(a) Front view (Left)



(b) Front view (Right)

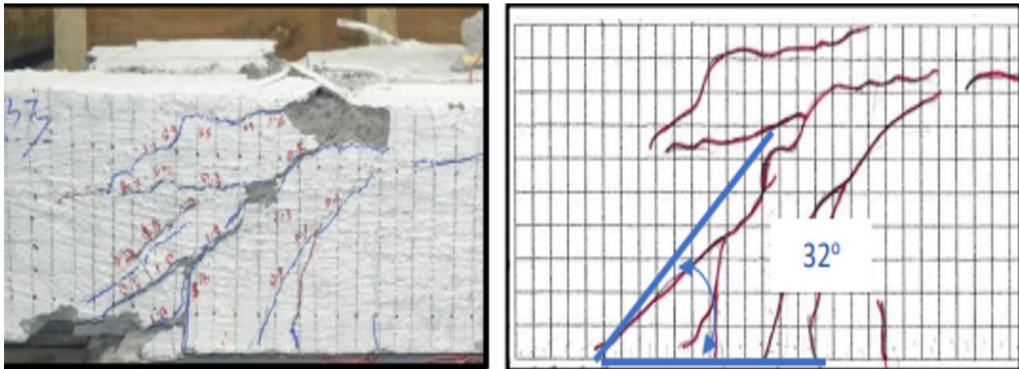


(c) Rear view (Left)

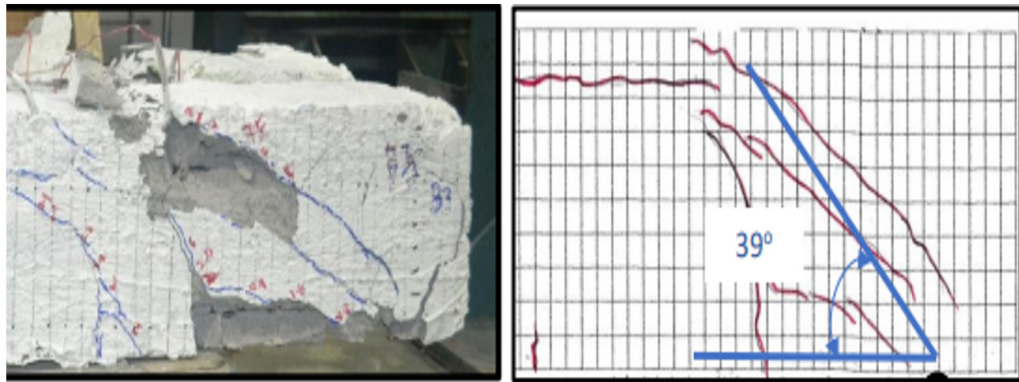


(d) Rear view (Right)

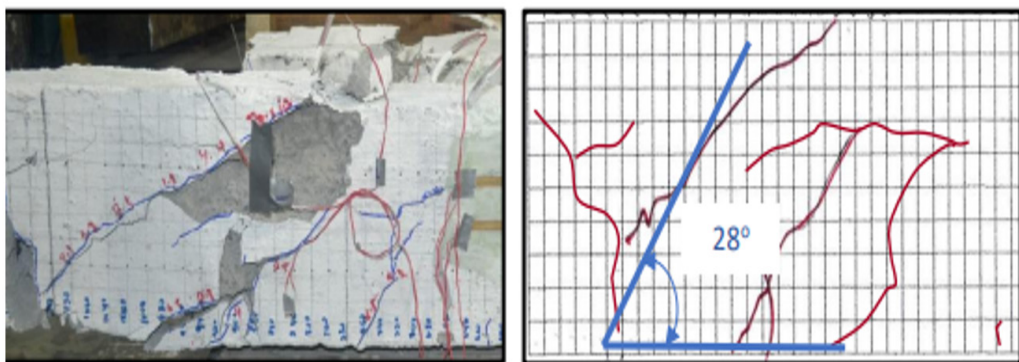
Figure 15. Critical crack width (CDC) of beam specimen (SCCBESP1.5)



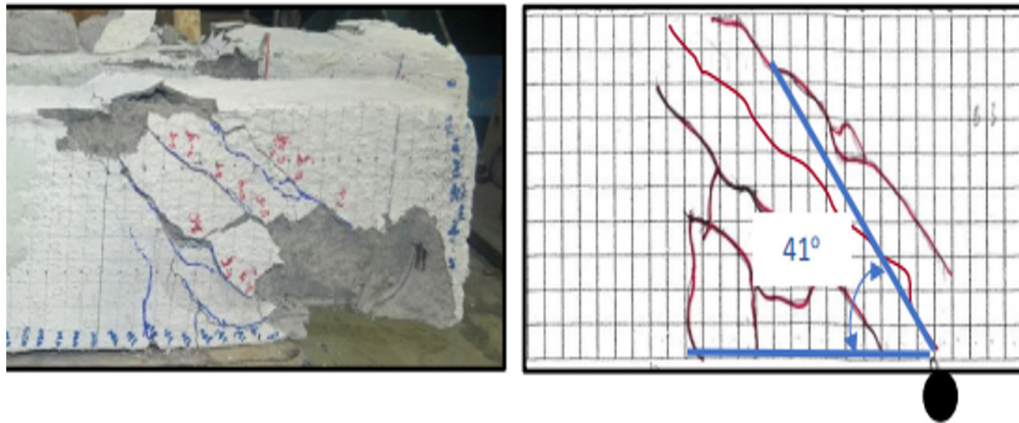
(a) Front view (Left)



(b) Front view (Right)



(c) Rear view (Left)



(d) Rear view (Right)

Figure 16. Critical crack width (CDC) of beam specimen (SCCBESP2.0)

The smallest critical diagonal crack (CDC) angle, as shown in Table 4 and detected from beam specimens, embodies as SCCBESP1.0, SCCBESP1.5, and SCCBESP2.0 was 28° [located at the SCCBESP2.0 rear view (right)]. In comparison, the largest CDC angle was 55° [located at the SCCBESP1.0 front view (left)]. Thus, the various types of cracks such as shear, flexural and combination of flexural-shear cracks caused a difference in angle between the front and rear views. With a mean value of 0.95, a standard deviation (SD) of 0.04 and a coefficient of variation (C.O.V) of 4.99 per cent, the experimental CDC angle located at the rearview (right) of all beam specimens is seen to correlate closely to the theoretically envisaged by Eurocode2 (EN 1992-1-1, 2004).

Table 4

Comparative analysis of the experimental and theoretical crack angle (Eurocode2)

Specimen designation	Inclination angle of CDC with regards to beam specimens longitudinal axis, θ_{CR} (°)				Theo. crack angle θ_{EC} (°)	$\theta_{CR} / \theta_{EC}$			
	Front view (left)	Front view (right)	Rear view (left)	Rear view (right)		Front view (left)	Front view (right)	Rear view (left)	Rear view (right)
SCCBESP1.0	55	55	53	45	22-45	1.22	1.22	1.18	1.00
SCCBESP1.5	49	44	44	42	22-45	1.09	0.98	0.98	0.93
SCCBESP2.0	32	39	28	41	22-45	0.71	0.87	0.62	0.91
Mean						1.01	1.02	0.93	0.95
Standard deviation (SD)						0.22	0.15	0.16	0.04
Coefficient of variation (C.O.V) (%)						26.3	17.5	30.6	4.99

CONCLUSION

The flexural behaviour and crack characteristics were assessed and observed, and the experimental outcomes were validated with the theoretical crack control value implied via Eurocode2 (EN 1992-1-1, 2004). The result of the study has directed to the subsequent conclusions:

1. The SCC beam can retain a higher load with enhanced deflection control when loads have been put near supports (lower a/d ratio).
2. On the SCC beam specimens, shear, flexural and shear-flexural cracks have been observed. Shear cracks were found mostly at the support, while flexural fractures were noticed at the centre of the beam span. At quarter points along the SCC beam, shear cracks were detected (diagonal cracks). Afterwards, cracks in the flexural shape developed vertically, and fractures in the form of flexure-shear (inclined) came into existence.
3. The crack width contour line was more toward the support when the a/d ratio dropped from 2.0 to 1.0. Nevertheless, once the SCC beam specimen was tested to failure subjected to a flexural test, the crack width contour line was detected more toward the central span of the SCC beam with a higher a/d ratio.
4. The outcomes of all SCC beams measurements found that the initial value of experimental crack width was well below the 0.3mm maximum crack control limit, as defined via Eurocode2 (EN 1992-1-1, 2004).
5. The experimental CDC angle located at the rearview (right) of all beam specimens has been seen to align closely to the theoretically proposed by Eurocode2 (EN 1992-1-1, 2004).

ACKNOWLEDGMENTS

The Ministry of Higher Education provided funding for the present work under the Fundamental Research Grant Scheme (FRGS) (600-IRMI/FRGS 5/3 (378/2019)). The authors are grateful to M. Fiqry Haziq Saharuddin for helping with the work of the laboratory. The authors also want to acknowledge the additional support of all technicians in the School of Civil Engineering laboratories, College of Engineering, Universiti Teknologi MARA (UiTM), Shah Alam in carrying out this work.

REFERENCES

- ACI CODE-318-14. (2014). *Building code requirements for structural concrete and commentary*. American Concrete Institute.
- Akinpelu, M. A., Odeyemi, S. O., Olafusi, O. S., & Muhammed, F. Z. (2019). Evaluation of splitting tensile and compressive strength relationship of self-compacting concrete. *Journal of King Saud University - Engineering Sciences*, 31(1), 19-25. <https://doi.org/10.1016/j.jksues.2017.01.002>

- Boel, V., Helincks, P., Desnerck, P., & Schutter, G. D. (2010). Bond behaviour and shear capacity of self-compacting concrete. *Design, Production and Placement of Self-Consolidating Concrete, RILEM Bookseries, 1*, 343-353. https://doi.org/https://doi.org/10.1007/978-90-481-9664-7_29
- BS 1881-125:2013. (2013). *Testing concrete Methods for mixing and sampling fresh concrete in the laboratory*. NBS Enterprise Ltd.
- Challagalli, R., & Hiremath, G. S. (2017). Comparative study on fresh and hardened concrete properties of ternary blend self compacting concrete. *International Journal of Advance Research, Ideas and Innovations in Technology, 3*(5), 13-17.
- Dinakar, P., Babu, K. G., & Santhanam, M. (2008). Durability properties of high volume fly ash self compacting concretes. *Cement and Concrete Composites, 30*(10), 880-886. <https://doi.org/10.1016/j.cemconcomp.2008.06.011>
- Dinakar, P., Reddy, M. K., & Sharma, M. (2013). Behaviour of self compacting concrete using Portland pozzolana cement with different levels of fly ash. *Materials & Design, 46*, 609-616. <https://doi.org/10.1016/j.matdes.2012.11.015>
- Domone, P. L. (2007). A review of the hardened mechanical properties of self-compacting concrete. *Cement and Concrete Composites, 29*(1), 1-12. <https://doi.org/10.1016/j.cemconcomp.2006.07.010>
- EPG. (2015). *The European guidelines for self-compacting concrete specification production and use*. European Project Group.
- EN 1992-1-1. (2004). *Eurocode 2: Design of concrete structures — Part 1-1: General rules and rules for buildings*. European Committee for Standardization.
- Faraj, R. H., Ali, H. F. H., Sherwani, A. F. H., Hassan, B. R., & Karim, H. (2020). Use of recycled plastic in self-compacting concrete: A comprehensive review on fresh and mechanical properties. *Journal of Building Engineering, 30*, Article 101283. <https://doi.org/10.1016/j.jobbe.2020.101283>
- Harkouss, R. H., & Hamad, B. S. (2015). Performance of high strength self-compacting concrete beams under different modes of failure. *International Journal of Concrete Structures and Materials, 9*(1), 69-88. <https://doi.org/10.1007/s40069-014-0088-x>
- Hassan, A. A. A., Hossain, K. M. A., & Lachemi, M. (2008). Behavior of full-scale self-consolidating concrete beams in shear. *Cement & Concrete Composites, 30*, 588-596. <https://doi.org/10.1016/j.cemconcomp.2008.03.005>
- Karthick, J., Jeyanthi, I. R., & Petchiyammal, M. (2014). Experimental study on usage of egg shell as partial replacement for sand in concrete. *International Journal of Advanced Research in Education Technology, 1*(1), 7-10.
- Mahmod, M., Hanoon, A. N., & Abed, H. J. (2018). Flexural behavior of self-compacting concrete beams strengthened with steel fiber reinforcement. *Journal of Building Engineering, 16*, 228-237. <https://doi.org/10.1016/j.jobbe.2018.01.006>
- Odaa, S. A., Hason, M. M., & Sharba, A. A. K. (2021). Self-compacting concrete beams reinforced with steel fiber under flexural loads: A ductility index evaluation. *Materials Today: Proceedings, 42*, 2259-2267. <https://doi.org/10.1016/j.matpr.2020.12.313>

- Oh, C. L., Lee, S. W., & Zain, M. R. M. (2019). Fresh properties and compressive strength of self-compacting concrete containing eggshells. *Malaysian Construction Research Journal*, 28(2), 1-10.
- Okamura, H., & Ouchi, M. (2003). Self-compacting concrete. *Journal of Advanced Concrete Technology*, 1(1), 5-15. <https://doi.org/https://doi.org/10.3151/jact.1.5>
- Olowofoyeku, A. M., Ofuyatan, O. M., Oluwafemi, J., & David, O. (2019). Effect of various types and sizes of aggregate on self-compacting concrete. *IOP Conference Series: Materials Science and Engineering*, 640, Article 012054. <https://doi.org/10.1088/1757-899X/640/1/012054>
- Panda, K. C., & Bal, P. K. (2013). Properties of self compacting concrete using recycled coarse aggregate. *Procedia Engineering*, 51, 159-164. <https://doi.org/10.1016/j.proeng.2013.01.023>
- Parthasarathi, N., Prakash, M., & Satyanarayanan, K. S. (2017). Experimental study on partial replacement of cement with eggshell powder and silica fume. *Rasayan Journal of Chemistry*, 10(2), 442-449. <https://doi.org/10.7324/RJC.2017.1021689>
- Safi, B., Saidi, M., Aboutaleb, D., & Maallem, M. (2013). The use of plastic waste as fine aggregate in the self-compacting mortars: Effect on physical and mechanical properties. *Construction and Building Materials*, 43, 436-442. <https://doi.org/10.1016/j.conbuildmat.2013.02.049>
- Sharifi, Y. (2012). Structural performance of self-consolidating concrete used in reinforced concrete beams. *KSCE Journal of Civil Engineering*, 16(4), 618-626. <https://doi.org/DOI 10.1007/s12205-012-1517-5>
- Siddique, R. (2011). Properties of self-compacting concrete containing class F fly ash. *Materials & Design*, 32(3), 1501-1507. <https://doi.org/10.1016/j.matdes.2010.08.043>
- Sonebi, M., Tamimi, A., & Bartos, P. J. M. (2003). Performance and cracking behaviour of reinforced beams cast with self-compacting concrete. *ACI Materials Journal*, 100(6), 492-500.
- Tang, W. C., Ryan, P. C., Cui, H. Z., & Liao, W. (2016). Properties of self-compacting concrete with recycled coarse aggregate. *Advances in Materials Science and Engineering*, 2016, 1-11. <https://doi.org/10.1155/2016/2761294>
- Tošić, N., Marinković, S., & Ignjatović, I. (2016). A database on flexural and shear strength of reinforced recycled aggregate concrete beams and comparison to Eurocode 2 predictions. *Construction and Building Materials*, 127, 932-944. <https://doi.org/https://doi.org/10.1016/j.conbuildmat.2016.10.058>
- Yerramala, A. (2014). Properties of concrete with eggshell powder as cement replacement. *The Indian Concrete Journal*, 88(10), 94-102.

A Privacy Preserving Framework for Health Records using Blockchain

Chitra Karunakaran, Kavitha Ganesh*, Sonya Ansar and Rohitha Subramani

Department of Information Technology, BSA Crescent Institute of Science & Technology, Chennai 600045, India

ABSTRACT

Electronic Health Records (EHR) is the electronic form of storing a patient's medical history. EHR contains patient's data such as progress notes, medications, prescriptions, vital signs, scan reports and laboratory data. Transferring EHR over the internet improves the quality of health care and reduces medical costs. However, in the traditional system, the EHR are stored across different decentralised hospitals, making data sharing difficult and increasing the risk of patient privacy. A privacy-preserving framework for electronic health records using blockchain technology is implemented to address these issues. The patient has complete control over the EHR, and the patient can share their health records with doctors of various medical institutions. The privacy and security of the patient's EHR are guaranteed by the verifiability and immutability property of the blockchain technology. The doctor upload the EHR, and it is encrypted using the SHA256 hashing algorithm and stored as a separate block. The patient shares the EHR with the doctor of any medical institution through the unique key shared via the doctor's email. The doctor can access and update the EHR using the shared key. The block validation is done using Delegated Proof

of Stake (DPoS) consensus algorithm, which guarantees the privacy of the patient's data. The proposed system based on the DPoS algorithm has considerable reduction in resource utilisation, computational capacity, time, and cost for EHR transactions.

Keywords: Blockchain, delegated proof of stake, electronic health records, healthcare, privacy, SHA256

ARTICLE INFO

Article history:

Received: 28 May 2021

Accepted: 9 August 2021

Published: 28 October 2021

DOI: <https://doi.org/10.47836/pjst.29.4.45>

E-mail addresses:

chitraashwin9896@gmail.com (Chitra Karunakaran)

gkavitha.78@gmail.com (Kavitha Ganesh)

sonya.yasmin152@gmail.com (Sonya Ansar)

srohitha23@gmail.com (Rohitha Subramani)

*Corresponding author

INTRODUCTION

Electronic Health Records (EHR) are digital health records of a patient created and managed by a medical practitioner or a staff in a health care organisation. EHR contains treatment given, medical history about a patient, and scan reports. Medical records of a patient are very useful because the doctors need to know the complete medical history of the patient prior to treatment in order to provide effective treatment. However, the patient cannot carry all the medical records every time they visit a doctor for consultation (Xia et al., 2017). It is convenient for both patients and doctors when the medical records are stored as EHR and transferred over the network to the doctor (Guo et al., 2018). The EHR is shared with doctors anywhere in the world, which makes the patient get consulted by the best doctors globally. However, maintaining the patient's data security and privacy are important as the data are transferred over the internet (Liu et al., 2018). Currently, the EHR is stored across different decentralised hospitals that make data sharing difficult with concern on patient privacy (Vedi et al., 2019). Blockchain is an efficient way to store and transfer data through the internet to guarantee privacy and security. In the healthcare sector, EHR plays a vital role in providing effective treatment, but it has to consider the privacy and security of patient data (Dagher et al., 2018). Blockchain has been implemented in many healthcare organisations for secure storage and transfer of medical data to monitor the complete shipping of drugs and store the shipping data (Wang et al., 2018).

Blockchain technology is a list of blocks where data is hashed and linked to the next block (Kadam et al., 2019). The data are hashed using a hashing algorithm such as MD, MD2, MD4, MD5, MD6, SHA1, SHA256, SHA3. The previous block's hash is linked to the next block, so, it cannot be changed once data is recorded, which provides immutability. If a hacker wants to change data in a particular block, then the corresponding hash value changes so the hacker has to change all the hash values of the blocks present after the modified block. It results in the wastage of computing power and cost for the hacker. The data blocks are replicated and stored in different decentralised nodes of a network (Zubaydi et al., 2019).

Blockchain is a decentralised network with peer to peer nodes, and there is no authorised node that decides (Christidis & Devetsikiotis, 2016). All the transactions in the blockchain are secure and verified using the consensus algorithm. Blockchain uses a consensus algorithm to reach an agreement and ensure the consistency and reliability of data (Alhaqbani & Fidge, 2008). The objective of the consensus algorithm is to provide an equal right to every node, mandatory participation of every node on reaching an agreement.

There is around 30 consensus algorithm that has been found in literature and some algorithms widely used are Proof of Work (PoW), Proof of Stake (PoS) and Proof of Delivery (PoD) (Tasatanattakool & Techapanupreeda, 2018). However, the Delegated Proof of Stake (DPoS) consensus algorithm is implemented in the proposed framework

because DPoS is more efficient, highly scalable and requires less energy than Proof of Work (Yang et al., 2018).

There are sensor-based health monitoring systems in which data generated by the Internet of Things (IoT) devices provide information about the patient's health condition (Guo et al., 2018). However, this method of gathering information would be difficult for the patients as they have to wear sensors 24/7. Furthermore, the sensor data are not highly reliable, and patients always prefer to meet the doctors for consultation in person. Here, the hospital maintains the health records, and the records can be accessed only by the doctors of that particular hospital. So, suppose a patient wants to consult a doctor of another medical institution. It is impossible to share those data with the expert doctors available in other hospitals and other countries.

The health care domain is improving using advanced technologies like blockchain, AI, and Machine learning (Ahram et al., 2017). In this work, a privacy-preserving framework using blockchain is developed, and it ensures the transfer of EHR with guaranteed privacy. Furthermore, the SHA256 algorithm is implemented for data encryption and Delegated Proof of Stack (DPoS) consensus algorithm is used for the secure transaction of EHR.

The rest of the paper is structured as follows: section 2 discusses the relevant literature related to this problem. Section 3 discusses the methodology of a privacy-preserving framework for EHR, and section 4 presents the results and performance analysis of the proposed framework. Finally, section 5 presents the conclusion and future work.

LITERATURE SURVEY

Many papers have discussed the privacy issues of EHR. Guo et al. (2018) have discussed a secure attribute-based signature scheme with multiple authorities for blockchain in Electronic Medical Records (EMR). In this paper, the EMR is stored in a separate server. There are many authorities among which data can be shared, such as hospitals, insurance companies, and medical research institute. Patients create, manage, control and sign their own EMR and share their data with any authority like doctors and insurance companies. The proposed work combines both blockchain and attribute-based schemes to share EMR records among multiple authorities. Each authority has a private key to view the data. The main advantage is that it supports multiple authorities and resists collision attacks on a cryptographic hash that finds two inputs producing the same hash value. The disadvantage of the system is that the cost and performance depend on the number of authorities.

Hosseini et al. (2019) have proposed a blockchain-based privacy-preserving healthcare architecture. Sensors are attached to the patient's body to gather blood pressure, heart rate, and ECG information. The data is transmitted through Bluetooth to the mobile phone or PDA of the patient. Hash and cryptographic operations are performed, and the miner creates a block. The blocks are verified using the Proof of Work (PoW) consensus algorithm.

Healthcare institutions are responsible for registering the patient and allocating a cluster miner to each patient. This work provides a high level of confidentiality, integrity and security. However, the problem is that the patients cannot wear the sensors 24/7, and the wearable sensors are not cost-effective.

Chen et al. (2019) have discussed blockchain-based secure storage for medical records and medical service frameworks. The three leading authorities in accessing medical data storage are the doctor, patient and third parties such as insurance companies. Data must be stored securely and shared between these authorities safely. The authors have proposed a framework to store and transfer EHR securely using blockchain and cloud technology. The blockchain uses a peer-peer propagation method to share resources such as medical data through a consensus algorithm. The medical records are not shared without the permission of the patient. The scheme does not depend on any third party such as a Healthcare care manager, admin and no single party has the authority to affect the processing of medical data, which is the main advantage of this work. Furthermore, the PoW consensus algorithm is implemented, which increases computational power, energy consumption and cost.

An enhanced architecture for privacy-preserving data integration in a medical research environment has been proposed by Jabeen et al. (2017). The reversible pseudonym technique is used in which artificial identifiers replace data records. In this scheme, a trusted third party generates a pseudonym termed Global Identifiers (GID). The GID allows linking patient's medical records from different hospitals. If a patient changes a care provider or hospital, all the medical records can still be linked, and the patient history is created. Thus, the patient health record can be revived as the medical records are not stored in any medical institution. The drawback of this approach is that there is a possibility of compromising the health records' privacy if the GID of a patient is known to attackers.

Blockchain-based personal data protection using a decentralised approach has been discussed by Zyskind et al. (2015). In this proposed approach, the patients are authorised to own and control their data. This framework provides full transparency to the user to view what is being done with the data and who accesses the data. This work implements a protocol that turns a blockchain into an automated access control manager and does not require trust in a third party. Only patients can change the user's permission in accordance with access control policies. All the nodes are equally trusted, and decision making is a collective process that leads to Sybil attacks, high latency and energy consumption.

All the above stated issues of the existing privacy-preserving models have been resolved in the proposed framework. As a result, the EHR can be shared across medical institutions globally with guaranteed privacy. In addition, the Delegated Proof of Stake (DPoS) consensus algorithm implemented in this work is efficient in energy consumption and cost compared to the other consensus algorithms like PoW and PoS.

METHODOLOGY

The health records of patients are generally managed by health care service providers and medical institutions. A privacy-preserving data sharing framework using blockchain is implemented in this work to assure data privacy in EHR. In the proposed framework, the patient has complete control over the EHR and can transfer the data to any doctor he visits, even outside the medical institution. The sensitive data are stored as blocks, and blockchain improves the transparency and immutability of the stored data in a decentralised network. Furthermore, the blockchain is a secured and trusted architecture and different consensus algorithms are implemented based on the application of domain-specific requirements (Zubaydi et al., 2019).

The proposed Privacy-Preserving Data Sharing Framework for EHR is depicted in Figure 1. The major components of this framework are User Authentication, Block Creation, Block Validation and Record Transaction. As a first step, the patient and the doctor get registered to the e-health centre. Then, when a patient consults a doctor, the EHR that contains information such as treatment given, medical history about the patient, scan reports, and prescribed medicines are generated by the doctor. The doctor then uploads the EHR to the webpage of the e-health centre. Next, the EHR is encrypted using the SHA256 hashing algorithm, and it will be stored as a separate block. Finally, the block ID is sent to both doctor and patient.

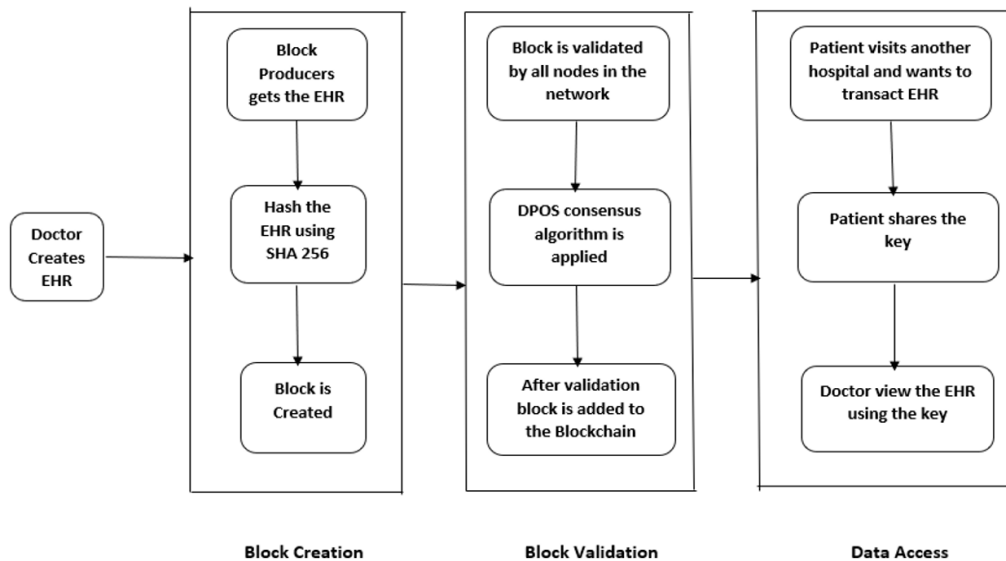


Figure 1. Privacy-Preserving Data Sharing Framework for EHR

Then a block is created by the transition node, and the hash value is generated for the current block using the SHA256 hashing algorithm (Shen et al., 2019). The hash value of the previous block is added to provide immutability, and the block is created. The block is then validated using Delegated Proof of Stake (DPoS) consensus algorithm. After validation, the block is added to the blockchain. In the proposed framework, the patient has complete control over accessing the EHR. Therefore, if a patient visits another doctor and consult with the previous health records, he can transfer the health record to any doctor through the e-health centre. The patient EHR are shared to the doctor’s mail id through a One-Time Password (OTP). The doctor is now permitted to log in, and using the generated OTP, the doctor can view the patient’s Electronic Health Record.

The implementation of blockchain technology over the traditional system of storing and retrieving EHR increases the system’s efficiency, reduces the risk of loss of EHR and avoids modification of information in EHR (Jin et al., 2019). The Delegated Proof of Stake (DPoS) consensus algorithm is employed over the Proof of Work (PoW) consensus algorithm due to the computational power and energy reduction. The DPoS consensus algorithm provides faster transactions than PoW and is also environmentally friendly (Judith et al., 2018).

A: User Authentication

The doctor and the patient are registered in the user authentication module by providing their name, mail ID, and contact number. The details are stored using the MySQL database. The user authentication process is shown in Figure 2. When a doctor or the patient logs in, the username and password are validated by fetching details from the database. If the username and password are correct, the homepage is displayed, or an error message is displayed. The doctor has a separate home page and performs tasks like viewing and updating EHR. The patient has a separate home page and has access permissions to share and view EHR. After authentication, the patients and doctors are allowed to access the web page of the e-health centre. The algorithm implemented for the authentication procedure is given below.

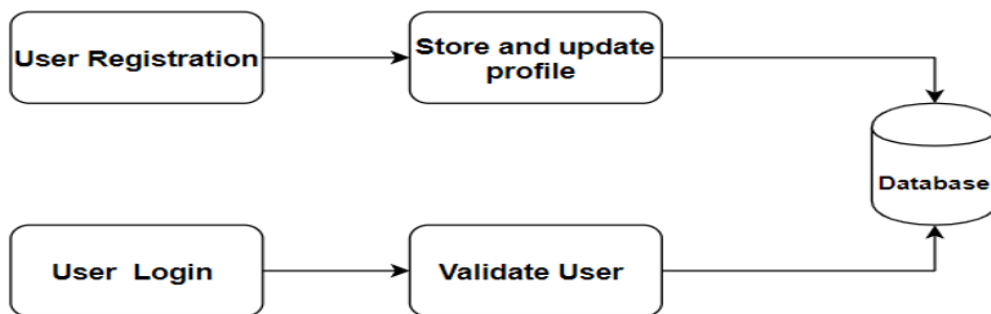


Figure 2. User authentication process

Algorithm 1: User Authentication - {Doctor D, Patient P}

```

Authentication(username(D,P),Password(D,P)){
    String user=username(D,P);
    String pass=password(D,P);
    if(user=database.username and password=database.pass){
        grant access(D,P);
    }
    else{
        deny access(D,P);
    }
}
    
```

B: Block Creation

The patient consults the doctor, and after the visit, the EHR of the patient will be uploaded as a new block. A new block is created for every visit, and the block is secured using the SHA256 hashing algorithm (Zubaydi et al., 2019). The previous block hash value is obtained whenever a new block is created. Thus, each block contains three segments: the data to be stored, the hash of the block and the hash of the previous block. The first block has no previous block, and hence, it has only the data and hash of the block, called the genesis block. When the next block is created, the previous block hash is calculated, and then a new block is inserted in the blockchain. The process of block creation is shown in Figure 3.

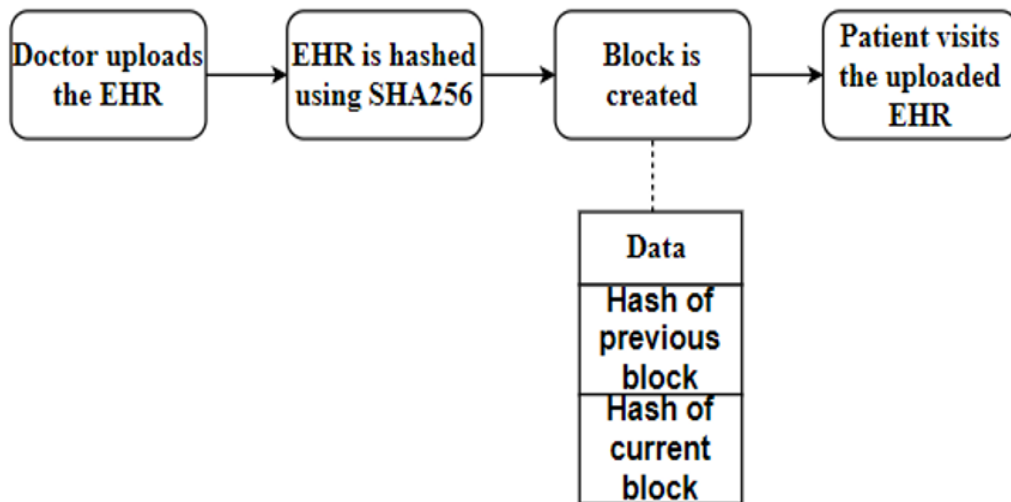


Figure 3. Block creation process

The block created cannot be modified because the hash value will change, making the blockchain immutable. A block ID has been generated for each block, and it is sent to the patient. Whenever the block is retrieved, the transaction details are updated, and a new block is created with reference to the previous hash value. The algorithm takes EHR as input and hashed using a SHA256 hashing algorithm and further converted to hash values.

Algorithm 2: Block creation using SHA256 algorithm

INPUT - EHR Record, OUTPUT - Hash of EHR record

```
Calculate Hash(S string){
    result=hashlib.sha256(str.encode(record))
    record=string(block.index)+block.timestring+block.preblockhash
return calculatedHash(record) }
```

C: Block Validation

As the blockchain is a decentralised network, there are many nodes in the blockchain network with the same copy of blocks. The newly created block has to be updated in all the nodes present in the network. Therefore, an agreement is reached between all nodes using a consensus algorithm and the newly created block is added to the nodes of the blockchain (Zheng et al., 2017). The proposed work employs Delegated Proof of Stake (DPoS) consensus algorithm. In DPoS, there are two types of nodes called consensus nodes and trading nodes. The trading nodes are responsible for creating a block, hashing the block of data, and storing the data block. The consensus node is responsible for validating a block and adding it to the blockchain. There are many nodes in a p2p network, and a consensus node is selected, which is responsible for verifying the block (Yang et al., 2018). After verification, the block is added to the blockchain. The consensus algorithm has three modules: selecting the consensus nodes, verifying blocks, and rejecting the malicious blocks.

For selecting the consensus node, the election process is held. There will be N number of nodes in a network, and a consensus node must be selected. A node conducts the election, and that node sends a broadcast message to all the nodes in the network. After voting, a node with majority votes is selected as the consensus node, which validates the newly created block. As a result, the DPoS algorithm can process the transactions faster and has reduced time complexity compared to Proof of Work (PoW) and Proof of Stake (PoS).

Algorithm 3: Selecting consensus node using Delegated Proof of Stake

```
Broadcast(voting msg){
while(HASH(current Blockhash),HASH(preBlockhash),nonce){
    Broadcast(Nodes)
    nonce = nonce+1 }
```

```

Nodes vote for a trusted node
V(n)=count votes
Node with max vote = consensus nodes
Node }
End
    
```

Algorithm 4: Algorithm for reaching consensus

```

Input :block , Output: block good or block error
block←(DATA,HASH(preblockhash,nounce,timestring) if(oldblockindex)≠NewBlockIndex)&&(oldblockhash≠New Block Hash)
{
broadcast(Block GOOD)
}
else{
broadcast(Block BAD)
}
    
```

D: Record Transaction

In the proposed methodology, the patient has complete control and authority over the transaction process of the EHR. The procedure for the EHR transactions between the patient and the doctor is given in Figure 4.

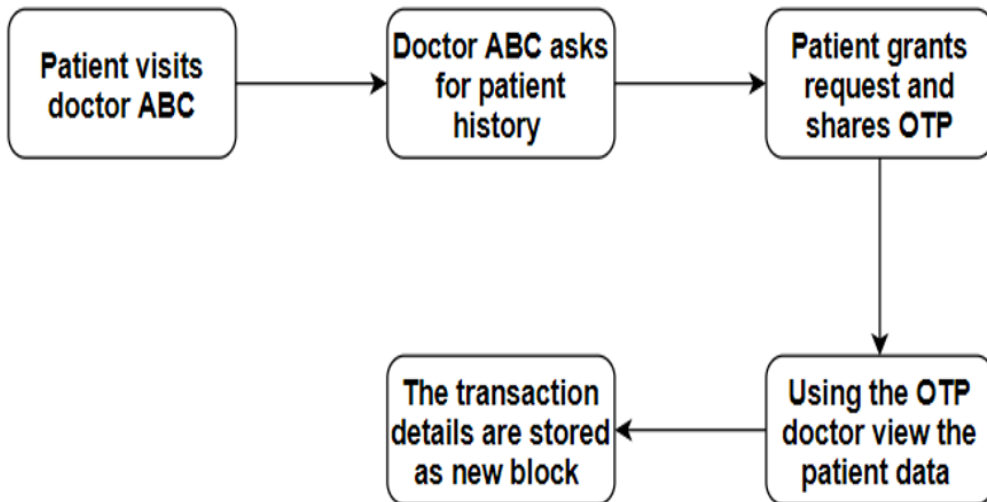


Figure 4. Record transaction process

The patient can share the EHR with the doctor, and after consultation, the doctor uploads the EHR. So, whenever a block transaction request is initiated, the patient logs into the account, chooses the transaction option and feeds the doctor's mail ID. The doctor receives OTP to his email. Then the doctor can view the EHR using the received OTP. During the transaction process, the system validates the doctor ID and all the transaction details such as doctor's name, transaction time and block ID are collected and stored in a new block. This block is validated using the DPoS consensus algorithm and added to the blockchain. Finally, the transaction ID is returned to the patient for future reference.

Thus, sharing of EHR among medical practitioners different medical institutions is achievable amidst preserving the privacy of patient's health records. The use of blockchain increases the system's efficiency, reduces the risk of loss of EHR and avoids malicious behaviour in EHR. DPoS is employed for reaching consensus. It is appropriate for applications that need a high level of scalability and hence applied for storing and maintaining EHR in an e-health care system.

RESULTS AND DISCUSSION

The proposed privacy-preserving framework for the EHR using blockchain is mostly developed for healthcare sectors, and it is implemented in this work using Anaconda, Python HTML and MySQL. The user interface is designed using HTML, and the database is set up using MYSQL 5.0.22. The complete system setup has been implemented, and deployed and the performance analysis is done.

A patient can transfer the EHR to any doctor who belongs to a different medical institution. However, only the authorised patients and doctors can access the data, and unauthorised entities will not gain access to patients' medical records.

Add Record

Nounce
234

Name
Malar

Reason
Fever

Detail
Patient came with high Fever and Body pain. She had 100 C fever. Blood test was taken. Paracetamol was prescribed.

Timestamp 06-11-2020

Submit

Figure 5. Doctor adding patient record

Figure 5 shows the log-in page where the doctor logs into his account and fill up the patient details such as patient name, nonce that is a unique value to the block, timestamp that is the date when the block is created. The reason for the visit and the brief description of patient health concerns are given by the doctor. These data are hashed using the SHA256 hashing algorithm, and a block is created.

View Record

Nounce
234

Name
Malar

Timestamp
12/04/2020

Reason
Fever

Detail
Patient came to the hospital with high fever and body pain. She had 100 C fever. Blood test was taken. Paracetamol was prescribed.

Hash Value
04839574389674567\$60669&98p56@56677y898)90734*93744096\$/ [p][8933664

Previous hash value
93053484389674567\$60669&98p56@56677y898)90734*937440963857384436^&

Cancel

Figure 6. Patient viewing medical record

After the doctor uploads the record, the patient can view it by logging in to their respective account. The details such as patient name, nonce, timestamp, hash value, previous block hash values are displayed as depicted in Figure 6.

Transfer Report

Enter mail address

Submit

Figure 7. The patient sends a key to the doctor through mail

If a patient wants to send a record to a doctor who belongs different medical institution, then he shares a unique key for that transaction. First, the email ID of the doctor is given then a OTP is generated and sent to the email. The validity for the OTP is for 24 hours and can be used for only one transaction. Finally, the patient mentioning the doctors' email is shown in Figure 7, and an OTP is generated.

View Report

Enter OTP

Submit

Figure 8. Doctor enters OTP

As shown in Figure 8, the OTP received through the doctor's email is entered, and if the OTP is valid, then patient details are displayed at the doctors' end, or an error message will be displayed.

View Record

Nounce	234
Name	Malar
Timestamp	23/04/2020
Reason	Fever
Detail	Patient came to the hospital with high fever and body pain. She had 100 C fever. Blood test was taken. Paracetamol was prescribed.

Cancel

Figure 9. Viewing patient records by doctor

After successfully validating OTP, the doctor is now allowed to view the patient health record and update the EHR after the consultation. The patient record as viewed and updated by the doctor is shown in Figure 9. After the successful data transaction, details such as doctor's names, time, patient details are collected, and a new block is created. The data has been hashed using SHA256 and validated using Delegated Proof of Stake (DPoS) consensus algorithm. Then the block is added to the blockchain. Likewise, for every transaction, a new block is created and added to the blockchain.

In health care sectors, the transfer of EHR requires an appropriate consensus algorithm with minimum time complexity and cost to reach an agreement between nodes in the block verification process. Hence, the DPoS algorithm is implemented to achieve a high processing speed with reduced expenses compared to PoW and PoS.

Performance Analysis

A. CIA Triad Analysis. *The performance of the proposed architecture is discussed in terms of storage, privacy and security. However, first, we can analyse the CIA triad.*

Confidentiality. Confidentiality of EHR is maintained as the data sharing is done only by the owner of the record (i.e.) the patient. Therefore, the doctors can only view the EHR and upload the EHR after the patient visit. However, the doctor is not permitted to share the EHR with any entity in e-health care.

Integrity. Integrity is the property where no one modifies the stored data without permission. Data integrity is one of the most important characteristics of blockchain, where the data once stored cannot be modified. So, blockchain technology provides 100% integrity for the data present in EHR.

Availability. Availability is managing all hardware software conflicts, thus ensure that the data is available 24/7. Furthermore, since blockchain is a decentralised network it has blocks stored in different P2P networks, which improves data availability.

The proposed system is compared with the existing systems for protecting personal data using blockchain (Zyskind et al., 2015), as given in Table 1.

B. Energy Consumption Analysis. The blockchain network requires many miners, and in PoW, all miners attempt to solve the complex problem, which consumes more energy, but only one can mine a block. As a blockchain network is implemented for preserving the privacy of patient's health records, the energy parameter of PoW and DPoS consensus algorithms are compared. The drawback of the PoW consensus algorithm is that it requires much energy, leading to higher costs, and it can be minimised by choosing the DPoS algorithm.

Table 1

Comparison of Privacy-Preserving Schemes for personal data

Attributes	Privacy-Preserving Data Sharing Framework (Proposed Model)	Decentralising Privacy & Protecting Personal Data (Existing Model)
Privacy Protection	Privacy is ensured through unique keys, and OTP shared for every transaction.	Adding records, updations and deletions are allowed, which compromises privacy.
Data Access	Complete access to user’s data for both the data owner and shared entity	Complete access to the data owner and restricted access to the shared entity.
Data Integrity	Users data cannot be compromised by hacker as the blocks are immutable.	A small fraction of data can be compromised if hacker gains signing and encryption keys.
Effectiveness	Efficient for processing data with less time and computation complexity.	Efficient for storing and processing queries and not for processing data.
Drawbacks	Less vulnerable to attacks, low energy consumption, low latency.	More vulnerable to Sybil attacks, excessive energy consumption, High latency.

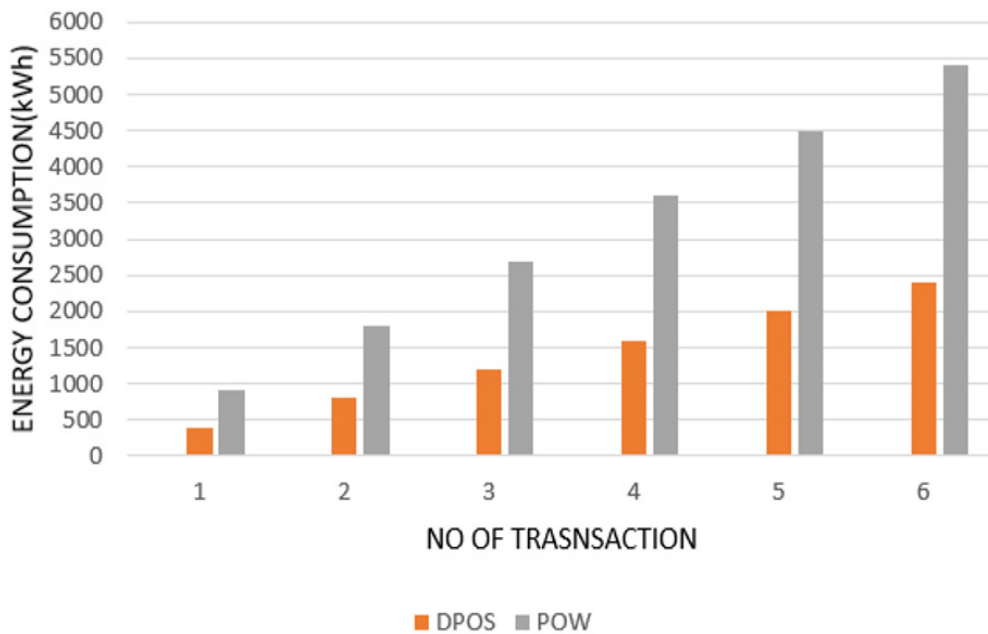


Figure 10. Energy consumption for transaction in PoW vs DPoS

The energy consumption for a record transaction using PoW and DPoS algorithm is given in Figure 10. The PoW consensus algorithm uses more energy to solve a problem as all nodes are involved. The one node that solves the mathematical problem is considered to validate a block. Thus, although one node validates a block, each node in the blockchain works on problem-solving, which leads to high energy consumption and computational capacity.

The energy consumption of the different consensus algorithms differs in terms of the total hash rate of the miners (Borzi & Salim, 2020). It is observed that PoW takes more energy, time and computation power in selecting a consensus node, but in DPoS, the consensus node is selected by a voting algorithm. Hence, applying the Delegated Proof of Stake (DPoS) consensus algorithm reduces the energy consumption by 40%, based on the number of block producers and energy consumed per block producer (Wh).

C. Time Complexity Analysis. The time required for generating and validating a block varies with different consensus algorithms. The existing system uses Proof of Work (PoW) consensus algorithm, and the proposed system implemented the Delegated Proof of Stake (DPoS). Figure 11 shows the time complexity of DPoS consensus algorithm. The average time for generating a block is high for PoW as each node must perform a mathematical calculation for validating a block. However, in DPoS, the validating node is selected based on the voting process that minimises time and cost.

The time complexity of the PoW consensus algorithm is depicted in Figure 12. The PoW algorithm takes 10 minutes to validate a block because of the computation process, whereas in DPoS, no such computation process is needed. Thus 50 blocks can be validated in 10 minutes.

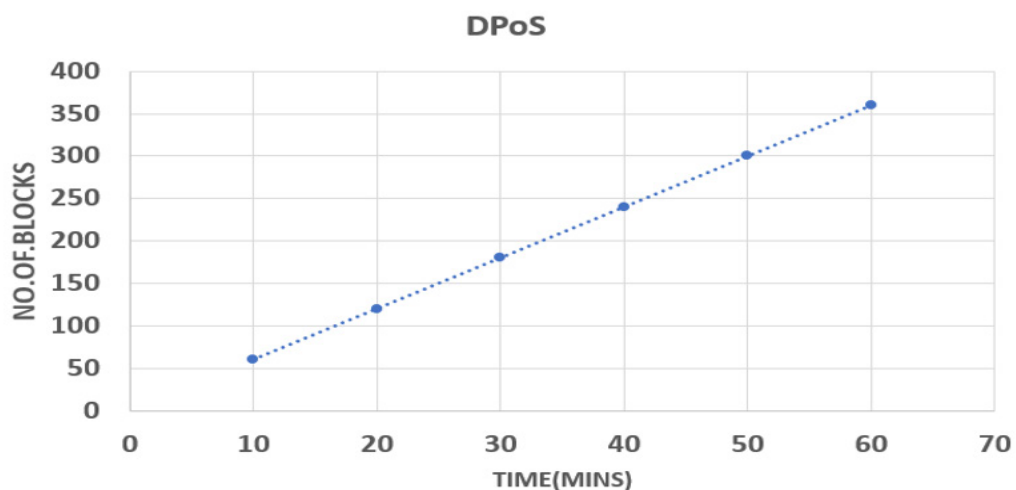


Figure 11. Time complexity of DPoS

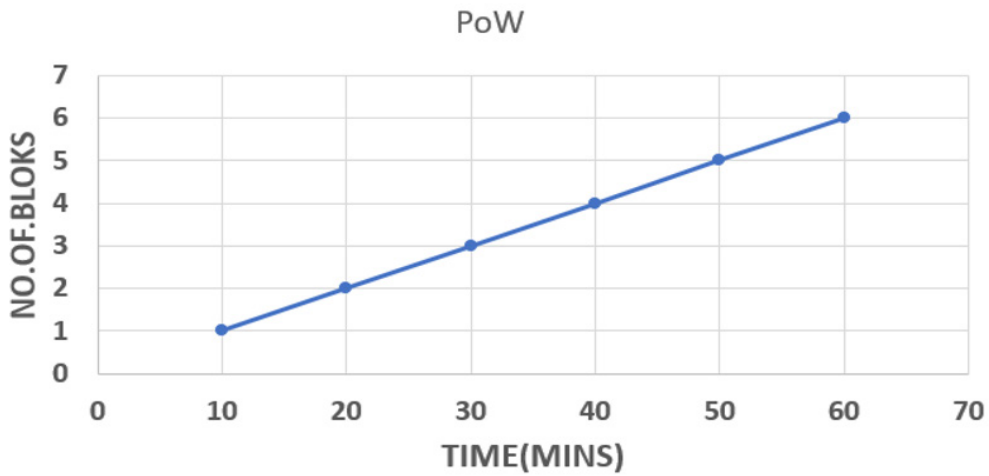


Figure 12. Time complexity of PoW

Table 2 shows the comparison of DPoS and PoW consensus algorithms. The validation node is selected based on the computing power in PoW, but in DPoS, the validating node is selected based on a number of votes. The time and cost are also high for PoW compared to DPoS.

Table 2
Performance of PoW and DPoS

Consensus algorithm	Proof of work	Delegated Proof of Stake
Basis for assigning accounting rights	Computing power	Stake votes
Resource consumption	High	Low
Average time to generate blocks	10min	5s
Cost	High	Low

CONCLUSION

Blockchain technology is an emerging technology used by most sectors such as banking, healthcare, AI, social media, etc. However, Electronic Health Records (EHR) are stored across different decentralised hospitals, making data-sharing difficult and increasing the risk of patient privacy. In this work, a data sharing framework that employs blockchain technology for storing and retrieving EHR across Medical Institutions is implemented. The decentralisation, transparency and immutability characteristics of blockchain guarantee secure storage and transfer of patients' health records. The EHR is encrypted using the

SHA256 hashing algorithm and stored as a separate block to ensure privacy. The block validation is done using Delegated Proof of Stake (DPoS) consensus algorithm.

In this system, the patient has complete ownership of the health record and is authorised to share the data with any medical practitioner without the intervention of third parties. Hence, the medical data cannot be compromised by any entity that participates in e-health care. The energy consumption and the time complexity are significantly reduced in the proposed model. The future work is to improve the downside of the DPoS consensus algorithm. The DPoS is more centralized, as the master node is responsible for block validation.

ACKNOWLEDGEMENT

The authors would like to thank the Management of B.S.A Crescent Institute of Science & Technology, Chennai, India, for providing the necessary research environment for carrying out this work.

REFERENCES

- Ahram, T., Sargolzaei, A., Sargolzaei, S., Daniels, J., & Amaba, B. (2017). Blockchain technology innovations. *In 2017 IEEE technology & engineering management conference (TEMSCON) (pp. 137-141)*. IEEE Publishing. <https://doi.org/10.1109/TEMSCON.2017.7998367>.
- Alhaqbani, B., & Fidge, C. (2008). Privacy-preserving electronic health record linkage using pseudonym identifiers. *In HealthCom 2008-10th International Conference on e-health Networking, Applications and Services (pp. 108-117)*. IEEE Publishing. <https://doi.org/10.1109/HEALTH.2008.4600120>.
- Borzi, E., & Salim, D. (2020). *Energy consumption and security in blockchain* (BSc Dissertation). KTH Royal Institute of Technology in Stockholm, Sweden
- Chen, Y., Ding, S., Xu, Z., Zheng, H., & Yang, S. (2019). Blockchain-based medical records secure storage and medical service framework. *Journal of Medical systems, 43*, 5-25. <https://doi.org/10.1109/s10916-018-1121-4>.
- Christidis, K., & Devetsikiotis, M. (2016). Blockchain and smart contract for internet of things. *IEEE Access, 4*, 2292-2303. <https://doi.org/10.1109/ACCESS.2016.2566339>.
- Dagher, G. G., Mohler, J., Milojkovic, M., & Marella, P. B. (2018). Ancile: Privacy-preserving framework for access control and interoperability of electronic health records using blockchain technology. *Sustainable Cities and Society, 39*, 283-297. <http://dx.doi.org/10.1016/j.scs.2018.02.014>.
- Guo, R., Shi, H., Zhao, Q., & Zheng, D. (2018). Secure attribute-based signature scheme with multiple authorities for blockchain in electronic health records. *IEEE Access, 6*, 11676-11686. <https://doi.org/10.1109/ACCESS.2018.2801266>.
- Hossein, K. M., Esmaili, M. E., Dargahi, T., & Khonsari, A. (2019). Blockchain-based privacy-preserving healthcare architecture. *In 2019 IEEE Canadian Conference of Electrical and Computer Engineering (CCECE) (pp. 1-4)*. IEEE. <https://doi.org/10.1109/CCECE.2019.8861857>.

- Jabeen, F., Hamid, Z., Abdul, W., Ghouzali, S., Malik, S. U. R., Khan, A., Nawaz, S., & Ghafoor, H. (2017). Enhanced architecture for privacy preserving data integration in a medical research environment. *IEEE Access*, 5,13308-13326. <https://doi.org/10.1109/ACCESS.2017.2707584>.
- Jin, H., Lyo, Y., Li, P., & Mathew, J. (2019). A review of secure and privacy preserving medical data sharing. *IEEE Access*, 7, 61656-61669. <https://doi.org/10.1109/ACCESS.2019.2916503>.
- Judith, A. G., Mitchel, L., Aleriot, N., & Armani, R. (2018). Electronic health records: An online medical records an asset or a liability under current condition? *Australian Health Review*, 42(1), 59-65. <https://doi.org/10.1071/AH16095>.
- Kadam, S., Meshram, A., & Suryavanshi, S. (2019). Blockchain for healthcare: Privacy preserving medical record. *International Journal of Computers and Applications*, 178(36), 5-9.
- Liu, J., Li, X., Ye, L., Zhang, H., & Guizani, M. (2018). BPDS-A blockchain based privacy preserving data sharing for electronic medical records. In *2018 IEEE Global Communications Conference (GLOBECOM)* (pp. 1-6). IEEE Publishing. <https://doi.org/10.1109/GLOCOM.2018.8647713>.
- Shen, B., Guo, J., & Yang, V. (2019), Medchain: Efficient healthcare data sharing via blockchain. *Applied Sciences*, 9(6), Article 1207. <https://doi.org/10.3390/app9061207>.
- Tasatanattakool, P., & Techapanupreeda, C. (2018). Blockchain: Challenges and applications. In *2018 International Conference on Information Networking (ICOIN)* (pp. 473-475). IEEE Publishing. <https://doi.org/10.1109/ICOIN.2018.8343163>.
- Vedi, A. D., Srivatsava,nG., Dhar, S., & Singh, R. (2019). A decentralised privacy preserving healthcare blockchain for IoT. *Sensors*, 19(2), 326-343. <https://doi.org/10.3390/s19020326>.
- Wang, S., Wang, J., Wang, X., Qiu, T., Yuan, Y., Ouyang, L., Guo, Y., & Wang, F. (2018). Blockchain-powered parallel healthcare systems based on the ACP approach. *IEEE Transactions on Computational Social Systems*, 5(4), 942-950. <https://doi.org/10.1109/TCSS.2018.2865526>.
- Xia, Q. I., Sifah, E. B., Assmoah, K. O., Guo, J., & Guizani, M. (2017). Medshare: Trustless medical data sharing among cloud service providers via blockchain. *IEEE Access*, 5,14757-14767. <https://doi.org/10.1109/ACCESS.2017.2730843>.
- Yang, F., Zhou, W., Wu, Q., Long, R., Xiong, N., & Zhou, M. (2018). Delegated proof of stake with downgrade: A secure and efficient blockchain consensus algorithm with downgrade mechanism. *IEEE Access*, 7, 118541-118555. <https://doi.org/10.1109/ACCESS.2019.2935149>.
- Zheng, Z., Xie, S., Dai, G., Chen, X., & Wang, H. (2017). An overview of blockchain technology: Architecture, consensus, and future trends. In *2017 IEEE international congress on big data (BigData congress)* (pp. 557-564). IEEE Publishing. <https://doi.org/10.1109/BigDataCongress.2017.85>.
- Zubaydi, H. D., Chong, Y. W., Ko, K., Hanshi, S. M., & Karuppayah, S. (2019). A review on the role of blockchain technology in healthcare domain. *Electronic*, 8(6), Article 679. <https://doi.org/10.3390/electronics8060679>.
- Zyskind, G., Nathan, O., & Pentland, A. (2015). Decentralizing privacy: Using blockchain to protect personal data. In *2015 IEEE Security and Privacy Workshops* (pp. 180-184). IEEE Publishing. <https://doi.org/10.1109/SPW.2015.27>.

Evaluation of Single Missing Value Imputation Techniques for Incomplete Air Particulates Matter (PM₁₀) Data in Malaysia

Zuraira Libasin¹, Wan Suhailah Wan Mohamed Fauzi², Ahmad Zia ul-Saufie^{3*}, Nur Azimah Idris¹ and Noor Azizah Mazeni¹

¹Department of Computer and Mathematical Sciences, Universiti Teknologi MARA, Cawangan Pulau Pinang, Permatang Pauh Campus, 13500 Permatang Pauh, Penang, Malaysia

²Faculty of Chemical Engineering with Environment, Universiti Teknologi MARA, 40450 Shah Alam, Selangor, Malaysia

³Faculty of Computer and Mathematical Sciences, Universiti Teknologi MARA, 40450 Shah Alam, Selangor, Malaysia

ABSTRACT

The missing value in the dataset has always been the critical issue of accurate prediction. It may lead to a misleading understanding of the scenario of air pollution. There might only be a small number of missing (5% to 10%) answers to each problem, but the missing details may vary. This research is focused mainly on solving long gap missing data. Single missing value imputation means replacing blank space in the monitoring dataset from chosen Department of Environment (DoE) monitoring station with the calculated value from the best technique for long gap hours. The variable that is mainly being a monitor is PM₁₀. The technique focused on this research is the single imputation technique. Furthermore, this technique was tested on the Tanjung Malim monitoring station dataset

by fitting with five performance indicators. The result was compared with the previous study, whether it is the best used for long gap hour data. Four stages need to be followed to complete this research. The steps are data acquisitions, characteristic analysis of missing value, single imputation approach, verification of approach and suggestion of the best technique. This research used four existing imputation techniques: series mean (SM), mean of nearby points (MNP), linear

ARTICLE INFO

Article history:

Received: 28 May 2021

Accepted: 9 August 2021

Published: 28 October 2021

DOI: <https://doi.org/10.47836/pjst.29.4.46>

E-mail addresses:

zuraira946@uitm.edu.my (Zuraira Libasin)

suhailahfauzi96@gmail.com (Wan Suhailah Wan Mohamed Fauzi)

ahmadzia101@uitm.edu.my (Ahmad Zia Ul-Saufie)

nurazimah7083@uitm.edu.my (Nur Azimah Idris)

noorazizah1103@uitm.edu.my (Noor Azizah Mazeni)

*Corresponding author

trend (LT), and linear interpolation (LIN). This research shows that the interpolation technique is the best technique to apply particulate matter missing data replacement with the least mean absolute error and better performance accuracy.

Keywords: Air pollution, imputation, linear interpolation, missing data, performance indicator

INTRODUCTION

Air pollution cases nowadays being a primary concern around the world. It is due to its effect on the environment and the human population's health when it accumulates in high concentrations in the atmosphere. The common pollutants mainly source from soot, smoke, mould, pollen, methane and even carbon dioxide (Ward, 2019).

These pollutants defected humans' health by irritating the eyes, nose, and throat. It can also cause wheezing, coughing, chest tighten also worsening the existing lung and heart disease. The worst-case can cause cancer and damage the immunization, neurological and reproductive systems (Department of Environment, 2018). The effects it brings to our environment also can be considered severe as it causes acid rain, eutrophication, haze, congenital disabilities and disease on wildlife, ozone depletion, crop and forest damage and finally, global climate change (Department of Environment, 2018).

Since many sources cause air pollution, air pollution monitoring is needed to control and monitor contamination. Of course, the way to monitor air pollution is by remote instrument. The data collected will be analysed by the researchers to know the exact statistics of pollution levels. However, sometimes when carrying the experiment, there are loopholes present. In this case, the missing data for analysis make the researchers facing difficulties.

This missing data occurs due to equipment failure, human errors, routine maintenance, and changes in sitting monitors or other factors (Ali & Darcy, 2017). It can be detected since there is much missing value in the data stream table collected from Tanjung Malim, Perak station. There are two types of missing data which are ignorable and non-ignorable. Ignorable data exist in three forms. The first is missing data that is linked to sampling. The second is missing at random, known as MAR data (Ali & Darcy, 2017). The third is missing completely at random (MCAR) (Norazian et al., 2008). The Missing Not at Random (MNAR) is considered not ignorable (Little & Rubin, 2019) if there are no present simple solutions for treating the missing data. A model must be postulated for MNAR missingness, which must be included in the study to avoid bias (De Leeuw & Meijer, 2008).

The missing value in the dataset has always been the critical issue of accurate prediction. It may lead to a misleading understanding of the scenario of air pollution. There might only be a small number of missing (5% to 10%) answers to each problem, but the missing details may be various (<https://www.bauer.uh.edu/jhess/documents/2.pdf>).

Previously research developed and enhanced new or existing imputation methods to solve for long gap missing data. However, few studies have tried to find an effective method to boost imputation output for long-term consecutive missing values (Anh et al., 2011).

Interpolation is a well-known technique used in numerical analysis and has different approaches in environmental data sets (Zainudin & Noor, 2009). The interpolation of the technique is introduced to overcome the problem of missing data. This research's chosen interpolation technique is single imputation, which replaces the calculated value in the blank space of the collected data set from the monitoring station. Recently, the previous study is only suitable for short gaps ($l < 3$ hours) and medium gaps (4 hours $< l < 18$ hours), where l is known as length. However, the previous techniques are unsuitable for the long gaps ($l > 19$ hours), due to poor performance and less accuracy. Therefore, this study aims to evaluate the single imputation technique in dealing with the long gaps of missing air pollution data to improve the performance. The single imputation approach was carried out using four different techniques and chose the best one by looking at their performance. This finding will overcome the misleading interpretation as well as inaccurate prediction due to the missing data. As a result, the chosen best single imputation technique will improve the accuracy in minimising the missing values problem, especially to the long gap's condition.

MATERIALS AND METHODS

This research's scope is to determine the missing value in air pollution data which variable stands from particulate matter (PM₁₀). Data were acquired from the Department of Environment (DoE) Malaysia. In this study, the Tanjung Malim monitoring station is chosen because it is strategically placed to detect transboundary haze pollution, harmful and affecting health quality (Latif et al., 2018).

The hourly data from 2002 until 2016 consists of variables sulfur dioxide (SO₂), carbon monoxide (CO), carbon dioxide (CO₂), ozone (O₃) and particulate matters (PM₁₀). However, data of PM₁₀ in the year 2005 only was considered in this study because it has the smallest missing value percentage and can support extensive data shown in Figure 1. Therefore, this variable will be calculated using the performance indicator at a different percentage of missing value.

Monitoring data of the year 2005 for PM₁₀ in Tanjung Malim were selected to simulate missing data. The data set consists of 8731 valid data set with 53 missing data counts. The mean and standard deviation values for the entire observed data set are 43.00882 and 28.860522, respectively. The missing data counts for the data ranging from 0.6% to 2.9%. The most extensive data set lies in 2005 with 8731 data, with the lowest missing values count. As a reason, this data set is used for the single imputation technique to know which of the techniques is the best fit for long gaps hours ($l > 19$ hours). The data will be split into three missingness groups: 2.5%, 5% and 10% within 24 hours.

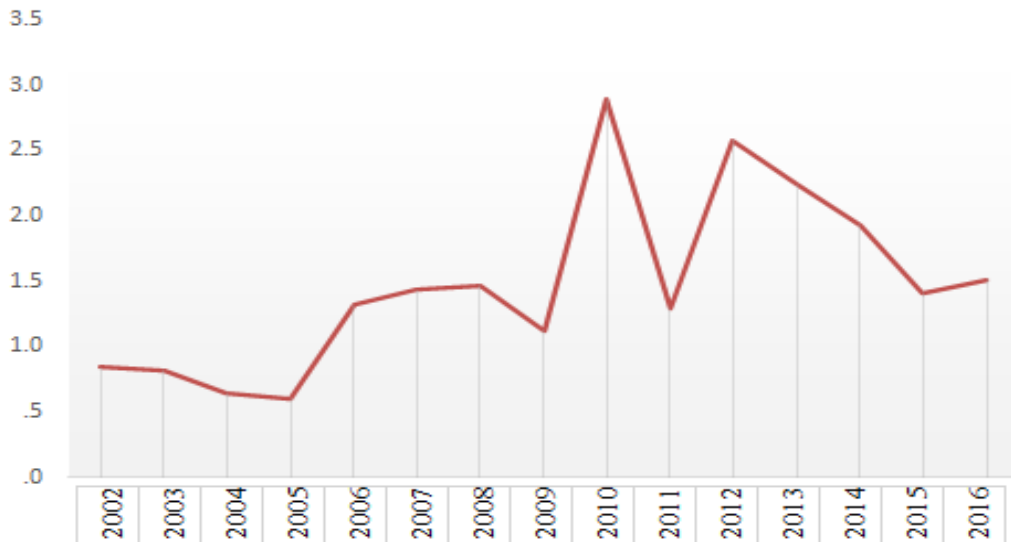


Figure 1. The percentage of PM₁₀ missing value from 2002 to 2016

Simulation of Missing Data

Once the data is divided into three missingness groups: 2.5%, 5% and 10%, it is ready to be served for simulations. The data will be used to compare four single imputation techniques. For 24 hours, in each per cent of missingness, the data will be grouped into a different level of complexity where it is divided by hour's gaps (length, l). There are the short gaps, consist of ($l < 3$ hours), medium gaps (4 hours $< l < 18$ hours) and long gaps ($l > 19$ hours). It serves as a purpose that shows the different hour gaps will have different best imputation techniques. However, mainly, the real purpose is to know the best fit technique for long gaps hours. Figure 2 illustrates the simulation process steps in general (Sukatis et al., 2019).

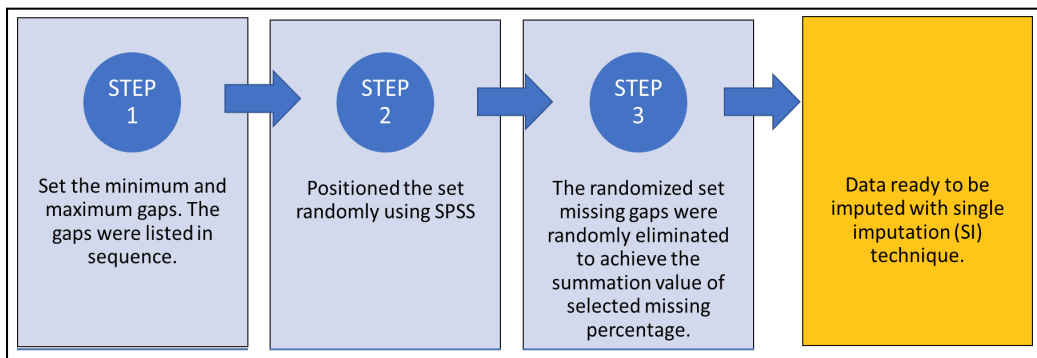


Figure 2. The steps of the simulation process in general

Single Imputation Technique

Single imputation uses only one value being substituted into each missing data with only one imputation effort to be carried out (Hirabayashi & Kroll, 2017). There are five different options for imputation in SPSS. However, the imputation techniques handled in this study is limited to four techniques. These techniques can be briefly summarised in Table 1. Each technique gives a different way and accuracy in stimulating the missing data. The missing value percentage stimulated randomly is 2.5%, 5%, and 10% (Norazian et al., 2008). These random missing data conditions will be generated using a random number generator in SPSS (Noor et al., 2006).

Table 1

Summary of four single imputation techniques

Single Imputation Technique	Description
Series Mean (SM)	The missing value places will be replaced by the mean value of the entire original data
Mean of Nearby Points (MNP)	The replacement of missing value by mean from data above or below the missing data datums.
Linear Interpolation (LIN)	The replacement of missing value is by interpolation, which in case if the series of data set has a missing value at first and last, the missing value will not be replaced.
Linear Trend (LT)	The missing value will be replaced by the current polynomial regression structure of the original data set.

Source. Cokluk and Kayri (2011)

Performance Indicators

Five performance indicators have been used to determine the best single imputation technique suitable for long gap missing data. In achieving this, the calculation using performance indicator was conducted to know the error value to ensure the best fit condition that can be applied for all variables of air pollution listed. The best fit condition is when there is the least error percentage shown from the calculation.

The importance of performance indicators are the values calculated being used to evaluate the best single imputation technique. The observed data (original data) will be merged with predicted data (impute data) in each equation of the performance indicator. The performance indicators used in this study are Mean Absolute Error (MAE), Root Square Mean Error (RSME), Index of Agreement (IA), Prediction Accuracy (PA) and Coefficient of Determination (R^2). MAE and RSME measure for errors. Meanwhile, IA, PA and R^2 are for measuring the accuracy. Below are the equations of performance indicators used in this study.

Mean Absolute Error (MAE). Predicted and the actual value determined the average differences. It ranges from 0 to infinity, with the best fit at 0 (Equation 1) (Ul-Saufie et al., 2011)

$$MAE = \frac{1}{N} \sum_{i=1}^N |P_i - O_i| \quad [1]$$

Root Mean Squared Error (RMSE). Commonly used for numeric prediction, the error result is dimensionally the same as predicted and the actual value (Equation 2) (Ul-Saufie et al., 2011).

$$RMSE = \left(\frac{1}{N} \sum_{i=1}^N [P_i - O_i]^2 \right)^{\frac{1}{2}} \quad [2]$$

Coefficient of Determination (R²). The range of value is between 0 to 1, which if the value gets closer to 1, it will be considered the best fit (Equation 3) (Ul-Saufie et al., 2011).

$$R^2 = \left[\frac{1}{N} \frac{\sum_{i=1}^N [(P_i - \bar{P})(O_i - \bar{O})]}{\sigma_P \sigma_O} \right]^2 \quad [3]$$

Prediction Accuracy (PA). The values range from 0 to 1, resulting in the higher value considering as the best fit (Equation 4) (Norazian et al., 2008)

$$PA = \sum_{i=1}^N \frac{[(P_i - \bar{P})(O_i - \bar{O})]}{(N-1)\sigma_P \sigma_O} \quad [4]$$

Index of Agreement (IA). The value range from 0 to 1, with the higher value as the best agreement (Equation 5) (Plaia & Bondi, 2006; Hirabayashi & Kroll, 2017)

$$IA = 1 - \left[\frac{\sum_{i=1}^N (P_i - O_i)^2}{\sum_{i=1}^N (|P_i - \bar{O}| + |O_i - \bar{O}|)^2} \right] \quad [5]$$

where,

N = Number of imputations

O_i = Observed data points

P_i = Imputed data points

- \bar{P} = Average of imputed data
- \bar{O} = Average of observed data
- σ_P = Population standard deviation of the imputed data
- σ_O = Population standard deviation of the observed data

RESULTS AND DISCUSSION

Figure 3 below shows the cases of missing values on particulate matter (PM₁₀) in 2005 from Tanjung Malim station, which has the most extended tail. The evidence can be related to the DoE statement, which said that the haze episode in August 2005 could be considered a severe case.

The concern involved the whole part of Klang Valley, which Air Pollution Index (API) reached about 500 on August 11. A few days later, the haze shifts to Malaysia’s northern states, causing the unhealthy API reading for northern states (Latif et al., 2018).

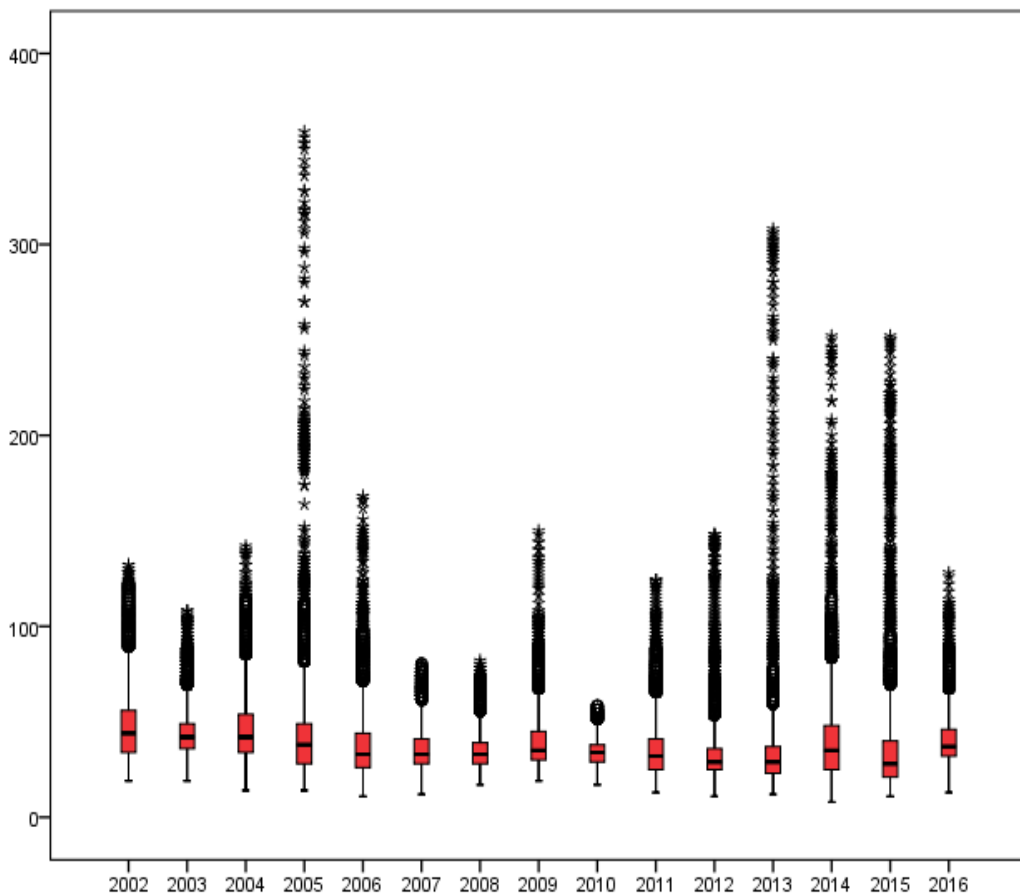


Figure 3. Distribution of particulate matter (PM₁₀) for the entire year from 2002 to 2016

An Evaluation of Single Imputation Technique by Gap Length

Data set from 2005 being simulated using SPSS by dividing it into three different per cent of missingness which is 2.5, 5 and 10. Each degree of percentage missingness simplifies into three different levels of complexity: short gap, medium gap, and long gap. Each gap being tested using four different single imputation techniques of techniques results in the finding, as shown in Table 2 and Figure 4.

From 2.5% missing value, at the short gap, the discovery of the best technique lies on Mean Nearby One Point, which has a slightly lower value of performance error of 0.028 and 1.118 depending on MAE and RSME compared to linear interpolation technique. However, it also needs to correlate with the performance accuracy, which the previous

technique has the highest value of PA of 0.981, indicated it is the best technique. Next, for the medium gap, the better technique that can be applied lies on Mean Nearby One Point, although, at the beginning of the early gap hours, the technique tends to be on Linear Interpolation. Finally, as for the long gap, the best fit technique falls on Linear Interpolation, with the lowest value of 0.009 of MAE and the highest value of 0.805 of IA in performance accuracy.

From the 5% missing value, at the short gap, the better techniques are Linear Interpolation and Mean Nearby Three Points, which have the same findings of 0.012 MAE and 0.944 IA. Therefore, it can be relatively said that the predicted data readings for both techniques from these gaps are almost the same. Next, for medium gaps, it also suggested Linear Interpolation and Mean Nearby Three Points as a better fit. Finally, as for the long gap, the best technique found is Mean Nearby Three-Point which has 0.559 RSME and 0.969 IA.

On the other hand, from the 10% missing value at the short gap, the Series Mean has a lower performance error which consists of 0.213 MAE and 11.907 RSME. However, the technique does not make accuracy since the performance accuracy is much better in Mean Nearby Three Points with an R^2 of 0.113. Next, for medium gaps, it also suggested that the Series Mean technique is a better fit. Finally, as for the long gap, the best technique found is Series Mean which has RMSE and IA of 13.005 and 0.409, respectively. This result has shown how close the results in RSME for predicting the missing value at the stated hours' gaps.

Table 3 shows the results for three patterns of missing data, each with their performance measuring performance error (MAE and RSME) and performance accuracy (IA, PA and R^2). At 2.5% missing data, linear interpolation technique rules out others technique as it has the lowest reading of performance error (MAE = 0.043233, RSME = 1.659556) and highest performance accuracy (IA = 0.975495, PA = 0.962742, R^2 = 0.918349). Next, at 5% missing data, it also showed that linear imputation technique fit best with (MAE = 0.038920, RSME = 2.159368) and (IA = 0.991016, PA = 0.982460, R^2 = 0.960815). Finally,

Table 2
 Result for 2.5%, 5%, and 10% Simulated Missing Data of PM₁₀ 2005 by Different Techniques at Different Gaps

Gaps	Method	2.5% simulated missing data					5% simulated missing data				
		MAE	RMSE	IA	PA	R ²	MAE	RMSE	IA	PA	R ²
Short	LIN	0.013	0.478	0.716	0.570	0.144	0.013	0.745	0.944	0.921	0.588
	SM	0.561	19.935	0.033	-0.500	0.111	0.144	8.575	0.352	0.656	0.299
	MN1P	0.028	1.118	0.713	0.982	0.429	0.015	0.894	0.920	0.881	0.539
	MN2P	0.359	17.004	0.011	-0.416	0.077	0.013	0.783	0.938	0.911	0.577
	MN3P	0.359	17.004	0.011	-0.416	0.077	0.013	0.745	0.944	0.921	0.588
Medium	LT	0.805	28.563	0.023	-0.499	0.111	0.208	12.367	0.255	0.620	0.267
	LIN	0.524	20.025	0.026	-0.472	0.100	0.106	6.309	0.559	0.748	0.400
	SM	0.579	21.032	0.031	-0.490	0.107	0.137	8.163	0.431	0.691	0.337
	MN1P	0.636	23.207	0.027	-0.487	0.106	0.150	8.946	0.415	0.686	0.335
	MN2P	0.580	21.422	0.028	-0.483	0.104	0.131	7.806	0.468	0.708	0.357
Long	MN3P	0.598	21.887	0.029	-0.487	0.106	0.140	8.305	0.438	0.695	0.343
	LT	0.594	21.827	0.028	-0.485	0.105	0.137	8.154	0.449	0.700	0.348
	LIN	0.010	0.313	0.806	0.759	0.400	0.015	0.599	0.966	0.959	0.773
	SM	0.686	19.633	0.027	-0.200	0.028	0.313	12.327	0.210	0.542	0.247
	MN1P	0.046	1.628	0.085	-0.257	0.046	0.012	0.674	0.955	0.933	0.732
Long	MN2P	0.532	18.404	0.045	0.446	0.138	0.012	0.584	0.967	0.947	0.753
	MN3P	0.532	18.404	0.045	0.446	0.138	0.012	0.560	0.970	0.950	0.758
	LT	0.497	14.206	0.036	-0.200	0.028	0.218	8.608	0.298	0.582	0.285

Table 2 (Continued)

Gaps	Method	10% simulated missing data				
		MAE	RMSE	IA	PA	R ²
Short	LIN	0.462	20.938	0.326	0.264	0.055
	SM	0.214	11.908	0.285	-0.114	0.010
	MN1P	0.452	20.606	0.332	0.155	0.019
	MN2P	0.452	20.520	0.337	0.265	0.055
	MN3P	0.451	20.435	0.341	0.379	0.114
	LT	0.344	16.340	0.320	-0.141	0.016
Medium	LIN	0.417	19.162	0.332	0.170	0.063
	SM	0.406	18.738	0.329	0.101	0.046
	MN1P	0.389	18.080	0.327	0.043	0.042
	MN2P	0.404	18.660	0.329	0.105	0.050
	MN3P	0.400	18.493	0.329	0.083	0.046
	LT	0.400	18.521	0.329	0.088	0.047
Long	LIN	0.448	19.364	0.341	0.157	0.022
	SM	0.283	13.005	0.409	0.235	0.049
	MN1P	0.449	19.462	0.338	0.019	0.000
	MN2P	0.449	19.414	0.341	0.112	0.011
	MN3P	0.449	19.367	0.343	0.210	0.039
	LT	0.452	19.556	0.339	0.096	0.008

at 10% missing data, with (MAE = 0.040230, RSME = 0.871611) and (IA = 0.998997, PA = 0.998313, R² = 0.996402), it also shown that linear interpolation (LIN) served as best fit technique for PM₁₀ variables at long hour gaps. The lowest performance error reading and the highest performance accuracy reading indicated that the technique could predict the data of missing value close to actual data supposedly being read by the machine.

Evaluation of Single Imputation for Incomplete PM10 Data

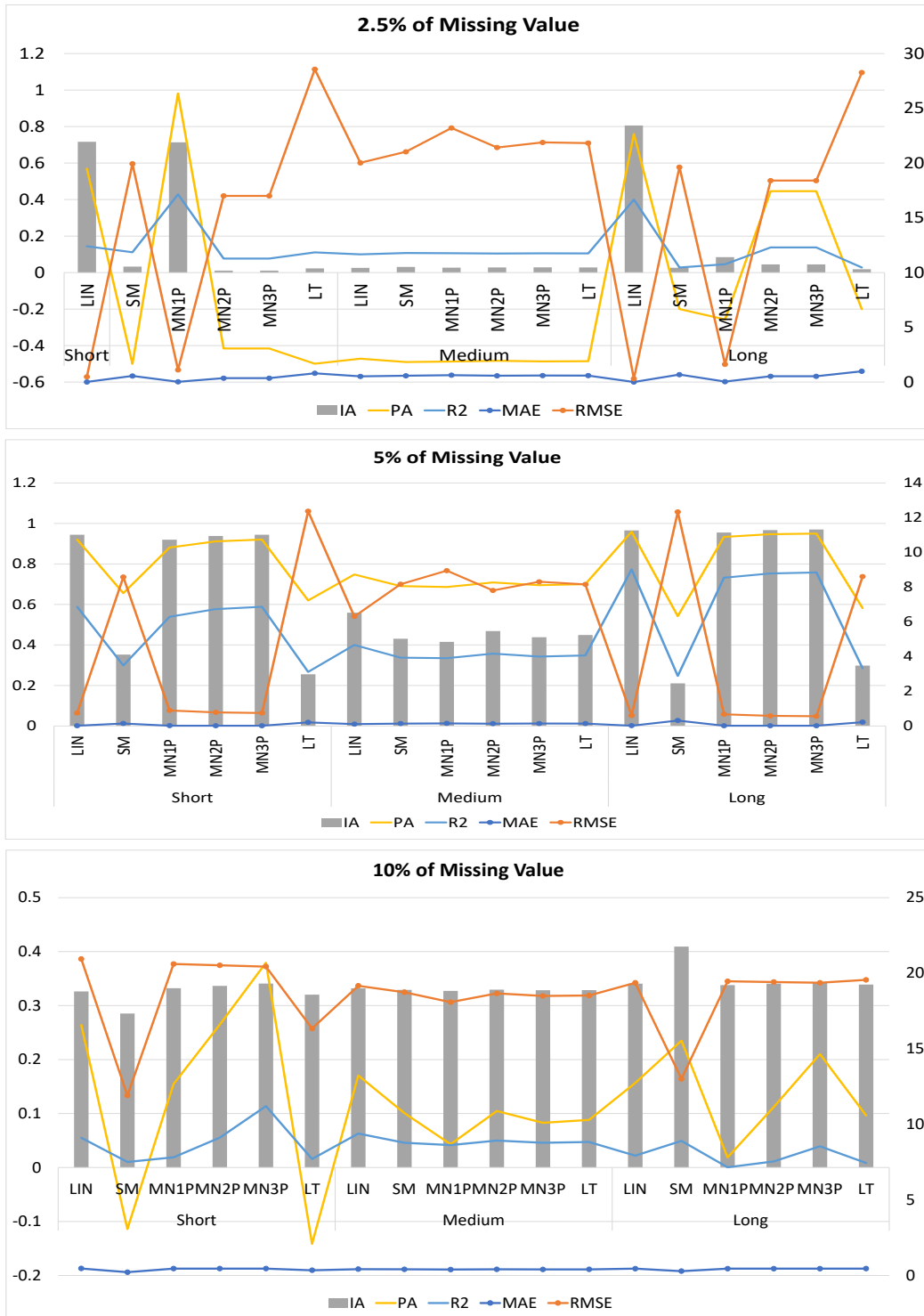


Figure 4. Performance indicator of 2.5%, 5% and 10% for PM₁₀ by different techniques at different gaps

Table 3

Values of performance indicators for every single imputation technique according to three different per cent of missingness

Missing Data	SI Technique	MAE	RMSE	IA	PA	R ²
2.5%	LIN	0.043233	1.659556	0.975495	0.962742	0.918349
	SM	0.593523	17.193990	0.336215	0.000000	0.000000
	MN2P	0.095029	5.423340	0.803035	0.699729	0.485118
	MN1P	0.055462	2.018434	0.962313	0.942526	0.880187
	MN3P	0.096861	5.448565	0.798063	0.691625	0.473946
	LT	0.898617	25.231054	0.261694	-0.515198	0.262989
5%	LIN	0.038920	2.159368	0.991016	0.982460	0.960815
	SM	0.256419	11.939487	0.285478	0.000000	0.000000
	MN2P	0.054667	2.914869	0.983292	0.967771	0.932299
	MN1P	0.055381	2.945380	0.982898	0.967092	0.930991
	MN3P	0.055480	2.940319	0.982823	0.967325	0.931441
	LT	0.337788	15.867781	0.431738	-0.679798	0.460012
10%	LIN	0.040230	0.871611	0.998997	0.998313	0.996402
	SM	0.313707	5.806496	0.950983	0.909237	0.826523
	MN2P	0.067985	1.567689	0.996726	0.993977	0.987764
	MN1P	0.063324	1.504180	0.996996	0.994413	0.988631
	MN3P	0.071544	1.626157	0.996466	0.993557	0.986931
	LT	0.377668	6.434816	0.948203	0.905342	0.819457

CONCLUSION

This paper discussed the use of a single imputation technique to estimate the missing data values. Four imputation techniques are being used, with also five performance indicators being calculated. The result confirmed that generally, the linear interpolation (LIN) technique served the best as the imputation technique that can replace the missing value in the observed (original) data set regardless of the percentage of missing data patterns. This study concludes that the efficiency of the linear interpolation (LIN) technique is used to predict the missing values closed to actual data for particulate matter (PM₁₀) variables for the long gaps with 2.5% of missingness (MAE = 0.010, RMSE = 0.313, IA = 0.806, PA = 0.759, R² = 0.400). However, for long gaps with 5% and 10% of missingness, the linear interpolation (LIN) technique indicates poor performance. The best imputation technique for the long gaps with 5% and 10% of missingness are the mean nearby three points (MN3P): MAE = 0.012, RMSE = 0.560, IA = 0.970, PA = 0.950, R² = 0.758, and

series mean (SM): MAE = 0.283, RMSE = 13.005, IA = 0.409, PA = 0.235, $R^2 = 0.049$, respectively.

Simulation results for this research demonstrate that the linear interpolation (LIN) technique produces the lowest performance error and is most accurate compared to other techniques for 2.5%, 5% and 10% of missingness without being separated into different gaps. Therefore, it is to be believed that when dealing with another data set for PM₁₀, the result produced will still be the same, which consists of the lowest MAE and RSME. It is also noticeable that the IA, PA and R^2 values approach to digit one, which is the best-fit conditions for performance accuracy. It proves the result obtained in the research by Norazian et al. (2008) that the linear interpolation (LIN) technique gives the best estimates for the 10%, 15%, and 25% missing values to the annual hourly monitoring records for PM₁₀ in Seberang Perai, Penang, Malaysia.

However, further research needs to be done since this research's limitation is the stated techniques of imputations already implemented in SPSS and are used vastly by previous researchers. Nevertheless, all in all, it can be said that if further experiment needs to be conducted, the Linear Interpolation technique is still the best among four available techniques in SPSS based on the experiment results.

Since this simulation only focuses on the PM₁₀ variable, it cannot be said the techniques are valid to be used for other pollutants variables such as SO₂, CO₂, CO, and O₃. However, in other previous literature from previous researchers, the result from different techniques apart from what is being programmed in SPSS already achieved success with some work limitations. In a nutshell, further study should be conducted for the other variables to determine the actual value for missing data to determine whether the different variables may affect this experiment results.

ACKNOWLEDGEMENT

The research was funded by 600-IRMI/FRGS 5/3 (289/2019). Thank you to the Faculty of Computer and Mathematical Sciences, Universiti Teknologi MARA, for their support and thanks to the Department of Environment Malaysia for providing air quality monitoring data.

REFERENCES

- Ali, S., & Dacey, S. (2017). Technical review: performance of existing imputation methods for missing data in SVM ensemble creation. *International Journal of Data Mining & Knowledge Management Process (IJDKP)*, 7(6), 75-91. <https://doi.org/10.5121/ijdkp.2017.7606>
- Anh, N. T. N., Kim, S. H., Yang, H. J., & Kim, S. H. (2011). Hidden dynamic learning for long-interval consecutive missing values reconstruction in EEG time series. In *2011 IEEE International Conference on Granular Computing* (pp. 653-658). IEEE Publishing. <https://doi.org/10.1109/grc.2011.6122674>

- Cokluk, O., & Kayri, M. (2011). The effects of methods of imputation for missing values on the validity and reliability of scales. *Educational Sciences: Theory and Practice*, 11(1), 303-309.
- De Leeuw, J., & Meijer, E. (2008). Introduction to multilevel analysis. In *Handbook of multilevel analysis* (pp. 1-75). Springer. https://doi.org/10.1007/978-0-387-73186-5_1
- Department of Environment. (2018). *Malaysia environmental quality report 2018*. DoE Publication.
- Hirabayashi, S., & Kroll, C. N. (2017). *Single imputation method of missing air quality data for i-tree eco analyses in the conterminous United States*. Retrieved January 1, 2021, from https://www.itreetools.org/documents/51/Single_imputation_method_of_missing_air_quality_data_for_i-Tree_Eco_analyses_in_the_conterminous_United_States.pdf
- Latif, M. T., Othman, M., Idris, N., Juneng, L., Abdullah, A. M., Hamzah, W. P., Khan, M. F., Sulaiman, N. M. N., Jewaratnam, J., Aghamohammadi, N., Sahani, M., Xiang, C. J., Ahamad, F., Amil, N., Darus, M., Varkkey, H., Tangang, F., & Jaafar, A. B. (2018). Impact of regional haze towards air quality in Malaysia: A review. *Atmospheric Environment*, 177, 28-44. <https://doi.org/10.1016/j.atmosenv.2018.01.002>
- Little, R. J., & Rubin, D. B. (2019). *Statistical analysis with missing data* (Vol. 793). John Wiley & Sons.
- Noor, N. M., Yahaya, A. S., Ramli, N. A., & Abdullah, M. M. A. (2006). The replacement of missing values of continuous air pollution monitoring data using mean top bottom imputation technique. *Journal of Engineering Research & Education*, 3, 96-105.
- Norazian, M. N., Shukri, Y. A., & Azam, R. N. (2008). Estimation of missing values in air pollution data using single imputation techniques. *ScienceAsia*, 34(3), 341-345. <http://doi.org/10.2306/scienceasia1513-1874.2008.34.341>
- Plaia, A., & Bondi, A. L. (2006). Single imputation method of missing values in environmental pollution data sets. *Atmospheric Environment*, 40(38), 7316-7330. <https://doi.org/10.1016/j.atmosenv.2006.06.040>
- Sukatis, F. F., Noor, N. M., Zakaria, N. A., Ul-Saufie, A. Z., & Suwardi, A. (2019). Estimation of missing values in air pollution dataset by using various imputation methods. *International Journal of Conservation Science*, 10(4), 791-804
- Ul-Saufie, A. Z., Yahya, A. S., Ramli, N. A., & Hamid, H. A. (2011). Comparison between multiple linear regression and feed forward back propagation neural network models for predicting PM10 concentration level based on gaseous and meteorological parameters. *International Journal of Applied*, 1(4), 42-49.
- Ward, N. (2019). *Air pollution*. Retrieved January 1, 2021, from <https://prezi.com/wyokg7n0uuru/air-pollution/>
- Zainudin, M. L., & Noor, N. M. (2009, June 20-22). The single interpolation and statistical technique: A review of application in air quality data sets. In *Proceedings of Malaysian Technical Universities Conference on Engineering and Technology (MUCEET2009)* (pp. 1-4). Pahang, Malaysia

Optimisation Design of Functionally Graded Sandwich Plate with Porous Metal Core for Buckling Characterisations

Emad Kadum Njim^{1*}, Sadeq Hussein Bakhy¹ and Muhannad Al-Waily²

¹ *University of Technology, Mechanical Engineering Department, Baghdad, 10066 Iraq*

² *University of Kufa, Faculty of Engineering, Mechanical Engineering Department, Najaf, 54001 Iraq*

ABSTRACT

This study presents the optimum operating parameters and geometrical of the functionally graded sandwich plate with porous materials (FGPMs), widely used in aircraft structures subjected to uniaxial critical buckling load. This process is developed design optimisation parameters by employing Multi-Objective Genetic Algorithm (MOGA) techniques. According to a simple power law, the assumption of varying material characteristics of the porous FG core through the plate thickness is considered. In addition, to evaluate the linear buckling behaviour, a new mathematical model based on the classical plate theory (CPT) is proposed. The impact of different design parameters on the performance of the functionally graded structure is studied. Then, finite element modelling is used to validate the results of the analytical solution. Finally, the optimisation method includes both design of experiments (DOE) and response surface methodology (RSM), which are used to find out the critical buckling load of the FG sandwich plate with porous metal core bonded

with two homogenous skins using suitable adhesion. The mandatory constraints are the maximum critical buckling and maximum total deformation. In this work, 100 design points are considered to determine the total deformation load multiplier, maximum deformation, and equivalent stress of sandwich plate with graded materials and even distribution of porosities. The buckling analyses of the FGPM sandwich plate subjected to the compression loading are presented by conducting an experimental program. The results show good convergence

ARTICLE INFO

Article history:

Received: 2 June 2021

Accepted: 30 July 2021

Published: 28 October 2021

DOI: <https://doi.org/10.47836/pjst.29.4.47>

E-mail addresses:

emad.njim@gmail.com (Emad Kadum Njim)

20093@uotechnology.edu.iq (Sadeq Hussein Bakhy)

muhanedl.alwaeli@uokufa.edu.iq (Muhannad Al-Waily)

*Corresponding author

between suggested analytical and FEA simulation with an average error percentage of no more than 2 %.

Keywords: Classical plate theory, critical buckling load, DOE, FEA, FGPMs, mathematical model, optimisation, RMS

INTRODUCTION

Functionally graded materials (FGMs) are known as new advanced materials can achieve higher performance by mixing two or more completely different components, the volume fraction of which is gradually changed in one or more directions, and combined with the required material properties, thus reducing the stress concentration found in laminated composites (Emad et al., 2021a). Due to the ability to produce materials with tailor-made properties, this material is suitable for various important applications, such as energy, aerospace, automobile, defence, marine, and biomedical, so people's interest in FGM is increasing. In addition, many researchers have been studying various aspects of static, vibration, buckling, and design (Bassiouny et al., 2020). The most popular FGMs are metal-ceramic constituents, usually showing a power-law distribution to describe their material properties.

In most fabrication processes, microvoids and porous may be found in the FGM structure leading to compatibility reduction of materials (Zhao et al., 2019). FGM structures with porous materials are essential and have unique attributes in many industrial and biomedical applications (Emad et al., 2021b). The classical plate theory (CPT) of sandwich structure is proposed considering the interrupted line hypothesis. A further improvement of this theory is considering the thin layer that combines the surface and the core (Krzysztof & Ewa, 2021). Numerous studies have been published in the literature on the stability analysis of functionally graded sandwich structures.

To predict the imperfect FGM sandwich plate's performance in post-buckling using in-plane mechanical compression load, Vuong and Chin (2018) introduced the concept of high-order shear deformation and the FEA meshfree method in their solution. They concluded that loading type and geometrical properties influence the stability of the FGM structure. Hessameddin and Farid (2020) investigated buckling characteristics of sandwich plates with different boundary conditions and proposed mathematical formulations according to modified shear deformation theory. They examined the sandwich plate performance against linear buckling by taking the effect of some input parameters and employing a response surface methodology (RSM) in their analysis. D. Chen et al. (2019) used the Chebyshev-Ritz method to study bending and buckling analyses of the FG plate with a different arrangement of porosity distribution. The results show that the proposed porous model can reduced interfacial failure and improved buckling and bending performances.

The buckling behaviours of a functional graded polymeric sandwich plate subjected to different load cases have been presented by Mine and Uğur (2020). Moreover, Abo-Bakr et al. (2021) used variable axial load conditions to investigate optimal weight for buckling loads of the two constituents functionally graded beams with volume fraction following the sigmoid function. Z. Chen et al. (2019) studied the flexural buckling problems of the FGMs sandwich structure considering thermal-induced non-uniform cross-sectional properties and taking into accounts the influence of transverse shear deformation. Michele (2020) analysed the impact of the uneven arrangement of the core-oriented fibres using various materials on buckling loads of functionally graded orthotropic plates. J. F. Wang et al. (2021) introduced the meshless method and discussed a composite quadrilateral plate's stability and thermal vibration features with the FG carbon reinforced with a nanotube. Yassir et al. (2021) proposed a high-order mathematical model to examine stability analysis of the FG plate structure using the finite element method. Recently, many important studies have been published and discussed the development and design problems of FGMs (Mrinal & Manish, 2021; Nikbakht et al., 2019; Yi et al., 2019). A comprehensive study in optimisation shape and material for stability and performance behaviour of functionally graded toroidal shells has been conducted by Thang et al. (2020).

C. Wang et al. (2021) presented an optimisation process to improve the performance of piezoelectric FG plates by analysing shape control using a multi-objective isogeometric integrated method. Jin and Masatoshi (2015) worked on minimising the flexibility of FG sandwich structures by conduct a reliable design and optimisation analysis using an interface shape method, taking into accounts the volume constraints of the FG part. Zhu et al. (2009) presented an optimal study of sandwich panels under impact loading conditions to study the buckling behaviour considering the effect of different design parameters. Additionally, to solve the stability problem of functionally graded plates work in a thermal environment and under the influence of mechanical loadings, multi-objective design optimisation is conducted by Moleiro et al. (2020). In order to generate a design of lightweight structures based on prospective yield performance, Bai et al. (2019) presented a new approach of topology optimisation considering maximum applied stress as a constraint to design graded lattice structures. According to the literature, many scientists have adopted great attention to study the static, dynamic, and stability problems of FGM structure. However, many limitations are still present and need further study. For example, the comprehensive study of eigenvalue buckling, design, and optimisation of FGM imperfect sandwich plate follow power-law variation by applying in-plane loads has not been studied previously.

The current study presents a linear buckling analysis of simply-supported FG sandwich plates with uniform porosity distribution. The mathematical formulations are developed by using the classical thin plate theory. In accordance with this aim, total deformation and critical stresses are obtained for various geometrical considerations. Many important

design parameters, such as porosity ratio, volume fraction index, and thickness ratio, are considered in detail—numerical results obtained by Ansys test the accuracy and validity of the proposed analytical solution. A new optimisation analysis using the concept of design of experiments (DOE) and Response Surface Method (RSM) are carried out to evaluate the stability characteristics of the FG sandwich plate with porous metal. The number of design points considered is 100. The chosen design variables include porosity ratio (Beta), gradient index (k), and core thickness (h), as while the Total Deformation, Equivalent Stress, and Total Deformation Load Multiplier are chosen as response functions. The ranges of the input variables considered in this study are porosity factor ($Beta= 0-0.5$), volume fraction index ($k= 0-5$), thickness of face sheet ($h_f=2-2.5$) mm, and FG core height ($h= 5-25$) mm. Moreover, to approximate the results, a dxrom software is combined with ANSYS DesignXplorer is presented. The main contribution of this work is that the paper reports a comprehensive study of the porous FGM material and provides useful analysis and results, which would be helpful for the usage of such materials in the engineering industry. The results obtained may encourage many researchers to conduct further works on porous FG sandwich structures.

MATERIALS AND METHOD

Consider the model of a supported, rectangular FGM plate with cartesian coordinates (x, y, z), composed of two constituents (Al_2O_3/Al) core bonded at top and bottom surfaces with isotropic metal skin as shown in Figure 1. The width a , length b , and total thickness h are the main dimensions of the plate. The plate is subjected to uniaxial force F_x acting on the plate boundaries along the x -direction. According to classical plate theory, the stress-strain relation for the FG plate is given by Equations 1a, 1b, and 1c (Phi et al., 2021; Arefi & Najafitabar, 2021),

$$\sigma_x = -\frac{Ez}{1-\nu^2} \left(\frac{\partial^2 w}{\partial x^2} + \nu \frac{\partial^2 w}{\partial y^2} \right) \tag{1a}$$

$$\sigma_y = -\frac{Ez}{1-\nu^2} \left(\frac{\partial^2 w}{\partial y^2} + \nu \frac{\partial^2 w}{\partial x^2} \right) \tag{1b}$$

$$\tau_{xy} = -\frac{Ez}{(1+\nu)} \frac{\partial^2 w}{\partial x \partial y} \tag{1c}$$

Similarly, the corresponding moment resultants components $M_x, M_y,$ and M_{xy} respectively can also be given as Equations 2, 3a, 3b, and 3c:

$$\begin{Bmatrix} M_x \\ M_y \\ M_{xy} \end{Bmatrix} = \int_{-h/2}^{h/2} \begin{Bmatrix} \sigma_x \\ \sigma_y \\ \tau_{xy} \end{Bmatrix} z \, dz \quad [2]$$

$$M_x = -D \left(\frac{\partial^2 w}{\partial x^2} + \nu \frac{\partial^2 w}{\partial y^2} \right) \quad [3a]$$

$$M_y = -D \left(\nu \frac{\partial^2 w}{\partial x^2} + \frac{\partial^2 w}{\partial y^2} \right) \quad [3b]$$

$$M_{xy} = -(1 - \nu) D \frac{\partial^2 w}{\partial x \partial y} \quad [3c]$$

Here, D indicates the flexural rigidity of the plate which is equal to $D = \frac{Eh^3}{12(1 - \nu^2)}$.

Now, the governing equation of the plate can be expressed as Equation 4:

$$\frac{\partial^2 M_{xx}}{\partial x^2} - 2 \frac{\partial^2 M_{xy}}{\partial x \partial y} + \frac{\partial^2 M_{yy}}{\partial y^2} = N_x w_{xx} \quad [4]$$

The axial force N_x can be obtained with respect to the generalized strains as Equation 5

$$D(\nabla^4 w) = N_x \frac{\partial^2 w}{\partial x^2} \quad [5]$$

Where ∇^4 is commonly called the biharmonic operator.

As indicated above, the core material of the sandwich plate is considered with two constituents (i.e. ceramic and metal). Taking into account the Voigt homogenisation rule, the ceramic volume fraction V_c can be expressed as Equation 6 (Latifi et al., 2013; Baferani et al., 2011),

$$V_c(z) = \left(\frac{z}{h} + \frac{1}{2} \right)^k \quad [6]$$

And the volume fraction V_c and V_m satisfy Equation 7:

$$V_m(z) + V_c(z) = 1 \quad [7]$$

Where V_m is the corresponding volume fraction of metal, h is the plate cross-section height, and k is a gradient index in which $k \in [0, \infty)$, organises plate flexibility behaviour. By employing Equations 6 and 7, the effective mechanical properties of FGMs across the thickness of plate, considering the distribution of constituents follow a power-law is given by Equations 8 and 9:

$$\varphi(z) = \varphi_c V_c + \varphi_m V_m \tag{8}$$

$$\varphi(z) = \varphi_m + (\varphi_c - \varphi_m) \left(\frac{z}{h} + \frac{1}{2}\right)^k \tag{9}$$

Here φ_c and φ_m denote to effective properties of the FG plate materials (i.e. ceramic and metal), respectively (Merdaci et al. 2019; Singh & Harsha, 2020).

Mathematical Model for Porous FGM Sandwich Plate

For FG sandwich plate with even distribution of porosities ($\beta < 1$) are considered to vary continuously within the thickness of the plate, expressions for, the elasticity modulus E and mass density of the imperfect FG core using the power-law distribution are described by Equations 10 and 11, while Poisson’s ratio ν is assumed not varies through-thickness direction (Nuttawit & Arisara, 2015; Kumar et al., 2021).

$$E(z) = E_m + (E_c - E_m) \left(\frac{z}{h} + \frac{1}{2}\right)^k - (E_c + E_m) \frac{\beta}{2} \tag{10}$$

$$\rho(z) = \rho_m + (\rho_c - \rho_m) \left(\frac{z}{h} + \frac{1}{2}\right)^k - (\rho_c + \rho_m) \frac{\beta}{2} \tag{11}$$

A rectangular sandwich plate assessed the linear buckling behaviour of an FGPM structure with total height H made of (Al/Al₂O₃) FG core with porous and two same isotropic face sheets is considered. As a result, the mechanical properties of upper and lower skins are the same (i.e. $E_1=E_2=E_f$ and $\nu_1= \nu_2= \nu$), and the thickness of both parts is the same (i.e., $h_1=h_2$), the corresponding flexural rigidity D_s can be represented in the following Equations 12, 13 and 14:

$$\begin{aligned} D_s &= \int_{-\left(\frac{h+h_1}{2}\right)}^{-\left(\frac{h}{2}\right)} \left\{ \frac{z^2}{(1-\nu^2)} E(z) \right\} dz \\ &+ \frac{1}{(1-\nu^2)} \left(\int_{-\left(\frac{h}{2}\right)}^{\left(\frac{h}{2}\right)} \left\{ E_m + (E_c - E_m) \left(\frac{z}{h} + \frac{1}{2}\right)^k \right. \right. \\ &\left. \left. - (E_c + E_m) \frac{\beta}{2} \right\} z^2 \right) dz + \int_{\left(\frac{h}{2}\right)}^{\left(\frac{h+h_2}{2}\right)} \left\{ \frac{z^2}{(1-\nu^2)} E(z) \right\} dz \end{aligned} \tag{12}$$

$$D_s = \left(\frac{(E_c - E_m)h^3}{(1 - \nu^2)} \left\{ \frac{1}{k + 3} - \frac{1}{k + 2} + \frac{1}{4(k + 1)} \right\} + \frac{E_m h^3}{12(1 - \nu^2)} - \frac{(E_c + E_m)\beta h^3}{24(1 - \nu^2)} \right) + \frac{E_f}{12(1 - \nu^2)} \{(h + 2h_1)^3 - h^3\} \quad [13]$$

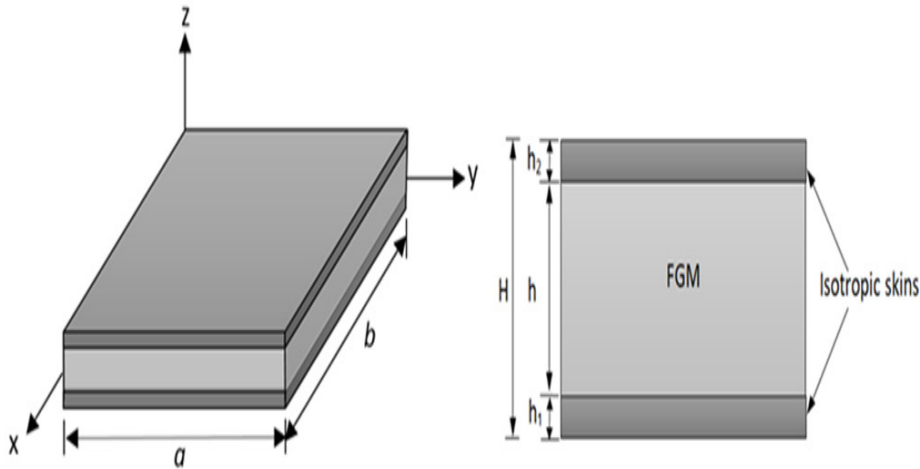


Figure 1. FGM Sandwich plate with porous core and homogenous skins

$$D_s \left(\frac{\partial^4 w}{\partial x^4} + 2 \frac{\partial^4 w}{\partial x^2 \cdot \partial y^2} + \frac{\partial^4 w}{\partial y^4} \right) = N_x \frac{\partial^2 w}{\partial x^2} \quad [14]$$

and we may represent Equation 14 as follows (Equation 15):

$$\left\{ \frac{(E_c - E_m)h^3}{(1 - \nu^2)} \left\{ \frac{1}{k + 3} - \frac{1}{k + 2} + \frac{1}{4(k + 1)} \right\} + \frac{E_m h^3}{12(1 - \nu^2)} - \frac{(E_c + E_m)\beta h^3}{24(1 - \nu^2)} \right\} + \frac{E_f}{12(1 - \nu^2)} \{(h + 2h_1)^3 - h^3\} \quad [15]$$

$$\times \left(\frac{\partial^4 w}{\partial x^4} + 2 \frac{\partial^4 w}{\partial x^2 \cdot \partial y^2} + \frac{\partial^4 w}{\partial y^4} \right) = N_x \frac{\partial^2 w}{\partial x^2}$$

Here, and as an approximate solution, the function may be used to describe the behaviour of rectangular plate in x and y directions, and the stability Equation 15 may be written as Equation 16 (Al-Waily et al., 2020)

$$w = A_{mn} \sin \frac{m\pi x}{a} \sin \frac{n\pi y}{b} \tag{16}$$

where: m, n natural numbers ($m, n=1, 2, 3, \dots$), also, A_{mn} is a constant coefficient, then by substituting the supported boundary conditions, into Equation 16, and putting through Equation 15,

we get Equations 17 and 18,

$$N_x = \left\{ D_s \times \left(\frac{m\pi}{a} \right)^2 + 2D_s \times \left(\frac{n\pi}{b} \right)^2 + D_s \times \left(\frac{n\pi}{b} \right)^4 \left(\frac{a}{m\pi} \right)^2 \right\} \tag{17}$$

$$N_x = \left\{ D_s \times \left(\frac{\pi}{a} \right)^2 + 2D_s \times \left(\frac{\pi}{b} \right)^2 + D_s \times \left(\frac{\pi}{b} \right)^4 \left(\frac{a}{\pi} \right)^2 \right\} \tag{18}$$

Consequently, the stability of an imperfect sandwich plate can be evaluated by determining the critical value of buckling load N_x . Moreover, in the case of the fundamental critical buckling occurs ($m = n = 1$), one may directly arrange Equation 18 for the square sandwich plate, which leads to getting Equation 19:

$$N_x = 4D_s \left(\frac{\pi}{a} \right)^2 \tag{19}$$

Using MATLAB code, the critical buckling load of Equation 17 may be determined, and different results can be recorded.

In consequence, the critical stress takes the following form as Equation 20,

$$\sigma_{x,cr} = \frac{N_{x,cr}}{h} \tag{20}$$

Furthermore, the associated dimensionless of the critical buckling load of thin porous FGM sandwich plates \bar{N} can be written as Equation 21:

$$\bar{N} = N_{x,cr} \frac{a^2}{E_m h^3} \tag{21}$$

Experimental Work

The experimental program covers the design of the specimens used as well as compression tests utilising samples with three porosity values ($\beta = 0.1, 0.2,$ and 0.3), a gradient index ($k=1$), and skins with a thickness of 1 mm using (Tinius Olsen H50KT) apparatus. In addition, a computer-controlled testing apparatus was used to measure maximum compression load and maximum total deflection at the mid-span of the plates.

Design and Preparation of the FG Test Specimens

In this study, two additively manufactured (AM) materials, Polylactic acid (PLA) and Thermoplastic polyurethane (TPU), produced by FlashForge (Zhejiang Hisun Biomaterials,

China), were used for 3D printing with a standard diameter of 1.75 mm. Each type has unique properties and applications that distinguish them from one another. All the samples were designed with porosity using Solid Works, then saved as a (.stl) file, then used to construct the sample with a CR-10 Max 3D printer. Throughout the current study, the face sheet was constructed mainly from aluminium alloy (AA6061-T6) plates with a thickness of 1 mm, the material most widely used for engineering applications and aerospace structures. On both top and bottom surfaces of the face sheet, extra adhesion (Epoxy) is used to bond it to the FG core, as shown in Figure 2. Table 1 summarises the mechanical properties of the FG core and face sheet (Arndt & Lechner, 2014; Balakrishna et al., 2020).



Figure 2. Manufacturing FG plate specimens using 3D printing

Table 1

Material properties of sandwich plates used in experimental work

Material	E (GPa)	ρ (Kg/m ³)	ν
PLA	1.2	1360	0.38
TPU	2.58	1450	0.35
AA6061-T6	70	2702	0.3

Experimental Setup and Procedure

Sandwich plates composed of functionally graded porous metals can be used for buckling experiments. The test specimens were fabricated from FGM with dimensions of 150 x 300 and 10 and 15 mm core heights. The plate is mounted on fixtures, and the experiment is conducted under (SFSF) boundary conditions. All experiments are carried out on

electromechanical universal testing equipment (UTM). The specimen was subsequently compressed unidirectionally at a displacement-controlled rate of 0.5 mm/min (in the direction of the y-axis). The force-extension curve drawn using UTM, as shown in Figure 3, can be used to establish the critical buckling load value for the plate structure under the impact of various parameters. The test technique was conducted three times on samples with the same attributes to ensure accuracy. Finally, the integral test method was repeated for all samples.

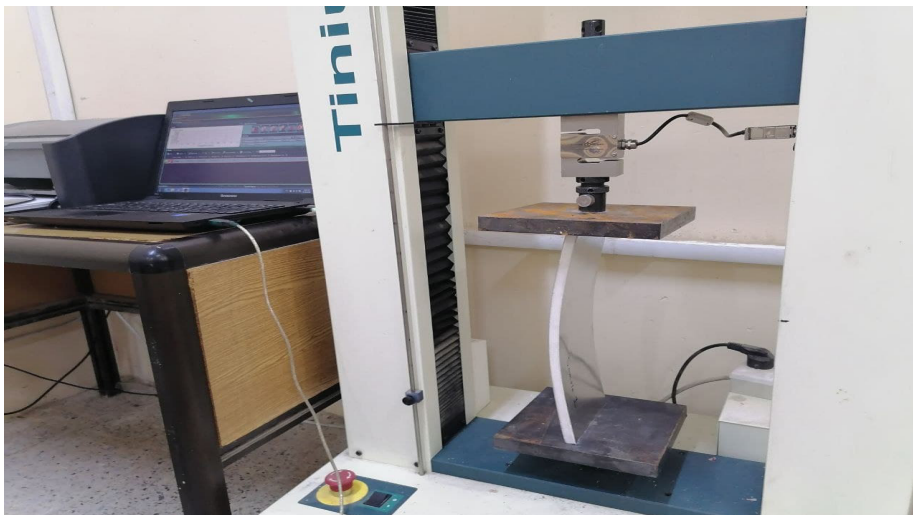


Figure 3. Experimental setup for FG sandwich plates

Numerical Investigation

The finite element method (FEM) is an excellent numerical way to analyse the dynamic response and the prediction of total deformation load, at which point stability can be observed in the FGMs sandwich plate (Emad et al., In Press; Vyacheslav & Tomasz, 2020). Accordingly, the numerical model of the sandwich plate with porous metal is carried out by employing the ANSYS software (Ver. 2021 R1). The 3D finite element model with dimensions $a=b=0.5$ m. The FG parameters include porosity coefficients Beta (0-0.3), the thickness of the core varies from (5-25) mm, and the gradient index k is (0-5). The skin thickness is kept to be 2.5 mm for upper and lower surfaces. For the mesh refinement process to work well, further mesh refining and convergence approach was carried out to get high accuracy numerical results, as shown in Figure 4, which uses 2536100 nodes. In the simulation, the material properties used in linear buckling analysis are calculated after mathematical operations, then involved as a new assignment into the model engineering data view. The desired model requires a thin layer of glue to pass through the connection area and between the layers to attain accurate results.

Furthermore, the glue prevents uneven thickness development between layers and skins caused by inconsistent settlement (Nguyen et al., 2020). In addition to the characteristics of the plate, the system also includes the mechanical characteristics of top and bottom skins. As such, apply the corresponding BC's under uniaxial compression on both plate sides. The square FG sandwich plate with supported boundary conditions subjected to uniaxial load case is illustrated in Figure 5. Next, buckling analysis of the selected models may be obtained to discover the stability behaviour in terms of total deformation load.

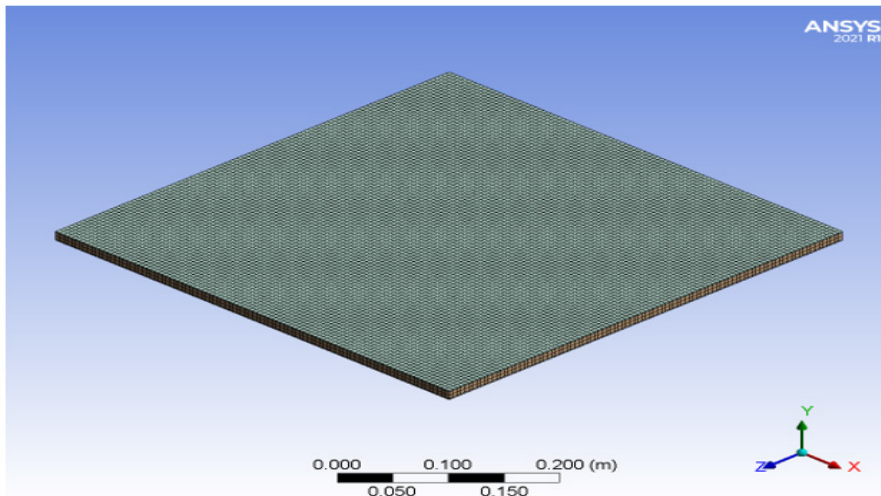


Figure 4. The model of FG system with Mesh

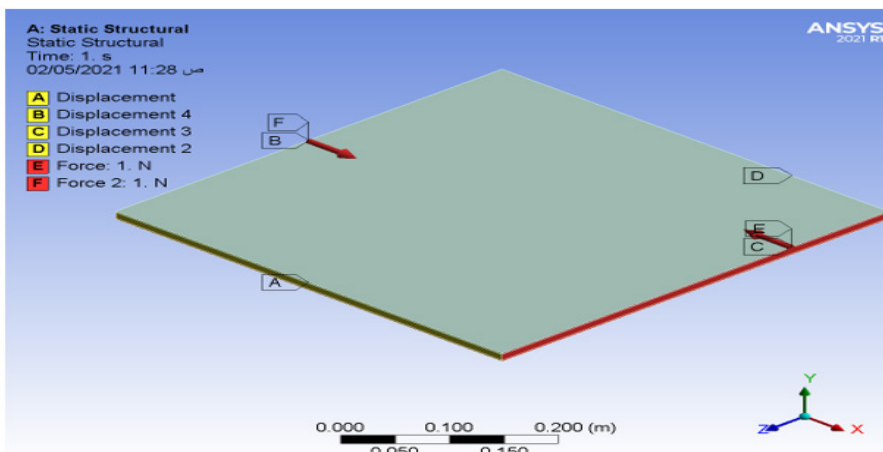


Figure 5. FGM Sandwich plate with S.S boundary conditions

Optimisation Problem Formulation

Topology optimisation can provide an optimised design and a better approximation based on a series of loads and constraints. Furthermore, by considering the buckling limit to minimise structural compliance, the buckling limit may determine an acceptable level of withstanding to total deformation of the structure (Mrinal & Manish, 2021; Sadiq et al., 2021; Lin et al., 2019). This work's scope optimisation includes a detailed design of a porous FG structure with specified boundary conditions under the influence of linear buckling using ANSYS 2021 R1, as shown in Figure 6. By including RSM, the model is built, meshed, and the design parameters are introduced, and the response results for total deformation, buckling load, and equivalent stresses are obtained.

Based on the fact that FG parameters have a considerable impact on handling the FGM sandwich structure stability problem, the design of experiment software (DOE) was employed: to study the influence of the FG parameters on stability, obtaining optimal parameters, and develop a mathematical model based on numerical data. The well-known optimisation procedure known as the MOGA method is used. It provides frequent purposes and constraints to determine the optimum global concept. The design variables involving skin thicknesses ($P1$), core height ($P3$), porous parameters ($P8$), and power-law index ($P9$) are selected with appropriate limits, as it is found in Table 2. The main objective of this study is the maximise Total Deformation Load Multiplier ($P15$), Total Deformation Maximum (mm) ($P18$), Equivalent Stress Maximum (MPa) ($P19$), and Force Magnitude 1 and 2 (N) ($P16$ & $P17$), respectively considering initial samples 4000 and the number of samples per iteration 800 with a maximum of 13 iterations for each process. Moreover, the number of candidates is 3. The most important convergence roles in optimisation work involve Pareto and stability criterion. The estimated number of evaluations is 19200. Numerical simulation cases were conducted based on the design matrix established by the design of experiment (DOE) software.

In particular, to get many results, special software known as dxrom combines with ANSYS DesignXplorer Add-in for Excel. One may select any variable of the input parameters, apply any sampling point from (1 to 100), and select X and Y values. We can generate frequent results represented by tables and plots through this scope. Furthermore, we can choose any response point and performed the same work. Also, the percentage error can be obtained for each solution.

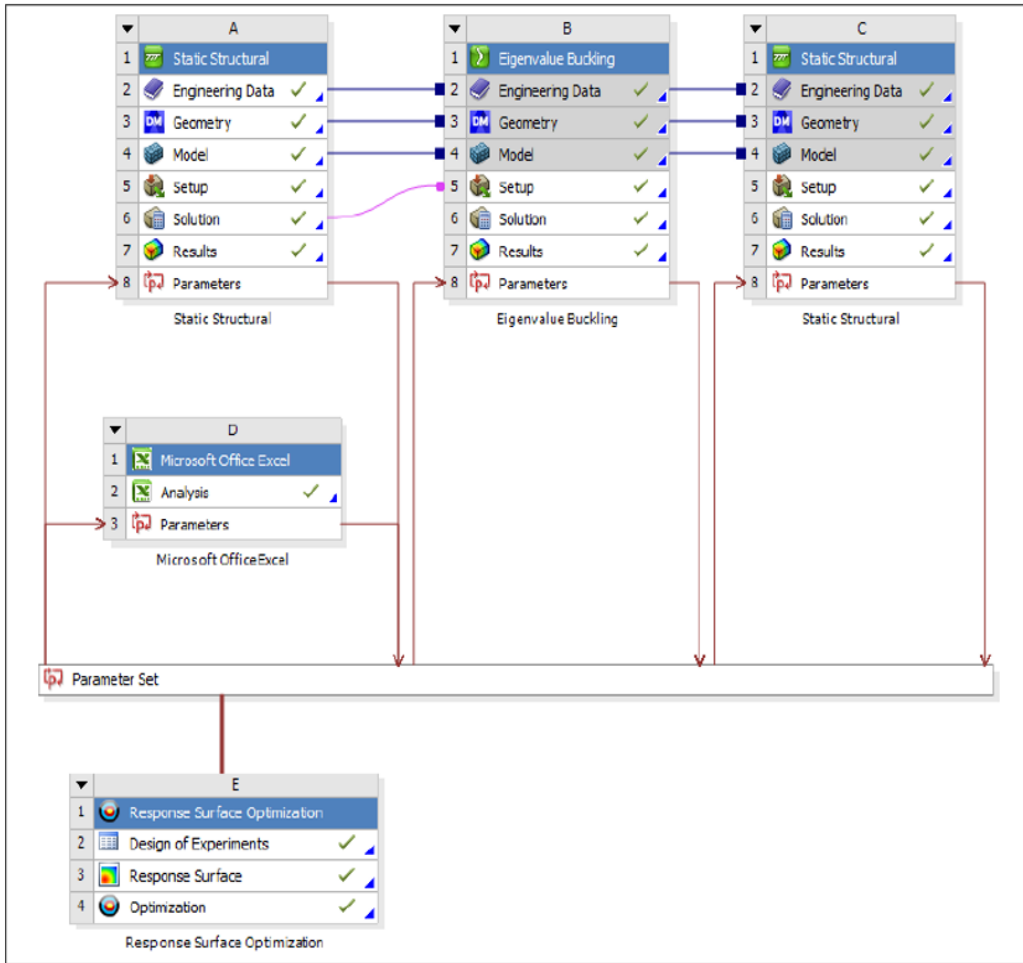


Figure 6. View of optimisation analysis via Ansys

Table 2

Limits of design parameters

Parameter	Symbol	Minimum value	Maximum value
Skin thickness (m)	$(P1 / a1)$	0.002	0.0025
Plate thickness (m)	$(P3 / b1)$	0.005	0.025
Porosity coefficient	$(P8 / Beta)$	0	0.5
Volume fraction index	$(P9 / K)$	0	5

RESULTS AND DISCUSSION

This paper presents buckling analysis and the stability problem of FGPMs. The FGM core layers are considered to be graded via the thickness direction of the plate with an even arrangement of porosities. A new mathematical formulation is carried out based on CPT, and the second-order differential equation is derived and solved. Many important parameters are tested to check their effects on the critical buckling load. These parameters include porosity ratio, gradient index, number of FGM platelayers, and aspect ratio. The analytical solution is validated by conduct a numerical investigation using the ANSYS 2021 R1. Various results are introduced and organised in multiple tables and figures. The mechanical properties for the FGM core, made from a mixture of (Al₂O₃/Al) and mild steel skins, are given in Table 3 (Cui et al., 2019). The plates have identical length and width ($a=b=0.5\text{m}$), the porosity ratio β (0 to 50%), the power-law distribution k (0 to 5), the FG core height h (5 to 25)mm, and two values of the skin thickness h_1 (2 and 2.5) mm.

Table 3

Material properties of the FG sandwich plate used in numerical and analytical solutions

Property	FG core		Face Sheets (Steel)
	Aluminium (Al)	Ceramic (Al ₂ O ₃)	
E (GPa)	70	380	210
ρ (Kg/m ³)	2700	3800	7800
ν	0.30	0.30	0.30

The nondimensional of critical buckling load is given as Equation 22:

$$\bar{N} = N_{x,cr} (a^2 / E_m h^3) \tag{22}$$

The proposed analytical solution capability for evaluating the linear buckling load of the functionally graded sandwich plate with porosity is examined. The dimensionless buckling load of the imperfect square sandwich plate is determined and compared with those calculated by FEA and introduced in Table 4. The dimensions of the plate are $a=b= 0.5$ m, and the (Al/Al₂O₃) constituents FG core height ($h = 10$ mm). Meanwhile various porosity factors $Beta$ (i.e., $Beta = 0.1,0.2,0.3, 0.4$ and 0.5) are considered and the power-law index $k=1$. The results were in good convergence with an average percentage error of 5%. One may discover that all models were utilising the critical value of buckling load induced in FG sandwich plate decrease with the increase of both power-law exponent and porosity parameters due to a clear decrease in material stiffness. Table 5 demonstrates the variation

of critical buckling loads of SFSF sandwich plate composed of PLA (Polylactic acid) and TPU (Thermoplastic Polyurethane) porous metal. The results show a good agreement between the UTM results and those obtained by the simulation procedure, with a maximum error percentage of 12% occurring at slenderness ratio $a/H = 30$ and porosity factor = 0.3. Furthermore, from the results, it may be concluded that TPU is an elastic polymer. Hence it may be used in various applications, such as car instrument panels and medical devices.

Table 4

Buckling load parameter results obtained by analytical and numerical solutions of supported Al/Al_2O_3 FGPMs sandwich plate ($a/b=1$)

No.	h_1	h	β	k	Buckling load parameter		Discrepancy %
					Analytical	Numerical	
1	2.5	10	0.0	0.5	11.347	11.75	3.429
2	2.5	10	0.1	0.5	11.104	11.476	3.241
3	2.5	10	0.2	0.5	10.65	10.95	2.739
4	2.5	10	0.3	0.5	10.317	10.624	2.889
5	2.5	10	0.4	0.5	10.174	10.365	1.842
6	2.5	10	0.5	0.5	9.931	9.995	0.640

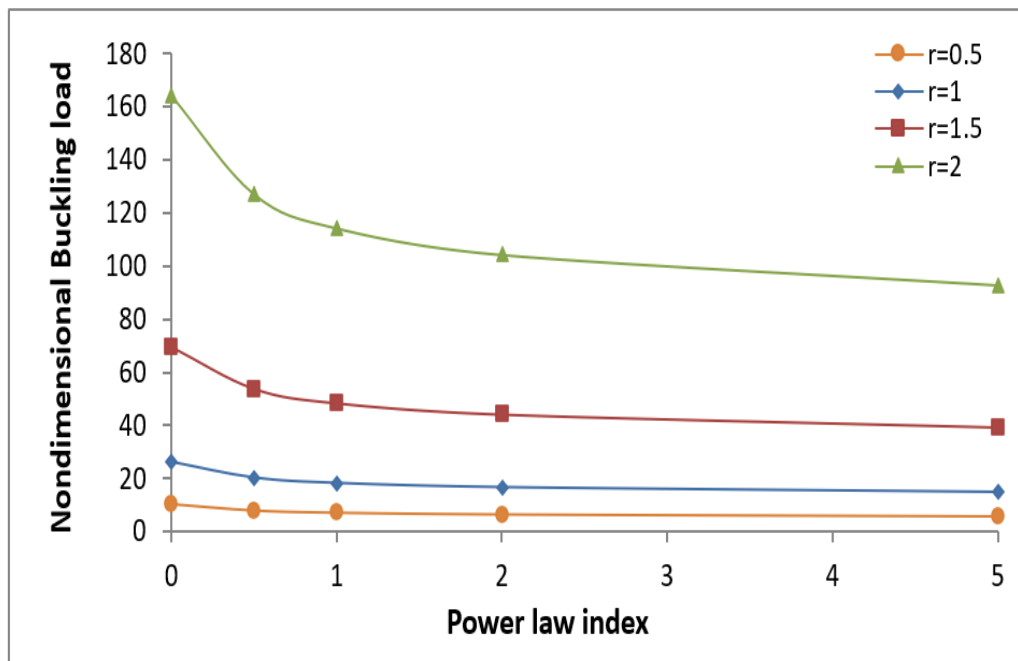


Figure 7. Convergence of the buckling load parameter results of supported (Al/Al_2O_3) FGPMs sandwich plates for different slenderness ratios.

Figure 7 shows the buckling load parameters results obtained by the proposed analytical solution of the supported porous FGM sandwich plate involving aspect ratio impact for five different values ($r=0.5, 1, 1.5,$ and 2) at porous factor ($\beta=0.1$), and the ratio of core to skin thickness ($h/h_1=5$). It can be seen from Figure 7 that as the volume fraction and aspect ratio gradually increase, (\bar{N}) increases, and the influence of the gradient index k is more significant as the aspect ratio increases (i.e. the effect of power-law exponent disappears at small values of aspect ratios). According to the details of Figure 8, the analytical solution results for the dimensionless parameter (\bar{N}) are given at porosity parameter ($\beta= 0, 0.1, 0.3$), for the various core to skin thickness ratio ($h/h_1 = 2, 4, 6, 8, 10$) at gradient index ($k=0.5$). It is observed that the critical buckling loads parameter is decreased with the increase of both cores to face-sheet thickness ratio (h/h_1) and porosity coefficient (β). Also, there is a clear convergence in results with an increased thickness ratio from 6 to 10. One may be concluded that the bending stiffness of the sandwich plate is significantly affected with the increase of core to face-sheet thickness ratio h/h_1 due to a decrease in overall stiffness. By considering the FGM sandwich plate comprised of layers up to 20, Figure 9 presents the buckling load parameter results due to the Ansys simulation at porosity coefficient ($\beta=0.25$). The results obtained for different aspect ratios including value of power-law index ($k= 1$), core height ($h=10$ mm), and face sheet thickness ($h_1 = 1.5$ mm). It is found that there are no obvious variations of buckling load parameters when the structure core is constructed by a few layers as well as a small aspect ratio. However, the performance of the whole structure offers high stability as the number of FG core layers increases.

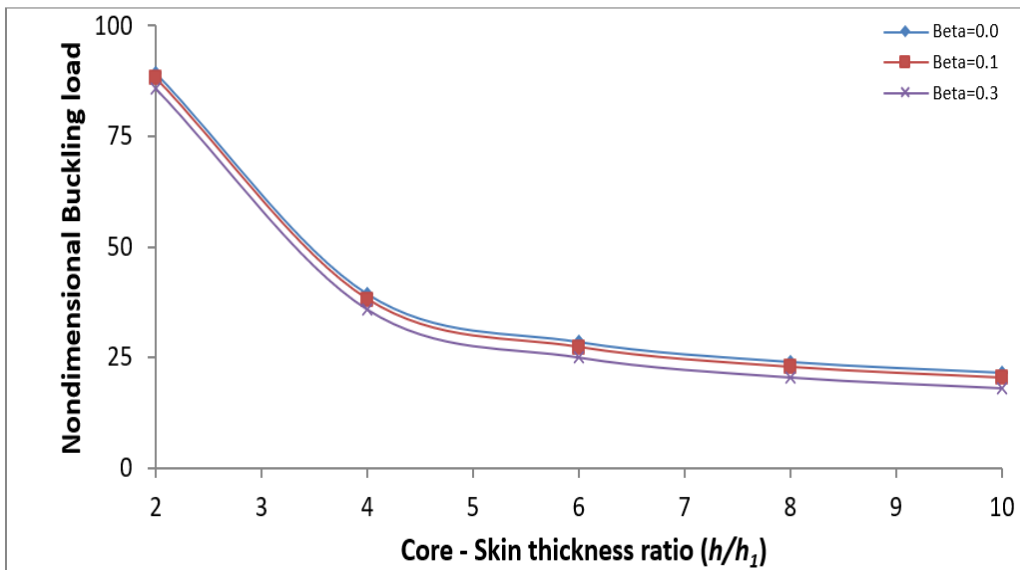


Figure 8. A comparison of the critical buckling load parameter of a square sandwich plate having three porosities, h/h_1 , in terms of the core to face-sheet thickness ratio.

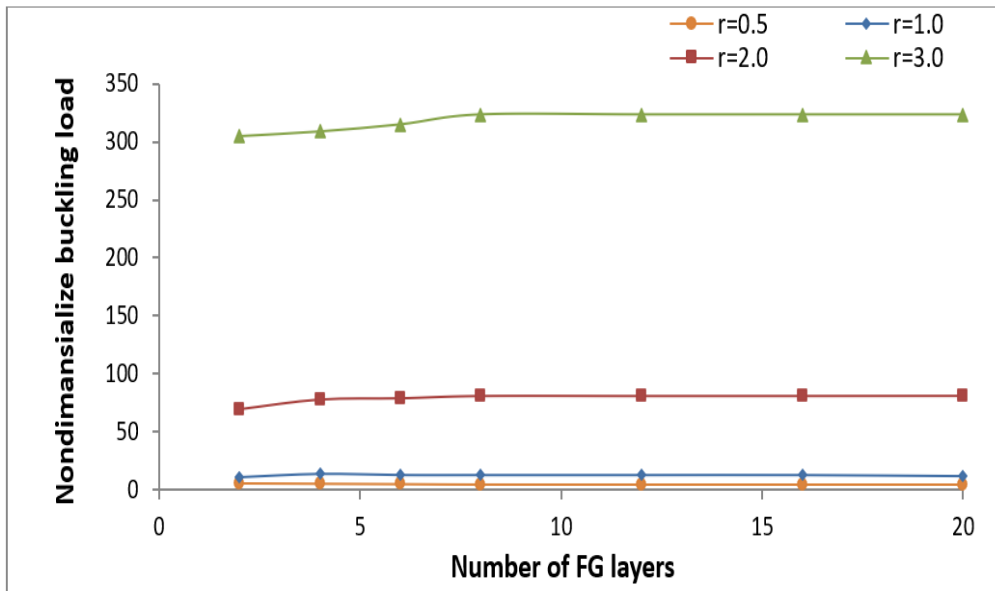


Figure 9. Results of the \bar{N} of rectangular FGM sandwich plate, for various aspect ratios at $k=1$

Table 5

Experimental and numerical variation of critical buckling loads of SFSF rectangular sandwich plate, skin thickness 1mm

Sandwich type	b/a	a/H	Porosity	Experimental (N)	Numerical (N)	Discrepancy %
PLA/Al	0.5	30	0	11750	12984.924	9.51
			0.1	11480	12362.883	7.14
			0.2	11179	11870.840	5.83
			0.3	10750	11618.802	7.48
	0.5	20	0	32100	33514.204	4.23
			0.1	31550	33396.080	5.53
			0.2	31000	33277.955	6.85
			0.3	30645	33159.831	7.58
TPU/Al	0.5	30	0	11200	11665.2	3.98
			0.1	10890	11635.38	6.41
			0.2	10455	11621.87	10.04
			0.3	10180	11568.37	12.00
	0.5	20	0	27175	28165.52	3.52
			0.1	26490	27982.29	5.33
			0.2	26750	27924.33	4.21
			0.3	26110	27866.37	6.30

Table 6 also shows Ansys’s critical buckling load parameter results for sandwich plates employing different porosity coefficients under five types of boundary conditions. For example, the plate thickness ratio $a/h = 50$, and thickness of face sheets 2mm. Influences of porosity coefficient and power-law index are investigated, and it is noticed that the higher buckling parameter value present at the model stronger constraints. As an example, taking into accounts the porosity coefficient ($\beta = 0.1$) and the gradient index ($k = 1$), The buckling parameter for the CCCC model is 17, while in CCCS, the buckling parameter is 15.75, also in CCCF, the buckling parameter is 13.79, as for SCSC, the buckling parameter is 12.79, and in SSSS, the value is 10.73. It is concluded that the critical buckling load increases with the increase in the constraints to the boundary conditions; for example, the frequency parameter for CCCC is higher than CCCS, and this condition is more than CSCS, and so on.

Table 6
Results of FEA solution of \bar{N} , with different boundary conditions at thickness ratio ($a/h = 100$)

B.C.'s	k	Porosity factor					
		0	0.1	0.2	0.3	0.4	0.5
CCCC	0	18.99	18.68	17.99	17.66	17.32	17.17
	0.5	17.87	17.67	17.46	17.13	16.99	16.69
	1	17.54	17.11	16.85	16.79	16.55	16.43
	2	17.11	16.78	16.52	16.38	16.10	15.99
	5	16.59	16.45	16.21	15.99	15.88	15.71
CCCF	0	14.85	14.65	14.42	14.21	14.09	13.93
	0.5	14.31	14.27	14.06	13.92	13.85	13.70
	1	14.01	13.95	13.72	13.61	13.50	13.12
	2	13.75	13.66	13.41	13.38	13.09	12.94
	5	13.50	13.22	13.15	12.95	12.74	12.42
SCSC	0	13.88	13.50	13.26	13.01	12.85	12.54
	0.5	13.35	13.12	12.97	12.71	12.49	12.11
	1	13.00	12.79	12.45	12.20	12.01	11.60
	2	12.50	12.20	12.07	11.87	11.40	11.20
	5	11.86	11.51	11.31	11.19	11.06	10.87
SSSS	0	12.34	12.13	11.94	11.71	11.53	11.32
	0.5	11.27	11.11	10.88	10.68	10.48	10.31
	1	10.97	10.73	10.53	10.35	10.16	9.920
	2	10.64	10.48	10.28	10.10	9.89	9.650
	5	10.37	10.16	9.967	9.750	9.58	9.380

Table 6 (Continued)

B.C.'s	k	Porosity factor					
		0	0.1	0.2	0.3	0.4	0.5
CCCS	0	16.84	16.59	16.26	16.09	15.87	15.71
	0.5	16.32	16.02	15.99	15.70	15.61	15.48
	1	15.81	15.75	15.61	15.55	15.31	15.00
	2	15.61	15.34	15.18	15.01	14.82	14.60
	5	15.09	14.88	14.79	14.58	14.37	14.12

Response Surface Results

Response surface methodology is another common statistical approach for process parameter optimisation. It includes 3D figures to display how certain input design values will impact the response view of resultant parameters. Figure 10 represents the total deformation buckling load response chart at gradient index $k=0$, while Figure 11 shows the maximum equivalent stress with varying porosity parameters and core height at gradient index $k=0.5$. From Figures 10 and 11, it is found that both buckling load and equivalent stress increase with the decrease of gradient index and porosity coefficients. Furthermore, a response chart for both equivalent stresses and deformation load is shown in Figures 12 and 13. In terms of the porosity parameter, it is demonstrated that the presence of pores influences the overall rigidity of functionally graded structures. We can also generate graphs of Local Sensitivity to display relationships of each input parameter with corresponding output parameters. Simultaneously by constructing a spider chart, changing the input parameters may visualise the effect on all the output parameters.

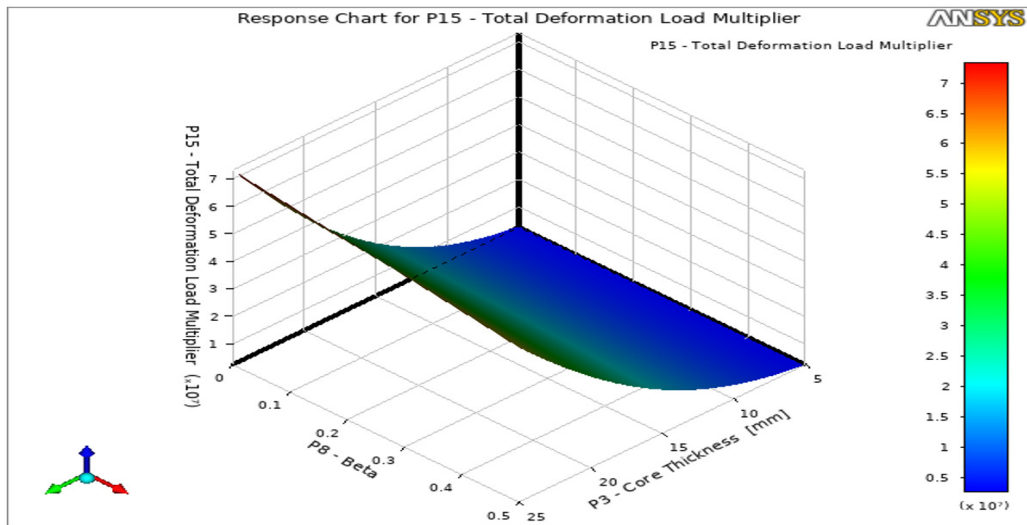


Figure 10. RSM with varying parameters for total deformation multiplier at $k=0$

Table 7

Optimisation results for three candidate points for total deformation load

Candidate points	P_1 (mm)	P_3 (mm)	P8	P9	Total Deformation Load Multiplier
1	2.5	20	0.3	3	353636
2	2.5	19.857	0.299	2.999	677775
3	2.5	19.678	0.299	3	785788

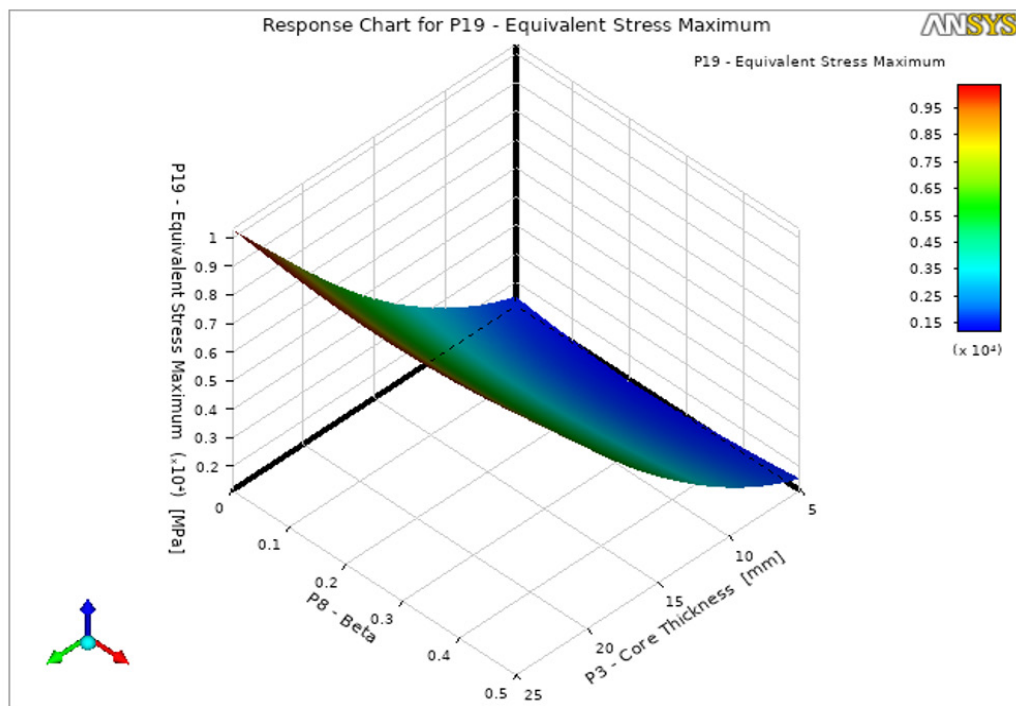


Figure 11. RSM with varying parameters for equivalent stresses at $k=0.5$

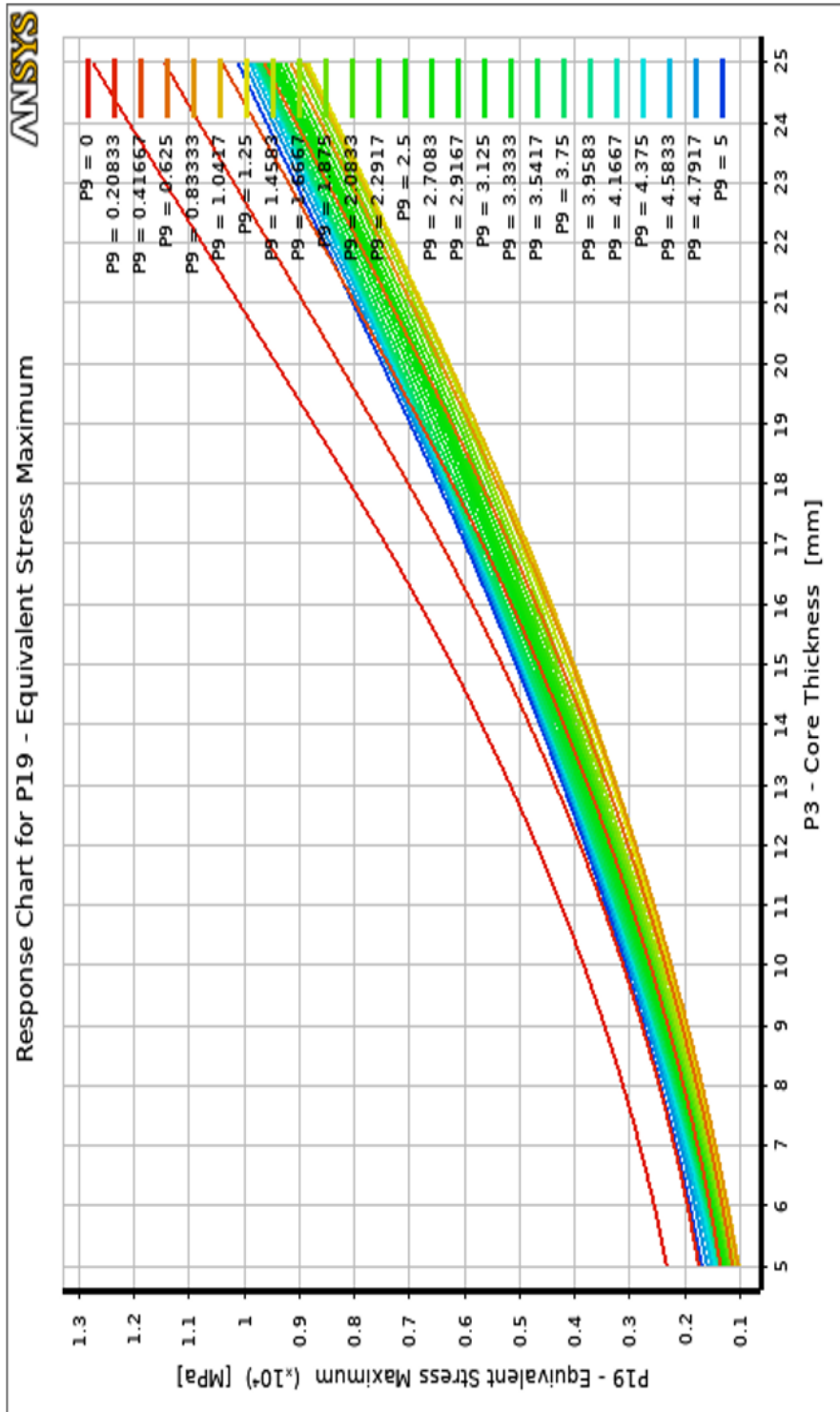


Figure 12. Response chart for Equivalent Stresses

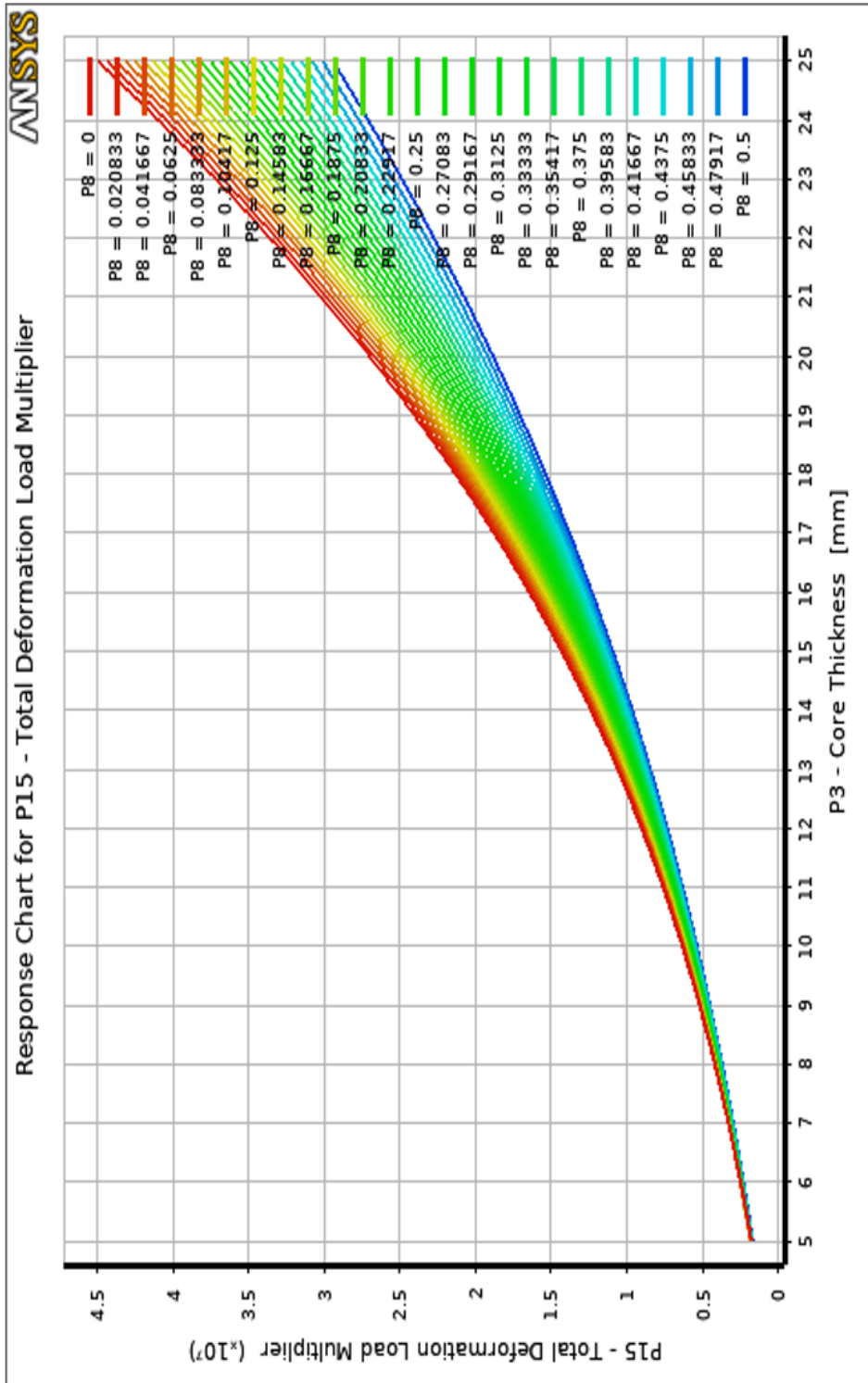


Figure 13. Response chart for Total Deformation Load

Optimisation Results and Discussion

This section deals with frequent results obtained by optimisation work. It is included but is not limited to the Tradeoff charts, Sensitivities, and Candidate points. Table 7 presents three candidate points results found by optimisation work. The results indicated that a generated design for all models has an excellent tendency to predict the stability of porous FG sandwich structures. Specifically, feasible points for total deformation load and equivalent stresses are introduced in the Tradeoff charts as shown in Figures 14 and 15, respectively. According to details in Figures 15 and 16, it is found that the gradient index $k = 0$ results in a sharp gradient in both total deformation and equivalent stress near the bottom surface of the plate, while $k = 2.9$ results in a steep gradient in total deformation equivalent stress near the top surface. The reason for this is the sharply varying material properties near the top and bottom surfaces for $k = 0$ and 3.

Figure 16 presents a graphical view of the global sensitivities for total deformation load multiplier, equivalent stresses, and force magnitude with respect to the input parameters such as skin, core heights, porosity coefficient, and FG constituent index. Sensitivity with positive response occurs when an apparent increase of the input parameter yields to an increase in output response. In contrast, a negative sensitivity can be seen when an inverse relationship between input and output occurs.

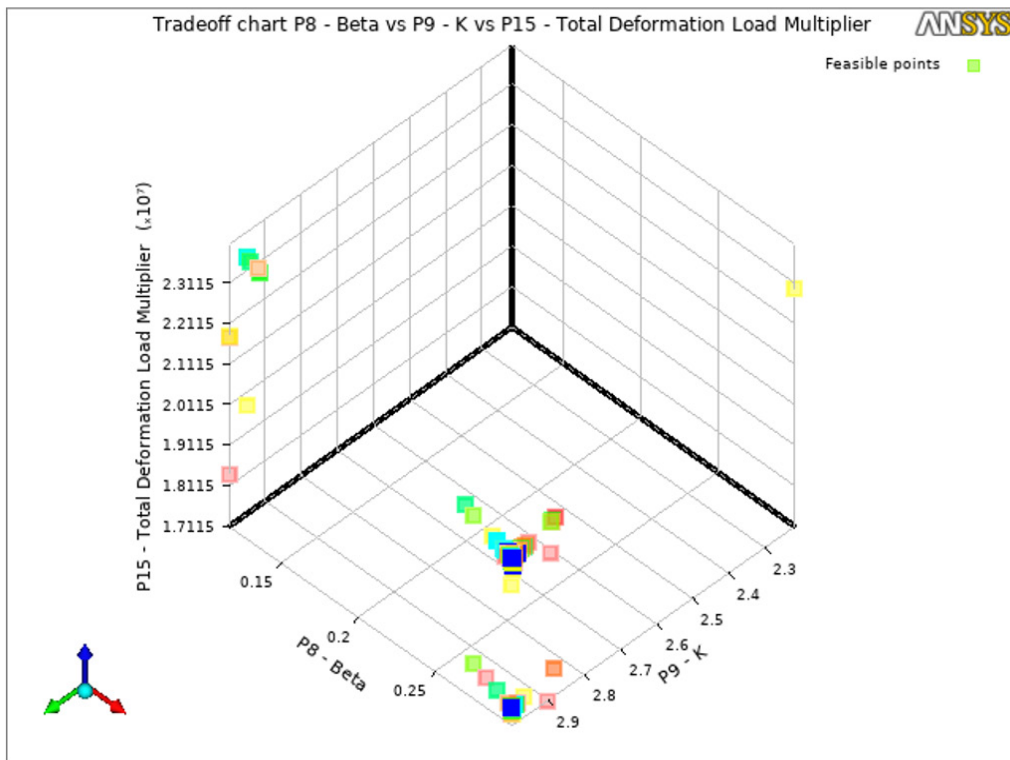


Figure 14. Tradeoff chart for Total deformation load at a number of Pareto to show 8 feasible points

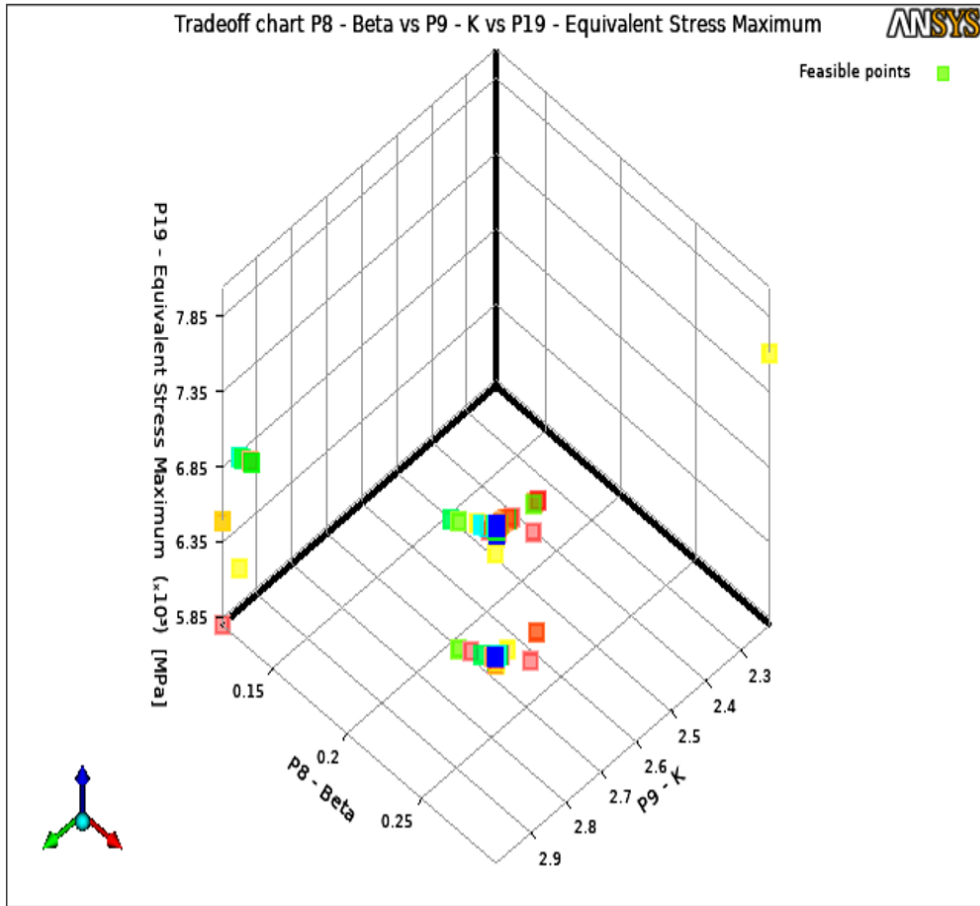


Figure 15. Tradeoff chart for Equivalent stress at a number of Pareto to show 8 feasible points

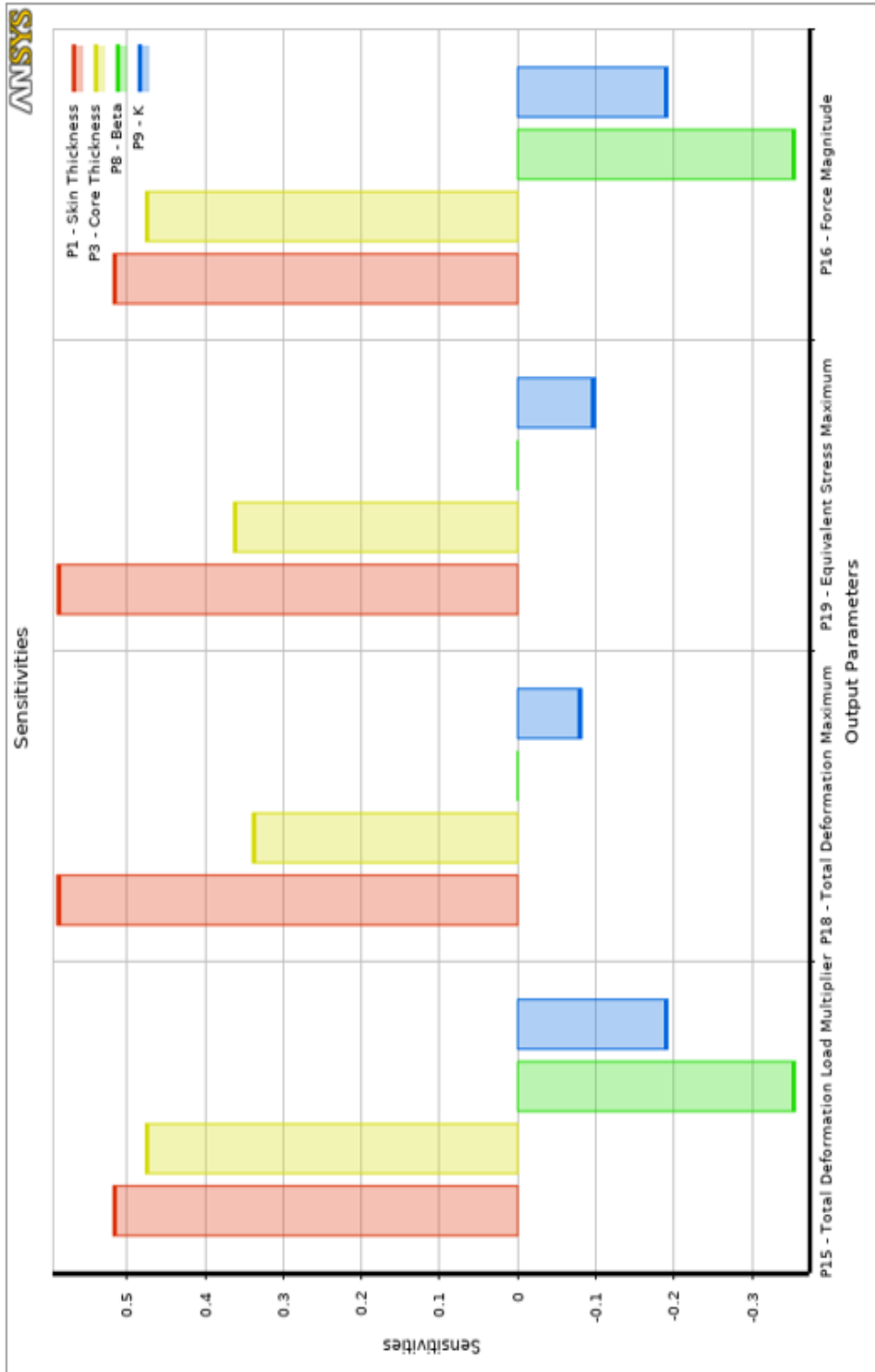


Figure 16. Sensitivities for various parameters

CONCLUSION

Porous FG materials are widely used in many applications such as tissue engineering, Biomedicine, and aerospace. The present work investigates the MOGA optimisation method for eigenvalue buckling analysis of supported functionally graded sandwich plate with Al/Al₂O₃ porous core and two homogeneous material skins. The presented generalised analytical model employing the classical plate theory of the sandwich structure is formulated. The FEA approach confirmed the correctness of the generalised analytical model of the sandwich structure with FGMs. Results for important parameters of FG core material and thickness and type of boundary conditions are evaluated. Some concluding observations from the investigation are given below.

- For all the boundary conditions, the buckling load increases with an increased aspect both thickness a/h and slenderness ratio (a/b).
- It can be observed that the performance of sandwich structures with porous FG is influenced by, type of the axial load, volume fraction characteristics, and boundary conditions. Also, it was found that the maximum critical buckling load of such a sandwich plate is gained when, pure ceramic surface, its supports are completely clamped, and the porosity factor is 0.1.
- The FEA models represented by Ansys software are a high-quality way to design, optimize, and predict critical buckling load. Hence it can identify the stability and level of performance of the FGM sandwich structure.
- A reasonable agreement was established between the experimental and finite element analysis using ANSYS software for buckling analysis, with a percentage error of no more than 15%, indicating that there was no delamination between the layers of FGM samples and that the test samples were well-fabricated.
- The behaviour of the sandwich structure is positively influenced by the ratio of core height to total sandwich plate height (i.e. h/H). It is because the rigidity of the sandwich panel is greatly affected by this ratio.
- According to the results obtained by the DOE and RSM, the resulted optimum value for the maximum porosity coefficient was found at 0.3, core height (0.019678 m), face sheet thickness (0.0025 m), and the maximum gradient index (3), where the optimum total deformation load multiplier value was found (785788).

ACKNOWLEDGEMENT

The authors appreciate the cooperation of the University of Kufa and the University of Technology/Iraq in completing the experimental work.

REFERENCES

- Abo-bakr, R. M., Abo-bakr, H. M., Mohamed, S. A., & Eltahir, M. A. (2021). Optimal weight for buckling of FG beam under variable axial load using Pareto optimality. *Composite Structures*, 258, Article 113193. <https://doi.org/10.1016/j.compstruct.2020.113193>
- Al-Waily, M., Al-Shammari, M. A., & Jweeg, M. J. (2020). An analytical investigation of thermal buckling behavior of composite plates reinforced by carbon nano-particles. *Engineering Journal*, 24(3), 11-21. <https://doi.org/10.4186/ej.2020.24.3.11>
- Arefi, M., & Najafitabar, F. (2021). Buckling and free vibration analyses of a sandwich beam made of a soft core with FG-GNPs reinforced composite face-sheets using Ritz Method. *Thin-Walled Structures*, 158, Article 107200. <https://doi.org/10.1016/j.tws.2020.107200>
- Arndt, K. F., & Lechner, M. D. (2014). *Polymer solids and polymer melts—mechanical and thermomechanical properties of polymers*. Springer. <https://doi.org/10.1007/978-3-642-55166-6>
- Baferani, H. A., Saidi, A. R., & Ehteshami, H. (2011). Accurate solution for free vibration analysis of functionally graded thick rectangular plates resting on elastic foundation. *Composite Structures*, 93(7), 1842-1853. <https://doi.org/10.1016/j.compstruct.2011.01.020>
- Bai, L., Yi, C., Chen, X., Sun, Y., & Zhang, J. (2019). Effective design of the graded strut of BCC lattice structure for improving mechanical properties. *Materials*, 12(13), Article 2192. <https://doi.org/10.3390/ma12132192>
- Balakrishna, A., Padmanav, D., & Singh, N. B., (2020). Buckling analysis of porous FGM sandwich plates under various types nonuniform edge compression based on higher order shear deformation theory. *Composite Structures*, 251, Article 112597. <https://doi.org/10.1016/j.compstruct.2020.112597>
- Bassiouny, S., Jinghua, J., Reham, F., Tareq, A., Qiong, X., Lisha, W., Dan, S., & Aibin, M. (2020). 30 years of functionally graded materials: An overview of manufacturing methods, applications, and future challenges. *Composites Part B: Engineering*, 201, Article 108376. <https://doi.org/10.1016/j.compositesb.2020.108376>
- Chen, D., Yang, J., & Kitipornchai, S. (2019). Buckling and bending analyses of a novel functionally graded porous plate using Chebyshev-Ritz method. *Archives of Civil and Mechanical Engineering*, 19(1), 157-170. <https://doi.org/10.1016/j.acme.2018.09.004>
- Chen, Z., Li, J., Sun, L., & Li, L. (2019). Flexural buckling of sandwich beams with thermal-induced non-uniform sectional properties. *Journal of Building Engineering*, 25, Article 100782. <https://doi.org/10.1016/j.jobbe.2019.100782>
- Cui, J., Zhou, T., Ye, R., Gaidai, O., Li, Z., & Tao, S. (2019). Three-dimensional vibration analysis of a functionally graded sandwich rectangular plate resting on an elastic foundation using a semi-analytical method. *Materials*, 12(20), Article 3401. <https://doi.org/10.3390/ma12203401>
- Emad, K. N., Al-Waily, M., & Sadeq, H. B. (In Press). Optimization design of vibration characterizations for functionally graded porous metal sandwich plate structure. *Materials Today: Proceedings*. <https://doi.org/10.1016/j.matpr.2021.03.235>
- Emad, K. N., Al-Waily, M., & Sadeq, H. B. (2021a). A review of the recent research on the experimental tests of functionally graded sandwich panels. *Journal of Mechanical Engineering Research and Developments*, 44(3), 420-441.

- Emad, K. N., Al-Waily, M., & Sadeq, H., B. (2021b). A critical review of recent research of free vibration and stability of functionally graded materials of sandwich plate. *IOP Conference Series: Materials Science and Engineering*, 1094, Article 012081. <https://doi.org/10.1088/1757-899X/1094/1/012081>
- Hessameddin, Y., & Farid T. (2020). Analytical solution and statistical analysis of buckling capacity of sandwich plates with uniform and non-uniform porous core reinforced with graphene nanoplatelets. *Composite Structures*, 252, Article 112700. <https://doi.org/10.1016/j.compstruct.2020.112700>
- Jin, X. S., & Masatoshi S. (2015). Interface shape optimization of designing functionally graded sandwich structures. *Composite Structures*, 125, 88-95. <https://doi.org/10.1016/j.compstruct.2015.01.045>
- Krzysztof, M., & Ewa, M., (2021). Generalization of a sandwich structure model: Analytical studies of bending and buckling problems of rectangular plates. *Composite Structures*, 255, Article 112944. <https://doi.org/10.1016/j.compstruct.2020.112944>
- Kumar, V., Singh, S. J., Saran, V. H., & Harsha, S. P. (2021). Vibration characteristics of porous FGM plate with variable thickness resting on Pasternak's foundation. *European Journal of Mechanics - A/Solids*, 85, Article 104124. <https://doi.org/10.1016/j.euromechsol.2020.104124>
- Latifi, M., Farhatnia, F., & Kadkhodaei, M. (2013). Buckling analysis of rectangular functionally graded plates under various edge conditions using Fourier series expansion. *European Journal of Mechanics - A/Solids*, 41, 16-27. <https://doi.org/10.1016/j.euromechsol.2013.01.008>
- Lin, C., Bai, J., & Albert, C. (2019). Functionally graded lattice structure topology optimization for the design of additive manufactured components with stress constraints. *Computer Methods in Applied Mechanics and Engineering*, 344, 334-359. <https://doi.org/10.1016/j.cma.2018.10.010>
- Merdaci, S., Belmahi, S., Belghoul, H., & Hadj, M. A. (2019). Free vibration analysis of functionally graded plates FG with porosities. *International Journal of Engineering & Technical Research*, 8(3), 143-147. <https://doi.org/10.17577/IJERTV8IS030098>
- Michele, B. (2020). Buckling analysis of three-phase CNT/polymer/fiber functionally graded orthotropic plates: Influence of the non-uniform distribution of the oriented fibers on the critical load. *Engineering Structures*, 223, Article 111176. <https://doi.org/10.1016/j.engstruct.2020.111176>
- Mine, U. U., & Uğur, G. (2020). Buckling of functional graded polymeric sandwich panel under different load cases. *Composite Structures*, 21, 182-196. <https://doi.org/10.1016/j.compstruct.2014.11.012>
- Moleiro, F., Madeira, J. F. A., Carrera, E., & Reddy, J. N. (2020). Design optimization of functionally graded plates under thermo-mechanical loadings to minimize stress, deformation and mass. *Composite Structures*, 245, Article 112360. <https://doi.org/10.1016/j.compstruct.2020.112360>
- Mrinal, G., & Manish, C. (2021). Optimization of functionally graded material under thermal stresses. *Materials Today: Proceedings*, 44(1), 1520-1523. <https://doi.org/10.1016/j.matpr.2020.11.733>
- Nguyen, N. V., Nguyen, X. H., Lee, D., & Lee, J. (2020). A novel computational approach to functionally graded porous plates with graphene platelets reinforcement. *Thin-Walled Structures*, 150, Article 106684. <https://doi.org/10.1016/j.tws.2020.106684>
- Nikbakht, S., Kamarian, S., & Shakeri, M. (2019). A review on optimization of composite structures Part II: Functionally graded materials, *Composite Structures*, 214, 83-102. <https://doi.org/10.1016/j.compstruct.2019.01.105>

- Nuttawit, W., & Arisara, C. (2015). Flexural vibration of imperfect functionally graded beams based on Timoshenko beam theory, Chebyshev collocation method. *Meccanica*, *50*, 1331-1342. <https://doi.org/10.1007/s11012-014-0094-8>.
- Phi, L. T. M., Nguyen, T. T., & Lee, J. (2021). Buckling analysis of open-section beams with thin-walled functionally graded materials along the contour direction. *European Journal of Mechanics-A/Solids*, *88*, Article 104217. <https://doi.org/10.1016/j.euromechsol.2021.104217>
- Sadiq, S. E., Bakhy, S. H., & Muhsin, J. J. (2021). Optimum vibration characteristics for honeycomb sandwich panel used in aircraft structure. *Journal of Engineering Science and Technology*, *16*(2), 1463-1479.
- Singh, S. J., & Harsha, S. P. (2020). Thermo-mechanical analysis of porous sandwich S-FGM plate for different boundary conditions using Galerkin Vlasov's method: a semi-analytical approach. *Thin-Walled Structures*, *150*, Article 106668. <https://doi.org/10.1016/j.tws.2020.106668>
- Thang, T. P., Nguyen, T. T., & Lee, J. (2020). Shape and material optimization for buckling behavior of functionally graded toroidal shells. *Thin-Walled Structures*, *157*, Article 107129. <https://doi.org/10.1016/j.tws.2020.107129>
- Vuong, N. V. D., & Chin, H. L. (2018). Numerical investigation on post-buckling behavior of FGM sandwich plates subjected to in-plane mechanical compression. *Ocean Engineering*, *170*, 20-42. <https://doi.org/10.1016/j.oceaneng.2018.10.007>
- Vyacheslav, N. B., & Tomasz, S. (2020). Free vibrations and static analysis of functionally graded sandwich plates with three-dimensional finite elements. *Meccanica*, *55*, 815-832. <https://doi.org/10.1007/s11012-019-01001-7>
- Wang, C., Yu, T., Shao, G., & Bui, T. Q. (2021). Multi-objective isogeometric integrated optimization for shape control of piezoelectric functionally graded plates. *Computer Methods in Applied Mechanics and Engineering*, *377*, Article 113698. <https://doi.org/10.1016/j.cma.2021.113698>
- Wang, J. F., Cao, S. H., & Zhang, W. (2021). Thermal vibration and buckling analysis of functionally graded carbon nanotube reinforced composite quadrilateral plate. *European Journal of Mechanics - A/Solids*, *85*, Article 104105. <https://doi.org/10.1016/j.euromechsol.2020.104105>
- Yassir, S., Khadija, M., Oussama, B., & Hassan, R. (2021) Buckling and post-buckling analysis of a functionally graded material (FGM) plate by the Asymptotic Numerical Method. *Structures*, *31*, 1031-1040. <https://doi.org/10.1016/j.istruc.2021.01.100>
- Yi, B., Zhou, Y., Yoon, G. H., & Saitou, K. (2019). Topology optimization of functionally-graded lattice structures with buckling constraints. *Computer Methods in Applied Mechanics and Engineering*, *354*, 593-619. <https://doi.org/10.1016/j.cma.2019.05.055>
- Zhao, J., Zhang, M., Zhu, Y., Li, X., Wang, L., & Hu, J. (2019). A novel optimization design method of additive manufacturing-oriented porous structures and experimental validation. *Materials & Design*, *163*, Article 107550. <https://doi.org/10.1016/j.matdes.2018.107550>
- Zhu, F., Wang, Z., Lu, G., & Zhao, L. (2009). Analytical investigation and optimal design of sandwich panels subjected to shock loading. *Materials & Design*, *30*(1), 91-100. <https://doi.org/10.1016/j.matdes.2008.04.027>



Case Study

Anomaly Detection of Grid Connected Photovoltaic System Based on Degradation Rate: A Case Study in Malaysia

Mohamad Zhafran Hussin^{1*}, Nor Diyana Md Sin¹, Hedzlin Zainuddin², Ahmad Maliki Omar³ and Sulaiman Shaari²

¹*Faculty of Electrical Engineering, Universiti Teknologi MARA (UiTM) Cawangan Johor, Kampus Pasir Gudang, 81750 Masai, Johor, Malaysia*

²*Faculty of Applied Sciences, Universiti Teknologi MARA (UiTM) Shah Alam, 41450 Shah Alam, Selangor, Malaysia*

³*Faculty of Electrical Engineering, Universiti Teknologi MARA (UiTM) Shah Alam, 41450 Shah Alam, Selangor, Malaysia*

ABSTRACT

This paper presents the characterization and performance of six-year field data for two different systems of PV module technologies from the rooftop grid-connected system installed at Universiti Teknologi MARA (UiTM) Shah Alam. Two different PV module technologies are used as case studies to establish a method of anomaly detection on the system performance. The selected parameters such as string voltage, string current and AC power output are used in the analysis, while solar irradiance and module temperature are used as a reference basis. Based on the results obtained, both systems having degradation rates differently. System A had shown stable performance before it degraded by 16.09%

after the 4th-year of operation, whereas system B continuously decreased by 39.35% during the monitored period. However, the string current of system A degraded up to 4.4% and, interestingly, no degradation for the string voltage. In contrast, system B has experienced a degradation of the string current by about 21.6%, whereas the string voltage was around 16.16%. Therefore, the string current and string voltage could identify the cause of the degradation rate of AC power. This analysis could be used to

ARTICLE INFO

Article history:

Received: 7 June 2021

Accepted: 22 August 2021

Published: 28 October 2021

DOI: <https://doi.org/10.47836/pjst.29.4.48>

E-mail addresses:

mzhafran@uitm.edu.my (Mohamad Zhafran Hussin)

diyana0366@uitm.edu.my (Nor Diyana Md Sin)

hedzl506@uitm.edu.my (Hedzlin Zainuddin)

maliki_omar@uitm.edu.my (Ahmad Maliki Omar)

solarman@uitm.edu.my (Sulaiman Shaari)

*Corresponding author

diagnose and identify the sources and causes of power degradation of grid-connected PV systems so that further action could be taken.

Keywords: Degradation, grid-connected, photovoltaic system, string current, string voltage

INTRODUCTION

The Government of Malaysia is committed to achieving the 20% target for the Renewable Energy (RE) sector in the national generation capacity mix by 2025. The preliminary Renewable Energy Transition Roadmap (RETR) 2035 developed by the Sustainable Energy Development Authority (SEDA) (<http://www.seda.gov.my/>) has projected that solar PV will contribute more than half of RE's target capacity by 2025 based on two key factors due to higher average solar irradiation and continuing decline trend in the price of solar PV technology (Velautham et al., 2019). As of 2019, the installed capacity of the solar PV installation is around 882.02 MW (Vaka et al., 2020). During the early stage of the Malaysia Building Integrated Photovoltaic (MBIPV) program, the PV cost index is approximately MYR32.00/Wp (Hussin et al., 2012). Almost all components in the grid-connected photovoltaic (GCPV) system were imported from European countries. However, once solar products from China were introduced in the Malaysia market around 2017, it witnessed a significant drop in PV cost index until 2019, where the average present cost is roughly MYR2.91 to MYR5.58/Wp for residential Building Integrated Photovoltaic (BIPV) until small centralised PV applications (Velautham et al., 2019).

At the end of 2011, Malaysia launched a Feed-in Tariff (FiT) scheme through The Renewable Energy Act 2011. The scheme obliges the Distribution Licensees (DLs) to buy the electricity produced from grid-connected renewable energy for 21 year period for solar PV and mini-hydro and a 16-years for biomass and biogas. However, by 2016, the FiT scheme will no longer be offered for solar PV quota allocation and replaced by a new Net Energy Metering programme (NEM1.0). NEM1.0 permits consumers to consume the energy generated by solar PV systems. Any surplus will be resold to the utility grid or distribution licensee (TNB/SESB) at the prevailing Displaced Cost prescribed by the Energy Commission instead of selling all harvested energy as in the FiT scheme. However, this mechanism does not help reduce consumer utility bills, especially for small-size residential.

As a result, the NEM2.0 scheme was updated to replace the previous scheme to overcome the drawbacks by making it a "one-to-one" energy offset mechanism instead of the previous net billing mechanism implemented from 2016 to 2018. Recently, NEM3.0 was introduced in December 2020 once NEM2.0 has been fully subscribed and will be effective from 2021 to 2023 (SEDA). Most GCPV system owners are only interested in monthly energy generation, which reflects their electricity bills. They are only interested in knowing in detail if their monthly electricity bill is not up to their expectations, especially

when they are engaged with the NEM scheme. If any problems occurred in their system, such as shading, solar panel defects, i.e., hotspots, micro-cracks, light-induced degradation (LID) or potential-induced degradation (PID) effects throughout the contract (Fouad et al., 2017), the return-on-investment (ROI) will not be achievable where most systems usually take 4 to 7 years if using FiT scheme (Husain et al., 2020; Yatim et al., 2014), and 10 to 22 years if using NEM1.0 scheme (Husain et al., 2020; Yatim et al., 2017) to get their investment back. For NEM2.0 and NEM3.0, ROI is expected to achieve in 6 to 7 years. Today, the PV cost index is around MYR4 to MYR 5/Wp for residential.

In harvesting free energy from the sun, some limitations contribute to power loss, such as geographical locations, climates and the reliability of BOS components such as PV module technology and inverter. Thus, generally, the power loss in the GCPV system could be divided into two categories, namely sub-system power loss and PV modules power loss. Sub-system power loss includes power losses in cables and inverters. The second category is the power loss within the PV module can be further classified into controllable and uncontrollable power loss. In a controllable power loss, the effect of heat, partial shading, faulty bypass diode and soiling are manageable. However, uncontrollable power loss due to the presence of snail trails, crack, or micro-crack, potential-induced degradation (PID), light-induced degradation (LID), ageing, decolourisation and hot spot are not manageable (Hussin et al., 2015; Islam et al., 2018; Jumien et al., 2015; Muhammad et al., 2017).

The reliability of the GCPV system is one of the major factors that determine the profitability of PV projects because the performance of the PV system has a huge impact on energy production. Thus, it is essential to evaluate the performance of the GCPV system continuously. Thus, the PV system integrators and owners could minimise the risks and losses over long-term investments. Many stakeholders, especially PV manufacturers, are interested to know their on-site product performance. Degradation of PV modules or systems can occur for many reasons. Most of the power warranty by PV manufacturers is 25-year for mono facial and 30-year for bi-facial double-glass PV modules. Currently, the lack of knowledge sharing, particularly under warm and humid climates related to degradation issues, becomes more pronounced when the owners are interested in their long-term risk investments, particularly in the reliability and longevity of installed systems (Halwachs et al., 2019; Köntges et al., 2017).

According to an extensive review by Phinikarides et al. (2014), the average degradation rate for mono-crystalline was 0.89%/year, poly-crystalline was 0.81%/year, while a-Si, CIGS, CdTe around 1.34%/year, 1.86%/year, 1.70%/year, and other thin-film technologies were found to be 2.24%/year. In the context of degradation rates, several researchers have investigated the outdoor performance of various PV module technologies at different locations under tropical and sub-tropical climates such as Thailand. The overall degradation rate is between 0.5% to 4.9%/ year, and for poly-crystalline (p-Si) is around 0.5% to 1.2%/

year (Limmanee et al., 2017; Limmanee et al., 2016). Such a trend is also reported in many other countries that use crystalline silicon (c-Si) types. For example, in Indonesia, Singapore, Ghana, Algeria and India, the PV degradation rate is equal to 1.6%/year in Indonesia (Kunaifi et al., 2020), 0.8% to 1.0%/year in Singapore (Ye et al., 2014), 1.3%/year in Ghana (Quansah, 2017), 0.76%/year in Algeria (Dahmoun et al., 2021) and 1.33%/year in India (Dubey et al., 2017). However, there is limited published literature on the long-term reliability of PV modules installed in the tropical region. Previous collections in the context of degradation studies in the tropics are primarily based on data collected under four-year, except in Ghana around 19 years.

From a global point of view, the average degradation rate varies from 0.89% to 6%/year, which depends on the types of PV module technology, geographical location and climate. If it exceeds the average value, it needs to be investigated further as it may be related to the uncontrolled power loss. Several case studies related to the uncontrollable power loss used three performance metrics: energy yield, performance ratio, and indoor power, to estimate the annual degradation rates for six types of c-Si PV modules (Ishii & Masuda, 2017). The authors have concluded that a small degradation of the newly PV modules was observed between 0.1%/year and 0.4%/year over three years of operation.

However, poly-crystalline and mono-crystalline declined by 2% due to light-induced degradation (LID) after initial exposure to sunlight. In comparison, the sc-Si heterojunction (SJH) and interdigitated back contact (IBC) sc-Si clearly showed the annual degradation of PR decreased by approximately 1.4% and 0.5%/year. In addition, the authors found that the IBC sc-Si experienced an open-circuit voltage which might cause by potential-induced degradation (PID) symptoms. Other issues were found from field-testing under the Malaysian environment. For example, nine-year-old PV modules using poly-crystalline suffered from PID, where it decreased by 42% due to on-site negative voltage stress and 17% for normal field ageing. Furthermore, all tested PV modules revealed several defects such as cracked propagation accelerating the PID by high voltage stress (Islam et al., 2018). Recently, several researchers used various methods to determine the rate of accuracy and identify the early stage of degradation, which such methods from statistical analysis methods (Malvoni et al., 2020; Phinikarides et al., 2014; Saleheen et al., 2021), commercial software tools (Malvoni et al., 2017; Okello et al., 2015), PV performance metrics or IV characterisation (Dahmoun et al., 2021; Kazem et al., 2020; Roumpakias & Stamatelos, 2019) and other visual or defect issues (Bansal et al., 2021; Lillo-Sánchez et al., 2021).

It is essential to know the sources of power degradation rates to help the PV industry decide on the manufacturing process, investment terms and warranties. Besides that, this can also help the user understand the power degradation factor in the actual situation. Although many existing developed techniques in PV systems are available in the market, most of the methods are highly technical and too complicated for ordinary users. Therefore,

it is essential to develop an analysis of degradation that is understandable by all users. The purpose of this paper is to introduce a new technique for determining the annual degradation of grid-connected photovoltaic (GCPV) systems. As a case study, two grid-connected systems are investigated, operating since 2012 in Malaysia (tropical rainforest climate, Af).

MATERIALS AND METHODS

This case study is based on an earlier model of PV modules installed in 2012 at Green Energy Research (GERC), UiTM Shah Alam, Selangor Darul Ehsan. There are two GCPV systems investigated with different technologies of PV modules installed, namely System A and System B. The electrical data were taken from a dedicated data logger from 2012 to 2017 with logging time at an interval of 5-minute. The characteristics of both systems as tabulated in Table 1.

Table 1

System characteristics of system A and system B

Description	System A	System B
System	Grid-connected	Grid-connected
Nominal Power (kWp)	5.405	10
Mounting	Retrofitted	Retrofitted
PV module technology	Polycrystalline (pc-Si)	Monocrystalline (mc-Si)
Array configuration	1p x 11s/1p x 12s	2p x 20s
Inverter	SB5000TL	STP8000TL

The electrical parameters used are alternating current (AC) power, string voltage, string current, the plane of array solar irradiance and module temperature. One-month data starting from the date of commissioning with one-year gaps are used in this analysis.

The AC power, DC voltage and DC current are normalised to its array capacity rating. Then, the predicted values are calculated using the following Equations 1-3:

$$P_{ac_predict} = P_{array_stc} \times \frac{G}{1000} \times K_{temp} \times K_{age} \times K_c \quad [1]$$

Where $P_{ac_predict}$ is the predicted value for AC power output, P_{array_stc} is PV array capacity, G is plane of array solar irradiance, K_{temp} is a de-rating factor due to temperature, K_{age} is an ageing factor, and K_c is a constant derate factor due to cable loss, inverter, shading, mismatch and soiling. Therefore, from Equation 1, AC power output is very much influenced by solar irradiance. V_{dc} significantly influences the K_{temp} besides small

influence by K_{mm_v} , voltage module mismatch factor as given in Equation 2.

$$V_{dc_predict} = V_{string} \times K_{temp} \times K_{mm_v} \quad [2]$$

In addition, I_{dc} during operating conditions is directly affected mainly by solar irradiance, G despite other factors, namely K_{mm_i} , current module mismatch, temperature, soiling and shading, as illustrated in Equation 3.

$$I_{dc_predict} = I_{mp_stc} \times \frac{G}{1000} \times K_{mm_i} \times K_{temp_i} \times K_{soiling} \times K_{shading} \quad [3]$$

The monitoring standard IEC61724 was referred to calculate the final yield and performance ratio. For final yield, Y_f is defined as the annual, monthly, or daily AC energy output in kWh, E_{ac} of the PV system per installed PV array power, P_o as shown in Equation 4.

$$Y_f = \frac{E_{ac}}{P_o} \quad [4]$$

Performance ratio (PR) is typically used to assess the installation quality of PV systems. The reference yield Y_r is the total amount of in-plane solar irradiation H (kWh/m²), divided by reference irradiance, G_{ref} (1 kW.m⁻²) and can be calculated as equated in Equation 5.

$$PR = \frac{Y_f}{Y_r} \quad [5]$$

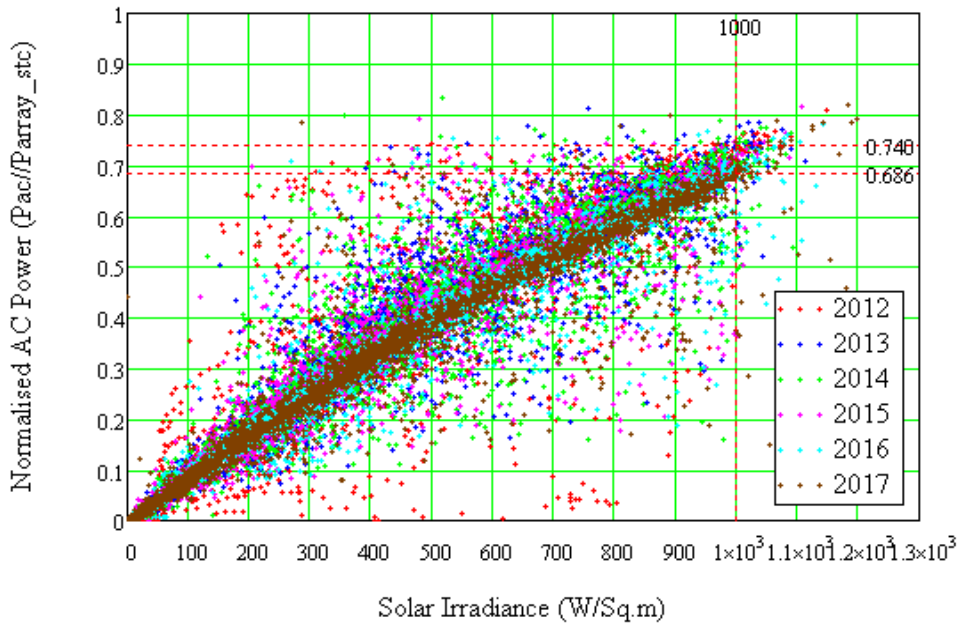
Thus, those five equations are used as a reference in this analysis. This study's selected parameters for degradation investigation are AC power, string voltage, string current, final yield and performance ratio.

RESULTS AND DISCUSSIONS

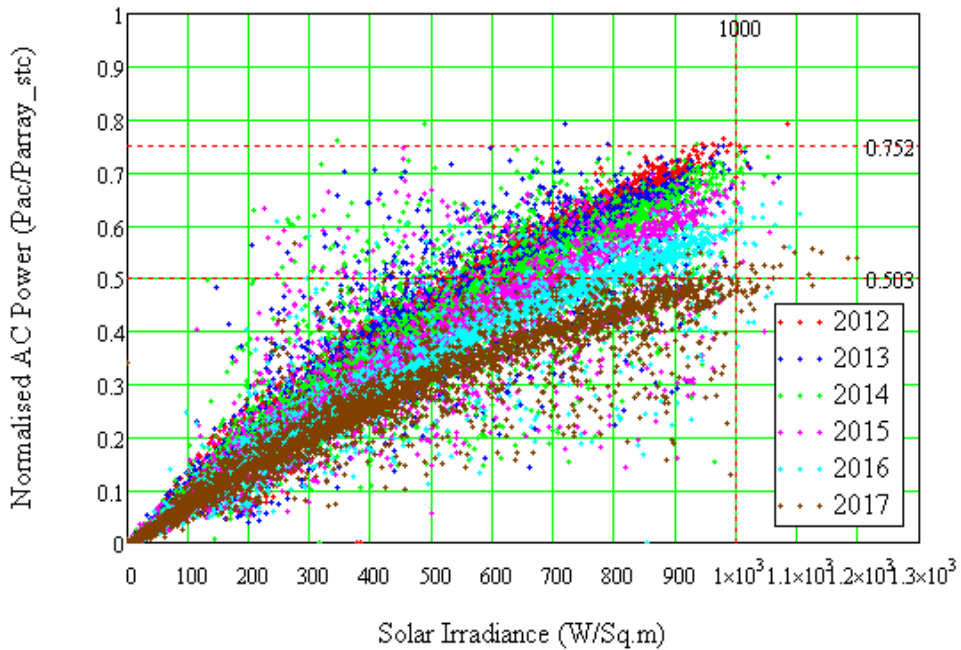
The PV modules are evaluated to address the degradation rate after six years of operation. Finally, the measurement results are presented in this case study.

AC Power Output

For system A, there is no significant degradation of AC power in the second year of operation. However, significant power degradation happened after the fourth year (2015) onwards, as shown in Figure 1(a). After that, the AC power appears to be stabilised at 16.09% in the fifth and the sixth year. However, system B shows continuous degradation of AC power output every year, as shown in Figure 1(b). This trend demonstrates anomaly conditions. It can be seen from Table 2. The AC power is dramatically degraded by 39.35% over six years of operation. For comparative purposes, analysis at solar irradiance 1000 W.m⁻² is used as a reference.



(a)



(b)

Figure 1. Degradation of AC power with solar irradiance (a) System A (b) System B

The amount of AC power output degradation with solar irradiance during six years of operation is tabulated in Figure 1.

Table 2

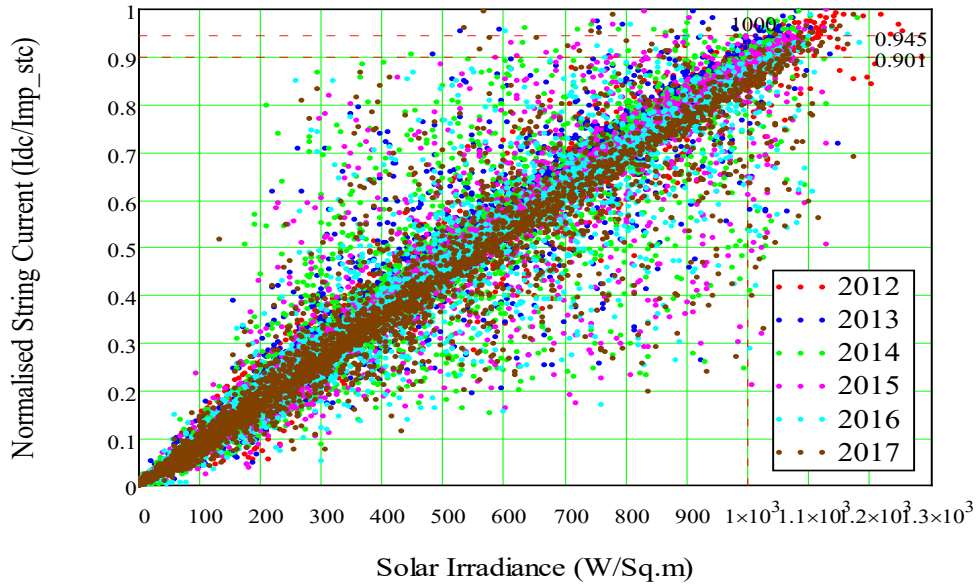
Comparative degradation of AC power

Year	System A	System B
	AC power drop, at G = 1,000 W/m ² (%)	AC power drop at G = 1,000 W/m ² (%)
2012 (1 st year)	0.0	0.0
2013 (2 nd year)	0.0	5.66
2014 (3 rd year)	1.03	8.42
2015 (4 th year)	13.34	19.14
2016 (5 th year)	16.09	28.57
2017 (6 th year)	16.09	39.35

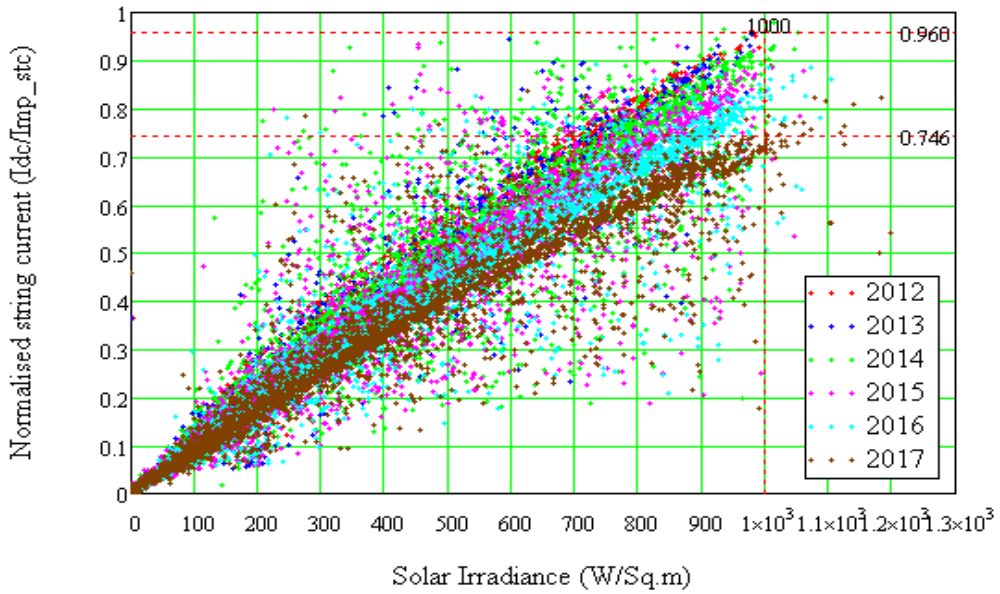
String Current

The degradation of string current with solar irradiance during six years of operation is shown in Figure 2. The degradation of string current for both systems contributes to power loss. The percentage of yearly string current degradation for system A and system B is tabulated in Table 3. For system A, it was found that there was no string current degradation for the first three years. However, after the fourth year, it was degraded by 3.3% to 4.4%, as shown in Figure 2(a). It is possibly due to natural ageing and soiling effect (Jamil et al., 2020).

On the other hand, system B demonstrated distinctive string current degradation, which is doubled every year consecutively until it reached 21.6%, as illustrated in Figure 2(b). It is possibly due to PV module failure, which needs further investigation, besides natural ageing and soil factors. Soil factors influence the penetration of sunlight into the PV module. Less string current can be seen because the PV modules installed in this area suffer from pollution problems such as new factories and construction sites. Thus, the modules need to be cleaned periodically even though both systems are exposed to natural cleaning via rainwater.



(a)



(b)

Figure 2. Degradation of string current with solar irradiance (a) System A (b) System B.

Table 3
Comparative degradation of string current

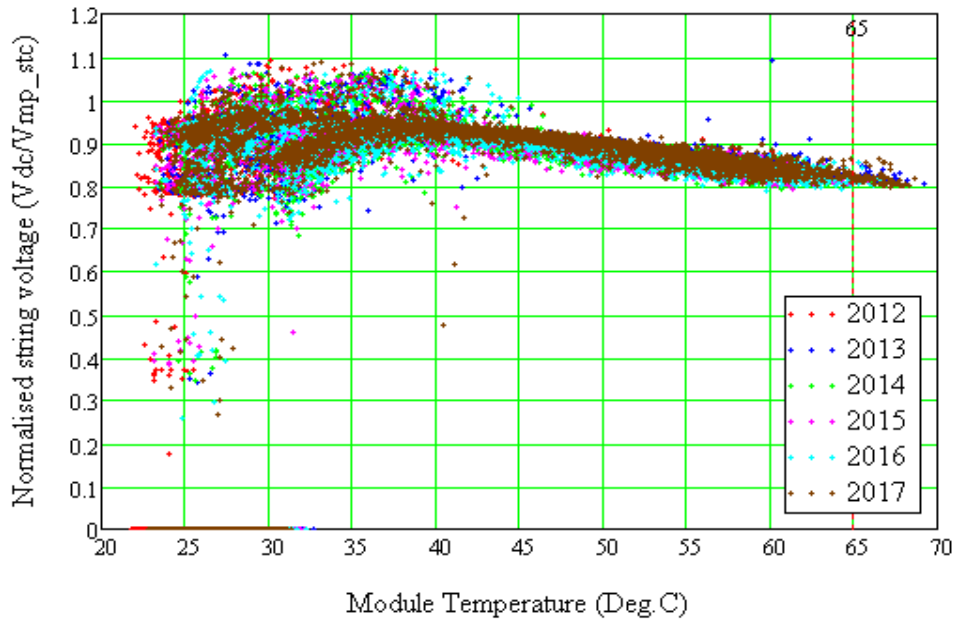
Year	System A	System B
	String current degradation at $G = 1,000 \text{ W/m}^2$ (%)	% String current degradation at $G = 1,000 \text{ W/m}^2$ (%)
2012 (1 st year)	0	0
2013 (2 nd year)	0	0
2014 (3 rd year)	0	3.1
2015 (4 th year)	3.3	7.2
2016 (5 th year)	4.4	13.4
2017 (6 th year)	4.4	21.6

String Voltage

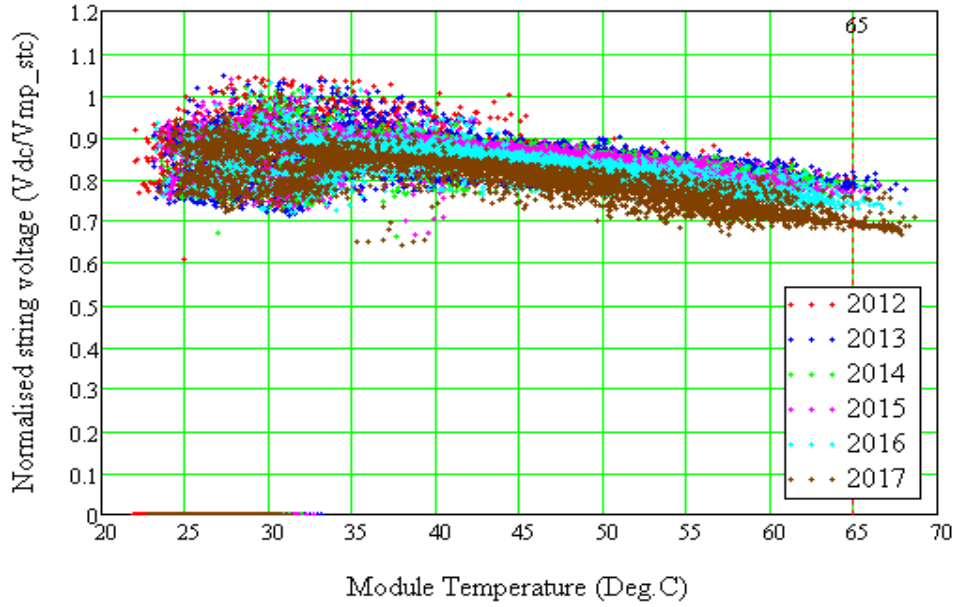
The degradation of string voltage with module temperature during six years of operation is illustrated in Figure 3. From Table 4, system A observed an insignificant drop of string voltage, whereas system B displayed significant degradation of string voltage in the fourth year, which is 13.27%. Thus, the degradation of AC power of system A is not due to string voltage. However, the voltage degradation for system B continued to decline until it reached 16.6% at the end of six years of operation in 2017. It clearly shows that the degradation of AC power of system B contributes to the degradation of string voltage. It is not the symptom of soiling or ageing effect, but possible indications of potential-induced degradation (PID) that occurs when PV modules operate at high voltages, combined with warm and humid weather conditions (Islam et al., 2018). The potential causes of PID are mostly due to a combination of factors from high voltage, high temperature and high humidity. This finding requires further investigation to establish its actual cause.

Table 4
Comparative degradation of string voltage

Year	System A	System B
	String voltage drop, at $T_m = 65^\circ\text{C}$ (%)	String voltage drop, at $T_m = 65^\circ\text{C}$ (%)
2012 (1 st year)	0.0	0.0
2013 (2 nd year)	0.0	0.0
2014 (3 rd year)	0.0	0.0
2015 (4 th year)	0.0	13.27
2016 (5 th year)	0.0	14.04
2017 (6 th year)	0.0	16.16



(a)

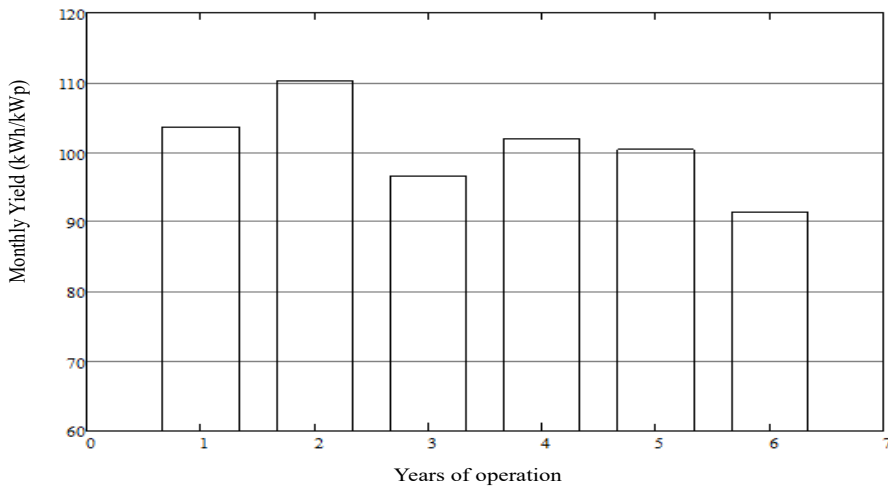


(b)

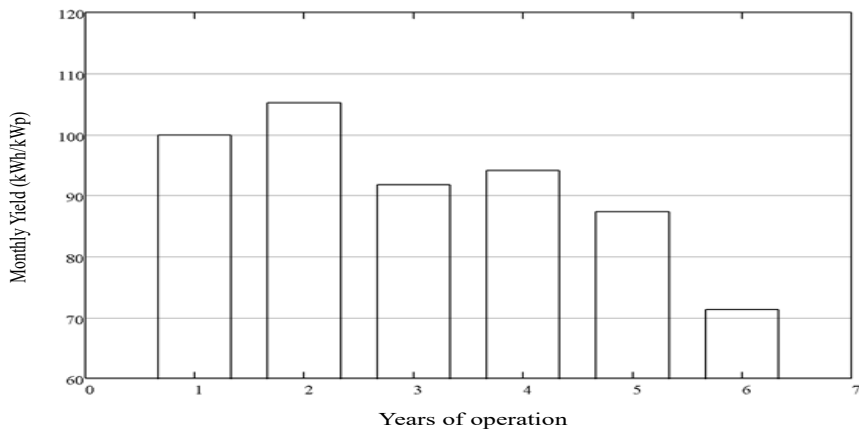
Figure 3. Degradation of string voltage with module temperature (a) System A (b) System B

Final Yield

The monthly final yield $Y_{f,m}$ for both systems during six years of operation is shown in Figure 4. The bar graph shows system A's average final yield is more than 100 kWh/kWp (benchmark Y_f used for Malaysia GCPV system [SEDA, 2016]) over its six years of operation. Thus, their excellent performance can be observed even though system A exhibits a fluctuation in yield generation. Meanwhile, system B keeps on dropping after the second year, where the overall final yield is less than 100 kWh/kWp during the monitoring period.



(a)

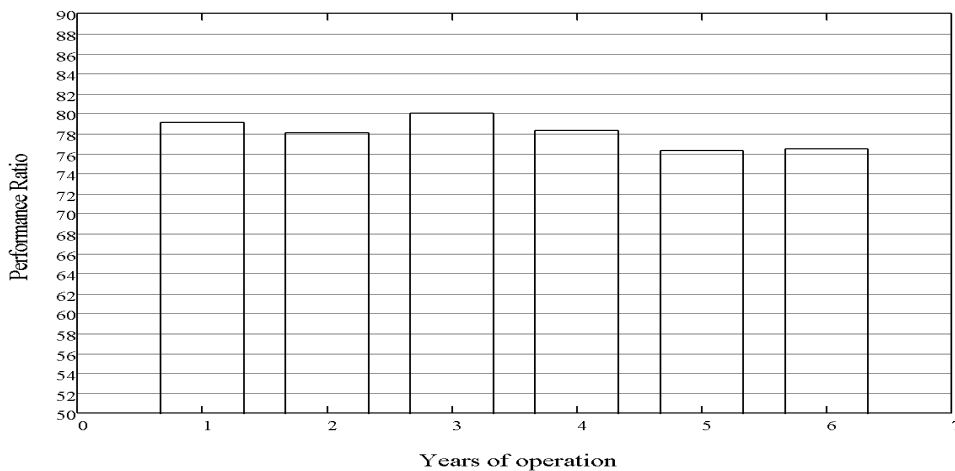


(b)

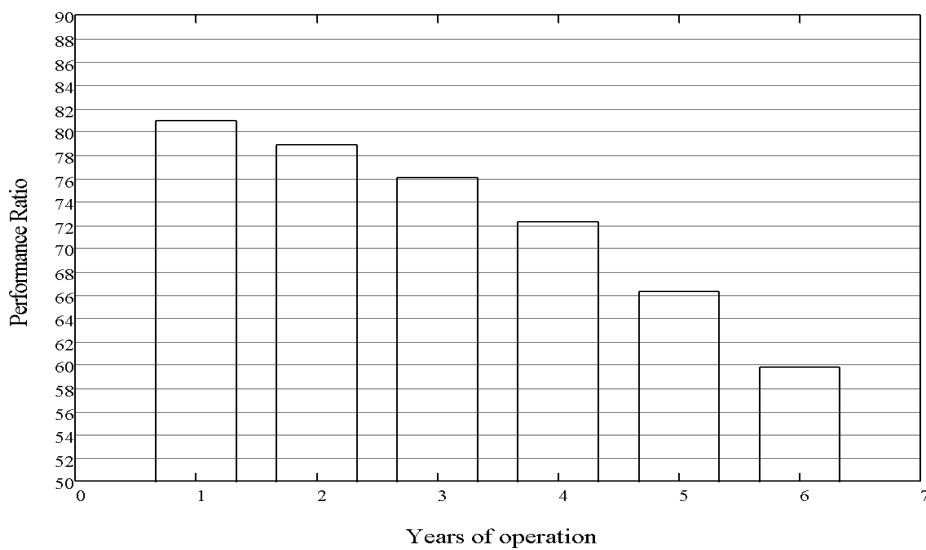
Figure 4. Final Yield (a) System A (b) System B

Performance Ratio

The degradation of Performance Ratio (PR) during six years of operation is as depicted in Figure 5. The results revealed that the performance ratio achieved by system A for six years of operation is consistently more than 75%, which is the benchmark for an accepted healthy GCPV system for Malaysia as stated in MS 2692:2020 (Department of Standards Malaysia, 2020). Meanwhile, system B shows a continuous declining trend of PR from the beginning of the operation.



(a)



(b)

Figure 5. Performance ratio (a) System A (b) System B

CONCLUSION

Both PV module technologies for two grid-connected PV systems under the same microclimate were monitored for over six years of operation, and performance parameters related to degradation factors were studied. Furthermore, both system performances were compared using selected parameters. From these findings, it could be concluded that system A works satisfactorily during the monitored period, while system B shows anomaly behaviour, mainly on the string voltage and marginal on the string current and other performance indices. Therefore, it is possible indications of potential-induced degradation (PID) that mostly occurs in a crystalline type of PV module technology.

The anomaly detection analysis for the GCPV system has been successfully demonstrated where the developed technique via string current and string voltage could be applied to any PV cell technology and PV system capacity. Furthermore, this technique could be used to rectify and identify the health of the GCPV system which required further detailed clarification.

ACKNOWLEDGEMENTS

The authors gratefully acknowledge the support of the Management of Universiti Teknologi MARA (UiTM) and are financially funded by the Malaysia Ministry of Education [600-RMI/FRGS 5/3 (083/2019) grant. Also, thanks to the Green Energy Research Centre (GERC) for providing facilities and data in this research.

REFERENCES

- Bansal, N., Pany, P., & Singh, G. (2021). Visual degradation and performance evaluation of utility scale solar photovoltaic power plant in hot and dry climate in western India. *Case Studies in Thermal Engineering*, 26, Article 101010. <https://doi.org/https://doi.org/10.1016/j.csite.2021.101010>
- Dahmoun, M. E. H., Bekkouche, B., Sudhakar, K., Guezgouz, M., Chenafi, A., & Chaouch, A. (2021). Performance evaluation and analysis of grid-tied large scale PV plant in Algeria. *Energy for Sustainable Development*, 61, 181-195. <https://doi.org/https://doi.org/10.1016/j.esd.2021.02.004>
- Department of Standards Malaysia. (2020). MS 2692:2020 Testing and commissioning of grid-connected photovoltaic system (GCPV). In *Malaysian Standard* (pp. 1-61). Department of Standards Malaysia.
- Dubey, R., Chattopadhyay, S., Kuthanazhi, V., Kottantharayil, A., Solanki, C. S., Arora, B. M., Narasimhan, K. L., Vasi, J., Bora, B., Singh, Y. K., & Sastry, O. S. (2017). Comprehensive study of performance degradation of field-mounted photovoltaic modules in India. *Energy Science & Engineering*, 5(1), 51-64. <https://doi.org/10.1002/ese3.150>
- Fouad, M. M., Shihata, L. A., & Morgan, E. I. (2017). An integrated review of factors influencing the performance of photovoltaic panels. *Renewable and Sustainable Energy Reviews*, 80, 1499-1511. <https://doi.org/https://doi.org/10.1016/j.rser.2017.05.141>

- Halwachs, M., Neumaier, L., Vollert, N., Maul, L., Dimitriadis, S., Voronko, Y., Eder, G. C., Omazic, A., Mühleisen, W., Hirschl, C., Schwark, M., Berger, K. A., & Ebner, R. (2019). Statistical evaluation of PV system performance and failure data among different climate zones. *Renewable Energy*, *139*, 1040-1060. <https://doi.org/https://doi.org/10.1016/j.renene.2019.02.135>
- Husain, A., Phesal, M., Kadir, Z., & Amirulddin, U. A. U. (2020). Short review on recent solar PV policies in Malaysia. *E3S Web of Conferences*, *191*, Article 01002. <https://doi.org/10.1051/e3sconf/202019101002>
- Hussin, M. Z., Hasliza, N., Yaacob, A., Zain, Z. M., Omar, A. M., & Shaari, S. (2012). A development and challenges of grid-connected photovoltaic system in Malaysia. In *2012 IEEE Control and System Graduate Research Colloquium* (pp. 191-196). IEEE Publishing. <https://doi.org/10.1109/ICSGRC.2012.6287160>
- Hussin, M. Z., Shaari, S., Omar, A. M., & Zain, Z. M. (2015). Amorphous silicon thin-film: Behaviour of light-induced degradation. *Renewable and Sustainable Energy Reviews*, *43*, 388-402. <https://doi.org/https://doi.org/10.1016/j.rser.2014.10.093>
- Ishii, T., & Masuda, A. (2017). Annual degradation rates of recent crystalline silicon photovoltaic modules. *Progress in Photovoltaics: Research and Applications*, *25*(12), 953-967. <https://doi.org/https://doi.org/10.1002/pip.2903>
- Islam, M. A., Hasanuzzaman, M., & Rahim, N. A. (2018). Investigation of the potential induced degradation of on-site aged polycrystalline PV modules operating in Malaysia. *Measurement*, *119*, 283-294. <https://doi.org/https://doi.org/10.1016/j.measurement.2018.01.061>
- Jamil, W. J., Rahman, H. A., Shaari, S., & Desa, M. K. M. (2020). Modeling of soiling derating factor in determining photovoltaic outputs. *IEEE Journal of Photovoltaics*, *10*(5), 1417-1423. <https://doi.org/10.1109/JPHOTOV.2020.3003815>
- Jumien, N. A., Hussin, M. Z., Omar, A. M., & Zulkapli, M. F. (2015). Performance of a 2.8 kWp monocrystalline free-standing grid-connected photovoltaic system at SIRIM berhad. In *2015 IEEE 6th Control and System Graduate Research Colloquium (ICSGRC)* (pp. 93-97). IEEE Publishing. <https://doi.org/10.1109/ICSGRC.2015.7412471>
- Kazem, H. A., Chaichan, M. T., Al-Waeli, A. H. A., & Sopian, K. (2020). Evaluation of aging and performance of grid-connected photovoltaic system northern Oman: Seven years' experimental study. *Solar Energy*, *207*, 1247-1258. <https://doi.org/https://doi.org/10.1016/j.solener.2020.07.061>
- Köntges, M., Oreski, G., Jahn, U., Herz, M., Hacke, P., Weiss, K. A., Razongles, G., Paggi, M., Parlevliet, D., & Tanahashi, T. (2017). *Assessment of photovoltaic module failures in the field*. International Energy Agency.
- Kunaifi, K., Reinders, A., Lindig, S., Jaeger, M., & Moser, D. (2020). Operational performance and degradation of PV systems consisting of six technologies in three climates. *Applied Sciences*, *10*(16), Article 5412.
- Lillo-Sánchez, L., López-Lara, G., Vera-Medina, J., Pérez-Aparicio, E., & Lillo-Bravo, I. (2021). Degradation analysis of photovoltaic modules after operating for 22 years. A case study with comparisons. *Solar Energy*, *222*, 84-94. <https://doi.org/https://doi.org/10.1016/j.solener.2021.04.026>
- Limmanee, A., Songtraai, S., Udomdachanut, N., Kaewniyompanit, S., Sato, Y., Nakaishi, M., Kittisontirak, S., Sriprapha, K., & Sakamoto, Y. (2017). Degradation analysis of photovoltaic modules under tropical climatic conditions and its impacts on LCOE. *Renewable Energy*, *102*, 199-204. <https://doi.org/https://doi.org/10.1016/j.renene.2016.10.052>

- Limmanee, A., Udomdachanut, N., Songtrai, S., Kaewnuyompanit, S., Sato, Y., Nakaishi, M., Kittisontirak, S., Sriprapha, K., & Sakamoto, Y. (2016). Field performance and degradation rates of different types of photovoltaic modules: A case study in Thailand. *Renewable Energy*, *89*, 12-17. <https://doi.org/https://doi.org/10.1016/j.renene.2015.11.088>
- Malvoni, M., Kumar, N. M., Chopra, S. S., & Hatziargyriou, N. (2020). Performance and degradation assessment of large-scale grid-connected solar photovoltaic power plant in tropical semi-arid environment of India. *Solar Energy*, *203*, 101-113. <https://doi.org/https://doi.org/10.1016/j.solener.2020.04.011>
- Malvoni, M., Leggieri, A., Maggioletto, G., Congedo, P. M., & De Giorgi, M. G. (2017). Long term performance, losses and efficiency analysis of a 960kWp photovoltaic system in the Mediterranean climate. *Energy Conversion and Management*, *145*, 169-181. <https://doi.org/https://doi.org/10.1016/j.enconman.2017.04.075>
- Muhammad, N., Zakaria, N., Shaari, S., & Omar, A. (2017). System performance and detectable faults of a 10-year old 1.1 kWp GCPV system in Malaysia. *Science Letters*, *11*(1), 10-17.
- Okello, D., van Dyk, E. E., & Vorster, F. J. (2015). Analysis of measured and simulated performance data of a 3.2kWp grid-connected PV system in Port Elizabeth, South Africa. *Energy Conversion and Management*, *100*, 10-15. <https://doi.org/https://doi.org/10.1016/j.enconman.2015.04.064>
- Phinikarides, A., Kindyni, N., Makrides, G., & Georghiou, G. E. (2014). Review of photovoltaic degradation rate methodologies. *Renewable and Sustainable Energy Reviews*, *40*, 143-152. <https://doi.org/https://doi.org/10.1016/j.rser.2014.07.155>
- Quansah, D. (2017). Reliability and degradation of solar PV modules - Case study of 19-year-old polycrystalline modules in Ghana. *Technologies*, *5*(2), Article 22. <https://doi.org/10.3390/technologies5020022>
- Roumpakias, E., & Stamatelos, A. (2019). Performance analysis of a grid-connected photovoltaic park after 6 years of operation. *Renewable Energy*, *141*, 368-378. <https://doi.org/https://doi.org/10.1016/j.renene.2019.04.014>
- Saleheen, M. Z., Salema, A. A., Islam, S. M. M., Sarimuthu, C. R., & Hasan, M. Z. (2021). A target-oriented performance assessment and model development of a grid-connected solar PV (GCPV) system for a commercial building in Malaysia. *Renewable Energy*, *171*, 371-382. <https://doi.org/https://doi.org/10.1016/j.renene.2021.02.108>
- SEDA. (2016). *SEDA Malaysia grid-connected photovoltaic (PV) systems design course* (2nd Ed.). Sustainable Energy Development Authority (SEDA) Malaysia.
- Vaka, M., Walvekar, R., Rasheed, A. K., & Khalid, M. (2020). A review on Malaysia's solar energy pathway towards carbon-neutral Malaysia beyond Covid'19 pandemic. *Journal of cleaner production*, *273*, 122834-122834. <https://doi.org/10.1016/j.jclepro.2020.122834>
- Velautham, S., Chen, W. N., & Han, T. W. (2019). *National survey report of PV power applications in Malaysia-2019* (National Survey Reports). IEA-PVPS.
- Yatim, Y., Hussin, F., Idris, M., Rahim, A., Baharudin, A., Mansur, T., & Alhassan, S. (2014). Economical analysis of grid-connected BiPV at UNIMAP building in Kuala Perlis, Malaysia. *International Journal of Renewable Energy Resources*, *4*(2), 42-45.

- Yatim, Y., Yahya, M. W., Tajuddin, M. F. N., Ismail, B., & Sulaiman, S. I. (2017). Tecno-economic analysis of PV module selection for residential BIPV with net metering implementation in Malaysia. In *2017 IEEE 15th Student Conference on Research and Development (SCORED)* (pp. 361-365). IEEE Publishing. <https://doi.org/10.1109/SCORED.2017.8305364>
- Ye, J. Y., Reindl, T., Aberle, A. G., & Walsh, T. M. (2014). Performance degradation of various PV module technologies in tropical Singapore. *IEEE Journal of Photovoltaics*, *4*(5), 1288-1294. <https://doi.org/10.1109/JPHOTOV.2014.2338051>



Serious Game Conceptual Model of Brain-Based Learning for Halus Student

Saffa Raihan Zainal Abidin, Siti Fadzilah Mat Noor* and Noraidah Sahari@Ashaari

Faculty of Information Science & Technology, Universiti Kebangsaan Malaysia, 43600 UKM, Bangi, Selangor, Malaysia

ABSTRACT

Malaysian society, including students who use technology in their daily lives, have made technology a necessity. Among the media technologies that have a place in students' hearts are serious games, convey information, emphasizing learning and not entertainment. A serious game is capable of creating self-directed active learning. In this study, the authors analyzed the key features of serious games that encourage learning in an academic environment. However, not many software specializes in problems for slow-reading students. This study aims to establish the elements used in in-game application software and the approaches and strategies used to develop a serious game design conceptual model for such students based on the acquired elements. The elements were obtained through two methods, i.e., systematic literature review and preliminary studies. This work identifies 48 potential studies in 2009-2020, using various well-known digital libraries. The analysis

of the selected documents applying the inclusion criteria resulted in 12 articles used to design serious games. This study integrates brain-based learning strategies into game and learning components. This serious game conceptual model expects to provide a meaningful learning experience for those children who are left behind to achieve their learning goals and increase their motivation to stay excited in learning.

Keywords: Brain-based learning, serious game, slow reader student

ARTICLE INFO

Article history:

Received: 19 June 2021

Accepted: 24 August 2021

Published: 28 October 2021

DOI: <https://doi.org/10.47836/pjst.29.4.49>

E-mail addresses:

saffaraihan@siswa.ukm.edu.my (Saffa Raihan Zainal Abidin)

fadzilah@ukm.edu.my (Siti Fadzilah Mat Noor)

nsa@ukm.edu.my (Noraidah Sahari@Ashaari)

*Corresponding author

INTRODUCTION

The technological integrations that have gotten teachers and students are serious games readily available at affordable prices. In a survey of online gaming by Rakuten Insight in March 2020, 73 percent of Malaysian respondents aged between 16 and 24 stated that they played online games (Hirschmann, 2020). The same survey found that a large portion of Malaysian gamers played games daily. Students born in the next generation or Gen Z (born between 1998 and the present) are modern students who grew up in digital times. However, the game to consider is that involving pedagogy, which is a serious game. Abidin et al. (2019) state that a serious game can refer to the game's purpose in imparting a message, whether in education or training. Serious games can help students learn flexibly regardless of time and place and reduce dependency on teachers. According to Auzar (2012), the process of T&L through a serious game is active learning because it promotes the active involvement of students through two-way interaction with software without relying entirely on teachers.

Abidin et al. (2019) state that designing games for children are challenging because they differ from adults in characteristics, and it is essential to understand their needs. Much software in the market are designed specifically for students with learning problems, and the rest are for children with normal learning abilities. These children need more consideration and the intervention of technology and aiding tools to enhance their learning to be equivalent to other normal children (Stanberry & Raskind, 2019). Past studies show that much software in the market proposes different design techniques and methods to help children with learning difficulties, especially reading literacy. Literacy was defined as the ability to read, write and use, simple and complex sentences and apply that knowledge in daily learning and communication (KPM, 2015). In this study, slow learner refers to students with low cognitive ability but not in the special needs' category called Halus students. In addition to the contents, the strategies used are also important to ensure the software's success. A strategy is an organized plan to achieve goals or success. In this serious game, the Brain-Based Learning (BBL) strategy is an appropriate strategy to be applied in the teaching medium to help students optimize their brain usage and enhance student attention in learning.

The use of BBL strategies can optimize the use of the left and right brain and activate the neuron cells of the user's brain. Halus students can have the same level of thinking as regular students if the strategies and methods used can stimulate their brains. This strategy applied to Halus students aims to achieve the three lowest levels in the low and medium levels of thinking of Anderson's Taxonomy, namely application, understanding and remembering. Past studies have found that conventional learning is considered more attractive if it incorporates appropriate technological elements. However, most of these serious games are not designed and tailored to users' needs (Ng et al., 2015), especially

for a slow learner. Serious games that have been used also do not have elements suitable for Halus students, such as less attractive, boring storylines and unattractive graphics. If the software is not optimized for its learning usage, it is deemed ineffective even though the content is excellent and appropriate. This strategy is chosen because the colour, shape, texture, sound, gameplay elements, and pedagogy can stimulate the entire left and right brain. The development of brain studies has introduced 12 principles of BBL via three instructional techniques associated with these principles (Caine & Caine, 1991). The BBL strategy Hileman (2006), which is B.R.A.I.N.B.A.S.E.D, into serious games, is seen to be helping students keep their attention in learning and improving their motivation. To outline this paper, we start with an introduction, background literature, methodology, model design, discussion and conclusion.

BACKGROUND LITERATURE

This section discusses the literature studies related to students left behind in learning or low cognitive students known as Halus students, serious game technology used, and brain-based learning (BBL) approach.

Halus Students (Slow Reading Students)

Reading is an essential skill, which helps students succeeding in their learning. Mastery in reading skills dramatically impacts students' daily performance, including examinations (Jamian, 2011). Conversely, students who are not interested and weak in learning are because of their incompetence in mastering reading and writing skills (Jamian, 2011). Thus, Halus students are one of the most challenging learning issues to overcome. In this study, Halus focuses on children who are not in the special learning category but the regular student category. Their cognitive ability might be slightly different from normal students, and they struggle to meet academic demands (Abidin et al., 2017). According to Chauhan (2011), Halus students need help to expedite their learning because they have limited capabilities involving symbols and abstracts such as languages, numbers and concepts.

Serious Game

The serious game has proven to motivate students and improve their learning performance effectively and interestingly (Masrop et al., 2015). Students prefer something enjoyable while learning, allowing them to play simultaneously (Su et al., 2016). Any game designed solely for consumer entertainment is not a serious game (Møller & Hansen, 2016). Serious games show great potential in stimulating the cognitive abilities of all ages, including children (Zaki et al., 2015).

However, a serious game designed has to have fine-tuned pedagogy (Bellotti et al., 2010). Among the critical issues in the game involving pedagogy is an insufficient

combination of educational and game design principles. The game mechanics that are not appropriate for certain target users causes the game's objective to fail. Besides, the use of games is proven to increase motivation, but students are likely to be passive in-class activities and performed badly on writing assignments (Domínguez et al., 2013). Thus, game elements have different positive effects on a gameplay concept, and the effectiveness of each of these elements needs to be reviewed to suit the user for a positive impact.

Many previous studies have discussed the positive aspects of using digital game software in learning which is: i) Improve cognitive and motor skills and help improve ICT skills (Peirce, 2013), ii) Learning is more effective (Martin & Shen, 2014); iii) Increase the focus of attention among students with short-term convergence problems (Boyler, 2010) and exacta.

Brain-based Learning

In addition to games and pedagogy for Halus students, the approaches used need to be considered when designing the game model in-game designs. Thus, the BBL approach is a good technique that motivates teachers to plan a teaching strategy to boost motivation and student performance.

As long as the brain is not restricted from fulfilling the normal processes, learning will take effect. BBL approach is based on the structure and function of the brain. BBLs can be applied in the T&L process by considering Halus student's needs and learning styles to assess and improve gaming software's delivery content (Binulal & Aravind, 2013). BBLs involve knowledge and teaching about the function and regulation of the brain for meaningful learning. Generally, all learning is brain-based, but BBL is a technique that considers the brain's optimal function compared to the traditional method (Caine & Caine, 1991). Optimal brain usage uses the entire brain by involving as many senses as possible simultaneously. In this BBL, students are fully engaged, in which the learning patterns are changed from relaxed to active learning patterns so that every part of the brain can play an optimal role (Mandar, 2011).

Caine and Caine (1991) have also issued 12 BBL principles to determine and select appropriate strategies and methodologies. According to Fazil and Saleh (2016), understanding the student's concept on the topic is emphasized based on a brain-based teaching strategy. Expose students to seven phases of BBL: activation, explaining the learning outcomes and learning process involved, creating relevance, carry out learning activities, demonstrating student understanding, reassess students' memory/make a conclusion, and preview new topics that have made them more focused and also give them more opportunities to engage throughout the learning process actively. This exposure has directly contributed to the optimum conditions for students learning.

Fazil and Saleh (2016) state, the BBL approach highlights the relevance between new information and students' prior knowledge to make students more aware of the T&L process. Through gameplay, inputs are given in various visual, audio and kinaesthetic forms to allow students to create relevance between the information obtained to build the desired meaning. This BBL can improve the comprehension and achievement of students in learning (Bawaneh et al., 2012). Based on Saleh and Halim (2016), BBL that focuses on overall brain function can self-potential and student achievement when brain function is used optimally with the help of the teacher's teaching method.

Based on BBL, can use principle strategies in T&L to encourage student engagement in the classroom and increase their motivation. According to Hileman (2006), if students are not motivated, they would not want to learn voluntarily, and meaningful learning will not happen. Meaning is when can link new knowledge to previous knowledge. This is supported by the study of Bawaneh et al. (2010) and She (2012), stating the meaningful learning can make learning more effective and be remembered longer. Furthermore, a study by Bawaneh et al. (2010) and She (2012) stated that the BBL method could speed up thinking, planning and execution processes that enhance the conceptual understanding and motivations to continue learning. Therefore, integrating the BBL strategy in a serious game is expected to improve Halus students' literacy skills by maintaining their attention and boosting their motivation to continue learning.

METHODOLOGY

This study used two methods; i) Systematic Literature Review (SLR), which is adapted from Ng et al. (2015), and ii) Preliminary studies to strengthen the findings of the study that involving questionnaires and observation that are conducted at two schools.

This study performed a targeted search of relevant studies to answer the research questions. Articles related to relevant elements in games, pedagogy and practical brain-based learning to build a model for the slow learner in literacy are gathered and studied extensively. The proposed SLR method has four phases. First, this method is intended to view existing studies specifically for slow reader children in Malaysia and looking for suitable components and elements in model design. After identifying the appropriate element, a preliminary study was conducted to strengthen the literature's initial findings.

A preliminary study has four phases comprising a questionnaire and observation: Phase 1 identifies the purpose of the study. Phase 2 examines past studies to find support and build a questionnaire instrument through journal readings. Phase 3 is the method used in the preliminary study (questionnaire with teachers and class observation). Finally, Phase 4 analyzes data to form a serious game model.

Systematic Literature Review

Four steps in the systematic literature review are discussed.

Identifying and Downloading Related Articles. The objective of the literature review was identified so that the related articles downloaded are a match. The selection of articles uses two methods. The first method, an initial selection, screened selected the articles from years 2009-2020. Then, implemented the search strategy based on four aspects: (a) serious games, (b) computer application, (c) educational games, (d) and (d) computer games relating to (“design” OR “methodology” OR “frameworks” OR “model”). To refine the selection of the works, applied the inclusion and exclusion criteria, a general review of each article’s title and abstract and conclusions are considered (Table 1).

Table 1

Selection Criteria

Selection Criteria	Exclusion Criteria
Papers that detail methodologies, models, frameworks and design of serious games.	Articles published on the company and websites.
Approaches that detail phases, stages or processes of development of serious games.	Articles that mention serious game design but do not define their details of the development.
Game-based learning	Computer applications such as simulation, voice recognition and augmented.
Articles relevant to the research questions.	Thesis, books, posters, and publishers
Focusing on the researcher in Malaysia especially, in Malay	Foreign Language

Electronic databases were used, including areas associated with education and Computing, Engineering and Technology, and Psychology. They were identified as sources of information: journals, conferences, and proceedings. The databases reviewed were: Science Direct Elsevier, IEEE eXplorer Digital Library, Springer, ACM Digital Library, Taylor & Francis, Proquest, and Google Scholar used for downloading articles. The downloaded articles were then managed and organized using the Mendeley program to more manageable references. Selected papers were written in Malay and English and focused only on researches in Malaysia. According to Bandara et al. (2011), the method used is the ‘primary’ articles focusing specifically on the title.

The second method, known as ‘secondary’ source as the search needed to be wider rather than look at the title. Usually, the article title does not mention the domain, but the contents are related. The search was done quickly, reading abstract and content before focusing on the critical content. Table 2 shows the downloaded articles; twelve studies belonging to a learning software application for slow-reading children, including specific

learning problems, have been identified. All downloaded software was specific for the Malay language because it conformed to Malaysia’s students’ patterns and cultures.

Analyzing Related Articles. The analysis started to look at the criteria and specifications of the articles. Target users were focused on children with difficulty in language literacy, either normal children or those with learning problems such as Down syndrome and dyslexia, to see additional elements or approaches used to suit the user. Bandara et al. (2011) state, the critical aspects observed during the analysis of literature studies include definitions, objectives, characteristics, historical analysis, success factors, failure/problem factors, research methods, theory, further studies, and contents.

Evaluating the Quality of A Study. For example, a study that was not documented in detail was not chosen, and the articles selected are from a reliable database to ensure the quality of a study. The chosen articles then were analyzed during the preliminary study.

Making Conclusions and Discussions. The elements obtained are listed in Table 2. In addition, Table 2 shows previous studies in developing technology for computer application, specifically in the mastery of reading skills for children with learning disabilities.

The researcher categorized the serious game component into three main parts from Table 2: game, learning, and BBL strategy. The selected game components consist of game objectives, storyline, avatars, emotions, feedback, interactivity, rules and challenges. The learning component consists of learning objectives, theory, content design, content structure design, serious game technology, teaching media, and BBL strategies. The BRAINBASED strategy by Hileman (2006) is applied into the serious game for the BBL strategy. All of these components will then be seen to suit the Halus students in the preliminary study conducted.

Table 2
Literature review of computer application in literacy for Halus students

Authors	Software Name/ Details	Details	Elements
Azid et al. (2020)	Evaluating User Experience of Using <i>Cerdik BM Series 1</i> Interactive Pedagogical Tool	1. The results conclude that <i>Cerdik BM</i> 's development based on the 4-D development study process enabled researchers to develop an interactive pedagogical tool that could stimulate students' thinking abilities, language skills, motivation and trust in the LINUS programmed.	1. Multiple Intelligences 2. Verbal Linguistics 3. Mathematical Logic 4. Kinesthetic 5. Music 6. Interpersonal 7. Intrapersonal 8. Naturalist

Table 2 (Continued)

Authors	Software Name/Details	Details	Elements
Ahmad et al. (2017)	Voice Recognition to overcome reading difficulties	1. This article suggested a process diagram that uses data from a learning portfolio and simultaneously considers the degree of difficulty in relational reading during the diagnostic test.	1. Voice recognition
Miswan and Adnan (2015)	Pembangunan Aplikasi Peranti Mudah Alih untuk Kemahiran Membaca Kanak-Kanak: Aplikasi Literasi LINUS (LiLIN)	1. The core features of the LiLIN framework include learning syllables and word spelling in immersive digital and multi-touch ways-responding to correct or incorrect answers automatically, incorporating audio spelling for alphabets and syllables, spelling and writing activities, and the engaged and collaborative learning game-like approach.	1. Pedagogy -Repetition -Conceptualization -Themed presentation -Coaching training -Closing 2. Content -LINUS teaching module unit 1 and 2 3. Technology -IOS system -Multi-touch -Multimedia -Interactive
Ng et al. (2016)	Perisian Pembelajaran bagi bahasa Melayu	1. The purpose of the study is to see the effectiveness of persuasive designs implemented in software for children with learning disabilities focused on the subject of Bahasa Melayu.	1. Goal-objective 2. Brain's Time Clock-Each exercise does not exceed 10 minutes 3. Lesson Content-Malaysian Ministry's syllabus 4. Game Mechanic-score 5. Reward 6. Emotion 7. Feedback

Table 2 (Continued)

Authors	Software Name/ Details	Details	Elements
Sidek et al. (2014)	Perisian ‘Saya Suka Belajar’	1. The software's objective is to enable students to build and read open/ closed syllabus, build words out of letters/syllables, select, match and copy syllables into meaningful words, read words constructed from syllables, spell and sound, and write simple syllables.	1. Text–minimal, understandable, simple and in the form of instructions 2. Graphic (image)– Caricature image, colourful, attractive graphic with colours usage. 3. Animation–attract students to focus 4. Navigation–consistent, simple and easy. 5. User Friendly–exciting and cheerful. 6. Focus– Content of the lesson related to everyday life.
Ahmad et al. (2013)	MyLINUS	1. Develop software for students under the LINUS program to overcome the difficulty of reading.	1. Goal–objective 2. Content–curriculum 3. Repetition 4. Colourful image 5. Recall 6. Storyline 7. Rule 8. Challenge 9. Active learning
Ramli and Zaman (2011)	Perisian AR BACA SindD	1. Multimedia software is explicitly designed for children with Down syndrome. 2. The Augmented Reality (AR) technique has been used in this software.	Goal–objective Immersive Feedback
Yusuf and Shima (2012)	MEL-SindD	1. Develop software for Down Syndrome children to learn Malay. This software applies scaffolding and multimedia techniques.	1. Goal– Objective 2. Game mechanic 3. Motivation 4. Emotion 5. Active learning 7. Multimedia elements 8. Feedback

Table 2 (Continued)

Authors	Software Name/ Details	Details	Elements
Amian (2012)	Multimedia Interaktif	1. Findings show that interactive multimedia improves reading skills' performance helps create an active learning environment, and is an effective teaching aid for teachers and students.	Combines various multimedia elements
Othman and Pakar (2011)	Interactive Storytelling Software Application	1. The t-test analysis findings show a significant difference in reading comprehension performance between middle-achieving students who follow the reading comprehension using computer applications interactively with medium-achieving students who follow the teaching using traditional methods in post-test.	1. Interactive 2. Colourful
Mahidin et al. (2011)	E-Z Disleksia	1. This software is devoted to Dyslexia children who have difficulty reading and learning Malay.	Goal–Objective Content–pedagogy and curriculum Interactive Colours–

Preliminary Study

A preliminary study involving questionnaire and observation methods was used to validate the elements obtained in the literature review and find suitable elements that suit Halus students. This preliminary study involved 4 phases.

Phase 1. The researcher identifies the preliminary study's objective by looking at the problems of conventional methods by teachers, game elements, pedagogy and brain-based learning appropriate for the serious game model based on literature.

Phase 2. Find support evidence for the findings by review related to previous studies. From the readings, one questionnaire instrument was produced by adaptations from several related journals.

Phase 3. Observations of LINUS and Pemulihan students and questionnaire methods with the teachers were done to collect the data.

Observation: The method was carried in two different schools and was made in classrooms to see and understand the T&L process conditions for Halus students. Driscoll (2011) states that two common ways to observe people are participant observation and unobtrusive observation. For this study, the researcher chooses unobtrusive observation. The researcher

does not interact with participants but rather record their behavior. Due to the Halus students inability to read and understand the questions well, this method is seen as the best method. Once the primary research data has been collected, the researcher will analyze the results.

The purpose of analyzing data is to look at what had been collected and create a cohesive, systematic interpretation to examine the validity of the elements. The observations were recorded in the form of a double-entry notebook and visual recording in the class. Before the class session started, the researcher wrote thick descriptions of what will observe, including descriptions of the scene, student’s behaviors, and overall conclusions about students in the class session.

Questionnaire: A questionnaire is a research instrument consisting of questions or other prompts aiming to collect information from a respondent. The researcher used a questionnaire of close-ended questions, and the data collected from a data collection questionnaire is quantitative. The questionnaire aims to look at existing problems and the need to use serious games in learning. The respondents consisted of 11 teachers involved in the subjects of Bahasa, LINUS and Recovery program in two schools, that 7 of the Sekolah Rendah Kebangsaan Proton City and 4 teachers of Sekolah Rendah Jenis Kebangsaan (Tamil) Ladang Kalumpang.

Phase 4. The results of the questionnaire, among the problems faced by students with a mean exceeding 3.40, which is the high category is High level of dependence on teachers (mean = 4.55), Repetition of the learning process frequently occurs (mean = 5.00), and Teaching Aids can attract students to learn (mean = 4.91). The questionnaire results proved the conventional method of Halus students who need teaching aids such as serious games.

The results obtained from the observation are listed in Table 3. The purpose of this observation is to strengthen the researcher’s findings in the literature review and explore the ideas and feelings of the respondents. The appropriate elements of the study are selected and formed into a serious game model for Halus students.

Table 3
The results of the preliminary study–Observation

	School	
	Sekolah Kebangsaan Proton City, Tanjong Malim, Perak	Sekolah Jenis Kebangsaan Tamil Ladang Kalumpang, Hulu Bernam, Selangor
Number of Halus students observed	Six students	Nine students

Table 3 (Continued)

	School	
	Sekolah Kebangsaan Proton City, Tanjong Malim, Perak	Sekolah Jenis Kebangsaan Tamil Ladang Kalumpang, Hulu Bernam, Selangor
Duration of Observation	20-25 minutes	15-20 minutes
Elements	<ol style="list-style-type: none"> 1. Create an active learning environment 2. Like colorful images 3. Limiting the time for a period of activity 	<ol style="list-style-type: none"> 1. Create an active learning environment 2. Like colorful images 3. Attracted to something new 4. Attracted to audio and music

This Prototype Conceptual Model was developed to ensure that the serious game applications developed meet the specifications of the needs of Halus students and become an effective aid tool for them. The design of the Prototype Conceptual Model is an adaptation of the elements and components of the model that contains a solid pedagogical foundation and game elements appropriate to the Halus students. This model is classified into two core elements, namely learning and game. Both elements match Anderson's ordered Thinking Skills, i.e. apply, understanding and retention. In addition, the BBL approach is also adapted and applied to give an adequate impression in helping the Halus students.

Elements of the Model

Kapp (2012) lists game elements commonly used: players, abstractions, rules, feedback, quantifying results, emotional results, and storytelling. The combination of game elements can make the difference in determining the success or failure of the game and enhancing motivation and interest in learning. Based on SLR and preliminary study, the elements corresponding to Halus students can be divided into core element learning mechanics and game mechanics. Therefore, this element is classified into core elements. Through literary reading and endorsed by preliminary study, it has proven that this element positively impacts maintaining a concentration, understanding and further enhancing student's interest in learning. The next subtopic will parse the selected element based on the shortlist in Table 4.

Design of the Model

Education is one of the critical aspects of human life. The BBL approach in learning is to optimize the brain's use and be aligned with how the brain works to learn. The assumption is that a human brain is highly potential, and every student can learn effectively if their

brains are allowed to function and play an optimal role (Jensen, 2008). The strategies applied in this gaming software are expected to help students in reading skills. In addition, the use of software facilitates the learning process by providing creative and innovative methods in teaching students with special needs rather than conventional methods (Suratin & Mahadi, 2016).

Figure 1 shows a proposed serious game model for Halus students that applies the BBL strategy (Hileman, 2006). The elements of the model are based on findings in SLR and preliminary studies. Based on Shapi'i and Ghulam (2016), designing a framework or model is to identify the core elements and pattern that make the game a success, where the fundamental objective is learning while enjoying the fun of playing. This model has two main plan, which is education and serious game. The education plan uses learning mechanics while serious games use game mechanics to acquire outcomes, skills and motivation. Those mechanics are assisted by the BBL approach (Hileman, 2006). Those strategies are applied in both teaching and serious game. Zhonggen (2019) states, learning and gaming attributes are interlinked and an important influencing factor in T&L in improving learning effectiveness and enhancing the learning experience in T&L in improving learning effectiveness and enhancing the learning experience.

Education and Serious Game

Two central part of this model is education and a serious game plan. A serious game is a classification of digital games designed with a main pedagogical goal for education and training. The serious game plan has the goal of the most serious game, making players learn higher-order thinking skills. Both education and serious game plan have been classified in Table 4 based on Bloom's ordered Thinking Skills.

Figure 2 shows Anderson's Taxonomy started by Anderson and Krathwohl (2001), adapted Bloom's idea, but few changes were made where replaced replaced 'knowledge' s replaced with 'remember'. In comparison, the higher-order levels of 'evaluation' and 'synthesis' we the place so that 'creating' or 'synthesis' were reflected as the highest order of thinking. This taxonomy evaluates the level of intelligence that people use to attain knowledge. It shows the different states of behavior that are required to learn information. For post-primary education, of the goals to achieve is critical or higher-order thinking skills. However, to reach that top level of thinking skills, one must first attain the lower order of thinking skills.

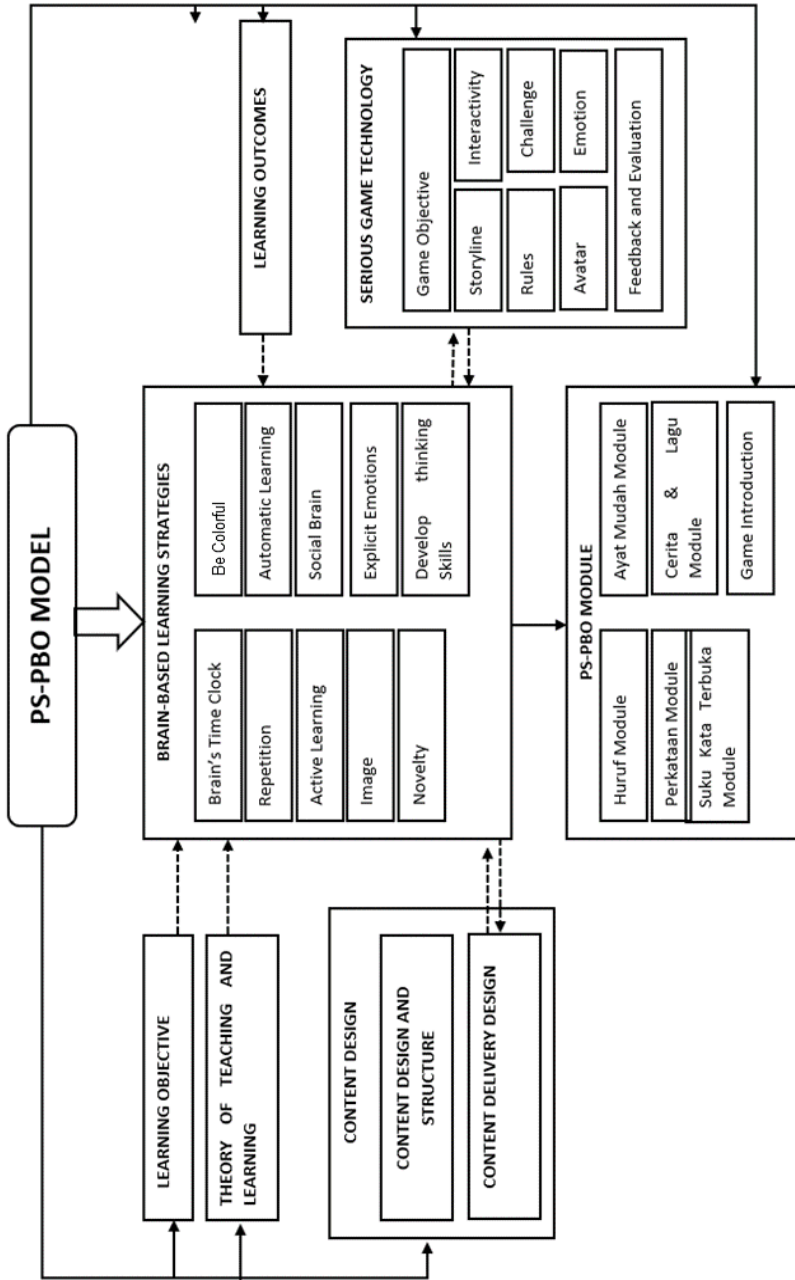


Figure 1. Serious game conception model for slow reading students

Table 4
 Classification based on Bloom's Ordered Thinking Skills

Learning Mechanics	Thinking Skills	Game Mechanics	Thinking Skills
Learning Objective	Understanding	Storyline	Retention
Learning Theory	Analyzing, Retention	Avatar	Retention
Content Design and Structure	Understanding	Feedback	Analyzing
Content Delivery Design	Understanding, Retention	Interactivity	Applying
Teaching aid used (Technology)	Evaluation	Emotional	Retention
Strategy used	Retention, Evaluation	Rules	Understanding
		Game Objective	Understanding
		Challenge	Retention

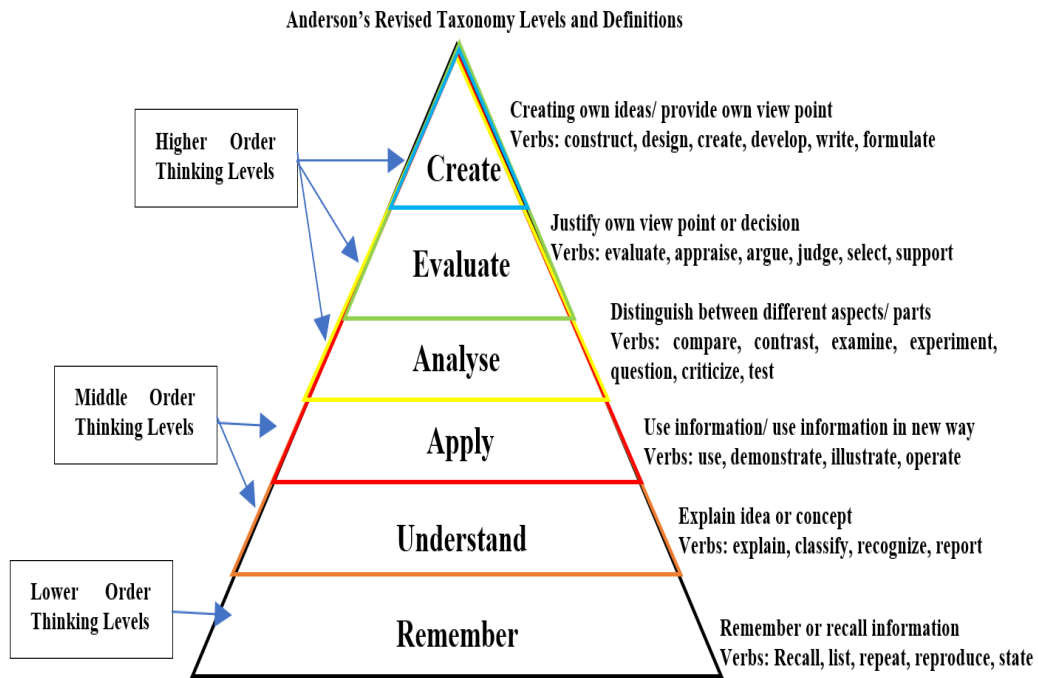


Figure 2. Anderson's Taxonomy and Level Descriptors; Adapted From (Sun, 2007)

Learning Components

The game component can be divided into six main elements, i.e. learning objective, learning theory, content design and structure, content delivery design, teaching aid used (Technology) and strategy used.

Instructional Objective. Instructional Objective: An instructional purpose is a statement that describes what the learner will do after the lesson is completed. A success goal is a comprehensive summary of what students will be expected to achieve after completing an instruction unit. For example, in this study, after completing the application, students expect to increase their motivation and skills in literacy skills.

Instructional Theories. The instructional theory describes how to help people learn, develop and create conditions that boost learning and improve instruction. There are three basic types of learning theory: behaviorist, cognitive constructivist, and social constructivist. In this application, we applied those learning theories using specific strategies and techniques: brain-based learning. Teachers need to understand learning theories to be prepared to utilize them in their classrooms.

Content Design and Structure. Lesson content design includes learning content according to the learning curriculum and presented in planned modules. Since teachers had no specific modules in learning, the researcher conducted content validation with five LINUS and Rehabilitation teachers to validate the game content. The Primary Integrated Skills (KBSR) curriculum is used as a guideline in determining the teaching goals and content of the model.

Content Delivery Design. The selected learning content is divided into submodules, while the learning objectives are included in each activity module as prescribed during the analysis phase. The steps involved in content structure design are navigation maps, logic flow charts, and storyboards. The navigation map links the contents of the modules and provides an interactive logic flow of the interface. Storyboards allow designers to get an overview of the structure of the courseware.

Serious Game Technology and Instructional Media. Instructional media are part of the instructional plan. It is a tool (other than teachers, textbooks and printed materials) that delivers lessons to students. It aims to produce an exciting and meaningful teaching and learning process while helping to achieve learning goals.

Teaching and Learning Strategies. The prototype model was designed by applying a Brain-Based Learning strategy. This BBL strategy is applied by Hileman (2006) in a game model.

Serious Game Component

The game component can be divided into six main elements, i.e. game objective, storyline, avatar, emotion, feedback, interactivity, rules, challenge.

Game Objective. A learning objective is the game's structure appropriate for the instructional objectives, for the audience's characteristics and intended use. As a result, it is essential to double-check that the games you plan to include align with your initial goals. For this application, the learning objective for the game is to increase the knowledge and skills in literacy for Halus students.

Storyline. The story is about the characters, of course. It is also about what the player sees. However, most importantly, it is about what the player does in the context of the narrative. To make the games have a good storyline, first; i) Outlines the major storyline, ii) Decide what type of game it will be, iii) Develop your world, iv) Create your main characters and v) Start writing the major story. This game is jungle and animal-themed, where players must help the animals that represent each module.

Avatar. Avatars in games are the player's representation in the game world. Users create avatars on various platforms to represent themselves when gaming, either serious or not serious. In this game, a bird represents the instructor to guide the users throughout the game.

Emotion. Game emotions are emotions generated due to winning, losing, accomplishment, and frustration. When you are playing a game, game emotions are directly related to your performance. Emotions are fundamental for players to engage with games deeply. Players' responses in a game are affected by their emotional states. If, in turn, it could affect the way the game responds, the player-game interaction could be augmented and enriched by magnitudes realizing affective loop-enabled games.

Interactivity. Interactivity is a dialogue between a computer and a user, and a user can interact with teaching materials. The game allows players to socialize either player with players or players with computers. Interactivity includes the speed of feedback or response to user activity, adaptability between humans and systems, instant feedback, and two-way communication between computer and human.

Rules. The effects of game mechanics are game rules, constraints in games that exist on each player's actions and abilities. Rules play an essential role in video games because they show how to win the game and how it works. In the game, there must be rules for increased learning. Clear instructions and methods for each game are essential. They are

a guideline and rules for players to follow. Rules mean the guidelines that describe the relationship between the player and the environment (Narayanasamy et al., 2006).

Challenge. Challenging can avoid boredom. Boredom can be avoided by challenging yourself. A challenging game would typically entice more learners to participate, resulting in increased participation and keeping in mind that the challenge should be suitable for the student's ability level. Introducing a challenge that is not easy to bore students with and is not too challenging to solve will increase student motivation, so be careful!

Feedback and Evaluation. Meaningful feedback in a game is critical to know whether learning goals are achieved, encourage knowledge construction, and reflect on existing and complete learning activities. Students' mistakes can be corrected, and students do not continue to make mistakes. In this serious game, the researcher used corrective feedback that helps with learning and provides guidance. It is called corrective feedback because if the learner did the wrong thing, they would be prompted or guided toward a more appropriate action (Kapp 2012). This corrective feedback informs the learner that their action was wrong, provides knowledge of the correct response, and indicates the right answer.

Brain-based Learning Component

For effective learning, serious games need to combine strategies and opportunities in-game designs to make them attractive. Hileman (2006) stated that the biological and chemical forces controlling the human brain are connected with learning. The human brain parts are intertwined to carry multiple brain functions such as thoughts, memories, sexuality, emotions, breathing, and creativity. Words, names, equations, vocabulary and facts are things that the brain cannot remember. The strategy by Hileman (2006) is a strategy that can be applied in the serious game and used by teachers in planning teaching activities so that brain use is in a state of readiness to learn. This strategy involves ten strategies known as BRAIN BASED.

B: Brain's Time Clock. Memory, interest, cognitive, attention, visual perception, stimulation, performance, mood and behavior are influenced by the brain cycle of 90 to 110 cycles called the ultra-ray rhythm. Therefore, it is essential to diversify teaching and learning activities or training sessions of not more than 12 to 15 minutes for active learning, especially for children aged 9-12.

R: Repetition. Memory Repetition of information reinforces the connections into the brain. When the content is repeated in various ways, the brain stores information efficiently. However, teachers need to be careful about using this strategy. If used correctly, knowledge

and skills can be used quickly and become more accurate because it is known. On the contrary, doing too much of the same thing causes the students to become bored.

A: Active Learning. This serious game requires students to be actively involved mentally and physically. When one learns through actions, they become more energetic and gain information more effectively. When the students are active, it can increase blood flow to the entire body and improve their memory. If the students sit for an extended period, it may cause low energy levels for them. An interactive game environment can add sensory stimulation to increase blood pressure and adrenaline levels to eliminate drowsiness, reduce anxiety, and strengthen information.

I: Images. Researches on the brain found that meaningful image concepts enable students to keep information in memory for the long term. In addition, visuals help students understand the content, attract attention and increase the students' percentage of remembrance. Hence, it is suggested that serious games need to be designed with text and graphics, diagrams, and videos.

N: Novelty. The level of dopamine increases in the brain as students know the stimulus that can reward them when they see something new. Therefore, it encourages students to look for rewards in whatever they do. For example, serious games apply a rewarding element to each level to stimulate the students' interest in playing.

B: Be Colorful. Color correlates with central nerves, and humans remember colors better than verbal or textual signals only. Colors also play a role in attracting attention, where black and white images can only draw one's attention for less than two seconds compared to colored images. Among the advantages of using the right colors in designs are; 1) Colors enhance software introduction up to 80%; 2) Colors can be read more frequently by 42%; 3) colors can increase the reader's interest by up to 40%; 4) Colors can increase learning from 55% to 78%; and 5) colors can increase understanding by 73%. Therefore, color compositions are essential for increased interest.

A: Automatic Learning. Automatic learning is information that is obtained through the use of electronic and mechanical tools. Indirect learning happens when students play games. Non-verbal communication is important in serious games. Designers need to stimulate students to enjoy learning by creating a positive environment with adequate resources. The components of games can enable students to play and learn at the same time indirectly.

S: Social Brain. Students have many opportunities to interact with teachers and other students through serious games, including students of different genders.

E: Elicit Emotions. Games can give players various emotions, ranging from frustration to excitement, from sad to anger and boredom to fun. Feelings are important for attention, perception, memory, and problem-solving. Acetylcholine in the synapse can be activated through the happy emotions generated from the game. Activating acetylcholine can help the received information be processed more quickly and memory stored better for the long term. By storytelling, students remember the stimulus more easily. Storytelling is one of the best ways to raise emotions like risk, happiness, insistence, and excitement. In addition, storytelling can help store information content.

D: Develop Thinking Skills. Problem-solving in serious games enables learning content to be related to the real world. Effective serious games allow students to collect information, generate results, and present the final decision. Before testing, students must follow the tutorials and training modules with an activity module that incorporates all the skills learned in this serious game.

RESULTS AND DISCUSSION

As the number of serious game users grows significantly and their social and educational impact is high, a review was conducted to analyze this topic's main aspects. As a result of this process, the game model was designed based on findings that suit a slow learner. Our research results indicate that games with Brain-based learning strategies apply in a serious game together with games and pedagogy elements. This model was created to suit students who are left out in learning, especially for slow-reading students. To produce students who master literacy skills, teaching aids and appropriate approaches to the 21st-century generation need to be aligned with technology development. Innovation in education begins with conventional methods. Computer-assisted learning through digital games embraces multimedia elements, which is the choice of T&L. Game emphasizes students to actively involved in the T&L process conducted by teachers and is known as a student-centered learning approach.

This model focuses on a serious game base of education and games that uses learning and game mechanics to acquire reading skills and motivation in learning. Based on the SLR conduct, components of games and learning are acquired. The BBL strategy component is also applied to the conception model. Preliminary studies were conducted to strengthen the findings in SLR to form a robust conceptual model. This component selection is selected based on their thinking skills. This serious game aims to help Halus students master lower-order thinking skills, including Remembering, Understanding, and Applying. Students

are not able to move to higher-order thinking when they skip the lower-order thinking skills. This person will not be prepared for real-life situations. Therefore, this is because lower-order thinking skills only need to be recalled and slightly understood. The serious game model focuses on lower-order thinking skills because it focuses on Halus students, especially the basic order thinking, which retention is and understanding.

Finally, this literature review helped identify research gaps in features related to approaches or strategies, pedagogical and game aspects that influence the serious game's design. This study's finding is significant for developing good quality serious games because aspects have not yet been explored extensively, especially for the strategies or approaches that have been applied. Besides, this work for new research projects is considered a basis for developing a serious game that integrates the most powerful game features to enhance literacy skills and increase motivation, especially for slow learners.

Besides, the BBL approach or strategy is used in learning and game mechanics. Student exposure to brain-based teaching strategies has helped students focus on learning and achieving the highest learning level. The findings show that BBL elements have already been used in conventional teaching but are not explicitly emphasized. Using game component and strategy application B.R.A.I.N.B.A.S.E.D into a serious game model can optimize the brain's use during the T&L process. Teaching strategies involving auditory, visual and kinesthetic provide the space for students to maximize their learning abilities to improve reading literacy skills and improve their learning motivation.

Education can significantly differ from school to school because of the lack of clear national policies related to digital gamers' engagement in game-based learning. As a result, the decision is left to school principals or individual teachers in many cases. Consequently, institutes focusing on game-based research must ensure a continuous two-way connection with teachers to integrate game-based learning into formal education.

For future work, the researcher will validate this conceptual model through the Delphi Technique. The Delphi technique is the best method to obtain expert consent in determining the elements included in the module's design. In addition, this technique will validate each element selected from the SLR Method and the preliminary study conducted.

CONCLUSION

In conclusion, this developed model is expected to guide developers in designing games compatible with Halus students. The game components and the strategies used are considered to have a good impact on Halus students.

ACKNOWLEDGEMENT

This study was funded by the Fundamental Research Grant Scheme FRGS/1/2019/ICT04/UKM/02/1. This work by the Faculty of Information Science and Technology, Universiti

Kebangsaan Malaysia, through the grant code FTM 1. The authors would like to thank the school principal of the two schools involved in this research, the LINUS and Pemulihan teachers, their valuable help, and the Faculty of Information Science and Technology, Universiti Kebangsaan Malaysia, for providing facilities and moral support.

REFERENCES

- Abidin, S. R. Z., Noor, S. F. M., & Ashaari, N. S. (2017). Guidelines of brain-based learning through serious game for slow reader students. In *2017 6th International Conference on Electrical Engineering and Informatics (ICEEI)* (pp. 1-6). IEEE Publishing. <https://doi.org/10.1109/ICEEI.2017.8312461>
- Abidin, S. R. Z., Noor, S. F. M., & Ashaari, N. S. (2019). Low-fidelity prototype design for serious game for slow-reading students. *International Journal of Advanced Computer Science and Application*, *10*(3), 270-276. <https://doi.org/10.14569/IJACSA.2019.0100335>
- Ahmad, N. A., Hashim, M., Al-Juboori, A. A. Z. A., & Zaidan, B. B. (2017). An effective diagnostic to overcome reading difficulties among learners with average reading ability. *International Journal of Arts & Sciences*, *10*(1), 299-303.
- Ahmad, W. F. W., Noordin, S. M., & Shariffudin, N. S. M. (2013). Development of a multimedia courseware for slow learner children with reading difficulties: MyLINUS. In *Advances in Visual Informatics, IVIC* (pp. 371-382). Springer. https://doi.org/10.1007/978-3-319-02958-0_34
- Anderson, L. W., & Krathwohl, D. R. (2001). *A taxonomy for learning, teaching, and assessing: A revision of bloom's taxonomy of educational objectives (Allyn & Ba)*. Pearson Education Group.
- Auzar, A. (2012). Keberkesanan penggunaan perisian asas membaca [Effectiveness of using basic reading software]. *GEMA OnlineTM Journal of Language Studies*, *12*(2), 629-644.
- Azid, N., Yusoff, N., Rawian, R., Sabarudin, N., & Ishak, M. Z. (2020). Evaluating user experience of using cerdas BM series 1 interactive pedagogical tool. *International Journal of Instruction*, *13*(4), 409-426. <https://doi.org/10.29333/iji.2020.13426a>
- Bandara, W., Miskon, S., & Fielt, E. (2011). A systematic, tool-supported method for conducting literature reviews in information systems. In *ECIS 2011 proceedings [19th European conference on information systems]* (pp. 1-13). AIS Electronic Library (AISeL)/Association for Information Systems.
- Bawaneh, A. K. A., Zain, A. N. M., & Ghazali, M. (2010). The effectiveness of conflict maps and the V-shape teaching method in science conceptual change among eighth-grade students in Jordan. *International Education Studies*, *3*(2), 96-108. <https://doi.org/10.5539/ies.v3n1p96>
- Bawaneh, A., Nurulazam, A., & Salmiza, S. (2012). The effect of a brain-based teaching method on conceptual change in students' understanding of electricity change agent. *International Journal of Physics & Chemistry Education*, *4*(2), 79-96.
- Bellotti, F., Berta, R., & Gloria, A. D. (2010). Designing effective serious games: Opportunities and challenges for research. *International Journal of Emerging Technologies in Learning (IJET)*, *5*, 22-35. <https://doi.org/10.3991/ijet.v5s3.1500>

- Binulal, K. R., & Aravind, A. (2013). Review of related literature on brain-based learning. *Indian Journal of Applied Research*, 3(7), 179-180.
- Boyler, S. (2010). Teaching toolkit: An introduction to games based learning. *UCD Teaching and Learning*, 5(January), 254-257.
- Caine, R. N., & Caine, G. (1991). *Making connections: Teaching and the human brain*. Addison-Wesley.
- Chauhan, S. (2011). Slow learners: Their psychology and educational programmes. *International Journal of Multidisciplinary Research*, 1(8), 279-289.
- Domínguez, A., Saenz-de-navarrete, J., Fernández-sanz, L., & Pagés, C. (2013). Gamifying learning experiences: Practical implications and outcomes. *Computers & Education*, 63, 380-392. <https://doi.org/10.1016/j.compedu.2012.12.020>
- Driscoll, L. (2011). Introduction to primary research: Observations, surveys, and interviews. In C. Lowe & P. Zemliansky (Eds.), *Writing spaces: Readings on writing* (Vol. 2, pp. 153-174). Parlor Press LLC.
- Fazil, F., & Saleh, S. (2016). Keberkesanan pendekatan pengajaran berasaskan otak dalam meningkatkan kefahaman pelajar tingkatan empat terhadap pembelajaran konsep dan mekanisme fotosintesis [The effectiveness of brain -based teaching approach in improving form four students' understanding of learning the concepts and mechanisms of photosynthesis]. *Asia Pacific Journal of Educators and Education*, 31, 69-83. <https://doi.org/10.21315/apjee2016.31.5>
- Hileman, S. (2006). Motivating students using brain-based teaching strategies. *The Agricultural Education Magazine*, 80(2), 1-28. <https://doi.org/10.1088/1742-6596/1157/2/022059>
- Hirschmann, R. (2020). *Share of online gamers in Malaysia in 2020, by age group*. Retrieved August 26, 2021, from <https://www.statista.com/statistics/1117575/malaysia-age-breakdown-of-online-gamers/>
- Jamian, A. R. (2011). Permasalahan kemahiran membaca dan menulis Bahasa Melayu murid-murid sekolah rendah di luar bandar [Problems reading and writing skills Malay primary school students in rural areas]. *Jurnal Pendidikan Bahasa Melayu*, 1(1), 1-1.
- Jensen, E. (2008). *Brain-based learning: The new paradigm of teaching*. Corwin Press.
- Kapp, K. (2012). *The gamification of learning and instruction: Game-based methods and strategies for training and education*. Pfeiffer.
- KPM. (2015). *Annual report 2015: Malaysia education blueprint 2013-2015*. Kementerian Pendidikan Malaysia. Retrieved August. 5, 2020, from [https://www.moe.gov.my/images/kpm/pemberitahuan/3-Laporan%20Tahunan%202015%20PPPM%202013-2025%20\(BM\).pdf](https://www.moe.gov.my/images/kpm/pemberitahuan/3-Laporan%20Tahunan%202015%20PPPM%202013-2025%20(BM).pdf)
- Mahidin, E. M. M., Umar, K., Ismail, S. S., Ismail, R., & Yusoff, M. Z. M. (2011). Preliminary testing on interactive Bahasa Melayu reading courseware for dyslexic children. In *2nd International Conference on Education and Management Technology* (Vol. 13, pp. 245-249). IACSIT Press.
- Mandar, S. D. (2011). Peranan cognitive neuroscience dalam dunia Pendidikan [The role of cognitive neuroscience in the world of education]. *Prosiding SNaPP: Sains, Teknologi*, 2(1), 369-376.
- Martin, M. W., & Shen, Y. (2014). The effects of game design on learning outcomes. *Computers in the Schools*, 31(1-2), 23-42. <https://doi.org/10.1080/07380569.2014.879684>

- Masrop, N. A. M., Din, H. A. M., Ariffin, A. N. Z., Salleh, N. M. M., & Ahmad, I. F. (2015, June 8-9). Kesan permainan digital dalam pendidikan [The effect of digital games in education]. In *Proceeding of International Conference on Information Technology & Society* (pp. 1-7). Kuala Lumpur, Malaysia.
- Miswan, M., & Adnan, H. M. (2015). Pembangunan aplikasi peranti mudah alih untuk kemahiran membaca kanak-kanak: aplikasi literasi linus (LILIN) [Development of mobile device applications for children's reading skills: Linus literacy application (LILIN)]. *Jurnal Pengajian Media Malaysia*, 17(2), 64-78.
- Møller, L., & Hansen, P. K. (2016). Framing serious games development as a matter of business. *International Journal of Serious Games*, 3(1), 33-40.
- Narayanasamy, V., Wong, K. W., Fung, C. C., & Rai, S. (2006). Distinguishing games and simulation games from simulators. *Computers in Entertainment*, 4(2), 9-es. <https://doi.org/10.1145/1129006.1129021>
- Ng, K. H., Bakri, A., & Rahman, A. A. (2015). A review on courseware for down syndrome children. *Journal of Information Systems Research and Innovation*, 8, 56-65.
- Ng, K. H., Bakri, A., & Rahman, A. A. (2016). Effects of persuasive designed courseware on children with learning difficulties in learning Malay language subject. *Education and Information Technologies*, 21(5), 1413-1431. <http://doi.org/10.1007/s10639-015-9391-7>
- Othman, Y., & Pakar, D. R. (2011). Kesan aplikasi perisian cerita interaktif semasa mengajarkan kemahiran bacaan dan kefahaman dalam kalangan murid tahun 4 di Brunei Darussalam [The impact of interactive story software application in teaching reading and comprehension skills among year 4 students in Brunei Darussalam]. *Jurnal Pendidikan Bahasa Melayu*, 1(1), 27-49.
- Peirce, N. (2013). *Digital game-based learning for early childhood: A state of the art report*. Learnovate Centre.
- Ramli, R., & Zaman, H. B. (2011). Designing usability evaluation methodology framework of augmented reality basic reading courseware (AR BACA SindD) for down syndrome learner. In *Proceedings of the 2011 International Conference on Electrical Engineering and Informatics* (pp. 1-5). IEEE Publishing. <https://doi.org/10.1109/ICEEL.2011.6021807>
- Saleh, S., & Halim, A. D. (2016). Kecenderungan otak dan hubungannya dengan pencapaian dan motivasi pelajar [Brain tendency and its relationship with student achievement and motivation]. *Jurnal Pendidikan Malaysia*, 41(1), 65-70.
- Shapi'i, A., & Ghulam, S. (2016). Model for educational game using natural user interface. *International Journal of Computer Games Technology*, 2016, 1-7. <https://doi.org/10.1155/2016/6890351>
- She, H. (2012). Promoting students' learning of air pressure concepts: The interrelationship of teaching approaches and student learning characteristics. *The Journal of Experimental Education*, 7(1), 29-51.
- Sidek, S. F., Fathil, N. S., Zain, N. Z. M., & Muhammad, K. (2014). Pembangunan perisian kursus [Courseware development]. *Jurnal Pendidikan Bahasa Melayu*, 4(1), 1-10.
- Stanberry, K., & Raskind, M. H. (2019). *Assistive technology for kids with learning disabilities: An overview*. Retrieved February 20, 2021, from <https://www.readingrockets.org/article/assistive-technology-kids-learning-disabilities-overview>
- Su, T. Y., Gates, P., & Harrison, I. (2016). Digital games and learning mathematics: Student, teacher and parent perspectives. *International Journal of Serious Games*, 3(4), 55-68.

- Sun, M. (2007). *Using the organizational and narrative thread structures in an e-book to support comprehension* (Doctoral dissertation). Robert Gordon University, UK.
- Suratin, S. F., & Mahadi, B. (2016). A review of learning courseware for children with learning disabilities in Malaysia. *Journal of Information Systems Research and Innovation*, 10(December), 1-8.
- Yussof, R. L., & Shima, T. P. T. N. (2012). Reading activities using the scaffolding in MEL-SindD for down syndrome children. *Procedia-Social and Behavioral Sciences*, 35, 121-128. <https://doi.org/10.1016/j.sbspro.2012.02.070>
- Zaki, N. A. A., Wook, T. S. M. T., & Ahmad, K. (2015, August). Analysis and classification of serious games for cognitive stimulation. In *2015 International Conference on Electrical Engineering and Informatics (ICEEI)* (pp. 612-617). IEEE Publishing. <https://doi.org/10.1109/ICEEI.2015.7352572>
- Zhonggen, Y. (2019). A meta-analysis of use of serious games in education over a decade. *International Journal of Computer Games Technology*, 2019, Article 4797032. <https://doi.org/10.1155/2019/4797032>



REFEREES FOR THE PERTANIKA JOURNAL OF SCIENCE & TECHNOLOGY

VoL. 29 (4) Oct. 2021

The Editorial Board of the Pertanika Journal of Science and Technology wishes to thank the following:

Abdul Samad Shibghatullah
(UCSI University, Malaysia)

Amirah Amalina Ahmad Tarmizi
(UiTM, Malaysia)

Edi Syams Zainudin
(UPM, Malaysia)

Abdullah Mat Rashid
(UPM, Malaysia)

Anusha Achuthan
(USM, Malaysia)

Edlic Sathiamurthy
(UMT, Malaysia)

Adi Irfan Che Ani
(UKM, Malaysia)

Arina Shairah Abdul Sukor
(UPM, Malaysia)

Elysha Nur Ismail
(UPM, Malaysia)

Adibah Mohd Amin
(UPM, Malaysia)

Athirah Nawawi
(UPM, Malaysia)

Emedya Murniwaty Samsudin
(UTHM, Malaysia)

Adriana Irawati Nur Ibrahim
(UM, Malaysia)

Baharuddin Abdullah
(USM, Malaysia)

Fadhilah Mat Yamin
(UUM, Malaysia)

Ahmad Baharuddin Abdullah
(USM, Malaysia)

Bijoy Kumar Mandal
(NSHM Knowledge Campus, India)

Fam Soo Fen
(UTeM, Malaysia)

Ahmad Kamil Arshad
(UiTM, Malaysia)

Chaiporn Thoppae
(EIT, Thailand)

Farshid Keynia
(GUAT, Iran)

Ahmad Sufriil Azlan Mohamed
(USM, Malaysia)

Che Maznah Mat Isa
(UiTM, Malaysia)

Farzaneh Mohamadpour
(USB, Iran)

Ahmed Al-Jumaili
(UFL, USA)

Che Zalina Zulkifli
(UPSI, Malaysia)

Gan Chin Kim
(UTeM, Malaysia)

Akbulut Bilal
(CFRI, Turkey)

Chua Han Bing
(Curtin University, Malaysia)

Haider Hadi Jasim
(University of Basrah, Iraq)

Ali Hajnaye
(SCU, Iran)

Chuan Zun Liang
(UMP, Malaysia)

Hari Krishnan
(NIOSH, Malaysia)

Aminu Rabiu
(UDUS, Nigeria)

Dian Darina Indah Daruis
(UPNM, Malaysia)

Haszianaliza Haslan
(UiTM, Malaysia)

Aminudin Abu
(UTM, Malaysia)

Dino Rimantho
(Pancasila University, Indonesia)

Irfan Ahmed Shaikh
(SAU, Pakistan)

Amir Izzwan Zamri
(UMT, Malaysia)

Dzati Athiar Ramli
(USM, Malaysia)

Isa Bala Muhammad
(FUTMinna, Nigeria)

Iskandar Ishak
(UPM, Malaysia)

Jamari Saidatul Shima
(UMP, Malaysia)

Jayaraj Vijaya Kumaran
(UMK, Malaysia)

Jobrun Nandong
(Curtin University, Malaysia)

Juliana Aida Abu Bakar
(UUM, Malaysia)

Kek Sie Long
(UTHM, Malaysia)

Khairil Anas Md Rezali
(UPM, Malaysia)

Lai Kee Huong
(Sunway University, Malaysia)

Maizatul Akmar Ismail
(UM, Malaysia)

Marina Kapitonova
(UNIMAS, Malaysia)

Marsyita Hanafi
(UPM, Malaysia)

Melody Kimi
(UNIMAS, Malaysia)

Mohammed Alias Yusof
(UPNM, Malaysia)

Mohammed Arifullah
(UMK, Malaysia)

Mohan Reddy Moola
(Curtin University, Malaysia)

Mohd Amrallah Mustafa
(UPM, Malaysia)

Mohd Asyraf Mansor
(USM, Malaysia)

Mohd Azreen Mohd Ariffin
(UTM, Malaysia)

Mohd Hudzari Haji Razali
(UiTM, Malaysia)

Mohd Khair Hassan
(UPM, Malaysia)

Mohd Rafee Baharudin
(UPM, Malaysia)

Mohd Shahrul Nizam Mohd
Danuri
(KUIS, Malaysia)

Mohd Tahir Ismail
(USM, Malaysia)

Mohd. Zaki Nuawi
(UKM, Malaysia)

Mostafa Abdulghafoor
Mohammed
(UPB, Romania)

Mus`ab Abd. Razak
(UPM, Malaysia)

Muzzneena Ahmad Mustapha
(UKM, Malaysia)

Nabilah Afiqah Mohd Radzuan
(UKM, Malaysia)

Ng Seng Beng
(UPM, Malaysia)

Nilotpai Banerjee
(NITDGP, India)

Noradila Nordin
(UUM, Malaysia)

Nur Farhayu Ariffin
(UMP, Malaysia)

Nuramidah Hamidon
(UTHM, Malaysia)

Nwankwo Wilson
(Edo University, Nigeria)

Ooi Lu Ean
(USM, Malaysia)

Othman A. Karim
(UKM, Malaysia)

P. Phung-Van
(HUTECH, Vietnam)

Payam Shafigh
(UM, Malaysia)

Peter David Kulyakwawe
(CAAS, China)

Poh Mau Ern
(UM, Malaysia)

Rajyalakshmi K
(KLU, India)

Riza Wirawan
(ITB, Indonesia)

Rosmiwati Mohd Mokhtar
(USM, Malaysia)

S Velmurugan
(CRRI, India)

Salang Musikasuwan
(PSU, Thailand)

Sara Yasina Yusuf
(UniMAP, Malaysia)

Sarina Sulaiman
(IIUM, Malaysia)

Sendilvelan Subramanian
(DRMGRDU, India)

Suhaidi Shafie
(UPM, Malaysia)

Surapati Pramanik
(NGBTC, India)

Tahereh Jafary
(IMCO, Oman)

Tan Tien Ping
(USM, Malaysia)

Ummu 'Atiqah Mohd Roslan
(UMT, Malaysia)

Wei-Chiang Hong
(JSNU, China)

Zulfa Hanan Ash'aari
(UPM, Malaysia)

Waida Ismail
(USIM, Malaysia)

Yap Wei Boon
(UKM, Malaysia)

Zurina Mohamad
(UTM, Malaysia)

Wan Mohd Nazmee Wan Zainon
(USM, Malaysia)

Zalisham Jali
(USIM, Malaysia)

Zurinahni Zainol
(USM, Malaysia)

Wang Seok Mui
(UiTM, Malaysia)

Zarani Mat Taher
(UTM, Malaysia)

CAAS – Chinese Academy of Agricultural Sciences
CFRI – Central Fisheries Research Institute
CRRI – Central Road Research Institute
DRMGRDU – Dr.M.G.R.Educational and Research Institute
EIT – The Engineering Institute of Thailand
FUTMinna – Federal University of Technology Minna
GUAT – Graduate University of Advanced Technology
HUTECH – Ho Chi Minh City University of Technology
IIUM – International Islamic University Malaysia
IMCO – International Maritime College Oman
ITB – Bandung Institute of Technology
JSNU – Jiangsu Normal University
KLU – Koneru Lakshmaiah Education
KUIS – Kolej Universiti Islam Antarabangsa Selangor
NGBTC – Nandalal Ghosh B.T. College
NIOSH – National Institute of Occupational Safety and Health
NITDGP – National Institute of Technology Durgapur
PSU – Prince of Songkla University
SAU – Sindh Agriculture University
SCU – Shahid Chamran University

UDUS – Usmanu Danfodiyo University Sokoto
UFL – University of Florida
UiTM – Universiti Teknologi MARA
UKM – Universiti Kebangsaan Malaysia
UM – Universiti Malaya
UMK – Universiti Malaysia Kelantan
UMP – Universiti Malaysia Pahang
UMT – Universiti Malaysia Terengganu
UniMAP – Universiti Malaysia Perlis
UNIMAS – Universiti Malaysia Sarawak
UPB – Politehnica University of Bucharest
UPM – Universiti Putra Malaysia
UPNM – Universiti Pertahanan Nasional Malaysia
UPSI – University Pendidikan Sultan Idris
USB – University of Sistan & Baluchestan
USIM – Universiti Sains Islam Malaysia
USM – Universiti Sains Malaysia
UTeM – Universiti Teknikal Malaysia Melaka
UTHM – Universiti Tun Hussein Onn Malaysia
UTHM – Universiti Teknologi Malaysia

While every effort has been made to include a complete list of referees for the period stated above, however if any name(s) have been omitted unintentionally or spelt incorrectly, please notify the Chief Executive Editor, *Pertanika* Journals at executive_editor.pertanika@upm.edu.my

Any inclusion or exclusion of name(s) on this page does not commit the *Pertanika* Editorial Office, nor the UPM Press or the university to provide any liability for whatsoever reason.



Pertanika Journal of Science & Technology

Our goal is to bring high-quality research to the widest possible audience

INSTRUCTIONS TO AUTHORS

(REGULAR ISSUE)

(Manuscript Preparation & Submission Guide)

Revised: November 2020

Please read the *Pertanika* guidelines and follow these instructions carefully. The Chief Executive Editor reserves the right to return manuscripts that are not prepared in accordance with these guidelines.

MANUSCRIPT PREPARATION Manuscript Types

Pertanika accepts submission of mainly 4 types of manuscripts

- that have not been published elsewhere (including proceedings)
- that are not currently being submitted to other journals

1. Regular article

Regular article is a full-length original empirical investigation, consisting of introduction, methods, results, and discussion. Original research work should present new and significant findings that contribute to the advancement of the research area. *Analysis and Discussion* must be supported with relevant references.

Size: Generally, each manuscript is **not to exceed 6000 words** (excluding the abstract, references, tables, and/or figures), a maximum of **80 references**, and **an abstract of less than 250 words**.

2. Review article

A review article reports a critical evaluation of materials about current research that has already been published by organising, integrating, and evaluating previously published materials. It summarises the status of knowledge and outlines future directions of research within the journal scope. A review article should aim to provide systemic overviews, evaluations, and interpretations of research in a given field. Re-analyses as meta-analysis and systemic reviews are encouraged.

Size: Generally, it is expected **not to exceed 6000 words** (excluding the abstract, references, tables, and/or figures), a maximum of **80 references**, and **an abstract of less than 250 words**.

3. Short communications

Each article should be timely and brief. It is suitable for the publication of significant technical advances and maybe used to:

- (a) reports new developments, significant advances and novel aspects of experimental and theoretical methods and techniques which are relevant for scientific investigations within the journal scope;
- (b) reports/discuss on significant matters of policy and perspective related to the science of the journal, including 'personal' commentary;
- (c) disseminates information and data on topical events of significant scientific and/or social interest within the scope of the journal.

Size: It is limited to **3000 words** and have a maximum of **3 figures and/or tables, from 8 to 20 references, and an abstract length not exceeding 100 words**. The information must be in short but complete form and it is not intended to publish preliminary results or to be a reduced version of a regular paper.

4. Others

Brief reports, case studies, comments, concept papers, letters to the editor, and replies on previously published articles may be considered.

Language Accuracy

Pertanika emphasises on the linguistic accuracy of every manuscript published. Articles can be written in **English** or **Bahasa Malaysia** and they must be competently written and presented in clear and concise grammatical English/Bahasa Malaysia. Contributors are strongly advised to have the manuscript checked by a colleague with ample experience in writing English manuscripts or a competent English language editor. For articles in Bahasa Malaysia, the title, abstract and keywords should be written in both English and Bahasa Malaysia.

Author(s) **may be required to provide a certificate** confirming that their manuscripts have been adequately edited. **All editing costs must be borne by the authors.**

Linguistically hopeless manuscripts will be rejected straightaway (e.g., when the language is so poor that one cannot be sure of what the authors are really trying to say). This process, taken by authors before submission, will greatly facilitate reviewing, and thus, publication.

MANUSCRIPT FORMAT

The paper should be submitted in **one-column format** with 1.5 line spacing throughout. Authors are advised to use Times New Roman 12-point font and *MS Word* format.

1. Manuscript Structure

The manuscripts, in general, should be organised in the following order:

Page 1: Running title

This page should **only** contain the running title of your paper. The running title is an abbreviated title used as the running head on every page of the manuscript. The running title **should not exceed 60 characters, counting letters and spaces.**

Page 2: Author(s) and Corresponding author's information

General information: This page should contain the **full title** of your paper **not exceeding 25 words**, with the name of all the authors, institutions and corresponding author's name, institution and full address (Street address, telephone number (including extension), handphone number, and e-mail address) for editorial correspondence. **The corresponding author must be clearly indicated with a superscripted asterisk symbol (*).**

Authors' name: The names of the authors should be named **in full without academic titles.** For Asian (Chinese, Korean, Japanese, Vietnamese), please write first name and middle name before surname (family name). The last name in the sequence is considered the surname.

Authors' addresses: Multiple authors with different addresses must indicate their respective addresses separately by superscript numbers.

Tables/figures list: A list of the number of **black and white/colour figures and tables** should also be indicated on this page. See **"5. Figures & Photographs"** for details.

Example (page 2):

Fast and Robust Diagnostic Technique for the Detection of High Leverage Points

Habshah Midi^{1,2*}, Hasan Talib Hendi¹, Jayanthi Arasan² and Hassan Uraibi³

¹*Institute for Mathematical Research, Universiti Putra Malaysia, 43400 UPM, Serdang, Selangor, Malaysia*

²*Department of Mathematics, Faculty of Science, Universiti Putra Malaysia, 43400 UPM, Serdang, Selangor, Malaysia*

³*Department of Statistics, University of Al-Qadisiyah, 88 -Al-Qadisiyah -Al-Diwaniyah, Iraq*

E-mail addresses

habshah@upm.edu.my (Habshah Midi)

h.applied.t88@gmail.com (Hasan Talib Hendi)

jayanthi@upm.edu.my (Jayanthi Arasan)

hssn.sami1@gmail.com (Hassan Uraibi)

*Corresponding author

List of Table/Figure: Table 1.

Figure 1.

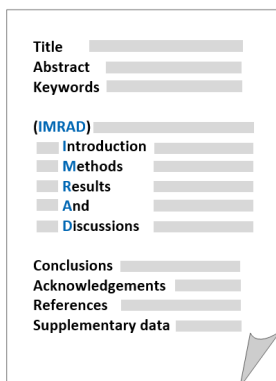
Page 3: Abstract

This page should **repeat** the **full title** of your paper with only the **Abstract**, usually in one paragraph and **Keywords**.

Keywords: *Not more than 8 keywords in alphabetical order must be provided to describe the content of the manuscript.*

Page 4: Text

A regular paper should be prepared with the headings *Introduction, Materials and Methods, Results and Discussions, Conclusions, Acknowledgements, References, and Supplementary data* (if any) in this order. The literature review may be part of or separated from the *Introduction*.



MAKE YOUR ARTICLES AS CONCISE AS POSSIBLE

Most scientific papers are prepared according to a format called IMRAD. The term represents the first letters of the words Introduction, Materials and Methods, Results, And, Discussion. It indicates a pattern or format rather than a complete list of headings or components of research papers; the missing parts of a paper are: Title, Authors, Keywords, Abstract, Conclusions, and References. Additionally, some papers include Acknowledgments and Appendices.

The Introduction explains the scope and objective of the study in the light of current knowledge on the subject; the Materials and Methods describes how the study was conducted; the Results section reports what was found in the study; and the Discussion section explains meaning and significance of the results and provides suggestions for future directions of research. The manuscript must be prepared according to the Journal's instructions to authors.

2. Levels of Heading

Level of heading	Format
1 st	LEFT, BOLD, UPPERCASE
2 nd	Flush left, Bold, Capitalise each word
3 rd	Bold, Capitalise each word, ending with .
4 th	Bold italic, Capitalise each word, ending with .

3. Equations and Formulae

These must be set up clearly and should be typed double-spaced. Numbers identifying equations should be in square brackets and placed on the right margin of the text.

4. Tables

- All tables should be prepared in a form consistent with recent issues of *Pertanika* and should be numbered consecutively with Roman numerals (Table 1, Table 2).
- A brief title should be provided, which should be shown at the top of each table (APA format):

Example:

Table 1

PVY infected Nicotiana tabacum plants optical density in ELISA

- Explanatory material should be given in the table legends and footnotes.
- Each table should be prepared on a new page, embedded in the manuscript.
- Authors are advised to keep backup files of all tables.

**** Please submit all tables in Microsoft word format only, because tables submitted as image data cannot be edited for publication and are usually in low-resolution.**

5. Figures & Photographs

- Submit an original figure or photograph.
- Line drawings must be clear, with a high black and white contrast.
- Each figure or photograph should be prepared on a new page, embedded in the manuscript for reviewing to keep the file of the manuscript under 5 MB.
- These should be numbered consecutively with Roman numerals (Figure 1, Figure 2).
- Provide a brief title, which should be shown at the bottom of each table (**APA format**):

Example: *Figure 1. PVY-infected in vitro callus of Nicotiana tabacum*

- If a figure has been previously published, acknowledge the original source, and submit written permission from the copyright holder to reproduce the material.
- Authors are advised to keep backup files of all figures.

**** Figures or photographs must also be submitted separately as TIFF or JPEG, because figures or photographs submitted in low-resolution embedded in the manuscript cannot be accepted for publication. For electronic figures, create your figures using applications that are capable of preparing high-resolution TIFF files.**

6. Acknowledgement

Any individuals and entities who have contributed to the research should be acknowledged appropriately.

7. References

References begin on their own page and are listed in alphabetical order by the first author's last name. Only references cited within the text should be included. All references should be in 12-point font and double-spaced. If a Digital Object Identifier (DOI) is listed on a print or electronic source, it is required to include the DOI in the reference list. Use Crossref to find a DOI using author and title information.

NOTE: When formatting your references, please follow the **APA-reference style** (7th edition) (refer to the examples). Ensure that the references are strictly in the journal's prescribed style, failing which your article will **not be accepted for peer-review**. You may refer to the *Publication Manual of the American Psychological Association* (<https://apastyle.apa.org/>) for further details.

Examples of reference style are given below:

Books		
	Insertion in text	In reference list
Book/E-Book with 1-2 authors	<p>Information prominent' (the author's name is within parentheses):</p> <p>... (Staron, 2020)</p> <p>... (Darus & Rasdi, 2019)</p> <p>... Or</p> <p>'Author prominent' (the author's name is outside the parentheses):</p> <p>(Starron, 2020)...</p> <p>Darus and Rasdi (2019) ...</p>	<p>Staron, M. (2020). <i>Action research in software engineering</i>. Springer International Publishing. https://doi.org/10.1007/978-3-030-32610-4</p> <p>Darus, A., & Rasdi, I. (2019). <i>Introduction to occupational health a workbook</i>. UPM Press.</p>
Book/E-Book with 3 or more authors	<p><i>For all in-text references, list only the first author's family name and followed by 'et al.'</i></p> <p>Information prominent' (the author's name is within parentheses):</p> <p>... (Yusof et al., 2020)</p> <p>... Or</p> <p>'Author prominent' (the author's name is outside the parentheses):</p> <p>Yusof et al. (2020) ...</p>	<p>Yusof, N. A., Azmi, U. Z. M., Ariffin, N., & Rahman, S. F. A. (2020). <i>Biosensors and chemical sensors: A practical approach</i>. UPM Press.</p>
Book/E-Book with more than 20 authors		<p>For books with more than 20 authors, please follow the guidelines for journal articles with more than 20 authors.</p>
Chapter in an edited Book/E-Book	<p>Inform ation pr ominent' (the author 's name is within parentheses):</p> <p>... (Mainzer, 2020) ...</p> <p>... (Tang et al., 2020) ...</p> <p>Or</p> <p>'Author prominent' (the author's name is outside the parentheses):</p> <p>Mainzer (2020) ...</p> <p>Tang et al. (2020) ...</p>	<p>Mainzer, K. (2020). Logical thinking becomes automatic. In K. Mainzer (Ed.), <i>Artificial intelligence-When do machines take over?</i> (pp. 15-45). Springer. https://doi.org/10.1007/978-3-662-59717-0_3</p> <p>Tang, W., Khavarian, M., Yousefi, A., & Cui, H. (2020). Properties of self-compacting concrete with recycled concrete aggregates. In R. Siddique (Ed.), <i>Self-Compacting Concrete: Materials, Properties, and Applications</i> (pp. 219-248). Woodhead Publishing. https://doi.org/10.1016/B978-0-12-817369-5.00009-X</p>

	Insertion in text	In reference list
Editor	<p>Information prominent' (the author's name is within parentheses): ... (Kesharwani, 2020) (Lanza et al., 2020) ... Or 'Author prominent' (the author's name is outside the parentheses): Kesharwani (2020) ... Lanza et al. (2020) ...</p>	<p>Kesharwani, P. (Ed.). (2020). <i>Nanotechnology based approaches for tuberculosis treatment</i>. Academic Press.</p> <p>Lanza, R., Langer, R., Vacanti, J. P., & Atala, A. (Eds.). (2020). <i>Principles of tissue engineering</i>. Academic press. https://doi.org/10.1016/C2018-0-03818-9</p>
Several works by the same author in the same year	<p>Information prominent' (the author's name is within parentheses): ... (Aggarwal & Aggarwal, 2020a, 2020b) ... Or 'Author prominent' (the author's name is outside the parentheses): Aggarwal & Aggarwal (2020a, 2020b) ...</p>	<p>Aggarwal, P., & Aggarwal, Y. (2020a). Strength properties of SCC. In R. Siddique (Ed.), <i>Self-Compacting Concrete: Materials, Properties, and Applications</i> (p. 83-115). Woodhead Publishing. doi: https://doi.org/10.1016/B978-0-12-817369-5.00004-0</p> <p>Aggarwal, P., & Aggarwal, Y. (2020b). Carbonation and corrosion of SCC. In R. Siddique (Ed.), <i>Self-Compacting Concrete: Materials, Properties, and Applications</i> (p. 147-193). Woodhead Publishing. doi: https://doi.org/10.1016/B978-0-12-817369-5.00007-6</p>
Journals		
Journal article with 1-2 authors	<p>Information prominent' (the author's name is within parentheses): ... (Laan & Fox, 2019) ... Or 'Author prominent' (the author's name is outside the parentheses): Laan and Fox (2019) ...</p>	<p>Laan, E., & Fox, J. W. (2019). An experimental test of the effects of dispersal and the paradox of enrichment on metapopulation persistence. <i>Oikos</i>, 129(1), 49-58. https://doi.org/10.1111/oik.06552</p>
Journal article with 3 or more authors	<p><i>For all in-text references, list only the first author's family name and followed by 'et al.'</i> Information prominent' (the author's name is within parentheses): ... (Midi et al., 2020) (Shagufta et al., 2017) ... Or 'Author prominent' (the author's name is outside the parentheses): Midi et al. (2020) ... Shagufta et al. (2017) ...</p>	<p>Midi, H., Hendi, H. T., Arasan, J., & Uraibi, H. (2020). Fast and Robust Diagnostic Technique for the Detection of High Leverage Points. <i>Pertanika Journal of Science & Technology</i>, 28(4), 1203-1220.</p> <p>Shagufta, B., Sivakumar, M., Kumar, S., Agarwal, R. K., Bhilegaonkar, K. N., Kumar, A., & Dubal, Z. B. (2017). Antimicrobial resistance and typing of Salmonella isolated from street vended foods and associated environment. <i>Journal of Food Science and Technology</i>, 54(8), 2532-2539. doi: https://doi.org/10.1007/s13197-017-2698-1</p>
Journal article with more than 20	<p>Information prominent' (the author's name is within parentheses): ... (Wiskunde et al., 2019) ... Or 'Author prominent' (the author's name is outside the parentheses): Wiskunde et al. (2019) ...</p>	<p>Wiskunde, B., Arslan, M., Fischer, P., Nowak, L., Van den Berg, O., Coetzee, L., Juárez, U., Riyaziyyat, E., Wang, C., Zhang, I., Li, P., Yang, R., Kumar, B., Xu, A., Martinez, R., McIntosh, V., Ibáñez, L. M., Mäkinen, G., Virtanen, E., ... Kovács, A. (2019). Indie pop rocks mathematics: Twenty One Pilots, Nicolas Bourbaki, and the empty set. <i>Journal of Improbable Mathematics</i>, 27(1), 1935-1968. https://doi.org/10.0000/3mp7y-537</p>
Journal article with an article number	<p>Information prominent' (the author's name is within parentheses): ... (Roe et al., 2020) ... Or 'Author prominent' (the author's name is outside the parentheses): Roe et al. (2020) ...</p>	<p>Roe, E. T., Bies, A. J., Montgomery, R. D., Watterson, W. J., Parris, B., Boydston, C. R., Sereno, M. E., & Taylor, R. P. (2020). Fractal solar panels: Optimizing aesthetic and electrical performances. <i>Plos One</i>, 15(3), Article e0229945. https://doi.org/10.1371/journal.pone.0229945</p>
Journal article with missing information	<p>Information prominent' (the author's name is within parentheses): ... (Alfirevic et al., 2017) (Hayat et al., 2020) (Fan et al., 2020) ...</p>	<p>Missing volume number Alfirevic, Z., Stampalija, T., & Dowswell, T. (2017). Fetal and umbilical Doppler ultrasound in high-risk pregnancies (review). <i>Cochrane Database of Systematic Reviews</i>, (6), 1-163. https://doi.org/10.1002/14651858.CD007529.pub4. Copyright</p>

	Insertion in text	In reference list
Journal article with missing information	Or 'Author prominent' (the author's name is outside the parentheses): Alfirevic et al. (2017) ... Hayat et al. (2020) ... Fan et al. (2020) ...	Missing issue number Hayat, A., Shaishta, N., Mane, S. K. B., Hayat, A., Khan, J., Rehman, A. U., & Li, T. (2020). Molecular engineering of polymeric carbon nitride based Donor-Acceptor conjugated copolymers for enhanced photocatalytic full water splitting. <i>Journal of colloid and interface science</i> , 560, 743-754. https://doi.org/10.1016/j.jcis.2019.10.088 Missing page or article number Fan, R. G., Wang, Y. B., Luo, M., Zhang, Y. Q., & Zhu, C. P. (2020). SEIR-Based COVID-19 Transmission Model and Inflection Point Prediction Analysis. <i>Dianzi Keji Daxue Xuebao/Journal of the University of Electronic Science and Technology of China</i> , 49(3). https://doi.org/10.12178/1001-0548.9_2020029
Several works by the same author in the same year	Information prominent' (the author's name is within parentheses): ... (Chee et al., 2019a, 2019b) ... Or 'Author prominent' (the author's name is outside the parentheses): Chee et al. (2019a, 2019b) ...	Chee, S. S., Jawaid, M., Sultan, M. T. H., Alothman, O. Y., & Abdullah, L. C. (2019a). Accelerated weathering and soil burial effects on colour, biodegradability and thermal properties of bamboo/kenaf/epoxy hybrid composites. <i>Polymer Testing</i> , 79, Article 106054. https://doi.org/10.1016/j.polymeresting.2019.106054 Chee, S. S., Jawaid, M., Sultan, M. T. H., Alothman, O. Y., & Abdullah, L. C. (2019b). Evaluation of the hybridization effect on the thermal and thermo-oxidative stability of bamboo/kenaf/epoxy hybrid composites. <i>Journal of Thermal Analysis and Calorimetry</i> , 137(1), 55-63. https://doi.org/10.1007/s10973-018-7918-z
Newspaper		
Newspaper article – with an author	... (Shamshuddin, 2019) ... Or ... Shamshuddin (2019) ...	Shamshuddin, J. (2019, September 23). Lynas plant waste residue can be used to boost oil palm growth? <i>New Straits Times</i> . https://www.nst.com.my/opinion/letters/2019/09/523930/lynas-plant-waste-residue-can-be-used-boost-oil-palm-growth
Newspaper article – without an author	("Zoonotic viruses," 2017). OR "Zoonotic viruses" (2017) ... Use a shortened title (or full title if it is short) in Headline Case enclosed in double quotation marks.	Zoonotic viruses like swine flu are ticking time bombs, say experts. (2020, July 4). <i>New Straits Times</i> , 3.
Dissertation/Thesis		
Published Dissertation or Thesis References	... (Rivera, 2016) ... Or ... Rivera (2016) ...	Rivera, C. (2016). <i>Disaster risk management and climate change adaptation in urban contexts: Integration and challenges</i> [Doctoral dissertation, Lund University]. Lund University Publications. https://lup.lub.lu.se/search/ws/files/5471705/8570923.pdf
Unpublished Dissertation or Thesis References	... (Brooks, 2014) ... Or ... Brooks (2014) ...	Brooks, J. D. (2015). <i>Bamboo as a strengthening agent in concrete beams for medium height structures</i> [Unpublished Doctoral dissertation]. The University of Washington.
Conference/Seminar Papers		
Conference proceedings published in a journal	... (Duckworth et al., 2019) ... Or Duckworth et al. (2019) ...	Duckworth, A. L., Quirk, A., Gallop, R., Hoyle, R. H., Kelly, D. R., & Matthews, M. D. (2019). Cognitive and noncognitive predictors of success. <i>Proceedings of the National Academy of Sciences, USA</i> , 116(47), 23499-23504. https://doi.org/10.1073/pnas.1910510116
Conference proceedings published as a book chapter	... (Bedenel et al., 2019) ... Or Bedenel et al. (2019) ...	Bedenel, A. L., Jourdan, L., & Biernacki, C. (2019). Probability estimation by an adapted genetic algorithm in web insurance. In R. Battiti, M. Brunato, I. Kotsireas, & P. Pardalos (Eds.), <i>Lecture notes in computer science: Vol. 11353. Learning and intelligent optimization</i> (pp. 225-240). Springer. https://doi.org/10.1007/978-3-030-05348-2_21

	Insertion in text	In reference list
Online	... (Gu et al., 2018) ... Or Gu et al. (2018) ...	Gu, X., Yu, J., Han, Y., Han, M., & Wei, L. (2019, July 12-14). <i>Vehicle lane change decision model based on random forest</i> . [Paper presentation]. 2019 IEEE International Conference on Power, Intelligent Computing and Systems (ICPICS), Shenyang, China. https://doi.org/10.1109/ICPICS47731.2019.8942520
Government Publications		
Government as author	First in-text reference: Spell out the full name with the abbreviation of the body. ... National Cancer Institute (2019) ... Or ... (National Cancer Institute, 2019) ... Subsequent in-text reference: ... NCI (2019) ... Or ... (NCI, 2019) ...	National Cancer Institute. (2019). <i>Taking time: Support for people with cancer</i> (NIH Publication No. 18-2059). U.S. Department of Health and Human Services, National Institutes of Health. https://www.cancer.gov/publications/patient-education/takingtime.pdf

8. General Guidelines

Abbreviations: Define alphabetically, other than abbreviations that can be used without definition. Words or phrases that are abbreviated in the *Introduction* and following text should be written out in full the first time that they appear in the text, with each abbreviated form in parenthesis. Include the common name or scientific name, or both, of animal and plant materials.

Authors' Affiliation: The primary affiliation for each author should be the institution where the majority of their work was done. If an author has subsequently moved to another institution, the current address may also be stated in the footer.

Co-Authors: The commonly accepted guideline for authorship is that one must have substantially contributed to the development of the paper and share accountability for the results. Researchers should decide who will be an author and what order they will be listed depending upon their order of importance to the study. Other contributions should be cited in the manuscript's *Acknowledgements*.

Similarity Index: All articles received must undergo the initial screening for originality before being sent for peer review. *Pertanika* does not accept any article with a similarity index exceeding **20%**.

Copyright Permissions: Authors should seek necessary permissions for quotations, artwork, boxes or tables taken from other publications or other freely available sources on the Internet before submission to *Pertanika*. The *Acknowledgement* must be given to the original source in the illustration legend, in a table footnote, or at the end of the quotation.

Footnotes: Current addresses of authors if different from heading may be inserted here.

Page Numbering: Every page of the manuscript, including the title page, references, and tables should be numbered.

Spelling: The journal uses American or British spelling and authors may follow the latest edition of the Oxford Advanced Learner's Dictionary for British spellings. Each manuscript should follow one type of spelling only.

SUBMISSION OF MANUSCRIPTS

All submissions must be made electronically using the **ScholarOne™ online submission system**, a web-based portal by Clarivate Analytics. For more information, go to our web page and click "**Online Submission (ScholarOne™)**".

Submission Checklist

1. MANUSCRIPT:

Ensure your manuscript has followed the *Pertanika* style particularly the first-4-pages as explained earlier. The article should be written in a good academic style and provide an accurate and succinct description of the contents ensuring that grammar and spelling errors have been corrected before submission. It should also not exceed the suggested length.

2. DECLARATION FORM:

Author has to sign a declaration form. In signing the form, authors declare that the work submitted for publication is original, previously unpublished, and not under consideration for any publication elsewhere.

Author has to agree to pay the publishing fee once the paper is accepted for publication in Pertanika.

3. COVER LETTER:

In Step 6 of the ScholarOne system, author is asked to upload a cover letter in *Pertanika* format. Please ignore this instruction and replace the cover letter with the **Declaration Form**.

Note:

COPYRIGHT FORM: Author will be asked to sign a copyright form when the paper is accepted. In signing the form, it is assumed that authors have obtained permission to use any copyrighted or previously published material. All authors must read and agree to the conditions outlined in the form and must sign the form or agree that the corresponding author can sign on their behalf. Articles cannot be published until a signed form (original pen-to-paper signature) has been received.

Visit our Journal's website for more details at <http://www.pertanika.upm.edu.my/>.

ACCESS TO PUBLISHED MATERIALS

Under the journal's open access initiative, authors can choose to download free material (via PDF link) from any of the journal issues from *Pertanika*'s website. Under "**Browse Journals**" you will see a link, "*Regular Issue*", "*Special Issue*" or "*Archives*". Here you will get access to all current and back-issues from 1978 onwards. No hard copy of journals or offprints are printed.

Visit our Journal's website at:

http://www.pertanika.upm.edu.my/regular_issues.php for "Regular Issue"
http://www.pertanika.upm.edu.my/cspecial_issues.php for "Special Issue"
http://www.pertanika.upm.edu.my/journal_archives.php for "Archives"

PUBLICATION CHARGE

Upon acceptance of a manuscript, a processing fee of RM 750 / USD 250 will be imposed on authors; RM 750 for any corresponding author affiliated to an institution in Malaysia; USD 250 for any corresponding author affiliated to an institution outside Malaysia. Payment must be made online at <https://paygate.upm.edu.my/action.do?do=>

Any queries may be directed to the **Chief Executive Editor's** office via email to executive_editor.pertanika@upm.edu.my

Morphological Characteristics and Plant Species for Noise Reducer and Pb Metal Absorbers at Adisucipto Airport: Yogyakarta, Indonesia <i>Chales Torang Pandapotan, Siti Nurul Rofiqo Irwan and Eka Tarwaca Susila Putra</i>	3043
Crack Behaviour of Self-Compacting Concrete (SCC) Beams Containing Eggshell in Flexural <i>Mohd Raizamzamani Md Zain, Oh Chai Lian, Lee Siong Wee, Norrul Azmi Yahya and Anizahyati Alisibramulisi</i>	3059
A Privacy Preserving Framework for Health Records using Blockchain <i>Chitra Karunakaran, Kavitha Ganesh, Sonya Ansar and Rohitha Subramani</i>	3081
Evaluation of Single Missing Value Imputation Techniques for Incomplete Air Particulates Matter (PM ₁₀) Data in Malaysia <i>Zuraira Libasin, Wan Suhailah Wan Mohamed Fauzi, Ahmad Zia ul-Saufie, Nur Azimah Idris and Noor Azizah Mazeni</i>	3099
Optimisation Design of Functionally Graded Sandwich Plate with Porous Metal Core for Buckling Characterisations <i>Emad Kadum Njim, Sadeq Hussein Bakhy and Muhannad Al-Waily</i>	3113
<i>Case Study</i> Anomaly Detection of Grid Connected Photovoltaic System Based on Degradation Rate: A Case Study in Malaysia <i>Mohamad Zhafran Hussin, Nor Diyana Md Sin, Hedzlin Zainuddin, Ahmad Maliki Omar and Sulaiman Shaari</i>	3143
Serious Game Conceptual Model of Brain-Based Learning for Halus Student <i>Saffa Raihan Zainal Abidin, Siti Fadzilah Mat Noor and Noraidah Sahari@Ashaari</i>	3161

Enhanced IoT-Based Climate Control for Oyster Mushroom Cultivation Using Fuzzy Logic Approach and NodeMCU Microcontroller <i>Muhammad Azizi Mohd Ariffin, Muhammad Izzad Ramli, Zarina Zainol, Mohd Nazrul Mohd Amin, Marina Ismail, Rosanita Adnan, Nor Diana Ahmad, Norhasiah Husain and Nursuriati Jamil</i>	2863
Participatory Design: Apps from The Older Adults to The Older Adults <i>Zaidatul Haslinda Abdullah Sani, Dinna@Ninna Mohd Nizam and Aslina Baharum</i>	2887
Development of Pulp Moulded Packaging Samples from Empty Fruit Bunch Fibre <i>Qiuyun Liu, Ceri Loxton, Amir Alzahari Mohamed, Mohammad Jawaid, Radek Braganca and Robert Elias</i>	2901
Empirical Model of Ground-Borne Vibration Induced by Commuter Railway Traffic <i>Mohd Khairul Afzan Mohd Lazi, Muhammad Akram Adnan and Norliana Sulaiman</i>	2913
<i>Review article</i>	
Impact of Climate Change on Migratory Birds in Asia <i>Nurhafizul Abu Seri and Azimah Abd Rahman</i>	2937
Enhanced Deep Hierarchical Long Short-Term Memory and Bidirectional Long Short-Term Memory for Tamil Emotional Speech Recognition using Data Augmentation and Spatial Features <i>Bennilo Fernandes and Kasiprasad Mannepalli</i>	2967
Proposed Methodology for End-of-Life Option using Multi Criteria Decision Analysis: A Study for General Paper Product <i>Salwa Mahmood, Muhammad Aizrul Ezuan Edirudzin and Nur Syamimi Jiran</i>	2993
Reduction of the Backing Gas Sequence as a Facile Method to Improve Corrosion Resistance in Duplex Stainless Steel (DSS) Weldment <i>Basuki Tri Laksono, Hendri Budi Kurniyanto, Purwa Sadewa and Riza Wirawan</i>	3013
Failure Rate Estimation for Transformer Population based on Health Index through Markov Model Approach <i>Nor Shafiqin Shariffuddin, Norhafiz Azis, Amran Mohd Selva, Muhammad Sharil Yahaya, Jasronita Jasni, Mohd Zainal Abidin Ab Kadir and Mohd Aizam Talib</i>	3029

The Demand Model of App-Based Transportation Household Scale in Semarang, Indonesia <i>Anita Ratnasari Rakhmatulloh, Diah Intan Kusumo Dewi, Wijayanti and Rosna Sari Pulungan</i>	2689
<i>Review article</i>	
Roles and Principles of Sterilisation Process in Palm Oil Mills <i>Yin Mee Thang, Robiah Yunus, Mohd Noriznan Mokhtar, David Ross Appleton, Ahmad Jaril Asis, Pei San Kong, Huey Fang Teh and Abdul Azis Ariffin</i>	2705
Utilisation of Oil Palm Fibre Biomass Waste as Additives in Foamed Concrete <i>Md Azree Othuman Mydin</i>	2723
Logistics and Freight Transportation Management: An NLP based Approach for Shipment Tracking <i>Rachit Garg, Arvind Wamanrao Kiwelekar and Laxman Damodar Netak</i>	2745
A Simulation Study on Modified Weibull Distribution for Modelling of Investment Return <i>Hamza Abubakar and Shamsul Rijal Muhammad Sabri</i>	2767
Analytical and Numerical Investigations of Mechanical Vibration in the Vertical Direction of a Human Body in a Driving Vehicle using Biomechanical Vibration Model <i>Maher Al-Baghdadi, Muhsin Jaber Jweeg and Muhannad Al-Waily</i>	2791
A Comparative Study on the Larvicidal Effects of <i>Piper sarmentosum</i> (Kaduk) Leaves Extracts against <i>Aedes aegypti</i> <i>Amelia Najiha Othman, Nur Farah Suryani Zainudin, Uswatun Hasanah Zaidan and Suhaili Shamsi</i>	2811
The Estimation of Iron Oxide Content in Soil based on Landsat 8 OLI TIRS Imagery in Wetland Areas <i>Deasy Arisanty, Aswin Nur Saputra, Akhmad Munaya Rahman, Karunia Puji Hastuti and Dedi Rosadi</i>	2829
Mathematical Modelling of Infra-Red Evaporation Characteristics of Wheat Straw Black Liquor <i>Surendra Pratap Singh, Mohammad Jawaaid, Bhoomika Yadav and Mohd Supian Abu Bakar</i>	2845

A Deep Learning Approach for Retinal Image Feature Extraction <i>Mohammed Enamul Hoque, Kuryati Kipli, Tengku Mohd Afendi Zulcaffle, Abdulrazak Yahya Saleh Al-Hababi, Dayang Azra Awang Mat, Rohana Sapawi and Annie Anak Joseph</i>	2543
Development of Micro-Spatial Electricity Load Forecasting Methodology Using Multivariate Analysis for Dynamic Area in Tangerang, Indonesia <i>Adri Senen, Christine Widyastuti, Oktaria Handayani and Perdana Putera</i>	2565
<i>Case study</i> Improving Performance in Construction Projects: A Case Study of Malaysian Public Projects <i>Aminah Md Yusof, Ali Raza Khoso, Samiullah Sohu, Shabir Hussain Khahro and Chang Saar Chai</i>	2579
Optimisation of Free Fatty Acid Removal in Nyamplung Seed Oil (<i>Callophyllum inophyllum</i> L.) using Response Surface Methodology Analysis <i>Ratna Dewi Kusumaningtyas, Haniif Prasetiawan, Radenrara Dewi Artanti Putri, Bayu Triwibowo, Siti Choirunisa Furi Kurnita, Nanda Dwi Anggraeni, Harumi Veny, Fazlena Hamzah and Miradatul Najwa Muhd Rodhi</i>	2605
A Comparative Study of Several EOF Based Imputation Methods for Long Gap Missing Values in a Single-Site Temporal Time Dependent (SSTTD) Air Quality (PM ₁₀) Dataset <i>Shamihah Muhammad Ghazali, Norshahida Shaadan and Zainura Idrus</i>	2625
Synthesis, Characterisation, and Density Functional Theory Study of Encapsulated Bioactive Components of Ginger <i>Triati Dewi Kencana Wungu, Damar Rastri Adhika, Meqorry Yusfi, Atsarina Larasati Anindya, Eduardus Bimo Aksono, Raden Roro Fosa Sarassina, Christofora Hanny Wijaya and Suprijadi</i>	2645
An Indoor Navigation Support for the Student Halls of Residence using Augmented Reality: A Design Perspective <i>Dinna Nina Mohd Nizam, Lim Wei Shin, Zaidatul Haslinda Abdullah Sani, Pornpon Thamrongrat and Nooralisa Mohd Tuah</i>	2659
Effects of Noise Pollution from Electric Backup Generators on the Operators' Health <i>Mahmmoud Ismail Mohammed and Muwafaq Ayesh Rabeea</i>	2675

A Novel Approach of Audio Based Feature Optimisation for Bird Classification <i>Murugaiya Ramashini, Pg Emeroylariffion Abas and Liyanage C De Silva</i>	2383
Behavioural Model for Decision-Makers' towards the Intention to Adopt Green Information Technology: A Preliminary Study <i>Abba Kyari Buba and Othman Ibrahim</i>	2409
Effect of Initial Carbon to Nitrogen Ratio on the Degradation of Oil Palm Empty Fruit Bunch with Periodic Addition of Anaerobic Palm Oil Mill Effluent Sludge <i>Muhamad Yusuf Hasan, Mohd Ali Hassan, Mohd Noriznan Mokhtar, Yoshihito Shirai and Azni Idris</i>	2435
Enhancement of Binding Affinity of Anti-Hapten Polyclonal IgG Recognizing Mitragnine using Affinity Purification <i>Radhiahtul Raehan Mustafa, Rashidah Sukor, Siti Mariam Mohd Nor, Nazamid Saari, Farina Mustaffa Kamal and Aliah Zannierah Mohsin</i>	2451
Response of Rubber Tree Saplings to Dolomite and Kieserite Application and K:Mg Ratio <i>Chakkrit Poonpakdee, Khwunta Khawmee and Jumpen Onthong</i>	2465
The Effect of the Operation Time, Orientation of Passenger and Body Mass Index on Passengers' Whole-Body Vibration on Urban Rail <i>Muhammad Nur Annuar Mohd Yunos, Mohd Azlis Sani Md Jalil, Nor Azali Azmir and Mifzal Nazhan Mazlan</i>	2481
Diffusion and Osmotic Permeability of Ion Exchange Membrane MK-40 Using Sodium Chloride Solution <i>Mohammed Qader Gubari, Haider Mohammed Zwain and Nadezda Vyacheslavovna Alekseeva</i>	2497
The Prediction of Chlorophyll Content in African Leaves (<i>Vernonia amygdalina</i> Del.) Using <i>Flatbed Scanner</i> and Optimised Artificial Neural Network <i>Retno Damayanti, Nurul Rachma, Dimas Firmanda Al Riza and Yusuf Hendrawan</i>	2509
The Effect of Storage Diversity on the Breaking Strength and Elongation of Polyamide Monofilament in Gill Net Fishing Gear <i>Herry Boesono, Fadhila Surya Layli, Agus Suherman, Bogi Budi Jayanto and Arief Yudhi Susanto</i>	2531

Pertanika Journal of Science & Technology

Vol. 29 (4) Oct. 2021

Content

Foreword <i>Mohammad Jawaid</i>	i
Mobile Application Development for Spectral Signature of Weed Species in Rice Farming <i>Nor Athirah Roslin, Nik Norasma Che'Ya, Nursyazyla Sulaiman, Lutfi Amir Nor Alahyadi and Mohd Razi Ismail</i>	2241
<i>Review article</i>	
Potential of <i>Syzygium polyanthum</i> (Daun Salam) in Lowering Blood Glucose Level: A Review <i>Nur Salsabeela Mohd Rahim, Ida Farah Ahmad and Terence Yew Chin Tan</i>	2261
Socio-Demographic Profile and Prevalence of Tuberculosis (TB) Treatment Outcomes among Tuberculosis/Human Immunodeficiency Virus (TB/HIV) Co-Infected Patients in Kelantan <i>Siti Romaino Mohd Nor, Mohd Rozi Husin, Mat Zuki Mat Jaeb and Nyi Nyi Naing</i>	2279
Physical Modelling of Flow and Head along with Dead-end and Looped Manifolds <i>Abdullah Amer, Thamer Ahmad Mohammad, Wissam Hameed Alawee and Nadhir Al-Ansari</i>	2295
A Combined Analytical Method for Intelligent Control of Friction Damped Structures <i>Kamyar Gharra, Karen Khanlari and Jafar Asgari Marnani</i>	2317
Classification of Existing Health Model of India at the End of the Twelfth Plan using Enhanced Decision Tree Algorithm <i>Ashok Kumar, Arun Lal Srivastav, Ishwar Dutt and Karan Bajaj</i>	2341
<i>Review Article</i>	
An Era of Recommendation Technologies in IoT: Categorisation by techniques, Challenges and Future Scope <i>Partibha Ahlawat and Chhavi Rana</i>	2355



Pertanika Editorial Office, Journal Division,
Putra Science Park,
1st Floor, IDEA Tower II,
UPM-MTDC Center,
Universiti Putra Malaysia,
43400 UPM Serdang,
Selangor Darul Ehsan
Malaysia

<http://www.pertanika.upm.edu.my>
Email: executive_editor@upm.edu.my
Tel. No.: +603- 9769 1622

PENERBIT
UPM
UNIVERSITI PUTRA MALAYSIA
PRESS

<http://www.penerbit.upm.edu.my>
Email: penerbit@upm.edu.my
Tel. No.: +603- 9769 8851

